PROCEEDINGS OF THE NINTH WORKSHOP ON GENERAL RELATIVITY AND GRAVITATION

Department of Physics, Hiroshima University,

November 3 - 6, 1999

edited by

Y. Eriguchi, T. Futamase, A. Hosoya, H. Ishihara,
M. Kasai, Y. Kojima, K. Maeda, T. Nakamura,
K. Nakao, Y. Nambu, K. Oohara, M. Sasaki,
J. Soda, K. Watanabe, K. Yamamoto

PREFACE

This volume is the proceedings of the ninth workshop on General Relativity and Gravitation. The purpose was to review the latest developments in general relativity and gravitation and related fields and to discuss future prospects. It was held from 3 to 6 November 1999 at the Department of Physics, Hiroshima University. The workshop of this year was timely concerning the site and date, since 50th anniversary of the funding of the Hiroshima University was celebrated during the period. There are a lot of Japanese researchers studying the general relativity and gravitation. Some pursued in the past their works as a professor or a graduate student in RITP (Research Institute for Theoretical Physics) at the Hiroshima University, which was integrated into the Yukawa Institute at Kyoto in 1990. This workshop gave a good chance to recall old days and visit the new campus in Higashi-Hiroshima. (See a brief note by Prof. Tomita.) The total number of the participants was 120, and 74 speakers gave talks including 10 invited talks. We wish to thank all the participants for their contributions to the workshop.

We would like to thank Mrs. Yokota, the secretary at the Department of Physics, Kyoto University, for her devoted transaction of various official works. We are also grateful to the graduate student of the astrophysics group in Hiroshima University for their cooperation in the management of the workshop. This workshop was supported by Grant-in-Aid for Creative Basic Research from the Japanese Ministry of Education, Science, Sports and Culture, which was the financial base of this workshop.

Y. Eriguchi	(University of Tokyo)
T. Futamase	(Tohoku University)
A. Hosoya	(Tokyo Institute of Technology)
H. Ishihara	(Tokyo Institute of Technology)
M. Kasai	(Hirosaki University)
Y. Kojima(*Secretary of the workshop*)	(Hiroshima University)
K. Maeda	(Waseda University)
T. Nakamura	(YITP)
K. Nakao	(Osaka City University)
Y. Nambu	(Nagoya University)
K. Oohara	(Niigata University)
M. Sasaki	(Osaka University)
J. Soda	(Kyoto University)
K. Watanabe	(Niigata University)
K. Yamamoto(*Secretary of the workshop*)	(Hiroshima University)

PROGRAM(TABLE OF CONTENTS)

PREFACE ii

Wednesday, November 3

Afternoon Session I (Chairperson: Y. Kojima)

Tsallis Statistics and Galaxy Distribution
Izumi Joichi ..... *

Multi-centered Solutions with a (very special) Warped Compactification
Mitsuru Ooho and Kiyoshi Shiraishi 1

Finite Temperature Field Theory of "Extreme Black Holes"
Yoshitaka Degura and Kiyoshi Shiraishi 5

Fermion Stars with an Extra Dimension
Nahomi Kan and Kiyoshi Shiraishi 13

AdS/CFT with non-trivial Dilaton
Shin'ichi Nojiri 20

Afternoon Session II (Chairperson: J. Soda)

Path Integral Measure in Higher-Derivative Gravity
Shinji Hamamoto and Makoto Nakamura 35

Massive Dirac Fields in Conformally Flat Spacetime
Nobukuni Hatayama and Koichi Hayashi 40

Neutrino Oscillations in Strong Gravitational Fields
Shinji Tsujikawa, Jun-ichiro Koga and Kei-ichi Maeda 45

String Excitation inside Generic Black Holes
Kengo Maeda, Takashi Torii and Makoto Narita 53

Semiclassical Approach to the Stability of Multidimensional Spacetime in Gravity Theory Depending on the Ricci Tensor
Hirofumi Iwasaki, Yasuo Ezawa and Tadashi Yano 61

Excitation of Kaluza-Klein Gravitational Mode
Kunihito Uzawa, Yoshiyuki Morisawa and Shinji Mukohyama 69

Comment on Non-Archimedean Character of Quantum Buoyancy
Takashi Okamura 77

BTZ Black Hole Entropy in Higher Curvature Gravity
Hiromi Saida and Jiro Soda 84

Aspects of Black Hole Entropy
Shinji Mukohyama 92

Black Hole Entropy in the Membrane Paradigm
Takeshi Shimomura, Takashi Okamura and Takashi Mishima 99

Motion of Cosmic String coupled to Gravitational Wave
Kouji Nakamura, Akihiro Ishibashi and Hideki Ishihara 107

Thursday , November 4
Morning Session I (Chairperson: Y. Kojima)

Observation of Black Hole Binary with ASCA and Test of Theoretical Model for Accretion Disk
Aya Kubota ..... *

Gravitational Effects on Neutrino Pair Annihilation in GRB Sources
Katsuaki Asano 115

Poynting Burst from a Collapsing Magnetized Star
Masayuki Nagamachi, Akira Tomimatsu and Masaaki Takahashi 123

Standing Shocks in MHD Accretions onto Black Holes
Masaaki Takahashi 131

Hypernovae and Black Hole Formation
Takayoshi Nakamura, Keiichi Maeda, Koichi Iwamoto, Tomoharu Suzuki, Ken'ichi Nomoto, Paolo A. Mazzali, Massimo Turatto, I. John Danziger and Ferdinando Patat 139

Morning Session II (Chairperson: M. Takahashi)

First Data from the TAMA300 Gravitational-Wave Detector
Seiji Kawamura and the TAMA collaboration 148

Searching for Gravitational Waves from Inspiralling Compact Binaries Using TAMA 300 Data
Hideyuki Tagoshi, Takahiro Tanaka, Nobuyuki Kanda, Daisuke Tatsumi, Souich Telada, Masatake Ohashi, and TAMA300 collaboration 162

Afternoon Session I (Chairperson: H. Tagoshi)

The Highest Energy Cosmic Rays
Masahiro Teshima 165

Structures of General Relativistic Binary Neutron Star Systems in Quasiequilibrium - A New Approach without the Conformally Flat Condition -
Fumihiko Usui, Koji Uryu and Yoshiharu Eriguchi 170

Almost Analytic Solution to Equilibrium Sequences of Irrotational Binary Polytropic Stars for $n = 1$
Keisuke Taniguchi and Takashi Nakamura 177

General Relativistic Simulations of Jet Formation in a Rapidly Rotating Black Hole Magnetosphere
Shinji Koide, David L. Meier, Kazunari Shibata and Takahiro Kudoh 182

Equation of Motion for the Relativistic Compact Binaries - Point Particle Limit Approach -
Yousuke Itoh, Toshifumi Futamase and Hideki Asada 190

Afternoon Session II (Chairperson: K. Nakamura)

Coalescing Binary Neutron Stars - 3D General Relativistic Simulations Using Conformal Slicing -

Ken-ichi Oohara and Takashi Nakamura 198

The post-Newtonian Equations of Spin Precession of Spinning Compact Objects to Second Post-Newtonian Order

Akira Ohashi 210

Gravitational Reaction Force on a Particle in the Schwarzschild Background

Hiroyuki Nakano and Misao Sasaki 215

Gravitational Radiation Reaction

Yasushi Mino ..... *

Gravitational Waves from Inspiralling Compact Binaries with Magnetic Dipole Moments

Kunihito Ioka and Keisuke Taniguchi 223

Inertial Modes of Rotating Stars

Shijun Yoshida and Umin Lee 231

Friday , November 5

Morning Session I (Chairperson: H. Asada)

Majumdar-Papapetrou Interior Field

Daisuke Ida 239

Relativistic Shell Crossing in the Wall of a Spherical Void

Ken-ichi Nakao ..... *

Morphology and Stability and Black Holes

Tatsuhiko Koike and Masaru Siino ..... *

Motion of Two Bodies in 2-dimensions and the Structure of Space-Time

Tadayuki Ohta and Robert Mann 247

Role of 5D Space-Time-Matter Theory in Modified GST Theory

Takao Fukui 256

Probe Particle, Force Balance and Exact Solution

Tetsuya Shiromizu 262

Quintessence without a Potential

Takahiro Okabe ..... *

Phantom Field: a Form of Dark Energy

Takeshi Chiba 268

Morning Session II (Chairperson: H. Asada)

Recent Development on Gamma-Ray Bursts
Nobuyuki Kawai ..... *

Afternoon Session I (Chairperson: M. Sasaki)

Cosmological Constant, Quintessence and Scalar-Tensor Theories of Gravity
Yasunori Fujii 274

Spherically Symmetric Self-Similar Solutions and their Astrophysical and Cosmological Applications
B.J.Carr 285

Afternoon Session II (Chairperson: N. Sugiyama)

On Average Properties of Inhomogeneous Cosmologies
Thomas Buchert 306

Lagrangian Description of Fluid Flow with Acceleration in Relativistic Cosmology
Hideki Asada 322

Can We See a Rotating Gravitational Lens ?
Masumi Kasai ..... *

Distance and Lensing in Cosmological Void Models
Kenji Tomita 328

GRG in Hiroshima
Kenji Tomita 334

Saturday , November 6

Morning Session I (Chairperson: M. Siino)

The Canonical Formulation of $N = 2$ Supergravity in terms of the Ashtekar Variable
Motomu Tsuda 335

Hyperbolic and Asymptotically Constrained Systems in the Ashtekar Formulation of General Relativity
Gen Yoneda and Hisa-aki Shinkai 342

Reinterpretations of the Vacuum C-metric
Masashi Egi 350

Properties of Locally $U(1) \times U(1)$ Symmetric Spacetimes
Masayuki Tanimoto ..... *

Analytic Description of Singularities in non-vacuum Gowdy Spacetimes
Makoto Narita, Takashi Torii and Kengo Maeda 358

Inversion of Spacetime with Maximally Charged Black Holes
Takashi Mishima, Hideki Ishihara and Takashi Okamura 366

Morning Session II (Chairperson: H. Ishihara)

Hawking Radiation with Modified High Frequency Dispersion Relation
Yoshiaki Himemoto and Takahiro Tanaka 373

Mass Spectrum of Scalar Field Fluctuation near Reissner-Nordstrom Black Hole
Hiroko Koyama and Akira Tomimatsu 381

Naked Singularities and Particle Creations
Akihiro Ishibashi and Akio Hosoya 386

Thurston's Geometrization Conjecture and Cosmological Models
Katsuhito Yasuno, Tatsuhiko Koike and Masaru Siino 391

Late Time Dynamics of Scalar Perturbations in Majumdar-Papapetrou Black Holes
Masaru Siino 395

Scaling of the Global String Network in the Matter Dominated Universe
Masahide Yamaguchi, Jun'ichi Yokoyama and Masahiro Kawasaki 403

Afternoon Session I (Chairperson: K. Nakao)

Phase Transition and Fractal in Self-Gravitating Ring Model
Yasuhide Sota, Osamu Iguchi and Masahiro Morikawa 411

Origin and Evolution of Stochastic Biasing
Atsushi Taruya and Yasushi Suto 418

Naked Singularity Explosion
Tomohiro Harada, Hideo Iguchi and Ken-ichi Nakao 425

Formation of Q-balls through Affleck-Dine Mechanism
Shinta Kasuya and Masahiro Kawasaki 430

Topological Defect Inflation
Nobuyuki Sakai 437

False Vacuum Decay with Gravity in Non-Thin-Wall Limit
Gen Uchida and Misao Sasaki 445

An Open Universe from Valley Bounce
Kazuya Koyama, Kayoko Maeda and Jiro Soda 453

Afternoon Session II (Chairperson: M. Kasai)

What Happens When the Inflaton Stops during Inflation
Osamu Seto, Jun'ichi Yokoyama and Hideo Kodama 461

Thick Domain Walls Interacting with a Black Hole
Yoshiyuki Morisawa, Ryo Yamazaki, Daisuke Ida, Akihiro Ishibashi and Ken-ichi Nakao 469

Theoretical Formulation for Two-Point Statistics on a Light Cone
Hiroaki Nishioka 474

Second Order Rotational Effects on the R-Mode Oscillations in GR
Masayasu Hosonuma and Yasufumi Kojima 482

General Relativistic Approach to Magnetized Stars
Kohkichi Konno, Tomohiro Obata and Yasufumi Kojima 488

Magnetized Stars on Relativistic Perturbation Theory
Tomohiro Obata, Kohkichi Konno and Yasufumi Kojima 496

Multi-centered Solutions with a (very special) Warped Compactification [1]

Mitsuru Ooho[2]

Graduate School of Science and Engineering, Yamaguchi University,
Yoshida, Yamaguchi 753-8512, Japan

Kiyoshi Shiraishi[3]

Graduate School of Science and Engineering, Yamaguchi University,
Yoshida, Yamaguchi 753-8512, Japan
and
Department of Physics, Yamaguchi University,
Yoshida, Yamaguchi 753-8512, Japan

Abstract

We find an exact solution for multi-black strings in the brane world with warped compactification.

1 Introduction

Recently it has been suggested by much work on unification theories that we live in a brane with three-dimensional spatial extension. Randall and Sundrum proposed a warped compactification scenaro [1]. They assumed the five-dimensional spacetime and the presence of a negative cosmological constant in the bulk space. Two branes with tension of individual values realize the compactification of an extra dimension on S^1/Z_2. The mass scale on a brane depends on the warp factor which is determined by the location of the brane in the extra dimension. Thus their model provides a novel solution to the hierarchy problem.

Extensions to many branes have been studied by many authors. (see, for example, [2].) [4]

The models including dilaton fields have been also studied [4] [5]. In the case, although the bulk space is not an anti-de Sitter space, similar warped compactification can be obtained.

On the other hand, the black hole solution on the brane was analyzed by Chamblin et al. [6]. Many other types of localized objects in the brane world may be considered, and we expect that physics on a brane will be clarified by study of them.

In this talk, we show an exact solution for charged objects in the brane world.

2 Brane world

We consider a model including a dilaton field governed by the following action:

$$\begin{aligned} S &= \int d^D x\sqrt{-g}\left[R - \frac{4}{D-2}(\nabla\phi)^2 - 2\Lambda e^{4b\phi/(D-2)}\right] \\ &- \sum_k \int_{brane_k} d^{D-1}x\sqrt{-g_{D-1}}2\sigma_k e^{2b\phi/(D-2)}, \end{aligned} \tag{1}$$

[1] A short talk presented by K.S. at JGRG '99 (November 3), at Hiroshima University, Japan.
[2] E-mail:c5024@sty.sv.cc.yamaguchi-u.ac.jp
[3] E-mail:shiraish@sci.yamaguchi-u.ac.jp
[4] A single brane scenario[3] has been also considered. We will not mention this scenario in detail here.

where Λ is a cosmological constant and σ_k is the tension of the kth brane. The metric is assumed to be

$$ds^2 = \Omega^2(\chi)\left[\eta_{\mu\nu}dx^\mu dx^\nu + d\chi^2\right], \tag{2}$$

where $\mu, \nu = 0, \cdots, D-2$. We also assume that the configuration of the dilaton field takes the form:

$$e^{4b\phi/(D-2)} = \Omega^{-2b^2}. \tag{3}$$

Under the assumptions, field equations derived from the previous action can be reduced to be

$$(D-2)(D-1-b^2)\left(\frac{\Omega'}{\Omega}\right)^2 = (-2\Lambda)\Omega^{2-2b^2}, \tag{4}$$

$$-\left(\frac{\Omega'}{\Omega}\right)' + (1-b^2)\left(\frac{\Omega'}{\Omega}\right)^2 = \frac{1}{D-2}\Omega^{1-b^2}\sum_k \sigma_k \delta(\chi - \chi_k), \tag{5}$$

where χ_k is a position of the kth brane.

For $b^2 \neq 1$, one can find the following solution:

$$\left(\Omega^{b^2-1}\right)' = \pm(1-b^2)\sqrt{\frac{(-2\Lambda)}{(D-2)(D-1-b^2)}}, \tag{6}$$

$$\left(\Omega^{b^2-1}\right)'' = (1-b^2)\frac{1}{D-2}\sum_k \sigma_k \delta(\chi - \chi_k). \tag{7}$$

This yields the brane solutions on tuning values for brane tensions. [5]

In particular, the case with $b^2 = 0$ corresponds to the Randall-Sundrum model. To see this more explicitly, we introduce a new coodinate $dz \equiv \Omega d\chi$. Then the metric takes the form:

$$ds^2 = e^{-2Kz}\eta_{\mu\nu}dx^\mu dx^\nu + dz^2, \tag{8}$$

where K is a certain constant.

For $b^2 = 1$, the solution is

$$\phi = \pm\frac{\sqrt{-2\Lambda}}{2}\chi, \quad \Omega = e^{-2\phi/(D-2)}. \tag{9}$$

In this case with $b^2 = 1$, we can simplifies the action, if we set $\bar{g}_{\mu\nu} = e^{4\phi/(D-2)}g_{\mu\nu}$, as

$$\begin{aligned} \bar{S} &= \int d^D x\sqrt{-\bar{g}}e^{-2\phi}\left[\bar{R} + 4\left(\bar{\nabla}\phi\right)^2 - 2\Lambda\right] \\ &- \sum_k \int_{\text{brane}_k} d^{D-1}x\sqrt{-\bar{g}_{D-1}}2\sigma_k e^{-2\phi} \end{aligned} \tag{10}$$

Therefore, the bulk solution for $b^2 = 1$ is the linear dilaton solution.

3 Black strings in the brane world

From now on, we concentrate our attention to the $b = 1$ case. We introduce an anti-symmetric tensor field into the model:

$$\begin{aligned} S &= \int d^D x\sqrt{-g}\left[R - \frac{4}{D-2}(\nabla\phi)^2 - \frac{1}{12}e^{-8\phi/(D-2)}H^2 - 2\Lambda e^{4\phi/(D-2)}\right] \\ &- \sum_k \int_{\text{brane}_k} d^{D-1}x\sqrt{-g_{D-1}}2\sigma_k e^{2\phi/(D-2)}, \end{aligned} \tag{11}$$

[5] For a single negative cosmological constant, one should choose $\sigma_k = \pm 2\sqrt{-2\Lambda}$.

where H_{MNL} is an anti-symmetric tensor field strength.

In this model, a solution in the bulk space is:

$$ds^2 = \Omega^2(\chi)\left[h^{-\frac{D-4}{D-3}}(-dt^2 + d\chi^2) + h^{\frac{2}{D-3}}\delta_{ij}dx^i dx^j\right], \tag{12}$$

$$e^{4b\phi/(D-2)} = \Omega^{-2}h^{-\frac{2}{D-3}}, \quad H_{t\chi i} = \partial_i h^{-1}, \tag{13}$$

$$(D-2)^2\left(\frac{\Omega'}{\Omega}\right)^2 = (-2\Lambda), \tag{14}$$

$$-\left(\frac{\Omega'}{\Omega}\right)' = \frac{1}{D-2}\sum_k \sigma_k \delta(\chi - \chi_k), \tag{15}$$

with

$$h = 1 + \frac{1}{\Omega^{D-2}}\sum_a \frac{\mu_a}{(D-4)|\mathbf{x} - \mathbf{x}_a|^{D-4}}, \tag{16}$$

where μ_a are arbitrary constants.

A spacetime slice with a constant χ appears to be extreme black holes with a dilaton and a scalar field:

$$ds_e^2 = h^{\frac{D-4}{(D-3)(D-3)}}\left[-h^{-\frac{D-4}{D-3}}dt^2 + h^{\frac{1}{D-3}}\delta_{ij}dx^i dx^j\right] + h^{-\frac{D-4}{D-3}}d\chi^2. \tag{17}$$

In particular, for $D = 5$, the metric seems

$$ds_e^2 = h^{\frac{1}{3}}\left[-h^{-\frac{1}{2}}dt^2 + h^{\frac{1}{2}}\delta_{ij}dx^i dx^j\right] + h^{-\frac{1}{3}}d\chi^2. \tag{18}$$

4 .Induced charge, energy density and pressure

When the black strings penetrate a brane perpendicularly, matter and dilatonic charge distributions are "induced" on the brane. For simplicity, we consider a single brane located at $\chi = 0$. The field equations are:

$$\begin{aligned} & R_{\mu\nu} - \frac{1}{2}Rg_{\mu\nu} - \frac{4}{D-2}\left[\nabla_\mu\phi\nabla_\nu\phi - \frac{1}{2}(\nabla\phi)^2 g_{\mu\nu}\right] \\ - & \frac{1}{4}e^{-8\phi/(D-2)}\left[H_{\mu\nu}^2 - \frac{1}{6}H^2 g_{\mu\nu}\right] + e^{4\phi/(D-2)}\Lambda g_{\mu\nu} + \frac{\sqrt{-g_{D-1}}}{\sqrt{-g}}e^{2\phi/(D-2)}\sigma g_{\mu\nu}\delta(\chi) \\ = & \frac{4}{D-2}\frac{\sqrt{-g_{D-1}}}{\sqrt{-g}}e^{2\phi/(D-2)}T_{\mu\nu}, \end{aligned} \tag{19}$$

$$\begin{aligned} & - \frac{8}{D-2}\nabla^2\phi - \frac{1}{12}\frac{8}{D-2}e^{-8\phi/(D-2)}H^2 \\ & + \frac{8}{D-2}e^{4\phi/(D-2)}\Lambda + \frac{4}{D-2}\frac{\sqrt{-g_{D-1}}}{\sqrt{-g}}e^{2\phi/(D-2)}\sigma\delta(\chi) \\ & = \frac{4}{D-2}\frac{\sqrt{-g_{D-1}}}{\sqrt{-g}}e^{2\phi/(D-2)}Q, \end{aligned} \tag{20}$$

where $T_{\mu\nu}$ represents the "induced" energy-momentum tensor and Q represents the "induced" dilatonic charge on the brane, when the bulk solution of black strings in the previous section is substituted into the equations.

We obtain:

$$\rho = -\sigma\left(1 - \frac{1}{\sqrt{h}}\right)\delta(\chi), \tag{21}$$

$$p = -\frac{\sigma}{2}\left(\sqrt{h} + \frac{1}{\sqrt{h}} - 2\right)\delta(\chi), \tag{22}$$

$$Q = -\rho, \tag{23}$$

where $T^{\mu}_{\nu} = diag.(-\rho, p, \cdots, p)$. Here we omitted the singularity of the string core.

In the case with a single black string at the origin in $D = 5$, ρ behaves as $1/r$ and p as $1/r^2$, asymptotically at a large distance r.

5 Summary

We have obtained an exact solution for multi-black strings in the brane world with warped compactification. Since the black strings "induce" matter and charge distributions on the brane, we suppose that the theory of gravity on the brane shoud be an "unusual" one.

In future work, we will examine the geodesic motion around the black strings in the brane world. We will also study black hole solutions with and without charges in the models including dilatonic fields, and in the case with a general number of extra dimensions. It is also interesting to study black holes in the case with thick domain walls.

Furthermore, we should investigate the possible relation to the string/M theory.

Note added After this talk, we found [7], in which various solitons are studied in the brane world with non-trivial dilatons.

References

[1] L. Randall and R. Sundrum, Phys. Rev. Lett. 83 (1999), 3370, hep-ph/9905221.

[2] H. Hatanaka et al., hep-th/9909076.

[3] L. Randall and R. Sundrum, Phys. Rev. Lett. 83 (1999), 4690, hep-th/9906064.

[4] A. Kehagias, hep-th/9906204.

[5] E. Halyo, hep-th/9909127.

[6] J. W. Chamblin, S. Hawking and Reall, hep-th/9909205.

[7] D. Youm, hep-th/9911218.

Finite Temperature Field Theory of "Extreme Black Holes"

Yoshitaka Degura[1] and Kiyoshi Shiraishi[2]

Graduate School of Science and Engineering, Yamaguchi University,
Yoshida, Yamaguchi-shi, Yamaguchi 753-8512, Japan

Abstract

We treat the model where "extreme black holes" move slowly. We derive an effective lagrangian in the low energy for this model and then investigate a statistical behavior of "extreme black holes" in the finite temperature.

1 Introduction

"Extreme black holes" are the objects (solitons) which have a certain condition between electric charge and mass; these two horizons coincide with each other. In other words, "extreme black holes" realize when three forces (the gravitational force, the electric force and the dilaton force) between dilatonic black holes are cancelled with each other. We regard "extreme black holes" as point particles, so we consider that the collection of these particles is expressed by the scalar field. For the static case, we know that the solution of "extreme black holes" is the Papapetrou-Majumdar-Myers solution [1, 2, 3]. On the other hand, we consider "extreme black holes" for the dynamical case, we derive a theoretical model of a (non-relastivistic) field including the low energy interaction of "extreme black holes". In the finite temperature, we examine the structure of the gas of "extreme black holes". As a result, we will show that the gas of "extreme black holes" lumps at the high temperature.

2 Effective Lagrangian

In this section, we derive an effective lagrangian for "extreme black holes" of which a typical velocity v is slow. In the classical theory, the action of particles, which have mass m and charge e, coupled to the gravitational field, the electromagnetic field and the dilaton field, is

$$I = -\int ds \left[m e^{a\phi} + eA_\mu \frac{dx^\mu}{ds} \right], \tag{1}$$

where ϕ is a dilaton field, a is the coupling constant of the dilaton field. Then, the four-momentum of the particle is

$$P_\mu = m e^{a\phi} g_{\mu\nu} \frac{dx^\nu}{ds} - eA_\mu. \tag{2}$$

This four-momentum satisfies the following equation:

$$g^{\mu\nu}(P_\mu + eA_\mu)(P_\nu + eA_\nu) + m^2 e^{2a\phi} = 0. \tag{3}$$

Next, in quantum theory, we can rewrite this equation (3) into a wave equation for a wave function φ:

$$\left[g^{\mu\nu}(P_\mu + eA_\mu)(P_\nu + eA_\nu) + m^2 e^{2a\phi} \right] \varphi = 0. \tag{4}$$

[1] E-mail:c1997@sty.sv.cc.yamaguchi-u.ac.jp
[2] E-mail:shiraish@sci.yamaguchi-u.ac.jp

So the action which gives this wave equation is

$$S_m = \int d^4x\sqrt{-g}\left[-\varphi^* e^{-a\phi} g^{\mu\nu}(P_\mu + eA_\mu)(P_\nu + eA_\nu)\varphi - m^2 e^{a\phi}\varphi^*\varphi\right], \tag{5}$$

where we regard φ as a "field" from now on. Therefore the total action including interactions is

$$S = \int d^4x \frac{\sqrt{-g}}{16\pi}\left[R - 2(\nabla_\mu\phi)(\nabla^\mu\phi) - e^{-2a\phi}F_{\mu\nu}F^{\mu\nu}\right] + S_m, \tag{6}$$

which leads to the following field equations,

$$\nabla^2\phi + \frac{a}{2}e^{-2a\phi}F^2 + 4\pi a\left[e^{-a\phi}\varphi^*(P+eA)^2\varphi - e^{a\phi}m^2\varphi^*\varphi\right] = 0, \tag{7}$$

$$\begin{aligned} R_{\mu\nu} - \frac{1}{2}g_{\mu\nu}R = 2\left[\nabla_\mu\phi\nabla_\nu\phi - \frac{1}{2}g_{\mu\nu}(\nabla\phi)^2\right] + e^{-2a\phi}\left[2F_{\mu\nu}^2 - \frac{1}{2}g_{\mu\nu}F^2\right] \\ +16\pi\Big\{e^{-a\phi}Re\Big[\varphi^*(P_\mu + eA_\mu)(P_\nu + eA_\nu)\varphi \\ -\frac{1}{2}g_{\mu\nu}\varphi^*(P+eA)^2\varphi\Big] - \frac{1}{2}g_{\mu\nu}e^{a\phi}m^2\varphi^*\varphi\Big\}, \end{aligned} \tag{8}$$

$$\nabla_\mu\left[e^{-2a\phi}F^{\mu\nu}\right] = 8\pi e\, e^{-a\phi}\varphi^* g^{\nu\lambda}(P_\lambda + eA_\lambda)\varphi. \tag{9}$$

From now on we consider in the lowest order of a typical velocity v of "extreme black holes", so we assume as follows:

$$ds^2 = -U^{-2}(dt + B_i dx^i)^2 + U^2 dx^2\ , \tag{10}$$

$$U = V(x)^{\frac{1}{1+a^2}}\ , \tag{11}$$

$$e^{-2a\phi} = V^{\frac{2a^2}{1+a^2}}\ , \tag{12}$$

$$A_0 = \frac{1}{\sqrt{1+a^2}}\left(1 - \frac{1}{V}\right)\ , \tag{13}$$

$$A_i \sim B_i = O(v). \tag{14}$$

Under these ansatze, for a static configuration ($A_i = B_i = 0$), a vacuum solution satisfies

$$\partial^2 V = 0, \tag{15}$$

which means that this vacuum solution represents an arbitrary number of "extreme black holes" [1, 2, 3]. One can find that the relation between mass m and electric charge e of a particle is, as seen from the correspondence of "extreme black holes",

$$\frac{e}{m} = \sqrt{1+a^2}. \tag{16}$$

Next, we consider the low energy limit, $-P_0 - m = E - m \ll m$. Then

$$\begin{aligned} P_0 + eA_0 &= P_0 + \frac{e}{\sqrt{1+a^2}}\left(1 - \frac{1}{V}\right) = P_0 + \left(1 - \frac{1}{V}\right) \\ &\approx -m\frac{1}{V}, \end{aligned} \tag{17}$$

$$\begin{aligned} P_i + eA_i - B_i(P_0 + eA_0) &\approx P_i + e\left(A_i + \frac{1}{\sqrt{1+a^2}}\frac{1}{V}B_i\right) \\ &\equiv P_i + e\hat{A}_i, \end{aligned} \tag{18}$$

where

$$\hat{A}_i \equiv A_i + \frac{1}{\sqrt{1+a^2}}\frac{1}{V}B_i\,, \tag{19}$$

and

$$\begin{aligned}\hat{F}_{ij} &\equiv \partial_i\hat{A}_j - \partial_j\hat{A}_i \\ &= \tilde{F}_{ij} - \frac{1}{\sqrt{1+a^2}}\frac{1}{V}G_{ij},\end{aligned} \tag{20}$$

where

$$\tilde{F}_{ij} \equiv F_{ij} + B_iF_{j0} - B_jF_{i0}, \tag{21}$$

$$G_{ij} \equiv \partial_iB_j - \partial_jB_i. \tag{22}$$

Taking the low energy and non-relativistic limit $-P_0 - m = E - m \ll m$, $|P_i + e\hat{A}_i|^2 \approx m^2v^2 \ll m^2$, we solve explicitly the field equations (7), (8) and (9). From the dilaton field equation (7), the (0 0) component of the gravitational field equation (8) and the time component of the electromagnetic field equation (9), in the lowest order, we obtain

$$\partial^2V + 8\pi(1+a^2)m^2U^3|\varphi|^2 = 0. \tag{23}$$

From the (0 i) component of the gravitational field equation (8), we get

$$\begin{aligned}\partial_t\Big[V^{\frac{2(a^2-1)}{1+a^2}}\frac{1}{V^2}G_{ti}\Big] &= 4\sqrt{\frac{1}{1+a^2}}\,\partial_t\Big[V^{\frac{2(a^2-1)}{1+a^2}}\frac{1}{V}\tilde{F}_{ti}\Big] - 4\sqrt{\frac{1}{1+a^2}}\frac{1}{V}\,\partial_t\Big[V^{\frac{2(a^2-1)}{1+a^2}}\tilde{F}_{ti}\Big] \\ &\quad + 32\pi\frac{m}{V}\,e^{-a\phi}\,\varphi^*(P_i + eA_i)\,\varphi,\end{aligned} \tag{24}$$

On the other hand, the space component of the electromagnetic field equation (9) reads

$$\partial_t\Big[V^{\frac{2(a^2-1)}{1+a^2}}\tilde{F}_{ti}\Big] = 8\pi e\,e^{-a\phi}\,\varphi^*(P_i + eA_i)\,\varphi. \tag{25}$$

We define an antisymmetric tensor field H_{ij} as

$$H_{ij} \equiv 4\sqrt{\frac{1}{1+a^2}}\tilde{F}_{ij} - \frac{1}{V}G_{ij}. \tag{26}$$

From eqs. (24) and (25), the antisymmetric tensor field equation is

$$\partial_t\Big[V^{\frac{2(a^2-1)}{1+a^2}}\frac{1}{V}H_{ti}\Big] = 0. \tag{27}$$

As stated, the (0 i) component of the gravitational field equation (8) and the space component of the electromagnetic field equation (9) are

$$-\frac{1+a^2}{3-a^2}\,\partial_t\Big[V^{\frac{2(a^2-1)}{1+a^2}}\hat{F}_{ti}\Big] = 8\pi e\,e^{-a\phi}\,\varphi^*(P_i + e\hat{A}_i)\,\varphi, \tag{28}$$

By the way, from eqs. (20) and (26), we can obtain the following relation:

$$\frac{1}{4}\frac{1}{V^2}G^2 - \tilde{F}^2 = \frac{1+a^2}{3-a^2}\Big(\hat{F}^2 - \frac{1}{4}H^2\Big). \tag{29}$$

Now we consider the effective lagrangian. From the total action (6),

$$\begin{aligned}
\mathcal{L} &= \sqrt{-g}\left\{\frac{1}{16\pi}\left[R - 2(\nabla\phi)^2 - e^{-2a\phi}F^2\right]\right. \\
&\qquad \left. + \left[-\varphi^* e^{-a\phi} g^{\mu\nu}(P_\mu + eA_\mu)(P_\nu + eA_\nu)\varphi - m^2 e^{a\phi}\varphi^*\varphi\right]\right\} \\
&\approx \frac{1}{16\pi} V^{\frac{2(a^2-1)}{1+a^2}}\left[\frac{1}{4}\frac{1}{V^2}G^2 - \tilde{F}^2\right] \\
&\quad + \left[V U^3 \varphi^*(P_0 + eA_0)^2\varphi - \frac{1}{V}m^2 U^3\varphi^*\varphi - \frac{1}{V}V^{\frac{2(a^2-1)}{1+a^2}} U^3\varphi^*(P_i + e\dot{A}_i)^2\varphi\right] \\
&= \frac{1}{16\pi} V^{\frac{2(a^2-1)}{1+a^2}}\left[\frac{1+a^2}{3-a^2}\left(\hat{F}^2 - \frac{1}{4}H^2\right)\right] \\
&\quad + \left[V U^3 \varphi^*(P_0 + eA_0)^2\varphi - \frac{1}{V}m^2 U^3\varphi^*\varphi - \frac{1}{V}V^{\frac{2(a^2-1)}{1+a^2}} U^3\varphi^*(P_i + e\dot{A}_i)^2\varphi\right]. \qquad (30)
\end{aligned}$$

In the first term of this effective lagrangian, H_{ij} can be regarded as an external field because H_{ij} does not couple to the scalar field φ. Because there is no external field in the model which we have considered, we consider only the interactions among black holes, thus $H_{ij} \equiv 0$.

We introduce a non-relativistic field ψ:

$$\psi \equiv \sqrt{2m}\, U^{3/2}\varphi, \qquad (31)$$

where since $(-g^{(3)})^{1/4} = U^{3/2}$, we obtain a correct measure. So the effective lagrangian in the low energy is

$$\begin{aligned}
\mathcal{L} &= \psi^*\left(-P_0 - m\right)\psi - \frac{1}{2m\, V^{(3-a^2)/(1+a^2)}}\psi^*\left(\boldsymbol{P} + e\hat{\boldsymbol{A}}\right)^2\psi \\
&\quad + \frac{1}{16\pi}\frac{1+a^2}{3-a^2}\frac{1}{V^{2(1-a^2)/(1+a^2)}}\hat{F}^2, \qquad (32)
\end{aligned}$$

where V satisfies the following equation:

$$\partial^2 V + 4\pi(1+a^2)\, m\,|\psi|^2 = 0. \qquad (33)$$

As a check, varying this effective lagrangian (32) with respect to $\hat{\boldsymbol{A}}$, we can derive again the field equation (28) in the low energy approximation:

$$-\frac{1+a^2}{3-a^2}\partial_t\left[V^{\frac{2(a^2-1)}{1+a^2}}\hat{F}_{ti}\right] = 8\pi e\, e^{-a\phi}\varphi^*(P_i + e\dot{A}_i)\varphi. \qquad (34)$$

3 Hartree-Fock Approximation in the Finite Temperature

First we rewrite the effective lagrangian (32) derived in the previous section as follows:

$$\mathcal{L} = \psi^* i\frac{\partial}{\partial t}\psi - \frac{1}{2M}\psi^*\left(\boldsymbol{P} + \tilde{e}\boldsymbol{A}\right)^2\psi + \frac{1}{16\pi}F_{ij}^2, \qquad (35)$$

where we omitted hat for simplicity. We have also used the notations:

$$M \equiv m V^{\frac{3-a^2}{1+a^2}}, \qquad (36)$$

$$\begin{aligned}
\tilde{e}^2 &\equiv \frac{3-a^2}{1+a^2}V^{\frac{2(1-a^2)}{1+a^2}}e^2 \\
&= (3-a^2)V^{\frac{2(1-a^2)}{1+a^2}}m^2. \qquad (37)
\end{aligned}$$

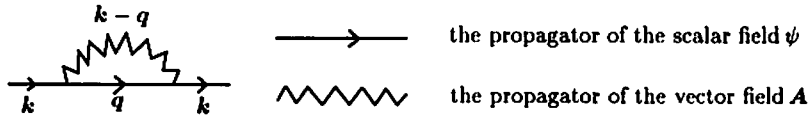

Fig. 1: Self-energy of the scalar field.

The relation between mass m and electric charge e is again

$$\frac{e}{m} = \sqrt{1+a^2}. \tag{38}$$

Next we consider the field theory in the finite temperature [4]. We define the propagator of the vector field $\boldsymbol{A}$:

$$\nu_{ij}(q) = \nu(q)\Big(\delta_{ij} - \frac{q_i q_j}{q^2}\Big). \tag{39}$$

In the lowest order, the self-energy of the scalar field is

$$\Sigma(k) \;=\; -\frac{1}{\beta\mathcal{V}}\frac{1}{4M^2}\sum_{q,\ell}\frac{\nu(k-q)}{i\omega_\ell - \epsilon'_q}\Big[(k+q)^2 - \frac{\{(k+q)\cdot(k-q)\}^2}{(k-q)^2}\Big], \tag{40}$$

(see Fig. 1) where $\mathcal{V}$ is the volume of the system, $\beta = 1/T$ (T is the temperature of the system), $\omega_\ell (= 2\ell\pi/\beta)$ is a frequency and

$$\epsilon'_k \;=\; \frac{1}{2M}k^2 + \Sigma(k) - \mu. \tag{41}$$

(μ : a chemical potential.)

In the lowest order, $\nu(q) = \tilde{e}^2/q^2$. We transform the sum over q, ℓ into integral representations; we can rewrite the self-energy of the scalar field (40) as

$$\begin{aligned}\Sigma(k) \;&=\; \frac{\tilde{e}^2}{4M^2}\frac{1}{(2\pi)^3}\int d^3q\, f_q \frac{1}{(k-q)^2}\Big[(k+q)^2 - \frac{\{(k+q)\cdot(k-q)\}^2}{(k-q)^2}\Big] \\ &=\; \frac{\tilde{e}^2}{M^2}\frac{1}{4\pi^2}\int_0^\infty dq\, q^2 f_q\left[-1 - \frac{k^2+q^2}{2kq}\ln\left|\frac{k-q}{k+q}\right|\right],\end{aligned} \tag{42}$$

where f_q is a distribution function of the scalar field:

$$f_q \;\equiv\; \frac{1}{e^{\beta\epsilon'_q} - 1}. \tag{43}$$

The self-energy of the scalar field $\Sigma(k)$ is, by non-relativistic treatment,

$$-1 - \frac{k^2+q^2}{2kq}\ln\left|\frac{k-q}{k+q}\right| \approx \frac{4k^2}{3q^2}. \tag{44}$$

From eq. (44), there is no constant term in terms of k, so can write approximately

$$\Sigma(k) \approx \frac{1}{2}Bk^2, \tag{45}$$

where B is a constant.

From now on we consider the high temperature approximation. Then the distribution function of the scalar field is

$$f_q \approx e^{-\beta\epsilon'_q} \tag{46}$$

Therefore (self-consistent) Hartree - Fock equation is

$$\begin{aligned}\Sigma(k) &\approx \frac{1}{2}Bk^2 \\ &\approx \frac{\tilde{e}^2}{4\pi^2M^2}\int_0^\infty dq\, q^2 f_q \frac{4k^2}{3q^2} \\ &= \frac{1}{2}\frac{4\tilde{e}^2 e^{\beta\mu}}{3(2\pi)^{3/2}M^2}\left[\beta\left(\frac{1}{M}+B\right)\right]^{-1/2}k^2.\end{aligned} \tag{47}$$

As a result, we get

$$B = \frac{4\tilde{e}^2 e^{\beta\mu}}{3(2\pi)^{3/2}M^2}\left[\beta\left(\frac{1}{M}+B\right)\right]^{-1/2}. \tag{48}$$

So the solution of eq. (48) in terms of B is

$$B = \frac{4\tilde{e}^2 e^{\beta\mu}}{3(2\pi)^{3/2}M^2}\sqrt{\frac{M}{\beta}}\left(\cos\frac{\theta}{3}+\frac{1}{\sqrt{3}}\sin\frac{\theta}{3}\right)^{-1}, \tag{49}$$

where

$$\theta = \sin^{-1}\frac{2\sqrt{3}\tilde{e}^2 e^{\beta\mu}}{(2\pi)^{3/2}\sqrt{\beta M}}. \tag{50}$$

On the other hand, the particle density n is

$$\begin{aligned}n &= \frac{1}{(2\pi)^3}\int d^3q\, f_q \\ &= \frac{e^{\beta\mu}}{(2\pi)^{3/2}}\left[\beta\left(\frac{1}{M}+B\right)\right]^{-3/2}.\end{aligned} \tag{51}$$

The particle density can also be written by $|\psi|^2$, therefore

$$|\psi|^2 = n = e^{\beta\mu}\left(\frac{M}{2\pi\beta}\right)^{3/2}\left[\cos\frac{\theta}{3}+\frac{1}{\sqrt{3}}\sin\frac{\theta}{3}\right]^{-3}. \tag{52}$$

Now we have to solve the following equation with this equation (52)

$$\partial^2 V + 4\pi(1+a^2)\,m\,|\psi|^2 = 0. \tag{53}$$

For solving explicitly eq. (53), let us assume the spherical symmetry and define the following quantities:

$$n_0 \equiv e^{\beta\mu}\left(\frac{m}{2\pi\beta}\right)^{3/2}, \tag{54}$$

$$\tilde{r} \equiv \sqrt{G\,m\,n_0}\,r, \tag{55}$$

$$\delta \equiv 2\sqrt{3}\,G\,n_0\beta, \tag{56}$$

where G is the Newton constant. Then eq. (53) for V is

$$\frac{1}{\tilde{r}^2}\left(\tilde{r}^2 V(\tilde{r})'\right)' = 4\pi(1+a^2)V(\tilde{r})^{\frac{3(3-a^2)}{2(1+a^2)}}\left(\cos\frac{\theta}{3}+\frac{1}{\sqrt{3}}\sin\frac{\theta}{3}\right)^{-3}, \tag{57}$$

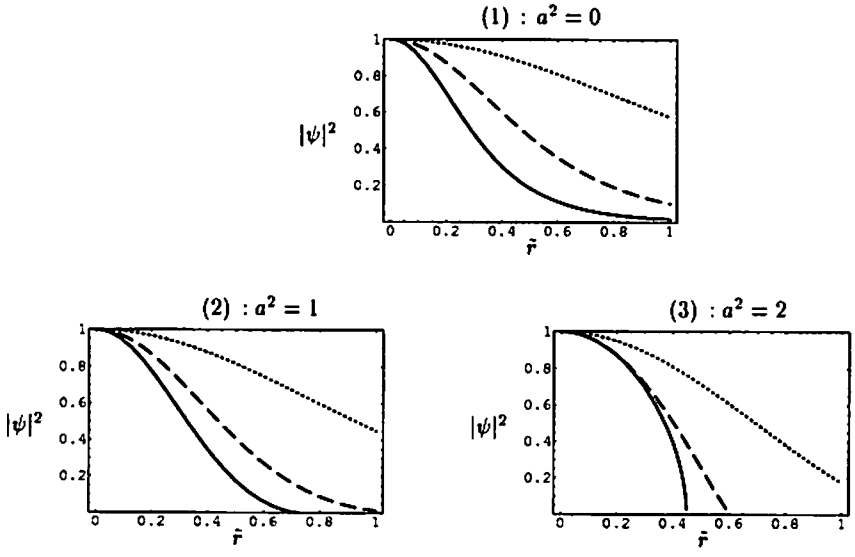

Fig. 2: The density distribution of the isothermal sphere of "extreme black holes" for different values of the coupling constant of the dilaton field; (1) $a^2 = 0$, (2) $a^2 = 1$ and (3) $a^2 = 2$. The solid line denotes $\delta = 0$ (the high temperature limit), the broken line $\delta = 1$ and the dotted line $\delta = 10$.

where prime denotes derivative with respect to $\tilde{r}$, and

$$\theta(\tilde{r}) = \sin^{-1}\left[(3-a^2)V(\tilde{r})^{\frac{(1-3a^2)}{2(1+a^2)}}\delta\right]. \tag{58}$$

From eqs. (52), (57) and (58), we have calculated numerically the relation between the radius $\tilde{r}$ and the particle density $|\psi|^2$ of the isothermal sphere of "extreme black holes". (see Fig. 2.) As seen from Fig. 2, we find that as δ is the smaller, that is, the temperature is the higher, the particles lump the more tightly, because the magnetic force acts among the particles as the attractive force in order v^2 from the electromagnetic field equation (9). And we see that as the coupling constant of the dilaton field is the larger, the particles lump the more tightly. In particular, there is a critical point whether an extent of the edge exists or not. For the case $a^2 = 3$, the effective lagrangian represents the free lagrangian, therefore the particles correspond to the free particles.

4 Conclusion

In this paper, we have derived the effective lagrangian of "extreme black holes" in the low energy. For the finite temperature, we have obtained Hartree - Fock equation and then we have seen the structure of the isothermal sphere distribution of "extreme black holes". In the high temperature, the gas of "extreme black holes" have been lumped by the attractive force. We have seen that there is the critical point at $a^2 \sim 1$ whether an extent of the edge exists or not.

In future work, we will evaluate the correction by the self-energy of the vector field $\boldsymbol{A}$ (see Fig. 3), consider the case of the low temperature, that is, the condensation, take the statistics of "extreme black

holes" into consideration and study the calculation by means of a lattice space.

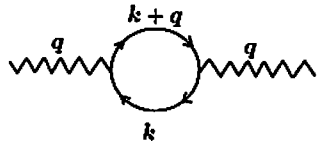

Fig. 3: Self-energy of the vector field

References

[1] A. Papapetrou, Proc. R. Irish Acad. **A51** (1947), 191.

[2] S. D. Majumdar, Phys. Rev. **72** (1947), 930.

[3] R. C. Myers, Phys. Rev. **D35** (1987), 455.

[4] A. L. Fetter and J. D. Walecka, *Quantum Theory of Many-Particle Systems* (McGraw-Hill, Inc., 1971).

Fermion Stars with an Extra Dimension

Nahomi Kan[1] and Kiyoshi Shiraishi[2]

Graduate School of Science and Engineering, Yamaguchi University,
Yoshida, Yamaguchi-shi, Yamaguchi 753-8512, Japan

Abstract

Many efforts have been devoted to the studies of the phenomenology in particle physics with extra dimensions. We propose the degenerate fermion star in the five dimensions, and study what effects caused by the geometry of extra dimensions should appear in its structure. We note that Kaluza-Klein excited modes have effects for the larger scale of extra dimensions and examine the conditions on which different layers should be caused in the inside of the stars. We expound how the effects of the extra dimensions appears on physical quantities.

1 Introduction

Recently, physics dealing with higher dimensions has been noted [1, 2]. Considering extra dimensions in GUT, one points out four forces could be unified at low energy scale. And these are closely related with superstring theories, supergravity, and the others. There are many works on extra dimensions. One of them is "Neutron stars and extra dimensions" by Liddle, Moorhouse and Henriques [3]. They considered the neutron stars in five dimensions of which the fifth one is compactified into S^1, and showed that the maximum mass of the stars decreases under the background. However there are some problems in their result. First, they did not consider Kaluza-Klein (K-K) excited modes caused by the geometry of extra dimensions. Secondly, they put some hypotheses both on the equation of state and on that of conservation, so arbitrariness is left. Whereas, in this paper, taking account of the K-K modes, we propose the star in the five dimensions, which is made of degenerate Dirac fermions, and indicated that the excited modes have effects to the inside of star. After asking for the maximum mass and the radius by use of numerical calculation, we will make it clear what the interior structure of star should be.

2 Matter

2.1 (3+1) dimensions

In the four dimensional theory, the thermodynamic potential of a fermion gas with mass m and half spin is

$$\Omega_4 = -2\frac{1}{\beta}V\int\frac{d^3\mathbf{p}}{(2\pi)^3}\left[\ln\left(1+e^{-\beta(\sqrt{\mathbf{p}^2+m^2}-\mu)}\right)+(\mu\leftrightarrow-\mu)\right], \tag{1}$$

where we put subscript to emphasize that it stands for a four dimensional quantity. We will restrict our system to degenerate fermion gas and take the zero temperature limit. Then, the thermodynamic potential becomes

$$\Omega_4(m) \equiv \begin{cases} -V\frac{m^4}{24\pi^2}\left[\frac{\mu}{m}\sqrt{\frac{\mu^2}{m^2}-1}\left(2\frac{\mu^2}{m^2}-5\right)+3\ln\left|\frac{\mu}{m}+\sqrt{\frac{\mu^2}{m^2}-1}\right|\right] & (m<\mu) \\ 0, & (m\geqq\mu) \end{cases}. \tag{2}$$

Thermodynamical quantities follow from Eq.(2).

[1] E-mail:b1834@sty.sv.cc.yamaguchi-u.ac.jp
[2] E-mail:shiraish@sci.yamaguchi-u.ac.jp

2.2 (4+1) dimensions

We will extend our argument into the five dimensional theory. Here we suppose that the fifith dimension is compactified into S^1 with a radius b, b is not so large. We impose the periodic boundary condition on a wave function in the fifth dimension:

$$\psi(\chi) \sim e^{ip_5 \cdot \chi} , \tag{3}$$

$$\psi(\chi + 2\pi b) \sim \psi(\chi) , \tag{4}$$

with the fifth coordinate χ and momentum p_5 , then

$$p_5 = \frac{n}{b} \quad (n\text{: integer}) . \tag{5}$$

Therefore the relativistic energy involving the fifth dimension is

$$E_5 = \sqrt{\mathrm{p}^2 + (\frac{n}{b})^2 + m^2} \tag{6}$$

$$= \sqrt{\mathrm{p}^2 + M^2} , \tag{7}$$

where

$$M^2 \equiv \left(\frac{n}{b}\right)^2 + m^2 , \tag{8}$$

(n is integer. Unless $n = 0$, the K-K modes become effective.) Using Eq.(7), the thermodynamic potential of the fermion gas with mass m and half spin in the (4+1) dimensional space-time is

$$\Omega_5 = -2\frac{1}{\beta}V_4 \int \frac{d^4\mathrm{p}}{(2\pi)^4} \left[\ln\left(1 + e^{-\beta(\sqrt{\mathrm{p}^2+M^2}-\mu)}\right) + (\mu \leftrightarrow -\mu)\right] , \tag{9}$$

If we turn the integral over the fifth dimensional momentum into the sum over quantum number n, that is :

$$\int dp_5 \to \frac{1}{b}\sum_n , \tag{10}$$

and in addition,

$$V_4 = 2\pi b V , \tag{11}$$

then the thermodynamic potential is

$$\Omega_5 = -2\frac{1}{\beta}V \sum_n \int \frac{d^3\mathrm{p}}{(2\pi)^3} \left[\ln\left(1 + e^{-\beta(\sqrt{\mathrm{p}^2+\frac{n^2}{b^2}+m^2}-\mu)}\right) + (\mu \leftrightarrow -\mu)\right]$$

$$= \sum_n \Omega_4\left(\sqrt{m^2 + \frac{n^2}{b^2}}\right) = \sum_n \Omega_4(M) . \tag{12}$$

As well as the previous section, we will deal with the degenerate fermion gas and low temperature near to zero. The thermodynamic potential, therefore,

$$\Omega_5 = \begin{cases} -Vb^{-4}f(\mu b, mb), & (\mu > M) \\ 0, & (\mu \leqq M) \end{cases} , \tag{13}$$

where

$$f \equiv \sum_{n=-\infty}^{\infty} \frac{(Mb)^4}{24\pi^2} \left\{ \frac{\mu b}{Mb} \left(2\left(\frac{\mu b}{Mb}\right)^2 - 5 \right) \sqrt{\left(\frac{\mu b}{Mb}\right)^2 - 1} + 3\ln \left| \sqrt{\left(\frac{\mu b}{Mb}\right)^2 - 1} + \frac{\mu b}{Mb} \right| \right\} \quad (\mu > M) \ . \tag{14}$$

From Eq.(13), thermodynamical quantities are as follows:

$$P = -\frac{1}{2\pi b}\frac{\partial \Omega_5}{\partial V} = -\frac{1}{2\pi b}\frac{\Omega_5}{V} = \frac{1}{2\pi b}\frac{1}{b^4} f \ , \tag{15}$$

$$P_5 = -\frac{1}{2\pi V}\frac{\partial \Omega_5}{\partial b} = \frac{1}{2\pi b}\frac{1}{b^4}\left(x\frac{\partial f}{\partial x} + y\frac{\partial f}{\partial y} - 4f \right) \ , \tag{16}$$

$$\rho = \frac{U}{V_4} = \frac{1}{2\pi b}\frac{1}{b^4}\left(x\frac{\partial f}{\partial x} - f \right) \ , \tag{17}$$

where P_5 is the pressure in the fifth dimension, and we put $x = \mu b, \ y = mb$.

3 Space-Time

We take the line element to be of the form

$$ds^2 = e^{-\Phi}\left[-e^{-2\delta}\Delta dt^2 + \frac{dr^2}{\Delta} + r^2(d\theta^2 + \sin^2\theta d\varphi^2) \right] + b_0^2 e^{2\Phi} d\chi^2 \ , \tag{18}$$

where we regard Δ, δ, and Φ ($b = b_0 e^{\Phi}$) as functions depending only on r, the distance from the origin. Next, the energy-momentum tensor is

$$T^{\mu}_{\nu} = diag.(-\rho, P, P, P, P_5) \ , \tag{19}$$

in which we suppose isotropic pressure in the space of three dimensions, and represent the fifth dimensional pressure as P_5. The equation of conservation is

$$\nabla_{\mu} T^{\mu r} = 0 \ . \tag{20}$$

From this, we find the chemical potential μ satisfies that

$$\mu b = \frac{e^{\frac{3}{2}\Phi + \delta}}{\sqrt{\Delta}} \mu_0 b_0 \ , \tag{21}$$

where μ depends on r and μ_0 and b_0 are each the value of μ and b when r is close to zero.

4 Equations

Now, we are just deriving Einstein equations. Before that, we will rewrite Eq.(14). After putting

$$x = \mu b, \quad y = mb,$$

Eq.(14) reduces to

$$\begin{aligned} f(x,y) &= {\sum_{n=-\infty}^{\infty}}' \frac{(y^2+n^2)^2}{24\pi^2} \left[\frac{x}{\sqrt{y^2+n^2}} \sqrt{\frac{x^2}{y^2+n^2} - 1} \left(2\frac{x^2}{y^2+n^2} - 5 \right) \right. \\ &\quad \left. + 3\ln \left| \frac{x}{\sqrt{y^2+n^2}} + \sqrt{\frac{x^2}{y^2+n^2} - 1} \right| \right] \\ &= {\sum_{n=-\infty}^{\infty}}' \tilde{f}(x,y) \qquad (\sqrt{x^2 - y^2} > n^2) \ , \end{aligned} \tag{22}$$

where the sum over n is done unless n^2 exceeds $\sqrt{x^2-y^2}$. (To remark this, we put prime on a sum symbol.) In addition, we put

$$Y = \sqrt{y^2+n^2} \, . \tag{23}$$

Using the leading formulae, Einstein equations are

$$\frac{\tilde{M}_\star'}{\tilde{r}^2} - \frac{3}{8}\tilde{\Delta}(\Phi')^2 = 4\pi \frac{1}{m^4 b_0^4} e^{-6\Phi} {\sum}' \left(x \frac{\partial \tilde{f}}{\partial x} - \tilde{f} \right) \, , \tag{24}$$

$$\frac{1}{\tilde{r}}\delta' + \frac{3}{4}(\Phi')^2 = -4\pi \frac{1}{m^4 b_0^4} \frac{e^{-6\Phi}}{\tilde{\Delta}} {\sum}' \left(x \frac{\partial \tilde{f}}{\partial x} \right) \, , \tag{25}$$

$$\begin{aligned} \Phi'' + \left(\frac{\tilde{\Delta}'}{\tilde{\Delta}} - \delta' + \frac{2}{\tilde{r}} \right) \Phi' \;\; = \;\; & -\frac{8\pi}{3} \frac{1}{m^4 b_0^4} \frac{e^{-6\Phi}}{\tilde{\Delta}} {\sum}' \left(\frac{3Y^2 - 2y^2}{Y^2} x \frac{\partial \tilde{f}}{\partial x} \right. \\ & \left. - \frac{12Y^2 - 8y^2}{Y^2} \tilde{f} \right) \, , \end{aligned} \tag{26}$$

where

$$\tilde{M}_\star = \sqrt{G_0^{(4)} m^2} G_0^{(4)} m M_\star \, , \tag{27}$$

$$\tilde{r} = \sqrt{G_0^{(4)} m^4} r \, , \tag{28}$$

$$\tilde{\Delta} = 1 - \frac{2\tilde{M}_\star}{\tilde{r}} \, . \tag{29}$$

In the above equations, we define a usual Newtonian constant $G_0^{(4)}$ as

$$G_0^{(4)} \equiv \frac{G_0^{(5)}}{2\pi b_0} \, , \tag{30}$$

in which $G_0^{(5)}$ stands for the Newtonian constant in the fifth dimension. And $M_\star$ is the mass of star depending on r. A prime means derivative with respect to $\tilde{r}$. We can solve these equations numerically. In the next section, we will show the result.

5 Results

We will exhibit the relationship between the mass and the central density in fermion stars in Fig.1, and the mass and the radius in Fig.2. It turns out that the larger the extra dimension grows, the smaller the maximum mass becomes. Furthermore, it is remarkable that two maximum points appeared when $mb_0 = 3, 4$.

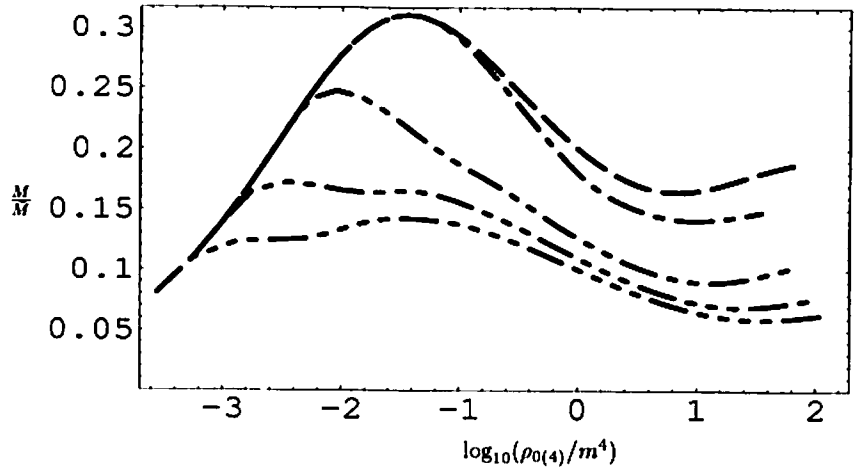

Fig 1: Plots of the mass M of the fermion stars versus its central density $\rho_{0(4)}$ for the various scales of the extra dimension. The dashed line corresponds to $mb_0 \approx 0$. The dot-dashed line corresponds to $mb_0 = 1$, the two dot-dashed line to $mb_0 = 2$, the three to $mb_0 = 3$, the four to $mb_0 = 4$.

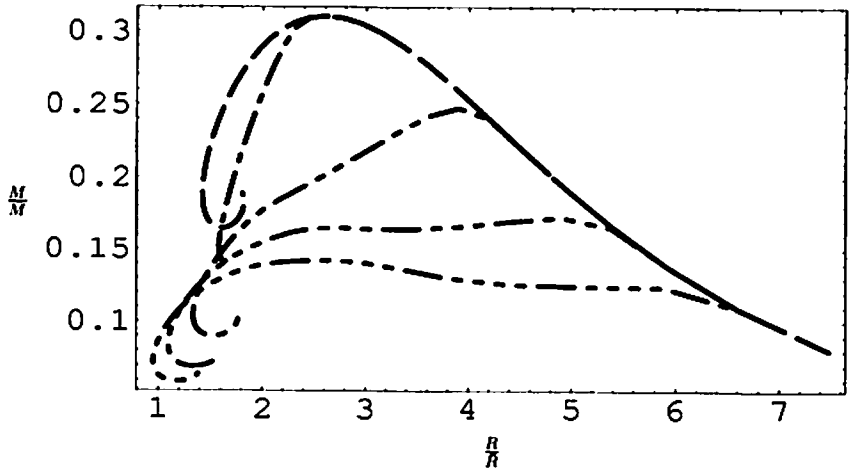

Fig 2: Plots of the mass M of the fermion stars versus its radius R for the various scales of the extra dimension. The correspondence between the dashed lines and the fifth dimension is the same as Fig.1.

Next, in Fig.3, we draw the interior structure of the stars having the maximum mass, which is based on Fig.2. We can read off it from Fig.3 that the excited modes have effects in the core of the stars with increase in the extra dimension. We have two solutions in the case of $mb_0 = 3, 4$. For $mb_0 = 3$, one of them is a larger star than that for $mb_0 = 2$ and its central density is lower, which is shown in Fig.1. While the other gets to be a smaller one and its central density is higher. In this solution, higher excited mode (n=2) is caused mainly in the center of stars and lower mode (n=1) in the vast region including the core. Proceeding to $mb_0 = 4$, this inclination appears more remarkably.

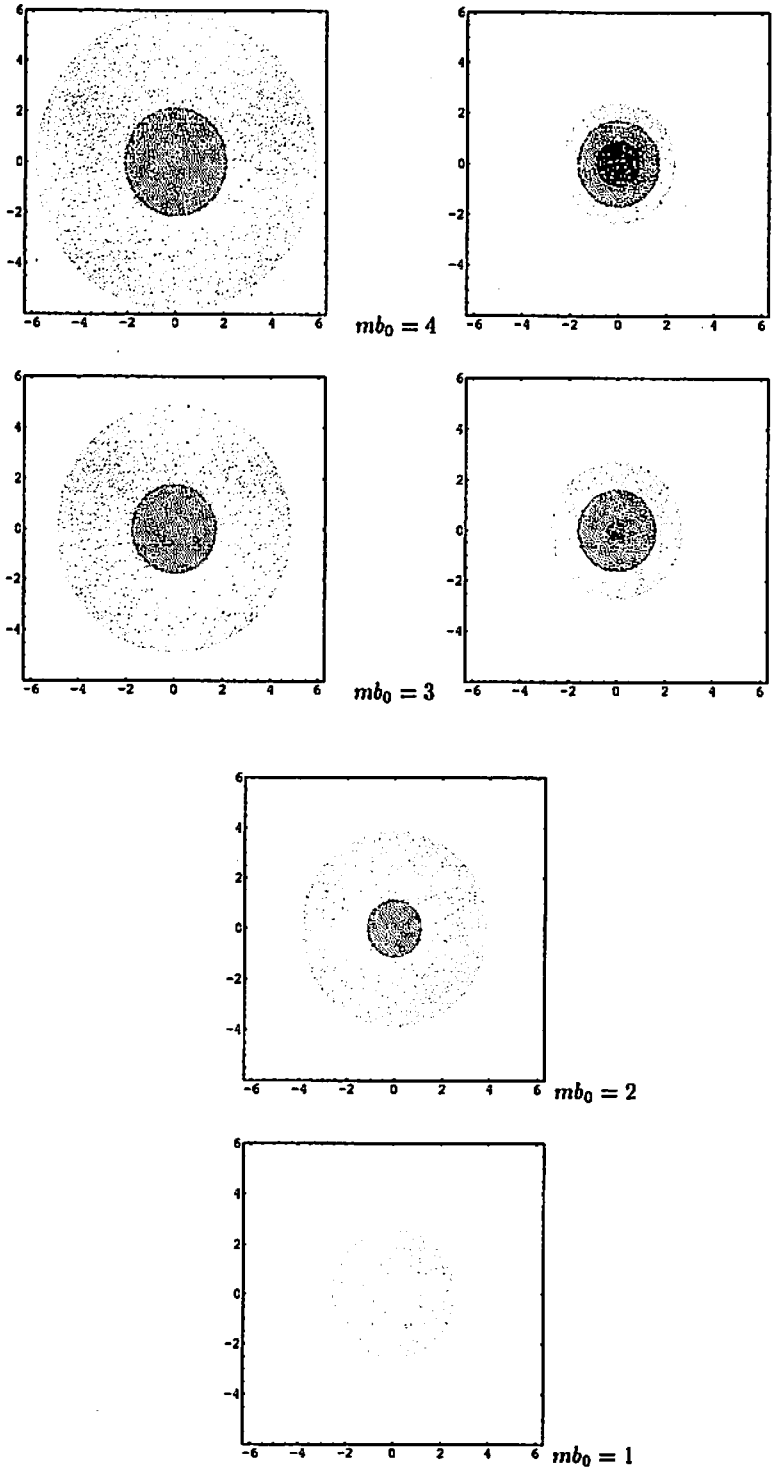

Fig 3: The evolutions of the fermion stars with the increase of the extra dimension. In the darkest circle, n=2 mode is most effective and n=1 mode in the middle one. The pale circle stands for no excited mode.

6 Conclusion

We have shown that considering K-K mode in the five dimensional theory, as the extra dimension becomes larger, the maximum mass more and more decreases. And also we have obtained two series of solutions. One is that the fermion star is getting larger and its central density lower with the increase of the extra dimension, that is, the larger and lighter star is formed. In these solutions, only n=1 mode is caused in the core of the stars. The other is that as the extra dimension grows, though the star once becomes larger and its central density lower for mb_0=2, it is getting smaller and smaller and its central density higher for the much larger dimension, namely, the smaller and heavier star is created. In these stars, n=2,1 modes is caused, the former is in the center of the stars and the latter is in the vast region including the core. As far as we examine, in this time, we have proved that the structure of the fermion stars depends on the scale of the fifth dimension, that is, the excited modes have effects to the inside of stars. Taking the scale of the fifth dimension much larger, however, we need to analyze the stability of stars explicitly. And, in this paper, we have imposed the periodic boundary condition on a wave function in the fifth dimension, while we can adopt the general one, that is: $\psi(\chi+2\pi b) \sim e^{i\varphi}\psi(\chi)$. For the anti-periodic one, $\psi(\chi+2\pi b) \sim -\psi(\chi)$, the effective mass of the fermion $M_{(h)}$ is $M_{(h)} = \sqrt{m^2+(\frac{n\pm\frac{1}{2}}{b})^2}$, on which we are working, so, the details will be explained elsewhere. Meanwhile, we can apply our topics to cosmology in which we will suppose the time dependence of the fifth dimension and think over how the stars should be created in the time-dependent process. Although we took the zero temperature limit in this paper, we can treat the finite one too. Furthermore we will try to extend our argument into higher dimensional theories (the six dimensions, the ten dimensions and the others), and consider what the star made of the bulk matter in the brane world should be, in which we are going to research as the next theme.

References

[1] N. Arkani-Hamed, S. Dimopoulos and G. Dvali, *Phys. Lett.* **B429**, 263 (1998); *Phys. Rev.* **D59**, 086004 (1999).

[2] K. Dienes, E. Dudas and T. Gherghetta, *Phys. Lett.* **B436**, 55 (1998); *Nucl. Phys.* **B537**, 47 (1999).

[3] A. R. Liddle, R. G. Moorhouse and A. B. Henriques, *Class. Quantum Grav.* **7**, 1009 (1990).

AdS/CFT with non-trivial Dilaton[1]

Shin'ichi Nojiri[2]

Department of Mathematics and Physics
National Defence Academy, Hashirimizu Yokosuka 239, Japan

Abstract

Recent developments on Anti-de Sitter/Conformal Field Theory (AdS/CFT) correspondence are reviewed. As applications of AdS/CFT correspondence to non-supersymmetric QCD, the roles of the non-trivial dilaton are also discussed

1 Introduction

AdS/CFT correspondence (or bulk/boundary) is conjectured in ref.[1] and after that it was well studied in [2, 3] (for a recent review, see [4]). When N p-branes in superstring theory or so-called M-theory coincide with each other and the coupling constant is small, the classical supergravity on $\mathrm{AdS}_{D=d+1=p+2}$, which is the low energy effective theory of superstring or M-theory, is, in some sense, dual to large N conformal field theory on M^d, which is the boundary of the AdS. For example, $d = 2$ case corresponds to $(4, 4)$ superconformal field theory, $d = 4$ case corresponds to $U(N)$ or $SU(N)$ $\mathcal{N} = 4$ super Yang Mills theory and $d = 6$ case to $(0, 2)$ superconformal field theory.

AdS/CFT correspondence may provide new insights to the understanding of non-perturbative QCD. For example, in frames of Type 0 String Theory the attempts[5] have been done to reproduce such well-known QCD effects as running gauge coupling and possibly confinement. It is among the first problems to get the description of well-known QCD phenomena from bulk/boundary correspondence.

In another approach one can consider IIB supergravity (SG) vacuum which describes the strong coupling regime of a non-supersymmetric gauge theory. This can be achieved by the consideration of deformed IIB SG vacuums, for an example, with non-constant dilaton which breaks conformal invariance and supersymmetry (SUSY) of boundary supersymmetric Yang-Mills (YM) theory. Such a background will be the perturbation of $\mathrm{AdS}_5 \times \mathrm{S}_5$ vacuum. The background of such a sort (with non-trivial dilaton) which interpolates between AdS (UV) and flat space with singular dilaton (IR) has been found in ref.[6] where also conformal dimensions for (dilaton coupled) scalar have been found.

This solution of IIB SG [6] has been used in ref.[7] with the interpretation of it as the one describing the running gauge coupling (via exponent of dilaton). It has been shown that running gauge coupling has a power law behavior with ultraviolet (UV) stable fixed point and quark-antiquark potential[8] has been calculated. QCD properties of such a background have been discussed in detail in refs.[9, 10]. Modifications of IIB SG solution with non-constant dilaton [6] due to presence of axion[11], constant self-dual vector[12] or world volume scalar [13] give further proof of the possible confinement and asymptotic freedom of the boundary non-SUSY gauge theory. Unfortunately, situation is very complicated here due to double role of IIB SG backgrounds. From one side they may indeed correspond to IR gauge theory (deformation of initial SUSY YM theory). On the same time such a background may simply describe another vacuum of the same maximally supersymmetric YM theory with non-zero vacuum expectation value (VEV) of some operator. Due to the fact that operators corresponding to deformation to another gauge theory are not known, it is unclear what is the case under discussion (interpretation of SG background). Only some indirect arguments as below may be given. As we see these arguments indicate that IIB SG background discussed in this work most probably corresponds to another vacuum of super YM theory under consideration. Then renormalization group (RG) flow is induced in the theory via giving a non-zero VEV to some operator.

In this report, we briefly review the mechanism of the AdS/CFT correspondence and after that we mention about the recent works by the author and his collaborator(s) [6, 10, 14, 15, 16, 17, 18]. The review part in this report is mainly based on [4, 19].

[1] based on the collaboration with Sergei D. Odintsov

[2] E-mail:nojiri@cc.nda.ac.jp, snojiri@yukawa.kyoto-u.ac.jp

2 Conformal transformation and AdS

Conformal field theories (CFTs) are, of course, field theories invariant under the conformal transformation, which is the coordinate transformation preserving the angle:

$$x^\mu \to x^{\mu\prime} = x^\mu + f^\mu(x) \implies g_{\mu\nu} \to g'_{\mu\nu} \propto g_{\mu\nu} \ . \tag{1}$$

Especially if $g_{\mu\nu} \propto \delta_{\mu\nu}$ in d-dimensional (Euclidean) space $g_{\mu\nu} \propto \delta_{\mu\nu}$, we obtain

$$\partial_i f_j + \partial_j f_i = \frac{2}{d}\delta_{ij} \sum \partial_k f_k \ . \tag{2}$$

For $d = 2$, the solutions of (2) are given by an analytic functions $f = f(z)$ if we define $f = f_1 + if_2$, $z = x^1 + ix^2$ ($i^2 = -1$). When $d \geq 3$, the general solution is given by

$$f_k = \sum_{i=1}^{d} \left\{ 2\left(c_i x^i\right) x^k - c_i \left(x^k\right)^2 + \omega_{ki} x^i \right\} + \epsilon x^k + a_k \ . \tag{3}$$

Here a_k corresponds to the translation, ω_{ij} to rotation (including Lorentz transformation in the Minkowski signature), ϵ to the scale transformation (dilatation) and c_k to conformal boost (special conformal). Under the conformal boost, we find $\frac{x^k}{x\cdot x} \to \frac{x^k}{x\cdot x} + c^k$, $(x \cdot x \equiv \sum_j (x^j)^2)$. Therefore the conformal boost is given by reflecting the coordinate with respect to the unit sphere ($x^k \to \frac{x^k}{x\cdot x}$) and after that, translating the reflected coordinate and finally reflecting the coordinate with respect to the sphere again.

Let the generators corresponding to the transformations be $P_i M_{ij} D K_i$ (here we choose them to be hermitian operators), then we obtain the following commutation relations :

$$\begin{aligned}
&[M_{ij}, P_k] = -i(\delta_{ik}P_j - \delta_{jk}P_i) \ , \quad [M_{ij}, K_k] = -i(\delta_{ik}K_j - \delta_{jk}K_i) \\
&[M_{ij}, M_{kl}] = -i\delta_{ik}M_{jl} + i\delta_{il}M_{jk} - i\delta_{jl}M_{ik} + i\delta_{jk}M_{il} \\
&[D, K_i] = iK_i \ , \quad [D, P_i] = -iP_i \ , \quad [P_i, K_j] = 2iM_{ij} - 2i\delta_{ij}D \ .
\end{aligned} \tag{4}$$

Other commutation relations vanish. If we redefine the following generators

$$J_{ij} = M_{ij} \ , \quad J_{i\,d+1} = \frac{1}{2}(K_i - P_i) \ , \quad J_{i\,d+2} = \frac{1}{2}(K_i + P_i) \ , \quad J_{d+2\,d+1} = D \ , \tag{5}$$

we find that the generators J_{ab} ($a, b = 1, 2, \cdots, d+1, d+2$) satisfy the algebra of $SO(d+1,1)$ ($SO(d,2)$ in the Lorentz signature).

The anti-de Sitter space (AdS) is the vacuum solution with constant curvature of the Einstein equation with negative cosmological constant. The D-dimensional AdS can be constructed by embedding it in the flat $D+1$-dimensional space:

$$-L^2 = \sum_{\mu=1}^{D} (X^\mu)^2 - \left(X^{D+1}\right)^2 \ , \quad ds^2 = \sum_{\mu=1}^{D} (dX^\mu)^2 - \left(dX^{D+1}\right)^2 \ . \tag{6}$$

(For Minkowski signature, we use analytic continuation: $x^d = -ix^0$). From the construction in (6), it is manifest that the AdS has a symmetry of $SO(D,1)$, which is the algebra of the conformal transformation ($D = d+1$). The transformation of the $SO(D,1)$ is linear for the coordinates X^M ($M = 1, \cdots, D+1$). If we change the coordinates by

$$U = X^D + X^{D+1} \ , \quad V = X^D - x^{D+1} \ , \quad x^i = \frac{X^i L}{U} \quad (i = 1, \cdots, d = D-1), \tag{7}$$

and delete V by using the constraint equation in (6), we find the following metric

$$ds^2 = \frac{L^2}{U^2} dU^2 + \frac{U^2}{L^2} \sum_{i=1}^{d} \left(dx^i\right)^2 \ . \tag{8}$$

By the identification (5) with the generators in the conformal transformation and those in $SO(D,1)$, we obtain the following transformation laws for the new coordinates in (7).

$$\begin{aligned}
&\text{dilatation} && \delta U = -\epsilon U\ , \quad \delta V = \epsilon V\ , \quad \delta x^i = \epsilon x^i \\
&\text{translation} && \delta U = 0\ , \quad \delta V = \frac{2a^i X_i}{L} = \frac{a^i x_i}{U}\ , \quad \delta x^i = a^i \\
&\text{conformal boost} && \delta U = -2c^i x_i U\ , \quad \delta V = 0\ , \quad \delta x^i = 2a^j x_j x^i - a^i x^j x_j - a^i \frac{L^4}{U^2}\ .
\end{aligned} \tag{9}$$

(Rotation is same as the usual one for x^i.) Then we find that x^i transforms as if they are the coordinates in the d-dimensional space (3) except the conformal boost. Even for the conformal boost, the transformation law of x^i coincides with (3) in the limit of $U \to \infty$, which tells that the conformal invariance is realized at the boundary ($U \to \infty$) of AdS.

3 AdS/CFT correspondence

The AdS/CFT correspondence can be found by identifying the extremal limit of the black p-brane, which appeared in the classical solution of the type IIB supergravity and Dp-brane (see [20]).

Type IIB superstring theory contains $2n$-rank ($n = 0, \cdots, 5$) anti-symmetric tensor. Then if we consider the classical solution of the type IIB supergravity, which is the low energy effective theory of type IIB superstring. We can assume the 5-dimensional part in 10 dimensional spacetime, where the superstring lives, to be S_5 (5 dimensional sphere) and rank 4 antisymmetric tensor $A_{\mu\nu\rho\sigma}$ is self-dual :

$$F_{\mu\nu\rho\sigma\tau} \equiv \partial_{[\mu} A_{\nu\rho\sigma\tau]}\ , \quad F^*_{\mu\nu\rho\sigma\tau} \equiv \frac{1}{5!}\epsilon_{\mu\nu\rho\sigma\tau\alpha\beta\gamma\delta\eta} F^{\alpha\beta\gamma\delta\eta}\ . \tag{10}$$

Here $\epsilon_{\mu\nu\rho\sigma\tau\alpha\beta\gamma\delta\eta}$ is a (constant) rank 10 anti-symmetric tensor. We also assume

$$\int_{S_5} F^* = N \quad (N \text{ is an integer.})\ , \quad F^* \equiv F^*_{\mu\nu\rho\sigma\tau} dx^\mu dx^\nu dx^\rho dx^\sigma dx^\tau \tag{11}$$

Then we find a black 3-brane solution, which is spatially 3 dimensional extended black hole like object. This solution has two horizons. We can consider an extremal limit, where two horizon coincides. The extremal solution has the following form:

$$ds^2 = \left(1 + \frac{R^4}{r^4}\right)^{-\frac{1}{2}} \left(-dt^2 + dx_1^2 + dx_2^2 + dx_3^2\right) + \left(1 + \frac{R^4}{r^4}\right)^{\frac{1}{2}} \left(dr^2 + r^2 d\Omega_5^2\right)\ . \tag{12}$$

Here $d\Omega_5^2$ expresses the metric tensor of the five-dimensional unit sphere and $R^4 \sim g_s N l_s^4$ (g_s is string coupling and l_s is string length). In the coordinate system in (12), the horizon lies at $r = 0$. Since the solution is extremal, the mass density M is equal to the charge density N of rank 4 antisymmetric field like charged black hole, which tells that the extremal black p-brane is BPS saturated state. Therefore the relation $M = N$ does not suffer the quantum correction. We can also show that N is quantized to be an integer, therefore both of N and M do not suffer the quantum correction. We should note that there is not any object which has the charge of the rank 4 anti-symmetric tensor at the level of the perturbation of the string theory. The D-brane is believed to correspond to the extremal limit of the black p-brane.

D-brane first appeared through T-duality. The T-duality is the symmetry where left-mover and right-mover in the string are exchanged. By exchanging left-mover and right-mover, the Neumann boundary condition at the ends of the open string is changed to the Dirichlet one. This suggests that there is an object where the ends of open string attach. This object is called D-brane. If the object is the (spatially) p-dimensional extended object, we call the object Dp-brane.

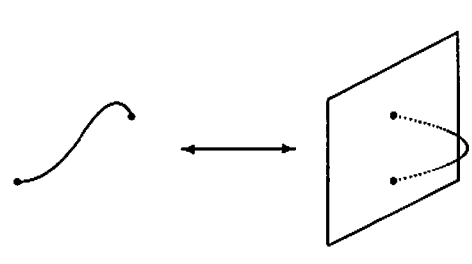

A conjecture that Dp-brane is nothing but the extremal limit of black p-brane can be given by the following things:

1. Dp-brane can naturally couple with rank $p+1$ antisymmetric tensor fields by considering the following interaction :

$$S_{DA} = q \int_{\text{D}p\text{-brane}} A \ . \tag{13}$$

2. If we consider a situation that two Dp-branes interact with each other by the closed string. This can be regarded as one loop vacuum amplitude of the open string (with Chan-Paton factor) by the T-duality. Due to the supersymmetry, the amplitude of the open string vanishes. This tells (especially when the distance between the 2 Dp-brane is large) that the interaction due to the graviton exactly cancels with that due to rank $p+1$ antisymmetric tensor fields. That is, the Dp-brane should be BPS saturated state.

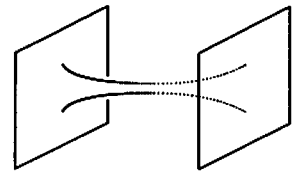

3. We can also show that the charge density of p-brane for rank $p+1$ antisymmetric tensor fields is quantized by the argument similar to Dirac's quantization condition for the electric and magnetic charges. Since Dp-brane is BPS saturated state, this tells the mass density is also quantized.

We now consider the dynamics on Dp-brane especially for $p = 3$. The D3-brane with charge and mass densities which are N times compared to the minimal ones can be regarded as the object composed of N D3-branes with minimal charge and mass densities. Then there exists an open string which connects i-th D3-brane and j-th D3-brane. By the T-duality, the open string can be regarded as an open string with Chan-Paton factor i and j. If the distance between the branes are very small, the open string becomes massless and corresponds to the vector fields A_μ^{ij}. If we consider the orientable string theory, we find $A_\mu^{ij} = (A_\mu^{ji})^*$, that is A_μ^{ij} is a hermitian matrix and can be regarded as the $U(N)$ or $SU(N)$ gauge fields. This gauge fields can be described by a non-linear action called the Born-Infeld action, which contains α' corrections but the leading order term is nothing but the usual (super) Yang-Mills action.

We now assume that the string theory with black p-brane is equivalent to that with Dp-brane and compare the low energy limits of the two theories.

In the low energy limit of the string theory with black p-brane, the theory are decoupled into two theories. The gravity theory becomes almost free in the region (called bulk) far from the brane. On the other hand, due to the red-shift, there can be any kind of configurations near the horizon of black p-brane ($r \sim 0$). The gravity theory in the bulk has long wave length and cannot observe the horizon. On the other hand, due to infinitely large red-shift, anything cannot leave from the horizon to the bulk. Therefore we have two decoupled theories, the free gravity theory in the bulk and the (full) gravity theory near the horizon.

On the other hand, in the string theory with Dp-brane, the gravity becomes free in the bulk and the gravitational wave does not observe the brane, again. On the brane, the α' corrections in the Born-Infeld action vanish and there remains (super) Yang-Mills action. In the low energy limit, the long string which has large energy, cannot appear and any interaction between the bulk and the brane vanishes.

In the low energy limit of two string theories, which is believed to be equivalent with each other, we have common free gravity theories in the bulk. Therefore the remaining decoupled two theories, the gravity theory near the horizon and (super) Yang-Mills theory on the brane, should be equivalent with each other. The Yang-Mills theory on the D3-brane is the $\mathcal{N} = 4$ supersymmetric $U(N)$ or $SU(N)$ gauge theory, which is only one known interacting theory with conformal symmetry in four dimensions. On the other hand, near the horizon of the black p-brane, the metric has the following form:

$$ds^2 = \frac{r^2}{R^2}\left(-dt^2 + dx_1^2 + dx_2^2 + dx_3^2\right) + \frac{R^2}{r^2}\left(dr^2 + r^2 d\Omega_5^2\right) \ . \tag{14}$$

Except the S_5 part, the metric is nothing but the one of AdS_5 ($r = UR = L$). Therefore we find AdS_5/CFT_4 correspondence; the (super)gravity theory in AdS_5 is equivalent to $\mathcal{N} = 4$ supersymmetric $U(N)$ or $SU(N)$ gauge theory.

In the further low energy limit, we can treat the AdS_5 (super)gravity theory classically. The low energy approximation would be valid when the (curvature) radius of the AdS_5 is large, which requires $R \gg l_s$. Since $R^4 \sim g_s N l_s^4$, the large R corresponds to the strong coupling region in $\mathcal{N} = 4$ gauge theory.

4 Conformal Field Theory in 4 Dimensions from AdS/CFT

In the AdS_5/CFT_4, the AdS is five dimensional spacetime but the corresponding CFT lives in four dimensions. The hint to solve the gap in the dimension could be given by the Bekenstein bound of the entropy

$$S \leq \frac{\text{Area}}{4G} . \tag{15}$$

The expression in (15) might tell that, in the gravity theory the degrees of the freedom in a region would be proportional to the area of the region, rather than the volume. If this is true, it might be consistent if the CFT lives on the boundary of AdS, which is a kind of holography. As it has been shown, the conformal symmetry is naturally realized on the boundary of the AdS. Then five dimensional gravity theory whose boundary value is given by ϕ_0 would correspond to the CFT where ϕ_0 is the source of the conformal primary operator $\mathcal{O}_\phi$, or by in terms of the path integral, we find the following relation:

$$\begin{aligned} Z_{\rm CFT}(\phi_0) &\equiv \int [d\varphi]\, e^{S_{\rm CFT}(\varphi)+\int d^4x\sqrt{g}\phi_0\mathcal{O}_\phi} \\ &= Z_{\rm AdS}(\phi_0) \equiv \int [d\phi]\, e^{S_{\rm AdS}(\phi)}\Big|_{\phi=\phi_0 \text{ at AdS boundary}} \simeq e^{S_{\rm AdS}(\phi_{\rm classical})}\Big|_{\phi=\phi_0 \text{ at AdS boundary}} . \end{aligned} \tag{16}$$

Here φ expresses the fields, which include fermion fields in general and is different from ϕ. In the strong coupling region, the path integral can be approximated by substituting the classical solution $\phi_{\rm classical}$ into the action $S_{\rm AdS}$ (WKB approximation). For example, the two point function $< \mathcal{O}_\phi(x)\mathcal{O}_\phi(y) >$ of the conformal primary operator $\mathcal{O}_\phi$ can be given by

$$< \mathcal{O}_\phi(x)\mathcal{O}_\phi(y) >= \frac{1}{Z_{\rm CFT}}\frac{\partial^2 Z_{\rm CFT}}{\partial\phi(x)\partial\phi(y)} = \frac{1}{Z_{\rm AdS}}\frac{\partial^2 Z_{\rm AdS}}{\partial\phi(x)\partial\phi(y)} . \tag{17}$$

We now choose the metric tensor of AdS_5 in the following form ($y = \frac{U^2}{L^2}$, $L = l$ in (8)):

$$ds^2 = \frac{l^2}{4y^2}dy^2 + y\sum_{i=0}^{3}\left(dx^i\right)^2 . \tag{18}$$

Let ϕ be a free scalar field on the AdS, whose action is given by

$$\begin{aligned} S_\phi &= -\int dx^5\sqrt{g}g^{\mu\nu}\left(\partial_\mu\phi\partial_\nu\phi + m^2\phi^2\right) = \int dx^5\sqrt{g}\phi\left(\Delta - m^2\right)\phi \\ \sqrt{g}\Delta\phi &\equiv \partial_\mu\left(\sqrt{g}g^{\mu\nu}\partial_\nu\phi\right) = \frac{2}{l}\partial_y\left(y^3\partial_y\phi\right) + \frac{l}{2}\sum_{i=0}^{4}\partial_i^2\phi \end{aligned} \tag{19}$$

Then the Green function $G(x_1, x_2)$ should satisfy

$$\sqrt{g}\left(\Delta_{x_1} - m^2\right)G(x_1, x_2) = \delta^5(x_1 - x_2) . \tag{20}$$

As we are interested in the case where both of x_1 and x_2 are on the boundary, first we put x_1 on the boundary and x_2 on the point off the boundary, which has finite but small y. The Green function G should be a function of y and $X^2 \equiv \sum_{i=1}^{4}\left(x_1^i - x_2^i\right)^2$. Furthermore since the metric in (18) has the following symmetry or a redundancy of the expression :

$$y \to e^{2c}y , \quad x^i \to e^{-c}x^i \quad (c \text{ is a constant}) , \tag{21}$$

G should be a function of only $Y \equiv yX^2$: $G = G(Y)$. Then (20) is rewritten as follows:

$$\frac{2}{l}\left(3YG' + Y^2G''\right) + \frac{l}{2}\left(2dG' + YG''\right) - \frac{m^2l}{2}G = 0 . \tag{22}$$

Since y and therefore Y is large near the boundary, we obtain

$$\frac{2}{l}\left(3YG' + Y^2G''\right) - \frac{m^2 l}{2}G \sim 0 \ , \tag{23}$$

which can be solved as

$$G \sim Y^b \ , \quad b^{\pm} = -1 \pm \sqrt{1 + \frac{m^2 l^2}{4}} \tag{24}$$

Then we find the conformal dimension of ϕ is given by $\Delta_\phi = -2b^{\pm}$ (usually we choose + sign). This tells that the conformal dimension of O_ϕ is given by $\Delta_{O_\phi} = 4 + 2b^{\pm} = 2b^{\mp}$.

5 IR-UV duality and Weyl anomaly

In the expression of AdS/CFT, the usual UV divergences appear in the CFT side but the IR divergences appear in the AdS side from the infinite volume even if we treat the gravity in the AdS classically. In this way, UV divergence and IR one are exchanged in the AdS/CFT, which can be understand from the expression (9) for the dilatation, where the sign for U and x^i is exchanged : $\delta U = -\epsilon U$, $\delta x^i = \epsilon x^i$, that is, the IR region far from the origin (large U) in AdS corresponds to small x^i (UV in CFT). This also tells that U can be regarded as the energy scale of the boundary field theory.

In the usual quantum field theory, there often appear phenomena called anomaly, where a classical symmetry is broken by regularizing UV divergence. In this section, we consider how the Weyl anomaly, corresponding to the breakdown of the dilatation symmetry, appears from the IR divergence in the AdS side.

We start with the action of the dilatonic gravity in $d+1$ $(=5)$ dimensions

$$\begin{aligned} S &= \frac{1}{16\pi G}\left[\int_{M_{d+1}} d^{d+1}x\sqrt{-\hat{G}}\left\{\hat{R} + X(\phi)(\hat{\nabla}\phi)^2 + Y(\phi)\hat{\Delta}\phi + 4\lambda^2\right\}\right. \\ &\quad \left. + \int_{M_d} d^d x\sqrt{-\hat{g}}\left(2\hat{\nabla}_\mu n^\mu + \alpha\right)\right] \ . \end{aligned} \tag{25}$$

Here ϕ is the dilaton, M_{d+1} is the $d+1$ dimensional manifold, corresponding to AdS_{d+1} and M_d is the d dimensional manifold which is the boundary of M_{d+1}. We denote the unit vector normal to M_d by n_μ. $X(\phi)$ and $Y(\phi)$ can be arbitrary dilaton function but the arbitrariness is not real one. In fact, if we define a new field φ by

$$\varphi \equiv \int d\phi\sqrt{2V(\phi)} \ , \quad V(\phi) \equiv X(\phi) - Y'(\phi) \tag{26}$$

the action in (25) can be rewritten in the following form:

$$S = \frac{1}{16\pi G}\left[\int d^{d+1}x\sqrt{-\hat{G}}\left\{\hat{R} + 2(\hat{\nabla}\varphi)^2 + 4\lambda^2\right\} + \int_{M_d} d^d x\sqrt{-\hat{g}}\left(2\hat{\nabla}_\mu n^\mu + \alpha + Y(\phi)n^\mu\partial_\mu\phi\right)\right] \ . \tag{27}$$

Since the boundary terms does not finally contribute to the Weyl anomaly, the result does not essentially depend on the form of $X(\phi)$ and $Y(\phi)$.

We now consider the fluctuation from the AdS and assume the following form for the metric of M_{d+1}:

$$\begin{aligned} ds^2 &\equiv \hat{G}_{\mu\nu}dx^\mu dx^\nu = \frac{l^2}{4}\rho^{-2}d\rho d\rho + \sum_{i=0}^{d-1}\rho^{-1}g_{ij}dx^i dx^j \\ (4\lambda^2 &= -d(d-1)/l^2) \ . \end{aligned} \tag{28}$$

Here g_{ij} can be regarded as the metric of M_d. When $g_{ij} = \eta_{ij}$ or $g_{ij} = \delta_{ij}$, the metric in (28) becomes that of AdS by identifying $\rho = y^{-1}$ in (18).

The expression in (28) has an arbitrariness and the expression is invariant under the following transformation:

$$\delta\rho = \delta\sigma\rho \ , \quad \delta g_{ij} = \delta\sigma g_{ij} \ . \tag{29}$$

Here $\delta\sigma$ is a constant parameter. The transformation (29) corresponds to the dilatation, which is the scale transformation on M_d, in (9).

We now expand ϕ and g_{ij} in the power series of ρ:

$$\phi = \phi_{(0)} + \rho\phi_{(1)} + \rho^2\phi_{(2)} + \cdots , \quad g_{ij} = g_{(0)ij} + \rho g_{(1)ij} + \rho^2 g_{(2)ij} + \cdots . \tag{30}$$

By using equations of motions, $\phi_{(l)}$ and $g_{(l)ij}$ $(l = 1, 2, \cdots)$ can be given by $\phi_{(0)}$ and $g_{(0)ij}$, which can be regarded as independent fields on M_d. By substituting the obtained forms of $\phi_{(l)}$ and $g_{(l)ij}$ in to the action of (25), we find the divergences coming from the infinite volume of AdS and we regularize them by introducing an infrared cutoff ϵ in the following way:

$$\int d^{d+1}x \to \int d^dx \int_\epsilon d\rho , \quad \int_{M_d} d^dx\Big(\cdots\Big) \to \int d^dx \left(\cdots\right)\Big|_{\rho=\epsilon} . \tag{31}$$

Then we find

$$S = S_0(\phi_{(0)}, g_{(0)ij})\epsilon^{-\frac{d}{2}} + S_1(\phi_{(0)}, \phi_{(1)}, g_{(0)ij}, g_{(1)ij})\epsilon^{\frac{d}{2}-1} + \cdots + S_{\ln}\ln\epsilon + S_{\frac{d}{2}} + O(\epsilon^{\frac{1}{2}}) . \tag{32}$$

We should note that the term proportional to $\ln\epsilon$ appears when d is even. Due to the symmetry in (29), the system is originally invariant the following transformation:

$$\delta g_{(0)\mu\nu} = 2\delta\sigma g_{(0)\mu\nu} , \quad \delta\epsilon = 2\delta\sigma\epsilon . \tag{33}$$

If we subtract the terms proportional the negative power of ρ in (32), as a renormalization, the system is still invariant under the transformation (33). If we, however, subtract the term proportional to $\ln\epsilon$ when d is even, the invariance is broken since the variation of $\ln\epsilon$ term is finite :

$$\ln\epsilon \to \ln\epsilon + \ln(2\delta\sigma) . \tag{34}$$

The original system is invariant under the transformation (33), the variation of $\ln\epsilon$ term should be cancelled by the variation of $S_{\frac{d}{2}}$, which is finite in the limit of $\epsilon \to 0$. Since $S_{\frac{d}{2}}$ can be renormalized (effective) action, the dilatation invariance in the system is broken. Since $S_{\ln}$ is the variation of the renormalized action $S_{\frac{d}{2}}$, we can find the Weyl anomaly T from the expression of $S_{\ln}$:

$$S_{\ln} = -\frac{1}{2}\int d^dx\sqrt{-g_{(0)}}T . \tag{35}$$

Then we find, when $d = 4$, [14]

$$\begin{aligned} S_{\ln} = \frac{l^3}{16\pi G}\int d^4x\sqrt{-g_{(0)}}\Bigg[&\frac{1}{8}R_{(0)ij}R^{ij}_{(0)} \\ &-\frac{1}{24}R^2_{(0)} + \frac{1}{2}R^{ij}_{(0)}\partial_i\varphi_{(0)}\partial_j\varphi_{(0)} - \frac{1}{6}R_{(0)}g^{ij}_{(0)}\partial_i\varphi_{(0)}\partial_j\varphi_{(0)} \\ &+\frac{1}{4}\left\{\frac{1}{\sqrt{-g_{(0)}}}\partial_i\left(\sqrt{-g_{(0)}}g^{ij}_{(0)}\partial_j\varphi_{(0)}\right)\right\}^2 + \frac{1}{3}\left(g^{ij}_{(0)}\partial_i\varphi_{(0)}\partial_j\varphi_{(0)}\right)^2\Bigg] . \end{aligned} \tag{36}$$

The first calculation without dilaton was given in [21]. And the conformal anomaly for the R^2 gravity is given in [15].

We can compare the result in (36) with the usual field theory calculation. In [22], the Weyl anomaly of $\mathcal{N} = 4$ supersymmetric $U(N)$ or $SU(N)$ Yang-Mills theory coupled with $\mathcal{N} = 4$ conformal supergravity is given by

$$\begin{aligned} T = -\frac{N^2}{4(4\pi)^2}\Bigg[&2\left(R_{ij}R^{ij} - \frac{1}{3}R^2\right) + F^{ij}F_{ij} \\ &+4\left\{2\left(R^{ij} - \frac{1}{3}Rg^{ij}\right)\partial_i\varphi^*\partial_j\varphi + \left|\frac{1}{\sqrt{-g}}\partial_i\left(\sqrt{-g}g^{ij}\partial_j\varphi\right)\right|^2\right\} + \cdots\Bigg] . \end{aligned} \tag{37}$$

Here F_{ij} is the field strength of $SU(4)$ gauge field, φ is a scalar field which is a combination of dilaton and RR scalar (axion) and "$\cdots$" expresses other fields and higher power of the fields. If we identify

$$\frac{l^3}{16\pi G} = \frac{2N^2}{(4\pi)^2}\,, \tag{38}$$

and consider a background where only gravity and the real part of φ is non-trivial, the result in (36) reproduces the result in (38). Recently the Weyl anomaly for the case where the axion fields, which is the imaginary part of φ, does not vanish is given in [18] and the result is consistent with (38).

6 $Q\bar{Q}$ potential

One of the old motivations for string theory was to explain the confinement of quark and anti-quark, which are the endpoints of open string. Since the energy of a string is proportional to its length, an infinite energy is necessary to separate quark and antiquark infinitely, which is the argument for the mechanism of the quark confinement. The string theory is described by the Nambu-Goto action:

$$S = \frac{1}{2\pi l^2}\int d\tau d\sigma \sqrt{\det\left(g^s_{\mu\nu}\partial_\alpha x^\mu \partial_\beta x^\nu\right)}\,. \tag{39}$$

Here $g^s_{\mu\nu}$ is called "string" metric and given by a product of the (Einstein) metric tensor and a dilaton function: $g^s_{\mu\nu} = g_{\mu\nu}e^{\Phi}$. As we consider, in this section, the case where the dilaton is constant, there is not any essential difference between the string metric and the Einstein metric. The action (39) is proportional to the area of the world sheet of the string. Let assume quark and anti-quark at the ends of the open string to be very heavy and the endpoints are fixed. When the period T of the time is finite, the action S is proportional T and the energy E of the system.

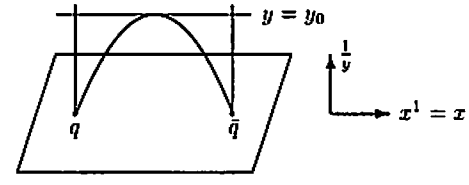

We choose the metric of AdS as in (18) and consider the configuration of string as $x^0 = \tau$, $x^1 \equiv x = \sigma$, $x^2 = x^3 = \cdots = x^{d-1} = 0$, $y = y(x)$ in AdS, then by substituting it into the action (39), we find

$$S = \frac{T}{2\pi l^2}\int dx y\sqrt{\frac{4l^2}{y^3}\left(\partial_x y\right)^2 + 1}\,. \tag{40}$$

The function $y = y(x)$ can be determined so that the action takes its minimum value, that is, by solving the Euler-Lagrange equation $\frac{\delta S}{\delta y} - \partial_x\left(\frac{\delta S}{\delta(\partial_x y)}\right) = 0$. From the Euler-Lagrange equation, we find the following integral :

$$E_0 = \frac{y}{\sqrt{\frac{4l^2}{y^3}\left(\partial_x y\right)^2 + 1}}\,. \tag{41}$$

If y has a finite minimum, where $\partial_x y|_{y=y_0} = 0$, we obtain $E_0 = y_0$. We now parameterize y by

$$y = y_0 \cosh t\,. \tag{42}$$

By taking the limit of $t \to +\infty$, we find the distance L between quark and antiquark:

$$L = \frac{C l y_0^{-\frac{1}{2}}}{2}\,, \quad C \equiv \int_{-\infty}^{\infty} dt \cosh^{-\frac{3}{2}} t = \frac{2^{\frac{1}{2}}\Gamma\left(\frac{3}{4}\right)^2}{\Gamma\left(\frac{3}{2}\right)}\,. \tag{43}$$

Then we find

$$S = \frac{T}{2\pi l^2}E(L)\,, \quad E(L) = \int_{-\infty}^{\infty} dt \frac{dx}{dt}\frac{y(t)^2}{y_0}\,. \tag{44}$$

Here $E(L)$ is the total energy of the system. We should note that $E(L)$ is divergent, which comes from the fact that $E(L)$ contains the self-energy of the infinitely heavy quark and anti-quark. The self-energy can be evaluated by considering the configuration of string given by $x^0 = \tau$, $x^1 = x^2 = x^3 = \cdots = x^{d-1} = 0$, $y = y(\sigma)$ (We should note $x_1 = 0$) and the minimum of y is y_D. We divide the region of y into two ones and $y_0 > y > y_D$, and we use the parameterization in (42) for the region $\infty > y > y_0$. Then we find the following expression for the self energy :

$$E_{\rm self} = \frac{1}{l^2}\int_{-\infty}^{\infty} dt\, y(t)\sqrt{\frac{4}{(y(t))^2}\left(\partial_t y(t)\right)^2} + 2\int_{y_D}^{y_0} dy\sqrt{\frac{4}{y}}\ . \tag{45}$$

Then the finite part of the quark-antiquark potential is given by

$$\begin{aligned} E_{q\bar{q}}(L) &\equiv E(L) - E_{\rm self} \\ &= \frac{CD}{4L} \\ D &\equiv 2\int_0^{\infty} dt \cosh^{-\frac{1}{2}} t\, e^{-t} - 4 = \frac{2^{-\frac{3}{2}}\Gamma\left(-\frac{1}{4}\right)^2}{\Gamma\left(-\frac{1}{2}\right)}\ . \end{aligned} \tag{46}$$

Here we neglected L independent terms. The potential (46) is proportional to $\frac{1}{L}$ as in the Coulomb potential, which reflects the conformal symmetry of the system. In the unit where $\hbar = 1$ and $c = 1$, the dimension of the energy is the inverse of the length. Since the conformal symmetry contains the dilatation, which is the scale transformation, CFT does not contain the dimensional parameter. Therefore the energy must be proportional to $\frac{1}{L}$.

7 Running Gauge Coupling and Quark-Antiquark Potential in Curved Spacetime

In this section, we briefly review the works in [6, 10, 17]. In these works, it was tried to investigate non-supersymmetric QCD by considering the background where the dilaton is non-trivial. We also consider the cases where the boundary manifold is not flat but has a constant curvature, then we can obtain the field theory on the curved background from AdS/CFT.

We start with the action of dilatonic gravity in $d+1$ dimensions:

$$S = -\frac{1}{16\pi G}\int d^{d+1}x\sqrt{-G}\left(R - \Lambda - \alpha G^{\mu\nu}\partial_\mu\phi\partial_\nu\phi\right)\ . \tag{47}$$

Here we assume $\alpha > 0$ and $\lambda^2 \equiv -\Lambda > 0$. The action (47) includes that of the low energy effective action ($d = 4$, $\alpha = \frac{1}{2}$) of type IIB string theory (type IIB supergravity) when the topology of the spacetime is $AdS_5 \times S^5$.

We now assume the following form of the metric tensor:

$$ds^2 = f(y)dy^2 + y\sum_{i,j=0}^{d-1} g_{ij}(x^k)dx^i dx^j \tag{48}$$

and g_{ij} is the metric of the Einstein manifold, which is defined by $r_{ij} = kg_{ij}$. Here r_{ij} is the Ricci tensor given by g_{ij} and k is a constant. We also assume that ϕ depends only on y. Then by using the equations of motion, we obtain

$$f = \frac{d(d-1)}{4y^2\lambda^2\left(1 + \frac{\alpha c^2}{\lambda^2 y^d} + \frac{kd}{\lambda^2 y}\right)}\ ,\quad \phi = c\int dy\sqrt{\frac{d(d-1)}{4y^{d+2}\lambda^2\left(1 + \frac{\alpha c^2}{\lambda^2 y^d} + \frac{kd}{\lambda^2 y}\right)}}\ . \tag{49}$$

As the string coupling is given by $g = g_s e^{\phi}$, the coupling depends on y: $g = g(y)$. If we define a new coordinate U by $y = U^2$. U can be regarded as the energy scale on the (boundary) d dimensional space

from the correspondence between long-distances/high-energy in the AdS/CFT scheme (see the arguments in the first paragraph in Sect.5). Then we obtain the following renormalization group equations

$$\begin{aligned} k \neq 0 \quad \beta(U) &\equiv U\frac{dg}{dU} \\ &= -d(g-g_s) - \frac{2kd\beta c\sqrt{\alpha}}{(d+2)\lambda^3}\left(-\frac{d\lambda}{2\beta c\sqrt{\alpha}}\right)^{\frac{3}{d}+1}\frac{(g-g_s)^{\frac{3}{d}+1}}{g_s^{\frac{3}{d}}} + \cdots \\ k = 0 \quad \beta(U) &= -d(g-g^*) - \left(d - \frac{d^2}{2\beta}\right)\frac{(g-g_s)^2}{g_s} + \cdots . \end{aligned} \tag{50}$$

In case of type IIB supergravity, $\alpha = \frac{1}{2}$ and $\beta = \sqrt{\frac{d(d-1)}{2}}$. Eqs.(50) tells that the theory would correspond to the theory with non-trivial UV fixed point.

We can also consider the static potential between "quark" and "anti-quark" by evaluating the Nambu-Goto action in (39). Then we find

$$\begin{aligned} k \neq 0 \quad E_{q\bar{q}}(L) &= \frac{1}{A}\left(\frac{C_{\frac{3}{2}}}{AL}\right)\left\{D_0 + B\left(\frac{C_{\frac{5}{2}}D_0}{C_{\frac{3}{2}}} + D_2\right)\left(\frac{AL}{C_{\frac{3}{2}}}\right)^2 + \cdots\right\} \\ A &\equiv \frac{2\lambda}{\sqrt{d(d-1)}}\ , \quad B \equiv -\frac{kd}{2\lambda^2} \\ D_d &\equiv 2\int_0^\infty dt \cosh^{-\frac{d+1}{2}} t\, e^{-t} + \frac{4}{d-1} = \frac{2^{d-\frac{3}{2}}}{(d-3)!!\sqrt{\pi}}\Gamma\left(\frac{d-1}{4}\right)^2 \\ k = 0 \quad E_{q\bar{q}}(L) &= \left(\frac{C_{\frac{3}{2}}}{AL}\right)\left\{D_0 \pm B_0\left(D_d + F_d + \frac{S_d D_0}{C_{\frac{3}{2}}}\right)\left(\frac{AL}{C_{\frac{3}{2}}}\right)^d + O(L^{2d})\right\} \\ B_0 &\equiv \frac{2\gamma c\sqrt{\alpha}}{d\lambda}\ , \quad F_d \equiv \int_{-\infty}^\infty dt \sinh^{-2} t \cosh^{\frac{1}{2}} t\left(1 - \cosh^{-\frac{d}{2}} t\right) \end{aligned} \tag{51}$$

Here L is the distance between "quark" and "anti-quark" . In case of type IIB supergravity, $\gamma = \sqrt{\frac{d(d-1)}{2}}$. When $k \neq 0$, the next-to-leading term is linear in L. The linear potential term is attractive if $k < 0$ and repulsive if $k > 0$.

We need to know the large L behavior of the potential when we discuss the confinement. When L is large, however, the orbit of the string would approach, in general, to the curvature singularity at $y = 0$, where the supergravity description would break down. By defining a new coordinate $\tilde{U}$ by

$$\tilde{U} \equiv y^{\mathrm{sgn}(c)\sqrt{\frac{d(d-1)}{2}}+\frac{d+1}{2}} \tag{52}$$

we find

$$\begin{aligned} k(\phi(y))\, y\sqrt{\frac{f(y)}{y}(\partial_x y)^2 + 1} &\sim y^{\mathrm{sgn}(c)\sqrt{\frac{d(d-1)}{2}}+1}\sqrt{\frac{d(d-1)}{4\alpha c^2}y^{d-3}(\partial_x y)^2 + 1} \\ &= \sqrt{\beta_0\left(\partial_x \tilde{U}\right)^2 + \left(\tilde{U}\right)^{\gamma_0}} \\ \beta_0 &\equiv \frac{d(d-1)}{4\alpha c^2\left(\mathrm{sgn}(c)\sqrt{\frac{d(d-1)}{2}} + \frac{d+1}{2}\right)^2}\ , \quad \gamma_0 \equiv \frac{2\mathrm{sgn}(c)\sqrt{\frac{d(d-1)}{2}} + 2}{\mathrm{sgn}(c)\sqrt{\frac{d(d-1)}{2}} + \frac{d+1}{2}}. \end{aligned} \tag{53}$$

In case of $d = 4$, $\gamma_0 = 1.39$ when $c > 0$ and $\gamma_0 = -57.4$ when $c < 0$.

By using the analysis in [9], we find that if $c > 0$ $(0 < \gamma_0 < 2)$, the orbit of the string goes straight to the region $y \sim 0$ and the potential becomes independent of L. In this case, however, the potential

would receive the α' correction from the string theory. On the other hand, if $c < 0$ ($\gamma_0 < 0$), there is an effective barrier which prevents the orbit of string from approaching into the curvature singularity and the potential would not receive the α' correction so much and the supergravity description would be reliable. Furthermore $c < 0$ ($\gamma < 0$) case predicts the confinement.

8 Axionic background with non-zero curvature and non-constant dilaton

As a generalization of the last section, we can consider non-constant axion. We start with the following action of type IIB supergravity ($\alpha = \frac{1}{2}$) with axion field χ.

$$S = -\frac{1}{16\pi G}\int d^{d+1}x\sqrt{-G}\left(R + \lambda^2 - \frac{1}{2}G^{\mu\nu}\partial_\mu\phi\partial_\nu\phi + \frac{1}{2}e^{2\phi}G^{\mu\nu}\partial_\mu\chi\partial_\nu\chi\right) . \tag{54}$$

Then by solving the eqs. of motion, we find

$$f = \frac{d(d-1)}{4y^2\lambda^2\left(1 + \frac{c_\phi}{2\lambda^2 y^d} + \frac{kd}{\lambda^2 y}\right)} . \tag{55}$$

If we replace c_ϕ with $\frac{\alpha c^2}{2}$, we obtain the previous result in (49). By defining a new coordinate η by

$$\eta = -\int dy\sqrt{\frac{f}{y^d}} = \int dy\sqrt{\frac{d(d-1)}{4y^{d+2}\lambda^2\left(1 + \frac{c_\phi}{2\lambda^2 y^d} + \frac{kd}{\lambda^2 y}\right)}} \tag{56}$$

we obtain the classical solution of ϕ and χ :

$$\begin{aligned} e^\phi &= \frac{c_\chi}{\sqrt{c_\phi}}\sinh\left(\sqrt{c_\phi}\,(\eta - \eta_0)\right) \\ \chi &= \chi_0 - \frac{\sqrt{c_\phi}}{c_\chi}\coth\left(\sqrt{c_\phi}\,(\eta - \eta_0)\right) . \end{aligned} \tag{57}$$

Here η_0 and χ_0 are constants of the integration. When $y \to +\infty$, $\eta \to 0$ and we obtain

$$e^\phi \to -\frac{c_\chi}{\sqrt{c_\phi}}\sinh\left(\eta_0\sqrt{c_\phi}\right) , \quad \chi \to \chi_0 + \frac{\sqrt{c_\phi}}{c_\chi}\coth\left(\eta_0\sqrt{c_\phi}\right) . \tag{58}$$

Then if we choose $\eta_0 = 0$, we find $e^\phi \to 0$. Since g_s is related with Yang-Mills coupling g_{YM} by $g_s e^\phi = g = g_{YM}^2$ and the limit $\rho \to 0$ ($y \to +\infty$) corresponds to the ultraviolet fixed point from AdS/CFT correspondence, $e^\phi \to 0$ means asymptotic free. Then the axion field describes running theta angle.

We also obtain the following potential between quark and anti-quark for asymptotically free ($\eta_0 = 0$) $d = 4$ case

$$\begin{aligned} E(L) &= \frac{R_s}{2}\left(\frac{C_{\frac{3}{2}}}{R_s L}\right)\left\{C_{\frac{1}{2}} + \frac{k}{\lambda^2}\left(\frac{C_{\frac{3}{2}}}{R_s L}\right)^{-2}\left(-\frac{16}{3}C_{\frac{3}{2}} + \frac{4}{3}E_{\frac{1}{2}} - \frac{4}{C_{\frac{3}{2}}}\left(C_{\frac{5}{2}} + \frac{E_{\frac{1}{2}}}{3}\right)\right) + \cdots\right\} \\ E_a &\equiv \int_{-\infty}^{\infty} dt\frac{\cosh^{-a} t}{\cosh t + 1} . \end{aligned} \tag{59}$$

We should note that a linear potential appears in the next-to-leading term, which is attractive if $k < 0$ and repulsive if $k > 0$.

The large L behavior can be found by the discussion similar to the previous section. When y is large, we find

$$\phi \sim -\sqrt{\frac{d(d-1)}{2}}\ln y , \tag{60}$$

which corresponds $c < 0$ case in the pure dilaton case. Therefore the potential would predict confinement.

9 Running Gauge Coupling and Quark-Antiquark Potential in Non-SUSY Gauge Theory at Finite Temperature

In this section, we discuss the non-constant dilaton deformed $AdS_5 \times S_5$ solutions of IIB supergravity where AdS sector is described by black hole. Due to the black hole, we can define the temperature T and we can discuss thermodynamical quantities (See [23, 24]). In this section, we restrict the case where $d = 4$ and $\alpha = \frac{1}{2}$.

We assume the $(d+1)$-dimensional metric in the following form:

$$ds^2 = -e^{2\rho}dt^2 + e^{2\sigma}dr^2 + r^2 \sum_{i,j=1}^{d-1} g_{ij}dx^i dx^j \ . \tag{61}$$

Here g_{ij} is the metric of $d-1$-dimensional Einstein manifold $r_{ij} = kg_{ij}$. When dilaton is non-trivial, black hole type solution can be given only by perturbation. When dilaton is constant, AdS Schwarzschild black hole is given by

$$e^{2\rho} = e^{-2\sigma} = \frac{1}{r^2}\left(\frac{kr^{d-2}}{d-2} + \frac{\lambda^2}{d(d-1)}r^d - \mu\right) \ . \tag{62}$$

We should note that in AdS background, the shape of the horizon is not always sphere but any kind of Einstein manifold, say flat plane or hyperboloid.

By the perturbation from the solution where $\mu = 0$ and $k < 0$, we obtain the following metric and the beta-function

$$\begin{aligned} e^{\phi} &= e^{\phi_0}\left(1 - \frac{cl^2}{4r^4} + \mathcal{O}\left(r^{-6}\right)\right) \\ \beta(g) &= r\frac{dg}{dr} = -4(g - g_s) + \frac{2^{\frac{5}{2}}}{3}(2\pi T)^2 l^3 g_s \left(\frac{g_s - g}{cg_s}\right)^{\frac{3}{2}} \ . \end{aligned} \tag{63}$$

We also find the following form for quark-antiquark potential

$$\begin{aligned} E_{q\bar{q}}(L) &= \frac{lAC}{L} - \frac{l^3(2\pi T)^2}{2}\left(\frac{BC}{A^2} + \frac{D}{A}\right)L + \mathcal{O}\left(L^3\right) \\ A &\equiv \int_{-\infty}^{\infty} \frac{dt}{\cosh^2 t\left(\cosh^2 t + 1\right)^{\frac{1}{2}}} = 1.19814... \\ B &\equiv \int_{-\infty}^{\infty} dt \frac{\cosh^4 t - \cosh^2 t - 1}{\cosh^4 t\left(\cosh^2 t + 1\right)^{\frac{3}{2}}} = -0.162061... \\ C &= 2\int_0^{\infty} dt \left\{\frac{\cosh^2 t}{\left(\cosh^2 t + 1\right)^{\frac{1}{2}}} - \sinh t\right\} - 2 = -1.19814... \\ D &= 2\int_0^{\infty} \frac{dt}{\left(\cosh^2 t + 1\right)^{\frac{3}{2}}} = 0.711959 \ . \end{aligned} \tag{64}$$

We find the next-to-leading term is linear in L. Since $\frac{BC}{A^2} + \frac{D}{A} > 0$ and $k < 0$, the linear potential is repulsive.

It is difficult to investigate the large L behavior of the potential when the dilaton is not constant. Here we investigate the $c = 0$ case (constant dilaton) to see what happens by the effect of the black hole. Then we find the following form of the potential

$$E_{q\bar{q}} = r_{\min}\int_{-\infty}^{\infty} dt \sinh t \left\{\left(1 - \frac{1}{\cosh^2 t}\cdot\frac{1 - \frac{r_0^2}{r_{\min}^2}}{\cosh^2 t - \frac{r_0^2}{r_{\min}^2}}\right)^{-\frac{1}{2}} - 1\right\} + 2(r_D - r_{\min}) \ . \tag{65}$$

Constant -1 in $\{\ \}$ and the last term correspond to the subtraction of the self-energy. The integration converges and the integrand is monotonically decreasing function of $\frac{1}{r_{\rm min}}$ if $r_{\rm min}$ is larger than the radius of the horizon r_0 : $r_{\rm min} > r_0$ and vanishes in the limit of $r_{\rm min} \to r_0$. Therefore if $r_{\rm min}$ decreases and approaches to r_0 when L is large, the potential $E_{q\bar{q}}$ approaches to a constant $E_{q\bar{q}} \to 2(r_D - r_0)$ and does not behave as a linear function of L. This tells that quark is not confined. This effect presumably would corresponds to deconfining phase of QCD at finite temperature.

By the perturbation from the solution where $\mu > 0$ and $k = 0$, we obtain

$$\begin{aligned} e^{\phi} &= e^{\phi_0}\left(1 - \frac{cl^2}{4r^4} + \mathcal{O}\left(r^{-8}\right)\right) \\ \beta(g) &= r\frac{dg}{r} = -4(g - g_*) + \frac{8(\pi T)^4 l^6}{g_* c}(g - g_*)^2 + \cdots \end{aligned} \tag{66}$$

and quark-antiquark potential

$$\begin{aligned} E_{q\bar{q}}(L) &= \frac{lAC}{L} + \frac{L^3}{lA^3}\left\{l^6(\pi T)^4\left(\frac{A}{2} - \frac{CB_1}{2}\right) + c\left(-\frac{5A}{12} - \frac{CB_2}{8}\right)\right\} + \mathcal{O}\left(L^7\right) \\ B_1 &\equiv \int_{-\infty}^{\infty} dt \frac{\sinh^2 t \left(\cosh^2 t + 1\right)^{\frac{1}{2}}}{\cosh^6 t} = 0.479256 \\ B_2 &\equiv \int_{-\infty}^{\infty} dt \frac{\cosh^4 t + 1}{\cosh^6 t \left(\cosh^2 t + 1\right)^{\frac{1}{2}}} = 1.91702\ . \end{aligned} \tag{67}$$

In the next-to-leading, there appears L^3 potential, which is attractive if $l^6(\pi T)^4 > \gamma c$ (high temperature or small dilaton) or repulsive if $l^6(\pi T)^4 < \gamma c$ (low temperature or large dilaton). Here γ is defined by

$$\gamma \equiv \frac{\frac{5A}{12} + \frac{CB_2}{2}}{\frac{A}{2} - \frac{CB_1}{2}} = -0.732589... \tag{68}$$

We can also obtain the free energy, entropy and energy (black hole mass) for $\mu = 0$ and $k < 0$ case

$$\begin{aligned} F &= -\frac{V_3}{2\pi G l^2}\left(\frac{5l^8(2\pi T)^4}{32} + \frac{c^2}{768 l^4 (2\pi T)^4}\right) \\ S &= -\frac{dF}{dT} = \frac{V_3}{2\pi G l^2 T}\left(\frac{25 l^8 (2\pi T)^4}{64} + \frac{49 c^2}{1536 l^4 (2\pi T)^4}\right) \\ E &= F + TS = \frac{V_3}{2\pi G l^2}\left(\frac{15 l^8 (2\pi T)^4}{64} + \frac{47 c^2}{1536 l^4 (2\pi T)^4}\right) \end{aligned} \tag{69}$$

and for $\mu > 0$ and $k = 0$ case

$$\begin{aligned} F &= -\frac{\tilde{V}_3}{2\pi^2}\left(\frac{5N^2(2\pi T)^4}{16} + \frac{c^2}{3072 l^4 g_{YM}^6 N \alpha'^6 (2\pi T)^4}\right) \\ S &= \frac{V_3}{2\pi^2 T}\left(\frac{25N^2(2\pi T)^4}{32} + \frac{49c^2}{6144 g_{YM}^6 N \alpha'^6 (2\pi T)^4}\right) \\ E &= \frac{V_3}{2\pi G l^2}\left(\frac{15N^2(2\pi T)^4}{32} + \frac{47c^2}{6144 g_{YM}^6 N \alpha'^6 (2\pi T)^4}\right)\ . \end{aligned} \tag{70}$$

Here V_3 expresses the volume of 3d Einstein manifold and we used the following relations in the string theory:

$$l^4 = 2 g_{YM}^2 N \alpha'^2\ ,\quad Gl = \frac{\pi g_{YM}^2 \alpha'^2}{N}\ . \tag{71}$$

10 Summary

In this report, we gave a very brief review for AdS/CFT and after that, we discuss the role of non-trivial dilaton in AdS/CFT. We find non-constant dilaton, non-zero curvature of four-dimensional space-time and with (or without) non-trivial axion background in type IIB supergravity. From AdS/CFT, the solution gives (power-like) running gauge coupling, which is curvature (k) dependent. In any case, there appears the potential linear to the distance L between quark and anti-quark. Furthermore by considering the black hole background, we investigate the finite temperature field theory on the boundary and find the temperature dependence of the running coupling and quark-antiquark potential and the thermodynamical quantities are calculated.

Acknowledgment

The author is indebted in S.D. Odintsov for the collaboration.

References

[1] J. Maldacena, Adv. Theor. Math. Phys. 2 (1998) 231.

[2] E. Witten, Adv. Theor. Math. Phys. 2 (1998) 253.

[3] S. Gubser, I. Klebanov and A. Polyakov, Phys. Lett. B428 105.

[4] O. Aharony, S. Gubser, J. Maldacena, H. Ooguri and Y. Oz, hep-th/9905111.

[5] I.R. Klebanov and A.A. Tseytlin, hep-th/9811035; hep-th/9812089; JHEP 03 (1999) 015; J.A. Minahan, JHEP 01 (1999) 020; hep-th/9902125; G. Ferretti and D. Martelli, hep-th/9811208; A. Armoni, E. Fuchs and J. Sonnenshein, hep-th/9903090; M. Alishahiha, A. Brandhuber and Y. Oz, hep-th/9903186; K. Ghoroku, hep-th/9907143.

[6] S. Nojiri and S.D. Odintsov, Phys. Lett. B449 (1999) 39.

[7] A. Kehagias and K. Sfetsos, hep-th/9902125.

[8] J. Maldacena, Phys. Rev. Lett. 80 (1998) 4859.

[9] L. Girardello, M. Petrini, M. Porrati and A. Zaffaroni, hep-th/9903026; S. Gubser, hep-th/9902155; R. de Mello Koch, A.Paulin-Campbell and J. Rodriques, hep-th/9903029. K. Ghoroku, hep-th/9907143.

[10] S. Nojiri and S.D. Odintsov, Phys. Lett. B458 (1999) 226.

[11] A. Kehagias and K. Sfetsos, hep-th/9903109.

[12] H. Liu and A.A. Tseytlin, hep-th/9903091.

[13] N. Constable and R.C. Myers, hep-th/9905081.

[14] S. Nojiri and S.D. Odintsov, Phys. Lett. B444 (1998) 92.

[15] S. Nojiri and S.D. Odintsov, hep-th/9903033, to appear in Int. J. Mod. Phys. A.

[16] S. Nojiri and S.D. Odintsov, to be published in Phys. Rev. D, hep-th/9906216.

[17] S. Nojiri and S.D. Odintsov, to be published in Phys. Rev. D, hep-th/9905200.

[18] S. Nojiri, S.D. Odintsov, S. Ogushi, A. Sugamoto, and M. Yamamoto, *Phys.Lett.* B

[19] Y. Kazama, Lecture Note at Ochanomizu Univ.

[20] J. Polchinski, *STRING THEORY*, Cambridge University Press, Cambridge (1998).

[21] M. Henningson and K.Skenderis, JHEP **9807** (1998), 023.

[22] H. Liu and A.A. Tseytlin, Nucl. Phys. **B533** (1998), 88.

[23] S. Gubser, I. Klebanov and A. Peet, *Phys.Rev.* **D54** (1996) 3915.

[24] S. Gubser, I. Klebanov and A. Tseytlin, *Nucl.Phys.* **B534** (1998) 202, hep-th/9805156

Path-Integral Measure in Higher-Derivative Gravity

Shinji Hamamoto[1] and Makoto Nakamura[2]

Department of Physics, Toyama University,
Toyama 930-8555, Japan

Abstract

A simple method of obtaining path-integral measures in higher-derivative gravities is presented. The measures are nothing but the generalized Lee-Yang terms.

1 Introduction

Path-integral measures in higher-derivative gravities have been calculated by Buchbinder and Lyahovich[1]. To obtain the results, they investigated the structure of constraints of the theories, performing canonical quatization straightforwardly.

In the present paper, we propose a simple method of deriving such measures. The measures are obtained by calculating the generalized Lee-Yang terms.

In §2 we treat a generic higher-derivative system. We review the canonical formalism and the path-integral quantization of the system, showing that the generalized Lee-Yang term gives the path-integral measure. In §3, the Lee-Yang terms are explicitly calculated for the higher-derivative gravities. The measures obtained there agrees with the ones of Buchbinder-Lyahovich. Section 4 gives summary and discussion.

2 Generalized Lee-Yang Term

We start with a generic system described by the Lagrangian containing up to n_a-th derivative of $x_a(t)(a = 1,\ldots,N)$

$$L = L(x_a, \dot{x}_a, \ddot{x}_a, \ldots, x_a^{(n_a)}), \tag{1}$$

where

$$x_a^{(r_a)} \stackrel{\mathrm{d}}{\equiv} \frac{d^{r_a} x_a}{dt^{r_a}}. \quad (r_a = 1,\ldots,n_a) \tag{2}$$

Canonical formalism of Ostrogradski[2] regards $x^{(s_a)}(s_a = 1,\ldots,n_a - 1)$ as independent coordinates q^{s_a+1}:

$$x^{(s_a)} \rightarrow q^{s_a+1}, \tag{3}$$

$$L(x_a, \dot{x}_a, \ldots, x_a^{(n_a)}) \rightarrow L_{\mathrm{q}}(q_a^1, \ldots, q_a^{n_a}, \dot{q}_a^{n_a}). \tag{4}$$

Momenta conjugate to $q_a^{n_a}$ are defined as usual:

$$p_{n_a}^a \stackrel{\mathrm{d}}{\equiv} \frac{\partial L_{\mathrm{q}}}{\partial \dot{q}_a^{n_a}}. \tag{5}$$

The Hessian matrix of L_{q} is

$$A^{ab} \stackrel{\mathrm{d}}{\equiv} \frac{\partial^2 L_{\mathrm{q}}}{\partial \dot{q}_a^{n_a} \partial \dot{q}_b^{n_b}}. \tag{6}$$

If the system is nonsingular $\det A^{ab} \neq 0$, which is the only case considered hereafter, the relation (5) can be inverted to give $\dot{q}_a^{n_a}$ as functions of $q^{r_a}(r_a = 1,\ldots,n_a)$ and p_{n_a}:

$$\dot{q}_a^{n_a} = \dot{q}_a^{n_a}(q^r, p_n). \tag{7}$$

[1] E-mail:hamamoto@sci.toyama-u.ac.jp
[2] E-mail:makoto@jodo.sci.toyama-u.ac.jp

The Hamiltonian is defined by

$$H_O \stackrel{d}{\equiv} p^a_{s_a} q^{s_a+1}_a + p^a_{n_a} \dot{q}^{n_a}_a(q^r, p_n) - L_q(q^r, \dot{q}^n(q^r, p_n)). \tag{8}$$

Canonical equations of motion $\dot{q}^r = (\partial H_O/\partial p_r)$, $\dot{p}_r = -(\partial H_O/\partial q^r)$ determine the time development of the system. Path integral is

$$Z_O = \int \mathcal{D}q^{r_a}_a \mathcal{D}p^a_{r_a} \exp\left\{ i \int dt \left[p^a_{r_a} \dot{q}^{r_a}_a - H_O(q^r, p_r) \right] \right\}. \tag{9}$$

After integrating with respect to $p^a_{s_a}$ and $q^{s_a+1}_a$, this reduces to[3]

$$Z_O = \int \mathcal{D}q^1_a \mathcal{D}p^a_{n_a} \exp\left\{ i \int dt \left[p^a_{n_a} q^{1(n_a)}_a - \hat{H}_O(q^1, q^{1(s)}, p_n) \right] \right\}, \tag{10}$$

where

$$\hat{H}_O(q^1, q^{1(s)}, p_n) \stackrel{d}{\equiv} p^a_{n_a} \dot{q}^{n_a}_a(q^1, q^{1(s)}, p_n) - L_q(q^1, q^{1(s)}, \dot{q}^n(q^1, q^{1(s)}, p_n)), \tag{11}$$

$$q^{1(s_a)}_a \stackrel{d}{\equiv} \frac{d^{s_a} q^1_a}{dt^{s_a}}. \tag{12}$$

To proceed further, take the following special case:

$$L_q = \frac{1}{2} A^{ab} \dot{q}^{n_a}_a \dot{q}^{n_b}_b + B^a \dot{q}^{n_a}_a + C, \quad \det A^{ab} \neq 0, \tag{13}$$

where A^{ab}, B^a and C are arbitrary functions of $q^{r_a}_a$. In this case, the conjugate momenta are

$$p^a_{n_a} = A^{ab} \dot{q}^{n_b}_b + B^a. \tag{14}$$

The Hamiltonian $\hat{H}_O$ in (11) becomes

$$\hat{H}_O = \frac{1}{2} A_{ab} p^a_{n_a} p^b_{n_b} - A_{ab} B^a p^b_{n_b} + \frac{1}{2} A_{ab} B^a B^b - C, \tag{15}$$

where A_{ab} represents the inverse matrix of A^{ab}. The integration with respect to $p^a_{n_a}$ can be carried out in (10). The result is

$$Z_O = \int \mathcal{D}q^1_a \Delta \exp\left(i \int dt L \right). \tag{16}$$

In this expression, L is the higher-derivative Lagrangian in the original configuration space

$$L \stackrel{d}{\equiv} \frac{1}{2} A^{ab} q^{1(n_a)}_a q^{1(n_b)}_b + B^a q^{1(n_a)}_a + C, \tag{17}$$

and the measure Δ is given as the generalized Lee-Yang term

$$\Delta \stackrel{d}{\equiv} [\det A_{ab}]^{-1/2} = [\det A^{ab}]^{1/2}. \tag{18}$$

3 Measures in Higher-Derivative Gravities

The Lagrangian of higher-derivative gravities is given by

$$\mathcal{L} = \mathcal{L}_E + \mathcal{L}_{HD} + \mathcal{L}_{BRS}, \tag{19}$$

$$\mathcal{L}_E = -\frac{1}{\kappa^2} \sqrt{-g} R, \tag{20}$$

$$\mathcal{L}_{HD} = \sqrt{-g} \left(a R^{\mu\nu} R_{\mu\nu} + b R^2 \right), \tag{21}$$

$$\mathcal{L}_{BRS} = \frac{1}{2\alpha_0 \kappa^2} \eta_{\mu\nu} \partial_\rho \bar{g}^{\mu\rho} \partial_\sigma \bar{g}^{\nu\sigma} - \frac{i}{2} (\partial_\mu \bar{c}_\nu + \partial_\nu \bar{c}_\mu) D^{\mu\nu}_\rho c^\rho. \tag{22}$$

Here κ, a, b are parameters of the theory; α_0 is a gauge parameter; $\eta_{\mu\nu}$ is the Minkowski metric; $c^\mu, \bar{c}_\mu$ are the FP ghosts; $\tilde{g}^{\mu\nu} \stackrel{\mathrm{d}}{\equiv} \sqrt{-g}g^{\mu\nu}$; and

$$D_\rho^{\mu\nu} \stackrel{\mathrm{d}}{\equiv} \tilde{g}^{\mu\sigma}\delta_\rho^\nu\partial_\sigma + \tilde{g}^{\nu\sigma}\delta_\rho^\mu\partial_\sigma - \tilde{g}^{\mu\nu}\partial_\rho - (\partial_\rho\tilde{g}^{\mu\nu}). \tag{23}$$

Because the BRS Lagrangian $\mathcal{L}_{\mathrm{BRS}}$ is introduced from the beginning, the system is made nonsingular.

In calculating the Hessian matrix it is convenient to use the ADM coordinates $\lambda, \lambda_i, e_{ij}$:

$$g_{\mu\nu} = \begin{pmatrix} \lambda^k\lambda_k - \lambda^2 & \lambda_j \\ \lambda_i & e_{ij} \end{pmatrix}, \quad \lambda^i \stackrel{\mathrm{d}}{\equiv} e^{ij}\lambda_j. \tag{24}$$

Expressing the Lagrangians (20)-(22) in terms of the ADM coordinates, we have

$$\mathcal{L}_{\mathrm{E}} = \frac{1}{\kappa^2}\frac{1}{4\lambda}\sqrt{e}\left(-P^{(2)ij,kl} + 2P^{(0)ij,kl}\right)\dot{e}_{ij}\dot{e}_{kl} + \ldots, \tag{25}$$

$$\mathcal{L}_{\mathrm{HD}} = \frac{1}{4\lambda^3}\sqrt{e}\left(aP^{(2)ij,kl} + 4(a+3b)P^{(0)ij,kl}\right)\ddot{e}_{ij}\ddot{e}_{kl} + \ldots, \tag{26}$$

$$\mathcal{L}_{\mathrm{BRS}} = \frac{1}{2\alpha_0\kappa^2}e\left(-\frac{1}{\lambda^4}(\dot{\lambda})^2 + \frac{1}{\lambda^2}\eta_{mn}e^{mi}e^{nj}\dot{\lambda}_i\dot{\lambda}_j + \ldots\right) + \frac{i}{2}\sqrt{e}\left(\frac{2}{\lambda}\dot{\bar{c}}_0\dot{c}^0 + \frac{1}{\lambda}\dot{\bar{c}}_i\dot{c}^i + \ldots\right), \tag{27}$$

where the projection operators

$$P^{(0)ij,kl} \stackrel{\mathrm{d}}{\equiv} \frac{1}{3}e^{ij}e^{kl}, \quad P^{(2)ij,kl} \stackrel{\mathrm{d}}{\equiv} \frac{1}{2}\left(e^{ik}e^{jl} + e^{il}e^{jk}\right) - \frac{1}{3}e^{ij}e^{kl} \tag{28}$$

have been introduced. In (25)-(27), only the highest-derivative terms have been written down explicitly. These terms are sufficient to read the Hessian matrix

$$M = \begin{array}{c} \\ e_{ij} \\ \lambda \\ \lambda_a \\ c^0 \\ \bar{c}_0 \\ c^i \\ \bar{c}_i \end{array} \begin{array}{c} \begin{array}{cccccc} e_{kl} & \lambda & \lambda_b & c^0 & \bar{c}_0 & c^j & \bar{c}_j \end{array} \\ \left(\begin{array}{c|c} A & \Gamma \\ \hline \Gamma^t & B \end{array}\right) \end{array}. \tag{29}$$

The submatrix A

$$A = \begin{pmatrix} A^{ij,kl} & * & * \\ * & A^{00} & * \\ * & * & A^{ab} \end{pmatrix} \tag{30}$$

has the main elements

$$A^{00} = \frac{e}{\lambda^4}, \quad , \tag{31}$$

$$A^{ab} = \frac{e}{\lambda^2}\eta_{mn}e^{ma}e^{nb}, \tag{32}$$

$$A^{ij,kl} = \alpha P^{(2)ij,kl} + \beta P^{(0)ij,kl}. \tag{33}$$

In (33) the parameters α, β have different values depending on the values of (a, b) as follows:

$$\begin{cases} \alpha = \beta = \dfrac{1}{\lambda}\sqrt{e} & \text{for } a = b = 0, \\ \alpha = \beta = \dfrac{1}{\lambda^3}\sqrt{e} & \text{for } a \neq 0,\ a + 3b \neq 0, \\ \alpha = \dfrac{1}{\lambda}\sqrt{e},\ \beta = \dfrac{1}{\lambda^3}\sqrt{e} & \text{for } a = 0,\ a + 3b \neq 0, \\ \alpha = \dfrac{1}{\lambda^3}\sqrt{e},\ \beta = \dfrac{1}{\lambda}\sqrt{e} & \text{for } a \neq 0,\ a + 3b = 0. \end{cases} \tag{34}$$

The submatrix B has the form

$$B = \begin{pmatrix} J & & & \\ & J & & \\ & & J & \\ & & & J \end{pmatrix}, \quad J \stackrel{\mathrm{d}}{\equiv} \frac{1}{\lambda}\sqrt{e}\begin{pmatrix} & -1 \\ 1 & \end{pmatrix}. \tag{35}$$

As shown in §2, the determinant of M gives the path-integral measure. This is calculated as follows:

$$\det M = \frac{\det(A - \Gamma B^{-1}\Gamma^t)}{\det B} = \frac{\det A}{\det B}, \tag{36}$$

where we have used the fact $\Delta B^{-1}\Gamma = 0$. Note that

$$\det A \sim \det(A^{ij,kl})e^2\lambda^{-10}, \tag{37}$$

$$\det B \sim e^4\lambda^{-8}, \tag{38}$$

and

$$\det(A^{ij,kl}) = \alpha^5\beta e^{-4}. \tag{39}$$

Then we arrive at the result:

$$\det M \sim \alpha^5\beta\lambda^{-2}e^{-6}, \tag{40}$$

which means

$$\det M = \begin{cases} \lambda^{-8}e^{-3} & \text{for } a = b = 0, \\ \lambda^{-20}e^{-3} & \text{for } a \neq 0,\ a + 3b \neq 0, \\ \lambda^{-10}e^{-3} & \text{for } a = 0,\ a + 3b \neq 0, \\ \lambda^{-18}e^{-3} & \text{for } a \neq 0,\ a + 3b = 0. \end{cases} \tag{41}$$

Returning field variables from the ADM coordinates $(\lambda, \lambda_i, e_{ij})$ to the original ones $g_{\mu\nu}$ gives

$$\begin{aligned} (g^{00})^m(-g)^n\mathcal{D}g_{\mu\nu} &= \lambda^{-2m+2n+1}e^n\mathcal{D}\lambda\mathcal{D}\lambda_i\mathcal{D}e_{ij} \\ &= (\det M)^{1/2}\mathcal{D}\lambda\mathcal{D}\lambda_i\mathcal{D}e_{ij}. \end{aligned} \tag{42}$$

Thus we arrive at the final expression for the path-integral measures Δ:

$$\Delta = (g^{00})^m(-g)^n \tag{43}$$

with

$$n = -\frac{3}{2}, \tag{44}$$

$$m = \begin{cases} 1 & \text{for } a = b = 0, \\ 4 & \text{for } a \neq 0,\ a + 3b \neq 0, \\ \frac{3}{2} & \text{for } a = 0,\ a + 3b \neq 0, \\ \frac{7}{2} & \text{for } a \neq 0,\ a + 3b = 0. \end{cases} \tag{45}$$

This is in agreement with the result of Buchbinder-Lyahovich.

4 Summary and Discussion

We have given a simple method of calculating path-integral measures in higher-derivative gravities. The measures are obtained as the generalized Lee-Yang terms. Our result agrees with that of Buchbinder-Lyahovich.

In this paper we have studied the 4-dimensional gravities with up-to-second order curvature terms. It is interesing to extend our investigation to higher dimensional and/or more-than-second order theories.

References

[1] I.L. Buchbinder and S.L. Lyahovich, Class. Quantum Grav. 4 (1987), 1487.

[2] M. Ostrogradski, Mem. Ac. St. Petersbourg V14 (1850), 385.

[3] T. Nakamura and S. Hamamoto, Prog. Theor. Phys. **95** (1996), 469.

Massive Dirac Fields in Conformally Flat Spacetime

Nobukuni Hatayama,[1] Koichi Hayashi[2]

Department of Physics, Faculty of Science and Technology,
Kinki University, Kowakae, Higashi Osaka 577-8502, Japan

Abstract

Massive Dirac fields in conformally flat spacetime are studied. It is shown that particle creation from the vacuum is possible in general. A concrete example for a given conformal factor is presented.

1 Introduction

At present, there exists no quantum theory of gravity in complete form. Only we can attack the problem satisfactory is the method of *Quantum Field Theory in Curved Spacetime*, i.e. the ordinary quantum field theory for matters in the classical gracitational background [1].

In a curved spacetime, we cannot define the vacuum state uniquely throughout the whole spacetime. We can take a local inertial frame at a spacetime point P, and can define the vacuum $|0\rangle$ at P with $a|0\rangle = 0$, where a is the annihilation operator in this frame. When we move to another spacetime point Q, and define a new inertial frame there. This new frame is not identical to the original frame at P, because the old frame is accelerated with respect to the new one. Accordingly, we must define a new vacuum $|0'\rangle$ at Q, with $a|0'\rangle \neq 0$, where a is the original annihilation operator defined at P. This means that particle creation from the vacuum is possible for curved spacetimes. An accelerated frame in curved spacetime is equivalent to a flat spacetime contact to the heat bath with a finite temperature (Unruh effect [2]). A clear example of this is manifest for the Rindler spacetime [1][3].

Particle creations from the vacuum in curved spacetimes are studied for various cases in the literatures. Most of them are, however, for scalar fields. We study here the case of massive Dirac fields (see, however, [4][5]). In fact, we restrict our considerations only to the conformally flat spacetime, $ds^2 = \Omega^2(x)(dt^2 - dr^2)$. Most of interesting cases are included to this class by an appropriate coordinate transformation, e.g. Rindler, Robartson-Walker, Milne, de Sitter, etc.

2 Dirac Equations in Curved Spacetime

With the Newman-Penrose formalism in curved spacetime, the Dirac equations are represented by a pair of spinors, P^A and $\overline{Q}^{A'}(A, A' = 0, 1)$;

$$\sigma^{\mu}_{AB'} P^{A}{}_{;\mu} + i\mu_* \overline{Q}^{C'} \epsilon_{C'B'} = 0 \tag{1}$$

$$\sigma^{\mu}_{AB'} Q^{A}{}_{;\mu} + i\mu_* \overline{P}^{C'} \epsilon_{C'B'} = 0 \tag{2}$$

$$\sigma^{\mu}_{AB'} = \frac{1}{\sqrt{2}} \begin{pmatrix} l^{\mu} & m^{\mu} \\ \overline{m}^{\mu} & n^{\mu} \end{pmatrix},$$

where $\sigma^{\mu}_{AB'}$ are generalized Pauli spin-matrices, $\sqrt{2}\,\mu_*$ is the mass of the particle, $\epsilon_{C'B'}$ is the two dimensional Levi-Civita symbol and $l^{\mu}, m^{\mu}, \overline{m}^{\mu}, n^{\mu}$ are the null basis vectors. We rewrite these equations in term of directional derivatives and spin coefficients. As a result, Dirac equations in curved spacetime reduce to

$$(D + \epsilon - \rho)F_1 + (\delta^* + \pi - \alpha)F_2 = i\mu_* G_2 \tag{3}$$

$$(\Delta + \mu - \gamma)F_2 + (\delta + \beta - \tau)F_1 = i\mu_* G_1 \tag{4}$$

[1] E-mail:hatayama@phys.kindai.ac.jp
[2] E-mail:hayashi@phys.kindai.ac.jp

$$(D+\epsilon^*-\rho^*)G_2+(\delta^*+\pi^*-\alpha^*)G_1=i\mu_* F_2 \tag{5}$$
$$(\Delta+\mu^*-\gamma^*)F_2+(\delta^*+\beta^*-\tau^*)F_1=i\mu_* F_1, \tag{6}$$

where $F_1=P^{(0)}, F_2=P^{(1)}, G_1=\overline{Q}^{(1')}, G_2=-\overline{Q}^{(0')}$.

3 Dirac Equations in Conformally Flat Spacetime

Using the conformal transformation, a metric tensor reduce to

$$\overline{g}_{\mu\nu}(x)=\Omega^2(x)\, g_{\mu\nu}(x), \tag{7}$$

where $\Omega(x)$ is non-zero, real function. In particular, when $g_{\mu\nu}=\eta_{\mu\nu}$, $\overline{g}_{\mu\nu}$ is conformally flat. Also a metric tensor is represented by the tetrad basis vectors $e_{(a)\mu}$; $a=1,2,3,4$. Therefore, we shall define new tetrad basis vectors

$$e_{(a)\mu} \equiv \Omega(x)\, e_{(a)\mu} \tag{8}$$
$$e_{(a)}{}^{\mu} \equiv \Omega^{-1}(x)\, e_{(a)}{}^{\mu}. \tag{9}$$

As described above, we shall use the Newman-Penrose formalism for the description of the Dirac equations. First, In conformally flat spacetime we give the tetrad vectors of null basis; $e_{(1)\mu}=l_\mu$, $e_{(2)\mu}=n_\mu$, $e_{(3)\mu}=m_\mu$, $e_{(4)\mu}=\overline{m}_\mu$. Thus, by equations (8) and (9), the components (t,r,θ,ϕ) of the null basis vectors are given by

$$\begin{aligned}
l^\mu &= \tfrac{\Omega^{-1}(x)}{\sqrt{2}}(1,1,0,0) & l_\mu &= \tfrac{\Omega(x)}{\sqrt{2}}(1,-1,0,0)\\
n^\mu &= \tfrac{\Omega^{-1}(x)}{\sqrt{2}}(1,-1,0,0) & n_\mu &= \tfrac{\Omega(x)}{\sqrt{2}}(1,1,0,0)\\
m^\mu &= \tfrac{\Omega^{-1}(x)}{\sqrt{2}}r^{-1}(0,0,1,i\,cosec\theta) & m_\mu &= \tfrac{\Omega(x)}{\sqrt{2}}r(0,0,-1,-i\sin\theta)\\
\overline{m}^\mu &= \tfrac{\Omega^{-1}(x)}{\sqrt{2}}r^{-1}(0,0,1,-i\,cosec\theta) & \overline{m}_\mu &= \tfrac{\Omega(x)}{\sqrt{2}}r(0,0,-1,i\sin\theta).
\end{aligned} \tag{10}$$

And directional derivatives and spin coefficients are written as

$$\begin{aligned}
D &= \tfrac{\Omega^{-1}(x)}{\sqrt{2}}\{\partial_t+\partial_r\} & \delta &= \tfrac{\Omega^{-1}(x)}{\sqrt{2}}r^{-1}\{\partial_\theta+i\,cosec\theta\partial_\varphi\}\\
\Delta &= \tfrac{\Omega^{-1}(x)}{\sqrt{2}}\{\partial_t-\partial_r\} & \delta^* &= \tfrac{\Omega^{-1}(x)}{\sqrt{2}}r^{-1}\{\partial_\theta-i\,cosec\theta\partial_\varphi\},
\end{aligned} \tag{11}$$

$$\begin{aligned}
&\kappa=\lambda=\sigma=\nu=0\\
&\epsilon=\tfrac{1}{2\sqrt{2}}\,\Omega^{-1}(x)\{(\ln\Omega(x))_{,t}+(\ln\Omega(x))_{,r}\},\ \gamma=-\tfrac{1}{2\sqrt{2}}\,\Omega^{-1}(x)\{(\ln\Omega(x))_{,t}-(\ln\Omega(x))_{,r}\}\\
&\pi=\tfrac{\Omega^{-1}(x)}{\sqrt{2}}r^{-1}\{(\ln\Omega(x))_{,\theta}-i\,cosec\theta(\ln\Omega(x))_{,\varphi}\},\ \tau=-\tfrac{\Omega^{-1}(x)}{\sqrt{2}}r^{-1}\{(\ln\Omega(x))_{,\theta}+i\,cosec\theta(\ln\Omega(x))_{,\varphi}\}\\
&\rho=-\tfrac{1}{\sqrt{2}}\Omega^{-1}(x)\{(\ln\Omega(x))_{,t}+(\ln\Omega(x))_{,r}+r^{-1}\},\ \mu=\tfrac{1}{\sqrt{2}}\Omega^{-1}(x)\{(\ln\Omega(x))_{,t}-(\ln\Omega(x))_{,r}-r^{-1}\}\\
&\alpha=-\tfrac{\Omega^{-1}(x)}{2\sqrt{2}}r^{-1}\{(\ln\Omega(x))_{,\theta}-i\,cosec\theta(\ln\Omega(x))_{,\varphi}+\cot\theta\}\\
&\beta=\tfrac{\Omega^{-1}(x)}{2\sqrt{2}}r^{-1}\{(\ln\Omega(x))_{,\theta}+i\,cosec\theta(\ln\Omega(x))_{,\varphi}+\cot\theta\}.
\end{aligned} \tag{12}$$

Substituting these results into the equations (3) ~ (6), we obtain the Dirac equations in conformally flat spacetime;

$$\begin{aligned}
&\left[\partial_t+\partial_r+r^{-1}+\tfrac{3}{2}\{(\ln\Omega(x))_{,t}+(\ln\Omega(x))_{,r}\}\right]F_1\\
&\quad+r^{-1}\left[\partial_\theta-i\,cosec\theta\,\partial_\varphi+\tfrac{1}{2}\cot\theta\right.\\
&\qquad\left.+\tfrac{3}{2}\{(\ln\Omega(x))_{,\theta}-i\,cosec\theta\,(\ln\Omega(x))_{,\varphi}\}\right]F_2=im_e\Omega(x)\,G_1
\end{aligned} \tag{13}$$

$$\left[\partial_t - \partial_r - r^{-1} + \tfrac{3}{2}\{(\ln\Omega(x))_{,t} - (\ln\Omega(x))_{,r}\} \right] F_2$$
$$+r^{-1}\left[\partial_\theta + i\,cosec\theta\ \partial_\varphi + \tfrac{1}{2}\cot\theta \right. \tag{14}$$
$$\left. +\tfrac{3}{2}\{(\ln\Omega(x))_{,\theta} + i\,cosec\theta\ (\ln\Omega(x))_{,\varphi}\} \right] F_1 = im_e\Omega(x)\ G_2$$
$$\left[\partial_t + \partial_r + r^{-1} + \tfrac{3}{2}\{(\ln\Omega(x))_{,t} + (\ln\Omega(x))_{,r}\} \right] G_2$$
$$-r^{-1}\left[\partial_\theta + i\,cosec\theta\ \partial_\varphi + \tfrac{1}{2}\cot\theta \right. \tag{15}$$
$$\left. +\tfrac{3}{2}\{(\ln\Omega(x))_{,\theta} + i\,cosec\theta\ (\ln\Omega(x))_{,\varphi}\} \right] G_1 = im_e\Omega(x)\ F_2$$
$$\left[\partial_t - \partial_r - r^{-1} + \tfrac{3}{2}\{(\ln\Omega(x))_{,t} - (\ln\Omega(x))_{,r}\} \right] G_1$$
$$-r^{-1}\left[\partial_\theta - i\,cosec\theta\ \partial_\varphi + \tfrac{1}{2}\cot\theta \right. \tag{16}$$
$$\left. +\tfrac{3}{2}\{(\ln\Omega(x))_{,\theta} - i\,cosec\theta\ (\ln\Omega(x))_{,\varphi}\} \right] G_2 = im_e\Omega(x)\ F_1,$$

where $m_e = \sqrt{2}\,\mu_*$.

4 Solution

Here, we shall consider a simple solution. We take conformal scale factor as $\Omega(x) = \Omega(t)$, the polar angle as $\theta = \pi/2$, and put the wave functions as

$$F_1(t,r,\varphi) = \frac{1}{r}\,e^{im\phi}\,\Omega(t)^{-\frac{3}{2}} f_1(t,r) \tag{17}$$
$$F_2(t,r,\varphi) = \frac{1}{r}\,e^{im\phi}\,\Omega(t)^{-\frac{3}{2}} f_2(t,r) \tag{18}$$
$$G_2(t,r,\varphi) = \frac{1}{r}\,e^{im\phi}\,\Omega(t)^{-\frac{3}{2}} g_2(t,r) \tag{19}$$
$$G_1(t,r,\varphi) = \frac{1}{r}\,e^{im\phi}\,\Omega(t)^{-\frac{3}{2}} g_1(t,r). \tag{20}$$

Then, equations (13) $\sim$ (16) reduce to

$$\left[\ \partial_t + \partial_r\ \right] f_1(t,r) + mr^{-1}\ f_2(t,r) = im_e\Omega(t)\ g_1(t,r) \tag{21}$$
$$\left[\ \partial_t - \partial_r\ \right] f_2(t,r) - mr^{-1}\ f_1(t,r) = im_e\Omega(t)\ g_2(t,r) \tag{22}$$
$$\left[\ \partial_t + \partial_r\ \right] g_2(t,r) + mr^{-1}\ g_1(t,r) = im_e\Omega(t)\ f_2(t,r) \tag{23}$$
$$\left[\ \partial_t - \partial_r\ \right] g_1(t,r) - mr^{-1}\ g_2(t,r) = im_e\Omega(t)\ f_1(t,r). \tag{24}$$

If we put the mass $m_e = 0$, above Dirac equations are invariant under the conformal transformation. This means that particle creations from vacuum don't occur for massless Dirac fields in conformally flat spacetime. Let us consider the case of $m_e \neq 0$. We restrict to radial trajectories, so that $m = 0$. Equations (21) $\sim$ (24) become

$$\left[\ \partial_t{}^2 - \partial_r{}^2\ \right] f_1(t,r) - (\ln\Omega(t))_{,t}\left[\ \partial_t + \partial_r\ \right] f_1(t,r) + m_e{}^2\Omega^2(t)\ f_1(t,r) = 0 \tag{25}$$
$$\left[\ \partial_t{}^2 - \partial_r{}^2\ \right] f_2(t,r) - (\ln\Omega(t))_{,t}\left[\ \partial_t - \partial_r\ \right] f_2(t,r) + m_e{}^2\Omega^2(t)\ f_2(t,r) = 0 \tag{26}$$
$$\left[\ \partial_t{}^2 - \partial_r{}^2\ \right] g_2(t,r) - (\ln\Omega(t))_{,t}\left[\ \partial_t + \partial_r\ \right] g_2(t,r) + m_e{}^2\Omega^2(t)\ g_2(t,r) = 0 \tag{27}$$
$$\left[\ \partial_t{}^2 - \partial_r{}^2\ \right] g_1(t,r) - (\ln\Omega(t))_{,t}\left[\ \partial_t - \partial_r\ \right] g_1(t,r) + m_e{}^2\Omega^2(t)\ g_1(t,r) = 0, \tag{28}$$

We should note that the second term of these equations are induced from $\Omega(x)$ of the right side of the equations (21) $\sim$ (24). Namely, these terms are the direct result of $m_e \neq 0$.

To solve these equations, we impose one more restriction that the mass m_e is small enough, so that, We neglect the second order terms. The equations become

$$[\,\partial_t{}^2 - \partial_r{}^2\,]\, f_1(t,r) - (\ln\Omega(t))_{,t}\,[\,\partial_t + \partial_r\,]\, f_1(t,r) = 0 \tag{29}$$

$$[\,\partial_t{}^2 - \partial_r{}^2\,]\, f_2(t,r) - (\ln\Omega(t))_{,t}\,[\,\partial_t - \partial_r\,]\, f_2(t,r) = 0 \tag{30}$$

$$[\,\partial_t{}^2 - \partial_r{}^2\,]\, g_2(t,r) - (\ln\Omega(t))_{,t}\,[\,\partial_t + \partial_r\,]\, g_2(t,r) = 0 \tag{31}$$

$$[\,\partial_t{}^2 - \partial_r{}^2\,]\, g_1(t,r) - (\ln\Omega(t))_{,t}\,[\,\partial_t - \partial_r\,]\, g_1(t,r) = 0. \tag{32}$$

The equation (29) has a solution;

$$f_1(t,r) = a\,\{\,e^{-i\omega t} + \left(-2i\omega\int_{-\infty}^{t}\Omega(t')\,e^{-2i\omega t'}\,dt'\right) e^{\,i\omega t}\,\}\,e^{-ikr}$$
$$b^\dagger\,\{\,e^{\,i\omega t} + \left(2i\omega\int_{-\infty}^{t}\Omega(t')\,e^{\,2i\omega t'}\,dt'\right) e^{-i\omega t}\,\}\,e^{\,ikr}. \tag{33}$$

From now on, we consider only the time-dependence, and abbreviate the factor $e^{\pm ikr}$. When $t \to -\infty$, the equation (33) reduces to the form

$$a\,e^{-i\omega t} + b^\dagger\,e^{\,i\omega t}, \tag{34}$$

so that we can interpret as the annihilation operator with $a|\,0\,\rangle = 0$ for the vacuum $|\,0\,\rangle$. When $t \to \infty$, we obtain

$$(\,a + b^\dagger\,\widetilde{\Omega}(2\omega)\,)\,e^{-i\omega t} + (\,b^\dagger + a\,\widetilde{\Omega}(-2\omega)\,)\,e^{\,i\omega t}, \tag{35}$$

where

$$\widetilde{\Omega}(2\omega) \equiv 2i\omega\int_{-\infty}^{+\infty}\Omega(t')\,e^{\,2i\omega t'}\,dt'. \tag{36}$$

Here, we define a new creation and annihilation operators, respectively;

$$\overline{a} = a + b^\dagger\,\widetilde{\Omega}(2\omega) \tag{37}$$

$$\overline{b}^\dagger = b^\dagger + a\,\widetilde{\Omega}(-2\omega). \tag{38}$$

Then, $\overline{a}\,|\,0\,\rangle = \widetilde{\Omega}(2\omega)\,b^\dagger|\,0\,\rangle \neq 0$. Thus, the vacuum in the far future $t \to +\infty$ is an excited state with respect to the vacuum in the far past $t \to -\infty$.

Let us take a concrete example. Consider the conformal scale factor

$$\Omega(t) = A + B\,\tanh(t/\alpha). \tag{39}$$

This is an asymptotically flat cosmological model(fig.1). A, B and α are constants. $A > B$, and $-\infty < t < +\infty$. Indeed, this conformally flat spacetime reduce to spatially flat Robertson-Walker spacetime by the transformation $dt = d\eta/a(\eta)$. Now the integrand $\Omega(t)$ of (33) becomes constant $A - B, A + B$ in the asymptotic regions $t \to \pm\infty$, respectively. So the integral in the asymptotic region shall ignore. Thus, we have only to consider non-static region; $-\alpha < t < \alpha$. Then, as $\tanh(t/\alpha) \sim t/\alpha$, becomes

$$\widetilde{\Omega}(2\omega) = 2i\omega\int_{-\infty}^{+\infty}\tanh(t'/\alpha)\,e^{\,2i\omega t'}\,dt' \tag{40}$$

$$= 2\cos 2\alpha\omega - \frac{1}{\alpha\omega}\sin 2\alpha\omega \equiv p(2\alpha\omega). \tag{41}$$

In particular, when $\alpha = 1$,

$$p(2\omega) = 2\cos 2\omega - \frac{1}{\omega}\sin 2\omega \tag{42}$$

(see fig.2).

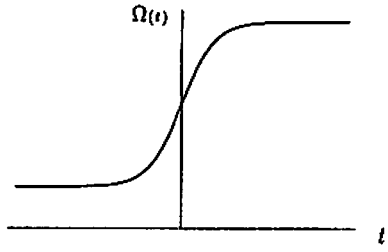

Figure 1: The conformal scale factor $\Omega(t) = A + B \tanh(t/\alpha)$ in asymptotically static universe

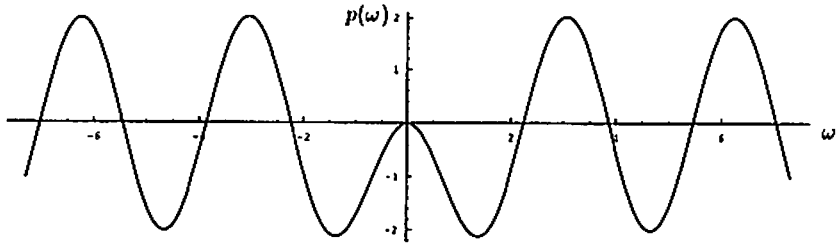

Figure 2: $p(\omega)$ for $\alpha = 1$

Therefore, this have obtained a simple example of $\omega-$dependent particle creations from the vacuum.

5 Discussion

We have derived simple solutions for massive Dirac fields in conformally flat spacetimes in general, and have shown that particle creations from the vacuum can occur for curved spacetimes also for Dirac fields, just as scalar cases. But it is interesting to compare our results with those for the scalar field on similar conditions. In the case of scalar fields, the conformal invariance is broken by the second order terms of the mass. For Dirac fields, particle creation can occur in the first order of the mass.

References

[1] N.D. Birell, P.C.W. Davies, *Quantum fields in curved spacetime* (Cambridge Univ. Press, 1982).

[2] W.G. Unruh, Phys.Rev.D, 14, 870 (1976).

[3] W. Rindler, *Essential Relativity* (NewYork: Springer-Verlag, 1969).

[4] F. Finelli, A. Gruppuso and G. Venturi, Class.Quantum Grav. 16, 3923 (1999).

[5] M. Wellmann, *Adiabatic vacuumstates of the Dirac-field on a curved spacetime*, hep-th/9802087.

Neutrino oscillations in strong gravitational fields

Shinji Tsujikawa,[1] Jun-ichiro Koga,[2] and Kei-ichi Maeda[3]

Department of Physics, Waseda University, 3-4-1 Ohkubo, Shinjuku-ku, Tokyo 169-8555, Japan

Abstract

We consider neutrino oscillations in strong gravitational fields by making use of the quantum field theory in curved spacetime. We investigate how a wave packet of a flavor neutrino emitted near the event horizon of the Schwarzschild black hole changes another flavor neutrino when it propagates toward the outgoing direction. The expectation values of number densities of two flavor neutrions are calculated, and we find that number densities of the center of wave packets decrease as neutrinos propagate, and the proper oscillation length becomes smaller as the position where neutrinos are generated is nearer to the event horizon. These results are due to the gravitational effects related with redshift.

1 Introduction

If neutrinos are massive and mixed, a flavor neutrino is generated by a weak-interaction process as a superposition of mass eigenstates. Neutrino oscillations occurs by the interference among the different eigenstates. Neutrino oscillations in the Minkowski spacetime have been much studied in the past in the case of vacuum[1] and matter[2] oscillations. Recently, several authors considered neutrino oscillations in strong gravitational fields in the vacuum case[3, 4, 5, 6, 7]. Since neutrinos can be emitted from strong gravitational sources such as supernova and neutron stars, it is important to investigate how gravitational effects will alter the standard vacuum oscillation formula of the Minkowski spacetime. They studied the quantum mechanical phase of neutrinos which are emitted around the Schwarzschild geometry and propagate in a radial trajectory, and found that gravitational effects due to the redshift play important roles for the calculation of the phase factor. However, these studies are based on the plane wave analysis which is valid for extremely relativistic neutrinos. We need to apply the wave packet treatment in order to know how neutrinos propagate in radial trajectories. Moreover, although they obtained the phase of neutrinos by quantum mechanical approach, it is worth questioning whether this classical picture will provide the correct description of neutrino oscillations. In this paper, motivated by these considerations, we investigate how wave packets of neutrinos generated around the Schwarzschild black hole propagate in outer directions by making use of the quantum field theory in curved spacetime[8, 9]. The expectation values of the number densities of flavor neutrinos will be calculated, and we mainly investigate how the results in strong gravitational fields are different from that in the Minkowski spacetime. In Sec. 2, we consider Dirac equations in the Schwarzschild geometry for massive neutrinos. In Sec. 3, we quantize neutrino fields and calculate the expectation values of the number densities of flavor neutrinos. In Sec. 4, the gravitational effect on neutrino oscillations is considered. We give our conclusions in the final section.

2 Dirac equations in the Schwarzschild spacetime

We consider a model where two flavor neutrinos ν_α and ν_β are mixing by the strength δ:

$$\mathcal{L} = \overline{\psi}_\alpha \left(\gamma^\nu \nabla_\nu + \mu_\alpha\right) \psi_\alpha + \overline{\psi}_\beta \left(\gamma^\nu \nabla_\nu + \mu_\beta\right) \psi_\beta + \delta \left(\overline{\psi}_\alpha \psi_\beta + \psi_\beta \overline{\psi}_\alpha\right), \tag{1}$$

where μ_α and μ_β are masses of neutrino fields ψ_α and ψ_β, respectively, and ∇_ν denotes a covariant derivative which is written as $\nabla_\nu = \partial_\nu - \Gamma_\nu$ with the spin connection Γ_ν[10]. The gamma matrix satisfies the relation

$$\gamma^\mu \gamma^\nu + \gamma^\nu \gamma^\mu = 2g^{\mu\nu}, \tag{2}$$

[1] E-mail:shinji@gravity.phys.waseda.ac.jp
[2] E-mail:koga@gravity.phys.waseda.ac.jp
[3] E-mail:maeda@gravity.phys.waseda.ac.jp

where $g_{\mu\nu}$ is the background metric. In this paper, we adopt the Schwarzschild metric,

$$ds^2 = -e^{\nu}dt^2 + e^{\lambda}dr^2 + r^2d\theta^2 + r^2\sin^2\theta d\phi^2, \tag{3}$$

with

$$e^{\nu} = 1 - \frac{2M}{r}, \quad e^{\lambda} = \left(1 - \frac{2M}{r}\right)^{-1}, \tag{4}$$

where M denotes the mass of the source of the gravitational field.

We obtain the following Dirac equations by the Lagrangian (1)

$$\mathbf{D}\Psi = \mathbf{M}\Psi, \tag{5}$$

with

$$\mathbf{D} = \gamma^{\nu}\nabla_{\nu} \ , \ \Psi = \begin{pmatrix} \psi_{\alpha} \\ \psi_{\beta} \end{pmatrix} \ , \ \mathbf{M} = \begin{pmatrix} -\mu_{\alpha} & -\delta \\ -\delta & -\mu_{\beta} \end{pmatrix}. \tag{6}$$

If we choose a unitary matrix U which diagonizes the matrix M as

$$\mathbf{U} = \frac{1}{A}\begin{bmatrix} \mu_{\beta} - \mu_{\alpha} + \sqrt{(\mu_{\beta} - \mu_{\alpha})^2 + 4\delta^2} & 2\delta \\ -2\delta & \mu_{\beta} - \mu_{\alpha} + \sqrt{(\mu_{\beta} - \mu_{\alpha})^2 + 4\delta^2} \end{bmatrix}, \tag{7}$$

where

$$A = \left[\left(\mu_{\beta} - \mu_{\alpha} + \sqrt{(\mu_{\beta} - \mu_{\alpha})^2 + 4\delta^2}\right)^2 + 4\delta^2\right]^{1/2}, \tag{8}$$

the Dirac equations yield

$$\mathbf{D}\Phi = \mathbf{P}\Phi, \tag{9}$$

with

$$\Psi = \mathbf{U}\Phi, \quad \mathbf{P} = \mathbf{U}^{-1}\mathbf{M}\mathbf{U}. \tag{10}$$

Expressing two matrixes Ψ and $\mathbf{P}$ in the form

$$\Phi = \begin{pmatrix} \psi_1 \\ \psi_2 \end{pmatrix}, \quad \mathbf{P} = \begin{pmatrix} \mu_1 & 0 \\ 0 & \mu_2 \end{pmatrix}, \tag{11}$$

the Dirac equations (9) in mass eigenstates can be written as

$$(\gamma^{\nu}\nabla_{\nu} + \mu_i)\,\psi_i = 0 \qquad (i = 1, 2). \tag{12}$$

Note that μ_1 and μ_2 correspond to the mass of neutrinos whose mass eigenstates are ψ_1 and ψ_2, respectively. As is found by the expression (7), flavor eigenstates Ψ and mass eigenstates Φ are connected by the relation

$$\begin{pmatrix} \psi_{\alpha} \\ \psi_{\beta} \end{pmatrix} = \begin{pmatrix} \cos\alpha & \sin\alpha \\ -\sin\alpha & \cos\alpha \end{pmatrix}\begin{pmatrix} \psi_1 \\ \psi_2 \end{pmatrix}, \tag{13}$$

where α is the so called mixing angle which satisfies $\tan\alpha = 2\delta/(\mu_{\beta} - \mu_{\alpha} + \sqrt{(\mu_{\beta} - \mu_{\alpha})^2 + 4\delta^2})$.

Let us consider the Dirac equation (12) in the Schwarzschild metric. Using the tetrad

$$e_a^{\mu} = \mathrm{diag}\left(e^{-\nu/2}, e^{-\lambda/2}, 1/r, 1/r\sin\theta\right), \tag{14}$$

and the gamma matrix in the Minkowski spacetime $\tilde{\gamma}^0 = (e_0^t)^{-1}\gamma^t, \tilde{\gamma}^1 = (e_1^r)^{-1}\gamma^r, \tilde{\gamma}^2 = (e_2^\theta)^{-1}\gamma^\theta, \tilde{\gamma}^3 = (e_3^\phi)^{-1}\gamma^\phi$, Eq. (12) can be written as

$$\left[\tilde{\gamma}^0 e^{-\frac{1}{2}\nu}\frac{\partial}{\partial t} + \tilde{\gamma}^1 e^{-\frac{1}{2}\lambda}\frac{1}{re^{\frac{1}{4}\nu}}\left(\frac{\partial}{\partial r}\left(re^{\frac{1}{4}\nu}\right)\right) + \tilde{\gamma}^2\frac{1}{r}\frac{1}{\sqrt{\sin\theta}}\left(\frac{\partial}{\partial\theta}\sqrt{\sin\theta}\right) + \tilde{\gamma}^3\frac{1}{r\sin\theta}\frac{\partial}{\partial\phi} + \mu_i\right]\psi_i = 0. \quad (15)$$

Setting the wave function as

$$\psi_i = \frac{1}{re^{\frac{1}{4}\nu}\sqrt{\sin\theta}}\mathrm{S}(r,\theta)e^{im\phi}e^{-i\omega t}, \quad (16)$$

with

$$\mathrm{S}(r,\theta) = {}^t\left[u_1(r)P_1(\theta), u_2(r)P_2(\theta), u_3(r)P_1(\theta), u_4(r)P_2(\theta)\right], \quad (17)$$

Eq. (15) is decoupled to the equations for r and θ directions. $P_1(\theta)$ and $P_2(\theta)$ are expressed by spin-s spherical harmonics ${}_sY_{lm}$, with $s = \pm 1/2$:

$$P_1(\theta) = \sqrt{\sin\theta}\,{}_{+\frac{1}{2}}Y_{lm}, \quad P_2(\theta) = \sqrt{\sin\theta}\,{}_{-\frac{1}{2}}Y_{lm}, \quad (18)$$

and satisfy the orthogonal relations. Introducing a tortoise coordinate r_* with $dr_*/dr = e^{\lambda/2-\nu/2} = 1 - 2M/r$, the equations for the r direction in the chiral representation of the gamma matrix are written by

$$\frac{du_1}{dr_*} - i\omega u_1 - i\mu\frac{\sqrt{\Delta}}{r}u_3 - \frac{k\sqrt{\Delta}}{r^2}u_2 = 0, \quad (19)$$

$$\frac{du_2}{dr_*} + i\omega u_2 + i\mu\frac{\sqrt{\Delta}}{r}u_4 - \frac{k\sqrt{\Delta}}{r^2}u_1 = 0, \quad (20)$$

$$\frac{du_3}{dr_*} + i\omega u_3 + i\mu\frac{\sqrt{\Delta}}{r}u_1 - \frac{k\sqrt{\Delta}}{r^2}u_4 = 0, \quad (21)$$

$$\frac{du_4}{dr_*} - i\omega u_4 - i\mu\frac{\sqrt{\Delta}}{r}u_2 - \frac{k\sqrt{\Delta}}{r^2}u_3 = 0, \quad (22)$$

where $\Delta = r^2 - 2Mr$ and k is a separation constant. In the limit of $r \to 2M$ ($r_* \to -\infty$), each component takes the following form

$$u_1 \sim e^{i\omega r_*}\ ,\ u_2 \sim e^{-i\omega r_*}\ ,\ u_3 \sim e^{-i\omega r_*}\ ,\ u_4 \sim e^{i\omega r_*}. \quad (23)$$

On the other hand, in the limit of $r \to \infty$, each component approaches the form

$$u_1\ ,\ u_2\ ,\ u_3\ ,\ u_4\ \sim e^{\pm i\sqrt{\omega^2-\mu^2}\,r}, \quad (24)$$

which correspond to the plane wave solution of the Minkowski spacetime.

Introducing the new variables

$$Z_+ = e^{-i\chi/2}(u_1 + u_4) + e^{+i\chi/2}(u_2 + u_3), \quad Z_- = e^{-i\chi/2}(u_1 + u_4) - e^{+i\chi/2}(u_2 + u_3), \quad (25)$$

with $\chi = \arctan(\mu r/k)$, we obtain the decoupled equations

$$\left(\frac{d^2}{d\hat{r}_*{}^2} + \omega^2\right)Z_\pm = V_\pm Z_\pm, \quad (26)$$

where $d\hat{r}_* = \left(1 - e^{-\frac{1}{2}(\lambda-\nu)}\frac{k\mu}{2\omega}\frac{1}{k^2+\mu^2r^2}\right)dr_*$ and

$$\begin{aligned} V_\pm &= \frac{\sqrt{\Delta}(k^2+\mu^2r^2)^{\frac{3}{2}}}{[r^2(k^2+\mu^2r^2) - k\mu\Delta/2\omega]^2}\left[\sqrt{\Delta}(k^2+\mu^2r^2)^{\frac{3}{2}} \pm \{(r-M)(k^2+\mu^2r^2) + 3\mu^2r\Delta\}\right] \\ &\mp \frac{\Delta^{\frac{3}{2}}(k^2+\mu^2r^2)^{\frac{3}{2}}}{[r^2(k^2+\mu^2r^2) - k\mu\Delta/2\omega]^3}\left[2r(k^2+\mu^2r^2) + 2\mu^2r^3 - k\mu(r-M)/\omega\right]. \end{aligned} \quad (27)$$

By choosing the following combinations,

$$Z_+{}' = e^{+i\chi/2}(u_1 - u_4) + e^{-i\chi/2}(u_2 - u_3), \quad Z_-{}' = e^{+i\chi/2}(u_1 - u_4) - e^{-i\chi/2}(u_2 - u_3), \tag{28}$$

the equations for Z'_+ and Z'_- yield

$$\left(\frac{d^2}{d\tilde{r}_*'^2} + \omega^2\right) Z_\pm{}' = V_\pm{}' Z_\pm{}', \tag{29}$$

where $d\tilde{r}'_* = \left(1 + e^{-\frac{1}{2}(\lambda-\nu)\frac{k\mu}{2\omega}\frac{1}{k^2+\mu^2r^2}}\right) dr_*$ and

$$\begin{aligned} V_\pm{}' &= \frac{\sqrt{\Delta}(k^2+\mu^2r^2)^{\frac{3}{2}}}{[r^2(k^2+\mu^2r^2)+k\mu\Delta/2\omega]^2}\left[\sqrt{\Delta}(k^2+\mu^2r^2)^{\frac{3}{2}} \pm \{(r-M)(k^2+\mu^2r^2)+3\mu^2r\Delta\}\right] \\ &\mp \frac{\Delta^{\frac{3}{2}}(k^2+\mu^2r^2)^{\frac{3}{2}}}{[r^2(k^2+\mu^2r^2)+k\mu\Delta/2\omega]^3}\left[2r(k^2+\mu^2r^2)+2\mu^2r^3+k\mu(r-M)/\omega\right]. \end{aligned} \tag{30}$$

In the limit of $r \to 2M$, $V_\pm$ and $V_\pm{}'$ vanish, and $Z_\pm$ and $Z'_\pm$ take the form

$$Z_\pm \sim e^{\pm i\omega r_*}, \quad Z'_\pm \sim e^{\pm i\omega \tilde{r}'_*}. \tag{31}$$

For the case of $r \to \infty$, $V_\pm$ and $V_\pm{}'$ approaches μ^2, and $Z_\pm$ and $Z'_\pm$ take the form

$$Z_\pm \sim e^{\pm i\sqrt{\omega^2-\mu^2}r_*}, \quad Z_\pm{}' \sim e^{\pm i\sqrt{\omega^2-\mu^2}\tilde{r}'_*}. \tag{32}$$

Making use of the decoupled equations (26) and (29), we analyze the evolution of wave packets of neutrinos in the subsequent sections.

3 Quantization of neutrino fields

Let us quantize the neutrino fields ψ_i $(i = 1, 2)$ with the mass μ_i,

$$\hat{\Psi}_i = \int_\omega d\omega \sum_{m,k,\lambda} \left[a_i(\omega,m,k,\lambda)\psi_i(\omega,m,k,\lambda) + b_i{}^\dagger(\omega,m,k,\lambda)\psi_i(-\omega,-m,k,\lambda)\right], \tag{33}$$

where a_i denotes the annihilation operators of the states with positive energy ω_i and mass μ_i, and $b_i^\dagger$ denotes the creation operators of the states with negative energy ω_i and mass μ_i. $\lambda = +, -$ means that neutrino waves from a black hole are outgoing or ingoing, respectively. Since the number density operator $\hat{j}^t$ of a neutrino field ψ is written in the form

$$\hat{j}^t = \bar{\hat{\psi}}\gamma^t\hat{\psi} = \frac{r}{\sqrt{\Delta}}\hat{\psi}^\dagger\hat{\psi}, \tag{34}$$

the number density operators for two flavor neutrinos ν_α and ν_β are expressed by two quantized neutrino fields $\hat{\Psi}_1$ and $\hat{\Psi}_2$ of mass eigenstates

$$\hat{j_\alpha}{}^t = e^{-\frac{1}{2}\nu}\left[\cos^2\alpha\cdot\hat{\Psi}_1^\dagger\hat{\Psi}_1 + \sin^2\alpha\cdot\hat{\Psi}_2^\dagger\hat{\Psi}_2 + \cos\alpha\sin\alpha\left(\hat{\Psi}_1^\dagger\hat{\Psi}_2 + \hat{\Psi}_2^\dagger\hat{\Psi}_1\right)\right], \tag{35}$$

$$\hat{j_\beta}{}^t = e^{-\frac{1}{2}\nu}\left[\sin^2\alpha\cdot\hat{\Psi}_1^\dagger\hat{\Psi}_1 + \cos^2\alpha\cdot\hat{\Psi}_2^\dagger\hat{\Psi}_2 - \cos\alpha\sin\alpha\left(\hat{\Psi}_1^\dagger\hat{\Psi}_2 + \hat{\Psi}_2^\dagger\hat{\Psi}_1\right)\right], \tag{36}$$

where we have used the relation (13).

Let us consider the case where a neutrino is emitted at the position of $r = r_0$ near the event horizon with $r_0 > 2M$. We give the initial energy dispersions of two massive neutrinos in the Gaussian form

$$C_\omega^{loc}(r_0) = P_1\exp\left[-\frac{(\omega^{loc}(r_0)-\omega_1^{loc}(r_0))^2}{2(\sigma_\omega{}^{loc}(r_0))^2}\right], \quad D_\omega^{loc}(r_0) = P_2\exp\left[-\frac{(\omega^{loc}(r_0)-\omega_2^{loc}(r_0))^2}{2(\sigma_\omega{}^{loc}(r_0))^2}\right], \tag{37}$$

where P_i is the normalization constant, $\omega^{loc}(r_0)$ is the local energy observed at r_0, $\omega_i^{loc}(r_0)$ is the center value of the distribution (37) and $\sigma_\omega^{loc}(r_0)$ denotes the width of energy dispersion. The local energies $\omega^{loc}(r_0)$ and $\sigma_\omega^{loc}(r_0)$ are related with the conserved energy ω and σ_ω observed from infinity as

$$\omega^{loc}(r_0) = \frac{r_0}{\sqrt{\Delta_0}}\omega \quad , \quad \sigma_\omega{}^{loc}(r_0) = \frac{r_0}{\sqrt{\Delta_0}}\sigma_\omega, \tag{38}$$

where $\Delta_0 = r_0^2 - 2Mr_0$.

We choose a state of a neutrino which has the positive energy

$$|\phi_+\rangle = \int d\omega^{loc}(r_0)\, C_\omega^{loc}(r_0) a_1{}^\dagger(\omega^{loc}(r_0))\ |0\rangle + \int d\omega^{loc}(r_0)\, D_\omega^{loc}(r_0) a_2{}^\dagger(\omega^{loc}(r_0))\ |0\rangle. \tag{39}$$

Then expectation values of the number densities of two flavor neutrinos ν_α and ν_β are written as

$$\begin{aligned} j_\alpha{}^t &= \langle\phi_+|\hat{j_\alpha}{}^t|\phi_+\rangle \\ &= \frac{r}{\sqrt{\Delta}}\cdot\frac{r_0^2}{\Delta_0}\left[\cos^2\alpha\int_{\mu_1}^\infty C_\omega{}^*\psi_1^\dagger(\omega)d\omega\int_{\mu_1}^\infty C_\omega\psi_1(\omega)d\omega + \sin^2\alpha\int_{\mu_2}^\infty D_\omega{}^*\psi_2^\dagger(\omega)d\omega\int_{\mu_2}^\infty D_\omega\psi_2(\omega)d\omega\right. \\ &\quad \left. + \cos\alpha\sin\alpha\times\left\{\int_{\mu_1}^\infty C_\omega{}^*\psi_1^\dagger(\omega)d\omega\int_{\mu_2}^\infty D_\omega\psi_2(\omega)d\omega + \int_{\mu_2}^\infty D_\omega{}^*\psi_2^\dagger(\omega)d\omega\int_{\mu_1}^\infty C_\omega\psi_1(\omega)d\omega\right\}\right], \end{aligned} \tag{40}$$

$$\begin{aligned} j_\beta{}^t &= \langle\phi_+|\hat{j_\beta}{}^t|\phi_+\rangle \\ &= \frac{r}{\sqrt{\Delta}}\cdot\frac{r_0^2}{\Delta_0}\left[\sin^2\alpha\int_{\mu_1}^\infty C_\omega{}^*\psi_1^\dagger(\omega)d\omega\int_{\mu_1}^\infty C_\omega\psi_1(\omega)d\omega + \cos^2\alpha\int_{\mu_2}^\infty D_\omega{}^*\psi_2^\dagger(\omega)d\omega\int_{\mu_2}^\infty D_\omega\psi_2(\omega)d\omega\right. \\ &\quad \left. - \cos\alpha\sin\alpha\times\left\{\int_{\mu_1}^\infty C_\omega{}^*\psi_1^\dagger(\omega)d\omega\int_{\mu_2}^\infty D_\omega\psi_2(\omega)d\omega + \int_{\mu_2}^\infty D_\omega{}^*\psi_2^\dagger(\omega)d\omega\int_{\mu_1}^\infty C_\omega\psi_1(\omega)d\omega\right\}\right]. \end{aligned} \tag{41}$$

Let us consider the number density which is observed by the local observer rest at r. $\hat{j}^t$ defined by Eq. (34) is different from the local number density operator $\hat{j}_{loc}^t$ as

$$\hat{j}_{loc}^t = |g_{tt}|^{1/2}\,\hat{j}^t = \frac{\sqrt{\Delta}}{r}\,\hat{j}^t. \tag{42}$$

We define the local energy density $J_{loc}^t(r)$ which is integrated in the θ, ϕ direction,

$$J_{loc}^t(r) = \int r^2\sin\theta\ j_{loc}^t d\theta d\phi. \tag{43}$$

Then $(J_\alpha^t)_{loc}(r)$ and $(J_\beta^t)_{loc}(r)$ are expressed as

$$\begin{aligned} (J_\alpha^t)_{loc}(r) &= \frac{r}{\sqrt{\Delta}}\cdot\frac{r_0^2}{\Delta_0}\left[\cos^2\alpha\int_{\mu_1}^\infty C_\omega{}^*u^\dagger(\omega)d\omega\int_{\mu_1}^\infty C_\omega u(\omega)d\omega + \sin^2\alpha\int_{\mu_2}^\infty D_\omega{}^*v^\dagger(\omega)d\omega\int_{\mu_2}^\infty D_\omega v(\omega)d\omega\right. \\ &\quad \left. + \cos\alpha\sin\alpha\times\left\{\int_{\mu_1}^\infty C_\omega{}^*u^\dagger(\omega)d\omega\int_{\mu_2}^\infty D_\omega v(\omega)d\omega + \int_{\mu_2}^\infty D_\omega{}^*v^\dagger(\omega)d\omega\int_{\mu_1}^\infty C_\omega u(\omega)d\omega\right\}\right], \end{aligned} \tag{44}$$

$$\begin{aligned} (J_\beta^t)_{loc}(r) &= \frac{r}{\sqrt{\Delta}}\cdot\frac{r_0^2}{\Delta_0}\left[\sin^2\alpha\int_{\mu_1}^\infty C_\omega{}^*u^\dagger(\omega)d\omega\int_{\mu_1}^\infty C_\omega u(\omega)d\omega + \cos^2\alpha\int_{\mu_2}^\infty D_\omega{}^*v^\dagger(\omega)d\omega\int_{\mu_2}^\infty D_\omega v(\omega)d\omega\right. \\ &\quad \left. - \cos\alpha\sin\alpha\times\left\{\int_{\mu_1}^\infty C_\omega{}^*u^\dagger(\omega)d\omega\int_{\mu_2}^\infty D_\omega v(\omega)d\omega + \int_{\mu_2}^\infty D_\omega{}^*v^\dagger(\omega)d\omega\int_{\mu_1}^\infty C_\omega u(\omega)d\omega\right\}\right], \end{aligned} \tag{45}$$

where we have used Eqs. (16), (17) for the field ψ_1 with mass μ_1, and (16) with $v(r)$ for the r direction for the field ψ_2 with mass μ_2.

4 Neutrino oscillations in the Schwarzschild metric

Let us consider the relativistic neutrino $\omega^2 \gg \mu^2$ emitted from a point near the event horizon. In this case, since the energy of the neutrino is much larger than the potential energy (27) and (30), we can apply the WKB approximation to analyze the evolution of neutrino fields. Then, the neutrino waves Z_+, Z_- which propagates in the outgoing direction is written by

$$Z_+ \approx C\frac{1}{(\omega^2 - V_+)^{\frac{1}{4}}} \exp\left(i\int_{r_*^0}^{r_*} \sqrt{\omega^2 - V_+}\, dr_*\right), \quad Z_- = \frac{1}{i\omega}\left(i\sqrt{\omega^2 - V_+} - W\right) Z_+, \tag{46}$$

where we have neglected the reflection wave. W is defined by $W = e^{\nu/2}(k^2 + \mu^2 r^2)^{3/2}/[r(k^2 + \mu^2 r^2) - e^{(\nu-\lambda)/2} k\mu r/2\omega]$. The solution for the waves Z_+', Z_-' are expressed as

$$Z_+{}' \approx D\frac{1}{(\omega^2 - V_+')^{\frac{1}{4}}} \exp\left(i\int_{r_*^0}^{r_*'} \sqrt{\omega^2 - V_+'}\, dr_*'\right), \quad Z_-{}' = \frac{1}{i\omega}\left(i\sqrt{\omega^2 - V_+'} - W'\right) Z_+', \tag{47}$$

where W' is defined by $W' = e^{\nu/2}(k^2 + \mu^2 r^2)^{3/2}/[r(k^2 + \mu^2 r^2) + e^{(\nu-\lambda)/2} k\mu r/2\omega]$. Making use of the relation $\omega^2 \gg Z_\pm, Z_\pm'$ and imposing the condition $D = -C$[11], we obtain the four components u_1, u_2, u_3, u_4 of the neutrino field ψ_1 with mass μ_1,

$$u_1 \approx 0, \tag{48}$$

$$u_2 = iC\frac{\mu_1}{2\omega}\frac{\sqrt{\Delta}}{r} e^{i\omega(r_* - r_*^0)} \frac{1}{\sqrt{\omega}}\left(1 + \frac{{\mu_1}^2}{8\omega^2}\frac{\Delta}{r^2}\right) \exp\left[-i\frac{{\mu_1}^2}{2\omega}(r - r_0)\right] \sin\chi, \tag{49}$$

$$u_3 = iC\frac{\mu_1}{2\omega}\frac{\sqrt{\Delta}}{r} e^{i\omega(r_* - r_*^0)} \frac{1}{\sqrt{\omega}}\left(1 + \frac{\mu_1^2}{8\omega^2}\frac{\Delta}{r^2}\right) \exp\left[-i\frac{\mu_1^2}{2\omega}(r - r_0)\right] \cos\chi, \tag{50}$$

$$u_4 = Ce^{i\omega(r_* - r_*^0)} \frac{1}{\sqrt{\omega}}\left(1 + \frac{\mu_1^2}{8\omega^2}\frac{\Delta}{r^2}\right) \exp\left[-i\frac{\mu_1^2}{2\omega}(r - r_0)\right]. \tag{51}$$

We obtain the solutions for the neutrino field ψ_2 with mass μ_2 by changing μ_1 to μ_2 in Eqs. (48)-(51). We choose the normalization constant as $C = \sqrt{\omega/2\pi}$ in order to satisfy the orthogonal relation for the outgoing wave $\overrightarrow{\psi}$:

$$(\overrightarrow{\psi}(\omega, m, k),\ \overrightarrow{\psi}(\omega', m', k')) = \delta(\omega - \omega')\delta_{mm'}\delta_{kk'}. \tag{52}$$

If we assume that the total numbers of neutrinos with mass μ_1 and μ_2 are $|A|^2$ and $|B|^2$, respectively, with a condition $|A|^2 + |B|^2 = 1$, then

$$\int r^2 \sin\theta\ j_1^t dr d\theta d\phi = |A|^2, \quad \int r^2 \sin\theta\ j_2^t dr d\theta d\phi = |B|^2. \tag{53}$$

From this we obtain the normalization constant P_i in Eq. (37) as follows

$$P_1 = \left(\frac{\Delta_0}{r_0^2}\frac{1}{\sqrt{\pi}\sigma_\omega}\right)^{1/2} A, \quad P_2 = \left(\frac{\Delta_0}{r_0^2}\frac{1}{\sqrt{\pi}\sigma_\omega}\right)^{1/2} B. \tag{54}$$

Then the local energy densities for two flavor neutrinos of Eqs. (44) and (45) yield

$$\begin{aligned}(J_\alpha{}^t)_{loc}(r) = {} & \frac{r}{\sqrt{\Delta}}\frac{\sigma_\omega}{\sqrt{\pi}} \times \left[\cos^2\alpha\,|A|^2\left(1 + \frac{{\mu_1}^2}{2{\omega_1}^2}\frac{\Delta}{r^2}\right)\exp\left(-\frac{\{r_* - r_*{}^0 - t + \mu_1^2/(2\omega_1^2)(r - r_0)\}^2}{1/{\sigma_\omega}^2}\right)\right. \\ & + \sin^2\alpha\,|B|^2\left(1 + \frac{{\mu_2}^2}{2{\omega_2}^2}\frac{\Delta}{r^2}\right)\exp\left(-\frac{\{r_* - r_*{}^0 - t + \mu_2^2/(2\omega_2^2)(r - r_0)\}^2}{1/{\sigma_\omega}^2}\right) + \cos\alpha\sin\alpha \times \\ & \left[A^* B\left\{1 + \frac{1}{8}\left(\frac{\mu_1}{\omega_1} + \frac{\mu_2}{\omega_2}\right)^2\frac{\Delta}{r^2}\right\} \times \exp\left\{i\left(\frac{{\mu_1}^2}{2\omega_1} - \frac{{\mu_2}^2}{2\omega_2}\right)(r - r_0) - i(\omega_1 - \omega_2)(r_* - r_*{}^0 - t)\right\}\right. \\ & \left.\left.\times \exp\left(-\frac{\{r_* - r_*{}^0 - t + \mu_1^2/(2\omega_1^2)(r - r_0)\}^2}{2/{\sigma_\omega}^2} - \frac{\{r_* - r_*{}^0 - t + \mu_2^2/(2\omega_2^2)(r - r_0)\}^2}{2/{\sigma_\omega}^2}\right) + \text{c.c.}\right]\right] \end{aligned} \tag{55}$$

$$(J_\beta{}^t)_{loc}(r) = \frac{r}{\sqrt{\Delta}}\frac{\sigma_\omega}{\sqrt{\pi}} \times \left[\sin^2\alpha\,|A|^2\left(1+\frac{{\mu_1}^2}{2{\omega_1}^2}\frac{\Delta}{r^2}\right)\exp\left(-\frac{\left\{r_* - {r_*}^0 - t + \mu_1^2/(2\omega_1^2)(r-r_0)\right\}^2}{1/{\sigma_\omega}^2}\right)\right.$$

$$+\cos^2\alpha\,|B|^2\left(1+\frac{{\mu_2}^2}{2{\omega_2}^2}\frac{\Delta}{r^2}\right)\exp\left(-\frac{\left\{r_* - {r_*}^0 - t + \mu_2^2/(2\omega_2^2)(r-r_0)\right\}^2}{1/{\sigma_\omega}^2}\right) - \cos\alpha\sin\alpha\times$$

$$\left[A^*B\left\{1+\frac{1}{8}\left(\frac{\mu_1}{\omega_1}+\frac{\mu_2}{\omega_2}\right)^2\frac{\Delta}{r^2}\right\}\times\exp\left\{i\left(\frac{{\mu_1}^2}{2\omega_1}-\frac{{\mu_2}^2}{2\omega_2}\right)(r-r_0) - i(\omega_1-\omega_2)(r_*-{r_*}^0-t)\right\}\right.$$

$$\left.\left.\times\exp\left(-\frac{\left\{r_* - {r_*}^0 - t + \mu_1^2/(2\omega_1^2)(r-r_0)\right\}^2}{2/{\sigma_\omega}^2} - \frac{\left\{r_* - {r_*}^0 - t + \mu_2^2/(2\omega_2^2)(r-r_0)\right\}^2}{2/{\sigma_\omega}^2}\right) + \text{c.c.}\right]\right] \quad (56)$$

We find that the centers of wave packets of different mass μ_1 and μ_2 move in different velocities. Namely,

$$t_i = r_* - {r_*}^0 + \frac{\mu_i^2}{2\omega_i^2}(r-r_0) \qquad (i=1,2). \quad (57)$$

This implies that two wave packets begin to split as time passes. We can consider that neutrino oscillations occur most significantly when

$$t = \frac{t_1+t_2}{2} = r_* - {r_*}^0 + \left(\frac{{\mu_1}^2}{4{\omega_1}^2}+\frac{{\mu_2}^2}{2{\omega_2}^2}\right)(r-r_0). \quad (58)$$

At this time, Eqs. (55) and (56) yield

$$(J_\alpha{}^t)_{loc}(r) = \frac{r}{\sqrt{\Delta}}\frac{\sigma_\omega}{\sqrt{\pi}}\exp\left[-\sigma_\omega^2\left(\frac{{\mu_1}^2}{4{\omega_1}^2}-\frac{{\mu_2}^2}{4{\omega_2}^2}\right)^2(r-r_0)^2\right]\times\left[\cos^2\alpha\,|A|^2\left(1+\frac{{\mu_1}^2}{2{\omega_1}^2}\frac{\Delta}{r^2}\right)+\right.$$

$$\sin^2\alpha\,|B|^2\left(1+\frac{{\mu_2}^2}{2{\omega_2}^2}\frac{\Delta}{r^2}\right)+\cos\alpha\sin\alpha\left[A^*B\left\{1+\frac{1}{8}\left(\frac{\mu_1}{\omega_1}+\frac{\mu_2}{\omega_2}\right)^2\frac{\Delta}{r^2}\right\}\right.$$

$$\left.\left.\times\exp\left\{i\left(\frac{{\mu_1}^2}{2\omega_1}-\frac{{\mu_2}^2}{2\omega_2}\right)(r-r_0)+i(\omega_1-\omega_2)\left(\frac{{\mu_1}^2}{4{\omega_1}^2}+\frac{{\mu_2}^2}{4{\omega_2}^2}\right)(r-r_0)\right\}+\text{c.c.}\right]\right], \quad (59)$$

$$(J_\beta{}^t)_{loc}(r) = \frac{r}{\sqrt{\Delta}}\frac{\sigma_\omega}{\sqrt{\pi}}\exp\left[-\sigma_\omega^2\left(\frac{{\mu_1}^2}{4{\omega_1}^2}-\frac{{\mu_2}^2}{4{\omega_2}^2}\right)^2(r-r_0)^2\right]\times\left[\sin^2\alpha\,|A|^2\left(1+\frac{{\mu_1}^2}{2{\omega_1}^2}\frac{\Delta}{r^2}\right)+\right.$$

$$\cos^2\alpha\,|B|^2\left(1+\frac{{\mu_2}^2}{2{\omega_2}^2}\frac{\Delta}{r^2}\right)-\cos\alpha\sin\alpha\left[A^*B\left\{1+\frac{1}{8}\left(\frac{\mu_1}{\omega_1}+\frac{\mu_2}{\omega_2}\right)^2\frac{\Delta}{r^2}\right\}\right.$$

$$\left.\left.\times\exp\left\{i\left(\frac{{\mu_1}^2}{2\omega_1}-\frac{{\mu_2}^2}{2\omega_2}\right)(r-r_0)+i(\omega_1-\omega_2)\left(\frac{{\mu_1}^2}{4{\omega_1}^2}+\frac{{\mu_2}^2}{4{\omega_2}^2}\right)(r-r_0)\right\}+\text{c.c.}\right]\right]. \quad (60)$$

The phase term $\Delta\varphi$ where two neutrinos are mixing is

$$\Delta\varphi = \left(\frac{{\mu_1}^2}{2\omega_1}-\frac{{\mu_2}^2}{2\omega_2}\right)(r-r_0), \quad (61)$$

where we have neglected the contributions by the term $i(\omega_1-\omega_2)\left(\frac{{\mu_1}^2}{4{\omega_1}^2}+\frac{{\mu_2}^2}{4{\omega_2}^2}\right)(r-r_0)$. The above result coincides with the results by the quantum mechanical treatment of neutrino oscillations[4, 5, 6, 7]. The difference appears in the term $1+\frac{1}{8}\left(\frac{\mu_1}{\omega_1}+\frac{\mu_2}{\omega_2}\right)^2\frac{\Delta}{r^2}$ of Eqs. (59) and (60). However, this term is approximately unity for the relativistic neutrinos, the difference between our method based on quantum field theory and the quantum mechanical treatment is very small. The phase $\Delta\varphi$ can be rewritten by the local energy ${\omega_i}^{loc}(r_0)$ as

$$\Delta\varphi = \left(\frac{{\mu_1}^2}{2{\omega_1}^{loc}(r_0)}-\frac{{\mu_2}^2}{2{\omega_2}^{loc}(r_0)}\right)\left(1-\frac{2M}{r_0}\right)^{-\frac{1}{2}}(r-r_0). \quad (62)$$

In the weak gravity approximation, this reads

$$\Delta\varphi \approx \left(\frac{{\mu_1}^2}{2\omega_1{}^{loc}(r_0)} - \frac{{\mu_2}^2}{2\omega_2{}^{loc}(r_0)} \right) L \left(1 + \frac{M}{r_0} - \frac{M}{L} \log \frac{r}{r_0} \right), \tag{63}$$

where $L \equiv \int_{r_0}^{r} e^{\lambda/2} dr$ is the proper length. Then we find from Eq. (63) that the proper oscillation length is smaller compared with that of the Minkowski spacetime in the presence of the term M/r_0. This effect is due to the gravitational redshift of the energy of neutrinos. We have numerically confirmed that the proper length decreases as r_0 approaches the horizon radius $r = 2M$. For example, it decreases about 10% for $r_0 = 10M$, and 30% for $r_0 = 4M$. Moreover, the number densities of the central parts of wave packets decrease as neutrinos propagate toward outgoing directions by the term $r/\sqrt{\Delta}$ in Eqs. (59) and (60). This also occurs by the effect of gravitational redshift.

An important factor in Eqs. (59) and (60) is the suppression factor,

$$f(r) \equiv \exp\left[-\frac{(r-r_0)^2}{L_{coh}^2} \right], \quad \text{with} \quad L_{coh} \equiv \frac{2/\sigma_\omega(r_0)}{\mu_1^2/2\omega_1(r_0)^2 - \mu_2^2/2\omega_2(r_0)^2} \frac{\sqrt{\Delta_0}}{r_0}. \tag{64}$$

The dumping of wave packets depends on the value r_0 where neutrinos are created, and L_{coh} approaches 0 in the limit of $r_0 \to 2M$. This suggests that the dumping effect by the treatment of wave packets becomes significant as r_0 approaches to the horizon radius.

5 Conclusions

We have investigated neutrino oscillations in strong gravitational fields making use of the quantum field theory in curved spacetime. We perform the wave packet treatment in order to know how flavor neutrinos propagate in outgoing directions from the Schwarzschild black hole. The expectation values of two flavor neutrino are calculated, and we find that the proper oscillation length becomes smaller compared with that of the Minkowski spacetime. The number densities of the central parts of wave packets decrease as neutrinos propagate. These are due to the gravitational redshift of the energy of neutrinos. We also find that the dumping of wave packets occurs relevantly as the position where neutrinos are produced is close to the horizon radius.

References

[1] B. Pontecorvo, Sov. Phys. JETP. **6** (1958) 429; Z. Maki, M. Nakazawa, and S. Sakata, Prog. Theor. Phys. **28**, 870 (1962).

[2] L. Wolfenstein, Phys. Rev. D **17**, 2369 (1978); Phys. Rev. D **20** 2634 (1979); S. P. Milheyev and A. Yu. Sminov, Sov. J. Nucl. Phys. **42**, 913 (1985).

[3] D. V. Ahluwalia and C. Burgard, Gen. Relativ. Gravit. **28**, 1161 (1996).

[4] N. Fornengo, C. Giunti, C. W. Kim, and J. Song, Phys. Rev. D **56**, 1895 (1997).

[5] C. Y. Cardall and G. M. Fuller, Phys. Rev. D **56**, 7960 (1997).

[6] Y. Kojima, Mod. Phys. Lett. A **11**, 2965 (1996).

[7] D. Piriz, M. Roy, and J. Wudka, Phys. Rev. D **54**, 1587 (1996).

[8] W. G. Unruh, Phys. Rev. D **10**, 3194 (1974).

[9] B. S. Dewitt, Phys. Repts. C **19** (1975).

[10] D. Brill and J. A. Wheeler, Rev. Mod. Phys **29**, 465 (1957).

[11] This condition means that u_1, u_2, u_3 vanish in the limit of $r \to 2M$.

String excitation inside generic black holes

Kengo Maeda[1]

Department of Physics, Waseda University, Shinjuku-ku, Tokyo 169, Japan,

Takashi Torii,[2]

Department of Physics, Tokyo Institute of Technology, Oh-Okayama, Meguro-ku, Tokyo 152, Japan

Makoto Narita,[3]

Department of Physics, Rikkyo University, Nishi-Ikebukuro, Toshima-ku, Tokyo 171, Japan

Abstract

We calculate how much a first-quantized string is excited after crossing the inner horizon of charged Vaidya solutions, as a simple model of generic black holes. To quantize a string suitably, we first show that the metric is approximated by a *plane-wave* metric near the inner horizon when the surface gravity of the horizon κ_I is small enough. Next, it is analytically shown that the string crossing the inner horizon is excited infinitely in an asymptotically flat spacetime, while it is finite in an asymptotically de Sitter spacetime and the string can pass across the inner horizon when $\kappa_I < 2\kappa := 2\min\{\kappa_B, \kappa_C\}$, where κ_B (κ_C) is the surface gravity of the black hole (cosmological) event horizon. This implies that the strong cosmic censorship holds in an asymptotically flat spacetime, while it is violated in an asymptotically de Sitter spacetime from the point of view of string theory.

1 Introduction

One of the interesting issues in general relativity is the inner structure of *generic* black holes, related to the strong cosmic censorship conjecture [1]. The conjecture states that every physically reasonable spacetime is globally hyperbolic, or it is uniquely determined by initial regular data on a spacelike hypersurface S. Therefore, if the conjecture is violated, the spacetime has a Cauchy horizon (CH), which is the boundary of the future (past) domain of dependence of S and we cannot predict what happens for an observer crossing the CH.

Over the past few years a considerable number of studies have been made on the internal structure of generic charged or rotating black holes both analytically and numerically. Poisson and Israel (PI) [2] showed that a scalar curvature singularity appears generically instead of the CH by using a simple model of spherically symmetric charged black holes. Ori [3] constructed an exact solution of the Einstein-Maxwell equations for the model, which suggests that the CH is transformed generically into a null weak singularity. This was verified numerically in charged black holes [4, 5]. Brady and Chambers [6] extended these arguments to the case of more realistic black hole models and suggested that the CH for Kerr-type vacuum black holes is transformed generically into a null weak singularity, where the local geometry and the strength of the singularity are quite similar to the spherically symmetric charged black holes. Thus, this series of works strongly suggests that the strong cosmic censorship holds in the framework of general relativity in the sense that there is no regular CH inside generic black holes. However, there remain unsettled questions. Is such a null weak singularity a real singularity, or the end of spacetime in a quantum theory of gravity? In particular, we have no precise knowledge about what happens from the point of view of quantum gravity in such a region where the curvature is very strong.

[1] E-mail:g_maeda@gravity.phys.waseda.ac.jp
[2] E-mail:torii@th.phys.titech.ac.jp
[3] E-mail:narita@se.rikkyo.ac.jp

One of the promising candidates for a quantum theory of gravity is string theory. Horowitz and Steif [7, 8] have proposed a new criterion for a singularity in terms of a first-quantized test string, namely if the expectation value of the mass associated with the test string diverges at a finite time, then spacetime is called singular. This is an extension of the classical definition of singularity [9]. As already shown in [7, 10, 11], all solutions to the vacuum Einstein equation with a covariantly constant null vector are also solutions to the classical equations of motion for the metric in string theory. These solutions are known as *plane-waves* [7]. Thus, if the metric for Kerr-type generic vacuum black holes is approximated by a plane-wave metric near the "singular CH" (hereafter, simply called CH), it is also the metric for a classical solution of string theory near the CH. In this case, it is worth testing whether such a null weak singularity is also a singularity for the first-quantized string, as a first step for considering the quantum corrections.

In this article, we test how much the first-quantized string gets excited after it crosses the CH in spherically symmetric charged black holes instead of Kerr-type generic ones for simplicity. As mentioned above, the spherically symmetric charged black hole is a good and simple model for describing the internal structure of the Kerr-type black hole because their internal structures are quite similar to each other. Firstly, we show that the spacetime near the CH is described approximately by a plane-wave metric if the surface gravity κ_I of the inner horizon is small enough. Secondly, we calculate explicitly the expectation value of the mass of the test string in two cases: (i) the charged black hole is embedded in flat spacetime; (ii) it is embedded in de Sitter spacetime. Finally, we discuss the strong cosmic censorship in the framework of string theory on the basis of the previous results.

2 Null weak singularities along the Cauchy horizon

When a physically realistic gravitational collapse with charge q and/or angular momentum a occurs, gravitational and/or electromagnetic waves propagate outward and some of them are back-scattered by the effective potential of the gravitational field outside a black hole. This implies that there exists, at least, two types of null flux near the CH; an ingoing null flux along the CH and an outgoing null flux produced by the scattering of the ingoing null flux inside the black hole.

PI [2] constructed a charged spherically symmetric model which well describes the interior of generic black holes with an inner horizon. They showed that once the CH is contracted by the outgoing flux, the invariantly defined quasi-local mass diverges and a curvature singularity inevitably appears. This is the consequence of the nonlinear interaction between the outgoing and the infinitely blue-shifted ingoing null fluxes. The outgoing null flux, however, is not important, as firstly pointed out by PI.

Before introducing the PI model, let us investigate a charged Vaidya solution, where only a purely-ingoing null flux exists. The spacetime is described by the metric

$$ds^2 = d\omega\,(2dr - f d\omega) + r^2 d\Omega^2, \qquad f = 1 - \frac{2m(\omega)}{r} + \frac{q^2}{r^2} - \frac{\Lambda}{3}r^2, \tag{1}$$

where q is an electric charge and Λ is the positive cosmological constant. The energy-momentum tensor is

$$T_{\mu\nu} \;=\; \rho_{\rm in}\, l_\mu l_\nu + 2F_{\mu\alpha}F_\nu{}^\alpha - \frac{1}{2}g_{\mu\nu}F^2, \tag{2}$$

where $\rho_{\rm in}$ represents the energy density of the ingoing null flux along the ingoing radial null vector, $l^\mu \equiv (\partial_r)^\mu$. Here, $F_{\mu\nu}$ is a purely electric Maxwell field $F = (q/r^2)\, d\omega \wedge dr$. From the conservation law, $\rho_{\rm in}$ is simply related to the mass $m(\omega)$ as follows,

$$\rho_{\rm in} = \frac{1}{4\pi r^2}\frac{dm}{d\omega}. \tag{3}$$

Now, we consider a freely-falling observer into the inner horizon along radial timelike geodesics whose tangent vector is $u = (\dot r, \dot\omega, 0, 0)$, where a dot denotes the derivative with respect to the proper time τ. The relation between ω and τ can be obtained by the following geodesic equation

$$2\ddot\omega = -f_{,r}\dot\omega^2. \tag{4}$$

Define the inner horizon $r = r_I$ and the surface gravity κ_I as

$$f(r_I, m_0) = 0, \quad \kappa_I := -\frac{1}{2} f_{,r}(r_I, m_0), \tag{5}$$

where m_0 is the asymptotic Bondi-like mass, i.e. $m_0 := m(\infty)$. It must be noted that the inner horizon corresponds to the CH in the Vaidya metric (1). By solving Eq. (4), $\dot{\omega}$ behaves as

$$\dot{\omega} \sim -\frac{1}{\kappa_I \tau} \tag{6}$$

near the CH. From Eqs. (2) and (3) the energy density $\rho_{\rm ob}$ seen by the freely-falling observer is given by

$$\rho_{\rm ob} = T_{\tau\tau} \sim T_{\omega\omega}\, \dot{\omega}^2 \sim \frac{1}{4\pi(\kappa_I r_I \tau)^2} \frac{dm}{d\omega}. \tag{7}$$

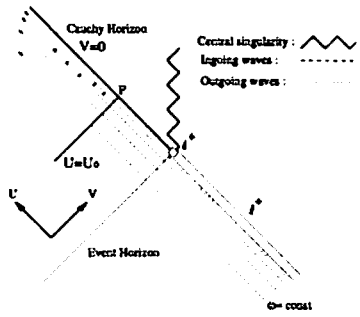

Figure 1: The Penrose diagram of a spherically symmetric charged black hole with outgoing and infinitely blue-shifted ingoing null fluxes for $U \geq U_0$. A null weak singularity appears along $V = 0$.

By introducing double null coordinates

$$ds^2 = -2e^{-\lambda(U,V)} dU dV + r(U,V)^2 d\Omega^2, \tag{8}$$

the asymptotic behavior of the quasi-local mass M near the CH ($V = 0$) is

$$M \sim \theta_- \theta_+ + (\text{finite terms}), \tag{9}$$

where θ_+ (θ_-) is the outgoing (ingoing) null expansion. The Raychaudhuri equation [9] along $U = U_0$ becomes

$$\frac{d\theta_+}{dV} = -\frac{1}{2}{\theta_+}^2 - T(\partial_V, \partial_V) \tag{10}$$

where we choose V such that $\lambda = \text{const.}$ along $U = U_0$. Because $\tau \sim V$ and $T(\partial_V, \partial_V) \sim \rho_{\rm ob}$, M near the CH can be estimated roughly as

$$M \sim \theta_- \int \rho_{\rm ob} d\tau + (\text{finite terms}) \tag{11}$$

through Eq. (10). Let us suppose that there exists a positive outgoing null flux $L(U) := T(\partial_U, \partial_U) > 0$ crossing the CH after $U \geq U_0$ and reparametrize the coordinate U such that U is the affine parameter of the null geodesic generator of the CH. Then, through the Raychaudhuri equation along the CH θ_- becomes negative after the outgoing flux passes through the CH because $\theta_- = 0$ before $U < U_0$. This implies that M diverges when the integral of $\rho_{\rm ob}$ with respect to τ becomes infinite. This is called *mass inflation*. The mass inflation corresponds to the scalar polynomial curvature singularity (*s.p. curvature singularity*) because the square of the Weyl curvature behaves as $C_{\alpha\beta\gamma\delta} C^{\alpha\beta\gamma\delta} \sim M^2$.

As shown in Ref. [3], this null singularity is a weak singularity in the sense that no null object falling into the singularity can be crushed to zero area, namely the 2-d area of the CH is non-zero. Here, we should not overlook the following facts; (i) the outgoing null flux can only contract the CH slowly, and the infinitely blue-shifted ingoing null flux is essential for the singular behavior along the CH, (ii) the Vaidya solution (1) contains a *p.p. curvature singularity* (any of the components of R_{abcd} diverges along a parallel propagated basis) [9] at the CH whenever ρ_{ob} diverges, although no s.p. curvature singularity appears in the metric. This implies that the Vaidya metric is a good approximation for representing the singular behavior along the CH near the timelike infinity i^+ where θ_- at the CH is negligibly small.

Hereafter, we shall consider the propagation of a test string on the Vaidya metric. In the next *section*, we will show that the Vaidya metric (1) is approximated by a plane-wave metric near the CH if κ_I is small enough.

3 The excitation of a test string

3.1 Plane symmetric approximation

Firstly, we shall consider the transformation from the Vaidya metric (1) to the double null metric (8). Let us define a null coordinate u such that

$$du = \frac{2g}{f}dr - g\,d\omega, \tag{12}$$

where g is a function of r and ω. From the coordinate condition $d^2u = 0$,

$$2\dot{G} + fG' = -f'G, \tag{13}$$

where G is defined by $g = fG$. A dot and a prime denote the derivatives with respect to ω and r, respectively. The general form of the solution of Eq. (13) is approximately given by

$$G \simeq e^{\kappa_I\omega}F[X], \qquad X := e^{\kappa_I\omega}y - \int_{\omega_o}^{\omega}\frac{m_0 - m(\omega')}{r_I}e^{\kappa_I\omega'}d\omega' \tag{14}$$

near the CH. By taking $g = 1$ for $\delta m(\omega) = 0$, $F[X]$ can be fixed as

$$F[X] = -\frac{1}{2\kappa_I X}. \tag{15}$$

Taking Eqs. (12), (14) into account, u behaves (in detail, see Ref. [12]) as

$$u \simeq -\omega - \frac{1}{\kappa_I}\ln\left|y - e^{-\kappa_I\omega}\int_{\omega_0}^{\omega}\frac{\delta m(\omega')}{r_I}e^{\kappa_I\omega'}d\omega'\right| \tag{16}$$

and the Vaidya metric (1) can be rewritten in terms of the new coordinate u as

$$ds^2 \simeq \frac{1}{G}du\,d\omega + (y + r_I)^2d\Omega^2 \simeq -\frac{2}{\kappa_I}dUdV + (y + r_I)^2d\Omega^2, \qquad U = -e^{-\kappa_I u}, \quad V = -e^{-\kappa_I\omega} \tag{17}$$

where

$$y \simeq UV - \frac{V}{\kappa_I r_I}\int_{V_0}^{V}\delta m\left(-\frac{\ln(-V)}{\kappa_I}\right)\frac{dV}{V^2}. \tag{18}$$

Thus, we bring the above metric into the plane-wave form, following the same procedure as in Ref. [13]. If r_I is large enough compared with the typical size of a test string crossing the CH, we can approximate the two sphere metric $(y + r_I)^2d\Omega$ by a flat metric $(y + r_I)^2dX_idX^i$. By using the coordinate transformation [14], *plane-wave* metric becomes

$$ds^2 \approx -du\,dv + H(v)x_ix^idv^2 + dx_idx^i, \qquad H(v) = \frac{y''}{y + r_I}. \tag{19}$$

Secondly, we shall see how much the first-quantized string gets excited after crossing the CH, or propagating through the spacetime region with the infinitely blue-shifted ingoing flux. Following the definition of singularity for the first-quantized string [8], we may say that the CH is singularity-free if the string can cross the CH without being excited infinitely. Conversely, if it is excited infinitely by the background field, then we may say that the CH has a real singularity and that it is the boundary of the spacetime. It is worth noting that all timelike geodesics end at the CH unless there is no curvature singularity (p.p. or s.p. curvature singularities) on it, according to the usual interpretation of singularity [9].

Let us introduce coordinates (τ, σ) on the world sheet of the test string. Then, we can take the light-cone gauge $v = P\tau$, which has the advantage of being unitary, where P is a positive constant. Hereafter, we will use the same approach and conventions as in Ref. [8].

In the light cone gauge, the motion of $u(\tau, \sigma)$ is given by

$$P\dot{u} = (\dot{x}^i)^2 + (x^{i\prime})^2 + HP^2, \qquad Pu' = 2\dot{x}_i x^{i\prime}. \tag{20}$$

where a dot and a prime mean the derivatives with respect to τ and σ, respectively. Thus, we quantize only x^i because x^i is the only independent variable in the light cone gauge. Because we consider closed strings here, x^i is decomposed as

$$x^i(\tau, \sigma) = \sum_{n=-\infty}^{+\infty} x_n^i(\tau) e^{in\sigma} \tag{21}$$

and the field equations are

$$\ddot{x}_n^i + n^2 x_n^i - HP^2 x_n^i = 0. \tag{22}$$

Because x^i is real, $x_{-n}^i = x_n^{i\,*}$. Let us denote the independent solutions ($H = 0$) of Eq. (22) by u_n^i and $\tilde{u}_n^i$ and write x_n^i as

$$x_n^i = \frac{i}{2\sqrt{n}}(a_n^i u_n^i - \tilde{a}_n^{i\dagger} \tilde{u}_n^i), \qquad u_n^i = e^{-in\tau}, \quad \tilde{u}_n^i = e^{in\tau} \tag{23}$$

for positive n, where a_n^i and $\tilde{a}_n^{i\dagger}$ are some coefficients, which are naturally interpreted as annihilation and creation operators, respectively, satisfying the standard canonical commutation relations.

We shall consider a spacetime with sandwich waves, namely $H = 0$ for $v < -v_0$ and $v \geq 0$, as in [13]. Physically, the latter condition implies that there is no flux from any pathological regions (if they exist) like timelike singularities or infinity when $v \geq 0$.

3.2 $\Lambda = 0$ case

For a generic perturbation in the $\Lambda = 0$ case [15], the decay of the ingoing null flux should be given by

$$\delta m(\omega) = \frac{\alpha r_I}{(p-1)} (\kappa_I \omega)^{-(p-1)}, \tag{24}$$

where α is a dimensionless positive constant and $p > 12$ is an integer.

After a simple calculation, $H(v)$ is found to be given by

$$H \simeq -\frac{\alpha}{\kappa_I r_I} \frac{[-\ln(-v)]^{-p}}{v^2}. \tag{25}$$

To calculate the Bogoliubov coefficients explicitly, we shall connect the sandwich wave region $H \neq 0$ with a "static" region $H = 0$ at $v = -P\epsilon$ ($\tau = -\epsilon$), where ϵ is an infinitely small positive value. After calculating the Bogoliubov coefficients, we will take the $\epsilon \to 0$ limit. Then, the solution of Eq. (22) can be written as

$$x_n^i = \frac{i}{2\sqrt{n}}(b_n^i v_n^i - \tilde{b}_n^{i\dagger} \tilde{v}_n^i), \qquad v_n^i = e^{-in(\tau+\epsilon)}, \qquad \tilde{v}_n^i = e^{in(\tau+\epsilon)} \tag{26}$$

for the $\tau \geq -\epsilon$ region. b_n^i and $\tilde{b}_n^{i\dagger}$ are linearly related to a_n^i and $\tilde{a}_n^{i\dagger}$ according to the Bogoliubov transformation

$$b_n^i = A_n^i a_n^i - B_n^{i\,*} \tilde{a}_n^{i\dagger}, \quad \tilde{b}_n^i = \tilde{A}_n^i \tilde{a}_n^i - \tilde{B}_n^{i\,*} a_n^{i\dagger}. \tag{27}$$

We can see the degree of excitation of a string for the $\tau \geq -\epsilon$ region which is initially in the ground state by calculating the total number of modes $\langle N_{\rm out}\rangle$ and the total mass-squared $\langle {M^2}_{\rm out}\rangle$. $\langle N_{\rm out}\rangle$ and $\langle {M^2}_{\rm out}\rangle$ are given by

$$\langle N_{\rm out}\rangle \;:=\; 2\sum_{i,n=1} \langle 0_{\rm in}|b_n^{i\,\dagger} b_n^i|0_{\rm in}\rangle = 2\sum_{i,n=1} |B_n^i|^2, \tag{28}$$

$$\langle {M^2}_{\rm out}\rangle := 4\sum_{i,n=1}^{\infty} \langle 0_{\rm in}|n(b_n^i b_n^{i\dagger} + \tilde{b}_n^{i\dagger}\tilde{b}_n^i)|0_{\rm in}\rangle = 8\sum_{i,n=1}^{\infty} n|B_n^i|^2 - 8, \tag{29}$$

where the last term in Eq. (29) corresponds to the Casimir energy. Because the differential equation (22) for x_n^i is independent of i, we have only to consider the $i = 1$ case.

Now, let us denote $x_n^1 = x_n$ by the following complex form,

$$x_n = e^{-in\omega}, \qquad \omega = S(\tau) + \frac{i}{n}\ln A(\tau), \tag{30}$$

where $A\ (\geq 0)$, S are real functions of τ. By substituting Eq. (30) into Eq. (22), we can obtain the following Bogoliubov coefficients.

$$|B_n|^2 = \frac{1}{4}\left(A_\epsilon - \frac{1}{A_\epsilon}\right)^2 + \frac{\dot{A}_\epsilon^2}{4n^2}, \tag{31}$$

where A_ϵ and $\dot{A}_\epsilon$ are the values of A and $\dot{A}$ at $\tau = -\epsilon$, respectively. The above equation means that when $\lim_{\epsilon\to 0} A_\epsilon = 0$, the Bogoliubov coefficient $|B_n|^2$ for each n diverges and hence the total number of modes $\langle N_{\rm out}\rangle$ and the total mass-squared $\langle {M^2}_{\rm out}\rangle$ also diverge in the limit $\epsilon \to 0$. Therefore we shall consider only the case $A_\epsilon \sim C > 0$.

As H diverges near the $\tau = -\epsilon$, the equation (22) is approximately

$$\ddot{A} \sim HP^2 A \sim HP^2 C. \tag{32}$$

By integrating it once, we obtain

$$\dot{A}_\epsilon \sim C\int^{-\epsilon} H(P\tau)P^2 d\tau \propto -\frac{[-\ln(\epsilon)]^{-p}}{\epsilon}, \tag{33}$$

which diverges in the $\epsilon \to 0$ limit. This causes again the divergence of $|B_n|^2$ and $\langle N_{\rm out}\rangle$, $\langle {M^2}_{\rm out}\rangle$. Thus we find that the CH is singular in terms of a first-quantized string, as mentioned before.

3.3 $\Lambda > 0$ case

For a generic perturbation in the $\Lambda > 0$ case [16], the decay of the ingoing flux should be dominated by

$$\delta m(\omega) \sim \frac{\kappa_I^2}{2\kappa_B} e^{-2\kappa_B\omega} + C(>0) \times \frac{\kappa_I^2}{2\kappa_C} e^{-2\kappa_C\omega}, \tag{34}$$

where κ_B and κ_C are the surface gravity of the black hole and of the cosmological event horizon, respectively. The first term of the r.h.s of Eq. (34) comes from the backscattering of the outgoing fluctuations close to the black hole event horizon, while the second term comes from the neighborhood of the cosmological event horizon. The dominant term for Eq. (34) depends on the values, κ_B and κ_C, i.e. for $\kappa_B \leq \kappa_C$ the first term is dominant, while it becomes subdominant for $\kappa_B > \kappa_C$. Defining $\kappa := \min\{\kappa_B, \kappa_C\}$, we

can easily find that the integral of ρ_{ob} in Eq. (7) diverges when $2\kappa \leq \kappa_I$ and the integral converges but ρ_{ob} itself diverges when

$$\kappa < \kappa_I < 2\kappa. \tag{35}$$

It must be noted that the first inequality in Eq. (35) is always satisfied because $\kappa_B < \kappa_I$ for $\kappa = \kappa_B$ unless $r_I = r_B$, and $\kappa_C < \kappa_B < \kappa_I$ for $\kappa = \kappa_C$. Therefore the Vaidya metric (1) always contains a p.p. curvature singularity at the CH.

By Eq. (34), we obtain

$$H(v) \sim -\frac{\alpha}{{r_I}^2}(-v)^{\frac{2(\kappa-\kappa_I)}{\kappa_I}}, \tag{36}$$

where α is a positive constant. As discussed in the $\Lambda = 0$ case, the Bogoliubov coefficient $|B_n|^2$ diverges when $\kappa_I \geq 2\kappa$ and hence $\langle N_{out} \rangle$, $\langle {M^2}_{out} \rangle$ also diverge, which implies that the singularity at the CH is also a singularity in terms of a first-quantized string.

Now, let us pay close attention to the $\kappa_I < 2\kappa$ case. As it can be easily verified, $\dot{A}$ is finite in this case. This implies that each $|B_n|^2$ is finite and that the solution of Eq. (22) can be represented perturbatively such as,

$$x_n = e^{-in\tau} + \delta x_n(\tau), \tag{37}$$

where we start with a purely positive frequency solution $x_n = e^{-in\tau}$ for $\tau \leq -\tau_0$. Substituting Eq. (37) into Eq. (22), we find

$$\delta\ddot{x}_n + n^2 \delta x_n \simeq H(P\tau)P^2 e^{-in\tau}. \tag{38}$$

After some calculations, the values of $|B_n|^2$ for the high frequency modes are as follows,

$$B_n \sim i^{2-\gamma}\frac{\alpha}{{r_I}^2}\left(\frac{P}{2n}\right)^{2-\gamma}\Gamma(1-\gamma), \qquad \gamma := -\frac{2(\kappa-\kappa_I)}{\kappa_I}, \tag{39}$$

where $\Gamma(x)$ is the gamma function. Because $0 < \gamma < 1$ by the definition of γ, $|B_n|^2$ is well defined and we obtain immediately

$$\langle N_{out} \rangle \propto \sum_n n^{-4+2\gamma} \sim \text{finite}, \qquad \langle {M^2}_{out} \rangle \propto \sum_n n^{-3+2\gamma} \sim \text{finite}. \tag{40}$$

This strongly suggests that a first-quantized string can cross the CH without infinite excitation and that the horizon can be singularity-free in terms of the quantized string.

4 Concluding remarks

We have examined whether a null weak singularity inside generic charged black holes is a real end of spacetime in terms of a first-quantized test string by using a charged Vaidya model. In an asymptotically flat spacetime ($\Lambda = 0$ case), the first-quantized test string falling into the CH is always excited infinitely, while it is not when $\kappa_I < 2\kappa$ in an asymptotically de Sitter spacetime ($\Lambda > 0$ case), in spite of the existence of a p.p. curvature singularity along the CH. We should note that the latter case occurs in the physically relevant range of parameters $m > q$. This implies that the asymptotically de Sitter spacetime can be extended through the CH and hence that the strong cosmic censorship is violated in string theory.

As already mentioned before, the internal structure of generic Kerr-type vacuum black holes is locally quite similar to that of spherically symmetric charged black holes. Thus, as verified in the charged Vaidya model, if the surface gravity of the inner horizon in the generic Kerr-type black holes is small enough, we naively expect that the spacetime near the CH is approximately described by a plane-wave metric. In this case, the metric is also a metric of the classical solution for string theory [7] and the same result as in the charged Vaidya model would be obtained.

In general, the back reaction from the first-quantized string and the quantum corrections for the background metric should be considered. However, such effects would be small in the case that a first-quantized test string is not excited infinitely by the following reason. Let us suppose that strings crossing the CH are simply null dust with outgoing null flux $L(U)(> 0)$ in section II. Thus, when the excited mass is small, $L(U)$ would also be small. As mentioned before, the small $L(U)$ can only contract the CH slowly and hence the background geometry after the outgoing flux is not significantly altered. This suggests that the strong cosmic censorship is violated in an asymptotically de Sitter spacetime in string theory, in contrast to general relativity.

Acknowledgment

This paper owes much to the thoughtful and helpful comments of Shigeaki Yahikozawa. We would like to thank Akio Hosoya, Hideo Kodama, Daniel Sudarsky, and Akira Tomimatsu for useful discussions. Our special thanks are due to Albert Carlini for reading our manuscript carefully. K. M. is also grateful to Kei-ichi Maeda for providing me with continuous encouragement. This work is supported in part by Scientific Research Fund of the Ministry of Education, Science, Sports, and Culture, by the Grant-in-Aid for JSPS (No. 199704162 and No. 199906147).

References

[1] R. Penrose, Riv. Nuovo Cimento **1**, 252 (1969).

[2] E. Poisson and W. Israel, Phys. Rev. D **41**, 1796 (1990).

[3] A. Ori, Phys. Rev. Lett. **68**, 2117 (1992).

[4] P. R. Brady and J. D. Smith, Phys. Rev. Lett. **75**, 1256 (1995).

[5] L. M. Burko, Phys. Rev. Lett. **79**, 4958 (1997).

[6] P. R. Brady, C. M. Chambers, Phys. Rev. D **51**, 4177 (1995).

[7] G. T. Horowitz and A. R. Steif, Phys. Rev. Lett. **64**, 260 (1990).

[8] G. T. Horowitz and A. R. Steif, Phys. Rev. D **42**, 1950 (1990).

[9] S. W. Hawking and G. F. R. Ellis, *The large scale structure of spacetime* (Cambridge University Press, Cambridge, 1973).

[10] R. Guven, Phys. Lett. B **191**, 275 (1987).

[11] D. Amati and C. Klimcik, Phys. Lett. B **219**, 443 (1989).

[12] K. Maeda, T. Torii, and M. Narita, Phys. Rev. D **61**, 024020 (2000).

[13] G. T. Horowitz and S. F. Ross, Phys. Rev. D **57**, 1098 (1998).

[14] G. W. Gibbons, Commun. Math. Phys. **45**, 191 (1975).

[15] R. H. Price, Phys. Rev. D **5**, 2419 (1972).

[16] P. R. Brady, I. G. Moss, and R. C. Myers, Phys. Rev. Lett. **80**, 3432 (1998).

[17] H. J. de Vega and N. Sánchez, Phys. Rev. D **45**, 2784 (1992).

[18] D. Mitchell and N. Turok, Nucl. Phys. **B294**, 1138 (1987).

Semiclassical Approach to the Stability of Multidimensional Spacetime in Gravity Theory Depending on the Ricci Tensor

Hirofumi Iwasaki,[1] Yasuo Ezawa[2] and Tadashi Yano[3]

[1] *Graduate School of Science and Technology, Ehime University*
Bunkyo-cho Matsuyama 790-8577, Japan

[2] *Department of Physics, Ehime University*
Bunkyo-cho Matsuyama 790-8577, Japan

[3] *Department of Electrical Engineering, Ehime University*
Bunkyo-cho Matsuyama 790-8577, Japan

Abstract

We have been investigating the stability of the extra-dimensional (internal) spaces required in unified theories such as the string, supergravity and Kaluza-Klein theories. The investigation is based on the Wheeler-DeWitt equation for multidimensional universe. In this paper we work with a gravity theory in which the Lagrangian depends on the square of the Ricci tensor of multidimensional spacetime. After dimensional reduction, the canonical formalism is carried out following the method of Buchbinder and Lyakhovich. Assuming that the inflation had ocurred and the extra-dimensional spaces had contracted to the Planck scale, we make the semiclassical approximation to the Wheeler-DeWitt equation. We can regard that the internal spaces are stable, if the Schrödinger equation for the state of the internal spaces derived in this approximation allows the ground state to exist.

1 Introduction

Unified theory of elementary objects is one of the major goals of fundamental physics. Among the candidates of such a theory are the superstring, supergravity and Kaluza-Klein (KK) theories. In these theories, extra-dimensional (internal) spaces other than the usual 4-dimensional spacetime are required. The internal spaces have not been detected and are supposed to be as small as the Planck scale. Recently interesting possibilities for detecting effects due to these spaces have been proposed assuming that the spaces are not so small as the Planck scale [1]. Cosmologically, the evolution of these spaces can induce the inflation of the 4-dimensional spacetime [2]. During inflation, the internal spaces would contract and after inflation they would continue to contract in the classical Einstein gravity. This is the problem of the stability of the internal spaces.

This problem could be resolved by the quantum theory as in the case of atoms. So we investigated the problem based on the Wheeler-DeWitt (WDW) equation. The problem arises in the evolutionary stage of the universe after inflation as noted above. Thus the semiclassical approximation to the WDW equation [3] would be appropriate since the 4-dimensional spacetime could be thought large enough. Then the Schrödinger equation is derived for the state of the internal spaces. If this equation would allow the ground state, the internal spaces could be thought to be sable.

In this approach, it is difficult for the internal spaces to be stable in Einstein gravity [4]. Then we investigated the problem in higher-curvature gravity theory whose Lagrangian density is a function of the scalar curvature [5]. With only one internal space, stability is attained under a certain condition. However, such a gravity theory is indistinguishable from the scalar-tensor gravity at least in classical theory and the relation is not clear in quantum theory.

In this work we investigate the problem in a gravity theory whose Lagrangian density depends on the square of the Ricci tensor. This theory is cleary different from the scalar-tensor gravity [6] and is expected to show the higher-curvature effects explicitely.

[1] E-mail:hirofumi@phys.sci.ehime-u.ac.jp
[2] E-mail:ezawa@sci.ehime-u.ac.jp
[3] E-mail:yanota@en2.ehime-u.ac.jp

The paper is organized as follows. In section 2 we start with the higher dimensional gravity and dimensionally reduce it to the theory in the external spacetime. In section 3 Lagrangian density is expressed in term of ADM decompsition [7]. After we introduce with higher order time derivative theory suitable for gravity [8], carry out canonical formulation by the ordinary procedure. In section 4 the WDW equation is derived when the external spacetime is the Robertson-Walker one. In section 5 is devoted to summary.

2 Dimensional Reduction

We start with the following action for a multidimensional higher-curvature gravity

$$S = \frac{1}{16\pi\hat{G}} \int d^{\hat{D}}\hat{x}\sqrt{-\det \hat{g}_{MN}}\left[\hat{R} + \xi f(\hat{S})\right], \tag{2.1}$$

where $\hat{D}$ is the number of multidimensions; M, N run from 0 to $\hat{D}-1$; G is the $\hat{D}$-dimensional gravitational constant. $\hat{R}$ is the scalar curvature of the $\hat{D}$-dimensional spacetime constracted from the metric tensor $\hat{g}_{MN}$, f is a function of $\hat{S}$ which is the square of $\hat{D}$-dimensional Ricci tensor (i.e., $\hat{S} = \hat{R}^{MN}\hat{R}_{MN}$,) and an ξ is a constant. (A hat denotes a quantity defined in $\hat{D}$-dimensional spacetime.) Forthermore, we assume that $\hat{g}_{MN}$ has the following block diagonal form

$$\hat{g}_{MN}(\hat{x}) = \begin{pmatrix} \hat{g}_{\mu\nu}(x) & & & 0 \\ & \hat{g}_{m_1 n_1}(x, y_1) & & \\ & & \ddots & \\ 0 & & & \hat{g}_{m_\alpha n_\alpha}(x, y_\alpha) \end{pmatrix} \tag{2.2a}$$

and that

$$\hat{g}_{m_i n_i}(x, y_i) = b_i^2(x)\tilde{g}_{m_i n_i}(y_i), \qquad i = 1, \ldots, \alpha, \tag{2.2b}$$

here $\mu, \nu = 0, 1, \ldots, d$ (which is eventuary set to 3); $m_i, n_i = 1, \ldots, d_i$; α is the number of d_i-dimensional internal spaces. x and y_i represent respectively the coodinates of $(d+1)$-dimensional spacetime and the i-th internal compact space. $\tilde{g}_{m_i n_i}(y_i)$ is assumed to be the metric tensor for the space of constant curvture. Under these assumptions non-vanishing components of the $\hat{D}$-dimensional Ricci tensor $\hat{R}_{MN}$ are expressed as [9]

$$\hat{R}_{\mu\nu} = \tilde{R}_{\mu\nu} - \sum_{i=1}^{\alpha} d_i\left[\nabla_\mu\nabla_\nu \ln b_i + (\partial_\mu \ln b_i)\partial_\nu \ln b_i\right] \tag{2.3}$$

and

$$\hat{R}_{m_i n_i} = \tilde{R}_{m_i n_i} - b_i^2\tilde{g}_{m_i n_i}\hat{g}^{\lambda\rho}\left[\nabla_\lambda\nabla_\rho \ln b_i + (\partial_\lambda \ln b_i)\sum_{j=1}^{\alpha} d_j\partial_\rho \ln b_j\right] \qquad i = 1, \ldots, \alpha, \tag{2.4}$$

where $\tilde{R}_{\mu\nu}$ and $\tilde{R}_{m_i n_i}$ are $(d+1)$-dimensional and d_i-dimensional Ricci tensors constructed from $g_{\mu\nu}$ and $\tilde{g}_{m_i n_i}$, respectively. The ∇ represents the covariant derivative with respect to $g_{\mu\nu}$. Thus the $\hat{D}$-dimensional scalar curvature $\hat{R}$ and $\hat{S}$ are written as

$$\hat{R} = \tilde{R} - \hat{g}^{\lambda\rho}\sum_{i=1}^{\alpha} d_i\left[2\nabla_\lambda\nabla_\rho \ln b_i + (\partial_\lambda \ln b_i)\partial_\rho \ln b_i + \sum_{j=1}^{\alpha} d_j(\partial_\lambda \ln b_i)\partial_\rho \ln b_j\right] + \sum_{i=1}^{\alpha} b_i^{-2}\tilde{R}_i \tag{2.5}$$

and

$$\hat{S} = \hat{R}_{\mu\nu}\hat{R}^{\mu\nu} + \sum_{i=1}^{\alpha} \hat{R}_{m_i n_i}\hat{R}^{m_i n_i}, \tag{2.6}$$

where $\tilde{R}$ and $\tilde{R}_i$ are the $(d+1)$-dimensional scalar curvature constructed from $\tilde{g}_{\mu\nu}$ and the scalar curvature of the i-th internal space constructed from $\tilde{g}_{m_i n_i}$, respectively.

Next a $(d+1)$-dimensional Lagrangian density $\mathcal{L}$ is obtained by dimensional reduction

$$\mathcal{L} = \int \prod_{i=1}^{a} d^{d_i} y_i \hat{\mathcal{L}}. \tag{2.7}$$

The action S corresponding to the Lagrangian density $\hat{\mathcal{L}}$ is then

$$S = \int d^D \hat{x} \hat{\mathcal{L}} = \int d^{d+1} x \mathcal{L}. \tag{2.8}$$

The Lagrangian density $\mathcal{L}$ has a factor $\prod_{i=1}^{a} b_i^{d_i}$ coming from $\sqrt{-\det \hat{g}_{MN}}$. This factor yields a gravity theory differing from the Einstein one for $f(\hat{S}) = 0$. Since we are interested in the universe after inflation, it is desirable that the $(d+1)$-dimensional gravity is the Einstein one for $f(\hat{S}) = 0$ or approximately so for arbitrary $f(\hat{S})$. One of the ways to assure this is to make a conformal (Weyl) transformation

$$g_{\mu\nu} = \Omega^2 \hat{g}_{\mu\nu}, \quad \Omega = \exp\left(\frac{1}{d-1} \sum_{i=1}^{a} d_i \ln b_i\right). \tag{2.9}$$

Accoding to this transformation, we have the following relations for the Ricci tensors

$$\hat{R}_{\mu\nu} = R_{(d+1)\mu\nu} + \frac{\kappa}{d-1} g_{\mu\nu} J^{\lambda}{}_{|\lambda} - \kappa^2 T_{\mu\nu} - \frac{\kappa^2}{d-1} J_\mu J_\nu \tag{2.10}$$

and

$$\hat{R}_{m_i n_i} = \tilde{R}_{m_i n_i} - \exp\left(\frac{2\kappa}{d-1}\Phi\right) \tilde{g}_{m_i n_i} \exp(2\kappa\phi_i) \Box \phi_i, \tag{2.11}$$

where $R_{(d+1)\mu\nu}$, $\tilde{R}_{m_i n_i}$ are the Ricci tensors of the $(d+1)$-dimensional spacetime formed from $g_{\mu\nu}$ and of the i-th internal space formed from $\tilde{g}_{m_i n_i}$, respectiviry. A stroke "|" denotes the covariant derivative with respect to $g_{\mu\nu}$, a square $\Box$ is the Laplacian constructed from the metric $g_{\mu\nu}$ and $\kappa \equiv \sqrt{8\pi G}$, where G is the $(d+1)$-dimensional gravitational constant related to $\hat{D}$-dimensional one by

$$G \equiv \hat{G} / \prod_{i=1}^{a} \left(\int d^{d_i} y_i \sqrt{\det \tilde{g}_{m_i n_i}} \right). \tag{2.12}$$

Also, for the scalar curvature we have

$$\hat{R} = \exp\left(\frac{2\kappa}{d-1}\Phi\right) \left[R_{(d+1)} + \frac{2\kappa}{d-1} g^{\lambda\rho} J_{\lambda|\rho} - \kappa^2 g^{\lambda\rho} (T_{\lambda\rho} + \frac{1}{d-1} J_\lambda J_\rho) \right] + \sum_{i=1}^{a} \tilde{R}_i \exp\left(-\frac{2\kappa}{d_i}\phi_i\right), \tag{2.13}$$

here $R_{(d+1)}$ is the scalar curvature of the $(d+1)$-dimensional spacetime formed from $g_{\mu\nu}$. We further define the following quantities

$$\phi_i \equiv \kappa^{-1} \ln b_i, \qquad i = 1, \ldots, a, \tag{2.14}$$

where we introduced the dimensional constant κ in order for the scalar fields ϕ_i to have the usual dimension. The following notation are used:

$$\Phi \equiv \sum_{i=1}^{a} d_i \phi_i, \quad J_\mu \equiv \sum_{i=1}^{a} d_i \partial_\mu \phi_i = \partial_\mu \Phi \quad \text{and} \quad T_{\mu\nu} \equiv \sum_{i=1}^{a} d_i \partial_\mu \phi_i \partial_\nu \phi_i. \tag{2.15}$$

Using these expressions, we have the following form for $\mathcal{L}$

$$\mathcal{L} = \frac{1}{2} \kappa^{-1} \sqrt{-\det g_{\mu\nu}} \exp\left(-\frac{2\kappa}{d-1}\right) \left[R + \xi f(S) \right]. \tag{2.16}$$

Here $\hat{S}$ is given by inserting (2.9) and (2.10) into (2.6).

3 Canonical Formalism

3.1 ADM Decomposition

The $(d+1)$-dimensional metric $g_{\mu\nu}$ is decomposed in terms of the ADM variables, a lapse function N, the shift vector N^m and the d-dimensional metric h_{mn} as

$$ds^2 = g_{\mu\nu}(x)dx^\mu dx^\nu = (-N^2 + N^k N_k)dt^2 + 2N_k dt\, dx^k + h_{kl}dx^k dx^l. \tag{3.1}$$

Then Non-vanishing components of $R_{(d+1)\mu\nu}$ and $R_{(d+1)}$ are expressed in the following $(d+1)$ form:

$$\begin{aligned} R_{(d+1)ij} &= F_{ij} + R_{ij}, \\ R_{(d+1)0i} &= N^k(F_{ki} + R_{ki}) - N(K^k{}_{;k} - \partial_i K), \\ R_{(d+1)00} &= N^k N^l(F_{kl} + R_{kl}) - N^2(F - K^2 + K^{kl}K_{kl}) - 2NN^k(K^l{}_{k;l} - \partial_k K), \end{aligned} \tag{3.2}$$

and

$$R_{(d+1)} = 2F - K^2 + K_{mn}K^{mn} + R, \tag{3.3}$$

where

$$F_{ij} = -N^{-1}(\partial_0 K_{ij} - N^k K_{ij;k} - N^k{}_{;i}K_{kj} - N^k{}_{;j}K_{ki} + N_{;ij}) + KK_{ij} - 2K_{ik}K^k{}_j, \tag{3.4}$$

R_{ij} is the d-dimensional Ricci tensor constructed from h_{mn}, R is the d-dimensional scalar curvature. K_{mn} is the extrinsic curvature,

$$K_{mn} \equiv -\frac{1}{2}\mathcal{L}_{\vec{n}}h_{mn} = -\frac{1}{2N}(\partial_0 h_{mn} - N_{m,n} - N_{n,m}), \tag{3.5}$$

$\vec{n}$ is the vector field normal to the hypersurface t =constant, the components of which are given as

$$\vec{n} = N^{-1}(1, -N^m),$$

$\mathcal{L}_{\vec{n}}$ denotes the Lie derivative with respect to the vector field $\vec{n}$; $K \equiv h^{mn}K_{mn}$, $F \equiv h^{mn}F_{mn}$, $R \equiv h^{mn}R_{mn}$, the scalar curvature of the d-dimensional space, $\Delta N \equiv h^{mn}N_{;mn}$ and a semicolon ";" denotes the covariant differentiation with respect to the metric h^{mn}. Then the D-dimensional scalar curvature $\hat{R}$ has the following form

$$\begin{aligned} \hat{R} = \exp\Big(\frac{2\kappa}{d-1}\Phi\Big)\Big[&-2N^{-1}h^{mn}\partial_0 K_{mn} \\ &+ \frac{2\kappa}{d-1}\{N^{-2}J_m\partial_0 N^m + N^{-3}(J_0 - N^m J_m)\partial_0 N - N^{-2}\partial_0 J_0\}\Big] - \hat{U}. \end{aligned} \tag{3.6}$$

So the $\hat{U}$ expression is long that we do not write down it.

3.2 Method of Buchbinder and Lyakhovich

Higher order time derivatives are treated following the method of Buchbinder and Lyakhovich (BL). The time derivatives of the metric h_{ij} and the scalar fields ϕ_i are replaced by new generalized coordinates Q_{ij} and Q_i, respectively, defined as

$$Q_{ij} \equiv K_{ij}, \quad Q_i \equiv \mathcal{L}_{\vec{n}}\phi_i = N^{-1}(\partial_0\phi_i - N^k\partial_k\phi_i). \tag{3.7a}$$

From (3.7a), we have

$$\partial_0 h_{ij} = 2NQ_{ij} + N_{i;j} + N_{j;i}, \quad \partial_0\phi_i = NQ_i + N^m\partial_m o_i. \tag{3.7b}$$

In terms of these new variables, the Lagrangian density (denoted as $\mathcal{L}_Q$) is expressed as

$$\mathcal{L}_Q = \frac{1}{2}\kappa^{-1}\sqrt{h}N\exp\Big(-\frac{2\kappa}{d-1}\Phi\Big)[\hat{R}_Q + \xi f(S_Q)], \tag{3.8}$$

here $h \equiv \det h_{ij}$ and

$$\hat{R}_Q = \exp\left(\frac{2\kappa}{d-1}\Phi\right)N^{-1}\left[2h^{ij}\partial_0 Q_{ij} - \frac{2\kappa}{d-1}\sum_{i=1}^{\alpha}\partial_0 Q_i\right] - U_Q \tag{3.9}$$

where $\hat{U}_Q = \hat{U} + 2\kappa\exp[2\kappa\Phi/(d-1)]N^{-1}N^k\partial_k J_0/(d-1)$ expressed in terms of the new variables. The $\hat{S}_Q$ expression is so long that we do not write down it. Using the Lagrange multiplier method, we modify the Lagrangian density to take into account the relations (3.7b) as follows

$$\mathcal{L}^* \equiv p^{ij}(\partial_0 h_{ij} - 2NQ_{ij} - N_{i;j} - N_{j;i}) + p^i(\partial_0\phi_i - NQ_i - N^k\partial_k\phi_i) + \mathcal{L}_Q, \tag{3.10}$$

where p^{ij} and p^i are Lagrange multipliers.

We carry out the canonical formalism based on the modified Lagrangian $\mathcal{L}^*$. It is seen that the Lagrange multipliers p^{ij} and p^i are the momenta canonically conjugate to the generalized coordinates h_{ij} and ϕ_i, respectively. The momenta Π^{ij} and Π^i which are canonically conjugate to Q_{ij} and Q_i, respectively, are given as

$$\begin{aligned}
\Pi^{kl} &\equiv \frac{\partial\mathcal{L}^*}{\partial\dot{Q}_{kl}} = \frac{\partial\mathcal{L}_Q}{\partial\dot{Q}_{kl}} \\
&= 2\mathcal{F}N^{-1}(G^{klmn}\dot{Q}_{mn} - \frac{2\kappa}{d-1}h^{kl}\sum_{i=1}^{\alpha}d_i\dot{Q}_i) + \kappa^{-2}\sqrt{h}h^{kl} + 2\mathcal{F}A_S^{kl}, \\
\Pi^i &\equiv \frac{\partial\mathcal{L}^*}{\partial\dot{Q}_i} = \frac{\partial\mathcal{L}_Q}{\partial\dot{Q}_i} \\
&= 2\mathcal{F}N^{-1}\Big[\kappa^2 d_i\Big\{\dot{Q}_i + \frac{d+1}{(d-1)^2}\sum_{j=1}^{\alpha}d_j\dot{Q}_j\Big\} - \frac{2\kappa}{d-1}d_i h^{kl}\dot{Q}_{kl}\Big] - \kappa^{-1}\frac{d_i}{d-1}\sqrt{h} + 2\mathcal{F}A_S^i.
\end{aligned} \tag{3.11}$$

where overdot denotes time derivative, $\mathcal{F} \equiv \frac{1}{2}\kappa^{-1}\sqrt{h}\,\xi f'\exp\Big(\frac{2\kappa}{d-1}\Phi\Big)$; $G_{ijkl} \equiv \frac{1}{2}(h_{ik}h_{jl} - h_{ij}h_{kl})$. A_{kl}, A^i are complex functions of the generalized coordinates. It is noted that there is no constraint contrary to the case where the Lagrangian density is a function of only the scalar curvature. Hamiltonian density $\mathcal{H}^*$ corresponding to $\mathcal{L}^*$ is given by

$$\begin{aligned}
\mathcal{H}^* &= p^{ij}\dot{h}_{ij} + p^i\dot{\phi}_i + \Pi^{ij}\dot{Q}_{ij} + \Pi^i\dot{Q}_i - \mathcal{L}^* \\
&= N(2p^{ij}Q_{ij} + p^iQ_i) + p^{ij}(N_{i;j} + N_{j;i}) + N^k p^i\partial_k\phi_i - \mathcal{L}_Q.
\end{aligned} \tag{3.12}$$

Relations among the time derivatives of the coordinates Q_{ij} , Q_i and the momenta Π^{kl}, Π^i can be written as

$$\begin{aligned}
N^{-1}\mathcal{F}\dot{Q}_{kl} &= \frac{1}{2}\Big[\Pi_{kl} - \frac{(d-1)^2 + (d-3)\tilde{D}}{(d-1)^2\tilde{D}}h_{kl}\Pi\Big] + \frac{1}{\kappa(d-1)\tilde{D}}h_{kl}\sum_{i=1}^{\alpha}\Pi^i \\
&\quad - \mathcal{F}\Big[A_{S\,kl} - \frac{(d-1)^2 + (d-3)\tilde{D}}{(d-1)^2\tilde{D}}h_{kl}h_{mn}A_S^{mn} + \frac{2}{\kappa(d-1)\tilde{D}}h_{kl}\sum_{i=1}^{\alpha}A_S^i\Big] \\
&\quad - \frac{\tilde{D}-2}{2\kappa^2(d-1)\tilde{D}}\sqrt{h}h_{kl} \\
\kappa^{-1}N^{-1}\mathcal{F}\dot{Q}_i &= \frac{1}{2\kappa}\Big(\frac{\Pi^i}{d_i} - \frac{1}{\tilde{D}}\sum_{j=1}^{\alpha}\Pi^j\Big) + \frac{1}{(d-1)D}\Pi \\
&\quad - \mathcal{F}\Big[\frac{2}{(d-1)\tilde{D}}h_{mn}A_S^{mn} + \kappa^{-1}\Big(\frac{A_S^i}{d_i} - \frac{1}{\tilde{D}}\sum_{j=1}^{\alpha}\Big)\Big] - \frac{1}{2\kappa^2 D}\sqrt{h}
\end{aligned} \tag{3.13}$$

These relations do not generally give the explicit expressions of Q_{ij} and Q_i since f contains an arbitrary function of them, $f(S_Q)$. We have to solve for these three derivatives equations consistently. Only for $f(S_Q) = S_Q$ this procedure is not necessary.

4 Wheeler-DeWitt equation

We are interested in stability of the internal space. In the cosmological context the problem of stability of the internal space occurs after the period of inflation. This makes simple the discussion as regards the 4-dimensional universe which can be described by the Robertson-Walker geometry (the spatially homogeneous part $n = 0$). By conformality with the metric, the matter source T_{ij} and Q_{ij} can be assumed to be only time. Secondly, the 3-dimensional universe would be so large that it could be described by the classical theory. This is just the situation in which the semi-classical approximation to the WDW equation is applicable.

We derive the WDW equation under the assumptions we do above. We start with the [illegible] equation

$$\sqrt{h}\,\mathrm{Ric}^{(3)} + \mathrm{Ric}^{(3)}Q_{ij} = \frac{1}{2}\mathrm{H}Q_{ij} + \frac{2}{D}p_{ij} - \frac{1}{D}Q\mathrm{H}_{ij} \tag{4.1}$$

[illegible] Then we choose the independent generalized coordinates that are the lapse n and the trace of Q_{ij}, $\beta_0 = \frac{1}{D}Q$. The momenta canonically conjugate to these coordinates, p_n and Π_β, are obtained by applying (3.1) to p_{ij} and Π_{ij}:

$$p_n = \frac{1}{2}\mathrm{H} - \frac{1}{3}Q\Pi_\beta \qquad \Pi_\beta = -\frac{1}{3}\mathrm{H} \tag{4.2}$$

or inversely

$$\mathrm{H} = 2p_n - 6Q\Pi_\beta \qquad Q = -3\Pi_\beta \tag{4.3}$$

In terms of these new variables, the Hamiltonian density $\mathcal{H}$ has a form

$$\mathcal{H} = \frac{1}{2}\mathrm{H}\mathcal{H} \tag{4.4}$$

This leads to the Hamiltonian constraint $\mathcal{H} = 0$ and $\mathcal{H}$ is given as

$$\mathcal{H} = \frac{Q}{3}p_n - Q\Pi_\beta + \frac{1}{2\kappa}\sqrt{h}\,e^{\beta}\left(\mathrm{Ric}^{(3)} + e^{\beta}\Pi_Q - 2\Lambda\right) \tag{4.5}$$

Here Π_Q and S_Q are expressed as follows:

$$R_Q = \frac{1}{D}\int d^3x \exp(\alpha\beta)\left[\frac{1}{D}Q - 2\Pi_Q + \kappa^2\sum_{i=1}^{n}\Pi^i - \kappa^2(D-1)\sqrt{h}\right]$$

$$\int d^3x \exp(\alpha\beta)\left[\frac{1}{D}(D-2)\beta_0 A_Q^{(0)} - 2\kappa^2\sum_{i=1}^{n}A_i\right] + \Gamma_Q \tag{4.6}$$

where

$$\Pi_Q = \frac{1}{\kappa^2}\int d^3x \exp(\alpha\beta)\left[\frac{1}{D}Q^2 + R\sqrt{h}\,e^{2\beta} + \kappa^2\left\{\sum_{i=1}^{n}d_iQ^i - \frac{1}{2}\Theta^2\right\}\right] \tag{4.7}$$

and

$$S_Q = \frac{1}{\kappa^2}\int d^3x\left[\frac{1}{D}Q - \frac{3\beta_0}{D}\Pi_Q^{(0)} - \frac{1}{D}\left(\kappa^2\sum_{i=1}^{n}\Pi^i - \Pi\right)^2 + \frac{1}{2}\sum_{i=1}^{n}\frac{\Pi_i}{d_i}\right] - \frac{1}{2\kappa^2\sqrt{h}}\int d^3x\left(\Pi_Q + \sum_{i=1}^{n}\Pi^i\right)$$

$$+ \exp(2\alpha\beta)\left[\frac{1}{D}(\beta_0 A_Q^{(0)})^2 - \frac{2}{\kappa D}\beta_0\sum_{i=1}^{n}A_i - A_Q^{(0)}\beta_0 Q - \kappa^2\sum_{i=1}^{n}\frac{A_i}{d_i}\right]$$

$$\mathrm{sgn}(\beta)\sqrt{h}\sum_{i=1}^{n}A_i + A_Q^{(0)}\frac{D}{D-2}\sqrt{h}\,e^{\beta}\Theta\Big] \tag{4.8}$$

where $\hat{\mathcal{F}} \equiv \frac{1}{2}\kappa^{-1}\sqrt{h}\,\xi f'$, $\Theta \equiv \sum_{i=1}^{\alpha} d_i Q_i$ and

$$A_S^{kl} = h^{kl}\Big[\frac{2k}{a^2} - \frac{2}{9}Q^2 - \kappa Q\Theta + \kappa^2\Big(\frac{1}{2}\Theta^2 + \sum_{i=1}^{\alpha} d_i {Q_i}^2\Big)\Big], \tag{4.8}$$

$$\begin{aligned}\kappa^{-1}A_S^i = -d_i\Big[\frac{3k}{a^2} - \kappa Q\Theta + \frac{\kappa^2}{2}\Big\{\frac{1}{2}\Big(\sum_{j=1}^{\alpha} Q_j\Big)^2 + \sum_{j=1}^{\alpha}\frac{{Q_j}^2}{d_j}\Big\}\Big] \\ + \exp(-\kappa\Phi)\tilde{R}_i\exp(-2\kappa\phi_i) + \kappa d_i Q Q_i,\end{aligned} \tag{4.9}$$

$$\begin{aligned}A_S = \exp(2\kappa\Phi)\Big[\frac{16}{27}Q^4 + 12\frac{k^2}{a^4} - 6\kappa\frac{kQ\Theta}{a^2}\kappa^2Q^2\Big(\Theta^2 + \frac{1}{2}\sum_{i=1}^{\alpha} d_i {Q_i}^2\Big) \\ - \kappa^3 Q\Theta\Big\{\frac{1}{2}\Big(\sum_{i=1}^{\alpha} Q_i\Big)^2 + \sum_{i=1}^{\alpha}\frac{{Q_i}^2}{d_i}\Big\} + \kappa^4\Big\{\frac{1}{2}\Big(\sum_{i=1}^{\alpha} Q_i\Big)^2 + \sum_{i=1}^{\alpha}\frac{{Q_i}^2}{d_i}\Big\}^2\Big] \\ + S_0 + 2\kappa\exp(\kappa\Phi)\,Q\sum_{i=1}^{\alpha}\tilde{R}_i Q_i\exp(-2\kappa\phi_i).\end{aligned} \tag{4.10}$$

Here

$$S_0 \equiv \sum_{i=1}^{\alpha}\tilde{S}_i\exp(-4\kappa\phi_i), \qquad \tilde{S}_i \equiv \tilde{R}_{m,n_i}\tilde{R}^{m,n_i} \tag{4.11}$$

From equations (4.7) – (4.11), we can in principle determine $\hat{S}_Q$ in terms of the canonical variables, the solution depending on the function $f(\hat{S}_Q)$. For $f(\hat{S}_Q) = \hat{S}_Q$, equation (4.7) gives the solution for $\hat{S}_Q$ since the right hand side involves only f' which is equal to one. So, hereafter we restrict ourselves to the case of $f = \hat{S}_Q$.

We decompose $\mathcal{H}$ into the kinematical part $\mathcal{K}$ and potential part $\mathcal{U}$:

$$\mathcal{H} = \mathcal{K} + \mathcal{U}, \tag{4.12}$$

where

$$\begin{aligned}\mathcal{K} = \frac{1}{3}Q(\frac{a}{2}p_a - Q\Pi_Q) - \frac{1}{2\kappa^2}\sqrt{h}\exp(-\kappa\Phi)\Big[\frac{1}{\hat{D}}\mathcal{F}^{-1}\exp(\kappa\Phi)\Big\{3(\hat{D}-2)\Pi_Q + \kappa^{-1}\sum_{i=1}^{\alpha}\Pi^i\Big\} \\ + \xi\frac{1}{4\mathcal{F}^2}\Big\{3(1-\frac{3\hat{D}}{\hat{D}})\Pi_Q^2 - \frac{1}{\hat{D}}(\kappa^{-1}\sum_{i=1}^{\alpha}\Pi^i - \Pi)^2 - \frac{1}{\kappa^2}\sum_{i=1}^{\alpha}\frac{{\Pi^i}^2}{d_i}\Big\} \\ + \frac{1}{2\kappa^2\mathcal{F}^2}\sqrt{h}(3\frac{D-2}{2}\Pi_Q + \kappa^{-1}\sum_{i=1}^{\alpha}\Pi^i)\Big]\end{aligned} \tag{4.13}$$

and

$$\begin{aligned}\mathcal{U} = \frac{1}{\hat{D}}\mathcal{F}^{-1}\exp(\kappa\Phi)\Big[-\kappa^2(\hat{D}-1)\sqrt{h} - \mathcal{F}\{(\hat{D}-2)h_{kl}A_S^{kl} - 2\kappa^{-1}\sum_{i=1}^{\alpha}A_S^i\}\Big] \\ + \exp(2\kappa\Phi)\Big[\frac{1}{\hat{D}}(h_{kl}A_S^{kl})^2 - \frac{2}{\kappa\hat{D}}A_S^{kl}\sum_{i=1}^{\alpha}A_S^i - A_S^{kl}A_{Skl} - \kappa^{-2}\sum_{i=1}^{\alpha}\frac{{A_S^i}^2}{d_i} \\ - 8\kappa^{-3}\mathcal{F}^{-1}\sqrt{h}\sum_{i=1}^{\alpha}A_S^i\Big] + A_S + \frac{D-1}{D}\xi^{-2} - U_Q\end{aligned} \tag{4.14}$$

The WDW equation is written as

$$\mathcal{H}_{op}\Psi = 0, \tag{4.15}$$

where $\mathcal{H}_{op}$ is obtained, as usual, by replacing p_a, Π_Q and p^i in $\mathcal{H}$ with $-i\partial/\partial a$, $-i\partial/\partial Q$ and $-i\partial/\partial\phi_i$, respectively.

5 Summary

We have been investigating the stability of the extra-dimensional spaces in the framework of canonical quantum gravity. Since it seems difficult to stabilize these spases in the Einstein gravity, we asked whether the higher-curvature effects stabilize these spaces. We begin with the Lagrangian density depending on the Ricci tensor of multidimensional spacetime . The Lagrangian density in $(d+1)$-dimensional spacetime was obtained by dimensional reduction. Canonical formalism with higher order time derivatives is treated following the method of Buchbinder and Lyakhovich. We obtained the Hamiltonian constraint. Then, we have written down the Wheeler-DeWitt equation when the four-dimensional universe is Robertson-Walker one. We adopt semiclassical approximation to the above Wheeler-DeWitt equation.

The remaining task and the prospect are as follows:

(1) Derivation of Schrödinger equation for the internal spaces

(2) Investigation whether the ground state exists or not. If there exists the ground state, the internal spaces are regarded to be stable.

References

[1] N. Arkani-Hamed, S. Dimopoulos, and G. Dvali, *Phys. Lett.* **B429** (1998), 263; *Phys. Rev.* **D59** (1999), 086004.

[2] Y. Okada, *Nucl. Phys.* **B264** (1986), 197.
Q. Shafi and C. Wetterlich, *Nucl. Phys.* **B289** (1987), 787; *Nucl. Phys.* **B297** (1988), 697.
Y. Ezawa, T. Watanabe and T. Yano, *Prog. Theor. Phys.* **86** (1991), 89.

[3] C. Kiefer, *Canonical Gravity: from Classical to Quantum* ed. L. Ehlers and H. Friedlich (Berlin: Springer, 1994), p.170.

[4] Y. Ezawa, F. Kakimoto, J. Soda and T. Yano, *Class. Quantum Grav.* **14** (1997), 257.

[5] Y. Ezawa, M. Kajihara, M. Kiminami, J. Soda and T. Yano, *Class. Quantum Grav.* **16** (1999), 1127; *Class.Quantum Grav.* **16** (1999), 1873.

[6] C. Magnano and L. M. Sokolowsky *Phys. Rev.* **D50** (1994), 5039.

[7] R. Aronwitt, S. Deser and C. Misner, *Gravitation: An Introduction to Current Research* ed. L. Witten (New York: Wikey, 1962), p.227.

[8] I. L. Buchbinder and S. L. Lyakhovich, *Class. Quantum Grav.* 4 (1987), 1487.
I. L. Buchbinder, I. Yu Karateva and S. L. Lyakhovich, *Class. Quantum Grav.* **8** (1991), 1113.

[9] M. Rainer and A. Zhuk, *Phys. Rev.* **D54** (1996), 6186.

Excitation of Kaluza-Klein gravitational mode

Kunihito Uzawa,[1]

Graduate School of Science and Technology, Chiba University
Chiba 263-8522, Japan

Yoshiyuki Morisawa[2]

Yukawa Institute for Theoretical Physics, Kyoto University,
Sakyo-ku, Kyoto 606-8502, Japan

Shinji Mukohyama[3]

Department of Physics and Astronomy, University of Victoria
Victoria BC, Canada V8W 3P6
Canadian Institute for Theoretical Astrophysics, University of Toronto
Toronto ON, Canada M5S 3H8

Abstract

We investigate excitation of Kaluza-Klein modes due to the parametric resonance caused by oscillation of radius of compactification. We consider a gravitational perturbation around a D-dimensional spacetime, which we compactify on a $(D-4)$-sphere to obtain a 4-dimensional theory. The perturbation includes the so-called Kaluza-Klein modes, which are massive in 4-dimension, as well as zero modes, which is massless in 4-dimension. These modes appear as scalar, vector and second-rank symmetric tensor fields in the 4-dimensional theory. Since Kaluza-Klein modes are troublesome in cosmology, quanta of these Kaluza-Klein modes should not be excited abundantly. However, if radius of compactification oscillates, then masses of Kaluza-Klein modes also oscillate and, thus, parametric resonance of Kaluza-Klein modes may occur to excite their quanta. In this paper we consider part of Kaluza-Klein modes which correspond to massive scalar fields in 4-dimension and investigate whether quanta of these modes are excited or not in the so called narrow resonance regime of the parametric resonance. We conclude that at least in the narrow resonance regime quanta of these modes are not excited so catastrophically.

1 Introduction

When we consider unified theories, spacetime may have more than four dimension. For example, the critical dimension of the superstring theories [1] is equal to ten, and the low-energy effective theory of M-theory [2] is the eleven-dimensional supergravity. On the other hand, we recognize only four dimensional spacetime. Therefore, in order to describe our universe we have to adopt some mechanism of dimensional reduction. Compactification of extra dimensions on some compact manifold (the Kaluza-Klein prescription [3]) has been conventionally adopted, while an alternative prescription was recently proposed by Randall and Sundrum [4]. Since the Randall-Sundrum prescription cannot be applied directly to more than 5-dimension, in this paper we consider the Kaluza-Klein prescription.

However, there are too many ways of compactification to specify a 4-dimensional theory from the higher dimensional unified theories. As for the superstring theory, although it is usually compactified on a Calabi-Yau manifold, there are so many Calabi-Yau manifolds.

[1] E-mail:uzawa@tc.chiba-u.ac.jp
[2] E-mail:morisawa@yukawa.kyoto-u.ac.jp
[3] E-mail:mukoyama@uvic.ca

Fortunately, in some cases it may be possible to judge which way of compactification is acceptable since different compactifications may give different 4-dimensional theories and, thus, different cosmologies. In particular, properties, eg. mass spectrum, of the so-called Kaluza-Klein modes reflect the manifold on which spacetime is compactified. Thus, it may be effective to investigate effects of Kaluza-Klein modes on the 4-dimensional cosmology.

In this respect, Kolb & Slansky [5] considered the effects of Kaluza-Klein modes on our 4-dimensional universe. For simplicity, they considered a scalar field in 5-dimensional spacetime of the form $M^4 \times S^1$, where M^4 is a 4-dimensional FRW universe and S^1 is a circle. They investigated Kaluza-Klein modes of the scalar field and showed that the Kaluza-Klein modes are dangerous in cosmology. To be precise, they showed that, if energy density of a Kaluza-Klein mode is not negligible compared with radiation density at an early epoch, then the Kaluza-Klein mode eventually dominate the universe. Thus, quanta of Kaluza-Klein modes should not be excited abundantly. It is expected that this result holds in quite general situation since their arguments are based on the momentum conservation along the compact direction. Thus, ***quanta of Kaluza-Klein modes of any fields should not be excited abundantly.***

However, there is a possibility that quanta of Kaluza-Klein modes may be excited. First, the radius of compactification appears as a scalar field in 4-dimension called a radion [6]. Hence, if the radion potential has a local minimum then it can oscillate around the local minimum. The oscillation of the radion leads to oscillation of masses of Kaluza-Klein modes since the masses are proportional to the inverse of the compactification radius. On the other hand, it is well-known that oscillation of mass leads to the so-called parametric resonance phenomenon [8, 9]. Hence, it is expected that, if the radion potential has a local minimum then quanta of Kaluza-Klein modes may be excited by parametric resonance [10].

Therefore, it is possible to obtain some knowledge about a way of compactification by investigating whether quanta of Kaluza-Klein modes are excited by the parametric resonance due to the radion oscillation. If the quanta are produced abundantly then the way of compactification should be rejected. In Ref. [10], the parametric resonance of Kaluza-Klein modes of a scalar field was investigated in the regime where the resonance band is narrow (the narrow resonance regime). It was shown that, for the case of compactification by a d-dimensional sphere, quanta of the Kaluza-Klein modes are not overproduced.

However, since there should be many other fields (eg. gravitational fields, anti-symmetric fields, spinor fields, and so on), the investigation of only a scalar field is not enough: in principle, ***we have to investigate Kaluza-Klein modes of all fields in the theory.*** In this paper, we investigate a gravitational field.

This paper is organized as follows. In section 2 we describe our model and derive the action for our system. In section 3 we investigate whether catastrophic creation of quanta of the Kaluza-Klein modes occur or not. In section 4 we summarize this paper.

2 Model construction

In this section we derive an effective action for Kaluza-Klein gravitational modes as well as for background fields. In subsection 2.1 we describe our model and basic assumptions verbally. In subsection 2.2 we calculate the tree action of our system from the Einstein-Hilbert action.

2.1 Basic assumptions

As already explained in Sec. 1, our purpose in this paper is to judge whether a particular model of dimensional reduction is acceptable or not by investigating parametric excitation of Kaluza-Klein modes. For this purpose, we have to specify higher dimensional theory in D-dimension somewhat. Moreover, in order to obtain the 4-dimensional effective theory from the D-dimensional theory, we have to specify a particular model of dimensional reduction. Namely, we consider the following setting.

(a) Let us consider a D-dimensional theory which includes gravity, N_s scalar fields, N_d Dirac fields, and other fields. The gravity, scalar fields and spinor fields are assumed to be described by the Einstein-Hilbert action with a cosmological constant, the Klein-Gordon action and the Dirac action, respectively. There may be interaction among these fields.

(b) We adopt the conventional Kaluza-Klein description of compactification: we compactify the D-dimensional spacetime on a d-dimensional compact manifold ($d = D-4$) to obtain the 4-dimensional

spacetime. As the compact manifold we take a d-dimensional sphere, which we shall denote by S^d.

(c) We consider the so-called Casimir effect to stabilize a radion potential, where the radion is a 4-dimensional scalar field corresponding to compactification radius [6]. In order to stabilize the radion potential by the Casimir effect, we have to assume that $d \geq 2$.

(d) We also consider perturbations of D-dimensional fields around the background given by the Kaluza-Klein prescription. These perturbations are described as 4-dimensional massive fields called Kaluza-Klein modes.

For this situation, in order to make calculations possible, we assume the following assumptions. (See the beginning of section 3 for further assumptions.)

(i) The number N_s (or N_d) of scalar fields (or Dirac fields) is sufficiently large compared with the number of other fields included in the D-dimensional theory.

(ii) The cosmological constant induced in 4-dimension is zero.

(iii) Terms in the 4-dimensional effective action which are order of $O(\varphi^3)$ can be neglected, where φ denotes Kaluza-Klein modes.

The assumption (i) makes it possible to calculate corrections to the radion potential due to the Casimir effect. In principle, all fields included in the D-dimensional theory should contribute to the Casimir effect. However, if N_s or N_d is large enough then contributions from other fields are small compared with those from the scalar fields and the Dirac fields. Hence, in this limit, the correction to the radion potential is parameterized by only N_s and N_d. In fact, we can show that, after redefining the D-dimensional cosmological constant, the corrected potential is parameterized by only two constants: the D-dimensional cosmological constant and a particular combination of N_s and N_d.

Therefore, the assumption (i) combined with the assumption (ii) determines the corrected radion potential uniquely up to only one constant. Hence, the potential is parameterized only by the present value b_0 of the compactification radius. Since b_0 can be eliminated from all equations of Kaluza-Klein modes by redefinition of variables, all information about the corrected radion potential can be obtained.

On the other hand, the assumption (iii) makes it possible to investigate each Kaluza-Klein mode independently, provided that kinetic terms and mass terms are properly diagonalized. In this paper, we consider only a particular class of Kaluza-Klein modes corresponding to D-dimensional gravitational perturbations. (In Ref. [10] a class of Kaluza-Klein modes corresponding to a D-dimensional scalar field was considered.) It is the assumption (iii) that makes it possible to consider these modes independently.

2.2 Perturbed Einstein-Hilbert action

We consider the D-dimensional Einstein-Hilbert action with a cosmological constant:

$$I_{EH} = \frac{1}{2\bar{\kappa}^2} \int d^D x \sqrt{-\bar{g}} (\bar{R} - 2\bar{\Lambda}), \tag{1}$$

where $\bar{\kappa}$ is a positive constant, $\bar{R}$ is the D-dimensional Ricci scalar, and $\bar{\Lambda}$ is the cosmological constant. We consider a gravitational perturbation h_{MN} around a background metric $\bar{g}^{(0)}_{MN}$, which we shall specify below.

$$\bar{g}_{MN} = g^{(0)}_{MN} + h_{MN}. \tag{2}$$

By substituting Eq.(2) into Eq.(1), we obtain the perturbed Einstein-Hilbert action as follows.

$$\begin{aligned} I_{EH} = \frac{1}{2\bar{\kappa}^2} \int d^D x \sqrt{-g^{(0)}} \Bigg[& \bar{R}^{(0)} - 2\Lambda - h^{MN} \left(\bar{R}^{(0)}_{MN} - \frac{1}{2} \bar{R}^{(0)} g^{(0)}_{MN} + \bar{\Lambda} g^{(0)}_{MN} \right) \\ & + \frac{1}{8} \left(h^2 - 2h^{MN} h_{MN} \right) \bar{R}^{(0)} + \frac{1}{2} \left(2h^{MM'} h^N_{M'} - h h^{MN} \right) \bar{R}^{(0)}_{MN} \\ & + \frac{1}{4} \left\{ h^{MN}{}_{;M'} \left(2h^{M'}_{M;N} - h_{MN}{}^{;M'} \right) + h_{;M} \left(h^{;M} - 2h^{MN}{}_{;N} \right) \right\} \\ & - \bar{\Lambda} \left(\frac{1}{4} h^2 - \frac{1}{2} h^{MN} h_{MN} \right) + O(h^3) \Bigg]. \end{aligned} \tag{3}$$

where ";" denotes the covariant derivative compatible with $g^{(0)}_{MN}$, and $\bar{R}^{(0)}_{MN}$ and $\bar{R}^{(0)}$ are the Ricci tensor and scalar constructed from $\bar{g}^{(0)}_{MN}$.

As for the background geometry, we compactify it on a d-dimensional sphere S^d ($d = D-4$) and it is convenient to analyze in the so called Einstein frame, we perform the following conformal transformation to make the new frame to be the Einstein frame. Note that, if we take b_0 to be the present value of b, then the conformal factor becomes unity after b settles to b_0. Hence, the change of the frame does not affect the final result, provided that all physical results are interpreted after b settles to b_0. On the other hand, our analysis becomes much easier if we adopt this conformal transformation. After the conformal transformation, the D-dimensional line element is written as :

$$\bar{g}^{(0)}_{MN}dx^M dx^N = \left(\frac{b}{b_0}\right)^{-d} g_{\mu\nu}dx^\mu dx^\nu + b^2\Omega^{(d)}_{ij}dx^i dx^j. \tag{4}$$

where $\hat{g}_{\mu\nu}$ and b are a 4-dimensional metric and a 4-dimensional scalar that depend only on the four-dimensional coordinate x^μ ($\mu = 0,1,2,3$), and Ω_{ij} is a metric of the unit d-sphere which depends only on the coordinates x^i ($i = 4,\cdots,D-1$). Hereafter, we denote D-dimensional, 4-dimensional and d-dimensional indexes by capital Latin ($M,N,\cdots$), Greek ($\mu,\nu,\cdots$) and small Latin ($i,j,\cdots$) letters, respectively. Note that the scalar b can be interpreted as radius of S^d.

For this particular background, the gravitational perturbation h_{MN} can be expanded by harmonics on S^d after gauge-fixing and redefining $g_{\mu\nu}$ and b as follows

$$h_{MN}dx^M dx^N = \sum_{lm}\left[h^{lm}_{\mu\nu}Y_{lm}dx^\mu dx^\nu + 2h^{lm}_{(T)\mu}(V_{(T)lm})_i dx^\mu dx^i + \{h^{lm}_{(T)}(T_{(T)lm})_{ij} + h^{lm}_{(Y)}(T_{(Y)lm})_{ij}\}dx^i dx^j\right], \tag{5}$$

where Y_{lm} is the scalar harmonics function; $V_{(T)lm}$ is the vector harmonics; $T_{(T)lm}$ is the tensor harmonics. Here, the coefficients $h^{lm}_{\mu\nu}$, $h^{lm}_{(T)\mu}$, $h^{lm}_{(T)}$,and $h^{lm}_{(Y)}$ depend only on the four-dimensional coordinates x^μ, while the harmonics depend only on the coordinates x^i on S^d and the summations are taken over $l \geq 1$ for the scalar and vector harmonics, and over $l \geq 2$ for the tensor harmonics.

Finally, by substituting this expression into Eq. (3), we obtain the following action.

$$I_{EH} = I^{(0)} + I^{(1)} + I^{(2)} + O(h^3), \tag{6}$$

where

$$I^{(0)} = \int d^4x\sqrt{-g^{(0)}}\left[\frac{1}{2\kappa^2}R^{(0)} - \frac{1}{2}g^{\mu\nu}\partial_\mu\sigma\partial_\nu\sigma - U_0(\sigma)\right], \tag{7}$$

$$I^{(2)} = \sum_{l,m}\int d^4x\sqrt{-g^{(0)}}\left(\mathcal{L}^{(T)}_{lm}[h^{lm}_{(T)}] + \mathcal{L}^{(V)}_{lm}[h^{lm}_{(T)\mu}] + \mathcal{L}^{(Y)}_{lm}[h^{lm}_{\mu\nu}, h^{lm}_{(Y)}],\right), \tag{8}$$

and $I^{(1)}$ is linear in h. When a total action of the system is considered (see the setting (a) in subsection 2.1), $I^{(1)}$ should be canceled by other linear terms in the total action because of the equations of motion. Hence, there is no need to consider $I^{(1)}$. The constant κ, the scalar field σ, the potential U_0, and Lagrangian densities $\mathcal{L}^{(T,V,Y)}_{lm}$ are defined as follows. First, the constant κ (> 0) is defined by $\kappa^2 = \frac{\bar{\kappa}^2}{2^d b_0^d \pi}$.

Next, σ is a scalar field defined by

$$\sigma = \sigma_0 \ln\left(\frac{b}{b_0}\right), \qquad \sigma_0 = \sqrt{\frac{d(d+2)}{2\kappa^2}}, \tag{9}$$

and is called a radion field [6]. The potential $U_0(\sigma)$ of σ is given by

$$U_0(\sigma) = \frac{\bar{\Lambda}}{\kappa^2}e^{-d\frac{\sigma}{\sigma_0}} - \frac{d(d-1)}{2\kappa^2 b_0^2}e^{-(d+2)\frac{\sigma}{\sigma_0}}. \tag{10}$$

Finally, the Lagrangian densities $\mathcal{L}^{(T)}_{lm}$ are given by

$$\mathcal{L}^{(T)}_{lm} = -\frac{1}{2}e^{-4\frac{\sigma}{\sigma_0}}g^{\mu\nu}\partial_\mu\chi^{lm}\partial_\nu\chi^{lm} - \frac{1}{2}\Lambda^{(T)}_{lm}\chi^{lm}\chi^{lm}, \qquad (l \geq 2) \tag{11}$$

where

$$\Lambda^{(T)}_{lm} = e^{-(d+6)\frac{\varphi}{\sigma_0}}\{l(l+d-1)+(d-1)(d-2)\}b_0^{-2} + e^{-4\frac{\varphi}{\sigma_0}}\left[(d+4)\nabla^2\left(\frac{\sigma}{\sigma_0}\right) - \left\{\frac{d(d+2)}{2}-4\right\}\nabla\left(\frac{\sigma}{\sigma_0}\right)^2 + \left\{R^{(0)} - 2e^{-d\frac{\varphi}{\sigma_0}}\bar{\Lambda}\right\}\right], \quad (12)$$

$$\chi^{lm} \equiv \sqrt{\frac{{b_0}^{-4}}{2^{d+2}\pi\kappa^2}}\, h^{lm}_{(T)} \qquad (l \geq 2). \quad (13)$$

(Since hereafter we analyze $h^{lm}_{(T)}$ (or χ^{lm}) only, we have not written down explicit form of $\mathcal{L}^{(V)}_{lm}$ and $\mathcal{L}^{(Y)}_{lm}$.) Hence, up to the second order in Kaluza-Klein modes, $h^{lm}_{(T)}$ (or χ^{lm}) is decoupled from all other Kaluza-Klein modes. (See the assumption (iii) in subsection 2.1.) In this paper, for simplicity, we investigate the parametric resonance of χ^{lm} (or $h^{lm}_{(T)}$) only. It should be stressed again that it is the assumption (iii) in subsection 2.1 that makes it possible to consider these modes independently.

Here, note that the constant b_0 is arbitrary at the moment and that we can eliminate it from all equations. However, in the next subsection, we chose b_0 to be the present value of b.

Moreover we assume that the Casimir effect [7] stabilizes the radion potential. In other words, we assume that quantum corrections to U_0 stabilize compactification. Thanks to the assumptions (i) and (ii) in subsection 2.1, we can easily calculate the stabilized radion potential, which we shall denote by U_1.

Finally, the perturbed Einstein-Hilbert action corrected by the Casimir effect is given by Eq. (6), provided that U_0 is replaced by U_1. Therefore, hereafter, we investigate the dynamics of the field χ^{lm} coupled to the radion field σ in the expanding universe. These fields are described by the following action.

$$I = I_\sigma + I_\chi, \quad (14)$$

where

$$I_\sigma = -\int d^4x\sqrt{-\bar{g}^{(0)}}\left[\frac{1}{2}g^{\mu\nu}\partial_\mu\sigma\partial_\nu\sigma + U_1(\sigma)\right],$$
$$I_\chi = -\frac{1}{2}\int d^4x\sqrt{-\bar{g}^{(0)}}\left[e^{-4\frac{\varphi}{\sigma_0}}g^{\mu\nu}\partial_\mu\chi^{lm}\partial_\nu\chi^{lm} + \Lambda^{(T)}_{lm}\chi^{lm}\chi^{lm}\right]. \quad (15)$$

Here, we mention that in the total action there may be other terms which are second order in χ^{lm}. In fact, there should appear other mass terms for χ^{lm} since some zero modes may couple to χ^{lm}. However, providing the assumption (vii) in the next section, these additional mass terms are small enough since zero modes are considered as usual low-energy matter whose energy density and pressure are bounded from above by 4-dimensional cosmological parameters. Therefore, the above action is enough for our purpose.

3 Parametric resonance

In this section we investigate parametric resonance of the field χ^{lm} due to the oscillation of the radion field σ in the expanding universe. For this purpose, we specify 4-dimensional geometry and initial condition somewhat.

(iv) The background 4-dimensional geometry is expressed by the flat FRW metric, and the radion field is homogeneous in the FRW universe.

(v) Initially, there is no excitation of Kaluza-Klein modes. Thus, the FRW universe is driven by the radion field as well as by usual homogeneous matter corresponding to zero modes.

Since the radion potential $U_1(\sigma)$ has exponential terms, it seems difficult to analyze oscillation of σ with large amplitude analytically. Hence, we assume that the amplitude of the oscillation is small enough. Moreover, for further simplicity, we assume that the time scale of the cosmological expansion is much longer than the time scale of the radion oscillation. Namely, we assume the following.

(vi) We assume that the amplitude of the radion oscillation around $\sigma = 0$ is small compared with σ_0.

(vii) The energy scale of the cosmological expansion is much lower than that of compactification: we assume that $Hb_0 \ll 1$ and $\dot{H}b_0^2 \ll 1$, where $H \equiv \dot{a}/a$ and the dot denotes the derivative with respect to the cosmological time.

Note that the assumption (vi) leads to the so called narrow resonance regime for the parametric resonance.

3.1 FRW background and homogeneous radion

According to the assumptions (iv) and (v), we consider the homogeneous radion field σ and the flat FRW universe, which is driven by the radion field and usual matter corresponding to zero modes.

Now, because of the symmetry of the background, it is convenient to analyze the field χ^{lm} in the momentum space. Hence, we decompose the field χ^{lm} as follows:

$$\chi_{lm} = a^{-\frac{3}{2}} \int \frac{\sqrt{2}\, d^3\boldsymbol{k}}{(2\pi)^3} [\chi^{(1)}_{lm\boldsymbol{k}}(t) \cos(\boldsymbol{k}\cdot\boldsymbol{x}) + \chi^{(2)}_{lm\boldsymbol{k}}(t) \sin(\boldsymbol{k}\cdot\boldsymbol{x})], \tag{16}$$

where $\chi^{(1,2)}_{lm\boldsymbol{k}}$ are real functions of the cosmological time t and the vector $\boldsymbol{x}$ represents (x, y, z) and $H \equiv \dot{a}/a$ and the dot denotes derivative with respect to the time t. Correspondingly, the action I_χ is rewritten as

$$I_\chi = \frac{1}{2} \sum_{l,m} \sum_{i=1,2} \int dt \int d^3\boldsymbol{k}\, e^{-4\frac{\sigma}{\sigma_0}} \left[\left\{ \partial_t\, \chi^{(i)}_{lm\boldsymbol{k}}(t) \right\}^2 - m^2(t) \left\{ \chi^{(i)}_{lm\boldsymbol{k}}(t) \right\}^2 \right], \tag{17}$$

where

$$m^2(t) = \Lambda^{(T)}_{lm} + e^{-4\frac{\sigma}{\sigma_0}} \frac{\boldsymbol{k}\cdot\boldsymbol{k}}{a^2} - \left\{ \frac{4}{9} H^2 + \frac{3}{2} \dot{H} - 6H \left(\frac{\dot{\sigma}}{\sigma_0} \right) \right\}. \tag{18}$$

Although the kinetic term in the above Lagrangian has time dependence, we can eliminate it by using a new time variable τ defined by

$$\frac{d\tau}{dt} = \exp\left[4 \frac{\sigma(t)}{\sigma_0} \right]. \tag{19}$$

In fact, the equations of motion for $\chi^{(1,2)}_{lm\boldsymbol{k}}$ are written as

$$\frac{\partial^2 Q}{\partial \tau^2} + \Omega^2(\tau) Q = 0, \tag{20}$$

where Q denotes $\chi^{(1,2)}_{lm\boldsymbol{k}}$ and Ω is defined by

$$\Omega^2(\tau) = m^2(t(\tau)) \exp\left[-4 \frac{\sigma(t(\tau))}{\sigma_0} \right]. \tag{21}$$

The hamiltonian with respect to the time τ is

$$\mathcal{H} \equiv \frac{f}{2} \left(P^2 + \Omega^2 Q^2 \right), \tag{22}$$

where P is the momentum conjugate to Q.

After the oscillation of σ ends up at $\sigma = 0$, the right hand side of Eq. (19) becomes unity. Thus, after the end of the oscillation, the hamiltonian $\mathcal{H}$ with respect to τ coincides with the hamiltonian with respect to the original cosmological time t. At the same time, those hamiltonians become conserved quantities. Hence, we can analyze the excitation of $\chi^{(1,2)}_{lm\boldsymbol{k}}$ by using the new time variable τ.

3.2 Small oscillation of the radion

Providing the assumptions (vi) and (vii), the equation of motion for σ gives

$$\frac{\sigma(t)}{\sigma_0} = \tilde{\sigma}(t)\cos\omega(t - t_0), \tag{23}$$

where t_0 is a constant, ω is defined by

$$\omega = \frac{1}{2}\sqrt{U_1''(0)} = \frac{1}{b_0}\sqrt{\frac{d-1}{2}}, \tag{24}$$

and $\tilde{\sigma}(t)$ ($\ll 1$) is a slowly varying amplitude:

$$\tilde{\sigma}(t) \propto a^{-3/2}. \tag{25}$$

Now, by using Eq. (23), we can express Ω^2 in terms of the new time variable τ up to the first order in $\tilde{\sigma}$:

$$\Omega^2(\tau) = \omega^2\left[A + B + \tilde{\epsilon}\cos\{2\omega(\tau - \tau_0)\} + O(\tilde{\epsilon}^2)\right], \tag{26}$$

where τ_0 is a constant and

$$A = \frac{2{b_0}^2(k^2/a)}{d-1} - \omega^2\left(\frac{9}{4}H^2 + \frac{3}{2}\dot{H}\right), \tag{27}$$

$$B = \frac{(d+4)\{l(l+d-1) + (d-2)(d-1)\} - d(d-1)(d+2)}{(d+4)b_0^2\,\omega^2}, \tag{28}$$

$$\tilde{\epsilon} = \tilde{\sigma}\left\{(d-1)\frac{d(d+2)(d+8) - l(l+d-1)(d-2)(d+10)}{b_0^2\omega^2} - \frac{8}{\omega^2}(k^2/a)^2 + 4(d+4)\right\}. \tag{29}$$

The first term in A is essentially the squared momentum along the three-dimensional spatial directions divided by ω^2, B is essentially the squared momentum along S^d divided by ω^2, and $\tilde{\epsilon}$ is the properly normalized amplitude of the radion oscillation.

3.3 Result

The expression (26) is of almost the same form as the expression of Ω^2 investigated in Ref. [10]. Hence, we can analyze the parametric resonance in the same way as in Ref. [10]. Thus, the necessary and sufficient condition for the catastrophic creation of quanta of the Kaluza-Klein mode is

$$\begin{aligned} B &\leq 1, \\ |B-1| &= O(\tilde{\epsilon}). \end{aligned} \tag{30}$$

However, it is easily shown that

$$B > 3 \tag{31}$$

for any values of d (≥ 2) and l (≥ 2). (See the setting (c) in subsection 2.1.) Therefore, it is concluded that quanta of the field χ^{lm} are not overproduced by the parametric resonance due to the small oscillation of the radion σ.

4 Summary and Discussions

We have investigated excitation of Kaluza-Klein modes due to the parametric resonance caused by oscillation of radius of compactification in the narrow resonance regime. In particular, we have considered a gravitational perturbation around a D-dimensional spacetime compactified on a $(D-4)$-sphere. Among many Kaluza-Klein modes of the gravitational perturbation we have investigated part of Kaluza-Klein modes which correspond to massive scalar fields in 4-dimension. We have obtained that quanta of these modes are not excited so catastrophically in the narrow resonance regime.

Now, several comments are in order.

First, we discuss about the consistency among the assumption (v), (vi) and (vii). Energy density ρ_σ and pressure p_σ of the radion is of the following order.

$$\rho_\sigma \sim p_\sigma \sim \tilde{\epsilon}^2 b_0^{-2} \kappa^{-2}, \tag{32}$$

where $\tilde{\epsilon} \sim \sigma/\sigma_0$. Thus, the condition $H^2 \sim \kappa^2 \rho_\sigma$ can be satisfied, even if $\tilde{\epsilon} \ll 1$, $Hb_0 \ll 1$ and $\dot{H} b_0^2 \ll 1$. In other words, the three assumptions (v), (vi) and (vii) can be satisfied simultaneously.

Next, we discuss about validity of our strategy. Although we have investigated only a particular class of Kaluza-Klein modes in this paper, in principle we have to investigate all Kaluza-Klein modes in order to judge whether a way of compactification is acceptable or not. If we find that one of these many Kaluza-Klein modes is excited abundantly, then the way of compactification should be rejected. In this respect, there may be an embarrassing expectation: it is easily expected that, even if we find that $N_{KK} \gg 1$, the result will be significantly changed by backreaction, where N_{KK} is the number of created quanta of a Kaluza-Klein mode. In fact, by the energy conservation and the assumptions (v) and (vii), it is easily concluded that $N_{KK} \ll 1$. Thus, it might be expected that under the assumptions (v) and (vii) we might not be able to judge whether a way of compactification is acceptable or not. However, this embarrassing consideration does *not* spoil our analysis. Actually, if we obtain $N_{KK} \gg 1$ by ignoring the backreaction, then this overestimating result implies at least that ρ_{KK} is not negligible compared with ρ_σ since the backreaction becomes effective only when ρ_{KK} is not negligible compared with ρ_σ, where ρ_{KK} is energy density of the Kaluza-Klein mode. Therefore, providing the assumption (v), the result $N_{KK} \gg 1$ obtained by ignoring the backreaction implies that ρ_{KK} is not negligible compared with energy density of radiation, which should be rejected as explained in Sec. 1.

References

[1] M. B. Green, J. H. Schwartz, E. Witten, *Superstring theory* (Cambridge University Press, 1987); J. Polchinski, *String Theory I& II* (Cambridge University Press, Cambridge, England 1998).

[2] J. H. Schwartz, Nucl. Phys. Suppl. **B55**, 1 (1997).

[3] T. Applquist, A. Chodos and P. G. O. Freund, *Modern Kaluza-Klein theories*, (Benjamin / Cummings, 1985).

[4] L. Randall and R. Sundrum, hep-th/9906064.

[5] E. W. Kolb and R. Slansky, Phys. Lett. **B135**, 378 (1984).

[6] N. Arkani-Hamed, S. Dimopoulos, N. Kaloper and J. March-Russell, hep-ph/9903224, 9903239; James M. Cline, hep-ph/9904495; E. Halyo, hep-ph9907223; E. E. Flanagan, S.-H. H. Tye and I. Wasserman, hep-ph/99099373; L. Mersini, hep-ph/9909494.

[7] P. Candelas and S. Weinberg, Nucl. Phys. **B237**, 397(1984)

[8] L. Landau and E. Lifschitz, *Mechanics* (Pergamon, Oxford, 1960).

[9] For example, L. Kofman, A. Linde and A. A. Starobinsky, Phys. Rev. **D56**, 3258 (1997), and references therein.

[10] S. Mukohyama, Phys. Rev. **D157**, 6191 (1998)

[11] For example, K. Maeda, Phys. Lett. **B186**, 33 (1987); L. Amendola, E. W. Kolb, M. Litterio and F. Occhionero, Phys. Rev. **D42**, 1944 (1990).

Comment on Non-Archimedean Character of Quantum Buoyancy

Takashi Okamura[1]

Department of Physics, Ochanomizu University,
1-1 Otsuka, 2 Bunkyo, Tokyo, 112-8610 Japan

Abstract

We review a *gedankenexperiment* about the generalized second law (GSL) and importance of buoyant force by black hole atmosphere (the acceleration radiation) for the GSL to be valid, which is pointed out by Unruh and Wald. In their argument, the buoyant force is estimated with fluid approximation. Recently, Bekenstein criticizes the application of the fluid approximation to the case that the size of the diffractor is much greater than a typical wavelength of the acceleration radiation, due to the diffractive effect of wave scattering. I argue that although his suggestion that the diffractive effect should be considered is right, he overlooked the contribution S-wave scattering by a scalar field to buoyant force. By reconsidering the diffractive effect by S-wave scattering, I show that if some massless scalar field exists, then the GSL holds without a new physics, such as an entropy bound for matter.

1 Introduction

It is well known that there exists a close mathematical analogy between black hole mechanics and the ordinary thermodynamics.

Law	Thermodynamics	BH mechanics
the zeroth	T = constant throughout body in thermal equilibrium	κ = constant over horizon of stationary black hole
the first	$dE = TdS + dW$	$dM = (\kappa/2\pi)(dA_{BH}/4) + ...$
the second	$\delta S > 0$ for any process	$\delta A_{BH} > 0$ for any process

The above correspondence suggests that a black hole is thermodynamical object with its temperature $T_{BH} = \alpha\kappa/2\pi$ and its entropy $S_{BH} = A_{BH}/4\alpha$, where α is a numerical constant.

The first law in the black hole mechanics is easily understood, because the first law is nothing but an energy balance equation and we can relate quantities at the event horizon and ones at the spatial infinity, thanks to divergence identities which exist in any gauge theory.

On the other hand, the second law has peculiar status even in the ordinary thermodynamics, because it refers to a direction in time. It is the second law that characterizes thermodynamics. Therefore it is important to establish the second law in the black hole mechanics, in order to transmute the mathematical analogy into physical one.

Since a black hole inevitably interacts with the external matters including graviton, we must consider the composite system of the black hole and the external matter as an isolated total system. And then, we are interested in the second law for the composite system, that is, the generalized second law (GSL) [1]: for any process,

$$\delta S_G > 0\,, \qquad S_G := S_{BH} + S_M = \frac{A_{BH}}{4\alpha} + S_M\,. \tag{1}$$

Considering a process which transfers an infinitesimal energy δE and entropy δS in the external region into the black hole, we obtain change in the total entropy $\delta S_G = \delta A_{BH}/4\alpha - \delta S = \delta E/T_{BH} - \delta S$. Since a black hole in classical theory has absolute zero temperature $T_{BH} = 0$ ($\alpha = 0$), the validity of the GSL in classical theory is nothing but the second law in the black hole mechanics $\delta A_{BH} > 0$. Thus, it is

[1]E-mail: okamura@skymint.phys.ocha.ac.jp

trivial for the GSL in classical theory to hold, provided that the energy condition is valid. However, once quantum processes are taken account into, the validity of the GSL is less trivial, owing to the breakdown of the energy condition.

Indeed, it is essential to incorporate quantum effects even semiclassically, in order for the black hole "thermodynamics" to make sense. If not, the physical analogy appears end in classical theory, since the thermodynamic temperature and entropy of a black hole are absolute zero and divergent, *respectively*. And then, taking account into quantum effects, the thermodynamic quantities of a black hole can be fixed as $T_{BH} = \kappa/2\pi$ and $S_{BH} = A_{BH}/4$ ($\alpha = 1$). Therefore, it is important to investigate the validity of the GSL by taking account into quantum effects.

Furthermore, the validity of the GSL strongly suggests that $A_{BH}/4$ is the thermodynamic entropy of a black hole, even though the underlying physical basis by which $A_{BH}/4$ arises as the black hole entropy remains unclear. Because the GSL can be viewed as nothing more than the ordinary second law of thermodynamics applied to a self-gravitating quantum system containing a black hole, it is natural to assign $A_{BH}/4$ to the black hole entropy.

Although an explicit general proof of the GSL has not been given until now, the various attempts for special cases have been performed. However, the question of the validity of the GSL is still be opened even in a simple gedankenexperiment . A breakdown of the GSL in the existing physics leads us to a new physics, such as an entropy bound for matter, if we take granted that the GSL holds.

In this report, we review the gedankenexperiment and its implication. And then we suggest that the GSL could hold even in the existing physics through reconsidering a recent reasoning by Bekenstein which supports the existence of an entropy bound for matter.

2 A gedankenexperiment and Its implication

2.1 A gedankenexperiment

We consider a gedankenexperiment involving a static black hole which area is $\mathcal{A}$ and a box of proper height b and geometrical cross-sectional area A. Far from the black hole, the box is filled with matter, so that the total energy of the box and contents is E_0 and its total entropy S_0. Then, the box is lowered adiabatically toward the black hole to some height l that corresponds to the proper distance between the horizon and the center of mass of the box. Because of the adiabaticity of the process, the total entropy of the box and contents remains constant. Therefore, the change in the total entropy becomes

$$\Delta S_G = \Delta S_{BH} - S_0 = \frac{\Delta M(l)}{T_{BH}} - S_0 \ , \tag{2}$$

where T_{BH} is the black hole temperature.

On the other hand, the energy $\Delta M(l)$ delivered to the black hole decreases because the gravitational energy of the box and contents is released by the work against the tension of the rope. Finally, we obtain the equation,

$$\Delta M(l) = E_0 + (\text{work done by the rope}) = E_0 + W_\infty(l) = E_0 + \int_\infty^l \left(-{F_\infty}^G\right)\, dl \tag{3}$$

$$= E_0 + E_0\,[\,\xi(l) - 1\,] = E_0\,\xi(l) \ , \tag{4}$$

where we use the relation $-{F_\infty}^G\, dl = dE_\infty = d(E_0\xi) = E_0\, d\xi$, that is derived from $E_\infty = E_0\,\xi$.

Thus, the energy delivered to the black hole is "redshiftened", due to the negative gravitational potential.

Therefore, the change in the total entropy is

$$\Delta S_G = \frac{E_0}{T_{BH}}\,\xi(l) - S_0 \ . \tag{5}$$

Because of $\xi \sim 0$ near the horizon, we can make the value of ΔS_G negative at will, if the box can be close to the horizon without limit.

2.2 Its implication

If we take granted that the GSL holds, then we need any mechanism which prevent the box from the horizon. There exist two reasonings: one is invoking to an entropy bound for matter and another makes use of the buoyant force by black hole atmosphere.

It is essential to recognize that the box must have a finite size which is greater than its Compton wavelength.

2.2.1 Entropy bound

The finiteness of the box size imposes a constraint, $l \geq b/2$, that is,

$$\xi(l) \sim \kappa\, l = 2\pi T_{BH} l \geq \pi T_{BH}\ b\ , \tag{6}$$

because the bottom of the box cannot touch the horizon. If we premise the validity of the GSL, we need an entropy bound for matter [2]

$$S \leq \pi E\ b\ . \tag{7}$$

Thus, the entropy of any matter is bounded above by its energy and size. Since, obviously, the size $b/2$ is greater than its gravitational radius $r_H = 2E$, we obtain

$$S \leq 2\pi E\ r_H \leq \frac{4\pi r_H^2}{4}\ . \tag{8}$$

Thus the maximum entropy of any matter is bounded above by its gravitational radius and the saturated state is attained by the black hole state.

Recently, the universal bound Eq.(8) is actively discussed in the different viewpoint, holographic principle [3].

2.2.2 Buoyant force

In the previous argument, we neglect the effect of the black hole atmosphere, that is, quantum fields outside the black hole.

We may start with two main working hypothesis [4];

A1. The black hole atmosphere is describable by radiation fluid of a thermal matter that maximizes entropy at a fixed energy.

A2. The buoyant force on the box exerted by the black hole atmosphere is the pressure gradient of the radiation fluid.

The assumption A1 means that the Gibbs-Duhem relation holds,

$$\begin{cases} \rho_{rad} + P_{rad} - (\ T_{BH}/\xi\ )\ s_{rad} = 0 \\ d\rho_{rad} = (\ T_{BH}/\xi\ )\ ds_{rad} \end{cases}\ , \tag{9}$$

and, by these equations, we obtain the equation

$$\frac{d}{dl}(\xi P_{rad}) = -\rho_{rad}(l)\ \frac{d\xi}{dl}\ . \tag{10}$$

And, because of the assumption A2, we obtain "Archimedean principle",

$$F_\infty{}^B = A\,[\ (\xi P_{rad})_{bottom} - (\xi P_{rad})_{top}\ ] = -V\frac{d}{dl}(\xi P_{rad}) = V\rho_{rad}(l)\ \frac{d\xi}{dl}\ . \tag{11}$$

Therefore, the work done by the total force $F_\infty = F_\infty{}^G + F_\infty{}^B$ become as

$$W_\infty = \int_\infty^l (-F_\infty)\ dl = E_0\,[\ \xi(l) - 1\ ] + V\ \xi(l)\ P_{rad}(l)\ . \tag{12}$$

And then, the energy delivered into the black hole is

$$\Delta M = E_0 + W_\infty = [\, E_0 + V P_{rad}(l) \,]\, \xi(l) \tag{13}$$

$$= V \left[\rho - \rho_{rad} + \frac{T_{BH}}{\xi} s_{rad} \right] \xi(l) \,, \tag{14}$$

where $\rho := E_0/V$ is the average density of the box and the contents.

It is the case of minimising ΔM that to hold the GSL is critical,

$$0 = \frac{d}{dl} W_\infty = {F_\infty}^G + {F_\infty}^B = V\,(\,\rho - \rho_{rad}\,)\,\frac{d\xi}{dl} \,, \tag{15}$$

so that, it is the most dangerous when the box is thrown into the black hole at the floating point $\rho = \rho_{rad}(l)$. And then

$$\Delta M = V \left[\rho - \rho_{rad} + \frac{T_{BH}}{\xi} s_{rad} \right] \xi(l) \geq V\, T_{BH}\, s_{rad} \,. \tag{16}$$

By definition of the radiation fluid, we can show the validity of the GSL [4]

$$\Delta S_G \geq V \left(s_{rad} - \frac{S_0}{V} \right) \geq 0 \,, \tag{17}$$

without a new physics.

Now we check the validity of our assumptions; especially, we suspect the validity of the assumption A2. It is natural to think that if $b \ll \lambda$, the assumption A2 is invalid due to the breakdown of the fluid picture. Therefore, it is doubtful to consider that the fluid picture is still valid far from the black hole, such as $b \sim \lambda \sim \xi(l)/T_{BH}$.

3 The buoyant force by scattering of long wavelength wave

Recently, Bekenstein have pointed out the breakdown of the fluid picture far from the horizon [5].

The pressure exerted on the surface of the box would be given by momentum flux T_{ii}, if the momentum flux were true, that is, it were estimated, inclusive of the boundary condition at the surface of the box. However, in the previous section, we estimated the pressure by the momentum flux, exclusive of the boundary condition (fictitious momentum flux). In order to get the true pressure by the fictitious momentum flux, we must multiply it by the reflection coefficient of the acceleration radiation by the box. For example, a perfectly transparent glass is not exerted by photons.

Thus, we need to estimate the scattering cross section of the box. If $b \ll R_H$, where R_H is the curvature radius at the horizon, then we can acquire large local Lorentz frame including the diffractor (the box). Therefore, it is possible to estimate the pressure by boosting estimation in the local Lorentz frame, so that it is enough to think the scattering problem in flat spacetime. Furthermore, if we consider a very massive black hole, we can approximate the region outside the horizon by the Rindler spacetime. For simplicity, hereafter we confine ourselves into the problem in Minkowski spacetime.

3.1 Momentum transfer in Minkowski spacetime

Especially, we are interested in scattering phenomena in the long wavelength limit. In this limit, the wave scattering is indifferent to details such as target's shape. Therefore we assume that the target's shape is spherically symmetric.

For example, for electromagnetic wave scattering by a conducting sphere, we have the differential cross-section as

$$\frac{d\sigma}{d\Omega'} \sim b^2\ (\,kb\,)^4\, F(\vec{n},\ \vec{n}') \,, \tag{18}$$

where $\vec{n}$ and $\vec{n}'$ are normalized incident wave vector and scattered one, respectively. The fourth order dependence of the cross-section on the wave vector is attributed to the fact that the dipole part is dominant in the scattering of the electromagnetic wave.

Given a distribution function such as $f(k) = \left[\exp\left(\frac{\hbar k}{T}\right) - 1 \right]^{-1}$, the incident momentum flux becomes

$$\vec{n}\, I(k,\vec{n})\, dkd\vec{n} \;:=\; f(k)\,(\hbar k)\,\vec{n}\,\frac{d^3k}{(2\pi)^3} = \vec{n}\, f(k)\,\hbar k^3\,\frac{dkd\vec{n}}{(2\pi)^3}\,. \tag{19}$$

Among the incident flux $I\, dkd\vec{n}$, the fraction $d\sigma/d\Omega'$ is scattered into the direction $\vec{n}'$. Thus we obtain the momentum transfer of the box in the local Lorentz frame,

$$\frac{d\vec{P}}{d\tau} = \int dkd\vec{n} \int d\vec{n}'\; I\;\frac{d\sigma}{d\Omega'}(\vec{n}-\vec{n}')\,. \tag{20}$$

Since the acceleration radiation has the temperature gradient, that going to the direction $\vec{n}$ hits on the box with the local temperature $T(l,\vec{n}) = T_{BH}/\xi(l,\vec{n}) = \hbar/2\pi[l + (\vec{e_l}\cdot\vec{n})b]$, where $\vec{e_l}$ is the normal vector that is directed to the center of mass of the box from the black hole. Therefore, the buoyant force by the dipole scattering in the global frame becomes

$$F_\infty{}^S = \xi(l)\left|\frac{d\vec{P}}{d\tau}\right| \sim T_{BH}\left[\frac{T(l)}{\hbar}\right]^8 (2\pi l)b^6 \int d\vec{n}\left[1+\frac{b}{l}(\vec{e_l}\cdot\vec{n})\right]^{-8} \sim \frac{T_{BH}}{b}\left(\frac{b}{l}\right)^8\,, \tag{21}$$

where we neglect numerical factor. Thus, the buoyant force by the dipole scattering is proportional to the seventh power of the size b, not to the volume (non-Archimedean) and proportional to the eighth inverse power of the distance l.

On the other hand, the buoyant force in fluid picture is estimated by,

$$F_\infty{}^B = V\rho_{rad}(l)\,\frac{d\xi}{dl} \sim b^3\,[T(l)]^4\,T_{BH} \sim \frac{T_{BH}}{b}\left(\frac{b}{l}\right)^4\,. \tag{22}$$

Thus, in the case of the dipole scattering, our intuition for "buoyant force", such that buoyant force is proportional to the volume of the box, does not work and the force rapidly decreases with the distance from the horizon.

Even in the case that the fluid picture is valid, it is possible to saturate the inequality Eq.(17) by lowering the radiation matter. Therefore the above implies that buoyant force alone is not enough for the GSL to be valid [5], because the inequality Eq.(17) does not hold for the process that lowering radiation matter is thrown to the black hole at the region $b \gg \xi(l)/T_{BH}$.

4 Long wavelength scattering revisited

We assume that a massless scalar field exists, so that S-wave scattering by the target occurs. By mode decomposition of the equation of motion of the scalar field $\Box\,\phi = 0$ in the local Lorentz frame, we obtain

$$\left[\, k^2 + \Delta \,\right]\,\Psi_{\vec{k}} = 0\,, \qquad \phi = \frac{\exp(-ik\tau)}{\sqrt{2k}}\,\frac{\Psi_{\vec{k}}(\vec{x})}{(2\pi)^{3/2}}\,, \tag{23}$$

where $k := |\vec{k}|$.

For simplicity, we would like to consider the case that the total entropy of the box and contents remains constant, we regard the surface of the box as infinite potential barrier. Our concern is equivalent to a scattering problem by the infinite potential barrier at the radius b in quantum mechanics. We obtain the result easily [6],

$$\Psi_{\vec{k}}(\vec{x}) \sim \exp(i\vec{k}\cdot\vec{x}) + g(\Omega)\frac{\exp(ikr)}{r}\,; \qquad \frac{d\sigma}{d\Omega} = |g(\Omega)|^2\,, \tag{24}$$

$$g(\Omega) = \sum_{l=0}^{\infty}\frac{2l+1}{2ik}\left(1+\frac{h_l^{(2)}(kb)}{h_l^{(1)}(kb)}\right)P_l(\cos\theta)\,. \tag{25}$$

In long wavelength limit, the reflection coefficient $g(\Omega)$ is approximated by

$$g(\Omega) \sim -b \sum_{l=0}^{\infty} \frac{(kb)^{2l}}{[(2l-1)!!]^2} P_l(\cos\theta) \ . \tag{26}$$

If S-wave scattering occurs, we have the differential cross section independent of wavelength,

$$\left(\frac{d\sigma}{d\Omega} \right)_0 \sim b^2 \sim \frac{\sigma_T}{4\pi} \ , \quad \sigma_T \sim 4\pi \, b^2 = 4A \ , \tag{27}$$

where σ_T is the total cross section.

In this connection, if scattering occurs only for higher multipole moment than S-wave, such as the electromagnetic field, we have the differential cross section

$$\left(\frac{d\sigma}{d\Omega} \right)_1 \sim b^2 (kb)^4 [\ P_1(\cos\theta) \ ]^2 \ , \tag{28}$$

which is depend on the fourth power of k, such as Eq.(18).

The contribution of the S-wave scattering to the momentum transfer of the diffractor in the local Lorentz frame is

$$\frac{d\vec{P}}{d\tau} = \int dk d\vec{n} \int d\vec{n}' \ I \left(\frac{d\sigma}{d\Omega'} \right)_0 (\vec{n} - \vec{n}') = \int d\vec{n} \, \sigma_T \int dk [\ \vec{n} \ I(k, \vec{n}) \ ] \ , \tag{29}$$

where the last equality is due to the spherical symmetric scattering of S-wave. Since the quantity $\sigma_T \int dk [\ \vec{n} \ I(k, \vec{n}) \ ]$ is nothing but the momentum flux across the surface with the area σ_T, Eq.(29) gives momentum transfer four times larger than the total momentum flux across the surface of the box.

Therefore, the buoyant force in the global frame exerted on the box by S-wave scattering is four times larger than that in the fluid picture, because of the diffractive effect,

$$F_\infty{}^S = 4 F_\infty{}^B (\text{fluid}) = 4V \rho_{rad}(l) \frac{d\xi}{dl} \ . \tag{30}$$

Thus, since the diffractive effect of S-wave scattering is favorable for the validity of the GSL, the GSL holds thanks to the buoyant force by black hole atmosphere without a new physics, such as an entropy bound for matter, if some massless scalar field exists.

For the completeness, we should check the validity of the fluid picture in short wavelength limit. In the limit, we obtain the differential cross section

$$\frac{d\sigma}{d\Omega} \sim \frac{A}{4\pi} \left[1 + \cot^2 \left(\frac{\theta}{2} \right) J_1^2(kb \sin\theta) \right] \ , \tag{31}$$

and using a formula,

$$J_1^2(z) \sim \frac{2}{\pi z} \sin^2 \left(z - \frac{\pi}{4} \right) \qquad \text{for } |z| \gg 1 \ , \tag{32}$$

we finally obtain the momentum transfer in the local Lorentz frame as

$$\begin{aligned} \frac{d\vec{P}}{dt} &= \int dk d\vec{n} \int d\vec{n}' \ I \left(\frac{d\sigma}{d\Omega'} \right) (\vec{n} - \vec{n}') \\ &= \int dk d\vec{n} [\vec{n} \ I(k, \vec{n})] \int d\vec{n}' \frac{A}{4\pi} \\ &= A \int dk d\vec{n} [\vec{n} \ I(k, \vec{n})] \ . \end{aligned} \tag{33}$$

As expected, the buoyant force in the geometrical optics approximation is equal to that in the fluid picture.

5 Summary

In this report, we reviewed a gedankenexperiment about the GSL and recognized importance of the buoyant force by black hole atmosphere. Since true pressure exerted on the diffractor is given by true momentum flux, inclusive of the boundary condition at the surface, it is necessary to multiply fictitious momentum flux estimated exclusive of the boundary condition by the reflection coefficient, in order to get the true buoyant force.

Because, in long wavelength limit, the dependence of the scattering cross section on wavelength much varies according to the spin of the scattered wave, whether we need a new physics, such as an entropy bound for matter, for the validity of the GSL or not, depends on the spin of massless fields in this world: If some massless scalar field exists in nature, then the GSL can hold, because of the buoyant force by black hole atmosphere. On the other hand, if not so, the validity of the GSL suggests the existence of some new physics, such as an entropy bound.

The above conclusion is based on the viewpoint of an accelerated observer. Although the energy-momentum tensor normalized by the accelerated observer is different from the true one, we can expect that the argument by the viewpoint of the accelerated observer gives right conclusion. Because the essential quantity in the argument is gradient of the energy-momentum tensor, not itself, and the difference between the energy-momentum tensor of the accelerated observer and the true one is divergence free.

By Unruh and Wald in 1982, it is shown that in two dimensional spacetime, the estimation of $\Delta M(l)$ delivered to the black hole by the viewpoint of inertial frame is equivalent to the estimation by the viewpoint of accelerated frame, which is based on the fictitious energy-momentum tensor exclusive of the boundary condition at the surface of the box. This result is ascribed to the fact that the reflection coefficient of any scattering problem by infinite potential in two dimensional spacetime is unity. For completeness, it is worthwhile to investigate in the viewpoint of inertial observer for higher dimensional spacetimes.

Furthermore, although we regard the sum of the black hole entropy and matter one as the total entropy, we have not yet obtained the foundation. Since the gravity is long range force, it may be doubtful to assume the additivity of entropies in self-gravitating system. It is interesting to reconsider the GSL without the assumption of the additivity of entropies [7].

References

[1] J.D. Bekenstein, Phys.Rev.**D7** (1973), 2333 ; **D9** (1974), 3292.

[2] J.D. Bekenstein, Phys.Rev.**D23** (1981), 287.

[3] G. 't Hooft, gr-qc/9310026 (1993) ; L. Susskind, J.Math.Phys.**36** (1995), 6377 ; R. Bousso, JHEP.**06** (1999), 078 ; **07** (1999), 004.

[4] W.G. Unruh and R.M. Wald, Phys.Rev.**D25** (1982), 942 ; **D27** (1983), 2271 ; M.A. Pelath and R.M. Wald, Phys.Rev.**D60** (1999), 104009-1

[5] J.D. Bekenstein, Phys.Rev.**D60** (1999), 124010.

[6] A. Messiah, *Quantum Mechanics* (Elsevier-North-Holland, Amsterdam, 1961).

[7] R.D. Sorkin, Phys.Rev.Lett.**56** (1986), 1885.

BTZ Black Hole Entropy in Higher Curvature Gravity

Hiromi SAIDA [1]

Graduate School of Human and Environmental Studies, Kyoto University, Sakyo-ku, Kyoto 606-8501, Japan

Jiro SODA [2]

Department of Fundamental Sciences, FIHS, Kyoto University, Sakyo-ku, Kyoto 606-8501, Japan

Abstract

For the BTZ black hole in the Einstein gravity, a statistical entropy has been calculated to be equal to the Bekenstein-Hawking entropy. In this paper, its statistical entropy in the higher curvature gravity is calculated and shown to be equal to the one derived by using the Noether charge method. This suggests that the equivalence of the geometrical and statistical entropies of the black hole is retained in the general diffeomorphism invariant theories of gravity. A relation between the cosmic censorship conjecture and the unitarity of the conformal field theory on the boundary of AdS_3 is also discussed.

1 Introduction

The profound understanding of the black hole thermodynamics is a clue for approaching the quantum gravity. Although the final form of the quantum gravity is covered with a veil of mystery, it would be legitimate to regard the diffeomorphism invariance as the key to the mystery. Hence the black hole thermodynamics in the diffeomorphism invariant theories of gravity should be studied to obtain the insights into the quantum gravity. The first law of black holes in such theories of gravity has already been established [1] [2]. The zeroth and second laws, especially in the higher curvature gravity, have been investigated, for example in ref. [3]. All the black hole entropies treated in the above works are of the integral of geometrical quantities on a spatial section of the event horizon. The geometrical entropy in an N-dimensional higher curvature gravity can be calculated by using the Noether charge method [1] [2] to give

$$S_{IW} = -\frac{1}{8G}\oint_H dx^{N-2}\sqrt{h}\,\frac{\partial f}{\partial R_{\mu\nu\alpha\beta}}\,\epsilon_{\mu\nu}\epsilon_{\alpha\beta}\,, \tag{1}$$

where H is the spatial section of the event horizon, h is the determinant of the induced metric on H, f is the higher curvature Lagrangian and $\epsilon_{\mu\nu}$ is the binormal to H [2]. When we denote $f = R$+(higher curvature terms), the first term of this Lagrangian contributes to the entropy (1) as the Bekenstein-Hawking term $A/4G$, where A is the area of H. The geometrical expression of the black hole entropy obtained in ref. [1] is consistent with the well known results previously obtained for the Einstein gravity, however it does not reveal statistical origin of the entropy. Statistical explanation of the entropy is remained as an open question.

For the Einstein gravity, a statistical derivation of the Bekenstein-Hawking entropy has been carried out [4] [5] for a black hole in three dimensional anti-de Sitter spacetime (AdS_3) which is called the BTZ black hole [6] [7] [8]. Although several issues remain open to be resolved [9], this is one of the important examples which demonstrate the equality between the Bekenstein-Hawking entropy and a statistical entropy. It is our central interest to give a statistical interpretation of the black hole entropy in the

[1] E-mail: saida@phys.h.kyoto-u.ac.jp
[2] E-mail: jiro@phys.h.kyoto-u.ac.jp

diffeomorphism invariant theories of gravity. In this paper, we attempt to derive the statistical entropy of the BTZ black hole in the higher curvature gravity, and the computation of it in refs. [4] and [5] is modified to be available for this case [10].

In section 2 we review the statistical derivation of the BTZ black hole entropy in the Einstein gravity. Section 3 is devoted to the computation of the entropy in the higher curvature gravity, and our results are illustrated with a concrete example. Finally we give summary and discussion in section 4. Throughout this paper we use the unit, $c = \hbar = 1$.

2 BTZ Black Hole Entropy in the Einstein Gravity

For the preparation of our purpose, in this section, we review the BTZ black hole [6] [7] [8] and its statistical entropy in the Einstein gravity [5]. The action we treat here is

$$I = \frac{1}{16\pi G}\int d^3x\,(R - 2\Lambda)\sqrt{-g} + B\,, \tag{2}$$

where Λ is the cosmological constant and B is a surface term which is needed to let the variation of I make sense [6].

2.1 BTZ Black Hole

Because three dimensional gravity have no dynamical degrees of freedom, the BTZ black hole spacetime is locally equivalent to AdS_3. Then it is enough for our purpose to consider only a constant negative curvature spacetime. The Riemann tensor of the constant curvature spacetime is expressed as

$$R_{\mu\nu\alpha\beta} = \frac{R}{6}(g_{\mu\alpha}g_{\nu\beta} - g_{\mu\nu}g_{\alpha\beta})\,, \tag{3}$$

where R is the Ricci scalar which is related to the cosmological constant through the Einstein equation: $R = 6\Lambda$. Further we can set $R = -6/l^2$ where l is the curvature radius of AdS_3. Note that l is related to the cosmological constant, $\Lambda = -1/l^2$. The BTZ black hole metric is [6]

$$ds^2 = -N^2dt^2 + \frac{1}{N^2}dr^2 + r^2\left[d\phi + N^\phi dt\right]^2\,, \tag{4}$$

where $\phi \sim \phi + 2\pi$, $N^2 = (r/l)^2 + (4GJ/r)^2 - GM/l$, $N^\phi = -4GJ/r^2$, and M and J are the mass and the angular momentum of the black hole, respectively. The event horizon is at the radius: $r_+ \equiv \sqrt{2Gl(M+J)} + \sqrt{2Gl(M-J)}$. Further the Bekenstein-Hawking entropy is calculated to be

$$S_{BH} = \frac{1}{4G}\oint_{r_+} d\phi\sqrt{g_{\phi\phi}} = \frac{\pi}{4G}\left[\sqrt{8Gl(M+J)} + \sqrt{8Gl(M-J)}\right]\,. \tag{5}$$

2.2 Statistical Entropy

The BTZ black hole entropy can be calculated by counting the number of states [5] [9]. The counted states are in the Hilbert space operated by the quantum counterparts (generators) of asymptotic symmetry of asymptotically AdS_3, whose definitions are described below [4]. The asymptotically AdS_3 metrics are defined as:

$$\begin{aligned} ds^2 &= \left[-\frac{r^2}{l^2} + O(1)\right]dt^2 + \left[\frac{l^2}{r^2} + O\left(\frac{1}{r^4}\right)\right]dr^2 + \left[r^2 + O(1)\right]d\phi^2 \\ &\quad + O\left(\frac{1}{r^3}\right)dtdr + O(1)dtd\phi + O\left(\frac{1}{r^3}\right)drd\phi\,, \end{aligned} \tag{6}$$

where $0 < \phi \leq 2\pi$. The global AdS_3, which denotes the AdS_3 spacetime without any source in it, is included in these metrics. It is obvious that the BTZ black hole is of asymptotically AdS_3. The

asymptotic symmetry of asymptotically AdS_3 is described by the following Killing vectors which preserve the boundary condition of the metric [4] [5]

$$\begin{aligned}
\xi^t &= l(T^+ + T^-) + \frac{l^3}{2r^2}(\partial_+^2 T^+ + \partial_-^2 T^-) + O\left(\frac{1}{r^4}\right), \\
\xi^r &= -r(\partial_+ T^+ + \partial_- T^-) + O\left(\frac{1}{r}\right), \\
\xi^\phi &= T^+ - T^- - \frac{l^2}{2r^2}(\partial_+^2 T^+ - \partial_-^2 T^-) + O\left(\frac{1}{r^4}\right),
\end{aligned} \tag{7}$$

where $T^\pm = T^\pm(x^\pm)$ and $x^\pm = t/l \pm \phi$. The Killing vectors in this form include those of the global AdS_3.

The algebra satisfied by the quantum counterparts (generators) of asymptotic symmetry of asymptotically AdS_3 should be of the quantization of the classical algebra satisfied by classical generators of the symmetry, which is just the Hamiltonian generating the diffeomorphism along the Killing vector ξ[4]. Such a Hamiltonian is expressed as $H[\xi] = \int_\Sigma d^2x\, \xi^a \mathcal{H}_a + Q[\xi]$, where Σ is the spatial hypersurface, ξ^a ($a = \perp, 1, 2$) are the vertical and parallel components of ξ with respect to Σ, $\mathcal{H}_a$ are the constraints and $Q[\xi]$ is the surface term which is needed to cancel the surface term in the variation $\delta H[\xi]$, that is, there is a freedom of additional constant to Q. Given two Hamiltonians, $H[\xi]$ and $H[\eta]$, the algebra of them is obtained by evaluating the Poisson bracket. It is shown in ref. [4] that such an algebra is the central extension of the commutation relation (Lie bracket) of ξ and η: $\{H[\xi], H[\eta]\}_P = H[\{\xi,\eta\}] + K[\xi,\eta]$, where $K[\xi,\eta]$ is the central extension, $\{\,\}_P$ is the Poisson bracket and $\{\xi,\eta\}$ is the Lie bracket. Further, because the constraints $\mathcal{H}_a$ is weakly zero, it reduces to the algebra: $\{Q[\xi], Q[\eta]\}_D = Q[\{\xi,\eta\}] + K[\xi,\eta]$, where $\{\,\}_D$ is the Dirac bracket. The central extension $K[\xi,\eta]$ can be calculated by setting the surface term Q for the global AdS_3 be zero [4]:

$$K[\xi,\eta] = \lim_{r\to\infty} \frac{1}{16\pi G} \oint dS_l \{ \widehat{G}^{ijkl} [\xi^\perp g_{ij|k} - \xi^\perp_{|k} (g_{ij} - \hat{g}_{ij})] + 2(\xi^i + N^i \xi^\perp)\pi^l_i \}, \tag{8}$$

where the latin indices denote the spatial coordinates, $\hat{g}_{\mu\nu}$ is the global AdS_3, $g_{\mu\nu}$ is the asymptotically AdS_3 of the form (6), $\widehat{G}^{ijkl} = (1/2)\sqrt{\det(\hat{g}_{ij})}(\hat{g}^{ik}\hat{g}^{jl} + \hat{g}^{il}\hat{g}^{jk} - 2\hat{g}^{ij}\hat{g}^{kl})$, dS_l is the line element of the circle of constant radius on the spatial hypersurface Σ, $\pi_i^{\,l} = g^{kl}\pi_{ik}$, π_{ij} is the conjugate momentum of g_{ij}, $A_{|k}$ is covariant derivative of quantity A with respect to spatial metric $\hat{g}_{ij}$, $\xi^\perp = N^\perp \xi^t$, and $N^\perp$ and N^i are the lapse function and the shift vector of $g_{\mu\nu}$ respectively. Here the variation of metric from $\hat{g}_{\mu\nu}$ to $g_{\mu\nu}$ is given by $\delta g_{\mu\nu} \equiv g_{\mu\nu} - \hat{g}_{\mu\nu} = \mathcal{L}_\eta \hat{g}_{\mu\nu}$.

When we define the Fourier components of ξ as $\xi^\pm_m \equiv (i/2)\xi$ with $T^\pm = \exp(imx^\pm)$ $(m = 0, \pm1, \pm2\cdots)$, the Lie brackets of the Killing vectors are calculated to be the Virasoro algebra without central extension: $\{\xi^\pm_m, \xi^\pm_n\} = (m-n)\xi^\pm_{m+n}$, $\{\xi^+_m, \xi^-_n\} = O(1/r)$. Then the classical algebra we are seeking can be expressed as the Virasoro algebra with the central extension given by eq. (8). That is, the algebra of the quantum generators is also the same algebra, which is obtained by quantizing the commutation relation through the replacement, $\{\,\}_D \to -i[\,]$, where $[\,]$ is the commutation relation of quantum operator [4]:

$$\begin{aligned}
[\, L_m, L_n \,] &= (m-n)\, L_{m+n} + \frac{C}{12} m(m^2-1)\delta_{m+n,0}, \\
[\, \tilde{L}_m, \tilde{L}_n \,] &= (m-n)\, \tilde{L}_{m+n} + \frac{C}{12} m(m^2-1)\delta_{m+n,0}, \\
[\, L_m, \tilde{L}_n \,] &= 0.
\end{aligned} \tag{9}$$

Here L_m and $\tilde{L}_m$ denote the quantum generators corresponding to ξ^+_m and ξ^-_m respectively, and the central charge C can be obtained by substituting the metric given by eq. (6) into $g_{\mu\nu}$ of eq. (8) to be a positive constant [4],

$$C = \frac{3l}{2G}. \tag{10}$$

Thus the quantum gravity of AdS_3 is related to the conformal field theory (CFT) on the boundary of the spacetime. Such a correspondence between the AdS and the CFT is called the AdS/CFT correspondence [11] [12].

With above preparations, we can proceed to a calculation of statistical entropy. The calculation follows the ordinary state counting of the conformal field theory, where the counted states are the eigen states of L_0 and $\tilde{L}_0$. For the case that the eigen values are large (semi-classical), we can obtain the number of states by Cardy's formula [9] [13] to give the statistical entropy:

$$S_C \approx 2\pi\sqrt{\frac{C\lambda}{6}} + 2\pi\sqrt{\frac{C\tilde{\lambda}}{6}}\,, \tag{11}$$

where λ and $\tilde{\lambda}$ are the (large) eigen values of L_0 and $\tilde{L}_0$ respectively.

Note that $\xi_0^+ + \xi_0^- = 2l\,\partial_t + O(1/r^4)$ and $\xi_0^+ - \xi_0^- = 2\partial_\phi + O(1/r^4)$, then a mass operator $\mathcal{M}$ and an angular momentum operator $\mathcal{J}$ are defined by $\mathcal{M} \equiv L_0 + \tilde{L}_0$ and $\mathcal{J} \equiv L_0 - \tilde{L}_0$, respectively [5]. For the BTZ black hole, we define a quantum state $|MJ\rangle$ by $\mathcal{M}\,|MJ\rangle = M\,|MJ\rangle$ and $\mathcal{J}\,|MJ\rangle = J\,|MJ\rangle$, further the ground state by $\mathcal{M}\,|00\rangle = 0$ and $\mathcal{J}\,|00\rangle = 0$, that is, $M = J = 0$. The spacetime of the ground state asymptotes to the AdS_3 as $r \to \infty$, thus this ground state can correspond to $\hat{g}_{\mu\nu}$ in eq. (8). Consequently, the above calculations of the central charge and the statistical entropy are available for the BTZ black hole [9]. The state, $|MJ\rangle$, provides the eigen values of L_0 and $\tilde{L}_0$ to be

$$\lambda = \frac{1}{2}(M + J) \quad , \quad \tilde{\lambda} = \frac{1}{2}(M - J)\,, \tag{12}$$

then the statistical entropy for the case of large M and J becomes

$$S_C = \frac{\pi}{4G}\left[\sqrt{8Gl(M+J)} + \sqrt{8Gl(M-J)}\right]. \tag{13}$$

This coincides with the Bekenstein-Hawking entropy S_{BH} given by eq. (5).

3 BTZ Black Hole Entropy in the higher Curvature Gravity

In this section, we calculate the statistical entropy of the BTZ black hole in the higher curvature gravity. The action we treat here is of the form:

$$I = \frac{1}{16\pi G}\int d^3x\, f(R_{\mu\nu}, g^{\mu\nu})\sqrt{-g} + B\,, \tag{14}$$

where $f(R_{\mu\nu}, g^{\mu\nu})$ is the Lagrangian of general higher curvature gravity and B is the surface term needed by the same reason as the action (2). This action is the most generic form of the three dimensional higher curvature gravity because the Weyl tensor vanishes in three dimensional spacetime, that is, the Riemann tensor can be expressed generally by the Ricci tensor, the Ricci scalar and the metric: $R_{\mu\nu\alpha\beta} = g_{\mu\alpha}R_{\nu\beta} + g_{\nu\beta}R_{\mu\alpha} - g_{\nu\alpha}R_{\mu\beta} - g_{\mu\beta}R_{\nu\alpha} - (1/2)(g_{\mu\alpha}g_{\nu\beta} - g_{\mu\beta}g_{\nu\alpha})\,R$.

When we are interested in the statistical entropy of the BTZ black hole in the higher curvature gravity, the entropy is given by the same formula as eq. (11) with the central charge and the eigen values of the Virasoro generators in the higher curvature gravity. The eigen values (12) can be easily obtained through the Noether charge form of the mass and the angular momentum constructed in ref. [1]. However, as reviewed in the previous section, the central charge is necessary to calculate the surface terms of the Hamiltonian, which should be corrected by the higher curvature terms in the Lagrangian to induce additional terms upon the central charge, eq. (8). The derivation and resultant form of the additional terms will be very complicated. To avoid this intricacy, we define new metric and transform the original higher curvature frame into the Einstein frame.

3.1 Frame Transformation

In this subsection, we review the transformation from the original higher curvature frame to the Einstein frame in preparation for calculating the central charge. The Euler-Lagrange equation in the original frame is obtained as

$$\frac{\partial f}{\partial g^{\mu\nu}} - \frac{1}{2}f g_{\mu\nu} = \frac{1}{2}\left[P_{\alpha\mu;\nu}{}^{;\alpha} + P_{\alpha\nu;\mu}{}^{;\alpha} - \Box P_{\mu\nu} - g_{\mu\nu}P_{\alpha\beta}{}^{;\alpha\beta}\right], \tag{15}$$

where $P_{\mu\nu} \equiv g_{\mu\alpha}g_{\nu\beta}(\partial f/\partial R_{\alpha\beta})$. This is obviously a fourth order differential equation of $g^{\mu\nu}$. The new *metric* which turns out to be that in the Einstein frame is defined by [14] [15]

$$\bar{g}^{\mu\nu} \equiv \left[-\det\left(\frac{\partial(f\sqrt{-g})}{\partial R_{\alpha\beta}}\right)\right]^{-1} \frac{\partial(f\sqrt{-g})}{\partial R_{\mu\nu}}. \tag{16}$$

We assume here that the relation (16) can be inverted to give $R_{\mu\nu}$ as a function of $\bar{g}^{\alpha\beta}$ and $g^{\alpha\beta}$ (including no derivative of them): $R_{\mu\nu} = R_{\mu\nu}(\bar{g}^{\alpha\beta}, g^{\alpha\beta})$.

The alternative action which is equivalent to the original action I and describes the Einstein frame can be defined through the Legendre transformation as [14] [15]

$$\bar{I} \equiv \frac{1}{16\pi G}\int d^3x\,\sqrt{-\bar{g}}\,\Big[\,\bar{g}^{\mu\nu}R_{\mu\nu}(g^{\alpha\beta}, \partial_\omega g^{\alpha\beta}, \partial_\tau\partial_\omega g^{\alpha\beta}) - \bar{g}^{\mu\nu}R_{\mu\nu}(\bar{g}^{\alpha\beta}, g^{\alpha\beta}) + \frac{\sqrt{-g}}{\sqrt{-\bar{g}}}f(R_{\mu\nu}(\bar{g}^{\alpha\beta}, g^{\alpha\beta}), g^{\mu\nu})\Big] + \tilde{B}. \tag{17}$$

Note that $\bar{g}^{\mu\nu}$ and $g^{\mu\nu}$ are treated as independent dynamical variables in this action. It can be easily checked that the Euler-Lagrange equations of $\bar{I}$ are equivalent to those of I.

In order to understand that $\bar{I}$ describes the Einstein frame, we rewrite it to an explicit form consisting of the Einstein-Hilbert action of $\bar{g}^{\mu\nu}$ and an auxiliary matter field. The following general relation is useful for such a purpose: $R_{\mu\nu}(g^{\alpha\beta}, \partial_\omega g^{\alpha\beta}, \partial_\tau\partial_\omega g^{\alpha\beta}) = \bar{R}_{\mu\nu}(\bar{g}^{\alpha\beta}, \partial_\omega \bar{g}^{\alpha\beta}, \partial_\tau\partial_\omega \bar{g}^{\alpha\beta}) + \bar{\nabla}_\alpha F^\alpha_{\mu\nu} - \bar{\nabla}_\nu F^\alpha_{\mu\alpha} + F^\alpha_{\alpha\beta}F^\beta_{\mu\nu} - F^\alpha_{\mu\alpha}F^\beta_{\alpha\nu}$, where $\bar{\nabla}_\mu$ is the covariant derivative with respect to $\bar{g}^{\mu\nu}$ and $F^\alpha_{\mu\nu} \equiv \Gamma^\alpha_{\mu\nu} - \bar{\Gamma}^\alpha_{\mu\nu} = (1/2)\,g^{\alpha\beta}(\bar{\nabla}_\nu g_{\mu\beta} + \bar{\nabla}_\mu g_{\beta\nu} - \bar{\nabla}_\beta g_{\mu\nu})$. By substituting this relation into $\bar{I}$, we obtain

$$\bar{I} = \frac{1}{16\pi G}\int d^3x\,\sqrt{-\bar{g}}\,\Big[\,\bar{g}^{\mu\nu}\bar{R}_{\mu\nu}(\bar{g}^{\alpha\beta}, \partial_\omega\bar{g}^{\alpha\beta}, \partial_\tau\partial_\omega\bar{g}^{\alpha\beta}) + \bar{g}^{\mu\nu}(F^\alpha_{\alpha\beta}F^\beta_{\mu\nu} - F^\alpha_{\mu\alpha}F^\beta_{\alpha\nu}) - \bar{g}^{\mu\nu}R_{\mu\nu}(\bar{g}^{\alpha\beta}, g^{\alpha\beta}) + \frac{\sqrt{-g}}{\sqrt{-\bar{g}}}f(R_{\mu\nu}(\bar{g}^{\alpha\beta}, g^{\alpha\beta}), g^{\mu\nu})\Big] + \text{surface terms}. \tag{18}$$

The Einstein frame described by $\bar{I}$ is understood as the system consisting of the Einstein gravity, $\bar{g}^{\mu\nu}$, and an auxiliary tensor matter field, $g^{\mu\nu}$.

3.2 Central charge in the higher curvature gravity

We restrict our treatment hereafter to the case that the right hand side of the Euler-Lagrange equation (15) vanishes, that is, the spacetime is of the constant curvature. Further we assume that the curvature R is of negative. Under such conditions, the BTZ black hole of the form given by eq. (4) can exist. Because the spacetime of the BTZ black hole is of constant curvature, the following quantity Ω is constant:

$$\Omega = \frac{1}{3}g^{\mu\nu}\frac{\partial f}{\partial R_{\mu\nu}}. \tag{19}$$

Eq. (16) gives the metric in the Einstein frame $\bar{g}^{\mu\nu}$ to be

$$\bar{g}^{\mu\nu} = \Omega^{-2}g^{\mu\nu} \quad , \quad \bar{g}_{\mu\nu} = \Omega^2 g_{\mu\nu}, \tag{20}$$

where $\bar{g}_{\mu\nu}$ is defined by $\bar{g}_{\mu\alpha}\bar{g}^{\alpha\nu} = \delta^\nu_\mu$. This is just a conformal transformation with constant conformal factor Ω. The calculation of the central charge in the Einstein frame can be carried out by relating the quantities in the Einstein frame to those in the original frame through the conformal transformation (20). Note that, because the isometries of the BTZ black hole in both frames are the same, the asymptotic symmetry Killing vectors (7) in both frames are the same. Further by definitions of $\widehat{G}^{ijkl}$, $\pi_i{}^j$, the lapse function and the shift vector, we can extract their relations between both frames: $\bar{\xi}^\mu = \xi^\mu$, $\bar{\widehat{G}}^{ijkl} = \Omega^{-2}\widehat{G}^{ijkl}$, $\bar{\pi}_i{}^j = \Omega\pi_i{}^j$, $\bar{N}^\perp = \Omega N^\perp$, $\bar{N}^i = \Omega^2 N^i$. Substituting these results into (8), the central charge is calculated to be

$$C = \frac{l}{2G}g^{\mu\nu}\frac{\partial f}{\partial R_{\mu\nu}}. \tag{21}$$

Although this is the central charge calculated in the Einstein frame, this central charge is equivalent to that in the original higher curvature frame.

3.3 Computation of the BTZ black hole entropy

With all the preparations done above, we can proceed to the calculation of the BTZ black hole entropy in the higher curvature gravity. The BTZ black hole is also of the asymptotically AdS_3 spacetime even in the higher curvature gravity. Hence the AdS/CFT correspondence is available [11] [12] to give the statistical entropy of the form (11). When we denote the BTZ black hole metric in the higher curvature gravity by the same notation as eq. (4), the mass and the angular momentum in the higher curvature gravity are calculated through the Noether charge form obtained in ref. [1] to be ΩM and ΩJ, respectively. Then the two Virasoro eigen values λ and $\tilde{\lambda}$ in the higher curvature gravity are given by the same procedure as eq. (12),

$$\lambda = \Omega\frac{1}{2}(M+J) \quad , \quad \tilde{\lambda} = \Omega\frac{1}{2}(M-J)\,. \tag{22}$$

Finally the statistical entropy of the BTZ black hole in the higher curvature gravity is obtained by eqs. (11), (21) and (22) as:

$$S_C = \frac{\pi}{12G}\,g^{\mu\nu}\frac{\partial f}{\partial R_{\mu\nu}}\left[\sqrt{8Gl(M+J)}+\sqrt{8Gl(M-J)}\right] \tag{23}$$

On the other hand, the geometrical entropy of the black hole can be calculated by eq. (1) to be

$$S_{IW} = -\frac{1}{8G}\oint_H d\phi\sqrt{g_{\phi\phi}}\,\frac{\partial f}{\partial R_{\mu\alpha}}\,g^{\nu\beta}\,\epsilon_{\mu\nu}\epsilon_{\alpha\beta} = \frac{1}{12G}\,g^{\mu\nu}\frac{\partial f}{\partial R_{\mu\nu}}\oint_{r_+} d\phi\sqrt{g_{\phi\phi}}\,, \tag{24}$$

By making use of the integral in (5), this formula (24) coincides with the statistical entropy S_C given by eq. (23).

3.4 Example: $f = R + aR^2 + bR_{\mu\nu}R^{\mu\nu} - 2\Lambda$

We apply the results obtained above to the case: $f = R + aR^2 + bR_{\mu\nu}R^{\mu\nu} - 2\Lambda$ (a, $b = const.$). For the constant curvature spacetime, the Euler-Lagrange equation (15) becomes

$$(1+2aR)R_{\mu\nu} + \frac{1}{2}(R + aR^2 + bR_{\alpha\beta}R^{\alpha\beta} - 2\Lambda)g_{\mu\nu} = 0\,. \tag{25}$$

For the BTZ black hole which is the negative constant curvature space, Λ is related to the Ricci scalar through eqs. (3) and (25): $\Lambda = \frac{R}{6}\left[1 + (b-a)R\right]$. The conformal transformation (20) becomes

$$\bar{g}_{\mu\nu} = \Omega^2 g_{\mu\nu} \quad , \quad \Omega = 1 - \frac{12a+4b}{l^2}\,, \tag{26}$$

where we have used the definition of the radius of AdS spacetime: $l = \sqrt{-6/R}$. This gives the central charge through eq. (21) as

$$C = \left(1 - \frac{12a+4b}{l^2}\right)\frac{3\,l}{2G}\,, \tag{27}$$

which is consistent with the results obtained in ref. [12]. We obtain the statistical entropy in the higher curvature gravity through eq. (23)

$$S_C = \left(1 - \frac{12a+4b}{l^2}\right)\frac{\pi}{4G}\left[\sqrt{8Gl(M+J)}+\sqrt{8Gl(M-J)}\right]. \tag{28}$$

The geometrical entropy given by eq. (1) is calculated to be

$$S_{IW} = \left(1 - \frac{12a+4b}{l^2}\right)\frac{1}{4G}\oint_{r_+} d\phi\sqrt{g_{\phi\phi}}\,. \tag{29}$$

By making use of the integral in (5), this equation (29) coincides with the statistical entropy S_C given by eq. (28).

4 Summary and Discussion

We have shown the statistical derivation of the BTZ black hole entropy in the higher curvature gravity. The resultant formula agrees with the one derived by the Noether charge method [1]. As a by-product, we have obtained the central charge, that is, the coefficient of the Weyl anomaly, in the higher curvature gravity. Although the statistical entropy is calculated in the higher curvature gravity, because the procedure of our calculation is essentially the same as the Einstein gravity, some issues which stemmed from the use of CFT on the boundary of AdS_3 [9] remain open to be resolved.

Provided that, instead of the higher curvature gravity, we adopt the BTZ black hole in diffeomorphism invariant theories of gravity which include symmetrized covariant derivatives of Riemann tensor like $R_{\mu\nu\alpha\beta;(\omega\tau)}$, the problem which arises in applying our procedure to calculate the central charge is that we do not have the formalism of transforming the frames in such theories. However, because the relation (3) denotes that the terms of covariant derivative of Riemann tensor in such Lagrangians vanishes for constant curvature spacetimes, it is expected that the frame transformation between the original and Einstein frames is also the conformal transformation with constant conformal factor. For the other case of Lagrangians include some matter fields coupling to the gravity, the factor Ω should depend on the matter fields. However it is possible to set such matter fields be constant without loss of consistency with the BTZ black hole. Then our computation of the statistical entropy of the BTZ black hole in this paper is available for the general diffeomorphism invariant theories of gravity which include the symmetrized covariant derivatives of Riemann tensor and the matter fields coupling to the gravity, provided that we can construct a well-defined transformation of the frames in such theories. Thus, it is natural to conjecture that the equality between the geometrical entropy and the statistical one is retained in the general diffeomorphism invariant theories of gravity. Further, with noting the ref. [16] which extends the computation of the statistical entropy of the BTZ black hole to any dimension in the Einstein gravity, it is expected that the equivalence between the geometrical and statistical entropies can be extended to any dimensional diffeomorphism invariant theories of gravity.

The derivation of the statistical entropy in this paper is heavily relied on the conformal field theory constructed on the boundary of the BTZ black hole spacetime. It has been well recognized that the unitarity of the conformal field theory requires the positivity of the central charge, which is consistent with eq. (10). Further it is required through eq. (21) that $\Omega > 0$. On the other hand, this relation, $\Omega > 0$, is required from the null energy condition in the Einstein frame and the weak cosmic censorship conjecture [17] in considering the second law of the Black hole thermodynamics for the geometrical entropy as mentioned below [3]. Both of these conditions are the essential assumptions in establishing the second law in the Einstein gravity (the area theorem). For the case of the Lagrangian polynomial in R, it has already been explicitly derived in ref. [3] that the null energy condition in the Einstein frame requires the positivity of the conformal factor Ω of the frame transformation. This suggests that this requirement can be extended to the case of general higher curvature gravity. Further, with making use of the frame transforation in considering the second law in the diffeomorphism invariant theories of gravity, the cosmic censorship conjecture will be required to be satisfied in the Einstein frame. It will also be necessary to retain the disappearance of naked singularities in the original frame. Then we require the positivity of Ω because, for the case that $\Omega \leq 0$, there is a possibility of appearing singularities in the original frame. Thus, the cosmic censorship conjecture and the null energy condition in the Einstein frame must have some relation with the unitarity of the conformal field theory on the boundary of spacetime. The issue about the details of such a relation is left as an interesting open question.

We turn our attention to some possible applications of our results to some interesting cases. As we have already seen, the statistical black hole entropy can be computed by using the data on the boundary of the black hole spacetime which asymptotes to that of anti-de Sitter spacetime. This kind of correspondence between the symmetry of the boundary of AdS spacetime and the conformal field theory (CFT) has been intensively studied recently. This correspondence can be used to deduce the entropy of the black string system in higher dimensions[18]. It is interesting to investigate whether or not our results of this paper can be extended to the higher dimensional black objects.

For the calculation of the statistical entropy through the AdS/CFT correspondence, the central importance exists in the correspondence between the symmetry of the boundary of AdS and the isometry of the bulk spacetime of a black hole, such as the stationarity and axisymmetry. Hence, it is not obvious

whether or not the statistical entropy which we have calculated can be extended to the dynamical cases such as the collapsing black holes and the evaporating black holes. As the geometrical entropy is extended with retaining its meaning even to the dynamical systems [1] [2], however, it is expected to be able to extend our results to the dynamical cases.

Acknowledgements

We would like to Thank M.Sakagami for his useful discussions. This work was supported in part by Monbusho Grant-in-Aid for Scientific Research No.10740118.

References

[1] R.Wald, Phys.Rev.D48 R3427(1993); V.Iyer and R.Wald, Phys.Rev.D50 846(1994), Phys.Rev.D52 4430(1995)

[2] T.Jacobson, G.Kang and R.Myers, Phys.Rev.D49 3518(1994)

[3] T.Jacobson, G.Kang and R.Myers, Phys.Rev.D52 3518(1995)

[4] J.Brown and M.Henneaux, Commun.Math.Phys.104 207(1986)

[5] A.Strominger, J.High Energy Phys.9802 009(1998), hep-th/9712251

[6] M.Bañados, M.Henneaux, C.Teitelboim and J.Zanelli, Phys.Rev.D48 1506(1993)

[7] O.Coussaert and M.Henneaux, Phys.Rev.Lett72 183(1994)

[8] S.Carlip, Class.Quantum Grav.12 2853(1995)

[9] S.Carlip, Class.Quantum Grav.15 3609(1998)

[10] H.Saida and J.Soda, gr-qc/9909061

[11] See for example: J.Maldacena, Adv.Theor.Math.Phys.2 231(1998); E.Witten, Adv.Theor.Math.Phys.2 505(1998); M.Henningson and K.Skenderis, J.High Energy Phys.9807 023(1998)

[12] S.Nojiri and S.Odintsov, hep-th/9903033

[13] J.Cardy, Nucl.Phys.B270 186(1986)

[14] G.Magnano, M.Ferraris, M.Francaviglia, General Rel.Grav.19 465(1987)

[15] G.Magnano, M.Ferraris, M.Francaviglia, Class.Quantum Grav.7 557(1990)

[16] S.Carlip, Phys.Rev.Lett.82 2828(1999)

[17] The null energy condition is expressed as $T_{\mu\nu}k^\mu k^\nu \geq 0$ for any null vector k^μ. The weak cosmic cesorship conjecture means that any naked singularities never appear in the interesting dynamical processes.

[18] See for example: N.Kaloper, Phys.Lett.B434 285(1998); Y.Myung, N.Kim and H.Lee, Mod.Phys.Lett.A14 575(1999); N.Deger, A.Kaya, E.Sezgin and P.Sundell, hep-th/9908089

Aspects of black hole entropy

Shinji Mukohyama [1]

Department of Physics and Astronomy, University of Victoria
Victoria, BC, Canada V8W 3P6
and
Canadian Institute for Theoretical Astrophysics, University of Toronto
Toronto, ON, M5S 3H8

Abstract

There have been many attempts to understand the statistical origin of black-hole entropy. Among them, entanglement entropy and the brick wall model are strong candidates. In this paper, first, we show that the entanglement approach reduces to the brick wall model when we seek the maximal entanglement entropy. After that, the stability of the brick wall model is analyzed in a rotating background. It is shown that in the Kerr background without horizon but with an inner boundary a scalar field has complex-frequency modes and that, however, the imaginary part of the complex frequency can be small enough compared with the Hawking temperature if the inner boundary is sufficiently close to the horizon, say at a proper altitude of Planck scale. Hence, the brick wall model is well defined even in a rotating background if the inner boundary is sufficiently close to the horizon. These results strongly suggest that the entanglement approach is also well defined in a rotating background.

1 Introduction

Black hole entropy is given by a mysterious formula called the Bekenstein-Hawking formula [1, 2]: $S_{BH} = A/4l_{pl}^2$, where A is area of the horizon. There have been many attempts to understand the statistical origin of the black-hole entropy [3].

Entanglement entropy [4, 5] is one of the strongest candidates of the origin of black hole entropy. It is originated from a direct-sum structure of a Hilbert space of a quantum system: for an element $|\psi\rangle$ of the Hilbert space $\mathcal{F}$ of the form

$$\mathcal{F} = \mathcal{F}_I \bar{\otimes} \mathcal{F}_{II}, \tag{1}$$

the entanglement entropy S_{ent} is defined by

$$S_{ent} = -\mathrm{Tr}_I[\rho_I \ln \rho_I], \quad \rho_I = \mathrm{Tr}_{II}|\psi\rangle\langle\psi|. \tag{2}$$

Here $\bar{\otimes}$ denotes a tensor product followed by a suitable completion and $\mathrm{Tr}_{I,II}$ denotes a partial trace over $\mathcal{F}_{I,II}$, respectively.

On the other hand, there is another strong candidate for the origin of black hole entropy: the brick wall model introduced by 'tHooft [6]. In this model, thermal atmosphere in equilibrium with a black hole is considered. In this situation, we encounter with two kinds of divergences in physical quantities. The first is due to infinite volume of the system and the second is due to infinite blue shift near the horizon. We are not interested in the first since it represents contribution from matter in the far distance. Hence we introduce an outer boundary in order to make our system finite. It is the second divergence that we would like to associate with black hole entropy. Namely, it can be shown by introducing a Planck scale cutoff that entropy of the thermal atmosphere near the horizon is proportional to the area of the horizon in Planck units.

In this paper, first, we show that the brick wall model seeks the maximal value of the entanglement entropy. In other words, the entanglement approach reduces to the brick wall model when we seek the maximal value of the entanglement entropy. After that, we analyze the stability of the brick wall model in a rotating background. We show that the time scale of the ergoregion instability is much longer than

[1] E-mail:mukoyama@uvic.ca

the relaxation time scale of the thermal state with the Hawking temperature. In the latter time scale ambient fields should settle in the thermal state. Thus, the brick wall model is well defined even in a rotating background. These results strongly suggest that the entanglement approach is also well defined in a rotating background.

This paper is organized as Follows. In Sec. 2 the relation between the entanglement entropy and the brick wall model is shown. In Sec. 3 the stability of the brick wall model is analyzed in the Kerr background. Sec. 4 is devoted to a summary of this paper.

2 Brick wall entropy as maximal entanglement entropy

For simplicity, we consider a minimally coupled, real scalar field described by the action

$$S = -\frac{1}{2}\int d^4x\sqrt{-g}\left[g^{\mu\nu}\partial_\mu\phi\partial_\nu\phi + \mu^2\phi^2\right], \tag{3}$$

in a spherically symmetric, static black-hole space-time

$$ds^2 = -f(r)dt^2 + \frac{dr^2}{f(r)} + r^2 d\Omega^2. \tag{4}$$

We denote the area radius of the horizon by r_0 and the surface gravity by κ_0 ($\neq 0$):

$$f(r_0) = 0, \quad \kappa_0 = \frac{1}{2}f'(r_0). \tag{5}$$

We quantize the system of the scalar field with respect to the Killing time t in a Kruskal-like extension of the black hole spacetime. The corresponding ground state is called the Boulware state and its energy density is known to diverge near the horizon. Although we shall only consider states with bounded energy density, it is convenient to express these states as excited states above the Boulware ground state for technical reasons. Hence, we would like to introduce an ultraviolet cutoff α with dimension of length to control the divergence. The cutoff parameter α is implemented so that we only consider two regions satisfying $r > r_1$ (shaded regions I and II in *Figure* 1), where r_1 ($> r_0$) is determined by

$$\alpha = \int_{r_0}^{r_1}\frac{dr}{\sqrt{f(r)}}. \tag{6}$$

[Evidently, the limit $\alpha \to 0$ corresponds to the limit $r_1 \to r_0$. Thus, in this limit, the whole region in which $\partial/\partial t$ is timelike is covered.] Strictly speaking, we also have to introduce outer boundaries, say at $r = L$ ($\gg r_0$), to control the infinite volume of the constant-t surface. However, even if there are outer boundaries, the following arguments still hold.

In this situation, there is a natural choice for division of the system of the scalar field: let $\mathcal{H}_I$ be the space of mode functions with supports in the region I and $\mathcal{H}_{II}$ be the space of mode functions with supports in the region II. Thence, the space $\mathcal{F}$ of all states are of the form (1), where $\mathcal{F}_I$ and $\mathcal{F}_{II}$ are defined as symmetric Fock spaces constructed from $\mathcal{H}_I$ and $\mathcal{H}_{II}$, respectively:

$$\mathcal{F}_{I,II} \equiv \mathbf{C} \oplus \mathcal{H}_{I,II} \oplus (\mathcal{H}_{I,II}\otimes\mathcal{H}_{I,II})_{sym} \oplus \cdots. \tag{7}$$

Here $(\cdots)_{sym}$ denotes the symmetrization.

Let us investigate what kind of condition should be imposed for our arguments to be self-consistent. A clear condition is that the backreaction of the scalar field to the background geometry should be finite. For the brick wall model this condition is satisfied. Namely, in Ref. [7], it was shown that the total mass of the thermal atmosphere of quantum fields is actually bounded. Thus, also for our system, we would like to impose the condition that the contribution ΔM of the subsystem $\mathcal{F}_I$ to the mass of the geometry should be bounded in the limit $\alpha \to 0$.

It is easily shown that ΔM is given by

$$\Delta M \equiv -\int_{x\in I} T_t^t 4\pi r^2 dr = H_I, \tag{8}$$

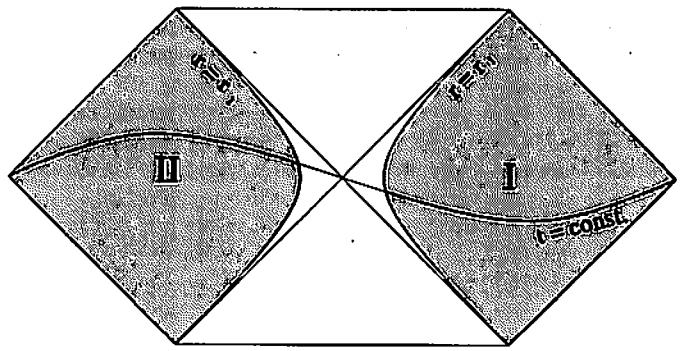

Figure 1: The Kruskal-like extension of the static, spherically symmetric black-hole spacetime. We consider only the regions satisfying $r > r_1$ (the shaded regions I and II).

where H_I is the Hamiltonian of the subsystem $\mathcal{F}_I$ with respect to the Killing time t. Hence, the expectation value of ΔM with respect to a state $|\psi\rangle$ of the scalar field is decomposed into the contribution of excitations and the contribution from the zero-point energy:

$$\langle\psi|\Delta M|\psi\rangle = E_{ent} + \Delta M_B, \tag{9}$$

where E_{ent} is entanglement energy defined by

$$E_{ent} \equiv \langle\psi| : H_I : |\psi\rangle, \tag{10}$$

and ΔM_B is the zero-point energy of the Boulware state. Here, the colons denote the usual normal ordering. [This definition of entanglement energy corresponds to $E_{ent}^{(I')}$ in Ref. [8] and $\langle : H_2 : \rangle$ in Ref. [3].]

Since the Boulware energy ΔM_B diverges as $\Delta M_B \sim -AT_H\alpha^{-2}$ in the limit $\alpha \to 0$ [7], we should impose the condition

$$E_{ent} \simeq |\Delta M_B|, \tag{11}$$

where $A = 4\pi r_0^2$ is the area of the horizon, $T_H = \kappa_0/2\pi$ is the Hawking temperature. We call this condition *the small backreaction condition (SBC)*. Note that the right hand side of SBC (11) is independent of the state $|\psi\rangle$.

Now, we shall show that the Hartle-Hawking state is a maximum of the entanglement entropy in the space of quantum states satisfying SBC. For this purpose, we have a more general statement for a quantum system with a state-space of the form (1): *a state of the form*

$$|\psi\rangle = \mathcal{N}\sum_n e^{-E_n/2T}|n\rangle_I \otimes |n\rangle_{II} \tag{12}$$

is a maximum of the entanglement entropy in the space of states with fixed expectation value of the operator E_I defined by

$$E_I = \left(\sum_n E_n|n\rangle_I \cdot {}_I\langle n|\right) \otimes \left(\sum_m |m\rangle_{II} \cdot {}_{II}\langle m|\right), \tag{13}$$

provided that the real constant T is determined so that the expectation value of E_I is actually the fixed value. Here, $\{|n\rangle_I\}$ and $\{|n\rangle_{II}\}$ $(n = 1, 2, \cdots)$ are bases of the subspaces $\mathcal{F}_I$ and $\mathcal{F}_{II}$, respectively, and E_n are assumed to be real and non-negative. (For a proof of this statement, see Ref. [9].) Note that this statement is almost the same as the following statement in statistical mechanics: a canonical state is a maximum of statistical entropy in the space of states with fixed energy, provided that the temperature of the canonical state is determined so that the energy is actually the fixed value.

Note that the expectation value of E_I is equal to the entanglement energy (10), providing that $|n\rangle_I$ and E_n are an eigenstate and an eigenvalue of the normal-ordered Hamiltonian $:H_I:$ of the subsystem $\mathcal{F}_I$. Hence, for the system of the scalar field, the above general statement insists that the state (12) is a maximum of the entanglement entropy in the space of states satisfying SBC, which corresponds to fixing the entanglement entropy. Off course, in this case, the constant T should be determined so that SBC (11) is satisfied. The value of T is easily determined as $T = T_H$ by using the well-known fact that the negative divergence in the Boulware energy density can be canceled by thermal excitations if and only if temperature with respect to the time t is equal to the Hawking temperature.

Finally, we obtain the statement that the Hartle-Hawking state [11] is a maximum of entanglement entropy in the space of quantum states satisfying SBC since the Hartle-Hawking state is actually of the form (12) with $T = T_H$ [12]. [Strictly speaking, in order to obtain the Hartle-Hawking state, we have to take the limit $\alpha \to 0$ (and $L \to \infty$). However, the following arguments still hold for a finite value of α (and L).] The corresponding reduced density matrix is the thermal state with temperature equal to the Hawking temperature. Therefore, the maximal entanglement entropy is equal to the thermal entropy with the Hawking temperature, which is sought in the brick wall model.

In summary the brick wall model seeks the maximal value of entanglement entropy [9, 14]. In other words, the entanglement approach reduces to the brick wall model when we seek the maximal entanglement entropy.

3 Stability of the brick wall model in a rotating background

Originally, the brick wall model was proposed in a spherically symmetric, static background, say, the Schwarzschild background. Hence, it seems interesting to see how this model is extended to a rotating background, say, the Kerr background [15, 16, 17, 18]. However, it is known that in a rapidly rotating spacetime without horizon a field has complex-frequency modes [19, 20] and that there is the so called ergoregion instability [21]. Thus, it might be expected that the brick-wall model in rotating background might be unstable and unsuitable for the origin of black hole entropy.

For simplicity, let us consider the Kerr spacetime as a background. The metric is given by

$$ds^2 = -\left(1 - \frac{2Mr}{\Sigma}\right)dt^2 + \frac{\Sigma}{\Delta}dr^2 + \Sigma d\theta^2 + R^2\sin^2\theta d\varphi^2 - \frac{4Mar}{\Sigma}\sin^2\theta d\varphi dt, \tag{14}$$

where

$$\begin{aligned} \Sigma &= r^2 + a^2\cos^2\theta, \\ \Delta &= r^2 + a^2 - 2Mr, \\ \Sigma R^2 &= (r^2 + a^2)^2 - a^2\Delta\sin^2\theta. \end{aligned} \tag{15}$$

We only consider the region $r \geq r_1$ in this spacetime: we impose the Dirichlet boundary condition on the field ϕ at $r = r_1$. (For more general boundary conditions, see Ref. [22].) Hereafter we assume that $r_1 > M + \sqrt{M^2 - a^2}$: there is no horizon in the region $r \geq r_1$.

It is well known that in this background the field equation of a massless real (Klein-Gordon) scalar field becomes separable. In fact, we can find a solution of the field equation of the form

$$f = \frac{u(r)}{\sqrt{r^2 + a^2}}S(\theta), \tag{16}$$

where S satisfies

$$\frac{1}{\sin\theta}\frac{d}{d\theta}\left(\sin\theta\frac{dS}{d\theta}\right) + \left[\lambda - a^2\mu^2(y^2 - 1)\sin^2\theta - \frac{m^2}{\sin^2\theta}\right]S = 0, \tag{17}$$

and the equation for u can be written as

$$\frac{d^2u}{dx^2} + (y - V_+)(y - V_-)u = 0 \tag{18}$$

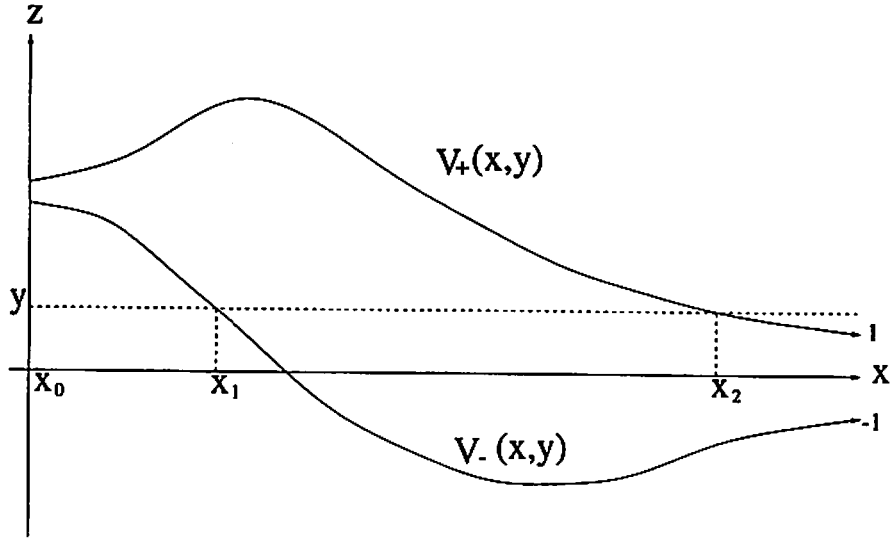

Figure 2: The typical form of the graphs $z = V_{\pm}(x, y)$ is written on a fixed y plane. Note that $V_{\pm}$ depend on y as well as x through the eigen value λ of equation (17). However, asymptotic behavior of $V_{\pm}$ in the limit $x \to \pm\infty$ does not depend on y.

by introducing the non-dimensional tortoise coordinate x by

$$\mu^{-1}\frac{dx}{dr} = \frac{r^2+a^2}{\Delta}, \tag{19}$$

or

$$\mu^{-1}x = r + \frac{M}{\sqrt{M^2-a^2}}\left[r_+ \ln\left(\frac{r-r_+}{r_+-r_-}\right) - r_- \ln\left(\frac{r-r_-}{r_+-r_-}\right)\right]. \tag{20}$$

Here, μ is the mass of the scalar field, $r_{\pm} = M \pm \sqrt{M^2-a^2}$, $y \equiv \omega/\mu$ and $V_{\pm}$ are defined by

$$\begin{aligned} \mu V_{\pm} &= \frac{2maMr}{(r^2+a^2)^2} \pm \sqrt{\frac{\Delta\bar{\mu}^2}{r^2+a^2}}, \\ \bar{\mu}^2 &= \mu^2 + \frac{\lambda}{(r^2+a^2)} - \frac{m^2a^2(r^2+a^2+2Mr)}{(r^2+a^2)^3} + \frac{2Mr+a^2}{(r^2+a^2)^2} - \frac{6Ma^2r}{(r^2+a^2)^3}. \end{aligned} \tag{21}$$

Note that in the horizon limit $r \to r_+$ (or $x \to -\infty$) both of $V_{\pm}$ approach to the same value

$$V_{\pm} \to \frac{ma}{2\mu M r_+}, \tag{22}$$

and that $V_{\pm}$ approaches to ± 1, respectively, in the limit $r \to \infty$ (or $x \to \infty$). (See Fig. 2.)

In Ref. [23], the existence of complex frequency modes was shown by examining a scattering amplitude for real-frequency waves. The strategy is based on the following expected form of the scattering amplitude S near a pole $y = y_R + iy_I$, providing that $|y_R| \gg |y_I|$ [20].

$$S = e^{2i\delta_0} \times \frac{y - y_R + iy_I}{y - y_R - iy_I}, \tag{23}$$

where δ_0 is a constant phase. Hence, if we can obtain this form of a scattering amplitude by analyzing real-frequency waves then we find an outgoing normal mode corresponding to $y = y_R + iy_I$ and an

incoming normal mode corresponding to $y = y_R - iy_I$. After that we should investigate whether these normal modes converge or diverge in the limit of $x \to \infty$. If these normal modes converge then they give complex-frequency mode functions.

By analyzing Eq. (18) in the WKB approximation and using the above strategy, we can obtain the following results [23].

(a) When $ma > 2\mu M r_+$ and $1 < y < V_-(x_1)$, we obtain a set of complex-frequency modes. However, the imaginary part $\Im\omega$ of the complex frequency is small enough:

$$T_{BH}^{-1}\Im\omega \sim \pm\pi e^{-2\eta}\left|\ln\left(\frac{r_1 - r_+}{r_+ - r_-}\right)\right|^{-1} \to 0 \quad (r_1 \to r_+), \tag{24}$$

where T_{BH} is the Hawking temperature of the Kerr background.

(b) When $ma < -2\mu M r_+$ and $V_+(x_1) < y < -1$, we obtain a set of complex-frequency modes. However, the imaginary part $\Im\omega$ of the complex frequency is small enough:

$$T_{BH}^{-1}\Im\omega \sim \pm\pi e^{-2\eta}\left|\ln\left(\frac{r_1 - r_+}{r_+ - r_-}\right)\right|^{-1} \to 0 \quad (r_1 \to r_+). \tag{25}$$

(c) In other cases, there is no complex-frequency modes.

In this section we have shown that in the Kerr background without horizon but with an inner boundary a scalar field has complex-frequency modes and that the imaginary part of the complex frequency is small enough compared with the Hawking temperature if the inner boundary is sufficiently close to the horizon, say at a proper altitude of Planck scale. Hence, the time scale of the ergoregion instability is much longer than the relaxation time scale of the thermal state with the Hawking temperature. In the latter time scale ambient fields should settle in the thermal state. In this sense ergoregion instability is not so catastrophic. Thus, the brick wall model is well defined if the inner boundary is sufficiently close to the horizon.

4 Summary and discussion

In this paper we have analyzed the entanglement entropy and the brick wall model. In Sec. 2 we have shown that the entanglement approach reduces to the brick wall model when we seek the maximal value of the entanglement entropy. In Sec. 3 we have shown that the brick wall model is well defined even in a rotating background. These two results strongly suggest that the entanglement approach is also well defined in a rotating background.

References

[1] J. D. Bekenstein, Phys. Rev. **D7**, 949 (19973).

[2] S. W. Hawking, Commun. Math. Phys. **43**, 199 (1975).

[3] S. Mukohyama, *"The origin of black hole entropy"*, Doctoral thesis, gr-qc/9812079.

[4] L. Bombelli, R. K. Koul, J. Lee and R. D. Sorkin, Phys. Rev. **D34**, 373 (1986).

[5] M. Srednicki, Phys. Rev. Lett. **71**, 666 (1993).

[6] G. 'tHooft, Nucl. Phys. **B256**, 727 (1985).

[7] S. Mukohyama and W. Israel, Phys. Rev. **D58**, 104005 (1998).

[8] S. Mukohyama, M. Seriu and H. Kodama, Phys. Rev. **D58**, 064001 (1998).

[9] S. Mukohyama, *"Hartle-Hawking state is a maximum of entanglement entropy"*, gr-qc/9904005, to appear in Phys. Rev. **D**.

[10] S. Mukohyama, Phys. Rev. **D58**, 104023 (1998).

[11] J. B. Hartle and S. W. Hawking, Phys. Rev. **D13**, 2188 (1976).

[12] W. Israel, Phys. Lett. **57A**, 107 (1976).

[13] S. Mukohyama, M. Seriu and H. Kodama, Phys. Rev. **D55**, 7666 (1997).

[14] S. Mukohyama, *"Entanglement/Brick-wall entropies correspondence"*, gr-qc/9907090, to appear in Proceedings of the 8th Canadian Conference on General Relativity and Relativistic Astrophysics.

[15] M. H. Lee and J. K. Kim, Phys. Rev. **D54**, 3904 (1996).

[16] J. Ho, W. T. Kim, Y. J. Park, and H. Shin, Class. Quant. Grav. **14**, 2617 (1997).

[17] J. Ho and G. Kang, Phys. Lett. **B445**, 27 (1998).

[18] V. P. Frolov and D. V. Fursaev, *"Statistical Mechanics of Axially-Symmetric Spacetimes with the Killing Horizon and Entropy of Rotating Black Holes in Induced Gravity"*, gr-qc/9907046.

[19] H. Sato and K. Maeda, Prog. Theo. Phys. **59**, 1173 (1978).

[20] N. Comins and B. F. Schutz, Proc. R. Soc. Lond. **A364**, 211 (1978).

[21] G. Kang, Phys. Rev. **D55**, 7563 (1997).

[22] S. N. Solodukhin, Phys. Rev. **D56**, 4968 (1997).

[23] S. Mukohyama, *"Is the brick-wall model unstable for a rotating background?"*, gr-qc/9910013.

Black hole entropy in the Membrane Paradigm

Takeshi Shimomura[1]

Department of Physics, Tokyo Institute of Technology,
Oh-okayama, Meguro-ku, Tokyo 152-8550, Japan

Takashi Okamura[2]

Department of Physics, Ochanomizu University,
1-1 Otsuka, 2 Bunkyo-ku, Tokyo 112-8610, Japan

Takashi Mishima[3]

Laboratories of Physics, College of Science and Technology,
Nihon University, Narashinodai, Funabashi, Chiba 274, Japan

Abstract

We study whether the black hole entropy can be understood in terms of physical properties of the membrane in the Membrane Paradigm. In particular, we calculate the entropy of the fluid membrane for generalized Einstein-Maxwell theory and higher curvature gravity theory within this framework and compare it with those derived by using the Noether charge method.

1 Introduction

There are many candidates for the statistical origin of the black hole entropy. In particular, the derivation of the black hole entropy $S_{BH} = A/4$ (A is the surface area of the black hole) [1] by counting the black hole microstates achieved remarkable results for some class of black holes, recently [2]. It might be true that, in order to understand the black hole entropy fully, we must know the quantum theory of gravity. However, it is widely believed that general feature of the black hole entropy can be understood by semiclassical approach, i.e., quantum field theory on fixed background. In fact, several attempts along this line was made in Refs. [3, 4]. Since the notion of the horizon is definite in semiclassical theory, the presence of the horizon as the boundary of information inside which we cannot see (or the boundary surface that is infinitely red-shifted) has an important role for the explanation of the black hole entropy at least in semiclassical theory.

On the other hand, aside from the entropy, there is a convenient view on black hole physics called membrane paradigm: The horizon of the black hole is replaced by a stretched horizon , which is viewed as a (2+1) dimensional time-like surface located slightly outside the true horizon in (3+1) dimensional spacetime and evolves in response to driving forces from the external universe. This membrane is regarded as, to an external observer, made from 2 dimensional viscous fluid that is electrically charged and has finite temperature. Further, this formalism can treat dynamical, evolving black holes and then the interaction of the membrane with the external universe is described in terms of familiar laws for the horizon's fluid, e.g., the Navier-Stokes equation, a tidal-force equation, Ohm's law, and so on. This view of a black hole as a dynamical timelike surface or membrane has been summarized in Ref. [5].

In this paper, we consider whether the black hole entropy can be understood in terms of physical properties of this fluid membrane. Of course, no direct insight into the statistical origins of black hole entropy can come from this approach. However, if the membrane paradigm is a effective description of

[1]E-mail:tshimomu@th.phys.titech.ac.jp
[2]E-mail:okamura@skymint.phys.ocha.ac.jp
[3]E-mail:tmishima@ns.phys.ge.cst.nihon-u.ac.jp

the black hole horizon to an external observer, we can expect that it accounts for such thermodynamic notions as entropy and then thermodynamics of the membrane can tell us its value.

In Section 2, we briefly summarize the action formulation of the membrane paradigm and gives several assumptions in order to calculate the entropy of the membrane in the following section. In Section 3, we calculate the entropy of the membrane by using the first law of thermodynamics and show that the desired results can be derived for the generalized Einstein-Maxwell theories and some class of higher curvature gravity theories. However, unfortunately, expected result cannot be obtained for the higher curvature gravity theories which involve the Ricci tensor terms explicitly. Section 4 is devoted to a summary and discussion of our results.

2 Action formulation for an external observer and several assumptions for membrane

The action formulation of the membrane paradigm has several advantage such as simplifying the derivations and making it easy when we extend this paradigm to the more general theories of gravity beyond the Einstein one. In this section, we reformulate the membrane paradigm as an action formulation [6].

Now since nothing can emerge from a black hole interior (classically), an observer who always stays outside the horizon cannot be affected by the dynamics inside the black hole. Thus, the physics for an external observer should be independent of the black hole interior and must follow from varying the action restricted to the spacetime outside the horizon. Hence, we rewrite the total action as

$$I_{total} = (I_{int} - I_{surf}) + (I_{ext} + I_{surf}), \tag{1}$$

where a surface term I_{surf} that cancel the residual boundary term is added to the external action in order to obtain the correct equation of motion. Therefore, we get the action principle for an external observer as

$$\delta I_{ext} + \delta I_{surf} = 0. \tag{2}$$

The added surface term I_{surf} corresponds to sources such as electromagnetic and gravitational ones residing on the stretched horizon. Although the sources are fictious ones, they are very useful article for an external observer and their presence is consistent with all external fields. In fact, an observer who remains outside the stretched horizon insist that the membrane is a perfectly real one.

The concrete application of Eq. (2) to the membrane interacting with the electromagnetic and gravitational fields was performed in Ref. [6]. It was shown that a dynamical membrane picture, obeying the Ohm's law and Navier-Stokes equation could be obtained as they were applied to the black holes.

In the next section, we calculate the entropy of a stationary fluid membrane located at the stretched horizon from a phenomenological point of view. In order to perform an actual calculation, we will here make several assumptions in advance.

We consider axisymmetric stationary geometries whose metric is of the form

$$ds^2 = -\alpha^2 dt^2 + \rho^2(d\psi - \Omega dt)^2 + q_{ab}dx^a dx^b. \tag{3}$$

where $(a,b) = (r,\theta)$. The lapse function α, the Bardeen angular velocity Ω, $(\psi\psi)$-component ρ^2 of the metric, and two dimensional metric q_{ab} are assumed to be functions of the coordinates $\{r,\theta\}$. The event horizon $r = r_+$ of the black hole is located at $\alpha(r_+) = 0$ and has area

$$\mathcal{A} = \int_{r_+} \sqrt{g_{\theta\theta}g_{\psi\psi}}d\theta d\psi. \tag{4}$$

This covers as special cases Schwarzschild, Reissner-Nordström and Kerr-Newman spacetimes.

When the fields the black hole interact with are not classical but quantum fields, the black hole radiates as a thermal black-body [7]. It can be understood as the fact that the zero angular momentum observers (ZAMOs [4]) located at fixed (r,θ), but move with angular velocity $d\psi/dt = \Omega$, in a black hole

[4]Hereafter, we call this observers FIDOs (hypersurface orthogonal fiducial observers) following Ref. [5]

spacetime sees the accelerated radiation whose temperature is given by [8, 9, 10]

$$T_{acc}(r) = \frac{a(r)}{2\pi} \equiv \frac{g_H}{2\pi\alpha}, \tag{5}$$

where the renormalized surface gravity g_H at the horizon is defined by using the null generator l^a as

$$l^c \nabla_c l^a = g_H l^a, \tag{6}$$

and α plays the role of redshift factor for this observer. Here, we assume that a membrane located at stretched horizon is in thermal equilibrium with the black hole and then its temperature is given by

$$T_m = T_{acc}(r_m) = \frac{1}{2\pi} a(r_m), \tag{7}$$

where r_m denotes the radial coordinate where stretched horizon, or membrane, is located. In fact, the FIDOs outside the horizon takes this picture: the horizon behaves as a membrane with very high temperature given by Eq. (7) [5]. Then, we further assume that both the first law of thermodynamics and the Gibbs-Duhem relation can be applied to this fluid membrane. The first law for the membrane is written as

$$T_m dS_m = d\mathcal{E}_m + P_m dA_m - \mathcal{Z}_m^{(\phi)} d\phi - \Phi_m dQ_m - \Omega_m d\mathcal{J}_m - \sum_i \mu_i d\mathcal{N}_i, \tag{8}$$

where Φ_m, Ω_m, ϕ and $\mathcal{Z}_m^{(\phi)}$, are the electric potential of the membrane, the angular momentum, intensive quantity as an external parameter and the corresponding generalized force, respectively. Although the physical significance of $\mathcal{N}_i$ and μ_i are irrelevant, for convenience we interpret them as the number of particles and the corresponding chemical potentials, respectively. The integrated Gibbs-Duhem relation [11] for the membrane is given by

$$S_m = \beta_m(\mathcal{E}_m + P_m A_m - \Phi_m Q_m - \Omega_m \mathcal{J}_m) - \sum_i \chi_i \mathcal{N}_i, \tag{9}$$

where $\beta_m = T_m^{-1}$, $\chi_i = \mu_i \beta_m$, respectively. Note that the quantity ϕ does not appear in this expression.

Next, we calculate the entropy of a fluid membrane for the generalized Einstein-Maxwell theories under these assumptions.

3 Entropy of fluid membrane

The most general action for 4 dimensional Einstein-Maxwell theory coupled to the scalar field ϕ is described by

$$I[g_{ab}, A_a, \phi] = \frac{1}{16\pi G} \int d^4x \sqrt{-g} \left[W(\phi) R + U(\phi)(\nabla\phi)^2 + V(\phi) + X(\phi) F^2 \right] + D_\infty, \tag{10}$$

where $W(\phi), U(\phi), V(\phi), X(\phi)$ are arbitrary functions of scalar field ϕ (but not contain derivative of the field), R is the Ricci scalar, F is the electromagnetic field strength, and D_∞ denotes the boundary terms at infinity which are necessary to obtain the equations of motion, respectively. We take Eq. (10) as the external action I_{ext}.

Varying this action with respect to arbitrary variations in g_{ab}, A_a and ϕ subject to the action principle for external observer (2), and evaluating it in the limit that the stretched horizon approaches the null horizon gives

$$\begin{aligned} \delta I_{ext}[g_{ab}, A_a, \phi] = & \frac{1}{16\pi G} \int d^4x \sqrt{-g} \left[A^{ab} \delta g_{ab} + B^a \delta A_a + C \delta\phi \right] \\ & - \frac{1}{16\pi G} \int d^3x \sqrt{-h} \left[W(K h^{ab} - K^{ab}) + n^c \partial_c W h^{ab} \right] \delta h_{ab} \\ & - \frac{1}{4\pi G} \int d^3x \sqrt{-h} X F^{ab} n_a \delta A_b - \frac{1}{8\pi G} \int d^3x \sqrt{-h} U n^c \partial_c \phi \delta\phi, \end{aligned} \tag{11}$$

where

$$A^{ab} = -WR^{ab} + \frac{1}{2}(WR + U(\nabla\phi)^2 + V)g^{ab} - U(\nabla^a\phi)(\nabla^b\phi) + \nabla^a\nabla^b W - \nabla^2 W g^{ab} - 2XF^a_c F^{cb} - \frac{1}{2}XF^2 g^{ab}, \quad (12)$$

$$B^a = -4\nabla_b(XF^{ba}), \quad (13)$$

$$\dot{C} = R\frac{\partial W}{\partial\phi} + \frac{\partial V}{\partial\phi} - 2\nabla^a(U\nabla_a\phi) + \frac{\partial U}{\partial\phi}(\nabla\phi)^2 + \frac{\partial X}{\partial\phi}F^2, \quad (14)$$

and h_{ab}, n^a are the determinant of the induced metric, the outward pointing spacelike unit normal to the stretched horizon, respectively.

While the bulk terms give the equations of motion, the residual boundary terms on the stretched horizon appear as it does the boundary of spacetime. We must add a surface terms that cancel these boundary terms to obtain the correct equations of motion. The variation of the required terms can be written as

$$\delta I_{surf}[h_{ab}, A_a, \phi] = +\frac{1}{16\pi G}\int d^3x\sqrt{-h}\left[W(Kh^{ab} - K^{ab}) + 2(n^c\partial_c W h^{ab} - n^a\partial^b W)\right]\delta h_{ab} + \frac{1}{4\pi G}\int d^3x\sqrt{-h}XF^{ab}n_a\delta A_b + \frac{1}{8\pi G}\int d^3x\sqrt{-h}Un^c\partial_c\phi\delta\phi. \quad (15)$$

Since we are interested in gravitational part of this source term, we vary (15) with respect to h_{ab} [12] and then get the surface stress tensor for gravity as

$$t_s^{ab} = \frac{2}{\sqrt{-h}}\frac{\delta I_{surf}}{\delta h_{ab}} = \frac{1}{8\pi G}\left[W(Kh^{ab} - K^{ab}) + 2(n^c\partial_c W h^{ab} - n^a\partial^b W)\right]. \quad (16)$$

The surface energy density and momentum surface density are defined by

$$\Sigma \equiv t_s^{ab}U_a U_b, \pi_A = -t_s^{ab}\gamma_{Aa}U_b, \quad (17)$$

where U^a and γ_{AB} denote FIDOs' four velocity and the 2 dimensional metric of the spacelike section of the stretched horizon, respectively.

We will see next that Eq. (16) can be regarded as the stress energy tensor of the two dimensional viscous fluid. To see this, note that both αU^a and αn^a approach the null generator l^a in the true horizon limit $\alpha \to 0$. Thus, αU^a and αn^a are equal in this limit, and then we can write the relevant components of K_{ab} in terms of the surface gravity g and the extrinsic curvature k_{AB} of a spacelike two section of the stretched horizon as [13]

$$K^U_U = g, \quad (18)$$

$$K^U_A = K^b_a\gamma^a_A U_b = -\Omega^H_A, \quad (19)$$

$$K^B_A = K^b_a\gamma^a_A\gamma^B_b = \alpha^{-1}k^B_A, \quad (20)$$

where $g \equiv g_H/\alpha$, Ω^H_A denotes the Hajicek field [14], which has the connection with the angular momentum J_m of the membrane via the relation (29), and k_{AB} is the extrinsic curvature of a spacelike two section of the true horizon defined by

$$k_{AB} \equiv \frac{1}{2}\mathcal{L}_{l^a}\gamma_{AB}. \quad (21)$$

Further, k_{AB} can be decomposed into a sum of a trace part and a traceless one as

$$k_{AB} = \sigma_{AB} + \frac{1}{2}\gamma_{AB}\theta, \quad (22)$$

where σ_{AB} and θ are the shear and expansion of the horizon, respectively.

Therefore, by using the relations (18)-(22), we can rewrite the surface stress tensor Eq. (16) as

$$t_s^{UU} = -\frac{1}{8\pi G}(W\theta + n^c\partial_c W), \tag{23}$$

$$t_s^{AU} = -\frac{1}{8\pi G}WK^{AU} = \frac{1}{8\pi G}W\Omega_H^A, \tag{24}$$

$$t_s^{AB} = \frac{1}{8\pi G}\left[-W\sigma^{AB} + (\frac{1}{2}W\theta + gW + n^c\partial_c W)\gamma^{AB}\right]. \tag{25}$$

These are just the stress energy tensor of a two dimensional viscous fluid with surface energy density Σ_m, surface pressure P_m, shear and bulk viscosity η_m and ζ_m, all as measured by the local static observer, given by

$$\Sigma_m = -\frac{1}{8\pi G}(W\theta + n^c\partial_c W), \tag{26}$$

$$P_m = \frac{1}{8\pi G}(gW + n^c\partial_c W), \tag{27}$$

$$\eta_m = \frac{W}{16\pi G}, \quad \zeta_m = -\frac{W}{16\pi G}. \tag{28}$$

Hence we may identify the horizon with a two dimensional dynamical fluid, or membrane. The fact that the bulk viscosity ζ_m is negative is connected with the acausael, teleological nature of a black hole horizon. Note that (AU)-component t_s^{AU} of the stress energy tensor is finite in the true horizon limit and gives the angular momentum of the membrane by the surface integral over the membrane

$$\mathcal{J}_m = \int_{r_m} \pi_A \xi^A d\mathcal{A}_m = \int_{r_m} (-\frac{1}{8\pi G}W\Omega_A^H)d\mathcal{A}_m, \tag{29}$$

where ξ^A denotes Killing vector field which generates a rotational symmetry.

Further, since we have assumed that the membrane is in thermal equilibrium, both the first law of thermodynamics and Gibbs-Duhem relation can be applied for the fluid membrane:

$$d\mathcal{S}_m = \beta_m(d\mathcal{E}_m + P_m d\mathcal{A}_m - \mathcal{Z}_m^{(\phi)}d\phi - \Phi_m dQ_m - \Omega_m d\mathcal{J}_m) - \sum_i \chi_i d\mathcal{N}_i, \tag{30}$$

$$\mathcal{S}_m = \beta_m(\mathcal{E}_m + P_m\mathcal{A}_m - \Phi_m Q_m - \Omega_m\mathcal{J}_m) - \sum_i \chi_i\mathcal{N}_i, \tag{31}$$

where

$$\mathcal{E}_m = \Sigma_m\mathcal{A}_m, \quad \Phi_m = \Phi(r_m), \quad \Omega_m = \Omega(r_m), \tag{32}$$

$$\mathcal{Z}_m^{(\phi)} = -\frac{1}{8\pi G}\frac{\partial W}{\partial\phi}g\mathcal{A}_m + \frac{\partial\Phi_m}{\partial\phi}Q_m + \frac{\partial\Omega_m}{\partial\phi}\mathcal{J}_m \tag{33}$$

are the mass of the membrane, electric potential and angular velocity, the generalized force corresponding to the scalar field ϕ, all as measured by FIDOs, respectively. Here, as the Eqs.(26)-(29) show, the scalar field ϕ plays the role of external parameter for the fluid membrane: The quantities which characterize the membrane, such as pressure and electric potential, depend on the scalar field ϕ via function $W(\phi)$. Thus, the term $\mathcal{Z}_m^{(\phi)}d\phi$ appears in the first law (30). Note that the physical significance of $\mathcal{N}_i$ and μ_i are irrelevant for our purpose: It is merely a mathematical implement to obtain a complete representation of the differential $d\mathcal{S}_m$ and have no more meaning then that.

Moreover, note that these expressions involve electric potential term corresponds to the fact that a black hole, or membrane, possesses a charge Q_m. The total charge Q_m is given by the integral of a surface charge q_m, which is determined by the electromagnetic source term, over the membrane as $Q_m = \int_{r_m} q_m d\mathcal{A}_m$. Although this term can be eliminated for a suitable choice of the chemical potential, it vanishes by imposing the regularity condition on the vector potential A_a at the horizon and then it does not appear in the expressions (30) and (31) in the true horizon limit: For a charged rotating black

hole with stationary axisymmetry, by using the gauge freedom, the electric field is described by the one form as

$$A_a dx^a = A_l(r)dl = -\frac{4\pi Q_m r_m}{\mathcal{A}_m} dl. \tag{34}$$

where l^a is defined by $l^a = k^a + \Omega(r_+)\xi^a$. In our description, in order that the action I_{surf} is a well-defined quantity, vector potential A_a must be bounded as measured by the local stationary frame on membrane. Hence, if we require that the stationary frame component of the potential one form $A_U = \alpha^{-1}A_l = \alpha^{-1}\Phi_m$ be bounded at the horizon, then because $\alpha(r_m) \to 0$ as $r \to r_+$, we must impose the regularity condition

$$A_l(r_m) = \Phi_m = 0 \quad \text{at the horizon} \quad r_m \to r_+. \tag{35}$$

It corresponds to the fact that we must shift the vector potential by using the gauge degrees of freedom such as it vanishes on the horizon in order to have a regular vector potential [15]. Therefore, we proceed our arguments with dropping this term below.

By using Eqs. (30) and (31), we get

$$\begin{aligned} \sum_i n_i d\chi_i &= \Sigma_m d\beta_m + d(\beta_m P_m) + \beta_m \mathcal{Z}_m^{(\phi)} d\phi - j_m d(\beta_m \Omega_m) \\ &= \frac{W\Sigma_m}{4G\gamma_m} d(\frac{1}{\Sigma_m}) + \beta_m j_m \frac{\partial \Omega_m}{\partial \phi} d\phi - j_m d(\Omega_m \beta_m), \end{aligned} \tag{36}$$

where $n_i = \mathcal{N}_i/\mathcal{A}_m$, $j_m = \mathcal{J}_m/\mathcal{A}_m$, $\gamma_m = gW/8\pi G\Sigma_m$, and we have used the explicit expression for β_m, P_m and $\mathcal{Z}_m^{(\phi)}$ in the second line. We must choose the functions n_i and χ_i subject to the restriction Eq. (36) in order that the right hand side of the Eq. (30) is a complete representation of the differential $d\mathcal{S}_m$. Here we take the simplest choice as follows:

$$\tilde{n}_1 = \frac{W\Sigma_m}{4G\gamma_m}, \quad \tilde{\chi}_1 = \frac{1}{\Sigma_m}, \tag{37}$$

$$\tilde{n}_2 = \beta_m j_m \frac{\partial \Omega_m}{\partial \phi}, \quad \tilde{\chi}_2 = \phi, \tag{38}$$

$$\tilde{n}_3 = -j_m, \quad \tilde{\chi}_3 = \beta_m \Omega_m, \tag{39}$$

Then, in this case, we get the relations for the chemical potentials as

$$\tilde{n}_1 \tilde{\mu}_1 = \Sigma_m, \tag{40}$$

$$\tilde{n}_2 \tilde{\mu}_2 = j_m \phi \frac{\partial \Omega_m}{\partial \phi}, \tag{41}$$

$$\tilde{n}_3 \tilde{\mu}_3 = -j_m \Omega_m \beta_m. \tag{42}$$

Hence, by substituting the Eqs. (40) - (42) into Eq. (31), we obtain the entropy of the fluid membrane as

$$\begin{aligned} \tilde{\mathcal{S}}_m &= \frac{\mathcal{A}_m}{4G_{eff}}(1 - \frac{1}{\gamma_m}(1 + \frac{J_m \phi}{\Sigma_m}\frac{\partial \Omega_m}{\partial \phi})) \\ &= \frac{\mathcal{A}}{4G_{eff}} \quad \text{as} \quad r_m \to r_+, \end{aligned} \tag{43}$$

where $G_{eff} \equiv G/W(\phi_+)$ is the effective gravitational constant in this theory. That is, the entropy of fluid membrane is one-quarter of its area (the Bekenstein-Hawking entropy) with effective gravitational constant. This result coincides with the black hole entropy which is derived by applying the Noether charge method to the theory (10).

Next, we study how sensitive is the result (43) to the choice of the functions n_i and χ_i. The general functions n_i and χ_i satisfying Eq. (36) are obtained by the following replacement:

$$\chi_i = f_i(\tilde{\chi}_i), \quad n_i = \frac{\tilde{n}_i}{f_i'(\tilde{\chi}_i)} \;\; ; \;\; i = 1, 2, \tag{44}$$

where f_i are arbitrary functions of $\tilde{\chi}_i$. This yields the relations

$$\frac{\mu_1 n_1}{\Sigma_m} = \frac{f_1}{\tilde{\chi}_1 f_1'}, \quad \frac{\mu_2 n_2}{j_m \frac{\partial \Omega_m}{\partial \phi}} = \frac{f_2}{f_2'}, \quad \frac{\mu_3 n_3}{j_m \Omega_m} = -\frac{f_3}{\tilde{\chi}_3 f_3'}, \tag{45}$$

Therefore, by using these Eqs. (44) and (45), the general expression for the entropy of the fluid membrane is given by

$$S_m = \frac{A_m}{4G_{eff}}[1 - \frac{1}{\Sigma_m \gamma_m}(\sum_i \mu_i n_i + \Omega_m j_m)]. \tag{46}$$

It shows that the result (43) is invariant, provided that the transformations (44) satisfy

$$\lim_{\beta_m \to 0} \beta_m \mu_i n_i = 0 \ ; \ i = 1, 2, 3. \tag{47}$$

Then, although it is not certain whether the transformations which violate the relation (47) are allowed or not, we can say that our result is valid for the broad class of choice for the functions n_i and χ_i which we assume for the membrane.

Finally we comment briefly on the entropy of black holes in higher curvature gravity theories. It is obvious that the above arguments can be applied, without changing any essential point, to the theory where the action is given by the form

$$I[g_{ab}] = \frac{1}{16\pi G}\int d^4x\sqrt{-g}f(\phi, g_{ab}, R) + D_\infty, \tag{48}$$

where the Lagrangian f is an arbitrary function of the scalar field ϕ, the metric g_{ab}, and a polynomial in the Ricci scalar R. This covers as special cases the constant curvature spacetimes. However, when the theory involves the Ricci tensor explicitly, things are not so simple. In fact, we can show that even in the case where the theory involves the quadratic term in Ricci tensor, the resultant entropy in our method does not coincide with that derived by using the Noether charge method. It might suggest that the membrane picture for the black hole physics breaks down for the general higher curvature gravity theories.

4 Summary and discussion

In this paper, we examined whether the black hole entropy can be understand in terms of physical properties of the fluid membrane. In particular, we used the first law of thermodynamics, or the integrated Gibbs-Duhem relation, for the membrane to derive the black hole entropy and compared it with those derived by the Noether charge method. We verified that the expected value of the entropy could be obtained for generalized Einstein-Maxwell theories and some class of higher curvature gravity theories within this framework. However, unfortunately, our methods do not give the desired result which is expected from the Noether charge method for the higher curvature gravity theories which involve the Ricci tensor terms explicitly. Although we concentrated only on the entropy in this paper, it is interesting to study how the Navier-Stokes equation, a tidal-force equation, and so on, are modified for the generalized theories of gravity and consider how these equations are interpreted for these theories.

Finally, we comment briefly on the entropy of dynamical black hole. If the black hole evolves dynamically, the shear and expansion of the corresponding fluid membrane take non-zero values and they are contribute to its entropy. However, in the membrane paradigm, since the problem in non-equilibrium black holes is replaced by the non-equilibrium thermodynamics of fluid membrane, whose properties are known better then those in black holes, it is tractable then those in non-equilibrium black hole physics. This is a future work of our research.

References

[1] J. D. Bekenstein, Phys. Rev. D7, 2333 (1973).

[2] A. Strominger and C. Vafa, Phys. Lett. **B379**, 99 (1996); G. Horowitz, "The Origin of Black Hole Entropy in String Theory", gr-qc/9604051.

[3] G. 'tHooft, Nucl. Phys. **B256**,727 (1985).

[4] M. Srednicki, Phys. Rev. Lett. **B71**, 666 (1993); C. Callan and F. Wilczek, Phys. Rev. Lett. **B333**, 55 (1994).

[5] K. S. Thorne, R. H. Price, and D. A. Macdonald, in *Black Holes: The Membrane Paradigm* (Yale University Press, New Haven, Connecticut, 1986).

[6] M. K. Parikh and F. Wilczek, Phys. Rev. **D58**, 064011 (1998).

[7] S. W. Hawking, Commun. Math. Phys. **43**, 199 (1975).

[8] W. G. Unruh, Phys. Rev. **D14**, 870 (1976).

[9] W. G. Unruh and R. M. Wald, Phys. Rev. **D29**, 1047 (1984).

[10] V. P. Frolov and K. S. Thorne, Phys. Rev. **D39**, 2125 (1989).

[11] For example, F. Reif, *Fundamentals of statistical and thermal physics* (McGraw-Hill, 1965).

[12] J. D. Brown and J. W. York, Jr., Phys. Rev. **D47**, 1407 (1993).

[13] R. H. Price and K. S. Thorne, Phys. Rev. **D33**, 915 (1986).

[14] P. Hajicek, J. Math. Phys. **15**, 1554 (1974).

[15] G. W. Gibbons and S. W. Hawking, Phys. Rev. **D15**, 2752 (1977).

[16] F. Pretorius, D. Vollick, and W. Israel, Phys. Rev. **D57**, 6311 (1998).

Motion of Cosmic String coupled to Gravitational Wave

Kouji Nakamura,[1] Akihiro Ishibashi[2*] and Hideki Ishihara[3**]

[*] *Department of Physics, Keio University, Hiyoshi, Yokohama 223-8521, Japan*

[**] *Yukawa Institute for Theoretical Physics, Kyoto University, Sakyo-ku, Kyoto 606-8502, Japan*

[***] *Tokyo Institute of Technology, Oh-Okayama Meguro-ku, Tokyo 152-0033, Japan*

Abstract

We study the dynamics of a gravitating thin Nambu-Goto string within the linear perturbation framework. To avoid singular spacetime, we first consider the perturbation around a thick string which is characterized by the specific energy momentum tensor. Considering the situation in which the thickness of the string is much smaller than the wavelength of gravitational waves or the scales of internal fluctuations, we obtain the dynamics of a self-gravitating thin Nambu-Goto string. We conclude that the "cosmic string traveling wave" is the unique solution which is independent of the internal fluctuations of the string and describes continuous string oscillations.

1 Introduction

There are significant interests in topological defects formed during phase transition in the early universe[1, 2]. In particular, it has been thought that these defects radiate gravitational wave by their rapid oscillation[3]. Thus, it is crucially important to study the precise dynamics of the defects and their gravitational effects.

In the simplest case, the defects are idealized by the infinitesimally thin Nambu-Goto membranes, i.e., their dynamics is governed by the minimization of their world hyper-volume. If the self-gravity of membranes is ignored (test membrane case), the Nambu-Goto action admits oscillatory solutions. It is considered that the test membranes gradually lose their kinetic energy by the gravitational wave emission[3]. However, by taking into account the self-gravity of the Nambu-Goto wall, it is shown that a self-gravitating wall coupled to gravitational wave behaves in a quite different manner[4].

How about self-gravitating Nambu-Goto strings? In this article, we consider the perturbation of the self-gravitating, straight and thin Nambu-Goto string. Since there is no simple prescription of an arbitrary line source where the metric becomes singular[5], we consider, first, a straight string with a finite thickness so that the singularity is regularized[1, 6]. We show that the perturbative equation of motion of the "thick string" has the same form as that derived from the Nambu-Goto action. We research all perturbations which are relevant to the Nambu-Goto string. Perturbations are classified into two types by their propagation. Considering the situation in which the thickness of string is much smaller than the wavelength of gravitational waves or the scale of internal fluctuations, we obtain the dynamics of a self-gravitating thin Nambu-Goto string. We conclude that the "cosmic string traveling wave" discussed in [7] is the unique solution which is independent of the internal fluctuations of the string and describes the continuous oscillations of a straight, thin Nambu-Goto string.

2 Regularized Self-Gravitating Nambu-Goto String

As the background for the perturbation, we consider a spacetime $(\mathcal{M}, g_{\mu\nu})$ containing a straight thick string. The surface $\mathcal{S}$ of the thick string divides $\mathcal{M}$ into two regions: $\mathcal{M}_{ex}$ and $\mathcal{M}_{in}$. Note that $\mathcal{M}_{in}$ describes the 'thick' world sheet of the string. We assume that the spacetime $\mathcal{M}$ is static and cylindrically

[1] E-mail:kouchan@phys-h.keio.ac.jp
[2] E-mail:akihiro@yukawa.kyoto-u.ac.jp
[3] E-mail:ishihara@th.phys.titech.ac.jp

symmetric. Then we divide $\mathcal{M}$ into two submanifolds so that $\mathcal{M} = \mathcal{M}_1 \times \mathcal{M}_2$ and write the background metric on $\mathcal{M}$ in the form

$$ds^2 = \gamma_{ab}dy^a dy^b + \eta_{pq}dz^p dz^q, \tag{1}$$

where γ_{ab}, the metric on $\mathcal{M}_1$, and η_{pq}, that on $\mathcal{M}_2$, are given by

$$\gamma_{ab}dy^a dy^b = d\rho^2 + r(\rho)^2 d\phi^2, \quad \eta_{pq}dz^p dz^q = -dt^2 + dz^2, \quad 0 \le \phi \le 2\pi. \tag{2}$$

We shall use the indices $a, ..., d$ for the tensors on $\mathcal{M}_1$ and $p, ..., s$ for that on $\mathcal{M}_2$. The string thickness is given by the circumference radius r_* of $\mathcal{S}$.

Since a Nambu-Goto string is characterized by a constant string tension σ_0, we consider the following energy-momentum tensor,

$$T_{\mu\nu} = -\sigma\eta_{\mu\nu}, \tag{3}$$

where $\sigma = \sigma_0$ for $r < r_*$ and $\sigma = 0$ for $r \ge r_*$ [1]. Here $\eta_{\mu\nu}$ is the four dimensional extension of η_{pq}.

The Einstein equations for the metric (1) and (2) are reduced to the single equation

$$\mathcal{R} = -2\frac{\partial_\rho^2 r}{r} = 16\pi G\sigma, \tag{4}$$

where $\mathcal{R}$ is the Ricci curvature on $\mathcal{M}_1$. The solution on $\mathcal{M}_{in} \cap \mathcal{M}_1$ is given by

$$\gamma_{ab}dy^a dy^b = \frac{dr^2}{1 - \hat{\alpha}^2 r^2} + r^2 d\phi^2, \quad \hat{\alpha}^2 = \frac{\mathcal{R}}{2} = 8\pi G\sigma_0, \tag{5}$$

and that on $\mathcal{M}_{ex} \cap \mathcal{M}_1$ is

$$\gamma_{ab}dy^a dy^b = \frac{dr^2}{(1-\alpha)^2} + r^2 d\phi^2, \tag{6}$$

where α is a deficit angle on $\mathcal{M}_{ex}$. These two solutions are joined along the surface $\mathcal{S}$ by Israel's junction condition[8]: $[K^\mu{}_\nu] := K^\mu{}_{\nu+} - K^\mu{}_{\nu-} = 0$, where $K^\mu{}_{\nu\pm}$ are the extrinsic curvature of $\mathcal{S}$ facing to $\mathcal{M}_{ex}$ and $\mathcal{M}_{in}$, respectively. For the solutions (5) and (6), this junction condition is reduced to $\alpha = 1 - \sqrt{1 - \hat{\alpha}^2 r_*^2}$.

3 Perturbative Equations

We consider the perturbations of the metric and the energy momentum tensor on the background geometry given by (1), (5) and (6). Let $h_{\mu\nu}$ be a perturbative metric and $t^\mu{}_\nu$ be a perturbed energy-momentum tensor. Since the metric η_{pq} on $\mathcal{M}_2$ is the two dimensional Minkowski metric, it is convenient to expand $h_{\mu\nu}$ and $t^\mu{}_\nu$ by the harmonics on $\mathcal{M}_2$. The harmonics are the eigen functions of the covariant derivative $\hat{D}_p$ associated with the metric η_{pq}. We classify the perturbations into two cases by the eigen value κ^2 of the differential operator $\eta^{pq}\hat{D}_p\hat{D}_q$: one is the $\kappa \neq 0$ case and the other is the $\kappa = 0$ case.

3.1 $\kappa \neq 0$ case

In this case, the independent tensor harmonics on $\mathcal{M}_2$ are given by as follows:

$$\begin{aligned} &S := e^{-i\omega t + ik_z z}, && V^p_{(e1)} := \eta^{pq}\hat{D}_q S, && V^p_{(o1)} := \epsilon^{pq}\hat{D}_q S, \\ &T_{(e0)pq} := \frac{1}{2}\eta_{pq}S, && T_{(e2)pq} := \left(\hat{D}_p\hat{D}_q - \tfrac{1}{2}\eta_{pq}D^r D_r\right)S, && T_{(o2)pq} := -\epsilon_{r(p}\hat{D}_{q)}\hat{D}^r S, \end{aligned} \tag{7}$$

where ϵ_{rs} is a two-dimensional antisymmetric tensor on $\mathcal{M}_2$, the symbols (o) and (e) refer to odd and even parity modes with respect to the inversion of (t, z), respectively. The eigen value of $\eta^{pq}\hat{D}_p\hat{D}_q$ is given by $\kappa^2 = \omega^2 - k_z^2$. By these tensor harmonics $h_{\mu\nu}$ and $t^\mu{}_\nu$ are expanded as follows:

$$h_{ab} = \int \left(F_{ab} + D_{(a}X_{b)}\right)S, \quad h_{ap} = \int \left\{\left(F_a + \tfrac{1}{2}D_a f_{(o2)}\right)V_{(o1)p} + \left(X_a + \tfrac{1}{2}D_a f_{(e2)}\right)V_{(e1)p}\right\}, \tag{8}$$

$$h_{pq} = \int \left\{f_{(o2)}T_{(o2)pq} + \left(F + \kappa^2 f_{(e2)}\right)T_{(e0)pq} + f_{(e2)}T_{(e2)pq}\right\}, \tag{9}$$

$$t^a{}_b = \int s^a{}_b S, \quad t^a{}_p = \int \left\{ s^a_{(o1)} V_{(o1)p} + \frac{1}{16\pi G} \left(V^a + \sigma X_a \right) V_{(e1)p} \right\}, \tag{10}$$

$$t^p{}_q = \int \left\{ s_{(o2)} T_{(o2)}{}^p{}_q + \frac{1}{16\pi G} \left(\Sigma - 2X^a D_a \sigma \right) T_{(e0)}{}^p{}_q + s_{(e2)} T_{(e2)}{}^p{}_q \right\}, \tag{11}$$

where $\int := \int d\omega dk_z$. The expansion coefficients are tensors on $\mathcal{M}_1$. The perturbative energy momentum tensor $t^\mu{}_\nu$ has its support only on $\mathcal{M}_{in}$. The variables F_{ab}, F_a, F are gauge invariant metric perturbation and the other variables in (8) and (9) are gauge dependent. V_a, Σ, $s^a{}_b$, $s^a_{(o1)}$, $s_{(o2)}$ $s_{(e2)}$ are all gauge invariant perturbations for the energy momentum tensor (3).

In this article, we consider the perturbative motion of a Nambu-Goto string, which is characterized by a constant string tension whose value is equal to the energy density. Then we concentrate only on Σ and V^a as the perturbation of the energy momentum tensor, since $\int \Sigma S$ and $i \int V^a \omega S$ are the perturbed energy density and the momentum perturbation of (3), which are induced by the string motion. We drop $s^a{}_b$, $s^a_{(o1)}$, $s_{(o2)}$ $s_{(e2)}$ in (10) and (11), which are irrelevant to the motion of a Nambu-Goto string as seen in the next section.

In terms of the gauge invariant variables, we write the linearized Einstein equations on $\mathcal{M}_{in}$: for odd modes,

$$D^a F_a = 0, \quad (\Delta + \kappa^2) F_a - D^c D_a F_c = 0, \tag{12}$$

and for even modes,

$$(\Delta + \kappa^2) F_{ab} = \mathcal{R} F_{ab} + 2 D_{(a} V_{b)} - \gamma_{ab} D_c V^c, \quad (\Delta + \kappa^2) F = 0, \tag{13}$$

$$D^c F_{ac} - \frac{1}{2} D_a F = V_a, \quad F^c{}_c = 0, \tag{14}$$

where $\Delta := D^a D_a$. The perturbative divergence of the energy momentum tensor are reduced to

$$\kappa^2 V^a + \frac{1}{2} \mathcal{R} D^a F = 0, \quad D_a V^a + \frac{1}{2} \Sigma = 0. \tag{15}$$

The first equation corresponds to the Euler equation and the second equation corresponds to the continuity equation for the energy density.

On $\mathcal{M}_{ex}$, the linearized Einstein equations are given by (12)-(14) with $\mathcal{R} = 0 = V^a$.

3.2 $\kappa = 0$ case

In this case, $V^p_{(o1)}$ and $T_{(o2)pq}$ fail to be independent of the other harmonics because the wave vector k_p defined by $D_p S = i k_p S$ is null: $k_p k^p = 0$. Then we introduce another null vector l_p and redefined the independent tensor harmonics on $\mathcal{M}_2$ as follows:

$$\begin{aligned} S &:= e^{-i\omega(t+\epsilon z)}, \qquad V^p_{(e1)} := \eta^{pq} D_q S, \qquad V^p_{(l1)} := i l^p S, \\ T_{(e0)pq} &:= \frac{1}{2} \eta_{pq} S, \qquad T_{(e2)pq} := D_p D_q S, \qquad T_{(l2)pq} := -l_p l_q S. \end{aligned} \tag{16}$$

where $\epsilon = \pm 1$ and l_p is defined by

$$l_p l^p = 0, \quad l_p k^p = -2\omega^2. \tag{17}$$

By these tensor harmonics, $h_{\mu\nu}$ and $t^\mu{}_\nu$ are expanded as follows:

$$h_{ab} = \int \left(H_{ab} + 2 D_{(a} X_{b)} \right) S, \quad h_{ap} = \int \left\{ \left(H_a + \frac{1}{4\omega^2} D_a f_{(e0)} \right) V_{(l1)p} + \left(X_a + \frac{1}{2} D_a f_{(e2)} \right) V_{(e1)p} \right\} \tag{18}$$

$$h_{pq} = \int \left\{ H T_{(l2)pq} + f_{(e0)} T_{(e0)pq} + f_{(e2)} T_{(e2)pq} \right\}. \tag{19}$$

$$t^a{}_b = \int s^a{}_b S, \quad t^a{}_p = \int \left\{ s^a_{(l1)} V_{(l1)p} + \frac{1}{16\pi G} \left(V^a + \sigma X_a \right) V_{(e1)p} \right\}, \tag{20}$$

$$t^p{}_q = \int \left\{ s_{(l2)} T_{(l2)}{}^p{}_q + \frac{1}{16\pi G} \left(\Sigma - 2X^a D_a \sigma \right) T_{(e0)}{}^p{}_q + s_{(e2)} T_{(e2)}{}^p{}_q \right\}, \tag{21}$$

where $\int := \Sigma_{\epsilon=\pm 1}\int d\omega$. The variables H_{ab}, H_a, H are gauge invariant metric perturbations and the other variables in (18) and (19) are gauge dependent. V_a, Σ, $s^a{}_b$, $s^a_{(l1)}$, $s_{(l2)}$ $s_{(e2)}$ are gauge invariant perturbations for the energy momentum tensor. Here again, we concentrate only on Σ and V^a as the perturbation of the energy momentum tensor and drop $s^a{}_b$, $s^a_{(l1)}$, $s_{(l2)}$ $s_{(e2)}$ in (20) and (21).

In terms of the gauge invariant variables, we write the linearized Einstein equations:

$$\Delta H_{ab} = \mathcal{R}H_{ab} + 2D_{(a}V_{b)} - \gamma_{ab}D_cV^c, \quad H^c{}_c = 0, \quad D^cH_{ac} + 2\omega^2 H_a = V_a, \tag{22}$$

$$\Delta H = 0, \quad D^aH_a + 2\omega^2 H = 0, \quad \Delta H_a - D^cD_aH_c - 2\omega^2 D_aH = 0, \tag{23}$$

The perturbative divergence of the energy momentum tensor are reduced to

$$\omega^2\mathcal{R}H_a = 0, \quad D_aV^a + \frac{1}{2}\Sigma = 0. \tag{24}$$

We note again that the first equation corresponds to the Euler equation and the second equation corresponds to the continuity equation for the energy density.

On $\mathcal{M}_{ex}$, the linearized Einstein equations are given by (22) and (23) with $\mathcal{R} = 0 = V^a$.

4 Equation of Motion as the bundle of Nambu-Goto String

Here we show that the Euler equations in (15) and (24) coincide with the equations derived from the Nambu-Goto action. We note that the background distribution of σ is regarded as the bundle of straight Nambu-Goto strings with the infinitesimally small energy density. Each string stays at the point with fixed ρ and ϕ in $\mathcal{M}_{in}$. The perturbation variables Σ and V^a is induced by the perturbative motion of each string in the bundle.

Let $\{x^\mu\}$ be a smooth coordinate system in a neighborhood of each string world sheet $\hat{\mathcal{S}}$ in $\mathcal{M}$. The embedding of the string world sheet $\hat{\mathcal{S}}$ into $\mathcal{M}$ is described by

$$x^\mu = x^\mu(\zeta^i), \tag{25}$$

where $\{\zeta^i\}$ (the indices $i, j, \cdots$ run over 0,1) is an intrinsic two-dimensional coordinate system on $\hat{\mathcal{S}}$. The Nambu-Goto action is given by

$$S_{NG} = -\tilde{\sigma}\int d\zeta^2\sqrt{-q}, \tag{26}$$

where $q = \det(q_{ij})$ and q_{ij} is the induced metric on $\hat{\mathcal{S}}$ defined by

$$q_{ij} := g_{\mu\nu}\frac{\partial x^\mu}{\partial\zeta^i}\frac{\partial x^\nu}{\partial\zeta^j}, \tag{27}$$

From (26), we obtain the equation

$$\Box_2 x^\mu + \Gamma^\mu{}_{\nu\lambda}q^{ij}\frac{\partial x^\mu}{\partial\zeta^i}\frac{\partial x^\lambda}{\partial\zeta^j} = 0, \tag{28}$$

where $\Box_2$ is the d'Alembertian on $\hat{\mathcal{S}}$, q^{ij} is the inverse of q_{ij} and $\Gamma^\mu{}_{\nu\lambda}$ is the Levi-Civita connection associated with the metric given by (1) and (5).

For the background string distribution x^μ and ζ^i are given by

$$x^0 = \zeta^0 = t, \quad x^1 = \zeta^1 = z, \quad x^2 = \rho, \quad x^3 = \phi, \tag{29}$$

and the induced metric q_{ij} is given by η_{pq}. Then we easily check that (28) is trivial by $D_px^\mu = \delta^\mu_p$ and $\Gamma^\mu{}_{\nu\rho}\eta^{\nu\rho} = 0$.

On the above background, we consider the metric perturbation $h_{\mu\nu}$ and the perturbation δx^μ of x^μ. We choose the coordinates on $\hat{\mathcal{S}}$ so that $\zeta^0 = t$ and $\zeta^1 = z$. The linear perturbation of (28) is given by

$$D^rD_p\delta x^a - \frac{1}{2}D^ah^r{}_p + D^rh^a{}_p = 0. \tag{30}$$

Since $i\int\omega(V^a+16\pi G\sigma X_a)S/(16\pi G)$ is the momentum perturbation, $-\int(V^a+16\pi G\sigma X_a)S/(16\pi G\sigma)$ is the perturbative displacement of each string. Indeed, one easily check that (30) coincide with the Euler equation in (15) (in (24)) by choosing

$$\delta x^a = -\int \frac{V^a + 16\pi G\sigma X_a}{16\pi G\sigma} S \tag{31}$$

Thus, our restriction for the mode coefficients of the perturbative energy momentum tensor is justified as the perturbation of the Nambu-Goto string bundle. If the other coefficients are included, one obtain additional equations of motion which are not derived from the Nambu-Goto action. Since (30) is the wave equation which admits oscillatory solutions. However, as seen below, these oscillatory solutions does not generate gravitational waves which reach to the region far from the string.

Further, we can extract the motion of the "single thick string" from the various motion of the string bundle. To see this, we use the metric perturbation variable X_a. When we fix the gauge freedom so that

$$X_a|_{\mathcal{S}} := X_a|_{\mathcal{S}+} = X_a|_{\mathcal{S}-} = -\frac{1}{\mathcal{R}} V_a\Big|_{\mathcal{S}-} \tag{32}$$

in the neighborhood of $\mathcal{S}$, where $X_{a\pm}$ are X_a on $\mathcal{S}$ facing to $\mathcal{M}_{ex}$ and $\mathcal{M}_{in}$, respectively. $X_a|_{\mathcal{S}}$ shows various deformations of the surface $\mathcal{S}$ instead of δx^a. We decompose these deformations by

$$X_a|_{\mathcal{S}} = \sum_m \hat{X}_a e^{im\phi}. \tag{33}$$

As the special deformation, the mode with $m = 1$ represents the displacement as the single string[9] which is relevant to a thin Nambu-Goto string. Henceforth, we concentrate only on the mode with $m = 1$.

5 Perturbative Solutions

Now, we construct the global solutions to the perturbed Einstein equations in $\mathcal{M}$. The exterior and the interior solutions to (13)-(15) and (22)-(24) should satisfy the perturbed junction conditions $[\delta q_{\mu\nu}] = 0$ and $[\delta K^{\mu}{}_{\nu}] = 0$ along the thick string surface $\mathcal{S}$ ($r = r_*$), where $\delta q_{\mu\nu\pm}$ is the perturbed intrinsic metric and $\delta K^{\mu}{}_{\nu\pm}$ is the perturbed extrinsic curvature of $\mathcal{S}$.

5.1 $\kappa \neq 0$ case

We consider here gravitational wave emission by the thick string motion which is excited by incident gravitational waves, i.e., the scattering problem of gravitational wave by a thick string.

(12)-(15) on $\mathcal{M}_{in}$ are reduced to the wave equations for two scalar variables $\Phi_{(o)}$ and $\Phi_{(e)}$:

$$(\Delta + \kappa^2)\Phi_{(o),(e)} = 0, \tag{34}$$

respectively, and all gauge invariant variables are given by

$$F_a = \epsilon_{ab} D^b \Phi_{(o)}, \quad F_{ab} = \mathcal{L}_{ab}\Phi_{(e)}, \quad F = \Delta\Phi_{(e)}, \quad V_a = \frac{1}{2}\mathcal{R} D_a \Phi_{(e)}, \quad \Sigma = -\mathcal{R}\Delta\Phi_{(e)}, \tag{35}$$

without loss of generality, where ϵ^{ab} is the two-dimensional antisymmetric tensor on $\mathcal{M}_1$ and $\mathcal{L}_{ab} := D_a D_b - \frac{1}{2}\gamma_{ab}\Delta$. On $\mathcal{M}_{ex}$, we also find that (12)-(14) are reduced to the same form as (34) and (35) with $\mathcal{R} = 0$. The exterior solutions $\Phi^{(ex)}_{(o),(e)}$ and the interior solutions $\Phi^{(in)}_{(o),(e)}$ to (34) are

$$\Phi^{(ex)}_{(o),(e)} = \sum_{m=0}^{\infty} e^{im\phi}\left\{AH^{(1)}_{\mu}(\beta r) + BH^{(2)}_{\mu}(\beta r)\right\}, \quad \Phi^{(in)}_{(o),(e)} = \sum_{m=0}^{\infty} e^{im\phi}\left\{CP^m_{\nu}(x) + DQ^m_{\nu}(x)\right\}, \tag{36}$$

where $H^{(1)}_{\mu}(\beta r)$ and $H^{(2)}_{\mu}(\beta r)$ are the Hankel function of the first and the second class, $P^m_{\nu}(x)$ and $Q^m_{\nu}(x)$ are the associated Legendre function of the first and second class, $\mu := m/(1-\alpha)$, $\beta := \kappa/(1-\alpha)$,

$\nu(\nu+1) := \kappa^2/\hat{\alpha}^2$ and $x := \sqrt{1-\hat{\alpha}^2 r^2}$. The coefficients A and B correspond to the amplitude of the outgoing and the incident wave, respectively. The regularity condition at the axis $r=0$ on $\Phi^{(in)}_{(o),(e)}$ leads $D=0$.

After some calculations, the perturbed junction conditions tell us

$$[\Phi_{(o,e)}] = 0, \quad [D_\perp \Phi_{(o,e)}] = 0, \tag{37}$$

where $D_\perp = n^a D_a$ and $n^a = (\partial/\partial\rho)^a$. Substituting (36) into (37), we have

$$A = UB, \tag{38}$$

$$U = -\frac{\kappa r_* H^{(2)}_{\mu+1}(\beta r_*) P^m_\nu(x_*) - \left(\sqrt{1-x_*^2} P^{m+1}_\nu(x_*) + \alpha m P^m_\nu(x_*)\right) H^{(2)}_\mu(\beta r_*)}{\kappa r_* H^{(1)}_{\mu+1}(\beta r_*) P^m_\nu(x_*) - \left(\sqrt{1-x_*^2} P^{m+1}_\nu(x_*) + \alpha m P^m_\nu(x_*)\right) H^{(1)}_\mu(\beta r_*)}, \tag{39}$$

where $x_* := \sqrt{1-\hat{\alpha}^2 r_*^2} = 1-\alpha$. The deformation of $\mathcal{S}$ is represented by V^a on $\mathcal{S}$. By the appropriate choice so that (32) is satisfied, we obtain

$$X_a|_{\mathcal{S}} = -\frac{1}{2} D_a \Phi_{(e)}\Big|_{\mathcal{S}}. \tag{40}$$

5.2 $\kappa = 0$ case

The solutions to (22)-(24) on $\mathcal{M}_{in}$ is given by

$$H_{ab} = \mathcal{L}_{ab}\Phi^{(in)}_{(\kappa 0)} + \mathcal{A}_{ab}\Psi^{(in)}_{(\kappa 0)}, \quad H = 0, \quad H_a = 0, \tag{41}$$

$$V_a = \tfrac{1}{2} D_a(\Delta + \mathcal{R})\Phi^{(in)}_{(\kappa 0)} + \tfrac{1}{2}\epsilon_{ac} D^c(\Delta+\mathcal{R})\Psi^{(in)}_{(\kappa 0)}, \quad \Sigma = -\Delta(\Delta+\mathcal{R})\Phi^{(in)}_{(\kappa 0)} \tag{42}$$

without loss of generality, where $\Phi^{(in)}_{(\kappa 0)}$ and $\Psi^{(in)}_{(\kappa 0)}$ are arbitrary scalar functions and $\mathcal{A}_{ab} = -\epsilon_{c(a} D_{b)} D^c$. We fix the gauge freedom so that (32) is satisfied. Evaluating some perturbative junction conditions and imposing the regularity at the infinity $r \to \infty$, we obtain the exterior solutions

$$H_{ab} = \mathcal{L}_{ab}\Phi^{(ex)}_{(\kappa 0)}, \quad H = 0, \quad H_a = 0, \tag{43}$$

where $\Phi^{(ex)}_{(\kappa 0)}$ is the solutions to the equation $\Delta\Phi^{(ex)}_{(\kappa 0)} = 0$. For $m=1$ mode, $\Phi^{(ex)}_{(\kappa 0)}$ is given by

$$\Phi^{(ex)}_{(\kappa 0)} = \left(A_1 \rho^{-\frac{1}{1-\alpha}} + B_1 \rho^{\frac{1}{1-\alpha}}\right) e^{i\phi} \quad \text{for} \quad \alpha \in [0, 1/2], \qquad \Phi^{(ex)}_{(\kappa 0)} = A_1 \rho^{-\frac{1}{1-\alpha}} e^{i\phi} \quad \text{for} \quad \alpha \in [1/2, 1). \tag{44}$$

The remaining junction conditions are

$$[H_{\parallel}] = 0, \quad [H_{\parallel\perp}] = 0. \tag{45}$$

We should join (41)-(44) at the string surface $\mathcal{S}$ by evaluating (45). Note that the term proportional to B_1 in (44) corresponds to the exact solution called a "cosmic string traveling wave" [7].

Here we show two examples of global solutions which satisfy the regularity at $r=0$ in $\mathcal{M}_{in}$, junction conditions (45) and the regularity at $r=\infty$ in $\mathcal{M}_{ex}$:

- $\Delta\Phi^{(in)}_{(\kappa 0)} = \Delta\Psi^{(in)}_{(\kappa 0)} = 0$ solution ($m=1$ mode):

$$\Phi^{(in)}_{(\kappa 0)} = C_1 \left(\frac{1-x}{1+x}\right)^{\frac{1}{2}} e^{i\phi}, \quad \Psi^{(in)}_{(\kappa 0)} = 0, \quad A_1 = 0, \quad B_1 = C_1 \left(\frac{1}{r_*}\right)^{\frac{1}{1-\alpha}} \left(\frac{\alpha}{2-\alpha}\right)^{\frac{1}{2}}. \tag{46}$$

- $\Delta\Phi^{(in)}_{(\kappa 0)} = -\lambda\Phi^{(in)}_{(\kappa 0)}$, $\Delta\Psi^{(in)}_{(\kappa 0)} = -\lambda\Psi^{(in)}_{(\kappa 0)}$ solution ($m=1$ mode):

$$\Phi^{(in)}_{(\kappa 0)} = C_1 P^1_\nu(x) e^{i\phi}, \quad \Psi^{(in)}_{(\kappa 0)} = D_1 P^1_\nu(x) e^{i\phi}, \quad \nu(\nu+1) = 2\lambda/\mathcal{R},$$

$$A_1 = \frac{1}{2}\left(\frac{1}{r_*}\right)^{-\frac{1}{1-\alpha}} (C_1 - iD_1)(\mathcal{I}_1 + \mathcal{J}_1), \quad B_1 = \frac{1}{2}\left(\frac{1}{r_*}\right)^{\frac{1}{1-\alpha}} (C_1 + iD_1)(\mathcal{I}_1 - \mathcal{J}_1). \tag{47}$$

$$\mathcal{I}_1 = \left(1 - \frac{\nu(\nu+1)}{2}\right) P^1_\nu, \quad \mathcal{J}_1 = (1-x_*^2)\frac{d}{dx} P^1_\nu + \frac{\nu(\nu+1)x_*}{2} P^1_\nu.$$

In these case, $X_a|_S$ is given by (32) and (42).

6 Fluctuating thin Nambu-Goto string

Now, we consider the thin string case. Physically, a "thin string" means a string whose thickness r_* is sufficiently smaller than the wavelength of gravitational wave or any scale of fluctuations inside the string. Here, in $\kappa \neq 0$ case, we consider the situation $\beta r_* \ll 1$ with the finite α and take the leading order of βr_* for a thin string. Further, in $\kappa = 0$ case, $\lambda^{-1/2}$ in (47) corresponds to the scale of the internal fluctuations and $\mathcal{R}^{-1/2}$ is the curvature scale of the background geometry. Then, we consider the situation $\lambda/\mathcal{R} \sim \nu \ll 1$ for a thin string in $\kappa = 0$ case.

6.1 $\kappa \neq 0$ case

The displacement X^a_S of a Nambu-Goto thin string by the gravitational wave scattering is given by

$$X^a_S := \int X^a|_S \,(m = 1, \beta r_* \ll 1)S = \int \frac{\kappa B_{m=1} S}{2(1-\alpha)\Gamma(\frac{2-\alpha}{1-\alpha})} \left(\frac{\beta r_*}{2}\right)^{\frac{\alpha}{1-\alpha}} e^{i\phi}(n^a + i\tau^a), \tag{48}$$

where $\tau^a = (1/r)(\partial/\partial\phi)^a$ and $n^a = (1-\alpha)(\partial/\partial r)^a$. (48) shows that the string is deformed while the incident wave exists on the string.

The order of magnitude of $|X^a_S| := \sqrt{\gamma_{ab} X^a_S X^b_S}$ is estimated by $|X^a_S|/r_* \sim \kappa^2 |B_{m=1}|(\beta r_*)^{\alpha/(1-\alpha)-1}$. The amplitude of gravitational wave (F or F_{ab}) is proportional to $|\kappa^2 B| \ll 1$. If $(\beta r_*)^{1-\alpha/(1-\alpha)} < \kappa^2|B| \ll 1$, then $|X^a_S| > r_*$. Therefore, the magnitude of the displacement may become larger than the string thickness within the linear perturbation framework.

In the same order calculation where X^a_S is given by (48), we obtain the trivial scattering data

$$U \sim 1 \tag{49}$$

from (39). Hence, there is neither resonance nor phase shift in the scattering problem, nevertheless the string is deformed by the gravitational waves.

6.2 $\kappa = 0$ case

In $\kappa = 0$ case, the arbitrariness of the functions $\Phi^{(in)}_{(\kappa 0)}$ and $\Psi^{(in)}_{(\kappa 0)}$ tells us that there are various solutions associated with the fluctuations of the string internal structure. For the thin string case, these internal fluctuations are irrelevant and the only solution (46) is relevant, because any solution described by the sum of (47) with the different λ and converges to (46) in the limit $\lambda/\mathcal{R} \to 0$. This is just the cosmic string traveling wave[7] and is the unique solution which is independent of the internal fluctuations of the string.

For the solution (46), the string displacement is given by

$$X^a_S := \int X^a|_S \,(m = 1, \nu \ll 1)S = -\int \frac{B_1}{2(1-\alpha)} \left(\frac{r_*}{1-\alpha}\right)^{\frac{\alpha}{1-\alpha}} S e^{i\phi}(n^a + i\tau^a). \tag{50}$$

We easily see that this string displacement X^a_S can be larger than the string thickness r_*.

7 Discussions

In this article, we have considered the perturbative motion of a self-gravitating, thin Nambu-Goto string. All perturbations are classified into two types : one is $\kappa \neq 0$ mode the other is $\kappa = 0$ mode. For $\kappa \neq 0$ mode, we considered the scattering problem of gravitational wave by a Nambu-Goto string. As the result, we obtained the string displacement (48) and the scattering data (49). For $\kappa = 0$ mode, we have shown that the solution (46) is the unique solution which is independent of the internal fluctuations of the string.

In the both case, we have found that the perturbative string displacement X^a_S is given by the degree of freedom of gravitational wave. Both (48) and (50) show that the string is bent while the gravitational wave exists on the string. This is analogous to the result for the self-gravitating Nambu-Goto wall [4].

For $\kappa \neq 0$ mode, the above result is consistent with our preliminary result in [10], nevertheless the background distribution of σ in (3) discussed here is different from that in [10]. We conclude again that there is neither resonance nor phase shift in the scattering problem, nevertheless the string is deformed by the gravitational waves. In particular, no resonance means the straight thin Nambu-Goto string does not emit gravitational wave spontaneously by its oscillatory motion. This result will be independent of the distribution of σ.

For $\kappa = 0$ mode, (46) is just the cosmic string traveling wave[7]. Since there is no degree of freedom for the continuous string oscillations in $\kappa \neq 0$ mode, we conclude that (46) is the unique solution which describes continuous oscillations of a thin Nambu-Goto string. Further, the cosmic string traveling wave is the pp-wave exact solution on the Minkowski spacetime with a deficit angle and the (46) is a exact solution itself. Hence this wave solution does not generate the other mode of gravitational wave by itself even if we consider the second order perturbation.

To obtained the above results, we have first considered the motion of a thick string coupled to gravity. We regard that a "thin string" is not a string with the thickness $r_* \to 0$ but that whose thickness r_* is sufficiently smaller than the wavelength of gravitational wave or the scale of the internal fluctuations. For a fixed amplitude of the outside gravitational wave, the magnitude of the string displacement X^a_S depends on r_*. If we take the limit $r_* \to 0$ for fixed the wavelength of gravitational wave, there is no response of the string motion for finite outside gravitational waves. This result is consistent with that obtained by Unruh et.al.[11]. Both their and our results show that the straight string cannot bend in the limit $r_* \to 0$. This mathematical limit will be irrelevant for strings formed during phase transition in the early universe, because they have finite thickness.

References

[1] A. Vilenkin and E.P.S Shellard, *"Cosmic Strings and Other Topological Defects"*, (Cambridge University Press, Cambridge, England, 1994) and the references therein.

[2] E.W. Kolb and M.S. Turner, *The Early Universe*, (Addison-Wesly Publishing Company, 1993) and the references therein.

[3] A. Vilenkin, and A.E. Everett Phys. Rev. Lett. **48** (1982), 1867. T. Vachaspati, A.E. Everett and A. Vilenkin, Phys. Rev. **D30** (1984), 2046.

[4] H. Kodama, H. Ishihara and Y. Fujiwara, Phys. Rev. **D50** (1994), 7292. A. Ishibashi and H. Ishihara, *ibid.* **D56** (1997), 3446.

[5] R. Geroch and J. Traschen, Phys. Rev. **D36**, (1987), 1017.

[6] J.R. Gott, Ap.J. **288**, (1985), 422. W.A. Hiscock, Phys. Rev. **D31**, (1985), 3288. B. Linet, Gen. Rel. Grav. **17**, (1985), 1109. B. Boisseau, C. Charmousis and B. Linet, Phys. Rev. **D55**, (1997), 616.

[7] T. Vachaspati, Nucl. Phys. **B277**, (1986), 593. D. Garfinkle, Phys. Rev. **D41**, (1990), 1112. D. Garfinkle, T. Vachaspati, *ibid*, **D42**, (1990), 1960. V.P. Frolov, D. Garfinkle, *ibid*, **D42**, (1990), 3980.

[8] W. Israel, Nuovo Cimento **B44** (1966). 1.

[9] K. Nakamura A. Ishibashi and H. Ishihara, in preparation.

[10] K. Nakamura A. Ishibashi and H. Ishihara, "Cosmic string coupled to gravitational waves " in PROCEEDINGS OF THE SEVENTH WORKSHOP ON GENERAL RELATIVITY, p124. (1997).

[11] W.G. Unruh, G. Hayward, W. Israel and D. McManus, Phys. Rev. Lett. **62**, (1989), 2897.

Gravitational Effects on Neutrino Pair Annihilation in GRB Sources

Katsuaki Asano [1]

Department of Physics, Ritsumeikan University,
Kusatsu, Shiga 525-8577, Japan

Abstract

We study semi-analytically the gravitational effects on the neutrino pair annihilation near the neutrinosphere and around the thin accretion disk. For the disk case, we assume that the accretion disk is isothermal and that the gravitational field is dominated by the Schwarzschild black hole. The general relativistic effects only near the rotation axis are studied. The energy deposition rate is enhanced by the effect of the orbital bending toward the center. However, the effects of the redshift and the gravitational trapping of the deposited energy reduce the effective energy of gamma ray bursts' source. Although each of these effects is substantial, the effects partly cancel each other. As a result, the gravitational effects do not substantially change the energy deposition rate for either the spherical symmetric case or disk case.

1 Introduction

The relativistic fireball is one of the most promising models of gamma ray bursts (GRBs). However, the central engine of GRBs is still beyond deep mist. The source of GRBs may be one super massive (failed) supernovae [1] or may be a merger of two neutron stars or of a neutron star and a black hole [2, 3].

In these compact high energy objects, the neutrino-antineutrino annihilation into electrons and positrons (hereafter neutrino pair annihilation) is a possible and important candidate to explain the energy source of GRBs [2, 3]. Motivated by the delayed explosion of Type II supernovae, the energy deposition rate due to the neutrino pair annihilation above the neutrinosphere has been calculated [4, 5].

One of the most possible candidates for the central engine of GRBs is the accretion disk around a black hole [1, 3, 6, 7]. The system of an accretion disk and a black hole may be formed by the merging of two neutron stars, the merging of a black hole and a neutron star, or the failed supernovae.

In various arguments on the energy deposition in the central engine of GRBs, the order estimation of the deposited energy is sufficient at least at present. In this article, based on simple models, we study semi-analytically the gravitational effects on the energy deposition rate for two cases. In one case neutrinos are emitted spherically symmetrically. In the other case the hot accretion disk emits neutrinos.

2 Neutrino Pair Annihilation near the Neutrinosphere

In this section we study the general relativistic effects on the neutrino pair annihilation near the neutrinosphere.

The number of the reaction, $\nu + \bar{\nu} \to e^+ + e^-$, per unit volume per unit time [4] is written by

$$\frac{dN(r)}{dtdV} = \int\int f_\nu(p_\nu, r) f_{\bar{\nu}}(p_{\bar{\nu}}, r) \sigma |v_\nu - v_{\bar{\nu}}| d^3p_\nu d^3p_{\bar{\nu}}. \tag{1}$$

Here f_ν ($f_{\bar{\nu}}$) is the number density of neutrinos (antineutrinos) in phase space. v_ν ($v_{\bar{\nu}}$) is the velocity of neutrinos (antineutrinos), and σ is the rest-frame cross section. The left handside of equation (1) is a Lorentz invariant. $\varepsilon_\nu \varepsilon_{\bar{\nu}} |v_\nu - v_{\bar{\nu}}| \sigma$ should be a Lorentz invariant, and be written in a manifest Lorentz invariant form as $\sigma c^3 (p_\nu \cdot p_{\bar{\nu}})$, where $(p_\nu \cdot p_{\bar{\nu}})$ is the inner product of the four-momenta. The standard model predicts that the cross section is expressed as

$$\sigma = 2c^2 K G_F^2 (p_\nu \cdot p_{\bar{\nu}}), \tag{2}$$

[1] E-mail:sph10001@se.ritsumei.ac.jp

where the dimensionless parameter, K, is written by

$$\begin{aligned} K(\nu_\mu\bar{\nu}_\mu) &= K(\nu_\tau\bar{\nu}_\tau) = \frac{1-4\sin^2\theta_W+8\sin^4\theta_W}{6\pi}, \\ K(\nu_e\bar{\nu}_e) &= \frac{1+4\sin^2\theta_W+8\sin^4\theta_W}{6\pi}. \end{aligned} \tag{3}$$

Here $G_F^2 = 5.29\times10^{-44}\mathrm{cm}^2\,\mathrm{MeV}^{-2}$ and $\sin^2\theta_W = 0.23$.

Let us incorporate the effects of gravitational force due to the neutron star or black hole on the neutrino pair annihilation rate. We assume that the gravitational field is described by the Schwarzschild metric:

$$ds^2 = g_{ij}dx^idx^j = \left(1-\frac{r_g}{r}\right)c^2dt^2 - \frac{1}{1-\frac{r_g}{r}}dr^2 - r^2\left(d\theta^2-\sin^2\theta d\varphi^2\right), \tag{4}$$

where $r_g = 2GM/c^2$ is the Schwarzschild radius. In this field the eikonal for a massless particle [8] is written by

$$\psi = -\omega_0 t + L\varphi + \psi_r(r), \tag{5}$$

where ω_0 and L are constants. $\psi_r(r)$ satisfies an equation

$$\frac{\partial\psi_r(r)}{\partial r} = \sqrt{\frac{\omega_0^2}{c^2}\left(1-\frac{r_g}{r}\right)^{-2} - \frac{L^2}{r^2}\frac{1}{1-\frac{r_g}{r}}}. \tag{6}$$

From equation (5), we can obtain the momentum of a neutrino by $p_i = \hbar\frac{\partial\psi}{\partial x^i}$.

Let us consider a neutrino and an antineutrino moving on the same surface, $\theta = \pi/2$. In this case, the inner product of the two particles is written by

$$(p_\nu\cdot p_{\bar{\nu}}) = g^{ij}p_{\nu i}p_{\bar{\nu}j} \tag{7}$$

$$= \frac{\varepsilon_\nu\varepsilon_{\bar{\nu}}}{c^2}\left(1-\sqrt{1-\left(\frac{\rho_\nu}{r}\right)^2\left(1-\frac{r_g}{r}\right)}\sqrt{1-\left(\frac{\rho_{\bar{\nu}}}{r}\right)^2\left(1-\frac{r_g}{r}\right)} - \frac{\rho_\nu\rho_{\bar{\nu}}}{r^2}\left(1-\frac{r_g}{r}\right)\right), \tag{8}$$

where

$$\rho_\nu \equiv \frac{cL_\nu}{\omega_{0\nu}}. \tag{9}$$

The proper energy of the neutrino has been written by

$$\varepsilon_\nu = \frac{\hbar\omega_{0\nu}}{\sqrt{1-\frac{r_g}{r}}} \equiv \frac{\varepsilon_{0\nu}}{\sqrt{1-\frac{r_g}{r}}}, \tag{10}$$

where $\varepsilon_{0\nu}$ is the energy observed at infinity. Defining an angle θ_ν by

$$\sin\theta_\nu = \frac{\rho_\nu}{r}\sqrt{1-\frac{r_g}{r}}, \tag{11}$$

equation (8) becomes a simple and natural form,

$$(p_\nu\cdot p_{\bar{\nu}}) = \frac{\varepsilon_\nu\varepsilon_{\bar{\nu}}}{c^2}\left(1-\cos\left(\theta\nu-\theta\bar{\nu}\right)\right). \tag{12}$$

The angle θ_ν ($\theta_{\bar{\nu}}$) represents the angle between p_ν ($p_{\bar{\nu}}$) and the position vector r (see Figure 1). We assume that the neutrinosphere emits neutrinos and antineutrinos isotropically. Then we can write the number densities as $f_\nu(p_\nu,r)d^3p_\nu = n(\varepsilon_\nu)\varepsilon_\nu^2d\varepsilon_\nu d\Omega$. Because ρ_ν is constant along a neutrino ray, the maximum angle, θ_M, is obtained by substituting $\pi/2$ for θ_ν at the radius of the neutrinosphere R_ν in equation (11). Thus we obtain

$$\sin\theta_M = \frac{R_\nu}{r}\sqrt{\frac{1-\frac{r_g}{r}}{1-\frac{r_g}{R_\nu}}}. \tag{13}$$

The effect of the orbital bending is apparent in this equation. Until now we have discussed the maximum angle on the surface of $\theta = \pi/2$. In general cases, the angles between p_ν and r or the inner product, $(p_\nu \cdot p_\flat)$, are expressed by the two angles, θ_ν and φ_ν. From the symmetry, the behaviour of θ_M is obviously the same as equation (13) and φ_ν varies from 0 to 2π.

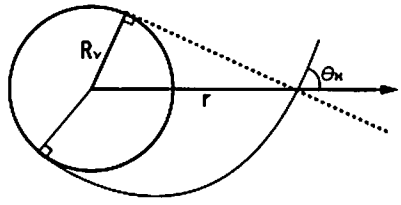

Figure 1. The maximum angle θ_M at a distance r from the center formed by neutrinos emitted from the surface of the neutrinosphere. The dashed line shows the orbit forming the maximum angle in the absence of gravitation.

Using the effective temperature of the neutrinosphere $T_{\rm eff} = T_0/\sqrt{g_{00}}$ with a constant T_0, we can write the density

$$n(\varepsilon_\nu) = \frac{g_\nu}{(hc)^3} \frac{1}{\exp\left(\frac{\varepsilon_\nu}{kT_{\rm eff}}\right) + 1}, \tag{14}$$

where g_ν is a statistical factor ($g_\nu = 1$ for a neutrino). $\varepsilon_\nu/(kT_{\rm eff})$ is constant along a neutrino ray since the redshift is cancelled out. Thus $n(\varepsilon_\nu)$ is conserved along a neutrino ray in accordance with Liouville's theorem in curved spacetime [9]. From the above formulation, one can find

$$\frac{dN(r)}{dtdV} = 2cKG_{\rm F}^2 F(r) \int\int d\varepsilon_\nu d\varepsilon_\flat n(\varepsilon_\nu) n(\varepsilon_\flat) \varepsilon_\nu^3 \varepsilon_\flat^3, \tag{15}$$

where the dimensionless factor $F(r)$ is written by

$$\begin{aligned} F(r) &= \int_0^{\theta_M} d\theta_\nu \sin\theta_\nu \int_0^{\theta_M} d\theta_\flat \sin\theta_\flat \int_0^{2\pi} d\varphi_\nu \int_0^{2\pi} d\varphi_\flat \\ &\quad \times (1 - \sin\theta_\nu \sin\theta_\flat \cos(\varphi_\nu - \varphi_\flat) - \cos\theta_\nu \cos\theta_\flat)^2 \qquad (16) \\ &= \frac{2\pi^2(1-X)^4}{3}(X^2 + 4X + 5), \qquad (17) \end{aligned}$$

where

$$X = \sqrt{1 - \left(\frac{R_\nu}{r}\right)^2 \frac{1 - \frac{r_g}{r}}{1 - \frac{r_g}{R_\nu}}}. \tag{18}$$

In our assumption, the energy deposited by the neutrino pair annihilation is propagated outward as a fireball or a shock wave, and observed as a GRB by a distant observer. Thus the energy we need to calculate is $\varepsilon_{0\nu}$, not the proper energy ε_ν. In this case the energy deposition rate is obtained by putting a factor $(\varepsilon_{0\nu} + \varepsilon_{0\flat})$ in the integrand in equation (15);

$$\begin{aligned} \frac{dE_0(r)}{dtdV} &= \frac{2cKG_{\rm F}^2}{\left(1 - \frac{r_g}{r}\right)^4} \int_0^\infty \int_0^\infty d\varepsilon_{0\nu} d\varepsilon_{0\flat} \\ &\quad \times n(\varepsilon_{0\nu}) n(\varepsilon_{0\flat}) \varepsilon_{0\nu}^3 \varepsilon_{0\flat}^3 (\varepsilon_{0\nu} + \varepsilon_{0\flat}) F(r) \qquad (19) \\ &= \frac{21\pi^4}{4} \zeta(5) \frac{KG_{\rm F}^2 g_\nu^2}{h^6 c^5} \frac{\left(1 - \frac{r_g}{R_\nu}\right)^{\frac{9}{2}}}{\left(1 - \frac{r_g}{r}\right)^4} (kT_{\rm eff})^9 F(r). \qquad (20) \end{aligned}$$

The factor, $(1-r_g/R_\nu)^{9/2}/(1-r_g/r)^4$, represents the effect of the gravitational redshift, and $F(r)$ includes the effect of the orbital bending.

As is understood from the Lorentz invariant, $dtdV = \sqrt{-g}d^4x$, if we integrate equation (20) over proper volume, $dV' = \sqrt{-g_{rr}g_{\theta\theta}g_{\varphi\varphi}}drd\theta d\varphi$, we can obtain the total energy deposition per unit proper time, $d\tau = \sqrt{g_{00}}dt$. It is natural to evaluate the energy deposition rate by the world time dt for a distant observer. We integrate over the volume, $dV = \sqrt{g_{\theta\theta}g_{\varphi\varphi}}drd\theta d\varphi$. Thus the energy deposition per unit world time is expressed as

$$\frac{dE_0}{dt} = \frac{21\pi^4}{4}\zeta(5)\frac{KG_F^2g_\nu^2}{h^6c^5}(kT_{\rm eff})^9\left(1-\frac{r_g}{R_\nu}\right)^{\frac{9}{2}}\int_{R_\nu}^{\infty}dr4\pi r^2\frac{F(r)}{\left(1-\frac{r_g}{r}\right)^4}C(r), \tag{21}$$

where we have put a factor,

$$C(r) = \frac{1}{2}\left(1+\sqrt{1-\frac{27}{4}\left(\frac{r_g}{r}\right)^2\left(1-\frac{r_g}{r}\right)}\right), \tag{22}$$

in the integrand. This is the escape probability of the deposited energy at r from the gravitational attraction [3, 10, 11]. The electrons, positrons and photons which are captured by the gravitational attraction can not contribute to the energy source of GRBs.

Let us investigate the effects of the redshift, orbital bending and gravitational capture. We integrate equation (21) and obtain the energy deposition rate for ν_e as

$$\frac{dE_0}{dt} = 1.27\times10^{42}\left(\frac{kT_{\rm eff}}{1{\rm MeV}}\right)^9\left(\frac{R_\nu}{10{\rm km}}\right)^3 f \quad {\rm ergs\ s^{-1}}, \tag{23}$$

where the dimensionless factor f expresses the effects of the general relativity ($f = 1$ when we neglect the gravitation). The energy deposition rates for ν_μ and ν_τ are 0.64 times of equation (23). We numerically estimate f including the effects of the redshift only, the orbital bending only, or both the redshift and orbital bending. The whole effects of the redshift, orbital bending and gravitational capture are lastly calculated. The results are listed in Table 1. As Table 1 or equation (21) indicates, the effect of the redshift reduces the energy deposition rate, and the effect of the orbital bending increases it. Although the each effect of the redshift and orbital bending is substantial, the effects partly cancel each other. As a result, the order of the energy deposition rate for the most probable case, $R_\nu/r_g = 2.5$, is not altered. When we neglect the general relativistic effects, the energy deposition rate increases by 1.3 times as R_ν becomes 10% larger, and also increases by 2.4 times as the temperature becomes 10% higher. Therefore, the gravitational effects are not so large in comparison with the errors due to the uncertainties of R_ν or $T_{\rm eff}$, and are overwhelmed by them. The effect of the gravitational capture becomes important as R_ν/r_g decreases. As is plotted in Figure 2, in both cases of the presence and absence of gravitation, the energy deposition mainly occurs near the neutrinosphere.

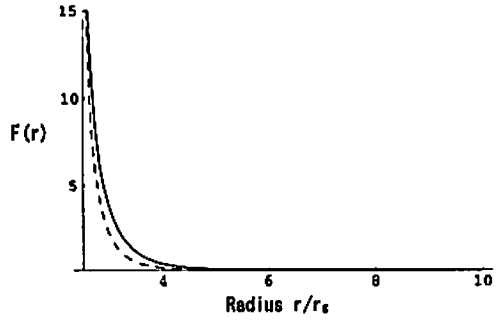

Figure 2. The plot of $F(r)$ against r for $R_\nu = 2.5r_g$ when neutrinos are emitted isotropically. The solid (dashed) line shows $F(r)$ for the case in the presence (absence) of gravitation. The origin is at $r = R_\nu$.

R_ν/r_g	f			
	redshift only	bending only	redshift and bending	whole
1.5	0.32	4.7	0.97	0.57
2.5	0.60	1.6	0.87	0.73
5	0.81	1.2	0.93	0.89 *

Table 1. The dimensionless factor f which represents the general relativistic effects (see equation (23)) when neutrinos are emitted isotropically from the neutrinosphere. f is normalized to one in the absence of gravitation. The words "redshift only" and so on indicate the incorporated effects of gravitation. "whole" on the rightest column means that we incorporate the all gravitational effects, the redshift, bending and trapping. The energy deposition rate is enhanced by the orbital bending and reduced by the redshift and trapping.

3 Neutrino Pair Annihilation around the Accretion Disk

In this section we investigate the neutrino pair annihilation around the accretion disk. In order to simplify our formulation we assume that the accretion disk is isothermal and that the gravitational field is dominated by the central Schwarzschild black hole. We neglect the rotation of the black hole. The accretion disk is assumed to be thin and its self-gravitational effects are neglected. In this case the equation of the energy deposition rate is the same as equation (20) provided that $F(r)$ is replaced by $F(r,\theta)$. The effect of the gravitational redshift can be easily incorporated, whereas the formulation of the neutrino bending is difficult to do because the accretion disk emits neutrinos anisotropically.

First, we calculate the dimensionless factor $F(r,\theta)$ without the effect of the gravity. The accretion disk is placed on the equatorial plane, $\theta = \pi/2$. The black hole is at the origin. We adopt $R_{\rm in} = 3r_g$, the innermost stable orbit, and $R_{\rm out} = 10r_g$ as Woosely [1] assumed. $F(r,\theta)$ derived from the numerical integral is plotted in Figure 3(a) and (b). As is shown from these figures, the energy deposition rate is maximized in the vicinity of the accretion disk, where $F(r,\theta) \simeq 30 - 33$. Let us calculate the energy deposition rate near the rotation axis, where is the lowest baryon density region. Thus we calculate in the region for $\theta \leq \pi/4$ and obtain

$$\frac{dE_0}{dt} = 5.22 \times 10^{43} \left(\frac{kT_{\rm eff}}{1{\rm MeV}}\right)^9 \left(\frac{r_g}{10{\rm km}}\right)^3 Gf \quad {\rm ergs\ s^{-1}}, \tag{24}$$

where the dimensionless quantity G shows the relative contributions from various regions in the absence of gravitation. G is normalized to one when we integrate over the volume for $\theta \leq \pi/4$ and $r = 2r_g - 10r_g$. The values of G in the other regions are summarized in Table 2, from which we can obtain the energy deposition rate in the respective region. We neglect the energy deposited inside $r = 2r_g$, since the baryon density in this region is very high and the energy contribution is small for the small volume and deposition rate. In the case of the spherical emitter in section 2, the deposition rate decreases as r^{-8}. On the other hand around the accretion disk, as is seen from Table 2, there leaves a marginal deposition rate even at regions relatively distant from the center. Of course the deposition rate per unit volume at distant positions is small. However large volume results in non-negligible contribution at the regions distant from the center.

(a) (b)

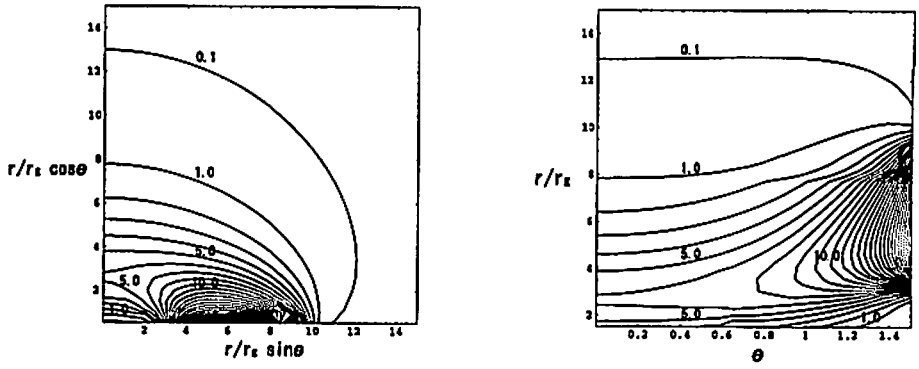

Figure 3. The contour plot of $F(r,\theta)$ where neutrinos are emitted from the disk. Here gravitation has been neglected. (a) is plotted in the Cartesian coordinates, $r\sin\theta$-$r\cos\theta$, and (b) is in the polar coordinates, r-θ. The contours are plotted at intervals of one except for the line of $F(r,\theta)=0.1$. $\theta=0$ and $\theta=\pi/2$ correspond to points on the rotation axis and on the disk, respectively.

Untill now we have neglected the gravitational effects. It is easy to incorporate the effects of the redshift and trapping by the central gravitational source in the preceding arguments of this section. However, the bending effect are difficult to treat unlike the case of the neutrinosphere since the accretion disk emits neutrinos anisotropically. Thus we are forced to take some approximation. As is shown from Figure 3(b), the θ-dependence of $F(r,\theta)$ is weak for a small θ. We may set $F(r,\theta)\simeq F(r,0)$ for $\theta\leq\pi/4$. In the absence of the gravitation if we adopt this approximation in the region for $\theta\leq\pi/4$ and $r=2r_g-10r_g$, we obtain $G=0.81$. The exact value of G is one and this approximation is not necessarily satisfactory. However, this approximation may be sufficient for the order estimate of the gravitational effects.

θ	$2r_g-5r_g$	$5r_g-10r_g$	$10r_g-20r_g$
$0-\pi/4$	0.35	0.65	0.22
$\pi/4-\pi/3$	0.32	0.77	0.17

Table 2. The dimensionless factor G which represents the fraction of the energy deposition rate for each region (see equation (24)) when neutrinos are emitted from the disk. G is normalized to one for the region surrounded by $r=2r_g-10r_g$ and $\theta=0-\pi/4$. Here we neglect the effects of gravitation.

We can obtain $F(r,0)$ including the effect of the orbital bending with comparative ease, since the geometry of this case maintain the symmetry. A neutrino is emitted from the disk at R and $\theta=\pi/2$, and it arrives at a point at r and $\theta=0$. The nearest distance, r_0, from the origin to the orbit of neutrinos [8] is numerically obtained from

$$\pi/2=\int_C \frac{dr'}{r'\sqrt{\left(\frac{r'}{r_0}\right)^2\left(1-\frac{r_g}{r_0}\right)-\left(1-\frac{r_g}{r'}\right)}}. \tag{25}$$

Here, in the case that a neutrino passes through r_0 until it arrives at a point at $\theta=0$, the integral for r' is performed from r_0 to R and r. When the distance from the origin to the neutrino monotonically varies, the integral is performed from the smaller one to the larger one of r and R. We can numerically get θ_ν at $\theta=0$ from r_0 and the following equation;

$$\sin\theta_\nu=\frac{r_0}{r}\sqrt{\frac{1-\frac{r_g}{r}}{1-\frac{r_g}{r_0}}}. \tag{26}$$

The constant, r_0, or θ_ν is a function of r and R in this case. As is easily understood, a neutrino coming from $R_{\rm in}$ forms the minimum value of θ_ν, $\theta_{\rm m}$, at $\theta = 0$ and that from $R_{\rm out}$ does the maximum value of θ, $\theta_{\rm M}$. Integrating equation (16) from $\theta_{\rm m}$ to $\theta_{\rm M}$, we obtain $F(r,0)$ involving gravitational effects. In Figure 4 we plot $F(r,0)$ for both cases when the bending is took into consideration or not into consideration. In comparison with the spherical case in Figure 2, the deposited energy at distant regions in the disk case is marginally substantial. In the presence of the bending, the peak of the energy deposition rate is shifted to a little bit larger r and the value of the rate at the peak is about two times larger in comparison with those in the absence of the bending.

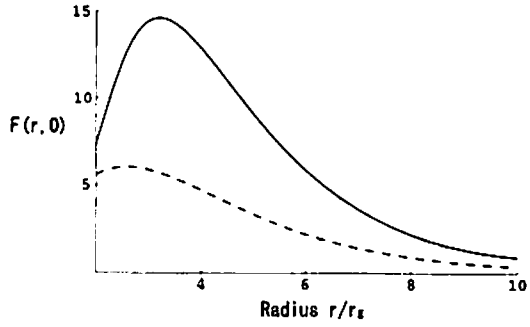

Figure 4. The diagram of $F(r,0)$ against r where neutrinos are emitted from the disk. The solid (dashed) line shows $F(r,0)$ for the case in which we consider (neglect) the effect of the gravitational bending.

Though the θ-dependence of the gravitational effects may not be necessarily small unlike $F(r,\theta)$ in the absence of gravitation, we assume it small here. Using $F(r,0)$ with the bending effect, we calculate the energy deposition rate in the range for $\theta \leq \pi/4$ and $r = 2r_g - 10r_g$. Table 3 is the list of the factor f which shows the gravitational effects. The θ-dependence is neglected in our calculation except for the case involving the redshift only. Thus f is normalized to one when $F(r,\theta)$ for the case involving the effect of the redshift only or $F(r,0)$ for the other cases is integrated over r and θ in the absence of gravitation. As is easily seen, the gravitational effects are canceled out each other. This is analogous to the neutrino sphere case in the previous section.

range	f			
	redshift only	bending only	redshift and bending	whole
$2r_g - 5r_g$	0.66	2.6	1.6	1.4
$5r_g - 10r_g$	0.31	2.5	0.78	0.75

Table 3. The dimensionless factor f for $\theta = 0 - \pi/4$ (see equation (24)) when neutrinos are emitted from the disk. f is normalized to one when $F(r,\theta)$ for the case involving the effect of the redshift only or $F(r,0)$ for the other cases is integrated over r and θ in the absence of gravitation.

4 Conclusions

In this article we have investigated semi-analytically the neutrino pair annihilation near the neutrinosphere and around the thin accretion disk assuming that the gravitational sources in both cases are described by the Schwarzschild metric. We have studied the general relativistic effects only near the rotation axis, because that region is specially of interest to the source of GRBs and to estimate the effect of the orbital bending for a large θ is difficult.

The general relativistic effects as a total do not enhance the neutrino energy deposition rate in either case. The energy deposition rate is enhanced by the effect of the orbital bending toward the center.

However, the enhancement is cancelled out by the effects of the redshift and capture by the gravitational attraction. Consequently, numerical simulations of the neutrino energy deposition rate in various models can correctly estimate the order of the rate without considering the gravitational effects since it is supposed that the thickness, shape or temperature distribution of the disk or sphere do not greatly affect on the gravitational effects themselves. We have also shown that the neutrinos emitted from the disk can deposit energy at more distant regions than the neutrinos emitted from the sphere.

References

[1] S.E. Woosley, ApJ **405** (1993), 273

[2] M. Ruffert and H.-T. Janka, A&A **338** (1998), 535

[3] M. Ruffert and H.-T. Janka, A&A **344** (1999), 573

[4] J, Goodman, A. Dar and S. Nussinov, ApJ **314** (1987), L7

[5] V.S. Berezinsky and O.F. Prilutsky, A&A **175** (1987), 309

[6] R. Popham, S.E. Woosley and C. Fryer, ApJ **518** (1999), 356

[7] A. MacFadyen and S.E. Woosley, submitted to ApJ (1998), (astro-ph/9810274)

[8] L.D. Landau and E.M. Lifshitz, *Classical Theory of Fields* (Pergamon, London 1979)

[9] C.W. Misner, K.S. Thorne and J.A. Wheeler, *Gravitation* (Freeman, New York 1975)

[10] S. Chandrasekhar, *The Mathematical Theory of Black Holes* (Oxford, New York 1983)

[11] S.L. Shapiro and S.A. Teukolsky, *Black Holes, White Dwarfs and Neutron Stars* (Wiley, New York 1983)

Poynting burst from a collapsing magnetized star

Masayuki Nagamachi,[1] Akira Tomimatsu[2]

Department of Physics, Nagoya University,
Chikusa-ku, Nagoya 464-8602, Japan

Masaaki Takahashi[3]

Department of Physics and Astronomy, Aichi University of Education,
Kariya, Aichi 448-8542, Japan

Abstract

We study electromagnetic radiation from a collapsing magnetized star, by solving wave equation on the Oppenheimer-Snyder background. In order to understand the effect of dynamics at the stellar interior, we adopt a uniform magnetic field as source of the wave. By using the Green's function technique and assuming pure outgoing junction condition at the stellar surface, wave equation is analytically solved. For initial radius $\rho_b \gg 3M$, we find that (1) at late time radiation is dominated by "ringing" and "wave tails" which are depend on the dynamics at the stellar interior, and (2) final burst of Poynting flux is independ on the dynamics at the stellar interior.

1 Introduction

By recent observations, many burst phenomena, like a gamma-ray burst, are observed, and a collapsing magnetized star has been given as a candidate for 'engine' of the burst. because real electromagnetic radiation from a collpasing magnetized star is depend on many factors, its behaviour is very complicated. In this report we study the fundamental properties of this radiation, using a simplified model.

As a fundamental work, there is a work of Cunningham, Price and Moncrieff [1]. They considered a case that magnetic field is generated by axissymmetric currents flowing inside star. In this case, because current density increase with collapsing, magnetic field is amplified, and so waves are generated. They ignored possible influence of the electromagnetic field upon the gravitational field, derived wave equations from the Maxwell equations on a given background, and numerically solved this equations. Particularly they studied radiation at late stages of collapse. They found that (1) the radiation generated is insensitive to dynamics of the stellar interiors, (2) the radiation spectrum is dominated by radiation of quasi-normal frequencies, and (3) l-pole fields fall off at very late times t in accordance with the predicted $t^{-(2l+2)}$ law.

The Model of Cunningham et al. [1] is valid in a case of high conductive star. But their model is not valid in a case of collapse of high resistive star surrounded a magnetic field. When this star start gravitational collapse, a gravity at the stellar interior become stronge, and so a magnetic field at the stellar interior is changed. This change generates electromagnetic waves. In this report, we investigate behaviour of this waves. In this case, it is expected that the radiation generated is sensitive to the dynamics of the stellar interiors.

We aim to analytically solve the wave equation, in order to see influence of the dynamics of the stellar interiors. So we use a simplified model for wave generation, and use the Green's function technique. In section 2 and 3, we talk about this model and analytic solution, respectively. In section 4 and 5, we talk about behaviour of wave generated at the stellar interior. Final section 6 is devoted to the summary.

[1]E-mail:nagamati@allegro.phys.nagoya-u.ac. jp
[2]E-mail:atomi@allegro.phys.nagoya-u.ac.jp
[3]E-mail:takahasi@phasms2.auephyas.aichi-edu. ac.jp

2 Model for wave generation

2.1 Background spacetime

We adopt the Oppenhimer-Snyder model [2] as a collapsing star. This model represents a spherically, homogeneous and marginally bound dust collapse. Because of pressure-less, it is impossible to stop the collapse, and so this star finally form a black hole with the stellar mass.

By using the conformal flat coordinate $(\eta, \rho, \theta, \phi)$, line element of this model is written as follow

$$ds^2 = \left(1 - \frac{p}{3}\eta\right)^4 \{-d\eta^2 + d\rho^2 + \rho^2(d\theta^2 + \sin^2\theta d\phi^2)\} \qquad \text{for} \qquad 0 \le \rho \le \rho_b\,, \tag{1}$$

where $p := \frac{3}{2}\left(\frac{8}{3}\pi\epsilon_0\right)^{1/2}$, and ϵ_0 and ρ_b denotes the initial energy density and the stellar surface in this coordinate. Also there is a following relation between (η, ρ) and the Schwarzschild radius r; $r = \rho\left(1 - \frac{p}{3}\eta\right)^2$.

Because of spherically gravitational collapse, the exterior line element is that of the Schwarzschild spacetime, and it is written by using the tortoise coordinate (t, r_*, θ, ϕ) [3]

$$ds^2 = \left(1 - \frac{2M}{r}\right)(-dt^2 + dr_*^2) + r^2(d\theta^2 + \sin^2\theta d\phi^2) \qquad \text{for} \qquad r \ge r_b\,, \tag{2}$$

where M and r_b respectively represent the stellar mass and the stellar surface.

2.2 Wave equations

We consider axissymmetric electromagnetic field. Then electromagnetic field is denoted by only A_ϕ which is ϕ-component of 4-potential A_μ, and the Maxwell equation become a single equation

$$\frac{1}{\sqrt{-g}}\partial_\mu(\sqrt{-g}g^{\mu\nu}g^{\phi\phi}\partial_\nu A_\phi) = 4\pi g^{\phi\phi} j_\phi\,, \tag{3}$$

where $g := \det[g_{\mu\nu}]$ and j_ϕ denotes current dencity. In Cunningham et al. [1], wave is generated by $j_\phi \neq 0$. But we consider a case for $j_\phi = 0$. Instead of currents flowing in the stellar interior, we adopt a uniform magnetic field $A_s := \frac{1}{2}B_0 r^2 \sin^2\theta$ as source of wave, where B_0 denotes the strength of magnetic field. At outside of the star this uniform field coincides Wald's solution [4] on the Schwarzschild spacetime, and at inside of the star it represents a decrease of the magnetic flux penetrating the collapsing star. Using this A_s, we devide A_ϕ into the source part A_s and wave part A_w

$$\begin{cases} A_\phi(\eta, \rho, \theta) = A_s + A_w = \frac{1}{2}B_0\rho^2\left(1 - \frac{p}{3}\eta\right)^4 \sin^2\theta + a(\eta, \rho)\sin^2\theta & \text{for} \quad 0 \le \rho \le \rho_b\,, \\ \tilde{A}_\phi(t, r_*, \theta) = \tilde{A}_s + \tilde{A}_w = \frac{1}{2}B_0 r^2 \sin^2\theta + \tilde{a}(t, r_*)\sin^2\theta & \text{for} \quad r \ge r_b\,, \end{cases} \tag{4}$$

$$a(0, \rho) = \tilde{a}(0, r_*) = \frac{\partial a(0, \rho)}{\partial \eta} = \frac{\partial \tilde{a}(0, r_*)}{\partial t} = 0\,, \tag{5}$$

where $\tilde{A}_\phi$ denotes the exterior field, a and $\tilde{a}$ denote amplitude of wave. Substituing (4) for (3), we obtain following wave equations

$$\left[-\frac{\partial^2}{\partial\eta^2} + \frac{\partial^2}{\partial\rho^2} - \frac{2}{\rho^2}\right] a(\eta, \rho) = 4\pi\epsilon_0 B_0 \rho^2 \left(1 - \frac{p}{3}\eta\right)^2 \qquad \text{for} \qquad 0 \le \rho \le \rho_b\,. \tag{6}$$

$$\left[-\frac{\partial^2}{\partial t^2} + \frac{\partial^2}{\partial r_*^2} - V(r)\right] \tilde{a}(t, r_*) = 0 \qquad \text{for} \qquad r \ge r_b\,, \tag{7}$$

$$V(r) := \frac{2}{r^2}\left(1 - \frac{2M}{r}\right)\,. \tag{8}$$

where V(r) represents curvature potencial. The interior wave equation denotes wave generation by dynamics of the stellar interior, and the exterior wave equation denotes wave propagation accompanying with the scatterring by the curvature potencial.

3 Analytical solution of wave equation

3.1 Junction condition

In order to understand behaviour of the waves, we must simultaneously solve the intrior and exterior wave equation under given junction conditions. But it is difficult to analytically solve these. So we approximate the junction condition.

The exterior equation denotes wave scattering by the curvature potencial . This potential has a peek at $r = 3M$, rapidly decreases as $r \to \infty$. So wave are hardly scatterd when the surface of collapsing star $r_b \gg 3M$. It is thought that effect of curvature scatterring is important only

For this reason, we only consider the initial stellar radius $\rho_b \gg 3M$, assume that it is possible to ignore the scatterring wav es. By this assumption, junction condition at the stellar surface is pure outgoing wave conditio n

$$\frac{\partial a(\eta, \rho_b)}{\partial \eta} + \frac{\partial a(\eta, \rho_b)}{\partial \rho} = 0 . \tag{9}$$

We solve the interior wave equation under this junction condition, investigate behaviour of the wave generated by dynamics of spacetime.

3.2 Green's function technique

Because of the form of The interior wave equation (6), it is possible to do the Laplace transeformation for η

$$\left[\frac{d^2}{d\rho^2} + \left(-\sigma^2 - \frac{2}{\rho^2}\right)\right] \bar{a}(\sigma, \rho) = 4\pi B_0 \rho^2 \int_0^\infty \left(1 - \frac{p}{3}\eta'\right)^2 e^{\sigma\eta'} d\eta' , \tag{10}$$

where $\bar{a}(\sigma, \rho)$ denotes the Laplaes transformed $a(\eta, \rho)$. We solve this equation (10) by using the Green's function technique.

The Green's function is constituted of $\rho^{1/2} J_{3/2}(i\sigma\rho)$ and $\rho^{1/2} N_{3/2}(i\sigma\rho)$ ($J_{3/2}$: Bessel's function, $N_{3/2}$: Neoman's function) which are linearly independent solutions of homogeneous equation of (6), and the Green's function is satisfied with next equation

$$\left[\frac{d^2}{d\rho^2} + \left(-\sigma^2 - \frac{2}{\rho^2}\right)\right] G(\sigma, \rho, \rho') = \delta(\rho - \rho') . \tag{11}$$

Since the regurality at $\rho = 0$ and (11), we constitute the Green's function as follow

$$G(\sigma, \rho, \rho') = \frac{\pi}{2} \begin{cases} \rho^{\frac{1}{2}} J_{\frac{1}{2}}(i\sigma\rho) \left[\rho'^{\frac{1}{2}} N_{\frac{1}{2}}(i\sigma\rho') + f(\sigma) \rho'^{\frac{1}{2}} J_{\frac{1}{2}}(i\sigma\rho')\right] & (0 \le \rho \le \rho') , \\ \rho'^{\frac{1}{2}} J_{\frac{1}{2}}(i\sigma\rho') \left[\rho^{\frac{1}{2}} N_{\frac{1}{2}}(i\sigma\rho) + f(\sigma) \rho^{\frac{1}{2}} J_{\frac{1}{2}}(i\sigma\rho)\right] & (\rho' \le \rho \le \rho_b) , \end{cases} \tag{12}$$

where $f(\sigma)$ is a arbitrary function decided by the junction condition (9). Using the Laplace inverse-transeformation and the junction condition (9), we obtain analytic solution for wave equation (6)

$$\frac{\dot{a}(z, \rho_b)}{M B_0} = \frac{3}{2\pi} \int_{-i\infty}^{+i\infty} g(x) \left\{ \left(1 - \frac{1}{\alpha x} + \frac{1}{2\alpha^2 x^2}\right) e^{xz} + \frac{1}{\alpha x} \left(1 - \frac{z}{2\alpha}\right) - \frac{1}{2\alpha^2 x^2} \right\} dx , \tag{13}$$

$$g(x) := \frac{1}{ix} \frac{\left(x - \frac{3}{x}\right)(e^x - e^{-x}) - 3(e^x + e^{-x})}{e^{-x} - (1 - 2x + 2x^2) e^x} , \tag{14}$$

where $\dot{a} := \partial a / \partial \eta$, $\alpha^2 := \rho_b / 2M$, $z := \eta / \rho_b$, $x := \sigma \rho_b$. From the form of solution (13), it is found that M and B_0 are only conserned with the amplitude of the wave. The factor deciding the wave form is α, which is the ratio between the initial radius and the gravitational radius of collapsing star.

4 Quasi-normal ringing and wave tails

In order to investigate this radiation, we numerically integrate (13). Figure 1 is the integral results.

4.1 Wave tails

At late time, $\dot{a}/MB_0$ is proportional to z. By analysing (13), it is found that this remarkable behaviour comes from distributions of the low-frequ encies

As $z \gg 1$, $x \ll 1$, we can approximate $\dot{a}/MB_0$ as follow

$$\begin{aligned} \left.\frac{\dot{a}(z,\rho_b)}{MB_0}\right|_{\text{tail.}} &:= \lim_{\alpha \gg 3M, z \gg 1, x \ll 1} \frac{\dot{a}(z,\rho_b)}{MB_0} \\ &\simeq \frac{3}{40\alpha^2}\{1+2(2\alpha - z)\}\,. \end{aligned} \tag{15}$$

This equation fit the late time behaviour of $\dot{a}/MB_0$ very well.

4.2 Quasi-normal ringing

Removing $\dot{a}/MB_0|_{\text{tail.}}$ from $\dot{a}/MB_0$, the behaviour of oscillation - "initial burst" and "ringing" - remains. In the following way, it is found that this behaviour is represented by the sum of the residues of Green's function.

For $z \gg 0$,

$$\begin{aligned} \left.\frac{\dot{a}(z,\rho_b)}{MB_0}\right|_{\text{ring.}} &:= \frac{3}{2\pi}\int_{-i\infty}^{+i\infty} g(x)\left(1 - \frac{1}{\alpha x} + \frac{1}{2\alpha^2 x^2}\right)e^{xz}dx \\ &= 3\mathrm{Re}\left[\sum_{\text{poles}}\left(1+\frac{2}{x}\right)\left(1 - \frac{1}{\alpha x} + \frac{1}{2\alpha^2 x^2}\right)e^{xz}\right] \\ &\simeq \frac{\dot{a}(z,\rho_b)}{MB_0} - \left.\frac{\dot{a}(z,\rho_b)}{MB_0}\right|_{\text{tail.}}\,. \end{aligned} \tag{16}$$

Figure 2 shows that the comparison between $\dot{a}/MB_0 - \dot{a}/MB_0|_{\text{tail.}}$ and $\dot{a}/MB_0|_{\text{ring.}}$. From this figure, it is found that $\dot{a}/MB_0|_{\text{ring.}}$ remarkably coincides with $\dot{a}/MB_0 - \dot{a}/MB_0|_{\text{tail.}}$.

5 Poynting flux

At the stellar surface $r = r_b$ $(\rho = \rho_b)$, Energy-momentum tensor $T_t{}^r$ which reach at the spacial infinity $r = \infty$ is written as

$$T_t{}^r(z,\rho_b) = -\frac{1}{4\pi}\frac{{\rho_b}^2}{{r_b}^4}\left\{1 - \left(\frac{2M}{r_b}\right)^{\frac{1}{2}}\right\}^2 \dot{a}^2 \sin^2\theta\,. \tag{17}$$

Poynting flux is defined as follow

$$\begin{aligned} \frac{S^r(z,\rho_b)}{16\pi M^2 {B_0}^2} &:= -\int_0^{2\pi}\left(\int_0^{\pi}\frac{T_t{}^r}{16\pi M^2 {B_0}^2}{r_b}^2\sin^2\theta\, d\theta\right)d\phi \\ &= \frac{1}{24\pi}\frac{\left(1 - \frac{1}{\alpha} - \frac{z}{2\alpha}\right)^2}{\left(1 - \frac{z}{2\alpha}\right)^6}\left(\frac{\dot{a}}{MB_0}\right)^2\,. \end{aligned} \tag{18}$$

Figure 3 is the numerical result of (18). From this picture, it is found that there is a final burst which is independ on α = (initial radius)/(gravitational radius). From calculation easily, the peek of final burst appear at $r_b \approx 8M > 3M$.

6 Summary

We have analytically solved the wave equaton on the Oppenheimer-Snyder background, and we have obtained two interesting results. The first, it has been found that for large initial radius the late time behaviour of the radiation is dominated by "ringing" and "wave tails". The "ringing" and the "wave tails" are different from that of the Schwarzschild black hole because the structure of the Green's function which we have obtained is different from that of the Schwarzschild black hole (Table 1 and Figure 4). The second, it has been found that there is a final burst which is independ on ratio between the initial radius and the gravitational radius.

References

[1] C.T. Cunningham, R.H. Price and V. Moncrief, Ap. J. **224** (1978), 643.

[2] J. R. Oppenheimer and H. Snyder, Phys. Rev. **56** (1939), 455.

[3] T. Regge and J. A. Wheeler, Phys. Rev. **108** (1957), 1063.

[4] R. M. Wald, Phys. Rev. D **10**, 1680.

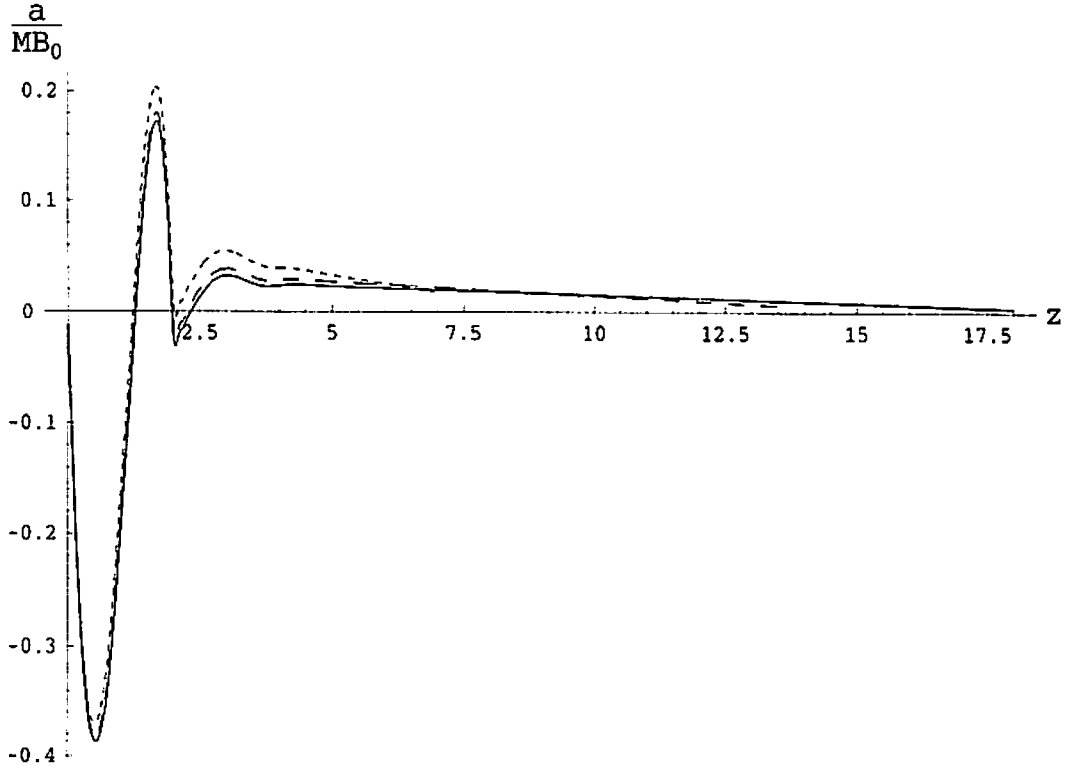

Figure 1: Plot of $\dot{a}/MB_0$ at the stellar surface ($\rho = \rho_b$). The results of $\alpha^2 = 100,\ 60,\ 20$ are ploted.

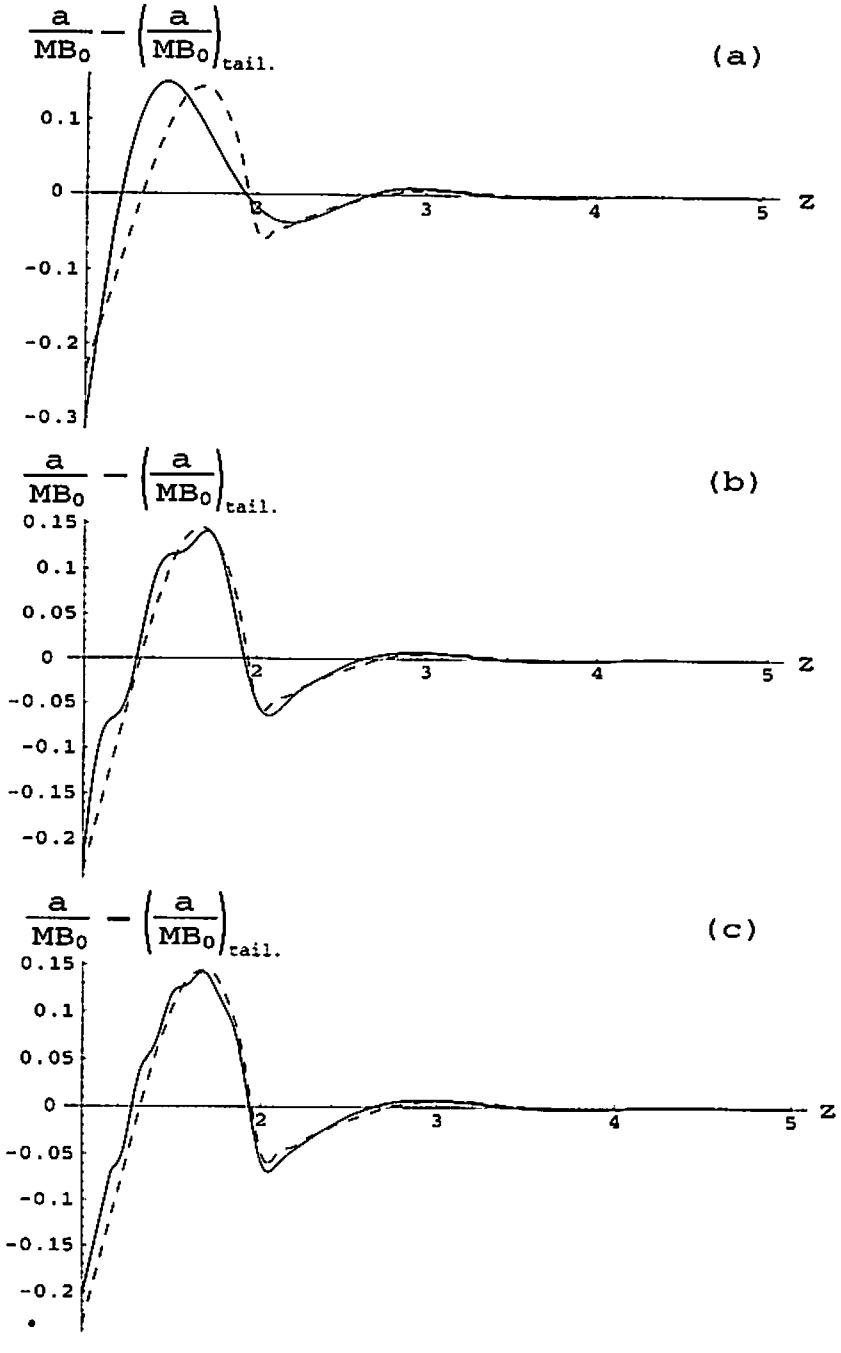

Figure 2: For $\alpha^2 = 100$, comparison between the 'ringing' and the residues summed up to (a) one pole, (b) five poles, and (c) ten poles.

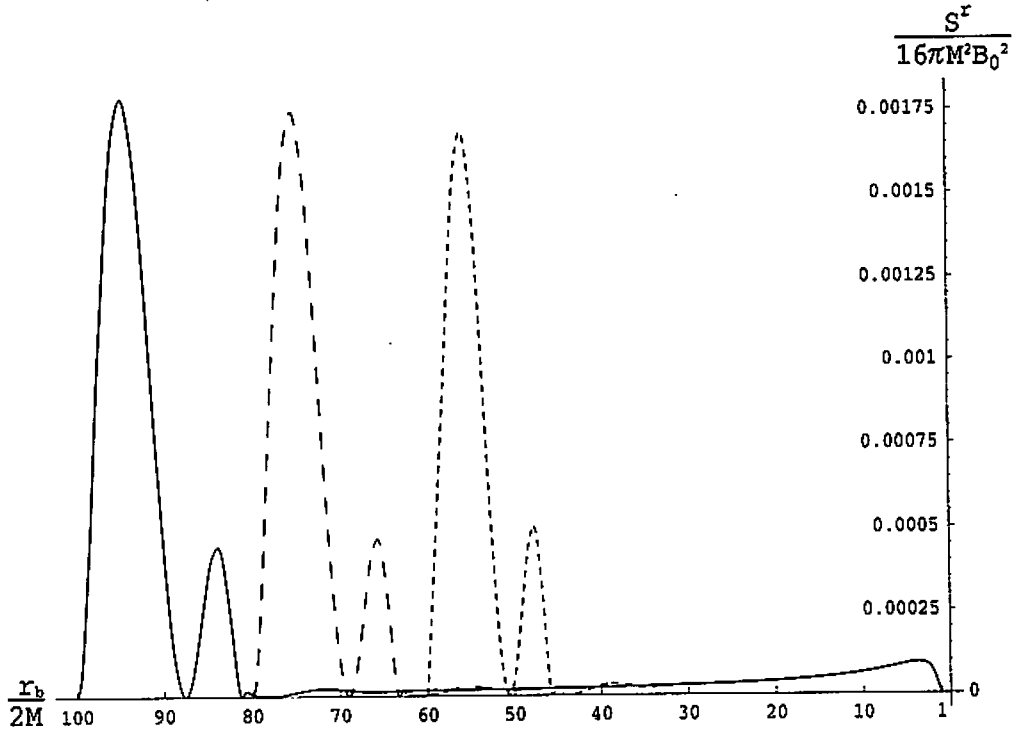

Figure 3: Plot of the Poynting flux. The results of $\alpha^2 = 100,\ 80,\ 60$ are ploted.

$\mathrm{Re}[2M\alpha^2\sigma]$	$\mathrm{Im}[2M\alpha^2\sigma]$
-1.91929	4.28341
-2.42868	7.47945
-2.760095	10.69925
-3.007745	13.8895
-3.206655	17.0647

Table 1: First five quasi-normal modes.

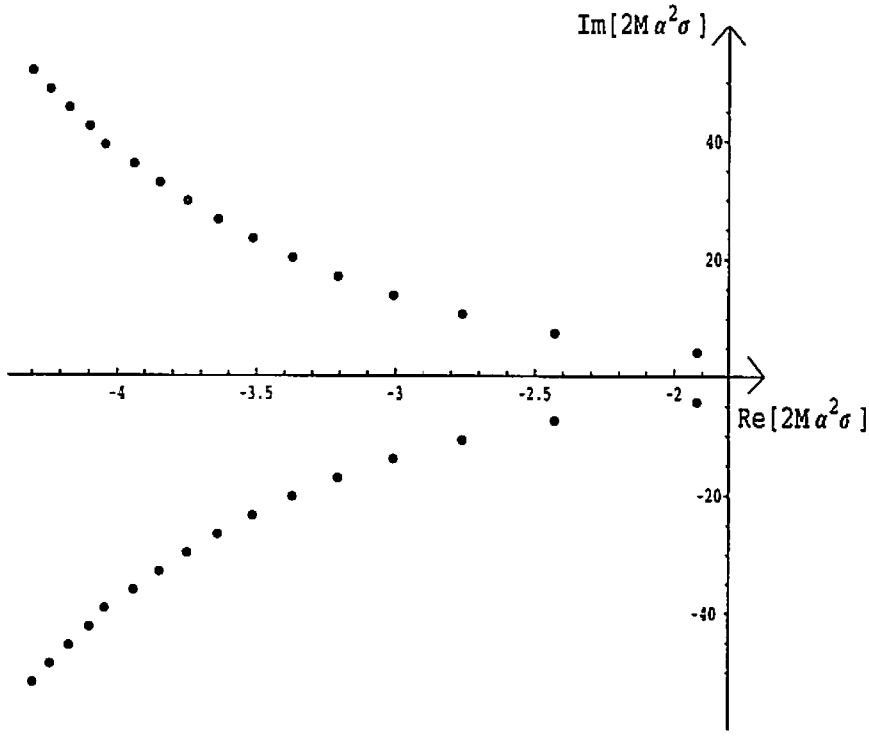

Figure 4: Plot of the QNMs in the $2M\alpha^2\sigma$-plane.

Standing Shocks in MHD Accretions onto Black Holes

Masaaki Takahashi [1]

Department of Physics and Astronomy, Aichi University of Education, Kariya, Aichi 448-8542, Japan

Abstract

We present a fully relativistic study on the standing shock formation for magnetohydrodynamical plasmas in a stationary and axisymmetric black hole magnetosphere. We express all the postshock physical quantities in terms of the relativistic compression ratio. The compression ratio can be obtained by depending on the preshock quantities. Then, the downstream state of a shocked plasma is determined by the upstream state of the accretion. We also discuss the dragging-effects of the rotating black hole on the shock conditions.

1 Introduction

We study the central engine of active galactic nuclei (AGNs). There are many suggestions for the existence of super massive black holes and accreting plasmas in the central regions. In this paper, to explain activities of AGNs, we introduce the effect of magnetic fields and discuss the central engine as "a black hole magnetosphere", where magnetized plasma (ex, an accretion disk and its corona) surrounds a black hole and an accretion and wind/jet would be generated from the surrounding plasma. We treat accreting plasmas onto a black hole and formulate the general relativistic magnetohydrodynamical (MHD) shock conditions. We expect that a very hot plasma area appears near the event horizon by the shock. The emission from this hot plasma would directly bring informations of the black hole to us.

The formation of shocks is based on the existence of multi-magnetosonic points in the accretion solution. This is because an accretion initially ejected from a plasma source with a low velocity must be terminally super-fast magnetosonic at the event horizon. At the shock front, the flow transits from super-magnetosonic to sub-magnetosonic, so the accretion with a shock must pass through a magnetosonic point on each side of the shock front.

The trans-magnetosonic MHD flow solution was discussed by Takahashi [1]. Along the magnetic field line, the five physical quantities are conserved; the total energy and angular momentum, the angular frequency of the magnetic field line, the particle number flux per magnetic flux tube and entropy (see, [2, 3, 4]). When these conserved quantities are given at the plasma source, the locations of the fast/slow magnetosonic points and the Alfvén points are determined. Takahashi [1] demonstrated multi-magnetetosonic points solutions, and found two regimes of accreting flows; that is, "hydro-like" and "magneto-like" accretion solutions. The hydro-like accretion would transit to magneto-like accretion by the shock formation.

In this paper, we apply the shock conditions for special relativistic MHD jets derived by Appl & Camenzind [5] to the shock conditions for general relativistic MHD accretions onto a Kerr black hole. Our main purpose of this extension is to be clear "the general relativistic effects" in MHD shock conditions. We try to express all the postshock physical quantities in terms of the relativistic compression ratio. This compression ratio is the solution of a polynomial of seventh degree; this situation is same as the special relativistic case.

2 Basic Equations of Relativistic Plasma Flow

We assume a stationary and axisymmetric magnetosphere and ignore its self-gravity. We also require infinite conductivity for the plasma flow. The background metric is written by the Boyer-Lindquest

[1] E-mail:takahasi@auephyas.aichi-edu.ac.jp

coordinates. We are using the geometrized units ($c = G = 1$). The basic equations of relativistic plasma flow are as follows:
(i) the particle number conservation

$$(nu^{\alpha})_{;\alpha} = 0 \; ; \tag{1}$$

(ii) the conservation of total energy and momentum

$$T^{\alpha\beta}_{\;\;;\beta} = 0 \; , \tag{2}$$

where the energy-momentum tensor is given by

$$T^{\alpha\beta} = n\mu u^{\alpha}u^{\beta} - Pg^{\alpha\beta} + \frac{1}{4\pi}\left(F^{\alpha}_{\;\lambda}F^{\lambda\beta} + \frac{1}{4}g^{\alpha\beta}F^2\right) \; , \tag{3}$$

n is the proper particle number density, μ is the relativistic specific enthalpy, P is the pressure and $F^2 = F^{\mu\nu}F_{\mu\nu}$;
(iii) MHD condition

$$u^{\beta}F_{\alpha\beta} = 0 \; . \tag{4}$$

The magnetic field and electric field seen by a distant observer are defined as

$$B_{\alpha} \equiv \frac{1}{2}\eta_{\alpha\beta\gamma\delta}k^{\beta}F^{\gamma\delta} \tag{5}$$

$$E_{\alpha} \equiv F_{\alpha\beta}k^{\beta} \tag{6}$$

where $k^{\alpha} = (1,0,0,0)$ is the time-like killing vector and $\eta_{\alpha\beta\gamma\delta} \equiv \sqrt{-g}\,\epsilon_{\alpha\beta\gamma\delta}$.

Further, we introduce the angular velocity of the magnetosphere (see, [2])

$$\Omega_F \equiv -\frac{F_{tr}}{F_{\phi r}} = -\frac{F_{t\theta}}{F_{\phi\theta}} \; . \tag{7}$$

Then, we obtain the following useful expressions

$$E_{\theta} = \frac{-\sqrt{-g}\,\Omega_F}{g_{tt} + g_{t\phi}\Omega_F}B^{r} \; , \tag{8}$$

$$E_{r} = \frac{\sqrt{-g}\,\Omega_F}{g_{tt} + g_{t\phi}\Omega_F}B^{\theta} \; , \tag{9}$$

3 MHD Flows

In this section, we summarize the relativistic MHD flows (the relativistic Bernoulli equation; see, [6, 7]). The energy and angular momentum of the fluid are

$$\mu u_t = \frac{M^2E - eG_t}{M^2 - \alpha} \; , \tag{10}$$

$$\mu u_{\phi} = -\frac{M^2L + eG_{\phi}}{M^2 - \alpha} \; , \tag{11}$$

where $M^2 \equiv 4\pi\eta^2(\mu/n)$ is the Alfvén Mach number, E and L are total energy and angular momentum seen by a distant observer, $e \equiv (E - \Omega_F L)$ is the total energy seen by a corotating observer with the magnetic field line, $G_t \equiv (g_{tt} + g_{t\phi}\Omega_F)$, $G_t \equiv (g_{t\phi} + g_{\phi\phi}\Omega_F)$ and $\alpha \equiv G_t + G_{\phi}\Omega_F$. The particle number flux per magnetic flux tube can be written as

$$\eta = -\frac{nu^{r}}{B^{r}}G_t \; . \tag{12}$$

The poloidal equation of the magnetized flow is written as

$$(1 + u_p^2) = (E/\mu)^2[(\alpha - 2M^2)f^2 - k] \; , \tag{13}$$

where

$$f \equiv -\frac{G_\phi + G_t \tilde{L}}{\rho_w (M^2 - \alpha)} , \tag{14}$$

$$k \equiv -(g^{tt} - 2g^{t\phi}\tilde{L} + g^{\phi\phi}\tilde{L}^2) , \tag{15}$$

u_p is the poloidal velocity defined by $u_p^2 \equiv -u^A u_A$ $(A = r, \theta)$ and $\tilde{L} \equiv L/E$. When we neglect dissipative effects and cooling in the plasma, the flow is adiabatic with a specific enthalpy of the form (see, [4])

$$\mu = m_p + \frac{\Gamma}{\Gamma - 1}\frac{P}{n} . \tag{16}$$

The toroidal component of the magnetic field is can be expressed

$$B_\phi = 4\pi\eta \frac{G_\phi E + G_t L}{M^2 - \alpha} . \tag{17}$$

4 The Jump Conditions

We discuss the properties of MHD shocks associated with accretion flows. The accretion is originated from the plasma source, which is the surface of a torus rotating around a black hole. We expect that the strong shock would be produced at somewhere between the plasma source and the event horizon.

In a complete solution of the accretion which includes a shock, the flow must satisfy a set of conditions on either side of the discontinuity. The jump conditions for arbitrary shocks in a relativistic MHD flow are

$$[nu^\alpha]n_\alpha = 0 , \quad \text{— the particle number conservation} \tag{18}$$

$$[T^{\alpha\beta}]n_\alpha = 0 , \quad \text{— the energy momentum conservation} \tag{19}$$

$$[\mathrm{E}] \times \mathrm{n} = 0 , \quad \text{— the continuity relations for the electric field} \tag{20}$$

$$[\mathrm{B}] \cdot \mathrm{n} = 0 , \quad \text{— the continuity relations for the magnetic field} \tag{21}$$

where $n^\alpha = (n_0, \mathrm{n})$ and the square brackets denote the difference between the values of a quantity on the two side of the shock. We assume that the downstream flow velocity is radial (normal to the event horizon) and the shock front is perpendicular to the downstream flow n=(1,0,0) as shown in Figure 1. Then, we set

$$u_1^\alpha = (u_1^t, u_1^r, u_1^\theta, u_1^\phi) , \tag{22}$$

$$u_2^\alpha = (u_2^t, u_2^r, 0, u_2^\phi) , \tag{23}$$

$$B_1^\alpha = (B^r, B_1^\theta, B_1^\phi) , \tag{24}$$

$$B_2^\alpha = (B^r, 0, B_2^\phi) , \tag{25}$$

$$E_1^\alpha = (E_1^r, E^\theta, 0) , \tag{26}$$

$$E_2^\alpha = (0, E^\theta, 0) , \tag{27}$$

where eqs. (20) and (21) have been used. From eq. (8), we see that Ω_F does not change across the shock. Equations (18) and (19) evaluated in the shock rest frame yield the following relations

$$n_1 u_1^r = n_2 u_2^r , \tag{28}$$

$$\begin{aligned} & n_1\mu_1(u^r u_r)_1 - P_1 + \frac{1}{8\pi g_{tt}}(-E_1^r E_{r1} + B_1^\theta B_{\theta 1} + B_1^\phi B_{\phi 1}) \\ = \; & n_2\mu_2(u^r u_r)_2 - P_2 + \frac{1}{8\pi g_{tt}}(B_2^\phi B_{\phi 2}) , \end{aligned} \tag{29}$$

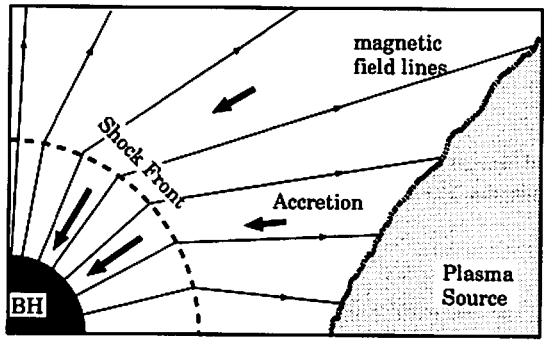

Figure 1: A schematic picture of accretion onto a black hole with a shock front.

$$n_1\mu_1 u_1^r u_1^\theta - \frac{1}{4\pi g_{tt}}\left(B^r B_1^\theta + E_1^r E^\theta\right) = 0\,, \tag{30}$$

$$n_1\mu_1 u_1^r u_1^\phi - \frac{1}{4\pi g_{tt}}\left(B_1^\phi B^r\right) = n_2\mu_2 u_2^r u_2^\phi - \frac{1}{4\pi g_{tt}}\left(B_2^\phi B^r\right)\,, \tag{31}$$

$$n_1\mu_1 u_1^r u_1^t - \frac{1}{4\pi g_{tt}}\left(\frac{B_{\phi 1}E_\theta}{\sqrt{-g}} + B_1^t B^r\right) = n_2\mu_2 u_2^r u_2^t - \frac{1}{4\pi g_{tt}}\left(\frac{B_{\phi 2}E_\theta}{\sqrt{-g}} + B_2^t B^r\right)\,, \tag{32}$$

where the subscripts "1" and "2" denote the preshock and the postshock quantities, respectively. From the MHD conditions, we also obtain

$$E_{r1}u_{t1} + \sqrt{-g}(B_1^\phi u_1^\theta - B_1^\theta u_1^\phi) = 0\,, \tag{33}$$

$$(B^r u_1^\phi - B_1^\phi u_1^r)\frac{1}{u_{t1}} = \frac{-E_\theta}{\sqrt{-g}} = (B^r u_2^\phi - B_2^\phi u_2^r)\frac{1}{u_{t2}}\,, \tag{34}$$

$$(g_{t\phi}E_\theta + \sqrt{-g}B^r)u_1^\theta + (g_{t\phi}E_{r1} - \sqrt{-g}B_1^\theta)u_1^r = 0\,, \tag{35}$$

$$E_{r1}u_1^r + E_{\theta 1}u_1^\theta = 0\,. \tag{36}$$

From the shock condition of $(T^{rt})_1 = (T^{rt})_2$, we obtain

$$(E - \omega L)_1 = (E - \omega L)_2\,, \tag{37}$$

where $\omega \equiv -g_{t\phi}/g_{\phi\phi}$ is the angular velocity of the zero angular momentum observer (ZAMO) with respect to a distant observer, and from the shock condition of $(T^{r\phi})_1 = (T^{r\phi})_2$, we also obtain

$$(g_{t\phi}E + g_{tt}L)_1 = (g_{t\phi}E + g_{tt}L)_2\,. \tag{38}$$

From these relations, we see $E_1 = E_2$ and $L_1 = L_2$.

5 Dimensionless Parameters

For any stationary and axisymmetric system we can define conserved flux vectors for energy and angular momentum about the axis of symmetry (see, [8]). From the conservation of total energy and momentum (2) and the Killing equation $\chi_{\mu;\nu} + \chi_{\nu;\mu} = 0$, where χ^μ is a Killing vector, it follows that $(\chi_\mu T^{\mu\nu})_{;\nu} = 0$. Thus, we define the conserved energy flux

$$\mathcal{E}^\mu = T^{\mu\nu}k_\nu = T_t^\mu = (T_t^\mu)_{\rm em} + (T_t^\mu)_{\rm fluid}$$

and angular momentum flux

$$-\mathcal{L}^{\mu} = T^{\mu\nu} m_{\nu} = T^{\mu}_{\phi} = (T^{\mu}_{\phi})_{\rm em} + (T^{\mu}_{\phi})_{\rm fluid}$$

where m^{ν} is the axial Killing vector with Boyer-Lindquist component (0,0,0,1). In the case of MHD flows, these fluxes is composed of the electromagnetic part labeled by "em" and fluid part labeled by "fluid". The fluid and electromagnetic parts of the radial component of energy flux $\mathcal{E}^{r}$ are

$$\mathcal{E}^{r}_{\rm fluid} \equiv (T^{r}_{t})_{\rm fluid} = n\mu u^{r} u_{t} , \tag{39}$$

$$\mathcal{E}^{r}_{\rm em} \equiv (T^{r}_{t})_{\rm em} = -\frac{B_{\phi} E_{\theta}}{4\pi\sqrt{-g}} = \frac{B_{\phi} B^{r} \Omega_{F}}{4\pi(g_{tt} + g_{t\phi}\Omega_{F})} , \tag{40}$$

respectively, and the fluid and electromagnetic parts of the radial component of angular momentum flux $\mathcal{L}^{r}$ are

$$-\mathcal{L}^{r}_{\rm fluid} \equiv (T^{r}_{\phi})_{\rm fluid} = n\mu u^{r} u_{\phi} , \tag{41}$$

$$-\mathcal{L}^{r}_{\rm em} \equiv (T^{r}_{\phi})_{\rm em} = -\frac{B_{\phi}}{4\pi g_{tt}} \left(\frac{g_{t\phi} E_{\theta}}{\sqrt{-g}} + B^{r} \right) = -\frac{B_{\phi} B^{r}}{4\pi(g_{tt} + g_{t\phi}\Omega_{F})} , \tag{42}$$

respectively, where we have used the relation (8).

From the energy momentum conservation at the shock front, we have $(T^{rt})_1 = (T^{rt})_2$. T^{rt} can be reduced as

$$T^{rt} = g^{tt}(\mathcal{E}^{r}_{\rm fluid} + \mathcal{E}^{r}_{\rm em}) - g^{t\phi}(\mathcal{L}^{r}_{\rm fluid} + \mathcal{L}^{r}_{\rm em}) \tag{43}$$

$$= g^{tt} \left\{ n\mu u^{r} u_{t} (1 - \omega\ell) + \frac{B_{\phi} B^{r} (\Omega_{F} - \omega)}{4\pi(g_{tt} + g_{t\phi}\Omega_{F})} \right\} , \tag{44}$$

where $\ell \equiv -u_{\phi}/u_{t}$ is the specific angular momentum of plasma.

Here, we define dimensionless parameters. First, we define the "magnetization parameter", which denotes the ratio of the Poynting flux and the total mass-energy flux seen by ZAMO,

$$\sigma \equiv \frac{(\mathcal{E}^{r} - \omega\mathcal{L}^{r})_{\rm em}}{(\mathcal{E}^{r} - \omega\mathcal{L}^{r})_{\rm fluid}} , \tag{45}$$

then we can express eq. (43) as

$$T^{rt} = g^{tt}(\mathcal{E}^{r} - \omega\mathcal{L}^{r})_{\rm fluid}(1 + \sigma) . \tag{46}$$

This magnetization parameter can be reduced to

$$\sigma = \frac{B_{\phi}}{4\pi\eta(\mu u^{t})} \frac{G_{\phi}}{\rho_{w}^{2}} . \tag{47}$$

By using (10) and (11), σ is denoted in terms of M^2, E, L, Ω_F; that is,

$$\sigma = -\frac{(G_{\phi}E + G_{t}L)G_{\phi}}{\rho_{w}^{2} e + (g_{\phi\phi}E + g_{t\phi}L)M^{2}} = -\frac{e - h\alpha}{e - hM^{2}} , \tag{48}$$

where $h \equiv g^{tt}(E - \omega L)$. We can also express M^2 in terms of σ, E, L, Ω_F.

Next, we define the following dimensionless parameters

$$q \equiv \frac{B_{\phi 2}}{B_{\phi 1}} = \frac{M_{1}^{2} - \alpha}{M_{2}^{2} - \alpha} . \tag{49}$$

$$\zeta \equiv \frac{\mu_{2} u_{2}^{t}}{\mu_{1} u_{1}^{t}} = \frac{e - hM_{2}^{2}}{e - hM_{1}^{2}} q , \tag{50}$$

$$\xi \equiv \frac{n_{2} u_{2}^{t}}{n_{1} u_{1}^{t}} = \frac{M_{1}^{2}}{M_{2}^{2}} \zeta . \tag{51}$$

where q is the amplification factor in the transverse magnetic field and ξ is the shock frame compression ratio, and from eqs. (28), (32), (34) we obtain the following relation

$$1-\zeta=\sigma_1(q-1)\ . \tag{52}$$

The normalisation of the 4-velocity gives an equation for u_2^t

$$u_2^t=\left\{g_{tt}+2g_{t\phi}\Omega_2+g_{\phi\phi}\Omega_2^2+\frac{(u^r u_r)_1}{\xi^2(u_1^t)^2}\right\}^{-1/2}\ , \tag{53}$$

where $\Omega\equiv u^\phi/u^t$ is the angular velocity of fluid, and

$$\Omega_2=\frac{e\Omega_F-\rho_w^{-2}(g_{t\phi}E+g_{tt}L)M_2^2}{e-hM_2^2}\ . \tag{54}$$

When other postshock quantities ξ or M_2 are determined, u_2^t can be obtained.

From eq. (29), we obtain

$$1-\frac{\zeta}{\xi}-\frac{P_1-P_2}{n_1\mu_1(u^r u_r)_1}+\frac{(-E^rE_r+B^\theta B_\theta+B^\phi B_\phi)_1-(B^\phi B_\phi)_2}{8\pi n_1\mu_1(u^r u_r)_1 g_{tt}}=0\ . \tag{55}$$

Using the relations

$$-E^rE_r+B^\theta B_\theta = \frac{g_{tt}\alpha}{(g_{tt}+g_{t\phi}\Omega_F)^2}B^\theta B_\theta\ , \tag{56}$$

$$(B^\phi B_\phi)_1-(B^\phi B_\phi)_2 = (B^\phi B_\phi)_1(1-q^2)\ , \tag{57}$$

we get

$$1-\frac{\zeta}{\xi}=\Pi-\mathcal{X}_1+(q^2-1)\mathcal{T}_1 \tag{58}$$

with

$$\Pi \equiv \frac{P_1-P_2}{n_1\mu_1(u^r u_r)_1}=1-\frac{1}{\xi}+\frac{\sigma_1}{\xi}(q-1)+\mathcal{X}_1-(q^2-1)\mathcal{T}_1\ , \tag{59}$$

$$\mathcal{X}_1 \equiv \frac{\alpha(B^\theta B_\theta)_1}{2B^r B_r M_1^2}\ , \tag{60}$$

$$\mathcal{T}_1 \equiv \frac{\sigma_1}{2}\left(\frac{u_t}{u^r}\right)_1^2\frac{\rho_w^2(\Omega_1-\Omega_F)}{g_{rr}G_\phi}\ , \tag{61}$$

which is dependent on ξ, q and upstream parameters M_1^2 (or σ_1), E, L, Ω_F. The relation between M_2^2 and M_1^2 are given by the poloidal equation (13). We will discuss this relation in the following sections.

Here, we restrict ourselves to cold accretions ($P_1=0$). Using the definition of ζ and the equation of state for a Boltzmann gas with polytropic index Γ

$$\mu_1 = m_p c^2 \tag{62}$$

$$\mu_2 = m_p c^2\left(1+\frac{\Gamma}{\Gamma-1}\frac{P_2}{n_2 m_p c^2}\right)\ , \tag{63}$$

we find with eq. (59)

$$1-\frac{u_2^t}{u_1^t}=\sigma_1(q-1)-\frac{\Gamma}{\Gamma-1}\frac{g_{rr}(u^r/u^t)_1^2(u_2^t)^2}{\xi}\Pi\ . \tag{64}$$

Combining eqs. (49) and (52) gives the quadratic equation for ζ

$$\zeta^2-\left\{1+\sigma_1+\left(\frac{G_t}{M_1^2}-\frac{\sigma_1\Omega_F}{\Omega_F-\Omega_1}\right)\xi\right\}\zeta+\left(\frac{G_t}{M_1^2}-\frac{\sigma_1\Omega_1}{\Omega_F-\Omega_1}\right)\xi=0\ . \tag{65}$$

We are now able to eliminate u_2^t and q from eq. (64) and after considerable manipulations we end up with a polynomial of seventh degree in ξ

$$\sum_{i=0}^{7} c_i(M_1^2, \Gamma; m, a, E, L, \Omega_F)\xi^i = 0 \ . \tag{66}$$

The coefficients c_i are dependent only on upstream parameters, except for Γ, which is a function of the downstream temperature (see, [5]). The polynomial (66) has in general several real solutions corresponding to the different shock transitions. Then, the downstream quantities ζ, q, u_2^t, u_2^r, Ω_2, Π are obtained from equations, (65), (49), (53), (28), (54), (59), respectively.

6 Shock Formation

Here, to obtain the trans-fast magnetosonic MHD flow solution including the shock formation, we introduce the "entropy related" mass flow rate defined by [9]

$$\dot{\mathcal{M}} \equiv K^N(m_p\eta) = (\rho K^N)(\eta/n) \ . \tag{67}$$

This quantity $\dot{\mathcal{M}}$ conserves for a shock-free flow, but can become larger at the shock due to the generation of entropy. To express $\dot{\mathcal{M}}$ in terms of r, M^2 with the conserved quantities, we obtain the following relations;

$$\rho K^N = \left\{\frac{Na_{sw}^2}{(1+N)(1-Na_{sw}^2)}\right\}^N = \left\{\frac{1}{1+N}\left(\frac{\mu}{m_p}-1\right)\right\}^N \tag{68}$$

and

$$\frac{\eta}{n} = \frac{M^2}{4\pi\mu\eta} \ . \tag{69}$$

Here, the sound velocity is defined by

$$a_{sw}^2 \equiv \left(\frac{dP}{d\epsilon}\right) = \frac{1}{N}\frac{\mu - m_p}{\mu} = \frac{\Gamma P}{n\mu} \ . \tag{70}$$

Thus, we can reduce eq.(67) to

$$\dot{\mathcal{M}} = \frac{M^2}{4\pi\mu\eta}\left\{\frac{1}{1+N}\left(\frac{\mu}{m_p}-1\right)\right\}^N \ . \tag{71}$$

From the poloidal equation (13), the enthalpy can be expressed in terms of r and M^2 with the conserved quantities

$$\mu^2 = E^2\left\{(\alpha - 2M^2)f^2 - k\right\} - \left(\frac{B_p M^2}{4\pi\eta}\right)^2 \ . \tag{72}$$

Then, using the relation (72), we can express the entropy related accretion rate as functions of r and M^2 with the conserved quantities; that is,

$$\dot{\mathcal{M}} = F(r, M^2; E, \tilde{L}, \Omega_F, \eta, N, m, a; \Psi), \tag{73}$$

where $\Psi = \Psi(r,\theta)$ is an assumed magnetic stream function. Thus, we can plot $\dot{\mathcal{M}}$ = constant lines on the r-M^2 plane. At the shock front, the line of $\dot{\mathcal{M}} = \dot{\mathcal{M}}_1$ connects to the line of $\dot{\mathcal{M}} = \dot{\mathcal{M}}_2$ by a vertical line on the r-M^2 plane, where the condition of $\dot{\mathcal{M}}_1 < \dot{\mathcal{M}}_2$ is required.

We can treat the poloidal equation (13) as functions of r and M^2 (or u_p) for the postshock flow. Then, at the shock location of $r = r_{sh}$, we would obtain two (or more) solutions of M^2 or u_p. We should consider a situation that a trans-fast MHD accretion ejected from the plasma source produces the shock front at $r = r_{sh}$ with the Mach number $M = M_1$, and then the postshock flow with the Mach number $M = M_2 < M_1$ accretes onto the black hole after passing the fast magnetosonic point again; of course, these Alfvén Mach number of M_1^2 and M_2^2 must satisfy the condition (66). To obtain the accretion passing through the fast magnetosonic point twice times by the shock formation, we must find the acceptable parameter ranges of conserved quantities carefully. This is the next step of this research.

7 Concluding Remarks

We have discussed about the general relativistic MHD shock conditions for the accretion onto a rotating black hole. Here, we introduce the magnetization parameter seen by ZAMO, because the shock conditions are related to local plasmas and the magnetosphere is dragged by the rotating black hole. Then, we can obtain the similar expressions of special relativistic case, while those formulas include the Kerr metric at many places.

We have seen that the compression ratio ξ is the solution of a polynomial of seventh degree. The concrete expressions of c_i and more detail analysis will be presented by Rilett et al. [10]. In future, we will be to discuss applications of the results for accreting plasma in a black hole magnetosphere; that is, we will treat a multi-magnetosonic points solution with the shock formation.

References

[1] M. Takahashi, in Proceedings of the 19th Texas Symposium on Relativistic Astrophysics and Cosmology, eds. J. Paul, T. Montmerle, and E. Aubourg, CEA Saclay (1998)

[2] J.D. Bekenstein and E. Oron, Phys. Rev. **D18** (1978) 1809.

[3] M. Camenzind, A&A, **156** (1986), 137.

[4] M. Camenzind, A&A, **184** (1987), 341.

[5] S. Appl and M. Camenzind, A&A, **206** (1988), 258.

[6] M. Camenzind, A&A, **162** (1986), 32.

[7] M. Takahashi, S. Nitta, Y. Tatematsu and A. Tomimatsu, ApJ, **363** (1990), 206.

[8] R.D. Blandford and R.L. Znajek, MNRAS, **179** (1977), 433.

[9] S.K. Chakrabarti, ApJ, **347** (1989), 365.

[10] D. Rilett, M. Takahashi, K. Fukumura and S. Tsuruta, (2000) in preparation.

Hypernovae and Black Hole Formation

Takayoshi Nakamura[1], Keiichi Maeda[1],Koichi Iwamoto[2],
Tomoharu Suzuki[1], Ken'ichi Nomoto[1], Paolo A. Mazzali[1,3],
Massimo Turatto[4] I. John Danziger[3], Ferdinando Patat[5]

[1] *Department of Astronomy and Research Center for the Early Universe, University of Tokyo, Japan*
[2] *Department of Physics, College of Science and Technology, Nihon University, Japan*
[3] *Osservatorio Astronomico di Trieste, via G. B. Tiepolo, Trieste, Italy*
[4] *Osservatorio Astronomico di Padova, vicolo dell'Osservatorio, Padova, Italy*
[5] *European Southern Observatory, Garching, Germany*

Abstract

We discuss the properties of the very energetic Type Ic supernovae (SNe Ic) 1998bw and 1997ef and Type IIn supernova (SN IIn) 1997cy. SNe Ic 1998bw and 1997ef are characterized by their large luminosity and the very broad spectral features. Their observed properties can be explained if they are very energetic SN explosions ($E_K \gtrsim 1 \times 10^{52}$ erg), originating probably from the core collapse of the bare C+O cores of massive stars ($\sim 30 - 40 M_\odot$). At late times, both the light curve and the spectra suggest that the explosion may have been asymmetric; this may help us understand the claimed connection with GRB's. Type IIn SN 1997cy is even more luminous than SN 1998bw and the light curve declines more slowly than the ^{56}Co decay. We model such a light curve with circumstellar interaction, which requires the explosion energy of $\sim 5 \times 10^{52}$ erg. Because these kinetic energies of explosion are much larger than in normal core-collapse SNe, we call objects like these SNe "hypernovae".

1 Introduction

The kinetic energies of core-collapse supernovae, i.e., Type II and Ib/c supernovae (SNe II, Ib/c), are fundamentally important quantities in relation to the explosion mechanism, impact on interstellar medium, nucleosynthesis. In this paper, we use E_K as the terminal kinetic energy of the ejecta. Typically $E_K \sim 1 \times 10^{51}$ ergs, and a good example is SN 1987A in the Large Magellanic Cloud, whose energy is estimated to be $E_K = (1.0 - 1.5) \times 10^{51}$ ergs from its early light curve and spectra (e.g., Shigeyama & Nomoto 1990).

However, SN Ic 1998bw clearly demonstrated that it is not always the case. This supernova was almost 10 times brighter than typical SN Ic 1994I and its spectra show unusually broad feature, which suggests a large explosion energy. More interestingly SN 1998bw was discovered in the error box of the gamma-ray burst GRB980425 one day after this GRB, which suggests a connection between these two events.

Other candidates for energetic supernovae, which we call "hypernovae" if $E_K \gtrsim 10^{52}$ ergs to distinguish from canonical supernovae, have been discovered recently. SN Ic 1997ef shows very broad spectral features similar to SN 1998bw. The Type IIn supernova (SN IIn) 1997cy, which might have been associated with GRB970514, is unusually bright (Germany et al. 1999; Turatto et al. 1999). In this paper, we study these three objects, SNe Ic 1997ef, 1998bw and SN IIn 1997cy, as hypernova candidates.

2 SN 1997ef

SN 1997ef has been noticed for its unique light curve and spectra. At early times, the spectra were dominated by broad oxygen and iron absorption lines, but did not show any clear feature of hydrogen or helium (Garnavich et al. 1997; Filippenko et al. 1997), which led us to classify SN 1997ef as a SN Ic. The most striking and peculiar feature of the spectra of SN 1997ef is the broadness of the line features, which suggests that SN 1997ef may have a large explosion energy. A possible connection with a GRB

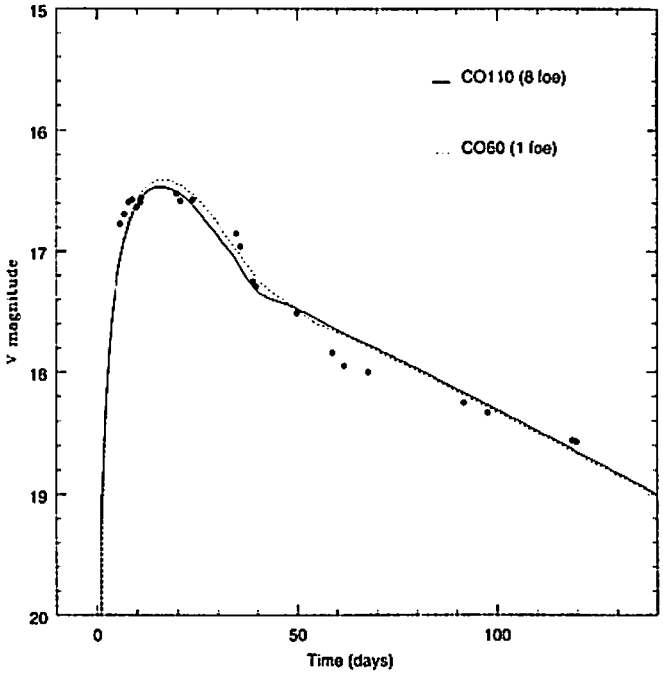

Figure 1: The V light curves of models CO100 (solid line) and CO60 (dashed line) compared with the observations of SN 1997ef. A distance modulus of $\mu = 33.6$ mag is adopted.

was also suggested for SN 1997ef: GRB971115 appears in fact to be compatible with SN 1997ef in the position and time occurrence of the SN (Wang & Wheeler 1998).

In order to clarify whether SN 1997ef is indeed a hypernova, we constructed hydrodynamical models for an ordinary SN Ic and for a hypernova (Iwamoto et al. 2000). For the ordinary SN Ic (model CO60), a C+O star with a mass $M_{\rm CO} = 6.0 M_\odot$ (the core of a 25 $M_\odot$ star) is exploded with a kinetic energy $E_{\rm K} = 1.0 \times 10^{51}$ ergs and an ejecta mass $M_{\rm ej} = 4.6 M_\odot$. For the hypernova model (CO100), a C+O star of $M_{\rm CO} = 10.0 M_\odot$ (the core of a 30 - 35 $M_\odot$ star) is exploded with $E_{\rm K} = 8.0 \times 10^{51}$ ergs and $M_{\rm ej} = 8.0 M_\odot$. The mass of ^{56}Ni is set to be 0.15 $M_\odot$ for both models to explain the observed peak brightness.

In Figure 1 we compare the synthetic V light curves for models CO60 and CO100 with the V light curve of SN 1997ef. A distance modulus of $\mu = 33.6$ mag and a color excess $E(B-V) = 0.00$ are adopted. Both models give synthetic light curves with quite a broad peak and a relatively slow tail, which reproduce the light curve of SN 1997ef reasonably well. We should note that the model light curve declines somewhat faster than the observed tail of SN 1997ef and, as shown later, of SN 1998bw. We will see in the next section that this might be due to some asymmetry in the explosion.

Light curve modeling provides important constraints on $M_{\rm CO}$ and $E_{\rm K}$. However, it is difficult to distinguish clearly between the ordinary SN Ic and the hypernova model from the light curve alone, since models with different values of $M_{\rm ej}$ and $E_{\rm K}$ can reproduce the observed light curve equally well if $M_{\rm ej}^{3/4} E_{\rm K}^{-1/4} = $ const. On the other hand, these models can be expected to produce different spectra, because of the different $E_{\rm K}$. Therefore, spectrum synthesis can tell these models apart, taking advantage of their differences.

Based on the hydrodynamical models CO60 and CO100, i.e., using their density structure and composition, we computed synthetic spectra using a Monte Carlo spectrum synthesis code (Mazzali & Lucy 1993; Lucy 1999; Mazzali 2000). Spectra computed with model CO60 for the first three epochs are compared to the observed spectra in Figure 2 (left). All synthetic spectra show narrow lines, much narrower

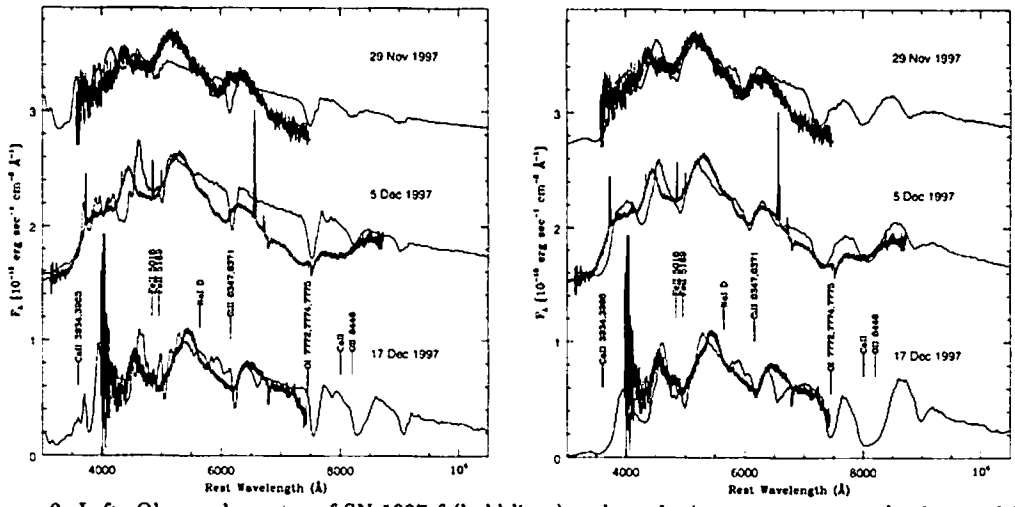

Figure 2: Left: Observed spectra of SN 1997ef (bold lines) and synthetic spectra computed using model CO60. The lines in the synthetic spectra are much too narrow. Right: Observed spectra of SN 1997ef (bold lines) and synthetic spectra computed using model CO100 (fully drawn lines).

than the observations. This clearly indicates a lack of material at high velocity in model CO60, and suggests that the kinetic energy of this model is too small. Synthetic spectra computed with model CO100 for the same three epochs are also shown in Figure 2 (right). The spectra have much broader lines, and are in good agreement with the observations.

Since the spectra of SN 1997ef are reproduced much better with the energetic model CO100 than with the ordinary SN Ic model CO60, We conclude that SN 1997ef is a hypernova.

3 SN 1998bw

SN 1998bw is very likely connected with GRB980425 (Galama et al. 1998; Kulkarni et al. 1998). This object was soon identified to be a supernova from its light curve, which was different from those of typical optical transients of gamma-ray bursts (Galama et al. 1998; Patat et al. 2000). Early spectra were rather blue and featureless, quite unlike any other known SNe. However, more careful inspection showed striking similarities with the spectra of Type Ic SNe, but with one major difference: the absorption lines are so broad in SN 1998bw that they blend together, giving rise to what could even be confused with an emission spectrum. Velocities in the Si II 6355Å line are as high as 30,000 km s^{-1}. Also, the SN was very bright for a SN Ic: the observed peak luminosity, $L \sim 1.4 \times 10^{43}$ erg s^{-1}, is almost ten times higher than that of previously known SNe Ib/Ic (Iwamoto et al. 1998; Woosley et al. 1999).

We calculate the light curves and spectra for various C+O star models with different values of E_K and M_{ej}. These parameters can be constrained by comparing the calculated light curves, the synthetic spectra, and the photospheric velocities with the data of SN 1998bw. Here we describe the best model, which is the explosion of a 13.8 $M_\odot$ C+O star with a large kinetic energy ($E_K = 6 \times 10^{52}$ erg). Such a massive C+O star progenitor is the product of a main-sequence star of $\sim 40\ M_\odot$ which lost its H/He envelope via a stellar wind or binary interaction. For a distance modulus of $\mu = 32.89$ mag, a ^{56}Ni mass of $\sim 0.63 M_\odot$ is necessary to reproduce the light curve maximum. Figure 4 shows the observed spectra of SN1998bw (solid lines) and synthetic spectra computed using model CO138 (dashed lines). We can see that the broad lines are well reproduced because we have enough material at high velocities in this model.

Despite the success of our 'hypernova' model in reproducing he early light curve of SN 1998bw ($t \lesssim 60$ days), the model light curve tail declines more rapidly than the observations. After day ~ 200 the

decline of the model light curve becomes slower, and it approaches the half-life of ^{56}Co decay around day 400. At $t \gtrsim 400$ days most γ-rays escape from the ejecta, while positrons emitted from the ^{56}Co decay are mostly trapped and their energies are thermalized. Therefore, positron deposition determines the light curve at $t \gtrsim 400$ days. If the observed tail should follow the positron-powered light curve, the ^{56}Co mass could be determined directly.

The deviation of the model light curve from the observation at $t \gtrsim 60$ days suggests that there might be a high density region in the ejecta of SN1998bw, where the γ-rays are efficiently trapped. Another unexpected features appeared in the late phase spectra. Measuring the velocity of each element (Patat et al. 1999), we note that iron expands faster than oxygen, which is contrary to expectations.

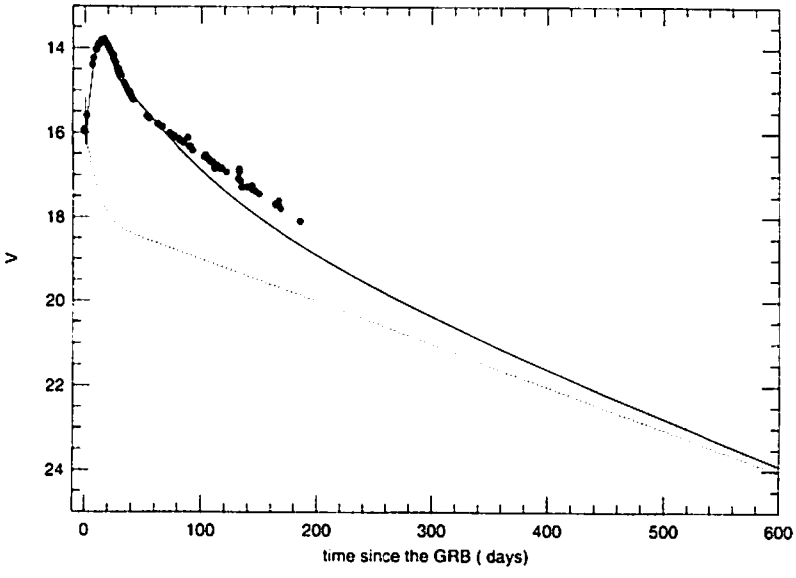

Figure 3: The light curve of model CO138 compared with the observations of SN1998bw. A distance modulus of $\mu = 32.89$ mag is adopted. The dotted line indicates the energy deposited by the positrons.

Both the need for a high density region and the velocity inversion might indicate that the explosion is aspherical (Höflich et al. 1999; MacFadyen & Woosley 1999). If the outburst in SN 1998bw took the form of a prolate spheroid, as also indicated by polarization measurements (Patat et al. 2000), the explosive shock along the long axis was probably strong, ejecting material with large velocities and producing abundant ^{56}Ni. In directions away from the long axis, on the other hand, oxygen is not consumed and the density is high enough for γ-rays to be trapped even at advanced phases, thus giving rise to the slowly declining tail (See §5).

4 SN1997cy

SN 1997cy was discovered on July 16, 1997 in the compact and faint galaxy of the cluster Abell 3266 Cluster at a distance modulus of $\mu = 37.40$ (Germany et al. 1999). The SN displayed narrow Hα emission, which lead to the classification of SN 1997cy as a Type IIn. It is noteworthy that the epoch of the SN explosion, constrained by a prediscovery limit on March 12, is consistent with the association of the SN with GRB 970514 (Germany et al. 1999).

SN 1997cy is the brightest SN II discovered so far (Turatto et al. 1999; Figure 5). Its light curve does not conform to the classical templates of SNe II, namely Plateau and Linear, but resembles the slow evolution of the Type IIn SN 1988Z (Turatto et al. 1993). SN 1997cy could be powered by either the radioactive decay of ^{56}Ni to ^{56}Co and ^{56}Fe or by circumstellar interaction. After about day 120 the SN

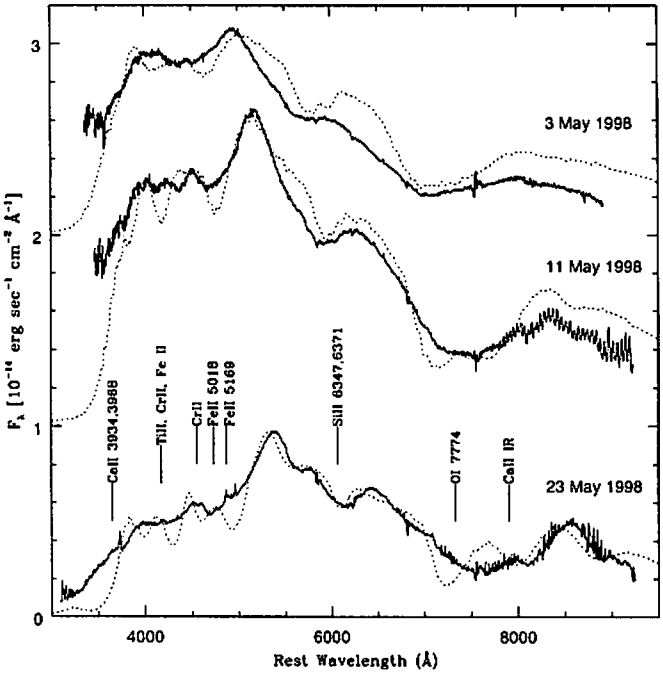

Figure 4: Observed spectra of SN1998bw (full lines) and synthetic spectra computed using model CO138 (dashed lines).

light decline becomes slower than the lifetime of ^{56}Co, suggesting circumstellar interaction for the energy source.

In the interaction model, collision of the SN ejecta with the slowly moving circumstellar matter (CSM) converts the kinetic energy of the ejecta into light, thus producing the observed intense light display of the SN. Our exploratory model considers the explosion of a massive star of $M = 25M_\odot$ with a parameterized kinetic energy E_K. We assume that the collision starts near the stellar radius at a distance r_1, where the density of the CSM is ρ_1, and adopt for the CSM a power-law for the density profile $\rho \propto r^n$. The parameters E_K, ρ_1, and n, are constrained by comparison with the observations.

The regions excited by the forward and reverse shock emit mostly X-rays. The density in the shocked ejecta is so high that the reverse shock is radiative and a dense cooling shell is formed (e.g., Suzuki & Nomoto 1995; Terlevich et al. 1992). The X-rays are absorbed by the outer layers and core of the ejecta, and re-emitted as UV-optical photons.

Figure 5 shows the model light curve which best fits the observations. The model parameters are: $E_K = 5 \times 10^{52}$ erg, $\rho_1 = 4 \times 10^{-14}$ g cm^{-3} at $r_1 = 2 \times 10^{14}$ cm (which corresponds to a mass-loss rate of $\dot{M} = 4 \times 10^{-4} M_\odot$ yr^{-1} for a wind velocity of 10 km s^{-1}), and $n = -1.6$. The large mass-loss episode giving rise to the dense CSM is supposed to have occurred after the progenitor made a loop in the HR diagram from BSG to RSG. In this model, the mass of the low-velocity CSM is $\sim 5M_\odot$, which implies that the transition from BSG to RSG took place about 10^4 yr before the SN event.

The large CSM mass and density are necessary to have large shocked masses and thus to reproduce the observed high luminosity, and so is the very large explosion energy. For models with low E_K and high ρ_1, the reverse shock speed is too low to produce a sufficiently high luminosity. For example, a model with $E_K = 10^{52}$ erg and ρ_1 as above yields a value of L_{UVOIR} lower than the observed luminosity by a factor of ~ 5. For high E_K or low ρ_1, the expansion of the SN ejecta is too fast for the cooling shell to absorb enough X-rays to sustain the luminosity. Thus in this model E_K and $\dot{M}$ are constrained within a factor of ~ 3 of the reported values.

The shape of the light curve constrains the circumstellar density structure. For $n = -2$, the case of

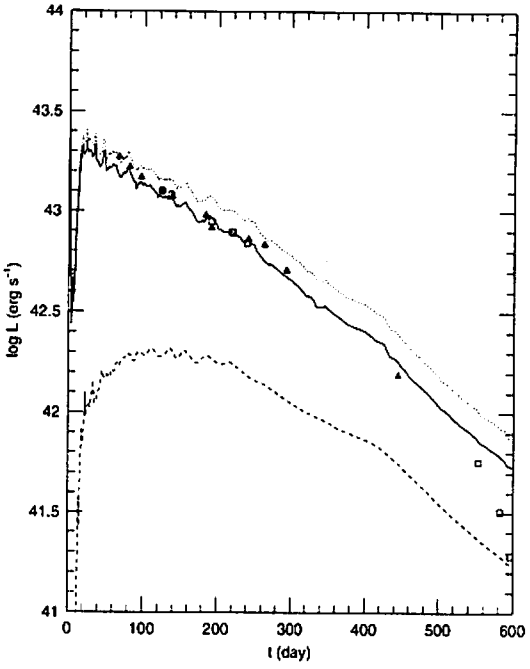

Figure 5: The *uvoir* bolometric light curve of SN 1997cy compared with the synthetic light curve obtained with the CSM interaction model.

a steady wind, $L_{\rm UVOIR}$ decreases too rapidly around day 200. To reproduce the observed decrease after day $\sim$ 300, the CSM density is assumed to drop abruptly at the radius the forward shock reaches at day 300, so that the collision becomes weaker afterwards. (Such a change of the CSM density corresponds to the transition from BSG to RSG of the progenitor $\sim 10^4$ yr before the SN explosion.) After day 550, The observed light curve drops more sharply than the model, which might indicate the development of clumps in the ejecta and the resulting decrease in the effective X-ray absorption.

The ejecta-CSM model with high explosion energy is thus able to reproduce the light curve. However, this does not necessarily mean that radioactive energy input is small, because of the uncertainty in the model fitting. To constrain the contribution from the radioactive decay, we calculate the optical light curve of the SN including shock heating and radioactive decay with various amount of ^{56}Ni. We find that a contribution of at most 0.7 $M_\odot$ of ^{56}Ni is allowed. We also note that the decline rate of the radioactive component is much faster than the half-life of the ^{56}Co decay because the explosion is so energetic that only a fraction of the γ-rays is trapped in the ejecta. This implies that radioactive decay cannot explain the slope of the observed light curve even between 60 and 120 days.

Its large kinetic energy gains SN 1997cy enrollment in the family of 'hypernovae'. While SN 1998bw and SN 1997ef are Type Ic, SN 1997cy is Type IIn. The recent SN 1999E (Turatto et al. 1999), whose spectrum is identical to that of SN 1997cy, may be another Type IIn hypernova, and so may be SN 1988Z, if a new study should lead to larger estimates for mass and kinetic energy.

5 Nucleosynthesis in asymmetric explosions

In §3, we speculate that the expansion velocity of Fe and O in SN 1998bw betrays the effect of the asymmetry in the explosion. To confirm this we calculate the explosive nucleosynthesis in an axisymmetric explosion. Our calculations are performed in two steps. The first step is a hydrodynamical simulation of explosions with a two-dimensional hydrodynamical code (Hachisu et al. 1991; Nagataki et al. 1997). In this calculation we follow tracks of a number of test particles and their density and temperature history.

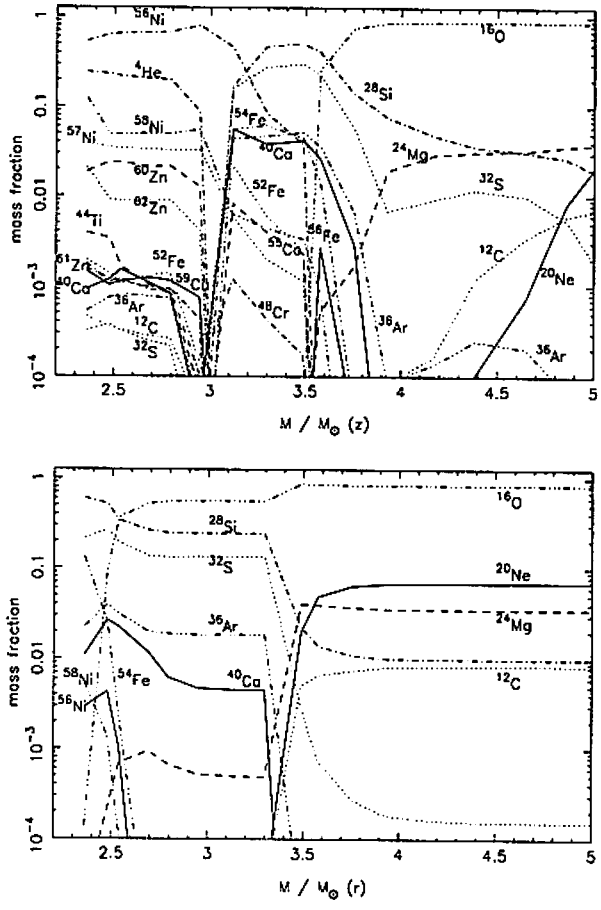

Figure 6: The isotopic compositions of the ejecta of the axisymmetric explosion in the direction of the jet (top) and the perpendicular to the jet (bottom).

This history is used in the second step to calculate the change in the chemical composition with a reaction network including a total of 222 isotopes up to ^{71}Ge (Thielemann, Nomoto, & Hashimoto 1996).

Figure 6 shows the isotopic compositions of the ejecta of the axisymmetric explosion in the direction of the jet (top) and the perpendicular to the jet (bottom). The progenitor model is the $16M_{\odot}$ He core of a $40M_{\odot}$ star (Nomoto et al. 1997; Nomoto & Hashimoto 1988). The the explosion energy is $E_{\rm K} = 1 \times 10^{51}$ erg. Starting the hydrodynamical simulation, we deposit the energy as 50% thermal energy and 50% kinetic energy toward the jet (z) below the mass cut that divides the ejecta and the collapsing core.

The shock is stronger and the post-shock temperatures are higher along the jet direction (z), so that explosive nucleosynthesis takes place in a more extended, lower density region compared with the perpendicular direction (r). A larger amount of ^{56}Ni, which decays into ^{56}Fe through ^{56}Co, is produced in the jet direction. In addition, elements produced by α-rich freezeout are enhanced because nucleosynthesis proceeds at higher entropies than in the region aside from the jet. Figure 6 clearly shows that in the jet direction a larger amount of ^{4}He is left after the shock decomposition. Hence, elements synthesized through capturing an α-particles such as ^{44}Ti and ^{48}Cr (decaying into ^{44}Ca and ^{48}Ti, respectively) become more abundant. Our results is consistent with previous similar calculations (Nagataki et al. 1997). In contrast, little ^{56}Ni is produced in the r direction. Also the expansion velocities are lower than those in the z direction. Therefore, the Fe velocities (mostly z direction) can exceed the O velocities

(in r direction), as observed in SN 1998bw. Oxygen in the z direction has the highest velocities but the densities may become too low to be excited by gamma-rays.

The above nucleosynthesis model might shed light on a problem in the the Galactic chemical evolution model. It has been pointed out that Ti is deficient in Galactic chemical evolution models with the usual supernova yields (Timmes et al. 1995, Ikuta 1998). However, if the contribution from hypernovae to the Galactic chemical evolution is relatively large, this problem could be relaxed. As we have seen, α-rich freezeout is enhanced in axisymmetric explosions and Ti is produced more abundantly. This possibility should be investigated further, together with more extensive nucleosynthesis calculation.

6 Summary

We have investigated the three peculiar supernovae SN Ic 1997ef, SN Ic 1998bw, and SN IIn 1997cy. We have shown that all of them have much larger explosion energies ($E_{\rm K} \gtrsim 10^{52}$ erg) than usual supernovae ($E_{\rm K} \sim 10^{51}$ erg), which leads us to call them 'hypernovae'. We have also suggested some degree of aspherical explosions for SN 1997ef and SN 1998bw from the comparison between our models and the observations. The polarization of SN 1998bw ($\lesssim 1$ %) indicates an axial ratio of 2:1 (Höflich et al. 1999). Thus our spherical models may overestimate $E_{\rm K}$ by a factor of a few, but still $E_{\rm K}$s are unusually large.

One may note that they all are candidates for GRB/SNe connection. SN Ic 1997ef might have been connected with GRB971115, SN Ic 1998bw with GRB980425, and SN IIn 1997cy with GRB970514. There are two other high redshift GRBs which might have been associated with a SN: GRB980326 (Bloom et al. 1999) and GRB970228 (Reichart 1999; Galama et al. 1999). To confirm these GRB/SN connections, relativistic asymmetric explosion models should be constructed (e.g., Aloy et al. 1999; MacFadyen & Woosley 1999).

References

[1] Aloy, M. A. et al. 1999, ApJ, 523, 125

[2] Bloom, J.S. et al. 1999, Nature, 401, 453

[3] Chugai, N., Danziger,I.J., 1994, MNRAS, 268, 173

[4] Filippenko, A.V. et al. 1997, IAU Circ. No.6783, 6809

[5] Galama, T. J. et al. 1998, Nature, 395, 670

[6] Galama, T. J. et al. 1999, ApJ, submitted (astroph/9907264)

[7] Garnavich, P. et al. 1997, IAU Circ. No. 6778, 6786, 6798

[8] Germany, L. et al. 1999, ApJ, submitted (astroph/9906096)

[9] Höflich, P., Wheeler, J.C., Wang, L., 1999, ApJ, 521, 179

[10] Hachisu, I. et al. 1991, 368, L27

[11] Ikuta, C., 1998, M. A. thesis, University of Tokyo

[12] Iwamoto, K. et al. 1998, Nature, 395, 672

[13] Iwamoto, K. et al. 2000, ApJ, in press (astroph/9807060)

[14] Kulkarni, S. R. et al. 1998, Nature, 395, 663

[15] Lucy, L.B. 1999, A&A, in press

[16] MacFadyen, A.I. & Woosley, S.E. 1999, ApJ, 524, 262

[17] Mazzali, P.A., & Lucy, L.B. 1993, A&A, 279, 447

[18] Mazzali, P.A. 1999, A&A, submitted

[19] Nagataki et al. 1997, ApJ, 486, 1026

[20] Nomoto, K. & Hashimoto, M. 1988, Phys. Rep., 256, 173

[21] Nomoto, K. et al. 1994, Nature, 371, 227

[22] Nomoto, K. et al. 1997, Nuclear Phys., A616, 79

[23] Patat, F. et al. 1999, Mem Sait, in press

[24] Patat, F. et al., 2000, ApJ, submitted

[25] Reichart, D.E. 1999, ApJ, 521, L111

[26] Shigeyama, T., & Nomoto, K. 1990, ApJ, 360, 242

[27] Suzuki, T., Nomoto, K., 1995, ApJ, 455, 658

[28] Terlevich,R., Tenorio-Tagle,G., Franco,J., Melnick,J., 1992, MNRAS, 255, 713

[29] Thielemann, F.-K., Nomoto, K., & Hashimoto, M. 1996, ApJ, 460, 408

[30] Thorsett, S.E. & Hogg, D.W. 1999, GCN Cir. 197

[31] Timmes, F. X., Woosley, S. E., Weaver, T. A. 1995, ApJS, 98, 617

[32] Turatto, M. et al. 1993, MNRAS 262, 128

[33] Turatto, M. et al. 1999, ApJ, submitted (astroph/9910324)

[34] Wang, L.-F.& Wheeler, J.C. 1998, ApJ, 504, L87

[35] Woosley, S.E., Eastman, R.G., Schmidt, B.P. 1999, ApJ, 516, 788

First Data from the TAMA300 Gravitational Wave Detector

Seiji Kawamura[1] and the TAMA collaboration

[1]*National Astronomical Observatory*
2-21-1 Osawa, Mitaka, Tokyo, Japan

Abstract

Laser interferometers have been considered the most promising means for detecting gravitational waves with a possibility of opening a new astronomy in the future, that is, the gravitational-wave astronomy. There are at present several on-going projects in the world for building medium- to large-scale (300m to 4km) laser interferometer gravitational wave detectors. TAMA is the Japanese project which is making the rapidest progress among those projects. Its detector, TAMA300 with an arm length of 300m employs a recycled Fabry-Perot Michelson interferometer illuminated by a 10W laser with a triangular mode cleaner. The whole interferometer (without recycling) has been successfully operated and the first set of data was already taken. These are also the first data from the medium- to large-scale gravitational wave detectors in the world. This first data taking is, thus, regarded as a significant milestone not only for the TAMA project but also for the world-wide gravitational wave detector network in the future.

1 Introduction

The detection of gravitational waves was pioneered by Weber in the early 1960s. He developed the first resonant bar detectors and announced that he had detected gravitational waves [1]. Although no convincing evidence for the detection was provided, his pioneering work inspired others to search for gravitational waves. In addition to the subsequent efforts on cooling bar detectors, Weiss and several other researchers had come to the idea of using laser interferometers to detect gravitational waves [2]. Since then several groups over the world have developed laser interferometer detectors and most experimentalists have come to believe that interferometers are the most promising means for detecting gravitational waves.

The detection principle of the laser interferometer gravitational wave detector is fairly simple. In a Michelson laser interferometer with suspended mirrors (Fig. 1), gravitational waves passing through the interferometer will modulate the lengths of the two arms differentially.[2] It results in changes in the intensity of the interfering light, which is detected by a photodetector. In the actual interferometer the intensity of the light at the detector port will be kept dark by controlling the arm length. Therefore the feedback signal to the mirrors should contain gravitational wave signals.

Laser interferometers are ideally suited for detecting gravitational waves, because the arm length changes caused by gravitational waves can be increased by simply scaling up the arm length. Therefore the larger interferometer will provide better sensitivity to gravitational waves. However, the signal would be cancelled if the arm length is too long. For example if the arm length is equal to a half the wavelength of the gravitational wave to be detected, in the TT coordinate system the light experiences modulation of the apparent speed of light positively half the time of its stay in the arm and negatively the rest of the time, resulting in a complete cancellation of the total phase change of the modulated light. It can be derived that the optimum arm length is a quarter the wavelength of the gravitational wave. For example

[1]E-mail:seiji.kawamura@nao.ac.jp

[2]It should be noted that the length change caused by gravitational waves can be regarded either as the consequence of the force applied to the end mirrors or that of the variation of the apparent speed of light, depending on the coordinate system considered. In the proper reference frame of an observer, where the apparent speed of light is constant, the force is applied to masses by gravitational waves with the amplitude of the force proportional to the mass's coordinate position. Therefore the end mirrors are shaken back and forth by the force, whereas the beamsplitter is sitting at rest. On the other hand, in the transverse traceless (TT) coordinate system, where any freely-falling mass with no initial velocity does not change its position, the apparent speed of light is modulated by gravitational waves. As a result the optical path difference, measured by such modulated light, is altered. In either coordinate system, the amount of changes in the intensity of the interfering light should be the same.

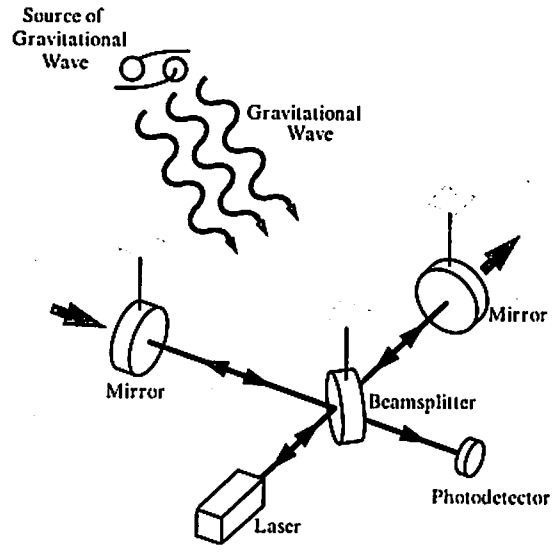

Figure 1: Michelson Interferometer with suspended mirrors for detecting gravitational waves

an arm length of 750km is optimum for the 100Hz gravitational wave. However, practical limitations, such as curvature of land and available budget, allow us to extend the arm length of the interferometers at most up to several kilometers on earth.

There are at present several on-going projects in the world for building medium- to large-scale (300m to 4km) laser interferometer gravitational wave detectors: LIGO [3] by the United States, VIRGO [4] by France and Italy, GEO [5] by Germany and England, and TAMA [6] by Japan. Although the detector (TAMA300) of the TAMA project is the smallest in its size among the detectors of those projects, TAMA is making the rapidest progress. We have already succeeded in operating the whole detector; TAMA300 is the only working detector in the world at present and it will be so for a while. Furthermore we have already had the first data run of the detector and the first set of data was successfully obtained.

In this paper after the TAMA project is briefly reviewed in section 2, the details of the TAMA300 gravitational wave detector and the first data taking of TAMA are described in section 3 and section 4, respectively. Finally the conclusions are derived in section 5.

2 TAMA Project

The TAMA project started in 1995 with the collaborating efforts of National Astronomical Observatory, The University of Tokyo, Institute for Cosmic Ray Research, Institute for Laser Science, High Energy Accelerator Research Organization, Yukawa Institute of Theoretical Physics, and Osaka University. Miyagi University of Education joined the project later.

The TAMA project has two objectives: to establish techniques necessary for the future km-class detector in Japan and to detect gravitational waves from near our galaxy if possible at all. In addition the TAMA project is expected to play an important role for the future gravitational wave detector network in the world, since any difficulties in experiment encountered first and overcome first by TAMA will be fed back to the other projects, which will lead to more effective and smooth realization of the future world network.

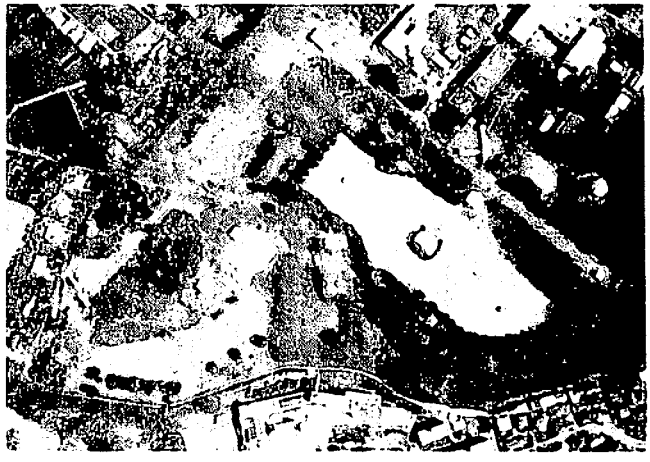

Figure 2: TAMA300 located on the campus of National Astronomical Observatory.

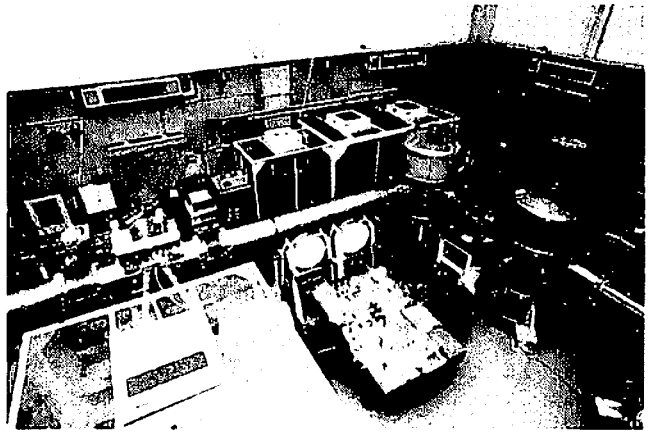

Figure 3: Vacuum system of the TAMA300 detector in the central building.

TAMA300 is located on the campus of National Astronomical Observatory in Tokyo (Fig. 2 and Fig. 3). The fundamental scheme of TAMA300 is a 300m Michelson interferometer illuminated by a 10W laser with three additional elements: Fabry-Perot arm cavities, a recycling system, and a mode cleaner (See Fig. 4).

Fabry-Perot arm cavity: Fabry-Perot arm cavities amplify the gravitational wave signals. In the Fabry-Perot arm cavity the light is bounced back and forth many times when the light is on resonance in the cavity. Thus the phase change of the light caused by gravitational waves is multiplied by the effective number of bounces. [3]

Recycling: A recycling system enhances the effective laser power and as a result it improves the signal to shot noise ratio. Since the interferometer is operated in such a way that the intensity of the light at the detection port is dark for optimization of the shot noise, all the light is reflected back to the laser. The recycling mirror inserted before the interferometer reflects this light coherently back to the interferometer so that the incident laser power effectively increases [4], which leads to better shot noise limit. This is because the signal to shot noise ratio is proportional to the square root of the incident laser power.

Mode Cleaner: A mode cleaner cleans the transverse mode of the light to reduce the noise related to the laser geometrical fluctuations, such as beam jitter and pulsation. When the fundamental transverse mode of the light is on resonance in the mode cleaner, other higher-order transverse modes cannot be transmitted through the mode cleaner because of the difference of the resonant condition between different modes. Since the laser geometrical fluctuations are the outcome of mixture between the fundamental mode and higher-order modes with time-varying relative amplitudes, the suppression of the higher-order mode results in reduction of the beam geometrical fluctuations. The mode cleaner also serves as a reference cavity for the coarse frequency stabilization.

The aimed sensitivity for gravitational waves is 3×10^{-21} in terms of the root-mean-square strain at 300Hz with a bandwidth of 300Hz. The interferometer sensitivity should be eventually limited by seismic noise at lower frequencies, by shot noise at higher frequencies, and by thermal noise at intermediate frequencies.

Seismic Noise: Ground motion shakes the mirrors directly. The mirrors should be well isolated from the ground motion to suppress the seismic noise.

Shot Noise: Shot noise exists because a photon has finite energy. Statistical fluctuations in the photon number in the detection process result in shot noise. The higher incident laser power provides the better signal to shot noise ratio.[5]

Thermal Noise: The mirrors show Brownian motion as a result of the energy exchange between the mirrors and the surrounding system. There are two important modes relevant to the suspended mirrors: the pendulum mode and internal mode. In either case, the thermal noise at frequencies off the resonances can be reduced by making the quality factor of the modes higher. This is because a mode with a higher quality factor has more energy concentrated around the resonances, thus lower thermal motion is engaged off the resonant frequencies, owing to the constant integrated thermal motion.

---

[3] Since most sensor noise such as laser frequency/intensity noise or shot noise does not explicitly depend on the effective number of bounces, the signal to noise ratio of the interferometer can be improved by using the Fabry-Perot arm cavity. However, this advantage does not hold for the displacement noise such as seismic noise or thermal noise of the mirrors, since the displace noise is also amplified by the Fabry-Perot arm cavity exactly in the same manner as the gravitational wave signal is.

[4] The extent to which the effective power can be increased depend on the loss of light in the interferometer. The lower loss of the light in the interferometer provides higher recycling gain. The transmission of the recycling mirror should be set nearly equal to the loss of the light in the interferometer to maximize the recycling gain for a given loss of light in the interferometer.

[5] The radiation pressure noise caused by quantum fluctuations of the intensity of the light hitting the mirrors could exceed the shot noise if the laser power is too high.

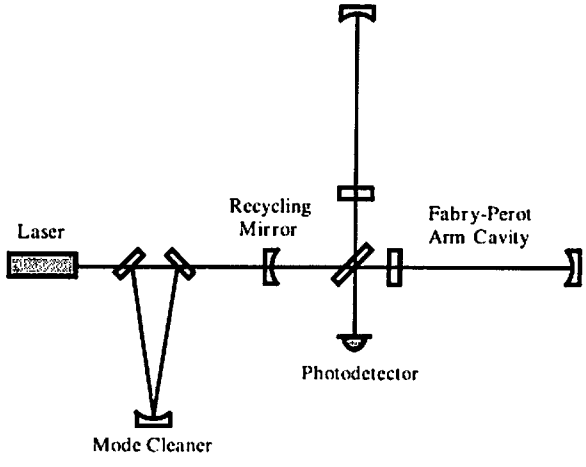

Figure 4: Standard optical configuration which has three elements: Fabry-Perot arm cavity, recycling, and mode cleaner.

TAMA300 has been commissioned step by step following the installation scenario as shown in Fig. 5. First the 10W Nd:YAG laser using the injection locking technique was developed by Sony Corporation. We also installed and characterized the ring-cavity mode cleaner using the 500mW Nd:YAG laser. As the next step, one arm cavity consisting of two suspended mirrors was installed and locked using the 700mW Nd:YAG laser with both mirrors controlled in orientation. We then installed the other arm cavity, the beamsplitter, and two pick-off mirrors. We successfully locked the Fabry-Perot Michelson interferometer using the 700mW Nd:YAG laser. In parallel with this effort, we have injected the 10W laser to the mode cleaner. In 1999 we finally connected the 10W laser and mode cleaner to the Fabry-Perot Michelson interferometer. The whole interferometer (without recycling) was successfully locked, and the first set of data was taken. We are now adjusting/refining the interferometer for better sensitivity and stability.

3 TAMA300 Detector

3.1 System Description

3.1.1 Laser

An injection-locked Nd:YAG laser with a wavelength of 1064nm, which was developed by a group at the research center of SONY corporation, is used as a light source of TAMA300. The slave laser pumped by two 10W laser diode is injection-locked to a master laser of a 700mW output power. The laser has an output power of 10W.

3.1.2 Optical and Length Control System

Figure 6 shows the schematic diagram of the TAMA300 detector. The light is phase-modulated to extract the signals corresponding to various length or frequency signals of the interferometer. The laser frequency is stabilized by the mode cleaner as a reference. The mode cleaner is, on the other hand, stabilized by the common-mode arm cavity length, which is detected by demodulating the signal in in-phase at the

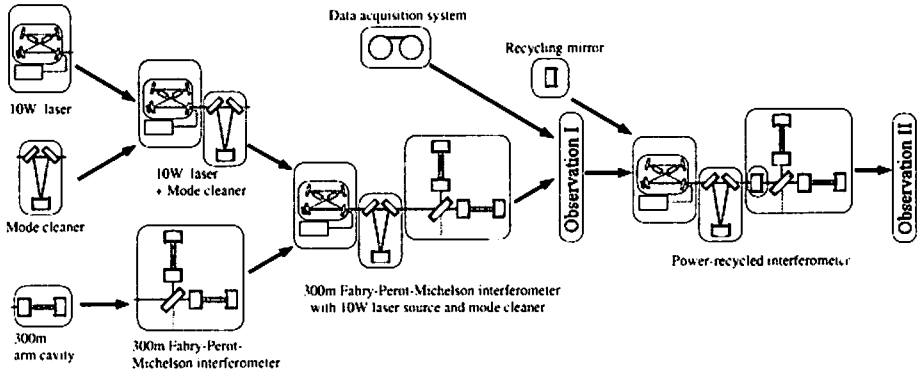

Figure 5: Installation Scenario of the TAMA300 interferometer

symmetric port. Therefore the laser frequency follows the common-mode arm cavity length. Since the bandwidth of the mode cleaner actuation is limited to no more than 1kHz because of the resonances of the mirrors, the high-frequency feedback signal of the common-mode arm length control system is injected into the error point of the mode cleaner control loop. The differential Michelson length is detected by demodulating the signal in quadrature-phase at the symmetric port, and is fed back to the beamsplitter. The differential arm cavity length is detected by demodulating the signal in quadrature phase at the anti-symmetric port, and is fed back to the two input mirrors differentially.

3.1.3 Lock Acquisition

For acquisition of the locking, the auxiliary signals which represent the two arm cavity lengths are used. They are obtained by demodulating the signals which are picked off from the two light paths between the beamsplitter and the two input mirrors. As shown in Fig. 7, the laser and mode cleaner are first acquired in locking using one arm length as a reference. After the other arm is locked independently, the differential Michelson length is locked. This procedure brings the whole interferometer in lock without any difficulty. The differential and common-mode arm cavity length signals obtained in above-mentioned method are then superimposed onto the existing feedback loop. The gain of those feedback loops have been adjusted so that the addition of the servo system does not make the system unstable. Finally the two independent arm cavity length signals are turned off, which makes the whole interferometer locked only with the differential and common-mode arm cavity length signals. This way the interferometer can be brought in full operation very smoothly.

3.1.4 Orientation Control System

The four mirrors are controlled in orientation by the wavefront sensing signals.Wavefront sensing technique is used to detect angular misalignments of the interferometer mirrors. This is an extension of the length sensing system. In the presence of angular misalignments, the length signal has a spatial gradients. This can be detected by using a segmented photodiode and differentiating the demodulated signals from the segments. Furthermore the angular information of each mirror in the interferometer can be independently extracted by sensing the spatial gradients at different positions, since the angular misalignment of each mirror causes wavefront deviation of the interfering light at different positions differently. [*]

[*] The advantage of the wavefront sensing compared with a conventional optical lever is that the optical lever senses the mirror angle only in the local frame, whereas the wavefront sensing detects the mirror orientation with respect to the incident beam. Therefore the wavefront sensing is not subject to the local disturbances of the system.

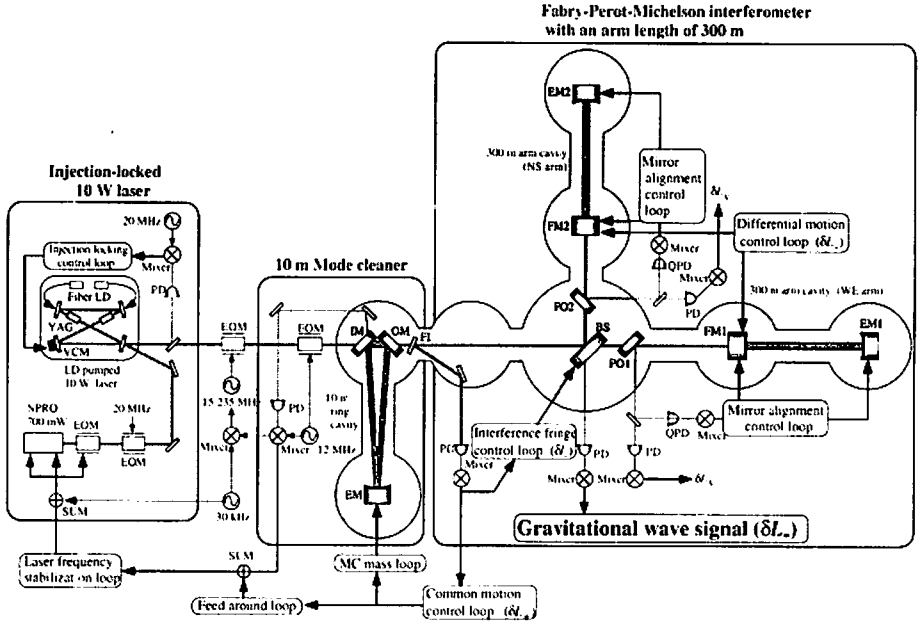

Figure 6: Schematic diagram of the recombined Fabry-Perot Michelson interferometer

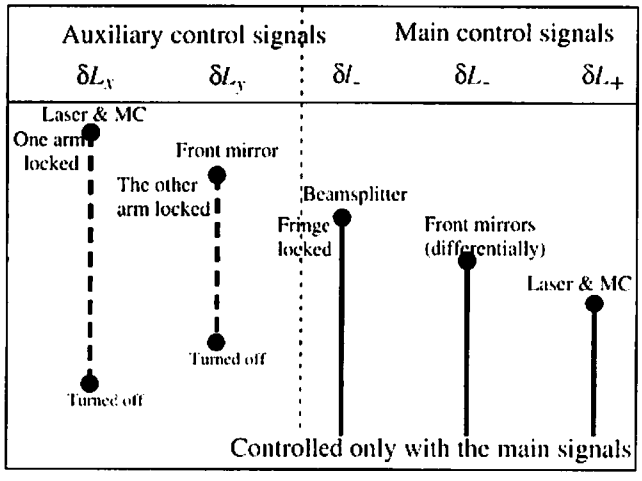

Figure 7: Acquisition procedure of the recombined Fabry-Perot Michelson Interferometer

3.1.5 Sidebands Transmission of Mode Cleaner

The phase modulation required to extract length signals of the interferometer should be imposed on the light before the mode cleaner, since an electro-optic modulator for phase modulation placed after the mode cleaner would impart the beam quality of the light coming out of the mode cleaner. The modulation sidebands were transmitted through the mode cleaner by making the modulation frequency exactly equal to the free spectral range (FSR) of the mode cleaner.

3.1.6 Suspension

The mirrors are suspended to make the freely falling masses. A double-pendulum system is used; the mirror is suspended from the upper mass which is in turn suspended from the suspension point of the suspension cage. The motion of the mirrors are damped by the eddy current in the upper masses produced by permanent magnets located closely to the upper mass.

3.1.7 Isolation

Suspending the mirrors also plays a role of isolating the mirrors from the ground motion. In addition the suspension system is placed on stacks consisting of three pairs of metal plates and elastomers accumulated alternately. The elastomers are housed in a metal-sealed bellows to avoid outgassing.

3.2 Sensitivity

The evolution of the sensitivity of TAMA300 is shown together with two goal sensitivities (Fig. ??): Phase I goal for the recombined interferometer and Phase II goal for the recycled interferometer.It can be seen that we have rapidly made a progress in improving the sensitivity since we obtained the first sensitivity spectrum in February 1999.

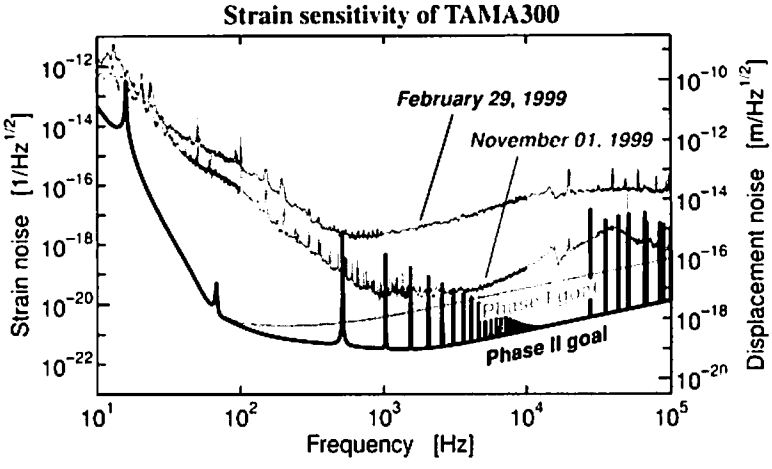

Figure 8: Evolution of the sensitivity of TAMA300 together with the goal sensitivity.

The current noise spectrum of the interferometer is shown in Fig. 9. The sensitivity is at present limited by seismic noise below 10Hz, by the alignment control system noise between 10Hz and 100Hz, and by the intensity and frequency noise above 1 kHz. We are currently trying to reduce the noise further down.

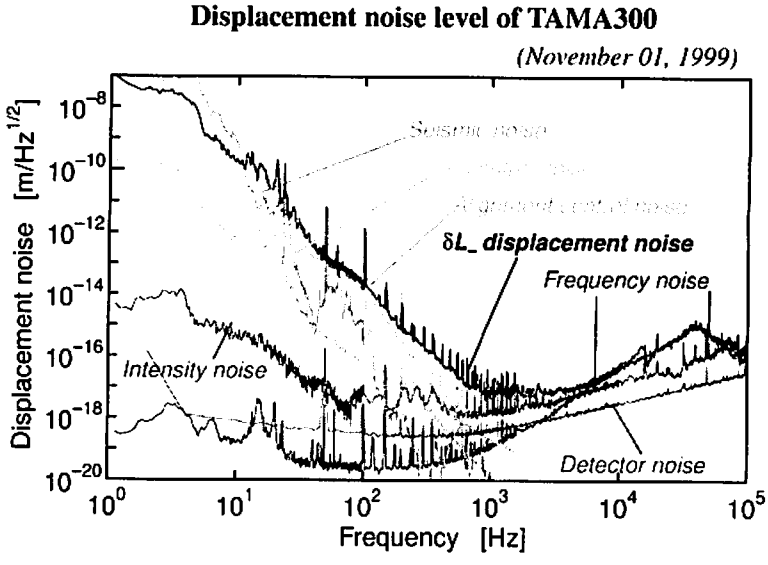

Figure 9: First sensitivity curve of TAMA300 in the recombined Fabry-Perot Michelson stage

3.3 Long-term Stability

Although the sensitivity of the detector is very important, comparably crucial is the stability of the instrument. In addition to the efforts of improving the sensitivity of the detector, we have been trying to make the system more stable and robust so that the interferometer can hold locking for a long time without any interruption. At present the detector behaves fairly stably especially at night, when the vibration level is significantly lower than that in the daytime. Figure 10 shows various feedback signals of the interferometer when the detector was held in lock for seven hours continuously. The longest continuous locking time of the interferometer recorded so far is approximately 8 hours.

4 Data from TAMA300

4.1 Data Taking System

The data taking system for TAMA300 has been developed to satisfy the following requirements:

1. The frequency range of the data taking system should be 50-5kHz.
2. Data should be recorded continuously without any dead time.
3. The arrival time should be determined within an accuracy of 10 micro seconds.
4. The frame format, which had been specifically developed for Interferometric Gravitational Wave Detector (IGWD) and is used and maintained by VIRGO and LIGO, should be adopted for the future coincidence analysis.
5. The detector environment signals should be also recorded.

The data taking system comprises a high-speed data acquisition (HDAQ) system and a low-frequency data acquisition system. The HDAQ system deals with the gravitational-wave related signals, while the EPICS system monitors the detector environment signals.

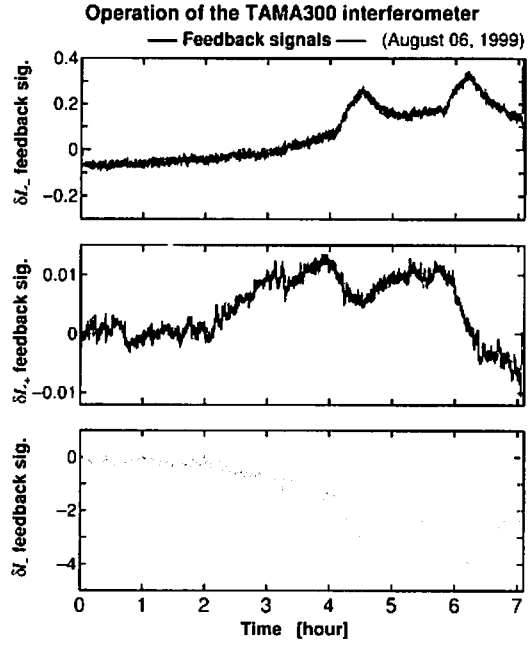

Figure 10: Feedback signals during the seven-hour continuous locking

4.1.1 High-speed Data Acquisition System

The gravitational-wave related signals such as the processed feedback signal of the differential arm length control system are taken with the HDAQ system as shown in Fig. 11. The feedback signal of the differential arm length control system, which would contain gravitational wave signals, are whitened and anti-aliased by appropriate filters before being analogue-to-digital (AD) converted. The whitening filter makes the signal, which is originally concentrated in power at low frequencies, rather white in spectrum, so that the low-power components at interesting frequencies can be larger than the AD conversion noise. The anti-aliasing filter has a cut-off frequency of 5kHz to avoid the aliasing effect of the AD conversion. The arrival time is determined using an atomic timer in the global positioning system (GPS). The AD-converted data are then transferred to the workstation and stored on the hard disk temporally. The data are finally copied to a digital linear tape automatically.

4.1.2 Low-speed Data Acquisition System

Experimental Physics and Industry Control System (EPICS), which had been developed for controlling particle accelerators and large experiments, is adopted to monitor the detector environment signals such as the ground vibration level. The EPICS system provides software tools and applications for making operator interfaces and interfaces to the instruments. The local area network is used for collecting data from the instrument interfaces which are distributed around the interferometer as shown in Fig. 12.

4.2 Calibration

The gravitational wave signals are calibrated by shaking the mirrors by a given amount (See Fig. 13). The relationship between the applied voltages to the mirror actuation system and the mirror displacement was measured in advance using the Michelson interferometer with the wavelength of the light as a reference. Then two monochromatic signals around 500Hz are applied to the mirror actuation system during the

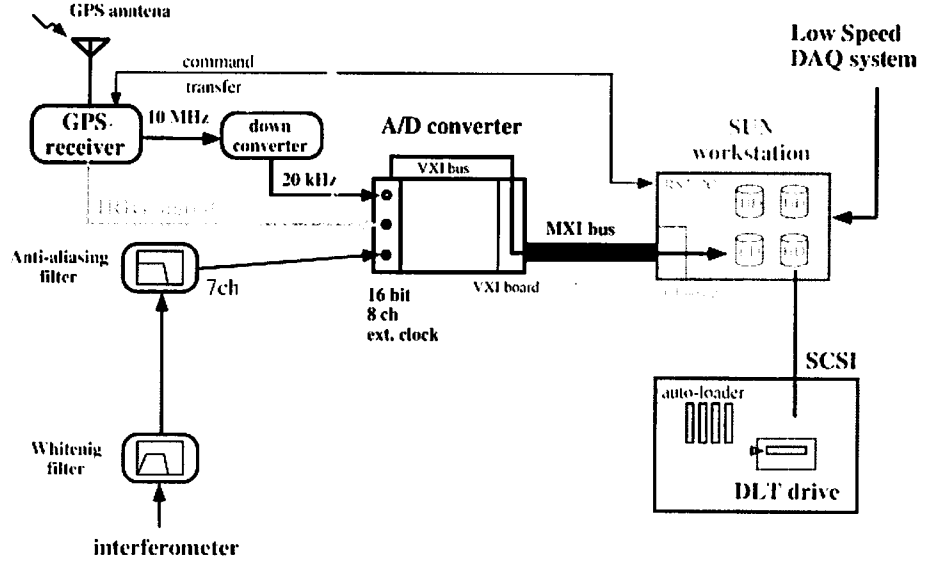

Figure 11: Schematic diagram of the HDAQ system.

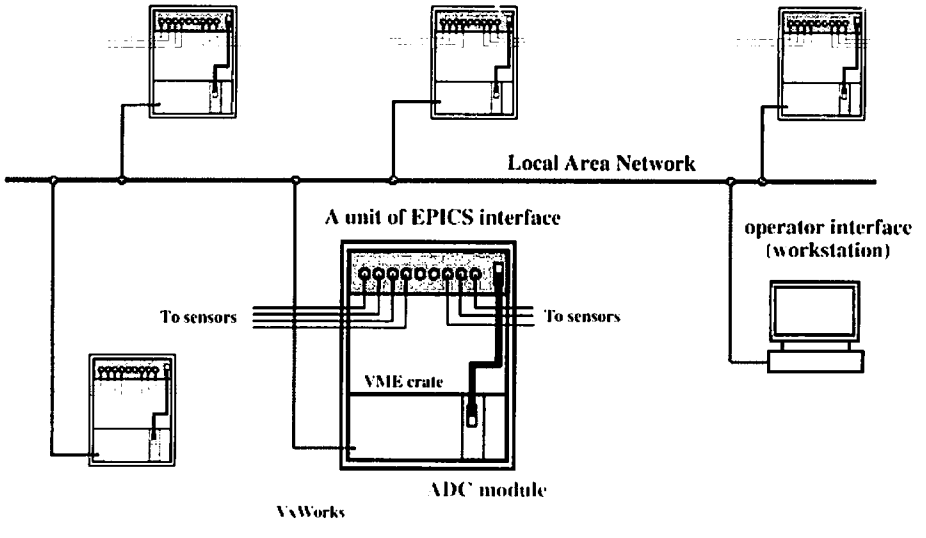

Figure 12: Schematic diagram of the EPICS system.

operation. The processed feedback signal of the differential arm length control system is converted into the gravitational wave strain signal by dividing the processed feedback signal by an appropriate transfer function, which contains the cavity pole of the arms, the closed loop gain of the control system, the whitening filter, the anti-aliasing filter, etc. This transfer function is a product of each transfer function, which is modeled after being verified in measurements. However, the transfer function strongly depends on the DC loop gain, which could vary mainly with the DC intensity level of the incident power, and the cavity pole, which could vary with the contamination of the mirror and the position of the beam spot on the mirrors. The response of the feedback signal to the two calibration signals are used to calculate and follow such variations of the transfer function. The transfer function is renewed from time to time to ensure that the transfer function is correct within a certain accuracy. The amplitude of the calibration signals and the integration time of the measurements were chosen in such a way that both the real fluctuation of the response of the interferometer to the calibration signals and that due to the noise around are within a required level in addition to that the outskirts of the calibration signals are not contaminated.

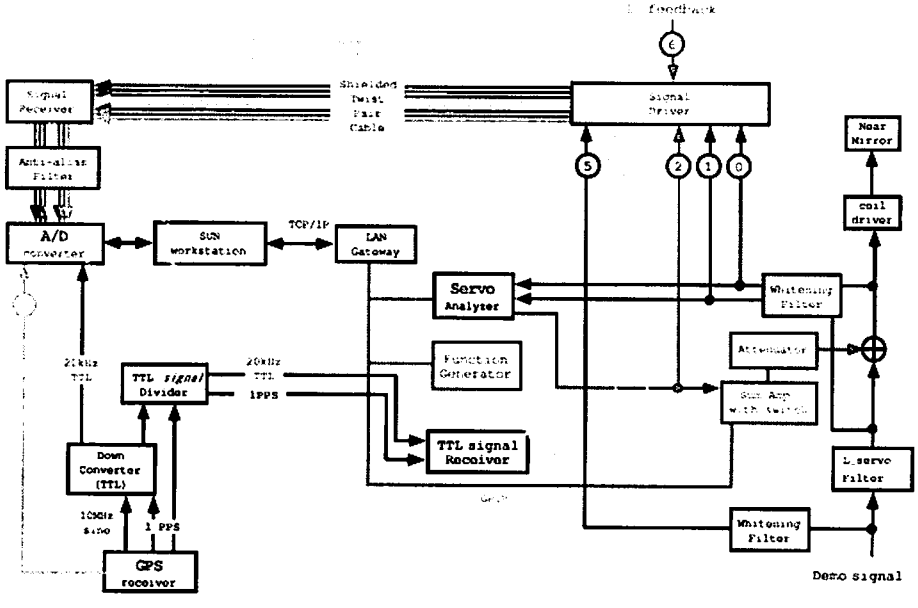

Figure 13: Calibration system of TAMA300.

4.3 Obtained Data

In August 1999 we performed a test data run to check the performance of the data taking system. In this run data of more than ten hours were obtained successfully. Encouraged by this result, we proceeded to the first scientific data run to search for gravitational waves in September 1999. The interferometer and the data taking system were operated for three nights. The transmitted light of one of the arm cavities is shown in Fig. 14. The typical continuous locking time during the data run was a few hours, and the longest one was almost 8 hours. The data obtained are currently analyzed by the members of the TAMA group. [7]

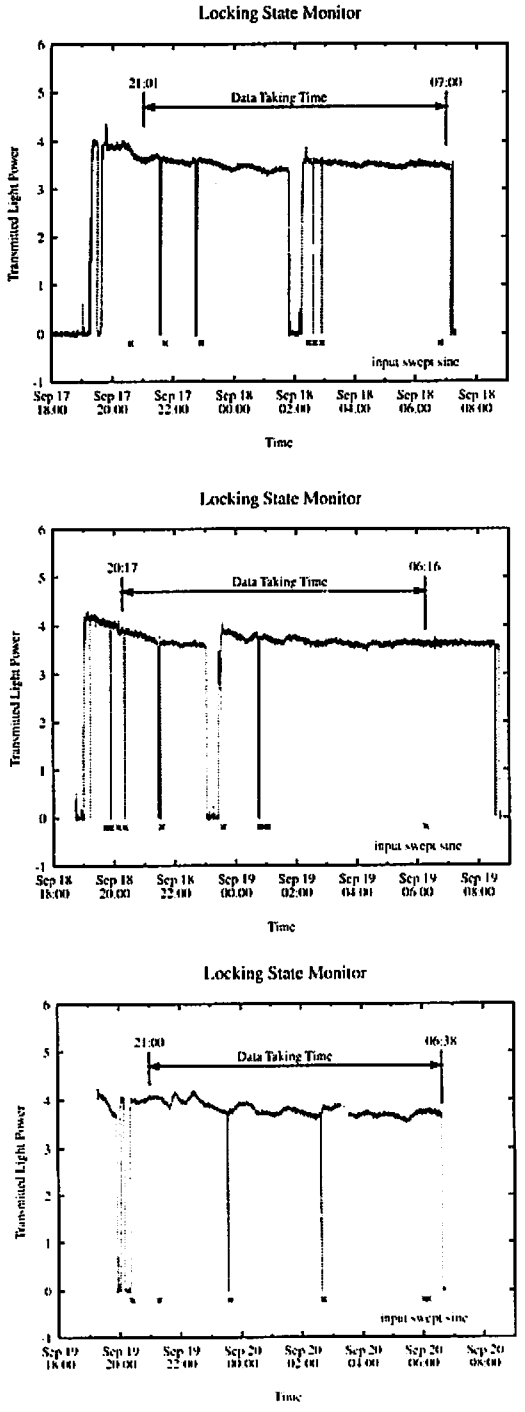

Figure 14: Power of the Transmitted light of the interferometer during the data run.

5 Conclusions

The TAMA project has been progressing very rapidly and smoothly. We have taken the first set of the data, and expect that data with even better sensitivity will be obtained in the near future. The big question is whether TAMA can detect gravitational waves. The answer to this question totally depends on how much and how often gravitational waves come to the earth. According to the estimate on the neutron star binary coalescence, however, the gravitational wave from the neutron star binary coalescence with a strain detectable by TAMA300 would come to the earth much less than once per a thousand years.

However, Nakamura [8] speculated that if MACHOs are black holes, there should be many black hole binaries in the universe, thus their coalescence rate should be very high. It was estimated that the gravitational wave from the black hole binary coalescence with a strain detectable by TAMA300 would come to the earth once per about twenty years. It means that if TAMA300 is operated for one full year, the possibility of detection is one-twentieth, which is not hopeless but not extremely high. Nevertheless, the operation of TAMA300, which will take place first in the world, is meaningful, because there might be unexpected strong gravitational wave sources the mechanism of which is still unknown.

The TAMA project started as a five-year project in 1995. The project will end in March 2000. We applied for an extension of the project for another two years, and we expect that it will be approved. In the next two year we should improve the performance of the detector by, for example, installing the recycling system to take better data in terms of sensitivity and duration. It might lead us to the first detection of gravitational waves.

References

[1] J. Weber, Phys. Rev. Lett. **22** (1969) 1320.

[2] R. Weiss, MIT Quarterly Progress Report (Research Laboratory of Electronics) **105** (1972), 54.

[3] A. Abramovici et. al., Science **256** (1992) 325.

[4] Virgo, CNRS-INFN, March (1992).

[5] The GEO600 Team, MPQ Report **190** (1994) 18.

[6] K. Tsubono, Proc. of the TAMA Workshop (1997) 183.

[7] H. Tagoshi, this workshop.

[8] T. Nakamura et. al., Astrophys. Jour. **487** (1997) L139.

Searching for gravitational waves from inspiraling compact binaries using TAMA300 data

Hideyuki Tagoshi[1], Takahiro Tanaka[1], Nobuyuki Kanda[2], Daisuke Tatsumi[3], Souich Telada[4], Masatake Ohashi[3], and TAMA300 collaboration

[1] *Department of Earth and Space Science, Osaka University, Toyonaka, Osaka 560-0043, Japan*
[2] *Department of Physics, Miyagi University of Education, Sendai, Miyagi 980-0845, Japan*
[3] *Institute of Cosmic Ray Research, University of Tokyo, Tanashi, Tokyo 181-0845, Japan*
[4] *TAMA project, National Astronomical Observatory, Mitaka, Tokyo 181-8588, Japan*

Abstract

We analyzed the 7 hours of continuous data from TAMA300 by using the matched filtering, searching for the gravitational waves from inspiraling compact binaries. For future long-term continuous operation, it is necessary to reduce the computation time. For this purpose, we introduced hierarchical search strategy. We also introduced a χ^2-test to avoid the loss of signal due to the non-Gaussian property of noise. In this paper, we report the results from our preliminary analysis.

Laser interferometric gravitational wave detector TAMA300 became ready to operate in the summer of 1999. The first long data acquisition was done between 17 and 20 September for three nights. The data length amounted to about 30 hours in total. The longest lock time of the interferometer reached nearly 8 hours. The best sensitivity was about $6 \times 10^{-18} m/\sqrt{\mathrm{Hz}}$ around 900kHz.

In this paper, we report the method and the first preliminary results of our search for the gravitational waves from coalescing compact binaries. Basically we used the matched filtering method to analyze the data stream. The detector output was converted to the strain equivalent amplitude $h(t)$ by using a transfer function. The details of the calibration will be reported somewhere else. We denote the strain equivalent one-sided power spectrum density of noise by $S_n(f)$. In order to calculate the expected wave forms, which are called *templates*, we used 2.5 restricted post-Newtonian wave forms, in which the phase evolution was correctly taken into account up to 2.5 post-Newtonian order, but the amplitude was evaluated by using the quadrupole formula. As for 2.5 post-Newtonian phase evolution, we used formulas derived in Blanchet et al.[1]. The gravitational wave form $h(t)$ is given by

$$h(t) = \mathcal{A}[\cos\alpha h_c(t - t_c) + \sin\alpha h_s(t - t_c)], \tag{1}$$

where t_c is the coalescence time, and $h_c(t)$ and $h_s(t)$ are two independent templates with different phases by $\pi/2$. The amplitude $\mathcal{A}$ depends on the distance and the direction to the source and on the orientation of the orbital plane relative to the detector arms. The phase α depends on the orbital phase and the orientation of the source. To construct filters, we need to calculate the Fourier transform of $h_{c,s}(t)$. It was computed directly by using the stationary phase approximation, the validity of which was established in Droz et al[2]. We neglected the effect of spin of the stars. Thus, the parameters to distinguish the wave forms are the amplitude $\mathcal{A}$, two masses m_1, m_2, the coalescence time t_c and the phase α.

We denote the data from the detector as $s(t)$. We define the filtered signal-to-noise ratio ρ after the maximization over α as

$$\rho = \sqrt{(s, h_c)^2 + (s, h_s)^2}, \tag{2}$$

$$(a, b) \equiv \int_{-\infty}^{\infty} df \frac{\tilde{a}(f)\tilde{b}^*(f)}{S_n(|f|)}, \tag{3}$$

where $\tilde{a}(f)$ denotes the Fourier transform of $a(t)$ and asterisk denotes the complex conjugation.

We searched the parameter space with $0.4M_\odot \leq m_1, m_2 \leq 3M_\odot$. In this parameter space, we prepared a mesh. The mesh points define the templates used for search. The spacing of the mesh points was determined so as not to lose more than 2 % of signal-to-noise due to the mismatch between the mass parameters for a signal and those for mesh points. Using geometrical arguments, we introduced new parameterization of masses which simplifies the algorithm to determine the mesh points[3]. By using these new parameters, the mesh in the parameter space can be taken as almost uniform Cartesian coordinates.

Analyzing real data from TAMA300, we found that the noise contains a large amount of non-stationary and non-Gaussian nature, whose statistical property has not been well understood yet. As a result, a lot of fake events with large ρ were generated. These fake events reduce the detector sensitivity significantly. In order to remove the influence of such noise, we introduced a χ^2 test[4], which was a test to discriminate fake events by checking the time-frequency behavior of the signal. Dividing the frequency band into n equal-weighted subintervals, we defined a statistic χ^2 in a standard manner. In the presence of Gaussian noise plus chirp, this statistic has a χ^2 distribution with $2n-2$ degrees of freedom. In the present analysis, we chose $n = 8$.

The parameter space defined by using our new mass parameters turned out to contain 700 templates in the present analysis. To perform the matched filtering, this number of templates is not very large. However, one of the purpose of this work is to develop a code for matched filtering which can be used to analyze future much more large-scale data stream with better quality. When the quality of data is improved, the necessary number of templates becomes larger. Thus, we introduced 2 step hierarchical search algorithm. The basic idea of it is simple. The templates for the 1st step search are chosen at the mesh points with coarse spacing. We perform the 1st step search with an appropriate threshold which must be chosen to be sufficiently low not to miss real detectable events. When there are 1st step mesh points at which the value of ρ exceeds the threshold, we search the points around them in detail. This is the 2nd step search.

Before starting the hierarchical search, we evaluated the values of ρ and χ^2 for all data with a few selected templates to obtain an estimate of the distribution of ρ and χ^2. Based on this distribution, we looked for several combinations of $(\rho^*_{\rm 2nd}, \chi^{*2}_{\rm 2nd})$ so that there were only a few fake events which satisfy $\rho > \rho^*_{\rm 2nd}$ and $\chi^2 < \chi^{*2}_{\rm 2nd}$ simultaneously. These values became our 2nd step threshold. The 1st step threshold and the 1st step length of the mesh separation were determined to satisfy the condition that "*when a data satisfies the 2nd step criterion at 2nd step mesh points, it must also satisfy the 1st step criterion at one of 1st step mesh points with more than 98 % probability*". By imposing this condition, it is guaranteed that the false dismissal rate of real detectable events was kept to be small. In this sense, we think that our criterion has much clearer meaning than that discussed in the paper by Mohanty[5]. We performed simulations by adding signals into real data, and looked for combinations of the 1st step threshold and the mesh separation which satisfy our criterion. We chose one of them which minimizes the computation time in total. In the present analysis, we introduced, at the 1st step, the χ^2 threshold as well as ρ threshold to select the candidates for the 2nd step, which reduced the computation time for the 2nd step. Also, we should note that we used multi-thresholds for (ρ, χ^2) taking into account the fact that events with large ρ tend to have large χ^2.

In order to reduce the computation time, we further introduced various techniques. First, we analyzed data with 2500Hz sampling rate of data at the 1st step, although we used 5000Hz sampling rate at the 2nd step. The reduction of the sampling rate produced only a small decrease of ρ due to mismatch of t_c which could be compensated easily by choosing a slightly lower 1st step threshold for ρ. The smaller sampling rate reduce the FFT length to calculate ρ and χ^2, which was effective to reduce the computation time.

We also introduced a new technique to reduce the computation time to calculate the correlation (s, h_c) and (s, h_s) for the 2nd step search. This technique makes use of the fact that we have already obtained a good guess for the coalescence time and the mass parameters as a result of the first step search at the time when we perform the second step search. We found that the length of FFT for the second step search could be reduced down to about 2048. We have also developed a technique to reduce the computation time to produce the templates in the frequency domain. These techniques are explained in the paper by Tanaka and Tagoshi[3].

The computers we used in this analysis were 9 Compaq Alpha machines. Each of them can perform

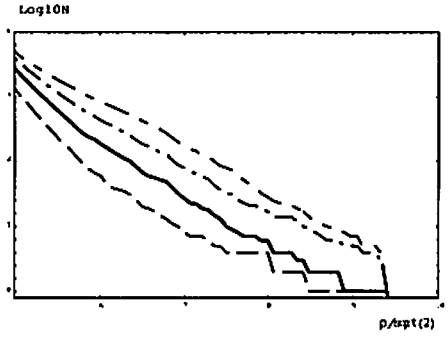

Figure 1: A result of the 2 step search. The number of events which exceed the threshold $\rho^*/\sqrt{2}$ are plotted. Different lines in the figure correspond to different values of χ^2 threshold at the 2nd step. From the top to the bottom, they correspond to 0.16%, 1.5%, 10%, and 50% false dismissal rate in Gaussian noise.

FFT of data consisting of $\sim 10^7$ single precision real numbers with 180MFlops. Among the 30 hours data, we analyzed 7 hours data with better quality taken on 19 September. For each time segment with length Δt seconds, we looked for the maximum of ρ over templates which satisfies the χ^2 threshold with the 2 step search discussed above. In Fig. 1, we only show a graph of the number of events, which exceed the ρ threshold for fixed χ^2 thresholds, and which are obtained by taking maximization of ρ over the templates in each time segment. The length of the time segment Δt was chosen so that the number of correlated events were small enough, but at the same time there were sufficiently large number of events to investigate the properties of its distribution. In Fig. 1, we have chosen $\Delta t \simeq 0.1$ seconds.

We can discuss the upper bound on the event rate, etc. using this figure. Further details of the analysis will be published elsewhere.

This work was supported by a Monbusho Grant-in-Aid 11740150 and by a Monbusho Grant-in-Aid for Creative Basic Research.

References

[1] L. Blanchet, T. Damour, B. Iyer, C.M. Will, and A.G. Wiseman, Phys. Rev. Lett. **74**, 3515 (1995); L. Blanchet, Phys. Rev. **D54**, 1417 (1996).

[2] S. Droz, D.J. Knapp, E. Poisson, and B.J. Owen, Phys. Rev. **D59**, 124016 (1999).

[3] T. Tanaka, and H. Tagoshi, in preparation.

[4] B. Allen et al. Phys. Rev. Lett. **83**, 1498 (1999).

[5] S.D. Mohanty Phys. Rev. **D57**, 630 (1998).

The Highest Energy Cosmic Rays

M. Teshima

Institute for Cosmic Ray Research, University of Tokyo
e-mail: mteshima@icrr.u-tokyo.ac.jp

Abstract. The existence of Super-GZK particles, cosmic rays above $10^{20}eV$, becomes clear by the AGASA experiment. However, its nature is still in mystery. We will discuss the interest and the importance of the highest energy cosmic-ray measurement and report the latest results of AGASA.

I INTRODUCTION

AGASA [1] [2] is the Akeno Giant Air Shower Array covering over 100km^2 area in operation at Akeno village about 130km west of Tokyo, in order to study extremely high energy cosmic rays (EHECR) above 10^{19}eV. In this energy region, distinctive features in the energy spectrum and arrival direction distribution are expected. First, for the extragalactic cosmic rays, photopion production between cosmic rays and primordial microwave background photons becomes important at energies above 6 $\times 10^{19}$eV with a mean free path of about 6Mpc. Therefore a cutoff in the spectrum should be observed around several times 10^{19}eV even if the primary cosmic ray energy spectrum extends beyond 10^{20}eV. This is called as the Greisen-Zatsepin-Kuzmin (GZK) cutoff [3].

Second, the effect of the magnetic field in the galactic and extra-galactic space becomes less significant at higher energy region. The deflection angle of $10^{20}eV$ cosmic ray becomes an order of 1 degree for the 30Mpc propagation. Therefore, the strong cosmic ray sources may be observed as point sources and the astronomy with neucleons can be possible above $10^{20}eV$.

Third, the acceleration site to accelerate cosmic rays up to $10^{20}eV$ is limitted significantly. The diffusive shock acceleration at radio lobes of relativistic jets from Active Galactic Neuclei, termination shocks in local group of galaxies, etc. are discussed to be possible sites [4]. The acceleration in dissipative wind of cosmological gamma-ray burst is proposed [5]. Since various difficulties are still anticipated in accelerating cosmic rays up to the highest observed energies, it is also discussed that these cosmic rays are possiblly the decay products of some massive particles produced at the collapse and/or annihilation of cosmic topological defects which could have been formed in a symmetry-breaking phase transiton in the early universe [6].

The details of the AGASA are described in Chiba et al. [1] and Ohoka et al. [2]. The array is operational since 1991 and the exposure is about 1000km^{2}year till the april of 1999. Here, we present the recent observational results of AGASA.

II AGASA RESULTS

In order to estimate the primary energy of giant air showers observed by the AGASA, the particle density at a distance of 600m from the shower axis (S(600)) is employed, which is known to be a good parameter [7]. The conversion factor from S(600) [per m^2] to primary energy E_0 [eV] is derived by simulation [8] as

$$E_0 = 2.0 \times 10^{17} \times S(600)^{1.0}. \quad (1)$$

The details of determination of arrival directions and S(600) are described in Yoshida et al. [9].

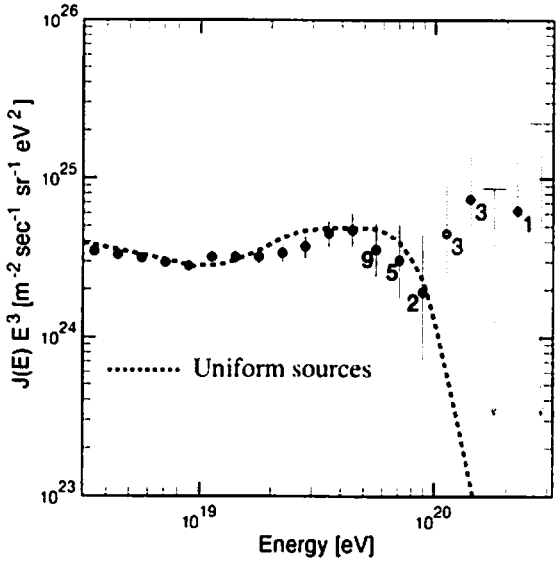

FIGURE 1. The energy spectrum observed with AGASA. The vertical axis is multipled by E^3. Error bars represent the Poisson upper and lower limits at 68% and arrows are 90% C.L. upper limits. Numbers attached to points show the number of events in each energy bin. The dashed curve represents the spectrum expected for extragalactic sources distributed uniformly in the Universe, taking account of the energy determination error. The primary spectrum is assumed $\propto E^{-2.3}$.

The differential energy spectra above $10^{18.5}$eV are shown in figure 1 [10]. The bars represent statistical errors only and the error in the energy determination is about 30% above 10^{19}eV, which is estimated from analyzing the artificial showers

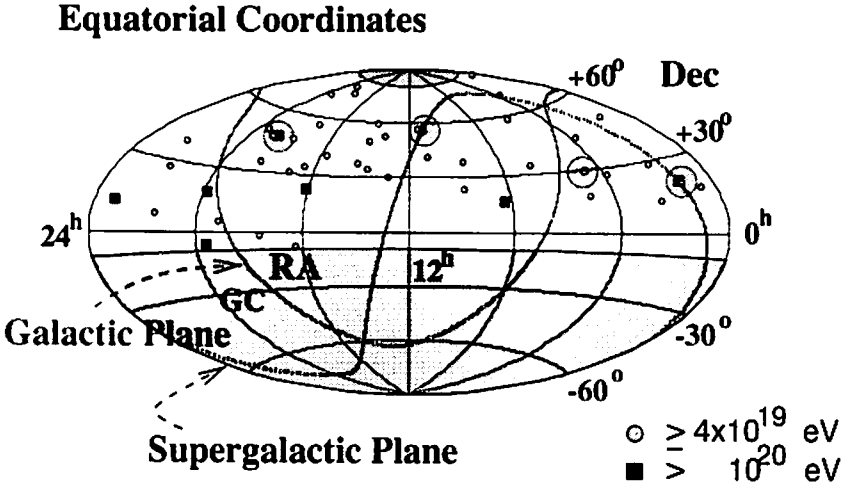

FIGURE 2. The arrival direction of the highest energy cosmic rays on the equatorial coordinate.

simulated considering shower development fluctuation and experimental errors in each detector [9].

The energy spectrum extends beyond 10^{20}eV and we observed 7 events above GZK cutoff energy. The expected energy spectrum with uniform source is show in figure 1 as the dashed curve. The expected number of events above 10^{20}eV is less than one, taking account of the energy resolution. The energy spectrum is therefore more likely to extend beyond 10^{20}eV without the GZK cutoff.

The arrival direction of the highest energy cosmic rays above $4 \times 10^{19} eV$ is shown in figure 2 on the equatorial coordinate [12]. Small dots and sqaures show events between $4 \times 10^{19} eV$ and $10^{20} eV$ and above $10^{20} eV$, respectively. Essentially they distribute uniformly in the observable sky. We have several test for the anisotropy. We could not find any large scale structures in this distribution. However, we found one tripplet and three doublets of events clustering within an angular resolution (2.5° circle) as indicated shadowed circles. The chance probability for this clustering effect was evaluated by the monte carlo simulation and found to be as small as $P_{ch} = 0.0032$. In the direction of triplet (the second cluster from the left in the figure), we found the interacting galacy VV141 at the distance of z = 0.02.

In order to explore of the galactic cosmic ray, the harmonic analysis in the right ascension was carried out using the comsic rays about 216,000 events observed by AGASA [11]. It is a traditional method to explore the global anisotropy of the cosmic-ray arrival direction distribution. The amplitude, the phase(peak direction in right ascension), and the rayleigh power k were determined in each differential energy bin as shown in table 1. The rayleigh power $k \sim 14$ around 10^{18}eV was found energy bin E5. It is surprisingly high, corresponding to a chance probability of 2.5×10^{-6}.

TABLE 1. The first harmonic analysis in right ascension.

Bin	Energy Range/EeV	#	Amplitude[%]	Phase	k	P_{prob}
E4	1/2 - 1.0	56658	0.5	272	0.42	0.65
E5	1.0 - 2.0	29207	4.2	297	12.9	2.5E-6
E6	2.0 - 4.0	10129	2.0	256	1.10	0.33
E7	4.0 - 8.0	2769	3.3	256	0.76	0.46

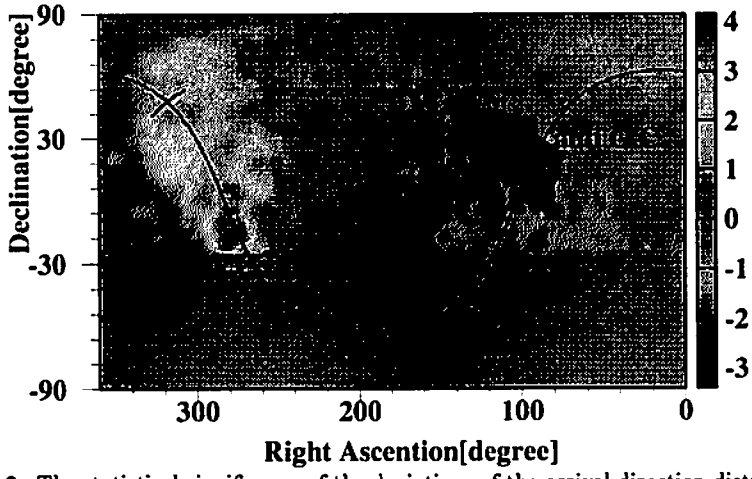

FIGURE 3. The statistical significance of the deviations of the arrival direction distribution of the cosmic rays above $10^{18}eV$ on the equatorial coorinate.

In figure 3 the arrival direction distributions in equatorial coordinates are shown. They show the statistical significance of the deviations from the expectation. Here, the energy region of $10^{18}eV \sim 10^{18.4}eV$ is selected which maximize the rayleigh power k-value. We can not observe events with declination less than $-25°$, as long as we use showers with zenith angles less than 60°. In this figure, we have chosen a circle of 20° radius to evaluate the excess. In the siginicance map, a 4.5σ excess (obs./exp. = 506/413.6) near the Galactice enter region can be seen. In contrast, near the direction of anti-Galactic Center we can see a deficit in the cosmic ray intensity (-4.0σ). An event excess from the direction of the Cygnus region is also seen with 3.9σ(obs./exp. = 3401/3148). This anisotropy can be considered as a clear evidence for the existence of galactic cosmic rays up to $10^{18}eV$.

III DISCUSSION

There are seven events whose energies exceed considerably the GZK cut-off energy (8th event was observed just after this conference, 26th ICRC). Their sources can't be very far and must be within a few tens of Mpc. However, there are no candidate, astronomical objects within a few tens of Mpc in the direction of the highest energy events which may be able to accelerate particles to more than 10^{20}eV.

These observations have led to suggestions that particles may be directly produced by decay from objects produced in phenomenon occurring on a higher energy scale [6,13]. For example, topological defects (TD's) left over from the phase transitions in the early universe, caused by the spontaneous breaking of symmetries, have been proposed as a candidate for production of extremely high energy cosmic rays. Such TD's are magnetic monopoles, cosmic strings, domain walls, superconducting strings etc. The remarkable result from this scenario is that bulk of cosmic rays above 10^{20}eV may be gamma-rays rather than protons and the energy spectrum is expected to extend up to the GUT scale $\sim 10^{25}$eV with a hard exponent such as 1.35 [13], which is based on the exponent of hadronization in QCD.

REFERENCES

1. N.Chiba et al., *Nucl. Instrum. Methods* A **311**, 388 (1992).
2. H.Ohoka et al., *Nucl. Instrum. Methods* A **A372**, 527 (1997).
3. K.Greisen, *Phys. Rev. Lett.* **16**, 748 (1966); G.T.Zatsepin and V.A.Kuzmin, *Pisma Zh. Eksp. Teor. Fiz.* **4**, 144 (1966).
4. Various acceleration models are discussed in *Astrophysical Aspects of the Most Energetic Cosmic Rays*, ed. M.Nagano and F.Takahara (World Scientific, Singapore, 1990) pp.252-334.
5. E.Waxman, *Phys. Rev. Lett.* **75**, 386 (1995); M.Vietri, *Ap. J.* **453**, 883 (1995); M.Milgrom and V.Usov, *Ap. J.* **449**, L37 (1995);
6. Recent summary and references are described in P.Bhattacharjee, *Proc. of ICRR Symp. on Extremely High Energy Cosmic Rays : Astrophysics and Future Observatories* ed. M.Nagano, (Inst. of Cosmic Ray Research, University of Tokyo., 1997) p.125.
7. A.M.Hillas et al, *Proc. 12th ICRC, Hobart* **3**, 1001 (1971).
8. H.Y.Dai et al., *J. Phys. G: Nucl. Part. Phys.* **14**, 793 (1988).
9. S.Yoshida et al., *J. Phys. G: Nucl. Part. Phys.* **20**, 651 (1994).
10. M.Takeda et al., *Phys. Rev. Lett.* **81**, 1163 (1998).
11. H.Hayashida et al., *Astroparticle Phys.* **10**, 303 (1999).
12. M.Takeda et al., *Ap. J.* **522**, 225 (1999).
13. P.Bhattacharjee, C.T.Hill and D.N.Schramm, *Phys. Rev. Lett.* **69**, 567 (1992).

Structures of general relativistic binary neutron star systems in quasiequilibrium

--- A new approach without the conformally flat condition —

Fumihiko Usui*

Department of Earth Science and Astronomy, Graduate School of Arts and Sciences, University of Tokyo, Komaba, Meguro, Tokyo 153-8902, Japan

Kōji Uryū

SISSA, Via Beirut 2-4, Trieste 34013, Italy

Yoshiharu Eriguchi

Department of Earth Science and Astronomy, Graduate School of Arts and Sciences, University of Tokyo, Komaba, Meguro, Tokyo 153-8902, Japan

Abstract

We present a new numerical scheme to obtain quasiequilibrium structures of non-axisymmetric compact stars and the space time around those systems in general relativity. Although all of the previous works of quasiequilibrium configurations in general relativity have been investigated by assuming *the conformally flat condition*, its validity is not fully understood. In our new scheme, on the other hand, Einstein equations are solved directly without assuming *the conformally flat condition*. Here we apply this scheme to binary neutron star systems. For $N = 2.0$ polytropes, we confirm that there is no tendency of individual collapse to black holes for synchronously rotating systems.

1 Introduction

One of the most important problems for theorists of relativistic astrophysics is constructing reliable models for quasiequilibrium configurations of binary neutron star systems. This is because such systems are the most promising sources of gravitational waves which can be observed by the gravitational wave detectors under construction, such as LIGO (USA), VIRGO (France/Italy), GEO (Germany/Great Britain), and TAMA (Japan).

In order to understand the final evolutional stages of compact binary star systems from gravitational wave observations, we need to know the detailed processes during inspiraling and merging phases. This can be done by performing dynamical computations of the evolution of binary star systems to a very high accuracy. It is, however, still difficult to perform highly accurate numerical computations of three-dimensional configurations in general relativity (GR), although many important results have been obtained (see, e.g., Oohara, Nakamura, and Shibata [1], Nakamura [2]).

Since the time scale of the orbital change due to gravitational wave emission is rather long compared with the orbital period except for the final stage of coalescence, we can neglect gravitational wave emission for the most stages of evolution. In other words, we can treat the systems in "quasiequilibrium".

The first numerical results for quasiequilibrium states of binary configurations in full general relativity have been obtained by Wilson, Mathews, and Marronetti [3]. In order to make the problem tractable, they have assumed that the spatial part of the metric is *conformally flat*. Hereafter we shall call this the conformally flat condition (CFC). One of their results was surprising: binary neutron stars become unstable and collapse into black holes individually prior to merging (see also, Mathews and Wilson [4]).

*E-mail:usui@provence.c.u-tokyo.ac.jp

In the framework of Newtonian gravity, as the binary stars approach each other, the central density of each star tends to decrease because each star expands by the tidal force of the companion star. When general relativistic effects are taken into account, the situation becomes more complicated. Recently Wilson *et al.*'s results are revised [5], but the outline of their results do not change. The same problem has been investigated by applying almost the same formulation but by using a different numerical scheme by Baumgarte *et al.* [6] (see also, Cook, Shapiro, and Teukolsky [7], Baumgarte *et al.* [8]). Baumgarte *et al.* [6] have found that there exist quasiequilibrium sequences of binary systems just prior to merger, i.e., the individual collapse to black holes does not occur (see also, [9, 10]).

All of these calculations are based on the CFC, although its validity is not fully understood [11]. It is already known that for axisymmetric rotating polytropes the scheme with the CFC gives reasonably accurate results [7]. However, it is uncertain whether results from axisymmetric configurations may be applied to nonaxisymmetric ones or not. In this sense, it is desirable to develop different schemes from that with the CFC and to compare results of two or many different schemes for nonaxisymmetric models.

It should be noted that quasiequilibrium configurations provide realistic initial conditions for dynamical computations of the final stage of coalescence [12].

We have developed a new numerical scheme to handle quasiequilibrium states of nonaxisymmetric configurations in general relativity without using the CFC [13]. This scheme is an extension of the numerical scheme for axisymmetric configurations developed by Komatsu, Eriguchi, and Hachisu (KEH scheme) [14]. In this paper, we calculate quasiequilibrium configurations of the binary systems using this new scheme and construct equilibrium sequences with constant baryon-mass which provide approximate evolutionary tracks.

2 Assumptions and basic equations

2.1 Assumptions

As mentioned in Introduction, we can neglect the effect of gravitational waves for almost all stages except for the last few milliseconds of the coalescence of binary systems and choose a rotating frame in which the system is in a stationary state.

We will make the following assumptions in this paper.

(1) We deal with a binary system which consists of two stars of equal masses in a circular orbit.

(2) The binary star system is in a stationary state in the rotating frame with the angular velocity Ω.

(3) Axes of spins of two stars and that of the orbital motion are parallel to one another. A schematic figure of the system is shown in Fig. 1.

(4) Spins of two stars are synchronized to the orbital motion. Each star is rigidly rotating with the angular velocity Ω if seen from a distant place.

(5) The matter of the star is a perfect fluid and a polytropic relation is assumed.

2.2 Metric and basic equations

In addition to the assumptions mentioned above, we further assume the following form for the metric in the spherical coordinates (r, θ, φ) (hereafter we use the units of $c = G = 1$):

$$ds^2 = -e^{2\nu}dt^2 + r^2\sin^2\theta e^{2\beta}(d\varphi - \omega dt)^2 + e^{2\alpha}dr^2 + r^2 e^{2\alpha'}d\theta^2 \ , \tag{1}$$

where ν, β, ω, α, and α' are the metric coefficients, which are functions of r, θ, and φ. This choice of the metric is not the most general one for quasiequilibrium states because we do not take into account (tr) and/or $(t\theta)$ components of the metric. However, since the purpose of this paper is to show the effectiveness of our new scheme and the $(t\varphi)$ component is considered to be the most dominant one among the nondiagonal components, we use the above form for the metric. Furthermore, for simplicity, we assume the following condition:

$$\alpha = \alpha' \ . \tag{2}$$

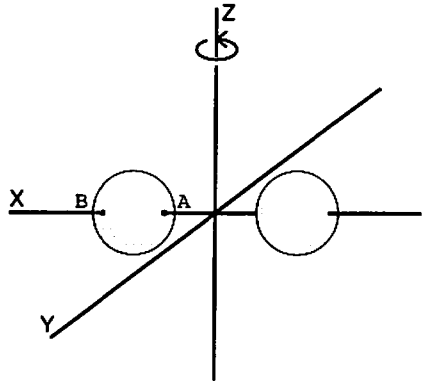

Figure 1: Schematic view of the binary system. The x axis is set along the line joining the two centers of mass of the two stars and the origin is set at their midpoint. The z axis is along the rotation axis. Points A, B are set at the intersections of the surface of the star and the x axis. The inner intersection is point A and the outer one is point B.

This form of the metric becomes exact for stationary axisymmetric configurations. Although the assumed metric form is incomplete for quasiequilibrium three-dimensional configurations, the essential and technical part of a new numerical scheme for three-dimensional configurations can be shown by choosing this kind of simplified metric and will be extended to a more general form of the metric.

The equation of state for the matter is assumed to be polytropic:

$$p = K\rho^{1+1/N} , \tag{3}$$

$$\varepsilon = \rho + Np , \tag{4}$$

where p, ρ, ε, and N are the pressure,the baryon mass density, the energy density, and the polytropic index, respectively. K is a proportional constant.

The energy-momentum tensor $T^{\zeta\eta}$ for the perfect fluid is written as

$$T^{\zeta\eta} = (\varepsilon + p)u^{\zeta}u^{\eta} + pg^{\zeta\eta} , \tag{5}$$

where u^{ζ} and $g^{\zeta\eta}$ are the four velocity of the matter and the metric, respectively. Concerning the four velocity, since an observer in the rotating frame sees that the matter is static, we can obtain the following relation by using the condition $u^{\zeta}u_{\zeta} = -1$:

$$u^{\zeta} = \frac{e^{-\nu}}{\sqrt{1-v^2}} \begin{pmatrix} 1 \\ 0 \\ 0 \\ 0 \end{pmatrix} , \tag{6}$$

where v is the proper velocity of the matter:

$$v = r(\Omega - \omega)\sin\theta e^{\beta-\nu} . \tag{7}$$

The hydrostatic equation is derived from the conservation law $T^{\zeta\eta}{}_{;\eta} = 0$ as follows:

$$\nabla p - (\varepsilon + p)\nabla \ln u^t = 0 . \tag{8}$$

By using the polytropic equation (3) and the rigid rotation law, it can be integrated to the following equation:

$$(1+N)\ln\left(K\varepsilon^{1/N}+1\right) + \nu + \frac{1}{2}\ln(1-v^2) = C , \tag{9}$$

where C is a constant of integration.

The Einstein equations are transformed to integral representations. This scheme is an extension of the numerical scheme for axisymmetric configurations developed by Komatsu, Eriguchi, and Hachisu (KEH scheme) [14]. The Einstein equations are explicitly derived after a lengthy but straightforward calculation. Combining the obtained Einstein equations appropriately, we can obtain the nonlinear Poisson-like equations for the metric functions (see, [13]). For nonaxisymmetric configurations, however, the Einstein equations for each metric component do not contain the Laplacian in the flat space even after proper arrangements. This can be done if we add appropriate terms to both sides of properly selected component equations of the Einstein equations, although the source terms of those equations contain extra derivatives in addition to the original sources. Since we can include the boundary condition into the Green's function, we only need to solve the integral equations by some means.

Here we solve four equations for the metric coefficients, ν, β, ω, and α, and the rest of the Einstein equations are not used. Therefore, our solutions are not numerically exact ones which satisfy all components of the Einstein equations. This is similar to the CFC approach [3, 6].

3 Method of calculations

3.1 Model parameters

For polytropes, the equation of state is fixed by choosing one parameter corresponding to the constant K in addition to the polytropic index N. Once the equation of state is fixed, we need to specify two parameters to determine a rotating equilibrium configuration: one for the strength of gravity and the other for the rotation rate. In our formulation, we choose the following two parameters: (1) the maximum energy density, ε_c, and (2) the ratio of the shortest distance r_A (distance from the origin to point A, see Fig. 1) to the largest distance r_B (distance from the origin to point B, see Fig. 1), q:

$$q \equiv \frac{r_A}{r_B} . \tag{10}$$

The quantity q indirectly specifies the rotation rate and is related to the distance between the two stars as $d = r_B(1+q)$, where d is the distance between the geometrical centers of the stars.

We can introduce dimensionless physical quantities by using the polytropic constant K as $M = K^{N/2}\bar{M}$ (mass), $\varepsilon = K^{-N}\varepsilon$ (energy density), $\Omega_0 = K^{-N/2}\bar{\Omega}_0$ (angular velocity), and $J = K^N\bar{J}$ (angular momentum).

Since the quantity K does not appear in the basic equations, we can treat the problem by specifying only two parameters, ε_c and q, in addition to the polytropic index N.

3.2 Solving scheme

Our formulation is almost the same as that used in Komatsu, Eriguchi, and Hachisu (KEH) [14] and we can adopt the HSCF (Hachisu's Self-Consistent Field) method [15] or the KEH method [14] as our solving scheme. That is, the nonlinear Poisson equations for the metric potentials and the hydrostatic equation are solved by an iterative procedure with two parameters ε_c and q kept constant. Thus we obtain the four metric coefficients ρ, γ, α, and ω, distributions of the energy density ε, the pressure p, and the angular velocity Ω of the system. In actual computations, we have used $(r \times \theta \times \varphi) = (128 \times 49 \times 81)$ grid points.

Since there exist no exact equilibrium or stationary states, it is impossible to define conserved quantities for nonaxisymmetric configurations in general relativity. Here we assume the quasiequilibrium states, the metric at infinity can be approximated by the flat space time as

$$\omega \sim 2J/r^3 \ , \ \partial\omega/\partial r \sim -6J/r^4 \ , \ \partial\nu/\partial r \sim M/r^2, \ \text{at } r \sim \infty. \tag{11}$$

For such a space time, we can define the approximate angular momentum and the approximate gravitational mass using these asymptotic behaviors (see, [13]).

4 Numerical results — Evolutions of constant baryon-mass binary systems —

During realistic evolution, the gravitational mass and the angular momentum are lost from the system. However, the baryon number of the system should be conserved. Therefore sequences of constant baryon-mass (rest-mass) provide approximate evolutionary tracks. In addition, the equation of state is assumed not to change during evolution, i.e., the polytropic index N and the constant K are fixed (cf. [6]).

In this paper, we show the results for $N = 2.0$ polytropes, although it may be too soft for neutron stars.

In Fig. 2, the dimensionless baryon-mass of each star is plotted against the dimensionless central energy density. Each line is the sequence along which the separation q is fixed but the energy density ε_c is varied. Three curves correspond to the sequence of $q = 0.0$ (contact), 0.125, and 0.375. From this figure, we can see that as the central energy density increases, the baryon-mass increases until a certain critical point. However, as the density increases further, the equilibrium configuration becomes unstable and the mass begins to decrease because of the general relativistic effects. Below the density corresponding to this maximum mass, the sequences near the contact phases ($q \sim 0$) are located above other two sequences. Hereafter, about the constant baryon-mass sequences,we will consider three evolutionary sequences of constant baryon-mass with three different compactnesses, i.e., $(M/R)_\infty = 0.0471, 0.0392$, and 0.0331.

In Fig. 3, the dimensionless angular velocity is shown against the dimensionless angular momentum. We see the change of the orbital motion from this figure. Three curves correspond to sequences with the compactness mentioned above. As the angular momentum decreases owing to gravitational wave emission, the binary system shifts to the left side along the curve. If the curve has a turning point, the system becomes secularly unstable at that point. However, as seen from this figure, there is no turning point and the system reaches the contact phase without suffering from any unstable phenomena.

In Fig. 4, the dimensionless central energy density is plotted against the separation q. From this figure, we can see the density decreases as the orbit shrinks, i.e., the evolution proceeds. In each sequence, the density decrease about $5 \sim 7\%$. In particular, for $(M/R)_\infty = 0.0471$ sequence which is located near the maximum mass configuration, there is no tendency to collapse individually prior to merging.

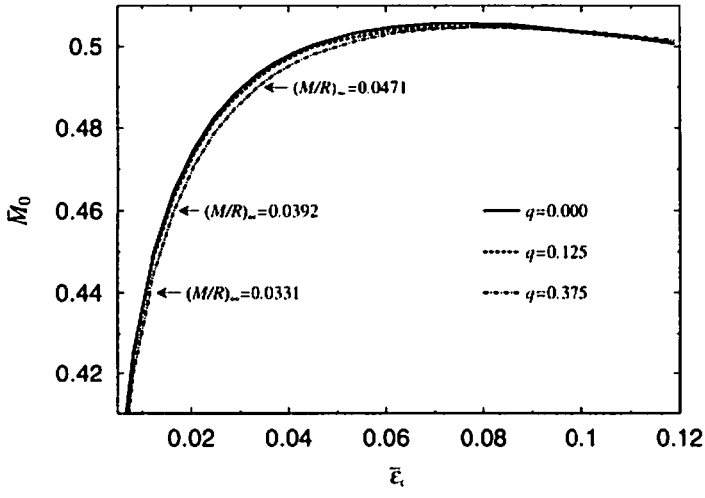

Figure 2: Dimensionless rest-mass of each star $\bar{M}_0$ is plotted against dimensionless central energy density ε_c for the quasiequilibrium $N = 2.0$ polytropic binary star systems with the separation $q = 0.0$ (contact), 0.125, and 0.375. Three arrows indicate the constant baryon-mass sequences discussed in Fig. 3 and Fig. 4.

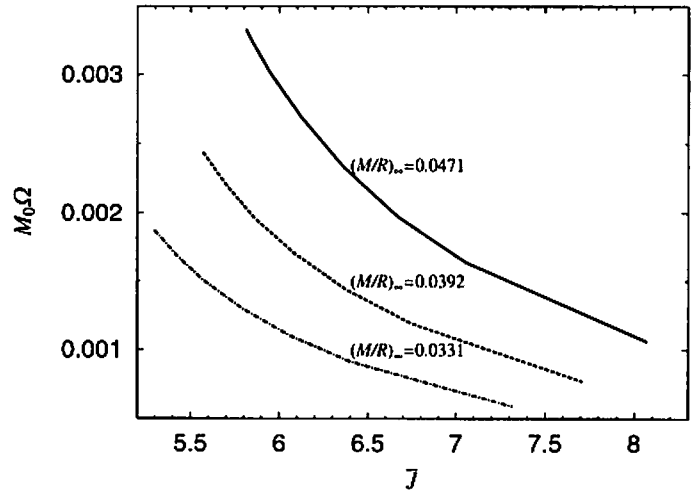

Figure 3: Dimensionless angular momentum J is plotted against dimensionless angular velocity $M_0\Omega$ for the sequences of constant baryon-mass polytropic binary systems with $N = 2.0$. Three curves correspond to sequences with the compactnesses $(M/R)_\infty = 0.0331$, 0.0392, and 0.0471.

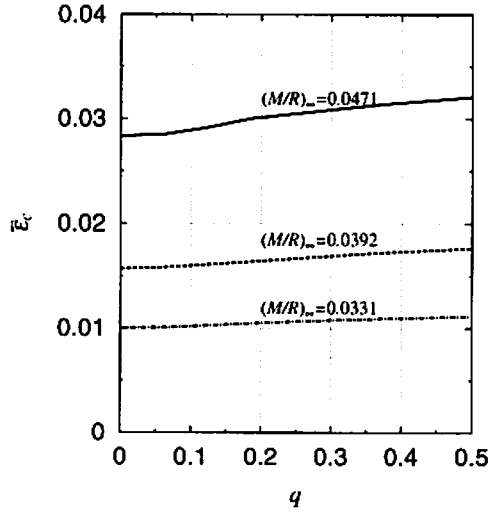

Figure 4: Dimensionless central energy density ε_c is plotted against the separation q (defined as Eq. (10)) for the sequences of constant baryon-mass polytropic binary systems with $N = 2.0$. Three curves correspond to sequences with the compactnesses $(M/R)_\infty = 0.0331$, 0.0392, and 0.0471.

5 Summary and Discussion

In this paper, we have calculated quasiequilibrium structures of synchronously rotating binary neutron star systems by integrating numerically the Einstein equations directly without assuming the CFC and constructed the sequences of constant baryon-mass polytropic binary star systems with $N = 2.0$. For these systems, we have shown that the central energy density of each star decreases as approaching each other. Our results agree well with other numerical computations [9, 10] and there is no tendency of individual collapse to black holes suggested by Wilson *et al.* [3].

Here we have used the polytropic relation as the equation of state and the polytropic index N and the constant K are fixed along the sequences. However, almost nothing is known about the behavior of N and/or K along the evolution. Furthermore, it should be noted that the realistic equation of state for the cold neutron star matter contains no parameter, i.e., if the density ε_c is specified, everything is determined. Since Wilson *et al.* [3, 5] used a kind of zero temperature equation of state, in order to examine their results, we must employ some realistic equations of state and investigate the behavior of evolutionary sequences in the future.

Since for realistic neutron stars the viscosity does not work enough, we need to extend our formulation to treat irrotational binary neutron star systems in order to give final answers to the individual collapse "problem".

Acknowledgments

We would like to thank Professor T. Nakamura for his useful comments.

References

[1] K. Oohara, T. Nakamura, and M. Shibata, Prog. Theor. Phys. Suppl. **128**, 183 (1997).

[2] T. Nakamura, in *Black Holes and High Energy Astrophysics*, edited by H. Sato and N. Sugiyama (Universal Academic Press, Tokyo, 1998), pp.249-268.

[3] J.R. Wilson, G.J. Mathews, and P. Marronetti, Phys. Rev. D **54**, 1317 (1996).

[4] G.J. Mathews and J.R. Wilson, Astrophys. J. **482**, 929 (1997).

[5] G.J. Mathews and J.R. Wilson, Phy. Rev. D. in press. (gr-qc/99011047)

[6] T.W. Baumgarte, G.B. Cook, M.A. Scheel, S.L. Shapiro and S.A. Teukolsky, Phys. Rev. D **57**, 7299 (1998).

[7] G.B. Cook, S.L. Shapiro, and S.A. Teukolsky, Phys. Rev. D **53**, 5533 (1996).

[8] T.W. Baumgarte, G.B. Cook, M.A. Scheel, S.L. Shapiro and S.A. Teukolsky, Phys. Rev. D **57**, 6181 (1998).

[9] F.A. Rasio and S.L. Shapiro, Class. Quantum Grav. **16**, R1 (1999).

[10] S. Bonazzola, E. Gourgoulhon, and J.-A. Marck, Phys. Rev. Lett. **82**, 892 (1999).

[11] H. Asada and M. Shibata, Phys. Rev. D **54**, 4944 (1996).

[12] M. Shibata and K. Uryū, Phy. Rev. in press. (gr-qc/9911058)

[13] F. Usui, K. Uryū, and Y. Eriguchi, Phy. Rev. D. in press. (gr-qc/9906102)

[14] H. Komatsu, Y. Eriguchi, and I. Hachisu, Mon. Not. R. Astron. Soc. **237**, 355 (1989).

[15] I. Hachisu, Astrophys. J. Suppl. **62**, 461 (1986).

Almost analytic solutions to equilibrium sequences of irrotational binary polytropic stars for n=1

Keisuke Taniguchi and Takashi Nakamura
Yukawa Institute for Theoretical Physics, Kyoto University, Kyoto 606-8502, Japan
(October 13, 1999)

A solution to an equilibrium of irrotational binary polytropic stars in Newtonian gravity is expanded in a power of $\epsilon = a_0/R$, where R and a_0 are the separation of the binary system and the radius of each star for $R = \infty$. For the polytropic index $n = 1$, the solutions are given almost analytically up to order ϵ^6. We have found that in general an equilibrium solution should have the velocity component along the orbital axis and that the central density should decrease when R decreases. Our almost analytic solutions can be used to check the validity of numerical solutions.

PACS number(s): 04.30.Db, 04.25.Dm, 97.80.Fk

Coalescing binary neutron stars are considered to be one of the most promising sources of gravitational waves for laser interferometers such as TAMA300, GEO600, VIRGO and LIGO [1]. We can determine the mass and the spin of neutron stars from the gravitational wave signals in the inspiraling phase. We may also extract the informations on the equation of state of a neutron star from the signals in the pre-merging phase [2]. For this purpose it is important to complete theoretical templates of gravitational waves in the pre-merging phase as well as in the inspiraling phase.

Recently Bonazzola, Gourgoulhon and Marck have numerically calculated quasi-equilibrium configurations of irrotational binary neutron stars in general relativity [3]*. Although their results seem to be reasonable, we do not have any analytic solutions in general relativity in order to check the validity of their results.

On the other hand, Uryū and Eriguchi have numerically constructed stationary structures of irrotational binary stars in Newtonian gravity [6]. We can use semi-analytic solutions produced by Lai, Rasio and Shapiro (hereafter LRS) [7] for checking the validity of the results. Even if there are differences in the appearance of the dynamical instability limits between the results of Uryū and Eriguchi and those of LRS, the integrated values, i.e., the total energy, the orbital angular velocity, and so on, are good approximate solutions.

However, in numerical solutions of Uryū and Eriguchi, the velocity component along the orbital axis exists while in those of LRS such a component is assumed to be zero from the beginning. When we extend the analytic solutions to the general relativistic ones [8], we should include this velocity component. This is because in the numerical calculation, there is a possibility to obtain another solution although the binding energy of the binary neutron stars is almost the same value, and to lead a different conclusion [9].

In order to include the velocity component along the orbital axis, we solve the equation of continuity with the other basic equations. The method we use in this Letter is that we seek a solution to an equilibrium of irrotational binary polytropic stars in Newtonian gravity by expanding all physical quantities in a power of $\epsilon \equiv a_0/R$, where R and a_0 are the separation of the binary system and the radius of each star for $R = \infty$. We extend the method developed by Chandrasekhar more than 65 years ago for corotating fluids [10] to the one for irrotational fluids.

Although a binary system consists of two stars, we pay particular attention to one of two stars. We call it star 1 whose mass is M_1 and the companion one star 2 whose mass is M_2. In this Letter, we adopt two corotating coordinate systems. First one is $\boldsymbol{X}$ whose origin is located at the center of mass of the binary system. For calculational convenience, we choose the orbital axis as X_3, and we take the direction of X_1 from the center of mass of star 2 to that of star 1. The second coordinate system is the spherical one $\boldsymbol{r} = (r, \theta, \varphi)$ whose origin is located at the center of mass of star 1. We use units of $G = 1$.

Since we treat irrotational fluids in Newtonian gravity, the basic equations are the equation of state, the Euler equation, the equation of continuity and the Poisson equation:

$$P = K\rho^{1+\frac{1}{n}}, \tag{1}$$

$$\nabla\left[\int \frac{dP}{\rho} - U + \frac{1}{2}v^2 - \boldsymbol{v}\cdot(\boldsymbol{\Omega}\times\boldsymbol{r})\right] = 0, \tag{2}$$

$$\nabla\cdot\boldsymbol{v} = -(\boldsymbol{v} - \boldsymbol{\Omega}\times\boldsymbol{r})\cdot\frac{\nabla\rho}{\rho}, \tag{3}$$

$$\Delta U = -4\pi\rho, \tag{4}$$

where P, ρ, n, U and Ω are the pressure, the density, the polytropic index, the gravitational potential and the orbital angular velocity, respectively. The gravitational

*The irrotational state is considered to be a realistic state for binary neutron stars before merger [4,5].

potential U is separated into two parts, i.e., the contribution from star 1 to itself $U^{1\to1}$ and that from star 2 to star 1 $U^{2\to1}$. $U^{2\to1}$ is written as

$$U^{2\to1} = \frac{M_2}{R}\sum_{l=0}^{\infty}(-1)^l\left(\frac{\alpha}{R}\right)^l \xi^l P_l(\sin\theta\cos\varphi) + \frac{3\mathcal{I}'_{11}}{2R^3}\left[1-3\left(\frac{\alpha}{R}\right)\xi\sin\theta\cos\varphi + O(R^{-2})\right] + \cdots. \quad (5)$$

Here, P_l and $\mathcal{I}_{11}$ denote the Legendre function and the reduced quadrupole moment, and the superscript $'$ means the term concerned with star 2. K is a constant related to entropy and v represents the velocity field in the inertial frame. In the irrotational fluid case, we can express v as a gradient of a scalar function Φ, i.e., $v = \nabla\Phi$.

Following the *Lane-Emden equation* we first express the density as $\rho = \rho_c\Theta^n$ with ρ_c being the central density and introduce $\xi = r/\alpha$ where

$$\alpha \equiv \left[\frac{K(1+n)\rho_c^{\frac{1}{n}-1}}{4\pi}\right]^{1/2}. \quad (6)$$

We expand Θ in a power series of a parameter ϵ as $\Theta = \sum_{i=0}^{\infty}\epsilon^i\Theta_i$. Since the shape of star 1 is spherical when R is large, the lowest order term of Θ is the solution of the *Lane-Emden equation*. Then we expand Θ_i by spherical harmonics as $\Theta_i = \sum_{l,m}{}^{(i)}\psi_{lm}(\xi)Y_l^m(\theta,\varphi)$. The radius of a spherical star a_0 is given by $a_0 = \alpha\xi_1$ as usual. Note here that $\xi_1 = \pi$ for $n = 1$ case.

Now we consider the orbital motion of star 1. In the spherical coordinate system, it becomes

$$\Omega\times r = \Omega R(\tilde{\Omega}\times\xi)_{orb} + \Omega\alpha(\tilde{\Omega}\times\xi)_{fig}, \quad (7)$$

where

$$(\tilde{\Omega}\times\xi)_{orb} = \frac{1}{1+p}(\sin\theta\sin\varphi,\ \cos\theta\sin\varphi,\ \cos\varphi), \quad (8)$$

$$(\tilde{\Omega}\times\xi)_{fig} = (0,\ 0,\ \xi\sin\theta), \quad (9)$$

and $p \equiv M_1/M_2$. The first term on the right-hand side of Eq. (7) comes from the orbital motion of the center of mass of star 1 and the second term comes from the fluid motion around the center of mass of star 1.

Next, we rewrite the equation of continuity (3) as

$$\Delta\Phi = -n(\nabla\Phi - \Omega\times r)\cdot\frac{\nabla\Theta}{\Theta}. \quad (10)$$

The condition for Φ at the stellar surface is

$$(\nabla\Phi - \Omega\times r)\cdot(\nabla\Theta)\big|_{surf} = 0, \quad (11)$$

since $\Theta = 0$ at the surface. We expand Φ also as $\Phi = \sum_{i=0}^{\infty}\epsilon^i\Phi_i$. The gradient of the lowest order term of Φ should agree with the orbital motion of the center of mass of star 1, i.e., $\Omega R(\tilde{\Omega}\times\xi)_{orb}$ because when R is large , the shape of star 1 is spherical and star 1 has only the orbital motion of the center of mass in the inertial frame with no intrinsic spin. This leads us to normalize Φ as $\tilde{\Phi} = \epsilon\Phi/(\Omega\alpha a_0)$. We again expand $\tilde{\Phi}_i$ by spherical harmonics as $\tilde{\Phi}_i = \sum_{l,m}{}^{(i)}\phi_{lm}(\xi)\tilde{Y}_l^m(\theta,\varphi)$.

The orbital angular velocity is derived from the first tensor virial relation defined by [11]

$$\int d^3x\frac{\partial P}{\partial x_1} = 0, \quad (12)$$

where $x_1 = r\sin\theta\cos\varphi$. If we substitute Eq. (7), Θ_0 and Φ_0 into Eq. (12), we obtain the orbital angular velocity in the lowest order as $\Omega_0^2 = M_{tot}/R^3$ where $M_{tot} = M_1 + M_2$. Note here that we also expand Ω^2 as $\Omega^2 = \sum_{i=0}^{\infty}\epsilon^i\Omega_i^2$.

Finally, we express the gravitational potential by rewriting Eq. (2) as

$$U = K(1+n)\rho^{\frac{1}{n}} + \frac{1}{2}v^2 - v\cdot(\Omega\times r) + U_0, \quad (13)$$

where U_0 is constant. Substituting Eq. (13) into the Poisson equation (4), we obtain the equation to determine the equilibrium figure as

$$\alpha^2\Delta\Theta = -\Theta^n - \frac{1}{8\pi\rho_c}\Delta\Big[(\nabla\Phi)^2 - 2(\nabla\Phi)\cdot(\Omega\times r)\Big]. \quad (14)$$

Now a solution can be obtained iteratively. Firstly, Θ_i is determined by demanding that the gravitational potential and its normal derivative are continuous at the stellar surface [10], that is, $U_{int}|_{\xi=\Xi} = U_{ext}|_{\xi=\Xi}$ and $\partial U_{int}/\partial\xi|_{\xi=\Xi} = \partial U_{ext}/\partial\xi|_{\xi=\Xi}$, where $\Xi(\theta,\varphi)$ expresses the surface ($\Theta(\xi = \Xi(\theta,\varphi)) = 0$). Substituting Θ_i and Eq. (7) into Eqs. (10) and (12), we obtain Φ_i and Ω_i^2. After that we substitute these equations into Eq. (14) and derive Θ_{i+1}. We continued this procedure up to order ϵ^6 in this Letter.

Since we would like to present almost *analytic* results, we only calculate $n = 1$ case in this Letter. The density profile up to $O(\epsilon^6)$ becomes

$$\Theta = \Theta_0 + \epsilon^3\Theta_3 + \epsilon^4\Theta_4 + \epsilon^5\Theta_5 + \epsilon^6\Theta_6, \quad (15)$$

where

$$\Theta_0 = \frac{\sin\xi}{\xi}, \quad (16)$$

$$\Theta_3 = \frac{5}{p}j_2(\xi)P_2(\sin\theta\cos\varphi), \quad (17)$$

$$\Theta_4 = -\frac{7\xi_1}{3p}j_3(\xi)P_3(\sin\theta\cos\varphi), \quad (18)$$

$$\Theta_5 = \frac{9\xi_1^2}{(15-\xi_1^2)p}j_1(\xi)P_1(\sin\theta\cos\varphi), \quad (19)$$

$$\Theta_6 = \frac{225}{7p^2\xi_1^2}j_2(\xi)P_2(\sin\theta\cos\varphi)$$

$$+{}^{(6)}\psi_{22}(\xi)P_2^2(\cos\theta)\cos 2\varphi + \frac{405}{7(15-\xi_1^2)p^2}j_4(\xi)P_4(\sin\theta\cos\varphi) - \frac{11\xi_1^3}{(105-10\xi_1^2)p}j_5(\xi)P_5(\sin\theta\cos\varphi). \quad (20)$$

Here j_l and P_l^m denote the spherical Bessel function and the associated Legendre function. The function ${}^{(6)}\psi_{22}$ is obtained by solving a differential equation:

$$\Big[\frac{1}{\xi^2}\frac{d}{d\xi}\Big(\xi^2\frac{d}{d\xi}\Big) - \frac{6}{\xi^2} + 1\Big]{}^{(6)}\psi_{22}(\xi) = \frac{2(1+p)}{p\xi_1}\Big[\frac{1}{\xi^2}\frac{d}{d\xi}\Big(\xi^2\frac{d}{d\xi}\Big) - \frac{6}{\xi^2}\Big]{}^{(4)}\phi_2(\xi), \quad (21)$$

where ${}^{(4)}\phi_2(\xi)$ will be defined later. We point out that the terms Θ_1 and Θ_2 disappear in Eq. (15) since there are no tidal terms to produce Θ_1 and Θ_2 in the gravitational potential.

We can write the velocity potential as

$$\tilde{\Phi} = \tilde{\Phi}_0 + \epsilon^4\tilde{\Phi}_4 + \epsilon^5\tilde{\Phi}_5 + \epsilon^6\tilde{\Phi}_6, \quad (22)$$

where

$$\tilde{\Phi}_0 = \frac{1}{1+p}\xi\sin\theta\sin\varphi, \quad (23)$$

$$\tilde{\Phi}_4 = {}^{(4)}\phi_2(\xi)P_2^2(\cos\theta)\sin 2\varphi, \quad (24)$$

$$\tilde{\Phi}_5 = {}^{(5)}\phi_3(\xi)\Big[P_3^1(\cos\theta)\sin\varphi - \frac{1}{2}P_3^3(\cos\theta)\sin 3\varphi\Big], \quad (25)$$

$$\tilde{\Phi}_6 = {}^{(6)}\phi_4(\xi)\Big[P_4^2(\cos\theta)\sin 2\varphi - \frac{1}{4}P_4^4(\cos\theta)\sin 4\varphi\Big]. \quad (26)$$

The functions ${}^{(4)}\phi_2$, ${}^{(5)}\phi_3$ and ${}^{(6)}\phi_4$ are determined by solving following differential equations:

$$\Big[\frac{d^2}{d\xi^2} + \Big(\frac{2}{\xi} + \frac{\Theta_0'}{\Theta_0}\Big)\frac{d}{d\xi} - \frac{6}{\xi^2}\Big]{}^{(4)}\phi_2 = -\frac{5j_2(\xi)}{2p\xi_1\Theta_0(\xi)}, \quad (27)$$

$$\Big[\frac{d^2}{d\xi^2} + \Big(\frac{2}{\xi} + \frac{\Theta_0'}{\Theta_0}\Big)\frac{d}{d\xi} - \frac{12}{\xi^2}\Big]{}^{(5)}\phi_3 = -\frac{7j_3(\xi)}{12p\Theta_0(\xi)}, \quad (28)$$

$$\Big[\frac{d^2}{d\xi^2} + \Big(\frac{2}{\xi} + \frac{\Theta_0'}{\Theta_0}\Big)\frac{d}{d\xi} - \frac{20}{\xi^2}\Big]{}^{(6)}\phi_4 = \frac{3\xi_1 j_4(\xi)}{4(15-\xi_1^2)p\Theta_0(\xi)}, \quad (29)$$

where Θ_0' denotes $d\Theta_0/d\xi$. Note that the terms $\tilde{\Phi}_1$, $\tilde{\Phi}_2$ and $\tilde{\Phi}_3$ disappear in Eq. (22). In Table I, we show the results of the velocity potentials. From the expressions of $\tilde{\Phi}_4$, $\tilde{\Phi}_5$ and $\tilde{\Phi}_6$, it is clear that the velocity has non-zero components along the orbital axis. Because since ${}^{(4)}\phi_2$ is not proportional to ξ^2, there remains the velocity component $\partial\tilde{\Phi}_4/\partial\tilde{x}_3$ where $\tilde{x}_3 = \xi\cos\theta$[†]. We can also show the existence of the velocity components along the orbital axis for $\tilde{\Phi}_5$ and $\tilde{\Phi}_6$. This analytic result does not agree with the semi-analytic solution given by Lai, Rasio and Shapiro [7] but qualitatively agrees with the numerical solutions given by Uryū and Eriguchi [6].

The orbital angular velocity is calculated as

$$\Omega^2 = \frac{M_{tot}}{a_0^3}\epsilon^3\Big[1 + \frac{9\epsilon^5}{2a_0^2}\Big(\frac{\bar{I}_{11}}{M_1} + \frac{\bar{I}_{11}'}{M_2}\Big) + O(\epsilon^7)\Big], \quad (30)$$

where $\bar{I}_{11} \equiv I_{11}/\epsilon^3$. The effect of the quadrupole moments in Ω^2 is $O(\epsilon^8)$. One can see from Eq. (5) that the quadrupole term is $O(\epsilon^5)$ higher than the monopole term since I_{11} is $O(\epsilon^3)$. In the case of a different mass binary stars, i.e., a neutron star-black hole binary, we can express the orbital angular velocity as

$$\Omega^2 = \frac{M_{tot}}{a_0^3}\epsilon^3\Big(1 + \frac{9\epsilon^5}{2a_0^2}\frac{\bar{I}_{11}}{M_1}\Big), \quad (31)$$

where we assume that a black hole is a point source.

Now it is ready to calculate relevant physical quantities. The mass of star 1 is calculated as

$$M_1 = \int_1 d^3x\rho = 4\pi\rho_c a^3\xi_1\Big(1 + \epsilon^6\frac{45}{2p^2\xi_1^2}\Big). \quad (32)$$

Since we consider the sequence for given baryon mass, the mass of star 1 should be the same one, which yields

$$\rho_c = \rho_{c0}\Big(1 - \frac{45}{2p^2\xi_1^2}\epsilon^6\Big), \quad (33)$$

where ρ_{c0} is the central density for $R = \infty$. We note that the central density of star 2 should be written by changing p into $1/p$ in Eq. (33). The equation (33) means that the central density of star 1 up to order ϵ^6 decreases from that of the spherical star as the separation decreases. Although we did not assume ellipsoidal figures like in Ref. [7], the result is essentially the same as that derived by Lai [12], since the calculation of the central density up to $O(\epsilon^6)$ includes only quadratic terms. In both calculations the central density of irrotational binary system decreases as R^{-6}. This dependence is different from that of corotating ones, i.e., R^{-3} [10].

Next, we calculate the total energy of the binary system, which is written as $E = \Pi_{tot} + (W_{self})_{tot} + (W_{int})_{tot} + T_{tot}$, where Π_{tot}, $(W_{self})_{tot}$, $(W_{int})_{tot}$ and T_{tot} denote the total internal energy, the total self-gravity energy, the total interaction energy and the total kinetic energy, respectively. They are given as

$$\Pi_{tot} = \frac{M_1M_2}{4a_0}\Big(p + \frac{1}{p}\Big) - \epsilon^6\frac{5M_1M_2}{4a_0}\Big(\frac{15}{\xi_1^2} - 1\Big)\Big(p + \frac{1}{p}\Big), \quad (34)$$

$$(W_{self})_{tot} = -\frac{3M_1M_2}{4a_0}\Big(p + \frac{1}{p}\Big)$$

[†]In the case of $n = 0$, ${}^{(4)}\phi_2$ is proportional to ξ^2.

$$+\epsilon^6 \frac{7M_1M_2}{4a_0}\Big(\frac{15}{\xi_1^2}-1\Big)\Big(p+\frac{1}{p}\Big), \tag{35}$$

$$(W_{int})_{tot} = -\frac{M_1M_2}{a_0}\epsilon - \epsilon^6 \frac{3M_1M_2}{2a_0^3}\Big(\frac{\bar{I}_{11}}{M_1}+\frac{\bar{I}'_{11}}{M_2}\Big), \tag{36}$$

$$T_{tot} = \frac{M_1M_2}{2a_0}\epsilon + \epsilon^6 \frac{9M_1M_2}{4a_0^3}\Big(\frac{\bar{I}_{11}}{M_1}+\frac{\bar{I}'_{11}}{M_2}\Big), \tag{37}$$

where the reduced quadrupole moment of star 1 is calculated as $\bar{I}_{11} = (2M_1a_0^2/3p)(15/\xi_1^2 - 1)$. The reduced quadrupole moment of star 2 is expressed by changing M_1 into M_2 and p into $1/p$. We note that the above energies satisfy the virial equation for $n = 1$; i.e. $3\Pi_{tot} + (W_{self})_{tot} + (W_{int})_{tot} + 2T_{tot} = 0$. Accordingly, the normalized total energy is given as

$$E = \frac{M_1M_2}{a_0}\Big[-\frac{1}{2}\Big(p+\frac{1}{p}\Big) - \frac{\epsilon}{2} + \Big(\frac{15}{\xi_1^2}-1\Big)\Big(p+\frac{1}{p}\Big)\epsilon^6\Big]. \tag{38}$$

In the case of a different mass binary stars, we obtain the total energy as

$$E = \frac{M_1^2}{a_0}\Big[-\frac{1}{2} - \frac{\epsilon}{2p} + \frac{\epsilon^6}{p^2}\Big(\frac{15}{\xi_1^2}-1\Big)\Big]. \tag{39}$$

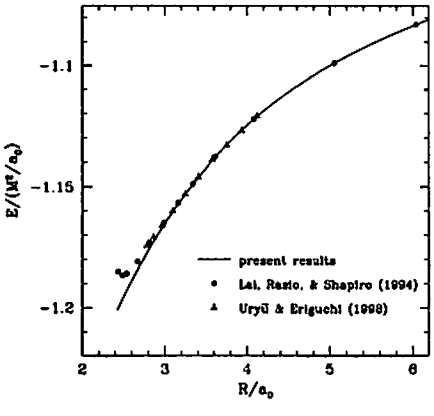

FIG. 1. The total energy as functions of the orbital separation for an identical star binary ($M_1 = M_2 = M$). Solid line denotes our result. Filled circles and open triangles are the results of Lai, Rasio, and Shapiro (1994) and Uryū and Eriguchi (1998).

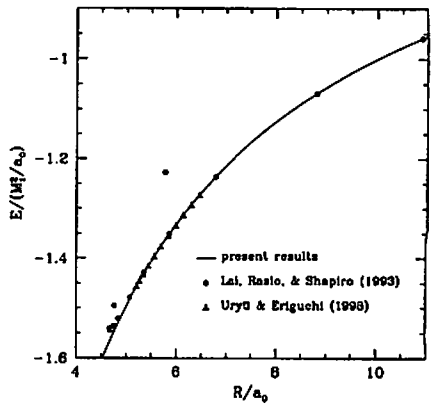

FIG. 2. The total energy as functions of the orbital separation for a different mass binary ($M_1/M_2 = 0.1$). Solid line and open triangles are the same notations in Fig. 1. Filled circles are the results of Lai, Rasio, and Shapiro (1993).

Our solution is correct if $\epsilon \ll 1$ so that it can be used to check the validity of numerical solutions. For any numerical codes, one can ask to solve an equilibrium for large R. One can compare numerically derived density and velocity distribution with our almost analytic solutions. For example, if a numerical solution has zero velocity component along the orbital axis, that is not correct.

For small R, our expansion up to ϵ^6 may not be enough. Nevertheless let us apply our present solution in this case. Consider an identical star binary ($p = 1$). Then the turning point of the total energy becomes $R = 1.657a_0$ in our solution up to order ϵ^6. This means that the turning point, i.e., the dynamical instability point, never appears before contact in the case of $n = 1$ and $p = 1$ since the contact condition becomes $R = 2a_1 = 2.426a_0$ taking into account the deformation. This agrees with the result of Uryū and Eriguchi [6] but not with Lai, Rasio, and Shapiro [7]. However, for the final conclusion, further higher order calculations in our scheme as well as the check of numerical codes using our almost analytic solutions for large R are urgently necessary.

One of the main results of this Letter are the simple equations of the total energy equation (38) and the orbital angular velocity (30).

In Figs. 1 and 2, we show the total energy for binary systems with $p = 1$ and $p = 0.1$ as functions of the orbital separation for an identical star binary. We find from these figures that the results of numerical and semi-analytic calculations coincide with our analytic solutions up to ϵ^6 rather well in the region $R/a_0 > 3$ for $p = 1$ and $R/a_0 > 5$ for $p = 0.1$ although they are quite different in details.

TABLE I. Velocity potentials

ξ	${}^{(4)}\phi_2$	$\partial_\xi {}^{(4)}\phi_2$	${}^{(5)}\phi_3$	$\partial_\xi {}^{(5)}\phi_3$	${}^{(6)}\phi_4$	$\partial_\xi {}^{(6)}\phi_4$
0.0	0.00	0.00	0.00	0.00	0.00	0.00
0.5	2.46(-2)	9.86(-2)	9.64(-4)	5.80(-3)	-3.40(-5)	-2.73(-4)
1.0	9.91(-2)	0.200	7.80(-3)	2.36(-2)	-5.52(-4)	-2.23(-3)
1.5	0.226	0.307	2.68(-2)	5.50(-2)	-2.87(-3)	-7.83(-3)
2.0	0.408	0.424	6.55(-2)	0.103	-9.40(-3)	-1.96(-2)
2.5	0.652	0.556	0.133	0.171	-2.41(-2)	-4.13(-2)
3.0	0.967	0.710	0.241	0.269	-5.33(-2)	-7.87(-2)
ξ_1	1.07	0.760	0.282	0.303	-6.55(-2)	-9.34(-2)

We would like to thank K. Ioka and K. Nakao for useful discussions. This work was partly supported by a Grant-in-Aid for Scientific Research Fellowship (No.9402; KT) and Grant-in-Aid of Scientific Research (No.09640351; TN) of the Japanese Ministry of Education, Science, Sports and Culture.

[1] K. S. Thorne, in Relativistic Cosmology, Proc. of the 8th Nishinomiya-Yukawa Memorial Symposium, ed. M. Sasaki (Tokyo Universal Academy), p.67 (1994).
[2] L. Lindblom, Astrophys. J. 398, 569 (1992).
[3] S. Bonazzola, E. Gourgoulhon, and J.-A. Marck, Phys. Rev. Lett. 82, 892 (1999).
[4] C. S. Kochanek, Astrophys. J. 398, 234 (1992).
[5] L. Bildsten and C. Cutler, Astrophys. J. 400, 175 (1992).
[6] K. Uryū and Y. Eriguchi, Astrophys. J. Suppl. Ser. 118, 563 (1998).
[7] D. Lai, F. A. Rasio, and S. L. Shapiro, Astrophys. J. 420, 811 (1994).
[8] J. C. Lombardi, F. A. Rasio, and S. L. Shapiro, Phys. Rev. D56, 3416 (1997).
[9] P. Marronetti, G. J. Mathews, and J. R. Wilson, Phys. Rev. D60, 087301 (1999).
[10] S. Chandrasekhar, Mon. Not. R. Astron. Soc. 93, 390 (1933); A. Kovetz, Astrphys. J. 154, 999 (1968).
[11] D. Lai, F. A. Rasio, and S. L. Shapiro, Astrophys. J. Suppl. Ser. 88, 205 (1993).
[12] D. Lai, Phys. Rev. Lett. 76, 4878 (1996).

General Relativistic Simulations of Jet Formation in a Rapidly Rotating Black Hole Magnetosphere

Shinji Koide[1]

Faculty of Engineering, Toyama University, Gofuku 3190, Toyama 930-8555, Japan

David L. Meier[2]

Jet Propulsion Laboratory, 4800 Oak Grove Dr. Pasadena, CA 91109, USA

Kazunari Shibata[3]

Kwasan and Hida Observatories, Kyoto University, Yamashina, Kyoto, 607-8471, Japan

Takahiro Kudoh[4]

National Astronomical Observatory, Mitaka, Tokyo 181-8588, Japan

Abstract

Recent observations of Galactic Black Hole Candidates (BHCs) suggest that superluminal jet sources have more rapid black hole spin rates than other normal BHCs. This provides observational support for models of relativistic jet formation that extract rotational energy of the central black hole. To investigate the formation mechanism of relativistic jets in active galactic nuclei and micro-quasars, we have developed a new general relativistic magnetohydrodynamic code in Kerr geometry. Here we report on the first numerical simulation of jet formation in a rapidly-rotating ($a = 0.95$) Kerr black hole magnetosphere. We study cases in which the Keplerian accretion disk in both co-rotating and counter-rotating with respect to the black hole rotation. In the co-rotating disk case, our results are almost the same as those in Schwarzschild black hole cases: a gas pressure-driven jet is formed by a shock in the disk, and a weaker magnetically-driven jet is also generated outside the gas pressure-driven jet. On the other hand, in the counter-rotating disk case, a new powerful magnetically-driven jet is formed inside the gas pressure-driven jet. The newly found magnetically-driven jet in the latter case is accelerated by a strong magnetic field created by frame dragging in the ergosphere. Through this process, the magnetic field extracts the energy of the black hole rotation.

1 Introduction

Radio jets ejected from radio loud active galactic nuclei (AGNs) sometimes show proper motion with apparent velocity exceeding the speed of light c [1, 2]. The widely-accepted explanation for this phenomenon, called superluminal motion, is relativistic jet flow in a direction along the observer's line-of-sight with a Lorentz factor greater than 2 [3]. Such relativistic motion is thought to originate from a region very close to the putative supermassive black hole which is thought to power each AGN [4, 5]. On the other hand, the great majority of AGNs are radio quiet and do not produce powerful relativistic radio jets [5]. These two classes of active objects (radio loud and quiet) are also found in the black hole candidates (BHCs)

[1]E-mail: koidesin@ecs.toyama-u.ac.jp
[2]E-mail: dlm@senjou.isaslan1.isas.ac.jp
[3]E-mail: shibata@kwasan.kyoto-u.ac.jp
[4]E-mail: kudo@solar.mtk.nao.ac.jp

in our own Galaxy. Objects with superluminal jets, such as GRS 1915+105 and GRO J1655-40, belong to the radio loud class [6, 7]. Other objects such as Cyg X-1 and GS 1124-68 are relatively radio quiet and produce little or no jet.

What causes the difference between the two classes? Recent observations of the BHCs in our Galaxy suggest that the Galactic superluminal sources contain very rapidly rotating black holes (normalized angular momentum, $a \equiv J/[GM_{\rm BH}^2/c] = 0.9 - 0.95$, where G and $M_{\rm BH}$ are the gravitational constant and black hole mass, respectively), while the black holes in Cyg X-1 and GS 1124-68 are spinning much less rapidly ($a = 0.3 - 0.5$) [8]. A similar rapidly rotating black hole is also suggested in the AGN of the Seyfert 1 galaxy MCG-6-30-15 by the X-ray satellite ASCA [9]. According to (nonrelativistic) studies of magnetically-driven jets from accretion disks [10, 11, 12, 13], the terminal velocity of the formed jet is comparable to the rotational velocity of the disk at the foot of the jet. Further nonrelativistic simulations of jet formation confirm these results [14, 15], except for the extremely large magnetic field/high jet-power case [16, 17] in which very fast jets can be produced. The rotation velocity at the innermost stable orbit of the Schwarzschild black hole ($r = 3r_S$) is $0.5c$, where $r_S = 2GM_{\rm BH}/c^2$ is the Schwarzschild radius. In addition, it appears that the poloidal magnetic field strength in disks around non-rotating black holes may be not extremely strong if the magnetic field energy density is comparable with that of the radiation [18, 5]. Therefore, a jet produced by MHD acceleration from an accretion disk around a non-rotating black hole should be sub-relativistic and very weak. In fact, numerical simulations of jet formation in a Schwarzschild metric show only sub-relativistic jet flow [19], except for the case when the initial black hole corona is in hydrostatic equilibrium rather than free fall [20].

Several mechanisms for relativistic jet formation from rotating black holes have been proposed [21, 22]. However, up until now no one has performed a self-consistent numerical simulation of the dynamic process of jet formation in a rotating black hole magnetosphere. To this end, we have developed a Kerr general relativistic magnetohydrodynamic (KGRMHD) code. In this paper we report briefly on what we believe are some of the first calculations of their kind — simulation of jet formation in a rotating black hole magnetosphere.

2 Numerical Method

We use a $3 + 1$ formalism of the general relativistic conservation laws of particle number, momentum, and energy and Maxwell equations with infinite electric conductivity [23]. The Kerr metric, which describes the spacetime around a rotating black hole, is used in the calculation. When we use Boyer-Lindquist coordinates, $x^0 = ct$, $x^1 = r$, $x^2 = \theta$, and $x^3 = \phi$, the Kerr metric $g_{\mu\nu}$ is written as follows,

$$ds^2 = g_{\mu\nu}dx^\mu dx^\nu = -h_0^2(cdt)^2 + \sum_{i=1}^{3} h_i^2(dx^i)^2 - 2h_3\Omega_3 cdtdx^3. \qquad (1)$$

By modifying the lapse function in our Schwarzschild black hole code ($\alpha = \sqrt{1 - r_S/r}$) to be $\alpha = \sqrt{h_0^2 + \Omega_3^2}$, and adding some terms of Ω_3 to the time evolution equations, we were able to develop a KGRMHD code relatively easily. (See Appendix C in [19] for more details on this procedure and the meaning of symbols used.)

We use the Zero Angular Momentum Observer (ZAMO) system for the 3-vector quantities, such as velocity $\mathbf{v}$, magnetic field $\mathbf{B}$, and so on. For scalars, we use the frame comoving with the fluid flow. The simulation is performed in the region $0.75r_S \le r \le 20r_S$, $0 \le \theta \le \pi/2$ with 210×70 mesh points, assuming axisymmetry with respect to the z-axis and mirror symmetry with respect to the plane $z = 0$. A free boundary condition is employed at $r = 0.75r_S$ and $r = 20r_S$. In the simulations, we use simplified tortoise coordinates, $x = \log(r/r_H - 1)$, where r_H is the radius of the black hole horizon. To avoid numerical oscillations, we use a simplified TVD method [24, 25, 26, 19]. We checked the KGRMHD code by computing Kepler motion around a rotating black hole and comparing with analytic results [27].

3 Results

The simulations were performed for two cases in which the disk co-rotates and counter-rotates with respect to the black hole rotation. Figures 1a-c illustrate the time evolution of the counter-rotating disk case and Fig. 1d the final state of the co-rotating case. These figures show the rest mass density (gray-scale), velocity (vectors), and magnetic field (solid lines) in $0 \leq R \equiv r\sin\theta \leq 7r_S$, $0 \leq z \equiv r\cos\theta \leq 7r_S$. The black region at the origin shows the inside of the black hole horizon. The angular momentum parameter of the black hole is $a = 0.95$ and the radius is $r_H = 0.656r_S$. The initial state in the simulation consists of a hot corona and a cold accretion disk around the black hole (Fig. 1a). In the corona, plasma is assumed to be in nearly stationary infall, with the specific enthalpy $h/\rho c^2 = 1 + \Gamma p/[(\Gamma - 1)\rho c^2] = 1.3$, where ρ is the rest mass density, p is the pressure, and Γ is specific heat ratio and set $\Gamma = 5/3$. Far from the hole, it becomes the stationary transonic solution exactly. The accretion disk is located at $|\cot\theta| \leq 0.125$, $r \geq r_D = 3r_S$ and the initial velocity of the disk is assumed to be the velocity of a circular orbit around the Kerr black hole. The co-rotating disk is stable, but the counter-rotating disk is unstable in the region $R \leq 4.4r_S$. Except for the disk rotation direction, we use the same initial conditions in both cases. The mass density of the disk is 100 times that of the corona at the inner edge of the disk. The mass density profile is given by that of a hydrostatic equilibrium corona with a scale height of $r_c \sim 3r_S$. The disk is in pressure balance with the corona, and the magnetic field lines are perpendicular to the accretion disk. We use the azimuthal component of the vector potential A_ϕ of the Wald solution to set the magnetic field, which provides a uniform magnetic field far from the Kerr black hole [28]. Here the magnetic field strength far from the black hole is $0.3\sqrt{\rho_0 c^2}$, where ρ_0 is the initial corona density at $r = 3r_S$. However, we do not use the time component of the vector potential A_t from Wald solution; instead, we use the ideal MHD condition $\mathbf{E} + \mathbf{v} \times \mathbf{B} = \mathbf{0}$ to determine the electric field $\mathbf{E}$. Here the Alfvén velocity and plasma beta value at the disk ($r = 3.5r_S$) are $v_A = 0.03c$ and $\beta \sim 3.4$, respectively.

Figure 1b shows the state at $t = 30\tau_S$, where τ_S is defined as $\tau_S \equiv r_S/c$. By this time the inner edge of the disk has rotated 0.75 cycles, *if* we assume the edge is at $R = 3r_S$.[5] Actually, the edge falls toward the black hole and rotates faster at $R = 2r_S$. The rapid infall produces a shock at $R = 3.1r_S$, and the high pressure behind it begins to produce the jet. This is the same pressure-driven jet formation process seen previously in the Schwarzschild case [19].

Figure 1c shows the final state of the counter-rotating disk case at $t = 47\tau_S$ when the inner edge of the disk rotated 1.2 cycles. The accretion disk continues to fall rapidly toward the black hole, with the disk plasma entering the ergosphere and then crossing the horizon, as shown by the crowded magnetic field lines near $r = 0.75r_S$. The magnetic field lines become radial due to dragging by the disk infall near the black hole. The jet is ejected almost along the magnetic field lines. Its maximum total and poloidal velocities are the same, $v = v_p = 0.44c$ at $R = 3.2r_S$, $z = 1.6r_S$. The mass density plot (gray-scale) shows that the jet consists of two layers. One is an inner, low density, fast, magnetically-driven jet and the other is an outer, high density, slow, gas pressure-driven jet. The latter comes from the disk near the shock at $R = 3.1r_S$ and is, therefore, similar to the gas pressure-driven jet of the Schwarzschild black hole case [20]. The former is new and has never been seen in the Schwarzschild black hole case. It comes from the disk near the ergosphere, and is accelerated as follows. As there is no stable orbit at $R \leq 4.4r_S$, the disk falls rapidly into the ergosphere. Inside the static limit , the velocity of frame dragging exceeds the speed of light ($c\Omega_3/\alpha > c$), causing the disk to rotate in the *same* direction of the black hole rotation (relative to the fixed Boyer-Lindquist frame), even though it was initially counter-rotating. The rapid, differential frame dragging greatly enhances the azimuthal magnetic field, which then accelerates the flow upward and pinches it into a powerful collimated jet.

Figure 1d shows a snapshot of the co-rotating disk case at $t = 47\tau_S$. The disk stops its infall near $R = 3r_S$ due to the centrifugal barrier with a shock at $r = 3.4r_S$. The high pressure behind the shock causes a gas pressure-driven jet with total and poloidal velocities of $v = v_p = 0.30c$ at $R = 3.4r_S$, $z = 2.4r_S$. A detailed analysis shows that a weak magnetically-driven jet is formed outside the gas pressure-driven jet with maximum total and poloidal velocities of $v = 0.42c$ and $v_p = 0.13c$, respectively. This two-layered shell structure is similar to that of Schwarzschild black hole case [20]. The centrifugal barrier makes the disk take much long time to reach the ergosphere, which causes the difference between

[5] To calculate inner disk rotation cycles, in this paper we always will assume that the inner edge is located at $R = 3r_S$, regardless of how far inward the edge actually has accreted.

the co-rotating and counter-rotating disk cases.

To more fully illustrate the physics of the jet formation mechanism, in figure 2 we show the plasma beta, $\beta \equiv p/(B^2/2)$ (gray-scale) and the toroidal component of the magnetic field, B_ϕ (contour) in the counter-rotating and co-rotating disk cases at $t = 47\tau_S$. The light-gray shows the region where magnetic field dominates the gas pressure; light dark-gray shows where gas pressure is dominant; and solid contour line shows negative azimuthal magnetic field ($B_\phi < 0$), while the broken line the positive value ($B_\phi > 0$). The toroidal component of the magnetic field B_ϕ is negative and its absolute value is very large above the black hole in both cases. The field increases to more than 10 times the initial magnetic field. This amplification is caused by the shear of the plasma flow in the Boyer-Lindquist frame due to the frame dragging effect of the rotating black hole [29, 30, 17]. Under the simplifying assumption that the plasma is at rest in the ZAMO frame, the general relativistic Faraday law of induction and ideal MHD condition yield,

$$\frac{\partial B_\phi}{\partial t} = f_1 B_r + f_2 B_\theta, \tag{2}$$

where $f_1 = c(h_3/h_1)\partial(\Omega_3/h_3)/\partial r$, and $f_2 = c(h_3/h_2)\partial(\Omega_3/h_3)/\partial\theta$. This expression is almost identical to that of ω-dynamo effect from the field of the terrestrial magnetism. Noted that f_2 is one order smaller than f_1 when $a \sim 1$.

Where does the magnetic field amplification energy comes from? It does not come from the gravitational energy or thermal energy of the disk, because frame dragging effect occurs even when the plasmas of the disk and corona are rest and cool. The only other possible energy source is the rotation of the black hole itself. Indeed, the increase in the azimuthal magnetic field component (eq. (2)) depends on the shear of the rotational variable Ω_3. We conclude that the amplification energy of the magnetic field is supplied by extraction of the rotational energy of the black hole.

The distribution of the plasma beta (β) and the azimuthal component of the magnetic field (B_ϕ) of the counter-rotating and co-rotating disk cases are quite different. In the co-rotating disk case, they are similar to those of the Schwarzschild black hole case. In the counter-rotating disk case, the outer part has a positive azimuthal component of the magnetic field ($B_\phi > 0$), which is caused by the counter-rotating disk, and the outer part has the high plasma beta. The inner part has a negative azimuthal magnetic field ($B_\phi < 0$) and low plasma beta. Note that the very high plasma beta region around $R = 2.5r_S$, $z = 2.5r_S$ is outside of the jet; at this point it has almost stopped and eventually will fall into the black hole. The negative azimuthal magnetic field is caused by the disk around the ergosphere, where the disk rotates in the same direction as the black hole in the Boyer-Lindquist frame.

To confirm the jet acceleration mechanism, we estimate the power from the electromagnetic field, $W_{EM} = \mathbf{v} \cdot (\mathbf{E} + \mathbf{J} \times \mathbf{B})$ and the gas pressure, $W_{gp} = -\mathbf{v} \cdot \nabla p$ along the line, $z = 1.1r_S$ which crosses the jet foot (Fig. 3). At $t = 47\tau_S$, the gas pressure is dominant in the co-rotating disk case (Fig. 3b). However, in the counter-rotating disk case, the electromagnetic power is dominant near the black hole even through the gas pressure power is the same as that of the co-rotating disk case (Fig. 3a). The magnetically-driven jet in this latter case is accelerated by the magnetic field anchored to the ergospheric disk. The frame dragging effect rapidly rotates the disk in the same direction as the black hole rotation, increasing the azimuthal component of the magnetic field and the magnetic tension which, in turn, accelerates the plasma by the magnetic pressure and centrifugal force, respectively. (A detailed analysis shows that both component of the magnetic forces are comparable.) This mechanism of jet production, therefore, is a kind of Penrose process that uses the magnetic field to extract rotational energy of the black hole and eject a collimated outflow from very near the horizon.

4 Discussion

We have presented general relativistic simulations of jet formation from both counter-rotating and co-rotating disks in a Kerr black hole magnetosphere. We have found that jets are formed in both cases. At the time when the simulations were stopped ($t = 47\tau_S$ ($53\tau_S$), after the inner edge of the disk had rotated 1.2 (1.4) cycles in the counter-rotating (co-rotating) disk case) the poloidal velocities of the jets were $v \sim 0.4c$ (counter-rotating), $\sim 0.3c$ (co-rotating), both sub-relativistic. In the co-rotating disk case, the jet has a two-layered structure: inner, gas pressure-driven jet and outer, magnetically-driven jet. On the other hand, in the counter-rotating case, a new magnetically-driven jet has been found inside the

gas pressure-driven jet. The new jet is accelerated by the magnetic field induced by the frame dragging effect in the ergosphere. In this case, existence of a magnetically-driven jet is not clear outside the gas pressure-driven jet. A longer term simulation may show a three-layered structure including the outer, magnetically-driven jet.

Unfortunately, the counter-rotating (co-rotating) disk case could not be continued beyond $t = 47\tau_S$ ($t = 53\tau_S$) because of numerical problems. We have performed one other case previously — the infall of a magnetized non-rotating disk into a rapidly-rotating black hole [31]. The disk falls toward the black hole more rapidly than the counter-rotating case. At later times (after almost two inner disk turns) it developed a *relativistic* jet with a velocity of $v \sim 0.9c$ (Lorentz factor ~ 2). We believe that, if we had been able to perform longer-term simulations here, in at least the counter-rotating disk case the magnetically-driven jet also would have been accelerated to relativistic velocities (and possibly the co-rotating case as well). Despite its low speed, the magnetically-driven jet in the counter-rotating disk case is nevertheless noteworthy because it extracts rotational energy from the black hole. While the process is similar to the Blandford-Znajek mechanism [21], it appears more closely related to the model of Takahashi *et al.* [22]. In our case, the electromagnetic field energy is transformed immediately into kinetic energy in the jet. A more detailed analysis and further calculations will be reported in our next paper.

Recently, Wardle *et al.* [32] detected circularly polarized radio emission from the jets of the archetypal quasar 3C279. They concluded that electron-positron pairs are important components of the jet plasma. Similar detections in three other radio sources have been made [33], which suggests that, in general, extragalactic radio jets may be composed mainly of an electron-positron pair plasma. The electron-positron plasma is probably produced very near the black hole. The mechanism we have investigated here, magnetically-driven jet powered by extraction of rotational energy of a black hole, is a strong candidate for explaining the acceleration of such electron-positron jets.

S. K. thanks M. Inda-Koide for discussions and important comments for this study. We thank K.-I. Nishikawa, M. Takahashi, A. Tomimatsu, P. Hardee, and J.-I. Sakai for discussions and encouragement. We appreciate the support of the National Institute for Fusion Science and the National Astronomical Observatory in the use of their super-computers. Part of this research was carried out at the Jet Propulsion Laboratory, California Institute of Technology, under contract with the National Aeronautics and Space Administrations.

References

[1] Pearson, J. J. 1981, *et al.* Nature **290**, 365.

[2] Hughes, P. A. 1991, eds., *Beams and Jets in Astrophysics* (Cambridge University Press, New York).

[3] Rees, M. J. 1966, Nature **211**, 468.

[4] Linden-Bell, D. 1969, Nature **223**, 690.

[5] Rees, M. J. 1984, Ann. Rev. Astron. Ap. **22**, 471.

[6] Mirabel, I. F. & Rodriguez, L. F. 1994, Nature **371**, 46.

[7] Tingay, S. J. 1995, *et al.* Nature **374**, 141.

[8] Cui, W., Zhang, S. N., & Chen, W. 1998, ApJ **484**, 383.

[9] Iwasawa, K., Fabian, A. C., Reynolds, C. S., Nandra, K., Otani, C. Inoue, H. Hayashida, K. Brandt, W. N., Dotani, T., Kunieda, H., Matsuoka, M., Tanaka, Y. 1996, MNRAS, **282**, 1038.

[10] Uchida, Y. & Shibata, K. 1985, PASJ **37**, 515.

[11] Shibata, K. & Uchida, Y. 1986, PASJ **38**, 631.

[12] Kudoh, T. & Shibata, K. 1995, ApJ **452**, L41.

[13] Kudoh, T. & Shibata, K. 1997, ApJ **474**, 362.

[14] Kudoh, T. & Shibata, K. 1997, ApJ **476**, 632.

[15] Ouyed, R., Pudritz, R. E., & Stone, J. M. 1997, Nature **385**, 409.

[16] Meier, D. L., Edgington, S., Godon, P., Payne, D. G., & Lind, K. R. 1997, Nature **388**, 350.

[17] Meier, D. L. 1999, ApJ **522**, in press.

[18] Begelman, .M.C., Blandford, R.D., Rees, M.J. 1984, Review of Modern Physics, **56**, 255.

[19] Koide, S., Shibata, K., & Kudoh, T., 1999, ApJ **522**, 175.

[20] Koide, S., Shibata, K., & Kudoh, T. 1998, ApJ **495**, L63.

[21] Blandford, R. D. & Znajek, R. 1977, MNRAS **179**, 433.

[22] Takahashi, M., Nitta, S., Tatematsu, Y., & Tomimatsu, A. 1990, ApJ **363**, 206.

[23] Thorne, K. S., Price, R. H., & Macdonald, D. A. 1986, *Membrane Paradigm* (Yale University Press, New Haven and London).

[24] Davis, S. F. 1984, NASA Contractor Rep. 172373, ICASE Rep. No. 84-20.

[25] Koide, S., Nishikawa, K.-I., & Mutel, R. L. 1996, ApJ **463**, L71.

[26] Koide, S. 1997, ApJ **478**, 66.

[27] Shapiro, S. L. & Teukolsky, S. A. 1983, *Black Holes, White Dwarfs, and Neutron Stars*, (John Wiley & Sons Inc., New York)

[28] Wald, R. M. 1974, Phys. Rev. D **10**, 1680.

[29] Yokosawa, M., Ishizuka, T., & Yabuki, Y. 1991, PASJ **43**, 427.

[30] Yokosawa, M. 1993, PASJ **45**, 207.

[31] Koide, S., Meier, D. L., Shibata, K., & Kudoh, T. 2000, in Proc. 19th Texas Symp. on Relativistic Astrophysics, ed. E. Aubourg, T. Montmerle, & J. Paul (World Scientific Press, Paris) in press.

[32] Wardle, J. F. C., Homan, D. C., Ojha, R., & Roberts, D. H. 1998, Nature **395**, 457.

[33] Homan, D. C., Wardle, J. F. C., Roberts, D. H., and Ojha, R. 1999, preprint.

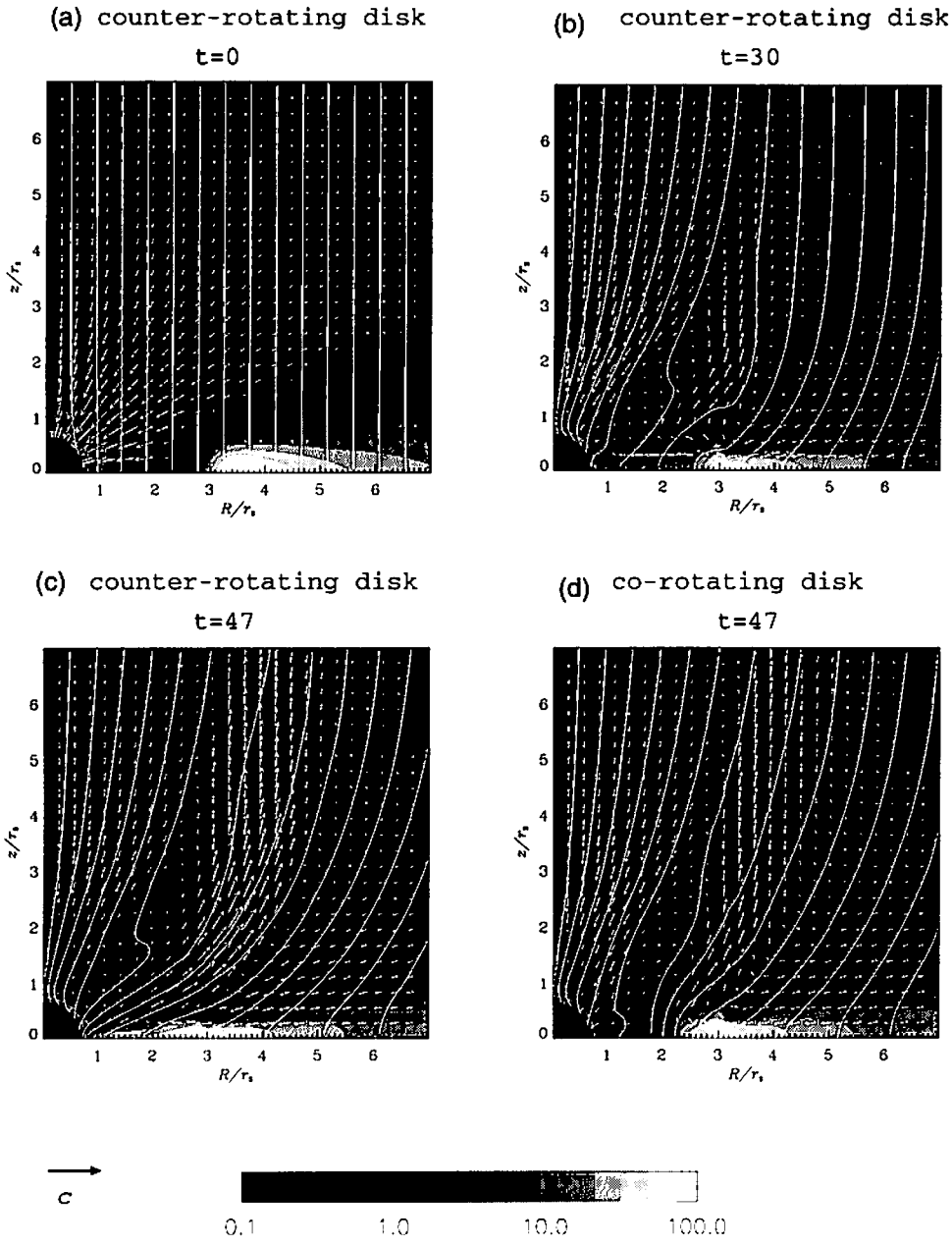

Fig. 1. Time evolution of jet formation in the counter-rotating disk case and the final state of the co-rotating disk case. Gray-scale shows the logarithm of the proper mass density; vectors indicate velocity; solid lines show the poloidal magnetic field. The black fan-shaped region at the origin shows the horizon of the Kerr black hole ($a = 0.95$). The dashed line near the horizon is the inner boundary of the calculation region. At $t = 0$ and $t = 30\tau_S$ the state of the co-rotating and counter-rotating disk cases are almost identical. However, at $t = 47\tau_S$, while the infall of the disk in the co-rotating disk stops (due to a centrifugal barrier), the unstable orbits of the counter-rotating disk plasma continue to spiral rapidly toward the black hole horizon. This difference causes the magnetohydrodynamic jet formation mechanisms in the two cases to differ drastically, resulting in a powerful jet emanating from deep within the ergosphere.

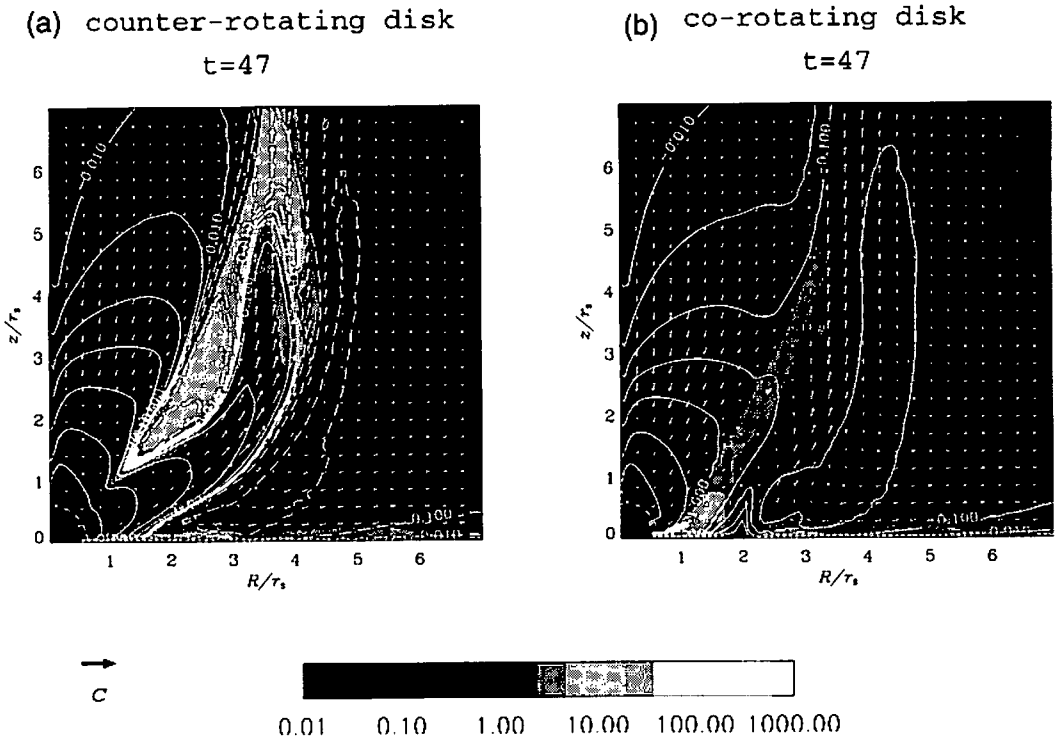

Fig. 2. Plasma beta (gray-scale) and azimuthal component of the magnetic field B_ϕ (contour) in the counter-rotating and co-rotating disk cases. Solid lines show negative value of B_ϕ and the dashed lines positive values. The two cases differ significantly in structure, with the jet in the counter-rotating case originating much closer to the black hole.

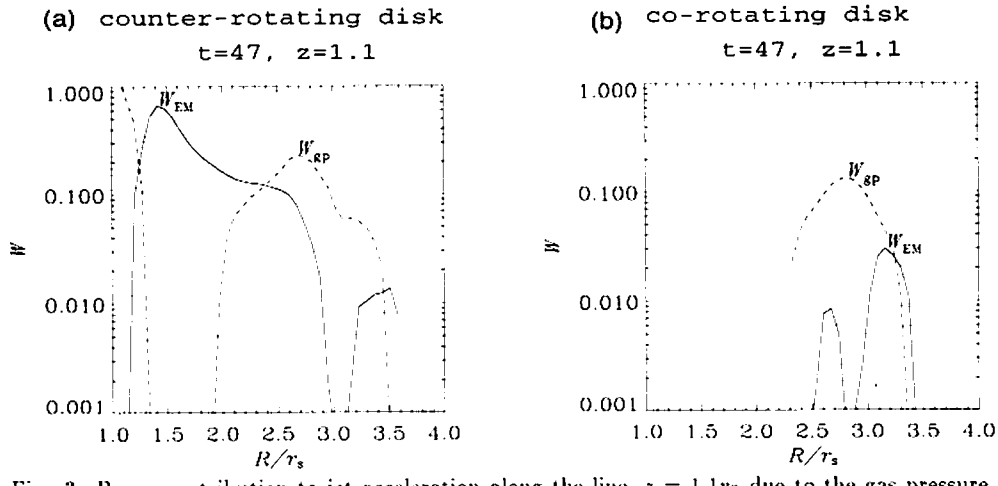

Fig. 3. Power contribution to jet acceleration along the line, $z = 1.1r_S$ due to the gas pressure (W_{GP}) and the electromagnetic force (W_{EM}) for both the counter-rotating and co-rotating disk cases. The jet in the counter-rotating disk case is accelerated mainly by electromagnetic forces, while that in the co-rotating disk is accelerated mainly by gas pressure. Note that, while the power in the gas jet component is comparable in the two cases, the power in the MHD jet component is nearly two orders of magnitude greater in the counter-rotating case than the co-rotating case.

Equation of motion for the relativistic compact binaries
— point particle limit approach —

Yousuke Itoh,[1] Toshifumi Futamase [2]

Astronomical Institute, Graduate School of Science, Tohoku University
Sendai 980-8578, Japan

Hideki Asada [3]

Faculty of Science and Technology, Hirosaki University,
Hirosaki 036-8561, Japan

Abstract

We study the equation of motion for the relativistic compact binaries in the post-Newtonian approximation. In order to take account of the strong internal gravity of the objects constituting the binary, we adopt the point particle limit and express the equation of motion in terms of surface intergrals. In our approach no singular term appears throughout all calculations, hence we need not resort to any regularization schemes. In addition, our approach naturally incorporate intrinsic mutipole moments of each object. Performing surface integrals carefully, We have derived the second and a half post-Newtonian (2.5 PN) equation of motion, the lowest order spin-orbit coupling force and the lowest order quadrupole-orbit coupling force.

1 Introduction

The problem of the motion of self gravitating systems have attracted much attention in general relativity. The gravitational detectors currently under construction (TAMA/LIGO/VIRGO/GEO) [1, 2, 3, 4] are going to realize the gravitational wave astronomy in the near future and this fact stimulate renewed interests in the problem of the motion for the binary consisting of compact objects, e.g. neutron stars and/or black holes. Actually a coalescing neutron stars binary system is expected to be one of the most promising sources of the gravitational waves.

In order to detect the extremely weak signals of the gravitational waves from the compact binaries, we need sufficiently accurate theoretical templates of the wave forms, and to obtain these templates we must know highly precise equations of motion for compact binaries[5, 6, 7, 8]. However, since Einstein equation is highly non-linear system as is well known, we must resort to some approximation schemes to describe a dynamical system such as a neutron star binary if we want to understand the dynamics of such a system as analytically as possible.

The inspiralling phase, where the evolution of the system can be roughly described by the Newtonian dynamics and the point particle limit is useful because the tidal effect is small, is a stage to which the post-Newtonian approximation, one of the most famous approximation schemes in general relativity, can be applied appropriately. Actually considerable efforts have been devoted to derive the equation of motion using the post-Newtonian approximation. Until now the 2.5 PN equation of motion is said to be standard [10, 11, 12, 13, 14] and the 3 PN equation of motion is now being tackled [15, 16]. The 3 PN and the higher order equation of motion is necessary for making accurate templates to detect the gravitational waves and the error estimate of the 2.5 PN equation of motion which contains the important effect, the radiation reaction effect.

However the previous derivations of the 2.5 PN equation of motion have some problems. To use mathematical regularization to make the point particle limit meaningful [9, 10, 11, 12, 14] or to resort to the strong equivalence principle [13, 17] are not conceivable enough.

[1] E-mail:yousuke@astr.tohoku.ac.jp
[2] E-mail:tof@astr.tohoku.ac.jp
[3] E-mail:asada@phys.hirosaki-u.ac.jp

Hence it is important to derive the equation of motion with another way, in which the strong internal gravity is explicitly taken into account and there is no need to use any mathematical regularization schemes though they are so elaborated, to confirm the 2.5 PN equation of motion. Also, it is important to derive the 3 PN and the higher order equation of motion using another way.

In this paper, in order to treat the strong self gravity, we take the point particle limit in which the size of the component object is reduced to a point keeping the strength of it's internal gravity[18, 19]. We apply the post-Newtonian approximation only to the gravitational field outside the bodies and their orbital motion. Hence we mean by the post-Newtonian approximation only the smallness of the ratio of the orbital velocity to the light velocity and the weakness of the gravitational field outside the compact objects, but not the weakness of the gravitational field inside them. This method has been used to derive the equation of motion only at the Newtonian order and the 2.5 PN order for compact binaries.

As stated above, one need to know higher post-Newtonian orders up to, say, the 4th post-Newtonian order to make sufficiently accurate predictions of the emitted waveform [20]. We wish to derive the equation of motion applicable to systems whose components, such as neutron stars, have strong internal gravity up to a sufficiently higher post-Newtonian orders using the point particle limit. In this paper we outline our approach to the derivation of the 2.5 PN equation of motion

Greek indices take from 0 to 3, and Latin indices from 1 to 3.

2 Formalism

2.1 The Strong Field Point Particle Limit

In the inspiralling phase, both the gravitational field outside the compact bodies forming the binary and their orbital velocities are small. Also there is a balance between the Newtonian gravitational force and the centrifugal force like $M/L \sim |dx^i/dt|^2$. Here $M, L, (t, x^i)$ is the mass of the compact body, separation between two bodies, and near zone coordinate, respectively.

It is convenient to introduce a post-Newtonian expansion parameter ϵ which represents the smallness of the orbital velocity, and Newtonian dynamical time $\tau = \epsilon t$ [21]. With τ we have $dx^i/dt = \epsilon dx^i/d\tau = O(\epsilon)$, hence M scales as ϵ^2 when we fix L.

In order to treat the strong internal gravity we introduce the point particle limit. Denoting a size of the body by R, we let R scale as ϵ^2 so that the internal gravity ($\sim M/R$) is of order unity. With this scaling, the density of the body is of order ϵ^{-4}.

From the scaling of R, we define the body zone B_A for each body ($A = 1, 2$) as $B_A = \{x^k | |\vec{x} - \vec{z}_A(\tau)| < \epsilon R_A\}$, here R_A is some length scale, $R_A << L$, and $\vec{z}_A(\tau)$ is the near zone coordinate representing each body. Also we define the body zone coordinate α^k_A

$$\vec{\alpha}_A = \epsilon^{-2}(\vec{x} - \vec{z}_A(\tau)), \tag{1}$$

so that in the body zone coordinate, the size of the body stays constant when we let ϵ go to zero. Hence it is useful to define physical quantities such as mass, spin with the body zone coordinate. Later, we derive the equation of motion for the objects by calculating surface integrals of the gravitational momentum flux through the body zone boundary to avoid the problem associated with the internal strong gravity. Since on the body zone boundary, ∂B_A, the gravitational filed caused by the mass A centered on the body zone B_A is small enough, we can calculate the gravitational momentum flux with the post-Newtonian expanded gravitational field.

In this paper we adopt the initial value approach as in [22, 19] and we choose two stationary uniformally rotating fluids with spatially compact support as the initial data for the matter. Also we choose zero initial data for the homogeneous solution of the Einstein equation for simplicity (see the discussion in [23]). Hence the time scale of the internal motion of the body is comparable with that of the orbital motion at least in the beginning of the evolution stage (i.e. near the initial hypersurface). All the violent internal motions are controlled to be caused by the tidal effect and gravitational waves and appear at the higher order than the $2.5PN$ order, the radiation reaction order.

Also, we assume that both objects rotate slowly, that is, the velocities of the spinning motion of the bodies scale as ϵ. We note that, with this scaling, the spin-orbit coupling force appears at the 2 PN order,

which is different from the usual result [12, 24, 25]. The initial data of the stress-energy tensor $T_A^{\mu\nu}$ of the body A is supposed to scale like

$$T_A^{\tau\tau} = \epsilon^2 T_A^{tt} \sim \epsilon^{-2}, \tag{2}$$

$$T_A^{\tau i} = \epsilon^{-1} T_A^{ti} \sim \epsilon^{-4}, \tag{3}$$

$$T_A^{ij} = \epsilon^{-4} T_A^{ij} \sim \epsilon^{-8}. \tag{4}$$

Note that as a slowly rotating fluid, the object is supported by the pressure. Also, note that the assumption that the densities of the fluids scale as ϵ^{-4} are applied to the components of $T_A^{\mu\nu}$ in the near zone coordinate, not in the body zone coordinate.

2.2 Basic Formulae : Field Equation and Equation of Motion

As discussed above, we need to know the metric on the body zone boundary where the metric deviates slightly from the flat metric. It is convenient to define the small deviation from the flat metric $\eta^{\mu\nu}$ as

$$\bar{h}^{\mu\nu} = \eta^{\mu\nu} - \sqrt{-g} g^{\mu\nu}, \tag{5}$$

where we denote the determinant of the metric $g_{\mu\nu}$ by g.

We choose the harmonic condition on the metric as $\bar{h}^{\mu\nu}{}_{,\nu} = 0$, where the comma denotes the partial derivative. Then, the Einstein's equation is rewritten as

$$\Box \bar{h}^{\mu\nu} = -16\pi \Lambda^{\mu\nu}, \tag{6}$$

where $\Box = \eta^{\mu\nu}\partial_\mu \partial_\nu$ is the flat wave operator and we defined

$$\Lambda^{\mu\nu} = \Theta^{\mu\nu} + \chi^{\mu\nu\alpha\beta}{}_{,\alpha\beta}, \tag{7}$$

$$\Theta^{\mu\nu} = (-g)(T^{\mu\nu} + t_{LL}^{\mu\nu}), \tag{8}$$

$$\chi^{\mu\nu\alpha\beta} = \frac{1}{16\pi}(\bar{h}^{\alpha\nu}\bar{h}^{\beta\mu} - \bar{h}^{\alpha\beta}\bar{h}^{\mu\nu}). \tag{9}$$

Here, $T^{\mu\nu}$ and $t_{LL}^{\mu\nu}$ denote the stress-energy tensor and the Landau-Lifshitz pseudotensor [26], respectively. The conservation law is expressed as

$$\Lambda^{\mu\nu}{}_{,\nu} = 0. \tag{10}$$

The reduced Einstein's equation is solved formally as

$$\bar{h}^{\mu\nu} = 4 \int_{C(\tau, x^k; \epsilon)} d^3y \frac{\Lambda_N^{\mu\nu}(\tau - \epsilon|\vec{x} - \vec{y}|, y^k; \epsilon)}{|\vec{x} - \vec{y}|}, \tag{11}$$

where $C(\tau, x^k; \epsilon)$ means the past light cone emanating from the event (τ, x^k). This equation must be solved iteratively to obtain an explicit form of the metric. The subscript N of $\Lambda^{\mu\nu}$ means that $\Lambda_N^{\mu\nu}$ are components in the near zone coordinate.

Let us define the four momentum of the object A as the integral over the body zone B_A like

$$P_A^\mu(\tau) = \epsilon^2 \int_{B_A} d^3\alpha_A \Lambda_N^{\tau\mu}. \tag{12}$$

Note that the volume integrals of $\chi^{\tau\nu\alpha\beta}{}_{,\alpha\beta}$ can be transformed into the surface integrals and appear at the $2PN$ and the higher order.

It should be noted that P_A^μ depends only on the time coordinate. We call the $\mu = \tau$ and i component of P_A^μ simply the energy and the momentum (density) of the object A, respectively. Note that we have not specified $z_A^i(\tau)$ yet.

Here, we define a dipole moment of the object as

$$D_A^i(\tau) = \epsilon^2 \int_{B_A} d^3\alpha_A \Lambda_N^{\tau\tau} \alpha_A^i. \tag{13}$$

To define the center of the mass $z^i_A(\tau)$ of the object A it is required that D^i_A takes a certain value. At the Newtonian and post-Newtonian order, we will require that D^i_A vanishes. But to derive the spin-orbit coupling force in the usual form [12, 24, 25], care must be taken when we define the center of the mass [27]. By taking the temporal derivative of D^i_A, we obtain the momentum velocity relation

$$P^i_A = P^\tau_A v^i_A + Q^i_A + \epsilon^2 \frac{dD^i_A}{d\tau}, \tag{14}$$

where $v^k_A = \dot{z}^k_A(\tau)$, and the dot denotes a temporal derivative.

Q^i_A is defined as

$$Q^i_A = \epsilon^{-4} \oint_{\partial B_A} dS_k \Lambda^{\tau k}_N \left\{ x^i - z^i_A(\tau) \right\} - \epsilon^{-4} v^k_A \oint_{\partial B_A} dS_k \Lambda^{\tau\tau}_N \left\{ x^i - z^i_A(\tau) \right\}. \tag{15}$$

Using the conservation law, Eq. (10), we obtain

$$\frac{d}{d\tau} P^\mu_A = -\epsilon^{-4} \oint_{\partial B_A} dS_k \Lambda^{k\mu}_N + \epsilon^{-4} v^k_A \oint_{\partial B_A} dS_k \Lambda^{\tau\mu}_N. \tag{16}$$

In order to obtain the equation of motion, an evolution equation for the momentum must be changed into an evolution equation for the velocity. Inserting Eq. (14) into the i-th component of Eq. (16), we obtain the general form of the equation of motion as

$$\begin{aligned} P^\tau_A \frac{d}{d\tau} v^i_A = \quad & -\epsilon^{-4} \oint_{\partial B_A} dS_k \Lambda^{ki}_N + \epsilon^{-4} v^k_A \oint_{\partial B_A} dS_k \Lambda^{\tau i}_N \\ & + \epsilon^{-4} v^i_A \Big(\oint_{\partial B_A} dS_k \Lambda^{k\tau}_N - v^k_A \oint_{\partial B_A} dS_k \Lambda^{\tau\tau}_N \Big) \\ & - \frac{d}{d\tau} Q^i_A - \epsilon^2 \frac{d^2 D^i_A}{d\tau^2}. \end{aligned} \tag{17}$$

The above set of our basic equations (15) and (17) consist only of the surface integrals when the representative point of the body A, z^i_A or equivalently, the value of the dipole moment D^i_A is specified. Therefore, all we must do is to evaluate these surface integrals perturbatively. This is a great advantage of our formalism, since our evaluations can be done outside the regions where the strong self gravitational field exists.

3 The 2.5 PN Gravitational Field

Due to lack of space, we can not write down here the 2.5 PN metric. We will show the outlines of the derivation only. More detailed derivation and the obtained gravitational field will be reported elsewhere.

Up to and including the 2.5 PN order, in the Eq. (11), we change the region of integration $C(\tau, x^k; \epsilon)$ to W, the τ constant spatial 3 hypersurface. Note that this dose not cause any divergences.

From Eq. (11), we evaluate integrals of the following type,

$$\begin{aligned} f(x) &= -\frac{1}{4\pi} \int_N d^3y \frac{g(\vec{y})}{|\vec{x} - \vec{y}|} \\ &= -\frac{1}{4\pi} \int_{N/B} d^3y \frac{g(\vec{y})}{|\vec{x} - \vec{y}|} - \frac{1}{4\pi} \epsilon^6 \sum_{A=1,2} \int_{B_A} d^3\alpha_A \frac{g(\epsilon^2 \vec{\alpha}_A)}{|\vec{x_A} - \epsilon^2 \vec{\alpha}_A|}. \end{aligned} \tag{18}$$

Here, we split the above integral into two parts, contribution from body zone B_A and contribution from elsewhere N/B.

As for the fist term in Eq.(18), we solve $\Delta G(\vec{x}) = g(\vec{x})$ and evaluate the following equation,

$$\int_{N/B} d^3y \frac{g(\vec{y})}{|\vec{x} - \vec{y}|} = -4\pi G(\vec{x}) + \oint_{\partial(N/B)} dS_k \left[\frac{\partial G(\vec{y})}{\partial y^k} - G(\vec{y}) \frac{\partial}{\partial y^k} \left(\frac{1}{|\vec{x} - \vec{y}|} \right) \right]. \tag{19}$$

For the second term in Eq.(18), we perform a multipole expansion. Up to and including the 2.5 PN order, we find the following multipoles,

$$P_A^\mu(\tau) = \epsilon^2 \int_{B_A} d^3\alpha_A \Lambda_N^{\tau\mu}, \tag{20}$$

$$\hat{I}_A^{ij} = \lim_{\epsilon\to 0}\epsilon^2 \int_{B_A} d^3\alpha_A \Lambda_N^{\tau\tau}(\alpha_A^{\langle i}\alpha_A^{j\rangle} - \frac{\delta^{ij}}{3}|\vec{\alpha}_A|^2), \tag{21}$$

$$M_A^{ij} = \lim_{\epsilon\to 0} 2\epsilon^4 \int_{B_A} d^3\alpha_A \alpha_A^{[i}\Lambda_N^{j]\tau}. \tag{22}$$

Here $\hat{I}_A^{ij}$ and M_A^{ij} are the reduced quadrupole moment and the spin of the body A, respectively.

In order to obtain the metric represented in terms of masses of the bodies, we must relate P_A^τ with the mass m_A. Noting that at the lowest order of ϵ, P_A^τ is the ADM mass of the body A, we write $P_A^\tau = m_A\Gamma_A$, where Γ_A is a correction due to the orbital motion and the gravitational field of the bodies. We can evaluate the functional dependence of Γ_A on the orbital velocities and the above defined masses of bodies explicitly by solving the time component of the equation of motion, Eq. (16) iteratively. With the above procedure we have successfully rederived the monopole part of the gravitational field up to and including the 2.5 PN order and which is exactly the same as derived in [14].

As for the spin part of the metric, care must be taken of the definition of the center of mass of each body. See [27] for detail.

We note that $\hat{I}_A^{ij}$ is mere parameter unless we provide the information on $\hat{I}_A^{ij}$, or more specifically, the equation of state of the body A and obtain functional dependence of the $\hat{I}_A^{ij}$ on the variables such as mass, spin and some constants which characterize the body A.

We obtain the spin and the quadrupole part of the metric which is the same as previously derived, e.g. [24].

4 The 2.5 PN Equation of Motion

Evaluating the surface integrals appearing in Eqs. (16) and (17), we obtain the equation of motion.

In the following equations, $\vec{r}_{12} = \vec{z}_1 - \vec{z}_2$, $r_{12} = |\vec{r}_{12}|$, $\vec{n}_{12} = \vec{r}_{12}/r_{12}$ and $\vec{V} = \vec{v}_1 - \vec{v}_2$.

4.1 Temporal Component

In the left hand side of Eq. (16), there are two contributions, from $\Theta^{\mu\nu}$ and $\chi^{\mu\nu\alpha\beta}$. In the following we split P_A^τ into corresponding parts.

$$P_{A,\Theta}^\mu(\tau) = \epsilon^2 \int_{B_A} d^3\alpha_A \Theta_N^{\tau\mu}, \tag{23}$$

$$P_{A,\chi}^\mu(\tau) = \epsilon^2 \int_{B_A} d^3\alpha_A \chi_N^{\tau\mu\alpha\beta}{}_{,\alpha\beta}. \tag{24}$$

$P_{A,\chi}^\mu$ can be explicitly evaluated by changing the volume integral into a surface integral.

Evaluating the Eq. (16) perturbatively, we obtain the evolution equation for $P_{A,\Theta}^\tau$ as

$$\begin{aligned}
\frac{dP_{1,\Theta}^\tau}{d\tau} &= -\epsilon^2\frac{m_1m_2}{r_{12}^2}[4(\vec{v}_1\cdot\vec{n}_{12}) - 3(\vec{v}_2\cdot\vec{n}_{12})] \\
&+ \epsilon^4\frac{m_1m_2}{r_{12}^2}\left[-\frac{9(\vec{v}_2\cdot\vec{n}_{12})^3}{2} + \frac{v_1^2(\vec{v}_2\cdot\vec{n}_{12})}{2} + 6(\vec{v}_1\cdot\vec{n}_{12})(\vec{v}_2\cdot\vec{n}_{12})^2 - 2v_1^2(\vec{v}_1\cdot\vec{n}_{12})\right. \\
&+ \left. 4(\vec{v}_1\cdot\vec{v}_2)(\vec{V}\cdot\vec{n}_{12}) + 5v_2^2(\vec{v}_2\cdot\vec{n}_{12}) - 4v_2^2(\vec{v}_1\cdot\vec{n}_{12})\right] \\
&+ \epsilon^4\frac{m_1m_2^2}{r_{12}^3}[-10(\vec{v}_1\cdot\vec{n}_{12}) + 11(\vec{v}_2\cdot\vec{n}_{12})] \\
&+ \epsilon^4\frac{m_1^2m_2}{r_{12}^3}[-4(\vec{v}_2\cdot\vec{n}_{12}) + 6(\vec{v}_1\cdot\vec{n}_{12})].
\end{aligned} \tag{25}$$

We find the functional dependence of $P^\tau_{A,\Theta}$ on the velocities v^i_A, masses m_A and separation r_{12} by integrate (functionally) the above equation (25),

$$p^\tau_{1,\Theta} = m_1\left[1+\epsilon^2{}_2\Gamma_1+\epsilon^4{}_4\Gamma_1\right]+O(\epsilon^6), \tag{26}$$

where

$$ {}_2\Gamma_1 = \frac{1}{2}v_1^2+\frac{3m_2}{r_{12}}, \tag{27}$$

$$ {}_4\Gamma_1 = -\frac{3m_2}{2r_{12}}(\vec{v}_2\cdot\vec{n}_{12})^2+\frac{2m_2}{r_{12}}v_2^2+\frac{7m_2}{2r_{12}}v_1^2-\frac{4m_2}{r_{12}}(\vec{v}_1\cdot\vec{v}_2)+\frac{3}{8}v_1^4+\frac{7m_2^2}{2r_{12}^2}-\frac{5m_1m_2}{2r_{12}^2}. \tag{28}$$

It is interesting to remark that up to and including the 2.5 PN order $P^\tau_{A,\Theta}$, Eq. (26) can be expressed as $P^\tau_{A,\Theta} = m_A[\sqrt{-g}u^\tau_A]_{reg}$, where u^τ_A is the temporal component of the four velocity of the body A normalized as $[g_{\mu\nu}u^\mu_A u^\nu_A]_{reg}=-1$ and the subscript "reg" means that the quantity in the $[\cdots]$ is regularized with the Hadamard regularization (or other regularization procedures as long as they reproduce the same result). Note that in order to obtain Eq. (26), we do not need any regularization schemes at all.

4.2 Spatial Component : Result

Performing procedures outlined in the preceding sections, we obtain the 2.5 PN equation of motion for the compact binaries in the following form,

$$m_1\frac{dv_1^i}{d\tau} = F^i_M+F^i_{SO}+F^i_{QP}, \tag{29}$$

where F^i_M, F^i_{SO} and F^i_{QP} are the force of monopole part , spin-orbit couplings and quadrupole-orbit couplings, respectively. The explicit formulae are as follows.

$$\begin{aligned}
F_M = & -\frac{m_1m_2}{r_{12}^2}n^i_{12}\\
&+\epsilon^2\frac{m_1m_2}{r_{12}^2}n^i_{12}\Big[-v_1^2-2v_2^2+4(\vec{v}_1\cdot\vec{v}_2)+\frac{3}{2}(\vec{v}_2\cdot\vec{n}_{12})^2+\frac{5m_1}{r_{12}}+\frac{4m_2}{r_{12}}\Big]\\
&+\epsilon^2\frac{m_1m_2}{r_{12}^2}V^i\Big[4(\vec{v}_1\cdot\vec{n}_{12})-3(\vec{v}_2\cdot\vec{n}_{12})\Big]\\
&+\epsilon^4\frac{m_1m_2}{r_{12}^2}n^i_{12}\Big[-2v_2^4+4v_2^2(\vec{v}_1\cdot\vec{v}_2)-2(\vec{v}_1\cdot\vec{v}_2)^2+\frac{3}{2}v_1^2(\vec{v}_2\cdot\vec{n}_{12})^2+\frac{9}{2}v_2^2(\vec{v}_2\cdot\vec{n}_{12})^2\\
&\qquad -6(\vec{v}_1\cdot\vec{v}_2)(\vec{v}_2\cdot\vec{n}_{12})^2-\frac{15}{8}(\vec{v}_2\cdot\vec{n}_{12})^4\\
&\qquad +\frac{m_1}{r_{12}}\Big(-\frac{15}{4}v_1^2+\frac{5}{4}v_2^2-\frac{5}{2}(\vec{v}_1\cdot\vec{v}_2)\\
&\qquad\qquad +\frac{39}{2}(\vec{v}_1\cdot\vec{n}_{12})^2-39(\vec{v}_1\cdot\vec{n}_{12})(\vec{v}_2\cdot\vec{v}_2)+\frac{17}{2}(\vec{v}_2\cdot\vec{n}_{12})^2\Big)\\
&\qquad +\frac{m_2}{r_{12}}\Big(4v_2^2-8(\vec{v}_1\cdot\vec{v}_2)\\
&\qquad\qquad +2(\vec{v}_1\cdot\vec{n}_{12})^2-4(\vec{v}_1\cdot\vec{n}_{12})(\vec{v}_2\cdot\vec{v}_2)+6(\vec{v}_2\cdot\vec{n}_{12})^2\Big)\\
&\qquad -\frac{57}{4}m_1^2-9m_2^2-\frac{69}{2}m_1m_2\Big]\\
&+\epsilon^4\frac{m_1m_2}{r_{12}^2}V^i\Big[v_1^2(\vec{v}_2\cdot\vec{n}_{12})+4v_2^2(\vec{v}_1\cdot\vec{n}_{12})-5v_2^2(\vec{v}_2\cdot\vec{n}_{12})-4(\vec{v}_1\cdot\vec{v}_2)(\vec{V}\cdot\vec{n}_{12})\\
&\qquad -6(\vec{v}_1\cdot\vec{n}_{12})(\vec{v}_2\cdot\vec{n}_{12})^2+\frac{9}{2}(\vec{v}_2\cdot\vec{n}_{12})^3\\
&\qquad +\frac{m_1}{r_{12}}\Big(-\frac{63}{4}(\vec{v}_1\cdot\vec{n}_{12})+\frac{55}{4}(\vec{v}_2\cdot\vec{n}_{12})\Big)\\
&\qquad +\frac{m_2}{r_{12}}\Big(-2(\vec{v}_1\cdot\vec{n}_{12})-2(\vec{v}_2\cdot\vec{n}_{12})\Big)\Big]
\end{aligned}$$

$$+\epsilon^5\frac{m_1^2m_2}{r_{12}^3}\Big[n_{12}^i(\vec{V}\cdot\vec{n}_{12})\Big(-6\frac{m_1}{r_{12}}+\frac{52}{3}\frac{m_2}{r_{12}}+3V^2\Big)+V^i\Big(2\frac{m_1}{r_{12}}-8\frac{m_2}{r_{12}}-V^2\Big)\Big], \tag{30}$$

and

$$F_{SO} = -\epsilon^4\frac{V^k}{r_{12}^3}\Big[\Big(2m_1M_2^{il}+m_2M_1^{il}\Big)\Delta^{lk}+2\Big(m_1M_2^{lk}+m_2M_1^{lk}\Big)\Delta^{li}\Big], \tag{31}$$

$$F_{QP} = \epsilon^4\frac{3}{2r_{12}^4}\Big(m_1\hat{I}_2^{kl}+m_2\hat{I}_1^{kl}\Big)\Big(2\delta^{il}n_{12}^k-5n_{12}^in_{12}^kn_{12}^l\Big). \tag{32}$$

Here $\Delta^{ij}=\delta^{ij}-3n_{12}^in_{12}^j$. These are exactly the same equations as the equations previously obtained (e.g. [10, 14, 12, 24]). Note that masses, spins and quadrupole moments are defined to involve the effect of the strong gravitational field inside the stars as can be seen from the definition. Hence it is found that the above equations can be applied to the stars even if whose internal gravity are strong.

5 Discussion and Conclusion

We study the equation of motion for a relativistic compact binary in the post-Newtonian approximation with the point particle limit. We can naturally incorporate multipole moments of each objects into this approach. When taking the point particle limit, we keep the internal gravity finite, hence multipole moments obtained in this limit include the effect of the self gravity explicitly, Eqs. (20), (21) and (22). In order to take the self gravity into account, besides the point particle limit, we express the equation of motion in terms of surface integrals, Eqs. (16), (15) and (17). Because we evaluate surface integrals only, there appears no singular term which has to be regularized. It is interesting to derive the 3 PN equation of motion using our approach.

In the actual calculation, we have derived the 2.5 PN metric and the 2.5 PN equation of motion. Also we obtain the spin-orbit coupling force and the quadrupole-orbit coulping force. All these obtained equations are exactly the same as derived previosly. Hence we have shown that these equations can be applied for the binary consisting of the compact objects.

We note two things about our approach. First, we take the (quasi-)stational initial data for the matter and zero homogeneous data for the gravitational field, so that the effects of the gravitational waves going through bodies and tidal forces are controlled to appear at the higher order than the 2.5 PN order at least. These effects will be difficult but very interesting problems. However they are beyond our scope in this paper.

Second, since we define the multipoles of each body as Eqs. (12) , (21) and (22), these multipoles depend on the body zone boundary, hence ϵR_A. As for the gravitational field, there are terms from integration over N/B which cancel out all R_A dependence of the multipoles or integration over B. While for the equation of motion (17) there seem no such terms. Then we must show the cancellation of the body zone boundary dependent terms in the equation of motion for the completeness. From a dimensional argument, in order to show that the n PN (n :integer) equation of motion is independent of R_A, we need to evaluate the (2n+0.5) PN gravitational field. Actually, we have proved the cancellation of terms depending on the R_A, appearing in the equation of motion (17), only for the 1 PN order equation of motion. If we wish to show similar cancellation at 2.5 PN order, then it seems that we must evaluate the 5.5 PN gravitational field. It is far away from our present status. However, in principle our approach can examine the validity of the use of some mathematical regularization [15, 28].

Acknowledgments. H.A. would like to thank Bernard F. Schutz for his hospitality at the Albert-Einstein-Institute, where a part of this work was done. Y.I. is deeply imbedted to Shijun Yoshida for useful discussion. This work was supported in part by the Japanese Grant-in-Aid for Scientific Research from the Ministry of Education, Science and Culture, No.11740130 (H.A.). Y.I. would like to acknowledge the support from JSPS Research Fellowships for Young Scientists.

References

[1] J. Hough, in *Proceedings of the Sixth Marcel Grossmann Meeting*, edited by H. Sato and T. Nakamura (World Scientific, Singapore, 1992), p.192.

[2] A. Abramovici et al., Science, **256**, 325 (1992).

[3] K. Kuroda et. al., in *Proceedings of the international conference on gravitational waves: Sources and Detections*, edited by I. Ciufolini and F. Fidecard (World Scientific, Singapore, 1997), p. 100.

[4] C. Bradaschia et al., Nucl. Instrum. Method Phys. Res. Sect. **A289**, 518 (1990).

[5] L. Blanchet, T. Damour, B. R. Iyer, C. M. Will and A. G. Wiseman, Phys. Rev. Lett. **74**, 3515 (1995).

[6] L. Blanchet, in *Proceedings of Les Houches School: Relativistic gravitation and gravitational radiation*, edited by J. A. Marck and J. P. Lasota (Cambridge Univ. Press, Cambridge, 1996)

[7] Y. Mino, M. Sasaki, M. Shibata, H. Tagoshi and T. Tanaka, Prog. Theor. Phys. Suppl. **128**, 1 (1997).

[8] H. Asada and T. Futamase, Prog. Theor. Phys. Suppl. **128**, 123 (1997).

[9] L. Bel, T. Damour, N. Deruelle, J. Ibanez and J. Martin, Gen. Rel. Grav. **13**, 963 (1981).

[10] T. Damour and N. Deruelle, Phys. Lett. **87A**, 81 (1981).

[11] T. Damour and N. Deruelle, C. R. Acad. Sci. Paris **293** II, 537 (1981); **293** II, 877 (1981).

[12] T. Damour, C. R. Acad. Sci. Paris **294** II, 1355 (1982).

[13] S. M. Kopejkin, Sov. Astron. **29**, 516 (1985).

[14] L. Blanchet, G. Faye and B. Ponsot, Phys. Rev. **D58**, 124002 (1998).

[15] R. Jaranowski and G. Schafer, Phys. Rev. **D57**, 7274 (1998); **D57**, 5948 (1998);**60**, 124003 (1999).

[16] C. M. Will, gr-qc/9910057, to be published in *the proceedings of Yukawa International Seminar on Blach Holes and Gravitational Waves : New Eyes in the 21st Century (YKIS 99)*, Kyoto, Japan, 28 June - 2 July.

[17] L. P. Grischuk and S. M. Kopejkin, Sov. Astron. Lett. 9, 230 (1983).

[18] T. Futamase, Phys. Rev. **D32**, 2566 (1985).

[19] T. Futamase, Phys. Rev. **D36**, 321 (1987).

[20] H. Tagoshi and T. Nakamura, Phys. Rev. **D49**, 4016 (1994).

[21] T. Futamase and B. F. Schutz, Phys. Rev. **D28**, 2363 (1983).

[22] B. F. Schutz, Phys. Rev. **D22**, 249 (1980).

[23] T. Futamase, Phys. Rev. **D28**, 2373 (1983).

[24] K. S. Thorne and J. B. Hartle, Phys. Rev. **D31**, 1815 (1985).

[25] L. E. Kidder, Phys. Rev. **D52**, 821 (1995).

[26] L. D. Landau and E. M. Lifshitz, *The Classical Theory of Fields* (Oxford: Pergamon 1962).

[27] Y. Itoh, T. Futamase and H. Asada, *Equation of motion for the relativistic compact binaries with the strong field point particle limit I: Formulation, the first post-Newtonian and multipole terms*, gr-qc/9910052.

[28] L. Blanchet, talk given at *Yukawa International Seminar on Blach Holes and Gravitational Waves : New Eyes in the 21st Century (YKIS 99)*, Kyoto, Japan, 28 June - 2 July.

Coalescing Binary Neutron Stars
— 3D General Relativistic Simulations Using Conformal Slicing —

Ken-ichi Oohara, [1]

Department of Physics, Niigata University, Niigata 950 2181, Japan

Takashi Nakamura[2]

Yukawa Institute for Theoretical Physics, Kyoto University, Sakyo-ku, Kyoto 606-8502, Japan

Abstract

We develop a 3 dimensional computer code to study a coalescing neutron star binary. The code can currently follow the evolution up to two stars begin to merge from two spherical stars of mass $1M_\odot$ and radius 8.9km with separation 35.4km. As for coordinate conditions, we use conformal slicing and pseudo-minimal distortion conditions. The evolution equations for the metric is integrated using the CIP method while the van Leer's scheme is used to integrate the equations for the matter. We present a few results of our simulations including gravitational radiation.

1 Introduction

We report on the present status of our computer code development to study the fully general relativistic evolution of spacetimes and matter. We solve the complete set of the Einstein equations in the absence of any symmetries. The main motivation of this project is studying promising sources of strong gravitational waves, such as coalescing neutron star or black hole binaries. The first detection by an interferometric detector of gravitational waves such as LIGO, VIRGO, GEO600 and TAMA may be the waves from a black hole binary, but the astrophysical importance of a coalescing neutron star binary is not smaller than a black hole binary. A detailed analysis of the detected waves near the merger of two stars, for example, will give information on the size of a neutron star and then on the equation of state of high density matter. On problems other than the gravitational wave physics, study on process of coalescence of a neutron star binary is helpful for models of a source of a gamma ray burst.

A compact star binary in the earliest stage is almost stationary but gravitational radiation reaction makes it evolve in the adiabatic manner. When the separation between stars is large enough, the stars can be regarded as point particles. As the separation is getting small, however, the size effect of the stars and the relativistic effects become important. Thus the complete set of the Einstein equations and the general relativistic hydrodynamics equations for a neutron star binary must be solved. In addition, the process of coalescence of a binary is not axisymmetric. Thus a three dimensional (in space) code is necessary and it requires a great power of computers. In 1994, we became able to use a supercomputer with memories of tens of GBytes and a peak speed of nearly a hundred GFLOPS. With this computer, we can manage a 200^3 grid. Then we started to make a 3D, fully general relativistic code for a coalescing neutron star binary. In this paper, we show the present status of our code development. The present code does not include a lot of realistic physics processes such as neutrino emission and a realistic equation of state near and beyond the nuclear density. So it is a milestone of 3D numerical relativity. In §2, we describe the mathematical framework of the calculation, including constraint equations, evolution equations of the metric, relativistic hydrodynamics equations, coordinate conditions and evaluation of the gravitational waves. In §3, numerical methods we use for elliptic equations and evolution equations are shown. In §4, we present numerical results of simulations of coalescing neutron star binaries obtained using the present code. In §5, we summarize and outline future work planned for this code.

[1] E-mail:oohara@astro.sc.niigata-u.ac.jp
[2] E-mail:takashi@yukawa.kyoto-u.ac.jp

2 The Mathematical Framework

2.1 Constraint equations

In the (3+1) (or ADM) formalism of general relativity, the spacetime metric is written as

$$ds^2 = -\alpha^2 dt^2 + \gamma_{ij}(dx^i + \beta^i dt)(dx^j + \beta^j dt), \tag{1}$$

where α, β^i and γ_{ij} are the lapse function, the shift vector and the intrinsic metric of three-metric. The Einstein equation reduces to the four constraint equations

$$R + K^2 - K_{ij}K^{ij} = 16\pi\rho_H, \tag{2}$$

$$D_j\left(K^j{}_i - \delta^j{}_i K\right) = 8\pi J_i \tag{3}$$

and 12 evolution equations

$$\partial_t \gamma_{ij} = -2\alpha K_{ij} + D_i\beta_j + D_j\beta_i, \tag{4}$$

$$\begin{aligned}\partial_t K_{ij} &= \alpha\left[R_{ij} - 8\pi\left\{S_{ij} + \tfrac{1}{2}\gamma_{ij}\left(\rho_H - S^\ell{}_\ell\right)\right\}\right] - D_iD_j\alpha \\ &\quad +\alpha\left(KK_{ij} - 2K_{i\ell}K^\ell{}_j\right) + K_{\ell i}D_j\beta^\ell + K_{\ell j}D_i\beta^\ell + \beta^\ell D_\ell K_{ij},\end{aligned} \tag{5}$$

where R_{ij} is the Ricci tensor, K_{ij} the extrinsic curvature tensor, $K = K^\ell{}_\ell$, and D_i the covariant derivative associated with γ_{ij}. The quantities ρ_H, J_i and S_{ij} are the energy density, the momentum density and the stress tensor, respectively, measured by the observer moving along the line normal to the spacelike hypersurface of t =constant.

In order to give an initial data, we should find a three-metric and extrinsic curvature which satisfy the constraint equations (2) and (3). It means that the constraint equations are solved giving ρ_H and J_i. Here we assume that $K = 0$ and γ_{ij} is conformally flat at $t = 0$

$$\gamma_{ij} = \phi^4\tilde{\gamma}_{ij}, \tag{6}$$

where $\tilde{\gamma}_{ij}$ is the flat space metric. Defining the conformal transformation as

$$\begin{aligned}&\tilde{K}_{ij} \equiv \phi^2 K_{ij}, \qquad \tilde{K}_i{}^j \equiv \phi^6 K_i{}^j, \qquad \tilde{K}^{ij} \equiv \phi^{10}K^{ij}, \\ &\rho_H \equiv \phi^6\rho_H \qquad \text{and} \qquad \tilde{J}_i \equiv \phi^6 J_i,\end{aligned} \tag{7}$$

Eq.(3) reduces to

$$\tilde{D}_j\tilde{K}^j{}_i = 8\pi\tilde{J}_i, \tag{8}$$

where $\tilde{D}_i$ is the covariant derivative associated with $\tilde{\gamma}_{ij}$[1]. The traceless extrinsic curvature can be decomposed with the transverse traceless part $\tilde{K}^{\rm TT}_{ij}$ and the longitudinal traceless part $(LW)_{ij}$ [2];

$$\tilde{K}_{ij} = \tilde{K}^{\rm TT}_{ij} + (LW)_{ij}, \tag{9}$$

where

$$(LW)_{ij} = \tilde{D}_iW_j + \tilde{D}_jW_i - \frac{2}{3}\tilde{\gamma}_{ij}\tilde{D}^\ell W_\ell. \tag{10}$$

Assuming $\tilde{K}^{\rm TT}_{ij} = 0$, Eq.(8) becomes

$$\tilde{\Delta}W_i + \frac{1}{3}\tilde{D}_i\tilde{D}^jW_j = 8\pi\tilde{J}_i, \tag{11}$$

where $\tilde{\Delta} \equiv \tilde{D}^i\tilde{D}_i$. Equation (11) is the coupled elliptic equation but can be reduced to four decoupled Poisson equations:

$$\Delta\chi = 6\pi\partial_i\tilde{J}_i, \tag{12}$$

$$\Delta W_i = 8\pi\tilde{J}_i - \frac{1}{3}\partial_i\chi, \tag{13}$$

where $\chi = \partial_iW_i$.

The Hamiltonian constraint equation (2) reduces to the nonlinear Poisson equation

$$\tilde{\Delta}\phi = -2\pi\phi^{-1}\rho_H - \frac{1}{8}\phi^{-7}\tilde{K}_{ij}\tilde{K}^{ij}. \tag{14}$$

2.2 Evolution equations of the metric

Defining the following variables

$$\phi = (\det(\gamma_{ij}))^{\frac{1}{12}}, \qquad \tilde{\gamma}_{ij} = \phi^{-4}\gamma_{ij}, \qquad \tilde{\gamma}^{ik}\tilde{\gamma}_{kj} = \delta^{i}{}_{j}, \tag{15}$$

$$\hat{K}_{ij} = \mathrm{STF}(\phi^{-4}K_{ij}), \qquad \hat{K}^{i}{}_{j} = \tilde{\gamma}^{ik}\hat{K}_{kj}, \qquad \hat{K}^{ij} = \tilde{\gamma}^{jk}\hat{K}^{i}{}_{k}, \tag{16}$$

where

$$\mathrm{STF}(A_{ij}) \equiv \frac{1}{2}\left(A_{ij} + A_{ji} - \frac{2}{3}\tilde{\gamma}_{ij}\tilde{\gamma}^{k\ell}A_{k\ell}\right), \tag{17}$$

the evolution equation (5) reduces to

$$\begin{aligned}\partial_t\hat{K}_{ij} - \beta^\ell\partial_\ell\hat{K}_{ij} &= \phi^{-4}\left[\mathrm{STF}\left\{\alpha\left(R_{ij} - 8\pi S_{ij}\right) - D_iD_j\alpha\right\}\right] \\ &\quad + \alpha\left(K\hat{K}_{ij} - 2\hat{K}_{i\ell}\hat{K}^{\ell}{}_{j}\right) \\ &\quad + \hat{K}_{i\ell}\partial_j\beta^\ell + \hat{K}_{j\ell}\partial_i\beta^\ell - \frac{2}{3}\hat{K}_{ij}\partial_\ell\beta^\ell,\end{aligned} \tag{18}$$

$$\partial_tK - \beta^\ell\partial_\ell K = \alpha\left[\hat{K}_{ij}\hat{K}^{ij} + \frac{1}{3}K^2 + 4\pi\left(\rho_{\scriptscriptstyle H} + S^{i}{}_{i}\right)\right] - D^iD_i\alpha, \tag{19}$$

and Eq.(4) to

$$\partial_t\tilde{\gamma}_{ij} = -2\left[\alpha\hat{K}_{ij} - \mathrm{STF}\left\{\tilde{D}_i\left(\phi^{-4}\beta_j\right)\right\}\right] \equiv A_{ij} \tag{20}$$

or

$$\partial_t\tilde{\gamma}_{ij} - \beta^\ell\partial_\ell\tilde{\gamma}_{ij} = -2\left[\alpha\hat{K}_{ij} - \mathrm{STF}\left(\tilde{\gamma}_{i\ell}\partial_j\beta^\ell\right)\right]. \tag{21}$$

The conformal factor ϕ obeys

$$\partial_t\phi - \beta^\ell\partial_\ell\phi = -\frac{\phi}{6}\left(\alpha K - \partial_\ell\beta^\ell\right) \tag{22}$$

or

$$\tilde{\Delta}\phi = -\frac{\phi^5}{8}\left(16\pi\rho_{\scriptscriptstyle H} + K_{ij}K^{ij} - K^2 - \phi^{-4}\tilde{R}\right). \tag{23}$$

Equation (22) follows from the trace of Eq.(4), while Eq.(23) from the Hamiltonian constraint (2).

2.3 Relativistic hydrodynamics equations

We assume the perfect fluid stress-energy tensor, which is given by

$$T_{\mu\nu} = (\rho + \rho\varepsilon + p)u_\mu u_\nu + pg_{\mu\nu}, \tag{24}$$

where ρ, ε and p are the proper mass density, the specific internal energy and the pressure, respectively, and u_μ is the four-velocity of the fluid. The energy density $\rho_{\scriptscriptstyle H}$, the momentum density J_i and the stress tensor S_{ij} of the matter measured by the normal line observer are, respectively, given by

$$\rho_{\scriptscriptstyle H} \equiv n^\mu n^\nu T_{\mu\nu}, \quad J_i \equiv -h_i{}^\mu n^\nu T_{\mu\nu} \quad \text{and} \quad S_{ij} \equiv h_i{}^\mu h_j{}^\nu T_{\mu\nu}, \tag{25}$$

where n_μ is the unit timelike four-vector normal to the spacelike hypersurface and $h_{\mu\nu}$ is the projection tensor into the hypersurface defined by

$$h_{\mu\nu} = g_{\mu\nu} + n_\mu n_\nu. \tag{26}$$

The relativistic hydrodynamics equations are obtained from the conservation of baryon number, $\nabla_\mu(\rho u^\mu)$, and the energy-momentum conservation law, $\nabla_\nu T_\mu{}^\nu$. In order to obtain equations similar to the Newtonian hydrodynamics equations, we define $\rho_{\scriptscriptstyle N}$ and u_i^N as

$$\rho_{\scriptscriptstyle N} \equiv \sqrt{\gamma}\alpha u^0\rho \quad \text{and} \quad u_i^N = \frac{J_i}{\alpha u^0\rho}, \tag{27}$$

respectively, where $\gamma = \det(\gamma_{ij})$. Then the equation for the conservation of baryon number takes the form

$$\partial_t \rho_N + \partial_\ell \left(\rho_N V^\ell\right) = 0, \tag{28}$$

where

$$V^\ell = \frac{u^\ell}{u^0} = \frac{\alpha J^\ell}{p + \rho_H} - \beta^\ell. \tag{29}$$

The equation for momentum conservation is

$$\begin{aligned}\partial_t(\rho_N u_i^N) + \partial_\ell \left(\rho_N u_i^N V^\ell\right) = & -\sqrt{\gamma}\alpha\partial_i p - \sqrt{\gamma}(p+\rho_H)\partial_i\alpha \\ & \frac{\sqrt{\gamma}\alpha J^k J^\ell}{2(p+\rho_H)}\partial_i\gamma_{k\ell} + \sqrt{\gamma}J_\ell\partial_i\beta^\ell.\end{aligned} \tag{30}$$

The equation for internal energy conservation becomes

$$\partial_t(\rho_N \varepsilon) + \partial_\ell \left(\rho_N \varepsilon V^\ell\right) = -p\partial_\nu\left(\sqrt{\gamma}\alpha u^\nu\right). \tag{31}$$

To complete hydrodynamics equations, we need an equation of state,

$$p = p(\varepsilon, \rho). \tag{32}$$

The right-hand side of Eq.(31) includes the time derivative. For a polytropic equation of state, $p = (\Gamma - 1)\rho\varepsilon$, however, the equation reduces to

$$\partial_t(\rho_N \varepsilon_N) + \partial_\ell \left(\rho_N \varepsilon_N V^\ell\right) = -p_N \partial_t V^\ell, \tag{33}$$

where

$$\varepsilon_N = \left(\sqrt{\gamma}\alpha u^0\right)^{\Gamma-1} \varepsilon, \tag{34}$$

$$p_N = (\Gamma - 1)\rho_N \varepsilon_N = \left(\sqrt{\gamma}\alpha u^0\right)^{\Gamma} p. \tag{35}$$

2.4 Coordinate conditions and gravitational waves

The choice of a shift vector β^i and a lapse function α is important because the stability of the code largely depends on it and because it is intimately related to the extraction of physically relevant information, including gravitational radiation, in numerical relativity.

Since the right-hand side of Eq.(20), A_{ij} is trace-free, the determinant of $\tilde{\gamma}_{ij}$ is preserved in time and the condition

$$D^j A_{ij} = 0 \tag{36}$$

produces the minimal distortion shift vector[3]. It must be a good choice of the spatial coordinate, but it is too complicated to be solved. Instead we replace the covariant derivative by the partial derivative

$$\partial_i A_{ij} = 0, \tag{37}$$

which yields an elliptic equation for the shift vector β^i:

$$\nabla^2\beta^i + \frac{1}{3}\partial_i\partial_\ell\beta^\ell = 2\partial_j\left[\alpha\hat{K}_{ij} - \mathrm{STF}(h_{i\ell}\partial_j\beta^\ell) - \frac{1}{2}\beta^\ell\partial_\ell h_{ij}\right], \tag{38}$$

where

$$h_{ij} = \tilde{\gamma}_{ij} - \delta_{ij}. \tag{39}$$

We call this condition as the pseudo-minimal distortion condition.

As for slicing condition, we choose the conformal slicing[4], where the lapse function α is given by

$$\alpha = \exp\left[-2\left(\hat{\phi} + \frac{\hat{\phi}^3}{3} + \frac{\hat{\phi}^5}{5}\right)\right] \tag{40}$$

with $\widehat{\phi} = \phi - 1$. Since in this slicing,

$$\alpha \approx \frac{1-\widehat{\phi}}{1+\widehat{\phi}} \to \frac{1-\frac{M}{2r}}{1+\frac{M}{2r}} \tag{41}$$

for large r, the space outside the central matter quickly approaches the Schwarzschild metric in the isotropic coordinates. Thus h_{ij} defined by Eq.(39) can be considered as gravitational wave parts for large r and the total energy of the gravitational waves is given by

$$E_{\rm GW} = \int dt \int_{r\to\infty} d\Omega\, r^2\, \rho_{\rm GW}, \tag{42}$$

$$\rho_{\rm GW} = \frac{1}{32\pi} A_{ij} A_{ij}, \tag{43}$$

since Eq.(37) means that A_{ij} is the transverse-traceless part of the time derivative of $\tilde{\gamma}_{ij}$ for large r.

3 Numerical Methods

3.1 Coordinate system

As for the spatial coordinates, we use a Cartesian coordinate system (x, y, z). We solve partial differential equations (PDEs) using a finite-difference scheme, where a finite grid is introduced and the PDEs are replaced by finite-difference approximations. It may be convenient to use a spherical coordinate system (r, θ, ϕ) with regard to saving of computer memory and an outer boundary condition at large distance from a compact source. But the use of spherical coordinates leads to a vexing problem of coordinate singularities at the origin and along the polar axis.

3.2 Elliptic equations

The constraint equations reduce four Poisson equations (12) and (13), and a nonlinear Poisson equation (14). These equations are solved once for initial data. The shift vector is given by the coupled elliptic equation (38), which is solved at every time step. The conformal factor ϕ is, in turn, determined either by the hyperbolic equation (22) or by the elliptic equation (Hamiltonian constraint) (23). However, since it is known that the conformal slicing yields instability in ϕ and α[5], we solve the Hamiltonian constraint (23) at every time step to prevent the onset of the instability caused by numerical errors from occurring quickly. Thus the solution of the elliptic equations consumes the greatest part of the CPU time.

A non-linear equation such as

$$\Delta\phi(t) = -4\pi S(\phi(t)), \tag{44}$$

where $S(\phi)$ is a non-linear function of ϕ, must be solved by an iterative method:

$$\phi^{(I+1)} = \Delta^{-1} S\left(\phi^{(I)}\right) \quad \text{for } I = 0, 1, 2, \cdots. \tag{45}$$

To solve Eq.(14) for initial data, we should made the iteration. For Eq.(23), however, we don't made the iteration to reduce the required CPU time. Instead, the right-hand side $S(\phi(t))$ is calculated using an approximate value of $\phi(t)$ evaluated by extrapolation from the values of ϕ at the previous two time steps $t - \Delta t$ and $t - 2\Delta t$. We examined the difference of the solution using the extrapolated source from the solution obtained by the iterative method, and found that it is small enough if Δt is as small as we use for our actual calculations.

We use the extrapolated value of β^i in calculating the right-hand side of Eq.(38), too. Note that terms including β^i vanish and we don't need the extrapolated value at $t = 0$, since $h_{ij} = 0$. Thus Eq.(38) reduces four Poisson equations (12) and (13), replacing W_i to β^i.

Now all the elliptic equations reduce Poisson equations, which are solved using a pre-conditioned conjugate gradient method[6]. The boundary condition of ϕ giving by Eq.(44) is that

$$\phi = \frac{M}{r} + \frac{d_x x^k}{r^3} + O\left(\frac{1}{r^3}\right), \tag{46}$$

for large r, where

$$M = \int S\, d^3x, \qquad d_k = \int S x^k\, d^3x. \tag{47}$$

The boundary condition of χ and W_i (or β^i) giving by Eqs.(12) and (13) is that[6]

$$\chi = \frac{P_i x^i}{2r^3} - \frac{3M_{ii}}{2r^3} + \frac{9M_{ij}x^i x^j}{2r^5} + O\left(\frac{1}{r^4}\right), \tag{48}$$

$$W_i = -\frac{P_k x^k x^i}{4r^3} - \frac{7P_i}{4r} - \frac{(7M_{ij} - M_{ji} - M_{kk}\delta_{ij})\, x^j}{4r^3} - \frac{3M_{jk}x^j x^k x^i}{4r^5} + O\left(\frac{1}{r^3}\right) \tag{49}$$

for large r, where

$$P_i = \int \tilde{J}_i\, d^3x, \qquad M_{ij} = \int \tilde{J}_i x^j\, d^3x. \tag{50}$$

3.3 Evolution of matter

Hydrodynamics equations Eqs.(28), (30) and (33) are written as

$$\partial_t Q + \partial_\ell (Q V^\ell) = F, \tag{51}$$

which is split into two phases:

$$\partial_t Q + \partial_\ell (Q V^\ell) = 0, \tag{52}$$

$$\partial_t Q = F. \tag{53}$$

Here we call Eq.(52) the advection phase and Eq.(53) the non-advection phase. The advection phase is solved using van Leer's scheme[7] to obtain $Q^{(n+1)*}_{ijk}$ from Q^n_{abc} and $(V^\ell)^n_{abc}$, where Q^n_{abc} is the value of Q at n-th time step $t = t^n$ and a spatial grid point (x^a, y^b, z^c). If the non-advection phase is solved as

$$Q^{n+1}_{ijk} = Q^{(n+1)*}_{ijk} + \Delta t \cdot F^n_{ijk} \tag{54}$$

with F^n_{ijk} calculated using quantities at $t = t^n$, it is of first-order accuracy in time. To achieve second-order accuracy, we use (1) a two-step algorithm

$$Q^{n+\frac{1}{2}}_{ijk} = Q^{(n+\frac{1}{2})*}_{ijk} + \frac{1}{2}\Delta t \cdot F^n_{ijk}, \tag{55}$$

$$Q^{n+1}_{ijk} = Q^{(n+1)*}_{ijk} + \Delta t \cdot F^{n+\frac{1}{2}}_{ijk}, \tag{56}$$

where $Q^{n+\frac{1}{2}}_{ijk}$ is used only in calculating $F^{n+\frac{1}{2}}_{ijk}$, or (2) a extrapolated source algorithm

$$Q^{n+1}_{ijk} = Q^{(n+1)*}_{ijk} + \Delta t \cdot \widetilde{F}^{n+\frac{1}{2}}_{ijk}, \tag{57}$$

where $\widetilde{F}^{n+\frac{1}{2}}_{ijk}$ given by

$$\widetilde{F}^{n+\frac{1}{2}}_{ijk} = F^n_{ijk} + \frac{1}{2}(F^n_{ijk} - F^{n-1}_{ijk}) \tag{58}$$

is the value of F at $t = t^n + \frac{1}{2}\Delta t$ evaluated by extrapolation from the values at $t = t^n$ and $t = t^n - \Delta t$. Since some test calculations indicated that these algorithms give almost the same results if Δt is small, we will use the extrapolated source algorithm.

Since the outer boundary is sufficiently far from the region of the matter distribution, we can safely set $Q = 0$ at the outer boundary.

3.4 Evolution of metric

The evolution equations for $\widehat{K}_{ij}$ (18), K (19) and $\tilde{\gamma}_{ij}$ (21) can be written as

$$\partial_t Q + v^\ell \partial_\ell Q = F, \tag{59}$$

with $v^\ell = -\beta^\ell$. It is solved using the CIP (Cubic-Interpolated Pseudoparticle/Propagation) *method[8]*. In the CIP method, both Eq.(59) and its spatial derivatives

$$\partial_t(\partial_a Q) + v^\ell \partial_\ell(\partial_a Q) = -(\partial_a v^\ell)(\partial_\ell Q) + \partial_a F \tag{60}$$

are solved. Numerical diffusion during propagation of Q can be reduced, since the time evolution of Q and its derivatives are traced. Equations (59) and (60) are split into the advection and the non-advection phases similarly to Eqs.(52) and (53). In the non-advection phase, F and $\partial_a F$ at $t = t^n + \frac{1}{2}\Delta t$ are evaluated by extrapolation from the values at previous two time steps.

By the way, special care must be taken to calculate the Ricci tensor appearing in the right-hand side of Eq.(18). With conformal transformation Eq.(15), the Ricci tensor R_{ij} associated with γ_{ij} is given by

$$R_{ij} = \tilde{R}_{ij} + R^{(\phi)}_{ij}, \tag{61}$$

where

$$R^{(\phi)}_{ij} = -2\phi^{-1}\left(\tilde{D}_j\tilde{D}_i\phi + \tilde{\gamma}_{ij}\tilde{\Delta}\phi\right) + 2\phi^{-2}\left(3(\tilde{D}_i\phi)(\tilde{D}_j\phi) - \tilde{\gamma}_{ij}(\tilde{D}_k\phi)(\tilde{D}^k\phi)\right) \tag{62}$$

and $\tilde{R}_{ij}$ is the Ricci tensor associated with $\tilde{\gamma}_{ij}$, which is given by

$$\tilde{R}_{ij} = \frac{1}{2}\left[\tilde{\gamma}^{k\ell}\left(h_{\ell i,jk} + h_{\ell j,ik} - h_{ij,k\ell}\right) + \tilde{\gamma}^{k\ell}{}_{,k}\left(h_{\ell i,j} + h_{\ell j,i} - h_{ij,\ell}\right)\right] - \tilde{\Gamma}^k_{\ell i}\tilde{\Gamma}^\ell_{jk}. \tag{63}$$

The second derivatives of h_{ij} are replaced by finite differences in numerical calculation but the numerical precision of terms such as $h_{ij,k\ell}$ with $k \neq \ell$ is not so good, while the degree of precision in calculation of $h_{ij,k\ell}$ with $k = \ell$ is the same as that of the first derivatives. Inaccuracies in $h_{ij,k\ell}$ will cause a numerical instability. The 'pseudo-minimal distortion condition', Eq.(37), however, leads $\delta^{jk}h_{ij,k} = 0$ and therefore

$$\tilde{\gamma}^{k\ell}\left(h_{\ell i,jk} + h_{\ell j,ik} - h_{ij,k\ell}\right) = -h_{ij,kk} + \psi^{k\ell}\left(h_{\ell i,jk} + h_{\ell j,ik} - h_{ij,k\ell}\right), \tag{64}$$

where $\psi^{ij} = \tilde{\gamma}^{ij} - \delta^{ij}$. Inaccuracies in numerical values of $\psi^{k\ell}h_{\ell i,jk}$ will not affect integration of Eq.(18) so seriously since both $\psi^{k\ell}$ and $h_{\ell i,jk}$ are smaller than unity.

Boundary conditions for $\widehat{K}_{ij}$ and $\tilde{\gamma}_{ij}$ are important, because the boundary is not so far from the stars and therefore inappropriate boundary conditions cause reflections of the outgoing waves. We apply outgoing conditions for $\widehat{K}_{ij}$ and $\tilde{\gamma}_{ij}$, since non-wave parts decrease rapidly in our coordinate conditions. The condition can be written as

$$Q(t, x^i) = \frac{H(\alpha t - \phi^2 r)}{r}, \tag{65}$$

where $r = \sqrt{x^2 + y^2 + z^2}$. Here H satisfies an advection equation

$$\partial_t H + c^\ell \partial_\ell H = 0, \tag{66}$$

where

$$c^\ell = \frac{\alpha x^\ell}{r\phi^2}. \tag{67}$$

It implies

$$\partial_t Q + c^\ell \partial_\ell Q = -\frac{\alpha}{r\phi^2}. \tag{68}$$

Equation (68) is solved along with Eq.(59) using the CIP method.

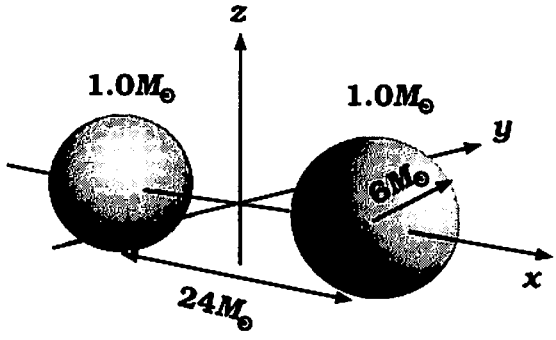

Figure 1: Initial configuration of a coalescing neutron star binary.

4 Numerical Simulations of Coalescing Binary Neutron Stars

Now we show numerical results on simulations of coalescing binary neutron stars. As for a equation of state, we use the $\gamma = 2$ polytropic equation of state. To reduce the required memory, we assume the symmetry with respect to the equatorial ($z = 0$) plane. A uniform grid of size $191 \times 191 \times 96$ with $\Delta x = \Delta y = \Delta z = 1GM_\odot/c^2 = 1.5$km is used. The numerical boundary is located at $95GM_\odot/c^2$ from the origin. In order to keep precision, we set the time step Δt as $0.01GM_\odot/c^3 = 5 \times 10^{-8}$ seconds. Calculations are performed on Fujitsu VPP500/80 at High Energy Accelerator Research Organization (KEK) and Fujitsu VPP300/16R at the National Astronomical Observatory (NAO), Japan. The required memory is approximately 8GBytes.

We performed calculations with two kinds of initial data. One is the corotation (synchronized rotation) case as for ordinary stellar binaries, in which the momentum density $\tilde{J}_i$ appearing in Eq.(8) of each star is given by

$$\tilde{J}_i = \rho_B \epsilon_{ijk} \Omega^j x^k, \tag{69}$$

where ϵ_{ijk} is the complete antisymmetric symbol and the angular velocity Ω^j is constant. The other is the irrotational (zero-circulation) case as for gravitational radiation driven compact stellar binaries, in which $\tilde{J}_i$ is given by

$$\tilde{J}_i = \rho_B \epsilon_{ijk} \Omega^j x_c^k, \tag{70}$$

where x_c^k is the position of each star and is constant for an individual star. In both cases, we assume that the binary consists of identical spherical stars of rest mass $1.0M_\odot$, radius 8.9km located at $(x_c, y_c, z_c) = (\pm 17.7\text{km}, 0, 0)$. The orbital angular momentum Ω points to the z-direction.

Here we show only results for the corotation case. Results for the irrotation case can be found at our Web site[9].

The parameters of initial data for the corotation case are shown in the second column of Table 1. It take about 10 hours on VPP500 using 64 processor units up to 26000 time steps. Figure 2 shows the evolution of the density and the velocity on the x-y plane. Movies for it including the evolution on x-z and y-z planes can be obtained from our Web site[9]. At the ~26000th time step, the onset of instability on ϕ in the central region occurs and it grows exponentially in a few time steps. At the time, only 3 grid points or so are included from the center to the surface of the star. So that numerical errors grow on account of unstable modes resident in the conformal slicing.

A thick disk around the merged star is likely to be formed as shown in Fig. 3. The mass of the disk is about a few percent of the total mass. In addition, there are indications of outflow along the rotation

Table 1: Parameters of initial data. The angular momentum parameter q is $J_t/(GM_{\rm tot}^2/c)$.

	Corotation	Irrotation
Orbital angular velocity Ω [sec^{-1}]	2.4×10^3	2.4×10^3
Angular momentum J_t [$GM_\odot^2/c$]	3.9	3.5
Collision velocity v_x [c]	0.074	0.071
Total gravitational mass $M_{\rm tot}$ [$M_\odot$]	1.96	1.95
Angular momentum parameter q	1.03	0.93

axis. However, since the precision of the numerical calculation at this time is not so good, these facts must be confirmed with more precise calculation.

The propagation of the "energy density of gravitational waves" $r^2\rho_{\rm GW}$ is shown in Fig. 4, movies of which are also provided on our Web site[9]. A spiral pattern appears on the x-y plane, while different patterns with peaks around z-axis appear on the x-z plane. This can be explained naively by the quadrupole wave pattern given by

$$r^2\rho_{\rm GW} = \frac{r^2}{32\pi}(A_{ij})^2 \propto \cos^2\theta + \sin^2\theta\sin^2(2\Omega(t-r)-2\varphi)/4. \tag{71}$$

On the x-y plane, where $\theta = \pi/2$, $\rho_{\rm GW}$ is constant along the spiral of $r + \varphi/\Omega$ = constant, while near z-axis, where $\theta \approx 0$, $\rho_{\rm GW} \propto \cos^2\theta$.

The waves pass through the numerical boundary with little reflection. It means that the boundary condition Eq.(68) behaves well. However, a small reflection on the x-, y- and z-axes interfere with the outgoing waves and interference patterns appears after $t \sim 0.8$msec.

Figures 5 shows the waveforms on the z-axis monitored between $75M_\odot$ and $85M_\odot$ from the origin. The emitted waveform falls off with r^{-1} as expected. The luminosity evaluated between $75M_\odot$ and $85M_\odot$ as functions of t and the total energy of the gravitational waves up to t are shown in Fig. 6. Comparing Figs. 4, 5 and 6 with Fig. 2, the main part of the waves begins to be emitted when the merger develops to a certain extend, but only the waves up to the time when the merger begins have arrived at the numerical boundary. The minor peak around $t - r = 0$ corresponds the waves included unexpectedly in the initial data.

The amplitude of gravitational waves is

$$h = 5 \times 10^{-22}\left(\frac{r}{10{\rm Mpc}}\right) \tag{72}$$

and the total energy emitted is

$$E_{\rm GW}(t < 1{\rm msec}) = 10^{-3}M_\odot c^2 = 2 \times 10^{51}{\rm erg} \sim 0.05\% \text{ of } M_{\rm tot}c^2. \tag{73}$$

The angular momentum of the emitted gravitational waves is given by

$$\Delta J = \int \frac{dJ}{dt}\,dt, \tag{74}$$

$$\frac{dJ}{dt} = \frac{1}{16\pi}\int \epsilon_{zjk}x^j(h^{\rm TT}_{km,p}\dot{h}^{\rm TT}_{mp} - \frac{1}{2}h^{\rm TT}_{mp,k}\dot{h}^{\rm TT}_{mp})\,dS, \tag{75}$$

to be

$$\Delta J(t < 1{\rm msec}) = 1.8 \times 10^{-2}GM_\odot^2/c \sim 0.5\% \text{ of } J_t. \tag{76}$$

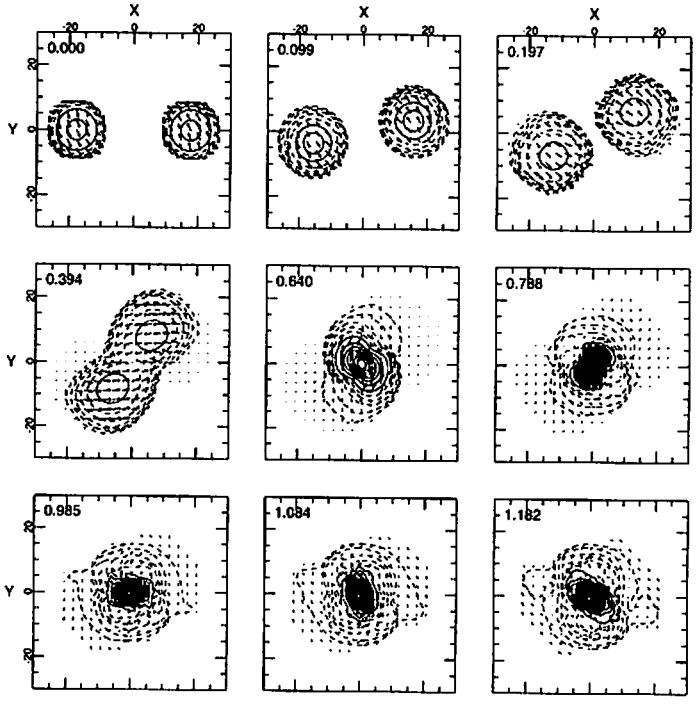

Figure 2: Density ρ_N and velocity V^i on the x-y plane for the corotation case. Time in units of milliseconds is shown. Solid lines are drawn from $\rho_{\min}$ through $\rho_{\max}$ in steps of $\rho_{\min}$, where $\rho_{\min} = 8 \times 10^{14}\mathrm{g{\cdot}cm^{-3}}$ and $\rho_{\max} = 4 \times 10^{16}\mathrm{g{\cdot}cm^{-3}}$. Dashed lines are at 1/2, 1/4, 1/8, 1/16, 1/32 of $\rho_{\min}$.

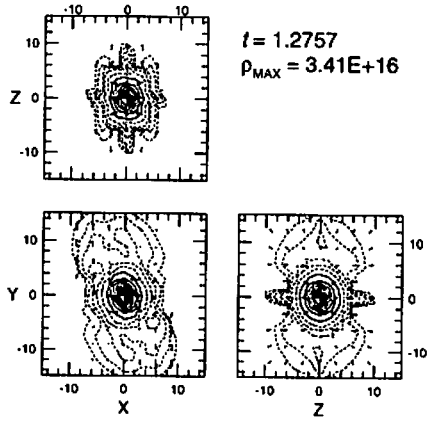

Figure 3: Density ρ_N and velocity V^i in the central region on the x-y, x-z and z-y planes for the corotation case. Parameters for contour lines are the same as Fig. 2 but $\rho_{\max} = 3.41 \times 10^{16}\mathrm{g{\cdot}cm^{-3}}$ and $\rho_{\min} = 0.1\rho_{\max}$.

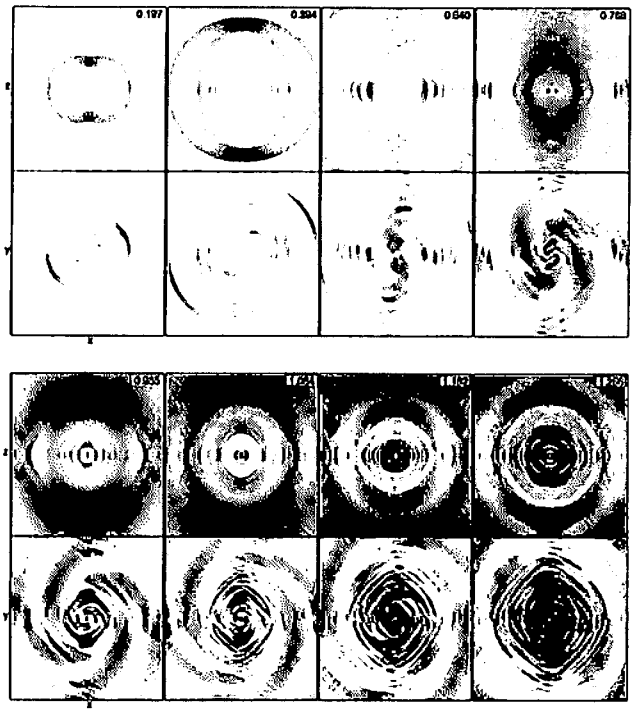

Figure 4: The propagation of the gravitational waves for the corotation case. The "energy densities of gravitational waves" $r^2\rho_{GW}$ on the x-y and x-z planes are shown as gray scale figures up to the numerical boundary. Time in units of milliseconds is shown. The upper figure of each time is on x-z plane and the lower one is on x-y plane.

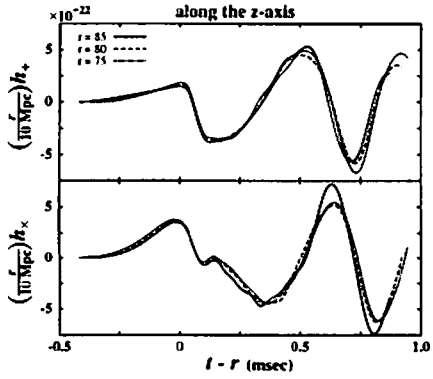

Figure 5: Waveforms h_+ and $h_\times$ observed on the z-axis for the corotation case. They have been monitored at $r = 75M_\odot, 80M_\odot$ and $85M_\odot$.

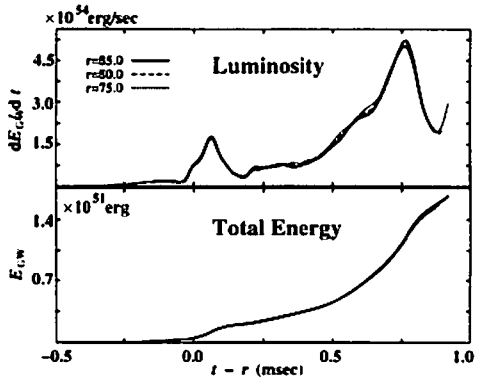

Figure 6: Luminosity (in units of erg/sec) and total energy (in units of erg) of the emitted gravitational waves. They are evaluated at $r = 75M_\odot, 80M_\odot$ and $85M_\odot$.

5 Summary

We have described a numerical code for simulations of coalescing binary neutron stars and presented some results with it. This code was developed after extensive study of a post-Newtonian code for coalescing binary neutron stars[6]. To solve hydrodynamics equations and elliptic equations, the general relativistic code uses the same methods as the post-Newtonian code does. For evolution equations for the metric, however, we adopted the CIP method, which made the evolution of the metric stable even with a coarse grid.

We faced instability when coalescence of two stars advanced to be probably a black hole. It is caused by a characteristics of the conformal slicing as well as by the coarseness of the grid. This fact may suggest that other slicing such as the maximal slicing must be adopted. Thus we are now making another code with the maximal slicing. With the maximal slicing, we must solve a elliptic equation for α, which is obtained by setteing the right-hand side of Eq.(19) equal to zero. The cost of solving this equation is great. In addition, to catch the wave form of gravitational waves, we have to apply a gauge-invariant wave extraction technique[10]. Since new super computer, 7 times faster with 20 times greater memory, will be available at KEK from the beginning of 2000, more precise calculation with the maximal slicing will be carried out. To calculate the right-hand side of Eq.(38), we used the extrapolated values for β^i as describe in §3.2, but the precision of the extrapolation will reduce in the highly dynamical phase of coalescence. We will be able to solve Eq.(38) more precisely by an iterative method on the new machine.

Acknowledgments

The calculations presented in this paper were carried out on Fujitsu VPP500/80 at High Energy Accelerator Research Organization as KEK Supercomputer Project No.99-52 and on Fujitsu VPP300/16R at the National Astronomical Observatory Japan. In addition, this work was in part supported by the Grant-in-Aid of Education, Culture, Science and Sports (09NP0801, 10640227).

References

[1] J.W. York Jr., *Source of Gravitational Radiation* (Cambridge University Press, Cambridge, 1979), p.83.

[2] J.W. York Jr., J. Math. Phys. **14** (1973), 456.

[3] L. Smarr and J.W. York Jr., Phys. Rev. **D17** (1978), 1945.

[4] M. Shibata and T. Nakamura, Prog. Theor. Phys. **88** (1992), 317.

[5] M. Shibata and T. Nakamura, Phys. Rev. **D52** (1995), 5428.

[6] K. Oohara, T. Nakamura and M. Shibata, Prog. Theor. Phys. Suppl. No. 128 (1997), 183.

[7] B. van Leer, J. Comput. Phys. **23** (1977), 276.

[8] T. Yabe, in *Computational Fluid Dynamics Review 1997* (Wiley, 1997).

[9] `http://astro.sc.niigata-u.ac.jp/~oohara/ykis99/`.

[10] A. Abrahams, D. Bernstein, D. Hobill, E. Seidel and L. Smarr, Phys. Rev. **D50** (1992), 3544.

The post-Newtonian equations of spin precession of spinning compact objects to second post-Newtonian order

Akira Ohashi,[1]

Department of Fundamental Science, FIHS, Kyoto University, Kyoto 606-8501, Japan

This work is collaborated with
Hideyuki Tagoshi (Dep. Earth and Space Science, Osaka Univ.) and
Benjamin J. Owen (Theoretical Astrophysics, Caltech and A. Einstein Institute).

Abstract

We derive the equation of spin precession to 2PN order in the case of binary systems using the post-Newtonian expansion method with the stress energy tensor of spinning particles.

1 Introduction

Gravitational waves from coalescing compact binaries are the most promising targets for detection by ground-based laser interferometers such as TAMA, LIGO, VIRGO etc. In order to detect signals and extract the information of the source system, we must analyze detail models of coalescing process which includes the inspiral phase and the merger phase of the gravitational waves. In the inspiral phase in detectable band, the binary cycles out roughly 10^3-10^4. This implies that highly accurate post-Newtonian calculations of the equation of motion and also the equation of spin precession if the objects are spinning.

Recently, we derived 2.5 post-Newtonian spin-orbit coupling force [1] and this new 2.5PN spin-orbit terms are necessary for calculation of 3PN energy flux. These are important to understand the gravitational evolution of the binary system and they affects on the gravitational waveform. If the objects of binary components are spinning, the precession of their spin also affects the waveform through changes of the orbital plane of the binary. Therefore in order to construct accurate templates of wave forms, we must derive the higher order equation of spin precession. In this article we derive the equation of spin precession up to 2PN order. In this calculation we use same techniques that we used in the calculation of 2.5PN spin-orbit terms of the equation of motion. These include energy-momentum tensor of spinning particles, regularization procedure and post-Newtonian expansion method. Finally, in our calculation we can reproduce the well-known 1PN spin precession equations.

This article is organized as follow. In Sec.2, we briefly review on the stress energy tensor of spinning particles and write down the relativistic equation of spin precession formally. In Sec.3 we summarize the 2PN metrics that we need in order to derive 2PN spin precession equations. In Sec.4 is a brief description of the regularization procedure. In Sec.5, we use the post-Newtonian metrics in order to expand basic variables. In Sec.6, we present the new 2PN equation of spin precession. In Sec.7, we summarize our result.

2 Energy-momentum tensor of spinning particles

We use the stress energy tensor given by Bailey and Israel [3] to express the spinning compact objects. Up to the order we need, it is given by

$$T^{\alpha\beta} = T^{\alpha\beta}_{(M)} + T^{\alpha\beta}_{(S)} + T^{\alpha\beta}_{(SA)}, \tag{1}$$

[1]E-mail:ohashi@phys.h.kyoto-u.ac.jp

where

$$T^{\alpha\beta}_{(M)}(x) = \sum_{A=1,2}\int d\tau m_A u^\alpha_A(\tau)\, u^\beta_A(\tau)\frac{\delta^{(4)}(x-y_A(\tau))}{\sqrt{-g}}, \tag{2}$$

$$T^{\alpha\beta}_{(S)}(x) = -\sum_{A=1,2}\nabla_\gamma\int d\tau \hat{S}^{\gamma(\alpha}_A(\tau)u^{\beta)}_A(\tau)\frac{\delta^{(4)}(x-y_A(\tau))}{\sqrt{-g}}, \tag{3}$$

$$T^{\alpha\beta}_{(SA)}(x) = -\frac{1}{2}\sum_{A=1,2}\nabla_\gamma\int d\tau \hat{S}^{\alpha\beta}_A(\tau)u^\gamma_A(\tau)\frac{\delta^{(4)}(x-y_A(\tau))}{\sqrt{-g}}. \tag{4}$$

In order to derive the spin-precession equations from this stress energy tensor, for the fact that generally the stress energy tensor must be symmetric, we calculate the following integral,

$$\int_{D_1} d^3x\sqrt{-g}T^{[\alpha\beta]} = 0, \tag{5}$$

where D_1 is a region including only the particle 1. By this integration, it is straightforward to derive the spin precession equations and we get the following equations

$$\frac{d}{dt}\hat{S}^{\alpha\beta}_1 + \left(\Gamma^\alpha_{\mu\nu}\right)_1\hat{S}^{\mu\beta}_1 u^\nu_1 + \left(\Gamma^\beta_{\mu\nu}\right)_1\hat{S}^{\alpha\mu}_1 u^\nu_1 = 0. \tag{6}$$

Here we introduce a spin vector related to the spin tensor by

$$\hat{S}^{\alpha\beta}_A = -\frac{1}{\sqrt{-g}}\varepsilon^{\alpha\beta\mu\nu}u_{A\mu}S_{A\nu}, \tag{7}$$

$$S^\mu_A u_{A\mu} = 0, \tag{8}$$

where $\varepsilon^{\mu\nu\rho\sigma}$ is the totally antisymmetric symbol with $\varepsilon^{0123} = 1$. For simplicity, we express the spin tensor in term of the spatial components of the spin 4-vector S^μ using the relation (8) that is, $S^0 = -\frac{g_{0m}+v^p_1 g_{pm}}{g_{00}+v^q_1 g_{q0}}S^m$, thus we get the following representation

$$\hat{S}^{0i}_1 \equiv A^i_{(1)m}S^m_1, \tag{9}$$

$$\hat{S}^{ij}_1 \equiv B^{ij}_{(1)m}S^m_1, \tag{10}$$

where

$$A^i_{(1)m} = \left(\tilde{A}^i{}_m\right)_1, \quad B^{ij}_{(1)m} = \left(\tilde{B}^{ij}{}_m\right)_1 \tag{11}$$

and

$$\tilde{A}^i{}_m \equiv -\frac{u^0_1}{\sqrt{-g}}\varepsilon^{ijk}\left[-\left(g_{0j}g_{0k}+g_{jl}g_{0k}v^l_1\right)\frac{g_{0m}+v^p_1 g_{pm}}{g_{00}+v^q_1 g_{q0}}+\left(g_{0j}g_{km}+g_{jl}g_{km}v^l_1\right)\right], \tag{12}$$

$$\tilde{B}^{ij}{}_m \equiv -\frac{u^0_1}{\sqrt{-g}}\varepsilon^{ijk}\left[\left(g_{00}g_{kl}-g_{0l}g_{0k}\right)v^l_1\frac{g_{0m}+v^p_1 g_{pm}}{g_{00}+v^q_1 g_{q0}}+\left\{\left(g_{00}g_{km}-g_{0k}g_{0m}\right)+\left(g_{0l}g_{km}-g_{kl}g_{0m}\right)v^l_1\right\}\right] \tag{13}$$

Using these quantities, we can rewrite the equation (6) into the following form as

$$\begin{aligned}\frac{d}{dt}S^{ij}_1 &= 2v^\gamma_1\left(\Gamma^{[i}{}_{\gamma\rho}\right)_1\hat{S}^{j]\rho}_1 \\ &= 2\left[\left(-\left(\Gamma^{[i}{}_{00}\right)_1 A^{j]}_{(1)m}+\left(\Gamma^{[i}{}_{0k}\right)_1 B^{j]k}_{(1)m}\right)+\left(-\left(\Gamma^{[i}{}_{0l}\right)_1 A^{j]}_{(1)m}+\left(\Gamma^{[i}{}_{kl}\right)_1 B^{j]k}_{(1)m}\right)v^l_1\right]S^m_1.\end{aligned} \tag{14}$$

These equations are for the time variations of the spin tensor S^{ij}_1, but it is more useful to express the equations for the time variations of the spatial components of the spin 4-vector. Using the relations,

$$\frac{d}{dt}S^{ij}_1 = \frac{d}{dt}\left(B^{ij}_{(1)m}S^m_1\right) = \frac{dB^{ij}_{(1)m}}{dt}S^m_1 + B^{ij}_{(1)m}\frac{dS^m_1}{dt}, \tag{15}$$

we obtain the following equations of the precession of the spin vector as

$$B^{ij}_{(1)m}\frac{dS^m_1}{dt} = \left[2\left\{\left(-\left(\Gamma^{[i}{}_{00}\right)_1 A^{j]}_{(1)m} + \left(\Gamma^{[i}{}_{0k}\right)_1 B^{j]k}_{(1)m}\right) + \left(-\left(\Gamma^{[i}{}_{0l}\right)_1 A^{j]}_{(1)m} + \left(\Gamma^{[i}{}_{kl}\right)_1 B^{j]k}_{(1)m}\right) v^l_1\right\} - \frac{dB^{ij}_{(1)m}}{dt}\right] S^m_1. \tag{16}$$

For simplicity, we will write the r.h.s. as $H^{ij}{}_m S^m_1$.

3 The second post-Newtonian metric

In harmonic coordinates we can write the Einstein equations as

$$\Box h^{\mu\nu} = 16\pi(-g)T^{\mu\nu} + \Lambda^{\mu\nu}(h), \tag{17}$$

$$h^{\mu\nu} \equiv \sqrt{-g}g^{\mu\nu} - \eta^{\mu\nu}, \tag{18}$$

where $\Box = \eta^{\mu\nu}\partial_\mu\partial_\nu$, $\eta^{\mu\nu} = \mathrm{diag}(-1,1,1,1)$, and $\Lambda^{\mu\nu}(h)$ represent the non-linear terms.

According to the ordinary procedure of post-Newtonian expansion [2], we can write the metric approximately as

$$g_{00} = -1 + 2V - 2V^2 + O(6)\,, \tag{19}$$

$$g_{0i} = -4V_i + O(5)\,, \tag{20}$$

$$g_{ij} = \delta_{ij}\left(1 + 2V + 2V^2\right) + 4\hat{W}_{ij} + O(6)\,, \tag{21}$$

where V,V_i and $\hat{W}_{ij}$ are post-Newtonian potentials defined by

$$V = \Box_R^{-1}\{-4\pi G\sigma\}\,, \tag{22}$$

$$V_i = \Box_R^{-1}\{-4\pi G\sigma_i\}\,, \tag{23}$$

$$\hat{W}_{ij} = \Box_R^{-1}\{-4\pi G(\sigma_{ij} - \delta_{ij}\sigma_{kk}) - \partial_i V\partial_j V\}\,, \tag{24}$$

(25)

and $\sigma,\sigma_i,\sigma_{ij}$ are defined by

$$\sigma \equiv T^{00} + T^{ii}\,, \tag{26}$$

$$\sigma_i \equiv T^{0i}\,, \tag{27}$$

$$\sigma_{ij} \equiv T^{ij}\,, \tag{28}$$

and the retarded integration $\Box_R^{-1}$ represents

$$\Box_R^{-1}\{-4\pi f\} \equiv \int \frac{d^3\vec{z}}{|\vec{x}-\vec{z}|} f(\vec{z}, t - |\vec{x}-\vec{z}|). \tag{29}$$

The concrete expression of the post-Newtonian potentials, $V, V_i, \hat{W}_{ij}$ can be seen in [2] in the case of monopole particles and in [1] in the case of spinning particles.

4 Regularization procedure

In the calculation of the equation of spin precession, we need to evaluate the gravitational field at the location of the objects. However the quantities that we need diverge because we adopt the point-like description for the objects. Therefore we must regularize them by an adequate method. In this article, we adopt the Hadamard finite part. This regularization procedure is the following:
(i)one expand the function as,

$$F(\vec{x}) = \sum_{-k_0\le k\le 0} r_1^k f_k(\vec{n}_1, \vec{y}_1) + O(r_1), \tag{30}$$

(ii)one defines the effective value of the function at the location of body 1 as the Hadamard finite part,

$$(F)_1 \equiv \int \frac{d\Omega(\vec{n}_1)}{4\pi} f_0(\vec{n}_1, \vec{y}_1). \tag{31}$$

The symbol $()_A$ denotes the Hadamard finite part at $\vec{x} = \vec{y}_A$. The reason why we adopt this Hadamard regularization is that it is adopted in [1] and [2] and it goes well in these cases expect that no problem would occur in this work although this procedure does not have Lorenz invariance.

5 the post-Newtonian expansion of basic variables

Here using 2PN metrics given in the section 3, we expand the basic variables. By substituting the 2PN metrics into the relation $g_{\mu\nu}u^\mu u^\nu = -1$ we obtain

$$u^0_A = 1 + \left(\frac{1}{2}v_A^2 + V\right)_A + \left(\frac{1}{2}V^2 + \frac{5}{2}v_A^2 V + \frac{3}{8}(v_A^2)^2 - 4v_A^i V_i\right)_A + O(6). \tag{32}$$

As same way, we subsituite the metrics into the equations (12),(13) and obtain

$$\tilde{A}^i{}_m = \delta_{mn}\varepsilon^{npi}\left\{\left(1 + \frac{1}{2}v_1^2 + 3V\right)v_1^p - 4V_p\right\} + O(5)\,, \tag{33}$$

$$\begin{aligned}\tilde{B}^{ij}{}_m &= \delta_{mn}\varepsilon^{nij}\left\{1 + \left(\frac{1}{2}v_1^2 - V\right) + \left(\frac{3}{8}(v_1^2)^2 + \frac{3}{2}v_1^2 V + \frac{1}{2}V^2 - 2\hat{W}_{pp}\right)\right\} \\ &\quad - \varepsilon^{pij}\left\{\delta_{mn}\left(v_1^p v_1^n + 3V v_1^p v_1^n - \frac{1}{2}v_1^2 v_1^p v_1^n\right) + 4\hat{W}_{pm}\right\} + O(6),\end{aligned} \tag{34}$$

We expand also the affine connections as

$$\Gamma^i{}_{00} = V_{,i} + 4VV_{,i} - 4V_{i,t}, \tag{35}$$

$$\Gamma^i{}_{0k} = \delta_{ik}V_{,t} + 4R_{k,i} - 4R_{i,k} + 2V_{k,i} - 2V_{i,k} - 4VV_{k,i} + 4VV_{i,k} + 2W_{ki,t} - 4V_{,k}V_i, \tag{36}$$

$$\Gamma^i{}_{kl} = \delta_{ik}V_{,k} + \delta_{il}V_{,l} - \delta_{kl}V_{,i} + 2W_{ik,l} + 2W_{il,k} - 2W_{kl,i}. \tag{37}$$

Then, by substituting concrete forms of the post-Newtonian potentials into the equations obtained above expansion, we can get the following expression as,

$$A^i{}_m = \varepsilon^{mpi}\left\{\left(1 + \frac{1}{2}v_1^2 + 3\frac{m_2}{r_{12}}\right)v_1^p - 4\frac{m_2}{r_{12}}v_2^p\right\}, \tag{38}$$

$$\begin{aligned}B^{ij}{}_m &= \varepsilon^{mij}\left\{1 + \left(\frac{1}{2}v_1^2 - \frac{m_2}{r_{12}}\right) + \left(\frac{3}{8}(v_1^2)^2 + \frac{3}{2}\frac{m_2}{r_{12}}v_1^2 + \frac{7}{2}\frac{m_1 m_2}{r_{12}^2} + \frac{1}{2}\frac{m_2^2}{r_{12}^2} + \frac{1}{2}\frac{m_2}{r_{12}}(n_{12}v_2)^2 - 2\frac{m_2}{r_{12}}v_2^2\right)\right. \\ &\quad \left. -\varepsilon^{pij}\left(v_1^p v_1^m\left[1 + 3\frac{m_2}{r_{12}} + v_1^2\right] + 8\frac{m_1 m_2}{r_{12}^2}n_{12}^p n_{12}^m - \frac{m_2^2}{r_{12}^2}n_{12}^p n_{12}^m - 4\frac{m_2}{r_{12}}v_2^p v_2^m\right)\right\}.\end{aligned} \tag{39}$$

Note that in these equation we have already applied the Hadamard regularization.

6 2PN equations of spin precession

Next, in order to write down PN order of the equations explicitly, we define following variables,

$$D_{am} = \frac{1}{2}\varepsilon_{aij}B^{ij}{}_m, \tag{40}$$

$$J_{am} = \frac{1}{2}\varepsilon_{aij}H^{ij}{}_m, \tag{41}$$

and we write the post-Newtonian expansion of these two variables such as

$$D_{am} = D^{(0)}_{am} + D^{(2)}_{am} + \cdots, \tag{42}$$

$$J_{am} = J^{(3)}_{am} + J^{(5)}_{am} + \cdots. \tag{43}$$

where numbers round-parenthesized indicate power of (v/c) and note $D^{(0)}_{am} = \delta_{am}$. By multipling ε_{aij} to the equation (16), we have

$$\frac{dS_1^{a\,(3)}}{dt} = J^{(3)}_{am} S_1^m, \tag{44}$$

$$\frac{dS_1^{a\,(5)}}{dt} = J^{(5)}_{am} S_1^m - D^{(2)}_{am} \frac{dS_1^{m\,(3)}}{dt} = \left(J^{(5)}_{am} - D^{(2)}_{ab} J^{(3)}_{bm} \right) S_1^m. \tag{45}$$

The equation (44) is the first post-Newtonian spin-precession equation and (44) is the new second post-Newtonian spin-precession equation. By substituting the potentials we have

$$J^{(3)}_{am} = \frac{m_2}{r_{12}^2} \left\{ \delta^{am} (n_{12} v_{12}) + n^m_{12} \left(v_1^a - 2 v_2^a \right) + 2 n^a_{12} \left(v_2^m - v_1^m \right) \right\}. \tag{46}$$

This agrees with well-known first post-Newtonian spin-precession equation.

Because the coordinate transformation to the center-of-mass system of the two-body system includes some post-Newtonian corrections, it is useful and comprehensible to change the velocity of the particles, v_1,v_2, to relative velocity v_{12} and also to change each masses of the particles m_1 and m_2 to the total mass $M \equiv m_1 + m_2$, the mass ratio $\eta \equiv m_1 m_2 / M^2$ and the difference of mass $\Delta \equiv (m_1 - m_2)/M$. Thus we have

$$J^{(3)}_{am} = \frac{M}{r^2} \left\{ \frac{1}{2} (1 - \Delta) \delta_{am} (nv) + (1 - \Delta + \eta) n^m v^a - (1 - \Delta) n^a v^m \right\} \tag{47}$$

$$\begin{aligned} J^{(5)}_{am} - D^{(2)}_{ab} J^{(3)}_{bm} = \frac{M}{r^2} \Bigg\{ & \frac{M}{r} \left(-\frac{1}{2} + \frac{1}{2}\Delta + \frac{3}{2}\eta - \frac{1}{2}\Delta\eta \right) \delta_{am} (nv) + \frac{M}{r} \left(1 - \Delta - \frac{73}{4}\eta + \frac{1}{4}\Delta\eta + \eta^2 \right) n^a n^m (nv) \\ & - \frac{3}{4}\eta (1 + \Delta) \delta_{am} (nv)^3 + \frac{M}{r} \left(-\frac{1}{2} + \frac{1}{2}\Delta + \frac{25}{4}\eta - \frac{1}{4}\Delta\eta + \eta^2 \right) n^m v^a \\ & - \frac{3}{2}\eta (1 + \Delta - \eta) n^m v^a (nv)^2 + 7 \frac{M}{r} \eta n^a v^m + \frac{3}{2} \frac{M}{r} \eta (1 + \Delta) n^a v^m (nv)^2 \\ & + \left(\frac{5}{2} - \frac{1}{2}\Delta \right) \eta v^a v^m (nv) + \left(\frac{5}{4} + \frac{3}{4}\Delta - \eta \right) \eta n^m v^a (nv) - 2\eta n^a v^m v^2 \\ & + \frac{1}{2} (1 + \Delta) \eta \delta_{am} (nv) v^2 \Bigg\}, \end{aligned} \tag{48}$$

where $n^a = n^a_{12}$ and $v^a = v^a_{12}$. What is multiplyed by the S^m to (48) is the new terms of 2PN correction on the equation of spin precession.

7 Summary

We have derived the equations of spin precession in the case of a binary system up to second post-Newtonian order. These terms are 1PN higher order correction to the well known the equation of spin precession because the leading one is already 1PN order. These spin precession effects influence on the inclination of the orbital plane of binary, thus do on the waveform of the gravitational waves emitted by the binary.

We have already written that the Hadamard regularization is not Lorenz invariant. Therefore we must check the Lorenz invariance of the our new result. This is under operation at present.

References

[1] H. Tagoshi, A. Ohashi and B. J. Owen, in preparation

[2] L. Blanchet, G. Faye and B. Ponsot, Phys. Rev. D 58, 124002 (1998)

[3] I. Bailey and W. Israel, Ann. Phys.130,188 (1980)

Gravitational reaction force on a particle in the Schwarzschild background

Hiroyuki Nakano[a],[1] Misao Sasaki[a,b2]

[a] *Department of Earth and Space Science, Graduate School of Science, Osaka University, Toyonaka, Osaka 560-0043, Japan*

[b] *Department of Physics, School of Science, University of Tokyo, Bunkyoku, Tokyo 113-0033, Japan*

Abstract

We formulate a new method for calculating the gravitational reaction force on a particle of mass μ orbiting a massive black hole of mass M. In this formalism, the tail part of the retarded Green function, which is responsible for the reaction force, is calculated at the level of the Teukolsky equation. Our method naturally allows a systematic post-Minkowskian (PM) expansion of the tail part at short distances. As a first step, we focus on the case of a Schwarzschild black hole and explicitly calculate the 1PM tail part. Then we apply it to a particle orbiting a black hole to obtain the reaction force of $O(\mu/M)$ at the 1st post-Newtonian level. The result agrees with the standard post-Newtonian calculation. ⇐ **This should be checked out!**

1 Introduction

In the black hole perturbation approach to the gravitational radiation from an inspiralling compact binary, one calculates the gravitational waves emitted by a point particle orbiting a black hole, assuming the mass of the particle (μ) is much less than the mass of the black hole (M). In the lowest order of μ/M, the particle moves along a geodesic trajectory on the black hole geometry. Already in this lowest order, this approach has been proved to be very powerful for evaluating general relativistic corrections to the gravitational wave forms from a compact binary, even for neutron star-neutron star (NS-NS) binaries. However, in such calculations one inevitably has to assume that the radiation reaction time scale is sufficiently long compared to the orbital period so that the adiabatic approximation to the orbital evolution is valid. That is, the orbital evolution is determined by the energy and angular momentum balance between the orbit and the graviational radiation.

However, there are several situations in which such an approximation cannot be justified. For example, when the particle is nearly in the last stable circular orbit, the radiation reaction time scale would become comparable to the orbital period. When the particle is in a very eccentric orbit or in a scattering orbit, presumably one has to know the orbital evolution not by averaging over many periods but by each scattering event.

Another case is when the massive object is in fact a rotating black hole. In this case the geometry is Kerr and the geodesic orbit is determined not only by the energy and the z-component of the angular momentum but also by the Carter constant. Since the Carter constant is not associated with the Killing vector field of the Kerr geometry, its evolution cannot be determined by evaluating the gravitational radiation at infinity even though the adiabatic approximation may be still valid.

In order to treat these situations, it is therefore necessary to evaluate the correction to the equation of motion of a particle on the background geometry. That is, we must know the reaction force of $O(\mu/M)$ acting on the particle,

$$\frac{D^2 z^\mu(\tau)}{d\tau^2} = F^\mu(z)\,. \tag{1}$$

[1] E-mail:denden@vega.ess.sci.osaka-u.ac.jp
[2] E-mail:misao@vega.ess.sci.osaka-u.ac.jp

Formally F^μ is given by

$$F^\mu = -\frac{1}{2}(g^{\mu\nu} + u^\mu u^\nu)\left(2h^{\rm tail}_{\nu\beta;\alpha} - h^{\rm tail}_{\alpha\beta;\nu}\right) u^\alpha u^\beta , \tag{2}$$

where $u^\mu = dz^\mu/d\tau$ and $h^{\rm tail}_{\mu\nu}$ is the tail part of the linear perturbation caused by the particle, i.e., the contribution from a part of the retarded Green function that has support inside the past lightcone. Thus our task is to evaluate the tail part of the Green function.[3]

However, since the tail part depends non-locally on the background geometry, it seems practically impossible to evaluate it directly. As a way to avoid this difficulty, Mino proposed a very interesting approach[2]. He noticed that the direct part of the Green function, which has support only on the light-cone, is determined by the local geometry, hence the corresponding metric perturbation can be evaluated solely with the knowledge of the local geometry. On the other hand, on the black hole background, the linear perturbation is known to be described by the Teukolsky formalism and there exist a method to obtain the general solution in a systematic manner. Hence, on the one hand, one may construct the full metric perturbation by solving the Teukolsky equation, and on the other hand, one can calculate the direct part of the metric perturbation by analyzing the local geometry. One can then obtain the tail part by subtracting the direct part from the full metric perturbation.

This approach was further pushed forward by Mino and Nakano[3], and they succeeded in obtaining some interesting results. Yet, their method seems rather cumbersome. It involves many steps of lengthy calculations, mainly caused by the different choice of gauges in which the full metric perturbation and the direct part of it are evaluated.

In this paper, we propose a new, improved method to evaluate the tail part of the perturbation. As Mino noticed, what one needs to do is to extract out the direct part of the retarded Green function. But it does not have to be done on the level of the metric perturbation. Instead, if one considers the Teukolsky equation in the spacetime domain, one can evaluate the direct part of the Green function for the Teukolsky equation directly, without transforming it to the metric perturbation. One can then systematically evaluate the tail part, from which the corresponding metric perturbation and subsequently F^μ can be calculated.

A potential problem in this approach is that the Teukolsky equation has a very non-trivial angular spin-weight dependence, even in the limit of flat spacetime, $M \to 0$. Thus the evaluation of the direct part would become very much involved. As a way to avoid this problem, we consider the transformation of the Teukolsky equation with spin-weight s to the Klein-Gordon type equation (i.e., with $s = 0$). In the case of the Schwarzschild background, this is essentially the Chandrasekhar transformation that brings the Teukolsky equation to the Regge-Wheeler equation. In the case of the Kerr background, there is no known transformation of this kind. One possibility is to use the transformation given by Sasaki and Nakamura in a perturbative way, with respect to the spin parameter a/M of the Kerr geometry. In this paper, however, we focus on the case of the Schwarzschild black hole background and defer the extension to the Kerr case to future work.

2 Chandrasekhar transformation in spacetime-domain

The Teukolsky equation in the spacetime domain is expressed as

$${}_s\Box\,{}_s\Psi \equiv \left[\nabla^\mu\nabla_\mu + \frac{2s}{r^2}\left\{\left(-r + \frac{Mr^2}{\Delta}\right)\partial_t + (r-M)\partial_r + i\frac{\cos\theta}{\sin^2\theta}\partial_\varphi + \frac{1 - s\cot^2\theta}{2}\right\}\right]{}_s\Psi = -4\pi\,{}_sT , \tag{3}$$

where $s = 0, \pm1$ or ±2. We note that ${}_s\Psi$ has the spin-weight s with respect to the spatial rotation of the tetrad, but it is a spacetime scalar. ${}_sT$ is the source term whose explicit form can be found in [4]. Although our interest is in the gravitational perturbation, and it is described by the Teukolsky equation with $|s| = 2$, we leave the value of s unfixed until we need to fix it. As we shall see later, this makes it easy to identify the tail part of the Green function.

[3]here and in the rest of the paper, the adjective 'retarded' will be omitted from the Green function unless confusion might arise.

The difficulty of directly dealing with the Teukolsky equation comes from the non-trivial angular-dependence in the zeroth and first derivative terms of it. In particular, this causes the non-conventional behavior of the Green function even in the flat spacetime limit. To overcome this difficulty, we consider a transformation of the Teukolsky equation. Since there is a one-to-one correspondence between the Teukolsky equation with spin-weight s and $-s$ (the Starobinsky-Teukolsky identities), we shall concentrate on negative spin weights; $s = 0, -1$ and -2. For $s \leq 0$, we introduce a new field variable ${}_sX$ by setting

$$ {}_s\Psi = \bar{\eth}^{|s|} \left(\frac{\Delta}{r}\right)^{|s|} \left(\partial_r - \frac{r^2}{\Delta}\partial_t\right)^{|s|} r^{|s|}\, {}_sX\,, \tag{4} $$

where

$$ \begin{aligned} \eth &= -\left(\partial_\theta + \frac{i}{\sin\theta}\partial_\varphi - s\cot\theta\right), \\ \bar{\eth} &= -\left(\partial_\theta - \frac{i}{\sin\theta}\partial_\varphi + s\cot\theta\right). \end{aligned} \tag{5} $$

It should be noted that $\eth$ ($\bar{\eth}$) operated on a quantity of spin-weight s yields a quantity of spin-weight $s+1$ ($s-1$). In particular, we have

$$ \begin{aligned} \eth\, {}_sY_{\ell m} &= [\ell(\ell+1) - s(s+1)]^{1/2}\, {}_{s+1}Y_{\ell m}\,, \\ \bar{\eth}\, {}_sY_{\ell m} &= -[\ell(\ell+1) - s(s-1)]^{1/2}\, {}_{s-1}Y_{\ell m}\,, \\ \bar{\eth}\eth\, {}_sY_{\ell m} &= -[\ell(\ell+1) - s(s+1)]\, {}_sY_{\ell m}\,, \end{aligned} \tag{6} $$

where ${}_sY_{\ell m}$ are the normalized spherical harmonics of spin-weight s. This implies ${}_sX$ has the spin-weight $s + |s| = 0$ for $s \leq 0$. If expanded in terms of $e^{-i\omega t}$ and ${}_sY_{\ell m}$, the radial part of the above transformation is just the Chandrasekhar transformation that relates homogeneous Teukolsky functions to Regge-Wheeler functions, apart from the overall normalization constant that depends on ℓ and ω. A conceptually important difference is that here we do not associate ${}_sX$ with the spin-weight s, but with $s = 0$.

Inserting (4) into (3), we find

$$ \begin{aligned} {}_s\Box\, {}_s\Psi &= \bar{\eth}^{|s|} \left(\frac{\Delta}{r}\right)^{|s|} \frac{1}{r^2} \left(\partial_r - \frac{r^2}{\Delta}\partial_t\right)^{|s|} r^{|s|+2} \left[\nabla^\mu\nabla_\mu + s^2\,\frac{2M}{r^3}\right] {}_sX = 0\,, \\ &\Rightarrow \quad \left[\nabla^\mu\nabla_\mu + s^2\,\frac{2M}{r^3}\right] {}_sX = 0\,. \end{aligned} \tag{7} $$

We see that the equation for ${}_sX$ has the standard Klein-Gordon type structure with the potential term that vanishes sufficiently rapidly at infinity irrespective of the spin-weight. Note that the radial part of it is just the Regge-Wheeler equation. It then follows that ${}_sX$ can be naturally expanded in terms of the scalar (i.e., $s = 0$) spherical harmonics even for nonzero s, in accordance with the discussion above. A very important point to be noted is the following. If one constructs the Green function of Eq. (7) for ${}_sX$, the direct part of it is exactly the same for all the spin-weights. This is because the local causal structure of a hyperbolic equation depends only on the derivative terms of the equation (i.e., the $\nabla^\mu\nabla_\mu$ part). This implies that the part that should be discarded from the Green function is independent of s if done for the variable ${}_sX$. In other words, any s-dependent terms in the Green function for ${}_sX$ belongs to the tail part.

3 1PM direct(instantaneous) part at short distances

As usual, we write the Green function in the Hadamard form,

$$ {}_sG^{\rm ret}(x,x') = \theta(\Sigma(x),x')\left\{\frac{u}{4\pi}\delta(\sigma) + \theta(-\sigma)\, {}_sv\right\}, \tag{8} $$

where σ is half the squared geodetic distance between x and x', u is a bi-scalar which depends only on the local geometry, and ${}_sv$ is a bi-scalar that describes the tail effects. As noted in the previous section, the direct part of ${}_sG^{\rm ret}$ is independent of s, and the bi-scalar u is given simply by that in the case of the scalar d'Alembertian[8],

$$u = \left(\frac{-\det |\sigma_{;\alpha;\beta'}|}{\sqrt{g(x)g(x')}} \right)^{1/2} \tag{9}$$

Let us denote the direct part of ${}_sG^{\rm ret}$ by $G^{\rm dir}$,

$$G^{\rm dir} = \theta(\Sigma(x), x') \frac{u}{4\pi} \delta(\sigma). \tag{10}$$

Our task is to explicitly evaluate $G^{\rm dir}$ at short distances.

To do so, it is more convenient to work in the isotropic coordinates than in the Schwarzschild coordinates. In terms of the isotropic coordinates, the Schwarzschild metric takes the form,

$$\begin{aligned} ds^2 &= -\frac{\left(1-\frac{M}{2r}\right)^2}{\left(1+\frac{M}{2r}\right)^2} dt^2 + \left(1+\frac{M}{2r}\right)^4 \delta_{ij} dx^i dx^j \\ &= \left(-1+\frac{2M}{r}+O(M^2)\right) dt^2 + \left(1+\frac{2M}{r}+O(M^2)\right) \delta_{ij} dx^i dx^j , \end{aligned} \tag{11}$$

where $r^2 = \delta_{ij} x^i x^j$. Here and in the rest of this section, r denotes the isotropic radial coordinate, while the conventional Schwarzschild radial coordinate will be denoted by r_s. These two radial coordinates are related as

$$r_s = r\left(1+\frac{M}{2r}\right)^2 = r + M + \frac{M^2}{4r} . \tag{12}$$

It should be noted that the isotropic coordinates satisfy the harmonic gauge condition to 1PM order.

The bi-scalar $\sigma(x,x')$ accurate to 1PM order can be found in a classic paper by Thorne and Kovacs[9], or in Leonard and Poisson[6]. To this order, the geodesic connecting x and x' can be approximated by a straightline on the flat background:

$$\xi^\mu(\lambda) = x'^\mu + \lambda X^\mu ; \quad X^\mu = x^\mu - x'^\mu , \tag{13}$$

where the affine parameter λ is normalized so that $\xi^\mu(0) = x'^\mu$ and $\xi^\mu(1) = x^\mu$. We then have

$$\begin{aligned} \sigma(x,x') &= \frac{1}{2}\left(\eta_{\mu\nu} + \int_0^1 h_{\mu\nu}(\xi(\lambda))d\lambda\right) X^\mu X^\nu \\ &= \frac{1}{2}\left(-\Delta t^2(1-F) + R^2(1+F)\right) ; \qquad F = \int_0^1 \frac{2M}{r(\lambda)} d\lambda , \end{aligned} \tag{14}$$

where $\Delta t = t - t'$ and $R^2 = \delta_{ij}(x^i - x'^i)(x^j - x'^j)$. The 1PM correction factor F can be calculated exactly:

$$\begin{aligned} F &= \frac{2M}{R} \ln \frac{(r+r'+R)}{(r+r'-R)} = \frac{2M}{r+r'} \sum_{n=0}^{\infty} \frac{2}{2n+1} \left(\frac{R}{r+r'}\right)^{2n} \\ &= \frac{4M}{r+r'} + \frac{4M}{3(r+r')} \left(\frac{R}{r+r'}\right)^2 + O(R^4). \end{aligned} \tag{15}$$

The bi-scalar u accurate to 1PM order is unity because of the Ricci flatness of the Schwarzschild geometry. Thus the direct part of the Green function to 1PM order becomes

$$\begin{aligned} G^{\rm dir} &= \frac{\theta(\Delta t)}{4\pi} 2\delta\left(-\Delta t^2(1-F) + R^2(1+F)\right) \\ &= \frac{\delta\left(\Delta t - R(1+F)\right)}{4\pi R} . \end{aligned} \tag{16}$$

To subtract the direct part from the full Green function, we take the Fourier-harmonic expansion of the direct part. The Fourier transformation of $G^{\rm dir}$ is

$$\begin{aligned}\tilde{G}^{\rm dir}_{\omega}(\mathrm{x},\mathrm{x}') &= \int G^{\rm dir} e^{i\omega\Delta t} d\Delta t = \frac{e^{i\omega R(1+F)}}{4\pi R} \\ &= \frac{e^{i\omega R}}{4\pi R}\left(1 + i\omega RF + O(M^2)\right) . \end{aligned} \tag{17}$$

The direct part of the Green function is explicitly expressed as

$$\tilde{G}_{\ell m\omega} = R^{dir}_{\ell m\omega}(r,r')\, Y_{\ell m}(\Omega)\overline{Y_{\ell m}(\Omega')}, \tag{18}$$

where

$$\begin{aligned} R^{dir}_{\ell m\omega}(r,r') &= \frac{1}{2r'}\left(\frac{r}{r'}\right)^{l} \\ &\quad \left(1 + \frac{M(l+1)}{r'} + \frac{1}{2}\frac{\omega^2 r'^2}{2l-1} - \frac{Ml}{r} - \frac{1}{2}\frac{\omega^2 r^2}{2l+3}\right) . \end{aligned} \tag{19}$$

Here we adopt so-called 'slow-motion' approximation, since a point particle moves sufficiently slower than the light. When v is the characteristic velocity of the velocity of the particle, $\omega r \sim v$ and $M\omega \sim v^3$. We note that this approximation is weaker than the 'post-Newtonian' approximation in the sense that it does not assume the weak gravitational potential. In the above equation, we neglect $o(v^3)$ for the leading term.

4 Regularized Green function

In this section we consider the Green function ${}_sG^{\rm ret}$ for Eq. (7). It satisfies

$$\left[\nabla^{\mu}\nabla_{\mu} + s^2\frac{2M}{r^3}\right] {}_sG^{\rm ret}(x,x') = -\frac{\delta(t-t')\delta(r-r')\delta^2(\Omega-\Omega')}{rr'} . \tag{20}$$

The Fourier-harmonic expansion of it is expressed as

$$\begin{aligned} {}_sG^{\rm ret}(x,x') &= \int \frac{d\omega}{2\pi} e^{-i\omega(t-t')} \sum_{\ell m} {}_sG_{\ell m\omega}(\mathrm{x},\mathrm{x}') ; \\ {}_sG_{\ell m\omega} &= -\frac{X^{\rm up}_{\ell}(r_>)\, X^{\rm in}_{\ell}(r_<)}{rr'\, W(X^{\rm up}_{\ell}, X^{\rm in}_{\ell})}\, Y_{\ell m}(\Omega)\overline{Y_{\ell m}(\Omega')} , \end{aligned} \tag{21}$$

where $r_> = \max\{r,r'\}$, $r_< = \min\{r,r'\}$, $W(X^{\rm up}_{\ell}, X^{\rm in}_{\ell})$ is the Wronskian,

$$W(X^{\rm up}_{\ell}, X^{\rm in}_{\ell}) = \left(\frac{d}{dr^*}X^{\rm up}_{\ell}\right) X^{\rm in}_{\ell} - X^{\rm up}_{\ell}\frac{d}{dr^*}X^{\rm in}_{\ell} , \tag{22}$$

and $X^{\rm up}_{\ell}$ and $X^{\rm in}_{\ell}$ are the homogeneous solutions of the Regge-Wheeler equation having the asymptotic behaviors,[4]

$$\begin{aligned} X^{\rm in}_{\ell} &\sim \begin{cases} \mathcal{A}^{\rm in}_{\ell\omega} e^{-i\omega r^*} + \mathcal{A}^{out}_{\ell\omega} e^{i\omega r^*} & (r\to\infty), \\ e^{-i\omega r^*} & (r\to 2M), \end{cases} \\ X^{\rm up}_{\ell} &\sim \begin{cases} e^{i\omega r^*} & (r\to\infty), \\ \mathcal{D}^{\rm in}_{\ell\omega} e^{-i\omega r^*} + \mathcal{D}^{out}_{\ell\omega} e^{i\omega r^*} & (r\to 2M). \end{cases} \end{aligned} \tag{23}$$

It then follows that $W = 2i\omega\mathcal{A}^{\rm in}_{\ell\omega} = 2i\omega\mathcal{D}^{out}_{\ell\omega}$.

[4] In this paper, we follow Chrzanowski and Misner[7] for notations of the homogeneous solutions.

We consider to derive the Green function explicitly. To the first post-Minkowskian order, the necessary formulas for the radial functions $X_\ell^{\rm in}$ and $X_\ell^{\rm up}$ may be found in Poisson and Sasaki[5] and Leonard and Poisson[6]. Using them, we find

$$\begin{aligned} X_\ell^{\rm in}(z) &= 2\mathcal{A}_{\ell\omega}^{\rm in}(-i)^{\ell+1}e^{i\epsilon(\ln(2\epsilon)-\beta_\ell)}(1+\frac{\pi}{2}\epsilon)\,z\left[j_\ell(z)+\epsilon\,\xi_\ell^{\rm in}(z)+O(\epsilon^2)\right], \\ \xi_\ell^{\rm in}(z) &= -A_\ell(z)j_\ell(z)+B_\ell(z)n_\ell(z)-\frac{\ell^2-s^2}{2\ell(2\ell+1)}j_{\ell-1}(z)+\frac{(\ell+1)^2-s^2}{2(\ell+1)(2\ell+1)}j_{\ell+1}(z), \quad (24) \\ X_\ell^{\rm up}(z) &= i^{\ell+1}e^{-i\epsilon(\ln(2\epsilon)-\beta_\ell)}(1-\frac{\pi}{2}\epsilon)\,z\left[h_\ell^{(1)}(z)+\epsilon\,\xi_\ell^{\rm up}+O(\epsilon^2)\right], \\ \xi_\ell^{\rm up}(z) &= (A_\ell(z)-iB_\ell(z))h_\ell^{(1)}(z)+C_\ell(z)j_\ell(z) \\ &\quad -\frac{\ell^2-s^2}{2\ell(2\ell+1)}h_{\ell-1}^{(1)}(z)+\frac{(\ell+1)^2-s^2}{2(\ell+1)(2\ell+1)}h_{\ell+1}^{(1)}(z), \quad (25) \end{aligned}$$

where $\epsilon = 2M\omega$, $z=\omega r$, and the functions $A_\ell(z)$, $B_\ell(z)$ and $C_\ell(z)$ are given by

$$\begin{aligned} A_\ell(z) &= \mathrm{Si}(2z)+z^2n_0(z)j_0(z)+\sum_{p=1}^{\ell-1}\left(\frac{1}{p}+\frac{1}{p+1}\right)z^2n_p(z)j_p(z), \\ B_\ell(z) &= \mathrm{Ci}(2z)-\gamma-\ln(2z)+z^2j_0(z)^2+\sum_{p=1}^{\ell-1}\left(\frac{1}{p}+\frac{1}{p+1}\right)z^2j_p(z)^2, \\ C_\ell(z) &= 2\left(\frac{\pi}{2}-A_\ell(z)+i\left(B_\ell(z)+\gamma+\ln(2z)\right)\right)-i\left(1+\sum_{p=1}^{\ell-1}\left(\frac{1}{p}+\frac{1}{p+1}\right)z(-1)^pR_{2p,\frac{1}{2}-p}(z)\right) \quad (26) \end{aligned}$$

for $\ell \geq 1$, and

$$\begin{aligned} A_0(z) &= \mathrm{Si}(2z), \\ B_0(z) &= \mathrm{Ci}(2z)-\gamma-\ln(2z), \\ C_0(z) &= 2\left(\frac{\pi}{2}-\mathrm{Si}(2z)+i\mathrm{Ci}(2z)\right), \quad (27) \end{aligned}$$

for $\ell = 0$. It should be noted that Expressions (24) and (25) are valid only for $\omega \geq 0$. For $\omega < 0$ (i.e, for $z<0$), they should be replaced by $\overline{X_\ell^{\rm in}(|z|)}$ and $\overline{X_\ell^{\rm up}(|z|)}$, respectively. With this understanding, we find

$${}_sG_{\ell m\omega} = i\omega\left[j_\ell(z_<)h_\ell^{(1)}(z_>)+\epsilon\left(j_\ell(z_<)\xi_\ell^{\rm up}(z_>)+\xi_\ell^{\rm in}(z_<)h_\ell^{(1)}(z_>)\right)+O(\epsilon^2)\right]Y_{\ell m}(\Omega)\overline{Y_{\ell m}(\Omega')}, \quad (28)$$

or

$$\begin{aligned} {}_sG_{\ell\omega} &:= \sum_m {}_sG_{\ell m\omega} \\ &= \frac{i\omega}{4\pi}(2\ell+1)\left[j_\ell(z_<)h_\ell^{(1)}(z_>)+\epsilon\left(j_\ell(z_<)\xi_\ell^{\rm up}(z_>)+\xi_\ell^{\rm in}(z_<)h_\ell^{(1)}(z_>)\right)+O(\epsilon^2)\right]P_\ell(\mu), \quad (29) \end{aligned}$$

where $\mu = \dfrac{\mathbf{x}\cdot\mathbf{x}'}{|\mathbf{x}|\,|\mathbf{x}'|}$.

The Radial part of the Green function ${}_sG_{\ell m\omega}(s=-2)$ is explicitly expressed as

$$\begin{aligned} {}_sR_{\ell m\omega}^{full}(r,r') &= \frac{1}{2r'}\left(\frac{r}{r'}\right)^l \\ &\quad \left(1-\frac{M\left(-l^2-2l-1+s^2\right)}{(l+1)\,r'}+\frac{1}{2}\frac{\omega^2r'^2}{2l-1}+\frac{M\left(-l^2+s^2\right)}{lr}-\frac{1}{2}\frac{\omega^2r^2}{2l+3}\right). \quad (30) \end{aligned}$$

Here we neglect $o(v^3)$ for the leading term under the slow motion approximation.

By the above analysis, we can obtain the regularized Green function for ${}_sX$ as the following. The regularized Green function, i.e., the tail part of the Green function is derived by subtracting the direct part from the full Green function.

$$ {}_sG_{\ell m\omega} = {}_sR^{tail}_{\ell m\omega}(r,r')\, Y_{\ell m}(\Omega)\overline{Y_{\ell m}(\Omega')}, \tag{31} $$

where

$$ {}_sR^{tail}_{\ell m\omega}(r,r') = \frac{1}{2r'}\left(\frac{r}{r'}\right)^l\left(-\frac{M s^2}{(l+1)r'} + \frac{M s^2}{l r}\right). \tag{32} $$

The tail part depend on only s^2-terms, so **the gravitational reaction force for a scalar field does not appear in the 1PM order**. The above equation is the result of this paper.

5 Summary and discussion

In this paper, we have proposed a new method to evaluate the tail part of the perturbation, and we have constructed the regularized Green function for Regge-Wheeler equation(s^2-terms). This is done easilier than the previous approach [3], since the Green function is regularized before integration with a source and summation of Fourier-harmonic expansion, and the 'gauge problem' does not appear since we regularize the Green function under the same gauge condition. But some procedures remain in order to derive the gravitational reaction force. In the following they are mentioned briefly.

* Transformation from Regge-Wheeler function to Teukolsky function

First, we consider the Chandrasekhar transformation. Here we assume the invariance of the causal structure under this transformation, that is to say, it is thought that the tail part of the Regge-Wheeler function bring about the one of the Teukolsky function. This invariance of the causal structure should be probed. And then, the point particle moving on a circular orbit is regarded as a source, the Weyl scalar Ψ_4 is calculated.

* Construction of metric and regularized force;

Using the method of Chrzanowski[1], we are able to derive the metric perturbation from Ψ_4 which is calculated by the above procedure. The gravitational reaction force is given by the formula (2). The reacton force at a point particle is evaluated by the coincidence limit $r \to r_0$ after summing over ℓ, m and ω in the Fourier-harmonic expansion.

We hope that the result agree with the standard post-Newtonian calculation, and moreover, by the higher order calculation it will be compared the energy and angular momentum loss with the balance equation which is derived up to now. Furthermore, The application of the consideration in this paper is limited to the simple case of a circlular orbit around a black hole, but the method constructed here can be extended to more complicated situations, for example, a slightly eccentric orbit around a black hole.

Acknowledgements

We thank all the members of the theoretical gravitational-wave physics group in Japan and all the members of the theoretical astrophysics group at Osaka University for fruitful conversations. Special thanks are due to T. Tanaka, H. Tagoshi, G. Uchida, Y. Himemoto and N. Sago for invaluable discussions. The author(H.N.) is supported by Research Fellowships of the Japan Society for the Promotion of Science for Young Scientists, No.2397.

References

[1] P.L. Chrzanowski, Phys. Rev. D11, 2042 (1975).

[2] Y. Mino, Prog. Theor. Phys. **99**, 79 (1998).

[3] Y. Mino and H. Nakano, Prog. Theor. Phys. **100**, 507 (1998).

[4] A. Teukolsky, Astrophys. J. **185**, 635 (1973).

[5] E. Poisson and M. Sasaki, Phys. Rev. **D51**, 5753 (1994).

[6] S.W. Leonard and E. Poisson, Phys. Rev. **D56**, 4789 (1997).

[7] P.L. Chrzanowski and C.W. Misner, Phys. Rev. **D10**, 1701 (1974).

[8] B.S. DeWitt and R.W. Brehme, Ann. Phys. (N.Y.) **9**, 220 (1960).

[9] K.S. Thorne and S.J. Kovacs, Astrophys. J. **200**, 245 (1975).

Gravitational waves from inspiralling compact binaries with magnetic dipole moments

Kunihito Ioka[1]

Department of Physics, Kyoto University, Sakyo-ku, Kyoto 606-8502, Japan

Keisuke Taniguchi[2]

Yukawa Institute for Theoretical Physics, Kyoto University, Kyoto 606-8502, Japan
Département d'Astrophysique Relativiste et de Cosmologie, UPR 8629 du C.N.R.S., Observatoire de Paris, F-92195 Meudon Cedex, France

Abstract

We investigate the effects of the magnetic dipole-dipole coupling and the electromagnetic radiation on the frequency evolution of gravitational waves from inspiralling binary neutron stars with magnetic dipole moments. This study is motivated by the discovery of the superstrongly magnetized neutron stars, i.e., magnetar. We derive the contributions of the magnetic fields to the accumulated cycles in gravitational waves as $N_{mag} \sim 6 \times 10^{-3}(H/10^{16}\mathrm{G})^2$, where H denotes the strength of the polar magnetic fields of each neutron star in the binary system. It is found that the effects of the magnetic fields will be negligible for the detection and the parameter estimation of gravitational waves, if the upper limit for magnetic fields of neutron stars are less than $\sim 10^{16}$G, which is the maximum magnetic field observed in the soft gamma repeaters and the anomalous X-ray pulsars up to date. We also discuss the implications of electromagnetic radiation from the inspiralling binary neutron stars for the precursory X-ray emission prior to the gamma ray burst observed by the Ginga satellite.

1 INTRODUCTION

Direct detection of gravitational waves (GWs) is one of the most exciting challenges in the history of science. Long baseline interferometers for detection of GWs such as TAMA300 [1], GEO600 [2], VIRGO [3], and LIGO [4] will be in operation within five years. One of the most promising sources of GWs for such detectors is the inspiralling binary neutron stars (BNSs), since we may expect several coalescing events per year within 200Mpc [5, 6, 7].

As the orbital radius of BNSs decays due to gravitational radiation reaction, the frequency of GWs sweeps upward in detector's sensitive bandwidth from $\sim$ 10Hz to $\sim$ 1000Hz. In the early inspiralling phase of BNSs, each neutron star (NS) can be treated as a point particle and the post-Newtonian (PN) expansion will converge [8] since the orbital separation of NSs is much larger than the NS's radius and the orbital velocity is much smaller than the velocity of light. This means that the theoretical templates of GWs in the inspiralling phase can be calculated with high accuracy by the PN approximation of general relativity using only several parameters: each mass and spin of NSs and the initial orbital elements. By cross correlating the observed noisy signals with the theoretical templates, the binary parameters, such as masses, spins [8, 9, 10, 11], and cosmological distances [12], are determined. The number of rotation of BNSs is about 16000 in the detector's sensitive bandwidth. Therefore, the quite accurate theoretical templates are needed in order to extract physical information about BNSs from GWs since any effect that causes only one cycle ambiguity over 16000 accumulated cycles in the theoretical templates will reduce the signal-to-noise ratio (SNR). For the inspiralling BNSs in the sensitive bandwidth, with $v^2 \sim m/r$ (hereafter $G = c = 1$) typically around 10^{-2}, the correction of $1/16000 \sim 10^{-4}$ corresponds to second PN

[1] E-mail:iokakuni@tap.scphys.kyoto-u.ac.jp
[2] E-mail:Keisuke.Taniguchi@obspm.fr

(2PN) order, $(m/r)^2 \sim 10^{-4}$ [13]. Many efforts are devoted to calculate higher-order PN corrections to theoretical templates [14]. However, these studies pay attention only to the gravitational effects on the theoretical templates, and it has not been studied how large corrections to the theoretical templates are caused by the electromagnetic effects, i.e., the magnetic fields of NSs, as far as we know.

NSs observed as radio pulsars are believed to have strong magnetic fields, typically $\sim 10^{12}$G, assuming that the spin-down of pulsars is due to magnetic dipole radiation. In addition, it begins to be recognized recently that NSs with superstrong magnetic fields $\gtrsim 10^{14}$G really exist (see below). We can crudely estimate the correction to the waveform due to magnetic dipole fields of NSs by comparing the gravitational force $F_G \sim m_1 m_2/r^2$ and the magnetic force $F_M \sim 3\mu_1\mu_2/r^4$ between BNSs of masses, m_1 and m_2, with magnetic dipole moments, μ_1 and μ_2, as

$$\frac{F_M}{F_G} = 1\times 10^{-4}\left(\frac{r}{6(m_1+m_2)}\right)^{-2}\left(\frac{H_1}{2\times 10^{16}\mathrm{G}}\right)\left(\frac{H_2}{2\times 10^{16}\mathrm{G}}\right) \times\left(\frac{R_1}{10^6\mathrm{cm}}\right)^3\left(\frac{R_2}{10^6\mathrm{cm}}\right)^3\left(\frac{1.4M_\odot}{m_1}\right)\left(\frac{1.4M_\odot}{m_2}\right)\left(\frac{2.8M_\odot}{m_1+m_2}\right)^2, \quad (1)$$

where $H_p = 2\mu_p/R_p^3$ $(p = 1, 2)$ are the magnetic fields at the pole of the star and R_p are radii of NSs. This corresponds to the 2PN order correction. Therefore, the magnetic fields of order $\sim 10^{16}$G might cause about one rotation error. Note that the r-dependence of the magnetic correction is the same as that of 2PN order, $v^4 \propto r^{-2}$, so that this argument is independent of the value of the separation r.

Theoretically, in a new born NS, such superstrong magnetic fields $\sim 10^{16}$ G can be generated if the initial spin is in millisecond range since the conditions for helical dynamo action are met during the first few seconds after gravitational collapse [15, 16]. Observationally, such a superstrongly magnetized NS, or "magnetar", may be found as the soft gamma repeaters (SGRs) and the anomalous X-ray pulsars (AXPs) [15, 17]. The dipolar magnetic fields of SGRs are estimated as $\sim 10^{15}$G by using the measured spin periods with spin-down rates for SGR1900+14 [18, 19] and SGR1806-20 [20], and with the peak luminosity for SGR1627-41 [21]. APXs that have measured the spin-down rate [22, 23, 24, 25, 26] can be considered to have magnetic fields of 10^{14}–10^{15}G. Although there are some other models for SGRs and AXPs, these objects are best understood within the framework of magnetar (see, e.g., [27, 20, 25]). Therefore, from both theoretical and observational results, it may be possible that a NS has superstrong magnetic fields $\sim 10^{16}$G.

In this paper we investigate the effects of the magnetic dipole fields of NSs on the frequency evolution of GWs from the inspiralling BNSs, since the magnetic fields of order $\sim 10^{16}$G might cause about one rotation error. Throughout the paper, we use the relation $H = 2\mu/R^3$ to connect the magnetic moment μ to the magnetic field at the magnetic pole H, and $R = 10^6$cm as the radius of a NS. For later convenience, note that $\mu = 1.4\times 10^9 (H/10^{16}\mathrm{G})$ cm^2 in units of $G = c = 1$.

2 EQUATIONS OF MOTION

We consider a binary system of two compact bodies of masses, m_1 and m_2, with magnetic dipole moments, μ_1 and μ_2, respectively. Since we pay particular attention to the effects of magnetic fields, we treat the orbital motion of BNSs in Newtonian gravity. Although a spherical symmetry of the stellar configuration is, in general, incompatible with the presence of magnetic fields [28], we ignore quadrupole effects which are caused by magnetic fields for a moment (see §5). We also neglect tidal effects which are expected to be small until pre-merging phase of BNSs [29].

By eliminating the motion of the center of mass of BNSs and setting the origin of the coordinate frame at the center of mass of BNSs, the effective one-body equations of motion can be derived from a Lagrangian,

$$\mathcal{L} = \frac{1}{2}\eta m v^2 + \frac{\eta m^2}{r} + \mathcal{L}_{DD}, \quad (2)$$

where

$$\mathcal{L}_{DD} = \mu_1 \cdot H_2 = \frac{1}{r^3}\left\{3(\hat{n}\cdot\mu_1)(\hat{n}\cdot\mu_2) - \mu_1\cdot\mu_2\right\}. \quad (3)$$

Here $m = m_1+m_2$, $\eta = m_1m_2/m^2$, $r = |\boldsymbol{x}|$, $\boldsymbol{x} = \boldsymbol{x}_1-\boldsymbol{x}_2$, $\hat{\boldsymbol{n}} = \boldsymbol{x}/r$, $\boldsymbol{v} = \dot{\boldsymbol{x}}$, and $\boldsymbol{H}_2 = \{3(\hat{\boldsymbol{n}}\cdot\boldsymbol{\mu}_2)\hat{\boldsymbol{n}} - \boldsymbol{\mu}_2\}/r^3$ is the magnetic field at $\boldsymbol{x}_1$ produced by the magnetic moment $\boldsymbol{\mu}_2$. By using the Euler-Lagrange equations, we obtain the equations of motion as

$$\boldsymbol{a} = -\frac{m}{r^2}\hat{\boldsymbol{n}} + \boldsymbol{a}_{DD}, \tag{4}$$

where $\boldsymbol{a} = \ddot{\boldsymbol{x}}$ and

$$\boldsymbol{a}_{DD} = \frac{3}{\eta m r^4}\left\{(\boldsymbol{\mu}_1\cdot\boldsymbol{\mu}_2)\hat{\boldsymbol{n}} + (\hat{\boldsymbol{n}}\cdot\boldsymbol{\mu}_2)\boldsymbol{\mu}_1 + (\hat{\boldsymbol{n}}\cdot\boldsymbol{\mu}_1)\boldsymbol{\mu}_2 - 5(\hat{\boldsymbol{n}}\cdot\boldsymbol{\mu}_1)(\hat{\boldsymbol{n}}\cdot\boldsymbol{\mu}_2)\hat{\boldsymbol{n}}\right\}. \tag{5}$$

From equation (2), the energy of this system is given by

$$E = \frac{1}{2}\eta m v^2 - \frac{\eta m^2}{r} + E_{DD}, \tag{6}$$

where

$$E_{DD} = -\frac{1}{r^3}\left\{3(\hat{\boldsymbol{n}}\cdot\boldsymbol{\mu}_1)(\hat{\boldsymbol{n}}\cdot\boldsymbol{\mu}_2) - \boldsymbol{\mu}_1\cdot\boldsymbol{\mu}_2\right\}. \tag{7}$$

The total angular momentum can be defined as $\boldsymbol{L} = \boldsymbol{L}_N + \boldsymbol{S}$ where $\boldsymbol{L}_N = \eta m(\boldsymbol{x}\times\boldsymbol{v})$ is the Newtonian orbital angular momentum and $\boldsymbol{S} = \boldsymbol{S}_1+\boldsymbol{S}_2$ is the total spin angular momentum. We can show explicitly $\dot{E} = \dot{\boldsymbol{L}} = 0$ with the equations of motion (4) and the evolution equations of the spins,[3]

$$\dot{\boldsymbol{S}}_p = \boldsymbol{\mu}_p\times\boldsymbol{H}_q = \frac{1}{r^3}\left\{3(\hat{\boldsymbol{n}}\cdot\boldsymbol{\mu}_q)(\boldsymbol{\mu}_p\times\hat{\boldsymbol{n}}) - \boldsymbol{\mu}_p\times\boldsymbol{\mu}_q\right\}. \quad (p,q = 1,2) \tag{8}$$

Assuming NSs as spherical compact bodies, the spin angular velocities $\boldsymbol{\Omega}_p$ are related to the spins $\boldsymbol{S}_p$ as $\boldsymbol{S}_p = I_p\boldsymbol{\Omega}_p$ where I_p is the principle moment of inertia of the bodies. Since the magnetic moments evolve as $\dot{\boldsymbol{\mu}}_p = \boldsymbol{\Omega}_p\times\boldsymbol{\mu}_p = \boldsymbol{S}_p\times\boldsymbol{\mu}_p/I_p$, the angular velocities of the magnetic moments Ω_p will be of order $\Omega_p \sim (\mu_1\mu_2/mR^2r^3)^{1/2}$ from dimensional analysis with equation (8). Note also that the orbital angular velocity w is of order $w \sim (m/r)^{3/2}/m$, and the orbital inspiral rate $w_{ins} = (dE/dt)_{GW}/E$ is of order $w_{ins} \sim (m/r)^4/m$.

3 GRAVITATIONAL WAVES AND ELECTROMAGNETIC WAVES

As a first step, we use the quadrupole formula to derive the rate of energy loss from a binary system due to GWs. The symmetric, trace-free parts of the quadrupole moments of this system are given by $I_{ij} = \eta m(x_ix_j - \frac{1}{3}r^2\delta_{ij})$. Taking third time derivatives of these quadrupole moments, we obtain the energy loss rate from the quadrupole formula as

$$\begin{aligned}\left(\frac{dE}{dt}\right)_{GW} &= -\frac{1}{5}\left\langle \dddot{I}_{ij}\dddot{I}_{ij}\right\rangle \\ &= -\frac{8}{15}\frac{\eta^2m^4}{r^4}\Bigg\{12v^2 - 11\dot{r}^2 \\ &\quad + \frac{1}{\eta m^2r^2}\Big[6(-12v^2+13\dot{r}^2)(\boldsymbol{\mu}_1\cdot\boldsymbol{\mu}_2) + 12(21v^2-34\dot{r}^2)(\hat{\boldsymbol{n}}\cdot\boldsymbol{\mu}_1)(\hat{\boldsymbol{n}}\cdot\boldsymbol{\mu}_2) \\ &\quad -36(\boldsymbol{v}\cdot\boldsymbol{\mu}_1)(\boldsymbol{v}\cdot\boldsymbol{\mu}_2) + 87\dot{r}\left\{(\hat{\boldsymbol{n}}\cdot\boldsymbol{\mu}_1)(\boldsymbol{v}\cdot\boldsymbol{\mu}_2) + (\boldsymbol{v}\cdot\boldsymbol{\mu}_1)(\hat{\boldsymbol{n}}\cdot\boldsymbol{\mu}_2)\right\}\Big]\Bigg\},\end{aligned} \tag{9}$$

where we have used the equations of motion (4) and assumed $\mu_1\mu_2/m^2r^2 \ll 1$.

[3]Note that there are no spin-orbit and spin-spin interactions since we consider Newtonian gravity. The spins are generated by the torque due to the magnetic dipole-dipole interaction.

On the other hand, electromagnetic (EM) waves are also emitted from this binary system since the magnetic moments are moving. Using the linearity in the EM fields, the radiation fields $\boldsymbol{B}_0^{rad}$ in equation (29) for this binary system are given by

$$\boldsymbol{B}_0^{rad} = \frac{1}{D}(\hat{\boldsymbol{d}} \cdot \boldsymbol{\mu}_{eff}) \left\{ (\hat{\boldsymbol{d}} \cdot \dot{\boldsymbol{a}}) \hat{\boldsymbol{d}} - \dot{\boldsymbol{a}} \right\}, \tag{10}$$

where

$$\boldsymbol{\mu}_{eff} = \frac{1}{m}(m_2 \boldsymbol{\mu}_1 - m_1 \boldsymbol{\mu}_2). \tag{11}$$

Therefore, since the radiated power is given by equation (31), the rate of energy loss due to the EM radiation is calculated as

$$\left(\frac{dE}{dt}\right)_{EM} = -\frac{2}{15}\frac{m^2}{r^6}\left[2\mu_{eff}^2 \left\{ v^2 - 6\dot{r}(\hat{\boldsymbol{n}} \cdot \boldsymbol{v}) + 9\dot{r}^2 \right\} - \left\{ \boldsymbol{\mu}_{eff} \cdot (\boldsymbol{v} - 3\dot{r}\hat{\boldsymbol{n}}) \right\}^2 \right], \tag{12}$$

where we have substituted $\boldsymbol{\mu}_{eff}$ into $\boldsymbol{\mu}$ in equation (31).

Note that the assumption of the constant magnetic moments in equations (9), (10) and (29) is valid since the angular velocities of the magnetic moments $\Omega_p \sim (\mu_1 \mu_2 / m R^2 r^3)^{1/2}$ are much smaller than the orbital angular velocities $w \sim (m/r)^{3/2}/m$ when $(H_1 H_2)^{1/2} \ll 10^{18}$G.

4 INSPIRAL OF CIRCULAR ORBITS

For calculational simplicity we assume that the orbital motion of BNSs has decayed to be circular apart from the adiabatic inspiral [30, 31]. In general, circular orbit solutions of equation (4) do not exit unless the magnetic moments are aligned perpendicular to the orbital plane. However, since the angular velocities of the magnetic moments $\Omega_p \sim (\mu_1 \mu_2 / m R^2 r^3)^{1/2}$ are much smaller than the orbital angular velocity $w \sim (m/r)^{3/2}/m$ when $(H_1 H_2)^{1/2} \ll 10^{18}$G, we can regard the magnetic moment vectors and $\hat{\boldsymbol{L}}$ as time-independent ones over an orbit where $\hat{\boldsymbol{L}}$ is a unit vector orthogonal to the orbital plane. Then, after taking an average of the magnetic term in the acceleration (5), we can obtain orbits of constant separation, $\ddot{r} = \dot{r} = \hat{\boldsymbol{n}} \cdot \boldsymbol{v} = 0$, $w = v/r$, $\boldsymbol{L}_N = \eta m r^2 w \hat{\boldsymbol{L}}$ (see similar discussions on spin precessions, [9, 32]). From the equations of motion for circular orbits, $\hat{\boldsymbol{n}} \cdot \boldsymbol{a} = \ddot{r} - r w^2$, we can calculate the orbital angular velocity as

$$w^2 = \frac{m}{r^3}\left[1 + \frac{3}{2\eta m^4}\left(\frac{m}{r}\right)^2 \left\{ \boldsymbol{\mu}_1 \cdot \boldsymbol{\mu}_2 - 3(\hat{\boldsymbol{L}} \cdot \boldsymbol{\mu}_1)(\hat{\boldsymbol{L}} \cdot \boldsymbol{\mu}_2) \right\}\right], \tag{13}$$

where we have used the orbit-averaged relation,

$$\overline{(\hat{\boldsymbol{n}} \cdot \boldsymbol{\mu}_1)(\hat{\boldsymbol{n}} \cdot \boldsymbol{\mu}_2)} = \frac{1}{2}\left\{ \boldsymbol{\mu}_1 \cdot \boldsymbol{\mu}_2 - (\hat{\boldsymbol{L}} \cdot \boldsymbol{\mu}_1)(\hat{\boldsymbol{L}} \cdot \boldsymbol{\mu}_2) \right\}. \tag{14}$$

The total energy and the energy loss rate for a circular orbit, averaged over an orbit, can be obtained as

$$-E = \eta \frac{m^2}{2r}\left[1 - \frac{1}{2\eta m^4}\left(\frac{m}{r}\right)^2 \left\{ \boldsymbol{\mu}_1 \cdot \boldsymbol{\mu}_2 - 3(\hat{\boldsymbol{L}} \cdot \boldsymbol{\mu}_1)(\hat{\boldsymbol{L}} \cdot \boldsymbol{\mu}_2) \right\}\right], \tag{15}$$

$$\begin{aligned} \frac{dE}{dt} &= \left(\frac{dE}{dt}\right)_{GW} + \left(\frac{dE}{dt}\right)_{EM} \\ &= -\frac{32}{5}\eta^2 \left(\frac{m}{r}\right)^5 \left[1 + \frac{9}{2\eta m^4}\left(\frac{m}{r}\right)^2 \left\{ \boldsymbol{\mu}_1 \cdot \boldsymbol{\mu}_2 - 3(\hat{\boldsymbol{L}} \cdot \boldsymbol{\mu}_1)(\hat{\boldsymbol{L}} \cdot \boldsymbol{\mu}_2) \right\} \right. \\ &\quad \left. + \frac{1}{96\eta^2 m^4}\left(\frac{m}{r}\right)^2 \left\{ 3\mu_{eff}^2 + (\boldsymbol{\mu}_{eff} \cdot \hat{\boldsymbol{L}})^2 \right\}\right], \end{aligned} \tag{16}$$

by using equations (6), (9), (12) and (13).

Combining equations (13), (15) and (16), we can express the change rate of the orbital angular velocity $\dot{w}$ as a function of w,

$$\dot{w} = \frac{96}{5}\eta m^{5/3} w^{11/3}\left\{1 + \sigma_{mag}(mw)^{4/3}\right\}, \tag{17}$$

where

$$\sigma_{mag} = \frac{5}{\eta m^4}\left\{\mu_1\cdot\mu_2 - 3(\hat{L}\cdot\mu_1)(\hat{L}\cdot\mu_2)\right\} + \frac{1}{96\eta^2 m^4}\left\{3\mu_{eff}^2 + (\mu_{eff}\cdot\hat{L})^2\right\}. \tag{18}$$

By using equation (17), we calculate the accumulated number of GW cycles $N = \int(f/\dot{f})df$, where $f = w/\pi$ is the frequency of the quadrupolar waves. For calculational simplicity, we assume that the two magnetic moments are aligned parallel to the orbital axis of the binary system. In this case, σ_{mag} becomes a constant value. Then, the accumulated number is integrated as

$$N = N_{grav} + N_{mag}, \tag{19}$$

where N_{grav} and N_{mag} denote the contributions from the Newtonian gravity term and the magnetic term respectively, and are expressed as

$$N_{grav} = -\frac{1}{32\pi\eta}(\pi m f)^{-5/3}\Big|_{f_{min}}^{f_{max}}, \tag{20}$$

$$N_{mag} = \frac{5}{32\pi\eta}\sigma_{mag}(\pi m f)^{-1/3}\Big|_{f_{min}}^{f_{max}}. \tag{21}$$

Here f_{max} is the exit frequency and f_{min} is the entering one of the detector's bandwidth.

5 ·DISCUSSION

Using 10Hz as the entering frequency and 1000Hz as the exit one, we obtain the contribution to the total number of GW cycles from the magnetic term as

$$N_{mag} = -5.9\times10^{-3}\left(\frac{H_1}{10^{16}\mathrm{G}}\right)\left(\frac{H_2}{10^{16}\mathrm{G}}\right)\left(\frac{m}{2\times1.4M_\odot}\right)^{-13/3}, \tag{22}$$

where we assume $\mu_1\cdot\mu_2 < 0$, $\mu_1 \parallel \hat{L}$, $\mu_2 \parallel \hat{L}$,[4] and $m_1 = m_2$. Note that the contribution of the EM radiation reaction (the second term in equation (18)) is much less than that of the dipole-dipole interaction (the first term in equation (18)). The maximum magnetic field allowed by the scalar virial theorem is $\sim 10^{18}$G for NSs [28, 33]. If NSs in the inspiralling BNSs have such magnetic fields $10^{17}\mathrm{G} \lesssim H \lesssim 10^{18}\mathrm{G}$, the effects of the magnetic fields can change more than one cycle in the accumulated cycles. However, if we consider that the maximum value of the observed fields $\sim 10^{16}$ G is the upper limit for the magnetic fields of NSs, the magnetic term will make negligible contributions to the accumulated phase, contrary to the crude estimate in §1 and equation (1). Consequently, the magnetic fields of NSs will not present difficulties for the detection of GWs from BNSs, if the upper limit for the magnetic fields of NSs is less than $\sim 10^{16}$G.

The magnetic term in equation (17) has the same dependence on the angular velocity w as 2PN terms. We can see this dependence from the 2PN expression for the frequency sweep [13],

$$\dot{w} = \frac{96}{5}\eta m^{5/3} w^{11/3}\left\{1 - \left(\frac{743}{336}+\frac{11}{4}\eta\right)(mw)^{2/3} + (4\pi-\beta)(mw) + \left(\frac{34103}{18144}+\frac{13661}{2016}\eta+\frac{59}{18}\eta^2+\sigma\right)(mw)^{4/3}\right\}, \tag{23}$$

[4]This set of configurations, $\mu_1\cdot\mu_2 < 0$, $\mu_1 \parallel \hat{L}$ and $\mu_2 \parallel \hat{L}$, is the most stable one, i.e., the EM interaction energy in equation (7) becomes the minimum value. However, note that the alignment rate of the magnetic moments w_{ali} is smaller than the orbital inspiral rate $w_{ins} \sim (m/r)^4/m$ when $H \lesssim 10^{16}(r/10^{11}\mathrm{cm})^{-1/4}$ G, since the alignment rate w_{ali} can be estimated as $w_{ali} \sim$ (energy loss rate due to magnetic dipole radiation)$/E_{DD} \sim (\mu\Omega_p^2)/(\mu^2/r^3) \sim \mu^4/r^3m^2R^4$ when $\mu_1 \sim \mu_2 \sim \mu$.

where the spin-orbit parameter is $\beta = \frac{1}{12}\Sigma_p(113m_p^2/m^2 + 75\eta)\hat{\boldsymbol{L}}\cdot\boldsymbol{\chi}_p$, the spin-spin parameter is $\sigma = (\eta/48)(-247\boldsymbol{\chi}_1\cdot\boldsymbol{\chi}_2 + 721\hat{\boldsymbol{L}}\cdot\boldsymbol{\chi}_1\hat{\boldsymbol{L}}\cdot\boldsymbol{\chi}_2)$ and $\boldsymbol{\chi}_p = \boldsymbol{S}_p/m_p^2$. As we can see from equations (17) and (23), we cannot distinguish the magnetic term σ_{mag} from the spin-spin term σ at 2PN order. Only the sum of the magnetic term and the spin-spin term can be deduced from the frequency evolution of 2PN order. This degeneracy might be broken by examining the wave-form modulations caused by the spin-induced precession of the orbit [34, 32]. However, the analysis of Poisson & Will [11] shows that the measurement error on the spin-spin term is $\Delta\sigma \sim 17.3$ assuming that the SNR is 10, $\beta = 0$, $\sigma = 0$ and there is no prior information. On the other hand, the contribution of the magnetic term is estimated as

$$\sigma_{mag} = 2.9\times10^{-3}\left(\frac{H_1}{10^{16}\mathrm{G}}\right)\left(\frac{H_2}{10^{16}\mathrm{G}}\right)\left(\frac{m}{2\times1.4M_\odot}\right)^{-4}, \tag{24}$$

where we assume $\boldsymbol{\mu}_1\cdot\boldsymbol{\mu}_2 < 0$, $\boldsymbol{\mu}_1 \parallel \hat{\boldsymbol{L}}$, $\boldsymbol{\mu}_2 \parallel \hat{\boldsymbol{L}}$ and $m_1 = m_2$. We can see from this equation that the contribution of the magnetic fields of NSs is much smaller than the measurement error on the spin-spin term. Therefore, the effects of the magnetic fields of NSs are also negligible for parameter estimation with moderate SNR if we consider that the maximum value of the observed fields $\sim 10^{16}$G is the upper limit for the magnetic fields of NSs.

In this paper, we regard NSs as spherical compact bodies. However, when we consider NSs as extended bodies, we have to take into account of the quadrupole effects induced by magnetic fields. The magnetic fields are a source of non-hydrostatic stress in the interiors of NSs. A magnetic dipole moment μ would give rise to moment differences of order

$$\epsilon := \frac{I_c - I_a}{I_a} \sim \frac{R^4H^2}{m^2}, \tag{25}$$

where I_c and I_a refer to the moments of inertia about the dipole axis and about an axis in the magnetic equator. Then, the gravitational potential $\eta m^2/r$ between NSs is modified by an amount of order $mI_a\epsilon/r^3 \sim \mu^2/r^3$. This is the same order as the EM interaction term in equation (2) when $\mu_1 \sim \mu_2$. Therefore, an accurate ellipticity ϵ in equation (25) is needed to determine the magnetic effects within a factor [33, 35]. Note that there are such quadrupole effects even if only one companion has magnetic moment.

Although the effects of the magnetic fields of NSs will be negligible for observations of GWs, they might be concerned with gamma ray bursts (GRBs). The BNS merger is one of models of GRB sources. (see, e.g., [36] for a review). If a NS in the binary system has strong magnetic fields, the total energy emitted by EM waves until coalescence can be estimated from equations (13), (16) and (17) as $-\int(dE/dt)_{EM}dt \sim \pi^2\mu_{eff}^2(f_{max}^2 - f_{min}^2)/144\eta m \sim 10^{46}(H/10^{16}\mathrm{G})^2(f_{max}/10^3\mathrm{Hz})^2$ ergs. This energy will be radiated at very low frequency $\sim 10^3$ Hz, which is difficult to be observed by the present radio telescope. Furthermore such radiation cannot propagate a plasma if an electron density is larger than $\sim 0.01\mathrm{cm}^{-3}$ since the plasma frequency is larger than the radiation frequency (e.g. [37]). However, this energy may be converted to the thermal energy of the surrounding plasma efficiently if the electron density n_e is sufficiently high since the electron-electron relaxation time is about $t_{rel} \sim 1(n_e/10^{11}\mathrm{cm}^{-3})^{-1}(kT_e/2\mathrm{keV})^{3/2}$ s where T_e is the electron temperature (e.g. [37]). Then, this thermal radiation might explain the precursory X-ray emission ~ 10 s before the onset of the GRB observed by the Ginga satellite, in which the total energy of the X-ray precursor emission is estimated to be about $\sim 10^{46}(d/100\mathrm{Mpc})^2$ ergs [38].

ACKNOWLEDGMENTS

We would like to thank H. Sato and T. Nakamura for continuous encouragement and useful discussions. We are also grateful to T. Tanaka, R. Nishi, K. Nakao, T. Harada and K. Omukai for useful discussions. This work was supported in part by Grant-in-Aid for Scientific Research Fellowship (No.9627: KI) and (No.9402: KT) of the Japanese Ministry of Education, Science, Sports and Culture.

A ELECTROMAGNETIC RADIATION FROM A MOVING MAGNETIC MOMENT

In this section we review the radiation from a moving magnetic dipole moment. We consider a particle with only a magnetic dipole moment μ' in its rest frame K'. A moving magnetic dipole moment with velocity $v = \dot{x}$ relative to an observer frame K also has an associated electric dipole moment. The apparent electric dipole moment is

$$p = v \times \mu, \tag{26}$$

where $\mu = \mu' - \frac{\gamma}{\gamma+1}(v \cdot \mu')v$ is the magnetic moment observed in K and $\gamma = (1-v^2)^{-1/2}$ [39]. Therefore, in the observer frame K the magnetization density M and electric polarization density P are given by

$$\begin{aligned} M(t,z) &= \mu(t)\delta[z - x(t)], \\ P(t,z) &= p(t)\delta[z - x(t)], \end{aligned} \tag{27}$$

where p is given by equation (26). Recalling that the moving magnetic moment is equivalent to a current $J = \nabla \times M + \dot{P}$ [39], we can calculate the electric and magnetic fields. For our purpose, it is sufficient to obtain the radiative parts which fall off as the inverse of the distance D^{-1}. The radiation field B^{rad} of this moving magnetic moment is given by (e.g. [40])

$$\begin{aligned} B^{rad}(t,z) &= \frac{3\hat{d}\times(\hat{d}\times\mu - p)(\hat{d}\cdot a)^2}{DW^5} + \frac{3\hat{d}\times(\hat{d}\times\dot{\mu} - \dot{p})(\hat{d}\cdot a)}{DW^4} \\ &\quad + \frac{\hat{d}\times(\hat{d}\times\mu - p)(\hat{d}\cdot\dot{a})}{DW^4} + \frac{\hat{d}\times(\hat{d}\times\ddot{\mu} - \ddot{p})}{DW^3}, \end{aligned} \tag{28}$$

where $D(t) = z - x(t)$, $\hat{d} = D(t)/|D(t)| = D(t)/D$, $W = 1 - v\cdot\hat{d}$, $a = \dot{v}$ and the right-hand side of this equation is evaluated at the retarded time t', i.e., $t' + D(t') = t$. When we assume that the magnetic dipole moment vector $\mu(t)$ is a constant one, the above equation (28) can be calculated as

$$\begin{aligned} B_0^{rad} &= \frac{1}{D}\left\{\hat{d}\times(\hat{d}\times\mu)(\hat{d}\cdot\dot{a}) - \hat{d}\times\ddot{p}\right\} \\ &= \frac{1}{D}(\hat{d}\cdot\mu)\left\{(\hat{d}\cdot\dot{a})\hat{d} - \dot{a}\right\}, \end{aligned} \tag{29}$$

up to the leading order term of v and $|x|/D$. Note that the radiation field B_0^{rad} becomes the same equation as (29) up to leading order even if we use μ' instead of μ. The power radiated per unit solid angle is given by

$$\frac{dP_0}{d\Omega} = \frac{1}{4\pi}\left(B_0^{rad}\right)^2 D^2 = \frac{1}{4\pi}(\hat{d}\cdot\mu)^2\left\{|\dot{a}|^2 - (\hat{d}\cdot\dot{a})^2\right\}. \tag{30}$$

The total instantaneous power is obtained by integrating equation (30) over all solid angle as

$$P_0 = \frac{2}{15}\left\{2\mu^2|\dot{a}|^2 - (\mu\cdot\dot{a})^2\right\}. \tag{31}$$

References

[1] Kuroda, K., et al. 1997, in Proceedings of International Conference on Gravitational Waves: Sources and Detectors, ed. Ciufolini, I., & Fidecaro, F. (World Scientific, Singapore), 100

[2] Hough, J. 1992, in Proceedings of the Sixth Marcel Grossmann Meeting, ed. Sato, H., & Nakamura, T. (World Scientific, Singapore), 192

[3] Bradaschia, C., et al. 1990, Nucl. Instrum. and Methods, A289, 518

[4] Abramovici, A., et al. 1992, Science, 256, 325

[5] Phinney, E. S., 1991, ApJ, 380, L17

[6] Narayan, R., Piran, T., & Shemi, A. 1991, ApJ, 379, L17

[7] van den Heuvel, E. P. J., & Lorimer, D. R. 1996, MNRAS, 283, L37

[8] Cutler, C., et al. 1993, Phys. Rev. Lett., 70, 2984

[9] Kidder, L. E., Will, C. M., & Wiseman, A. G. 1993, Phys. Rev. D, 47, R4183

[10] Cutler, C., & Flanagan, E. E. 1994, Phys. Rev. D, 49, 2658

[11] Poisson, E., & Will, C. M. 1995, Phys. Rev. D, 52, 848

[12] Schutz, B. F. 1986, Nature, 323, 310

[13] Blanchet, L., Damour, T., Iyer, B. R., Will, C. M., & Wiseman, A. G. 1995, Phys. Rev. Lett., 74, 3515

[14] Blanchet, L. 1996, Phys. Rev. D., 54, 1417

[15] Duncan, R. C., & Thompson, C. 1992, ApJ, 392, L9

[16] Thompson, C., & Duncan, R. C. 1993, ApJ, 408, 194

[17] Thompson, C., & Duncan, R. C. 1996, ApJ, 473, 322

[18] Kouveliotou, C., et al. 1999, ApJ, 510, L115

[19] Woods, P. M., et al. 1999b, astro-ph/9907173

[20] Kouveliotou, C., et al. 1998, Nature, 393, 235

[21] Woods, P. M., et al. 1999a, ApJ, 519, L139

[22] Israel, G. L., et al. 1999, A&A, 346, 929

[23] Mereghetti, S., Israel, G. L., & Stella, L. 1998, MNRAS, 296, 689

[24] Baykal, A., Swank, J. H., Strohmayer, T., & Stark, M. J. 1998, A&A, 336, 173

[25] Vasisht, G., & Gotthelf, E. V. 1997, ApJ, 486, L129

[26] Haberl, F., Motch, C., Buckley, D. A. H., Zickgraf, F. -J., & Pietsch, W. 1997, A&A, 326, 662

[27] Thompson, C., & Duncan, R. C. 1995, MNRAS, 275, 255

[28] Chandrasekhar, S. 1981, Hydrodynamics and Hydromagnetic Stability (Dover, New York), §VIII.

[29] Bildsten, L, & Cutler, C. 1992, ApJ, 400, 175

[30] Peters, P. C., & Mathews, J. 1963, Phys. Rev., 131, 435

[31] Peters, P. C., 1964, Phys. Rev., 136, B1224

[32] Kidder, L. E. 1995, Phys. Rev. D, 52, 821

[33] Bocquet, M., Bonazzola, S., Gourgoulhon, E., & Novak, J. 1995, A&A, 301, 757

[34] Apostolatos, T. A., Cutler, C., Sussman, G. J., & Thorne, K. S. 1994, Phys. Rev. D, 49, 6274

[35] Bonazzola, S., & Gourgoulhon, E. 1996, A&A, 312, 675

[36] Piran, T. 1999, Phys. Rep., in press (astro-ph/9810256)

[37] Spitzer, L., Jr. 1962, Physics of Fully Ionized Gases (New York: Wiley)

[38] Murakami, T., et al. 1991, Nature, 350, 592

[39] Jackson, J. D. 1998, Classical Electrodynamics (New York: Wiley), §14.5.

[40] Heras, J. A. 1994, Am. J. Phys., 62, 1109

Inertial modes of rotating stars

Shijun Yoshida[1] and Umin Lee[2]

Astronomical Institute, Graduate School of Science, Tohoku University, Sendai 980-8578, Japan

Abstract

We investigate inertial mode oscillations of slowly and uniformly rotating, isentropic, Newtonian stars. Using the slow rotation approximation, we study the properties of the inertial modes and r-modes, by taking account of the effect of the rotational deformation of the equilibrium on the eigenfrequencies and eigenfunctions. We also estimate the dissipation timescales due to the gravitational radiation and several viscous processes for polytropic neutron star models. We find that for the inertial modes, the mass multipole gravitational radiation dominates the current multipole radiation, which is dominating in the case of the r-modes.

1 Introduction

Since Andersson [1] suggested and Friedman and Morsink [2] analytically verified that the r-modes of rotating stars are unstable due to the gravitational radiation reaction, much attention has been paid to oscillation modes of rotating neutron stars because of their possible importance in a field of astrophysics. Lindblom et al. [3] argued that due to this instability, the maximum angular rotation velocity of hot young neutron stars is strongly restricted. Owen et al. [4] also suggested that the gravitational radiation emitted from hot young neutron stars due to the r-mode instability is expected to be one of the potential sources for the gravitational wave detectors, e.g. LIGO. Following these earlier investigations on the r-mode instability, there have appeared a number of papers which study the properties of the r-modes of rotating stars (see, e.g., Ref. [5]).

It is well known that r-modes form a sub-class of the modes called "inertial modes", for which the restoring force is the Coriolis force and the characteristic frequency is comparable to the angular rotation frequency Ω of the star [6]. As the prominent characteristics of the r-modes, we know that the toroidal motion dominates the spheroidal motion in the velocity field, and that the frequency ω observed in the corotating frame of the star is given by $\omega = 2m\Omega/(l(l+1))$ in the limit of $\Omega \to 0$, where m and l are the indices of a spherical harmonic function Y_l^m representing the toroidal component of the velocity field [7] [8]. As shown by Lee et al [9], however, the inertial modes in general have the spheroidal component of the velocity field comparable with the toroidal component and do not have any analytical formula to give ω/Ω in the limit of $\Omega \to 0$, except for the case of the Maclaurin spheroids [10][11]. In this paper, to distinguish these two classes of inertial modes, we use the term of "inertial modes" to refer to the inertial modes with the comparable spheroidal and toroidal components of the velocity field, and the term of "r-modes" to refer to the inertial modes whose toroidal component of the velocity field is dominating the spheroidal component.

Very recently, Lockitch and Friedman [12] calculated the inertial modes, assuming an ordering law given by $S_l \sim O(1)$, $H_l \sim O(1)$, $iT_{l'} \sim O(1)$, $\delta\rho \sim O(\Omega^2)$, $\delta p \sim O(\Omega^2)$, $\delta\Phi \sim O(\Omega^2)$, and $\sigma \sim O(\Omega)$, where S_l and H_l are the spheroidal components and $iT_{l'}$ is the toroidal component of the displacement vector, and $\delta\rho$, δp, and $\delta\Phi$ are the Eulerian perturbations of the density, pressure, and gravitational potential, and σ is the oscillation frequency observed in an inertial frame. For r-modes, we may assume an ordering law given as $\sigma \sim O(\Omega)$, $iT_{l'} \sim O(1)$, and $S_l \sim H_l \sim \delta\rho \sim \delta p \sim \delta\Phi \sim O(\Omega^2)$. Lockitch and Friedman [12] showed that a number of inertial modes are unstable because of the gravitational radiation reaction, just as r-modes are, and estimated the dissipation timescales due to the gravitational radiation and some viscous processes for slowly rotating polytropic neutron star models, where they made use of eigenfrequencies and eigenfunctions for slowly rotating Maclaurin spheroids to classify the inertial

[1] E-mail:yoshida@astr.tohoku.ac.jp
[2] E-mail:lee@astr.tohoku.ac.jp

modes. Notice that Lindblom and Ipser [11] obtained analytically eigenfrequencies and eigenfunctions of the inertial mode for the Maclaurin spheroids (see also [10]). Lockitch and Friedman [12] and Lindblom and Ipser [11] called the inertial modes "rotation modes" or "generalized r-modes", which are exactly the same as the inertial modes that will be discussed in this paper.

In this paper, we study the inertial modes and r-modes of slowly rotating stars, by employing a different numerical approach to the problem [13] from the calculations by, e.g., Lindblom et al. [14], and Lockitch and Friedman [12]. Newtonian gravity, uniform rotation, and isentropic structure of the equilibrium are assumed for adiabatic perturbations in this paper. The effects of the rotational deformation of the equilibrium structure on the eigenfunctions and eigenfrequencies are included in the analysis, where the formulation by Lee and Saio [13] has been improved so that the eigenmodes are consistent up to the order of Ω^3.

2 Method of Solutions

We consider oscillations of uniformly rotating Newtonian stars. Thus the angular rotation frequency of the star, Ω is constant. We assume the polytropic relation for the equilibrium structure of the model, and the relation between the pressure p and the mass density ρ is given by

$$p = K\,\rho^{1+\frac{1}{n}}\,, \tag{1}$$

where n and K are the polytropic index and the structure constant determined by giving the mass and the radius of the model, respectively. In this investigation, assuming slow rotation, we employ the Chandrasekhar-Milne expansion (see, e.g., Ref. [15]) to obtain the equilibrium structure of rotating stars. In this technique the effects of the centrifugal force and the equilibrium deformation are treated as small perturbations to the non-rotating spherical symmetric structure of the star. The small expansion parameter due to rotation is chosen as $\tilde{\Omega} = \Omega(R^3/GM)^{1/2}$, where R and M are the radius and the mass of the non-rotating star, respectively. The equilibrium configurations are constructed with accuracy up to the order of $\tilde{\Omega}^2$. For simplicity, we consider a sequence of slowly rotating stars whose central density is the same as that of the non-rotating star.

The governing equations of nonradial oscillations of a rotating star are obtained by linearizing the basic equations used in fluid mechanics (e.g., Ref. [16]). Since the equilibrium state is assumed to be stationary and axisymmetric, the perturbations may be represented by a Fourier component proportional to $e^{i(\sigma t+m\varphi)}$, where σ is the frequency observed in an inertial frame and m is the azimuthal quantum number. In this study, we consider only adiabatic oscillations.

In order to solve the governing equations of nonradial oscillations, we employ the series expansion in terms of spherical harmonics to represent the angular dependence of the perturbed quantities. The Lagrangian displacement vector, ξ^i is expanded in terms of the vector spherical harmonics as

$$\xi^a = \sum_{l\geq|m|}^{\infty} a\,S_l(a)Y_l^m(\theta,\varphi)e^{i\sigma t}\,, \tag{2}$$

$$\xi^\theta = \sum_{l,l'\geq|m|}^{\infty}\left\{H_l(a)Y_l^m{}_{,\theta} + T_{l'}(a)\frac{1}{\sin\theta}\,Y_{l'}^m{}_{,\varphi}\right\}e^{i\sigma t}\,, \tag{3}$$

$$\xi^\varphi = \frac{1}{\sin^2\theta}\sum_{l,l'\geq|m|}^{\infty}\left\{H_l(a)Y_l^m{}_{,\varphi} - T_{l'}(a)\sin\theta\,Y_{l'}^m{}_{,\theta}\right\}e^{i\sigma t}\,, \tag{4}$$

where we employ the parameter a that is constant on a distorted effective potential surface of the star as the radial coordinate, instead of the polar radial coordinate r. The perturbed scalar quantity such as $\delta\Phi$ is expressed as

$$\delta\Phi = \sum_{l\geq|m|}^{\infty}\delta\Phi_l(a)\,Y_l^m(\theta,\varphi)e^{i\sigma t} \tag{5}$$

[17]. Here, the expansion coefficients T_l are called "axial" (or "toroidal") and the other coefficients are called "polar" (or "spheroidal"). It is known that these two set of components are decoupled when $\Omega = 0$.

Substituting the perturbed quantities expanded in terms of the spherical harmonics into the linearized basic equations, we obtain an infinite system of coupled linear ordinary differential equations for the expansion coefficients. Notice that the system of differential equations employed in this paper is arranged to give eigenfunctions and eigenfrequencies consistent up to the order of $\bar{\Omega}^3$ for slow rotation. The explicit expressions for the governing equations are given in Appendix of Yoshida and Lee [18].

Since the equilibrium state of a rotating star is invariant under the parity transformation defined by $\theta \to \pi - \theta$, the linear perturbations have definite parity for that transformation. In this paper, a set of modes whose scalar perturbations such as $\delta\Phi$ are symmetric with respect to the equator is called "even" modes, while the other set of modes whose scalar perturbations are antisymmetric with respect to the equator is called "odd" modes. Note that we do not use the term of the even (the odd) parity mode to refer to the polar (the axial) mode, although this terminology is used traditionally in relativistic perturbation theory (e.g., Ref. [17]).

For numerical calculations, we truncate the infinite set of linear ordinary differential equations to obtain a finite set by discarding all the expansion coefficients associated with l higher than l_{max}. This truncation determines the number of the expansion coefficients kept in the spherical harmonic expansion of each perturbed quantity. We denote this number as k_{max}. Our basic equation becomes a system of $4 \times k_{max}$-th order linear ordinary differential equations, which, together with the boundary conditions, are numerically solved as an eigenvalue problem of $\omega \equiv \sigma + m\Omega$ by using a Henyey type relaxation method (e.g., Ref. [16]).

3 Inertial Modes

We compute the eigenvalues and eigenfunctions of inertial modes and r-modes of rotating polytropic stars with accuracy up to the order of $\bar{\Omega}^3$. In this study, we concentrate our attention to the case of isentropic stars. Since the rotational deformation is of the order of $\bar{\Omega}^2$, the effects on the frequencies ($\propto \bar{\Omega}$) of the inertial modes and r-modes appear as terms of the order of $\bar{\Omega}^3$. For sufficiently small values of $\bar{\Omega}$, therefore, we may expand the eigenfrequency ω of the inertial modes and r-modes of a rotating star in powers of $\bar{\Omega}$ as

$$\frac{\omega}{\Omega} = \kappa_0 + \kappa_2 \bar{\Omega}^2 + O(\bar{\Omega}^4) . \tag{6}$$

In this study, the expansion coefficients κ_0 and κ_2 are obtained by fitting the eigenfrequencies computed for a mode at several small values of $\bar{\Omega}$.

To our knowledge, no well-established classification scheme for inertial modes of a rotating star exists, except for the case of the Maclaurin spheroids, for which exact eigensolutions are known [10][11]. As shown by Bryan [10], eigenmodes of the Maclaurin spheroid can be characterized by the eigenvalue ω/Ω and the angular quantum numbers l_0 and m of the associated Legendre functions of the spheroidal coordinate defined on a surface form of the spheroid. The functional forms of the eigenfunctions in the spheroidal coordinate, which depends on the eigenvalue ω/Ω, are specified by l_0 and m. Since the the spheroidal coordinate employed is dependent on ω/Ω, the functional forms in the actual spatial coordinate are different for different eigenvalues ω/Ω for given l_0 and m. In fact, Lindblom and Ipser [11] have shown that, for given l_0 and m, the eigenvalue κ_0 for inertial modes of the Maclaurin spheroid can be determined, to lowest order of $\bar{\Omega}$, by solving the algebraic equation given by

$$m \frac{d^m}{dx^m} P_{l_0}(\kappa_0/2) + \left(\frac{\kappa_0}{2} - 1\right) \frac{d^{m+1}}{dx^{m+1}} P_{l_0}(\kappa_0/2) = 0 , \tag{7}$$

where $P_l(x)$ is a Legendre polynomial. Here, $m \geq 0$ is assumed. They also have shown that

$$-2 < \kappa_0 < 2 , \tag{8}$$

and that the number of the roots of equation (7) is equal to $l_0 - m$.

In this paper, as a classification scheme for inertial modes of uniformly rotating polytropic stars with $n \neq 0$, we follow the scheme used for the inertial modes of the Maclaurin spheroid, and we pick up

the inertial modes that are similar in the mode character to those of the Maclaurin spheroid, labeling them with the quantum numbers l_0 and m. In practice, the value of l_0 is determined by examining the properties of the eigenfunctions, such as the number of radial nodes of the expansion coefficients, and the number of the dominant expansion coefficients of the eigenfunctions. A similar procedure was employed by Lockitch and Friedman [12]. Notice that our definition of l_0 is not the same as that of Lockitch and Friedman [12], but the same as that of Lindblom and Ipser [11].

In Table 1 we tabulate the eigenvalues (κ_0, κ_2) for inertial modes and r-modes of a polytropic model with $n = 1$. As expected from the results for the Maclaurin spheroid, the value of $l_0 - |m|$ is odd for odd modes and even for even modes. The modes which satisfy the condition $\sigma(\sigma + m\Omega) < 0$ are unstable to the gravitational radiation reaction (see, e.g. [3]), and are marked with an asterisk $*$. We find that a number of inertial modes are unstable to the gravitational radiation reaction, as first shown by Lockitch and Friedman [12]. The modes with $l_0 - |m| = 1$ are r-modes and the frequency to lowest order in Ω is given by $\kappa_0 = 2/(|m| + 1)$, which is independent of the structure of the star. Only the r-modes with $l_0 - 1 = |m|$, for which the toroidal component $iT_{l'}$ associated with $Y^m_{l'=|m|}$ is dominating, are found in isentropic stars, as suggested by Saio [8].

In Table 2, the eigenfrequencies (κ_0, κ_2) of inertial modes and r-modes with $m = 2$ are tabulated for several values of the polytropic index n, to see the dependence of the eigenfrequencies on the equation of state, where the eigenfrequencies for the case of $n = 0$ are obtained by using the results by Lindblom and Ipser [11]. As shown by Table 2, the eigenvalues (κ_0,κ_2) of the inertial modes depend on the polytropic index n, while only the eigenvalue κ_2 of the r-modes is dependent on the index n.

4 Dissipation Timescales

For isentropic stars, we find that a number of inertial modes are unstable to the gravitational radiation reaction in the sense that the frequency σ satisfies the condition $\sigma(\sigma + m\Omega) < 0$. Let us determine the stability of the inertial modes of the isentropic models against the gravitational radiation driven instability, taking account of the dissipative processes due to the shear and bulk viscosity, where we will follow the method of calculation almost the same as that employed in the previous stability analyses of the r-mode and the inertial modes [3][12].

The damping timescale of the inertial modes for sufficiently small $\bar{\Omega}$ may be estimated by [12]

$$\begin{aligned}\frac{1}{\tau} &= \frac{1}{\tilde{\tau}_S}\left(\frac{10^9K}{T}\right)^2 + \frac{1}{\tilde{\tau}_B}\left(\frac{T}{10^9K}\right)^6\left(\frac{\pi G\bar{\rho}}{\Omega^2}\right) \\ &+ \sum_{l=2}^{\infty}\frac{1}{\tilde{\tau}_{J,l}}\left(\frac{\Omega^2}{\pi G\bar{\rho}}\right)^{l+1} + \sum_{l=2}^{\infty}\frac{1}{\tilde{\tau}_{D,l}}\left(\frac{\Omega^2}{\pi G\bar{\rho}}\right)^{l+2}, \end{aligned} \tag{9}$$

where $\bar{\rho}$ is the average density of the star, and the dissipative timescales $\tilde{\tau}$ are calculated for each oscillation mode in the limit of $\bar{\Omega} \to 0$ and are considered not to depend on the rotation frequency Ω. Here, the first, second, third and fourth terms in the right-hand side of equation (9) are contributions from the shear viscosity, the bulk viscosity, the current multipole radiation and the mass multipole radiation, respectively.

In Table 4, we tabulate the timescales in the unit of second for various dissipative processes for a polytropic model with the index $n = 1$, where the radius and the mass at $\Omega = 0$ are chosen to be $R = 12.57$km and $M = 1.4M_\odot$, respectively. As shown by Table 4, for inertial modes the mass multipole radiation dominates the current multipole radiation for both the even and odd parity modes. Note that for r-modes with $l_0 - |m| = 1$, only the current multipole moment is relevant to the gravitational radiation. We also find that for even parity inertial modes, the fastest growth time due to the mass multipole radiation is of the order of 10^3 seconds for the parameters 10^9K and $\Omega = \sqrt{\pi G\bar{\rho}}$.

As seen from equation (9), the total dissipation timescale τ is given as a function of the angular velocity Ω and the temperature T of a star. For a given temperature T, we can define the critical angular velocity Ω_c such that

$$\frac{1}{\tau(\Omega_c, T)} = 0 \qquad \text{for} \qquad 0 < \Omega_c < (\pi G\bar{\rho})^{1/2}. \tag{10}$$

With this critical Ω_c, we may say that a rotating neutron star is unstable due to the gravitational radiation when $\Omega > \Omega_c$ because the gravitational radiation reaction dominates the viscous damping processes. In Figure 1, the critical angular rotation velocities Ω_c for two inertial modes and an r-mode are plotted against the temperature of the star. From this figure we can see that the instability of the $m = 2$ even parity inertial mode with $\kappa_0 = 1.100$ is strong, although this instability is weaker than that of the r-mode. At about $T = 10^9 K$ the critical angular velocity of this mode is about 25% of $(\pi G\bar{\rho})^{1/2}$.

5 Summary

In this paper, we have investigated the properties of inertial mode and r-mode oscillations in rotating isentropic Newtonian stars, using the slow rotation approximation. By taking account of the effects of the rotational deformation of the equilibrium state, we have evaluated the eigenfrequencies of the inertial modes and the r-modes with an accuracy up to the order of $\bar{\Omega}^3$. We have also estimated the dissipation timescales due to the gravitational radiation and the viscosity for a simple neutron star model. We show that the inertial modes emit gravitational radiation mainly by the mass multipole rather than the current multipole. It is also found that the instability due to the gravitational radiation reaction is strong for the most unstable inertial mode, although the instability associated with the inertial modes is not as strong as that with the r-modes.

In spite of the recent improvements in our understanding about the instability of the inertial modes and the r-modes, it seems that the fundamental properties of these modes have not yet been sufficiently understood, considering that most of the previous investigations of the inertial modes and the r-modes, including the present paper, are restricted to the case of uniformly and slowly rotating, isentropic, Newtonian stars. In this sense, we do not have any clear understanding about the inertial modes and the r-modes of, for example, differentially and rapidly rotating, non-isentropic, relativistic stars. As a first step to relax these restrictions, several studies have already appeared (see, e.g., Refs. [5]). Therefore it is highly desirable to investigate the properties of the inertial modes and the r-modes in the more general case than that investigated previously, to conclude that the instability does have an importance in astrophysics.

References

[1] N. Andersson, Astrophys. J. **502**, 708 (1998)

[2] J. L. Friedman and S. M. Morsink, Astrophys. J. **502**, 714 (1998)

[3] L. Lindblom, B. J. Owen, and S. M. Morsink, Phys. Rev. D **80**, 4843 (1998)

[4] B. J. Owen, L. Lindblom, C. Cutler, B. F. Schutz, A. Vecchio, and N. Andersson, Phys. Rev. D **58**, 084020 (1998)

[5] J. L. Friedman and K. H. Lockitch, gr-qc/9908083

[6] H. P. Greenspan, *The Theory of Rotating Fluids* (Cambridge: Cambridge University Press, Cambridge, England, 1964)

[7] J. Papaloizou and J. E. Pringle, Mon. Not. R. Astron. Soc. **182**, 423 (1978); J. Provost, G. Berthomieu, and A. Rocca, Astron. Astrophys. **94**, 126 (1981)

[8] H. Saio, Astrophys. J. **256**, 717 (1982)

[9] U. Lee, T. D. Strohmayer, and H. M. Van Horn, Astrophys J. **397**, 647 (1992)

[10] G. H. Bryan, Phil. Trans. Roy. Soc. London **A180**, 187 (1889)

[11] L. Lindblom and J. R. Ipser, Phys. Rev. D **59**, 044009 (1998)

[12] K. H. Lockitch and J. L. Friedman, Astrophys. J. **521**, 764 (1999)

[13] U. Lee and H. Saio, Mon. Not. R. Astron. Soc. **221**, 365 (1986); U. Lee, Astrophys J. **405**, 359 (1993)

[14] L. Lindblom, G. Mendell, and B. J. Owen, Phys. Rev. D 60, 064006 (1999)

[15] J.-L. Tassoul, *Theory of Rotating Stars* (Princeton University Press, Princeton, 1978)

[16] W. Unno, Y. Osaki, H. Ando, H. Saio, and H. Shibahashi, *Nonradial Oscillations of Stars*, 2nd ed. (University of Tokyo Press, Tokyo, Japan, 1989)

[17] T. Regge and J. A. Wheeler, Phys. Rev. **108**, 1063 (1957)

[18] S, Yoshida and U. Lee, Astrophys J. in press (2000)

Table 1. Eigenvalues (κ_0, κ_2)[a] of inertial modes and r-modes for the $p = K\rho^2$ Polytrope.

$l_0 - \lvert m\rvert$[b]	$m = 1$	$m = 2$	$m = 3$
1[c]	(1.00000, -0.00018)	(0.66667, 0.39827)*	(0.50000, 0.42727)*
2	(-0.40137, 0.20020)	(-0.55659, 0.12248)	(-0.63164, 0.05993)
	(1.41300, 0.23767)	(1.10003, 0.46560)*	(0.90491, 0.54494)*
3	(-1.03238, -0.21090)	(-1.02588, -0.22877)	(-1.01487, -0.23750)
	(0.69059, 0.36221)*	(0.51734, 0.37950)*	(0.41265, 0.35766)*
	(1.61373, 0.26999)	(1.35778, 0.45492)*	(1.17674, 0.55092)*
4	(-1.31227, -0.32577)	(-1.27289, -0.33970)	(-1.23863, -0.34435)
	(-0.17879, 0.01402)	(-0.27533, 0.00051)	(-0.33327, -0.01537)
	(1.05153, 0.45459)	(0.86295, 0.50140)*	(0.73430, 0.50562)*
	(1.72626, 0.24391)	(1.51957, 0.41210)*	(1.36056, 0.51593)*

[a] $\Omega(\kappa_0 + \kappa_2\tilde{\Omega}^2) = \omega$ is the mode frequency in the corotating frame up to the order of $\tilde{\Omega}^3$. The modes marked with an asterisk * satisfy the condition $\sigma(\sigma + m\Omega) < 0$ to the lowest order in Ω, and are considered to be unstable to the gravitational radiation reaction in the absence of viscous dissipation.

[b] Our definition of the angular quantum number l_0 is not the same as that of Lockitch and Friedman [12], but the same as that of Lindblom and Ipser [11]. Eigenmodes having odd (even) values of $l_0 - |m|$ are odd (even) parity modes.

[c] These modes are r-modes. To the lowest order in Ω, $\kappa_0 = 2/(m+1)$ [7] and is independent of the equation of state.

Table 2. Eigenvalues $(\kappa_0,\ \kappa_2)^a$ of $m = 2$ inertial modes and r-modes for several values of the polytropic index n.

$l_0 - \lvert m\rvert$[b]	$n = 0$	$n = 1$	$n = 1.5$	$n = 2$
1[c]	(0.66667, 0.76543)*	(0.66667, 0.39827)*	(0.66667, 0.28248)*	(0.66667, 0.19701)*
2	(-0.23193, 0.02930)	(-0.55659, 0.12248)	(-0.69646, 0.13213)	(-0.82771, 0.12773)
	(1.23193, 0.88145)*	(1.10003, 0.46560)*	(1.06259, 0.33590)*	(1.03438, 0.24322)*
3	(-0.76334,-0.55320)	(-1.02588,-0.22877)	(-1.12777,-0.15318)	(-1.21712,-0.11767)
	(0.46690, 0.62847)*	(0.51734, 0.37950)*	(0.53563, 0.29081)*	(0.55163, 0.22228)*
	(1.49644, 0.77599)*	(1.35778, 0.45492)*	(1.31003, 0.34136)*	(1.27054, 0.25749)*
4	(-1.09257,-0.77973)	(-1.27289,-0.33970)	(-1.34194,-0.24015)	(-1.40134,-0.18109)
	(-0.10179, 0.00439)	(-0.27533, 0.00051)	(-0.36424,-0.01189)	(-0.45689,-0.02235)
	(0.88425, 0.89693)*	(0.86295, 0.50140)*	(0.85863, 0.38371)*	(0.85688, 0.29910)*
	(1.64344, 0.63981)*	(1.51957, 0.41210)*	(1.47219, 0.32232)*	(1.43071, 0.25292)*

[a] $\Omega(\kappa_0 + \kappa_2\Omega^2) = \omega$ is the mode frequency in the corotating frame up to the order of Ω^3. The modes marked with an asterisk * satisfy the condition $\sigma(\sigma + m\Omega) < 0$ to the lowest order in Ω, and are considered to be unstable to the gravitational radiation reaction the absence of viscous dissipation.

[b] Our definition of the angular quantum number l_0 is not the same as that of Lockitch & Friedman [12], but the same as that of Lindblom & Ipser [11]. Eigenmodes having odd (even) values of $l_0 - |m|$ are odd (even) parity modes.

[c] These modes are r-modes. To the lowest order in Ω, $\kappa_0 = 2/(m+1)$ [7] and is independent of the equation of state.

Table 3. Dissipative timescales of inertial modes[a] and r-modes for $n = 1$ polytropic model at $T = 10^9 K$ and $\Omega = \sqrt{\pi G\bar{\rho}}$.

m	$l_0 - \lvert m\rvert$	κ_0	$\tilde{\tau}_B$(s)	$\tilde{\tau}_S$(s)	$\tilde{\tau}_2$(s)[b]	$\tilde{\tau}_3$(s)	$\tilde{\tau}_4$(s)	$\tilde{\tau}_5$(s)
1	3	0.691	5.89×10^9	9.23×10^7	-2.46×10^5†	-1.27×10^8	...	...
2	1[c]	0.667	2.03×10^{11}	2.50×10^8	-3.31×10^0	-3.49×10^2†	...	...
	2	1.100	3.35×10^9	1.23×10^8	-1.71×10^3†	-3.43×10^4	...	...
	3	0.517	6.47×10^9	6.18×10^7	-1.31×10^8	-8.39×10^4†	-1.88×10^6	...
		1.358	4.13×10^9	7.14×10^7	-7.12×10^9	-1.69×10^7†	-1.63×10^9	...
	4	0.863	1.94×10^9	4.92×10^7	-1.63×10^5†	-1.12×10^7	...	...
		1.520	4.82×10^9	4.87×10^7	-3.35×10^7†	-1.90×10^{11}	...	...
3	1[c]	0.500	6.63×10^{10}	1.43×10^8	...	-3.17×10^1	-1.88×10^3†	...
	2	0.905	1.88×10^9	9.41×10^7	...	-8.62×10^3†	-2.77×10^4	...
	3	0.413	6.97×10^9	4.78×10^7	...	-1.86×10^{10}	-5.30×10^5†	-4.07×10^6
		1.177	2.49×10^9	6.11×10^7	...	-1.65×10^{11}	-5.11×10^6†	-6.11×10^7
	4	0.734	1.29×10^9	4.10×10^7	...	-2.00×10^6†	-1.16×10^7	...
		1.361	3.06×10^9	4.18×10^7	...	-3.45×10^7†	-1.75×10^{10}	...

[a] We present dissipative timescales only for those modes that are unstable to gravitational radiation reaction.

[b] We present dissipative timescales $\tilde{\tau}_l$ due to the gravitational radiation reaction only for those of the dominant multipole moments, where for modes with odd l_0 $\tilde{\tau}_{2k+1} = \tilde{\tau}_{D,2k+1}$ and $\tilde{\tau}_{2k} = \tilde{\tau}_{J,2k}$, and for modes with even l_0 $\tilde{\tau}_{2k+1} = \tilde{\tau}_{J,2k+1}$ and $\tilde{\tau}_{2k} = \tilde{\tau}_{D,2k}$. Here $k = 1, 2, 3, \ldots$. Dissipative timescales due to the mass multipole radiation are marked with a dagger †.

[c] This mode is the r-mode. Since the expansion of perturbations vanishes to the lowest order in Ω for r-modes, the definition of the bulk viscosity timescale $\tilde{\tau}_B$ for this mode is not the same as that of equation (9), but that of Lindblom et al. [3].

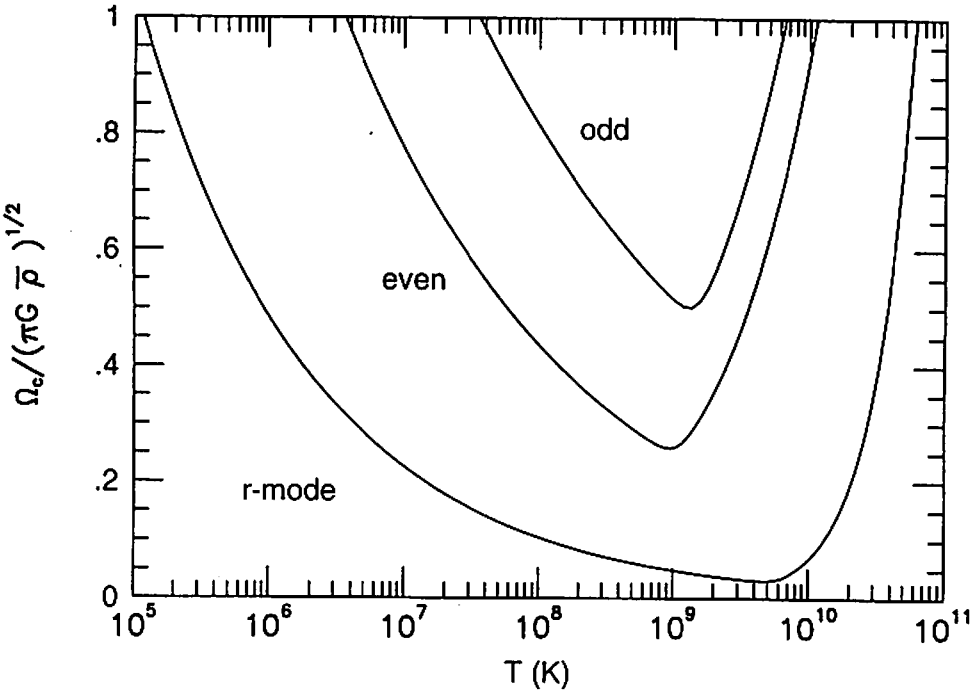

Figure 1: Critical angular velocities Ω_c for the r-mode and two inertial modes are plotted against the temperature of a neutron star. The curve labeled "r-mode" is for the $m = 2$ r-mode with $\kappa_0 = 0.667$. The curve labeled "even" is for the $m = 2$ even parity inertial mode with $\kappa_0 = 1.100$. The curve labeled "odd" is for the $m = 2$ odd parity inertial mode with $\kappa_0 = 0.517$. Here, the critical angular velocity is normalized by using $(\pi G\bar{\rho})^{1/2}$ and the unit of the temperature is Kelvin.

Majumdar-Papapetrou interior field

Daisuke Ida[1]

Department of Physics, Kyoto University,
Kitashirakawa, Sakyo-ku, Kyoto 606-8502, Japan

Abstract

Equilibrium configurations of charged perfect fluid have been studied. It is shown that the gravitational potential and the electrostatic potential have the Weyl-Majumdar relation, then the background spatial metric is the space of constant curvature, and the field equations reduce to a single non-linear partial differential equation. The solution does not any spatial symmetry, and the regular interior metric of the extremely charged black holes is found.

1 Introduction

In Newtonian theory, there are static equilibrium configurations of charged particles in which the gravitational attractions and the electric repulsions among the particles exactly balance. In general relativity, it is well known that the Einstein equation has such a static solution corresponding to these Newtonian situations, namely there is the Majumdar-Papapetrou solution [2, 3] describing an equilibrium state of many charged black holes [4].

Majumdar [2] studied the static Einstein-Maxwell system which is described by the static metric

$$g = f dt \otimes dt - f^{-1} h \tag{1}$$

and the vector potential

$$A = -\psi dt, \tag{2}$$

subject to the coupled Einstein and source-free Maxwell equations. The function $f < 0$ is the square of the timelike Killing vector field ∂_t, h the Riemannian 3-metric, and the function ψ denotes the electrostatic potential. Majumdar [2] proved that if there is a functional relationship between f and ψ, this must be of the form

$$f = -\psi^2 + c \tag{3}$$

with a constant c, generalizing Weyl's result [1] in axial symmetry. Moreover, he showed that if

$$f = -\psi^2, \tag{4}$$

then the 3-metric h is flat metric, i.e., $h = dx^2 + dy^2 + dz^2$, and the field equations reduces to a single Laplace equation in the 3-dimensional flat space. Solutions of this type were studied by Papapetrou [3] also. Later Hartle and Hawking [4] investigated the global structure of the Majumdar-Papapetrou solution, and showed that this can be interpreted as describing an equilibrium state of extremely charged black holes.

For the system of a charged dust in Newtonian theory, similar equilibrium between gravitational and Coulomb forces is possible, whenever mass density μ and charge density σ of the charged dust satisfy

$$\sigma = \pm\mu. \tag{5}$$

Das [5] studied corresponding situation in general relativity, and showed that the condition (5) besides (3) implies Weyl-Majumdar relation (4), and then the field equations reduces to a single non-linear equation, i.e., the balance condition (5) makes sense in precisely the same form in general relativity. Further discussion concerning the generality of the assumption (3) can be found in De and Raychaudhuri

[1] E-mail: ida@tap.scphys.kyoto-u.ac.jp

[6]. Explicit solutions for this system have been found by many authors, e.g., Ref. [9, 10, 11, 12] with spherical symmetry, and the recent papers [13] without spatial symmetry.

The blance equations and the Weyl-Majumdar relationship are closely related to each other, and moreover, it seems that the force balance condition largely simplifies the Einstein equation. The most typical examples are Weyl and Majumdar-Papapetrou metrics stated above, and recent Gürses metric with static charged-dust source [13]. In the pure Einstein-Maxwell or the charged-dust case, however, there are only two relevant forces, i.e. the gravitational attractive and the Coulomb repulsive forces, so that the Weyl-Majumdar relation, which implies that these two forces are parallel, leading to a scalar balance equation. In the precence of an additional force, however, the static configuration may be impossible in general; the exception is the spherically symmetric case [14, 15, 16], in which case the balance equation will be a radial scalar equation explaining that the field equations are rather simple in this case. A natural generalization may be the precence of the magnetic field or the matter pressure. The configuration of the magnetic field parallel to the electric field is easily obtained by duality rotation of pure electric field, however, there will be a magnetic monopole in this case. While the precence of non-parallel magnetic and electric fields generates Poynting flux, contributing to the energy-flux component of the stress-energy tensor, which is the character of the stationary field rather than static one. On the other hand, the (isotropic) matter pressure itself does not generates any energy (heat) fluxes, i.e., effectively contributes only to the energy-density and momentum-flux parts of the stress-energy tensor by definition, one may expect that there might be a large class of static configuration generated by the charged perfect-fluid. Such a configuration may be considered as the interior metric of Majumdar-Papapetrou multi black-holes. Since the Majumdar-Papapetrou metrics describe multiple (extremely) charged black-holes, they inevitably have timelike singularities in each horizon, so that the consideration of the regular interior metric might be interesting. Gautreau and Hoffman [8] generalized the balance equation in the presence of the matter pressure assuming the equation (3), showing

$$\sigma = \pm(\mu + 3p)\left(1 + \frac{c}{\psi^2}\right)^{\frac{1}{2}}, \tag{6}$$

where p is the isotropic pressure of the fluid, though they did not consider the rest of field equations. However, the existence of such a balance equation seems to imply that there are many unknown static configurations from the above observation. In fact, Guilfoyle [17] recently studied this system of charged perfect fluid with Weyl-Majumdar relationship, and obtained a large class of algebraically special (type D) metrics.

In this paper, we shall investigate the system of the pure-electric charged perfect fluid with Weyl-Majumdar relation from a general point of view, and show that there exists a still large class of exact solutions, which can be algebraically general (type I) and need not have any spatial symmetries. As will be shown later, if the Weyl-Majumdar relation (4) is assumed, then the 3-metric h must be that of a space of constant curvature, and the field equation reduces to a single non-linear equation. Moreover, if the fluid obeys the linear equation of state: $p = \text{const.} \times \mu$, then the field equation becomes a Helmholtz equation on the space of constant curvature (Sec. 2). Therefore, solutions are expressed in terms of the eigenfunction of the Laplace operator. Some of the explicit solutions are given in Sec. 3.

2 Field equations

The metric of static spacetimes is expressed in the form

$$g = -\frac{1}{\phi^2} dt \otimes dt + \phi^2 h, \tag{7}$$

where neither the function $\phi > 0$ nor the Riemannian 3-metric h depends on the coordinate t, i.e., the vector field $\xi = \partial_t$ satisfies the Killing equation

$$\mathcal{L}_\xi g = 0. \tag{8}$$

The Killing vector field ξ of a static spacetime is hypersurface orthogonal, or twist-free, i.e., it satisfies the Frobenius's condition

$$\xi \wedge d\xi = 0, \tag{9}$$

where $\xi = -\phi^{-2}dt$ is the Killing 1-form. (Here and in what follows, we use the same symbol for vector fields and their corresponding 1-forms.)

Maxwell field is assumed to be pure electric,

$$\xi \wedge F = 0 \tag{10}$$

which is equivalent to the condition that the charged fluid is also static. Then, the electric field is described by a real function ψ, which is the electrostatic potential, through $\iota_\xi F = d\psi$. The Maxwell equation $dF = 0$ and $d * F = 4\pi\sigma * u$ then becomes a Poisson equation

$$*d * d\psi = 2\frac{g^{-1}(d\psi, d\phi)}{\phi} - 4\pi\sigma g^{-1}(\xi, u). \tag{11}$$

where u and σ denote the velocity and the charge density of the fluid, respectively. The stress-energy tensor of the Maxwell field T_F is

$$8\pi T_F(\partial_\mu, \partial_\nu) = g^{-1}(\iota_{\partial_\mu} F, \iota_{\partial_\nu} F) + g^{-1}(\iota_{\partial_\mu} * F, \iota_{\partial_\nu} * F). \tag{12}$$

The stress-energy tensor of the fluid has the form

$$T_m = (\mu + p)u \otimes u + pg, \tag{13}$$

or equivalently

$$\tilde{T}_m = T_m - \frac{1}{2}\mathrm{tr}(T_m)g = (\mu + p)u \otimes u + \frac{1}{2}(\mu - p)g. \tag{14}$$

The fluid velocity u must be proportional to ξ, i.e., $u = \phi\xi$ (which is a consequence of the time–space components of the Einstein equation).

Now we consider the Einstein equation

$$Ric = 8\pi(T_F + \tilde{T}_m). \tag{15}$$

Here we show only the result, see [26] for details. Non-vanishing components of the Einstein equation are

$$*d * d\phi = -\frac{g^{-1}(d\phi, d\phi)}{\phi} + \phi^3 g^{-1}(d\psi, d\psi) + 4\pi\phi(\mu + 3p), \tag{16}$$

which is regarded as Poinsson equation for gravitation, and

$$Ric[h] + 16\pi\phi^2 ph = 2\phi^{-2}d\phi \otimes d\phi - 2\phi^2 d\psi \otimes d\psi. \tag{17}$$

The equations (11), (16) and (17) form a complete set of the field equations.

To solve equation (17), assume the Weyl-Majumdar relation (4), or

$$\psi + \epsilon\phi^{-1} = 0, \quad (\epsilon = \pm 1), \tag{18}$$

then the r.h.s. of the equation (17) vanishes, and the 3-dimensional manifold with metric h becomes an Einstein space, i.e., the Ricci tensor has only a trace part (scalar curvature). Since in three or higher dimensional Einstein space, the scalar curvature must constant, which can be seen by the contracted Bianchi identity, the matter pressure p is proportional to ϕ^{-2} with a constant ratio. Without loss of generality, we may take $p = -\kappa/8\pi\phi^2$, $(\kappa = 0, \pm 1)$. Since a 3-dimensional Einstein space is a space of constant curvature (namely Riemann tensor has only a Ricci trace-part), we have

$$h = \frac{dx^2 + dy^2 + dz^2}{\left[1 + \frac{1}{4}\kappa(x^2 + y^2 + z^2)\right]^2}. \tag{19}$$

Then, the equations (11) and (16) reduce to

$$(\Delta + \lambda)\phi = 0 \tag{20}$$

and

$$\sigma = \epsilon(\mu + 3p), \tag{21}$$

where Δ denotes the Laplacian with respect to h, and $\lambda = 4\pi\phi^2(\mu + 3p)$. This equation is non-linear, however, it can be made linear if we assume a linear (isothermal-type) equation of state for the fluid, i.e., $\mu = \text{const.} \times p (= \text{const.} \times \phi^{-2})$. Then, λ becomes constant and equation (20) is simply a Helmholtz equation on the space of constant curvature, whose solutions are known (see e.g. [20]).

3 Examples

Here we shall study some explicit solutions of the equation (20). We mainly consider the spherically symmetric solutions as simple examples. As an energy condition, we shall assume the dominant energy condition, which requires $\mu \geq |p|$.

3.1 positive pressure ($\kappa = -1$)

In this case, the dominant energy condition requires $\lambda \geq 2$. In the spherical polar coordinate system $\{r, \vartheta, \varphi\}$, the 3-metric h can be written as

$$h = \eta(r)^2[dr^2 + r^2(d\vartheta^2 + \sin^2\vartheta d\varphi^2)], \tag{22}$$

where $\eta = (1 - r^2/4)^{-1}$, $(0 < r < 2)$. The equation (20) for the function $\phi(r)$ becomes

$$\frac{1}{\eta^3 r^2}\frac{d}{dr}\eta r^2 \frac{d}{dr}\phi + \lambda\phi = 0. \tag{23}$$

The general solution of this equation are

$$\phi = l\frac{1 - r^2/4}{r}\sin\left[(\lambda - 1)^{\frac{1}{2}} \ln\frac{2 + r}{2 - r} + \delta\right], \tag{24}$$

where $l > 0$ and $0 \leq \delta \leq \pi$ are integration constants. In general, the set at which $\phi = 0$ is a singularity, since for example a field invariant $F : F = -\phi^{-2}g^{-1}(d\phi, d\phi)$ blows up there (only the exception is $\delta = 0$, $r = 0$, in which case the metric comes close to flat near the origin $r = 0$), so that this solution mast have a singularity, and the situation is same even without spherical symmetry. The locations of the singularities are

$$r = 2\tanh\frac{(n\pi - \delta)}{2(\lambda - 1)^{\frac{1}{2}}}, \quad (n = 0, \pm 1, \pm 2, \cdots) \tag{25}$$

at which the area radius $R = |\phi\eta r|$ vanishes, so that these singularities are actually point-like, and each connected component of the spacetime has in general topology S^3 minus two points. (Without spherical symmetry, the singularity might be line- or surface-like, and the spacetime topology would be S^3 minus several such sets.)

Next, let consider the solution (24) in the neighborhood of $r = 0$. We may assume that $0 \leq \delta \leq \pi/2$, since the transformation $r \mapsto -r$ corresponds to $\delta \mapsto \pi - \delta$, and let consider the region $r < 0$. Whenever $\delta \neq 0$, this solution diverges at $r = 0$ like $l\sin\delta/r$, however, it is only a coordinate singularity. The hypersurface $r = 0$ is a null hypersurface, on which the Killing vector becomes null, and it is generated by spheres of radius $R = l\sin\sigma$. In fact, whenever $\delta \neq 0, \pi/2$, the region $r < 0$ is extended analytically to the region $r > 0$ across this null hypersurface. To see this, let consider the coordinate transformation

$$v = t + \int^r \phi^2\eta dr. \tag{26}$$

Then the metric transforms to

$$g = -\frac{dv^2}{\phi^2} + \frac{2}{1 - r^2/4}dvdr + l^2\sin^2\left[(\lambda - 1)^{\frac{1}{2}} \ln\frac{2 + r}{2 - r}\right](d\vartheta^2 + \sin^2\theta d\phi^2), \tag{27}$$

which is manifestly non-singular at $r = 0$.

Moreover, we can consider a class C^1 extension of the region $r < 0$ to the exterior field of a black-hole spacetime. The Misner-Sharp mass m_H (which coincides with Hawking mass or Kodama mass in spherical symmetry) with respect to the surface $r = 0$ is

$$m_H = \frac{l\sin\delta}{2}. \tag{28}$$

On the other hand, the electric charge inside a two-surface S is evaluated by

$$q = -\frac{1}{4\pi}\int_S *F. \tag{29}$$

Especially, when the surface $r = \text{const.}$ is chosen as S, we find

$$q = \epsilon \frac{r^2}{1 - r^2/4}\frac{d|\phi|}{dr}, \tag{30}$$

where 'inside' means smaller r, so that the electric charge inside the surface $r = 0$ is

$$q_H = \epsilon l \sin\delta = 2\epsilon m_H. \tag{31}$$

This relationship is the very same as that the extreme Reissner-Nordström spacetime has on the horizon. Furthermore, mass density and matter pressure of the fluid vanishes on the surface $r = 0$. These evaluations suggest that the region $r < 0$ of the metric with respect to the equation (24) can be matched at $r = 0$ to the exterior field of the extreme Reissner-Nordström metric. By the rescaling of the coordinates $\tilde{r} = l(\lambda - 1)^{\frac{1}{2}} \cos\delta\, r$, $\tilde{t} = t/[l(\lambda - 1)^{\frac{1}{2}} \cos\delta]$ the metric transforms into the form

$$g = -\frac{d\tilde{t}^2}{\tilde{\phi}^2} + \tilde{\phi}^2\tilde{\eta}^2\left[d\tilde{r}^2 + \tilde{r}^2(d\vartheta^2 + \sin^2\vartheta d\varphi^2)\right]. \tag{32}$$

Note that $\tilde{\phi}$ behaves near $\tilde{r} = 0$ like $\tilde{\phi} = 1 + l\sin\delta/\tilde{r} + O(\tilde{r}^2)$. Next, introduce the advanced time coordinate

$$v = \tilde{r} + \int^{\tilde{r}} \tilde{\phi}^2\tilde{\eta}d\tilde{r}, \tag{33}$$

then the metric (32) becomes

$$g = -\frac{dv^2}{\tilde{\phi}^2} + 2\tilde{\eta}dvd\tilde{r} + \tilde{\phi}^2\tilde{\eta}^2\tilde{r}^2(d\vartheta^2 + \sin^2\theta d\varphi^2), \tag{34}$$

while the metric of the extreme Reissner-Nordström has a form

$$\begin{aligned} g_{RN} &= -\left(1 + \frac{m}{\tilde{r}}\right)^{-2} dv^2 + 2dvd\tilde{r} \\ &\quad + \left(1 + \frac{m}{\tilde{r}}\right)^2 \tilde{r}^2(d\vartheta^2 + \sin^2\vartheta d\varphi^2). \end{aligned} \tag{35}$$

If the mass parameter (ADM mass) of the metric (35) is

$$m = l\sin\delta, \tag{36}$$

then these two metrics are matched on the hypersurface $\tilde{r} = 0$, and it is easily seen that this extension is class C^1. In this case, the exterior metric (35) and the interior metric (34) correspond to $\tilde{r} > 0$ and $\tilde{r} < 0$, respectively. We can similarly verify that the region $r > 0$ of (24) can be matched to the $m = l\sin\delta$ interior metric (i.e., the metric (35) for $m = -l\sin\delta < 0$, $\tilde{r} > 0$), and if $l\sin\delta < 0$, then the region $r < 0$ and $r > 0$ of (24) can be matched to the interior ($m = -|l\sin\delta|$) and exterior ($m = |l\sin\delta|$) metric (35), respectively.

Of course, we may also obtain solutions without spherical symmetry by the method of multipole expansion. Alternatively, we show an example by superposing monopole solutions with respect to different centers (x_i, y_i, z_i):

$$\phi = \sum_i l_i \frac{1 - r_i^2/4}{r_i}\sin\left[(\lambda - 1)^{\frac{1}{2}} \ln\frac{2 + r_i}{2 - r_i} + \delta_i\right], \tag{37}$$

where $r_i = [(x - x_i)^2 + (y - y_i)^2 + (y - y_i)^2]^{\frac{1}{2}}$, and l_i's and δ_i's are constants. Each hole $r_i = 0$ can be matched to the Reissner-Nordström metric with $m = l_i\sin\delta_i$.

3.2 dust $\kappa = 0$

The dust case is obtained by taking appropriate limit of possitive pressure case. Recently, Gürses [13] also found this class, so that we shall briefly collect the result.

The general spherically symmetric solution is

$$\phi = l\frac{\sin(\lambda^{\frac{1}{2}}r + \delta)}{r}, \tag{38}$$

The solution without spatial symmetry can be expressed in terms of the spherical harmonics and the spherical Bessel functions. For more information, see Ref. [13].

3.3 negative pressure ($\kappa = 1$)

In this case the dominant energy condition requires $\lambda \geq -1$. Consider the solution of the equation (23) with $\eta = (1 + r^2/4)^{-1}$. The general solution is

$$\phi = l\frac{1 + r^2/4}{r}\sin\left[(1+\lambda)^{\frac{1}{2}}\arcsin\frac{r}{1+r^2/4} + \delta\right], \tag{39}$$

where $l > 0$ and $0 \leq \delta \leq \pi$ are integration constants, and the arcsin above should be regarded as

$$\arcsin\frac{r}{1+r^2/4} = \begin{cases} -\pi - \mathrm{Arcsin}\frac{r}{1+r^2/4} & (r < -2) \\ \mathrm{Arcsin}\frac{r}{1+r^2/4} & (-2 \leq r \leq 2) \\ \pi - \mathrm{Arcsin}\frac{r}{1+r^2/4} & (r > 2) \end{cases} \tag{40}$$

in terms of the Arcsin which takes principal value. Unlike the case of positive pressure or dust, these solutions need not have any singularity in the appropriate range of λ, in fact, if $-1 \leq \lambda \leq -3/4$ ($|p| \leq \mu \leq 3/2|p|$) and $(1+\lambda)^{\frac{1}{2}}\pi \leq \delta \leq \pi - (1+\lambda)^{\frac{1}{2}}\pi$, ϕ gives a regular solution for all r, and if $\delta = 0$ and $-1 \leq \lambda \leq 0$ ($|p| \leq \mu \leq 3|p|$), then it gives a regular solution for $r \geq 0$.

Similar to the other cases, we can match the solution to the exterior metric ($\tilde{r} > 0$) of the extreme Reissner-Nordström spacetime (35) at $r = 0$ whenever $\delta \neq 0, \pi/2, \pi$. Note that we may assume $0 < \delta < \pi/2$, since δ is transformed to $\pi - \delta$ by $r \mapsto -r$. Let consider the coordinate transformation $\tilde{r} = l(1+\lambda)^{\frac{1}{2}}\cos\delta\, r$, $\tilde{l} = l/[l(1+\lambda)^{\frac{1}{2}}\cos\delta]$, then the metric can be written as

$$g = -\frac{d\tilde{l}^2}{\tilde{\phi}^2} + \tilde{\phi}^2\tilde{\eta}^2\left[d\tilde{r}^2 + \tilde{r}^2(d\vartheta^2 + \sin^2\vartheta d\varphi^2)\right]. \tag{41}$$

Furthermore, the transformation $v = \tilde{l} + \int^{\tilde{r}} \tilde{\phi}^2\tilde{\eta}d\tilde{r}$ makes the metric in the form

$$g = -\tilde{\phi}^{-2}dv^2 + 2\tilde{\eta}dvd\tilde{r} + \tilde{\phi}^2\tilde{\eta}^2\tilde{r}^2(d\vartheta^2 + \sin^2\vartheta d\varphi^2). \tag{42}$$

The region $\tilde{r} < 0$ of this metric can be matched to the region $r > 0$ of the metric (35) with

$$m = l\sin\delta, \tag{43}$$

and in this case also, the extension is class C^1, since $\tilde{\phi} = 1 + l\sin\delta/\tilde{r} + O(\tilde{r}^2)$, $\tilde{\eta} = 1 + O(\tilde{r}^2)$.

Unlike the positive pressure fluid, the metric (39) or (42) can be regular for all $r < 0$ ($\tilde{r} < 0$), if $\delta \geq (1+\lambda)^{\frac{1}{2}}\pi$ is satisfied. In this case, the surface $r = -\infty$ is neither infinity nor singularity, in fact it can be shown that this surface is a null hypersurface, and that the spacetime is extendable beyond $r = -\infty$, unless $\delta = (1+\lambda)^{\frac{1}{2}}\pi$, in which case, $r = -\infty$ simply corresponds to a regular center. To see this, consider the inverse of the radial coordinate

$$\bar{r} = 4/r, \tag{44}$$

then the metric transforms to

$$g = -\frac{dt^2}{\phi^2} + \bar{\phi}^2\bar{\eta}^2\left[d\bar{r}^2 + \bar{r}^2(d\vartheta^2 + \sin^2\vartheta d\varphi^2)\right], \tag{45}$$

where

$$\bar{\phi} = l\frac{1+\bar{r}^2/4}{\bar{r}}\sin\left[(1+\lambda)^{\frac{1}{2}}\arcsin\frac{\bar{r}}{1+\bar{r}^2/4} + \pi + (1+\lambda)^{\frac{1}{2}}\pi - \delta\right] \tag{46}$$

and

$$\bar{\eta} = \left(1+\frac{1}{4}\bar{r}^2\right)^{-1}, \tag{47}$$

namely, the effect of this transformation is simply

$$\delta \mapsto \pi + (1+\lambda)^{\frac{1}{2}}\pi - \delta, \tag{48}$$

so that the metric can be analytically extended across the null hypersurface $\bar{r} = 0$ in a similar manner explained above, and it can be also matched to the interior region ($\bar{r} < 0$) of the Reissner-Nordström metric (35) with $m = l\sin[\delta - (1+\lambda)^{\frac{1}{2}}\pi]$.

Finally, we give a multi-center solution in an obvious way:

$$\phi = \sum_i l_i\frac{1+r_i^2/4}{r_i}\sin\left[(1+\lambda)^{\frac{1}{2}}\arcsin\frac{r_i}{1+r_i^2/4} + \delta_i\right]. \tag{49}$$

4 Conclusions

We have investigated the static field of charged perfect fluid, and then shown that only two assumptions, i.e. Weyl-Majumdar relation (4) and the linear equation of state, reduce the field equations to a single linear equation. Thus, any solution of this type can be described by an eigenfunction of the Laplacian on the 3-dimensional space of constant curvature and the eigenvalue determines the equation of state, i.e., the ratio of energy density to pressure. These solutions have some good properties, for example, they obey simple equation of state as required, both mass density and matter pressure do not change their sign, and they need not have any spatial symmetry.

The mechanism of this simplification of field equations may be explained in terms of force balance among gravitational force, Coulomb force and the pressure gradient. The function ϕ^{-2} is the norm of the static Killing vector, so can be interpreted as the gravitational potential. Then the equation (4) gives a functional relationship between the gravitational and electrostatic potential, which implies that the gravitational and Coulomb force are parallel. This property characterizes the Weyl[1] and Majumdar-Papapetrou[2, 3] solutions, and explains why they permitts a large class of solutions without spherical symmetry. The point in this paper is that the pressure gradient automatically becomes parallel to both gravitational and Coulomb forces by the Einstein equation, even in the presence of perfect fluid, which is implicit in the spherically symmetric case. Thus, the balance equation among three relevant forces, which is originally a vector equation, becomes a scalar equation (21), explaining why a large class of inhomogeneous metrics are obtained. Though we have discussed only in the case when the equipotential surfaces of the gravitational potential, electrostatic potential, and matter pressure, this is not a necessary condition for the static configuration; there would be a situation in which the vector balance equation holds at each point, however, such a spacetime might have some spatial symmetry such as axial or cylindrical symmetry, or equation of state might depend on spacetime points. The static configuration considered here may be regarded as a final state of the non-rotating object composed of charged fluid. Through the realistic contraction of such an object with given equation of state, the scalar balance equation might be satisfied in the final equilibrium state, even if it were not spherically symmetric.

Another characterization of the solution is given in terms of the Ernst potentials[21]. In a similar way to the stationally Einstein-Mawell system, we can define the Ernst potential by $\mathcal{E} = 1/\phi^2 - \psi^2$, then the equation (16) can be replaced with the Poisson equations for $\mathcal{E}$. However, the assumption (4) implies that $\mathcal{E} = 0$, so that this equation reduces to an algebraic equation, which is just a balance equation (21).

We have also shown that solutions corresponding to the equations (24), (38) and (39) can be matched to the extreme Reissner-Nordström metric at the horizon, however though this interior solution has central singularity unless the matter pressure is negative. In the negative pressure case, the interior solution (49) can be regular for appropriate range of parameters, and then $r \to -\infty$ is not conformal infinity, but represents another 'hole' connected by another interior metric, or regular center. Since the

matching conditions are determined by the behavior near the horizon, solutions (49), (??) and (37) could be matched to an appropriate Majumdar-Papapetrou metric [2, 3, 4] at $r_i = 0$ in a similar manner given here.

Acknowledgements.

We would like to acknowledge many helpful discussions with Prof. Humitaka Sato, Prof. Ken-ichi Nakao and Dr. Akihiro Ishibashi. The author is supported by Research Fellowships of the Japan Society for the Promotion of Science of Young Scientists.

References

[1] H. Weyl, Ann. Physik **54**, 117 (1917).

[2] S.D. Majumdar, Phys. Rev. **72**, 390 (1947).

[3] A. Papapetrou, Proc. Roy. Irish Acad. **A51**, 191 (1947).

[4] J.B. Hartle and S.W. Hawking, Commun. Math. Phys. **26**, 87 (1972).

[5] A. Das, Proc. R. Soc. London, Ser. A **267**, 1 (1962).

[6] U.K. De and A.K. Raychaudhuri, Proc. R. Soc. London, Ser. A **303**, 47 (1968).

[7] R.M. Misra, Phys. Rev. **D15**, 2125 (1970).

[8] R. Gautreau and R.B. Hoffman, Nuovo Cimento **16B**, 162 (1973).

[9] W.B. Bonnor, Mon. Not. R. Astr. Soc. **129**, 443 (1965).

[10] C.F. Kyle and A.W. Martin, Nuovo Cimento **50**, 583 (1967).

[11] S.J. Wilson, Can. J. Phys. **47**, 2401 (1969).

[12] P.S. Florides, Nuovo Cimento **42A**, 343 (1977).

[13] M. Gürses, Phys. Rev. **D58**, 044001 (1998).

[14] M. Omote, Letters Nuovo Cimento **6**, 49 (1973).

[15] A. Banerjee and N.O. Santos, J. Math. Phys. **22**, 824 (1981).

[16] T. Singh, G.P. Singh, and A.M. Helmi, Astrophys. Space Sci. **199**, 113 (1993).

[17] B.S. Guilfoyle, J. Math. Phys. **40**, 2032 (1999).

[18] B. Carter, in *Black holes*, ed. C. DeWitt and B.S. DeWitt (New York, Gordon and Breach, 1973).

[19] R. Geroch, J. Math. Phys. **12**, 918 (1971).

[20] E.R. Harrison, Rev. Mod. Phys. **39**, 862 (1967).

[21] F.J. Ernst, Phys. Rev. **168**, 1415 (1968).

[22] H.A. Buchdahl, Phys. Rev. **116**, 1027 (1959).

[23] F. de Felice, Y. Yu and J. Fang, M.N.R.A.S. **277**, L17 (1995).

[24] Y. Yu and S. Liu, gr-qc/9904050.

[25] F. de Felice, gr-qc/9905099.

[26] D. Ida, gr-qc/9906071.

Motion of Two Bodies in 2-dimensions and the Structure of Space-Time

Tadayuki Ohta[1]

Department of Physics, Miyagi University of Education
Aoba-Aramaki, Sendai 980, Japan

Robert Mann[2]

Department of Physics, University of Waterloo
Waterloo, Ontario, N2L 3G1, Canada

Abstract

In the framework of 2-dimensional theory of dilaton gravity with the cosmological constant and the charges we investigate the change of the spacetime structure along the motion of two bodies. The exact solution of the motion is obtained by solving the canonical equations which are derived from the determining equation of the Hamiltonian in the canonical reduction of the theory. The causal relationship between particles is demonstrated for both bounded and unbounded motions.

1 Introduction

As a model of self-gravitating N-body system (1+1)-dimensional theories have yielded quite fruitful insights into many problems in gravity. Such lineal gravity theories admit a considerably simpler level of computational and analytic analysis that can be applied to star systems (small $N \geq 2$) and galactic evolution (large N), whilst avoiding a number of difficulties inherent in (3+1)-dimensions, including singularities, evaporation, and energy dissipation in the form of gravitational radiation.

We have already formulated the canonical theory of (1+1)-dim dilaton gravity with the cosmological constant for a system of N bodies, deriving the determining equation of the Hamiltonian and the exact solutions to the canonical equations for the 2-body case [1, 2, 3]. Here we extend the theory to include the charges. Since the Einstein action is a topological invariant in (1+1) dimensions, we must incorporate a scalar (dilaton) field into our action which is

$$I = \int dx^2 \left[\frac{1}{2\kappa}\sqrt{-g}g^{\mu\nu}\left\{ \Psi R_{\mu\nu} + \frac{1}{2}\nabla_\mu\Psi\nabla_\nu\Psi + \frac{1}{2}g_{\mu\nu}\Lambda \right\} - A_\mu \mathcal{F}^{\mu\nu}{}_{,\nu} + \frac{1}{4\sqrt{-g}}\mathcal{F}^{\mu\nu}\mathcal{F}^{\alpha\beta}g_{\mu\alpha}g_{\nu\beta} \right.$$
$$\left. + \sum_a \int d\tau_a \left\{ -m_a \left(-g_{\mu\nu}(x)\frac{dz_a^\mu}{d\tau_a}\frac{dz_a^\nu}{d\tau_a} \right)^{1/2} + e_a \frac{dz_a^\mu}{d\tau_a} A_\mu(x) \right\} \delta^2(x - z_a(\tau_a)) \right], \qquad (1)$$

where Ψ is the dilaton field, A_μ and $\mathcal{F}^{\mu\nu}$ are the vector potential and the field strength, $g_{\mu\nu}$ and g are the metric and its determinant, R is the Ricci scalar, and e_a and τ_a are the charge and the proper time of a-th particle, respectively, with $\kappa = 8\pi G/c^4$. The symbol ∇_μ denotes the covariant derivative associated with $g_{\mu\nu}$.

On transforming the action (1) in the first order form and eliminating the redundant variables we get

$$I = \int dx^2 \left\{ \sum_a p_a \dot{z}_a \delta(x - z_a(t)) + \pi\dot{\gamma} + \Pi\dot{\Psi} + N_0 H^0 + N_1 H^1 \right\}. \qquad (2)$$

[1]E-mail:t-ooi@ipc.miyakyo-u.ac.jp
[2]E-mail:mann@avatar.uwaterloo.ca

where π and Π are conjugate momenta to γ and Ψ, respectively, with $\gamma = g_{11}$, $N_0 = (-g^{00})^{-1/2}$, $N_1 = g_{10}$ and

$$R^0 = -\kappa\sqrt{\gamma}\gamma\pi^2 + 2\kappa\sqrt{\gamma}\pi\Pi + \frac{1}{4\kappa\sqrt{\gamma}}(\Psi')^2 - \frac{1}{\kappa}\left(\frac{\Psi'}{\sqrt{\gamma}}\right)' - \frac{1}{2}\sqrt{\gamma}(E^2 - \frac{\Lambda}{\kappa}) - \sum_a \sqrt{\frac{p_a^2}{\gamma} + m_a^2}\,\delta(x - z_a(t))\,, \tag{3}$$

$$R^1 = \frac{\gamma'}{\gamma}\pi - \frac{1}{\gamma}\Pi\Psi' + 2\pi' + \sum_a \frac{p_a}{\gamma}\delta(x - z_a(t))\,. \tag{4}$$

From the analysis of the generator arising from the variation of the action at the boundary we find that we can consistently choose the coordinate condition $\gamma = 1$ and $\Pi = 0$. The action (2) then reduces to

$$I = \int d^2x \left\{ \sum_a p_a \dot{z}_a \delta(x - z_a) - \mathcal{H} \right\}\,. \tag{5}$$

where the reduced Hamiltonian is $H = \int dx\mathcal{H} = -\frac{1}{\kappa}\int dx \Delta\Psi$, with $\Delta \equiv \partial^2/\partial x^2$. The field $\Psi = \Psi(x, z_a, p_a)$ is understood to be determined from the constraint equations which are now

$$\Delta\Psi - \frac{1}{4}(\Psi')^2 + \kappa^2\pi^2 + \frac{1}{2}(\kappa E^2 - \Lambda) + \kappa\sum_a \sqrt{p_a^2 + m_a^2}\,\delta(x - z_a) = 0\,, \tag{6}$$

$$2\pi' + \sum_a p_a \delta(x - z_a) = 0\,. \tag{7}$$

2 Solution for a system of two particles

In (1+1) dimensions the electromagnetic field strength is a 2-form, and so in compact spatial regions contributes to the stress-energy like a cosmological constant. We therefore set $V(x) \equiv E^2 - \frac{1}{4}(\sum_a e_a)^2$ and $\Lambda_c \equiv \Lambda - \frac{\kappa}{4}(\sum_a e_a)^2$, so that $V(x)$ vanishes in the outer regions and Λ_c is an effective cosmological constant. With these replacements, we divide spacetime into three regions ($z_1 < x$, $z_2 < x < z_1$, $x < z_2$, respectively the $+, 0, -$ regions) and solve for $N = 2$ the constraints equations for $\Psi = -4\log|\phi|$ and $\pi = \chi'$, matching the solutions at the boundaries of each region. We adopt at infinity boundary conditions which ensure that the surface terms obtained in passing from (1) to (5) vanish and the Hamiltonian remains finite – this is tantamount to requiring that in the $\pm$ regions $\Psi^2 - 4\kappa^2\chi^2$ must be a quadratic function of x . This is sufficient to ensure that all constants of integration in the constraint equations can be expressed in terms of the momenta and positions of the bodies. This procedure is sufficient to solve all remaining dynamical equations exactly. Repeating the analysis for $z_1 < z_2$ yields a similar solution with $p_i \to -p_i$, and so the full solution is a function of $(z_i, \tilde{p}_i)$, where $\tilde{p}_i = p_i \mathrm{sgn}(z_1 - z_2)$.

Although the resultant expressions are rather cumbersome, the canonical equations imply conservation of the total momenta $p_1 + p_2$. Setting $p_1 = -p_2 = p$ considerably simplifies the exact solution, which is

$$\phi_\pm(x) = A_\pm e^{\pm\frac{1}{2}Kx}, \quad \phi_0(x) = A_0 e^{\frac{1}{2}K_0 x} + B_0 e^{-\frac{1}{2}K_0 x}\,, \tag{8}$$

for the the $(+)$, $(-)$ and (0) regions respectively, where $K = \sqrt{(\kappa X)^2 - \frac{\Lambda_c}{2}}$, $K_0 = \sqrt{Y_0^2 - \frac{\kappa}{2}\epsilon_1\epsilon_2 - \frac{\Lambda_c}{2}}$ with $Y_0 \equiv \kappa\left[X - \frac{\epsilon}{2}\tilde{p}\right]$ and X is determined by the matching conditions. The parameter $\epsilon = \pm 1$ is a constant of integration associated with the metric degree of freedom and changes sign under time reversal. The coefficients $A_{\pm,0}$ and $B_{\pm,0}$ are

$$A_\pm = \left(\frac{K_{1,2}}{\mathcal{M}_{1,2}}\right)^{1/2} e^{-\frac{\kappa}{4}(z_1 - z_2) \mp \frac{1}{2}Kz_{1,2}}\,, \tag{9}$$

$$\{A_0, B_0\} = \frac{(K_{2,1}\mathcal{M}_{2,1})^{1/2}}{4K_0} e^{-\frac{\kappa}{4}(z_1 - z_2) \mp \frac{1}{2}K_0 z_{2,1}}\,,$$

where

$$K_{1,2} \equiv 2K_0 + 2K - \kappa\sqrt{p^2 + m_{2,1}^2}, \qquad \hat{K} \equiv K_0 - K + \frac{\kappa\epsilon}{2}\tilde{p}\,.$$

$$\mathcal{M}_{1,2} \equiv \kappa\sqrt{p^2 + m_{1,2}^2} + 2K_0 - 2K\,.$$

The metric components are

$$\begin{aligned} N_{0(\pm)} &= A\phi_\pm^2\,, \qquad N_{0(0)} = A\phi_{(0)}^2\,, \\ N_{1(\pm)} &= \pm\epsilon\frac{\kappa X}{K}\left(A\phi_\pm^2 - 1\right)\,, \\ N_{1(0)} &= \epsilon\left\{AY_0\left[2A_0B_0x + \frac{A_0^2\,e^{K_0x} - B_0^2\,e^{-K_0x}}{K_0}\right] + D_0\right\}\,. \end{aligned} \tag{10}$$

where $A = \frac{16\kappa K_0 X}{J_+ K}\,e^{\frac{1}{2}\hat{K}(z_1-z_2)}$, $D_0 = \kappa\frac{J_- X}{J_+ K}$ and

$$J_\pm = 2\left(\frac{Y_0}{K_0} + \frac{\kappa X}{K}\right)(K_1 \pm K_2) - 2K_1K_2\left(\frac{Y_0}{K_0} - \frac{\kappa X}{K}\right)\left(\frac{1}{\mathcal{M}_1} \pm \frac{1}{\mathcal{M}_2}\right) - \frac{Y_0}{K_0}K_1K_2(z_1 \mp z_2). \tag{11}$$

The solution for $z_1 < z_2$ is obtained by interchanging the suffices 1 and 2 in the preceding solution. The Hamiltonian is straightforwardly computed to be $H = -\frac{1}{\kappa}\int dx\Delta\Psi = \frac{4K}{\kappa}$, whereas the matching conditions at $x = z_1, z_2$ in turn force the relation

$$K_1K_2 = \mathcal{M}_1\mathcal{M}_2e^{K_0|z_1-z_2|}\,, \tag{12}$$

which determines X and then H. The above relation yields

$$\tanh(\frac{\kappa\mathcal{J}}{8}|r|) = \frac{\mathcal{J}(B_1 + B_2)}{\mathcal{J}^2 + B_1B_2} \tag{13}$$

where $B_{1,2} = H - 2\sqrt{p^2 + m_{1,2}^2}$, $\mathcal{J}^2 = \left(\sqrt{H^2 + \frac{8\Lambda}{\kappa^2}} - 2\epsilon\tilde{p}\right)^2 - \frac{8\epsilon_1\epsilon_2}{\kappa} - \frac{8\Lambda}{\kappa^2}$ and $r \equiv z_1 - z_2$. For a given $\Lambda \geq -(\kappa H)^2/8$, the equation (13) describes the surface in (r, p, H) space of all allowed phase-space trajectories. Since H is a constant of the motion, (a fact easily verified by differentiation of (13) with respect to t) a given trajectory in the (r, p) plane is uniquely determined by setting $H = H_0$ in (13).

Although the solution for the field components is formally the same as that obtained in ref. [3] , the equations of motion

$$\dot{p}_a = -\frac{\partial N_0}{\partial z_a}\sqrt{p_a^2 + m_a^2} + \frac{\partial N_1}{\partial z_a}p_a + \frac{1}{2}\sum_b \epsilon_a\epsilon_b N_0\frac{\partial}{\partial z_a}|z_a - z_b|\,, \tag{14}$$

$$\dot{z}_a = N_0\frac{p_a}{\sqrt{p_a^2 + m_a^2}} - N_1\,. \tag{15}$$

where $\frac{\partial N_{0,1}}{\partial z_i} \equiv \frac{1}{2}\left\{\frac{\partial N_{0,1}}{\partial x}\Big|_{x=z_i+0} + \frac{\partial N_{0,1}}{\partial x}\Big|_{x=z_i-0}\right\}$ have an additional Lorentz-force term which yields qualitatively new features. Although the equations in the unequal mass case can be solved exactly , the expression cannot be given in terms of elementary functions.

However in the equal mass case an explicit exact solution to (14) can be obtained, which is

$$p(\tau) = \frac{\epsilon m}{2}\left(f(\tau) - \frac{1}{f(\tau)}\right) \tag{16}$$

with

$$f(\tau) = \begin{cases} \dfrac{\frac{\mu}{m}\left(1+\sqrt{\gamma_H}\right)\left\{1-\eta\,e^{\frac{\epsilon\kappa m}{4}\sqrt{\gamma_m}(\tau-\tau_0)}\right\}}{\gamma_e+\sqrt{\gamma_m}+\left(\sqrt{\gamma_m}-\gamma_e\right)\eta\,e^{\frac{\epsilon\kappa m}{4}\sqrt{\gamma_m}(\tau-\tau_0)}} & \gamma_m > 0\,, \\ \dfrac{1+\sqrt{\gamma_H}}{\frac{m}{\mu}\gamma_e+\frac{\epsilon\kappa H}{4}(\tau-\tau_0)} & \gamma_m = 0\,, \\ \dfrac{\frac{\mu}{m}\left(1+\sqrt{\gamma_H}\right)}{\gamma_e+\sqrt{-\gamma_m}\frac{\nu+\frac{m^2}{H}\sqrt{-\gamma_m}\tan\left[\frac{\epsilon\kappa m}{4}\sqrt{-\gamma_m}(\tau-\tau_0)\right]}{\frac{m^2}{H}\sqrt{-\gamma_m}-\nu\tan\left[\frac{\epsilon\kappa m}{4}\sqrt{-\gamma_m}(\tau-\tau_0)\right]}} & \gamma_m < 0\,, \end{cases} \tag{17}$$

where $d\tau = d\tau_1 = d\tau_2 = \frac{m}{\sqrt{p^2+m^2}}\frac{\mathcal{J}^2}{C}dt$ is the proper time of each particle and

$$\begin{aligned} \gamma_H &= 1 + \tfrac{8\Lambda_e}{\kappa^2 H^2}\,, & \gamma_e &= 1 + \tfrac{2e_1e_2}{\kappa m^2}\,, \\ \gamma_m &= \gamma_e^2 + \tfrac{8\Lambda_e}{\kappa^2 m^2}\,, & \sigma &= (1+\sqrt{\gamma_H})(\sqrt{p_0^2+m^2} - cp_0) - \tfrac{m^2}{H}\gamma_e\,, \\ \eta &= \tfrac{\sigma - \frac{m^2}{H}\sqrt{\gamma_m}}{\sigma + \frac{m^2}{H}\sqrt{\gamma_m}}\,. \end{aligned} \qquad (18)$$

with p_0 the initial momentum at $\tau = \tau_0$. It is then straightforward to obtain an exact expression for r as a function of τ, either directly from the second of eqs. (15) or by inserting the expression for $p(\tau)$ into (13) and solving for r as a function of τ.

3 Classification of the solutions

A number of different types of motion are possible, depending upon a combination of four factors: gravitational attraction, the electric force between charges, the effect of the cosmological constant and relativistic effects. The solution is characterized by the signs of γ_m and $\kappa^2\left(H_0 - mf(\tau) + \frac{m}{f(\tau)}\right)^2 - 8\kappa e_1 e_2 - 8\Lambda_e$.

Here we show only the brief analysis of the case of $\Lambda_e < 0$ and the repulsive charges. (A full analysis of all the cases will be reported in another occasion.) The solutions are classified in terms of the $(|q|, p)$ diagram, where the shaded area $\mathcal{J}_\Lambda^2 > 0$ and $B > 0$ correspond to the bounded motions and the area of $\mathcal{J}_\Lambda^2 < 0$ does to the unbounded motions. The boundary of $\mathcal{J}_\Lambda^2 = 0$ is given by

$$p = \sqrt{\left(\frac{H}{2}\right)^2 - \frac{2|\Lambda_e|}{\kappa^2}} \pm \sqrt{\frac{2}{\kappa}\left(q^2 - \frac{|\Lambda_e|}{\kappa}\right)} \qquad (19)$$

There are two types of $(|q|, p)$ diagram depending on whether the vertex $(q_0 = \sqrt{\frac{|\Lambda_e|}{\kappa}}, \sqrt{\left(\frac{H}{2}\right)^2 - \frac{2|\Lambda_e|}{\kappa^2}})$ of $\mathcal{J}_\Lambda^2 = 0$ is within the region $-p_0 \le p \le p_0 : p_0 = \sqrt{(H/2)^2 - m^2}$, or not. Fig.1 is the diagram for $m > \sqrt{2|\Lambda_e|}/\kappa$ where the vertex is outside the region $-p_0 \le p \le p_0$. The q_c and q_d are the values of $|q|$ at the intersections of $\mathcal{J}_\Lambda^2 = 0$ with $p = \pm p_0$, namely,

$$q_{c,d} = \sqrt{\frac{\kappa}{2}\left\{\sqrt{(H/2)^2 - 2|\Lambda_e|/\kappa^2} \mp \sqrt{(H/2)^2 - m^2}\right\} + |\Lambda_e|/\kappa}.$$

The motions corresponding to this diagram are classified into three categories according to the $|q|$ value:
(i) $|q| \le q_0$: bounded motion,
(ii) $q_0 < |q| < q_c$: both bounded and unbounded motions,
(iii) $q_c \le |q|$: unbounded motion.

In Fig.2 the $r(\tau)$ plot for each category is depicted for the parameters $H_0 = 3, m = 1.2$ and $\Lambda_e = -0.1$ with $q_0 = 0.316$ and $q_c = 0.491$: $|q| = 0.1, 0.4$ and 0.6 for the categories (i), (ii) and (iii), respectively. As $|q|$ becomes large, both the period and the amplitude of the motion increase and finally the motion becomes unbounded, because the repulsive force between charges prevails over the attractive forces of gravity and the cosmological constant. Fig.3 shows the corresponding phase space trajectories.

For $m \le \sqrt{2|\Lambda_e|}/\kappa$, the $(|q|, p)$ diagram is given in Fig.4 and the vertex of $\mathcal{J}_\Lambda^2 = 0$ is within the region $-p_0 \le p \le p_0$. The motions are classified into two categories:
(i) $|q| \le q_0$: bounded motion or unbounded motion,
(ii) $q_0 < |q|$: unbounded motion.
The physical region of the category (i) belongs to the shaded area of $\mathcal{J}_\Lambda^2 > 0$ and $B > 0$. A typical phase space trajectory for $q_0 < |q| < q_c$ is shown in Fig.5. Here between two split nonperiodic trajectories (solid curves) there appear an infinite series of tan-type A, B solutions of the unbounded motions.

4 Causal relationships between particles

In general-relativistic theory the spacetime and the motion of the particles are closely related with each other. In our formalism the structure of the spacetime is represented by the lapse-shift functions $N_0(x, z_1(t), z_2(t), p(t))$ and $N_1(x, z_1(t), z_2(t), p(t))$. In Figs. 6 and 7 N_0 and N_1 are plotted $H = 2.1, m = 1, \Lambda = 1.5$ and $q = 0$. These functions change as the positions of the particles 1 and 2 move with time t. The plots on the x axis in the figures represent the positions of the particles.

To see the causal relationships between particles and the space-time structure we try to pursue the path of light signal emitted from particle 2. The path $x(t)$ of the light is governed by $d\tau = 0$, which reads

$$\left(\frac{dx}{dt}\right)^2 + 2N_1\frac{dx}{dt} - (N_0^2 - N_1^2) = 0\,. \tag{20}$$

The equation of the light signal emitted inward (directed to particle 1) is

$$\frac{dx}{dt} = N_0(x(t), z_1(t), z_2(t), p(t)) - N_1(x(t), z_1(t), z_2(t), p(t))\,, \tag{21}$$

and the light emitted outward is described by

$$\frac{dx}{dt} = -N_0(x(t), z_1(t), z_2(t), p(t)) - N_1(x(t), z_1(t), z_2(t), p(t))\,. \tag{22}$$

Let's take first a typical bounded motion in the case of $\Lambda_e = 0$ and the attractive charges for the parameters of $H_0 = 3, m = 1$ and $q = 1$. In Fig.8 the trajectories of light signals emitted from particle 2 at various times T are plotted. The two particles are always in causal contact, because the inward light signal from particle 2 reaches particle 1. We see one striking feature for the case of $\Lambda_e = 0$, namely that the outward light pulse has a constant velocity c, since the equations (21) and (22) become $dx/dt = \pm 1$, where the plus and the minus signs correspond to the light emitted outward from the particle 1 and 2, respectively.

Next we look into the effect of the cosmological constant on the path of the light signal. Fig.9 shows the trajecories of light for the case of a negative cosmological constant $\Lambda_e = -1$ and the same values of the parameters H_0, m and q. The outward light behaves as if it is subjected to a repulsive force, in significant contrast to the particles' trajectories on which the cosmological constant acts effectively as an attractive force. On the other hand, while the positive cosmoligical constant causes a repulsive force between particles, the outward light behaves as if it undergoes an attractive force and approaches a kind of horizon given by the line $N_0(x, z_1(t), z_2(t), p(t)) \pm N_1(x, z_1(t), z_2(t), p(t)) = 0$ which is shown in Fig.10 as a narrow solid line for the case of $\Lambda_e = 0.5$.

When the cosmological constant exceeds a critical value, the particles' motion becomes unbounded and the light signals emitted from the particle 2 exhibit new characteristics as shown in Fig.11 for the case of $\Lambda_e = 2.5$. For small $T(T < 0.9)$, the particles are in causal contact (the inward dotted curve), but for $T \approx 0.9$ the signal just barely catches up with particle 1, which is almost in light-like motion (the inward dashed curve). For $T = 2$ the inward world line $x(t)$ is parallel to $z_1(t)$ at large t and in the outward direction it goes nearly on the same trajectory with the particle 2. For large T $(T > 2)$ the particles are out of causal contact with each other : a light ray sent from particle 2 toward particle 1 receives a strong repulsive effect and ultimately reverses direction, following behind particle 2.

References

[1] T. Ohta and R.B. Mann, Class. Quant. Grav. **13** 2585 (1996).

[2] R.B. Mann and T. Ohta, Phys. Rev. **D57** (1997) 4723; Class. Quant. Grav. **14** (1997) 1259.

[3] R.B. Mann, D. Robins and T. Ohta, Phys. Rev. Lett. **82** (1999)3738; Phys. Rev. **D60** (1999)104048.

Figure Captions

Fig. 1 The $(|q|, p)$ diagram for $\Lambda_e < 0$ and repulsive charges under the condition $m > \sqrt{2|\Lambda_e|}/\kappa$. The dashed line represents $\mathcal{J}_\Lambda - B = 0$.
Fig. 2 The $r(\tau)$ plots for the categories (i)-(iii) for the parameters $H_0 = 3, m = 1.2$ and $\Lambda_e = -0.1$.
Fig. 3 The phase space trajectories corresponding to the plots in Fig.2.
Fig. 4 The $(|q|, p)$ diagram for $\Lambda_e < 0$ and repulsive charges
under the condition $m \leq \sqrt{2|\Lambda_e|}/\kappa$. The dashed line represents $\mathcal{J}_\Lambda - B = 0$.
Fig. 5 The phase space trajectories for $H_0 = 10, m = 0.02, \Lambda_e = -0.5$ and $q_0 < |q| < q_c$.
Fig. 6 N_0 for $H = 2.1, m = 1, \Lambda = 1.5$ and $q = 0$ at various times t.
Fig. 7 N_1 for $H = 2.1, m = 1, \Lambda = 1.5$ and $q = 0$ at various times t.
Fig. 8 The trajectories of light signals emitted from the particle 2 for the case of $\Lambda_e = 0$.
Fig. 9 The trajectories of light signals emitted from the particle 2 for the case of $\Lambda_e = -1$.
Fig. 10 The trajectories of light signals emitted from the particle 2 for the case of $\Lambda_e = 0.5$. The narrow solid line denotes $N_0(x, z_1(t), z_2(t), p(t)) + N_1(x, z_1(t), z_2(t), p(t)) = 0$.
Fig. 11 The trajectories of light signals emitted from the particle 2 for the case of $\Lambda_e = 2.5$.

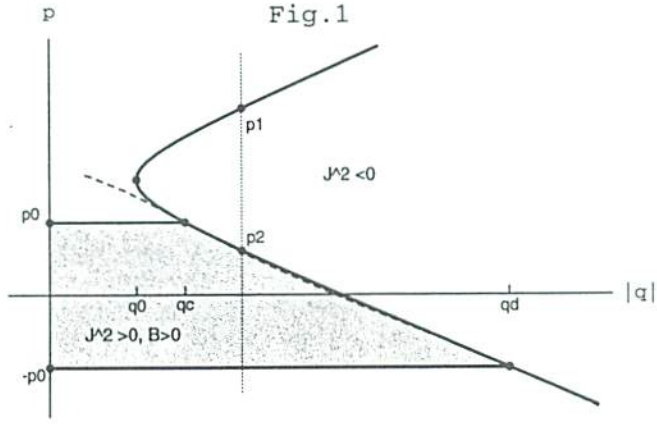

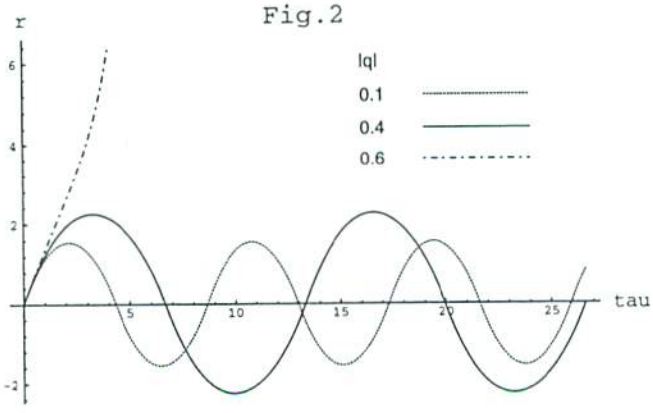

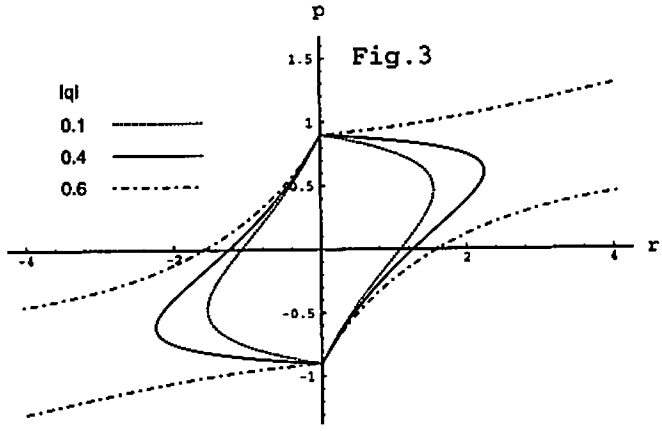
p
Fig.3
|q|
0.1
0.4
0.6
r

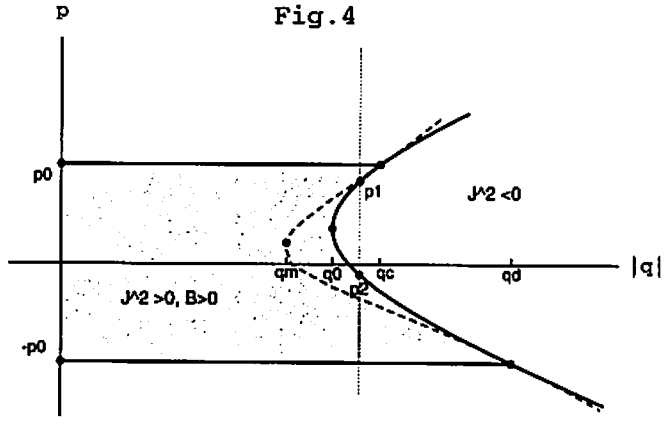
p
Fig.4
p0
-p0
p1
p2
J^2 <0
J^2 >0, B>0
qm
q0
qc
qd
|q|

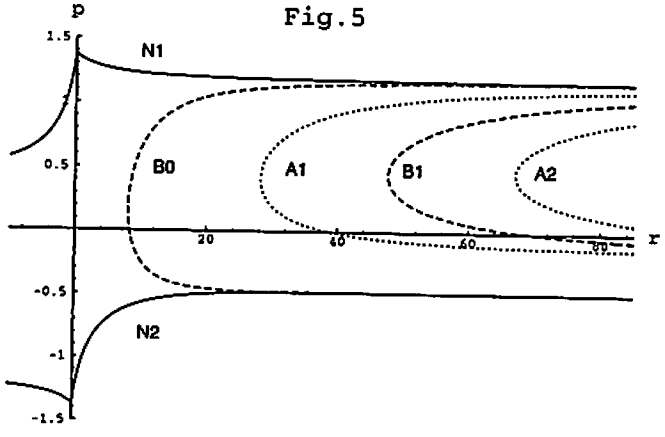
p
Fig.5
N1
N2
B0
A1
B1
A2
r

Fig.6

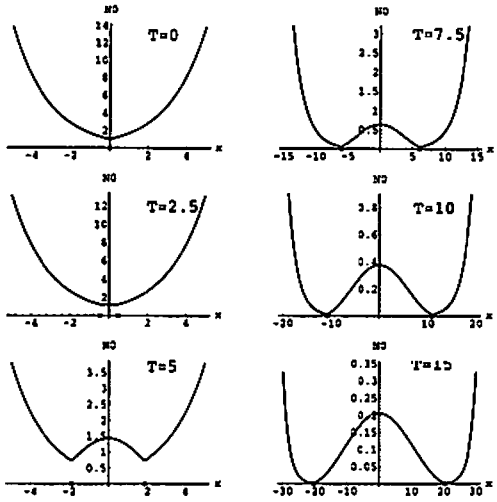

Fig.7

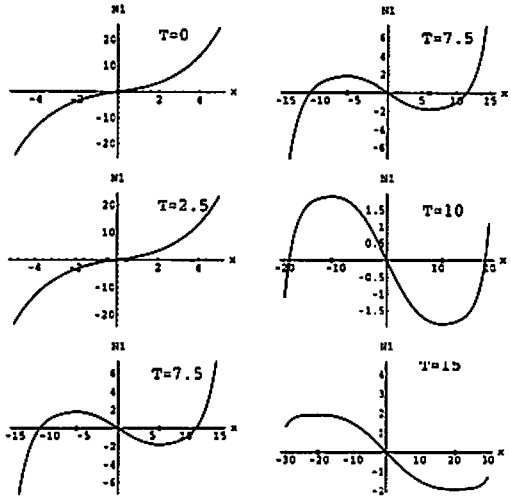

Fig.8

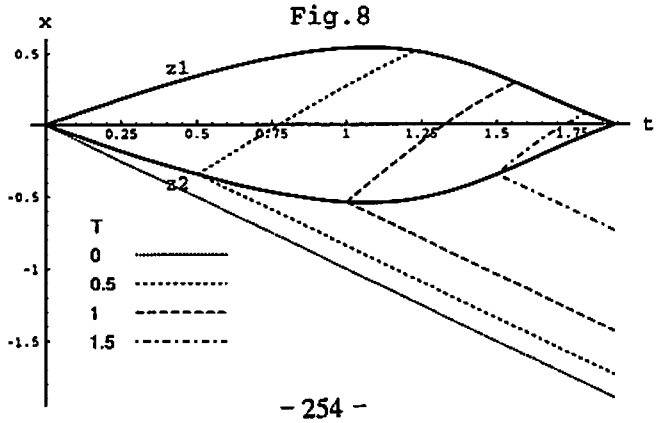

Fig.9

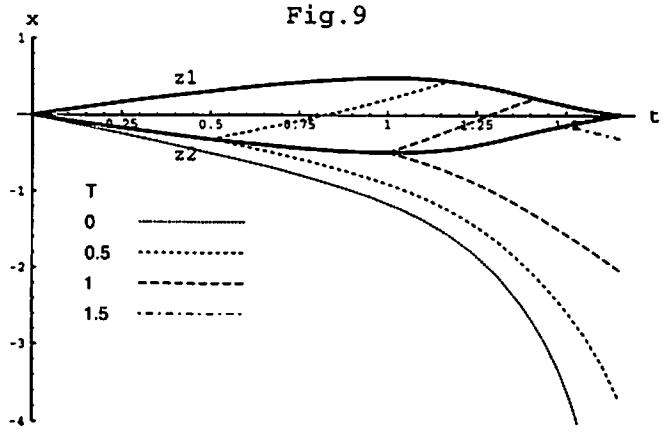

Fig.10

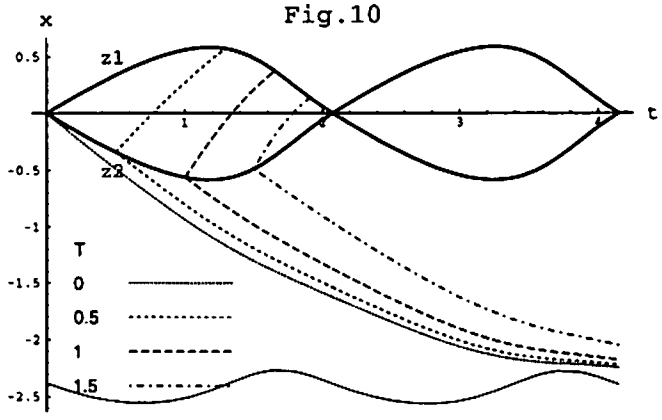

Fig.11

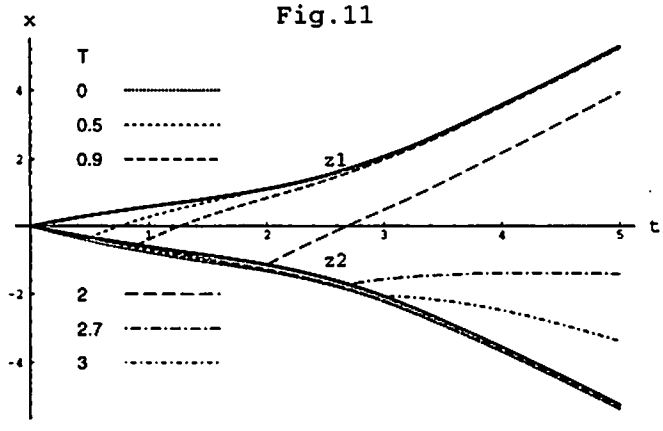

Role of 5D STM Theory in Modified GST Theory

Takao Fukui[1]

Department of Language and Culture, Dokkyo University
Soka, Saitama 340-0042, Japan

Abstract

The 5D Space-Time-Matter cosmology gives a solution of the scale factor. The comparison of the cosmology with the Modified Generalized Scalar-Tensor Cosmology enables us to obtain solutions of the scalar field and of the cosmological term which is assumed to depend not only on the scalar field ϕ but also on its time derivative $\dot{\phi}^2$. The flatness problem is touched upon with a simple solution among the solutions.

1 INTRODUCTION

In order to give a geometrical interpretation to physical quantities, Wesson introduced the 5D Space-Time-Matter theory of gravity[1], or equivalently the induced-matter theory[2]. In the theory, the fifth coordinate of matter in combination with the dimension transposing constants G and c is added to the 4D space-time. The 5D STM is along the same line as the 4D Minkowsky Space-Time where the fourth coordinate of time in combination with c is added to the 3D space. The theory enables us to interpret most properties of matter[3]. Therefore the induced matter theory is a promising idea in studying the physical quantities of the 4D space-time universe in terms of geometrical properties.

Recently, generalized scalar-tensor theory[4] has come back because a self-interaction potential of the scalar field, or the variable cosmological term, in the GST theory might cause the universe to expand with an inflationary fashion. The inflationary era is expected to have existed in the early universe for solving the monopole problem, the flatness problem and the horizon problem[5]. The variable cosmological term in relation to the scalar field has been studied to solve the cosmological"constant" problem too[6,7]. But a new extended inflationary theory has been demanded for examining another problem, an exit problem which the conventional theories are confronting [8]. Therefore, it is necessary to modify the GST theory a little.

A new approach to the cosmological constant problem is then made by assuming that the term is a function of a kinetic term of a scalar field as well as its potential term[9] through modification of the GST theory. The same assumption is made to examine the dark matter problem[10].

Here we study the role of the promising induced matter theory in the modified GST theory and see how much the 5DSTM theory will play a role in solving some of the cosmological problems.

2 MODIFIED GST THEORY

The following variational principle is employed first,

$$0 = \delta \int \left\{ \varphi \left(R - 2\Lambda(\varphi, \partial_i \varphi, \partial^i \varphi) \right) + \frac{16\pi}{c^4} L_m - \omega(\varphi) \frac{\partial_i \varphi \partial^i \varphi}{\varphi} \right\} \sqrt{-g} d\Omega, \tag{1}$$

where Latin index i runs over 0,1,2 and 3. The scalar field ϕ is taken here to be a function of time $x^0 = ct$ alone, $\dot{\phi} \equiv \dot{\phi}(ct)$. We emphasize the cosmological term Λ is assumed to be a function of $\partial_i \varphi \partial^i \varphi$ as well as φ, to give more freedom to the functional forms of Lambda and the scalar field as well. That is, Lambda thus depends on the kinetic energy of BD type scalar field too. That is a generalization of the previous work[6] in which $\Lambda = \Lambda(\phi)$ was assumed. A similar idea has been considered by Moffat[11] in connection

[1] E-mail:tfukui@dokkyo.ac.jp

with the age problem. And a quite recent "quintessence" scenario[9] has a common aspect with this idea. The field equation for the metric field g_{ij} is obtained by varing g_{ij},

$$R_{ij} - \frac{1}{2}g_{ij}R + g_{ij}\Lambda - 2\frac{\partial\Lambda}{\partial b}\phi_{,i}\phi_{,j} = \frac{8\pi}{\phi c^4}T_{ij} + \frac{\omega}{\phi^2}\left(\phi_{,i}\phi_{,j} - \frac{1}{2}g_{ij}b\right) + \frac{1}{\phi}(\phi_{,i;j} - g_{ij}\Box\phi), \tag{2}$$

where $b = \phi_{,l}\phi^{,l}$ and T_{ij} is the energy momentum tensor of matter,

$$T^{ij} = \frac{2}{\sqrt{-g}}\frac{\partial(\sqrt{-g}L_m)}{\partial g_{ij}}.$$

The vacuum energy momentum tensor is defined here as follows,

$$\frac{8\pi}{\phi c^4}T_{ij}^{vac} \equiv \frac{\omega}{\phi^2}\left(\phi_{,i}\phi_{,j} - \frac{1}{2}g_{ij}b\right) + \frac{1}{\phi}(\phi_{,i;j} - g_{ij}\Box\phi) - g_{ij}\Lambda + 2\frac{\partial\Lambda}{\partial b}\phi_{,i}\phi_{,j}. \tag{3}$$

The field equation for ϕ is obtained by varing ϕ and $\phi_{,i}$,

$$R - 2\Lambda - 2\phi\frac{\partial\Lambda}{\partial\phi} + 4\frac{\partial}{\partial x^l}\left(\phi\frac{\partial\Lambda}{\partial b}\right)\phi^{,l} + 4\phi\frac{\partial\Lambda}{\partial b}\Box\phi = \frac{\omega}{\phi^2}b - \frac{2\omega}{\phi}\Box\phi - \frac{b}{\phi}\frac{\partial\omega}{\partial\phi}. \tag{4}$$

Eq.(4) ensures that the conservation law $T^k_{i;k} = 0$ holds as required. Eqs.(2) and (4) are the basic equations for the tensor and scalar fields.

3 APPLICATION TO COSMOLOGY

The field equations in the homogeneous and isotropic perfect fluid cosmologies are derived from the time-time and space-space components of Eq.(2) as follows: (0,0) component of Eq.(2),

$$\left(\frac{\dot{a}}{a}\right)^2 + \frac{kc^2}{a^2} - \frac{\Lambda c^2}{3} + \frac{2}{3}\frac{\partial\Lambda c^2}{\partial\dot{\phi}^2}\dot{\phi}^2 = \frac{8\pi}{3\phi c^2}\epsilon + \frac{\omega}{6}\left(\frac{\dot{\phi}}{\phi}\right)^2 - \frac{\dot{a}}{a}\frac{\dot{\phi}}{\phi}, \tag{5}$$

(1,1) = (2,2) = (3,3) components of Eq.(2),

$$2\frac{\ddot{a}}{a} + \left(\frac{\dot{a}}{a}\right)^2 + \frac{kc^2}{a^2} - \Lambda c^2 = -\frac{8\pi}{\phi c^2}p - \frac{\omega}{2}\left(\frac{\dot{\phi}}{\phi}\right)^2 - \frac{\ddot{\phi}}{\phi} - 2\frac{\dot{a}}{a}\frac{\dot{\phi}}{\phi}. \tag{6}$$

From Eq.(4), we have

$$\begin{aligned}\frac{\ddot{a}}{a} + \left(\frac{\dot{a}}{a}\right)^2 + \frac{kc^2}{a^2} - \frac{\Lambda c^2}{3} - \frac{\phi}{3}\frac{\partial\Lambda c^2}{\partial\phi} + \frac{2}{3}\frac{\partial}{\partial t}\left(\phi\frac{\partial\Lambda c^2}{\partial\dot{\phi}^2}\right)\cdot\dot{\phi} + \frac{2}{3}\phi\frac{\partial\Lambda c^2}{\partial\dot{\phi}^2}\left(\ddot{\phi} + 3\frac{\dot{a}}{a}\dot{\phi}\right) \\ = \omega\frac{\dot{a}}{a}\frac{\dot{\phi}}{\phi} + \frac{\omega}{3}\frac{\ddot{\phi}}{\phi} + \frac{1}{6}\frac{\partial\omega}{\partial\phi}\frac{\dot{\phi}^2}{\phi} - \frac{\omega}{6}\left(\frac{\dot{\phi}}{\phi}\right)^2.\end{aligned} \tag{7}$$

Since a and ϕ are independent of each other, the cross term of a and ϕ in the right and left hand sides of Eq.(7) should be equated, that is,

$$\frac{\partial\Lambda c^2}{\partial\dot{\phi}^2} = \frac{\omega}{2\phi^2}. \tag{8}$$

Then Eq.(7) is separable with a and ϕ as follows,

$$\frac{\ddot{a}}{a} + \left(\frac{\dot{a}}{a}\right)^2 + \frac{kc^2}{a^2} = \frac{1}{3}\left\{\Lambda c^2 + \phi\frac{\partial\Lambda c^2}{\partial\phi} - \frac{1}{2}\frac{\partial\omega}{\partial\phi}\frac{\dot{\phi}^2}{\phi} + \frac{\omega}{2}\left(\frac{\dot{\phi}}{\phi}\right)^2\right\}. \tag{7}'$$

We use Eqs.(5),(6), and (7)' with the assumption Eq.(8) to solve ϕ and Λc^2.

4 5D STM THEORY AND COSMOLOGY

The vacuum field equation of 5D STM theory is obtained by applying the variational principle to $\int R\sqrt{-g}d^5x$, as follows,

$$R_{AB} - \frac{1}{2}g_{AB}R = 0, \tag{9}$$

where capital Latin indices A and B run over 0,1,2,3, and 5. The FRW metric $d^{(4)}s^2$ is extended to a 5D manifold as follows,

$$d^{(5)}s^2 = d^{(4)}s^2 + e^{\mu}(dx^5)^2, \tag{10}$$

where μ is a function of both x^0 and x^5. The field equations in the vacuum 5D universe are obtained from Eq.(9) as follows,

$$\left(\frac{\dot{a}}{a}\right)^2 + \frac{kc^2}{a^2} + \frac{1}{2}\frac{\dot{a}}{a}\dot{\mu} = 0, \tag{11}$$

$$2\frac{\ddot{a}}{a} + \left(\frac{\dot{a}}{a}\right)^2 + \frac{kc^2}{a^2} + \frac{\ddot{\mu}}{2} + \frac{\dot{\mu}^2}{4} + \frac{\dot{a}}{a}\dot{\mu} = 0, \tag{12}$$

$$\frac{\ddot{a}}{a} + \left(\frac{\dot{a}}{a}\right)^2 + \frac{kc^2}{a^2} = 0. \tag{13}$$

Eq.(13)is easily solved [12] as follows,

$$a = \sqrt{-kc^2t^2 + \alpha t + \beta}, \tag{14}$$

where α and β are constants. From Eq.(13)−Eq.(11), the following relation is obtained,

$$\dot{\mu} = 2\frac{\ddot{a}}{\dot{a}}, \tag{15}$$

With Eqs.(11) and (14), the metric coefficient of the fifth coordinate is obtained [12] as,

$$e^{\mu} = C(x^5)\frac{(-2kc^2t + \alpha)^2}{-kc^2t^2 + \alpha t + \beta} \tag{16}$$

where $C(x^5)$ is an integration parameter which is a function of x^5. The solutions Eqs.(14) and (16) satisfy Eq.(12).

5 5D STM THEORY AND GST THEORY

In this section, we see a role of the 5D STM theory in the GST theory. Then we use Eqs.(5), (6), (7)′, and (8) of the GST theory, and Eqs.(14) or equivalently (13), and (16) of the 5D STM theory. Since LHS of Eq.(7)′ is zero by virtue of Eq.(13), the cosmological term is obtained by solving Eqs.(7)′ and (8),

$$\Lambda c^2 = \frac{\omega}{2}\left(\frac{\dot{\phi}}{\phi}\right)^2 + \frac{f_0}{\phi}, \tag{17}$$

where f_0 is a constant. Eq.(17) shows that in the standard FRW universe of ϕ being a constant, Λc^2 is a constant. In the BD theory of constant ω on the other hand, the first term of RHS decreases as t^{-2} for the power-law evolution of ϕ with t. Then Eq.(17) implies the possibility to solve the cosmological

"constant" problem, that is, the big discrepancy in the values of Λc^2 between now and then. A simple example of Λc^2 is shown in Section 6.

The scalar field $\phi(ct)$ is obtained by solving Eqs.(5) and (6). Both Eq.(5) and Eq.(6) happen to give an identical equation for ϕ under the relation, Eq.(8).

From the conservation law, $T^k{}_{i;k} = 0$, the well known equation is derived,

$$\epsilon = \epsilon_\gamma a^{-3(1+\gamma)}, \tag{18}$$

where $\gamma = p/\epsilon$ and ϵ_γ is a constant.

Both Eq.(5) and Eq.(6) with Eqs.(14)-(18) give the following differential equation for ϕ,

$$\dot{\phi} + \frac{a^2+4k\beta c^2}{2(-2kc^2t+\alpha)a^2}\phi = \frac{2a^2}{-2kc^2t+\alpha}\left(\frac{8\pi\epsilon_\gamma}{3c^2}a^{-3(1+\gamma)} + \frac{f_0}{3}\right). \tag{19}$$

Eq.(19) is a linear differential equation of first order. Therefore it can easily be solved for each case of $k = \pm 1, 0$ and $\gamma = -1, 1, 1/3$ and 0 to yield functional forms of the scalar field with time.

We solve Eq.(19) for $k = \pm 1$ as follows,

$$\gamma = -1, \quad \phi = \frac{\mp 2c^2t+\alpha}{a}\left(\frac{16\pi\epsilon_{-1}}{3c^2}\Phi_{k=\pm1} + \frac{2f_0}{3}\Phi_{k=\pm1} + \phi_0\right), \tag{20}$$

$$\gamma = 1, \quad \phi = \frac{32\pi\epsilon_1\left(-8c^4t^2 \pm 8\alpha c^2t - \alpha^2 \pm 4\beta c^2\right)}{3c^2(\alpha^2 \pm 4\beta c^2)^2a^2} + \frac{\mp 2c^2t+\alpha}{a}\left(\frac{2f_0}{3}\Phi_{k=\pm1} + \phi_0\right), \tag{21}$$

$$\gamma = \frac{1}{3}, \quad \phi = \frac{32\pi\epsilon_{1/3}}{3c^2(\alpha^2 \pm 4\beta c^2)} + \frac{\mp 2c^2t+\alpha}{a}\left(\frac{2f_0}{3}\Phi_{k=\pm1} + \phi_0\right), \tag{22}$$

$$\gamma = 0, \quad \phi = \pm\frac{8\pi\epsilon_0}{3c^4a} + \frac{\mp 2c^2t+\alpha}{a}\left(\frac{2f_0}{3}\Phi_{k=\pm1} + \phi_0\right), \tag{23}$$

where

$$\Phi_{k=\pm1} \equiv \frac{a^3}{-4c^4t \pm 2\alpha c^2} + \frac{3}{16c^4}\left\{(\mp 2c^2t+\alpha)a - \frac{\alpha^2 \pm 4\beta c^2}{2}I_F\right\},$$

with

$$I_F \equiv -\frac{1}{c}\arcsin\frac{-2c^2t+\alpha}{\sqrt{\alpha^2+4\beta c^2}} \qquad (k=1),$$

$$I_F \equiv \frac{1}{c}\ln|2c^2t+\alpha+2ca| \qquad (k=-1).$$

We solve Eq.(14) for $k = 0$ as follows,

$$\gamma = -1, \quad \phi = \frac{32\pi\epsilon_{-1}}{15\alpha^2c^2}a^4 + \frac{4f_0}{15\alpha^2}a^4 + \frac{\phi_0}{a}, \tag{24}$$

$$\gamma = 1, \quad \phi = -\frac{32\pi\epsilon_1}{3\alpha^2c^2a^2} + \frac{4f_0}{15\alpha^2}a^4 + \frac{\phi_0}{a}, \tag{25}$$

$$\gamma = \frac{1}{3}, \quad \phi = \frac{32\pi\epsilon_{1/3}}{3\alpha^2c^2} + \frac{4f_0}{15\alpha^2}a^4 + \frac{\phi_0}{a}. \tag{26}$$

$$\gamma = 0, \quad \phi = \frac{16\pi\epsilon_0 t}{3\alpha c^2 a} + \frac{4f_0}{15\alpha^2}a^4 + \frac{\phi_0}{a}. \tag{27}$$

When we take an increasing function of ϕ with an expansion of the universe as is usually expected, an integration constant ϕ_0 should be zero.

6 COMMENTS AND DISCUSSION

In the present work, we have modified the generalized scalar-tensor theory by taking the cosmological term as a function not only of the scalar field but also of the gradient of the scalar field. Since we regard the scalar field as a function only of time, the cosmological term depends on $\dot{\phi}^2$ and ϕ as well. This

means that we regard both the second and the third terms of the Wagoner's Lagrangian density, Eq.(2) in Ref.[3] as a variable cosmological term. This recognition would be justified when we think of the origin of the scalar field. That is, the scalar field appears in 4D space-time as a physical manifestation of the extra part of the higher dimensional universe[13]. The physical manifestation altogether could be recognized as a cosmological term. We in the 4D universe then scrutinize the term as a constant for the de-Sitter universe or a dependence on the temperature for spontaneous symmetry breaking[14] or a kinetic energy-like term in connection with the dark matter[10] or with the age problem[11].

Recently Fukui and Overduin studied the relation of the modified GST theory in the same Lagrangian as that of the present work, Eq.(1), to Wesson's 5D STM theory[9]. There the term plays a role in the periods of false-vacuum energy and stiff matter. The present cosmological term Eq.(17) which is obtained upon the other assumption in the relation of a and ϕ than that made in Ref[9], shows another dependency on the scalar field and its time derivatve. As is seen in Eq.(17), the cosmological term evolves differently with time for each period because ϕ is obtained for each γ. The cosmological term presents a mechanism to create a new cosmological term for succesive cosmological phase transitions and is a way to approach the cosmological "constant" problem[6,7].

Here we see the flatness problem. From Eq.(3), the vacuum energy density is obtained as follows,

$$\epsilon_{vac} = \frac{\phi c^2}{8\pi}\left(-3\frac{\dot{a}}{a}\frac{\dot{\phi}}{\phi} + \frac{f_0}{\phi}\right),$$

and the vacuum pressure is

$$p_{vac} = \frac{\phi c^2}{8\pi}\left(\frac{\ddot{\phi}}{\phi} + 2\frac{\dot{a}}{a}\frac{\dot{\phi}}{\phi} - \frac{f_0}{\phi}\right).$$

From Eq.(5), we derive

$$\frac{kc^2}{H^2a^2} = \Omega + \Omega_{vac} - 1,$$

where H is the Hubble parameter, and the energy density parameter of matter is defined as

$$\Omega \equiv \frac{8\pi}{3H^2\phi c^2}\epsilon,$$

and also the vacuum energy density parameter is

$$\Omega_{vac} \equiv \frac{8\pi}{3H^2\phi c^2}\epsilon_{vac} = -\frac{1}{H}\frac{\dot{\phi}}{\phi} + \frac{f_0}{3H^2\phi}.$$

In the simple case of $k = 0$, $\beta = 0$ during the matter era, Ω_{vac} is obtained as

$$\Omega_{vac} = 1 - \frac{2}{1 + Et^{3/2}},$$

where

$$E \equiv \frac{f_0\Omega^{3/2}c^2}{20\pi\epsilon_0}.$$

The cosmological term is given by Eq.(17) as

$$\Lambda c^2 = \frac{\omega}{8t^2}\left(\frac{1 + 4Et^{3/2}}{1 + Et^{3/2}}\right)^2 + \frac{15E}{4(t^{1/2} + Et^2)}. \tag{28}$$

When we apply the post-Newtonian approximation of the gravitational "constant" G to the required accuracy, G is given in the approximation, by Eqs.(2),(8) and (17), as

$$G = \frac{1}{3\phi}\left(4 - \frac{f_0c^2}{4\pi\dot{T}^{00}}\right), \tag{29}$$

where $\hat{T}_{00}$ is the density of rest-mass[15]. When we use Eq.(29) in the present time $\hat{T}_{00} \sim \epsilon_0$, we obtain $f_0 \sim 4\pi\epsilon_0/c^2$. Then $Et_0^{3/2}$ is about $10^{25}\alpha^{3/2}$ for the present age of the universe, $t_0 \sim 10^{17}$ s, and therefore Ω_{vac} at the present time is slightly less than 1, in the approximation. At the same time, Eq.(28) in the approximation tells us that during the present era Ac^2 decays as t^{-2} in case of a constant ω. In this sipmle case, Eq.(16) tells us that the 5th dimension can be very small, although in general we can alternatively think that the present 4D ST universe is embedded in the 5D STM universe.

The present work with the new assupmtion Eq.(8) widens the role of the 5D STM theory to more periods.

Acknowledgements

The author is grateful to J.M. Overduin, K. Arai, and M. Hashimoto for their useful comments and discussion, and to P.S. Wesson for his constant encouragement.

References

[1] P.S. Wesson. Astron. Astrophys.**119**(1983), 145.

[2] P.S. Wesson, *Space-Time-Matter, Modern Kaluza-Klein Theory* (World Scientific,Singapore 1999).

[3] J.M. Overduin and P.S. Wesson, phys. Rep.**283**(1997), 283.

[4] P.G. Bergmann, Int. J. Theor. Phys.**1**(1968), 25.
R.V. Wagoner, Phys. Rev.**D1**(1970), 3209.

[5] B. Ratra and P.J.E. Peebles, Phys. Rev.**D37**(1988), 3407.
J.D. Barrow and K. Maeda, Nucl. Phys.**B341**(1990), 294.
J.A. Frieman,C.T. Hill, A. Stebbins and I. Waga, Phys. Rev. Lett.**75**(1995), 2077.

[6] M. Endo and T. Fukui, Gen. Rel. Grav.**8**(1977), 833.
K. Arai, M. Hashimoto and T. Fukui, Astron. Astrophys.**179**(1987), 17.
T. Etoh, M. Hashimoto, K. Arai and S. Fujimoto, Astron. Astrophys.**325**(1997), 893.

[7] S. Weinberg, Rev. Mod. Phys.**61**(1989), 1.
Y. Fujii and T. Nishioka, Phys. Rev.**D42**(1990), 361.

[8] S.K. Blau and A.H. Guth, in *300 Years of Gravitation*, ed. S. Hawking and W. Israel (Cambridge 1987), p.524.

[9] T. Fukui and J.M. Overduin, Gen. Rel. Grav.**31**(1999), 1159.

[10] R.P. Caldwell,R. Dave, and P.J. Steinhard, Phys. Rev. Lett.**80**(1998), 1582.

[11] W. Moffat, Phys. Lett.**B357**(1995), 526.

[12] A. Banerjee, B.K. Bhui, and S. Chaterjee, Astron. Astrophys.**232**(1990), 305.

[13] P. Jordan, in *Cosmological Models, Proc. of International Summer Institute. Lisbon, September 1963.* ed. Centro de Cálculo Cientifico Instituto Gulbenkian de Ciência (Lisboa), p.117.

[14] A.D. Linde, JETP Lett.**19**(1974), 183.

[15] S. Weinberg, *Gravitation and Cosmology* (Wiley, New York 1972), p.211.

Probe Particle, Force Balance and Exact Solution[1]

Tetsuya Shiromizu

DAMTP, Centre for Mathematical Sciences,
University of Cambridge
Wilberforce Road, United Kingdom

Abstract

We discuss the relation between the force balance via the spin-spin interactions and the existence of exact solutions which describes spinning multi-black-holes. Moreover we give an exact solution in the string theory.

1 Introduction

A cosmological multi-black hole solution has been discovered by Kastor and Traschen[5](KT solution) in the Einstein-Maxwell theory with a positive cosmological constant Λ(EM-Λ). The solution describes collisions of several black holes(BHs) in asymptotically deSitter space-times. It is worth noting that the solution is the first exact solution such that describes BH-BH collision. It also provides the test of the cosmic censorship and cosmic no-hair conjectures in the inflationary universe.

One may be greatly interested in the spinning version of the KT solution because the rotating cases are generic. Apart from the cosmological cases, the spinning multi-soliton solution was found by Israel & Wilson[7] and Perjes[8](IWP solution) in asymptotically flat space-times. Unfortunately, the solution has naked singularities due to the force balance condition $Q = M$. On the other hand, we can expect that there are cases without singularities in asymptotically deSitter space-times even if $Q = M$. This expectation relies on the causal structure of the single Kerr-Newman-deSitter space-time. So we can obtain the physical advantage of the cosmological version because of no singularity.

The existence of the spinning multi-soliton solution is deeply related to the force balance up to the gravitational spin-spin interaction. The force cancellation has been confirmed for the IWP solution[9].

In this presentation, we will show the force balance including spin-spin interactions by using the probe particle for a stringy black hole and the Kerr-Newman-deSitter(KNdS) spacetimes. The former is consistent with the exact solution of the Einstein-Maxwell-dilaton-axion(EMDA) systems[10]. The latter strongly indicates the existence of the spinning version of the KT solution. In fact we found the exact solution in the string theory with a positive cosmological constant.

2 Force Balance via Spin-Spin Interaction in String Theory

In this section, we firstly derive the EOM for the stringy probe particle by using the Nambu-Goto action with $B_{\mu\nu}$ field. The low energy effective action is the Einstein-Maxwell-dilaton-axion(EMDA) theory, which has the action

$$S_4 = \int d^4x\sqrt{-g}\Big[R - 2g^{\mu\nu}\partial_\mu\phi\partial_\nu\phi - \frac{1}{12}g^{\mu\nu}g^{\alpha\beta}g^{\rho\sigma}e^{-4\phi}H_{\mu\alpha\rho}H_{\nu\beta\sigma} + \frac{1}{2}e^{-2\phi}g^{\mu\nu}g^{\alpha\beta}F_{\mu\alpha}F_{\nu\beta}\Big]. \tag{1}$$

After length calculation, we are resulted in

$$\frac{\mathcal{D}^2\overline{X}^\mu}{d\tau^2} - \frac{q}{m}F^\mu{}_\nu\dot{\overline{X}}^\nu - \frac{q}{2m}{}^{(4)}\nabla^\mu F_{\alpha\beta}S^{\alpha\beta} + \frac{1}{2}{}^{(4)}R^\mu{}_{\nu\alpha\beta}\dot{\overline{X}}^\nu S^{\alpha\beta} - \frac{1}{4}\Big({}^{(4)}\nabla^\mu H_{\alpha\nu\beta} - {}^{(4)}\nabla_\nu H^\mu{}_{\alpha\beta}\Big)\dot{\overline{X}}^\nu S^{\alpha\beta} = 0, \tag{2}$$

where $\mathcal{D}/d\tau := \dot{\overline{X}}^\mu{}^{(4)}\nabla_\mu$.

[1] This talk is based on Refs. [1, 2, 3, 4]

Now we can confirm the force balance between the gravitational spin-spin, dipole-spin and axion-spin interactions when the Bogomol'nyi type bound is saturated. he spinning multi-soliton solution exists in the $D = 4$ EMDA system. This solution is the straightforward extension of the IWP solution and saturates the Bogomol'nyi bound, *i.e.*, $|Q| = \sqrt{2}M$. We expect that the force balance holds via the gravitational spin-spin interaction therein. To check the force balance, we consider the motion of a stringy probe particle on the background geometry of the single soliton with $Q = \sqrt{2}M$. In the limit of the slow rotating the metric, vector potential and axion field are written as

$$ds^2 = -\Big(1+\frac{2M}{r}\Big)^{-1}dt^2 + \Big(1+\frac{2M}{r}\Big)d\mathbf{x}^2 + \frac{4\epsilon_{ijk}J^j x^k}{r^3}dtdx^i + O(a^2), \tag{3}$$

$$A \simeq \frac{1}{\sqrt{2}}e^{2\phi}dt - \frac{Q}{r^3 M}\epsilon_{ijk}J^j x^k dx^i \tag{4}$$

and

$$a = \frac{2J^i x^i}{r^3} + O(a^2), \tag{5}$$

where a is the parameter of the angular momentum so that $\vec{J} = (0, 0, Ma)$. One can find the exact expression of the above solution in Ref. [10].

In the order of $O(1/r^3)$, the spatial components of the equation of the motion for a probe is given by

$$\begin{aligned} \partial_\tau^2 \overline{X}^i &\simeq -{}^{(4)}\Gamma^i_{\alpha\beta}\dot{\overline{X}}^\alpha\dot{\overline{X}}^\beta + \frac{q}{m}F^i{}_\alpha\dot{\overline{X}}^\alpha \\ &\simeq -\Big(2-\sqrt{2}\frac{q}{m}\Big)\partial^i\phi \end{aligned} \tag{6}$$

because of $g_{S00} = e^{2\phi}g_{00} = -e^{4\phi}$. Hence we can see the force cancellation between the Newtonian-like gravitational and the Coulombic electrostatic forces when $q = \sqrt{2}m$ holds.

Let us confirm the force balance via the gravitational spin-spin interaction. The spin-spin, dipole-spin and axion-spin interaction forces are

$$F^i_{\rm spin} = -\frac{1}{2}R^i{}_{0jk}S^{jk} + O\Big(\frac{1}{r^5}\Big) \tag{7}$$

$$F^i_{\rm dipole} = \frac{q}{2m}S^{jk(4)}\nabla^i F_{jk} + O\Big(\frac{1}{r^5}\Big) \tag{8}$$

and

$$F^i_{\rm axion} = -\frac{1}{4}\partial^i H_{j0k}S^{jk} + O\Big(\frac{1}{r^5}\Big). \tag{9}$$

respectively. Thus the total force in the order of $O(1/r^4)$ becomes

$$F^i_{\rm spin} + F^i_{\rm dipole} + F^i_{\rm axion} = \Big(2-\frac{qQ}{mM}\Big)\partial_i\Big[\frac{-\mathbf{J}\cdot\mathbf{S} + 3(\mathbf{S}\cdot\mathbf{r})(\mathbf{J}\cdot\mathbf{r})}{r^3}\Big] + O\Big(\frac{1}{r^5}\Big), \tag{10}$$

where $S^i := (1/2)\epsilon^{ijk}S^{jk}$ and $\mathbf{r} := \mathbf{r}/r$. As we can easily see, the above total force exactly vanishes when the Bogomol'nyi type bound is saturated, that is, $Q = \sqrt{2}M$ and $q = \sqrt{2}m$. This is related to the exact multi-soliton solution in EMDA system[10].

3 Force Balance via Spin-Spin Interaction in Cosmos

In this section we show the force balance between the charged probe particle and the Kerr-Newman-deSitter black hole. The equation of motion for a spinning charged particle was derived by Dixon[11] based on the Papapetrou's work[12]. The basic equations are

$$v^\nu\nabla_\nu p^\mu = -\frac{1}{2}R^\mu{}_{\nu\alpha\beta}v^\nu S^{\alpha\beta} + qF^\mu{}_\nu v^\nu + \frac{gq}{4m}\Big(\frac{p\cdot v}{-m}\Big)\nabla^\mu F_{\alpha\beta}S^{\alpha\beta} \tag{11}$$

and

$$v^\mu \nabla_\mu S^{\alpha\beta} = p^\alpha v^\beta - p^\beta v^\alpha + \frac{gq}{2m}\Big(-\frac{p\cdot v}{m}\Big)\Big(S^{\mu\alpha}F_\mu{}^\beta - S^{\mu\beta}F_\mu{}^\alpha\Big), \tag{12}$$

where $\mu = 0,1,2,3$ and $v^\mu = dx^\mu(\tau)/d\tau$. p^μ and $S^{\mu\nu}$ are the 4-momentum and the angular momentum tensor, respectively. g is the gyromagnetic ratio of the probe particle. " $\cdot$ " denotes the inner product with respect to the metric, that is, $X\cdot Y = g_{\mu\nu}X^\mu Y^\nu$. We adopt the normalisation $v\cdot v = -1$. As we want to set the orbit $x^\mu(\tau)$ to be the center of the mass, we impose the "supplementary condition" such that

$$p^\mu S_{\mu\nu} = 0. \tag{13}$$

It is well known in general that p^μ is not parallel to v^μ due to the spin. ¿From Eqs. (11) and (12) with the condition (13), we obtain the relation between v^μ and p^μ,

$$v^\mu \simeq \frac{1}{mf}\Big[p^\mu - \frac{q}{m^2 f^2}S^{\mu\nu}F_{\nu\alpha}p^\alpha\Big(1-\frac{g}{2}f\Big)\Big] \tag{14}$$

in the lowest order needed for the later evaluation of the gravitational spin-spin interaction and the slow rotating limit of the background space-time. In Eq. (14), the function, f, is defined by

$$f = \frac{1}{m}\frac{p\cdot p}{v\cdot p}. \tag{15}$$

Now we can confirm the force cancellation including the gravitational spin-spin interaction between a probe particle and the central Kerr-Newman-deSitter(KNdS) black hole. For this purpose we omit the higher order term of the angular momentum. Namely, we take the slow rotating limit and the metric becomes

$$ds^2 = -V(r)dt^2 + \frac{1}{V(r)}dr^2 + r^2 d\Omega_2^2 + 2a(V-1)\sin^2\theta dt d\varphi + O(a^2), \tag{16}$$

where a is the parameter of the angular momentum and $V(r) = 1 - 2M/r + Q^2/r^2 - (\Lambda/3)r^2$. $\Lambda = 3H^2$ is a positive cosmological constant. The vector potential is

$$A = -\frac{Q}{r}(dt - a\sin^2\theta d\varphi) + O(a^2). \tag{17}$$

This system has two Killing vectors $\xi = \partial_t$ and $\psi = \partial_\varphi$. These Killing vectors satisfy $\pounds_\kappa A^\mu = 0$ and $\pounds_\kappa F_{\mu\nu} = 0$ and thus we have two constants of motion.

The constants of the motion related to the Killing vectors, ξ and ψ, become

$$\begin{aligned} -Q_\xi &= -\xi^\mu(p_\mu + qA_\mu) - \frac{1}{2}S^{\mu\nu}\nabla_\mu\xi_\nu \\ &= Vp^0 - a(V-1)\sin^2\theta p^\varphi + \frac{qQ}{r} - \frac{aS}{r^2}(V-1)\cos^2\theta \end{aligned} \tag{18}$$

and

$$\begin{aligned} Q_\psi &= \psi^\mu(p_\mu + qA_\mu) + \frac{1}{2}S^{\mu\nu}\nabla_\mu\psi_\nu \\ &= a(V-1)\sin^2\theta p^0 + r^2\sin^2\theta p^\varphi + \frac{aqQ}{r}\sin^2\theta + S\cos^2\theta, \end{aligned} \tag{19}$$

respectively. Now we assume $v^\vartheta = p^\vartheta = 0$. Setting $Q_\xi = -m$ and $Q_\psi = S\cos^2\theta$, p^0 and p^φ can be written as

$$p^0 = \frac{m}{V}\Big(1-\frac{qQ}{mr}\Big) \quad \text{and} \quad p^\varphi = -\frac{aqQ}{r^3} - \frac{ma(V-1)}{r^2 V}\Big(1-\frac{qQ}{mr}\Big). \tag{20}$$

For simplicity we also assume that the spin vector $\tilde{S}$ of the probe particle is parallel to that of the background space-time, $\tilde{S} = (0, 0, S)$ in a sort of Cartesian coordinate. In the present coordinate of Eq. (16), each components of the spin tensor $S^{\mu\nu}$ are written as

$$S^{\theta\varphi} = \frac{\cos\theta}{\sin\theta}\frac{S}{r^2}$$

and $S^{r\theta} = S^{r\varphi} = 0$. In this case, we can show

$$v^\mu \nabla_\mu (p \cdot p) = \frac{gq}{m}\left(\frac{p \cdot v}{-m}\right) p^\mu \nabla_\mu F_{\theta\varphi} S^{\theta\varphi} + O(aS^2). \tag{21}$$

Let us determine the reading order of the function, f, defined by Eq. (15). First of all, Eq. (14) yields

$$v^0 = \frac{1}{mf}p^0, \quad v^r = \frac{1}{mf}p^r, \quad v^\theta = \frac{1}{mf}p^\theta + O(a^2), \quad v^\varphi = \frac{1}{mf}p^\varphi + O(a^2 S) \tag{22}$$

which implies

$$p^\mu p_\mu = (mf)^2 v_\mu v^\mu + O(a^2) = -(mf)^2 + O(a^2). \tag{23}$$

Substituting these approximate expression into Eq. (21), we obtain the equation for the function f:

$$v^\mu \partial_\mu \ln f^2 = -\frac{gaSqQ}{m^2} v^\mu \partial_\mu \left(\frac{1}{r^3}\right)\cos^2\theta + O(a^2), \tag{24}$$

and then

$$\begin{aligned} f &\simeq e^{-\frac{gaSqQ}{m^2 r^3}\cos^2\theta} \\ &\simeq 1 - \frac{gaSqQ}{m^2 r^3}\sin\theta\cos\theta =: 1 - g\tilde{f}, \end{aligned} \tag{25}$$

where $\tilde{f} = \frac{aSqQ}{m^2 r^3}\cos^2\theta$.

Now we can calculate the force acting on the probe particle. Noting

$$\begin{aligned} v^\mu \partial_\mu p^r &= m v^\mu \partial_\mu (f v^r) \\ &= m f v^\mu \partial_\mu v^r + m (v^r)^2 \partial_r f, \end{aligned} \tag{26}$$

we see that the equation of motion becomes

$$\begin{aligned} mf v^\mu \partial_\mu v^r &= -m(v^r)^2 \partial_r f - \Gamma^r_{\alpha\beta} v^\alpha p^\beta - \frac{1}{2} R^r{}_{\nu\alpha\beta} v^\nu S^{\alpha\beta} + q F^r{}_\nu v^\nu + \frac{gq}{4m}\left(-\frac{p \cdot v}{m}\right)\nabla^r F_{\alpha\beta} S^{\alpha\beta} \\ &=: mf F^r, \end{aligned} \tag{27}$$

where F^μ denotes the force per unit mass. Using Eqs. (22) $\sim$ (25), we obtain the total force,

$$F^r = \frac{d^2 r}{d\tau^2} \simeq \frac{1}{3}\Lambda r - \frac{Mm - Qq}{mr^2} + \frac{(m^2 - q^2)Q^2}{m^2 r^3} + \frac{3aS(2Mm - gQq)}{m^2 r^4}\cos^2\theta. \tag{28}$$

Eq (28) obviously yields $F^r \simeq \frac{1}{3}\Lambda r = H^2 r$ as $Q = M, q = m$ and $g = 2$. This expression of the force is same as pure deSitter space-time case. That is, the force cancellation holds including the order of the gravitational spin-spin interaction except for the repulsive force due to the cosmological constant. We can show that F^θ and F^φ are negligible under the approximation used here.

4 A New Exact Solution in 'String Theory'

we will give an exact solution in the four dimensional Einstein-Maxwell-Dilaton-Axion(EMDA) theory with a positive Λ(EMDA-Λ) which describe a low energy string theory except for a positive Λ.

In the Einstein frame the action of the four dimensional EMDA-Λ theory is

$$S_4 = \int d^4x\sqrt{-g}\Big[R - 2(\nabla\phi)^2 - e^{-2\phi}F_{\mu\nu}F^{\mu\nu} - \frac{1}{12}e^{-4\phi}H_{\mu\nu\sigma}H^{\mu\nu\sigma} - e^{2\phi}\Lambda\Big], \tag{29}$$

where ϕ, $F_{\mu\nu}$ and $H_{\mu\nu\sigma}$ are the dilaton, field strength of the electromagnetic and three form tensor fields, respectively. In this paper, Λ is assumed to be a positive constant.

Firstly, we give the expression of the exact solution without the explanation of the derivation. The metric $g_{\mu\nu}$, vector potential A_μ and the three form $H_{\mu\nu\sigma}$ are

$$g_{\mu\nu}dx^\mu dx^\nu = a^2\Big[-F(d\tau + \omega_i dx^i)^2 + F^{-1}\delta_{ij}dx^i dx^j\Big] \tag{30}$$

$$A = \frac{F}{\sqrt{2}}(d\tau + \omega_i dx^i) \tag{31}$$

and

$$H_{\mu\nu\sigma} = 24A_{[\mu}\partial_\nu A_{\sigma]}, \tag{32}$$

where

$$F^{-1} = 1 + \mathrm{Re}\Big[\sum_i \frac{M_i}{a^2|\mathbf{x} - \mathbf{x}_i|}\Big] \tag{33}$$

$$\omega = \mathrm{Re}\Big[\sum_i \frac{N_i}{a^2|\mathbf{x} - \mathbf{x}_i|}\Big] \tag{34}$$

and the relation between ω_i and the above harmonic function ω is given by

$$\epsilon_{ijk}\partial_j\omega_k = \partial_i\omega. \tag{35}$$

M_i and N_i are real parameters. $\mathbf{x}_i$ are complex constant vectors. The dilaton field is

$$e^{2\phi} = \frac{F}{a^2}. \tag{36}$$

a is the function of the time coordinate τ so that

$$a(\tau) = e^{H_0\tau}, \tag{37}$$

where $H_0 := \pm\sqrt{\Lambda}/2$. This solution apparently induces the non-cosmological dilatonic IWP solution[10] in the limit of $H_0 = 0$.

In the same way as the non-rotating dilatonic KT solution[13], we can see that the solution given by us here, the rotating dilatonic KT solution, has the timelike singularities which surrounds solitons. This is the reason why we say dashed 'Black Hole' in the title and the abstract of this paper. Rigourously speaking, the solution does not describe black holes.

5 Discussion

We confirmed the force cancellation including the gravitational spin-spin interaction between a probe particle and the slow rotating Kerr-Newman-deSitter(KNdS) space-time. We remind readers that the KNdS space-time with $Q = M$ is free from naked singularities in the slow rotating limit. The force balance holds when $Q = M$, $q = m$ and $g = 2$. As we said, this fact may suggest the existence of the exact solution which is the spinning version of the Kastor-Traschen solution. It is important to remind

you that one of the present authors found a new exact solution which is the spinning dilatonic version of the Kastor-Traschen solution in the Einstein-Maxwell-dilaton-axion theory with a positive cosmological constant[3].

Even in asymptotically deSitter space-times, the force balance indicates the existence of a symmetry which might be slightly related to supersymmetry. The symmetry should give the relation between components of the metric and the electromagnetic field and help us to solve the Einstein equation. More precisely, the energy bound as the Bogomol'nyi bound holds and a symmetry appears when the bound is saturated. The saturation yields the Killing spinor like equation related to supersymmetry and the equation gives a relation between components. In fact, we can easily show the bound nature in certain case.

References

[1] T. Shiromizu, Phys. Lett. **B460**141(1999)

[2] T. Shiromizu, Phys. Rev. **D60**, 104046(1999)

[3] T. Shiromizu, Prog. Theor. Phys. **102**, 1207(1999)

[4] T. Shiromizu and U. Gen, to be published in CQG[gr-qc/9912040]

[5] D. Kastor and J. Traschen, Phys. Rev. **D47**, 5370(1993)

[6] D. R. Brill, G. T. Horowitz, D. Kastor and J. Traschen, Phys. Rev. **D49**, 840(1994)

[7] W. Israel and G. A. Wilson, J. Math. Phys. **13**, 865(1972)

[8] Z. Perjes, Phys. Rev. Lett. **27**, 1668(1971)

[9] J. Tiomno, Phys. rev. **D7**,356(1973);
D. Kastor and J. Traschen, Class. Quantum Grav. **16** (1999),1265

[10] R. Kallosh, D. Kastor, T. Ortin and T. Torma, Phys. Rev. **D50**, 6374(1994)

[11] W. G. Dixon, Proc. Roy. Soc. Lond. **A314**, 499(1970)

[12] A. Papapetrou, Proc. Roy. Soc. Lond. **A209**, 248(1951)

[13] J. H. Horne and G. T. Horowitz, Phys. Rev. **D48**,5457(1993)

Phantom Field: a form of dark energy[1]

Takeshi Chiba[2]

Department of Physics, University of Tokyo,
Tokyo 113-0033, Japan

Abstract

We present a model for the "phantom" component which has an equation of state with $w = p/\rho < -1$ in which the dynamics is driven solely by (non-canonical) kinetic terms rather than by potential terms.

1 Introduction

Recent indirect or direct observations suggest that the Universe is currently dominated by an energy component with negative pressure[2, 3, 4, 5]. One possibility for such a component is the cosmological constant. Another possibility is dynamical vacuum energy or quintessence, a temporary decreasing and spatially inhomogeneous component with negative pressure[6, 7, 8, 9, 10, 11, 12, 13, 14, 15, 16, 17]. Only recently, a more radical candidate (called "phantom" component) has been proposed which is "growing" in time[18].

Two problems arise from such a vacuum energy. The first is the fine-tuning problem: the vacuum energy density of order $\sim 10^{-47}\mathrm{GeV}^4$ requires the introduction of a new mass scale about 14 orders of magnitude smaller than the electroweak scale. The second is the coincidence problem: the conditions in the early universe have to be set very carefully in order for the energy density of the vacuum and that of the matter to be comparable today. These problems are degenerate for the cosmological constant, however, they are separated in quintessence. A class of quintessence can avoid the coincidence problem by means of the attractor solution[7, 13]. It is shown that the quintessence field approaches a common evolutionary track for a very wide range of initial conditions, so that the cosmology is extremely insensitive to the initial conditions.

Usually the quintessence field is modeled by a scalar field with a canonical kinetic term and a potential term. However, we show that a scalar field with solely kinetic terms can (even without potential terms), albeit they are non-canonical, mimic such a (canonical) quintessence field. Our model is a natural extension of the kinetically driven inflation model proposed recently[19]. A mechanism is proposed by which a dilaton remains massless[20]. Assuming universality of the dilaton coupling functions, it has been shown that the dilaton evolves cosmologically towards values where it decouples from matter (so called "Least Coupling Principle")[20].

Unlike the usual potentially driven quintessence model which automatically satisfies the weak energy condition, allowing non-canonical kinetic terms enables us to model the missing energy component which violates even the weak energy condition (so called "phantom field"[18]). Only recently, Caldwell draw our attention to consider more general equation of state with $w = p/\rho < -1$[18]. As he noted, since such a "phantom" equation-of-state cannot be achieved with a canonical Lagrangian and Einstein gravity, considering the phantom field requires some extension: either (i) non-canonical Lagrangian or (ii) non-Einstein gravity (or both). The latter possibility seems unlikely since the deviation from general relativity at the present time is strongly constrained by the solar system experiments[21]. Our attempt is minimal one: non-canonical kinetic terms without a potential term. We intend to develop a more general study by including potential terms as well in the near future.

The organization of the paper is as follows. In Sec.2, we present our model. In Sec.3, we give a model which has a scaling solution with a constant equation of state of $w < -1$, and show that the scaling solution is a late-time attractor. Sec.4 is devoted to summary.

[1] This work is based on [1].

[2] E-mail: chiba@utap.phys.s.u-tokyo.ac.jp

2 basics

We consider the following action of a single scalar field ϕ minimally coupled with gravity:

$$S = \int d^4x\sqrt{-g}\left(\frac{1}{2\kappa^2}R + p(\phi, \nabla\phi)\right) + S_B, \tag{1}$$

where $\kappa^2 \equiv 8\pi G$ and S_B denotes the action of the background matter and/or radiation. Following[19], for simplicity, we only consider Lagrangians which depend only on the scalar field ϕ and its derivative squared[3]

$$X \equiv -\frac{1}{2}\nabla^\mu\phi\nabla_\mu\phi. \tag{2}$$

For the general action of the scalar field (1), the field equations are given by

$$R_{\mu\nu} - \frac{1}{2}g_{\mu\nu}R = \kappa^2\left(\frac{\partial p(\phi, X)}{\partial X}\nabla_\mu\phi\nabla_\nu\phi + p(\phi, X)g_{\mu\nu} + T^B_{\mu\nu}\right) \tag{3}$$

where $T^B_{\mu\nu}$ denotes the energy-momentum tensor of the background. Eq.(3) shows that $p(\phi, X)$ in the action (1) actually corresponds to the "pressure", p_ϕ, of the scalar field[19], while the energy density, ρ_ϕ, is given by $\rho_\phi = 2X\partial p/\partial X - p$. Hence the extrema of $p(\phi, X)$ with respect to X correspond to the same equation of state as that of a cosmological constant: $\rho_\phi + p_\phi = 2X\partial p/\partial X = 0$.

We assume that the universe is described by a flat homogeneous and isotropic universe model with the scale factor a. The time coordinate is so normalized that $a = 1$ at present. The field equations are then

$$H^2 := \left(\frac{\dot{a}}{a}\right)^2 = \frac{\kappa^2}{3}(\rho_B + \rho_\phi) = \frac{\kappa^2}{3}\left(\rho_B + 2X\frac{\partial p}{\partial X} - p\right), \tag{4}$$

$$\frac{\ddot{a}}{a} = -\frac{\kappa^2}{6}(\rho_B + 3p_B + \rho_\phi + 3p_\phi), \tag{5}$$

$$\dot{\rho}_B = -3H(\rho_B + p_B) =: -3H(1 + w_B)\rho_B, \tag{6}$$

$$\ddot{\phi}\left(\frac{\partial p}{\partial X} + \dot{\phi}^2\frac{\partial^2 p}{\partial X^2}\right) + 3H\frac{\partial p}{\partial X}\dot{\phi} + \frac{\partial^2 p}{\partial X\partial\phi}\dot{\phi}^2 - \frac{\partial p}{\partial\phi} = 0 \tag{7}$$

where ρ_B and p_B are the energy density and the pressure of the background matter and/or radiation, respectively.

Since we only consider kinetic terms, we must impose that the function $p(\phi, X)$ vanishes when $X \to 0$.[4] Near $X = 0$, a generic Lagrangian may be expanded as

$$p(\phi, X) = K(\phi)X + L(\phi)X^2 + \cdots. \tag{8}$$

3 phantom field

In this section, we construct a model of a power-law phantom field which is recently proposed as an alternative to the dark energy component[18]. In fact, in Ref.[18], a scalar field with a kinetic term of inverted sign is introduced as a toy model of such a component: the Lagrangian density is given by $\mathcal{L}_P = +\frac{1}{2}\nabla_\mu\phi\nabla^\mu\phi - V(\phi)$. The concern is the tachyonic instability for ϕ. However, as shown in [18], as long as $V_{,\phi\phi}$ is negative, such an instability is not developed. For example, for a constant equation of state, one can show $V_{,\phi\phi} = \frac{3}{2}(1 - w_P)[\dot{H} - \frac{3}{2}H^2(1 + w_P)]$, thus it is negative as long as $-2 < w_P < -1$. Our model will not suffer from such a restriction even for a constant equation of state.

[3] We use the metric signature $(- + ++)$.

[4] This amounts to assuming some resolution of the cosmological constant problem. The situation is the same as assuming the minimum energy of the potential is zero in the (canonical) quintessence field with a potential term.

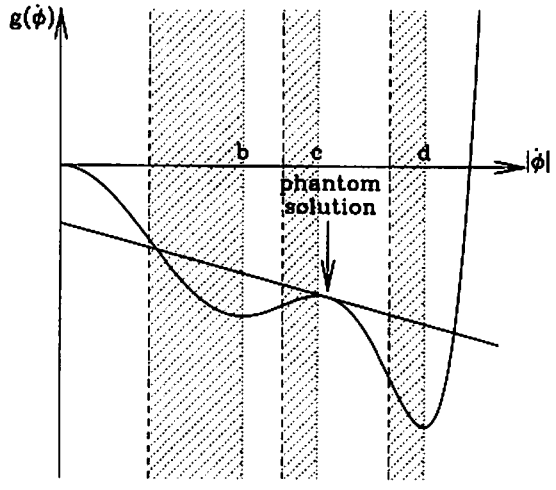

Figure 1: A sketch of the function $g(\dot{\phi})$. $c_s^2 < 0$ in the shaded regions. The phantom solution is one of the solutions of Eq.(13) at which $\dot{\phi} g_{,\dot{\phi}} < 0$ and $g_{,\dot{\phi}}/\dot{\phi} g_{,\dot{\phi}\dot{\phi}} > 0$ and the intersection of the tangent with the vertical axis is negative.

3.1 scaling solution

As an Ansatz for a kinetic Lagrangian, we consider $p(\phi, X) = f(\phi)g(X)$. One can show the equation of motion Eq.(7) has a solution $X_0 = \text{const.}$ with the function $f(\phi)$ being of form

$$f(\phi) \propto \phi^{-\alpha} \tag{9}$$

if X_0 satisfies

$$2\frac{\partial \ln g}{\partial \ln X}\bigg|_{X=X_0} = \frac{1+w_Q}{w_Q}. \tag{10}$$

The equation of state is characterized by

$$w_P \equiv \frac{p_P}{\rho_P} = \frac{(1+w_B)\alpha}{2} - 1, \tag{11}$$

then the phantom field which violates the weak energy condition, $w_P < -1$, corresponds to $\alpha < 0$.

We determine the function $g(X)$ which has a phantom solution. We impose the following conditions on $g(X)$ other than $g(X) \to 0$ for $X \to 0$(vacuum triviality) and $g(X) > 0$ for $X \to \infty$(positivity of the energy density for large X): (i) the positivity of the energy density $\rho_P = f(2Xg_{,X} - g) > 0$ because we are considering the missing energy component; (ii) the violation of the weak energy condition, $\rho_P + p_P = 2fXg_{,X} < 0$; (iii) the stability against perturbations, $c_s^2 = g_{,X}/(g_{,X} + 2Xg_{,XX})$.

In terms of $\dot{\phi}$ (so that $X = \dot{\phi}^2/2$) these conditions are rewritten as: (i') $g_{,\dot{\phi}}\dot{\phi} - g > 0$, which is geometrically interpreted as the intersection of the tangent to the curve $g = g(\dot{\phi})$ at the point $\dot{\phi}$ with the vertical axis is negative; (ii') $\dot{\phi} g_{,\dot{\phi}} < 0$; (iii') $g_{,\dot{\phi}}/(\dot{\phi} g_{,\dot{\phi}\dot{\phi}}) > 0$. Thus, for $\dot{\phi} > 0$, $g(\dot{\phi})$ should satisfy $g_{,\dot{\phi}} < 0$ and $g_{,\dot{\phi}\dot{\phi}} < 0$. Therefore, $g(\dot{\phi})$ must have at least three extrema for $\dot{\phi} > 0$ and hence be an eighth-order

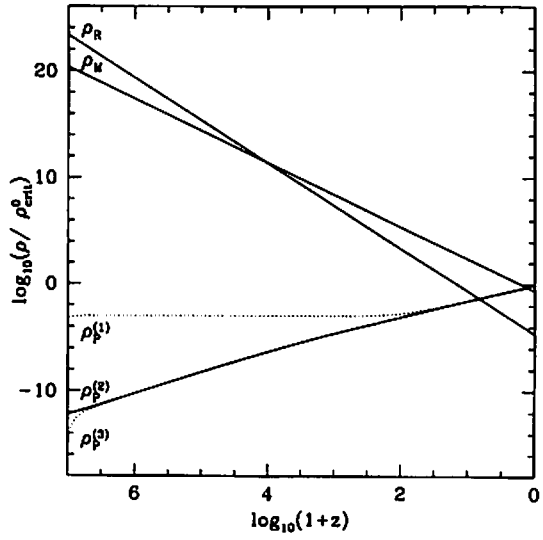

Figure 2: Energy densities of radiation, ρ_R, matter, ρ_M, and phantom field for various initial conditions, $\rho_P^{(i)}$, $i = 1, 2, 3$, against the redshift. The initial conditions for $\rho_P^{(2)}$ correspond to that of the phantom solution in the radiation dominated universe. The initial energy density of the phantom field which converges on the phantom solution spans more than 10 orders of magnitude.

function of $\dot{\phi}$. We parameterize $g(\dot{\phi})$ as[5]:

$$\begin{aligned} g(\dot{\phi}) &= \int_0^{\dot{\phi}} \dot{\phi}(\dot{\phi}^2 - b^2)(\dot{\phi}^2 - c^2)(\dot{\phi}^2 - d^2)d\dot{\phi} \\ &=: \frac{1}{8}\dot{\phi}^8 - \frac{1}{6}A\dot{\phi}^6 + \frac{1}{4}B\dot{\phi}^4 - \frac{1}{2}C\dot{\phi}^2, \end{aligned} \tag{12}$$

where b, c and d are constants corresponding to the extrema of $g(\dot{\phi})$ as shown in FIG. 1. A sketch of $g(\dot{\phi})$ which satisfies the above conditions (i'), (ii") and (iii') is shown there. In the shaded regions, $c_s^2 < 0$ so that the solution is unstable for perturbations on all length scale. From the above equation, the scaling solutions satisfy

$$w_P = \frac{C\dot{\phi}^2/2 - B\dot{\phi}^4/4 + A\dot{\phi}^6/6 - \dot{\phi}^8/8}{C\dot{\phi}^2/2 - 3B\dot{\phi}^4/4 + 5A\dot{\phi}^6/6 - 7\dot{\phi}^8/8}. \tag{13}$$

Then there are six scaling solutions at most.

One can show that the phantom solution is an attractor of the equation of motion for the scalar field by means of both a linear perturbation analysis and a numerical analysis. For the details, see [1].

The cosmological evolution of the scalar field is obtained by solving Eqs.(5) and (7) numerically. In FIG. 2, we show the time evolution of energy densities of radiation, matter and phantom field for various initial conditions. We choose $\Omega_{M,0} = 0.25$ and set $\alpha = -1$. Since the scaling solution is growing in time and bounded by the instability regions (in which $w > -1$) as shown in FIG. 1, the initial energy density should be chosen to be below the present energy scale. Hence, there remains a severe fine-tuning problem of the initial conditions. We expect that including potential terms or introducing additional fields may allow initially decaying solutions. We note, however, that the condition (ii), $\rho + p = 2fXg_{,X} < 0$, remains unchanged even if we include potential terms.

[5]We take negative sign for the coefficient of $\dot{\phi}^2$ as a minimal extension. If we take positive sign, then the polynomial should be at least of tenth-order.

4 summary

We have shown that a scalar field with only non-canonical kinetic terms can, without the help of potential terms, behave like quintessence or phantom energy component.

We have also given a model of a power-law "phantom" field with arbitrary w of $w < -1$ which is stable against perturbation, and have shown that the phantom solution is a late-time attractor. In our model of the phantom field, the initial conditions have to be set carefully because there are a number of scaling solutions. Moreover, the initial energy density should be chosen to be below the present energy scale because the decaying lambda region corresponds to the unstable region. Therefore, there remains a fine-tuning problem of the initial conditions, which is no more severer than that of the cosmological constant. The situation may be improved by including potential terms or by introducing additional fields.

The violation of the weak energy condition is required to construct wormholes[22]. Our model of a phantom field may be used to explore such a fascinating possibility.

Acknowledgement

This work was supported in part by JSPS Fellowship for Young Scientists under grant No.3596 (TC) and No.4558 (MY).

References

[1] T. Chiba, T. Okabe, and M. Yamaguchi, *Kinetically Driven Quintessence*, UTAP-352.

[2] J.P. Ostriker and P.J. Steinhardt, Nature **377**, 600 (1995); L. Wang, R.R. Caldwell, J.P. Ostriker, and P.J. Steinhardt, astro-ph/9901388.

[3] L.M. Krauss and M.S Turner, Gen. Rel. Grav. **27**, 1137 (1995).

[4] S. Perlmutter *et al.*, ApJ. **517**, 565 (1999).

[5] B.P. Schmidt *et al.*, ApJ. **507**, 46 (1998); A.G. Riess *et al.*, Astron. J. **116**, 1009 (1998).

[6] A.D. Dolgov, in *The Very Early Universe*, edited by G.W.Gibbons, S.W.Hawking, and S.T.Siklos (Cambridge University Press, Cambridge, 1983).

[7] B. Ratra and P.J.E. Peebles, Phys. Rev. D **37**, 3406 (1988); P.J.E. Peebles and B. Ratra, Astrophys. J. **325**, L17.

[8] Y. Fujii and T. Nishioka, Phys. Rev. D **42**, 361 (1990).

[9] J.A. Frieman, C.T. Hill, and R. Watkins, Phys. Rev. D **46**, 1226 (1992).

[10] T. Chiba, N. Sugiyama, and T. Nakamura, Mon. Not. Roy. Astron. Soc. **289**, L5 (1997); T. Chiba, N. Sugiyama, and T. Nakamura, Mon. Not. Roy. Astron. Soc. **301**, 72 (1998).

[11] M.S. Turner and M. White, Phys. Rev. D **56**, 4439 (1997).

[12] R.R. Caldwell, R. Dave, and P.J. Steinhardt, Phys. Rev. Lett. **80**, 1582 (1998).

[13] I. Zlatev, L. Wang, and P.J. Steinhardt, Phys. Rev. Lett. **82**, 896 (1999).

[14] M. Bucher and D. Spergel, Phys. Rev. D **60**, 043505 (1999); R.A. Battye, M. Bucher and D. Spergel, astro-ph/9908047.

[15] T. Chiba, Phys. Rev. D **60**, 083508 (1999).

[16] P. Binétruy, Phys. Rev. D **60**, 063502 (1999); A. Masiero, M. Pietroni, and F. Rosati, hep-ph/9905346.

[17] A. Albrecht and C. Skordis, astro-ph/9908085; V. Sahni and L. Wang, astro-ph/9910097; T. Barreiro, E.J. Copeland, and N.J. Nunes, astro-ph/9910214.

[18] R.R. Caldwell, astro-ph/9908168.

[19] C. Armendáriz-Picón, T. Damour and V. Mukhanov, Phys. Lett. **B458**, 209 (1999).

[20] T. Damour and A.M. Polyakov, Nucl. Phys. **B423**, 532 (1994).

[21] C.M. Will, *Theory and experiment in gravitational physics*, (Rev.Ed., Cambridge University Press, Cambridge, 1993); C.M. Will, gr-qc/9811036.

[22] F.J. Tipler, Phys. Rev. Lett. **37**, 879 (1976); M.S. Morris, K.S. Thorne, and U. Yurtsever, Phys. Rev. Lett. **61**, 1446 (1988).

Cosmological Constant, Quintessence and Scalar-Tensor Theories of Gravity

Yasunori Fujii,*

Nihon Fukushi University, Handa, 475-0012, Japan

Abstract

We show how the scalar field, a candidate of quintessence, in a proposed model of the scalar-tensor theories of gravity provides a way to understand a small but nonzero cosmological constant as indicated by recent observations. A particular emphasis is placed on the effort to inherit the success of the scenario of a decaying cosmological constant. Discussions of a possible link to non-Newtonian gravity, the coincidence problem, the issue of time-variability of coupling constants as well as the chaos-like nature of the solution are also included in a new perspective.

I Introduction

For the last few years we have heard much about indications, coming from such observations like age problem, large-scale structure, lens statistics and type Ia supernovae, for the presence of a small but nonzero cosmological constant. The expected size is measured in units of the parameter $\Omega_\Lambda \equiv \Lambda/\rho_{\rm crit}$, with the most favored number somewhere around $0.6 - 0.7$ [1].

Acceptance of the conclusion from a theoretical point of view is limited, however, because Λ has been considered to be highly artificial, unnatural and arbitrary. Alternative ideas have been discussed to produce nearly the same end result. One of the key observations is that in the language of ideal fluid in cosmology, introducing Λ is equivalent to assuming an equation of state, $p = -\rho$. This aspect of negative pressure is what one can implement in terms of a scalar field that couples to ordinary matter roughly as weakly as gravity.

The study of this type of a "gravitational scalar field" has a long history. Recently, Chiba *et al.* presented a detailed analysis showing how the assumed negative pressure can be compared with observations [2]. They did not confine themselves to a scalar field, calling it X-matter. Caldwell *et al.* were the first to use a new name "quintessence," as the fifth element of the universe in addition to the four; baryons, radiation, dark matter and neutrinos [3]. They focussed more on the scalar field, discussing what the potential of the field should be like in order to fit the observations. An inverse-power potential is preferred over the exponential potential, for example.

We complain, however, that many of the analyses are too much phenomenological-oriented. We are talking about Λ which has been much discussed, often under such a grandeur name like the "cosmological constant problem," at the center of which lies a question why the observed value or its upper bound is so small compared with what we expect naturally from a theoretical point of view, by as much as 120 orders of magnitude.

In this connection we remind the audience that some progress has been achieved in terms of scalar-tensor theories. We believe that these theories are promising because they might have important aspects shared by attempts toward unified theories, and also because they provide the simplest derivation of an exponential potential of the scalar field, allowing us to implement the "scenario of a decaying cosmological constant" [4]. According to this scenario, we find Λ not to be a true constant, but to decay like $\Lambda(t) \sim t^{-2}$. In the (reduced) Planckian unit system of $c = \hbar = 8\pi G = M_{\rm P}^{-2} = 1$, the present age of the universe, $t_0 \sim 10^{10}$y is about 10^{60}, hence giving $\Lambda(t_0) \sim 10^{-120}$; today's cosmological constant is small only because our universe is old, not because of an unnatural fine-tuning of the parameters to the accuracy of 120 orders of magnitude.

This "success," however, is not good enough for understanding the accelerated universe as suggested by the recent observations, which indicates $\Lambda(t)$ that behaves nearly constant for some duration of time

*E-mail:fujii@handy.n-fukushi.ac.jp

toward the present epoch, or at least falling off more slowly than $\sim t^{-2}$. This requires a deviation from the purely exponential potential, though without losing its advantage of implementing the scenario of a decaying $\Lambda(t)$. Proposed modification of the prototype Brans-Dicke (BD) model will be presented in Section V, which will be preceded, however, by Sections II–IV. In Section II, we show that the prototype BD model with Λ added entails a serious drawback. A remedy is proposed in Section III. A possible link to non-Newtonian gravity is suggested in Section IV. Section VI is for discussion including the novel view on the coincidence problem, the expected chaos-like nature of the solution, and possible extensions of the model.

The present article is based on the talk intended to outline basic ideas and main conclusions of Refs. [5-8], in which more details and references will be found.

II Prototype BD model with Λ

We start with the Lagrangian [5]

$$\mathcal{L}_{\rm BD} = \sqrt{-g}\left(\frac{1}{2}\xi\phi^2 R - \epsilon\frac{1}{2}g^{\mu\nu}\partial_\mu\phi\partial_\nu\phi - \Lambda + L_{\rm matter}\right), \tag{1}$$

where we use symbols similar to but slightly different from the original ones [9];

$$4\xi\omega = \epsilon = {\rm Sign}(\omega), \quad \varphi_{\rm BD} = (\xi/2)\phi^2.$$

We use the reduced Planckina unit system, in which Λ is naturally expected to be of the order unity, as suggested in many of theoretical models of unification.

An important assumption is made that the scalar field is decoupled from ordinary matter fields at the level of the Lagrangian. This feature distinguishes the prototype BD model [9] from the preceding model due to Jordan [10]. In the field equation, however, we find that the scalar field does couple to the trace of the matter energy-momentum tensor. This is due to the mixing interaction between the scalar field and the spinless component of the metric tensor implied by the nonminimal coupling term. The scalar field couples to matter only via the metric field. This explains why the scalar field in this model respects Weak Equivalence Principle (WEP) which is a privilege of the force endowed with spacetime geometry.

Conformal transformations defined by

$$g_{\mu\nu} \rightarrow g_{*\mu\nu} = \Omega^2(x)g_{\mu\nu}, \tag{2}$$

always provide a powerful tool in analyzing theories with a nonminimal coupling, like the first term on the right-hand side of (1). Of particular importance is the choice

$$\Omega = \xi^{1/2}\phi, \tag{3}$$

by which we eliminate the nonminimal coupling. In fact the same Lagrangian (1) can be put into the form

$$\mathcal{L}_{\rm BD} = \sqrt{-g_*}\left(\frac{1}{2}R_* - \frac{1}{2}g_*^{\mu\nu}\partial_\mu\sigma\partial_\nu\sigma - V(\sigma) + L_{*\rm matter}\right), \tag{4}$$

in which the term of the curvature scalar is the standard Einstein-Hilbert (EH) term, and the *canonical* scalar field is now σ related to the original ϕ by

$$\phi = \xi^{-1/2}e^{\zeta\sigma}, \tag{5}$$

where

$$\zeta^{-2} = 6 + \epsilon\xi^{-1}. \tag{6}$$

We assume that the right-hand side is positive;

$$\epsilon\xi^{-1} > -6. \tag{7}$$

Notice also that the term of Λ acts now as an exponential potential as alluded before;

$$V(\sigma) = \Lambda\Omega^{-4} = \Lambda e^{-4\zeta\sigma}. \tag{8}$$

We say that we have moved from the original Jordan conformal frame, abbreviated by J frame, to Einstein (E) frame. Generally speaking, quantities in different conformal frames (CFs) are related to each other in an unambiguous manner. For this reason different CFs are sometimes called to be equivalent to each other. Physics may look different, however. Then a question may arise how we can single out a particular CF out of (infinitely many) CFs. We do it according to what clock or meter stick we use. Remember that (2) represents a local change of units [11], as will be evident if it is put into the form $ds_*^2 = \Omega^2(x)ds^2$. These features will be demonstrated later by explicit examples.

Let us choose E frame for convenience of mathematical analysis, for the moment. Consider spatially flat Robertson-Walker cosmology. Looking for the solution in which the scalar field is spatially uniform, we find analytic solution;

$$a_*(t_*) = t_*^{1/2}, \tag{9}$$

$$\sigma(t_*) = \bar{\sigma} + \zeta^{-1}\frac{1}{2}\ln t_*, \tag{10}$$

$$\rho_{m*}(t_*) = \left(1 - \frac{1}{4}\zeta^{-2}\right)t_*^{-2} \times \begin{cases} \frac{3}{4}, \\ 1, \end{cases} \tag{11}$$

$$\rho_\sigma(t_*) = t_*^{-2} \times \begin{cases} \frac{3}{16}\zeta^{-2}, \\ \frac{1}{4}\left(-1 + \zeta^{-2}\right), \end{cases} \tag{12}$$

where t_* is the cosmic time in E frame, ρ_{m*} is the ordinary matter density, while $\rho_\sigma \equiv \dot{\sigma}^2/2 + V(\sigma)$ may be interpreted as an effective cosmological constant $\Lambda_{\rm eff}$. The upper and lower lines in (11) and (12) are for radiation- and dust-dominated universe, respectively. We first notice that (12) shows that the $\Lambda_{\rm eff}$ decays like t_*^{-2}, thus implementing the scenario of a decaying cosmological constant.

The solution (9)-(12), which is in fact an attractor reached asymptotically, differs in many ways from the one obtained from the equation without Λ. For example, (9) for the scale factor holds true not only for radiation-dominance but also for dust-dominance; the exponent for dust dominance without Λ is given by $2/(3 + 2\zeta^2)$ which is close to 2/3 if $\zeta^2 \ll 1$.

More important is, however, that particle masses depend on σ, and hence on time. The mass term of the quark, for example, is given by

$$\mathcal{L}_{mq} = -m_0\bar{q}q, \tag{13}$$

with a *constant* m_0, due to the assumed absence of ϕ in the matter Lagrangian. In E frame, however, we have

$$\mathcal{L}_{mq} = -m_*\bar{q}_*q_*, \tag{14}$$

with $q_* = \Omega^{-3/2}q$, while

$$m_* = m_0\Omega^{-1} = m_0e^{-\zeta\sigma} \sim t_*^{-1/2}, \tag{15}$$

where we have used (10) to derive the last expression in (15).

If we consider the period of primordial nucleosynthesis, for example, (15) would imply the decrease of nucleon mass, say, as much as ∼ 70%. This is unacceptable because the physical processes are analyzed in terms of quantum mechanics in which particle masses are taken as constant. The physical CF corresponding to this situation is J frame. We should then study the solution in J frame.

We may restart with the cosmological equations in J frame. There is, however, another interesting approach by using the relations

$$dt_* = \Omega dt, \tag{16}$$

$$a_* = \Omega a \tag{17}$$

which can be obtained directly from (2). Combining $\Omega \sim \phi \sim t_*^{1/2}$ obtained from (3), (5) and (10), we derive

$$a = \text{const}, \tag{18}$$

implying that the universe looks *static* in J frame. This can be understood even in E frame by noting that a_* and m_*^{-1} grow in the same way $\sim t_*^{1/2}$, and that assuming time-independent mass is equivalent to choosing the inverse mass as the time unit.

We have a dilemma; varying mass in E frame and static scale factor in J frame. We admit that the conclusion is not final, because we assumed the simplest nonminimal coupling term and a purely constant Λ in J frame. These can be modified. More detailed study shows, however, that we must accept rather extreme choices of parameters. We would find it increasingly difficult and unnatural to understand why the simple standard cosmology works so well. It seems better to modify the model at the more fundamental level, still based on simple physical principles.

III Dilaton model

In view of (9) which happens to coincide with the standard result for radiation-dominated universe, we try to see if we can have a constant mass in E frame instead of J frame. Let us assume the E frame mass term,

$$\mathcal{L}_{mq} = -m_{q\dagger}\sqrt{-g_*}\,\bar{q}_* q_*, \tag{19}$$

where $m_{q\dagger}$ is chosen to be constant. This can be transformed back to J frame;

$$\mathcal{L}_{mq} = -\xi^{1/2} m_{q\dagger}\sqrt{-g}\bar{q}q\phi, \tag{20}$$

a simple Yukawa interaction, with the coupling constant $\xi^{1/2}m_{q\dagger}$ which is in fact dimensionless as will be confirmed by re-installing $M_{\rm P}^{-1}$. We have no mass term in the starting Lagrangian. The nonminimal coupling implies that we have no dimensional gravitational constant either. For this reason we have scale invariance, or dilatation symmetry, which might be chosen as a simple physical principle we mentioned above. We have a conserved dilatation current in J frame. The presence of mass term (19) and the EH term in E frame suggests that dilatation symmetry is *broken spontaneously* with σ a massless Nambu-Goldstone boson, called a *dilaton*.

Allowing ϕ to be present in the J frame Lagrangian implies that WEP is violated. We still maintain Equivalence Principle at the more fundamental level as stated that tangential space of curved spacetime be Minkowskian. WEP as a *phenomenological* law can be tolerated within the limit allowed by the fifth-force type experiments [12]. We have now E frame as a physical CF in which we develop radiation-dominated cosmology showing standard result with constant particle masses. The scalar field is left decoupled from ordinary matter in E frame. This simple situation changes, however, once we take the effect of interaction among matter fields into account.

Consider the quark-gluon interaction, for example. Calculation based on relativistic quantum field theory suffers always from divergences. To put this under control we use the recipe of dimensional regularization. We start with spacetime dimension N which we choose off the physical value 4. Divergences can be represented by poles $\sim (N-4)^{-1}$ if we confine ourselves to 1-loop diagrams for the moment. After applying renormalization techniques with $N \neq 4$, we finally go to the limit $N = 4$ at the end of the calculation. We now observe that the scalar field is decoupled from matter only at $N = 4$. In other words, we have the coupling proportional to $N - 4$ which may cancel the pole coming from divergences, thus leaving a nonzero finite result. This is a typical way we obtain "quantum anomalies," which play important roles in particle physics. In the same way, we are left with nonzero matter coupling of the scalar field in general.

The QCD calculation yields

$$\mathcal{L}_{mq1} = \sqrt{-g_*}\zeta_q m_{q\dagger}\bar{q}_* q_* \sigma, \tag{21}$$

where

$$\zeta_q = \zeta\frac{5\alpha_s}{\pi} \approx 0.3\zeta, \tag{22}$$

with $\alpha_s \approx 0.2$ is the QCD counterpart of the fine-structure constant. The occurrence of α_s which is specific to the quark implies composition-dependence of the force mediated by σ, in accordance with violation of WEP, as discussed before.

For more-loop diagrams we obtain terms of higher power of σ. Combined with the mass term (19), these coupling terms will give σ-dependent mass, as before. We will show, however, that the dependence

might be reasonably weaker than in the prototype model. Consider a nucleon which constitutes a major component of the real world, but is composite to make the same calculation as to the quark not applicable. In view of a rather small content of the quark mass contribution ($\sim$ 60MeV) [13] out of the total nucleon mass $\sim$ 940MeV, we estimate an effective coupling strength of the nucleon;

$$\zeta_N \approx 0.02\zeta. \tag{23}$$

The smallness of $\zeta_N/\zeta \ll 1$ seems to justify E frame as a physical CF to a good approximation, although strictly speaking we should move to anther CF in which the nucleon mass is truly constant. By this process ϕ reappears in front of scalar curvature, thus making the gravitational constant time-dependent. The predicted rate of change based on (23) is $\dot{G}/G \sim 10^{-12}\mathrm{y}^{-1}$, in roughly consistent with the observational upper bound obtained so far [14].

We also find that the exponent of the scale factor in dust-dominated universe is given by

$$\alpha_* = \frac{2}{3}\left(1 - \frac{\bar{\zeta}}{\zeta}\right) \sim \frac{2}{3}, \tag{24}$$

where $\bar{\zeta}$ is an average of ζ's for particles that comprise dust matter. In this way we are in a better status compared with the model discussed in Section II.

We also add that scale invariance is broken explicitly finally when the quantum effect is included. σ is now a pseudo NG boson which acquires a nonzero mass. This seems to raise a tempting possibility that σ provides yet another origin of non-Newtonian gravity [15], as will be further pursued.

IV Non-Newtonian gravity

We decompose σ into the cosmological background part and the locally fluctuating component;

$$\sigma(x) = \sigma_b(t_*) + \sigma_f(x). \tag{25}$$

Substituting this into (21) yields the matter coupling of each component.

Consider the σ_f-coupling. A 1-quark-loop diagram will give a self-mass μ_f basically given by

$$\mu_f^2 \sim m_{*q}^2 M_{*b}^2, \tag{26}$$

where we assumed the cut-off energy of the order of M_{*b}, the mass scale of supersymmetry breaking. We use the values $m_{*q} \sim 5\mathrm{MeV}$ and $M_{*b} \sim 1\mathrm{TeV}$, which are $\sim 2\times 10^{-21}$ and $\sim 4\times 10^{-16}$, respectively in the reduced Planckian unit system, obtaining $\mu_f \sim 0.84\times 10^{-36} \sim 2.1\times 10^{-9}\mathrm{eV}$, and the corresponding force-range $\lambda = \mu^{-1} \sim 1.2\times 10^{36} = 9.6\times 10^{3}\mathrm{cm} \approx 100\mathrm{m}$. This turns out to be a macroscopic size considered typically as the force-range of non-Newtonian gravity [16], though obviously latitudes of several orders of magnitude should be allowed.

On the other hand, it has been argued that the force of σ should be of long-range. A simple estimate of this kind can be obtained by considering a component of the Einstein equation $3H_*^2 = \rho_\sigma + \rho_{m*}$. The left-hand side would be $\sim t_*^{-2}$, giving $\rho_\sigma \sim V \sim t_*^{-2}$. We may also expect that the mass-squared μ^2 will be given by $\mu^2 \sim V'' \sim V$. Combining these we reach a conclusion $\lambda \sim t_*$ which is the size of the whole visible universe, in sharp contrast with the previous estimate.

In this connection we point out that the latter argument applies to σ_b, a classical solution of a *nonlinear* equation, while μ_f^2 in the former is a squared mass of a quantized field, which is based on the solution of a *linear* harmonic oscillator. These two can be simply different from each other. An example is provided by the sine-Gordon equation in 2 dimensions, featuring a quantized mesonic excitation *and* the classical soliton solution, which show behaviors entirely different from each other [17].

We do not know if the 2-dimensional model provides an appropriate analogy, nor if our cosmological equations in 4 dimensions allow a soliton-type solution. Nevertheless the lesson learned from this example seems highly suggestive. Without any further details at this moment, we offer a conjecture that σ_f mediates an intermediate-range force between local objects, with σ_b still rolling down the exponential slope slowly.

We also point out that σ_b may also acquire self-energy through its own matter coupling. As it turns out, this amounts to be part of the vacuum energy of matter fields. In the sense of quantum field theory, this contribution is given roughly by $\sim M_{*b}^4$ which provides another origin of the cosmological constant with the size represented by Ω_Λ as large as $\sim 10^{60}$. Since M_{*b} depends on σ, we would have the potential too large by the same amount. The same "success" for the contribution from Λ in the J frame Lagrangian dose not seem expected. An entirely different mechanism based perhaps on nonlinearly or topological nature is called for. If a solution is discovered finally, however, we would be likely left with non-Newtonian gravity featuring finite force-range and WEP violation. Quintessence might be quintessentially a fifth force.

The phenomenological aspects of this putative force have been analyzed in terms of the static potential between two nuclei;

$$V_{5ab}(r) = -\frac{Gm_a m_b}{r}\left(1 + \alpha_{5ab} e^{-r/\lambda}\right). \tag{27}$$

The size of the coefficient α_{5ab} is given essentially by

$$\alpha_{5ab} \sim \alpha_{5N} = 2\zeta_N^2 \sim 10^{-3}, \tag{28}$$

where the estimate at the far right-side is based on (23) together with $\zeta \sim 1$ assumed. Given the experimental constraints [12], we are on the verge of immediate exclusion, though it might be premature to draw a final conclusion before more detailed analyses are completed on various kinds of uncertainties.

V Two-scalar model

We now discuss how the exponential potential should be modified to understand the accelerated universe. We start with a clue which we find in a *transient* solution for the exponential potential.

Suppose $\sigma(t)$ starts moving ahead even slightly. The potential will decrease rapidly, and then the frictional force coming from the cosmological expansion will decelerate σ until it comes to an almost complete stop. ρ_σ will fall off much faster than ρ_{m*} to reach a near constant. This state lasts until ρ_{m*} comes down to be comparable again with this constant when the system enters the asymptotic phase, described by (9)-(12). The plateau of ρ_σ thus formed is expected to mimic a cosmological constant.

Detailed numerical simulation shows, however, that σ starts moving again toward the asymptotic behavior a little too early, before ρ_σ crosses ρ_{m*}. Remember that this crossing, if it occurs, would imply $\Omega_\Lambda = 0.5$. As a consequence Ω_Λ would reach short of values as "large" as 0.6-0.7. We must invent a mechanism to prevent this premature departure of σ.

After somewhat random effort on a try-and-error basis, we came across a proposal [18]. We introduce another scalar field Φ which couples to σ through the E frame potential,

$$V(\sigma, \Phi) = e^{-4\zeta\sigma}\left(\Lambda + \frac{1}{2}m^2\Phi^2[1 + \gamma\sin(\kappa\sigma)]\right), \tag{29}$$

as shown graphically in Fig. 1, where m, γ and κ are constants roughly of the order unity. We will study the consequences simply for the success, without any discussion on the theoretical origin, at this moment. In Fig. 2, we show an example of the solution in which quantities are plotted against $u \equiv \log t_*$.

We notice that σ and Φ in the upper diagram show alternate occurrence of rapid changes and near standstills. Corresponding to this we find plateau behaviors of ρ_s, the energy density of the $\sigma - \Phi$ system, in the lower diagram. There are two of them in this particular example. In both of them ρ_s crosses ρ_{m*}, resulting in sufficient acceleration of the scale factor, as clearly recognized as two mini-inflation's in the upper diagram.

We moderately fine-tuned initial values and parameters such that the second mini-inflation takes place around the present epoch, $u \approx 60$. It is rather easy to "predict" values like $t_{*0} = (1.1 - 1.4) \times 10^{10}$y, $\Omega_\Lambda = 0.6 - 0.8$ and $h = 0.6 - 0.8$, with more details described in Ref. [7].

We provide an intuitive explanation briefly on how we understand this result. The decelerated σ settles at a place which is determined only by the "initial" values, quite independent of where it is with respect to the sinusoidal potential which had sunk so much. As the time elapses, the potential grows in terms of the strength relative to the frictional force. It may happen that σ finds itself near one of

the minima of the sinusoidal potential. σ is then trapped, tighter and tighter, as the potential strength proportional to Φ^2 builds up again in the relative sense as above. This serves to prevent σ from escaping too early, and consequently to have the plateau behavior to last sufficiently long. The growing potential implies, however, that also Φ is attracted toward the central valley $\Phi = 0$ stronger and stronger. Finally the time will come when Φ starts moving downward. This entails a sudden collapse of the potential wall that has confined σ. With the accumulated energy σ is catapulted forward. See Fig. 3 showing a magnified view of this behavior. In short this "trap-and-catapult mechanism" is a result of a superb collaboration of the two scalar fields.

The decelerated σ may find itself again near a potential minima. Then nearly the same pattern of the behavior will repeat itself, as in the above example. Otherwise, σ and Φ will make a smooth transition to the asymptotic phase, as in the model without Φ. No mini-inflation and hence no extra acceleration take place. There are many different combinations of these typical behaviors.

VI Discussion

Our argument in Section IV for a possible link to non-Newtonian gravity will remain unchanged for σ even in the two-scalar model. Experimental searches for the non-Newtonian force with improved accuracy are strongly encouraged. On the other hand, Φ will most likely stay extremely massive leaving virtually no trace in the macroscopic physics.

In Fig. 2 we find ρ_s and ρ_{m*} fall off interlacing each other, maintaining the dependence $\sim t_*^{-2}$ as an overall behavior. In this way we inherit the scenario of a decaying cosmological constant, unlike many other models of quintessence.

We have not attempted to determine the parameters and initial values uniquely. We add some remarks, however. They should be determined such that a plateau behavior has lasted long enough to cover the present epoch and the period of nucleosynthesis, as shown in Fig. 2. By requiring this we can guarantee that particle masses must have been the same as today, also keeping the period well in the radiation-dominated epoch. There is a wide area in parameter space where this is not the case, thus endangering one of the most successful part of standard cosmology.

Some of the coupling constants, including G, may depend on time probably through its dependence on scalar fields. Assuming that we are today during the period of a plateau behavior entails no time variability of the coupling constants, or below the level of $t_{*0}^{-1} \approx 10^{-10}\mathrm{y}^{-1}$ by perhaps several orders of magnitude, apparently in good agreement with the upper bounds obtained so far [19]. The previous argument on $\dot{G}/G$ in Section III is no longer relevant in the present context.

Given the required long plateau behavior, one may wonder if the modification of the model proposed in Sections II-III loses its ground. No need is present to distinguish CFs from each other during a plateau behavior. The argument still holds true, however, for epochs much earlier than nucleosynthesis. We must avoid concluding a contracting universe, for example, at the very early epochs [5].

Suppose we are really witnessing an extra acceleration of the universe. Suppose also this is due to a fixed constant Λ. It then follows that we are in a truly remarkable, special once-for-all era throughout the whole history of the universe. Taking aside a special version of the Anthropic Principle, this should be too arrogant a view, a way of representation of the coincidence problem. From the point of view of the two-scalar model, on the other hand, we are looking at only one of the repeated events. We still face the coincidence problem but certainly to a lesser degree.

We can show that the analytic solution (9)-(12) supplemented with $\Phi = 0$ is still an asymptotic solution. Before reaching this fixed-point attractor, however, there can be many different types of transient behaviors, depending sensitively on the initial values. In particular we have many different possibilities with respect to the number showing how many plateau behaviors we experience before the solution finally enters the asymptotic phase. This number, and hence the qualitative characteristics of the solution changes suddenly as an initial value changes smoothly. This reminds us of the well-known chaotic behavior in nonlinear dynamics. The presence of the fixed-point attractor rather than the strange attractor in phase space, however, implies that the behavior is not genuinely chaotic, but only chaos-like. The dependence on initial values and parameters is still so sensitive that the system seems to deserve further scrutiny. It may provide a new type of dissipative structure.

In this sense we are leaving the traditional view that the universe we see now should depend as little as possible on initial values. Nothing seems seriously wrong if, on the contrary, today's universe is still in a complicated transient state of evolution affected quite strongly by what the universe was like in the very early time [6].

We finally add a comment on a possible extension of the model. The starting Lagrangian in J frame may be thought of as the theoretical one obtained by the process of dimensional reduction from the still more fundamental Lagrangian perhaps in higher dimensions. It is then likely that A is multiplied by a monomial of ϕ. This provides a possible extension of the simplest model considered so far. As we find, we still reach an exponential potential with ζ in (8) replaced by another factor depending on the exponent of the monomial. This suggests that the analyses carried out here can be applied to more general models.

References

[1] For the most recent result, see, for example, A.G. Riess *et al.*, Astron. J. **116** (1998), 1009: S. Perlmutter *et al.*, Astroph. J. **517** (1999), 565.

[2] T. Chiba, N. Sugiyama and T. Nakamura, Mon. Not. R. Astron. Soc. **289** (1997), L5.

[3] R.R. Caldwell, R. Dave and P.J. Steinhardt, Phys. Rev. Lett. **80** (1998), 1582.

[4] A.D. Dolgov, *The very early universe*, Proceedings of Nuffield Workshop, 1982, Cambridge University Press, 1982; Y. Fujii and T. Nishioka, Phys. Rev. **D42** (1990), 361.

[5] Y. Fujii, Prog. Theor. Phys. **99** (1998), 599.

[6] Y. Fujii, *Fundamental parameters in cosmology*, Proceedings of the XXXIIIrd Rencontres de Moriond, Editions Frontieres, 1998, p. 93, gr-qc/9806089.

[7] Y. Fujii, *A two-scalar model for a small but nonzero cosmological constant*, gr-qc/9908021.

[8] Y. Fujii, *Quintessence, scalar-tensor theories and non-Newtonian gravity*, gr-qc/9911064.

[9] C. Brans and R.H. Dicke, Phys. Rev. **124** (1961), 925.

[10] P. Jordan, Z. Phys. **157** (1959), 112.

[11] R.H. Dicke, Phys. Rev. **125** (1962), 2163.

[12] E. Fischbach and C.L. Talmadge, *The search for non-Newtonian gravity*, AIP Press-Springer, 1998.

[13] M.P. Locher, Nucl. Phys. **A527** (1991), 73c.

[14] R.W. Hellings *et al.*, Phys. Rev. Lett. **51** (1983), 1609.

[15] See also R.D. Peccei, J. Sola and C. Wetterich, Phys. Lett. **B195** (1987), 183.

[16] Y. Fujii, Nature Phys. Sci. **234** (1971), 5: Int. J. Mod. Phys. **A6** (1991), 3505.

[17] See, for example, S.V. Ketov, Fortsch. Phys. **45** (1997), 237.

[18] Y. Fujii and T. Nishioka, Phys. Lett. **B254** (1991), 347; Y. Fujii, Astropart. Phys. **5** (1996), 133.

[19] See, for example, Y. Fujii, M. Omote and T. Nishioka, Prog. Theor. Phys. **92** (1992), 521; Y. Fujii, A. Iwamoto, T. Fukahori, T. Ohnuki, M. Nakagawa, H. Hidaka, Y. Oura and P. Möller, *The nuclear interaction at Oklo 2 billion years ago*, hep-ph/9809549, and papers cited therein.

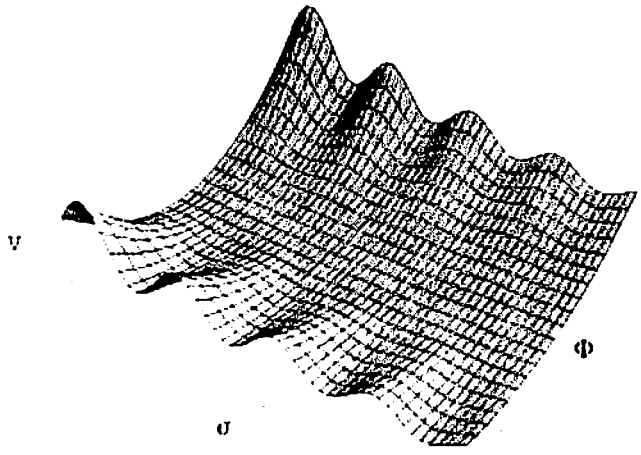

Figure 1: The potential $V(\sigma, \Phi)$ given by (29). Along the central valley with $\Phi = 0$, the potential reduces to the simpler behavior $\Lambda e^{-4\zeta\sigma}$ as given by (8), but with $\Phi \neq 0$, it shows an oscillation in the σ direction.

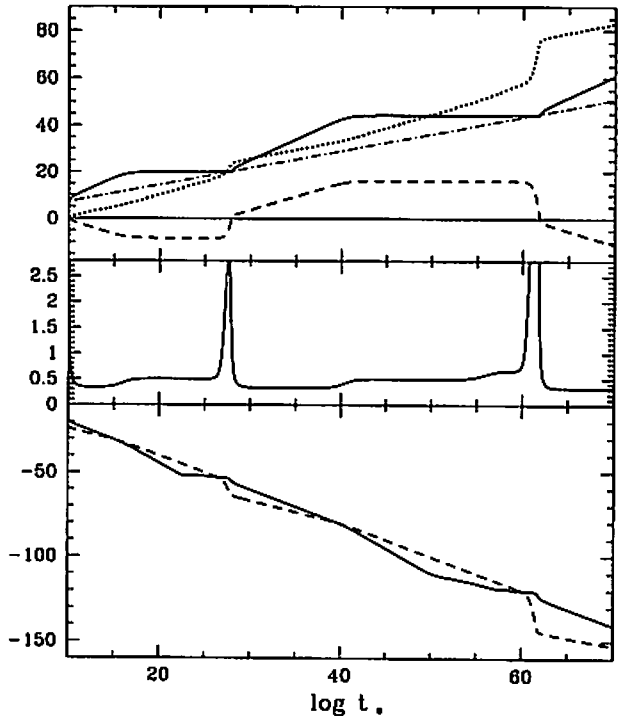

Figure 2: An example of the solution. Upper diagram: $b = \ln a_*$ (dotted), σ (solid) and 2Φ (dashed) are plotted against $\log t_*$. The present epoch corresponds to $\log t_* = 60.1 - 60.2$, while the primordial nucleosynthesis must have taken place at $\log t_* \sim 45$. The parameters are $\Lambda = 1, \zeta = 1.5823, m = 4.75, \gamma = 0.8, \kappa = 10, \zeta_d = 0.002$. The initial values at $t_{1*} = 10^{10}$ are $\sigma_1 = 6.7544, \sigma_1' = 0$ (a prime implies differentiation with respect to $\tau = \ln t_*$),$\Phi_1 = 0.21, \Phi_1' = -0.005, \rho_{1\mathrm{rad}} = 3.7352 \times 10^{-23}, \rho_{1\mathrm{dust}} = 4.0 \times 10^{-45}$. The dashed-dotted straight line represents the asymptote of σ given by $\tau/(2\zeta)$. Notice long plateaus of σ and Φ, and their rapid changes during relatively "short" periods. Middle diagram: $\alpha_* = b' = t_* H_*$ for an effective exponent in the local power-law expansion $a_* \sim t_*^{\alpha_*}$ of the universe. Notable leveling-offs can be seen for 0.333, 0.5 and 0.667 corresponding to the epochs dominated by the kinetic terms of the scalar fields, the radiation-matter and the dust-matter, respectively. Lower diagram: $\log \rho_s$ (solid), the total energy density of the $\sigma - \Phi$ system, and $\log \rho_{m*}$ (dashed), the matter energy density. Notice an interlacing pattern of ρ_s and ρ_{m*}, still obeying $\sim t_*^{-2}$ as an overall behavior. Nearly flat plateaus of ρ_s precede before ρ_s crosses ρ_{m*}, hence with Ω_Λ passing through 0.5.

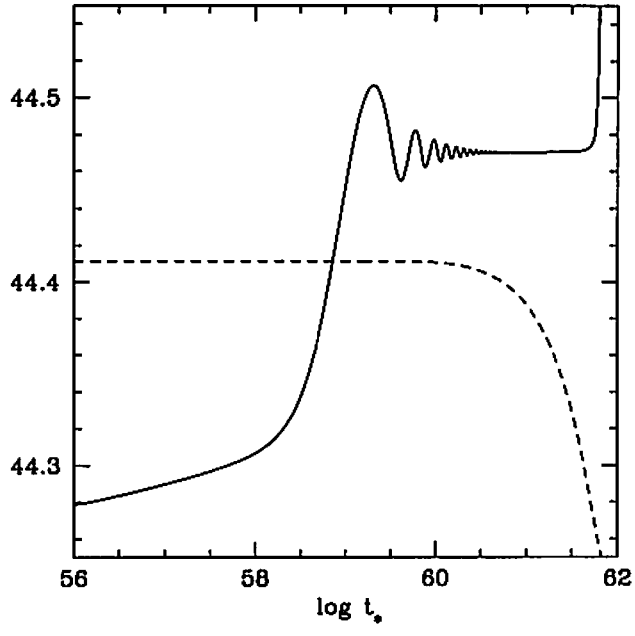

Figure 3: Magnified view of σ (solid) and $0.02\Phi+44.25$ (dashed) in the upper diagram of Fig. 2. Note that the vertical scale has been expanded by approximately 330 times as large compared with Fig. 2. With the time variable $\tau = \ln t_*$, the potential V grows relatively to the frictional force as the multiplying factor $t_*^2 = e^{2\tau}$. The potential wall for σ becomes increasingly steeper, thus confining σ further to the bottom of the potential, as noticed by an oscillatory behavior of σ with ever increasing frequency measured in τ. (In this particular example, σ was trapped finally long after it had been decelerated to settle near one of the maxima of the potential.) The growing V causes Φ eventually to fall downward, resulting in the collapse of the confining potential wall. The stored energy is then released to unleash σ.

Spherically Symmetric Self-Similar Solutions and their Astrophysical and Cosmological Applications

B.J.Carr[1]

Astronomy Unit, Queen Mary and Westfield College,
Mile End Road, London E1 4NS, England

Abstract

We discuss spherically symmetric perfect fluid solutions of Einstein's equations which have equation of state ($p = \alpha\mu$) and which are self-similar in the sense that all dimensionless variables depend only upon $z \equiv r/t$. For each value of α, such solutions are described by two parameters and have now been completely classified. There is a 1-parameter family of solutions asymptotic to the flat Friedmann model at large values of z. These represent either black holes or density perturbations which grow as fast as the particle horizon; the underdense solutions may be relevant to the existence of large-scale cosmic voids. There is also a 1-parameter family of solutions asymptotic to a self-similar Kantowski-Sachs model at large z. These are probably only physically realistic for $-1 < \alpha < -1/3$, in which case they may relate to the formation of bubbles in an inflationary universe. There is a 2-parameter family of solutions associated with a self-similar static solution at large z. This family contains solutions with naked singularities and this includes the "critical" solution discovered in recent collapse calculations for $\alpha < 0.28$. Finally, for $\alpha > 1/5$, there is a family of solutions which are asymptotically Minkowski. These asymptote either to infinite z, in which case they are described by one parameter, or to a finite value of z, in which case they are described by two parameters and this includes the "critical" solution for $\alpha > 0.28$. We discuss the stability of spherically symmetric similarity solutions to more general (non-self-similar) spherically symmetric perturbations.

1 Introduction

Self-similar models have proved very useful in General Relativity because the similarity assumption reduces the complexity of the partial differential equations. Even greater simplification is achieved in the case of spherical symmetry (Cahill & Taub 1971) since the governing equations then reduce to comparatively simple ordinary differential equations. In this case, the solutions can be put into a form in which every dimensionless variable is a function of some dimensionless combination z of the time coordinate t and the comoving radial coordinate r. In the simplest situation, a similarity solution is invariant under the transformation $r \rightarrow ar, t \rightarrow at$ for any constant a, so the similarity variable is $z = r/t$. Geometrically this corresponds to the existence of a homothetic vector and is sometimes termed similarity of the "first" kind.

Although we will focus almost exclusively on this kind of similarity here, it should be stressed that there are various ways of generalizing the concept. For example, there are also similarity solutions of the "second" kind, which involve an intrinsic scale. A particularly important application of this is *kinematic* self-similarity (Carter & Henriksen 1991, Coley 1997), in which the similarity variable is of the form $z = r/t^{\beta}$ for some constant β. Ponce de Leon (1993) has also introduced the concept of *partial homothety*, in which the Killing condition is only satisfied with spatial hypersurfaces. In this case, the similarity variable has the form $z = r/F(t)$ for some general function F and it reduces to self-similarity of the first kind only if F is linear in t. However, this approach is not covariant. There are also solutions which possess *discrete* self-similarity, in the sense that dimensionless variables repeat themselves on some spacetime scale Δ, i.e. they are invariant under the transformation $r \rightarrow e^{-n\Delta}r, t \rightarrow e^{-n\Delta}t$ for any integer n. One recovers the *continuous* type of self-similarity discussed above in the limit $\Delta \rightarrow 0$. Although

[1]E-mail:B.J.Carr@qmw.ac.uk

discrete self-similarity is much harder to deal with mathematically, Choptuik (1997) has emphasized its crucial role in the context of critical phenomena.

What makes similarity solutions of more than mathematical interest is the fact that they are often relevant to the real world dynamics (Barenblatt & Zeldovich 1972). This is because, in a variety of astrophysical and cosmological situations, solutions may naturally evolve to self-similar form even if they start out more complicated. For example, an explosion in a homogeneous background produces fluctuations which may be very complicated initially but which tend to be described more and more closely by a spherically symmetric similarity solution as time evolves (Sedov 1967). This applies even if the explosion occurs in an expanding cosmological background (Schwartz et al. 1975, Ikeuchi et al. 1983). The evolution of cosmic "voids" is also described by a similarity solution at late times (Hoffman et al. 1983, Hausman et al. 1983, Maeda & Sato 1984, Bertschinger 1985). In the hierarchically clustering scenario gravitationally bound clouds tend to form self-similar cosmic structures (Gunn & Gott 1972, Gunn 1977, Fillmore & Goldreich 1984, Bertschinger & Watts 1984) and a cloud collapsing from an initially uniform static configuration may also evolve towards self-similarity (Larson 1969, Penston 1969). Recently it has become clear that spherically symmetric self-similar solutions also play a crucial role in the context of the "critical" phenomena (Choptuik 1993, Evans and Coleman 1994, Gundlach 1995, Koike et al. 1995, Maison 1996, Carr et al. 1999).

These examples suggest that self-similar solutions may play the same sort of role in describing the asymptotic properties of spherically symmetric models as they do in the *spatially homogeneous* context (Hsu & Wainwright 1986). In the cosmological context, these considerations have led to the "similarity hypothesis" (Carr 1993), which proposes that - under certain circumstances (e.g. non-zero pressure, non-linearity, shell-crossing etc.) - cosmological solutions may naturally evolve to a self-similar form. One might also extend this hypothesis to the more general spherically symmetric context.

The possibility that self-similar models may be singled out in this way from more general spherically symmetric solutions means that it is essential to understand the full family of similarity solutions. This paper will focus exclusively on the situation in which the source of the gravitational field is a perfect fluid with equation of state of the form $p = \alpha\mu$ (where α is a constant). Indeed, Cahill & Taub (1971) have shown that this is the only equation of state compatible with the similarity assumption. In this case, it is well known that, for a given value of α, spherically symmetric similarity solutions are described by two parameters. Such solutions have now been classified completely (Carr & Coley 1999a; CC). We describe the characteristics of these solutions in Section 2 and discuss some of their cosmological and astrophysical applications in Section 3. In completing this introduction, we also summarize the main results here.

CC find that there are four classes of solutions and each of these relate to a specific application. The first class consists of the 1-parameter family of solutions asymptotic to the exact $k = 0$ Friedmann model at large z and these are obviously relevant in the cosmological context (Section 2.3). Some of them contain black holes which grow at the same rate as the particle horizon (Carr & Hawking 1974, Bicknell & Henriksen 1978a). Others represent density perturbations in a Friedmann background which always maintain the same form relative to the particle horizon (Carr & Yahil 1990). The latter all contain a sonic point and the requirement that they be regular there severely restricts their form (Bogoyavlenski 1985). While there is a continuum of regular underdense solutions, regular overdense solutions only occur in narrow bands. The underdense solutions may be relevant to the existence of large-scale cosmic voids (Section 3.3). The overdense solutions do not seem to describe features in the present Universe but they may relate to the formation of overdense blobs at an early phase transition.

The second class of models are asymptotic to a self-similar member of the Kantowski-Sachs (KS) family (Section 2.4). For each non-zero α there is a unique self-similar KS solution and there also exists a 1-parameter family of solutions asymptotic to this at both large and small values of z (Carr & Koutras 1992). Solutions with $-1/3 < \alpha < 1$ are probably unphysical because they are tachyonic and the mass is negative. Solutions with $-1 < \alpha < -1/3$ avoid these problems and are therefore more interesting. Although this equation of state violates the strong energy condition, it could could well arise in the early Universe. Indeed, such models may be related to the growth of bubbles formed at a phase transition in an inflationary model (Wesson 1986). Generalized negative-pressure KS solutions, in which the similarity is of the second kind, have been studied by Ponce de Leon (1988) and Wesson (1989); in these the equation of state deviates from $p = \alpha\mu$ and the fluid can be interpreted as a mixture of false vacuum and dust.

The third class of models are associated with self-similar static models. There is just one static self-

similar solution for each positive value of α (Misner & Zapolsky 1964) and there is also a 1-parameter family of solutions asymptotic to this. However, there is a 2-parameter family of solutions which are asymptotically "quasi-static" in the sense that they have an isothermal density profile at large values of z (Section 2.5). Since the asymptotically Friedmann and asymptotically KS solutions are described by only one parameter, this third class of models play a crucial role in understanding the full family of similarity solutions. Some asymptotically quasi-static solutions have been studied by Foglizzo & Henriksen (1993) and a more extensive analysis is being carried out by Carr et al. (1999). Such solutions are of particular interest because they are are associated with the formation of naked singularities (Section 3.1) and, for $\alpha < 0.28$, the occurrence of critical phenomena (Section 3.2).

The fourth class of solutions, which only exist for $\alpha > 1/5$, are asymptotically Minkowski and have not been previously analysed at all. They were originally found numerically by Goliath et al. (1998b) and this led CC to "predict" them analytically. There are actually two such families and they are described in more detail elsewhere (Carr et al. 1999). Members of the first family are described by one parameter and are asymptotically Minkowski as $|z| \to \infty$; members of the second family are described by two parameters and are asymptotically Minkowski as z tends to some finite value (though this corresponds to an infinite physical distance unless $\alpha = 1$). As with the asymptotically Friedmann and asymptotically quasi-static solutions, these may be either supersonic everywhere (in which case they contain a black hole or naked singularity) or attached to $z = 0$ via a sonic point (in which case they are asymptotically Friedmann or exactly static at small $|z|$). The transonic ones are associated with critical phenomena for $\alpha > 0.28$ (Carr et al. 1999).

2 Spherically Symmetric Similarity Solutions

One can analyse self-similar spherically symmetric models using three possible approaches. The first one uses "comoving" coordinates and was pioneered by Cahill & Taub (1973) and then followed by Carr and Henriksen and coworkers. The second approach, followed by Bogoyavlenski (1977) and coworkers, uses "homothetic" coordinates in which the homothetic Killing vector is along either the time or space axis. In this case, the equations can be reduced to those of a dynamical system and one can exploit results derived from the study of hypersurface homogeneous models (cf. Goliath et al. 1998a, 1998b). A third approach uses "Schwarzschild" coordinates and was included in the analysis of Ori & Piran (1990) and Maison (1996). This is useful if one is matching the solution to an asymptotically flat spacetime and wishes to find its global structure. All of these approaches are complementary and which is most suitable depends on what type of problem one is studying. In this paper we wish to emphasize the form of the solutions explicitly and it is most convenient to use the first approach.

2.1 General features of similarity solutions

In the spherically symmetric situation one can introduce a time coordinate t such that surfaces of constant t are orthogonal to fluid flow lines and comoving coordinates (r, θ, ϕ) which are constant along each flow line. The metric can be written in the form

$$ds^2 = e^{2\nu}\, dt^2 - e^{2\lambda}\, dr^2 - R^2\, d\Omega^2, \quad d\Omega^2 \equiv d\theta^2 + \sin^2\theta\, d\phi^2 \tag{1}$$

where ν, λ and R are functions of r and t. The equations have a first integral

$$m(r,t) = \tfrac{1}{2} R \left[1 + e^{-2\nu} \left(\frac{\partial R}{\partial t} \right)^2 - e^{-2\lambda} \left(\frac{\partial R}{\partial r} \right)^2 \right] \tag{2}$$

and this can usually be interpreted as the mass within comoving radius r at time t:

$$m(r,t) = 4\pi \int_0^r \mu R^2 \frac{\partial R}{\partial r'}\, dr'. \tag{3}$$

There is also a dimensionless quantity $E(r,t)$ which represents the total energy per unit mass for the shell with comoving coordinate r. Unless $p = 0$, both these quantities decrease with increasing t because of the work done by the pressure.

Spherically symmetric homothetic solutions were first investigated by Cahill & Taub (1971), who showed that by a suitable coordinate transformation they can be put into a form in which all dimensionless quantities such as ν, λ, E and

$$S \equiv \frac{R}{r}, \quad M \equiv \frac{m}{R}, \quad P \equiv pR^2, \quad W \equiv \mu R^2 \tag{4}$$

are functions only of the dimensionless variable $z \equiv r/t$. Values of z for which $M = 1/2$ correspond to a black hole or cosmological apparent horizon since the congruence of outgoing null geodesics have zero divergence. Another important quantity is the function

$$V(z) = e^{\lambda - \nu} z \tag{5}$$

which represents the velocity of the spheres of constant z relative to the fluid. These spheres contract relative to the fluid for $z < 0$ and expand for $z > 0$. Special significance is attached to values of z for which $|V| = \sqrt{\alpha}$ and $|V| = 1$. The first corresponds to a sonic point (where the pressure and density gradients are not uniquely determined), the second to a Cauchy horizon (either a black hole event horizon or a cosmological particle horizon).

The only barotropic equation of state compatible with the similarity ansatz is one of the form $p = \alpha\mu$, where causality requires $-1 \leq \alpha \leq 1$. It is convenient to introduce a dimensionless function $x(z)$ defined by

$$x(z) \equiv (4\pi\mu r^2)^{-\alpha/(1+\alpha)}. \tag{6}$$

The conservation equations $T^{\mu\nu}{}_{;\nu} = 0$ can then be integrated to give

$$e^{\nu} = \beta x z^{2\alpha/(1+\alpha)}, \quad e^{-\lambda} = \gamma x^{-1/\alpha} S^2 \tag{7}$$

where β and γ are integration constants. The remaining field equations reduce to a set of ordinary differential equations in x and S (given explicitly in CC). These specify integral curves in the 3-dimensional $(x, S, \dot{S})$ space (where a dot denotes $z d/dz$). For a given equation of state parameter α, there is therefore a 2-parameter family of spherically symmetric similarity solutions.

In $(x, S, \dot{S})$ space the sonic condition $|V| = \sqrt{\alpha}$ specifies a 2-dimensional surface. Where a curve intersects this surface, the equations do not uniquely determine $\dot{x}$ (i.e. the pressure gradient), so there can be a number of different solutions passing through the same point. However, only integral curves which pass through a line Q on the sonic surface are "regular" in the sense that $\dot{x}$ is finite, so that they can be extended beyond there. The equations permit just two values of $\dot{x}$ at each point of Q and these values will be real only on a restricted part of it. On this part, there will be two corresponding values of $\dot{V}$, at least one of which will be positive. If both values of $\dot{V}$ are positive, the smaller one is associated with a 1-parameter family of solutions, while the larger one is associated with an isolated solution. If one of the values of $\dot{V}$ is negative, both values are associated with isolated solutions. This behaviour has been analysed in detail by Bogoyavlenski (1977), Bicknell & Henriksen (1978a), Carr & Yahil (1990) and Ori & Piran (1990).

On each side of the sonic point, $\dot{x}$ may have either of the two values. If one chooses different values for $\dot{x}$, there will be a discontinuity in the pressure gradient. If one chooses the same value, there may still be a discontinuity in the higher derivatives of x, in which case the solutions are described as "weakly discontinuous". Only the isolated solution and a single member of 1-parameter family of solutions are *analytic*. This contrasts with the case of a shock where x is itself discontinuous (Cahill & Taub 1971, Bogoyavlenski 1985, Anile et al. 1987). One can show that the part of Q for which there is a 1-parameter family of solutions corresponds to two ranges of values for z. One range $(z_1 < z < z_2)$ lies to the left of the Friedmann sonic point z_F and includes the static sonic point z_S. The other range $(z > z_3)$ includes the Friedmann sonic point. The ranges for $\alpha = 1/3$ are indicated in Figure (1); in this case, $z_2 = z_S$ and $z_3 = z_F$.

Carr & Coley (1999a; CC) have classified the $p = \alpha\mu$ spherically symmetric similarity solutions completely. The key steps in their analysis are: (1) a complete analysis of the dust solutions, since this provides a qualitative understanding of the solutions with pressure in the supersonic regime; (2) an elucidation of the link between the $z > 0$ solutions and the $z < 0$ solutions; (3) a proof that, at large and small values of $|z|$, all similarity solutions must have an asymptotic form in which x and S have

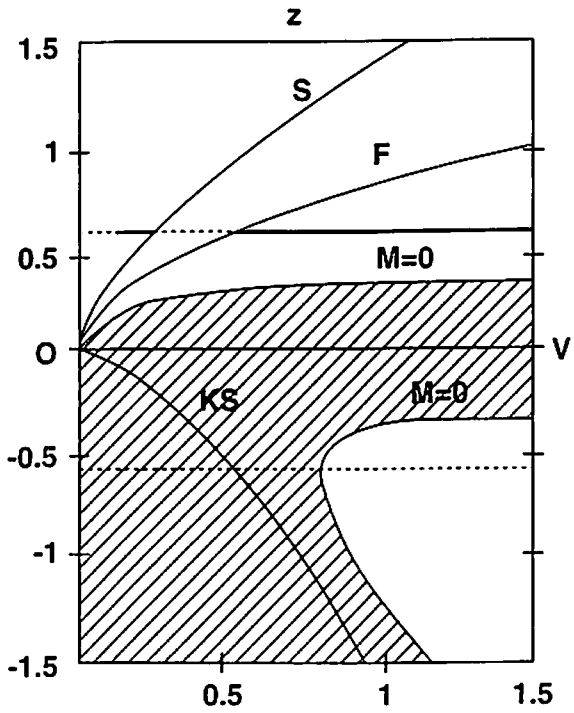

Figure 1: The form of $V(z)$ for the exact Friedmann, static and Kantowski-Sachs solutions in the $\alpha = 1/3$ case. Also shown are the curves corresponding to $M = 0$ (solid), the sonic lines $|V| = 1/\sqrt{3}$ (broken) and the range of values of z in which there is a 1-parameter family of regular solutions at the sonic point.

a power-law dependence on z; (4) a demonstration that there are only three such power-law solutions; and (5) a proof that solutions whose asymptotic behaviour is associated with a *finite* value of z have a power-law dependence on $\ln z$. We first discuss the power-law solutions and then the asymptotic ones. We will assume $z > 0$ in the first case but we will need to consider both signs of z in the second. The equations can be extended to the $z < 0$ regime by replacing z by $|z|$ and reversing the sign of V. Except in the case of the KS or asymptotically KS solutions, we also assume $\alpha > 0$.

2.2 Power-law solutions

• The $k = 0$ Friedmann solution. For this one can choose β and γ in eqn (7) such that

$$x = z^{-2\alpha/(1+\alpha)}, \quad S = z^{-2/[3(1+\alpha)]} \tag{8}$$

and then

$$\mu = \frac{1}{4\pi t^2}, \quad V = \left(\frac{1+3\alpha}{\sqrt{6}}\right) z^{(1+3\alpha)/[3(1+\alpha)]}. \tag{9}$$

One can put the metric in a more familiar form by making the coordinate transformation

$$\hat{t} = \beta t, \quad \hat{r} = \beta^{-2/[3(1+\alpha)]} r^{(1+3\alpha)/[3(1+\alpha)]} \tag{10}$$

which gives

$$ds^2 = d\hat{t}^{\,2} - \hat{t}^{4/[3(1+\alpha)]}[d\hat{r}^2 + \hat{r}^2 d\Omega^2]. \tag{11}$$

Only the $k = 0$ Friedmann model is self-similar since the $k = \pm 1$ models contain an intrinsic scale.

• A self-similar Kantowski-Sachs model. For each α there is a unique self-similar KS solution and this can be put in the form

$$S = S_0 z^{-1}, \quad x = x_0 z^{-2\alpha/(1+\alpha)} \tag{12}$$

where x_0 and S_0 are determined by α. It is convenient to take β and γ to have the same values as for the Friedmann solution if $\alpha < 0$ and i times those values if $\alpha > 0$. In this case, one has

$$\mu t^2 = \frac{1}{4\pi}\left(\frac{1}{3|\alpha|}\right)^{(1+\alpha)/(\alpha-1)}, \quad V = -\frac{(1-\alpha)(1+3\alpha)^2}{2\sqrt{6}\alpha}\left(\frac{1}{3|\alpha|}\right)^{-2\alpha/(1-\alpha)} z^{(1+3\alpha)/(1+\alpha)} \tag{13}$$

V is negative for $z > 0$, corresponding to tachyonic solutions, if $0 < \alpha < 1$; this means that the t coordinate is spacelike and the r coordinate is timelike. For $-1/3 < \alpha < 0$, V is positive but S is imaginary. The mass m, which depends only on t in the KS case, is also negative for $-1/3 < \alpha < 0$. [The KS solution has no origin, so eqn (3) is inapplicable.] Therefore probably only solutions with $\alpha < -1/3$ are physical. One can put the metric in a more familiar form by making the coordinate transformation

$$\hat{t} = \beta x_0 t, \quad \hat{r} = \gamma^{-1}(\beta x_0)^{2\alpha/(1+\alpha)} x_0^{\,1/\alpha} S_0^{-2}\, r^{(1+3\alpha)/(1+\alpha)}. \tag{14}$$

This gives

$$ds^2 = d\hat{t}^2 - \hat{t}^{-4\alpha/(1+\alpha)} d\hat{r}^2 - (S_c/\beta x_c)^2 \hat{t}^2 d\Omega^2 \tag{15}$$

although it should be noted that the new coordinates may not be real for $\alpha > -1/3$.

• A self-similar static solution. In this case

$$x = x_0, \quad S = S_0 \tag{16}$$

where the constants x_0 and S_0 are determined uniquely by α, so there is just one static solution for each equation of state. One also has

$$\mu = x_0^{-(1+\alpha)/\alpha}(4\pi r^2)^{-1}, \quad V = \sqrt{3\alpha}\, x_0^{(1-\alpha)/2\alpha} z^{(1-\alpha)/(1+\alpha)}, \tag{17}$$

where the density profile has the usual isothermal form. Note that there is a naked singularity at the origin. By introducing the variables

$$\hat{r} = rS_0, \quad \hat{t} = \left(\frac{1+\alpha}{1-\alpha}\right)\beta x_0 S_0^{-2\alpha/(1+\alpha)}, \tag{18}$$

the metric can be put in an explicitly static form

$$ds^2 = \hat{r}^{4\alpha/(1+\alpha)} d\hat{t}^2 - \gamma^{-2} x_0^{2/\alpha} S_0^{-6} d\hat{r}^2 - \hat{r}^2 d\Omega^2. \tag{19}$$

The existence of the self-similar static solution has been noted by several authors (Misner & Zapolsky 1964, Henriksen & Wesson 1978a & 1978b, Carr & Yahil 1990). There is an interesting connection between the static and KS solutions: if one interchanges the r and t coordinates in the static metric and also changes the equation of state parameter to

$$\alpha' = -\frac{\alpha}{1+2\alpha}, \tag{20}$$

one obtains the KS metric. For a static solution with a normal equation of state ($1 > \alpha > 0$), α' must lie in the range $-1/3$ to 0, so negative pressure (negative mass) KS solutions can also be interpreted as positive pressure (positive mass) static solutions.

The forms of $V(z)$ for the Friedmann, KS and static solutions in the $\alpha = 1/3$ case are shown in Figure (1). To study the family of similarity solutions asymptotic to these or the associated $z < 0$ solutions at large and small $|z|$, one introduces functions $A(z)$ and $B(z)$ defined by

$$x \equiv x_i e^A, \quad S \equiv x_i e^B \tag{21}$$

where x_i is given by eqn (8) in the Friedmann case, eqn (12) in the KS case and eqn (16) in the static case. The ordinary differential equations for x and S then become ordinary differential equations for A and B. The solutions in each family can be specified by the values of A and B as $|z| \to \infty$ and $|z| \to 0$, although these values may not be independent. The form of the complete family of solutions in the $\alpha = 1/3$ case is summarized in Figure 6.

2.3 Asymptotically Friedmann solutions

In the supersonic (large z) regime, one linearizes the equations in A, $\dot{A}$ and $\dot{B}$ and obtains the 1st order solution

$$A = -\frac{\alpha(1+3\alpha)}{(1+\alpha)} k z^{-2(1+3\alpha)/3(1+\alpha)}, \quad B = B_\infty - k z^{-2(1+3\alpha)/3(1+\alpha)} \tag{22}$$

where B_∞ and k are integration constants related by

$$k = \frac{3(1+\alpha)(e^{-2B_\infty} - e^{4B_\infty})}{2(1+3\alpha)(5+3\alpha)}. \tag{23}$$

Thus there is a 1-parameter family of asymptotically Friedmann solutions and one can take this parameter to be B_∞. Eqns (6), (21) and (23) show that solutions are overdense relative to the Friedmann solution for $B_\infty < 0$ and underdense for $B_\infty > 0$.

If B_∞ is sufficiently negative, V reaches a minimum value and then rises again to infinity as z decreases. Such solutions contain black holes and were originally studied because there was interest in whether black holes could grow at the same rate as the particle horizon. Carr & Hawking (1974) showed that such solutions exist for radiation ($\alpha = 1/3$) and dust ($\alpha = 0$) but only if the universe is asymptotically rather than exactly Friedmann ($B_\infty \neq 0$), i.e. one cannot attach a black hole to an exact Friedmann model via a sound-wave. This means that black holes formed through purely local processes in the early Universe cannot grow as fast as the particle horizon. Carr (1976) and Bicknell & Henriksen (1978a) then extended this result to a general $0 < \alpha < 1$ fluid. Lin et al. (1978) claimed that a black hole similarity solution *can* be attached to an exact Friedmann model for the special case of a stiff fluid ($\alpha = 1$) but Bicknell & Henriksen (1978b) showed that this requires the inflowing material to turn into a radiation fluid at the event horizon. In fact, for fixed α, it is now known that *all* subsonic solutions which can be attached to an exact Friedmann model via a sound wave are non-physical: as one goes inward from the sound wave they either enter a negative mass regime or reach another sonic point at which the pressure diverges (Bicknell & Henriksen 1978a).

It is likely that asymptotically Friedmann solutions which contain black holes are supersonic everywhere (in the sense that V never falls below $1/\sqrt{\alpha}$), although this has not been rigorously proved. However, all the solutions with B_∞ exceeding some critical negative value B_∞^{crit} reach the sonic surface and those for which the value of z at the sonic point lies within the ranges $z_1 < z < z_2$ and $z > z_3$ [indicated in Figure (1) for $\alpha = 1/3$] may be attached to the origin by subsonic solutions. The latter are also described by a single parameter: A and B tend to related constants as $z \to 0$, so we can take the parameter to be A_0, the value of A at $z = 0$. This is a measure of the overdensity at the origin since eqns (6) and (21) imply

$$A_0 = \left[\frac{\alpha}{1+\alpha}\right] \log\left[\frac{\mu_F(0)}{\mu(0)}\right], \tag{24}$$

where μ_F is the density in the Friedmann solution. Thus solutions are overdense relative to the Friedmann solution for $A_0 < 0$ and underdense for $A_0 > 0$. These transonic solutions represent density fluctuations in a flat Friedmann background which grow at the same rate as the particle horizon (Carr & Yahil 1990). While there is a continuum of regular underdense solutions, regular overdense solutions only occur in narrow bands (with just one solution per band being analytic). The overdense solutions exhibit oscillations inside the sonic point, with the number of oscillations labelling the band. The existence of these bands was first pointed out by Bogovalenski (1985) and also studied by Ori & Piran (1990). The band structure arises even in the Newtonian situation (Whitworth & Summers 1985). The higher bands are all nearly static near the sonic point ($z_1 = z_S$ if $\alpha = 1/3$), although they deviate from the static solution as one goes towards the origin. The form of the solutions near the sonic point is qualitatively similar for all values of α. It is illustrated in Figure (2) for $\alpha = 1/3$, the case most likely to pertain in the early Universe, although this shows only the first overdense band explicitly.

The overall form of $S(z)$ and $V(z)$ in the $\alpha = 1/3$ asymptotically Friedmann solutions is indicated in Figure (3). For comparison with the other similarity solutions, the curves are here parametrized by the "asymptotic energy" parameter (E), which is related to B_∞ by

$$E = \frac{1}{2}(e^{6B_\infty} - 1). \tag{25}$$

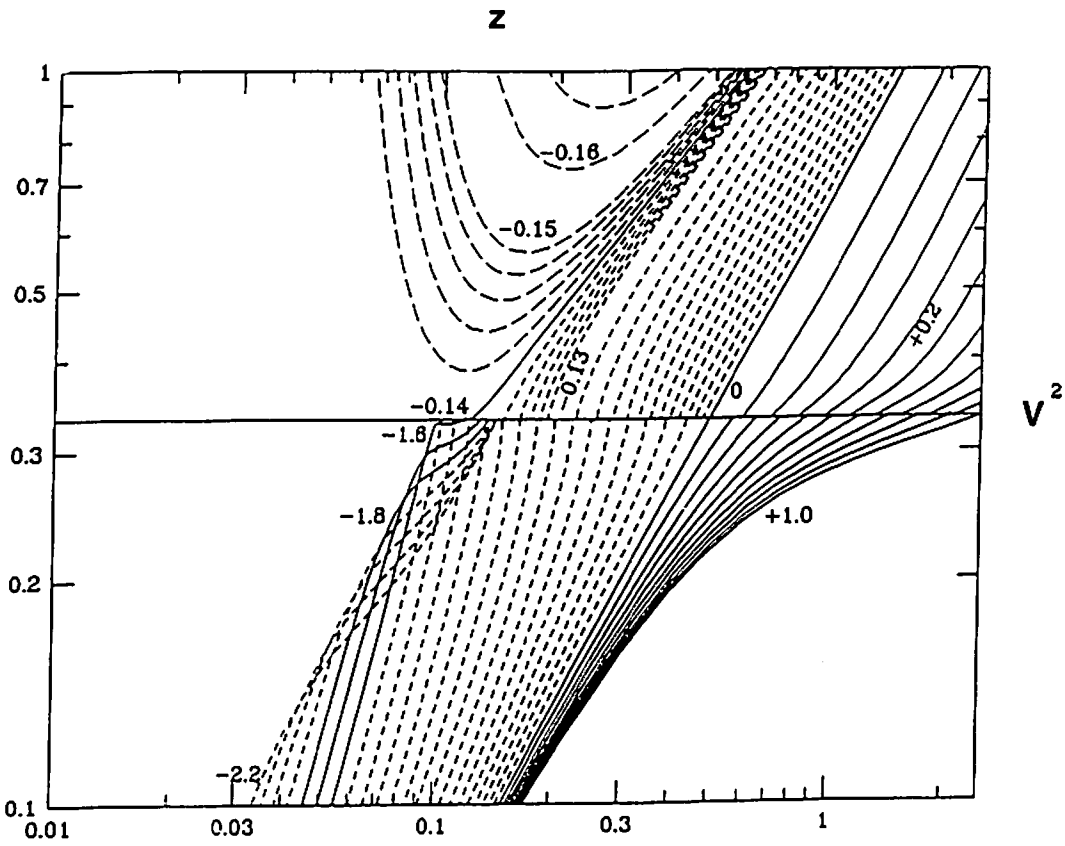

Figure 2: The form of the velocity function $V(z)$ near the sonic line for the asymptotically Friedmann solutions with $\alpha = 1/3$. In the supersonic regime, they are described by the parameter B_∞. The spacing is 0.05 for $B_\infty > 0$ and 0.01 for $B_\infty < 0$, except in the range between 0.13 and 0.15, where it is 0.02. In the subsonic regime, solutions are described by the parameter A_0 with spacing 0.1. The solutions which are regular on both sides of the sonic point are shown by solid curves; otherwise they are shown dashed, with long dashes for solutions containing black holes.

The $z > 0$ solutions correspond to inhomogeneous models which start from an initial Big Bang singularity at $z = \infty$ ($t = 0$) and then, as z decreases, either expand to infinity for $E > E_{crit}$ or recollapse for $E < E_{crit}$; here E_{crit} is the (negative) value associated with B_∞^{crit}. The recollapsing solutions contain a black hole event horizon and a cosmological particle horizon for values of E exceeding another negative value E_* such that V_{min} is below 1. In this case, the mass of the black hole is

$$m_{BH} = (MSz)_{BH}\, t, \tag{26}$$

so it forms with zero mass at $t = 0$ and then grows as t. We have seen that there are overdense oscillating solutions without black holes providing E lies in narrow bands between E_{crit} and 0 but Figure (3) does not show these oscillations explicitly. The analysis is trivially extended to the $z < 0$ regime. The $z < 0$ solutions are merely the time-reverse of the $z > 0$ ones: $E > E_{crit}$ models collapse from an infinitely dispersed initial state to a Big Crunch singularity as z decreases from 0 to $-\infty$ (i.e. as t increases from $-\infty$ to 0), while $E < E_{crit}$ models emerge from a white hole and are never infinitely dispersed.

2.4 Asymptotically Kantowski-Sachs solutions

The asymptotically KS models were studied by Carr & Koutras (1992). At large values of $|V|$, linearizing the equations in A, $\dot{A}$ and $\dot{B}$ gives the 1st order solution

$$A = A_\infty z^{-p_{1,2}}, \quad B = A_\infty \left[\frac{1}{2\alpha} - \left(\frac{1-\alpha}{1+\alpha}\right)\frac{1}{p_i}\right] z^{-p_{1,2}}, \tag{27}$$

where A_∞ is an integration constant and

$$p_{1,2} = \frac{-1+\alpha \pm \sqrt{(1-\alpha)(24\alpha^2+7\alpha+1)}}{2(1+\alpha)}. \tag{28}$$

There is thus a 1-parameter famly of solutions. For $\alpha > 0$, the KS solution has $|V| \to \infty$ as $z \to \infty$, so we must choose the positive root p_1. For $-1 < \alpha < -1/3$, the KS solution has $|V| \to \infty$ as $z \to 0$, so we must choose the negative root p_2. For $-1/3 < \alpha < 0$, one again has $|V| \to \infty$ as $z \to \infty$ but both p_1 and p_2 are negative, so there are no solutions. At small values of $|V|$, A and B must be constant but their values are related, so there is again a 1-parameter family of solutions. The parameter may be taken to be A_0 and is a measure of the underdensity or overdensity relative to the KS solution.

Solutions with $\alpha > 0$, like the KS similarity solution itself, are probably unphysical since the mass is negative. It also turns out that there are only isolated solutions at a sonic point in this case, so solutions which hit the sonic surface are unlikely to be regular there. However, these solutions are still of mathematical interest, since they fill in the negative V quadrant in Figure (6). The solutions with $-1 < \alpha < -1/3$ may be more physical since this equation of state could arise in the early Universe due to inflation or particle production. Such models may be related to the growth of $p > 0$ bubbles formed at a phase transition in a $p < 0$ cosmological background (Wesson 1986). Note that the asymptotic energy in all these solutions is $E = -1/2$, which from eqn (25) corresponds to the limit of the asymptotically Friedmann solutions as $B_\infty \to -\infty$.

A rather peculiar feature of the asymptotically KS solutions is that the mass can go negative. Indeed this is a general feature of similarity solutions which can occur even for $V > 0$. This may seem unphysical but - in the context of the Big Bang model - Miller (1976) has given a possible interpretation of this in terms of "lagging" cores. She gives an explicit example of a self-similar solution for which the mass goes negative in the stiff ($\alpha = 1$) case. In the $\alpha = 1/3$ case (but only this case), one can show that there is a well-defined curve in the $V(z)$ diagrams where $M = 0$:

$$V^3 = -\sqrt{3/2}\, z^{3/2}(V^2 - 1/9). \tag{29}$$

This curve is shown in Figure (1) and has two parts. The upper part (with $V > 0$) is relevant for asymptotically Friedmann solutions, while the lower part (with $V < 0$) is relevant for asymptotically KS solution. M is negative in between the two parts and this region includes KS itself (as expected).

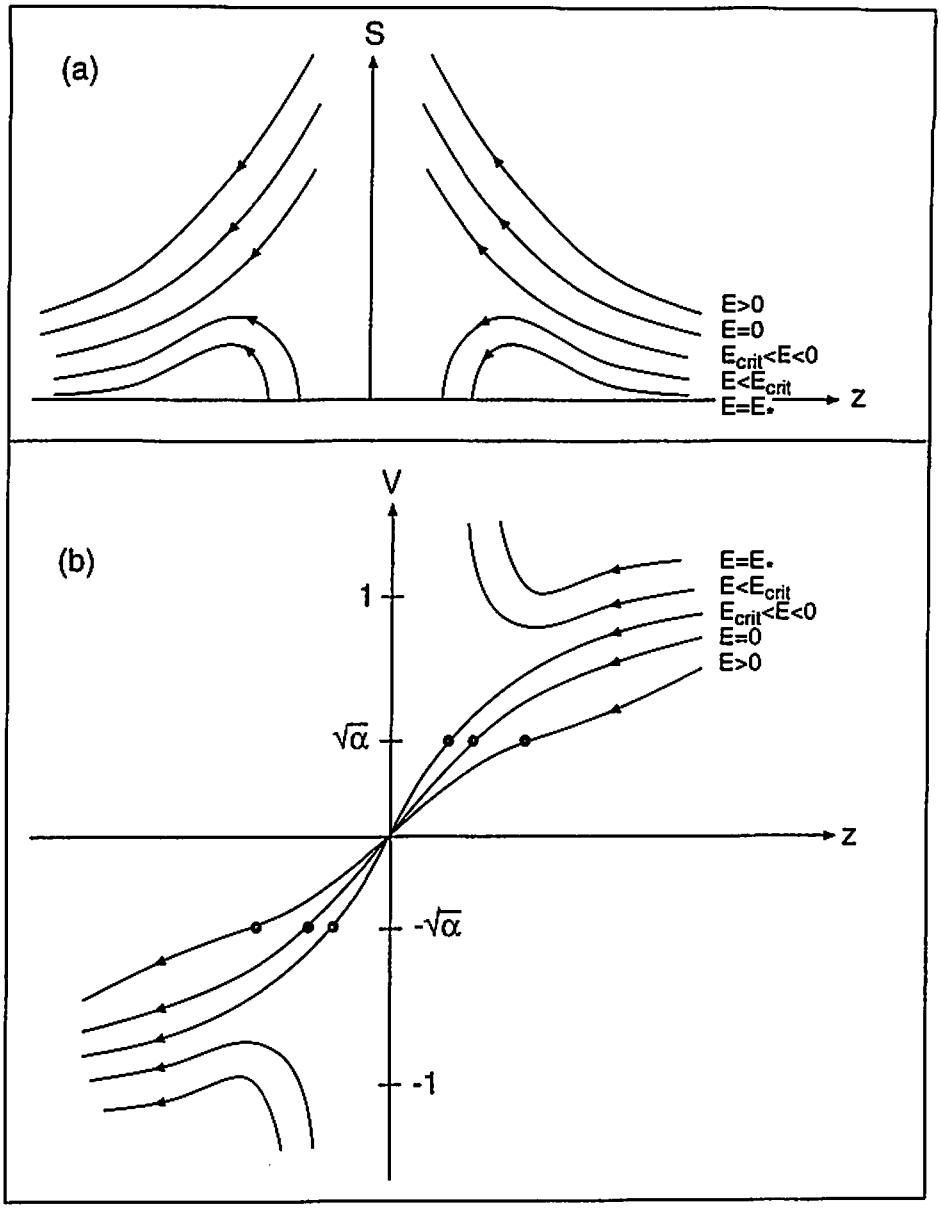

Figure 3: This shows the form of the scale factor $S(z)$ and the velocity function $V(z)$ for the asymptotically Friedmann solutions with different values of E. The $z > 0$ ($z < 0$) solutions contain black (white) holes for $E* < E < E_{crit}$, so that the minimum of $|V|$ lies between 1 and $\sqrt{\alpha}$. The solutions with $E > E_{crit}$ contain a sonic point (bold).

2.5 Asymptotically quasi-static solutions

For $0 < \alpha < 1$, the 1st order solution as $V \to \infty$ (i.e. as $z \to \infty$), is

$$A = A_\infty + Cz^{-(1-\alpha)/(1+\alpha)}, \quad B = B_\infty + \left(\frac{C}{2\alpha}\right) z^{-(1-\alpha)/(1+\alpha)} \tag{30}$$

where C is determined by the arbitrary integration constants A_∞ and B_∞. These constants also determine the asymptotic energy parameter

$$E_\infty = \frac{(1+\alpha)^2}{2(1+6\alpha+\alpha^2)} e^{6B_\infty - 2A_\infty/\alpha} - \frac{1}{2}. \tag{31}$$

This shows that asymptotically static solutions are described by *two* parameters at infinity for a given equation of state. They are therefore of particular interest since they represent the most general solution.

Describing these solutions as "asymptotically static" is rather misleading because one can show that the velocity of the fluid relative to the constant R surfaces is

$$V_R \approx -\frac{(1-\alpha)}{2\alpha(1+\alpha)} C, \tag{32}$$

at large z, so only the 1-parameter family of solutions with $C = 0$ are strictly static at infinity. This agrees with the description of Foglizzo & Henriksen (1993), who term $C = 0$ solutions "symmetric". (The exact static solution has $A_\infty = B_\infty = C = 0$ and is just one member of this family.) CC describe the more general solutions with $V_R \neq 0$ as asymptotically "quasi-static" since they still have $\dot{S}$ and $\dot{x}$ tending to 0 at infinity and one can show that they also have an isothermal density profile there.

These solutions can be straightforwardly extended to the $z < 0$ regime; indeed they *need* to be since the complete asymptotically quasi-static solutions necessarily span both positive and negative values of z. This is illustrated by the form of $S(z)$, given in Figure (4). If E exceeds some critical negative value E_{crit}, there are monotonically expanding and collapsing solutions, each of which start in the $z < 0$ region and then cross to $z > 0$. (This contrasts with the asymptotically Friedmann case, in which the expanding and collapsing solutions are confined to $z > 0$ and $z < 0$, respectively.) The expanding solutions can be interpreted as inhomogeneous Big Bang models but with the initial singularity at $z = -1/D$ rather than $z = \infty$ (i.e. for each fluid element the singularity occurs before $t = 0$). Here D is a positive constant which depends implicitly on A_∞ and B_∞, although it cannot be expressed in terms of them explicitly. The collapsing solutions are the time reverse of the expanding ones and describe the collapse of an inhomogeneous gas cloud to a Big Crunch singularity at $z = +1/D$ (i.e. after $t = 0$). For $E < E_{crit}$, S never reaches infinity, so the models either expand from a Big Bang singularity at $z = -1/D$ and then recollapse to another singularity at z_S or they expand from a white hole singularity at $-z_S$ and then recollapse to a Big Crunch singularity at $z = 1/D$. There is a minimum value of E, associated with the symmetric solution for which $z_S = 1/D$, and this is denoted by E_{sym} in Figure (4).

The form of $V(z)$ in these solutions is also indicated in Figure (4). The monotonically collapsing solutions start with $V = 0$ at $z = 0$ and then, as z decreases, pass first through a sonic point (where $V = -\sqrt{\alpha}$) and then a Cauchy horizon (where $V = -1$), before tending to the quasi-static form at $z = -\infty$. They then jump to $z = +\infty$ and enter the $z > 0$ regime. As z further decreases, V first reaches a minimum and then diverges to infinity when it encounters the singularity at $z = 1/D$. The minimum of V will be below 1 if E exceeds some value $E_+(D)$ and, in this case, one necessarily has a naked singularity. The singularity forms with zero mass at $t = 0$ but its mass m_S then grows as t since

$$m_S = (MSz)_S\, t. \tag{33}$$

As pointed out by Ori & Piran (1990), such solutions have an analogue in Newtonian theory (Larson 1969, Penston 1969). Solutions in which the minumum of V falls below $\sqrt{\alpha}$ can probably be excluded since there would need to be two sonic points and the solution is unlikely to be regular at both of them. The monotonically expanding solutions are just the time reverse of the collapsing ones. The expanding-recollapsing solutions with $E < E_{crit}$ have no sonic points. The ones which expand from $z = -1/D$ (where $V = -\infty$) and collapse to $z = z_S$ (where $V = +\infty$) will have a black hole event horizon and cosmological particle horizon for $E_* < E < E_{crit}$, corresponding to the minimum of V being less than 1.

It should be noted that the introduction of the "second" parameter D has relatively little effect on the form of the solutions in the subsonic regime. Indeed one can show that all solutions must be either *exactly* static or asymptotically Friedmann at small $|z|$, so one can still use the analysis in Section 2.3 here.

2.6 Asymptotically Minkowski Solutions

For $\alpha > 1/5$ there are also two families of asymptotically Minkowski self-similar solutions which were only discovered very recently, one associated with infinite z and the other with a finite value. These solutions are discussed in more detail by Carr et al. (1999) and turn out to play an important role in the context of critical phenomena. The forms of $S(z)$ and $V(z)$ are illustrated in Figure (5).

The first family is associated with the limit $z \to \infty$ and is characterized by the fact that V tends to a finite value

$$V_* = \frac{\alpha(1+\alpha) + \sqrt{\alpha(\alpha^3 - \alpha^2 + 3\alpha + 1)}}{1-\alpha}. \tag{34}$$

This exceeds 1 if $\alpha > 1/5$; solutions with $\alpha < 1/5$ are unphysical in the sense that the mass is negative. In addition,

$$x = x_o z^a, \quad S = S_o z^b \tag{35}$$

where a and b have a complicated dependence on α. Both exponents are positive for $\alpha > 1/5$, so the scale factor tends to infinity, while the density tends to zero as $z \to \infty$. The mass function M also tends to zero, so these solutions are asymptotically flat, although it requires a complicated coordinate transformation to demonstrate this explicitly. Eqns (34) and (35) impose a relationship between x_0 and S_0, so these solutions are described by just one independent parameter.

The second family of asymptotically flat solutions has $V \to 1$ at some finite value z_*. In this case, it can be shown that

$$S = S_0 L^{(1-\alpha)/(1-5\alpha)}, \quad x = x_0 L^{2\alpha/(1-5\alpha)}, \quad L \equiv ln(z/z_*). \tag{36}$$

Thus the scale factor diverges and the density goes to zero providing $\alpha > 1/5$. $M \to 0$ at $z = z_*$ but the product MS tends to a constant, so the mass itself is not zero. These solutions can be regarded as asymptotically Schwarzschild. The condition $V_* = 1$ gives a relationship between the constants x_0, S_0 and z_*, so they are described by two independent parameters.

3 Applications of Spherically Symmetric Similarity Solutions

3.1 Gravitational collapse and naked singularities

Until recently most counter-examples to the cosmic censorship hypothesis have been restricted to spherically symmetric spacetimes which involve shell-crossing or shell-focussing and have usually involved homothetic solutions (Eardley et al. 1986, Zannias 1991). Indeed it has been argued that one might expect a naked singularity to *generally* have a horizon structure similar to that of the global homothetic solution (Lake 1992). The occurrence of naked singularities in spherically symmetric, perfect fluid, self-similar collapse has been studied by Ori & Piran (1987, 1990), Waugh & Lake (1988, 1989), Lake & Zannias (1990), Henriksen & Patel (1991), Foglizzo & Henriksen (1993), Joshi and Dwivedi (1993), Joshi and Singh (1995) and Dwivedi and Joshi (1997). Their occurrence in the spherically symmetric collapse of a self-similar massless scalar field has also been studied by Brady (1995).

Most of the early work, including the analytical studies of Eardley & Smarr (1979) and Christodolou (1984), focussed on self-similar dust solutions of the Tolman-Bondi class. Ori & Piran (1990; OP) extended this work by studying spherically symmetric homothetic solutions with pressure. For reasonable equations of state, it might be expected that pressure gradients would prevent the formation of shell-crossing singularities but OP proved the existence of a "significant" class of self-similar solutions with a globally-naked central singularity. These are the subset of asymptotically quasi-static solutions discussed in Section 2.5 with $E_{crit} > E > E_*$. They explicitly studied the causal nature of these solutions by analysing the equations of motion for the radial null geodesics, thereby demonstrating that the null geodesics emerge to infinity.

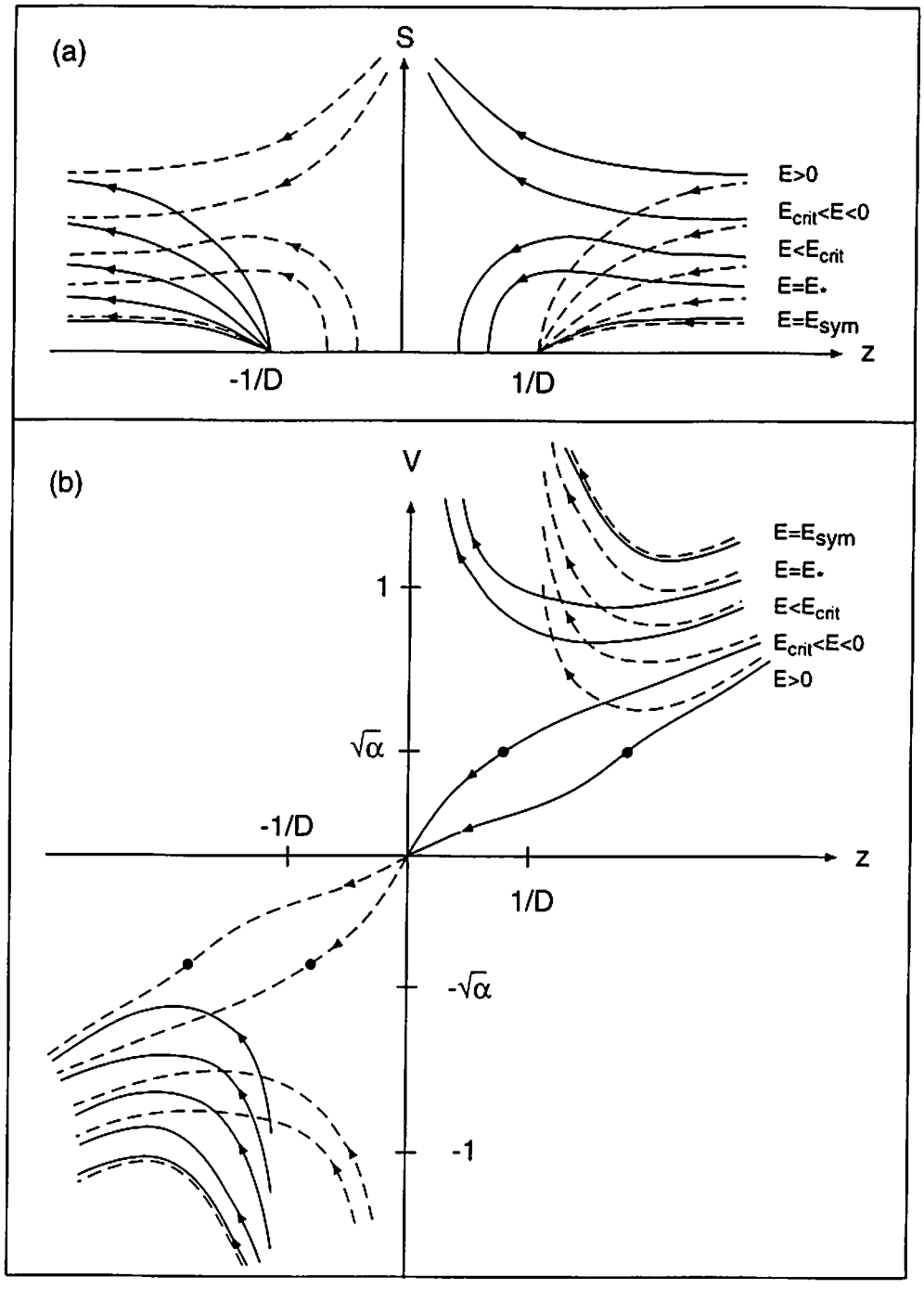

Figure 4: This shows the form of the scale factor $S(z)$ and the velocity function $V(z)$ for the asymptotically quasi-static solutions with different values of E and D. The solid curves show solutions which expand from an initial singularity at $z = -1/D$ and then either expand forever if $E > E_{crit}(D)$, in which case they pass through a sonic point (bold), or recollapse to another singularity if $E < E_{crit}(D)$. There is an event horizon and particle horizon for $E_*(D) < E < E_{crit}(D)$. The last recollapsing solution is the symmetric one for which $E = E_{sym}$. The broken curves are the time reverse of the solid ones.

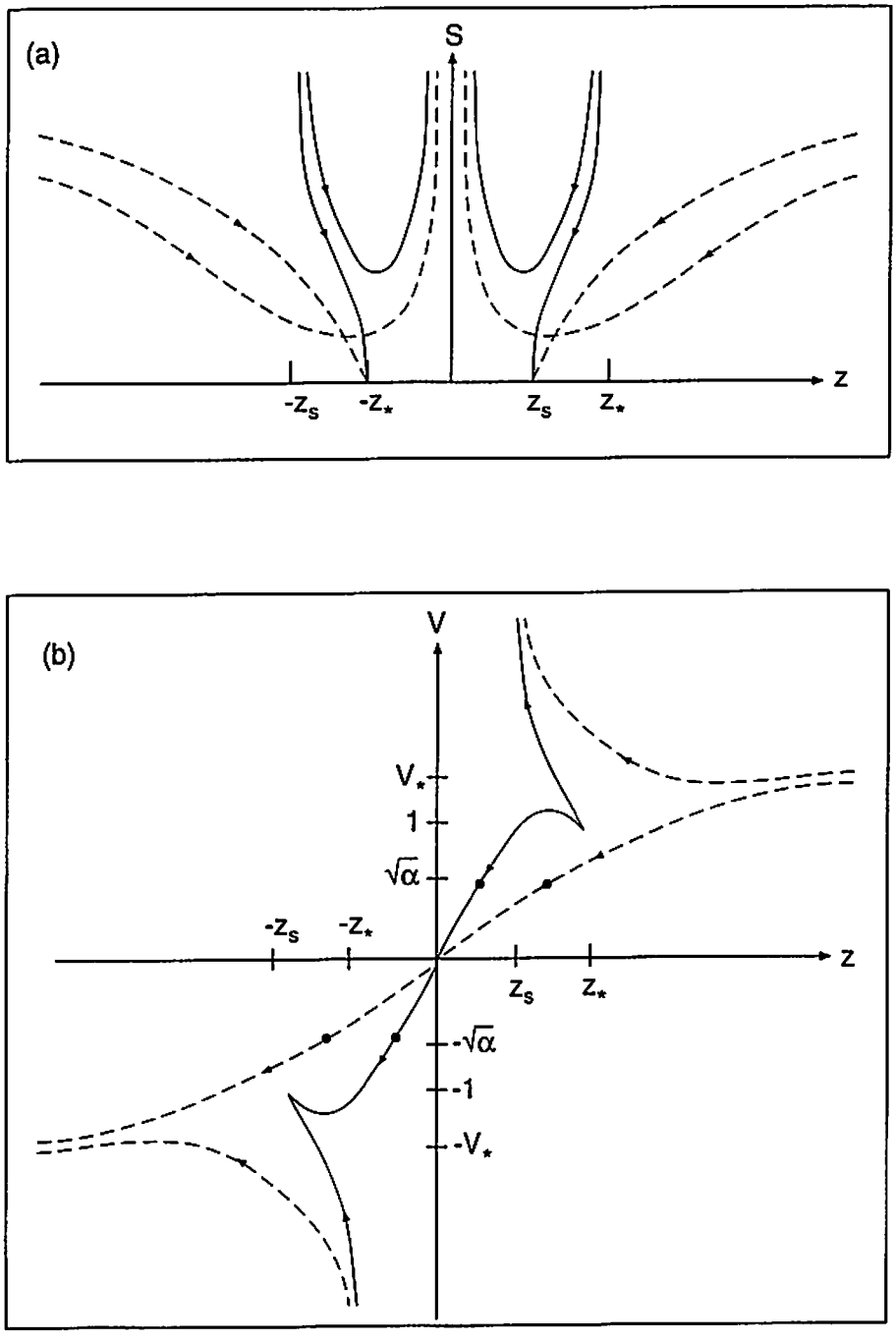

Figure 5: This shows the form of the scale factor $S(z)$ and the velocity function $V(z)$ for the ($\alpha > 1/5$) asymptotically Minkowski solutions. One family (solid lines) asymptotes to the finite value z_* with $V \to 1$; the other family (broken lines) asymptotes to infinite z with $V \to V_* > 1$. In both cases, there are solutions which collapse monotonically to a central singularity (z_S) and solutions which collapse and then bounce into an expansion phase.

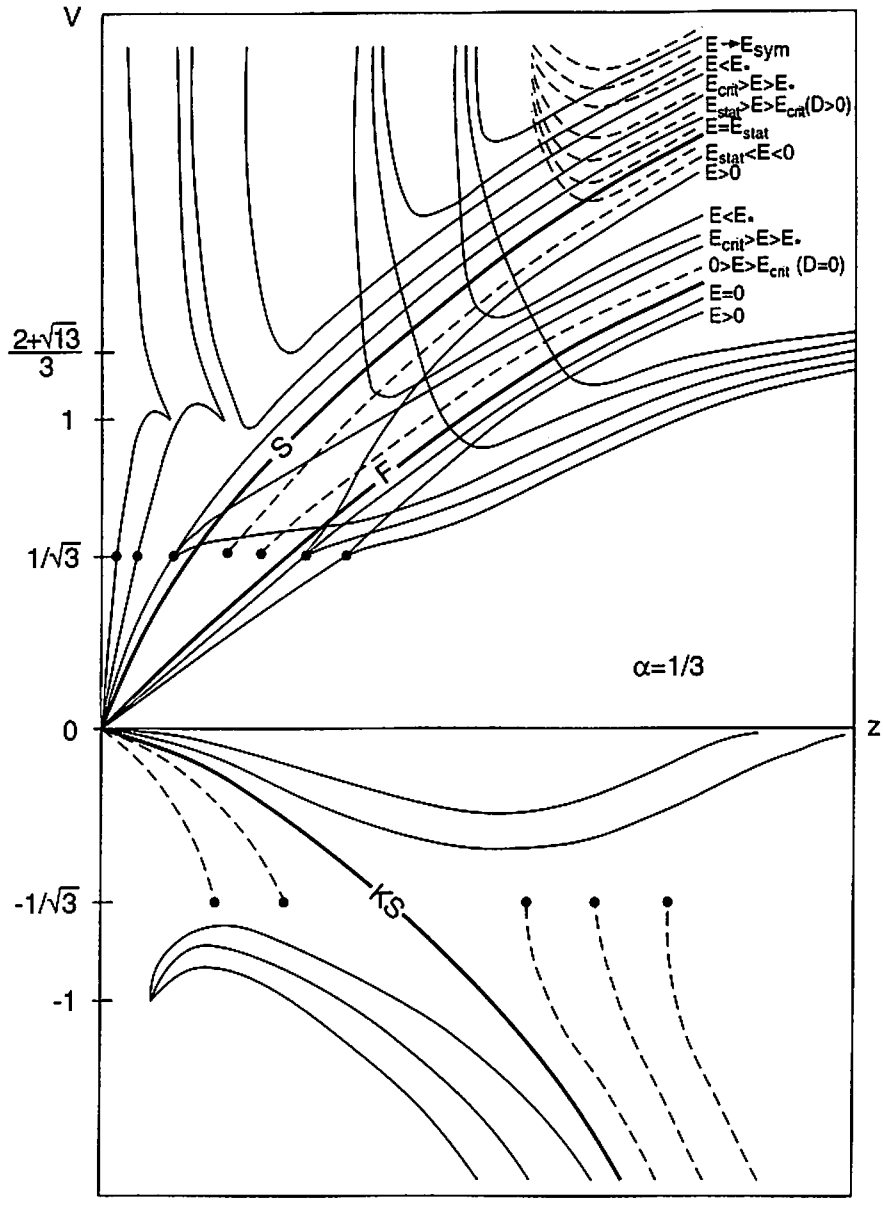

Figure 6: This shows the form of the velocity function $V(z)$ for the full family of spherically symmetric similarity solutions with $\alpha = 1/3$. The exact Friedmann, Kantowski-Sachs and static solutions are indicated by the bold lines. Also shown (for different values of E) are the asymptotically Friedmann solutions and (for different values of E and fixed D) the asymptotically quasi-static solutions. For each value of E, the latter have two branches and the branches given by the broken curves all have a singularity at $z = 1/D$. The negative V region is occupied by the asymptotically Kankowski-Sachs solutions, although these may not be physical since the mass is negative. Solutions shown by dashed lines are irregular at the sonic point and cannot be extended beyond there. Also shown are the two families of asymptotically flat solutions: for one of these V asymptotes to 1 at finite value of z; for the other V asymptotes to $(2 + \sqrt{13})/3$ at infinite z.

Foglizzo & Henriksen (1993; FH) extended OP's analysis of the gravitational collapse of homothetic perfect fluid gas spheres with $p = \alpha\mu$ to all values of α between 0 and 1, partially utilizing the powerful dynamical systems approach of Bogoyavlenski (1985). Their solutions can be characterized by the number of oscillations they contain in the subsonic region n_α. As n_α increases, the minimum value V_{min} obtained by V in the region $z > 0$ where the singularity z_S lies decreases. Thus there is always a first n_α for which V_{min} falls below 1 and this value, n_α^* say, labels the threshold for the formation of massless black holes and naked singularities. FH give $n_\alpha^* = 1$ for $\alpha = 1/16$, 4 for $\alpha = 1/3$ and 6 for $\alpha = 9/16$. They surmise that $n_\alpha^* \to \infty$ as $\alpha \to 1$ but do not prove this assertion. For sufficiently small α, $n_\alpha^* = 0$ (Ori & Piran 1990).

3.2 Critical phenomena

One of the most exciting developments in general relativity in recent years has been the discovery of critical phenomena in gravitational collapse. This first arose in studying the gravitational collapse of a spherically symmetric massless (minimally coupled) scalar field (Choptuik 1993). If one considers a family of imploding scalar wave packets whose strength is characterized by a continuous parameter l, one finds that the final outcome is either gravitational collapse for $l > l^*$ or dispersal leaving behind a regular spacetime for $l < l^*$. For $(l - l^*)/l^*$ positive and small, the final black hole mass obeys a scaling law

$$M_{BH} = C(l - l^*)^\gamma \tag{37}$$

where C is a family-dependent parameter and $\gamma = 0.37$ is family-independent. Initial data with $l = l^*$ evolve towards a critical solution which exhibits "echoing". This is a discrete self-similarity in which all dimensionless variables Ψ repeat themselves on ever-decreasing spacetime scales:

$$\Psi(t, r) = \Psi(e^{-n\Delta}t, e^{-n\Delta}r) \tag{38}$$

where n is a positive integer and $\Delta = 3.44$. Near-critical initial data first evolves towards the critical solution, showing some echoing on small space scales, but then rapidly evolves away from it to either form a black hole ($l > l^*$) or disperse ($l < l^*$).

The structure of this critical solution has been studied by Gundlach (1995). He claims that the solution is unique providing the metric is regular at the origin ($r = 0$) and analytic across the past null-cone of $r = t = 0$. (The null cone is also a sonic surface since the speed of sound is the speed of light for a scalar field.) The solution has a naked singularity at $r = t = 0$. Gundlach also shows that the critical solution is unstable, spherically symmetric perturbations about it containing a single growing mode. A similar picture has emerged from the numerical analysis of spherically symmetric field collapse for a non-minimally coupled scalar field and for a self-interacting scalar field (Choptuik 1994).

Obtaining analytical results with a discrete self-similarity is difficult, so attempts have been made to elucidate critical phenomena by studying spherically symmetric solutions which possess continuous self-similarity. There is evidence that continuous self-similarity is a good approximation in the near-critical regime, so mathematical simplification is not the only motivation for these studies. Spherically symmetric homothetic spacetimes containing radiation have been investigated by Evans & Coleman (1994). They study models containing ingoing Gaussian wave packets of radiation numerically and find analogous non-linear behaviour to the scalar case. The scaling law even has the same exponent $\gamma = 0.36$, although this appears to be a coincidence since the exponent is different for other equations of state. They also obtain an exact self-similar critical solution which is qualitatitively similar to the scalar DSS critical solution; in particular, it has a curvature singularity at $t = r = 0$ but is regular at $r = 0$ and the sonic point. As in the scalar case, they find that the critical solution is an intermediate attractor: as the critical point is approached, the evolution of the fluid and gravitational field develops a self-similar region (given by the exact critical solution) near the centre of collapse. However, only a precisely critical model is described by this solution everywhere. A rather puzzling feature of the Evans-Coleman solution is claimed to be "type 2" since the similarity variable is r/t^n. However, as discussed by Carr & Henriksen (1998), this claim is misleading. The index n appears in their calculations only because their solution is asymptotically flat and this entails matching a non-self-similar region to a self-similar region across an ingoing sound-wave.

Maison (1996) has extended Evans and Coleman's work to the more general $p = \alpha\mu$ case. By considering spherically symmetric non-self-similar perturbations to the critical solution, he manages to

obtain the scaling behaviour indicated by eqn (33) analytically. If $\alpha = 1$, corresponding to a "stiff" fluid, the similarity equations are singular and so the Maison analysis cannot be straightforwardly applied to a scalar field itself. Even though a *homogeneous* scalar field can be described as a stiff fluid, the presence of inhomogenieties forces the equation of state to deviate from $p = \mu$. However, spherically *symmetric* self-similar spacetimes with a massless scalar field have been investigated by a number of authors (Brady 1995, Koike et al. 1995, Hod & Piran 1997, Frolov 1997). The self-similar solution of Roberts (1989) is also relevant in this context. This describes the implosion of scalar radiation from past null infinity. The solution is described by a single parameter: it collapses to a black hole when this parameter is positive, disperses to future null infinity - leaving behind Minkowski space - when it is negative, and exhibits a null singularity when it is zero. Although this is reminiscent of the usual critical behaviour, the critical solution is not an intermediate attractor since nearby solutions do not evolve towards it.

It is clearly important to relate these studies of self-similar solutions to the earlier ones and to identify the critical solutions among the complete CC family. The overdense asymptotically Friedmann solutions already exhibit some of the features of the critical solution in that they are nearly static inside the sonic point and exhibit oscillations. They are also regular at the origin and at the sonic point. However, they cannot be identified with the critical solution itself since they do not contain a naked singularity at the origin. Nor can the static solution itself be so identified since it has a naked singularity at $r = 0$ for all t, whereas the critical solution only has a singularity at the origin for $t = 0$.

To identify the critical solution, we need to consider the full 2-parameter family of spherically symmetric similarity solutions. If one confines attention to solutions which are analytic at the the sonic point, then Carr et al. (1999) have shown numerically that, for all α, the critical solution starts from a regular centre, passes through a sonic point and enters the spatially self-similar region (with $|V| > 1$). For $0 < \alpha \lesssim 0.28$, the critical solution is of the asymptotically quasi-static kind: it passes through the spatially self-similar region and enters a second timelike self-similar region, finally reaching another sonic point, which is generally irregular. However, this does not invalidate the solution as being the critical one, since the solution describing the inner collapsing region is usually matched to an asymptotically flat exterior geometry sufficiently far from the centre. For $0.28 \lesssim \alpha < 1$, the critical solution belongs to the asymptotically Minkowski solutions associated with finite z. For the limiting case $\alpha \approx 0.28$, the critical solution is also asymptotically Minkowski but of the kind associated with infinite z.

3.3 Self-similar voids

Measurements of the Hubble constant H_0 obtained through studying Cepheid variables in galaxies in the Virgo and Leo clusters give values of around 80 $km\ s^{-1} Mpc^{-1}$ (Pierce et al. 1994, Freedman et al. 1994). As is well known, in the standard Big Bang model without a cosmological constant this makes it hard to reconcile the age of the Universe with the ages of the globular clusters (at least 12 Gyr). More recent estimates of H_0 using Cepheids yield values closer to 70 $km\ s^{-1} Mpc^{-1}$ (Freedman 1998) but there may still be an age problem. However, it must be stressed that these large values of H_0 are all obtained within the relatively local distance of 100 Mpc, which is much less than the horizon size of order 10 Gpc. Observations based on the Sunyaev-Zeldovich effect for clusters and the time delay in gravitational lensed quasars at much larger distances give lower values for the Hubble constant, which would be compatible with the standard cosmological age.

Several people have pointed out that the apparent discrepancy between the local and distant values of the Hubble constant can be reconciled if we live in a region of the Universe for which the local density is considerably less than its global value (Moffat & Tatarski 1992 & 1995, Nakao et al. 1995, Shi et al. 1996). This could also explain why the local density parameter (e.g. the density inferred dynamically from galaxy motions) is less than the global value required by inflation. We will describe such a region as a "void", even though it is not completely empty. This suggestion might not seem too radical since we already know that the Universe contains large-scale voids (Geller & Huchra 1989). However, to resolve the age problem, we need the local void to extend to at least 100 Mpc (so that it includes the Coma cluster, which is assumed to have negligible deviation from the Hubble flow in the Cepheid estimates of H_0) and this is much larger than the typical void.

In analysing this proposal, one needs to assume a particular model for the void. Most authors use the Tolman-Bondi solution to model the local region as an underdense sphere embedded in a flat Universe

and then determine the ratio of the global and local Hubble and density parameters (Suto et al. 1995, *Wu et al.* 1995). However, we have seen that density perturbations in an asymptotically Friedmann Universe may naturally evolve to a spherically symmetric self-similar form and this has motivated Carr & Whinnett (1999; CW) to consider the possibility that we are located at the centre of a self-similar void.

The precise form of the self-similar void depends upon the equation of state. After the time of decoupling at around 10^5 y, the Universe can be treated as pressureless "dust" ($\alpha = 0$). In this case, there is no sonic point and the underdense self-similar solutions can be analysed analytically as a special case of the Tolman-Bondi solutions (cf. Tomita 1995, 1997). CW express the various Hubble and density parameter profiles in terms of the (negative) energy parameter E. Although they find that the local values of these parameters may indeed differ considerably from their global values, they also note that the self-similar dust solution is non-regular at the origin in that the circumference function is non-zero in the limit $r \to 0$ unless $E = 0$. Thus the coordinate origin is an expanding 2-sphere and must be patched onto a non-self-similar region at the centre. This produces anomalous behaviour in the r-dependence of the Hubble parameter, which is in contradiction with the observations.

Although the self-similar dust solution is not a viable model for a void in the real Universe, the similarity hypothesis is not really expected to apply in the dust situation since Carr (1993) speculates that one needs the effects of pressure to impose these features. It is therefore more natural to assume that the voids only tend to self-similar form in the radiation-dominated ($\alpha = 1/3$) era before decoupling. Since the special conditions required for self-similar evolution in the radiation era are incompatible with self-similar evolution after decoupling, this suggests that one should merely use the self-similar radiation solution to set the initial conditions for the non-self-similar Tolman-Bondi evolution in the dust era. More precisely, the similarity solutions specify the form of R, m and E as functions of r along the decoupling hypersurface and the Tolman-Bondi equations then give the evolution of $R(t, r)$ for each shell of constant r. From this one can calculate the various Hubble parameters at any given epoch.

CW find models that are in agreement with the observational data and clearly show a variation of Hubble parameter with distance. However, these models have a drawback. From eqn (24), the strength of the initial radiation perturbation is determined by the single parameter A_0, which fixes both the density contrast and the size of the void relative to the particle horizon. To obtain a void that is large enough to contain the Coma cluster at the present epoch, it is necessary to choose a value for A_0 which implies that the density contrast at decoupling exceeds the mean perturbations allowed by the COBE data. In addition, at the current epoch, the void has a local density parameter much lower than the observed value. One can select a smaller value of A_0 to produce the required density contrast but, in this case, the void radius is too small.

3.4 The similarity hypothesis

In Section 1 we emphasized that there are a variety of astrophysical and cosmological situations in which spherically symmetric solutions naturally evolve to self-similar form, leading to the "similarity hypothesis". Presumably a necessary (but not sufficient) condition for the validity of this hypothesis is that spherically symmetric similarity solutions (or at least some subset of them) be stable to non-self-similar perturbations. As a first step to investigating the similarity hypothesis, Carr & Coley (1997b) have therefore investigated the stability of the spherically symmetric similarity solutions within the more general class of spherically symmetric solutions.

Following Cahill & Taub (1971), we express all functions in terms of the similarity variable z and the radial coordinate r and regard these as the independent variables rather than r and t. We also assume that the perturbations in S and x (defined in Section 2.1) can be expressed in the form

$$S(z, r) = S_0(z)[1 + S_1(r)], \quad x(z, r) = x_0(z)[1 + x_1(r)] \tag{39}$$

where a subscript 0 indicates the form of the function in the exact self-similar case and a subscript 1 indicates the fractional perturbation in that function (taken to be small; i.e. $S_1 << 1$ and $x_1 << 1$). The perturbations equations for $S_1(r)$ and $x_1(r)$ can then be expressed as 2nd order differential equation in r and we test whether a particular similarity solution is stable by examining whether the perturbation terms grow or decay at large values of r. It might seem more natural to examine whether the solution grows or decays at large values of time, since the similarity hypothesis only requires that the general solution

tends to similarity as $t \to \infty$. However, the t evolution is entirely contained within the z evolution, so if one wrote the perturbation equations in terms of t and z (instead of r and z), one would get equivalent results.

Carr & Coley come to the following conclusions:

• The asymptotically Friedmann solutions are stable providing $\alpha > -1/3$. This directly relates to the original similarity hypothesis (i.e. to the issue of whether density perturbations naturally evolve to self-similar form). Of course, this does not prove the similarity hypothesis since they only consider *small* perturbations of self-similar models. Nor do they consider non-spherical perturbations.

• The asymptotically Kantowski-Sachs solutions are unstable for $1 > \alpha > -1/3$ but stable for $-1 < \alpha < -1/3$. The latter corresponds precisely to the range in which the solution may be physically permissible. This may relate to the formation of bubbles in an inflationary scenario and hence to the stability of the inflationary phase itself.

• The overdense asymptotically Friedmann solutions which are non-analytic at the sonic point are unstable. This relates to the well-known "kink" instability: non-analytic solutions either develop shocks or are driven towards analytic ones (Ori & Piran 1988, Whitworth & Summers 1985).

• The asymptotically quasi-static solutions which contain naked singularities are unstable. This clearly relates to the cosmic censorship hypothesis since this states that such singularities are physically forbidden. It also relates to the instability of the critical solutions which arise in gravitational collapse calculations (Maison 1996).

ACKNOWLEDGEMENTS

Some of the results described in this review derive from work done in collaboration with Alan Coley, Martin Goliath, Stephen Hawking, Andreas Koutras, Ulf Nilsson, Claes Uggla, Andrew Whinnett and Amos Yahil. The author thanks them for many stimulating interactions.

References

[1] A. M. Anile, G. Moschetti and O. I. Bogoyavlenski, 1987, J. Math. Phys. **28**, 2942.

[2] G. I. Barenblatt and Ya B. Zeldovich, 1972, Ann. Rev. Fluid Mech. 4, 285.

[3] E. Bertschinger, 1985, Ap. J. **268**, 17.

[4] E. Bertschinger and P. N. Watts, 1984, **328**, 23.

[5] G. V. Bicknell and R. N. Henriksen, 1978a, Ap. J. **219**, 1043.

[6] G. V. Bicknell and R. N. Henriksen, 1978b, Ap. J. **225**, 237.

[7] O. I. Bogoyavlenski, 1977, Sov. Phys. JETP **46**, 634.

[8] O. I. Bogoyavlenski, 1985, *Methods in the Qualitative Theory of Dynamical Systems in Astrophysics and Gas Dynamics* (Springer-Verlag).

[9] P. Brady, 1995, Phys. Rev. D **51**, 4168 .

[10] M.E. Cahill and A.H. Taub,1971, Comm.Math.Phys., **21**, 1.

[11] B. J. Carr, 1976, Cambridge, Ph.D. thesis.

[12] B. J. Carr, 1993, *The Origin of Structure in the Universes*, ed. E. Gunzig & P. Nardone, Reidel; omitted from Proceedings.

[13] B. J. Carr and S. W. Hawking, 1974, MNRAS **168**, 399.

[14] B. J. Carr and A. Koutras, 1992, Ap. J. **405**, 34.

[15] B.J. Carr and A. Yahil, 1990, Ap.J., **360**, 330.

[16] B. J. Carr and A. A. Coley, 1999a, Phys. Rev. D., in press (CC).

[17] B. J. Carr and A. A. Coley, 1999b, preprint.

[18] B. J. Carr and A. A. Coley, 1999c, Class. Quant. Grav., 16, R31-R71.

[19] B. J. Carr and R. N. Henriksen, 1998, preprint.

[20] B. J. Carr and A. Whinnett, 1999, preprint (CW).

[21] B. J. Carr, A. A. Coley, M. Goliath, U. S. Nilsson and C. Uggla, 1999, preprint.

[22] B. Carter and R. N. Henriksen, 1991, J. Math. Phys. **32**, 2580.

[23] M. W. Choptuik, 1993, Phys. Rev. Lett. **70**, 9.

[24] M. W. Choptuik, 1994, in *Deterministic Chaos in General Relativity*, ed. D. Hobill et al. (Plenum, New York).

[25] D. Christodoulou, 1984, Commun. Math. Phys. **93**, 171.

[26] A. A. Coley, 1997, Class. Quantum Grav. **14**, 87.

[27] I. H. Dwivedi and P. S. Joshi, 1997, Class. Quant. Grav., **47**, 5357.

[28] D. M. Eardley and L. Smarr, 1979, Phys. Rev. D **19**, 2239.

[29] D. M. Eardley, J. Isenberg, J. Marsden and V. Moncrief, 1986, Comm. Math. Phys. **106**, 137.

[30] C. R. Evans and J. S. Coleman, 1994, Phys. Rev. Lett. **72**, 1782.

[31] J. A. Fillmore and P. Goldreich, 1984, Ap. J. **281**, 1.

[32] T. Foglizzo and R. N. Henriksen, 1993, Phys. Rev. D. **48**, 4645 (FH).

[33] W. L. Freedman et al., 1994, Nature **371**, 757.

[34] W. L. Freedman, 1998, Phys. Rep. **307**, 45.

[35] A. V. Frolov, 1997, Phys. Rev. D. **56**, 6433.

[36] M. J. Geller and J. P. Huchra, 1989, Science **246**, 897.

[37] M. Goliath, U. S. Nilsson and C. Uggla, 1998a, Class. Quant. Grav. **15**, 167.

[38] M. Goliath, U. S. Nilsson and C. Uggla, 1998b, Class. Quant. Grav. **15**, 2841.

[39] C. Gundlach, 1995, Phys. Rev. Lett. **75**, 3214.

[40] J. E. Gunn, 1977, Ap. J. **218**, 592.

[41] J. E. Gunn and J. R. Gott, 1972, Ap. J. **176**, 1.

[42] M. A. Hausman, D.W. Olson and B. D. Roth, 1983, Ap. J. **270**, 351.

[43] R. N. Henriksen and K. Patel, 1991, Gen. Rel. Grav. **23**, 527.

[44] L. Hsu and J. Wainwright, 1986, Class. Quant. Grav. **3**, 1105.

[45] S. Hod and T. Piran, 1997, Phys. Rev. D. **55**, R440.

[46] G.L. Hoffman, E. E. Salpeter and I. Wasserman, 1983, Ap. J. **268**, 527.

[47] S. Ikeuchi, K. Tomisaka and J. P. Ostriker, 1983, Ap. J. **265**, 583.

[48] P. S. Joshi and I. H. Dwivedi, 1993, Phys. Rev. D. **47**, 5357.

[49] P. S. Joshi and T. P. Singh, 1995, Phys. Rev. D. **51**, 6778.

[50] T. Koike, T. Hara and S. Adachi, 1995, Phys. Rev. Lett. **74**, 5170.

[51] K. Lake, 1992, Phys. Rev. Lett. **68**, 3129.

[52] K. Lake and T. Zannias, 1990, Phys. Rev. D **41**, 3866.

[53] R. B. Larson, 1969, MNRAS **145**, 271.

[54] D. N. C. Lin, B. J. Carr and S. D. M. Fall, 1978, MNRAS **177**, 151.

[55] K. Maeda and H. Sato, 1984. Prog. Theor. Phys. **71**, 1.

[56] D. Maison, 1996, Phs. Lett. B. **366**, 82.

[57] B.D. Miller, 1976, Ap.J., **208**, 275.

[58] C. W. Misner and H. S. Zapolsky, 1964, Phys. Rev. Lett. **12**, 635.

[59] J. W. Moffat and D. C. Tatarski, 1992, Phys. Rev. D. **45**, 3512.

[60] J. W. Moffat and D. C. Tatarski, 1995, Ap. J. **353**, 17.

[61] K. Nakao et al., 1995, Ap. J. **453**, 541.

[62] A. Ori and T. Piran, 1987, Phys. Rev. Lett. **59**, 2137.

[63] A. Ori and T. Piran, 1988, Mon. Not. R. Astron. Soc. **234**, 821.

[64] A. Ori and T. Piran, 1990, Phys. Rev. D. **42**, 1068 (OP).

[65] M. V. Penston, 1969, MNRAS **144**, 449.

[66] M. J. Pierce et al., 1994, Nature **371**, 211.

[67] J. Ponce de Leon, 1988, J.Math.Phys., **29**, 2479.

[68] J. Ponce de Leon, 1993, Gen. Rel. Grav. **25**, 865.

[69] M. D. Roberts, 1989, Gen. Rel. Grav. **21**, 907.

[70] J. Schwartz, J. P. Ostriker and A. Yahil, 1975, Ap. J. **202**, 1.

[71] L. I. Sedov, 1967, *Similarity and Dimensional Methods in Mechanics* (New York, Academic).

[72] X. Shi, L. M. Widrow and L. J. Dursi, 1996, MNRAS **281**, 565 (1996).

[73] Y. Suto et al., 1995, Prog. Theor. Phys. **93**, 839.

[74] K. Tomita, 1995, Ap. J. **451**, 1.

[75] K. Tomita, 1997, Phys. Rev. D. **56**, 3341.

[76] B. Waugh and K. Lake, 1988, Phys. Rev. D **38**, 1315.

[77] B. Waugh and K. Lake, 1989, Phys. Rev. D **40**, 2137.

[78] P.S. Wesson, 1986, Phys.Rev. D, **34**, 3925.

[79] P. S. Wesson, 1989, Ap. J. **336**, 58.

[80] A. Whitworth and D. Summers, 1985, MNRAS, **214**, 1.

[81] X-P. Wu et al., 1995, Astrophys. J. **448**, L65.

[82] T. Zannias, 1991, Phys. Rev. D **44**, 2397.

On Average Properties of Inhomogeneous Cosmologies

Thomas Buchert[1]

Theoretical Astrophysics Division, National Astronomical Observatory
2-21-1 Osawa, Mitaka, Tokyo 181-8588, Japan

Abstract

The present talk summarizes the recently progressed state of a systematic re-evaluation of cosmological models that respect the presence of inhomogeneities. Emphasis is given to identifying the basic steps towards an effective (i.e. spatially averaged) description of structural evolution, also unfolding the various facets of a "smoothed-out" cosmology. We shall highlight some results obtained within Newtonian cosmology, discuss expansion laws in general relativity within a covariant fluid approach, and put forward some promising directions of future research.

1 Motivation and Results in Newtonian Cosmology

1.1 Bridging the Gap

Does an inhomogeneous model of the Universe evolve *on average* like a homogeneous solution of Einstein's or Newton's laws of gravity ? This question is not new, at least among relativists who think that the answer is certainly *no*, not only in view of the nonlinearity of the theories mentioned [26]. The problem was and still is the notion of *averaging* whose specification and unambiguous definition turned out to be an endeavor of high magnitude, mainly because it is not straightforward to give a unique meaning to the averaging of tensors, e.g., a given metric of spacetime. This problem seems to lie in the backyard of relativists who, from time to time, add another effort towards a solution of this problem. On the other hand, the community of cosmologists "should" locate exactly this problem at the basis of their evolutionary models of the Universe. Although there are many exceptions (e.g. [28], [3], [4], [29], [43], [37], [47]; [23], [31], [44], a certainly incomplete list), most researchers in this field are drawn back to the historical development of cosmologies starting with Friedmann, Einstein and de Sitter at the beginning of the last century. Despite the drastic changes of our picture of structures in the Universe on large scales, still, the cosmologist's thinking rests on the hegemony of the so-called "standard model" (i.e. the family of FLRW models for homogeneous and isotropic matter distributions). This standard model, up to the present state of knowledge, explains (or better is employed to explain) a wide variety of orthogonal observations, and it is therefore hard to beat due to its (suggestively) established status of resistance against observational tests. Therefore, most discussions in this field are based on the vocabulary of the standard model, aiming to constrain its "cosmological parameters", often on the basis of observations of structure in the regional Universe that is very different from homogeneous and isotropic.

Bridging the gap between an involved mathematical problem of general relativity and the practical modeling of cosmological dynamics is possible, if ambiguities of averagers could be removed, and results related to contemporary discussions in observational cosmology. In the sequel we shall follow a line of thought that will match this need and could intensify work directed to mastering an inhomogeneous spacetime.

1.2 Setting the Pace

Averaging procedures can be defined in a vast variety of ways (see, e.g., a recent summary by Stoeger *et al.* [45]). A smoothing out operator can live on different foliations of spacetime; it can leave an averaged field space-dependent, thus operating on a given spatial scale; it can also smooth out all inhomogeneities.

[1] E-mail:buchert@theorie.physik.uni-muenchen.de

It could involve statistical ensemble averaging. It can act on scalars, vectors or tensors; it can smooth matter variables or, most elegantly, the geometry of spacetime itself [21], [22]. It can average spacetime variables and not merely spatial variables, etc. To remove ambiguity here, it is best to work within the framework of Newtonian cosmology as a first step of understanding, since there the choice of foliation is not a problem and spatial averaging can be simply put into practice by Euclidean volume integration. As a second step, we confine ourselves to scalar variables. This allows us to get at least some corresponding answer in general relativity, since the averaging of scalars is, for a given foliation, a covariant operation. We therefore propose to look at the simplest (mass-conserving) averager as follows.

1.3 A Newtonian Averager

Consider any simply-connected spatial domain in Newtonian spacetime. With $\langle\cdot\rangle_{\mathcal{D}}$ we denote spatial averaging in Eulerian space, e.g., for a spatial tensor field $\mathcal{A}(\mathbf{x},t) = \{\mathcal{A}_{ij}(\mathbf{x},t)\}$ we simply have the Euclidean volume integral normalized by the volume of the domain:

$$\langle\mathcal{A}\rangle_{\mathcal{D}}(t) = \frac{1}{V(t)}\int_{\mathcal{D}} \mathrm{d}^3x\, \mathcal{A}(\mathbf{x},t)\ . \tag{1}$$

(Here, $\mathbf{x}$ are non-rotating Eulerian coordinates.) Since, with this averager, the averaged field is only time-dependent, the space-dependence is only implicit by a functional dependence on the domain's morphology and position. We shall evolve the domain in time by preserving its mass content. This is a natural assumption, if we also want to extend the domain to the whole Universe.

Now, consider the volume of an Eulerian spatial domain $\mathcal{D}$ at a given time, $V = \int_{\mathcal{D}} \mathrm{d}^3x$, and follow the position vectors $\mathbf{x} = \mathbf{f}(\mathbf{X},t)$ of all fluid elements (indexed by the Lagrangian coordinates $\mathbf{X}$) within the domain. Then, the volume elements are deformed according to $\mathrm{d}^3x = J\mathrm{d}^3X$, where J is the Jacobian determinant of the transformation from Eulerian to Lagrangian coordinates. The total rate of change of the volume of the same collection of fluid elements may then be calculated as follows:

$$\frac{d_t V}{V} = \frac{1}{V}\mathrm{d}_t\int_{\mathcal{D}_{\mathrm{i}}} \mathrm{d}^3X\ J = \frac{1}{V}\int_{\mathcal{D}_{\mathrm{i}}} \mathrm{d}^3X\ d_t J = \frac{1}{V}\int_{\mathcal{D}_{\mathrm{i}}} \mathrm{d}^3X\ \theta J = \langle\theta\rangle_{\mathcal{D}} =: 3H_{\mathcal{D}}, \tag{2}$$

where d_t is the total (Lagrangian) time-derivative, $\theta = \nabla\cdot\mathbf{v} = \frac{\dot{J}}{J}$ the local expansion rate of a given velocity model $\mathbf{v}(\mathbf{x},t)$; $\mathcal{D}_{\mathrm{i}}$ denotes the initial domain found by mapping back $\mathcal{D}$ with the help of $\mathbf{f}^{-1}$ (provided $\mathbf{f}^{-1}$ exists), and $H_{\mathcal{D}} = \dot{a}_{\mathcal{D}}/a_{\mathcal{D}}$ naturally defines an effective Hubble-parameter on the domain.

1.4 Commuting Averaging and Evolution

From the point of view of the standard model of cosmology it makes no difference, if we smooth the initial inhomogeneities (say, at a time in the matter dominated epoch) and then evolve the smoothed data with a FLRW solution, or if we evolve these inhomogeneities until present and then smooth the distribution. The conjecture is held that both ways produce the same values for the characteristic parameters of a FLRW cosmology.

However, averaging, as defined above, and evolving inhomogeneities are non-commuting operations. To see this we have to notice that the total (Lagrangian) time-derivative does not commute with spatial averaging in Eulerian space. For an arbitrary tensor field $\mathcal{A}$ we can readily derive, with the help of the above definitions, the following *Commutation Rule* [18]:

$$\mathrm{d}_t\langle\mathcal{A}\rangle_{\mathcal{D}} - \langle\mathrm{d}_t\mathcal{A}\rangle_{\mathcal{D}} = \langle\mathcal{A}\theta\rangle_{\mathcal{D}} - \langle\theta\rangle_{\mathcal{D}}\langle\mathcal{A}\rangle_{\mathcal{D}}\,. \tag{3}$$

This tells us that exchanging the operators for averaging and time evolution produces a source due to the presence of inhomogeneities (that we will discuss to consist of positive-definite fluctuations). As an example consider the expansion rate itself. Setting $\mathcal{A} = \theta$, we get

$$\mathrm{d}_t\langle\theta\rangle_{\mathcal{D}} - \langle\mathrm{d}_t\theta\rangle_{\mathcal{D}} = \langle\theta^2\rangle_{\mathcal{D}} - \langle\theta\rangle_{\mathcal{D}}^2 = \langle(\theta - \langle\theta\rangle_{\mathcal{D}})^2\rangle_{\mathcal{D}} \geq 0\ . \tag{4}$$

i.e., the source is the averaged mean square fluctuation of the expansion rate. It vanishes for the case where the local rate equals the global one, which is true for homogeneous isotropic matter distributions.

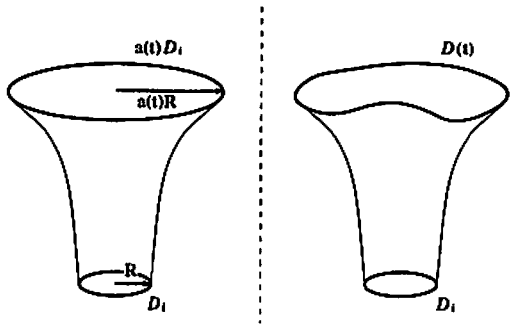

Figure 1: The evolution of an initial domain $\mathcal{D}_i$ within the Hubble flow of a FLRW cosmology with global scale factor $a(t)$ (left) and for a general inhomogeneous setting (right).

1.5 Formulating the General Expansion Law of Newtonian Cosmology

As suggested by Eq. (2) we may measure the effective expansion of a portion of the Universe with the help of the rate of volume change. Let us introduce an effective dimensionless scale-factor $a_{\mathcal{D}}$ via the domain's volume $V(t) = |\mathcal{D}|$ and the initial volume $V_i = V(t_i) = |\mathcal{D}_i|$ (compare Fig. 1):

$$a_{\mathcal{D}}(t) = \left(\frac{V(t)}{V_i}\right)^{\frac{1}{3}} \quad , \text{ i.e. } , \quad H_{\mathcal{D}} = \frac{\dot{a}_{\mathcal{D}}}{a_{\mathcal{D}}} \quad . \tag{5}$$

For domains $\mathcal{D}$ with constant mass $M_{\mathcal{D}}$, as for Lagrangian defined domains, the average mass density evolves as:

$$\langle \varrho \rangle_{\mathcal{D}} = \frac{\langle \varrho(t_i) \rangle_{\mathcal{D}_i}}{a_{\mathcal{D}}^3} = \frac{M_{\mathcal{D}}}{a_{\mathcal{D}}^3 V_i}. \tag{6}$$

Looking at the *Commutation Rule*, Eq. (4), we appreciate that this rule furnishes a purely kinematical relation provided we give a velocity model. Dynamics enters by saying how this velocity model is generated by gravity. In Eq. (4) we can express most of the terms already through the scale-factor and its time-derivatives. The only unknown is the evolution equation for the local expansion rate. This is furnished by Raychaudhuri's equation (which employs the Newtonian field equation $\nabla \cdot \mathbf{g} = \Lambda - 4\pi G\varrho$ for the gravitational field strength of dust matter $\mathbf{g} = \dot{\mathbf{v}}$).

Inserting Raychaudhuri's equation,

$$\dot{\theta} = \Lambda - 4\pi G\rho - \frac{1}{3}\theta^2 + 2(\omega^2 - \sigma^2) \ : \ \sigma := \sqrt{\frac{1}{2}\sigma_{ij}\sigma_{ij}} \ , \ \omega := \sqrt{\frac{1}{2}\omega_{ij}\omega_{ij}} \ . \tag{7}$$

into Eq. (4), we find that the scale-factor $a_{\mathcal{D}}$ *in general* obeys the dynamical expansion law [18]:

$$3\frac{\ddot{a}_{\mathcal{D}}}{a_{\mathcal{D}}} + 4\pi G \langle \varrho \rangle_{\mathcal{D}} - \Lambda = Q_{\mathcal{D}} \ . \tag{8}$$

with Newton's gravitational constant G, the cosmological constant Λ, and the source term $Q_{\mathcal{D}}$, which we may call "backreaction term", since it measures the departure from the standard model due to the influence of inhomogeneities.

$Q_{\mathcal{D}}$ depends on the kinematical scalars, the expansion rate θ, the rate of shear σ, and the rate of vorticity ω featuring three positive-definite fluctuation terms:

$$Q_{\mathcal{D}} = \frac{2}{3}\left(\langle \theta^2 \rangle_{\mathcal{D}} - \langle \theta \rangle_{\mathcal{D}}^2\right) + 2\langle \omega^2 \rangle_{\mathcal{D}} - 2\langle \sigma^2 \rangle_{\mathcal{D}} \ . \tag{9}$$

1.6 The Quintessence of Inhomogeneities and Anisotropies

It is easily verified that $Q_{\mathcal{D}} = 0$ is a necessary and sufficient condition for having $a_{\mathcal{D}} = a(t)$, with the global scale-factor $a(t)$ solving the standard Friedmann equations. Assuming for the moment that the averaged Universe would be described by the standard model, then the universal expansion rate would be determined by four components: the average mass density (commonly conceived to have baryonic and non-baryonic "dark" components), the value of the cosmological constant, and the global "curvature parameter" k, which arises as an integration constant by integrating the second-order Friedmann equation (Eq. (8) for $Q_{\mathcal{D}} = 0$) in order to get the global expansion rate $3H(t) = 3\frac{\dot{a}}{a}$.

Upon integrating the actual expansion law, Eq. (8), we instead obtain ([13] used a different sign convention for $Q_{\mathcal{D}}$):

$$3\frac{\dot{a}_{\mathcal{D}}^2}{a_{\mathcal{D}}^2} + 3\frac{k_{\mathcal{D}}}{a_{\mathcal{D}}^2} - 8\pi G\,\langle\varrho\rangle_{\mathcal{D}} - \Lambda = \frac{1}{a_{\mathcal{D}}^2}\int_{t_i}^{t} \mathrm{d}t'\; Q_{\mathcal{D}}\frac{\mathrm{d}}{\mathrm{d}t'}a_{\mathcal{D}}^2(t') \;. \tag{10}$$

where $k_{\mathcal{D}}$ enters as a domain-dependent integration constant. The effective Hubble-parameter $H_{\mathcal{D}} = \frac{\dot{a}_{\mathcal{D}}}{a_{\mathcal{D}}}$ is now determined by the previous (now domain-dependent) components, but also by a fifth component due to the presence of inhomogeneities.

Since there are many unresolved conundrums of the standard model (see, e.g., [27], [46]), cosmologists are searching for a fifth parameter that may resolve them (see the talk by Prof. Fujii on "Quintessence" in the present Proceedings). The use of the letter Q for the "backreaction" is coincidential, but it may possibly be a working coincidence.

1.7 Cosmic Triangle or Cosmic Quartett ?

The vocabulary of the standard model may be condensed into the picture of a "cosmic triangle" [2], consisting of three cosmological parameters, which are constructed by normalizing the mass density, the cosmological constant, and the "curvature parameter" by the square of the Hubble-parameter.

As suggested by Eq. (10) we are led to define an additional dimensionless "kinematical backreaction parameter" through

$$\Omega_Q^{\mathcal{D}} := \frac{1}{3\,a_{\mathcal{D}}^2 H_{\mathcal{D}}^2}\int_{t_i}^{t} \mathrm{d}t'\; Q_{\mathcal{D}}\frac{\mathrm{d}}{\mathrm{d}t'}a_{\mathcal{D}}^2(t') \;. \tag{11}$$

in addition to the common cosmological parameters:

$$\Omega_m^{\mathcal{D}} := \frac{8\pi G\,\langle\varrho\rangle_{\mathcal{D}}}{3H_{\mathcal{D}}^2} \;,\quad \Omega_\Lambda^{\mathcal{D}} := \frac{\Lambda}{3H_{\mathcal{D}}^2} \;,\quad \Omega_k^{\mathcal{D}} := -\frac{k_D}{a_{\mathcal{D}}^2 H_{\mathcal{D}}^2} \;. \tag{12}$$

However, contrary to the standard model, all $\Omega^{\mathcal{D}}$ parameters are now domain-dependent and transformed into fluctuating fields on the domain: for $Q_{\mathcal{D}} = 0$ the "cosmic triangle" is undistorted and the parameters acquire their global standard values.

Comparing these definitions with Eq. (10) we have

$$\Omega_m^{\mathcal{D}} + \Omega_\Lambda^{\mathcal{D}} + \Omega_k^{\mathcal{D}} + \Omega_Q^{\mathcal{D}} = 1 \;. \tag{13}$$

i.e., there are four players in the game (or five, respectively, if we split $\Omega_m^{\mathcal{D}}$ into baryonic matter and non-baryonic "dark matter").

In Friedmann-Lemaître cosmologies there is by definition no backreaction: $\Omega_Q^{\mathcal{D}} = 0$. In this case a universe model with $\Omega_m = 1$ conserves the matter parameter. Also, the initial value of the "curvature parameter" $\Omega_k = 0$ remains so during the entire evolution. This changes, if "backreaction" is taken into account. $\Omega_Q^{\mathcal{D}}$ itself may act as a "kinematical dark matter", or as a "kinematical cosmological term", respectively, depending on the relative strength of shear-, epansion- and vorticity-fluctuations.

As we have learned [19] and as we shall illustrate below, the parameters corresponding to the "cosmic triangle" can experience large changes, even in situations when the "backreaction parameter" is seemingly negligible, but non-zero.

1.8 Construction Principle for Evolution Models

In order to obtain quantitative results on the value and impact of the "backreaction parameter", we have to employ evolution models for the inhomogeneities. Their implementation seems not to be straightforward, since cosmological evolution models (analytical or N-body simulations) are constructed in such a way that they evolve an initial power spectrum of density- and velocity-fluctuations on a given global background (a solution of the standard Friedmann equations), implying a vanishing "backreaction" by construction. However, the framework of Newtonian cosmology offers the possibility of making use of contemporary evolution schemes by assigning sense to a global background within the general expansion law of an averaged inhomogeneous model. We shall now elaborate on this fact by demonstrating the validity of the following *Construction Principle*:

The average expansion of a generic inhomogeneous matter distribution on (topologically) closed Newtonian space sections is given by the solution of the standard Friedmann equations.

This principle, although usually not explicitly stated, lies at the basis of any evolution model in Newtonian cosmology. It appears to be very restrictive in light of the general relativistic framework (see Subsection 2.5).

In order to proof this principle let us work with the invariants of the gradient of the velocity field[2]. They are expressible in terms of kinematical scalars and can be written as total divergences of vector fields, which has been used and discussed in the context of perturbation solutions ([11], [25]):

$$\mathrm{I}(v_{i,j}) = \nabla\cdot\mathbf{v} = \theta \quad , \quad \mathrm{II}(v_{i,j}) = \frac{1}{2}\nabla\cdot\Big(\mathbf{v}(\nabla\cdot\mathbf{v}) - (\mathbf{v}\cdot\nabla)\mathbf{v}\Big) = \omega^2 - \sigma^2 + \frac{1}{3}\theta^2 \quad . \tag{14}$$

The "backreaction term" can be entirely expressed in terms of the first and second invariants:

$$Q_{\mathcal{D}} = 2\left\langle \mathrm{II}(v_{i,j})\right\rangle_{\mathcal{D}} - \frac{2}{3}\left\langle \mathrm{I}(v_{i,j})\right\rangle^2_{\mathcal{D}} \quad . \tag{15}$$

Now, let us formally assume that there exists a global, homogeneous and isotropic reference model with scale-factor $a(t)$. We introduce the following variables with respect to this reference background. With the global Hubble-parameter $H = \dot{a}/a$ we define comoving Eulerian coordinates $\mathbf{q} := \mathbf{x}/a$ and peculiar-velocities $\mathbf{u} := \mathbf{v} - H\mathbf{x}$ as usual. Using the derivative $\partial_{q_j} u_i \equiv \partial u_i/\partial q_j$ with respect to comoving coordinates we obtain for the first and second invariants:

$$\mathrm{I}(v_{i,j}) = 3H + \frac{1}{a}\mathrm{I}\left(\partial_{q_j} u_i\right) \quad , \quad \mathrm{II}(v_{i,j}) = 3H^2 + \frac{2H}{a}\mathrm{I}\left(\partial_{q_j} u_i\right) + \frac{1}{a^2}\mathrm{II}\left(\partial_{q_j} u_i\right) \quad . \tag{16}$$

The "backreaction term" remains form-invariant (note: $\frac{1}{a}\partial_{q_j} u_i = u_{i,j}$):

$$Q_{\mathcal{D}} = \frac{1}{a^2}\left(2\left\langle \mathrm{II}\left(\partial_{q_j} u_i\right)\right\rangle_{\mathcal{D}} - \frac{2}{3}\left\langle \mathrm{I}\left(\partial_{q_j} u_i\right)\right\rangle^2_{\mathcal{D}}\right) \quad . \tag{17}$$

Thus, all terms correponding to the background flow cancel in this expression, and only inhomogeneities contribute to "backreaction".

Using Eq. (14) we write the "backreaction term" as a volume-average over divergences. Hence, using the theorem of Gauss we obtain:

$$Q_{\mathcal{D}} = \frac{1}{a^2}\left[2\,\frac{1}{V_q}\int_{\partial\mathcal{D}_q} \mathrm{d}\mathbf{S}\cdot\left(\mathbf{u}(\nabla_q\cdot\mathbf{u}) - (\mathbf{u}\cdot\nabla_q)\mathbf{u}\right) - \frac{2}{3}\left(\frac{1}{V_q}\int_{\partial\mathcal{D}_q}\mathrm{d}\mathbf{S}\cdot\mathbf{u}\right)^2\right], \tag{18}$$

with the surface $\partial\mathcal{D}_q$ bounding the comoving domain $\mathcal{D}_q$, the surface element $\mathrm{d}\mathbf{S}$, and the comoving differential operator ∇_q.

From Eq. (18) we directly obtain $Q_{\mathcal{D}} = 0$ for a domain with empty boundary, e.g., for toroidal space sections, or periodic peculiar-velocity fields, respectively. In turn, the assumed reference solution is a standard Hubble-flow and may serve as a global background. (For more details see [18].)

This establishes the *Construction Principle* q.e.d.

[2] A comma denotes partial derivative with respect to Eulerian coordinates $\partial/\partial x_i \equiv ,_i$.

1.9 Generalization of the Top-Hat Model

The *Construction Principle* provides room for employing the language of standard theories of structure formation. As an example we apply the general expansion law to domains within a global Hubble-flow.

Assuming an Einstein-de-Sitter background for this example we subtract a standard Friedmann equation, $3\frac{\ddot{a}}{a} + 4\pi G\varrho_H = 0$, from Eq. (8), with the background density $\varrho_H = \frac{3H^2}{8\pi G}$, and obtain the following differential equation for $a_{\mathcal{D}}(t)$ [19]:

$$3\left(\frac{\ddot{a}_{\mathcal{D}}}{a_{\mathcal{D}}} - \frac{\ddot{a}}{a}\right) + \frac{3}{2}\left(\frac{\dot{a}}{a}\right)^2 \langle\delta\rangle_{\mathcal{D}} = Q_{\mathcal{D}} \ . \tag{19}$$

with $\langle\delta\rangle_{\mathcal{D}} = (\langle\varrho\rangle_{\mathcal{D}} - \varrho_H)/\varrho_H$ specifying the averaged density contrast δ in $\mathcal{D}$. For $Q_{\mathcal{D}} = 0$ and $\langle\delta\rangle_{\mathcal{D}} = 0$ this equation simply states that the time evolution of a domain follows the global expansion, $a_{\mathcal{D}}(t) = a(t)$. For $Q_{\mathcal{D}} = 0$ and $1 + \langle\delta\rangle_{\mathcal{D}} = \frac{\langle\varrho\rangle_{\mathcal{D}} a^3}{\varrho_H a_{\mathcal{D}}^3}$ the evolution of $a_{\mathcal{D}}$ is still of Friedmann type, but with a mass different from the background mass. An important subcase with $Q_{\mathcal{D}} = 0$ and $\langle\delta\rangle_{\mathcal{D}} \neq 0$ is the well-known spherical top-hat model [36]. In Eq. (19) there are two sources determining the deviations from the Friedmann acceleration, the over/under-density *and* the "backreaction term". This shows that, in general, the evolution of a Newtonian portion of the Universe is triggered by an over/under-density *and* velocity-fluctuations.

1.10 An Averaged Lagrangian Perturbation Scheme

As a second example we apply the *Construction Principle* to the widely used and well-tested Lagrangian perturbation schemes (see: [38], [25] for reviews, and [12] for a tutorial).

The trajectory field in the mostly employed "Zel'dovich approximation" [49], [50] (which can be derived as a subcase of the first-order Lagrangian perturbation scheme [10]), is given by:

$$\mathbf{f}^Z(\mathbf{X}, t) = a(t)\Big(\mathbf{X} + \xi(t)\nabla_0 \psi(\mathbf{X})\Big) . \tag{20}$$

$\psi(\mathbf{X})$ is the initial displacement field, ∇_0 the gradient with respect to Lagrangian coordinates and $\xi(t)$ a global time-dependent function (given for all background models in [5]).

Given this trajectory field we can already approximate the rate of volume change by the volume deformation that is caused by the field. For the effective scale-factor we obtain [19]:

$$(a_{\mathcal{D}}^{\text{kin}})^3 = a^3\left(1 + \xi\langle \mathrm{I_i}\rangle_{\mathcal{D}_i} + \xi^2\langle \mathrm{II_i}\rangle_{\mathcal{D}_i} + \xi^3\langle \mathrm{III_i}\rangle_{\mathcal{D}_i}\right) . \tag{21}$$

A better estimate is to calculate the "backreaction term" from the approximation of the velocity field $\mathbf{v}^Z = \dot{\mathbf{f}}^Z$ and solve the dynamical expansion law, Eq. (8), for $a_{\mathcal{D}}$. The "backreaction term" separates into its time-evolution given by $\xi(t)$ and the spatial dependence on the initial displacement field given by averages over the invariants of the displacement gradient $\mathbf{I_i}, \mathbf{II_i}$, and $\mathbf{III_i}$:

$$Q_{\mathcal{D}}^Z = \frac{\dot{\xi}^2}{\left(1 + \xi\langle \mathrm{I_i}\rangle_{\mathcal{D}_i} + \xi^2\langle \mathrm{II_i}\rangle_{\mathcal{D}_i} + \xi^3\langle \mathrm{III_i}\rangle_{\mathcal{D}_i}\right)^2} \times \tag{22}$$

$$\left[\left(2\langle \mathrm{II_i}\rangle_{\mathcal{D}_i} - \frac{2}{3}\langle \mathrm{I_i}\rangle_{\mathcal{D}_i}^2\right) + \xi\left(6\langle \mathrm{III_i}\rangle_{\mathcal{D}_i} - \frac{2}{3}\langle \mathrm{I_i}\rangle_{\mathcal{D}_i}\langle \mathrm{II_i}\rangle_{\mathcal{D}_i}\right) + \xi^2\left(2\langle \mathrm{I_i}\rangle_{\mathcal{D}_i}\langle \mathrm{III_i}\rangle_{\mathcal{D}_i} - \frac{2}{3}\langle \mathrm{II_i}\rangle_{\mathcal{D}_i}^2\right)\right] .$$

The numerator of the first term is global and corresponds to the damping factor that also arises in the Eulerian linear theory of gravitational instability; in an Einstein-de-Sitter universe $\dot{\xi}^2 \propto a^{-1}$. The denominator of the first term is the volume effect discussed above, whereas the second term in brackets features the initial "backreaction" as a leading term and higher-order terms.

A property of this approximation that renders it very useful as an averaged evolution model should be emphasized: it is exact for two orthogonal symmetry assumptions: for the evolution of plane-symmetric inhomogeneities, which is a consequence of the known properties of the first-order Lagrangian approximation [9], and for the evolution of spherically symmetric inhomogeneities, as will be shown below.

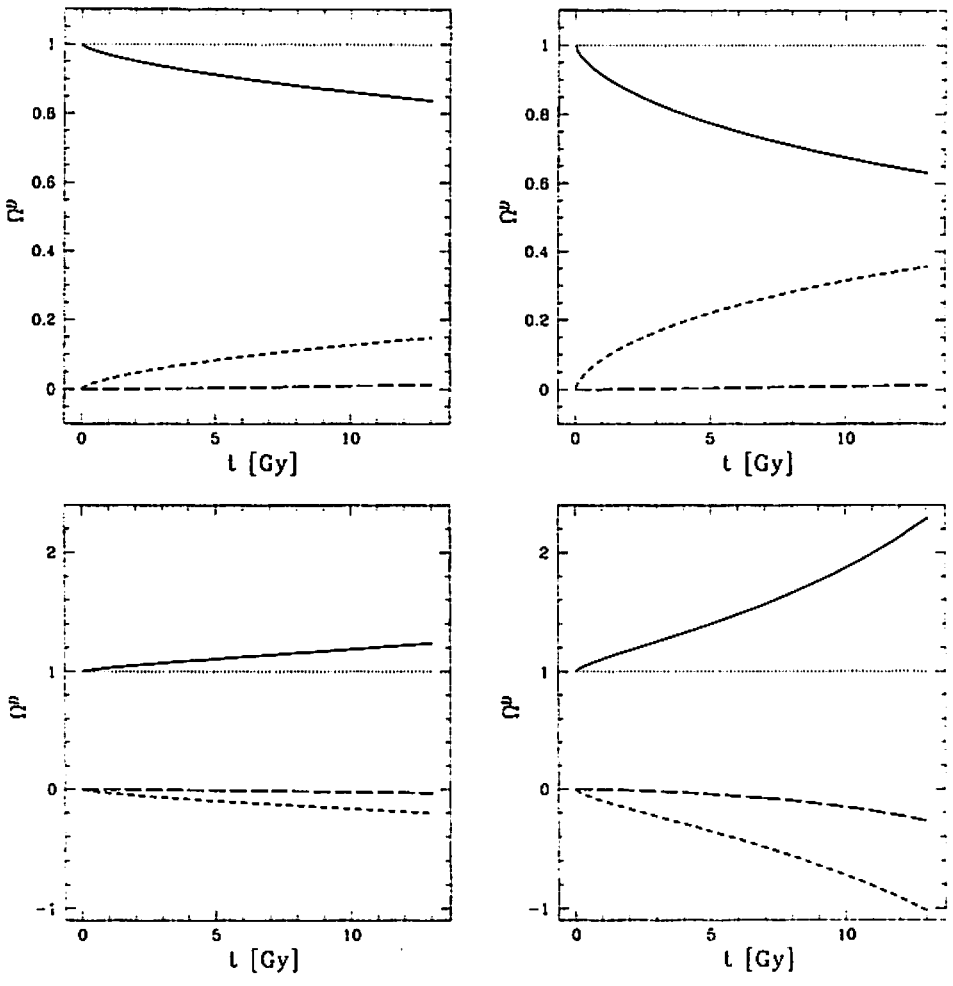

Figure 2: The evolution of the "cosmological parameters" $\Omega_m^{\mathcal{D}}$ (solid line), $\Omega_k^{\mathcal{D}}$ (short dashed), and $\Omega_Q^{\mathcal{D}}$ (long dashed) in an expanding (under-dense) domain with initial radius 0.5Mpc (a scaled radius of 100Mpc today). The dotted line is marking $\Omega_m^{\mathcal{D}} + \Omega_k^{\mathcal{D}} + \Omega_Q^{\mathcal{D}}$. The upper left plot is for one-σ, the upper right plot is for three-σ fluctuations (assigned to the expected amplitudes of the initial invariants in a Gaussian random field of standard Cold-Dark-Matter fluctuations). The lower plots show the result for a collapsing domain. We see here that the "backreaction parameter" is quantitatively more important than in an expanding domain – an interpretation of this result will be offered below: a collapsing domain experiences more drastic changes in shape.

Employing the averaged Lagrangian scheme we can quantify the impact of backreaction on the domain-dependent "cosmological parameters". For details the reader may look at a recent work [19]. Here, I would like to mention the remarkable result that for an accelerating, i.e., under-dense region, $\Omega_Q^{\mathcal{D}}$ may be numerically negligible as seen in (Fig. 2, upper plots), but dramatic changes in the other parameters are observed. For a collapsing domain with a present-day radius of 100Mpc the mass parameter of the domain may even differ by more than 100% from the global mass parameter (Fig. 2, lower plots).

1.11 Newton's Iron Spheres

Looking at the general expansion law, Eq. (8), the careful reader may object that Friedmann's equations also hold, if we study the motion of a spherically symmetric domain, although the matter distribution inside the sphere may be inhomogeneous. This fact is known as Newton's "Iron Sphere Theorem". Let us show that the general expansion law respects this theorem.

We note that, for a spherically symmetric distribution of matter within the domain, the invariants of the velocity gradient, averaged over a ball $\mathcal{B}_R$, obey relations resulting in [19]:

$$\langle \mathrm{II}(v_{i,j})\rangle_{\mathcal{B}_R} = \frac{1}{3}\langle \mathrm{I}(v_{i,j})\rangle^2_{\mathcal{B}_R}, \quad \text{and} \quad \langle \mathrm{III}(v_{i,j})\rangle_{\mathcal{B}_R} = \frac{1}{27}\langle \mathrm{I}(v_{i,j})\rangle^3_{\mathcal{B}_R}. \tag{23}$$

Inserting this into the "backreaction term", Eq. (15), shows that $Q^{\text{spherical}}_{\mathcal{B}_R} = 0$ in accordance with Newton's theorem. The inhomogeneous model discussed in the last subsection also has this property: inserting the above expressions into Eq. (22) (using the proportionality of displacement gradient and initial velocity gradient), we also obtain $Q^{\mathcal{Z}}_{\mathcal{B}_R} = 0 = Q^{\text{spherical}}_{\mathcal{B}_R}$.

1.12 Averaging and the Evolution of Form

The expansion law, Eq. (8), is built on the rate of change of a simple morphological quantity, the volume content of a domain. Although functionally it depends on other morphological characteristics of a domain, it does not explicitly provide information on their evolution. An evolution equation for the "backreaction term" is missing. This fact touches on the problem of closing the hierarchy of dynamical evolution equations considered as a set of coupled ordinary differential equations in Lagrangian space. The problem of closing such a hierarchy of equations is often considered in the literature and various closure conditions are formulated (e.g., [30]), one of them being the "Silent Universe Model" in general relativity, which assumes a vanishing magnetic part of the Weyl tensor [6]. Averaging such a hierarchy would result in evolution equations for the "backreaction term" and would, with some local closure condition, also close the system of averaged equations. Here, we will not pursue this problem further, but instead begin to develop the morphological point of view that eventually implies an alternative proposition of a morphological closure condition.

Let us focus our attention on the boundary of the spatial domain $\mathcal{D}$. A priori, the location of this boundary in space enjoys some freedom which we may constrain by saying that the boundary coincides with a velocity front of the fluid (hereby restricting attention to irrotational flows). This way we employ the Legendrian point of view of velocity fronts that is dual to the Lagrangian one of fluid trajectories. Let $S(x, y, z, t) = s(t)$ define a velocity front at Newtonian time t, $\mathbf{v} = \nabla S$. Below, we shall need that the three principal scalar invariants of the velocity gradient $v_{i,j} =: S_{,ij}$ can be transformed into divergences of vector fields as written explicitly in Eqs. (14,26).

Defining the unit normal vector $\mathbf{n}$ on the front, $\mathbf{n} = \pm\frac{\nabla S}{|\nabla S|}$ (the sign depends on the direction of its motion), the average expansion rate can be written as a flux integral using Gauss' theorem:

$$\langle\theta\rangle_{\mathcal{D}} = \frac{1}{V}\int_{\mathcal{D}} d^3x\, \nabla\cdot\mathbf{v} = \frac{1}{V}\int_{\partial\mathcal{D}} \mathbf{dS}\cdot\mathbf{v}\ . \tag{24}$$

and, with the surface element $d\sigma$, $\mathbf{dS} = \mathbf{n}d\sigma$, we obtain the intuitive result that the average expansion rate is related to another morphological quantity of the domain, the total area of the enclosing surface:

$$\langle\theta\rangle_{\mathcal{D}} = \frac{1}{V}\int_{\partial\mathcal{D}} d\sigma|\nabla S|\ . \tag{25}$$

Inserting the velocity potential also into the other invariants, Eq. (14) and

$$\mathbf{III}(v_{i,j}) = \frac{1}{3}\nabla\cdot\left(\frac{1}{2}\nabla\cdot\Big(\mathbf{v}(\nabla\cdot\mathbf{v}) - (\mathbf{v}\cdot\nabla)\mathbf{v}\Big)\mathbf{v} - \Big(\mathbf{v}(\nabla\cdot\mathbf{v}) - (\mathbf{v}\cdot\nabla)\mathbf{v}\Big)\cdot\nabla\mathbf{v}\right) \quad . \tag{26}$$

and performing the spatial average, we obtain [17]:

$$\langle\mathbf{II}\rangle_{\mathcal{D}} = \frac{1}{V}\int_{\mathcal{D}} d^3x\,\mathbf{II} = \int_{\partial\mathcal{D}} d\sigma|\nabla S|^2\,\mathbf{H}\;;\quad \langle\mathbf{III}\rangle_{\mathcal{D}} = \frac{1}{V}\int_{\mathcal{D}} d^3x\,\mathbf{III} = \int_{\partial\mathcal{D}} d\sigma|\nabla S|^3\,\mathbf{K}\quad . \tag{27}$$

where $\mathbf{H}$ is the mean curvature and $\mathbf{K}$ the Gaussian curvature of the 2–surface bounding the domain. $|\nabla S| = \frac{ds}{dt}$ equals 1, if the instrinsic arc-length s of the trajectories is used instead of the extrinsic Newtonian time t. The averaged invariants comprise, together with the volume a complete set of morphological characteristics related to the *Minkowski functionals of a body*.

$$W_0(s) := \int_{\mathcal{D}} d^3x = V\;;\; W_1(s) := \frac{1}{3}\int_{\partial\mathcal{D}} d\sigma\;;\; W_2(s) := \frac{1}{3}\int_{\partial\mathcal{D}} d\sigma\,\mathbf{H}\;;\; W_3(s) := \frac{1}{3}\int_{\partial\mathcal{D}} d\sigma\,\mathbf{K} = \frac{4\pi}{3}\chi\quad . \tag{28}$$

The Euler-characteristic χ determines the topology of the domain and is assumed to be an integral of motion ($\chi = 1$), if the domain should remain simply-connected (a morphological closure condition).

Thus, we have gained a morphological interpretation of the "backreaction term": it can be entirely expressed through three of the four Minkowski functionals:

$$Q_{\mathcal{D}}(s) = 6\left(\frac{W_2}{W_0} - \frac{W_1^2}{W_0^2}\right)\quad . \tag{29}$$

The $W_\alpha\;;\;\alpha = 0,1,2,3$ have been introduced as "Minkowski functionals" into cosmology by Mecke *et al.* ([35]) in order to statistically assess morphological properties of cosmic structure. Minkowski functionals proved to be useful tools to also incorporate information from higher-order correlations, e.g., in the distribution of galaxies, galaxy clusters, density fields or cosmic microwave background temperature maps ([34], [33], [40], [41]; see the review by Kerscher [32] and ref. therein). Related to the morphology of individual domains is the study of building blocks of large-scale cosmic structure [39], [42].

For a ball with radius R we have for the Minkowski functionals:

$$W_0^{\mathcal{B}_R}(s) := \frac{4\pi}{3}R^3\;;\; W_1^{\mathcal{B}_R}(s) := \frac{4\pi}{3}R^2\;;\; W_2^{\mathcal{B}_R}(s) := \frac{4\pi}{3}R\;;\; W_3^{\mathcal{B}_R}(s) := \frac{4\pi}{3}\quad . \tag{30}$$

Inserting these expressions into the "backreaction term", Eq. (29), shows that $Q_{\mathcal{D}}^{\mathcal{B}_R}(s) = 0$, and we have confirmed Newton's "Iron Sphere Theorem" once more. Moreover, we can understand now that the "backreaction term" encodes the deviations of the domain's morphology from that of a ball, a fact which we shall illustrate now with the help of Steiner's formula of integral geometry (see also [35]).

Let $d\sigma_0$ be the surface element on the unit sphere, then (according to the Gaussian map) $d\sigma = R_1R_2d\sigma_0$ is the surface element of a 2–surface with radii of curvature R_1 and R_2. Moving the surface a distance ε along its normal we get for the surface element of the parallel velocity front:

$$d\sigma_\varepsilon = (R_1+\varepsilon)(R_2+\varepsilon)d\sigma_0 = \frac{R_1R_2 + \varepsilon(R_1+R_2) + \varepsilon^2}{R_1R_2}d\sigma = (1 + \varepsilon 2\mathbf{H} + \varepsilon^2\mathbf{K})d\sigma\quad , \tag{31}$$

where

$$\mathbf{H} = \frac{1}{2}\left(\frac{1}{R_1} + \frac{1}{R_2}\right)\quad ,\quad \mathbf{K} = \frac{1}{R_1R_2}\quad . \tag{32}$$

are the mean curvature and Gaussian curvature of the front as before.

Integrating Eq. (31) over the whole front we arrive at a relation between the total surface area A of the front and A_ε of its parallel front. The gain in volume may then be expressed by an integral of the resulting relation with respect to ε (which is known as *Steiner's formula* defining the Minkowski functionals of a (convex) body in three spatial dimensions):

$$V_\varepsilon = V + \int_0^\varepsilon d\varepsilon' A_{\varepsilon'} = V + \varepsilon A + \varepsilon^2\int_{\partial\mathcal{D}} d\sigma\,\mathbf{H} + \varepsilon^3\int_{\partial\mathcal{D}} d\sigma\,\mathbf{K}\quad . \tag{33}$$

2 Average Models in General Relativity

2.1 An Averager for Scalars

The key to reducing ambiguity of choosing an averager in general relativity is to confine ourselves to scalars, since spatially averaging a scalar field Ψ is a covariant operation. However, we have to make sure that we understand the word "spatial" physically. Geometrically, we shall introduce a foliation of spacetime, but we shall encounter ambiguity in choosing it. Suppose for the moment that we insist on *spatial* averaging and consider for all what follows a foliation of spacetime as given. The simplest averager is then immediately written down as follows:

$$\langle \Psi(X^i,t)\rangle_{\mathcal{D}} := \frac{1}{V}\int_{\mathcal{D}} J d^3X \;\; \Psi(X^i,t) \;\; : \;\; V = \int_{\mathcal{D}} J d^3X \;\; . \tag{34}$$

with $J := \sqrt{\det(g_{ij})}$, where g_{ij} is the metric of the spatial hypersurfaces, and X^i are coordinates in the hypersurfaces, conveniently chosen such that they are constant along flow lines.

2.2 Foliating Spacetime: Covariant Fluid Approach

We wish to conserve mass inside a spatial domain of spacetime. Therefore, let us first consider the (conserved) restmass flux vector[3]

$$M^\mu := \varrho u^\mu \;\; : \;\; M^\mu{}_{,\mu} = 0 \;\; : \;\; \varrho > 0 \;\; . \tag{35}$$

where ϱ is the restmass density and the flow lines are integral curves of the 4-velocity u^μ. We shall confine ourselves to irrotational perfect fluids with energy density ε and pressure p, which allows us to simplify the splitting of spacetime, e.g. the spatial hypersurfaces can be chosen flow-orthogonal in this case, the unit normal on the hypersurfaces coincides with the 4-velocity and the shift vector vanishes. Irrotationality guarantees the existence of a scalar function S, such that

$$u^\mu =: \frac{-\partial^\mu S}{h} \;\; , \tag{36}$$

In general, we identify the magnitude h with the "injection energy per fluid element and unit restmass",

$$h := \frac{\varepsilon + p}{\varrho} \;\; . \tag{37}$$

which is related to the relativistic enthalpy $\eta := \frac{\varepsilon+p}{n}$ by $h = \eta/m$ with m the unit restmass of a fluid element, and n the baryon density. Note that $d\varepsilon = h d\varrho$. For a barotropic fluid we can easily see that ε is a function of the restmass density only and, hence, h is a function of ϱ. h is identical to 1 in the case of dust. The magnitude h normalizes the 4-gradient $\partial^\mu S$ so that $u^\mu u_\mu = -1$.

$$h = \sqrt{-\partial^\alpha S \partial_\alpha S} = u^\mu \partial_\mu S = \dot{S} \; > \; 0 \;\; . \tag{38}$$

The overdot stands for the material derivative operator along the flow lines of any tensor field $\mathcal{F}$ as defined covariantly by $\dot{\mathcal{F}} := u^\mu \mathcal{F}_{,\mu}$. It reduces in the case of a scalar function in a flow-orthogonal slicing (which we want to envisage) to the partial time-derivative multiplied by $\frac{1}{N}$, where N is the lapse function (for more details see: [16]).

It can be shown that S is spatially homogeneous. Thus, $S(t)$ and $h(X^i,t)$ play the role of "phase" and "amplitude" of the fluid's wave fronts. Foliating the spacetime into hypersurfaces $S(t) = const.$ is a gauge condition that is naturally adapted to the fluid itself and, therefore, this foliation can be given a covariant meaning ([7], [8] and ref. therein).

[3] Greek indices run through 0...3, while latin indices run through 1...3 as before; summation over repeated indices is understood. A semicolon will denote covariant derivative with respect to the 4-metric with signature $(-,+,+,+)$; the units are such that $c = 1$.

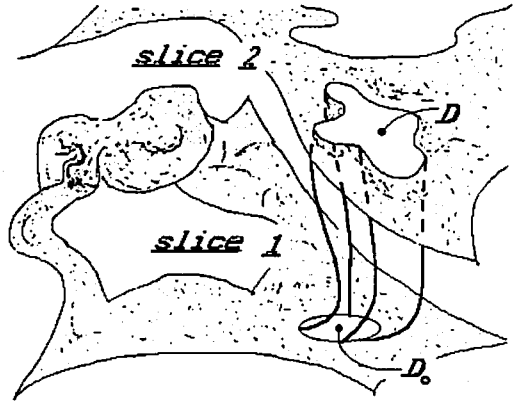

Figure 3: The evolution of an initial domain $\mathcal{D}_o$ within a simply-connected tube of spacetime. The figure visualizes the restrictions implied by the topological requirement of simple connectivity throughout the evolution of the domain. Note that the boundary of the domain may break in the coarse of structure formation (occurence of a Legendrian singularity), which may induce topology changes.

2.3 A Commutation Rule in General Relativity

The rate of change of the volume $V(t)$ in the hypersurfaces $S(t) = const.$ is evaluated by taking the partial time-derivative of the volume and dividing by the volume. Since ∂_t and d^3X commute (but not $\frac{d}{d\tau} := \frac{\partial_t}{N}$ and d^3X !) we obtain:

$$\frac{\partial_t V}{V} = \frac{1}{V}\int_{\mathcal{D}} d^3X \partial_t J = \frac{1}{V}\int_{\mathcal{D}} d^3X N\dot{J} = \frac{1}{V}\int_{\mathcal{D}} d^3X N\theta J = \langle N\theta\rangle_{\mathcal{D}} \ . \tag{39}$$

Introducing the scaled (t-)expansion $\tilde{\theta} := N\theta$ we define an effective (t-)Hubble function in the hypersurfaces by

$$\langle\tilde{\theta}\rangle_{\mathcal{D}} = \frac{\partial_t V}{V} = 3\frac{\partial_t a_{\mathcal{D}}}{a_{\mathcal{D}}} =: 3\tilde{H}_{\mathcal{D}} \ . \tag{40}$$

With the help of these definitions we readily derive the *Commutation Rule*:

$$\partial_t \langle\Psi\rangle_{\mathcal{D}} - \langle\partial_t\Psi\rangle_{\mathcal{D}} = \langle\Psi\tilde{\theta}\rangle_{\mathcal{D}} - \langle\Psi\rangle_{\mathcal{D}}\langle\tilde{\theta}\rangle_{\mathcal{D}} \ . \tag{41}$$

The lapse-weighted quantities have to be introduced only in the case of non-vanishing pressure, since the pressure gradient induces deviations from a geodesic flow implying an inhomogeneous lapse function. In the much simpler case of a dust matter model, the lapse function is homogeneous and can be chosen equal to 1, and the covariant fluid gauge is identical to the comoving and synchronous gauge, which makes the correspondence to the Newtonian investigation most transparent.

In the sequel we shall, for simplicity, discuss the case of a pressure-less fluid only and resume the discussion of the more general case thereafter.

2.4 Expansion Law of General Relativity: Dust Models

Employing the averaging procedure outlined above and following the line of thought of the Newtonian investigation in Section 1, we derive the general expansion law for dust matter in the synchronous and comoving gauge. The result will be covariant with respect to this foliation.

I here give the result derived in [15]: the spatially averaged equations for the scale-factor $a_{\mathcal{D}}$, respecting mass conservation, read:

averaged Raychaudhuri equation:

$$3\frac{\ddot{a}_{\mathcal{D}}}{a_{\mathcal{D}}}+4\pi G\frac{M_{\mathcal{D}}}{V_{\mathcal{I}}a_{\mathcal{D}}^3}-\Lambda=Q_{\mathcal{D}}\ ; \tag{42}$$

averaged Hamiltonian constraint:

$$\left(\frac{\dot{a}_{\mathcal{D}}}{a_{\mathcal{D}}}\right)^2-\frac{8\pi G}{3}\frac{M_{\mathcal{D}}}{V_{\mathcal{I}}a_{\mathcal{D}}^3}+\frac{\langle\mathcal{R}\rangle_{\mathcal{D}}}{6}-\frac{\Lambda}{3}=-\frac{Q_{\mathcal{D}}}{6}\ , \tag{43}$$

where the mass $M_{\mathcal{D}}$, the averaged spatial Ricci scalar $\langle\mathcal{R}\rangle_{\mathcal{D}}$ and the "backreaction term" $Q_{\mathcal{D}}$ are domain-dependent and, except the mass, time-dependent functions. The backreaction source term is given by

$$Q_{\mathcal{D}}:=2\langle\mathrm{II}\rangle_{\mathcal{D}}-\frac{2}{3}\langle\mathrm{I}\rangle_{\mathcal{D}}^2=\frac{2}{3}\left\langle(\theta-\langle\theta\rangle_{\mathcal{D}})^2\right\rangle_{\mathcal{D}}-2\langle\sigma^2\rangle_{\mathcal{D}}\ . \tag{44}$$

Here, I and II denote the invariants of the extrinsic curvature tensor that correspond to the kinematical invariants we employed earlier. The same expression (except for the vorticity) as in Eq. (9) follows by introducing the split of the extrinsic curvature into the kinematical variables shear and expansion (second equality above).

We appreciate an intimate correspondence of the GR equations with their Newtonian counterparts (Eq. (8) and Eq. (10)). The first equation is formally identical to the Newtonian one, while the second delivers an additional relation between the averaged curvature and the "backreaction term" that has no Newtonian analogue. This implies an important difference that becomes manifest by looking at the time-derivative of Eq. (43). The integrability condition that this time-derivative agrees with Eq. (42) is non-trivial in the GR context and reads:

$$\partial_t Q_{\mathcal{D}}+6\frac{\dot{a}_{\mathcal{D}}}{a_{\mathcal{D}}}Q_{\mathcal{D}}+\partial_t\langle\mathcal{R}\rangle_{\mathcal{D}}+2\frac{\dot{a}_{\mathcal{D}}}{a_{\mathcal{D}}}\langle\mathcal{R}\rangle_{\mathcal{D}}=0\ . \tag{45}$$

The correspondence between the Newtonian $k_{\mathcal{D}}$-parameter and the averaged spatial Ricci curvature is more involved in the presence of a "backreaction term":

$$\frac{k_{\mathcal{D}}}{a_{\mathcal{D}}^2}-\frac{1}{3}a_{\mathcal{D}}^2\int_{t_i}^{t}dt'\,Q_{\mathcal{D}}\,\frac{d}{dt'}a_{\mathcal{D}}^2(t')=\frac{1}{6}\left(\langle\mathcal{R}\rangle_{\mathcal{D}}+Q_{\mathcal{D}}\right). \tag{46}$$

The time-derivative of Eq. (46) is equivalent to the integrability condition Eq. (45). Eq. (45) shows that averaged curvature and "backreaction term" are directly coupled unlike in the Newtonian case, where the domain-dependent $k_{\mathcal{D}}$-parameter is fixed by the initial conditions.

For dust models in general relativity we may therefore introduce dimensionless average characteristics that are slightly different from those in Newtonian cosmology, the difference being that the "backreaction parameter" is now directly expressible in terms of the "backreaction source term", and not just as an integral expression:

$$\Omega_m^{\mathcal{D}}:=\frac{8\pi G M_{\mathcal{D}}}{3V_{\mathcal{D}_i}a_{\mathcal{D}}^3H_{\mathcal{D}}^2}\ ;\ \Omega_\Lambda^{\mathcal{D}}:=\frac{\Lambda}{3H_{\mathcal{D}}^2}\ ;\ \Omega_k^{\mathcal{D}}:=-\frac{\langle\mathcal{R}\rangle_{\mathcal{D}}}{6H_{\mathcal{D}}^2}\ ;\ \Omega_Q^{\mathcal{D}}:=-\frac{Q_{\mathcal{D}}}{6H_{\mathcal{D}}^2}\ . \tag{47}$$

which also obey Eq. (13).

The evolution of these parameters is intimately related, unlike the situation in the standard model, as may be illustrated by the following equation [15]:

$$\dot{\Omega}_Q^{\mathcal{D}}+6H_{\mathcal{D}}\Omega_Q^{\mathcal{D}}(1-\Omega_k^{\mathcal{D}}-\Omega_Q^{\mathcal{D}})+\dot{\Omega}_k^{\mathcal{D}}+2H_{\mathcal{D}}\Omega_k^{\mathcal{D}}(1-\Omega_k^{\mathcal{D}}-\Omega_Q^{\mathcal{D}})-3H_{\mathcal{D}}(1-\Omega_\Lambda^{\mathcal{D}}-\Omega_k^{\mathcal{D}}-\Omega_Q^{\mathcal{D}})(\Omega_k^{\mathcal{D}}+\Omega_Q^{\mathcal{D}})=0\ . \tag{48}$$

It is, e.g., a good excercise to show with the help of this equation that an inhomogeneous model (including "backreaction"), in which the matter parameter stays 1 like in the standard Einstein-de Sitter cosmos, does not exist.

2.5 Liberation from Strict Meter

Let us now hold in for a moment and sort out what the Newtonian and the relativistic expansion laws for dust matter distinguish. Their close correspondence bears the temptation of overlooking a crucial conceptual challenge for the modeling of inhomogeneities in general relativity.

Given the Newtonian average model, Eq. (8), and its quantitative consequences (elaborated in detail in [19]), we can draw the conclusion that we only have to consider spatial scales that are large enough to have a negligible influence from the "backreaction term". This term, which brought the higher voltage of having mastered a generic inhomogeneous Newtonian cosmology, shows no global relevance, and it seems that we are drawn back to the previous state of low visibility of the standard cosmological models.

The key-reason for this outcome is the validity of the *Construction Principle*. We force a globally vanishing "backreaction" by the way we construct inhomogeneous evolution models. (Remember that the majority of cosmological N-body simulations and analytical approximations are Newtonian and assume periodic boundary conditions for inhomogeneities on a FLRW background.) The apparent global irrelevance of "backreaction" should not be a surprise, since our evaluations have taken place within a periodic cube into which the universe model was forced: the scale of this cube introduces a "strict meter" governed by the scale-factor of a standard FLRW universe, the action of fluctuations of inhomogeneities is confined to the interior of this cube.

The relativistic average model not only has a somewhat richer tone by linking the averaged spatial Ricci curvature to the "backreaction term" as a result of the Hamiltonian constraint, it also places an equal stress on both of them in the following sense. Suppose we let the self-gravitating fluid evolve freely and link its structure to the curvature of space sections through Einstein's equations. Let now the inhomogeneities evolve out of an almost homogeneous and isotropic state on almost flat space sections. Naturally, the inhomogeneities grow in the coarse of structure formation. The average Ricci curvature of the space sections, however, is dictated by the fluid structure unlike in the standard model which would suggest an evolution inversely proportional to the "strict meter" $a(t)$. In contrast, the value of the averaged curvature is an outcome rather than a model assumption. Thus, a genuine property of the relativistic model, also globally, is a change of the average curvature that does not follow a predesigned global law; a priori it is not constrained on some large scale, because the link to the "backreaction term" makes sure that, at any time, the "interior" of a universe model (below this scale) also determines the global curvature. In other words: there is no analogue of the *Construction Principle*. This comment is not entirely correct, since further study may reveal that it could be possible to formulate an analoguous principle on the basis of topological constraints that may be imposed on the space sections. In any case, research should not lack commitment to the challenge of constructing inhomogeneous evolution models on curved space sections, since this is evidently the generic case. We note that existing work on general relativistic evolution models and their averages relies in most cases on assumptions that are closely designed after the Newtonian case in order to rescue standard procedures like periodic boundary conditions, decomposition of inhomogeneities into plane waves and set-ups of initial conditions on locally flat space sections (compare [37] and comments in [15] and [14]).

2.6 What Einstein Wanted

In the previous subsection we advocated a viewpoint that concentrates on the physics of fluids, which (actively) determines the geometry of spacetime, in particular its average properties. As a showcase we learned in the Newtonian framework that the morphological properties of spatial domains are determined by the averages over fluctuations in the kinematical variables (Subsection 1.12). A similar view may also apply to the relativistic context and, most interestingly, also to the global morphology of space sections.

Turning this around, we may alternatively take the (passive) viewpoint of understanding the global world structure as given in terms of geometrical (and topological) conjectures (which may themselves be subjected to observational falsification; an example is the possibility of falsifying possible topological spaceforms on the basis of microwave background observations ([24]; see also [48] and ref. therein).

Einstein's vision of a globally static universe model stands out as a famous example. His "prejudice" that the Universe as a whole should be static and all evolution (assigning sense to the notion of time) should take place in the "interior" of this world model entails a strong determination of the model's average properties. Only his invention of the cosmological term made this vision possible resulting in the beautiful

structure of a spherical space in which, apart from topological degeneracies, many characteristics (like the radius of the universe model) are practically fixed. Hence, according to what we have learned about average models, the fluid's fluctuations are "slaved" to the global predetermined structure. This global model even guarantees strong evolution, because fluctuations evolve exponentially in a static cosmos.

The problem that his model is unstable (within the class of FLRW models) applies also to the other expanding candidates, if the class is widened to include inhomogeneities. Einstein's example so serves as a guide to think about the average model we have discussed in a geometrical way. The assumption of a static model (the general expansion law allows for a static cosmos even without the cosmological term) should be taken as an example for the possible slaving of fluctuations to global structural assumptions. Of course, other such assumptions are possible. This illustrates how global geometrical and topological constraints on spaceforms could provide "boundary conditions" for the evolution of fluctuations. Since, in Newtonian cosmology, we are always working on a toroidal space without further questioning this assumption, this point of view is not exotic, but plants the seed for possibly fruitful research directions. That these directions are mathematically very involved can be made obvious by pointing out the relation between the average curvature and its compatibility with topological spaceforms (a spaceform with globally negative spatial curvature is not compatible with simply-connected space sections). Due to the process of structure formation the boundary of the domain may break, or it may self-intersect and split into two domains (these events are topologically classified in the framework of Legendrian singularities, [1] and ref. therein). Since the spatial metric is linked to the fluid, a singular dynamics could induce topology changes. Contrary to the existence of such natural metamorphoses, the averager we have defined relies on the assumption that the domain remains simply-connected (Fig. 3).

2.7 Expansion Law of General Relativity: Perfect Fluid Models

As an outlook I briefly give one of the results obtained by averaging a perfect fluid cosmology on hypersurfaces $S(t) = const.$ as explained above.

The averaged equations can be summarized in the following way [16]:

Let us define effective densities as sources of an expansion law,

$$\varepsilon_{\mathrm{eff}} := \langle\tilde{\varepsilon}\rangle_{\mathcal{D}} - \frac{\tilde{\mathcal{Q}}_{\mathcal{D}}}{16\pi G} \quad , \quad p_{\mathrm{eff}} := \langle\tilde{p}\rangle_{\mathcal{D}} - \frac{\tilde{\mathcal{Q}}_{\mathcal{D}}}{16\pi G} - \frac{\tilde{\mathcal{P}}_{\mathcal{D}}}{12\pi G} \quad , \tag{49}$$

with the scaled matter sources $\tilde{\varepsilon} := N^2\varepsilon$ and $\tilde{p} := N^2 p$. Then, the averaged equations can be cast into a form similar to the standard Friedmann equations:

$$3\frac{\partial_t^2 a_{\mathcal{D}}}{a_{\mathcal{D}}} + 4\pi G\left(\varepsilon_{\mathrm{eff}} + 3p_{\mathrm{eff}}\right) = 0 \quad : \tag{50}$$

$$6\tilde{H}_{\mathcal{D}}^2 + \langle\tilde{\mathcal{R}}\rangle_{\mathcal{D}} - 16\pi G\varepsilon_{\mathrm{eff}} = 0 \quad , \tag{51}$$

and the integrability condition of Eq. (50) to yield Eq. (51) has the form of a balance equation between the effective sources and the averaged spatial (t-)Ricci scalar $\tilde{\mathcal{R}} := N^2\mathcal{R}$:

$$\partial_t\varepsilon_{\mathrm{eff}} + 3\tilde{H}_{\mathcal{D}}\left(\varepsilon_{\mathrm{eff}} + p_{\mathrm{eff}}\right) = \frac{1}{16\pi G}\left(\partial_t\langle\tilde{\mathcal{R}}\rangle_{\mathcal{D}} + 2\tilde{H}_{\mathcal{D}}\langle\tilde{\mathcal{R}}\rangle_{\mathcal{D}}\right) \quad . \tag{52}$$

The effective densities obey a conservation law, if the domains' curvature evolves like in a "small" FLRW cosmology, $\langle\tilde{\mathcal{R}}\rangle_{\mathcal{D}} = 0$, or $\langle\tilde{\mathcal{R}}\rangle_{\mathcal{D}} \propto a_{\mathcal{D}}^{-2}$, respectively.

The expressions $\tilde{\mathcal{Q}}_{\mathcal{D}}$ and $\tilde{\mathcal{P}}_{\mathcal{D}}$ are given in [16]. As can be seen above, $\tilde{\mathcal{Q}}_{\mathcal{D}}$ (the "kinematical backreaction") acts like a fluid component with "stiff" equation of state, similar to the action of a minimially coupled scalar field, while $\tilde{\mathcal{P}}_{\mathcal{D}}$ (the "dynamical backreaction") is due to the non-vanishing pressure gradient in the hypersurfaces.

It is interesting that the "kinematical backreaction" of the inhomogeneities could play the role of a free scalar field component that is commonly introduced when early evolutionary stages of the Universe are studied. It is also interesting that the expansion law in the case of a minimally coupled scalar field source gets particularly simple. This case will be investigated in a forthcoming work [20].

Acknowledgements

I would like to thank the organizers of this workshop for their invitation and support during a pleasant and inspiring stay at Hiroshima University. I also appreciate generous support and hospitality by the National Astronomical Observatory in Tokyo, as well as hospitality at Tohoku University in Sendai. Also, I would like to thank my collaborators with whome I share some of the reported results.

References

[1] V. I. Arnol'd, S. M. Gusein-Sade, A. N. Varchenko, *Singularities of Differentiable Maps* Vol.I.II, Birkhäuser, Boston (1985, 1988).

[2] N. Bahcall, J. P. Ostriker, S. Perlmutter, P. J. Steinhardt, Science **284**, 1481 (1999).

[3] S. Bildhauer and T. Futamase, Mon. Not. Roy. Astron. Soc. **249**, 126 (1991).

[4] S. Bildhauer and T. Futamase, G. R. G. **23**, 1251 (1991).

[5] S. Bildhauer, T. Buchert, M. Kasai, Astron. Astrophys. **263**, 23 (1992).

[6] M. Bruni, S. Matarrese, O. Pantano, Ap. J. **445**, 958 (1995).

[7] M. Bruni, P. K. S. Dunsby, G. F. R. Ellis, Ap. J. **395**, 34 (1992).

[8] M. Bruni, G. F. R. Ellis, P. K. S. Dunsby, Class. Quant. Grav. **9**, 921 (1992).

[9] T. Buchert, Astron. Astrophys. **223**, 9 (1989).

[10] T. Buchert, Mon. Not. Roy. Astron. Soc. **254**, 729 (1992).

[11] T. Buchert, Mon. Not. Roy. Astron. Soc. **267**, 811 (1994).

[12] T. Buchert, in *Proceedings of the International School of Physics Enrico Fermi. Course CXXXII: Dark Matter in the Universe*, edited by S. Bonometto, J. Primack, and A. Provenzale (Società Italiana di Fisica, Varenna sul Lago di Como, IOS Press Amsterdam 1996), pp. 543–564.

[13] T. Buchert, in *Mapping, measuring and modelling the Universe*, edited by P. Coles, V. Martínez, and M. J. Pons Bordería (University of València, ASP Conference Series 1996), pp. 349–356.

[14] T. Buchert, in *2nd SFB workshop on Astro-particle physics*, Report SFB/P002, Ringberg. Tegernsee (F.R.G.), edited by R. Bender, T. Buchert, P. Schneider, F.v. Feilitzsch (Technical University of Munich, 1996), pp. 71–82.

[15] T. Buchert, G. R. G. **32**, 105 (2000).

[16] T. Buchert, G. R. G. , to be submitted.

[17] T. Buchert, in preparation.

[18] T. Buchert and J. Ehlers, Astron. Astrophys. **320**, 1 (1997).

[19] T. Buchert, M. Kerscher, C. Sicka, Phys. Rev. D, submitted (1999), Preprint: astro-ph/9912347.

[20] T. Buchert and G. Veneziano, in preparation.

[21] M. Carfora and A. Marzuoli, Class. Quant. Grav. **5**, 659 (1988).

[22] M. Carfora, J. Isenberg, M. Jackson, J. Diff. Geom. **31**, 249 (1990).

[23] M. Carfora and K. Piotrkowska, Phys. Rev. D **52**, 4393 (1995).

[24] N. J. Cornish, D. N. Spergel, G. D. Starkman, Class. Quant. Grav. **15**, 2657 (1998).

[25] J. Ehlers and T. Buchert, G. R. G. **29**, 733 (1997).

[26] G. F. R. Ellis, in *General Relativity and Gravitation* (D. Reidel Publishing Co., Dordrecht, 1984), pp. 215–288.

[27] G. F. R. Ellis (Rapporteur), G. Börner, T. Buchert, J. Ehlers, C. J. Hogan, R. P. Kirshner, W. H. Press, G. Raffelt, F.-K. Thielemann, S. van den Bergh, in *The Evolution of the Universe*, Dahlem Workshop Report ES19, Berlin (F.R.G.) 1995, edited by G. Börner, S. Gottlöber, (Chichester: Wiley, New York, 1997), pp. 51–78.

[28] T. Futamase, Mon. Not. Roy. Astron. Soc. **237**, 187 (1989).

[29] T. Futamase, Phys. Rev. D **53**, 681 (1996).

[30] L. Hui and E. Bertschinger, Ap. J. **471**, 1 (1996).

[31] O. Iguchi, A. Hosoya, T. Koike, Phys. Rev. D **57**, 3340 (1998).

[32] M. Kerscher, in *Statistical Physics and Spatial Statistics*, edited by K. R. Mecke and D. Stoyan, Lecture Notes in Physics, (Springer, Berlin 2000), in press.

[33] M. Kerscher, J. Schmalzing, J. Retzlaff, S. Borgani, T. Buchert, S. Gottlöber, V. Müller, M. Plionis, H. Wagner, Mon. Not. Roy. Astron. Soc. **284**, 73 (1997).

[34] M. Kerscher, J. Schmalzing, T. Buchert, H. Wagner, Astron. Astrophys. **333**, 1 (1998).

[35] K. R. Mecke, T. Buchert, H. Wagner, Astron. Astrophys. **288**, 697 (1994).

[36] P. J. E. Peebles, *The Large Scale Structure of the Universe* (Princeton University Press, Princeton, New Jersey, 1980).

[37] H. Russ, M. H. Soffel, M. Kasai, G. Börner, Phys. Rev. D **56**, 2044 (1997).

[38] V. Sahni and P. Coles, Physics Rep. **262**, 1 (1995).

[39] V. Sahni, B. S. Sathyaprakash, S. F. Shandarin, Ap. J. **495**, L5 (1998).

[40] J. Schmalzing and T. Buchert, Ap. J. **482**, L1 (1997).

[41] J. Schmalzing and K. M. Gorski, Mon. Not. Roy. Astron. Soc. **297**, 355 (1998).

[42] J. Schmalzing, T. Buchert, A.L. Melott, V. Sahni, B.S. Sathyaprakash, S.F. Shandarin, Ap. J. **526**, 568 (1999).

[43] U. Seljak and L. Hui, in *Clusters, Lensing and the Future of the Universe*, edited by V. Trimble and A. Reisenegger, (University of Maryland, ASP Conference Series, Vol. 88, 1996), pp. 267–270.

[44] Y. Sota, T. Kobayashi, K. Maeda, T. Kurokawa, M. Morikawa, A. Nakamichi, Phys. Rev. D **58**, 3502 (1998).

[45] W. R. Stoeger, A. Helmi, D. F. Torres, Preprint: gr-qc/9904020 (1999).

[46] N. Straumann, Eur. J. Phys. **20**, 419 (1999).

[47] M. Takada and T. Futamase, G. R. G. **31**, 461 (1999).

[48] J.-P. Uzan, R. Lehoucq, J.-P. Luminet, Astron. Astrophys. **351**, 766 (1999).

[49] Ya. B. Zel'dovich, Astron. Astrophys. **5**, 84 (1970).

[50] Ya. B. Zel'dovich, Astrophysics **6**, 164 (1973).

Lagrangian description of fluid flow with acceleration in relativistic cosmology

Hideki Asada,[1]

Faculty of Science and Technology, Hirosaki University, Hirosaki 036-8561, Japan

Abstract

The Lagrangian description in relativistic cosmology is extended to fluids flow with acceleration, which is generated by the pressure. In the description, the entropy and the vorticity are obtained exactly, when we assume the barotropic equation of state. In order to obtain the metric, the Einstein equation is solved perturbatively. Thus, the present formalism is applicable to the case when the inhomogeneities are small in the large scale but locally nonlinear.

1 Introduction

Understanding the evolution of fluids in the expanding universe is of great interest in the cosmology. First, let us consider the Eulerian description and the Lagrangian one. In the Eulerian approach, all variables are expanded in series, so that the density contrast should be small. On the other hand, the Lagrangian framework is based on the description along the fluid flow. As a result, we can solve exactly the continuity equation for the density and so on. This is a great advantage, since we can tackle with the nonlinear dynamics. Next, we compare the Newtonian treatment with the general relativistic one. The Newtonian treatment is often used as a good approximation for the region $l/L \ll 1$, where l is the length scale of fluctuations of fluids and L corresponds to the Hubble radius. Thus, it is restricted within small scales, though it enables us to understand its results quite intuitively. On the other hand, there are no restrictions on scales in the general relativistic treatment. It is found that the relativistic version of the Lagrangian description is most powerful for studying highly nonlinear region in the expanding universe up to the caustic formation. For the dust case, the Lagrangian description is formulated generally [1, 2, 3]. Now, it is extended to the case of the fluid with the pressure. This case may correspond to the radiation dominated era.

A key idea inherent in the Lagrangian description of the universe is as follows [4, 5]: We illustrate it in the Newtonian cosmology for simplicity. The density is *exactly* obtained along the fluid flow. The Poisson equation for the cosmological Newtonian potential ϕ is

$$\nabla^2\phi = 4\pi G(\rho - \rho_b), \tag{1}$$

where ρ_b denotes a density in a background universe. This is estimated as

$$\left(\frac{L}{l}\right)^2 \phi \sim \delta, \tag{2}$$

where δ denotes the density contrast. In the cosmological situation, ϕ can be safely considered as small. The above equation, however, shows that the density can become large. Actually, this occurs when l/L goes to zero, namely in the small scale. We expect that the above idea works well, if ϕ is replaced by the metric. The fluid flow approach has been discussed by several authors [6, 7, 8, 9]. However, their treatment is not satisfactory, since their formulations are based on the fluid flow but they solve their equations perturbatively by splitting the flow into the background and perturbed parts.

In section 2, we consider the perfect fluid. It is shown that the entropy and the vorticity are determined exactly based on the Lagrange condition. Under this condition, section 3 presents a perturbative Lagrangian approach. Discussion is given in section 4. Greek indices run from 0 to 3, and Latin indices from 1 to 3. We use the unit, $c = 1$.

[1] E-mail:asada@phys.hirosaki-u.ac.jp

2 Lagrangian description - *General Formalism*

Let us consider a universe filled with the perfect fluid, whose energy momentum tensor is written as

$$T^{\mu\nu} = (\varepsilon + P)u^\mu u^\nu + Pg^{\mu\nu}. \tag{3}$$

The conservation law becomes

$$(\varepsilon u^\mu)_{;\mu} + Pu^\mu{}_{;\mu} = 0, \tag{4}$$
$$(\varepsilon + P)u_{\mu;\nu}u^\nu + P_{,\nu}\gamma^\nu_\mu = 0, \tag{5}$$

where we defined the projection tensor as

$$\gamma^\mu_\nu = \delta^\mu_\nu + u^\mu u_\nu. \tag{6}$$

Here, we assume the barotropic equation of state as $P = P(\varepsilon)$, so that we can introduce the entropy and the enthalpy respectively as [10, 11]

$$s = \exp\int \frac{d\varepsilon}{\varepsilon + P}, \tag{7}$$
$$h = \exp\int \frac{dP}{\varepsilon + P}. \tag{8}$$

Then, the conservation law is re-expressed as

$$(su^\mu)_{;\mu} = 0, \tag{9}$$
$$u_{\mu;\nu}u^\nu + (\ln h)_{,\nu}\gamma^\nu_\mu = 0. \tag{10}$$

Furthermore, we define the vorticity as

$$\omega^\mu = \frac{1}{2}\epsilon^{\mu\alpha\beta\gamma}u_\alpha u_{\beta;\gamma}. \tag{11}$$

Then, the Beltrami's equation for the vorticity is written as

$$\left(\frac{h\omega^\mu}{s}\right)_{;\nu}\frac{u^\nu}{h} = \left(\frac{u^\mu}{h}\right)_{;\nu}\frac{h\omega^\nu}{s}. \tag{12}$$

So far the treatment is fully covariant. In the following, we introduce the Lagrangian coordinate,

$$x^\mu = (\tau, x^i), \tag{13}$$

where τ is the proper time and x^i is constant along the fluid flow. This gives us the Lagrangian condition (e.g. [12]), in which the matter 4-velocity take components of

$$u^\mu = (1, 0, 0, 0). \tag{14}$$

Under this condition, we have $g_{00} = -1$ and $u_\mu = (-1, g_{0i})$. In the Lagrangian description, the conservation equation for the entropy, Eq. (9) is simply

$$(s\sqrt{-g})_{,0} = 0. \tag{15}$$

Therefore,

$$s(x, t) = \sqrt{\frac{g(x, t_0)}{g(x, t)}}s(x, t_0). \tag{16}$$

The relativistic Beltrami equation (12) also becomes simply

$$\left(\frac{h\omega^i}{s}\right)_{,0} = 0, \tag{17}$$

which is integrated to give

$$\frac{h\omega^i}{s} = \left.\frac{h\omega^i}{s}\right|_{t_0}. \tag{18}$$

This is also expressed as

$$h\omega^i(x,t) = \sqrt{\frac{g(x,t_0)}{g(x,t)}}\, h\omega^i(x,t_0). \tag{19}$$

The ω^0 component is not independent of ω^i. Using the relation $\omega^\mu u_\mu = 0$, we obtain

$$\omega^0 = g_{0i}\omega^i, \tag{20}$$

The result Eq. (18) tells us that the vorticity is coupled to the entropy enhancement and vice versa. In particular, if the vorticity does not vanish exactly at an initial time, the vorticity will blow up as the entropy grows larger and larger (i.e. in the collapsing region), even if it has only the decaying mode in the linear perturbation theory. It should also be emphasized that our results Eqs. (16) and (18) in the fully general relativistic treatment precisely correspond to those in the Newtonian case.

3 Perturbative approach

In the previous section, we solved exactly the equations for the entropy and the vorticity. The results Eqs. (16) and (19) show that s and ω^i are completely written in terms of the determinant of the metric tensor and their initial values. Here, we shall obtain the metric perturbatively.

The Einstein equation is decomposed with respect to the fluid flow:

$$G_{\mu\nu}u^\mu u^\nu = 8\pi G\varepsilon, \tag{21}$$

$$G_{\mu\nu}u^\mu \gamma^\nu{}_\alpha = 0, \tag{22}$$

$$G_{\mu\nu}\gamma^\mu{}_\alpha \gamma^\nu{}_\beta = 8\pi G P \gamma_{\alpha\beta}. \tag{23}$$

The Euler equation is rewritten as

$$(hu_i)_{,0} + \left(\frac{h}{u^0}\right)_{,i} = 0, \tag{24}$$

As a simple illustration, let us take the equation of state as

$$P = \frac{1}{3}\varepsilon. \tag{25}$$

We assume that the background is spatially flat Friedmann-Lemaître-Robertson-Walker (FLRW) universe. The extension to the spatially non-flat case must be a straightforward task. The perturbed metric is decomposed into

$$g_{0i} = B_{,i}(x) + b_i(x), \tag{26}$$

$$g_{ij} = a^2\Big(\delta_{ij} + 2H_L\delta_{ij} + 2H_{T,ij} + (h_{i,j} + h_{j,i}) + 2H_{ij}\Big),$$

where B, H_L, and H_T are scalar mode quantities, b_i and h_i are the vector (transverse) mode, and H_{ij} is the tensor (transverse-traceless) mode satisfying

$$b^i{}_{,i} = 0, \tag{27}$$

$$h^i{}_{,i} = 0, \tag{28}$$

$$H^i{}_i = 0, \tag{29}$$

$$H^{ij}{}_{,j} = 0. \tag{30}$$

Raising and lowering indices of the perturbed quantities are done by δ^{ij} and δ_{ij}.

3.1 Residual gauge freedom in the Lagrange condition

The general gauge transformation to the first order is induced by the infinitesimal coordinate transformation

$$\tilde{x}^\mu = x^\mu + \xi^\mu. \tag{31}$$

The changes due to the gauge transformation are

$$\delta_\xi g_{\mu\nu} = -g_{\mu\nu,\alpha}\xi^\alpha - g_{\mu\alpha}\xi^\alpha{}_{,\nu} - g_{\nu\alpha}\xi^\alpha{}_{,\mu}, \tag{32}$$

$$\delta_\xi u^\mu = \xi^\mu{}_{,\nu}u^\nu - u^\mu{}_{,\nu}\xi^\nu. \tag{33}$$

In order to leave the Lagrangian condition unchanged, we have $\delta_\xi u^\mu = 0$, which leads to $\xi^\mu{}_{,0} = 0$. Therefore,

$$\xi^\mu = \xi^\mu(\boldsymbol{x}). \tag{34}$$

For the spatially flat background, ξ^μ are decomposed into each mode,

$$\xi^\mu(\boldsymbol{x}) = (T, \delta^{ij}L_{,j} + \ell^i), \tag{35}$$

where the vector mode quantity ℓ^i satisfies $\ell^i{}_{,i} = 0$. Hence we obtain

$$\tilde{B} = B + T(\boldsymbol{x}), \tag{36}$$

$$\tilde{H}_L = H_L - \frac{\dot{a}}{a}T(\boldsymbol{x}), \tag{37}$$

$$\tilde{H}_T = H_T - L(\boldsymbol{x}), \tag{38}$$

$$\tilde{h}_i = h_i - \ell_i(\boldsymbol{x}), \tag{39}$$

where an overdot ($\dot{}$) denotes $\partial/\partial t$. The vector mode quantity b_i and the tensor mode quantity H_{ij} are gauge-invariant.

3.2 Scalar perturbations

The Einstein equations for the scalar perturbations are

$$\left(\frac{\dot{a}}{a}\right)^{\cdot} B + \dot{H}_L = 0, \tag{40}$$

$$\ddot{H}_L + 4\frac{\dot{a}}{a}\dot{H}_L - \frac{2}{3}\frac{\dot{a}}{a}\nabla^2 H_L + \frac{1}{3}\frac{\dot{a}}{a}\nabla^2\dot{H}_T + \frac{1}{3}\left(\frac{\dot{a}}{a}\right)^{\cdot}\nabla^2 B = 0, \tag{41}$$

$$\ddot{H}_T + 3\frac{\dot{a}}{a}\dot{H}_T = \frac{1}{a^2}\left(H_L + \frac{1}{a}(aB)^{\cdot}\right), \tag{42}$$

where $\nabla^2 = \delta^{ij}\partial_i\partial_j$. We introduce the conformal time η as

$$d\eta = \frac{dt}{a}. \tag{43}$$

We expand all quantities in a Fourier's series, for instance

$$\Psi = \int d^3k \Psi_{\boldsymbol{k}}(\eta)\exp(i\boldsymbol{k}\cdot\boldsymbol{x}), \tag{44}$$

where the subscript $\boldsymbol{k}$ denotes the Fourier coefficient. We define θ as

$$\theta = \frac{k\eta}{\sqrt{3}}, \tag{45}$$

where $k = |\boldsymbol{k}|$. We are in position to solve Eqs. (40)-(42) and obtain

$$B_{\boldsymbol{k}} = \frac{1}{4}\left(\frac{k}{\sqrt{3}}\right)^2\left[\Psi_{\boldsymbol{k}}(-2 + \cos\theta + \theta\sin\theta) + \Phi_{\boldsymbol{k}}(-2\sin\theta + \theta\cos\theta)\right], \tag{46}$$

$$H_{L\boldsymbol{k}} = \Psi_{\boldsymbol{k}}\theta^{-2}(1 - \cos\theta) + \Phi_{\boldsymbol{k}}\theta^{-2}\sin\theta, \tag{47}$$

$$H_{T\boldsymbol{k}} = \left(\frac{k}{\sqrt{3}}\right)^2\left[\Psi_{\boldsymbol{k}}\left(\theta^{-1}\sin\theta - \frac{1}{2}\cos\theta - \frac{1}{2}\right) + \Phi_{\boldsymbol{k}}\left(\theta^{-1}\cos\theta + \frac{1}{2}\sin\theta - \theta_0^{-1}\right)\right], \tag{48}$$

where θ_0 denotes θ at the initial time and we used the residual gauge freedom to set initially $H_{Tk} = 0$.

The initial density field $\rho(\boldsymbol{x}, t_0)$ is also expressed by the metric. When the density contrast $\delta \equiv (\rho - \rho_b)/\rho_b$ is sufficiently small, we obtain from Eq. (21)

$$\delta_k(\eta_0) = \frac{4}{3}\left[\Psi_{\vec{k}}\left(3\theta_0^{-2}(\cos\theta_0 - 1) + 3\theta_0^{-1}\sin\theta_0 - \frac{3}{2}\cos\theta_0\right) + \Phi_{\vec{k}}\left(-3\theta_0^{-2}\sin\theta_0 + 3\theta_0^{-1}\cos\theta_0 - \frac{3}{2}\sin\theta_0\right)\right]. \tag{49}$$

3.3 Vector perturbations

The Einstein equations for the vector perturbations are

$$\nabla^2\left(\dot{h}_i - \frac{1}{a^2}b_i\right) = 4\left(\frac{\dot{a}}{a}\right)^{\cdot} b_i, \tag{50}$$

$$\left(a^3\dot{h}_i - ab_i\right)^{\cdot} = 0. \tag{51}$$

Introducing β_i as

$$b_i(\boldsymbol{x}) = t^{1/2}\nabla^2\beta_i(\boldsymbol{x}), \tag{52}$$

Eq. (50) is solved to give

$$h_i = 2(t - t_0)^{1/2}\nabla^2\beta_i(\boldsymbol{x}) + 4(t - t_0)^{-1/2}\beta_i(\boldsymbol{x}), \tag{53}$$

where we again used the residual gauge freedom (cf. Eq. (39)) to set $h_i(\boldsymbol{x}, t_0) = 0$.

3.4 Tensor perturbations

The equation for the tensor perturbations is

$$\ddot{H}_{ij} + 3\frac{\dot{a}}{a}\dot{H}_{ij} - \frac{1}{a^2}\nabla^2 H_{ij} = 0. \tag{54}$$

This is a homogeneous wave equation in the expanding universe. The solutions are well known and we will not discuss the detail here. See, e.g., [11].

As for the metric, our result is identical to that of the linear perturbation theory (e.g. [13]). However, there is an important difference to be emphasized: In Bardeen's paper, it is essential to linearize the density contrast. On the other hand, our Lagrangian approach does not rely on the assumption that *the density contrast should be small.* It is actually an important advantage of the Lagrangian approach that it uses (or extrapolates) the well-known solutions of the linear theory to express the non-linear behavior of the entropy.

4 Discussion

The Lagrangian description in the relativistic cosmology has been extended to the case of the fluid with the pressure [14]. The present formulation contains the dust cosmology as a special case ($P = 0$) [3]. It is applicable to even highly nonlinear regions up to the caustic formation, since the entropy and the vorticity are obtained exactly along the fluid flow. In this approach, dynamical variables are the metric but not material variables thanks to the Lagrange condition. The metric is obtained by solving perturbatively the Einstein equation.

It is worthwhile to mention that there are several choices of a temporal coordinate. Here, we adopted the proper time, since it seems the simplest choice. However, we have another choice [15]

$$u^\mu = (h, \vec{0}), \tag{55}$$

so that Eq. (24) is solved as

$$g_{0i} = \frac{f_i(\boldsymbol{x})}{h^2}, \tag{56}$$

where $f_i(\boldsymbol{x})$ is independent of time. Then, we find

$$g_{00} = -\frac{1}{h^2}. \tag{57}$$

In this case, it might be rather troublesome to solve the Einstein equation, since g_{00} is not constant.

As future subjects along this Lagrangian approach, it may be interesting to study the primordial black hole formation [16] and the averaging problem in inhomogeneous cosmologies (e.g. [17]).

Acknowledgment

The author would like to thank M. Kasai for fruitful discussion. He is also grateful to T. Buchert, N. Sugiyama and K. Yamamoto for useful conversation.

References

[1] M. Kasai, Phys. Rev. D **52**, 5605 (1995).

[2] H. Russ, M. Morita, M. Kasai and G. Börner, Phys. Rev. D **53**, 6881 (1996).

[3] H. Asada and M. Kasai, Phys. Rev. D **59**, 0123515 (1999).

[4] Y. B. Zel'dovich, Astron. Astrophys. **5**, 84 (1970).

[5] T. Buchert, Astron. Astrophys. **223**, 9 (1989); Mon. Not. R. Astron. Soc. **254**, 729 (1992); Mon. Not. R. Astron. Soc. **267**, 811 (1994).

[6] S. W. Hawking, Astrophys. J. **145**, 544 (1966).

[7] G. F. R. Ellis. in *General Relativity and Cosmology*, edited by R. K. Sachs (Academic, New York, 1971).

[8] D. W. Olson, Phys. Rev. D **14**, 327 (1976).

[9] D. H. Lyth and M. Mukherjee, Phys. Rev. D **38**, 485 (1988).

[10] J. Ehlers, Proc. Math. Nat. Sci. Sect. Mainz Acad. Sci. Lit. **11**, 792 (1961); English translation in Gen. Rel. Grav. **25**, 1225 (1993).

[11] S. Weinberg, *Gravitation and Cosmology* (John Wiley & Sons, New York, 1972).

[12] H. Friedrich, Phys. Rev. D **57**, 2317 (1998).

[13] J. M. Bardeen, Phys. Rev. D **22**, 1882 (1980).

[14] H. Asada, in preparation.

[15] G. F. R. Ellis. in *Cargese Lectures in Physics, vol. bf 6*, edited by E. Schatzman (Gordon and Breach, New York, 1973).

[16] B. J. Carr, Astrophys. J. **201**, 1 (1975).

[17] T. Buchert, Gen. Rel. Grav. *in press* (1999).

Distances and lensing in cosmological void models

Kenji Tomita[1]

Yukawa Institute for Theoretical Physics, Kyoto University,
Sakyo-ku, Kyoto, 606-8502, Japan

Abstract

To explain the puzzling situation in the observed bulk flows on scales $\sim 150h^{-1}$ Mpc ($H_0 = 100h^{-1}$ km sec^{-1} Mpc^{-1}), we consider the observational behavior of spherically symmetric inhomogeneous cosmological models, which consist of inner and outer homogeneous regions connected by a shell or an intermediate self-similar region. It is assumed that the present matter density parameter in the inner region is smaller than that in the outer region, and the present Hubble parameter in the inner region is larger than that in the outer region. Then galaxies in the inner void-like region can be seen to have a bulk motion relative to matter in the outer region, when we observe them at a point O deviated from the center C of the inner region. Their velocity v_p in the CD direction is equal to the difference of two Hubble parameters multiplied by the distance between C and O. It is found also that the velocity v_d corresponding to CMB dipole anisotropy observed at O is by a factor ≈ 10 small compared with v_p. This behavior of v_d and v_p is consistent with the observed cosmic flow of cluster galaxies, when the radius of the inner region and the distance CD are about 200 h^{-1} Mpc and 40 h^{-1} Mpc, respectively, and when the gaps of density and Hubble parameters are ≈ 0.5 and 18%, respectively. Moreover, the $[m, z]$ relation in these models is discussed in connection with SNIa data.

1 Introduction

The dipole moment in the cosmic microwave background radiation (CMB) is thought to come mainly from the Doppler shift due to the motion of the Local Group (LG), relative to the cosmic homogeneous expansion. As the main gravitational source which brings the velocity vector of LG, the existence of the Great Attractor (GA) was found by Lynden-Bell et al.(1988) and Dressler et al. (1987). It has the position at the redshift of 4300 km sec^{-1}. On the other hand, the motion of LG relative to the inertial frame consisting of many clusters on larger-scales was studied observationally by several groups: A bulk flow of ~ 700 km sec^{-1} was found by Lauer and Postman (1994, 1995) and Colless (1995) as the motion of the Abell cluster inertial frame relative to LG in the region with redshift < 15000 km sec^{-1}, but in the other approach the different result was derived by Giovanelli et al. (1998), Dale et al. (1999) and Riess et al. (1997) in the regions with similar redshifts. Lauer and Postman's work is based on the assumption that the brightest cluster galaxies as standard candles and the Hoessel relation can be used, but at present these assumptions have been regarded as questionable or unreliable.

Independently of these works, the motion of cluster frames relative to CMB was measured by Husdon et al. (1999) and Willick (1999) due to the global Hubble formula using the Tully-Fisher distances of clusters and their redshifts with respect to CMB, and the flow velocity vector was derived in the region with about $150h^{-1}$ Mpc ($H_0 = 100h^{-1}$ km sec^{-1} Mpc^{-1}). The remarkable and puzzling properties of these flows are that the flow velocity reaches a large value ~ 700 km/sec on a large scale, while the dipole velocity (not due to GA) corresponding to the CMB dipole anisotropy seems to be much small, compared with the above flow velocity.

In the present note we first consider inhomogeneous models on sub-horizon scale, corresponding to matter flows on scales $\sim 150h^{-1}$ Mpc. They are assumed to be spherically symmetric inhomogeneous models which consist of inner and outer homogeneous regions connected by a shell being a singular layer, and the behavior of large-scale motions caused in the inner region is considered. Next we consider light rays which are emitted at the last scattering surface and reach an observer situated at a point O (inthe

[1]E-mail:tomita@yukawa.kyoto-u.ac.jp

inner region) deviated from the center C, and the CMB dipole anisotropy for the observer is shown. On the basis of these results we show the consistency with various observations of cosmic flows. Moreover the $[m, z]$ relation is discussed in connection with SNIa data, and the lensing effect is examined. Finally concluding remarks are presented.

2 Cosmological models and the bulk motions

In previous papers (Tomita 1995, 1996) we treated spherically symmetric inhomogeneous models which consist of inner homogeneous region ($V^{\rm I}$) and outer homogeneous region ($V^{\rm II}$) connected with an intermediate self-similar region and have the boundary on a super-horizon scale. Here we consider a similar spherically symmetric inhomogeneous model ("single-shell model") which consists of inner and outer homogeneous regions, but is connected by a shell being a singular layer on a sub-horizon scale $\sim 150h^{-1}$ Mpc (cf. Fig. 1). This shell may be associated with large-scale structures or excess powers observed by Broadhurst et al.(1990), Landy et al.(1996), and Einasto et al.(1997). The physical state in each region is specified by the Hubble constant density and the density parameter. It is assumed that the present Hubble parameter in the inner region ($H_0^{\rm I}$) is larger than that in the outer region ($H_0^{\rm II}$), and the present inner density parameter ($\Omega_0^{\rm I}$) is smaller than the present outer density parameter ($\Omega_0^{\rm II}$). The evolution of physical states in each region and the boundary has been studied in the form of void models (e.g., Sakai et al. 1993).

The average motion of CMB is comoving with matter in the outer region ($V^{\rm II}$), while it is not comoving with matter in the inner region ($V^{\rm I}$) or matter in the inner region moves relative to CMB, because their Hubble constants are different. The bulk motion appears as the result of this relative motion to CMB. The relative velocity (Δv) is $(H_0^{\rm I} - H_0^{\rm II})r$ in the radial direction, where r is the radial distance from the center C to an arbitrary point (a cluster's position) in the inner region. When an observer O sees this velocity vector Δv, it can be divided into two parts: the component in the observer's line of sight ($\Delta v_{\rm ls}$) and the bulk-velocity component in the direction of C $\rightarrow$ O (v_p). The latter component v_p is constant, irrespective of the cluster's position. In the case when the present radius of the boundary and the distance from C to O are $\sim 200(h^{\rm I})^{-1}$ and $40(h^{\rm I})^{-1}$ Mpc, respectively, we have $v_p \sim 700$ km sec^{-1}, where $H_0^{\rm I} = 100h^{\rm I}$ and $H_0^{\rm II} = 100h^{\rm II}$ km sec^{-1} Mpc^{-1}.

Fig. 1. A model with a single shell. z and $\bar{z}$ are the redshifts for observers at O and C.

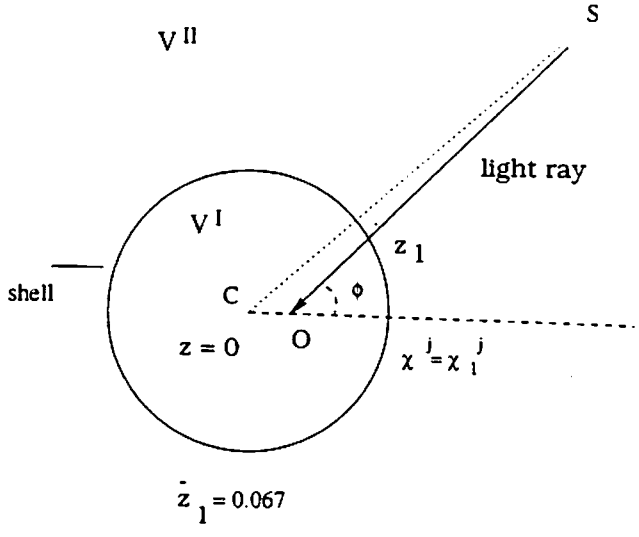

Table 1: Model parameters in single-shell models.

Model	$\Omega_0^{\rm I}$	$\Omega_0^{\rm II}$	$h^{\rm I}$	$h^{\rm II}/h^{\rm I}$
1	0.2	0.56	0.7	0.82
2	0.2	0.88	0.7	0.82

3 Dipole anisotropy and the consistency with various observations of cosmic flows

If the observer were in the center C, he never sees any CMB anisotropy, as long as the two regions are homogeneous. For the non-central observer O we have nonzero dipole anisotropy D which is derived by calculating curved paths from the last scattering surface to O and the directional variation of the temperature T_r. The velocity v_d corresponding to D is defined by $v_d \equiv c[(3/4\pi)^{1/2}D]$ and derived. As the result it was found that v_d is small compared with v_p, if O is near to C. In our above example, $r({\rm OC})/r({\rm boundary}) \sim 1/5$, we obtain $v_d \sim 0.1v_p$, where we assumed model parameters as shown in Table 1.

As described in §2, the bulk velocities at arbitrary two points are equal and so their difference is zero. Accordingly the relative velocity of the Local Group (LG) to the frame of clusters (v_{LG}) is only the peculiar velocity (v_{GA}) caused by the small-scale nonspherical gravitational field of the Great Attracter. The above result gives the dipole velocity of LG, $v_d({\rm LG}) = v_{GA} + v_d$, so that v_{GA} and $v_d({\rm LG})$ are comparable and the diffrence is v_d ($\sim 0.1v_p$). This situation in the present models is consistent with the observations (Giovanelli et al. (1998), Dale et al. (1999) and Riess et al. (1997)) for relative velocities of LG to the cluster frame , and the observations (Husdon et al. (1999) and Willick (1999)) for the bulk flows of clusters, since the observed values of v_{LG}, $v_d({\rm LG})$ and v_p are 565 km sec^{-1}, 627 km sec^{-1} and $\sim$ 700 km sec^{-1}, respectively, in the similar directions. The observed difference of first two velocities is about $0.1 \times v_p$.

The detail derivation of the contents in §2 and §3 is shown in Tomita (2000a).

4 $[m, z]$ relation and SNIa data

Here the behavior of distances in the present models is studied. First we treat the distances from a virtual observer who is in the center C of the inner void-like region in models with a single shell, and derive the [magnitude m - redshift z] relation. This relation is compared with the counterpart in the homogeneous models. Then the relation in the present models is found to deviate from that in the homogeneous models with $\Lambda = 0$ at the stage of $z < 1.5$. It is partially similar to that in the nonzero-Λ homogeneous models, but the remarkable difference appears at the high-redshift stage $z > 1.0$. Moreover, we consider a realistic observer who is in the position O deviated from the center, and calculate the distances from him. The distances depend on the direction of incident light and the area angular diameter distance is different from the linear angular diameter distances. It is shown as the result that the $[m, z]$ relation is anisotropic, but the relation averaged with respect to the angle is very near to the relation by the virtual observer (at C). When we compare these theoretical relations with SNIa data (Riess et al.(1998), Garnavich et al.(1998), and Schmidt et al.(1998)), we can determine which of the present models and nonzero-Λ homogeneous models are better, and the fittest model parameters. At present, however, there are few data at $z \sim 1.0$, so that the model selection may be impossible. But in near future many data at $z \sim$ or > 1.0 will be accumulated and the above model selection will be performed. The detail description of the content in this section is given in Tomita (2000b).

Fig. 2. The relation between the luminosity distance d_L and z. A solid line (a) and a short dash line (b) represent the single-shell model with $(\Omega_0^{\rm I}, \Omega_0^{\rm II}, h^{\rm I}, h^{\rm II}/h^{\rm I}) = (0.2, 0.56, 0.7, 0.82)$. (a) denotes the ϕ averaged value by the observer O and (b) denotes the case of the virtual observer C. (c) and (d) stand for the homogeneous models with $(\Omega_0, \lambda_0) = (0.2, 0)$ and $(0.2, 0.8)$, respectively.

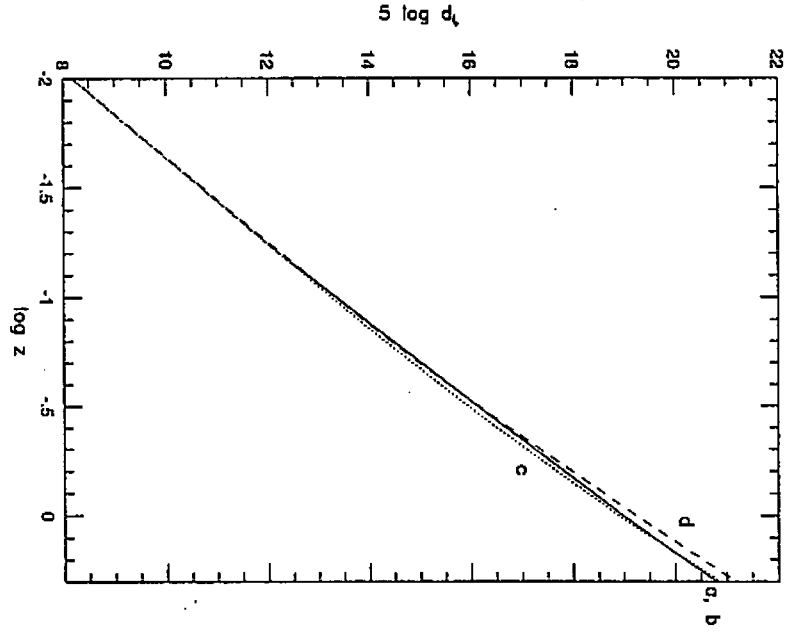

Fig. 3. The relation between the luminosity distance d_L and z. A solid line (a) and a short dash line (b) represent the single-shell model with $(\Omega_0^{\rm I}, \Omega_0^{\rm II}, h^{\rm I}, h^{\rm II}/h^{\rm I}) = (0.2, 0.88, 0.7, 0.82)$. The other meaning of lines is the same as that in Fig. 2.

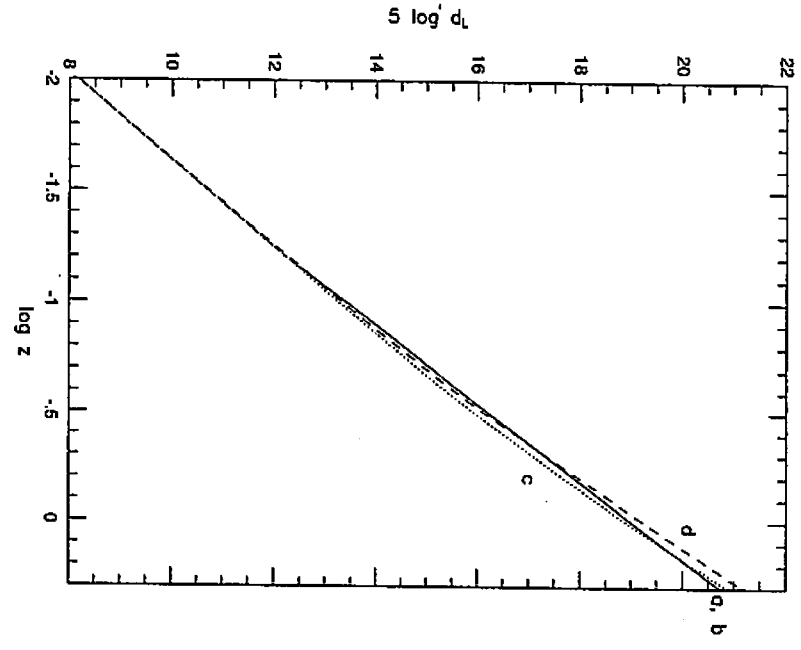

Fig. 4. Hubble diagram for 42 high-redshift Type Ia supernova from Supernova Cosmology Project, and 18 low-redshift Type Ia supernova from the Calan/Tololo Supernova Survey. The solid curves are the theoretical $m(z)$ for a range of cosmological models with zero cosmological constant: $(\Omega_M N, \Omega_\Lambda) = (0,0)$ on top, $(1,0)$ in middle and $(2,0)$ on bottom. The dashed curves are for a range of flat cosmological models: $(\Omega_M N, \Omega_\Lambda) = (0,1)$ on top, $(0.5, 0.5)$ second from top, $(1,0)$ third from top, and $(1.5, -0.5)$ on bottom.

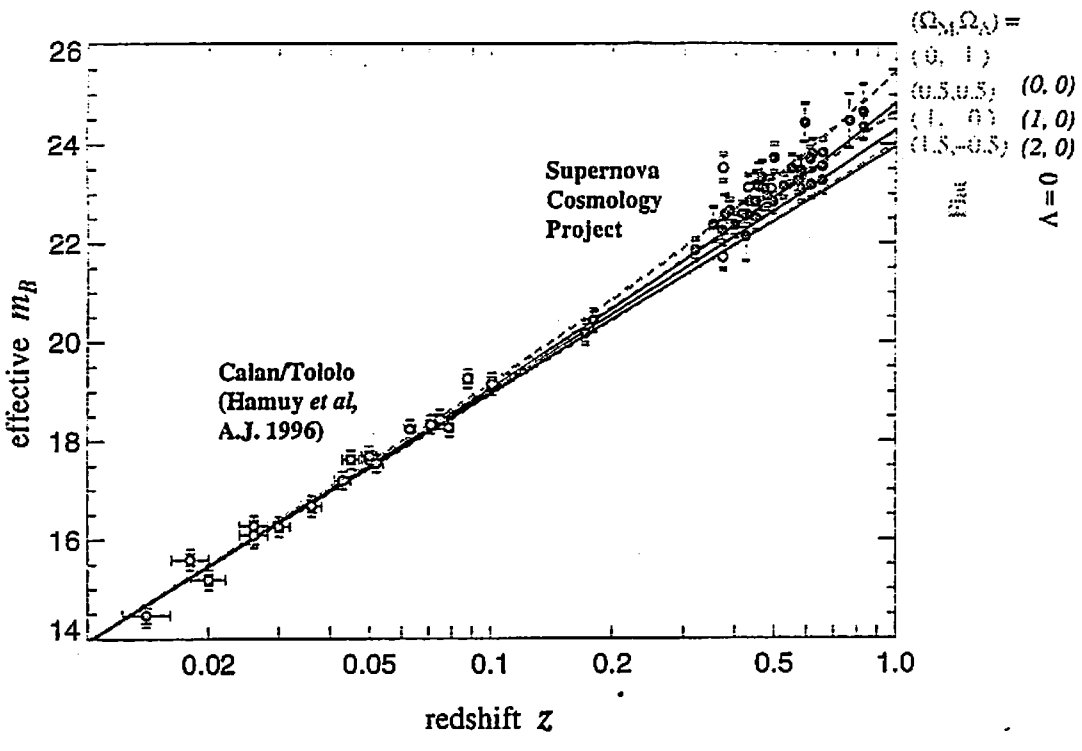

In Fig.2 and Fig. 3 the relation is shown in Model 1 and 2, respectively. Here the ordinate is $5 \ln d_L$ which is used for the apparent magnitude m, because m is expressed as

$$m = -\frac{5}{2} \log \frac{L}{4\pi (d_L)^2} = 5 \log d_L + \text{const.}$$

The luminosity distance d_L is related to the area angular diameter distance d_A by $d_L = (1+z)^2 d_A$. In Fig. 4 the SNIa data with homogeneous models are shown. The arrows denote the corresponding points in the theoretical relations.

5 Concluding remarks

The density perturbations in the inner region and their influence of on CMB anisotropy are another important factor to the selection of model parameters, which should be studied next.

References

[1] Lynden-Bell, D., Faber, S.M., Burstein, D., Davies, R. L., Dressler, A., Terlevich, R. J. and Wegner, G., Astrophys. J. 326 (1988), 19.

[2] Dressler, A., Faber, S.M., Burstein, D., Davies, R. L., Lynden-Bell, D., Terlevich, R. J., and Wegner, G., Astrophys. J., 313 (1987), L37.

[3] Lauer, T. R. and Postman, M. , Astrophys. J., 425 (1994), 418; Postman, M. and Lauer, T. R., Astrophys. J., 440 (1995), 28.

[4] Colless, M. , Astron. J., 109 (1995), 1937.

[5] Giovanelli, R., Haynes, M. P., Freudling, W., da Costa, L. N., Salzer, J. J., and Wegner, G., Astrophys. J., 505 (1998), L91.

[6] Dale, D. A., Giovanelli, R., and Haynes, M.P., Astrophys. J., 510 (1999), L11.

[7] Riess, A. G., Davis, M., Baker, J., and Kirshner, R. P. , Astrophys. J., 488 (1997), L1.

[8] Hudson, M. J., Smith, R. J., Lucey, J. R., Schlegel D. J. and Davies, R. L. Astrophys. J., 512 (1999), L79.

[9] Willick, J. A. , Astrophys. J., 516 (1999), 47.

[10] Tomita, K. , Astrophys. J., 461 (1996), 507.

[11] Tomita, K. , Astrophys. J., 451 (1995), 541; Tomita, K., Astrophys. J., 464 (1996), 1054 for Erratum.

[12] Broadhurst, T. J., Ellis, R. S., Koo, D.C., Szalay, A. S. , Nature, 343 (1990), 726

[13] Landy, S. D., Shectman, S. A., Lin, H., Kirshner, R. P., Oemler, A., and Tucker, D., Astrophys. J., 456 (1996), L1 .

[14] Einasto, J. et al. , Nature, 385 (1997), 139.

[15] Sakai, N., Maeda, K. and Sato, H. , Prog. Theor. Phys., 89 (1993), 1193.

[16] Tomita, K., Astrophys. J., 529(2000), No.1.

[17] Riess, A. G. et al. , Astron. J., 116 (1998), 1009.

[18] Garnavich, P. M. et al., Astrophys. J., 493(1998), L53.

[19] Schmidt, B. P. et al., Astrophys. J., 507(1998), 46.

[20] Tomita, K., Astrophys. J., 529 (2000), No.1.

A special note:

GRG in Hiroshima

Kenji Tomita

Yukawa Institute for Theoretical Physics, Kyoto University,
Sakyo-ku, Kyoto, 606-8502, Japan

In the 9th GRG meeting at Hiroshima University, I had a talk on RITP, GRG groups in Hiroshima University, and the "Golden Oldie" in the GRG journal.

RITP means Research Institute for Theoretical Physics (Hiroshima University), which was one of centers of studies on general relativity and gravitation in Japan. Originally it was in the old campus (in Hiroshima city) of Hiroshima University and the first director Y. Mimura tried to fuse general relativity and quantum field theory by developing the theory of "wave geometry." Most workers during WWII died or were injured, and the building was broken, under the strong influence of A-bomb. After WWII a new building was constructed in Takehara city. Workers in RITP before 1990 include H. Nariai, T. Kimura, K. Tomita, A. Tomimatsu, A. Hosoya, M. Sasaki, Y. Suto (stuffs), T. Azuma, M. Kasai, M. Den, J. Soda, H. Ishihara, Y. Nambu, K. Nakao, N. Sugiyama, K. Yamamoto, K. Watanabe, H. Ueda, N. Makino, and T. Matsubara (graduate school). In June, 1990 this institute was united with RIFP (= Research Institute for Fundamental Physics, Kyoto University), and a new institute: Yukawa Institute for Theoretical Physics (Kyoto University) was born. In the 6th Marcel Grossmann Meeting held at Kyoto next year (in June 1991), the MG Institutional Award was given to RITP for its acitivity in GRG research.

Another GRG group started in 1995 in Department of Physics, Hiroshima University. Their present members are Y. Kojima, K. Yamamoto (stuffs), H. Nishioka, M. Hosonuma, K. Kaneno, and T. Obata (graduate school).

In the articles of "Golden Oldie", various old valuable papers are being introduced and reproduced, which were published in unpopular journals in the past. Nariai's papers (Sci. Rep. Tohoku Univ., 34(1950), 160 and 35(1951), 62) are one of them, which derived the so-called Nariai solution and showed its physical meaning. We can see them in the GRG journal 31(1999), 945.

The canonical formulation of $N = 2$ supergravity in terms of the Ashtekar variable

Motomu Tsuda *

Laboratory of Physics, Saitama Institute of Technology

Okabe-machi, Saitama 369-0293, Japan

Abstract

We reconsider the Ashtekar's canonical formulation of $N = 2$ supergravity (SUGRA) derived from the $N = 2$ chiral Lagrangian, which has been constructed in our previous work following the method employed in the usual SUGRA.

The nonperturbative canonical treatment of supergravity (SUGRA) in terms of the Ashtekar variable [1] was firstly discussed about the simplest $N = 1$ theory in [2]. In this theory the chiral Lagrangian is constructed by using the self-dual connection which couples to only a right-handed spin-3/2 field, and this has two kinds of right- and left-handed supersymmetry (SUSY) invariances in the first-order formalism. Therefore two types of the SUSY constraints, which generate those SUSY transformations appear in the canonical formulation. Recently, D. Armand-Ugon *et al.* [3] have shown that, in $N = 1$ chiral SUGRA, the $SU(2)$ algebra generated by the Gauss-law constraint is graded by means of the right-handed SUSY constraint. They also have rewritten all the constraints in a simple form towards a loop representation of quantum canonical SUGRA, by using "super" configuration space variables associated with the graded group which is called the $GSU(2)$ group [4]. [1]

The extension of the Ashtekar's canonical formulation to $N = 2$ extended SUGRA was mainly developed in the context of the 2-form gravity [6, 7, 8]. The chiral Lagrangian of $N = 2$ SUGRA is constructed in [6, 7] based on $N = 1$ 2-form SUGRA [9] with auxiliary fields which are needed to write the chiral (2-form) Lagrangian. They proved that the SUSY algebra is not closed at the level of transformation algebra on auxiliary fields but actually closes at the level of the canonical formulation. In [8] the structure of the graded algebra in $N = 2$ theory, which was reffered to as the $G^2SU(2)$ algebra, was discussed in the relation of the 2-form SUGRA with the so-called "BF-theory".

In this paper we focus on the $N = 2$ chiral Lagrangian which has been constructed in our previous work [10] following the method employed in the usual SUGRA, and reconsider

*e-mail: tsuda@sit.ac.jp

[1] In Ref.[5] it is pointed out that the algebra of $GSU(2)$ is corresponds to the super Lie algebra, $Osp(1/2)$.

the Ashtekar's canonical formulation of $N = 2$ SUGRA. The chiral Lagrangian with a nonvanishing cosmological constant we adopted in this paper does not contain any auxiliary fields of the 2-form SUGRA, and the supersymmetry (SUSY) transformation parameters are not constrained at all. Therefore the canonical formulation are derived in a straightforward manner in contrast with the 2-form SUGRA. We particularly study the algebra of the Gauss, $U(1)$ gauge and right-handed SUSY constraints, and show that they form a graded algebra, so-called the $G^2SU(2)$ algebra. We then introduce "super" configuration space variables associated with the graded group and rewrite the canonical constraints in a simple form in terms of these variables.

Firstly we present the chiral Lagrangian of $N = 2$ SUGRA constructed in [10]. The independent variables are a tetrad e^i_μ, two (Majorana) Rarita-Schwinger fields $\psi^{(I)}_\mu$, a Maxwell field A_μ and a self-dual connection $A^{(+)}_{ij\mu}$ which satisfies $(1/2)\epsilon_{ij}{}^{kl}A^{(+)}_{kl\mu} = iA^{(+)}_{ij\mu}$. [2] The $N = 2$ chiral Lagrangian density in terms of these variables is written in the following first-order, global $O(2)$ invariant form as

$$\begin{aligned}\mathcal{L}^{(+)}_{N=2} &= -\frac{i}{2}\epsilon^{\mu\nu\rho\sigma}e^i_\mu e^j_\nu R^{(+)}_{ij\rho\sigma} - \epsilon^{\mu\nu\rho\sigma}\overline{\psi}^{(I)}_{R\mu}\gamma_\rho D^{(+)}_\sigma \psi^{(I)}_{R\nu} - \frac{e}{2}(F^{(-)}_{\mu\nu})^2 \\ &+ \frac{1}{4\sqrt{2}}\overline{\psi}^{(I)}_\mu\{e(F^{\mu\nu} + \hat{F}^{\mu\nu}) + i\gamma_5(\tilde{F}^{\mu\nu} + \tilde{\hat{F}}^{\mu\nu})\}\psi^{(J)}_\nu\epsilon^{(I)(J)} \\ &+ \frac{i}{8}\epsilon^{\mu\nu\rho\sigma}(\overline{\psi}^{(I)}_{L\mu}\psi^{(J)}_{R\nu})\overline{\psi}^{(K)}_{R\rho}\psi^{(L)}_{L\sigma}\epsilon^{(I)(J)}\epsilon^{(K)(L)},\end{aligned} \tag{1}$$

where e denotes $\det(e^i_\mu)$, $\epsilon^{(I)(J)} = -\epsilon^{(J)(I)}$ and $F^{(-)\mu\nu} := (1/2)(F^{\mu\nu} - ie^{-1}\tilde{F}^{\mu\nu})$ with $\tilde{F}^{\mu\nu} = (1/2)\epsilon^{\mu\nu\rho\sigma}F_{\rho\sigma}$. The covariant derivative $D^{(+)}_\mu$ and the curvature $R^{(+)ij}{}_{\mu\nu}$ are

$$\begin{aligned}D^{(+)}_\mu &:= \partial_\mu + \frac{i}{2}A^{(+)}_{ij\mu}S^{ij}, \\ R^{(+)ij}{}_{\mu\nu} &:= 2(\partial_{[\mu}A^{(+)ij}{}_{\nu]} + A^{(+)i}{}_{k[\mu}A^{(+)kj}{}_{\nu]}),\end{aligned} \tag{2}$$

while $\hat{F}_{\mu\nu}$ in the second line of (1) is defined as

$$\hat{F}_{\mu\nu} := F_{\mu\nu} - \frac{1}{\sqrt{2}}\overline{\psi}^{(I)}_\mu\psi^{(J)}_\nu\epsilon^{(I)(J)}. \tag{3}$$

Let us briefly explain about the role of the last four-fermion contact term in (1). This term is pure imaginary but it is needed to reproduce the Lagrangian of the usual $N = 2$ SUGRA in the second-order formalism: Indeed, if we take the self-dual connection

[2] Greek letters $\mu, \nu, \ldots$, are spacetime indices, Lattin letters $i, j, \ldots$, are local Lorentz indices and $(I), (J), \ldots = 1, 2$, denote $O(2)$ internal indices. We take the Minkowski metric $\eta_{ij} = \mathrm{diag}(-1, +1, +1, +1)$ and the totally antisymmetric tensor ϵ_{ijkl} is normalized as $\epsilon_{0123} = +1$. We define $\epsilon_{\mu\nu\rho\sigma}$ and $\epsilon^{\mu\nu\rho\sigma}$ as tensor densities which take values of $+1$ or -1.

$A^{(+)}_{ij\mu}$ in $\mathcal{L}^{(+)}_{N=2}$ as the function of the tetrad and spin-3/2 fields by solving the equation $\delta\mathcal{L}^{(+)}_{N=2}/\delta A^{(+)} = 0$, then the torsion part of the chiral Lagrangian density in the second-order formalism, which we denoted by $\mathcal{L}^{(+)}_{N=2}$[second order], involves a four-fermion contact term

$$\frac{i}{8}\epsilon^{\mu\nu\rho\sigma}T_{\lambda\mu\nu}T^{\lambda}{}_{\rho\sigma} = -\frac{i}{16}\epsilon^{\mu\nu\rho\sigma}(\overline{\psi}^{(I)}_{R\mu}\gamma_\lambda\psi^{(K)}_{R\nu})\overline{\psi}^{(J)}_{R\rho}\gamma^\lambda\psi^{(L)}_{R\sigma}\epsilon^{(I)(J)}\epsilon^{(K)(L)}, \tag{4}$$

since the torsion tensor is defined by $T^i{}_{\mu\nu} = -2D_{[\mu}e^i_{\nu]}$ with $D_\mu e^i_\nu = \partial_\mu e^i_\nu + A^i{}_{j\mu}e^j_\nu$. However, since the last term in (1) can be rewritten as

$$\begin{aligned}&\frac{i}{8}\epsilon^{\mu\nu\rho\sigma}(\overline{\psi}^{(I)}_{L\mu}\psi^{(J)}_{R\nu})\overline{\psi}^{(K)}_{R\rho}\psi^{(L)}_{L\sigma}\epsilon^{(I)(J)}\epsilon^{(K)(L)}\\ &= \frac{i}{16}\epsilon^{\mu\nu\rho\sigma}(\overline{\psi}^{(I)}_{R\mu}\gamma_\lambda\psi^{(K)}_{R\nu})\overline{\psi}^{(J)}_{R\rho}\gamma^\lambda\psi^{(L)}_{R\sigma}\epsilon^{(I)(J)}\epsilon^{(K)(L)}\end{aligned} \tag{5}$$

by using a Fierz transformation, this exactly cancels with the term of (4). Therefore the $\mathcal{L}^{(+)}_{N=2}$[second order] of $N = 2$ chiral SUGRA is reduced to that of the usual one up to imaginary boundary terms; namely, we have

$$\begin{aligned}\mathcal{L}^{(+)}_{N=2}[\text{second order}] = \;& \mathcal{L}_{N=2\text{ usual SUGRA}}[\text{second order}]\\ & -\frac{1}{4}\partial_\mu\{\epsilon^{\mu\nu\rho\sigma}(\overline{\psi}^I_\nu\gamma_\rho\psi^I_\sigma + 2iA_\nu\partial_\rho A_\sigma)\}.\end{aligned} \tag{6}$$

Note that the boundary term with respect to the Maxwell field A_μ is adopted in (6).

The global $O(2)$ invariance of (1) can be gauged by introducing the minimal coupling for $\psi^{(I)}_\mu$ and A_μ, which automatically requires a spin-3/2 mass-like term and a cosmological term in the Lagrangian [11]. These additional terms are written as

$$\begin{aligned}\mathcal{L}_{\text{cosm.}} = \;& \lambda\epsilon^{\mu\nu\rho\sigma}\overline{\psi}^{(I)}_{R\mu}\gamma_\rho\psi^{(J)}_{R\nu}\,A_\sigma\epsilon^{(I)(J)}\\ & -\sqrt{2}i\lambda e\,\overline{\psi}^{(I)}_\mu S^{\mu\nu}\psi^{(I)}_\nu + 6\lambda^2 e\end{aligned} \tag{7}$$

with the gauge coupling constant λ, in which the cosmological constant Λ is related to λ as $\Lambda = -6\lambda^2$. The chiral Lagrangian, $\mathcal{L}^{(+)}_{N=2} + \mathcal{L}_{\text{cosm.}}$ of (1) and (7), is invariant under the SUSY transformation of the usual "gauged" $N = 2$ SUGRA [11] in the second-order formalism because of Eq.(6). On the other hand, the first-order (i.e.,"off-shell") SUSY invariance of the chiral Lagrangian may be realized by introducing the right- and left-handed SUSY transformations as in the case of $N = 1$ chiral SUGRA [2, 12].

Starting with the chiral Lagrangian,

$$\mathcal{L}^{(+)} := \mathcal{L}^{(+)}_{N=2} + \mathcal{L}_{\text{cosm.}}, \tag{8}$$

we derive the canonical formulation of $N = 2$ SUGRA in terms of the Ashtekar variable by means of the (3+1) decomposition of spacetime. For this purpose we assume that the

topology of spacetime M is $\Sigma \times R$ for some three-manifold Σ so that a time coordinate function t is defined on M. Then the time component of the tetrad can be defined as [3]

$$e_i^i = Nn^i + N^a e_a^i. \tag{9}$$

Here n^i is the timelike unit vector orthogonal to e_{ia}, i.e. $n^i e_{ia} = 0$ and $n^i n_i = -1$, while N and N^a denote the lapse function and the shift vector, respectively. Furthermore, we give a restriction on the tetrad with the choice $n_i = (-1, 0, 0, 0)$ in order to simplify the Legendre transform of (8). Once this choice is made, e_{Ia} becomes tangent to the constant t surfaces Σ and $e_{0a} = 0$. Therefore we change the notation e_{Ia} to E_{Ia} below. We also take the spatial restriction of the totally antisymmetric tensor $\epsilon^{\mu\nu\rho\sigma}$ as $\epsilon^{abc} := \epsilon_t{}^{abc}$, while $\epsilon^{IJK} := \epsilon_0{}^{IJK}$.

Under the above gauge condition the tetrad, the (3+1) decomposition of Eq.(8) yields the kinetic terms in the two-component spinor notation,

$$\tilde{E}_I^a \dot{\mathcal{A}}^I{}_a + \tilde{\pi}^{(I)}{}_A{}^a \dot{\psi}^{(I)A}{}_a + {}^+\tilde{\pi}^a \dot{A}_a, \tag{10}$$

where $\mathcal{A}^I{}_a := -2A^{(+)}{}_0{}^I{}_a$ and we define $\tilde{\pi}^{(I)}{}_A{}^a$ and ${}^+\tilde{\pi}^a$ as

$$\begin{aligned} \tilde{\pi}^{(I)}{}_A{}^a &:= \frac{\delta \mathcal{L}}{\delta \dot{\psi}^{(I)A}{}_a} = \sqrt{2} i\, \epsilon^{abc} E_c^I \overline{\psi}^{(I)A'}{}_b \sigma_{IAA'}, \\ {}^+\tilde{\pi}^a &:= \tilde{\pi}^a + i\, \tilde{B}^a \end{aligned} \tag{11}$$

with $\tilde{\pi}^a$ and $\tilde{B}^a$ being defined by

$$\begin{aligned} \tilde{\pi}^a &:= \frac{\delta \mathcal{L}}{\delta \dot{A}_a} \\ &= \frac{e}{2N^2} q^{ab} \{ 2\,(F_{tb} - N^d F_{db}) \\ &\quad - \sqrt{2}\,(\overline{\psi}_t^{(I)} \psi_b^{(J)} - N^d \overline{\psi}_d^{(I)} \psi_b^{(J)}) \epsilon^{(I)(J)} \} \\ &\quad - \frac{i}{2\sqrt{2}}\, \epsilon^{abc} \overline{\psi}_b^{(I)} \gamma_5 \psi_c^{(J)} \epsilon^{(I)(J)}, \\ \tilde{B}^a &= \frac{1}{2}\, \epsilon^{abc} F_{bc}. \end{aligned} \tag{12}$$

The following constraints are also obtained in the canonical formulation; namely, in particular, the Gauss, $U(1)$ gauge, right- and left-handed SUSY constraints are

$$\mathcal{G}_I = \mathcal{D}_a \tilde{E}_I^a + \frac{i}{\sqrt{2}}\, \tilde{\pi}^{(I)}{}_A{}^a \sigma_I{}^A{}_B \psi^{(I)B}{}_a$$

[3] Latin letters $a, b, \cdots$ are the spatial part of the spacetime indices $\mu, \nu, \cdots$, and capital letters $I, J, \cdots$ denote the spatial part of the local Lorentz indices $i, j, \cdots$.

$$
\begin{aligned}
g = \;& \partial_a{}^{+}\tilde{\pi}^a - \lambda\ \psi^{(I)A}{}_a\tilde{\pi}^{(J)}{}_A{}^a\epsilon^{(I)(J)} \\
{}^{R}\mathcal{S}_A^{(I)} = \;& \mathcal{D}_a\pi^{(I)}{}_A{}^a - \frac{1}{\sqrt{2}}\,{}^{+}\tilde{\pi}^a\ \psi^{(J)B}{}_a\epsilon_{AB}\epsilon^{(I)(J)} \\
{}^{L}\mathcal{S}_A^{(I)} = \;& \sqrt{2}\ \tilde{E}_I^a\tilde{E}_J^b(\sigma^I\sigma^J)_A{}^B\Bigg[\,2(\mathcal{D}_{[a}\psi^{(I)}_{|B|b]} - \lambda\ A_{[a}\psi^{(J)}_{|B|b]}\epsilon^{(I)(J)}) \\
& + \frac{i}{\sqrt{2}}\lambda\ \epsilon_{abc}\tilde{\pi}^{(I)}{}_B{}^c\Bigg] \\
& - \frac{i}{2}E^{-2}\epsilon_{def}\epsilon_{agh}(\sigma^I\sigma^J\sigma^K\sigma^L)_A{}^B\epsilon^{(I)(J)}\tilde{E}_I^e\tilde{E}_J^f\tilde{E}_K^g\tilde{E}_L^h\tilde{\pi}^{(J)}{}_B{}^d \\
& \left[\epsilon^{abc}\left\{F_{bc} + \frac{\kappa}{\sqrt{2}}\,\epsilon_{CD}(\psi^{(K)C}{}_b\psi^{(L)D}{}_c)\epsilon^{(K)(L)}\right\} + i\ {}^{+}\tilde{\pi}^a\right]
\end{aligned}
\tag{13}
$$

with

$$
\begin{aligned}
\mathcal{D}_a\tilde{E}_I^a &:= \partial\tilde{E}_I^a + i\epsilon_{IJK}\mathcal{A}^J{}_a\tilde{E}^{Ka}, \\
\mathcal{D}_a\pi^{(I)}{}_A{}^a &:= \partial\pi^{(I)}{}_A{}^a - \frac{i}{\sqrt{2}}\mathcal{A}_A{}^B{}_a\pi^{(I)}{}_B{}^a.
\end{aligned}
\tag{14}
$$

Note that these canonical constraints up to the Gauss constraint have the slightly different forms from the results of the $N = 2$ 2-form SUGRA [6, 7].

Let us now calculate the algebra of the Gauss, $U(1)$ gauge and right-handed SUSY constraints, and show that they form a graded Lie algbra by using the Poisson brackets among the canonical variables,

$$
\begin{aligned}
&\{\mathcal{A}^I{}_a(x), \tilde{E}_J{}^b(y)\} = \delta^I_J\delta^b_a\delta^3(x-y), \\
&\{\psi^{(I)A}{}_a(x), \tilde{\pi}^{(J)}{}_B{}^b(y)\} = \delta^{(I)(J)}\delta^A_B\delta^b_a\delta^3(x-y), \\
&\{A_a(x), {}^{+}\pi^b(y)\} = \delta^b_a\delta^3(x-y).
\end{aligned}
\tag{15}
$$

Indeed, if we define the smearing functions,

$$
\begin{aligned}
\mathcal{G}_I[\Lambda^I] &:= \int_\Sigma d^3x\ \Lambda^I\mathcal{G}_I, \\
g[a] &:= \int_\Sigma d^3x\ a\ g, \\
{}^{R}\mathcal{S}_A^{(I)}[\xi^{(I)A}] &:= \int_\Sigma d^3x\ \xi^{(I)A}\ {}^{R}\mathcal{S}_A^{(I)}
\end{aligned}
\tag{16}
$$

for convenience of the calculation, the Poisson brackets of $(\mathcal{G}_I, g, {}^{R}\mathcal{S}_A^{(I)})$ are obtained as

$$
\begin{aligned}
&\{\mathcal{G}_I[\Lambda^I],\ \mathcal{G}_J[\Gamma^J]\} = \mathcal{G}_I[\Lambda'^I], \\
&\{\mathcal{G}_I[\Lambda^I],\ g[a]\} = 0 = \{g[a],\ g[b]\}, \\
&\{\mathcal{G}_I[\Lambda^I],\ {}^{R}\mathcal{S}_A^{(I)}[\xi^{(I)A}]\} = {}^{R}\mathcal{S}_A^{(I)}[\xi'^{(I)A}],
\end{aligned}
$$

$$\{g[a],\ {}^{R}\mathcal{S}_A^{(I)}[\xi^{(I)A}]\} = \lambda\ {}^{R}\mathcal{S}_A^{(I)}[\xi''^{(I)A}],$$
$$\{{}^{R}\mathcal{S}_A^{(I)}[\xi^{(I)A}],\ {}^{R}\mathcal{S}_B^{(J)}[\eta^{(J)B}]\} = \lambda\ \mathcal{G}_I[\Lambda''^I] + g[a'] \tag{17}$$

with the parameters, $\Lambda'^I, \Lambda''^I, \xi'^{(I)A}, \xi''^{(I)A}$ and a', being defined as

$$\Lambda'^I := i\ \epsilon^{IJK}\Lambda_J\Gamma_K,$$
$$\Lambda''^I := 2i\ \xi^{(I)A}\eta^{(J)B}\sigma^I{}_{AB}\delta^{(I)(J)},$$
$$\xi'^{(I)A} := \frac{i}{\sqrt{2}}\ \Lambda^I\xi^{(I)B}\sigma_{IB}{}^A,$$
$$\xi''^{(I)A} := -a\ \xi^{(J)A}\epsilon^{(I)(J)},$$
$$a' := \frac{1}{\sqrt{2}}\ \xi^{(I)A}\eta^{(J)B}\epsilon_{AB}\epsilon^{(I)(J)}. \tag{18}$$

These algebra of (17) is just the graded Lie algebra associated with the $G^2SU(2)$ group as stated in [8].

Based on (17), we introduce graded variables $(\mathcal{A}_a, \tilde{\mathcal{E}}^a)$ of $G^2SU(2)$ defined by

$$\mathcal{A}_a := \mathcal{A}^{\dot{i}}{}_a J_{\dot{i}} = \mathcal{A}^I{}_a J_I + \psi^{(I)A}{}_a J_A^{(I)} + A_a J, \tag{19}$$
$$\tilde{\mathcal{E}}^a := \tilde{\mathcal{E}}_{\dot{i}}{}^a J^{\dot{i}} = \tilde{E}_I{}^a J^I - \frac{1}{2\sqrt{2}\lambda}\tilde{\pi}^{(I)}{}_A{}^a J^{(I)A} + \frac{1}{4\lambda^2}{}^{+}\tilde{\pi}^a J. \tag{20}$$

Here $(J_I, J_A^{(I)}, J)$ stand for the generators which correspond to the constraints $(\mathcal{G}_I, {}^{R}\mathcal{S}_A^{(I)}, J)$ satisfying the algebra of (17), and their $G^2SU(2)$-invariant bilinear forms are expressed by using the supertrace, which is denoted by "STr", as

$$\mathrm{STr}(J_IJ_J) = \delta_{IJ},\ \ \mathrm{STr}(J_A^{(I)}J_B^{(J)}) = 2\sqrt{2}\lambda\epsilon_{AB}\delta^{(I)(J)},\ \ \mathrm{STr}(JJ) = 4\lambda^2,$$
$$\mathrm{STr}(J_IJ_A^{(I)}) = 0 = \mathrm{STr}(J_IJ) = \mathrm{STr}(J_A^{(I)}J). \tag{21}$$

By virtue of the definition for the graded variables, (19) and (20), the Gauss, $U(1)$ gauge and right-handed SUSY constraints are written as a $G^2SU(2)$ Gauss law,

$$\mathcal{D}_a\tilde{\mathcal{E}}^a = \partial\tilde{\mathcal{E}}^a + [\mathcal{A}_a, \tilde{\mathcal{E}}^a\} = 0. \tag{22}$$

The left-handed SUSY constraint, on the other hand, cannot be written as a $G^2SU(2)$ invariant form, but can be expressed by using the graded variables, $\mathcal{A}^{\dot{i}}{}_a = (\mathcal{A}^I{}_a, \psi^{(I)A}{}_a, A_a)$ and $\tilde{\mathcal{E}}_{\dot{i}}{}^a = (\tilde{E}_I{}^a, \tilde{\pi}^{(I)}{}_A{}^a, {}^{+}\tilde{\pi}^a)$ as in the case of $N = 1$ theory.

An exact state that solves all the constraint equations can be easily studied because the Gauss, $U(1)$ gauge and right-handed SUSY constraints particularly take the simple form as $G^2SU(2)$ Gauss law as explained above. The result of the solution coincides with

the $N = 2$ supersymmetric-extended Chern-Simons solution obtained in [6, 7, 8]. The extension to higher N supergravity is now investigated.

Acknowledgments

I am grateful to Professor T. Shirafuji for useful discussions. I also would like to thank the members of Physics Department at Saitama University for discussions and encouragements. This work was supported by the High-Tech Research Center of Saitama Institute of Technology.

References

[1] A. Ashtekar, *Phys. Rev. Lett.* **57**, 2244 (1986); *Phys. Rev.* D **36**, 1587 (1987).

[2] T. Jacobson, *Class. Quantum Grav.* **5**, 923 (1988).

[3] D. Armand-Ugon, R. Gambini, O. Obregón and J. Pullin, *Nucl. Phys.* B **460**, 615 (1996).

[4] A. Pais and V. Rittenberg, J. Math. Phys. **16**, 2062 (1975).

[5] Y. Ling and L. Smolin, Report No. hep-th/9904016.

[6] T. Sano, Report No. hep-th/9211103.

[7] H. Kunitomo and T. Sano, *Int. J. Mod. Phys.* **D** 1, 559 (1993).

[8] K. Ezawa, *Prog. Theor. Phys.* **114**, 31 (1996).

[9] R. Capovilla, J. Dell, T. Jacobson and L. Mason, *Class. Quantum Grav.* **8**, 41 (1991).

[10] M. Tsuda and T. Shirafuji, *Class. Quantum Grav.* **16**, 69 (1999).

[11] D. Z. Freedman and A. Das, *Nucl. Phys.* B **120**, 221 (1977).

[12] M. Tsuda and T. Shirafuji, *Phys. Rev.* D **54**, 2960 (1996).

Hyperbolic and asymptotically constrained systems in the Ashtekar formulation of general relativity

GEN YONEDA[†] and HISA-AKI SHINKAI[‡]

[†] *Dept. of Mathematical Science, Waseda University, Shinjuku, Tokyo 169-8555, Japan*
[‡] *Center for Gravitational Physics and Geometry, 104 Davey Lab., Department of Physics, The Pennsylvania State University, University Park, Pennsylvania 16802-6300, USA*

(December 22, 1999)

Abstract

Hyperbolic formulations of the equations of motion are essential technique for proving the well-posedness of the Cauchy problem of a system, and are also helpful for implementing stable long time evolution in numerical applications. We, here, present three kinds of hyperbolic systems in the Ashtekar formulation of general relativity for Lorentzian vacuum spacetime. We exhibit several (I) weakly hyperbolic, (II) diagonalizable hyperbolic, and (III) symmetric hyperbolic systems, with each their eigenvalues, and discuss how gauge conditions and reality conditions are constrained toward constructing a symmetric hyperbolic system. As an application of this formulation, we present a set of dynamical equations which forces the space-time to evolve to the manifold that satisfies the constraint equations or the reality conditions or both as the attractor against perturbative errors. The obtained systems may be useful for future numerical studies using Ashtekar's variables. Several current works are also described.

1 Introduction

1.1 Hyperbolic formulations in General Relativity

Developing hyperbolic formulations of the Einstein equation is growing into an important research areas in general relativity (see e.g. [1]). These formulations are used in the analytic proof of the existence, uniqueness and stability (well-posedness) of the solutions of the Einstein equation [2]. So far, several first order hyperbolic formulations have been proposed; some of them are flux conservative [3, 4], some of them are symmetrizable or symmetric hyperbolic systems [5, 6, 7, 8]. The recent interest in hyperbolic formulations arises from their application to numerical relativity. One of the most useful features is the existence of characteristic speeds in hyperbolic systems. We expect more stable evolutions and expect improved boundary conditions in their numerical simulation. Some numerical tests have been reported along this direction [9, 10]. It might be worth remarking that the standard Arnowitt-Deser-Misner (ADM) formulation cannot be a first-order hyperbolic form, since there are curvature terms in the r.h.s. of dynamical equations.

For the reader's convenience, we provide our definitions of hyperbolic systems here.

Definition 1 *We assume a certain set of (complex) variables u_α $(\alpha = 1, \cdots, n)$ forms a first-order (quasi-linear) partial differential equation system,*

$$\partial_t u_\alpha = J^{l\beta}{}_\alpha(u)\partial_l u_\beta + K_\alpha(u), \tag{1}$$

where J (the characteristic matrix) and K are functions of u but do not include any derivatives of u. We say that the system (1) is:

(I). **weakly hyperbolic**, *if all the eigenvalues of the characteristic matrix are real.*

(II). **diagonalizable hyperbolic**, *if the characteristic matrix is diagonalizable and has all real eigenvalues.*

(III). **symmetric hyperbolic**, *if the characteristic matrix is a Hermitian matrix.*

We treat $J^{l\beta}{}_\alpha$ as a $n \times n$ matrix when the l-index is fixed. We say λ^l is an eigenvalue of $J^{l\beta}{}_\alpha$ when the characteristic equation, $\det(J^{l\beta}{}_\alpha - \lambda^l \delta^\beta{}_\alpha) = 0$, is satisfied. The eigenvectors, p^α, are given by solving $J^{l\alpha}{}_\beta\, p^{l\beta} = \lambda^l p^{l\alpha}$.

These three classes have the relation (III) $\in$ (II) $\in$ (I). The symmetric hyperbolic system gives us the energy integral inequalities, which are the primary tools for studying well-posedness of the system. As was discussed

[†]Email: yoneda@mn.waseda.ac.jp
[‡]Email: shinkai@gravity.phys.psu.edu

by Geroch [11], most physical systems can be expressed as symmetric hyperbolic systems. In order to define the symmetric hyperbolic system, (III), we need to declare an inner product $\langle u|u\rangle$ to judge whether $J^{l\beta}{}_{\alpha}$ is Hermitian. In other words, we are required to define the way of lowering the index α of u^{α}. We say $J^{l\beta}{}_{\alpha}$ is Hermitian with respect to this index rule, when $J^{l}{}_{\beta\alpha} = \bar{J}^{l}{}_{\alpha\beta}$ for every l, where the overhead bar denotes complex conjugate.

For more concrete descriptions for each systems, please refer our paper [12].

1.2 Ashtekar's formulations of General Relativity

Ashtekar's formulation of general relativity [13] has many advantages. By using his special pair of variables, the constraint equations which appear in the theory become low-order polynomials, and the theory has the correct form for gauge theoretical interpretation. These features suggest the possibility for developing a nonperturbative quantum description of gravity. The detail equations are reviewed in Sec.2.

From the point of hyperbolicity of the system, Ashtekar's original set of equations of motion already forms a weakly hyperbolic system, as we will show in §3. A symmetric hyperbolic formulation of Ashtekar's variables was first developed by Iriondo, Leguizamón and Reula (ILR) [14]. Unfortunately, in their first short paper [14], they did not discuss the consistency of their system with the reality conditions, which are crucial in the study of the Lorentzian dynamics using the Ashtekar variables. We considered this point in [15], and found that there are strict reality constraints (alternatively they can be interpreted as gauge conditions). There are also another debates between ILR's system and ours: on the definition of the symmetric hyperbolic systems and on the treatment of the triad lapse freedom. These are described in [16] and [12].

As can been seen above, there is always a problem of reality conditions in applying Ashtekar formulation to classical dynamics. Fortunately, it was shown that the secondary condition of the reality of the metric will be automatically preserved during the evolution, if the initial data satisfies both primary and secondary metric reality conditions [17]. If we impose the reality condition on the triad (triad reality condition), then we have additional conditions that can be controlled by a part of a gauge variable, triad lapse $\mathcal{A}_0^a$ (defined later) [18]. Therefore the reality conditions are controllable, and we think that applying the Ashtekar formulation to dynamics is quite attractive, and broadens our possibilities to attack dynamical issues. It is, however, also the case that preliminary numerical simulations of the spacetime using Ashtekar's variables show that the system will not normally recover real-valued spacetime if we relax the metric reality condition locally during the evolution [19]. Therefore, we desire a system that is robust for controlling both the reality conditions and the constraint equations for stable long-term integration. We present a new dynamical system to solve these problems in §4.

1.3 Short description of this report

In this *report*, we summarize our recent works [15, 12, 20], and comments on our current directions.

The first main results obtained are the several levels of hyperbolic formulations of Ashtekar's system. There are two reasons to consider (I) weakly and (II) diagonalizable hyperbolic systems, rather than (III) symmetric hyperbolic system. First, as we found in [15], the symmetric hyperbolic system we obtained has strict restrictions on the gauge conditions, while the original Ashtekar equations constitute a weakly hyperbolic system. We are interested in these differences, and show how additional constraints appear during the steps toward constructing a symmetric hyperbolic system. Second, many numerical experiments show that there are several advantages if we apply a certain form of hyperbolic formulation. Therefore, we think that presenting these three hyperbolic systems is valuable to stimulate the studies in this field. To aid in possibly applying these systems in numerical applications, we present characteristic speeds of each system we construct.

The second result is a proposal of a new dynamical systems, which is robust for the perturbative error for violations of the constraint equations and the reality conditions. This is an extension of the idea by Brodbeck, Frittelli, Hübner and Reula (BFHR) [21] who constructed an asymptotically *stable* system (i.e., it approaches to the constraint surface) for the Einstein equation. (A similar effort can be found also in [22].) BFHR introduced additional dynamical variables, λs, which obey dissipative dynamical equations and which evolve the spacetime to the constraint surface of general relativity as the attractor in the extended spacetime.

The layout of this paper is as follows: In §2, we briefly review Ashtekar's formulation and the way of handling reality conditions. In §3, we show several classes of hyperbolic system, including the construction of symmetric hyperbolic system. In §4, we show a dynamical system which asymptotically evolves to constrained manifold. Summary and discussion are in §5.

In this report, we discuss only the case of a vacuum spacetime, but including matter is straightforward.

2 Ashtekar formulation

We start by giving a brief review of the Ashtekar formulation and the way of handling reality conditions.

2.1 Variables and Equations

The key feature of Ashtekar's formulation of general relativity [13] is the introduction of a self-dual connection as one of the basic dynamical variables. Let us write the metric $g_{\mu\nu}$ using the tetrad E^I_μ as $g_{\mu\nu} = E^I_\mu E^J_\nu \eta_{IJ}$ [1]. Define its inverse, E^μ_I, by $E^\mu_I := E^J_\nu g^{\mu\nu}\eta_{IJ}$ and we impose $E^0_a = 0$ as the gauge condition. We define SO(3,C) self-dual and anti self-dual connections ${}^\pm\mathcal{A}^a_\mu := \omega^{0a}_\mu \mp (i/2)\epsilon^a{}_{bc}\omega^{bc}_\mu$, where ω^{IJ}_μ is a spin connection 1-form (Ricci connection), $\omega^{IJ}_\mu := E^{I\nu}\nabla_\mu E^J_\nu$. Ashtekar's plan is to use only the self-dual part of the connection ${}^+\mathcal{A}^a_\mu$ and to use its spatial part ${}^+\mathcal{A}^a_i$ as a dynamical variable. Hereafter, we simply denote ${}^+\mathcal{A}^a_\mu$ as $\mathcal{A}^a_\mu$.

The lapse function, N, and shift vector, N^i, both of which we treat as real-valued functions, are expressed as $E^\mu_0 = (1/N, -N^i/N)$. This allows us to think of E^μ_0 as a normal vector field to Σ spanned by the condition $t = x^0$ =const., which plays the same role as that of ADM formulation. Ashtekar treated the set $(\tilde{E}^i_a, \mathcal{A}^a_i)$ as basic dynamical variables, where $\tilde{E}^i_a$ is an inverse of the densitized triad defined by $\tilde{E}^i_a := eE^i_a$, where $e := \det E^a_i$ is a density. This pair forms the canonical set.

In the case of pure gravitational spacetime, the Hilbert action takes the form

$$S = \int d^4x[(\partial_t\mathcal{A}^a_i)\tilde{E}^i_a + (i/2)\underset{\sim}{N}\tilde{E}^i_a\tilde{E}^j_b F^c_{ij}\epsilon^{ab}{}_c - e^2\Lambda\underset{\sim}{N} - N^i F^a_{ij}\tilde{E}^j_a + \mathcal{A}^a_0\mathcal{D}_i\tilde{E}^i_a], \tag{2}$$

where $\underset{\sim}{N} := e^{-1}N$, $F^a_{\mu\nu} := 2\partial_{[\mu}\mathcal{A}^a_{\nu]} - i\epsilon^a{}_{bc}\mathcal{A}^b_\mu\mathcal{A}^c_\nu$ is the curvature 2-form, Λ is the cosmological constant, $\mathcal{D}_i\tilde{E}^j_a := \partial_i\tilde{E}^j_a - i\epsilon_{ab}{}^c\mathcal{A}^b_i\tilde{E}^j_c$, and $e^2 = \det\tilde{E}^i_a = (\det E^a_i)^2$ is defined to be $\det\tilde{E}^i_a = (1/6)\epsilon^{abc}\underset{\sim}{\epsilon}_{ijk}\tilde{E}^i_a\tilde{E}^j_b\tilde{E}^k_c$, where $\epsilon_{ijk} := \epsilon_{abc}E^a_i E^b_j E^c_k$ and $\underset{\sim}{\epsilon}_{ijk} := e^{-1}\epsilon_{ijk}$ [2].

Varying the action with respect to the non-dynamical variables $\underset{\sim}{N}$, N^i and $\mathcal{A}^a_0$ yields the constraint equations,

$$\mathcal{C}_H := (i/2)\epsilon^{ab}{}_c\tilde{E}^i_a\tilde{E}^j_b F^c_{ij} - \Lambda\det\tilde{E} \approx 0, \tag{3}$$

$$\mathcal{C}_{Mi} := -F^a_{ij}\tilde{E}^j_a \approx 0, \tag{4}$$

$$\mathcal{C}_{Ga} := \mathcal{D}_i\tilde{E}^i_a \approx 0. \tag{5}$$

The equations of motion for the dynamical variables ($\tilde{E}^i_a$ and $\mathcal{A}^a_i$) are

$$\partial_t\tilde{E}^i_a = -i\mathcal{D}_j(\epsilon^{cb}{}_a\underset{\sim}{N}\tilde{E}^j_c\tilde{E}^i_b) + 2\mathcal{D}_j(N^{[j}\tilde{E}^{i]}_a) + i\mathcal{A}^b_0\epsilon_{ab}{}^c\tilde{E}^i_c, \tag{6}$$

$$\partial_t\mathcal{A}^a_i = -i\epsilon^{ab}{}_c\underset{\sim}{N}\tilde{E}^j_b F^c_{ij} + N^j F^a_{ji} + \mathcal{D}_i\mathcal{A}^a_0 + \Lambda\underset{\sim}{N}\tilde{E}^a_i, \tag{7}$$

where $\mathcal{D}_j X^{ij}_a := \partial_j X^{ij}_a - i\epsilon_{ab}{}^c\mathcal{A}^b_j X^{ij}_c$, for $X^{ij}_a + X^{ji}_a = 0$.

2.2 Reality conditions

In order to construct the metric from the variables $(\tilde{E}^i_a, \mathcal{A}^a_i, \underset{\sim}{N}, N^i)$, we first prepare the tetrad E^μ_I as $E^\mu_0 = (1/e\underset{\sim}{N}, -N^i/e\underset{\sim}{N})$ and $E^\mu_a = (0, \tilde{E}^i_a/e)$. Using them, we obtain the metric $g^{\mu\nu}$ such that $g^{\mu\nu} := E^\mu_I E^\nu_J \eta^{IJ}$.

This metric, in general, is not real-valued in the Ashtekar formulation. To ensure that the metric is real-valued, we need to impose real lapse and shift vectors together with two *metric reality* conditions;

$$\mathrm{Im}(\tilde{E}^i_a\tilde{E}^{ja}) = 0, \tag{8}$$

$$W^{ij} := \mathrm{Re}(\epsilon^{abc}\tilde{E}^k_a\tilde{E}^{(i}_b\mathcal{D}_k\tilde{E}^{j)}_c) = 0, \tag{9}$$

where the latter comes from the secondary condition of reality of the metric $\mathrm{Im}\{\partial_t(\tilde{E}^i_a\tilde{E}^{ja})\} = 0$ [17], and we assume $\det\tilde{E} > 0$ (see [18]).

For later convenience, we also prepare stronger reality conditions, *triad reality* conditions. The primary and secondary conditions are written respectively as

$$U^i_a := \mathrm{Im}(\tilde{E}^i_a) = 0, \tag{10}$$

$$\text{and } \mathrm{Im}(\partial_t\tilde{E}^i_a) = 0. \tag{11}$$

---

[1] We use $\mu,\nu = 0,\cdots,3$ and $i,j = 1,\cdots,3$ as spacetime indices, while $I,J = (0),\cdots,(3)$ and $a,b = (1),\cdots,(3)$ are $SO(1,3)$, $SO(3)$ indices respectively. We raise and lower $\mu,\nu,\cdots$ by $g^{\mu\nu}$ and $g_{\mu\nu}$ (the Lorentzian metric); $I,J,\cdots$ by $\eta^{IJ} = \mathrm{diag}(-1,1,1,1)$ and η_{IJ}; $i,j,\cdots$ by γ^{ij} and γ_{ij} (the 3-metric); $a,b,\cdots$ by δ^{ab} and δ_{ab}. We also use volume forms ϵ_{abc}: $\epsilon_{abc}\epsilon^{abc} = 3!$.

[2] When $(i,j,k) = (1,2,3)$, we have $\epsilon_{ijk} = e$, $\underset{\sim}{\epsilon}_{ijk} = 1$, $\epsilon^{ijk} = e^{-1}$, and $\tilde{\epsilon}^{ijk} = 1$.

Using the equations of motion of $\tilde{E}^i_a$, the gauge constraint (5), the metric reality conditions (8), (9) and the primary condition (10), we see that (11) is equivalent to [18]

$$\mathrm{Re}(\mathcal{A}^a_0) \;=\; \partial_i(\underset{\sim}{N})\tilde{E}^{ia} + (1/2e)E^b_i \underset{\sim}{N}\tilde{E}^{ja}\partial_j\tilde{E}^i_b + N^i\mathrm{Re}(\mathcal{A}^a_i), \tag{12}$$

or with un-densitized variables,

$$\mathrm{Re}(\mathcal{A}^a_0) = \partial_i(N)E^{ia} + N^i\,\mathrm{Re}(\mathcal{A}^a_i). \tag{13}$$

From this expression we see that the secondary triad reality condition restricts the three components of the "triad lapse" vector $\mathcal{A}^a_0$. Therefore (12) is not a restriction on the dynamical variables ($\tilde{E}^i_a$ and $\mathcal{A}^a_i$) but on the slicing, which we should impose on each hypersurface.

Throughout the discussion in this report, we assume that the initial data of $(\tilde{E}^i_a, \mathcal{A}^a_i)$ for evolution are solved so as to satisfy all three constraint equations and the metric reality condition (8) and (9). Practically, this is obtained, for example, by solving ADM constraints and by transforming a set of initial data to Ashtekar's notation.

3 Constructing hyperbolic systems

We have constructed several hyperbolic systems based on the Ashtekar formulation of general relativity, together with discussions of the required gauge conditions and reality conditions. We summarize their features in Table 1. For details, see [12].

system	Eqs of motion	reality condition	gauge conditions required	first order	all real eigenvals	diagonal-izable	sym. matrix
Ia	original	metric	-	yes	yes	no	no
Ib	original	triad	$\mathcal{A}^a_0 = \mathcal{A}^a_i N^i,\ \partial_i N = 0$	yes	yes	no	no
IIa	original	metric	$N^i \neq 0,\ \pm N\sqrt{\gamma^{ii}}\ (\gamma^{ii} \neq 0)$	yes	yes	yes	no
IIb	modified	metric	$\mathcal{A}^a_0 = \mathcal{A}^a_i N^i$	yes	yes	yes	no
IIIa	modified	triad	$\mathcal{A}^a_0 = \mathcal{A}^a_i N^i,\ \partial_i N = 0$	yes	yes	yes	yes

Table 1: List of obtained hyperbolic systems. The system *I*, *II* and *III* denote weakly hyperbolic, diagonalizable hyperbolic and symmetric hyperbolic systems, respectively.

For the later convenience, we show the explicit form of the system (*IIIa*). For a pair of $u^{(D)}_a = (\tilde{E}^i_a, \mathcal{A}^a_i)$, a symmetric hyperbolic system is obtained by modifying the right-hand-side of the dynamical equations using appropriate combinations of the constraint equations. The modification we made is to add terms to the original evolution equation (6) and (7) as:

$$\begin{aligned}
\text{adding term to } \partial_t\tilde{E}^i_a &= (N^i\delta_{ab} + i\underset{\sim}{N}\epsilon_{ab}{}^c\tilde{E}^i_c)\mathcal{C}^b_G, \\
\text{adding term to } \partial_t\mathcal{A}^a_i &= e^{-2}\underset{\sim}{N}\tilde{E}^a_i\mathcal{C}_H - ie^{-2}\underset{\sim}{N}\epsilon^{abc}\tilde{E}_{bi}\tilde{E}^j_c\mathcal{C}_{Mj}.
\end{aligned}$$

Then the principal part of evolution equation becomes

$$\partial_t\begin{pmatrix}\tilde{E}^i_a \\ \mathcal{A}^a_i\end{pmatrix} \;\cong\; \begin{pmatrix}A^{ia}{}_{bj} & 0 \\ 0 & D^{ia}{}_{bj}\end{pmatrix}\partial_t\begin{pmatrix}\tilde{E}^j_b \\ \mathcal{A}^b_j\end{pmatrix},$$

where $\cong$ means that we have extracted only the terms which appear in the principal part of the system, and the actual block diagonal components are

$$A^{iajb} = i\epsilon^{abc}\underset{\sim}{N}\tilde{E}^i_c\gamma^{ij} + N^i\gamma^{ij}\delta^{ab}, \tag{14}$$

$$\begin{aligned}
D^{iajb} &= i\underset{\sim}{N}(\epsilon^{abc}\tilde{E}^j_c\gamma^{ii} - \epsilon^{abc}\tilde{E}^i_c\gamma^{ji} \\
&\quad -e^{-2}\tilde{E}^{ia}\epsilon^{bcd}\tilde{E}^j_c\tilde{E}^i_d - e^{-2}\epsilon^{acd}\tilde{E}^i_d\tilde{E}^j_c\tilde{E}^{jb} + e^{-2}\epsilon^{acd}\tilde{E}^i_d\tilde{E}^j_c\tilde{E}^{ib}) + N^i\delta^{ab}\gamma^{ij}.
\end{aligned} \tag{15}$$

The inner product of a set of the variables is

$$\langle(\tilde{E}^i_a, \mathcal{A}^a_i)|(\tilde{E}^i_a, \mathcal{A}^a_i)\rangle = \gamma_{ij}\delta^{ab}\tilde{E}^i_a\tilde{E}^j_b + \gamma^{ij}\delta_{ab}\mathcal{A}^a_i\mathcal{A}^b_j. \tag{16}$$

We note that this symmetric hyperbolic system is obtained under the assumption of the triad reality condition, together with gauge conditions, $\mathcal{A}^a_0 = \mathcal{A}^a_i N^i$ and $\partial_i N = 0$.

4 Asymptotically constrained system

4.1 Propagations of constraints

Frittelli [23] showed that the propagation of the constraint equations in the standard ADM system of the Einstein equation forms a symmetric hyperbolic system. This fact suggests that a small violation of the constraint equations such as a truncation error in numerical simulation does not behave in a fatal way immediately.

Similarly, we can show the set of constraint equations (3), (4) and (5), forms a symmetric hyperbolic system in its evolution equations. The principal part of the time derivatives of $\mathcal{C}_H$, $\tilde{\mathcal{C}}_{M_i} := e\,\mathcal{C}_{M_i}$ and $\mathcal{C}_{G_a}$ become

$$\partial_t \begin{pmatrix} \mathcal{C}_H \\ \tilde{\mathcal{C}}_{M_i} \\ \mathcal{C}_{G_a} \end{pmatrix} \cong \begin{pmatrix} N^l & -e\underset{\sim}{N}\gamma^{li} & 0 \\ -e\underset{\sim}{N}\delta_i{}^l & N^l\delta_i{}^j + i\underset{\sim}{N}\tilde{e}^{lj}{}_i & 0 \\ 0 & 0 & i\underset{\sim}{N}\epsilon_a{}^{bc}\tilde{E}^l_c + N^l\delta_a{}^b \end{pmatrix} \partial_l \begin{pmatrix} \mathcal{C}_H \\ \tilde{\mathcal{C}}_{M_j} \\ \mathcal{C}_{G_b} \end{pmatrix}, \tag{17}$$

which forms a Hermitian matrix under the inner product rule of

$$\langle (\mathcal{C}_H, \mathcal{C}_{M_i}, \mathcal{C}_{G_a}) | (\mathcal{C}_H, \mathcal{C}_{M_i}, \mathcal{C}_{G_a}) \rangle := \mathcal{C}_H \bar{\mathcal{C}}_H + \gamma^{ij}\mathcal{C}_{M_i}\bar{\mathcal{C}}_{M_j} + \delta^{ab}\mathcal{C}_{G_a}\bar{\mathcal{C}}_{G_b}. \tag{18}$$

We note that non-principal parts of the dynamical equations of a set of $u_a^{(C)} = (\mathcal{C}_H, \tilde{\mathcal{C}}_M, \mathcal{C}_G)$ include the terms of $u_a^{(D)}$ and $u_a^{(C)}$. These facts suggest that all constraint equations have a well-posed feature. Iriondo *et al* [16] present a similar result, but our definition of the inner product does not include any coefficients. We also remark that all other occurrences of the inner products throughout this report also do not include any coefficients (i.e., obey the normal index notation). Thus we omit to express the inner product hereafter.

4.2 Asymptotically constrained system

Following the BFHR procedure [21], we next construct a dynamical system which evolves the spacetime to the constrained surface, $\mathcal{C}_H \approx \mathcal{C}_{M_i} \approx \mathcal{C}_{G_a} \approx 0$ as the attractor. We introduce new variables $(\lambda, \lambda_i, \lambda_a)$, as they obey the dissipative evolution equations

$$\partial_t \lambda = \alpha_1 \mathcal{C}_H - \beta_1 \lambda, \tag{19}$$

$$\partial_t \lambda_i = \alpha_2 \tilde{\mathcal{C}}_{M_i} - \beta_2 \lambda_i, \tag{20}$$

$$\partial_t \lambda_a = \alpha_3 \mathcal{C}_{G_a} - \beta_3 \lambda_a, \tag{21}$$

where $\alpha_i \neq 0$ (allowed to be complex numbers) and $\beta_i > 0$ (real numbers) are constants.

If we take $u_a^{(DL)} = (\tilde{E}^i_a, \mathcal{A}^a_i, \lambda, \lambda_i, \lambda_a)$ as a set of dynamical variables, then the principal part of (19)-(21) can be written as

$$\partial_t \lambda \cong -i\alpha_1 \epsilon^{bcd}\tilde{E}^j_c\tilde{E}^l_d(\partial_t \mathcal{A}^b_j), \tag{22}$$

$$\partial_t \lambda_i \cong \alpha_2[-e\delta^l_i\tilde{E}^j_b + e\delta^j_i\tilde{E}^l_b](\partial_t \mathcal{A}^b_j), \tag{23}$$

$$\partial_t \lambda_a \cong \alpha_3 \partial_l \tilde{E}^l_a. \tag{24}$$

The characteristic matrix of the system $u_a^{(DL)}$ does not form a Hermitian matrix. However, if we modify the right-hand-side of the evolution equation of $(\tilde{E}^i_a, \mathcal{A}^a_i)$, then the set becomes a symmetric hyperbolic system. This is done by adding $\bar{\alpha}_3\gamma^{il}(\partial_l\lambda_a)$ to the equation of $\partial_t\tilde{E}^i_a$, and by adding $i\bar{\alpha}_1\epsilon^a{}_c{}^d\tilde{E}^c_i\tilde{E}^l_d(\partial_l\lambda) + \bar{\alpha}_2(-e\gamma^{lm}\tilde{E}^a_i + e\delta^m_i\tilde{E}^{la})(\partial_l\lambda_m)$ to the equation of $\partial_t\mathcal{A}^a_i$. The final principal part, then, is written as

$$\partial_t \begin{pmatrix} \tilde{E}^i_a \\ \mathcal{A}^a_i \\ \lambda \\ \lambda_i \\ \lambda_a \end{pmatrix} \cong \begin{pmatrix} A^l{}_a{}^b{}_m & 0 & 0 & 0 & \bar{\alpha}_3\gamma^{il}\delta_a{}^b \\ 0 & D^{la}{}_{ib}{}^m & i\bar{\alpha}_1\epsilon^a{}_c{}^d\tilde{E}^c_i\tilde{E}^l_d & \bar{\alpha}_2 e(\delta^m_i\tilde{E}^{la} - \gamma^{lm}\tilde{E}^a_i) & 0 \\ 0 & -i\alpha_1\epsilon_b{}^{cd}\tilde{E}^m_c\tilde{E}^l_d & 0 & 0 & 0 \\ 0 & \alpha_2 e(\delta^m_i\tilde{E}^l_b - \delta^l_i\tilde{E}^m_b) & 0 & 0 & 0 \\ \alpha_3\delta_a{}^b\delta^l{}_m & 0 & 0 & 0 & 0 \end{pmatrix} \partial_l \begin{pmatrix} \tilde{E}^m_b \\ \mathcal{A}^b_m \\ \lambda \\ \lambda_m \\ \lambda_b \end{pmatrix}. \tag{25}$$

Clearly, the solution $(\tilde{E}^i_a, \mathcal{A}^a_i, \lambda, \lambda_i, \lambda_a) = (\tilde{E}^i_a, \mathcal{A}^a_i, 0, 0, 0)$ represents the original solution of the Ashtekar system. If the λs decay to zero after the evolution, then the solution also describes the original solution of the Ashtekar system in that stage. Since the dynamical system of $u_a^{(DL)}$, (25), constitutes a symmetric hyperbolic form, the solutions to the λ-system are unique. BFHR showed analytically that such a decay of λs can be seen for λs sufficiently close to zero with a choice of appropriate combination of αs and βs. and that statement can be also applied to our system. Therefore, the dynamical system, (25), is useful for stabilizing numerical simulations from the point that it recovers the constraint surface automatically.

4.3 Experiments of λ-system using linearized equations

In order to show the system (25) evolves into asymptotically constrained manifold, we here demonstrate the eigenvalues in the case of linearized system. This process is in accordance with the process of section 3 of [21].

The linearization, we mean, is obtained by truncating higher order deviations from the background (0th order) spacetime, $(\tilde{E}^i_a, \mathcal{A}^a_i) = (\delta^i_a, 0)$. That is, we expand

$$\begin{aligned} \tilde{E}^i_a &= \delta^i_a + {}^{(1)}\tilde{E}^i_a + {}^{(2)}\tilde{E}^i_a + \cdots \\ \mathcal{A}^a_i &= 0 + {}^{(1)}\mathcal{A}^a_i + {}^{(2)}\mathcal{A}^a_i + \cdots \end{aligned}$$

and take only up to the terms which has 1st order contributions. For example, 2-form curvature F^a_{ij} becomes $F^a_{ij} = \partial_i \mathcal{A}^a_j - \partial_j \mathcal{A}^a_i - i\epsilon^a{}_{bc}\mathcal{A}^b_i\mathcal{A}^c_j \simeq \partial_i({}^{(1)}\mathcal{A}^a_j) - \partial_j({}^{(1)}\mathcal{A}^a_i)$.

Applying this linearization procedure to the evolution equations of $\mathcal{C}_H, \hat{\mathcal{C}}_{Mi}, \mathcal{C}_{Ga}$ (and λs), we obtain

$$\partial_t \mathcal{C}_H = -\partial_k \hat{\mathcal{C}}_{Mk} + 2\tilde{\alpha}_1(\partial_k \partial_k \lambda), \tag{26}$$

$$\partial_t \hat{\mathcal{C}}_{Mi} = -\partial_i \mathcal{C}_H - i\epsilon^a{}_{ij}(\partial_a \hat{\mathcal{C}}_{Mj}) + \tilde{\alpha}_2(\partial_i \partial_l \lambda_l) + \tilde{\alpha}_2(\partial_l \partial_l \lambda_i), \tag{27}$$

$$\partial_t \mathcal{C}_{Ga} = -i\epsilon^{jb}{}_a \partial_j \hat{\mathcal{C}}_{Gb} - 2\hat{\mathcal{C}}_{Ma} + 2\tilde{\alpha}_1(\partial_a \lambda) - i\tilde{\alpha}_2 \epsilon^{alm}(\partial_l \lambda_m) + \tilde{\alpha}_3(\partial_i \partial_i \lambda_a). \tag{28}$$

Fourier transformation yields the equations for transformed variables $(\hat{\mathcal{C}}, \hat{\mathcal{C}}_{Mi}, \hat{\mathcal{C}}_{Ga}, \hat{\lambda}, \hat{\lambda}_i, \hat{\lambda}_a)$,

$$\partial_t \hat{\mathcal{C}}_H = -ik_m \hat{\mathcal{C}}_{Mm} - 2\tilde{\alpha}_1 k_m k^m \hat{\lambda}, \tag{29}$$

$$\partial_t \hat{\mathcal{C}}_{Mi} = -ik_i \hat{\mathcal{C}}_H + k_l \epsilon^l{}_i{}^m \hat{\mathcal{C}}_{Mm} - k_i k^m \tilde{\alpha}_2 \hat{\mathcal{C}}_{Mm} - \tilde{\alpha}_2 k_p k^p \delta^{mi} \hat{\lambda}_i, \tag{30}$$

$$\partial_t \hat{\mathcal{C}}_{Ga} = +\epsilon^{jb}{}_a k_j \hat{\mathcal{C}}_{Gb} - 2\hat{\mathcal{C}}_{Mi}\delta^i_a + 2i\tilde{\alpha}_1 k_a \hat{\lambda} + \tilde{\alpha}_2 \epsilon^{alm} k_l \hat{\lambda}_m - \tilde{\alpha}_3 k_m k^m \hat{\lambda}_a, \tag{31}$$

$$\partial_t \hat{\lambda} = \alpha_1 \hat{\mathcal{C}}_H - \beta_1 \hat{\lambda}, \tag{32}$$

$$\partial_t \hat{\lambda}_i = \alpha_2 \hat{\mathcal{C}}_{Mi} - \beta_2 \hat{\lambda}_i, \tag{33}$$

$$\partial_t \hat{\lambda}_a = \alpha_3 \hat{\mathcal{C}}_{Ga} - \beta_3 \hat{\lambda}_a. \tag{34}$$

We can show that the eigenvalues of this coefficient matrix are all negative (real part), for certain pairs of αs and βs. Such example can be obtained from a combination of $\alpha_1 = \alpha_2 = \alpha_3 = 1$, and $\beta_1 = \beta_2 = \beta_3 = 1$ in one dimensional situation $k_1 = 1, k_2 = k_3 = 0$. This suggests that λ-system, (25), works for decreasing the errors of constraints.

5 Future issues

Up to the previous sections, we summarized our recent works. These are, (1) efforts for constructing several levels of hyperbolic formulations of Ashtekar's dynamical equations [15, 12], and (2) a proposal of a new set of dynamical variables which force the spacetime evolution onto its constrained manifold asymptotically [20]. Here as the concluding remarks of this report, we mention some current status of our future works together with these backgrounds.

5.1 Relation between hyperbolic formulations and stabilities in numerics

First issue to concern is the relation between hyperbolic formulations and stabilities in numerical simulations. Up to a couple of years ago, ADM decomposition was taken as the standard formulation for numerical relativists. Difficulties in stable long-term evolutions were supposed to be solved by choosing proper gauge conditions and boundary conditions.

As we mentioned in the introduction, one of the alternative approaches to ADM is to formulate Einstein equations as they reveal hyperbolicity. Several numerical tests show nice properties than those by original ADM (e.g. tests [4] of Bona-Massó's flux conservative form [3], tests [10] of Choquet-Bruhat and York (95)'s symmetrizable form [7]). It is worth remarking the following two points here. (i) These numerical tests were performed using spherical symmetric spacetime. Therefore these advantages in full three-dimensional simulations are not yet confirmed. (ii) Both two hyperbolic formulations are not of first-order symmetric hyperbolic form. Therefore a question arises: Is a symmetric hyperbolic form necessary for numerical relativity?

The recent studies can be checked from another direction. There are also several papers which mention that the original ADM formulation is not the best one to be used. For example, a modified ADM formulation that was applied by Shibata and Nakamura (SN) [24] was shown to give us stable time evolutions than those of the original ADM [25]. The propagation of the original ADM constraint equations obeys well-posed behavior [23] (and this

fact can be applied also to SN's modified version), but dynamical equations of both ADM and ADM-SN are not a first-order hyperbolic formulation. Therefore another question arises: Will hyperbolic formulations really help for numerical relativity?

Alcubierre *et al* [26] analyzed eigenvalues of both ADM and ADM-SN equations of their linearized version, and found that ADM-SN does not have zero-eigenvalues in its characteristic matrix. They conjectured that non-zero eigenvalues in the evolution system contribute stable long-term numerical evolution. This, we think, implies a certain kind of hyperbolicity as a threshold for stable simulations.

In order to answer these questions, we are now preparing numerical tests using our three-levels of hyperbolic equations based on the Ashtekar formulation. Such comparisons are suitable when the fundamental equations cast on the similar interface, and that is available only in our formulations in any gravity theories at this moment.

5.2 Towards an initial boundary value problem

The second issue is a direction to understand the system as an initial boundary value problem (IBVP). All the numerical simulations are of IBVP, that is we have to impose proper boundary conditions at the edges of numerical region during the time evolution, together with data on initial hypersurface. In order not to pick up unphysical reflected information from the boundaries, several techniques (such as out-going wave conditions) are so far developed. However, we have not yet obtained a "well-posed" boundary condition based on the mathematical consideration.

The actual researches of IBVP in general relativity began only recently. A satisfactory theory of IBVP is only available currently for linearized problems, and from this reason the base system is preferred to be a symmetric hyperbolic form. Therefore the discussion is available only limited cases. As far as we know, there are only two references on this topic: Stewart [27] studied IBVP for Frittelli and Reula's symmetric hyperbolic formulation [8], and Friedrich and Nagy [28] for Friedrich's system [6]. Along to this IBVP, we are now trying to find out a proper additional conditions for our symmetric hyperbolic formulation based on Ashtekar's variables.

5.3 Asymptotically constrained systems

In §4, we showed a set of dynamical equations, which has the constraint surface as its attractor, by introducing new additional variables that obey dissipative equations of motion. Based on BFHR's analytical proof [21], we expect that this set of equations is robust against a perturbative error of the constraint equations. Thus, the system may be useful for future numerical studies with its stability property.

In [20], we also showed an advanced set of equations that has its attractor also in the real-valued surface. Since our symmetric hyperbolic system of the original Ashtekar's variables requires the reality condition on the triad, the new system is designed as such a way. The same above discussion can be applied to this advanced set, and we expect the asymptotically real-valued feature in its evolution.

The problem of these systems might be that they require many additional variables. From a view point of numerical applications, this claim would not be so serious a problem, as we see a success of a dissipative maximal slicing condition [29] ('K-driver' in the literature). Actually, the λ-system of the Einstein equations was already tested and confirmed to work appropriately in numerical applications at least in one dimensional space evolution models [30]. Therefore we expect our system also shows the desired asymptotic behaviors. We are in preparation of presenting such a numerical result. We are also trying to reduce the number of the variables in order to find out clear geometrical meanings of our λ-system. We will report these efforts elsewhere.

Acknowledgments

HS would like to thank Abhay Ashtekar and CGPG group members for their hospitality. HS is supported by the Japan Society for the Promotion of Science (JSPS) as a research fellow abroad.

References

[1] Recent review is given by O. A. Reula, Livng Rev. Relativ. **1998-3** at http://www.livingreviews.org/.

[2] Y. Choquet-Bruhat and J.W. York. Jr., in *General Relativity and Gravitation* , vol. 1, ed. by A. Held, (Plenum, New York, 1980).

[3] C. Bona, J. Massó, Phys. Rev. Lett. **68**, 1097 (1992).

[4] C. Bona, J. Massó, E. Seidel and J. Stela, Phys. Rev. Lett. **75**, 600 (1995); Phys. Rev. **D56**, 3405 (1997).

[5] A. E. Fischer and J. E. Marsden, Commun. Math. Phys. **28**, 1 (1972).

[6] H. Friedrich, Proc. Roy. Soc. **A375**, 169 (1981); Proc. Roy. Soc. **A378**, 401 (1981); Comm. Math. Phys **100**, 525 (1985); J. Diff. Geom. **34**, 275 (1991); Class. Quantum Grav. **13**, 1451 (1996).

[7] Y. Choquet-Bruhat and J.W. York, Jr., C. R. Acad. Sci. Paris, **t. 321**, Série I, 1089 (1995) [gr-qc/9506071]; A. Abrahams, A. Anderson, Y. Choquet-Bruhat and J.W. York, Jr., Phys. Rev. Lett. **75**, 3377 (1995); C. R. Acad. Sci. Paris, **t. 323**, Série II b, 835 (1996); Class. Quantum Grav. **14**, A9 (1997); A. Anderson and J.W. York, Jr. Phys. Rev. Lett. **82**, 4384 (1999).

[8] S. Frittelli and O.A. Reula, Phys. Rev. Lett. **76**, 4667 (1996).

[9] M. Alcubierre, Phys. Rev. **D55**, 5981 (1997); M. Alcubierre and J. Massó, Phys. Rev. **D57**, 4511 (1998).

[10] M.A. Scheel, T.W. Baumgarte, G.B. Cook, S.L. Shapiro, and S.A. Teukolsky, Phys. Rev. **D56** 6320 (1997); *ibid.* **D58**, 044020 (1998).

[11] R. Geroch, *Partial Differential Equations in Physics*, gr-qc/9602055.

[12] G. Yoneda and H. Shinkai, to be published in Int. J. Mod. Phys. D. (gr-qc/9901053).

[13] A. Ashtekar, Phys. Rev. Lett. **57**, 2244 (1986); Phys. Rev. **D36**, 1587 (1987); *Lectures on Non-Perturbative Canonical Gravity* (World Scientific, Singapore, 1991).

[14] M.S. Iriondo, E.O. Leguizamón and O.A. Reula, Phys. Rev. Lett. **79**, 4732 (1997).

[15] G. Yoneda and H. Shinkai, Phys. Rev. Lett. **82**, 263 (1999).

[16] M.S. Iriondo, E.O. Leguizamón and O.A. Reula, Adv. Theor. Math. Phys. **2**, 1075 (1998).

[17] A. Ashtekar, J. D. Romano and R. S. Tate, Phys. Rev. **D40**, 2572 (1989).

[18] G. Yoneda and H. Shinkai, Class. Quantum Grav. **13**, 783 (1996).

[19] G. Yoneda, H. Shinkai and A. Nakamichi, Phys. Rev. **D56**, 2086 (1997).

[20] H. Shinkai and G. Yoneda, Phys. Rev. **D60**, 101502 (1999).

[21] O. Brodbeck, S. Frittelli, P. Hübner and O.A. Reula, J. Math. Phys. **40**, 909 (1999).

[22] S. Detweiler, Phys. Rev. **D35**, 1095 (1987).

[23] S. Frittelli, Phys. Rev. **D55**, 5992 (1997).

[24] M. Shibata and T. Nakamura, Phys. Rev. **D52**, 5428 (1995).

[25] T. W. Baumgarte and S. L. Shapiro, Phys. Rev. **D59**, 024007 (1999).

[26] M. Alcubierre, G. Allen, B. Brügmann, E. Seidel and W-M. Suen, gr-qc/9908079.

[27] J.M. Stewart, Class. Quant. Grav. **15**, 2865 (1998).

[28] H. Friedrich and G. Nagy, Comm. Math. Phys. **201**, 619 (1999).

[29] J. Balakrishna *et al*, Class. Quant. Grav. **96**, L135 (1997).

[30] In private commucations with P. Hübner and with G. Cook.

Reinterpretation of the vacuum C metric

Masashi Egi,[1]

Department of Physics, Nagoya University,
Chikusa-ku, Nagoya 464-8602, Japan

Abstract

We re-examine the vacuum C-metric and propose eminently suitable coordinates and parameterizations to describe two Schwartzschild-type black holes with equal mass uniformly accelerated by a spring between them in the form of a conical singularity. The metric referring to the situation is uniquely determined by two independent constants A and M which are arranged to have physically meaningful definition contrasting to the well-known work of Kinnersley and Walker [5]. In the co-accelerating frame attached to one of the black holes, the space-time is static and so admits the time-like Killing vector. There, the space-time asymptotically approaches the Rindler space-time with the acceleration constant A at large distances from the black hole, and the time-like Killing vector defines the conserved energy M inside an arbitrary 2-sphere enclosing the black hole. The compression force F on the spring, which is interpreted as the external mechanical force necessary for the uniform acceleration of the particle, is found to be simply $F = MA$, which leads us to interpret M as the inertial mass of the black hole.

1 Introduction

The vacuum C-metric has a very long history. It was firstly discovered in 1918 [1] as a class of static and axi-symmetric exact solutions for the vacuum Einstein equations. In 1960s it was rediscovered again and again [2, 3, 4], nevertheless no physical interpretations were suggested at that stage. This was manly due to the lack of understanding of geometrical meanings of original coordinates and the groundless choice of parameterization of the solution. In 1970, pointing out such the difficulties, Kinnersley and Walker (hereafter KW) overcome them by introducing a novel parameterization which we refer to as the KW representation of the vacuum C-metric, and showed that the metric describes the space-time of uniformly accelerating Schwarzschild-type black holes [5]. Since their work, various different aspects of the metric have been extensively studied; for example, horizon structure[8], gravitational radiation [9, 10, 12, 13], and source structure [6, 7, 14]. All of these works are entirely based on the KW parameterization. However, as we will show in section 2, the KW parameterization is still in the stage of rough drafts of the more appropriate one. We will give it in section 3. We will show that the new parameterization marvelously clarifies physical interpretation in section 3 and 4.

2 The vacuum C-metric and the KW class

In this section, we give an overview of the general properties of the vacuum C-metric and the standard KW parameterization, and then point out the imperfection of the KW parameterization.

2.1 General properties

The vacuum C-metric is generally given by the form

$$ds^2 = \frac{1}{a^2(y-x)^2}\left\{f(y)d\tau^2 - \frac{dy^2}{f(y)} + \frac{dx^2}{f(x)} + f(x)d\phi^2\right\}. \tag{1}$$

[1] E-mail:emasashi@allegro.phys.nagoya-u.ac.jp

where a is an arbitrary constant with a dimension of inverse of length and

$$f(w) := b_0 + b_1 w + b_2 w^2 + b_3 w^3, \tag{2}$$

where $b_0, \cdots, b_3$ are arbitrary dimensionless constants. It should be noticed that all the parameters $a, b_0, \cdots, b_3$ are not independent because of the following consideration. If we transform the original coordinates (t, y, x, ϕ) into the new coordinates $(\bar{t}, \bar{y}, \bar{x}, \bar{\phi})$ via

$$\tau = \alpha\beta^{-1}\bar{\tau},\ y = \alpha\beta\bar{y} + \gamma,\ x = \alpha\beta\bar{x} + \gamma,\ \phi = \alpha\beta^{-1}\bar{\phi}, \tag{3}$$

where α, β and γ are arbitrary constants, then the transformed metric assumes the same form as (1)(2) with another set of constants $\bar{a}, \bar{b}_0, \cdots, \bar{b}_3$ given by

$$\bar{a} = a\beta, \tag{4}$$

and

$$\begin{aligned}\bar{f}(w) &= \beta^{-2} f(\alpha\beta w + \gamma), \\ &= \beta^{-2} f(\gamma) + \alpha\beta^{-1} f'(\gamma) w + \frac{1}{2}\alpha^2 f''(\gamma) w^2 + \alpha^3 \beta b_3 w^3, \\ &= \bar{b}_0 + \bar{b}_1 w + \bar{b}_2 w^2 + \bar{b}_3 w^3.\end{aligned} \tag{5}$$

In other words, the metric characterized by a set of constants $a, b_0, \cdots, b_3$ is identical to that of $\bar{a}, \bar{b}_0, \cdots, \bar{b}_3$, if there exists a set of constants α, β, γ which satisfies (4)(5). This identification is relevant for later discussions.

According to the choice of the signature +2, the metric has following profiles. The signature is valid in the range of x satisfying $f(x) > 0$, there $\partial/\partial\phi$ is a space-like Killing vector of the angular direction, and the boundaries $x = x_*$ satisfying $f(x_*) = 0$ are symmetry axes. The space-time is static in the range of y satisfying $f(y) < 0$ in addition to $f(x) > 0$, there $\partial/\partial t$ is a time-like Killing vector and the boundaries $y = y_*$ satisfying $f(y_*) = 0$ are Killing horizons. On the other hand, the only non-vanishing complex curvature scalar is found to be

$$\Psi_2 := -\frac{1}{2} C_{\alpha\beta\gamma\delta} k^\alpha l^\beta k^\gamma l^\delta = -\frac{a^2 b_3 (y - x)^3}{2}, \tag{6}$$

where the principle null directions are given by

$$l^\alpha := \left(-f(y)^{-1}, -a, 0, 0\right),\ k^\alpha := (y - x)^2/2\,(1., -af(y), 0, 0), \tag{7}$$

and so the C-metric is a type-D solution. Hence, the space-time is flat if $b_3 = 0$, and in general the space-time is asymptotically flat in the limit $y - x \to 0$ and has curvature singularity at $y - x = \pm\infty$.

As an example, a space-time configuration is illustrated in figure 1 for the case that $b_3 > 0$ and the algebraic equation $f(w) = 0$ on w has three real distinct roots $w_1 < w_2 < w_3$.

2.2 Physically interesting classes

In the previous subsection, we have seen that the vacuum C-metric has somewhat entangled parameter dependences. By virtue of the relations (3)(4)(5), one might naively expect that the vacuum C-metric entirely depends on two independent parameters. However, we should pay attention to the fact that the coordinate transformation (3) can only deform $f(w)$ into $\bar{f}(w)$ by rectangularly enlargement or reduction. Therefore we rather start with the classification of $f(w)$. We are not interested in merely flat space-time associated with $b_3 = 0$, and taking into account of (4)(5) we can choose $a > 0$ and $b_3 > 0$ without loss of generality.

Let us consider a class of $f(w)$ such that $f(w)$ takes a positive local maximum value at $w = w_*$. Then, choosing the constants α, β and γ as

$$(\alpha,\ \beta,\ \gamma) = \left(\sqrt{-2/f''(w_*)},\ \sqrt{f(w_*)},\ w_*\right), \tag{8}$$

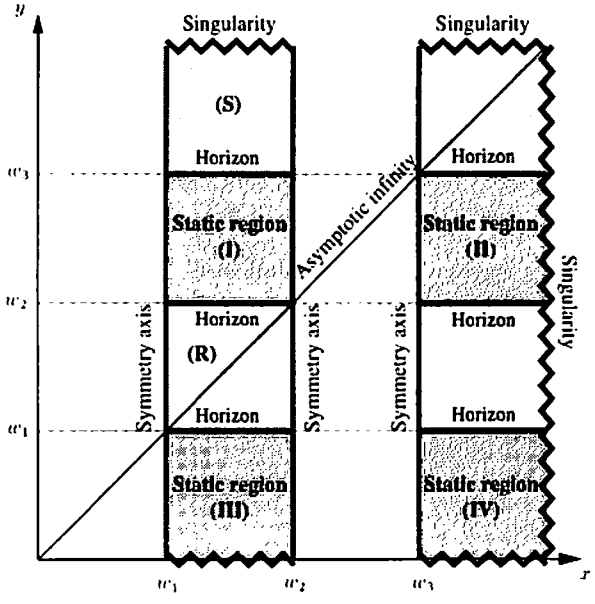

Figure 1: The signature of the metric is +2 in slight-grey and dark-grey regions. There are four static regions from (I) to (IV) and each of which refers to a completely different kind of space-time.

we obtain

$$ds^2 = \frac{1}{\bar{a}^2(y-x)^2}\left\{\bar{f}(y)d\tau^2 - \frac{dy^2}{\bar{f}(y)} + \frac{dx^2}{\bar{f}(x)} + \bar{f}(x)d\phi^2\right\}, \tag{9}$$

$$\bar{f}(w) = 1 - w^2 + 2m\bar{a}, \tag{10}$$

where we notice that $\bar{a} := a\beta > 0$ and $m := \alpha^3 b_3/(2a) > 0$. This class can be expressed in terms of the two independent positive constants $\bar{a}$ and m. Inversely, this form (9)(10) for $\bar{a}$, $m > 0$ do not include other classes, because $\bar{f}(w)$ always takes a positive local maximum value at $w = 0$.

This is the well-known form of the vacuum C-metric proposed by KW, and so we refer to this class as the KW class and refer to (9)(10) as the KW parameterization. However, we emphasize that KW did not recognize the necessity of this classification, on the contrary, they even stated as if the metrics for any set of constants $(a, b_0, \cdots, b_3)$ can be transformed into this form via (3)(4)(5), which is impossible as mentioned above.

KW and subsequent papers investigated this class with an additional condition $m\bar{a} < 1/\sqrt{27}$ which is the condition that the algebraic equation $\bar{f}(w) = 0$ has three real distinct roots, as we saw in the previous example. See the figure 1. There are four static regions from (I) to (IV). Among them, there is a physically interesting static region (I) only which is not suffering from naked singularity. If $m\bar{a} > 1/\sqrt{27}$, (I) disappears and there is no such the physically interesting static region. After some proper coordinates transformation, it was shown that

1. In the limit $\bar{a} \to 0$ the region (I) accompanied by the region (S) reduces to the Schwarzchild space-time of the mass m, then the Killing horizon given by $y = w_3$ is discovered as a black hole horizon.

2. In the limit $m \to 0$ the region (I) reduces to the Rindler space-time of the acceleration constant $\bar{a}$ and the region (I) accompanied by the region (R) reduces to the Minkowski space-time, then the Killing horizon given by $y = w_2$ is discovered as a Rindler horizon.

Accordingly, the vacuum C-metric in the KW parameterization associated with the additional condition $m\bar{a} < 1/\sqrt{27}$ has been understood to describe the space-time of a uniformly accelerated Schwarzschild-type black hole.

However, the KW parameterization has a congenital defect that it is no more an ansatz and is not determined by some proper boundary conditions. The defect results in that the physical meanings of the parameters $\bar{a}, m$ can be given only in the limits $m\bar{a} \searrow 0$ as mentioned above. Although it is true that we can approximately extrapolate the interpretations into the narrow range $m\bar{a} \ll 1$ [5, 6, 7], further extrapolations into the range $m\bar{a} \sim O(1)$ are just confronted with an apparent violation of the equivalence principle [8]. Hence, we assert that the KW parameterization is still in the stage of a rough draft of more appropriate one in which we expect that the independent parameters should be given physically meaningful definitions and the extra condition on them like $m\bar{a}$ should be naturally eliminated.

3 New class and its parameterization

Our strategy is as follows. Going back to the original form of the vacuum C-metric (1)(2), we can easily survey all form of $f(w)$ for $b_3 > 0$, and understand that such the physically meaningful static region appears iff the algebraic equation $f(w) = 0$ on w has three real distinct roots. Then it is quite reasonable to consider the class of $f(w)$ such that $f(w) = 0$ has three real distinct roots and start with the form of $f(w)$ as

$$f(w) = c(w - w_1)(w - w_2)(w - w_3), \tag{11}$$

where $c > 0$ and $w_1 < w_2 < w_3$.

3.1 Boundary conditions

As the mathematical preliminary for the boundary condition, we consider the Rindler space-time of the acceleration constant A in the bipolar coordinates. The metric of the Rindler space-time in the cylindrical coordinates $(\tilde{t}, \tilde{\rho}, \tilde{z}, \tilde{\phi})$ is given by

$$ds^2 = -A^2\tilde{z}^2 d\tilde{t}^2 + d\tilde{\rho}^2 + d\tilde{z}^2 + \tilde{\rho}^2 d\tilde{\phi}^2, \tag{12}$$

which is associated with the Minkowski space-time in the cylindrical coordinate $(\tilde{T}, \tilde{R}, \tilde{Z}, \tilde{\phi})$ via

$$\tilde{T} = \tilde{z}\sinh A\tilde{t}, \quad \tilde{Z} = \tilde{z}\cosh A\tilde{t}. \tag{13}$$

The time-like coordinate $\tilde{t}$ and the constant parameter A are understood as the proper-time of the world line $(\tilde{\rho}, \tilde{z}) = (0, \pm 1/A)$ which is found to be a pair of hyperbola of the acceleration constant A in the Minkowski space-time. However, it should be noticed that the directions of proper-time are opposite as in the figure 2. In terms of the bipolar coordinates $(\tilde{\mu}, \tilde{\eta})$ given by

$$\tilde{\rho} = \frac{\sin\tilde{\eta}}{A(\cosh\tilde{\mu} - \cos\tilde{\eta})}, \quad \tilde{z} = \frac{\sinh\tilde{\mu}}{A(\cosh\tilde{\mu} - \cos\tilde{\eta})}, \tag{14}$$

the metric is rewritten as

$$ds^2 = \frac{1}{A^2(\cosh\tilde{\mu} - \cos\tilde{\eta})^2}\left(-A^2\sinh^2\tilde{\mu}d\tilde{t}^2 + d\tilde{\mu}^2 + d\tilde{\eta}^2 + \sin^2\tilde{\eta}d\tilde{\phi}^2\right), \tag{15}$$

and the world lines $(\tilde{\rho}, \tilde{z}) = (0, \pm 1/A)$ are mapped to $\tilde{\mu} = \pm\infty$. The geometrical configuration of the bipolar coordinates is plotted in figure 3. At large distances from the world line, that is $\tilde{\rho}, \tilde{z} \gg 1/A$ equivalently $\tilde{\mu}, \tilde{\eta} \ll 1$, the metric is approximately

$$ds^2 = \frac{4}{A^2(\tilde{\mu}^2 + \tilde{\eta}^2)^2}\left\{-A^2\tilde{\mu}^2 d\tilde{t}^2 + d\tilde{\mu}^2 + d\tilde{\eta}^2 + \tilde{\eta}^2 d\tilde{\phi}^2 + O(\tilde{\mu}^3, \tilde{\eta}^3)\right\}. \tag{16}$$

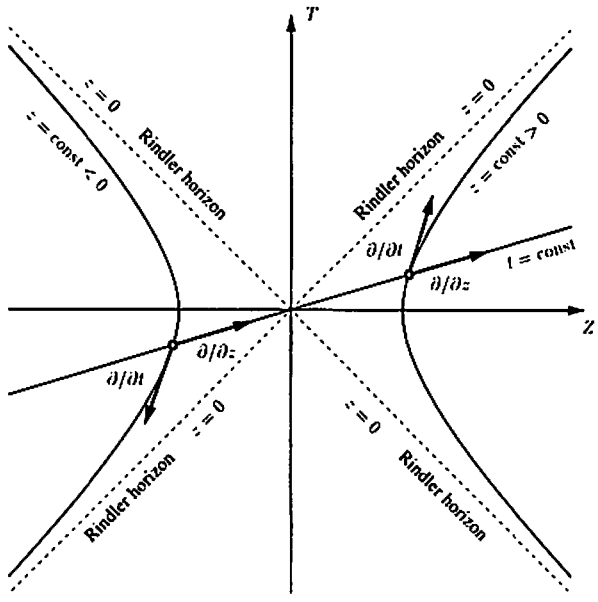

Figure 2: This schematic picture represents the relation between the Minkowski and Rindler space-times.

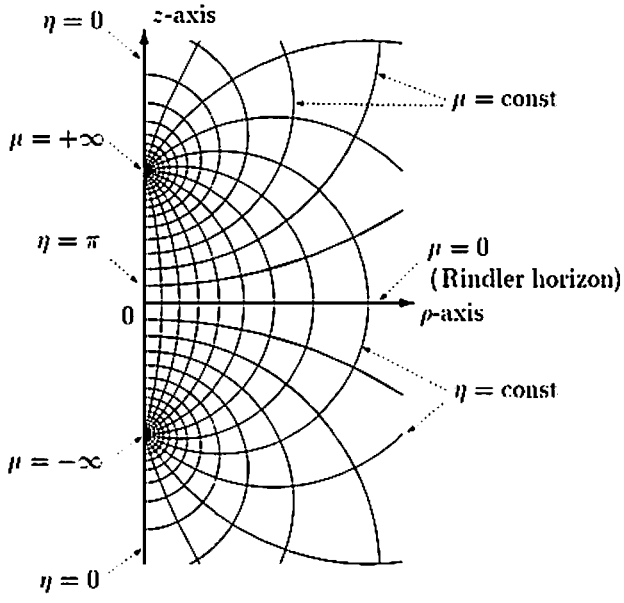

Figure 3: The geometrical configuration of the bipolar coordinates on the ρ-z plane.

Now, we are in a stage to consider the vacuum C-metric. One of our novel idea to clarify the geometrical structure of the vacuum C-metric is to introduce the bipolar coordinates (μ, η) via

$$y = \frac{w_2 + w_1}{2} + \frac{w_2 - w_1}{2}\cosh\mu, \tag{17}$$

$$x = \frac{w_2 + w_1}{2} + \frac{w_2 - w_1}{2}\cos\eta, \tag{18}$$

where $-\infty \le \mu \le +\infty$ and $0 \le \eta \le \pi$, so the (μ, η) coordinates cover the region (I)(S) in the figure 1.

The curvature singularities are located at both poles given by $\mu = \pm\infty$. Two Killing horizons given by $y = w_2, w_3$ are mapped to $\mu = 0$ and $\mu = \pm 2\sinh^{-1}\sqrt{(w_3 - w_2)/(w_2 - w_1)}$, respectively. The asymptotic region given by $y - x \to 0$ is now given by $\mu \to 0$ and $\mu \to 0$, there the metric is approximately

$$ds^2 = \frac{4}{a^2(\mu^2 + \eta^2)^2}\left\{c(w_3 - w_2)(-a^2\mu^2 dt^2 + \eta^2 d\phi^2) + \frac{d\mu^2 + d\eta^2}{c(w_3 - w_2)(w_2 - w_1)^2/4} + O(\mu^3, \eta^3)\right\} \tag{19}$$

where we redefine $t = a^{-1}\tau$. Comparing (16) and (19), we can impose that the vacuum C-metric approaches the Rindler metric of the acceleration constant A at large distances from the black hole, that is, $a = A$ and $(t, \mu, \eta, \phi) \to (\tilde{t}, \tilde{\mu}, \tilde{\eta}, \tilde{\phi})$, which requires

$$\frac{w_2 - w_1}{2} = 1, \ c(w_3 - w_2) = 1. \tag{20}$$

Furthermore $\xi = \partial/\partial t$ is a time-like Killing vector in the region (I) and so we can define the conserved energy M inside a μ =constant 2-sphere denoted by $S[\mu]$ enclosing the singularity $\mu = +\infty$, by the Komar integral [15] as follows

$$M = \frac{1}{8\pi}\int_{S[\mu]} \nabla^\alpha \xi^\beta d\sigma_{\alpha\beta} = \frac{c(w_3 - w_1)}{4a}, \tag{21}$$

where $\sigma_{\alpha\beta}$ represents a surface element, and we emphasize that M is obviously independent of μ, and will be interpreted as the inertia of the black hole in section 4. We adopt the relation as a boundary condition on the constants a, c, w_1, w_2, w_3.

We can uniquely solve (20)(21) on $a, c, w_2 - w_1, w_3 - w_2$ in terms of A, M as

$$a = A, \ c = 2MA, \ w_2 - w_1 = 2, \ w_3 - w_2 = \frac{1}{2MA}. \tag{22}$$

Without loss of generality we can put $w_2 = 1$, then we obtain

$$ds^2 = \frac{1}{A^2(y - x)^2}\left\{A^2 f(y)dt^2 - \frac{dy^2}{f(y)} + \frac{dx^2}{f(x)} + f(x)d\phi^2\right\}, \tag{23}$$

$$f(w) = 2MA(w + 1)(w - 1)\left(w - 1 - \frac{1}{2MA}\right). \tag{24}$$

Inversely the new class given by (11) is always transformed into this form by choosing α, β, γ as

$$(\alpha, \ \beta, \ \gamma) = \left(\{c(w_3 - w_2)\}^{-1/2}, \ \frac{1}{2}(w_2 - w_1)\{c(w_3 - w_2)\}^{1/2}, \ \frac{1}{2}(w_2 + w_1)\right), \tag{25}$$

then A and M is given by

$$(A, \ M) = \left(\frac{a}{2}(w_2 - w_1)\{c(w_3 - w_2)\}^{1/2}, \ \frac{c}{2a}\{c(w_3 - w_2)\}^{-3/2}\right). \tag{26}$$

Therefore our physically meaningful class is uniquely determined by the two independent parameters A and M, each of which is designed to have physically meaningful definitions. We close this section with rewriting the metric the previous bipolar coordinates as

$$ds^2 = \frac{1}{A^2(\cosh\mu - \cos\eta)^2}\left\{-A^2\left(1 - 4MA\sinh^2\frac{\mu}{2}\right)\sinh\mu^2 dt^2 + \left(1 - 4MA\sinh^2\frac{\mu}{2}\right)^{-1}d\mu^2 \right.$$
$$\left. + \left(1 + 4MA\sin^2\frac{\eta}{2}\right)^{-1}d\eta^2 + \left(1 + 4MA\sin^2\frac{\eta}{2}\right)\sin\eta^2 d\phi^2\right\}, \tag{27}$$

whose the geometrical configuration is illustrated in figure 4.

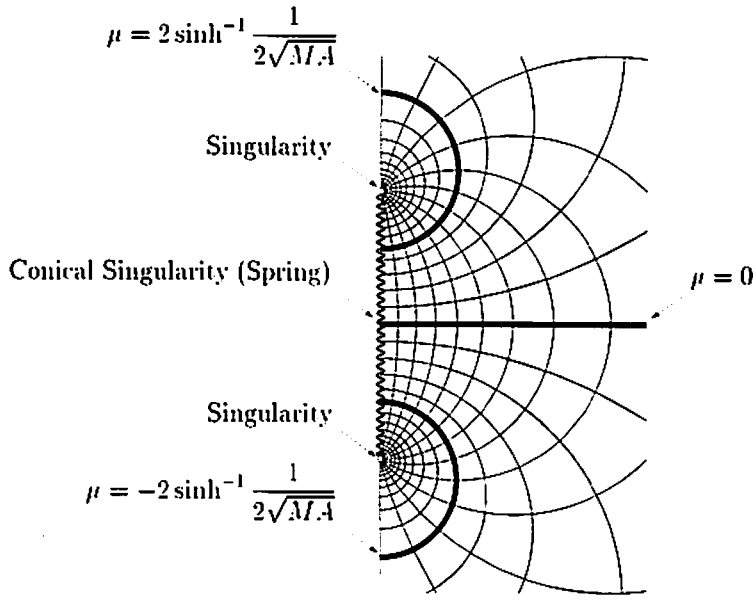

Figure 4: There are three Killing horizons, that is, the Rindler horizon $\mu = 0$ and the Schawrzschild-type black hole horizons $\mu = \pm 2\sinh^{-1} 1/(2\sqrt{MA})$.

4 The dynamical property

Finally, we discuss the physical interpretation of the new parameter M and the driving force necessary to accelerated the black holes. Evaluating the quantities

$$\lim_{\eta \to 0} \sqrt{g_{\phi\phi}/g_{\eta\eta}} = 1, \tag{28}$$

$$\lim_{\eta \to \pi} \sqrt{g_{\phi\phi}/g_{\eta\eta}} = 1 + 4MA, \tag{29}$$

we find that there is a conical singularity along the $\eta = \pi$ as in figure 4. The detail consideration leads to

$$T^t{}_t = T^\mu{}_\mu = -MA\delta^{(2)}(\eta - \pi). \tag{30}$$

We understand that the conical singularity has negative energy density and drives the uniform acceleration of the black holes. If we define the external mechanical force F as

$$F := \int (-T^\mu{}_\mu) d\sigma, \tag{31}$$

where the integration is performed over the small disk crossing the conical singularity, we obtain a quite simple relation $F = MA$, which is accordance with the equations of motion for the particle uniformly accelerated in the Minkowski space-time. Thus we can reasonably interpret M as the inertia of the black hole.

References

[1] D. Kramer, H. Stephani, E. Herlt, M. MacCallum and E. Schmutzer (Ed.), *Exact Solutions of Einstein's field equations*, Cambridge University, Cambridge (1980).

[2] E. Newman and L. Tamburino, J. Math. Phys. **2**, 667 (1961).

[3] I. Robinson and A. Trautman, Proc. Roy. Soc. (London) **A265**, 463 (1962).

[4] J. Ehlers and W. Kundt, in *Gravitation, an Introduction to Current Research*, edited by L. Witten (Wiley, New York, 1962).

[5] W. Kinnersley and M. Walker, Phys. Rev. **D2**, 1359 (1970).

[6] W. B. Bonner, Gen. Rel. Grav. **15**, 535(1983).

[7] F. H. J. Cornish and W. J. Uttley, Gen. Rel. Grav. **27**, 439 (1995).

[8] H. Farhoosh and R.L. Zimmerman, Phys. Rev. **D21**, 317 (1980).

[9] H. Farhoosh and R.L. Zimmerman, J. Math. Phys. **20**, 2272 (1979).

[10] A. Ashtekar and T. Dray, Commun. Math. Phys. **79** 581 (1981).

[11] T. Dray, Gen. Rel. Grav. **14**, 109 (1980).

[12] A. Tomimatsu, Phys. Rev. **D57**, 2623 (1998).

[13] J. Bičák and V. Pravda, Phys. Rev. **D60**, 0440004 (1999).

[14] W. Yongcheng, Phys. Rev. **D55**, 7977 (1997).

[15] A. Komar, Phys. Rev. **113**, 934, (1959).

Analytic description of singularities in non-vacuum Gowdy spacetimes

Makoto Narita[1]

Department of Physics, Rikkyo University, Nishi-Ikebukuro, Toshima, Tokyo 171-8501, Japan

Takashi Torii[2]

Department of Physics, Tokyo Institute of Technology, Oh-Okayama, Meguro, Tokyo 152-8551, Japan

Kengo Maeda[3]

Department of Physics, Waseda University, Ohkubo, Shinjuku, Tokyo 169-8555, Japan

Abstract

We show that T^3 Gowdy spacetimes in Einstein-Maxwell-dilaton-axion system have asymptotically velocity-term dominated singularities by using the Fuchsian algorithm. This means that the spacetimes are not Mixmaster necessarily even if the dilaton field is exponentially coupled to the Maxwell and/or the axion fields like the "potential" of Bianchi IX spacetimes which have Mixmaster singularities.

1 Introduction

The singularity theorem gives us some sufficient conditions for the existence of spacetime singularities which are defined as a endpoint of incomplete geodesics [15, 14]. Those conditions fall into (1) the strong energy condition; (2) the generic condition; (3) the chronology condition and (4) the existence of trapped regions. After the discovery of the singularity theorem, some attempts of generalization were performed by replacing these conditions with some others (see e.g. Refs.[27, 20, 25]). Although we have new many variations of the singularity theorem, they give no information on the nature of the singularity.

To the best of our knowledge, the first research about the nature of the singularity was done by Belinskii, Khalatnikov and Lifshitz (BKL) [5]. They investigated how the spacetime evolves to the singularity and predicted that the dynamics would spatially decouple near singularities. BKL have described a vacuum and spatially homogeneous (mainly Bianchi IX) spacetime singularity as an infinite sequence of Kasner epochs ("oscillatory approach to the singularity"). Independently, Misner showed the same behavior in term of exponentially growing "potential" terms constructed by the spatial curvature. The spacetime is bounced by the potentials infinite times. This is called the *Mixmaster dynamics* [23]. Then, BKL gives a conjecture which stated that a generic singularity would be locally of the Mixmaster type. It is *BKL conjecture*.

Up to now BKL conjecture is neither validated nor invalidated by rigorous arguments. For example, even the dynamics of Bianchi IX spacetimes is not known precisely. There is, however, a special case for BKL conjecture, that is, the *asymptotically velocity-term dominated* (AVTD) singularity. It is not described by a infinite sequence of Kasner epochs but by only one epoch (i.e., "no oscillatory approach to the singularity") [17, 29]. Hence, Kasner spacetimes are necessarily (A)VTD. In brief, the characteristic feature of the AVTD singular behavior is that at sufficiently close to the singularity, the functions behave as if all spatial derivative terms are dropped from the field equations. It is possible to make exact arguments on the nature of the AVTD singularity since the AVTD solutions are more simple than the Mixmaster solutions in the sense that there is no complicated oscillation. Our interest is to verify BKL conjecture and clarify whether spacetimes is AVTD or not in non-vacuum and/or spatially inhomogeneous cases.

In order to attack the above issue, we will consider Gowdy spacetimes [12]. They are spatially compact spacetimes which have $U(1) \times U(1)$ symmetry and vanishing twist. Gowdy spacetimes are adopted in various investigations because they are one of the most manageable inhomogeneous spacetimes and can give an essential feature of inhomogeneity in spite of its simpleness. Until now, the behavior near the singularity in Gowdy spacetime are also discussed in various situations. In the vacuum case, Isenberg and Moncrief have shown that polarized Gowdy spacetimes are AVTD [17]. Grubišić and Moncrief (GM) [13] and Kichenassamy and Rendall (KR) [19] have shown that non-polarized T^3 Gowdy spacetimes have AVTD singularities if the *low velocity condition* is satisfied. Using numerical method, Berger, Garfinkle, Isenberg and Moncrief confirmed that non-polarized T^3 Gowdy spacetimes have AVTD singularities even in the situation that the low velocity condition is broken initially [6]. Recently, Garfinkle has shown that $S^2 \times S^1$ Gowdy spacetimes have AVTD singularities numerically [11].

The effect of the matter field are also discussed and AVTD solutions are found in, for example, polarized Gowdy spacetimes admitting scalar fields minimally coupled with the Maxwell field [8], and Einstein-dilaton-axion (EDA) system in polarized Gowdy spacetimes [3]. Weaver et al. have shown numerically, however, that magnetic Gowdy spacetimes are not AVTD but Mixmaster [6]. Hence, it is nontrivial whether the spacetime is Mixmaster or AVTD type and these facts drive us to study the non-vacuum and spatially inhomogeneous case.

There is a further point which needs to be clarified. Belinskii and Khalatnikov (BK) have suggested that the existence of massless scalar fields suppresses Mixmaster behavior by examining the Bianchi I cosmology [4]. It is due to the fact that the scalar field is algebraically equivalent to the stiff matter in some cases. Recently, Berger confirmed this suggestion by numerical analysis [7]. BK and Berger also have suggested, however, exponential coupling of the scalar field to the Maxwell field restores Mixmaster behavior which is suppressed initially by the scalar field [4, 7]. It is important to note that such matter fields arises naturally from the low energy effective superstring theory [28], i.e. Einstein-Maxwell-dilaton-axion (EMDA) system. The EMDA system was discuss actively in the context of the black hole solutions and singularities, and gives characteristic features different from Einstein-maxwell system.

Our purpose in this paper is to explore into the nature of singularities in EMDA system with Gowdy spacetimes on $T^3 \times \mathbf{R}$. We make use of the Fuchsian algorithm developed by Kichenassamy and Rendall [19]. Although the system treated here is very complicated, the Fuchsian algorithm is powerful enough for the system since this algorithm is independent of non-linearity, number of functions and dimension of space. We will show that there exist families of AVTD singular solutions of EMDA field equations, which is generic in the sense that they depend on the maximal number of arbitrary functions. Hence, our result shows that exponential coupling of the scalar field to the Maxwell field does not necessarily restore the Mixmaster behavior. The matter is not quite as simple as was suggested.

Organization of this paper is as follows. In Sec. 2, an appropriate definition of AVTD is given. In Sec. 3, we discuss importance to study EMDA system. Sec. 4 is devoted to introduce T^3 Gowdy spacetimes in EMDA system. Sec. 5 presents a brief review of the Fuchsian algorithm. Finally, results and summary are given in Sec. 6.

2 Asymptotically velocity-term dominated (AVTD) singularity

In this section, we gives precise definition of AVTD. In contrast to Mixmaster which is a complicated singularity, AVTD is called a simple singularity [10, 17]. An essential difference between Mixmaster and AVTD singularities is whether spatial curvature terms in Einstein's equations becomes dominant or not as the system approaches the singularities. As mentioned in the previous section, the "potentials" constructed by the spatial curvatures grow exponentially in the Mixmaster case. These "potentials" give rise to the infinite times of reflection and the spacetime will approach oscillating, i.e. Mixmaster singularities as an infinite sequence of Kasner epochs. On the other hand, such a "potential" does not exist in the AVTD case. Therefore, reflection by the potential does not occur and the spacetime will approach Kasner one.

Now, let us define AVTD. Suppose that a four-dimensional spacetime (M, g) with the signature $(-+++)$ satisfies Einstein's equations, $G_{\mu\nu} = T_{\mu\nu}$, where $G_{\mu\nu} \equiv {}^{(4)}R_{\mu\nu} - \frac{1}{2}\,{}^{(4)}Rg_{\mu\nu}$ is the Einstein tensor

and $T_{\mu\nu}$ is the energy-momentum tensor. For any $3+1$ decomposition, we can obtain the constraint equations,

$$ {}^{(3)}R - K^{ab}K_{ab} + (trK)^2 = 2T^0_0, \tag{1} $$

$$ {}^{(3)}\nabla_a K^a_b - {}^{(3)}\nabla_b(trK) = -T^0_b, \tag{2} $$

and the evolution equations,

$$ \partial_t h_{ab} = -2NK_{ab} + \mathcal{L}_{\mathbf{N}} h_{ab}, \tag{3} $$

$$ \partial_t K^a_b = N\left[{}^{(3)}R^a_b + (trK)K^a_b\right] - {}^{(3)}\nabla^{(3)}_b\nabla^a N + \mathcal{L}_{\mathbf{N}} K^a_b + 2N\left[T^a_b + \frac{1}{2}h^a_b(T^0_0 - T^c_c)\right], \tag{4} $$

where h_{ab}, K_{ab} and (trK) are the first, second fundamental form and mean curvature of the 3-dimensional spacelike hypersurface, respectively. Also, ${}^{(3)}\nabla$, ${}^{(3)}R_{ab}$ and ${}^{(3)}R$ are the spatial covariant derivative, spatial Ricci and scalar curvature, respectively. N and $\mathbf{N}$ are the lapse function and shift vector. $\mathcal{L}_{\mathbf{N}}$ is the Lie derivative along the vector field $\mathbf{N}$. From the full Einstein equations, we define the velocity term dominated (VTD) equations as follows.

$$ -K^{ab}K_{ab} + (trK)^2 = 2\tilde{T}^0_0, \tag{5} $$

$$ {}^{(3)}\nabla_a K^a_b - {}^{(3)}\nabla_b(trK) = -\tilde{T}^0_b, \tag{6} $$

$$ \partial_t h_{ab} = -2NK_{ab}, \tag{7} $$

$$ \partial_t K^a_b = N\left[(trK)K^a_b\right] + 2N\left[\tilde{T}^a_b + \frac{1}{2}h^a_b(\tilde{T}^0_0 - \tilde{T}^c_c)\right], \tag{8} $$

where $\tilde{\bullet}$ is modification of $\bullet$. (Generally, the spatial derivatives are removed.)

Now we define the AVTD singularity.

Definition 1 (Isenberg and Moncrief [17]) *A spacetime (M,g) is AVTD if*

1. *it is a solution to Einstein's equations;*
2. *there exists another $(M,\tilde{g})$ and there exists a foliation $i_t : \Sigma^3 \to M$ such that*
   (a) *$(M,\tilde{g})$ obeys the VTD equations relative to i_t;*
   (b) *metric g asymptotically approaches $\tilde{g}$ as $t \to 0$ in the sense that, for an appropriate norm $\|\bullet\|$ on the space of $3+1$ quantities $\bullet$, for any $\epsilon > 0$ there exists $T > 0$ such that for all $t < T$, $\|\bullet - \tilde{\bullet}\| < \epsilon$.*

Furthermore, a spacetime (M,g) has the AVTD singularity if

1. *it contains a spacelike singularity;*
2. *it is AVTD.*

To sum up, singularities are called AVTD if all spatial curvature and spatial derivative terms in Einstein's equations can be neglected as $t \to 0$. Then, near AVTD singularity, AVTD solutions can be interpreted as a different spatially homogeneous cosmology at each point in space [6].

In order to see an example of the AVTD singularity, let us consider Bianchi I (Kasner) spacetimes. Since these spacetimes are spatially homogeneous, there is no spatial derivative terms. Furthermore, Bianchi I spacetimes are spatially flat, i.e. ${}^{(3)}R = 0$. Therefore, the singularity is necessarily AVTD. On the other hand, Bianchi IX spacetimes are not AVTD but Mixmaster [5, 23] since the spatial curvature is not vanish and the "potential" term constructed by the spatial curvature cannot be neglected as approaching to the singularity (See Sec. 3).

3 Influence of matter fields

BKL assumed the vacuum spacetimes originally in the investigation of the singularity. The reason for putting such assumption is illustrated as follows. For simplicity, consider Kasner spacetimes with a perfect fluid whose equation of state is $p = (\gamma - 1)\rho$, where ρ and p are the energy density and the pressure, respectively. The metric ds_I^2 of the spacetimes is

$$ds_I^2 = -dt^2 + A^2(t)dx^2 + B^2(t)dy^2 + C^2(t)dz^2,$$

where $A = t^{p_1}$, $B = t^{p_2}$, $C = t^{p_3}$ and $p_1 + p_2 + p_3 = p_1^2 + p_2^2 + p_3^2 = 1$. The square of shear σ is estimated as

$$\sigma^2 \sim \left(\frac{\dot{A}}{A} - \frac{\dot{B}}{B}\right)^2 + \left(\frac{\dot{B}}{B} - \frac{\dot{C}}{C}\right)^2 + \left(\frac{\dot{C}}{C} - \frac{\dot{A}}{A}\right)^2 \sim t^{-2} \sim S^{-6},$$

where $S^3 = ABC \sim t$ is a volume element. Hence, the contribution from the shear is more dominant than that of the energy density $\rho \sim S^{-3\gamma}$ near singularities ($t = 0$) if $1 \leq \gamma < 2$ for natural matters such as a dust ($\gamma = 1$) and a radiation ($\gamma = 4/3$). Thus, the effect of the matter field is negligible for the behaviors of the spacetime near singularities, and we can mainly consider the vacuum case.

We must, however, look more carefully into the influence of the energy density in the case $\gamma = 2$, where time dependence of the energy density and shear are equivalent. The matter with $\gamma = 2$ is a stiff matter [2], and is not realistic matter in the relativistic sense. However, it is known that a scalar field ϕ is algebraically equivalent to a stiff matter if $\nabla\phi$ is timelike [29], where ∇ is covariant derivative with respect to g. Therefore, the existence of scalar fields will give strong influence on the nature of singularities.

Actually, BK found that massless scalar fields can suppress Mixmaster oscillations in Bianchi I spacetimes [4]. Numerically, Berger verified BK's result in Bianchi IX spacetimes and furthermore, she showed that Mixmaster oscillations are suppressed also in non-polarized $U(1)$-symmetric and magnetic Gowdy spacetimes which are Mixmaster if there exist no scalar fields [7].

On the contrary, there is a possibility that the existence of exponential potentials of scalar fields drastically change the behavior of singularities, i.e. the Mixmaster dynamics may comes back. Recall the mechanism of the Mixmaster dynamics. The metric ds_{IX}^2 and the Hamiltonian $\mathcal{H}_{IX}$ for Bianchi IX spacetimes [23, 7] are

$$ds_{IX}^2 = -dt^2 + e^{2\Omega}(e^{2\beta})_{ij}\sigma^i\sigma^j$$

and

$$2\mathcal{H}_{IX} = -p_\Omega^2 + p_+^2 + p_-^2 + V(\Omega, \beta_\pm),$$

where Ω is $1/3$ of the logarithm of the spatial volume, $\beta = \mathrm{diag}(-2\beta_+, \beta_+ + \sqrt{3}\beta_-, \beta_+ - \sqrt{3}\beta_-)$ is the anisotropic shear and $d\sigma^i = \epsilon^i_{jk}\sigma^j \wedge \sigma^k$. p_Ω and $p_\pm$ are conjugate momenta of Ω and $\beta_\pm$, respectively. The "potential" term $V(\Omega, \beta_\pm)$ is given by

$$V(\Omega, \beta_\pm) = e^{4\Omega}\left[e^{-8\beta_+} + e^{4\beta_+ + 4\sqrt{3}\beta_-} + e^{4\beta_+ - 4\sqrt{3}\beta_-} - 2\left(e^{4\beta_+} + e^{-2\beta_+ - 2\sqrt{3}\beta_-} + e^{-2\beta_+ + 2\sqrt{3}\beta_-}\right)\right].$$

It is known that Bianchi IX spacetime has singularity as $\Omega \to -\infty$. If this spacetime is AVTD, the "potential" must vanish as $\Omega \to -\infty$. When $V(\Omega, \beta_\pm) = 0$, we have the solution $\beta_\pm = \beta_\pm^0 + v_\pm$ by varying the Hamiltonian $\mathcal{H}_{IX}$ and the Hamiltonian constraint $\mathcal{H}_{IX} = 0$ is $v_+^2 + v_-^2 = 1$, where $v_\pm \equiv p_\pm/|p_\Omega|$. Then,

$$V \approx e^{-4|\Omega|(1+2\cos\theta)} + e^{-4|\Omega|(1-\cos\theta-\sqrt{3}\sin\theta)} + e^{-4|\Omega|(1-\cos\theta+\sqrt{3}\sin\theta)},$$

where $v_+ = \cos\theta$ and $v_- = \sin\theta$. For generic θ (except for $\theta = 0, 2\pi/3, 4\pi/3$), the term V exponentially grows as $\Omega \to -\infty$. This is a contradiction. Thus, Bianchi IX spacetimes are not AVTD since the "potential" term becomes dominated near singularities. As a result, reflections by the potential cause the Mixmaster dynamics.

As we can learn from the above discussion, the essential point is the existence of exponentially growing "potential" terms. Then, BK have claimed that scalar fields exponentially coupled to the Maxwell field

restores Mixmaster oscillations in Bianchi I spacetimes [4]. Berger also suggested that if there exists a "potential"

$$V(\phi) = a^2 e^{\alpha\phi} + b^2 e^{-\beta\phi}, \quad \alpha, \beta > 0, \tag{9}$$

where a and b are functions, then Mixmaster oscillations can be retained in homogeneous and further inhomogeneous spacetimes [7].

At a glance, these suggestions are plausible since it seems that Mixmaster can not be avoided whenever $\phi \to \pm\infty$ as $t \to 0$ in Eq.(9). However, is this true? In our opinion, the circumstance is not so simple in any inhomogeneous spacetimes since the nonlinear gravitational effect may not necessarily be even for both terms in Eq.(9). That is, if the gravitational effect is dominated rather than influences of the scalar field in one term and the situation is the reverse in another term, the behavior of each "potential" terms would be independent. Therefore, whole "potential terms may dump in some cases even if $\phi \to \pm\infty$ as $t \to 0$. As a result, such spacetimes are AVTD not Mixmaster. Thus, the AVTD singularity is probable even though there is a "potential" term like Eq.(9) in inhomogeneous spacetimes.

It should be noted that this form of potential arises from the low energy effective superstring theory. It contains the dilaton and axion field which are non-minimally couples to the Maxwell field. Form the unified theoretical point of view, it is believed that the distinction between gravity and matter fields cannot be maintained near spacetime singularities and the superstring theory is the most promising candidate of such unified theories [28]. Also, it is pointed out that EMD system with a positive cosmological constant has new mechanism forming singularities [21]. Hence, it is important to investigate the behavior around the singularity in EMDA system.

4 Einstein-Maxwell-Dilaton-Axion system in Gowdy spacetimes on $T^3 \times R$

In this section we introduce a model and assumptions. First we adopt Gowdy spacetimes. Gowdy proposed spatially compact and inhomogeneous spacetimes with the following metric [12];

$$ds^2 = e^{\lambda(t,\theta)/2} t^{-1/2}(-dt^2 + d\theta^2) + R(t,\theta)\left[e^{-Z(t,\theta)}(dy + X(t,\theta)\,dz)^2 + e^{Z(t,\theta)}dz^2\right]. \tag{10}$$

Gowdy spacetimes have two twist free spacelike Killing vectors $\partial/\partial y$ and $\partial/\partial z$. Spatial topology of the spacetimes are classified into three types, T^3, $S^2 \times S^1$ and S^3. We will consider only the simplest case T^3 since the isometry group action has no degenerate orbits and therefore Einstein's equations have no corresponding singularities [24].

Properties of the metric (10) depend on whether ∇R is timelike, spacelike or null. When the metric Eq. (10) describes a cosmological model, i.e. ∇R is globally timelike and the spatial topology is T^3, one can take the function $R(t,\theta)$ for t without loss of generality by Gowdy's corner theorem if the spacetime is vacuum [12]. This fact can be led from Einstein's equations, that is

$$G_{tt} - G_{\theta\theta} = \ddot{R} - R'' = 0, \tag{11}$$

where dot and prime denotes t and θ derivatives, respectively. Also in EDA system, Eq. (11) holds [3]. In Einstein-Maxwell system, Eq. (11) is not satisfied generically. However in the case that the field strength $F_{\mu\nu} = \partial_\mu A_\nu - \partial_\nu A_\mu$ has only the following components [22];

$$F_{ty} = \dot{\omega}, \quad F_{\theta y} = \omega', \quad F_{tz} = \dot{\chi}, \quad F_{\theta z} = \chi',$$

it is satisfied. This situation does not change even if the dilaton field is exponentially coupled with the Maxwell field. Thus, in EMDA system, we can put $R(t,\theta) = t$. Hereafter, we will choose this gauge. In this case, Gowdy spacetimes have spacelike singularities at $t = 0$ [12].

The action of the EMDA theory is

$$\begin{aligned} S &= \int d^4x\sqrt{-g}\left[-{}^{(4)}R + e^{-2a\phi}F^2 + 2(\nabla\phi)^2 + \frac{1}{3}e^{-4a\phi}H^2\right] \\ &= -\frac{1}{2}t\left[\ddot{\lambda} - \lambda'' + \dot{Z}^2 - Z'^2 + e^{-2Z}\left(\dot{X}^2 - X'^2\right)\right] \end{aligned}$$

$$-2e^{-2a\phi}\left[\left(e^{-Z}X^2+e^{Z}\right)\left(\dot{\omega}^2-\omega'^2\right)+e^{-Z}\left(\dot{\chi}^2-\chi'^2\right)-2Xe^{-Z}\left(\dot{\omega}\dot{\chi}-\omega'\chi'\right)\right]$$
$$-2t\left(\dot{\phi}^2-\phi'^2\right)-\frac{1}{2}e^{4a\phi}t\left(\dot{\kappa}^2-\kappa'^2\right),$$

where $\phi = \phi(t,\theta)$ is the dilaton field, $H = dB \equiv -\frac{1}{2}e^{4a\phi} * d\kappa(t,\theta)$ is the three-index antisymmetric tensor field being dual to the axion field κ and a is a coupling constant [28]. In the case of the effective superstring theory, $a = 1$. If we neglect the axion field, $a = \sqrt{3}$ gives Kaluza-Klein theory. If $a = 0$, the dilaton and axion fields decouple with the gravity and the system becomes equivalent to the vacuum case.

Note that the metric function λ is decoupled with other functions, and that λ appears only in the Hamiltonian and momentum constraints. Then, we focus on evolution equations. If one need λ, we can calculate it by evaluating that the integral of λ' from 0 to 2π vanishes after obtaining other functions,.

Gowdy spacetimes are called *polarized* if $X \equiv 0$, while *non-polarized* if they are not polarized.

5 Review of the Fuchsian algorithm

The above system is very complicated and give rise to the highly nonlinear partial differential equations which are nontrivially couples to the matter fields. In order to investigate this system, we adopt the Fuchsian algorithm. This algorithm is developed by Kichenassamy and Rendall. One of the advantages of this algorithm is to be able to use for general (nonlinear and/or singular) partial differential equations (PDEs). Another advantage of the Fuchsian algorithm is to be able to apply for arbitrary spatial dimension. (Spatial dimension in Gowdy spacetimes is one since these spacetimes have two spacelike Killing vector fields.) This fact suggests that the Fuchsian algorithm is applicable to fewer or no symmetry spacetimes [26, 1].

In this section, we briefly review the Fuchsian algorithm. Its precise and complete arguments are entrusted to Refs. [19, 16, 18]. Let us consider a PDE system

$$F\left[u(t,x^a)\right] = 0. \tag{12}$$

Generically, u can have any number of components. Here, we will assume that the PDE is singular with respect to the argument t. The Fuchsian algorithm consists of three steps as follows.

1st step. Identify the leading (singular) terms $a(t,x)$ which is a part of the desired expansion for u. This means that the most singular terms cancel each other when $a(t,x)$ is substituted in Eq. (12).

2nd step. Introduce a renormalized unknown v, which is given by

$$u = a + t^m v. \tag{13}$$

If $a \sim t^k$, we should set $m = k + \epsilon$, where $\epsilon > 0$.

3rd step. Obtain a *Fuchsian system* for v by substituting Eq. (13) in Eq. (12). That is,

$$(D + A)v = t^{\epsilon} f(t, x, v, \partial_x v), \tag{14}$$

where $D \equiv t\partial_t$ and A is a matrix which does not depend on t. f can be assumed to be analytic in all of arguments except t and continuous in t.

Once we have the Fuchsian system, we can show the existence of a unique solution for prescribed singular part a by the following theorem.

Theorem 1 (Theorem 3 of Ref. [19]) *Let us consider a system Eq. (14), where A is an analytic matrix near $x = 0$, such that $\|\sigma^A\| \leq C$ for $0 < \sigma < 1$ and f is analytic in space x and continuous in time t. Then the system (14) has exactly one solution which is defined near $x = 0$ and $t = 0$, and which is analytic in space and continuous in time, and tend to zero as $t \to 0$.* □

Applying the Fuchsian algorithm to our problem of Gowdy spacetimes in EMDA system, the procedure is summarized as follows.

1. Solve VTD equations as ordinary differential equations with respect to t.

2. Substitute solutions obtained above into full Einstein's equations. Here, make integral constants unknown functions of spatial arguments x.

3. Obtain a Fuchsian system for unknown functions and see every eigenvalues of A and powers of f.

4. Apply Theorem 1 to the system.

If every eigenvalues of A are non-negative and powers of f are positive, renormalized unknown functions are identically zero as $t \to 0$ by Theorem 1. Thus, we have AVTD singular solutions. Essentially, the above argument is a singular version of the Cauchy-Kowalevskaya theorem [1].

6 Results and summary

We are now ready to examine the singularity in EMDA system. EMDA system with Gowdy symmetry, however, has six functions (Z, X, ω, χ, ϕ, κ), and it is very complicated to treat all of them at the same time. Hence, we will reduce the system by selecting four functions from them for simplicity. As a selection rule, it is important to leave exponential coupling between the dilaton and other fields since, as mentioned in Sec.3, an essential part to analyze the nature of singularities is whether or not potential terms in Einstein's equations exponentially grow as $t \to 0$ [6, 7]. Therefore, we examined three cases, which are non-polarized EMD ($\chi = 0$, $\kappa = 0$), non-polarized EDA ($\omega = 0$, $\chi = 0$) and polarized EMDA ($X = 0$, $\chi = 0$). In any case, Our results state that T^3 Gowdy spacetimes in EMDA system have AVTD singularities in general in the sense that these AVTD singular solutions depend on the maximal number of singular data. This fact supports BKL conjecture as a special case, that is, the dynamics of spatially different points effectively decouples but the spacetimes do not oscillate like Mixmaster near cosmological singularities.

Let us compare to the results of GM and KR in the (non-)polarized and vacuum case [13, 19]. If spacetimes are vacuum, then non-polarized T^3 Gowdy spacetimes are AVTD under the low-velocity condition. Also, when $X \equiv 0$ (polarized), the spacetimes are AVTD without the low-velocity condition. In any case, our results clearly include GM and KR's. That is, when all of matter fields vanish, theorems of GM and KR are reproduced.

Our results are counterexamples for Berger's suggestion since the existence of a "potential" like Eq.(9) does not cause necessarily the Mixmaster behavior [7]. Our results, however, indicate that the existence of the "potential" narrows down a set of families of AVTD solutions. Thus, Berger's suggestion may be correct in the weak sense that the AVTD behavior is controlled by a "potential" like Eq.(9).

We can verify that the Kretschemann invariant $R^{\mu\nu\lambda\sigma}R_{\mu\nu\lambda\sigma}$ of all of our AVTD solutions is blow up like $t^{-(Z_0^2+2\phi_0^2+3)}$. Thus, our AVTD singularity is the curvature singularity. This indicates the validity of the strong cosmic censorship for T^3 Gowdy spacetimes in EMDA system since the spacetimes cannot be extended beyond the singularity similar to the vacuum case [13, 17, 24].

Finally, we would like to comment on study in the future. To avoid complicated calculation we focused only four functions among six functions (Z, X, ω, χ, ϕ and κ). In the next step we should try the case that all of six functions are not zero. Even this case, we expect that T^3 Gowdy spacetimes in EMDA system have AVTD singularities. The power of the leading parts for the Fuchsian system are $2Z$, $-4a\phi$, $2-2Z$, $2+4a\phi$, $1 \pm 2a\phi \pm Z$ and/or $1 \pm 2a\phi \mp Z$ in any case as seen from the action of EMDA theory. We can make all of these values positive. Thus, T^3 Gowdy spacetimes in EMDA system would be AVTD at the singularity in general.

Another object for further investigation is to study asymptotic behavior of $U(1)$-symmetric spacetimes. Einstein's equations for $U(1)$-symmetric spacetimes are very complicated since these spacetimes have only one spacelike Killing vector. However, the Fuchsian algorithm is independent on space dimension and then it is applicable with low symmetry assumptions like $U(1)$-symmetry. Recently, the Fuchsian algorithm is used for vacuum polarized $U(1)$-symmetric and for diagonal spacetimes in Einstein-scalar field system [16, 1]. Our interest is to know whether non-polarized $U(1)$-symmetric spacetimes in EMDA system are AVTD or not. This subject is in progress.

References

[1] Andersson L 1999 *The global existence problem in general relativity* gr-qc/9911032

[2] Barrow J D 1978 Nature **272** 211

[3] Barrow J D and Kunze K E 1997 Phys. Rev. **D56** 741

[4] Belinskii V A and Khalatnikov I M 1973 JETP **36** 591

[5] Belinskii V A, and Khalatnikov I M and Lifshitz E M 1982 Adv. Phys. **31** 639

[6] Berger B K 1998 *Numerical Approaches to Spacetime Singularities* Living Reviews in Relativity **1** 7

[7] Berger B K 2000 Phys. Rev. **D61** 023508

[8] Carmeli M, Charach C and Malin S 1981 Phys. Rep. **76** 79

[9] Collins C B and Ellis G F R 1979 Phys. Rep. **56** 65

[10] Eardley D, Liang E and Sachs R 1972 J. Math. Phys. **13** 99

[11] Garfinkle D 1999 Phys. Rev. **D60** 104010

[12] Gowdy R H 1974 Ann. Phys. **83** 203

[13] Grubišić B and Moncrief V 1993 Phys. Rev. **D47** 2371

[14] Hawking S W and Ellis G F R 1973 *The large scale structure of space-time* (Cambridge: Cambridge University Press)

[15] Hawking S W and Penrose R 1970 Proc. Roy. Soc. Lond. A. **314** 529

[16] Isenberg J and Kichenassamy S 1999 J. Math. Phys. **40** 340

[17] Isenberg J and Moncrief V 1990 Ann. Phys. **199** 84

[18] Kichenassamy S 1996 *Nonlinear Wave Equations* (New York: Marcel Dekker)

[19] Kichenassamy S and Rendall A D 1998 Class. Quantum Grav. **15** 1339

[20] Maeda K, Ishibashi A and Narita M 1998 Class. Quantum Grav. **15** 1637

[21] Maeda K, Torii T and Narita M 1998 Phys. Rev. Lett. **81** 5270

[22] Mansfield P A 1989 dissertation Yale University

[23] Misner C W 1969 Phys. Rev. Lett. **29** 1071

[24] Moncrief V 1981 Ann. Phys. **132** 87

[25] Narita M 1998 Phys. Rev. **D58** 127501

[26] Rendall A D 1998 *The structure of singularities in inhomogeneous cosmological models* gr-qc/9804036

[27] Senovilla J M M 1998 Gen. Rel. Grav. **30** 701

[28] Shapere A, Trivedi S and Wilczek F 1991 Mod. Phys. Lett. **A6** 2677

[29] Wainwright J and Ellis G F R 1997 *Dynamical systems in Cosmology* (Cambridge: Cambridge University Press)

Inversion of Spacetime with Maximally Charged Black Holes

Takashi Mishima [1]

Laboratories of Physics, College of Science and Technology, Nihon University, Narashinodai, Funabashi, Chiba274-8501, Japan

Hideki Ishihara[2]

Department of Physics, Tokyo Institute of Technology, Oh-okayama, Meguro-ku, Tokyo 152-8550, Japan

Takashi Okamura[3]

Department of Physics, Ochanomizu University, Ochanomizu, Bunkyo-ku, Tokyo 169-8555, Japan

Abstract

We consider the transfotmation properties of spacetime with maximally charged black holes under inversion transformation which replace the event horizon with the infinity, following the suggestion of our previous work. First We find the spacetime of Reissner-Nordström solution has conformal invariance under the inversion. Secod we extend the investigation to the spacetime with an assemblage of black holes (Majumdar-Papapetorou solution) and the behavior of massless scalar field equation on the spacetime. In the case of many black holes, the spacetime does not return to the original one up to conformal factor, but changes into other spacetime with a different assemblage of black holes. The field equation on the original spacetime also is transformed into the equation on the spacetime changed. we also suggest the perturbative equations of Einsten-Maxwell system have the same behavior.

1 Introduction

General relativity allows various kinds of solution of spacetime including black holes. The solutions corresponding to extreme black holes form the boundary of the set of black hole solutions. Near or on the boundary, we expect new phenomena to occur like the case of critical phenomena. During these decades, theoretical physisists have clarified several aspects of extremality. For example, extremality is the signal of the BPS states connected with supersymmetry[1, 2]. Recently the theoretical physisists believe such extremal solutions have crucial roles to construct a fundamental theory like stringy theories[3]. So the extremal black holes have important and interesting properties to study the fundamental physics[4].

Today many kinds of extremal black hole solutions have been found and many reseachers try to understand their properties vigorously[5]. Compared with these extremal black holes in generalized gravitational theories, the original extremal solutions in Einstein gravitational theory are the simplest ones(*i.e.* extreme Kerr solution, extreme Reissner-Nordstörm one, Majumdar-Papapetorou solution and etc., See Ref.[6, 7] for examples) and interesting enough to study.

Previously we investigated the behavior of fields around extreme Reissner-Nordström black hole spacetime, especially of perturbation equations of Einstein-Maxwell system. We first numerically found that quasinormal frequencies of gravitational waves and electromagnetic waves about extreme Reissner-Nordström black hole coincide with some shift of angular momentum parameters[8]. In the second paper

[1] E-mail:tmishima@phys.ge.cst.nihon-u.ac.jp
[2] E-mail:ishihara@th.phys.titech.ac.jp
[3] E-mail:okamura@skymint.phys.ocha.ac.jp

we show that spin 3/2 fields also have the same behavior and make a trio with gravitational waves and electromagnetic waves[9]. At the same time we give an explanation of the coincidence by finding some relation between the potentials of radial part of perturbation equations. Following this discovery, one of the authors succeeded to give another explanation from supersymmetric viewpoint[10], which seems to have no relation to the former explanation apparently.

As described in the next section, the former explanation above is related to a certain kind of inversion transformation which reverse the positions of the event horizon and the infinity, so that naturally lead to the thought that the background spacetime itself has some interesting properties under the inversion. In this article, we study the transfotmation property of spacetime with maximally charged black holes under the inversion. After the brief review of the explanation, first we study the case of Reissner-Nordström solution. Second we extend the investigation to the spacetime with an asseblage of black holes(Majumdar-Papapetorou solution). Next we try to study the behavior of the field equaitons in the spacetime with maximally charged black holes under the inversion. Although the full treatment has not been established for perturbation equations of Einstein-Maxwell system, we give some clues to develop the study finally.

2 Behavior of Zerilli-Moncrief Potentials

For the case of a stationary black hole the perturbative equations are decoupled into ordinary differetial equations by separation of variables. In particular the radial equations can be reduced to the 1-dimensional Schrödinger-type equations

$$\left[\frac{d^2}{dr_*^2}+\omega^2-V_s(r)\right]Z_s(r_*)=0, \quad dr_*=\frac{r^2}{\Delta}dr \tag{1}$$

where r_* is the tortoise coordinate, $\Delta = r^2 - 2Mr + Q^2$ in the case of a charged black hole (the parameters M and Q are black hole mass and charge respectively) and $V_s(r)$ is Zerilli-Moncrief potential with some dependence on angular momentum parameter. The subscript s takes 1 or 2 which coresponds to electromagnetic fields or gravitational fields respectively. We can see the behavior of perturbations about the black hole by solving or evaluating the radial equations.

In the previous first paper, we showed numerically that the quasinormal frequencies of gravitational waves and those of electromagnetic waves are equal with a suitable shift of angular momentum parameter in the case of extremal charged black hole[8]. And subsequently we gave the proof of the coincidence as follows[9]. In the extremal case the Zerilli-Moncrief potentials of Eq.(1) are

$$V_1 = (j_1+1)\frac{df}{dr_*}-4f^3+(j_1+1)^2f^2 \tag{2}$$

$$V_2 = j_2\frac{df}{dr_*}-4f^3+j_2^2f^2 \tag{3}$$

$$j_s = l+s \ \ (l=0,1,2,\cdots), \quad f=\frac{r-M}{r^2}.$$

Here r_* and r have the following relation

$$r_* = r - M + \ln(r-M)^2 - \frac{1}{r-M}. \tag{4}$$

Hence the following relation is valid

$$V_1(-r_*\,;\, j_1=j) = V_2(r_*\,;\, j_2=j+1), \tag{5}$$

under the reflection

$$r_* \longmapsto -r_* \ \ (r-M \longmapsto \frac{1}{r-M}). \tag{6}$$

Thus we can see that the scattering amplitudes of both perturbative equations are essentially equal so that the quasinormal frequencies have the same behavior.

For the explanation above, the simple behavior of the perturbed equations under the reflection of the tortoise coordinate is essential. We consider the massless scalar field as an another example. In this case we also obtain the analogous Schrödinger-type equation

$$\left[\frac{d^2}{dr_*^2} + \omega^2 - V_0(r)\right] Z_0(r_*) = 0, \tag{7}$$

where $V_0 = 2f^3 + j_0(j_0+1)f^2$. From this equation we can easily find that under the reflection the potential is invariant so that the massless scalar field equation with any curvature coupling is too. Consequently we are naturally led to the idea that the backgroud geometry has some symmetry under the transformation.

3 Inversion of Extreme Reissner-Nordstörm solution

Following the suggestion in the previous section, first we investigate the behavior of the spacetime with an extremal charged black hole(i.e. extreme Reissner-Nordstörm solution). The metric of extreme Reissner-Nordstörm solution is as follows

$$ds^2 = -\left(1 - \frac{M}{r}\right)^2 dt^2 + \left(1 - \frac{M}{r}\right)^{-2} dr^2 + r^2 d\Omega^2. \tag{8}$$

Under the transformation (6); $r - M \longmapsto \tilde{r} = \frac{1}{r-M}$, the metric (8) is transformed into

$$ds^2 = \left(\frac{M}{\tilde{r} - M}\right)^2 \left[-\left(1 - \frac{M}{\tilde{r}}\right)^2 dt^2 + \left(1 - \frac{M}{\tilde{r}}\right)^{-2} dr^2 + \tilde{r}^2 d\Omega^2\right]. \tag{9}$$

These equations clearly tell us that the spacetime is conformally invariant under the transformation.

When we introduce the new coordinate $r' = r - M$, the transformation above can be interpreted as more familiar transformation in mathematics(i.e. inversion). The transformation is then described as

$$r' \longmapsto \tilde{r}' = \frac{M}{r'}. \tag{10}$$

The metric is described as

$$ds^2 = -\left(1 + \frac{M}{r'}\right)^{-2} dt^2 + \left(1 + \frac{M}{r'}\right)^2 \left[dr'^2 + r'^2 d\Omega^2\right] \tag{11}$$

$$= \left(\frac{M}{\tilde{r}'}\right)^2 \left\{-\left(1 + \frac{M}{\tilde{r}'}\right)^{-2} dt^2 + \left(1 + \frac{M}{\tilde{r}'}\right)^2 \left[d\tilde{r}'^2 + \tilde{r}'^2 d\Omega^2\right]\right\}, \tag{12}$$

where the first metric form is just a single black hole case of Majumdar-Papapetorou solution. From now on we use Majumdar-Papapetoru form so that $'$ is omitted.

The explicit form of the inversion is the same as of 3 dimensional Euclidian space E^3,

$$\tilde{r} = \left(\frac{M}{r}\right)^2 r \quad (\tilde{r}r = M^2) \tag{13}$$

where $\boldsymbol{r}$ and $\tilde{\boldsymbol{r}}$ are position vectors and r and $\tilde{r}$ are lengths of $\boldsymbol{r}$ and $\tilde{\boldsymbol{r}}$ in E^3. It must be noticed that the black hole spacetime is not conformally invariant unless the inversion is done with respect to the black hole event horizon $r = 0$ and parameter M, while the inversion in E^3 is not restricted to the paticular points.

4 The Case of an assemblage of Extremal Black Holes

Majunda-Papapetorou solution (abbreviated to MP solution) represents an assemblage of extremal black holes whose configuration is static due to the balance of gravitational forces and Coulomb forces. The metric of MP solution corresponding to $N + 1$ black holes is

$$ds^2 = -U^{-2}dt^2 + U^2 dr^2 \tag{14}$$

$$U = 1 + \frac{M}{r} + \sum_{i=1}^{N} \frac{M_i}{|r - r_i|} \tag{15}$$

where dr^2 is the metric of E^3. Mass of the black hole sited on the origin is M. The indices i,j,k are assigned to other N black holes in the system. Mass of i-th black hole is represented by $M_i (i = 1, ..., N)$ and $|r - r_i|$ is the Euclidean length from i-th black hole.

Now we apply the inversion (13) with respect to the origin to the metric above. Then the metirc becomes

$$ds^2 = \left(\frac{M}{\tilde{r}}\right)^2 \left[-\tilde{U}^{-2}dt^2 + \tilde{U}^2 d\tilde{r}^2\right] \tag{16}$$

$$\tilde{U} = 1 + \frac{M}{\tilde{r}} + \sum_{i=1}^{N} \frac{\tilde{M}_i}{|\tilde{r} - \tilde{r}_i|} \tag{17}$$

where $\tilde{M}_i = \frac{MM_i}{r_i}$. From Eq.(16), we can say that the inversion transforms original MP spacetime(the spacetime corresponding to MP solution) into another $\widetilde{MP}$ spacetime conformally.

5 Transformation Property of Wave Equations in MP Spacetime

In this section, we anlyze the behavior of the wave equaitons in MP spacetime under the inversion introduced in the previous section. As the case of extreme Reissner-Nordström solution, we can expect characteristic behavior of the field equations in MP spacetime under the inversion. First we treat massless scalar field equation as the simplest example

$$^{(mp)}g^{\mu\nu}\nabla_\mu\nabla_\nu\phi = 0 \tag{18}$$

where $^{(mp)}g^{\mu\nu}$ is the metric form of MP spacetime. We apply the inversion (13) to the massless scalar field (18), and at the same time transform the scalar field as follows

$$\tilde{\phi}(\tilde{x}) = \left(\frac{M}{\tilde{r}}\right)\phi(x(\tilde{x})). \tag{19}$$

This transformation is known as Kelvin transformation in mathematics. Then the equation (18) change into

$$\widetilde{^{(mp)}g}^{\mu\nu}\tilde{\nabla}_\mu\tilde{\nabla}_\nu\tilde{\phi} = 0. \tag{20}$$

This fact is nothing but the property of conformal scalar field in under the general conformal transformation (See Ref.[11] for an example), Although no distinction between conformal case and non-conformal one appears due to the Ricci scalar free. Here we note that as a particular property of the MP spacetime a weight-free part Z can be extracted from the scalar field ϕ,

$$\begin{aligned} Z(x) &= (r + M)\phi(x) \\ &= (\tilde{r} + \tilde{M})\tilde{\phi}(\tilde{x}) \\ &= Z(\tilde{x}). \end{aligned}$$

In the case of single black hole, the equation of $Z(x)$ corresponds to Eq.(7). The extension of the analysis to the case of free fields with spin 1/2 or 1 is straightforwards. We easily expect the same behavior as that of the scalar field.

Next we must discuss whether the perturbation equations of the Einstein-Maxwell system have the same behavior as above. Einstein-Maxwell system has no conformal invariance under the general conformal transformation, and so we cannot directly say that generalization of the behavior in the single black hole case is possible. And further it seems to be too complicated to handle the perturbative equaitons directly. But we think that a certain simple property is hidden behind such intricasy. In the last of this paper, we analyze the perturbation equations by the use of geometrical optics approximation[7, 12] as an evidence.

Let $h_{\mu\nu}$ and a_μ be small perturbations against backgroud spacetime. And expand the Einsten-Maxwell system about the background to linear order in $h_{\mu\nu}$ and a_μ with gauge fixing conditions $\nabla_\mu k^{\mu\nu} = 0$ and $\nabla_\mu a^\mu = 0$ where $k_{\mu\nu} = h^{\mu\nu} - \frac{1}{2}g^{\mu\nu}h$. Then we use the geometrical optics approximation under the assumption $\lambda \ll L$ where λ is the typical wavelength and L is the typical radius of curvature of the background. We substitute the perturbations a_μ and $k_{\mu\nu}$ in the follwing form into the linearized Einstein-Maxwell equations,

$$a_\mu = \mathrm{Re}\left[(\alpha_\mu + \epsilon\beta_\mu + \cdots)e^{iS/\epsilon}\right] \tag{21}$$

$$k_\mu = \mathrm{Re}\left[(\kappa_{\mu\nu} + \epsilon\pi_{\mu\nu} + \cdots)e^{iS/\epsilon}\right] \tag{22}$$

where ϵ is a parameter of order λ/L. We obtain the set of equaitons in geometric optics by picking out the terms of order ϵ^{-1} and ϵ^{-2} as follws

$$l_\mu l^\mu = 0 \tag{23}$$

where $l_\mu = \partial_\mu S$, and

$$l^\mu \kappa_{\mu\nu} = 0, \quad l^\mu \alpha_\mu = 0 \tag{24}$$

$$\nabla_\rho l^\rho \alpha^\mu + 2l^\rho \nabla_\rho \alpha^\mu = l_\rho \left(\frac{1}{2}F^{\mu\rho}\kappa - F^{\rho\sigma}\kappa^\mu_\sigma\right) \tag{25}$$

$$\nabla_\rho l^\rho \kappa_{\mu\nu} + 2l^\rho \nabla_\rho \kappa_{\mu\nu} = -4\left(F^\rho_\mu l_{[\nu}\alpha_{\rho]} + F^\rho_\nu l_{[\mu}\alpha_{\rho]} + \frac{1}{2}g_{\mu\nu}F^{\rho\sigma}l_\rho\alpha_\sigma\right). \tag{26}$$

Next we introduce the set of null tetrad $(l^\mu, n^\mu, m^\mu, \bar{m}^\mu)$ which obey the equations $l^\mu m_\mu = -1$, $m^\mu \bar{m}_\mu = 1$, $l^\mu \nabla_\mu n^\nu = 0$, $l^\mu \nabla_\mu n^\nu = 0$ and then represent α_μ, $\kappa_{\mu\nu}$ as

$$\alpha_\mu = A\bar{m}_\mu + \tilde{A}m_\mu \tag{27}$$

$$\frac{1}{2}\kappa_{\mu\nu} = H\bar{m}_\mu\bar{m}_\nu + \tilde{H}m_\mu m_\nu. \tag{28}$$

Finally from Eqs.(25), (26) the following equations are obtained

$$l^\mu \partial_\mu A - \rho A = \tilde{\Phi}_0 H \tag{29}$$

$$l^\mu \partial_\mu H - \rho H = -\Phi_0 A \tag{30}$$

where $\rho = -\frac{1}{2}\nabla_\nu l^\nu$ and $\Phi_0 = F^{\mu\nu}l_\mu\alpha_\nu$.

Now we transform the basic equations (29), (30) under the inversion

$$r \mapsto \left(\frac{M}{r}\right)^2 r,$$

and the following transformations (i.e. Generalized Kelvin transformation) are also done

$${}^{(mp)}g_{\mu\nu} \mapsto {}^{(\widetilde{mp})}g_{\mu\nu} = \left(\frac{r}{M}\right)^2 {}^{(mp)}\tilde{g}_{\mu\nu} \tag{31}$$

$${}^{(mp)}A_\mu \mapsto {}^{(\widetilde{mp})}A_\mu = -\left(\frac{r}{M}\right) {}^{(mp)}\tilde{A}_\mu \tag{32}$$

$${}^{(mp)}l_\mu \mapsto {}^{(\widetilde{mp})}l_\mu = {}^{(mp)}\tilde{l}_\mu \tag{33}$$

$$
{}^{(mp)}n_\mu \mapsto {}^{(\widetilde{mp})}n_\mu = \left(\frac{r}{M}\right)^2 {}^{(mp)}\tilde{n}_\mu \tag{34}
$$

$$
{}^{(mp)}m_\mu \mapsto {}^{(\widetilde{mp})}m_\mu = \left(\frac{r}{M}\right) {}^{(mp)}\tilde{m}_\mu \tag{35}
$$

$$
{}^{(mp)}A \mapsto {}^{(\widetilde{mp})}A = -\left(\frac{M}{r}\right) {}^{(mp)}\tilde{H} \tag{36}
$$

$$
{}^{(mp)}H \mapsto {}^{(\widetilde{mp})}H = \left(\frac{M}{r}\right) {}^{(mp)}\tilde{A}. \tag{37}
$$

Here the quantity with superscript (mp) or $(\widetilde{mp})$ mean the quantity is defined on the MP spacetime or $(\widetilde{MP})$ spacetime respectively. As a result the basic equations defined on the MP spacetime

$$
{}^{(mp)}l^\mu \partial_\mu {}^{(mp)}A - {}^{(mp)}\rho {}^{(mp)}A = {}^{(mp)}\tilde{\Phi}_0 {}^{(mp)}H \tag{38}
$$

$$
{}^{(mp)}l^\mu \partial_\mu {}^{(mp)}H - {}^{(mp)}\rho {}^{(mp)}H = -{}^{(mp)}\Phi_0 {}^{(mp)}A \tag{39}
$$

$$
\tag{40}
$$

is transformed into the equaitons defined on the $\widetilde{MP}$

$$
{}^{(\widetilde{mp})}l^\mu \partial_\mu {}^{(\widetilde{mp})}A - {}^{(\widetilde{mp})}\rho {}^{(\widetilde{mp})}A = {}^{(\widetilde{mp})}\tilde{\Phi}_0 {}^{(\widetilde{mp})}H \tag{41}
$$

$$
{}^{(\widetilde{mp})}l^\mu \partial_\mu {}^{(\widetilde{mp})}H - {}^{(\widetilde{mp})}\rho {}^{(\widetilde{mp})}H = -{}^{(\widetilde{mp})}\Phi_0 {}^{(\widetilde{mp})}A \tag{42}
$$

This behavior under the inversion suggests existence of a certain simple property in the full perturbative equations.

6 Summary

We found interesting properties of the background spacetime with extremally charged black holes under the inversion transformation which replace the event horizon with the infinity. The spacetime of Reissner-Nordström solution(the case of single black hole) has conformal invariance under the inversion. Majumdar-Papapetorou solution(the case of many black holes) is transformed into another Majumdar-Papapetorou solution. The behavior of wave propagations on the background also have simple transformation property. The behavior of perturbative equations of Einstein-Maxwell system has not been completely analyzed. However the behavior in the geometrical optics approximation is so impressive that we strongly expect the full perturbative equaitons have a certain symmetry or a simple transformation property on the background. Full analysis of the behavior is significant as a future problem.

On the other hand the Majumdar-Papapetorou solution is a BPS state so that the solution is supersymmetric. At pesent the relation between the supersymmetry and the behavior discussed in this paper is not clear. If any unexpected relation is found, new prospect will be open.

References

[1] E. Witten and D. Olive, Phys. Lett. **B78**, 97(1978).

[2] G. W. Gibbons and C. M. Hull, Phys. Lett. **B109**, 190(1982).

[3] J. Polchinski, *String Theory* (Cambridge University Press, Cambridge, 1998).

[4] J. M. Maldacena, Nucl. Phys. Proc. Suppl. **61A** 111(1998)

[5] R. D'Auria and P. Fre, *Lecture Notes for the SIGRAV Graduate School in Contemporary Relativity* hep-th/9807171(1998)

[6] S. Chandrasekhar, *The Mathematical Theory of Black Holes* (Oxford University Press, Oxford, 1983).

[7] V. P. Frolov and I. D. Novikov, *Black Hole Physics* (Kluwer Academic Publishers, The Netherlands,1998).

[8] H. Onozawa, T. Mishima, T. Okamura and H. Ishihara, Phys. Rev. **D53**, 7033(1966).

[9] H. Onozawa, T. Okamura, T. Mishima and H. Ishihara, Phys. Rev. **D55**, R4549(1997).

[10] T. Okamura, Phys. Rev. **D56**, 4927(1997).

[11] R. M. Wald, *General Relativity* (The University of Chicago Press, Chicago, 1984).

[12] C. W. Misner, K. S. Thorne and J. A. Wheeler, *Gravitation* (Freeman, San Francisco, 1973).

Hawking radiation with modified high frequency dispersion relation

Yoshiaki Himemoto[a1] and Takahiro Tanaka[a,b2]

[a] *Department of Earth and Space Science, Graduate School of Science Osaka University, Toyonaka 560-0043, Japan*
[b] *IFAE, Departament de Física, Universitat Autònoma de Barcelona, 08193 Bellaterra, Spain*

Abstract

The Hawking radiation is one of the most interesting phenomena predicted by the theory of quantum field in curved space. The origin of Hawking radiation is closely related to the fact that a particle which marginally escapes from collapsing into a black hole is observed at the future infinity with infinitely large redshift. In other words, such a particle had a very high frequency when it was near the event horizon. Motivated by the possibility that the property of Hawking radiation may be altered by some unknowned physics which may exist beyond some critical scale, Unruh proposed a model which has higher order spatial derivative terms. In his model, the effects of unknown physics are modeled so as to be suppressed for the waves with a wavelength much longer than the critical scale, k_0^{-1}. Surprisingly, it was shown that the thermal spectrum is recovered for such modified models. To introduce such higher order spatial derivative terms, the Lorentz invariance must be violated because one special spatial direction needs to be chosen. In previous works, the rest frame of freely-falling observers was employed as this special reference frame. We gave, furthermore, an extension by allowing a more general choice of the reference frame and showed that the resulting spectrum of created particles again becomes the thermal one at the Hawking temperature even if the choice of the reference frame is generalized in our recent work. In this paper, using the technique of the matched asymptotic expansion, we show that the correction to the thermal radiation stays of order k_0^{-2} or smaller when the spectrum of radiated particle around its peak is concerned.

1 Introduction

The thermal radiation from a black hole was first predicted by Hawking [1], which phenomenon became widely known as the Hawking radiation. This prediction is based on quantum field theory in curved space, which is thought of as an effective theory valid for low energy physics. However, when we consider the mechanism of the Hawking radiation, crucial role is played by wave packets which left the past null infinity with very high frequency. Such wave packets propagate through the collapsing body just before the horizon formed, and undergo a large redshift on the way out to the future null infinity. Here arises one question. Can it be justified to apply quantum field theory in curved space, an effective theory at low energy, to the phenomenon which involves the infinitely high frequency regime? There may exist some unknown physics which invalidates the application of the standard quantum field theory in curved space [2].

One of such possibilities is that the spacetime may reveal its discrete nature at such high frequencies. To take account of the effect of possible modification of theory in the high frequency regime, Unruh proposed a simple toy model by a sonic analog of a black hole [3, 4]. In Unruh model, the dispersion relation of fields at high frequencies are modified so as to eliminate very short wavelength modes. In some sense, this modification is arranged to reflect the atomic structure of fluid which propagates sound waves. Usually, the group velocity of sound waves drops to values much less than the low frequency value when the wavelength becomes comparable to the atomic scale. In performing such modifications [4], one must assume the existence of a reference frame because the concept of high frequencies can never be a Lorentz invariant one. Namely, the Unruh's model manifestly breaks the Lorentz invariance. To our surprise,

[1] E-mail:himemoto@vega.ess.sci.osaka-u.ac.jp
[2] E-mail:tama@vega.ess.sci.osaka-u.ac.jp

even with such a drastic change of theory, the spectrum observed at the future infinity was turned out to be kept unaltered [4, 5, 6].

In order to introduce the modified dispersion relation we need to specify one special reference frame. In previous works [4, 5, 6, 7], the rest frame of freely-falling observers was employed as the special reference frame. In this case, the thermal spectrum of the Hawking radiation was shown to be reproduced. However, it is still uncertain whether the same thing remains true even when we adopt another reference frame as the special reference frame. In our paper [8], we gave a generalization of previous works [4, 5, 6, 7] by allowing a more general choice of the reference frame and found that the resulting spectrum of created particle stays thermal one at the Hawking temperature as long as we mildly change the choice of the special reference frame. In the present paper, by a systematic use of the technique of the so-called matched asymptotic expansion, we evaluate how small the leading correction to the thermal radiation is. On the other hand, for some extreme modification of the reference frame, in which case the analytic treatment is no longer valid, the spectrum is numerically shown to deviate from the thermal one significantly.

This paper is organized as follows. First we introduce a generalization of the Unruh's model in Sec.2. We briefly review what quantities need to be evaluated in computing the spectrum of particle creation in our model and how to construct a solution of the field equation, and we finally show that the resulting spectrum of created particles become the thermal one at the Hawking temperature in Sec.2. In Sec.3, we also demonstrate some results of numerical calculation to verify our analytic results. In addition, we display the results for some extreme cases which are out of the range of validity of our analytic treatment. Section 4 is devoted to conclusion. In the present paper, we use units with $\hbar = c = 1$.

2 Computing the spectrum of black hole radiation

First, we explain how we generalize the model that was investigated in the earlier works [4, 5, 6]. Following these references, we consider a massless scalar field propagating in a 2-dimensional spacetime given by

$$ds^2 = -d\tilde{t}^2 + (d\tilde{x} - \tilde{v}(\tilde{x})d\tilde{t})^2, \tag{1}$$

where $\tilde{v}(x)$ is a function which goes to a constant at $\tilde{x} \to \infty$ and satisfies $\tilde{v}(\tilde{x}) \geq -1$ for $\tilde{x} \geq 0$. The equality holds at $\tilde{x} = 0$. Since the line element $d\tilde{x} = 0$ is null at $\tilde{v} = -1$, we find that the event horizon is located at $\tilde{v} = -1$. In this coordinate system, the unit vector perpendicular to the $\tilde{t}$ =constant hypersurfaces is given by $\tilde{u}_\alpha := \partial_\alpha \tilde{t}$, and the differentiation in this direction is given by $\tilde{u}^\alpha \partial_\alpha = (\partial_{\tilde{t}} + \tilde{v}\partial_{\tilde{x}})$. We denote the unit outward pointing vector normal to $\tilde{u}_\alpha$ by $\tilde{s}^\alpha$. In order to examine the effect on the spectrum of the Hawking radiation due to a modification of theory in the high frequency regime, they investigated a system defined by the modified action of a scalar field,

$$S = \frac{1}{2}\int d^2\tilde{x}\sqrt{-g}\, g^{\alpha\beta}\mathcal{D}_\alpha\phi^*\mathcal{D}_\beta\phi, \tag{2}$$

where the differential operator $\mathcal{D}$ is defined by $\tilde{u}^\alpha\mathcal{D}_\alpha = \tilde{u}^\alpha\partial_\alpha, \tilde{s}^\alpha\mathcal{D}_\alpha = \hat{F}(\tilde{s}^\alpha\partial_\alpha)$. If we set $\hat{F}(z) = z$, the action (2) reduces to the standard form. Since we are interested in the effect caused by the change in the high frequency regime, we assume that $\hat{F}(z)$ differs from z only for large z.

In the above model, the dispersion relation for the scalar field manifestly breaks the Lorentz invariance, and there is a special reference frame specified by $\tilde{u}$. One can easily show that this reference frame is associated with a set of freely-falling observers. As noted in Introduction, it was shown that the spectrum of the Hawking radiation is reproduced in this model. Here we consider a further generalization of this model allowing to adopt other reference frames as the special reference frame.

However, because of technical difficulties, we restrict our consideration to stationary reference frames. As we are working on a 2-dimensional model, the reference frame is perfectly specified by choosing one time-like unit vector, which we denote by u. Since $\partial_{\tilde{t}}$ in the original coordinate system $(\tilde{t}, \tilde{x})$ is a time-like Killing vector, the condition for the reference frame to be stationary becomes $\mathcal{L}_{\partial_{\tilde{t}}} u^\alpha = 0$, where $\mathcal{L}_{\partial_{\tilde{t}}}$ is the Lee derivative in the direction of $\partial_{\tilde{t}}$. This condition can be simply written as $\partial u^{\hat{\alpha}}/\partial\tilde{t} = 0$, where we used indices associated with $\hat{}$ to represent the components in the $(\tilde{t}, \tilde{x})$−coordinate. Furthermore, the covariant components $u_{\hat{\alpha}}(\tilde{x}) = g_{\hat{\alpha}\hat{\beta}}(\tilde{x})u^{\hat{\beta}}(\tilde{x})$ is also independent of $\tilde{t}$. Thus, if we introduce a new time coordinate t by

$$dt = u_{\hat{0}}^{-1}(\tilde{x})\left(u_{\hat{0}}(\tilde{x})d\tilde{t} + u_{\hat{1}}(\tilde{x})d\tilde{x}\right) = d\tilde{t} - \gamma(\tilde{x})d\tilde{x}, \tag{3}$$

the t−constant hypersurfaces become manifestly perpendicular to u_α. Here we introduced $\gamma(\tilde{x}) := -u_{\tilde{1}}(\tilde{x})/u_{\tilde{0}}(\tilde{x})$. Further, it is convenient to choose a new spatial coordinate x so that ∂_t coincide with the Killing vector. Since $\partial_{\tilde{t}} = \partial_{\tilde{t}} + \frac{\partial x}{\partial t}\partial_{\tilde{x}}$, x should be chosen as a function which depends only on $\tilde{x}$. Hence, we set $x := \int_0^{\tilde{x}} \zeta(\tilde{x}')d\tilde{x}'$. By using such a new coordinate (t, x) with $\zeta(\tilde{x}') = (1 - \tilde{v}\gamma)^2 - \gamma^2$, the metric (1) can be written in the form[3] ,

$$ds^2 = \Omega^2(x)\left[-dt^2 + (dx - v(x)dt)^2\right], \tag{4}$$

where we set

$$\Omega^2(x) := \frac{1}{(1 - \tilde{v}\gamma)^2 - \gamma^2}, \tag{5}$$

$$v(x) := \gamma + \tilde{v}(1 - \tilde{v}\gamma). \tag{6}$$

Then, by using the new coordinate system ,we find $u^\alpha\partial_\alpha = \frac{1}{\Omega}(\partial_t + v\partial_x)$, $s^\alpha\partial_\alpha = \frac{1}{\Omega}\partial_x$, $g^{\alpha\beta} = -u^\alpha u^\beta + s^\alpha s^\beta$, and $g = -\Omega^4$.

Here we mention the constraint on Ω. If we explicitly write down the condition that u is a time-like unit vector, i.e., $u_\alpha u^\alpha = -1$, we find that $\Omega^2 = u_{\tilde{0}}^2$ holds. Hence $\Omega^2 > 0$ is guaranteed as long as u is time-like. Also, directly from the metric (4), we can easily verify $\Omega^2 > 0$ if and only if the t−constant hypersurfaces are space-like. Hence, it will be appropriate to assume $\Omega^2 > 0$. Then, we find that Ω^2 has a finite minimum value when $|\tilde{v}| < 1$. The minimum value is $1 - \tilde{v}^2$ which is realized when $v = 0$.

Now, we find that to generalize the choice of the special reference frame introduced to set the modified dispersion relation is equivalent to generalize the metric form given in (1) to the one given in (4) replacing $\tilde{u}$ and $\tilde{s}$ with u and s in the defining equations of the differential operator $\mathcal{D}$. As a result, the action (2) becomes

$$S = \frac{1}{2}\int dtdx\left[|(\partial_t + v\partial_x)\phi|^2 - \Omega(x)^2\left|\hat{F}\left(\frac{1}{\Omega}\partial_x\right)\phi\right|^2\right]. \tag{7}$$

If we set $\Omega^2 \equiv 1$, the models are reduced to the original one discussed in Ref. [6].

Then, let us derive the field equation by taking the variation of the action (7). Assuming that $\hat{F}(z)$ is an odd function of z, we obtain

$$(\partial_t + \partial_x v)(\partial_t + v\partial_x)\phi = \Omega\hat{F}\left(\frac{1}{\Omega}\partial_x\right)\Omega\,\hat{F}\left(\frac{1}{\Omega}\partial_x\right)\phi. \tag{8}$$

To proceed further calculations, we need to assume a specific dispersion relation. Following Ref. [6], we adopt here

$$\hat{F}(z) = z + \frac{1}{2k_0^2}z^3, \tag{9}$$

where k_0 is a constant. Since the model should be arranged to differ from the ordinary one only in the high frequency regime, the critical wave number k_0 is supposed to be sufficiently large. With this choice of $\hat{F}$, neglecting the terms that are inversely proportional to the fourth power of k_0, the field equation becomes

$$(\partial_t + \partial_x v)(\partial_t + v\partial_x)\phi = \left[\partial_x^2 + \frac{1}{2k_0^2}\left(\partial_x^2\frac{1}{\Omega}\partial_x\frac{1}{\Omega}\partial_x\right) + \frac{1}{2k_0^2}\left(\partial_x\frac{1}{\Omega}\partial_x\frac{1}{\Omega}\partial_x^2\right)\right]\phi. \tag{10}$$

We briefly discuss the meaning of the functions Ω and v. It is easy to understand that v is the coordinate velocity of the integration curves of u. To understand the meaning of Ω, we further calculate the covariant acceleration of the integral curves of u, $|u^\alpha{}_{;\beta}u^\beta|$, where semicolon represents the covariant differentiation. After a straightforward calculation, we see that the covariant acceleration is given by $|\partial_x\Omega^{-1}|$. Hence, we find that the derivative of Ω^{-1} gives the acceleration of the reference frame.

To evaluate the spectrum of Hawking radiation, we need to solve the field equation (10) with an appropriate boundary condition. However, owing to the time translation invariance with the Killing vector

[3] Here, we should mention one important relation for the later use. The temperature of the Hawking spectrum is determined by the surface gravity κ defined by $\kappa := d\tilde{v}/d\tilde{x}|_{\tilde{x}=0}$. The surface gravity κ can also be represented as [9] $\kappa = dv/dx|_{x=0}$.

∂_t, we do not have to solve the partial differential equation (10) directly. By setting $\phi(t,x) = e^{-i\omega t}\psi(x)$, Eq. (10) reduces to an ordinary differential equation (ODE),

$$\left[(-i\omega + \partial_x v)(-i\omega + v\partial_x) - \left\{\partial_x{}^2 + \frac{1}{2k_0{}^2}\left(\partial_x{}^2\frac{1}{\Omega}\partial_x\frac{1}{\Omega}\partial_x\right) + \frac{1}{2k_0{}^2}\left(\partial_x\frac{1}{\Omega}\partial_x\frac{1}{\Omega}\partial_x{}^2\right)\right\}\right]\psi = 0. \tag{11}$$

From the above ODE, the asymptotic solution at $x \to \infty$ is easily obtained by assuming the plane wave solution like $\psi(x) \propto e^{ikx}$. As shown in Ref. [5], two wave numbers at $x \to \infty$ have large absolute values, which we denote by $k_\pm$, and the other two have small absolute values, which we denote $k_{\pm s}$. For each pair, one is positive and the other is negative. The subscript $\pm$ represents the signature of the solution. Then, the general solution of Eq. (11) at $x \to \infty$ is given by a superposition of these plane wave solutions as

$$\psi(x) = \sum_{l=\pm,\pm s} c_l(\omega)e^{ik_l(\omega)x}. \tag{12}$$

By such a local analysis, however, the coefficients $c_l(\omega)$ are not determined. To determine them, we need to find the solution that satisfies the boundary condition corresponding to no ingoing waves plunging into the event horizon. Finally, for a wave packet which is peaked around a frequency ω, the expectation value of the number of created particles is given Ref. [5] by

$$N(\omega) = \frac{|\omega'(k_-)v_g(k_-)c_-^2(\omega)|}{|\omega'(k_{+s})v_g(k_{+s})c_{+s}^2(\omega)|}, \tag{13}$$

where $v_g(k) := \partial\omega(k)/\partial k$ is the group velocity measured by a static observer and ω' is related to the frequency measured by the observers in the special refrence frame.

Next to determine the coefficients c_l, we solve the field equation (11) by using several approximations. (For the details, see Ref. [8])

In the region close to the horizon, we use the method of Fourier transform. The solution is found to be uniquely determined by imposing the boundary condition discussed in the preceding section. On the other hand, in the region sufficiently far from the horizon, we construct four independent solutions which become $e^{ik_l(\omega)x}$ at $x \to \infty$. We use the WKB approximation for the two short-wavelength modes and we use the simple $1/k_0^2$ expansion for the other two long-wavelength modes. Since these two different regions of validity have an overlapping interval as long as k_0 is taken to be sufficiently large Ref. [8], the requirement that the solutions obtained in both regions match in this overlapping interval determines the coefficients $c_l(\omega)$.

The respective resulting solutions in the overlapping regions are given by such as following,

$$\psi(x) = \psi_1(x) + \psi_2(x) + \psi_3(x), \tag{14}$$

and

$$\begin{aligned}
\psi_\pm &= \frac{1}{\sqrt{k_0\Omega_0}}(2\kappa x)^{-\frac{3}{4}-\frac{i\omega}{2\kappa}}\exp\left(\pm i\frac{2}{3}k_0\Omega_0\sqrt{2\kappa}x^{\frac{3}{2}} + W_{1,2} + O(\epsilon^2,\delta^2)\right),\\
\psi_{+s}(x) &= x^{\frac{i\omega}{\kappa}}\exp\left(-\frac{i\omega}{2\kappa}\tilde{\delta}_1 + O(\epsilon^2,\delta^2)\right),
\end{aligned} \tag{15}$$

where

$$\begin{aligned}
\psi_{1,2}(x) &= e^{\mp\pi\omega/2\kappa}\frac{1}{\sqrt{k_0\Omega_0}}(k_0\Omega_0)^{-\frac{i\omega}{\kappa}}\sqrt{2\pi\kappa}(2\kappa x)^{-\frac{3}{4}-\frac{i\omega}{2\kappa}}\exp\left(\mp i\frac{2}{3}\sqrt{2\kappa}k_0\Omega_0x^{3/2} + W_{1,2} + O(\epsilon^2,\delta^2)\right),\\
\psi_3(x) &= -2\sinh(\pi\omega/\kappa)\Gamma(-i\omega/\kappa)\,x^{i\omega/\kappa}\left(1 - \frac{i\omega}{2\kappa}\tilde{\delta}_1 + O(\epsilon^2,\delta^2)\right),\\
W_{1,2} &= \mp i\frac{\sqrt{2}}{\tilde{\epsilon}}\left(-\frac{1}{10}\tilde{\delta}_0 + \frac{1}{10}\tilde{\delta}_1 - \frac{2}{5}\tilde{\delta}_2\right) + \left(\frac{i\omega}{4\kappa} + \frac{3}{8}\right)\tilde{\delta}_0 + \left(\frac{i\omega}{4\kappa} - \frac{3}{8}\right)\tilde{\delta}_1 + \frac{1}{2}\tilde{\delta}_2\\
&\quad \mp i\frac{\tilde{\epsilon}}{\sqrt{2}}\left[\left(-\frac{41}{48} - \frac{i\omega}{\kappa} - \frac{1}{4}\left(\frac{i\omega}{\kappa}\right)^2\right) + \left(\frac{11}{64} + \frac{1}{4}\frac{i\omega}{\kappa} + \frac{1}{16}\left(\frac{i\omega}{\kappa}\right)^2\right)\tilde{\delta}_0\right.
\end{aligned}$$

$$+\left(-\frac{11}{64}+\frac{3}{4}\frac{i\omega}{\kappa}+\frac{15}{16}\left(\frac{i\omega}{\kappa}\right)^2\right)\tilde{\delta}_1+\left(-\frac{5}{16}-\frac{i\omega}{\kappa}-\frac{3}{4}\left(\frac{i\omega}{\kappa}\right)^2\right)\tilde{\delta}_2\Bigg]. \tag{16}$$

Here we introduced four small parameters. When we assume that $v(x)$ and $1/\Omega(x)$ can be expanded around the horizon like $v(x) \approx -1+\kappa x+\frac{1}{2}\kappa_1^2 x^2+\cdots$, $\left(\frac{1}{\Omega}\right) \approx \frac{1}{\Omega_0}+\frac{1}{\Omega_1}x+\cdots$, these parameters in overlapping region are expressed by

$$\tilde{\delta}_0 := \kappa x, \quad \tilde{\delta}_1 := \frac{\kappa_1^2 x}{\kappa}, \quad \tilde{\delta}_2 := \frac{\Omega_0}{\Omega_1}x, \quad \tilde{\epsilon} := \sqrt{\frac{1}{k_0^2\Omega_0^2\kappa x^3}}. \tag{17}$$

By comparing (14) with (15), we can determine the coefficients c_l. Finally the expectation value of the number of created particle is evaluated as

$$N(\omega)=\frac{1}{e^{2\pi\omega/\kappa}-1}(1+O(\epsilon^2,\delta^2)), \tag{18}$$

a thermal spectrum at the Hawking temperature $\kappa/2\pi$ up to $O(\epsilon^1,\delta^1)$.

3 Analytic and numerical studies of the deviation from hawking spectrum

	ϵ^{-1}	ϵ^0	ϵ^1	ϵ^2
δ^0	$x^{3/2}$	x^0	$x^{-3/2}$	x^{-3}
δ^1	$x^{5/2}$	x^1	$x^{-1/2}$	x^{-2}
δ^2	$x^{7/2}$	x^2	$x^{1/2}$	x^{-1}
δ^3	$x^{9/2}$	x^3	$x^{3/2}$	x^0

TABLE I. Table to explain the matching procedure.

In the preceding section, to obtain the flux of the created particles observed in the asymptotic region, where $v(x)$ is essentially constant, we propagated the near-horizon solution (14), which satisfies the appropriate boundary condition, to the infinity by matching it with the outer-region solutions (15), which are valid in the region distant from the horizon. As a result, we could determine the coefficients c_l and we found that the thermal spectrum is reproduced up to $O(\epsilon^1,\delta^1)$.

Here, let us look at the above table. For each element in the table, we have assigned a power of x that the corresponding corrections possess. As we mentioned above, we need to choose an appropriate superposition of the four independent outer-region solutions to achieve a successful matching. The coefficients which determine the weight of this superposition is nothing but c_l. Now we should note that the condition to determine the coefficients c_l will be completely supplied by matching the x-independent elements. Once these coefficients are determined, the agreement of the other x-dependent terms must be automatic from the consistency. The leading order x-independent elements consists of the terms of $O(\epsilon^0\delta^0)$, and it is easy to see that the second lowest one consists of the terms of $O(\epsilon^2\delta^3)$. This fact tells us that the possible modification of the coefficients c_{+s} and c_- is at most of $O(\epsilon^2\delta^3)$, and hence the possible deviation from the thermal radiation starts only from this order. Thus we find

$$N(\omega)=\frac{1}{e^{2\pi\omega/\kappa}-1}(1+O(\epsilon^2\delta^3)). \tag{19}$$

Next we investigate the deviation from thermal radiation $\delta N/N := (N-N_{thermal})/N_{thermal}$ in more detail. There are three different quantities of $O(\delta)$ as mentiond previous section. We write them down

as $\tilde{\delta}_0 = xv'|_{x=0} = \kappa x$, $\tilde{\delta}_1 = x\kappa^{-1}v''|_{x=0} =: (\kappa x)b_1$, $\tilde{\delta}_2 = x\Omega_0\left(\frac{1}{\Omega}\right)'_{x=0} =: (\kappa x)b_2$, where we introduced non-dimensional model parameters b_1 and b_2. We also have various quantities of $O(\delta^2)$ and of $O(\delta^3)$ consisted of higher derivatives of v and $1/\Omega$. They are $x^2\kappa^{-1}v'''|_{x=0} =: (\kappa x)^2 b_3$, $x^2\Omega_0\left(\frac{1}{\Omega}\right)'_{x=0} =: (\kappa x)^2 b_4$, and $x^3\kappa^{-1}v^{(4)}|_{x=0} =: (\kappa x)^3 b_5$, $x^3\Omega_0\left(\frac{1}{\Omega}\right)''_{x=0} =: (\kappa x)^3 b_6$, respectively. Also, b_3, b_4, b_5 and b_6 are non-dimensional model parameters. One may suspect that terms including factors proportional to κ^{-2} such as $x\kappa^{-2}v'''|_{x=0}$ might appear among the correction terms of $O(\epsilon^2\delta^3)$. However, by repeating the same calculation that was given in Sec.2 with extra higher order derivative terms, we can verify that such factors do not appear. From this notion, we can expect that the deviation from the thermal spectrum is given by

$$\frac{\delta N}{N} = \frac{\kappa^2}{k_0^2\Omega_0^2}\Big[\quad (a_{000} + a_{001}b_1 + a_{002}b_2 + (7 \text{ other terms})) \\ + (a_{03} + a_{13}b_1 + a_{23}b_2)\, b_3 + (a_{04} + a_{14}b_1 + a_{24}b_2)\, b_4 + a_5 b_5 + a_6 b_6 \Big] + O(\epsilon^4\delta^6), \quad (20)$$

where "a"s are some functions of ω/κ which are independent of model parameters.

Now, we numerically confirm that the deviation actually starts from this order. The following results are obtained by using *MATHEMATICA*. As an example, let us consider a model given by

$$v = -\frac{1}{2}e^{-2x-3x^2} - \frac{1}{2}, \quad (21)$$

$$\Omega = 9e^{-x-x^2/2} + 1. \quad (22)$$

For this model, we have $\kappa = 1$, $b_1 = 1$ and $b_2 = 9/10$, and the other parameters also do not vanish. For this fixed model, we numerically calculated the deviation from the thermal spectrum for various values of $1/k_0^2$. The frequency ω was fixed to 1 since our main interest is in the modes whose observed frequency at infinity becomes comparable with Hawking temperature ($= \kappa/2\pi$). The results of the numerical calculation are shown in Fig.1 by the filed circles. The horizontal axis is $\log(1/k_0)$ and the vertical one is $\log \delta N/N$. The data points are fitted well by a liner function (the solid line) with its gradient, 1.99742, which perfectly agrees with the expectation represented by Eq.(20).

At this point, one may notice that the deviation we obtained here is much larger than that given by Corley and Jacobson[5], in which a model with

$$v = \frac{1}{2}\{\tanh[(2\kappa x)^2]\}^{1/2} - 1, \quad (23)$$

and $\Omega \equiv 1$ was considered [4]. The outstanding feature of their model is that $b_1 = b_2 = b_3 = b_4 = b_5 = b_6 = 0$. Hence, the terms of $O(\epsilon^2\delta^3)$ in Eq.(20) reduce to $a_{000}\kappa^2/k_0^2\Omega_0^2$. If $a_{000} \equiv 0$, all the terms of $O(\epsilon^2\delta^3)$ in the deviation $\delta N/N$ disappear, and it turns out to be $O(\epsilon^4\delta^6)$. If so, the discrepancy between two calculations can be understood. To show that this is certainly the case, we repeated the numerical calculation for the same model that was discussed in Ref.[5]. The resulting $\delta N/N$ calculated for various values of $1/k_0$ were also plotted in Fig.2 by the open squares. Again, the data points in logarithmic plot are fitted well by a linear function. But, this time, its gradient is 4.06935, which indicates that the deviation is actually caused by the terms of $O(\epsilon^4\delta^6)$.

Now, we can conclude that $a_{000} \equiv 0$. Although this result might be interesting, we do not pursue this direction of study in this paper. Here, we would like to focus on another interesting aspect that is anticipated by the expression (20). With moderate values of model parameters, the deviation $\delta N/N$ stays small for a sufficiently large k_0. However, conversely, we can expect that the deviation from the thermal spectrum becomes large if we consider some extreme modifications of the special reference frame. Especially, when we consider the limiting case in which $\Omega_0^2 \to 0$, the expression (20) diverges. Although the approximation used to obtain the analytic expression (20) is no longer valid in this limit, we can still expect that the resulting spectrum will significantly differ from the thermal one. As we mentioned below Eq.(6), there is a lower bound on $\Omega^2(x)$. The possible smallest value of $\Omega^2(x)$ is $1 - \tilde{v}^2$, which is

[4] T. Jacobson suggested us the existence of this discrepancy.

realized when $v(x) = 0$. Hence, we find $v(x) \approx 0$ near $x = 0$ in this limiting case. Recall that $v(x)$ was the coordinate velocity of the integration curves of u. Hence, vanishing $v(x)$ means that we adopt the reference frame corresponding to the static observers.

Here, we present the results of our numerical calculation, which shows that the deviation $\delta N/N$ can be large for some cases. Since we also want to demonstrate that the drastic change of spectrum can occur just in the consequence of the change of the special reference frame, we varies only the function $\gamma(\tilde{x})$, which was defined in Eq.(3). The model of $\tilde{v}(\tilde{x})$ is kept unchanged. As for a model of $\tilde{v}(\tilde{x})$, we assume the same form that is given in Eq.(21). As for $\gamma(\tilde{x})$, we adopt

$$\gamma = \frac{-\tilde{v} - (1/2)}{\rho^{-1} - \tilde{v}}, \tag{24}$$

with $\rho \in [0, 1)$. $\rho = 0$ corresponds to the original model associated with the freely falling observers, and $\rho = 1$ corresponds to the case with $\Omega_0^2 = 0$. With this choice of $\gamma(\tilde{x})$, the following two conditions are satisfied. One is that $v(x)$ stays negative for all positive x. The other is that $\Omega_\infty^2 = 1$. We calculated the deviation $\delta N/N$ for various values of ρ, and the results were shown in Fig.2. As was expected, the deviation becomes large for small Ω_0^2. This plot raises an interesting speculation that N might converge to 0 in the $\Omega_0^2 \to 0$ limit. Although we have not confirmed it yet, it is very likely that this is the case because the situation in this limit is very similar to the case in which we set a static mirror surrounding the event horizon of the black hole. The calculation for small Ω_0^2 were tried, but it was found to be out of validity of our present computation code. Anyway, we conclude that, even if κ/k_0 is sufficiently small, the deviation from the thermal spectrum can be large if the combination $\kappa/k_0\Omega_0$ becomes large. It should be noted that the integration curves of u are not required to be suffered from infinite acceleration to achieve such a small but non-zero Ω_0^2.

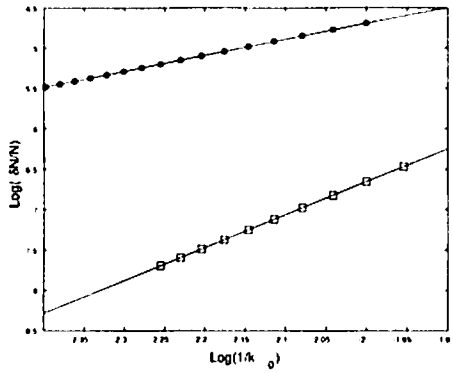

Figure 1: The logarithmic plot of $\delta N/N$ as a function of $1/k_0$ for two different choice of $v(x)$. The filled circles(our model) and the open squares(model in Ref.[5]) represent the numerical data points for respective models. Each solid line corresponds to a linear function which fits the data points.

4 Conclusion

In the original model, the dispersion relation is modified on the basis of the freely falling observers. In our present work, we generalized the choice of the reference frame with respect to which we set the non-standard dispersion relation. Extending the analytic method developed by Corley [6], we have shown that the thermal spectrum of radiation from a black hole is almost reproduced as long as the modification of the special reference frame is not too extreme. In this analysis, we assumed $\omega \approx \kappa$, where ω is the frequency of the emitted photon observed at the spatial infinity and κ is the surface gravity of the black hole. We have also obtained a strong suggesting that the deviation from the exact thermal spectrum appears from $O(\kappa^2/k_0^2)$, where k_0 is the typical wave number corresponding to the modification of the dispersion relation. This speculation has been confirmed numerically.

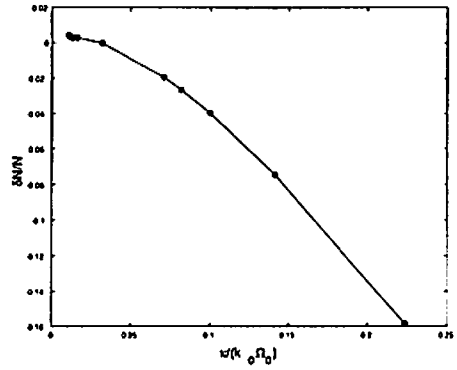

Figure 2: A plot of $\delta N/N$ as a function of $1/\Omega_0$ for the model given by Eq.(24).

Of course, we should not stress this small deviation from the Hawking spectrum. In the ordinary model with the Lorentz invariant dispersion relation, the thermal radiation at the temperature T for the static observer is observed as the thermal radiation at the temperature $\sqrt{\frac{1-\beta}{1+\beta}}T$ for the observer moving with the radial velocity β. This argument holds in general whatever the source of the outward pointing radiation is because it is a direct consequence of $\omega = k$. However, in the present modified model, the Lorentz invariance is violated from the beginning. We can easily see that $(\omega - k)/\omega$ is also of $O(\omega^2/k_0^2)$. Hence, even if the exact Hawking spectrum is reproduced for one specific free-falling observer, it cannot be so for the other free-falling observers.

On the other hand, the result that we obtained analytically also suggests that the deviation from the thermal spectrum can be large if we consider some extreme situations. With the aid of numerical methods, we also examined one of such extreme situations. We considered a sequence of different special reference frames which ranges from the case in which the observers associated with the special reference frame are freely falling into black hole to the case in which they are kept from falling into it. We found that, in the latter limiting case, the spectrum of radiation can significantly differ from the thermal one, even though ω^2/k_0^2 is small. It will be important to study the physical meaning of this result. But, since the central issue of this paper is to develop the analytic treatment of our new model, we have not performed detailed numerical studies yet. We will return to this issue in future publications.

References

[1] S.W. Hawking, Commun. Math. Phys. **43**, 199 (1975); Nature **248**, 30 (1974).

[2] N.D. Birrel and P.C.W. Davies, *Quantum fields in curved space*, Cambridge University Press, Cambridge, (1982).

[3] W.G. Unruh, Phys. Rev. Lett. **46**, 1351 (1981).

[4] W.G. Unruh, Phys. Rev. **D51**, 2827 (1995).

[5] S. Corley and T. Jacobson, Phys. Rev. **D54**, 1568 (1996).

[6] S. Corley, Phys. Rev. **D57**, 6280 (1998).

[7] R. Brout, S. Massar, R. Parentani, and Ph. Spindel Phys. Rev. **D52**, 4559 (1995).

[8] Y. Himemoto and T. Tanaka, gr-qc 9904076, (accepted to PRD October 1999)

[9] T. Jacobson and G. Kang, Class. Quant. Grav., **10**, L201 (1993).

Mass spectrum of scalar field fluctuation near Reissner-Nordstrom black hole

Hiroko Koyama,[1] and Akira Tomimatsu[2]

Department of Physics, Nagoya University, Chikusa-ku, Nagoya 464-8602, Japan

Abstract

Vacuum polarization of massive scalar fields on the horizon of Reissner-Nordstrom black hole is studied. We calculate the regularized $\langle\phi^2\rangle$ in the thermal state with black hole to investigate the dependence of $\langle\phi^2\rangle$ on field mass. We find that in the case of nearly extreme black hole vacuum polarization of massive field is enhanced in comparison with that of massless field. The enhancement of $\langle\phi^2\rangle$ arrives at the peak where compton length of scalar field and horizon radius are same order. This non-thermal behavior can be interpreted as a kind of resonance.

1 Introduction

Since Hawking's discovery of black holes radiation [8], it has been an important subject to investigate quantum effects in black hole spacetimes and a great deal of effort has been done. Vacuum polarization $\langle\phi^2\rangle$ describes quantum fluctuations and is a clue to understand effects on the black hole spacetime. In black hole spacetimes we can construct the model that scalar field is a state in thermal equilibrium with a black hole. This thermal state is called the Hartle-Hawking state [7], and the temperature of the scalar field in the state is called the Hawking temperature. The regularized $\langle\phi^2\rangle$ in the Hartle-Hawking state has a finite regular value on the horizon.

In this paper we investigate the behavior of vacuum polarization on the horizon in the Hartle-Hawking state. For massless scalar field the magnitude of $\langle\phi^2\rangle$ on the horizon is proportional to surface gravity of the black hole. This indicates that temperature of the black hole in terms of surface gravity is an important parameter for vacuum polarization. For large mass scalar fields, the magnitude of $\langle\phi^2\rangle$ is the order of the second powers of the compton length. This indicates that in general vacuum polarization of large mass field is much smaller than that of massless field at first sight. It is expected intuitively the picture that particles with heavy mass are dull for thermal excitations.

Here we present a question whether the role of mass parameter is only to suppress thermal excitations. If it is true, field mass is not very interesting parameter for back reaction problem. It is true in the case of Schwarzschild black hole. It may not be true, however, in the case of low-temperature black hole such as nearly extreme Reissner-Nordstrom. In nearly extreme Reissner-Nordstrom whose surface gravity is nearly zero, the magnitude of $\langle\phi^2\rangle$ of massless field on the horizon is suppressed to be zero, whereas that of large mass field become a finite positive value. This indicates that the effect of field mass is not only to suppress the thermal excitations.

Our purpose in this paper is to point out that there is an another effect of the field mass except the effect to suppress the thermal excitations, and to investigate what kind of features the nontrivial effect has. We calculate $\langle\phi^2\rangle$ of massive field with arbitrary mass. We are interested in the case of low-temperature black hole in particular, because we expect that the effects of field mass may emerge clearly under low-temperature where the effects of thermal excitation are quite suppressed. Thus we consider Reissner-Nordstrom spacetime as background, because it expresses the case of the low-temperature black hole keeping the horizon radius finite.

In Sec.2 we describe the derivation for $\langle\phi^2\rangle$ and show the results in the case of massless and large mass field as the characteristic examples. In Sec.3 we investigate the dependence of vacuum polarization on the horizon of the nearly extreme Reissner-Nordstrom black hole on field mass. The results are expressed as the mass spectrum. Sec.4 is devoted to the conclusion and discussion. Throughout this paper we use units such that $G = c = \hbar = k_B = 1$.

[1] E-mail:hiroko@allegro.phys.nagoya-u.ac.jp
[2] E-mail:atomi@allegro.phys.nagoya-u.ac.jp

2 Vacuum polarization on the horizon

In this section the expression for $\langle\phi^2\rangle$ is derived. We consider a scalar field with mass m, in thermal equilibrium with Reissner-Nordstrom black hole. The metric in Euclidean section $\tau = -it$ is given by

$$ds^2 = f d\tau^2 + \frac{1}{f}dr^2 + r^2 d\Omega^2, \tag{1}$$

where $f = (r - r_+)(r - r_-)/r^2$, r_+ and r_- are the location of inner and outer horizon and the surface gravity $\kappa = (r_+ - r_-)/2r_+^2$. The temperature of the field is the Hawking temperature, $\kappa/2\pi$. Vacuum polarization $\langle\phi^2\rangle$ can be computed from the Euclidean Green's function by noting the identities

$$\langle\phi^2\rangle_{unreg} = \frac{1}{2}G^{(1)}(x,x) = iG_F(x,x) = G_E(x,x), \tag{2}$$

where $G^{(1)}$ is the Hadamard Green's function, G_F is the Feynman Green's function, and G_E is the Euclidean Green's function respectively. G_E is divergent at coincident limit and must be regularized. In this paper the covariant point-splitting method is employed for the regularization of ultraviolet divergences. We start from an expression for $G_E(x,x')$ when the points x and x' are separated. Next we prepare an appropriate counterterm, finally take coincident limit. This procedure is shown schematically as

$$\langle\phi^2\rangle = \lim_{x'\to x}\left[G_E(x,x') - G_{DS}(x,x')\right]. \tag{3}$$

where $G_{DS}(x,x')$ is the point-splitting counterterm needed to regularize $G_E(x,x')$ and given by

$$\begin{aligned} G_{DS}(x,x') &= \frac{1}{8\pi^2\sigma} + \frac{m^2 + (\xi - \frac{1}{6})R}{8\pi^2}\left[\gamma + \frac{1}{2}\ln\left[\frac{m^2\sigma}{2}\right]\right] \\ &\quad - \frac{m^2}{16\pi^2} + \frac{1}{96\pi^2}R_{\alpha\beta}\frac{\sigma^{;\alpha}\sigma^{;\beta}}{\sigma}, \end{aligned} \tag{4}$$

where σ is the one half the square of distance between the points x and x' along the shortest geodesic connecting them and γ is the Euler's constant. For a scalar field $G_E(x,x')$ obeys the equation

$$\left[\Box - m^2\right]G_E(x,x') = -\frac{\delta^4(x,x')}{g^{1/2}(x)} \tag{5}$$

with $\Box$ evaluated using the Euclidean metric (1). When the points (x,x') have the same values of r,θ, and ϕ, and different values of τ, such that $\tau - \tau' = \epsilon$ for Eq.(5), $G_E(x,x')$ is given by

$$G_E(x,x') = \frac{\kappa}{8\pi^2}\sum_{l=0}^{\infty}(2l+1)p_{0l}(r)q_{0l}(r) + \frac{\kappa}{4\pi^2}\sum_{n=1}^{\infty}\cos(n\kappa\epsilon)\sum_{l=0}^{\infty}(2l+1)p_{nl}(r)q_{nl}(r), \tag{6}$$

where p_{nl} and q_{nl} are independent solutions of the mode equation

$$\frac{d^2\chi_{nl}}{dr^2} + \left[\frac{2}{r} + \frac{1}{f}\frac{df}{dr}\right]\frac{d\chi_{nl}}{dr} - \left[\frac{n^2\kappa^2}{f^2} + \frac{l(l+1)}{r^2 f} + \frac{m^2}{f}\right]\chi_{nl} = 0 \tag{7}$$

and satisfy the Wronskian condition

$$p_{nl}\frac{dq_{nl}}{dr} - q_{nl}\frac{dp_{nl}}{dr} = -\frac{1}{r^2 f}. \tag{8}$$

Now we show the results in the case of massless $m = 0$ and large mass limit $mr_+ \gg 1$ as characteristic examples. For massless scalar fields of $\langle\phi^2\rangle$ on the horizon reduces to

$$\langle\phi^2\rangle_{massless} = \frac{\kappa}{24\pi^2 r_+} \tag{9}$$

by the analytical approximation in [3]. It is found that the magnitude of vacuum polarization of massless field on the horizon is proportional to the surface gravity of the black hole. On the other hand for large mass field, $mr_+ \gg 1$, $\langle\phi^2\rangle$ reduces to

$$\langle\phi^2\rangle_{large\ mass} = \frac{1}{720\pi^2 m^2 r_+^4}(16\kappa^2 r_+^2 - 4\kappa r_+ + 1) \tag{10}$$

using the DeWitt-Schwinger expansion [5, 6]. The justification that $\langle\phi^2\rangle_{large\ mass}$ using the DeWitt-Schwinger expansion is that in the Hartle-Hawking state on the horizon is proved in [9].

From Eq.(9) and Eq.(10), it is found that $\langle\phi^2\rangle_{large\ mass}$ is much smaller than $\langle\phi^2\rangle_{massless}$ in Schwarzschild black hole. It is noting, however, in the extreme limit $\kappa \to 0$, $\langle\phi^2\rangle_{massless}$ goes to zero, whereas $\langle\phi^2\rangle_{large\ mass}$ becomes a finite positive value. The magnitude of vacuum polarization of large massive field on the horizon of extreme Reissner-Nordstrom black hole is subtle larger than that of massless field. It suggests that field mass has an another effect on the vacuum polarization except to suppress the thermal excitation in the case of low-temperature black hole. Thus it is interesting to investigate $\langle\phi^2\rangle$ of arbitrary field mass in the case of nearly extreme Reissner-Nordstrom.

3 Mass spectrum of scalar field fluctuation

In this section we investigate the dependence of $\langle\phi^2\rangle$ on the horizon of nearly extreme Reissner-Nordstrom black hole on field mass. The case of nearly extreme limit, $\kappa r_+ \to 0$, is considered. The details of the derivation are described in [10]. In this paper we present only the results.

We express $8\pi^2 r_+^2\langle\phi^2\rangle$ on the horizon of massive field with arbitrary mass as a mass spectrum in Fig. 1. The dots curve is in the case of Schwarzschild background in [1]. These data indicate that the larger field mass is, the smaller the magnitude of vacuum polarization is. It can be said that thermal excitation is suppressed by field mass. The solid curve is our results in the case of nearly extreme limit. Unlike the case of Schwarzschild, it is shown that vacuum polarization is enhanced together with the increase of field mass. The enhancement arrives at the peak at $mr_+ \sim 0.38$.

4 Conclusion and discussion

In this paper we investigate the dependence of $\langle\phi^2\rangle$ in the Hartle-Hawking state on the horizon of nearly extreme Reissner-Nordstrom black hole on field mass. The results are expressed as a mass spectrum in Fig.1. It is found that $\langle\phi^2\rangle$ on the horizon of nearly extreme Reissner-Nordstrom black hole has a peculiar behavior; the magnitude of $\langle\phi^2\rangle$ becomes maximum at $mr_+ \sim O(1)$, where compton length of scalar field and horizon radius are same order. This feature is not seen in the case of Schwarzschild black hole. We interpret it as non-thermal effect and a kind of resonance.

Our results suggest that not only temperature of black hole, that is its surface gravity, but also field mass is an important factor for quantum effects in black hole spacetime. The latter emerges in the case of low-temperature black hole. The calculations in the case of arbitrary Reissner-Nordstrom black hole, that is, in the case that the value of κr_+ is arbitrary, have not been carried yet from the difficulty. Nevertheless it is interesting to investigate in what region of κr_+ the enhancement feature of $\langle\phi^2\rangle$ by scalar mass occurs and the value of mr_+ when the enhancement arrives at the peak.

We consider that the quantum fluctuation in the nearly extreme limit is important for the analysis of the stability of extreme Reissner-Nordstrom black hole. From the results here, we have no idea whether finite vacuum polarization effects induce the decrease of mass of the black hole as back reaction effects. It is a future work to investigate how the non-thermal fluctuations in nearly extreme black hole act on the black hole spacetime.

References

[1] P.R. Anderson, Phys. Rev.D 39, 3785 (1989).

[2] P.R. Anderson, Phys. Rev.D 41, 1152 (1990).

[3] P.R. Anderson, W.A. Hiscock, and D.A. Samuel, Phys. Rev. Lett.70, 1739 (1993).

[4] S.M. Christensen, Phys. Rev.D 14, 2490 (1976).

[5] V.P. Frolov, Phys. Rev.D 26, 954 (1982).

[6] V.P. Frolov, in Quantum Gravity, edited by M. A. Markov and P. C. West (Plenum, New York, 1984), p.303.

[7] J. B. Hartle and S. W. Hawking, Phys. Rev. D **13**, 2188 (1976).

[8] S.W. Hawking, Commun. Math. Phys.**43**, 199 (1975).

[9] Hiroko Koyama, Yasusada Nambu, and Akira Tomimatsu, in preparation.

[10] Akira Tomimatsu and Hiroko Koyama, in preparation.

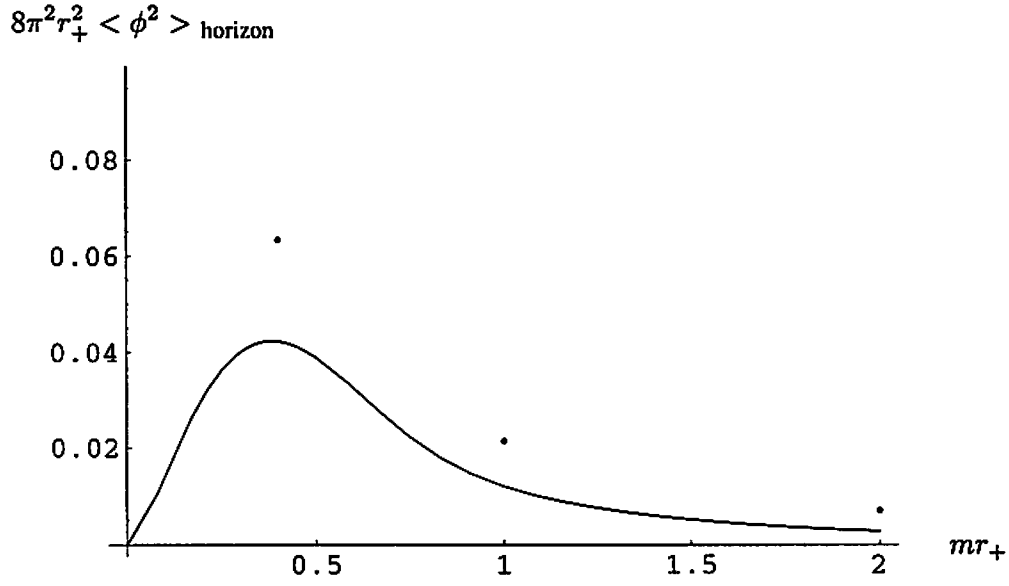

Figure 1: The dots curve is in the case of Schwarzschild black hole [1]. The solid curve is our results in the case of nearly extreme Reissner-Nordstrom black hole.

Naked singularities and particle creations

Akihiro Ishibashi[1] and Akio Hosoya[2]

[1] *Yukawa Institute for Theoretical Physics,*
Kyoto University,
Sakyo-ku, Kyoto 606-8502, Japan

[2] *Department of Physics,*
Tokyo Institute of Technology,
Oh-Okayama Meguro-ku, Tokyo 152-0033, Japan

Abstract

We consider quantum theoretical effects of the occurrence of naked singularities. We calculate the vacuum expectation value of the energy-momentum tensor for a massless scalar field and explicitly show that the singular waves or the *thunderbolts* appear along the Cauchy horizon.

1 Introduction

In the previous work [1] we have studied the wave propagation in the spacetimes with naked singularities. The issue was that the self-adjoint extension of the time-translation operator and its uniqueness. We call the classical singularity wave-regular if the self-adjoint extension is unique and so is the boundary condition at the singularity depending on the Hilbert space of initial value that we choose. In the wave-regular case there exists a unique solution of wave equation for a given initial value.

In the present work we shall focus our attention on the wave-singular case in which the timelike singularity emerges at some stage and the boundary condition is not a priori specified. This feature may manifest itself when the singularity appears in occasion of gravitational collapse. A simplified version will be the case that the boundary condition suddenly changes at some time so that the boundary become naked timelike singularities.

We consider such a case in the context of quantum field theory. The time-translation operator $(A, \mathcal{D}(A))$ changes in time by the change of the domain so that we naturally expect particle creations from vacuum state. We shall first show that this is indeed the case in the perhaps simplest example: a massless scalar field theory in a $(1+1)$ dimensional spacetime $R \times [0, \pi]$. The boundary condition at 0 and π suddenly changes from the Neumann to Dirichlet boundary condition. Intuitively, we study possible quantum effects when the free ends of a string are suddenly pinned down. We shall compute the energy-momentum tensor and see that it just gives the standard Casimir energy inside the domain of dependence while it is divergent at the Cauchy horizon of the initial hypersurface $t = 0$. The thunderbolt effect is observed in the sense that there appears a delta function like singularity which has a support only on the Cauchy horizon. We have also studied the unitary implementability of the Bogoliubov transformation and have found that the Hilbert space are orthogonal to each other before and after the emergence of the naked singularity.

We shall also study the effect of the most general boundary conditions in the same model and give an explicit form of the vacuum expectation value of the energy momentum tensor.

Long ago Anderson and DeWitt [2] discussed a similar problem in the context of topology change in spacetime which exhibits a splitting of the universe. In a sense the emergence of the naked singularity is a kind of topology change which altered the domain of quantum fields. Not surprisingly their result is very similar to ours.

[1] E-mail address: akihiro@yukawa.kyoto-u.ac.jp
[2] E-mail address: ahosoya@th.phys.titech.ac.jp

2 Hair of wave-singular naked singularity

For self-containedness we recapitulate the self-adjoint extension of the time translation operator in the wave-singular case in the previous work.

In the wave-singular case, the preliminary time translation operator A has many different self-adjoint extensions. Each self-adjoint extension corresponds to the different boundary condition at the singularity and accordingly describes different time evolution of the wave for the same initial data. In other words, a wave-singular naked singularity has degrees of freedom for the possible choice of the time translation operator. The degrees of freedom can be interpreted as the character or the *hair* of the wave-singular naked singularity and described by the isometries U between the deficiency subspaces $\mathcal{K}_\pm$ of A.

Consider solutions of $A^*\phi_\pm = \pm i\phi_\pm$ and the sets $\mathcal{K}_\pm$ of the solutions $\phi_\pm$, respectively, which are called the *deficiency subspaces* of A. The pair of numbers $(n_+, n_-) := (\dim \mathcal{K}_+, \dim \mathcal{K}_-)$ is called the *deficiency indices* of A. If A is a closed symmetric operator with the deficiency indices $n_+ = n_-$, then A has self-adjoint extensions, and if $n_+ = n_- = 0$, A is self-adjoint. Let U be the partial isometries $\mathcal{K}_+ \to \mathcal{K}_-$. Then, the self-adjoint extensions A_E can be obtained by taking the domains as

$$\mathcal{D}(A_E) := \{\phi_0 + \phi_+ + U\phi_+ \,|\, \phi_0 \in \mathcal{D}(A),\ \phi_+ \in \mathcal{K}_+\}. \tag{1}$$

When probing timelike singularities in static spacetimes, we will find the preliminary time translation operator as a symmetric operator of the form $A = -VD^iVD_i$ with domain $C_0^\infty(\Sigma)$. Then the deficiency indices n_+, n_- of A are equal and self-adjoint extensions can be made. If the naked singularity is wave-singular, then $n_+ = n_- = N \neq 0$ and hence the partial isometry U is represented by an $N \times N$ unitary matrix $U(N)$.

One of the simplest examples is a scalar field theory in $(1+1)$-dimensions with the boundary conditions at the ends $x = 0, \pi$ of the finite interval $[0, \pi]$. The hair is then $U(2)$. In what follows we shall consider only its subgroup $U(1) \times U(1)$ with each $U(1)$ corresponding to the arbitrariness of the boundary conditions at $x = 0$, $x = \pi$.

We shall consider quantum theoretical effects in the situation that the hair $U(1) \times U(1)$ suddenly changes at some time which can be interpreted as emerging timelike singularities at $x = 0$, $x = \pi$ for $t > 0$.

3 A simple example

In this section we consider a quantum field theory of a scalar field in the $(1+1)$-dimensional Minkowski spacetime $R \times [0, \pi]$. The scalar field ϕ obeys the Klein-Gordon equation:

$$\frac{\partial^2}{\partial t^2}\phi = -A\phi, \qquad A := -\frac{\partial^2}{\partial x^2}. \tag{2}$$

We require the square integrability for the scalar field, i.e., $\phi \in L^2(0,\pi) = \{\phi \,|\, \int_0^\pi dx|\phi|^2 < \infty\}$. Then A with $\mathcal{D}(A) = C_0^\infty(0,\pi)$ is regared as a positive symmetric operator in the Hilbert space $L^2(0,\pi)$ and the solution for any initial data $(\phi_0, \dot{\phi}_0)$ is given by

$$\phi(t,x) = \cos(\sqrt{A_E}t)\ \phi_0(x) + \frac{\sin(\sqrt{A_E}t)}{\sqrt{A_E}}\ \dot{\phi}_0(x), \tag{3}$$

with A_E being a suitable self-adjoint extension of A. Note that in the wave approach the wave-regularity depends on the choice of Hilbert space. In this article we consider in $L^2(0,\pi)$ for a simple demonstration. It is straight forward to generalize the present analysis in the case that the Sobolev space is chosen as the Hilbert space.

Now, let us consider the situation that the boundary conditions at $x = 0$, $x = \pi$ are the Neumann boundary conditions $\partial\phi/\partial x = 0$ before $t = 0$ but they will change to the Dirichlet boundary conditions $\phi = 0$ after $t = 0$. This sudden change of the boundary conditions can be viewed as a particular case of emerging the naked timelike singularities at $x = 0$, $x = \pi$ after $t = 0$.

Before $t = 0$ the positive frequency mode functions which satisfy the Neumann boundary condition are

$$f_n^{(in)}(t<0,x) = \frac{e^{-int}}{\sqrt{\pi n}}\cos nx. \tag{4}$$

After $t = 0$, the positive mode functions must satisfy the Dirichlet boundary condition, hence are

$$f_m^{(out)}(t>0,x) = \frac{e^{-imt}}{\sqrt{\pi m}}\sin mx. \tag{5}$$

We can take the initial data at $t = 0$ as

$$f_n^{(in)}(0,x) = \frac{1}{\sqrt{\pi n}}\cos nx = \frac{1}{\pi}\sqrt{\frac{2}{n}}\sum_{m=1}^{\infty}\left(\frac{1}{m+n}+\frac{1}{m-n}\right)\sin mx \tag{6}$$

$$\dot{f}_n^{(in)}(0,x) = \partial_t f_n^{(in)}(t,x)|_{t=0} = -in\, f_n^{(in)}(0,x), \tag{7}$$

where $m \pm n$ are odd numbers and we use the Fourier expansion of $\cos nx$ by $\sin mx$ in the second line.

The evolution of the mode function $f_n^{(in)}$ into $t > 0$ region is obtained by inserting the above initial data in Eq. (3) in which $\mathcal{D}(A_E)$ is taken so as to respect the Dirichlet boundary condition. Then, by an explicit calculation, we obtain

$$f_n^{(in)}(t>0,x) = \sum_m \left\{\alpha_{nm}\, f_m^{(out)}(t>0,x) + \beta_{nm}\, f_m^{*(out)}(t>0,x)\right\}, \tag{8}$$

where the coefficients α_{nm} and β_{nm} are given by

$$\alpha_{nm} = \sqrt{\frac{2}{\pi}}\sqrt{\frac{m}{n}}\,\frac{1}{m-n}, \quad \beta_{nm} = \sqrt{\frac{2}{\pi}}\sqrt{\frac{m}{n}}\,\frac{1}{m+n}, \tag{9}$$

where $(m \pm n)$ is odd. This clearly exhibits the mode mixing of positive and negative frequency parts hence the particle creations.

3.1 Particle creations

The Klein-Gordon field is quantized by the standard way. The quantum field ϕ is expanded by the mode functions f as

$$\phi(t,x) = \sum_n \{a_n^{(in)} f_n^{(in)} + a_n^{\dagger(in)} f_n^{*(in)}\} = \sum_m \{a_m^{(out)} f_m^{(out)} + a_m^{\dagger(out)} f_m^{*(out)}\} \tag{10}$$

The expansion coefficients a and $a^\dagger$, which are annihilation and creation operators, respectively, satisfy the canonical commutation relations

$$[a_n^{(in,\,out)},\, a_{n'}^{\dagger(in,\,out)}] = \delta_{nn'},\ [a_n^{(in,\,out)},\, a_{n'}^{(in,\,out)}] = [a_n^{\dagger(in,\,out)},\, a_{n'}^{\dagger(in,\,out)}] = 0. \tag{11}$$

Then the (in -) vacuum state corresponding to the positive frequency mode $f_n^{(in)}$ is defined by

$$a_n^{(in)}|0_{in}> = 0. \tag{12}$$

The expectation value of the number operator of the m -mode particle in $|0_{in}>$ is evaluated as

$$N_m := <0_{in}|a_m^{\dagger(out)} a_m^{(out)}|0_{in}> = \sum_n |\beta_{mn}|^2 = \sum_n \frac{m}{n}\,\frac{1}{(m+n)^2}, \tag{13}$$

and the total number is

$$\sum_m N_m = \sum_m\sum_n \frac{m}{n}\,\frac{1}{(m+n)^2} \sim \log\infty. \tag{14}$$

The number of created particles is therefore logarithmically divergent so that the Bogoliubov transformation cannot be unitarily implementable. This means the final Fock space is not equivalent to but completely different from the initial Fock space and suggests that the physics completely changes by the emerging wave-singular naked singularities. We can see this also from the study of the vacuum expectation value of the energy-momentum tensor before and after of the incident at $t = 0$.

3.2 The vacuum expectation value of the energy-momentum tensor

We see the physical effects of the particle creations by the sudden change of the boundary conditions. We compute the vacuum expectation value of the energy-momentum tensor. First, we obtain in $t < 0$ region

$$\begin{aligned} < T_{\pm\pm} > &= \frac{1}{4} < 0_{in}| \dot{\phi}^2 + \phi'^2 + 2\dot{\phi}\phi' |0_{in} > \\ &= -\frac{1}{96}, \end{aligned} \tag{15}$$

where $\pm$ denote the advanced and retarded time, $z_\pm := t \pm x$, respectively. This is the Casimir energy. On the other hand, after some calculation we have in $t > 0$ region,

$$< T_{\pm\pm} >= -\frac{1}{96} + \frac{1}{2}\left(\sum_{n=1}^{\infty}\frac{1}{n}\right) \times \{\delta(z_\pm) - \delta(z_\pm - \pi)\}^2 . \tag{16}$$

The first term is the Casimir energy. From the second term, it turns out that the energy density diverges along the null boundaries $z_+ = \pi$ and $z_- = 0$, which form the Cauchy horizon for the $t = 0$ initial surface as illustrated in Fig. 1. Besides the logarithmically divergent factor, the square of the delta function implies that not only the energy density but also the total energy will be unbounded.

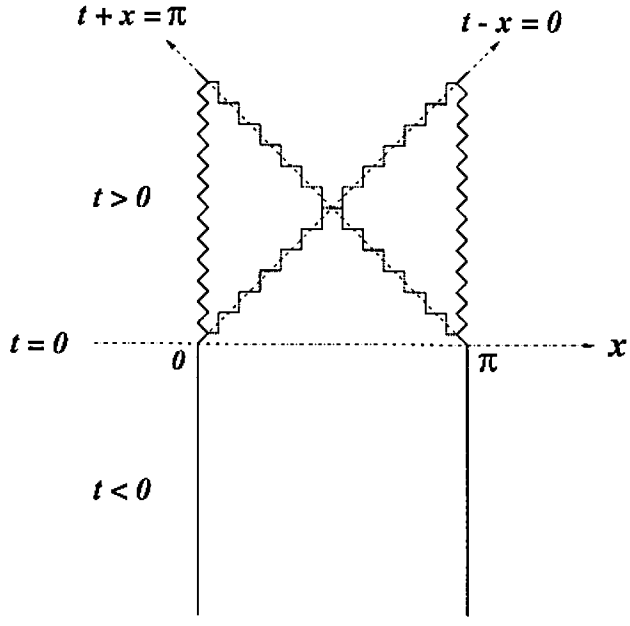

Figure 1: Thunderbolts appear along the null lines.

4 Summary

We have examined quantum effects of the sudden change of the boundary conditions which mimic the situation of the occurrence of wave-singular naked singularities. We have dealt with the massless scalar field in (1 + 1) -dimensional Minkowski spacetime with finite spatial interval. We explicitly showed that the singular null waves or the *thunderbolts* appear along the null lines coming from the edges of the

emerging singularities, while the energy-momentum tensor is zero inside the future domain of dependence of the initial hypersurface $\{t = 0\} \times [0, \pi]$.

This result suggests that the Cauchy horizon associated with wave-singular naked singularities will be destroyed by the thunderbolts and the global hyperbolicity will be restored by the quantum effects.

In the present analysis we restricted ourselves to the simple case such that the boundary conditions change from the Neumann condition to the Dirichlet condition. We can also compute the case that the boundary conditions change from the Neumann condition to general one.

Acknowledgments

We are very grateful to Dr. H. Kobayashi and Prof. A. Inoue for a number of fruitful discussions. A.I. also thank Prof. H. Kodama for discussions. This work was supported in part by Yukawa Shogakukai (A.I.) and also by a grant-in-aid by the Ministry of Science, Sports, and Culture of Japan (A.H., 09640341).

References

[1] A. Ishibashi and A. Hosoya, *Phys. Rev. D* **60** (1999) 104028.

[2] A. Anderson and B. DeWitt, *Found. Phys.* **16** (1986) 91.

Thurston's Geometrization Conjecture and Cosmological Models

Katsuhito Yasuno[1]

Department of Physics, Tokyo Institute of Technology, Oh-Okayama, Megro-ku, Tokyo 152-0033, Japan

Tatsuhiko Koike[2]

Department of Physics, Keio University, Hiyoshi, Kohoku, Yokohama 223-8522, Japan

Masaru Siino[3]

Department of Physics, Tokyo Institute of Technology, Oh-Okayama, Megro-ku, Tokyo 152 0033, Japan

Abstract

One way to generalize the investigation of spatially compact, locally homogeneous universes (CHUs) is proposed. Assuming spatial compactness and local homogeneity, we can construct a kind of *globally inhomogeneous* cosmological model with the help of a widely believed conjecture for 3-manifolds which states that any compact 3-manifolds can be glued together from certain basic building blocks. For technical simplicity, we employ the thin-shell approximation for the construction. The timelike hypersurfaces appearing in gluing two *different* CHUs together are assumed to be spatially homogeneous and homeomorphic to *tori*. This study will be a support in dealing with more generic 3-manifold as the spatial section of the universe.

1 Introduction

Observations of our local region of the universe imply that the early universe must have been homogeneous and isotropic. It is a classical problem of cosmology to provide an explanation for it. As for the initial condition of the universe, we have no reason to restrict ourselves to consider only isotropic geometries. However, at the last scattering surface, the universe should be homogeneous and isotropic in sufficiently large scale. Is there no possibility to include anisotropic geometries in the initial surface?

In this respect, we should begin with the situation that possible topologies and geometries diverge. We restrict ourselves to spatially compact universes. When the spatial compactness of the universe is assumed, the problem can be simplified comparatively with the help of a widely believed conjecture for compact 3-manifolds. This conjecture, called the *Geometrization Conjecture*, states that any compact 3-manifolds can be decomposed by cutting along embedded 2-spheres and tori into domains, each of which admits a locally homogeneous metric [1]. That is, a compact 3-manifold consists of locally homogeneous building blocks and 'wormholes', each of which is homeomorphic to either the 2-sphere or torus, connecting them. The Geometrization Conjecture may implies that the study of spatially compact universes is classified into two parts, that of CHUs and that of 'wormholes'.

We can see such composite 3-manifolds as follows. A man is making a journey from a locally homogeneous 'patch' to the outside world by isometry. After a long time, suddenly he will be faced with a wormhole connecting his patch with another locally homogeneous patch, where he will no longer be able

[1]E-mail:kyasuno@th.phys.titech.ac.jp
[2]E-mail:koike@rk.phys.keio.ac.jp
[3]E-mail:msiino@th.phys.titech.ac.jp

to pass through the wormhole without the entry permit. 'The entry permit' is described mathematically as the isometry that the induced metrics on the boundary between different two patches have. We are of particular interest to such wormholes.

In this paper, we investigate the gluing two CHUs together under the thin-shell approximation, and the dynamics of the boundaries. The boundary hypersurfaces are assumed to be spatially homogeneous and homeomorphic to tori.

2 A model

Our strategy is based on the results for construction of spatially compact locally homogeneous universes, developed by Tanimoto, Koike and Hosoya [2]. Let us summarize here a part of their results for later use. Let $({}^4M_I, g_I)$ and $({}^4M_{VI_0}, g_{VI_0})$ be the Bianchi type I and VI_0 universes of which solutions for the vacuum Einstein equation with vanishing cosmological constant are given, respectively [3]:

$$g_I = -dt_I^2 + t_I^{2p_1}dx_I^2 + t_I^{2p_2}dy_I^2 + t_I^{2p_3}dz_I^2, \tag{1}$$

$$g_{VI_0} = t_{VI_0}^{-1/2}e^{Q^2t_{VI_0}^2}[-dt_{VI_0}^2 + Q^{-2}dz_{VI_0}^2] + t_{VI_0}[e^{2z_{VI_0}}dx_{VI_0}^2 + e^{-2z_{VI_0}}dy_{VI_0}^2], \tag{2}$$

where $\sum_i p_i = \sum_i p_i^2 = 1$, and Q is a curvature parameter which is constant. Further, assume that the spatial (initial) identification of them have been completed by using a discrete subgroup of their *extendible isometries*, respectively. Assume that topologies of compactified Bianchi type I and VI_0 are a2/1 and f/1(n), respectively [4]. They have a common structure, T^2 bundle over S^1. Representations of their fundamental groups up to conjugations are given by [2]

$$\Gamma_I = \{a, b, c\} = \left\{ \begin{pmatrix} a_1 \\ a_2 \\ a_3 \end{pmatrix}, \begin{pmatrix} b_1 \\ b_2 \\ b_3 \end{pmatrix}, \begin{pmatrix} c_1 \\ c_2 \\ c_3 \end{pmatrix} \right\}, \tag{3}$$

$$\Gamma_{VI_0} = \{l, m, n\} = \left\{ \begin{pmatrix} a_0u_1 \\ a_0u_2 \\ 0 \end{pmatrix}, \begin{pmatrix} a_0v_1 \\ a_0v_2 \\ 0 \end{pmatrix}, \begin{pmatrix} 0 \\ 0 \\ n_3 \end{pmatrix} \right\}, \tag{4}$$

where n_3 corresponds to c_3 in [2]. We restrict ourselves to the case $n > 2$.

The gluing of given two CHUs can be proceeded as follows.

- The first step is to fix the initial identification. It can be done by using the fact that there exists commuting local Killing vector fields spanning fiber tori in a2/1 and f/1(n). By cutting a2/1 and f/1(n) along a fiber torus, and matching resulting boundaries each other, we obtain a compact locally homogeneous but globally inhomogeneous 3-manifold. It can be represented algebraically as follows. Representations of a2/1 and f/1(n) are identified at the boundaries such that

  $$l = a, m = b. \tag{5}$$

  Therefore, a representation of the boundary torus is expressed as

  $$l|_{T^2} = \begin{pmatrix} a_0u_1 \\ a_0u_2 \end{pmatrix}, m|_{T^2} = \begin{pmatrix} a_0v_1 \\ a_0v_2 \end{pmatrix}. \tag{6}$$

  This characterizes the initial identification of the boundary torus. In this way, we can obtain (topologically) a compact locally homogeneous but globally inhomogeneous 3-manifold.

- The next step is to determine local dynamics of the boundary by applying Israel's junction conidition under the thin-shell approximation [5], i.e., there exists, on the boundary, a distributional energy momentum tensor described in terms of the jump in the extrinsic curvature across the boundary. Let M_I and M_{VI_0} be timelike hypersurfaces homeomorphic to $T^2 \times \mathbb{R}$ embedded in ${}^4M_I$ and ${}^4M_{VI_0}$ and be characterized by $z_I = \zeta_I(t_I)$ and $z_{VI_0} = \zeta_{VI_0}(t_{VI_0})$, respectively. Induced metrics of them

are denoted by q_I and $q_{\mathrm{V}I_0}$, respectively. Then the gluing M_I and $M_{\mathrm{V}I_0}$ together requires to satisfy the following equations (we denote the glued surface as M):

$$q_{Iab} = q_{\mathrm{V}I_0ab} =: q_{ab}, \tag{7}$$

$$[K_{ab}] = -8\pi\left(S_{ab} - \frac{1}{2}q_{ab}S\right), \tag{8}$$

where q_{ab} is the induced metric on M, $[K_{ab}] := \lim_{\epsilon\to 0}(K_{Iab}|_\epsilon - K_{\mathrm{V}I_0ab}|_{-\epsilon})$ is the jump in the extrinsic curvature, $K_{\Lambda ab} := q_{\Lambda a}{}^m q_{\Lambda b}{}^n \nabla_m n_{\Lambda n}$, where n^a_Λ is the normal to M and Λ denotes I and VI_0, on both sides of the boundary, S_{ab} is the surface energy momentum tensor on M, and $S = q^{ab}S_{ab}$.

For simplicity, we consider here the case that $q_{Ixx} = q_{\mathrm{V}I_0xx}$ and $q_{Iyy} = q_{\mathrm{V}I_0yy}$. In fact, we should take into consideration the degree of freedom of rotating x_Iy_I-plane relative to $x_{\mathrm{V}I_0}y_{\mathrm{V}I_0}$-plane when we proceed the gluing $M_I = M_{\mathrm{V}I_0}$. General treatment will be given in [6].

The result is summarized as follows. First, from the metric continuity condition (7), we can find a trajectory of the boundary torus, i.e., the embedding of M into ${}^4M$ is determined. It is not because the simplification mentioned above but because the geometrical property of the Bianchi type I, i.e., there is no characteristic scale that determine the position of M_I in ${}^4M_I$. Next, from (8), we obtain an expression for the surface energy momentum tensor S_{ab}. In fact, the surface energy density and principal pressure are represented by certain functions of time, e.g., $t_{\mathrm{V}I_0}$. In particular, we see that it must have the anisotropic principal pressure. As for the energy condition, the obtained surface energy momentum tensor can violate the weak energy condition.

- The final step is to solve global deformation of the boundary torus. The global deformation is described by the *Teichmüller parameters* which span the *Teichmüller space*. (For the definition of them, see [2].) Since the Teichmüller space of the torus is the upper half-plane, the Teichmüller parameters are represented up to the global conformal isometries of $\mathrm{Isom}^+\Xi^2$ as,

$$r = \begin{pmatrix} r_1 \\ 0 \end{pmatrix}, \quad s = \begin{pmatrix} s_1 \\ 1/r_1 \end{pmatrix}, \quad r_1 > 0. \tag{9}$$

Thus, the Teichmüller parameters are two real parameters $r_1(>0)$ and s_1.

In fact, whereas q_{ab} is not a conformally $\mathrm{Isom}^+\Xi^2$-invariant metric, we can take conjugations of $l|_{T^2}$ and $m|_{T^2}$ by the global conformal isometries of $\mathrm{Isom}^+\Xi^2$ [2]. The reason is explained as follows. Introduce the proper time τ on q_{ab} and the unit normal vector τ^a of τ-constant 2-surface Σ. Then the induced metric on Σ can be written as $\sigma_{ab} = \tau_a\tau_b + q_{ab}$. Moreover, since Σ is locally homogeneous, we can introduce the synchronous coordinate system, i.e., we can take $\tau_a = (d\tau)_a$. Since, on Σ, components of σ_{ab} are constant, σ_{ab} can be transformed into a conformally $\mathrm{Isom}^+\Xi^2$-invariant metric by a homogeneity preserving diffeomorphism [7].

Therefore, we can relate the Teichmüller parameters with the parameters of the initial identification and the components of q_{ab}. Finally, we obtain the global deformation of the boundary:

$$r_1 = \frac{\sqrt{(u_1)^2\, t_{\mathrm{V}I_0}^{\frac{p_1-p_2}{p_1+p_2}} + (u_2)^2\, t_{\mathrm{V}I_0}^{-\frac{p_1-p_2}{p_1+p_2}}}}{\alpha_0|u_1v_2 - v_1u_2|}, \tag{10}$$

$$s_1 = \frac{u_1v_1\, t_{\mathrm{V}I_0}^{\frac{p_1-p_2}{p_1+p_2}} + u_2v_2\, t_{\mathrm{V}I_0}^{-\frac{p_1-p_2}{p_1+p_2}}}{\alpha_0|u_1v_2 - v_1u_2|\sqrt{(u_1)^2\, t_{\mathrm{V}I_0}^{\frac{p_1-p_2}{p_1+p_2}} + (u_2)^2\, t_{\mathrm{V}I_0}^{-\frac{p_1-p_2}{p_1+p_2}}}}. \tag{11}$$

3 Discussion

We have succeeded to construct a spatially compact, locally homogeneous but globally inhomogeneous universe whose spatial topology is homeomorphic to *Sol*. It is worth noting that our construction does

not give the torus sum of 3-manifolds. For a comapct 3-manifold to be the torus sum, it is necessary to contain at least one *incompressible* torus [1]. The way of construction given here is applicable to compact 3-manifolds modeled on $\mathbb{E}^3$, Nil and Sol, i.e., any compact 3-manifolds which are T^2 bundle over S^1. (As for compact 3-manifolds modeled on Nil, not all of them have that structure. See, e.g., [4]) In terms of the Bianchi types, we can apply our method to I, II, VI_0 and VII_0. Other models we did not deal with, for example, Nil vs. Sol (Bianchi II vs. Bianchi VI_0) will appear in [6]. While we glued only two different manifolds together in the above example, we can deal with various combinations of compact 3-manifolds listed above.

The 'generic' topology of the universe mentioned above was previously investigated by Morrow-Jones and Witt [8] under an assumption of the local spherical symmetry. Their treatment of sewing spaces was done by interpolating a reasonable function. On the other hand, our construction is based on the thin-shell approximation such that inhomogeneity of the universe is compressed on the boundary hypersurfaces. So, one may suppose that the appearance of the anisotropic principal pressure will be cured by finding certain 'surgery' like that of [8]. However, anisotropy of the torus makes such challenges difficult. It can be suspected that backreactions of smoothing effect, for example, propagation of the gravitational wave, might violate the local homogeneity of the universe. However, to understand the reason why the isotropic region survives at the last scattering surface, it is necessary to find a 'surgery' which realizes the torus sum. It remains as a future work.

Acknowledgments

K.Y. is very greatful to M. Tanimoto for helpful discussions and for detailed comments. He thanks H. Kodama, A. Ishibashi, and D. Ida for stimulated discussions, and A. Hosoya and H. Ishihara for continuous encouragement. He would like to acknowledge the hospitality of Yukawa Institute of Theoretical Physics during the month of December, 1999. He also acknowledges financial support from the Japan Society for the Promotion of Science and the Ministry of Education, Science, Sports and Culture.

References

[1] W.P. Thurston, Bull. Amer. Math. Soc. 6 (1982), 357.

[2] M. Tanimoto, T. Koike, and A. Hosoya, J. Math. Phys. 38 (1997), 350.

[3] See, e.g., D. Kramers, H. Stephani, M. MacCallum, and E. Herlt, *Exact solutions of Einstein's field equations* (Cambridge University Press, Cambridge, 1980).

[4] T. Koike, M. Tanimoto, and A. Hosoya, J. Math. Phys. 35 (1994), 4855.

[5] W. Israel, IL Nuovo Ciment 44B (1966), 1.

[6] K. Yasuno, T. Koike, and M. Siino, in preparation.

[7] A. Ashtekar, and J. Samuel, Class. Quantum Grav. 8 (1991), 2191.

[8] J. Morrow-Jones, and D.M. Witt, Phys. Rev. D48 (1993), 2516.

Late time dynamics of scalar perturbations in Majumdar-Papapetrou black holes

Masaru Siino[1]

Department of Physics, Tokyo Institute of Technology, Oh-Okayama, Megro-ku, Tokyo 152-0033, Japan

Abstract

We examine the late time dynamics of scalar perturbation in the Majumdar-Papapetrou black holes. Numerical simulation of the scalar field evolution with axial symmetry is done to determine the power-low index of the late time decaying tail of a scalar perturbation. The power-low index is also evaluated analytically using Barack's scheme.

1 Introduction

The uniqueness theorem of the black hole is the one of the most remarkable results in theoretical studies of black hole spacetimes. Related to it, it is well believed that the general black hole spacetime relaxes to a Kerr-Newmann geometry characterized only by the black hole mass, charge and angular momentum. Especially it have been revealed that a class of gravitational field relaxes to Schwarzschild black holes through the late time era with the power-low decaying tail[1]. Similar relaxation is expected to occur in general black hole spacetimes and numerically and analytically confirmed in some spherically symmetric cases[2][3]. The case of perturbations in spherically symmetric backgrounds is well understood.

The remaining trials are to discuss the axially symmetric cases. In the Kerr geometry background, recently some authors attempt to examine the late time dynamics of the scalar-, electro magnetic-, or gravitational-perturbation. A remarkable difference from the spherically symmetric black holes is the existence of a mode coupling between modes of spherical harmonics with different angular momentum l. It have made analytical study more complicated[12][11]. Their results does not agree in a delicate way.

The numerical analysis also have been entered an axially symmetric stage. Powerful numerical codes are developed and detailed studies about the late-time dynamics are carried out. The results do not agree with the analytical estimation partially. The differences should be resolved soon.

On the other hand, the uniqueness theorem includes some intolerable exceptions, i.e. the existence of the black hole with degenerate or topological event horizon e.g. the Majumdar-Papapetrou (MP) spacetime. The MP-spacetime contains several charged black holes whose masses are equal to their charge, respectively. Against such exceptions, two attitude would be possible. One is to consider conditions which can exclude such a unpleasant case. Imposing the non-degeneracy or trivial topology of their event horizon, one will exclude the exceptions. For example, discussion about the stability of these aspects will justifies the validity of such conditions. The other is to study the variety and regularity of such a exceptions rigorously. Those who have this attitude classified the electrovacuum spacetime supposing that $|Q| = M$, where Q is total charge and M is ADM mass[10] and discovered that only MP-series of electrovacuum solution does not contain naked singularity.

In the present article, we examine the late-time dynamics of a scalar-perturbation in the background of the MP black holes. This investigation is meaningful in the following two points of view. First, our investigation reveals whether there exist a class of gravitational field which relaxes to the MP black holes as the exception of the uniqueness theorem of the black hole. The other view point is interested in the universality of the power-low index of the late-time decaying tail. As stated above, spherical black holes which is target of the uniqueness theorem are accompanied by the same power-low index of the late-time decaying tail since the potentials of the fields equation of the perturbations possesses the same leading form to that of Schwarzschild black hole. So, a question arises, how widely such a universality observed. Of course, even with the spherical symmetry, the power-low index is different provided that the leading

[1]E-mail address:msiino@th.phys.titech.ac.jp

form of the potential is different. It is mysterious, however, that they are same even for the spherical black holes allowed by the uniqueness theorem. The fact that the power-low index is independent of any parameter of black hole on the contrast of the quasi normal mode of a black hole perturbation, seems that the index implicitly depends on the global aspects of spacetime.

To answer this question, it is extremely proper to investigate the perturbations of the Kerr black hole expecting the mode coupling changes the situation. Nevertheless, we could further expect the topology of the black hole (the topology of the MP's event horizon is 'two disconnected S^2' which is different from that of the Schwarzschild horizon) changes the result. The topology of black hole affect the field as the boundary condition and is affected by the anisotropy of the gravitational field. Since an integrated effect of the gravitational radiation might changes the region around future null infinity if the anisotropy is brought by the gravitational radiation contains sufficiently slow decaying tail without oscillation.

Then the purpose of the present article is to examine the power-low index of the scalar-perturbation decaying tail using axially symmetric numerical code and Barack's analytical method to estimate it.

The plan of this article is as follows. Sec. II presents our numerical analysis. In Sec. III, we analytically evaluate the power-low index of the late time tail using Barack's scheme. The final section is devoted to summary and discussions.

2 Numerical analysis

We consider the evolution of a scalar-perturbation field outside extremely charged two black holes with a congruent mass and charge. Such a background spacetime was discovered by Majumdar and Papapetrou[9], which takes the form

$$\begin{aligned} ds^2 &= -U^{-2}dt^2 + U^2(dr^2 + r^2(d\theta^2 + \sin^2\theta d\varphi^2) \\ U &= 1 + \Sigma\frac{m_j}{|r - r_j|} \\ &= 1 + \frac{a}{r} + \frac{a}{\sqrt{r^2 + z_0^2 - 2rz_0\cos\theta}}, \end{aligned} \tag{1}$$

where m_j is a mass of j-th black hole and both are set to a. z_0 is a separation of the two black holes in this conformally flat spatial coordinates. Of course, this is a axially symmetric spacetime. It possesses appropriate symmetry to make numerical analysis possible. In this coordinate $r = r_j$ corresponds to an event horizon of j-th black hole, for example a coordinate transformation $r_R = r + a$ gives a extreme Reissner Nordström metric for a single black hole case.

2.1 numerical scheme

A field equation governing the evolution of scalar perturbations is given by a (massless) Klein-Gordon equation and in the coordinate of Majumdar-Papapetrou it takes the form

$$\begin{aligned} 0 &= \frac{1}{\sqrt{-g}}\partial_\mu g^{\mu\nu}\sqrt{-g}\partial_\nu\phi \\ &= \left[-U^2\partial_t^2 + U^{-2}\Delta_{flat}\right]\phi, \end{aligned} \tag{2}$$

where Δ_{flat} is Laplacian operator in terms of a flat metric.

To adapt it for an axially symmetric code, ϕ is expanded with $e^{im\varphi}$, and one obtains a wave equation for each value of m:

$$0 = \left[\partial_t^2 + U(r,\theta)^{-4}\left(\frac{1}{r^2}\partial_r r\partial_r + \frac{1}{r^2\sin\theta}\partial_\theta\sin\theta\partial_\theta - \frac{m^2}{r^2\sin\theta^2}\right)\right]\phi. \tag{3}$$

We numerically solve this partial differential equation in Two-Step Lax-Wendorff scheme. To solve the equation on the spherical coordinate is accompanied by a coordinate singularity. With another coordinate singularity, i.e. the event horizons, we can remove such a singular nature by make them at a same position.

The contribution from an angular differentiation with factor r^-2 is diminished by the factor $U^{-4} \sim r^4$ in equation 3.

If we analyzed the field in the frequency domain, a trial to separate the field in r and θ coordinates might be possible and worth in this 'two black holes' case. For instance, many works on the dynamics of perturbations of the Kerr black hole has been performed in the frequency domain (or with the assumption of harmonic time dependence) by this variable decomposition. This has certainly been the case for studying quasi normal mode[6], wave scattering[7], and the motion of test particles[8] in the Kerr background.

In principle, one can Fourier transform the initial data and perform the evolution of such data for each frequency. Transforming the data back to the real space, however, it would become hard to keep sufficient accuracy. The reason is because the number of frequencies that one has to consider is much larger than the number of angular components to resolve the θ-direction. Focusing on the investigation of the power-low tails, one would first of all expect that one needs quite a fine resolution near the $\omega = 0$ point in order to be able to correctly resolve the tails. With this in mind, we have chosen to solve the equation 3 in t, r and θ coordinates[5].

To set up the numerical analysis, we also give an appropriate boundary condition at spatial infinity and the event horizon. For simplicity and convenience, we set Dirichlet boundary condition at the event horizon and for outer boundary condition we make a sufficiently large computational domain and a distant outer boundary, which cannot affect the result in time of calculation. Consequently, we set the field arbitrary to zero at there. Of course, it is valid to impose ingoing wave boundary condition at the event horizon. Nevertheless, the accurate ingoing condition is difficult in this system and we can avoid it, in the following reasons. The Dirichlet boundary condition on the event horizon is justified by the fact that the event horizon is infinitely far from the static observer in terms of the proper length. The ingoing wave condition $U^2\partial\phi/\partial t = U^{-2}\partial\phi/\partial x_r$ degenerates and $\dot{\phi}$ vanishes there as long as the gradient of ϕ with respect to affinely parametrized coordinate is finite.

Moreover it is suggested by some authors that the boundary condition does not affect the result basically[2][3]. Depending on the behavior of the angular eigenfunction indicated by m, one imposes either $\phi = 0$ or $\partial_\theta\phi = 0$. All these set up are similar to reference [5] though our case is simpler than it. Our results are computed only from information inside the maximal Cauchy development of the initial data surface.

Finally it might be claimed by someone that to calculate on the spatially conformally flat coordinates, i.e. the MP coordinates, cause problem since the mesh of the coordinates is larger than that of the tortoise coordinate around the event horizon. Nevertheless, we consider that the gradient of the potential is not so steep. On the contrary, it is favorable to keep the relativistic Courant condition $\sqrt{g_{00}}dt < \sqrt{g_{ij}dx_i dx_j}$ around its coordinate singularity.

2.2 numerical result

We can now solve Eq. (3) numerically. This equation is discretized on a uniform two-dimensional rectangular grid:$0 \leq r_i \leq 4000a$, $0 \leq \theta_j \leq \pi$, $0 \leq i \leq 8192$, $0 \leq j \leq 32$. δt is set $\sim \delta r/2$ and is sufficient to keep numerical stability. (It is verified for 100,000steps.) The accuracy of the code is checked using a exact propagating wave in a flat background. The relative error is under 0.04 for evolution times $t < 3000a$.

Mainly we examine the decaying and mode coupling of each Y_{lm} mode around the Majumdar-Papapetrou black hole. An initial conditions of the field are given with the bell shape packet in radial distribution and a spherical harmonics in angular distribution, and its time derivative is set to zero:

$$\phi_{ini} = c_1((c_2 r - r_{in})(c_2 r - r_{out}))^8 Y_{lm}, \quad \dot{\phi} = 0, \tag{4}$$

where each parameters are set as $c_1 = 100, c_2 = 0.02, r_{in} = 1.0, r_{out} = 3.0$.

Fig. 1 (a)$\sim$(d) are snap-shots of the distribution of ϕ at $t = 0, 500, 1000, 2000$ with initial condition $\phi_{ini}[l = 1, m = 0]$. In this calculation a boundary condition at z-axis is $\partial_\theta\phi = 0$ so that there is no excitation of $m \neq 0$ mode because of the axial symmetry of the back ground. Since there would be a mode coupling between the different l-mode with the same m, a Y_{00}-mode is excited before $t = 500$,

and then the ratio of the Y_{00}-mode to the Y_{10}-mode increases. The reason of this aspect will be that the Y_{10}-mode decays faster than the Y_{00}-mode as in the case of spherically symmetric background, e.g. Schwarzschild or Reisner-Nordström black hole.

To confirm this we estimate the time evolution of each mode. Supposing that there is no other mode than the two mode, the amplitude of the Y_{00}-mode is determined by $A_0 = \phi(r_0, \theta = \pi/2)$ and Y_{10}-mode by $A_1 = \phi(r_0, \theta = 0) - A_0$, where r_0 is the radial coordinate for a static observer. Fig. 3 shows the time evolution of A_0 at $r_0 = r_{max}/4$ for $z_0 = 0$ (RN – BH), $200\delta r$, $1000\delta r$ and Fig. 4 A_1.

From these figures, it can be observed that the power-low tails of each mode in two black hole backgrounds are not different from that is the spherically symmetric background corresponding to the extreme Reissner-Nordström black hole. Furthermore, the fact that there is not so much amplitude of other mode can be confirmed by the expansion of the angular distribution at $r = r_1, t = t_1$ with spherical harmonics (with $m = 0$). Fig. 2 displays amplitude of each l-mode. From this figure, we can conclude that only Y_{00}-mode and Y_{10}-mode are relevant.

In the case of $m = 1$, ϕ_{ini} is chosen to have Y_{21}-angular distribution. The snap-shots are Fig. 5 which reveals that there also be mode excitation of lower l-mode by axially symmetric mode-coupling. The spherical harmonics expansion is Fig. 6. There are the contributions of only Y_{11}-mode and Y_{21}-mode. The late time evolutions of $B_1 = \phi(r_0, \theta = \pi/2)$ and $B_2 = \phi(r_0, \pi/4) - \sin(\pi/4)B_1$ are shown in Fig. 7 and Fig. 8, respectively. The difference from the case of $m = 0$ is not notable.

To complete the analysis we should examine the late time evolution of the field for ingoing null observer. However it is not sufficient to report here, since it is hard to find the radiative zone to evaluate the power-low index. Moreover, we fail to ϕ between different angles, since it is hard to synchronize the zeros of ingoing null coordinates belonging to observers with different θ.

The following is the table of the power low index for all these calculations.

l	m	extreme RN	MP ($z_0 = 200dr$)	MP ($z_0 = 1000dr$)
0	0		-3.04	-4.78
1	0	-2.85	-2.84	-2.79
1	1		-3.36	-2.41
2	1	-2.02	-2.01	-2.02

From these results, we cannot discuss its qualitative aspects. To discuss it, we need more long calculation which will provide more accurate power-low index in sufficiently asymptotic region.

3 Analytical evaluation with Barack's scheme (in Majumdar-Papapetrou black holes)

In this section, we analytically estimate the power-low index of the late time tail, considering a mode coupling between different l-modes. Barack[11] estimated the effect of the coupling in the Kerr back ground with an iterative framework. Their way is very simple and does not require finding concrete solution and its asymptotic form, unlike other methods[12]. So, we apply this method to the Majumdar-Papapetrou (MP) black holes.

First of all, we decompose the metric function U, eq.(1) into a spherical part and multi pole moments.

$$U = U_0 + \delta U$$
$$\begin{cases} U_0 = 1 + \frac{2a}{r} \\ \delta U = \frac{a}{r} \sum_{l=1} P_l(\cos\theta)(\frac{z_a}{r})^l \end{cases} \tag{5}$$

By this decomposition, the Klein-Gordon equation can be decomposed into a spherical part, which is in terms of an extreme Reissner Nordström metric and the rest including mode couplings.

$$\begin{aligned} 0 &= \left[-U^{-4}\partial_t^2 + \Delta_{flat}\right]\phi \\ &= \left[-U_0^{-4}\partial_t^2 + \Delta_{flat} - (U^{-4} - U_0^{-4})\partial_t^2\right]\phi \\ &= \left[U_0^{-2}{}_{RN} - (U^{-4} - U_0^{-4})\partial_t^2\right]\phi \end{aligned} \tag{6}$$

where $_{RN}$ is a d'Alembertian operator in terms of the extreme Reissner Nordstrom metric whose mass parameter is $2a$.

Introducing a tortoise coordinate r_* of the $_{RN}$-part and $\psi = \phi/r_R$, by spherical harmonics expansion the field equation becomes

$$-\partial_t^2\psi_{lm} + \partial_{r_*}^2\psi_{lm} - \left[U_0^{-2}\left(\frac{l(l+1)}{(r+a)^2} + \frac{2}{U_0 r_R}\frac{\partial(U_0^{-1})}{\partial r_R}\right)\right] + I_{MC}(\phi, tt) = 0 \tag{7}$$

$$\begin{cases} dr_* = dr_R\dot{U}_0^2, r_R = r + a_1 + a_2 = r + a \\ \phi/r_R =: \psi =: \psi_{lm}Y_{lm} \end{cases} \tag{8}$$

The reason we avoid a expansion with a appropriate harmonics, which can decompose the radial and angular coordinate is that it is not convenient since the late time tail is not related to the eigenfunction rather to the cut of Green function[13].

Here we consider an asymptotic form of the mode coupling since the result depends only on it as in the following. For large r, the mode coupling is caused by

$$I_{MC} = \Sigma_{n=-l}^{\infty}\left[\frac{c_{l,+n}}{r^{|n|+1}}\psi_{l+n\ m,tt} - \frac{c'_n}{r^{|n|+1}}\psi_{lm,tt}\right], \tag{9}$$

where $c_\sim$ are certain coefficients.

3.1 power at future null infinity

Now we estimate the power low index at future null infinity according to Ref. [11]. Following iterative expansion is essential:

$$\begin{aligned} \Psi &= \sum_{N=0}\Psi_N \\ (\partial_t^2 - \partial_{r_*}^2 + V_0)\Psi_N &= \begin{cases} 0 & (N=0) \\ -(\delta V(r_*)\Psi_{N-1} + I_{MC}[\Psi_{N-1}] & (N \neq 0) \end{cases} \\ V &= V_0 + \delta V \\ V_0 &= \begin{cases} 0 & (r < r_0) \\ \frac{l(l+1)}{r_*^2} & (r \geq r_0) \end{cases}. \end{aligned} \tag{10}$$

It is given by the region $v < v', u' < u, u < v'$ that the significant contribution to estimate $\Psi_1(u,v) = \int du \int^{'} dv' G(u,v;u',v')V(u',v')\Psi_0(u',v')$. Ψ l_0 which is l-component of Ψ_0 is given by

$$\Psi_0^l = \sum_{j=0}^{l} A_j^l \frac{g_0^{(j)}(u)}{(u-v)^{l-j}}, \tag{11}$$

with the function

$$g_0^{l\neq 0}(u) = \theta(-u) \times \frac{1}{(l-1)!}\int_{u_0}^{u}(u/u')^{l+1}(u-u')^{l-1}\Gamma(u')du', \quad g_0^0 = \Gamma(u), \tag{12}$$

where A_j^l are constant coefficients given by

$$A_j^l = \frac{(2l-j)!}{j!(l-j)!}. \tag{13}$$

The Green function for eqs.(10), $[\partial^2/\partial t^2 - \partial^2/\partial r_*^2 - V_0]G = \delta$, is also given by

$$G^l(u,v;u',v') = \sum_{j=0}^{l} A_j^l \frac{g^{(j)}(u;u',v')}{(v-u)^{l-j}}\theta(u-u')\theta(v-v')\theta(v'-u), \tag{14}$$

where the function $g(u;u',v')$ is

$$g(u;u',v') = \frac{1}{l!}\frac{(v'-u)^l(u-u')^{l^l}}{v'-u'}, \tag{15}$$

and where the j-differentiations of this function are with respect to u.

Here it should be noted that though $\theta(...)$ originate from causality it does not rigorously reflect the causality of MP black holes, since u, v are not null coordinates of the MP spacetime but of only its spherical part. In this estimation, it can be seen a well-known result that the power-low index of Schwarzschild or Reissner Nordström black hole at future null infinity, i.e. $-(l+2)$, is caused by leading term of δV which behaves as $r_*^{-3}\ln r_*$ as $\Psi_l^{\infty}[\delta V] = -\int du' \int dv' G[\delta V(\sim r_*^{-3}\ln r_*)]\Psi_0 \sim u^{-l-2}$.

To evaluate the contribution from δV and I_{MC} totally, we expand these terms in the power of r_*

$$\begin{aligned} \delta V &= V - \frac{l(l+1)}{r_*^2} \sim \frac{a+b\ln r_*}{r_*^3} + ... \\ I_{MC}^{l\leftarrow l'} &\sim \frac{c}{r_*^{|l-l'|+1}}\frac{d^2}{dt^2}\Psi_{0\,l'} + ... \end{aligned} \tag{16}$$

Then we consider the source of the iterative equation with the following form,

$$S_{l\leftarrow l'} = r_*^{-P}[\alpha + \beta\ln r_*]\left(\frac{d}{dt}\right)^d \Psi_0^{l'}. \tag{17}$$

Using equations 11 and 14, the contribution to Ψ_0 from this source is evaluated[11] as

$$\begin{aligned} \Psi &= \int du' \int dv' G(u,u',v,v') S_{l\leftarrow l'} \\ &\sim [A + B\ln u]u^{-(l'+P-1-d)}, \quad (A=0, \text{for} P < l-l'+2), \end{aligned} \tag{18}$$

Collecting the contribution from all of the terms in eqs. 9, the late time tail at the future null infinity is given by

$$\sim u^{-l-2}. \tag{19}$$

3.2 late time tail with fixed r

To compare the analytical calculation to the numerical result, it is convenient to interpret the above late time tail at the future null infinity into that with fixed r. The method is given in [11]. However, the result does not agree with our numerical result. We would understand that the estimation given in [11] is only valid for the dominant mode. In the estimation at the future null infinity, the effect of the mode coupling does not change the index. This will agree with the numerical result that the index is not be affected by the mode coupling at the future null infinity and with fixed r.

4 summary and conclusion

We have numerically calculated the late time behavior of scalar perturbations in the background of Majumdar-Papapetrou black holes. We see that the lower l-modes are excited by the mode coupling and it dominate the evolution since the lower l mode decays more slowly than the higher. Nevertheless, the power-low index we evaluated is no difference from that of the perturbation in the Reissner-Nordström (or Schwarzschild) background.

To discuss this result, we also analytically calculated the index. The analytical index also is not affected in future null infinity but is affected for a observer with fixed r. The in-coincidence between numerical and analytical estimation may occur when we relate the index at future null infinity and a observer with fixed r.

Finally we briefly comment on the effect of the accumulation of the quasi normal modes of an extreme black hole. As some author pointed out[15][5], in an extreme Kerr black hole background, the accumulation of the quasi normal modes occurs and it changes the power-low index. Then one may expect that

in MP black holes background, similar aspects since MP black holes are corresponding to extreme black hole with $m = |q|$. Nevertheless, such a situation stands only for charged fields[14]. This will become clear by writing down a potential of it.

Acknowledgments

The author thanks Prof. T. Nakamura and Prof. K. Oohara for useful advises about numerical technique. We are also grateful to Prof. M. Sasaki and Prof. T. Mishima for comments about the accumulation of the quasi normal mode. Finally we want to express thanks to Prof. Hosoya and Prof. Ishihara for their continuous encouragement.

References

[1] R. H. Price, *Phys. Rev.* **D5**, 2419 (1972); **5**, 2439 (1972).

[2] C. Gundlach, R. H. Price, and J. Pullin, *Phys. Rev. D* **49**,883 (1994).

[3] E. S. C. Ching, P. T. Leung, W. M. Suen, and K. Young, *Phys. Rev. D* **52** 2118 (1995).

[4] W. Krivan, P. Laguna and P. Papadopoulos, *Phys. Rev. D* **54**, 4728 (1996).

[5] W. Krivan, P. Laguna, P. Papadopoulos and N. Andersson, *Phys. Rev. D* **56**, 3395 (1997).

[6] S. Detweiler, *Astrophys. J.* **238**,292 (1980), E.W. Leaver, *Proc. R. Soc. London* **A402**,285 (1985), E. Seidel and S. Iyer, *Phys. Rev. D* **41**, 374 (1990), K. D. Kokkotas, *Class. Quantum Grav.* **8**, 2217 (1991),

[7] J. A. H. Futterman, F. A. Handler, and R. A. Matzner, *Scattering from Black holes* (Cambridge University Press, Cambridge, England, 1988).

[8] M. Sasaki and T. Nakamura, Prog. Theor. Phys. **67**,1788 (1982), Y. Kojima and T. Nakamura, *Phys. Lett.* **96A**, 335 (1983); **99A**, 37 (1983), Y. Kojima and T. Nakamura, *Prog. Theor. Phys.* **71**, 79 (1984); **72**, 494 (1984).

[9] S. D. Majumdar, *Phys. Rev.* **72**, 390 (1947), A. Papapetrou, *Proc. Roy. Irish Acad.* **A51**, 191 (1945).

[10] P. T. Chruściel and N. S. Nadirashvili, *Class. Quantum Grav.* **12**, L17 (1995).

[11] L. Barack, *Phys. Rev. D* **61**, 024026 (1999).

[12] S. Hod, *Phys. Rev. D* **58**, 104022 (1998).

[13] E. W. Leaver, *Phys. Rev. D* **34**, 384 (1986).

[14] private communication with Prof. T. Mishima

[15] M. Sasaki and T. Nakamura, *Gen. Rel. Gra.* **22** 1351 (1990).

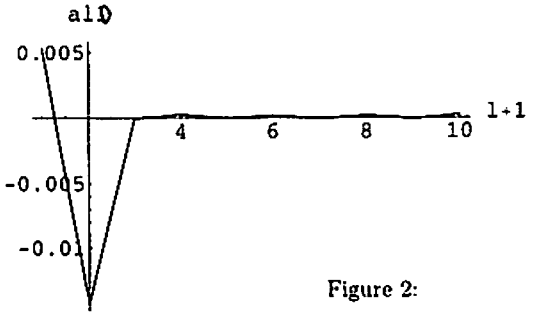

Figure 2:

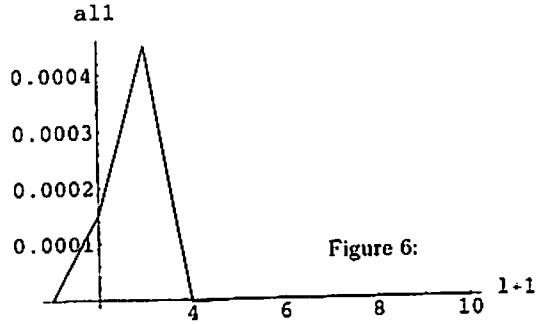

Figure 6:

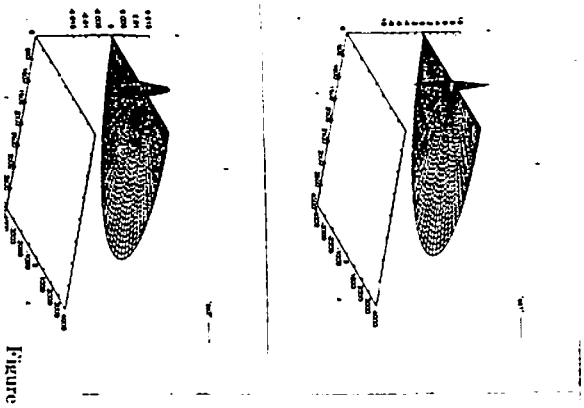

Figure 5:

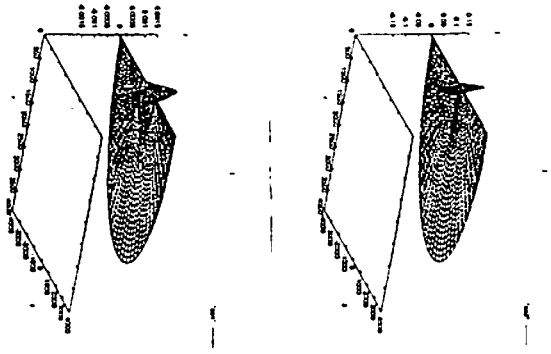

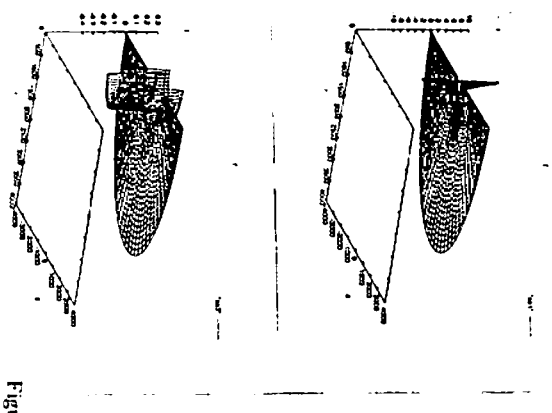

Figure 1:

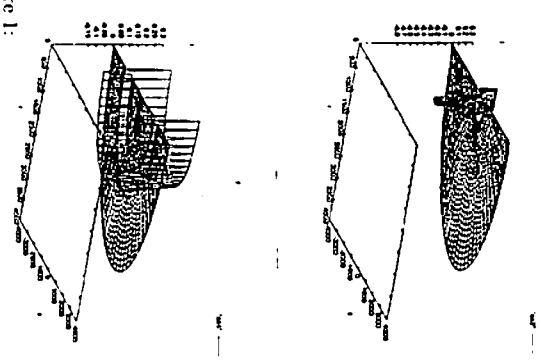

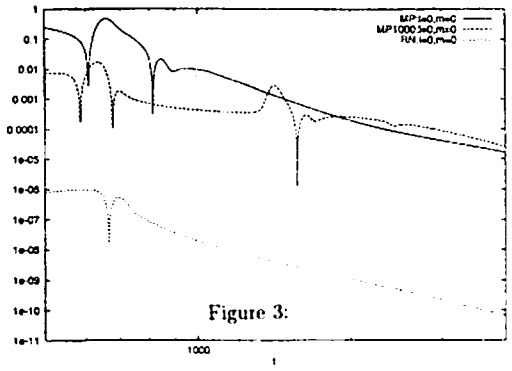

Figure 3:

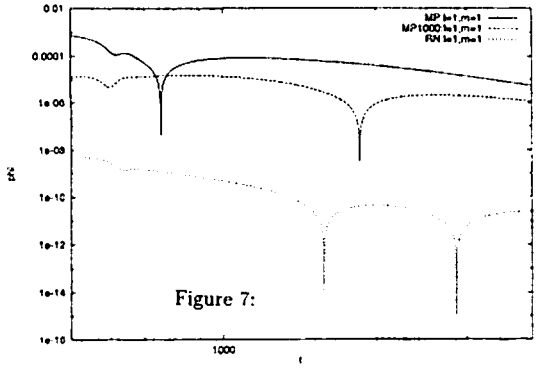

Figure 7:

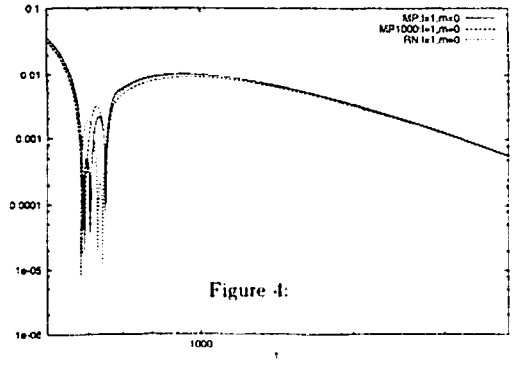

Figure 4:

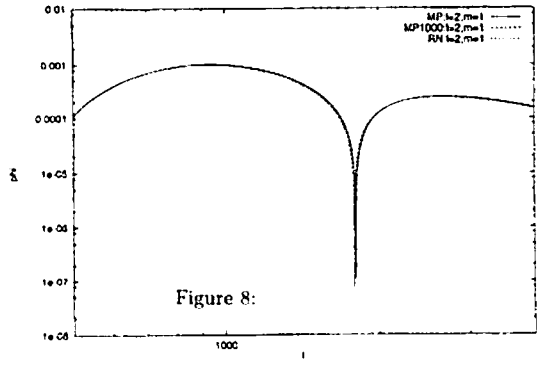

Figure 8:

Scaling of the global string network in the matter dominated universe

Masahide Yamaguchi[1]

Department of Physics, School of Science, University of Tokyo, Tokyo 113-0033, Japan

Jun'ichi Yokoyama[2]

Department of Earth and Space Science, Graduate School of Science, Osaka University, Toyonaka 560-0043, Japan

M. Kawasaki[3]

Research Center for the Early Universe, School of Science, University of Tokyo, Tokyo 113-0033, Japan

Abstract

We evolve the network of global strings in the matter dominated universe by means of numerical simulations. The existence of the scaling solution is confirmed as in the radiation dominated universe but the scaling parameter, ξ, takes a slightly smaller value, $\xi \simeq 0.6 \pm 0.1$, which is defined as $\xi = \rho_s t^2/\mu$ with ρ_s the energy density of global strings and μ the string tension per unit length. The change of ξ from the radiation to the matter dominated universe is consistent with that obtained by Albrecht and Turok by use of the one scale model. We also study the loop distribution function and find that it can be well fitted with that predicted by the one scale model, where the number density, $n_l(t)$, of the loop with the length, l, is given by $n_l(t) = \nu/(t^2(l+\kappa t)^2)$ with $\nu \sim 0.040$ and $\kappa \sim 0.48$. Thus, the evolution of the global string network in the matter dominated universe can be well described by the one-scale model as in the radiation dominated universe.

1 Introduction

Cosmic strings are formed in a class of cosmological phase transitions [1]. Among them, gauged or local strings have been extensively studied because they could produce density fluctuations responsible for the large-scale structure formation and the cosmic microwave background anisotropy [2]. A lot of analytical and numerical studies have been done to confirm that after some relaxation period, a local string network enters the scaling regime. In this regime, the large-scale behavior of a network scales with the Hubble radius and the energy density of a network is given by

$$\rho_{\rm string} = \xi\mu/t^2 \,, \tag{1}$$

where ξ is a constant irrespective of cosmic time. [3, 4, 5, 6]. Long strings intercommute to make loops [5, 6, 7], which decay through radiating gravitational waves [8]. But, an alternative scenario was recently proposed that long strings directly emit massive particles and lose their own energy [9]. Thus, though the mechanism to drive a network to the scaling regime is still in dispute, the existence of the scaling solution is undoubted.

On the other hand, global strings has been less investigated and considered only in the context of axion cosmology [10, 11, 12, 13, 14, 15]. It was assumed without direct verification that a global string network relaxes into the scaling solution just as the local counterpart, where long strings intercommute to

[1] E-mail:gucci@utap.phys.s.u-tokyo.ac.jp
[2] E-mail:yokoyama@vega.ess.sci.osaka-u.ac.jp
[3] E-mail:kawasaki@resceu.s.u-tokyo.ac.jp

create loops with typical size comparable with the horizon scale and loops decay through emitting Nambu-Goldstone(NG) bosons. However, since global strings have a long-range interaction their dynamics could be different from that of local strings. In fact our numerical analysis of the evolution of a complex scalar field in 2+1 dimensions revealed that the global "strings" do not relax into the scaling solution but the number of defects per horizon volume increases logarithmically with time due to the long-range interaction [16]. In the previous paper [17] we examined the evolution of a global string network in the radiation dominated universe by numerically solving the equation of motion for a complex scalar field representing a global string. Then the above picture was confirmed. The scaling parameter, ξ, takes a constant value and becomes $\xi \sim (0.9 - 1.3)$, irrespective of the cosmic time. Furthermore, one of the authors (MY) [18] further have found that the number density, $n_l(t)$, of the loop with the length, l, can be well fitted by the formula predicted from the so-called one scale model, that is, $n_l(t) = \nu/[t^{3/2}(l + \kappa t)^{5/2}]$ with $\nu \sim 0.0865$ and $\kappa \sim 0.535$. Thus, the evolution of a global string network in the radiation dominated universe is well described by the one scale model proposed by Kibble [19, 20, 21].

In this paper, for a complete understanding, we study the evolution of a global string network in the matter-dominated universe, concretely, whether it can be well described by the one scale model as in the radiation dominated universe, and if at all, we clarify relation between scaling parameters in both eras.

2 Formulation of numerical simulations

We consider the following Lagrangian density for a complex scalar field $\Phi(x)$,

$$\mathcal{L}[\Phi] = g_{\mu\nu}(\partial^\mu\Phi)(\partial^\nu\Phi)^\dagger - V_{\rm eff}[\Phi, T]\,, \tag{2}$$

where $g_{\mu\nu}$ is identified with the Robertson-Walker metric and the effective potential $V_{\rm eff}[\Phi, T]$ is given by

$$V_{\rm eff}[\Phi, T] = \frac{\lambda}{2}(\Phi\Phi^\dagger - \eta^2)^2 + \frac{\lambda}{3}T^2\,\Phi\Phi^\dagger\,, \tag{3}$$

which represents a typical second order phase transition and the $U(1)$ symmetry is broken below the critical temperature, $T_c = \sqrt{3}\eta$.

For cosmological purposes, it would be desirable to trace the evolution of strings in the transition regime from the radiation dominated era to the matter dominated era. Due to the limitation of our computer powers, however, we concentrate on the evolution of a global string network during the matter domination alone in this paper. Since the scaling property, if at all, is expected to be reached irrespective of initial conditions, we start simulations from a symmetric state with the equations of motion given in the matter domination. Then, strings are formed soon and they evolve in the matter domination. As will be shown later, we confirm the scaling behavior in the matter dominated regime and find that ξ in this era is not different from that in the radiation domination by more than a factor of 2. Hence we expect transition from the radiation era to the matter era does not give rise to any significant cosmological effects, justifying our approach.

In the matter-dominated universe, the equation of motion is given by

$$\ddot{\Phi}(x) + 3H\dot{\Phi}(x) - \frac{1}{R(t)^2}\nabla^2\Phi(x) = -V'_{\rm eff}[\Phi, T]\,, \tag{4}$$

where the prime represents the derivative $\partial/\partial\Phi^\dagger$ and $R(t)$ is the scale factor which grows in proportion to $t^{2/3}$. We define $\alpha(T)$ ($\alpha(T) > 1$) as $\alpha(T) \equiv \rho_{\rm mat}(T)/\rho_{\rm rad}(T)$ with $\rho_{\rm mat}(T)$ being the contribution to the energy density from non-relativistic particles and $\rho_{\rm rad}(T)$ that from relativistic particles at the temperature T. Then,

$$\alpha(T) = \alpha_c\left(\frac{T_c}{T}\right)\,, \tag{5}$$

with $\alpha_c \equiv \rho_{\rm mat}(T_c)/\rho_{\rm rad}(T_c)$. Therefore, the Hubble parameter $H = \dot{R}(t)/R(t)$ and the cosmic time t are given by

$$H^2 = \alpha(T)\frac{8\pi}{3m_{\rm pl}^2}\frac{\pi^2}{30}g_*T^4 = \alpha_c\frac{4\sqrt{3}\pi^3\eta g_*}{45m_{\rm pl}^2}T^3, \tag{6}$$

$$t = \frac{2}{3H} \equiv \frac{\epsilon}{T^{3/2}}\,, \tag{7}$$

where $m_{\rm pl} = 1.2 \times 10^{19}$GeV is the Plank mass, g_* is the total number of degrees of freedom for the relativistic particles. We define the dimensionless parameter ζ as

$$\zeta \equiv \frac{\epsilon}{\eta^{1/2}} = \left(\frac{5 m_{\rm pl}^2}{\sqrt{3} \alpha_c \pi^3 g_* \eta^2} \right)^{1/2} . \tag{8}$$

In our simulation, we take $\zeta = 8$ and 4 to investigate ζ dependence on the result. We take the initial time $t_i = t_c/(2\sqrt{2})$ corresponding to $T_i = 2T_c$ and the final time $t_f = 70(140)\, t_i$, where t_c is the epoch with $T = T_c$. Since the $U(1)$ symmetry is restored at the initial time $t = t_i$, we adopt as the initial condition the thermal equilibrium state with the mass squared,

$$m^2 = \left. \frac{d^2 V_{\rm eff}[|\Phi|, T]}{d|\Phi|^2} \right|_{|\Phi|=0} , \tag{9}$$

which is the inverse curvature squared of the potential at the origin at $t = t_i$.

Below we measure all physical quantities in units of t_i. Then, the equation of motion is given by

$$\ddot{\Phi}(x) + \frac{2}{t}\dot{\Phi}(x) - \frac{1}{t^{4/3}} \nabla^2 \Phi(x) = - \left(|\Phi|^2 + \frac{\zeta^2}{6\sqrt{3}\, t^{4/3}} - \frac{\zeta^2}{24\sqrt{3}} \right) \Phi^\dagger , \tag{10}$$

where λ is set to unity for brevity. The scale factor $R(t)$ is normalized as $R(1) = 1$.

Using the second-order leap-frog method (See Ref. [18] for details), we evolve the global string networks in the matter-dominated universe. In order to judge whether the global string network relaxes into the scaling regime in the matter-dominated universe, we give time development of the scaling parameter ξ defined as $\rho = \xi \mu / t^2$. In our simulations, a lattice is identified with a part of a string core if the potential energy density there is larger than that corresponding to the field value of a static cylindrically-symmetric solution at $r = \delta x_{\rm phys}/\sqrt{2}$.

We perform the simulations in seven different sets of lattice sizes, spacings, and ζ (See TABLE 1, 2.). In the case (1) and (5), the box size is nearly equal to the horizon volume $(H^{-1})^3$ and the lattice spacing to a typical width $\delta \sim 1.0/(\sqrt{2}\eta)$ of a string at the final time t_f. For each case, we simulate the system from 10 ((1)-(6)) or 300 ((7)) different thermal initial conditions.

If the simulation box is much larger than the horizon volume, it is reasonable to think that the boundary effect is negligible. But, in our simulation, the simulation box is comparable with or at most 4^3 times as large as the horizon volume at the final time of the simulation so that we should be careful to avoid possible boundary effects. In fact, a long-range force works between global strings so that the boundary effect cannot necessarily be neglected if the number of long strings in the simulation box is very small. As shown later, there are only a few long strings in our case so that the boundary effect could be significant. Hence in this paper we run simulations with two different boundary conditions of distinct features and employ a large enough simulation box so that the results with the different boundary conditions converge to each other. We thereby obtain a result free from the boundary effects.

3 Results

First, we adopt the periodic boundary condition, under which a string feels an attractive force from the boundary and there exists no infinite string so that strings can completely disappear in the simulation box if the Hubble radius becomes larger than the dimension of the simulation box. Figs. 1 represent time development of ξ with $\zeta = 8$ (case(1),(3),(4)) under this boundary condition. In the case (1) with the smallest box, the boundary effect is so significant that strings tend to disappear, which is inconsistent with [19, 20, 21]. The larger the box size is, the less important the boundary effect is. In the case (3) corresponding to the largest box simulations, the boundary effect is less significant so that ξ seems to relax to a constant with $\xi \sim 0.49 \pm 0.02$.

Next, we adopt the reflective boundary condition, where $\nabla^2 \Phi(x)$ on the boundary points disappears. Under this boundary condition, a string suffers a repulsive force from the boundary so that a string near the boundary intercommutes less often than that near the center of the simulation box because the partner to intercommute only lies in the inner direction of the boundary. Thus, the number of the

Table 1: Three different sets of the simulations under the periodic boundary condition

case	lattice number	lattice spacing (unit $= t_i R(t)$)	ζ	realization	box size/H^{-1} (at final time)	ξ
(1)	128^3	$\sqrt[3]{70}/85$	8	10	1(at 70)	Disappearance
(3)	256^3	$\sqrt[3]{70}/85$	8	10	2(at 70)	0.50 ± 0.02
(4)	256^3	$2\sqrt[3]{70}/85$	8	10	4(at 70)	0.49 ± 0.02

Table 2: Seven different sets of the simulations under the reflective boundary condition

case	lattice number	lattice spacing (unit $= t_i R(t)$)	ζ	realization	box size/H^{-1} (at final time)	ξ
(1)	128^3	$\sqrt[3]{70}/85$	8	10	1(at 70)	1.93 ± 0.04
(2)	128^3	$2\sqrt[3]{70}/85$	8	10	2(at 70)	1.03 ± 0.03
(3)	256^3	$\sqrt[3]{70}/85$	8	10	2(at 70)	1.13 ± 0.02
(4)	256^3	$2\sqrt[3]{70}/85$	8	10	4(at 70)	0.72 ± 0.03
(5)	128^3	$\sqrt[3]{140}/85$	4	10	1(at 140)	1.36 ± 0.06
(6)	256^3	$\sqrt[3]{140}/85$	4	10	2(at 140)	1.21 ± 0.02
(7)	128^3	$2\sqrt[3]{70}/85$	4	300	2(at 70)	1.25 ± 0.02

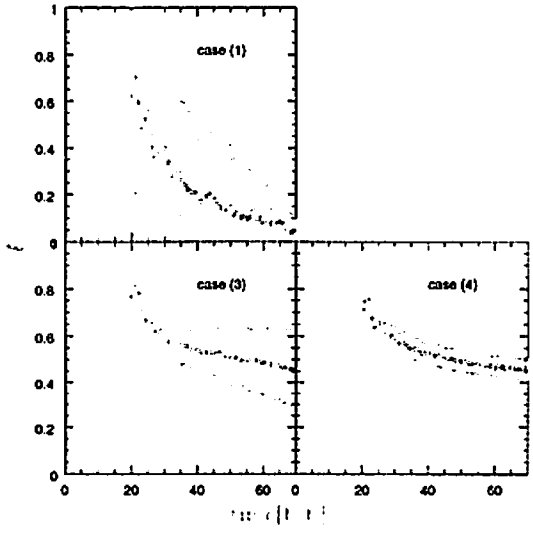

Figure 1: Time development of ξ under the periodic boundary condition. Symbols(□) represent time development of ξ. The vertical lines denote a standard deviation.

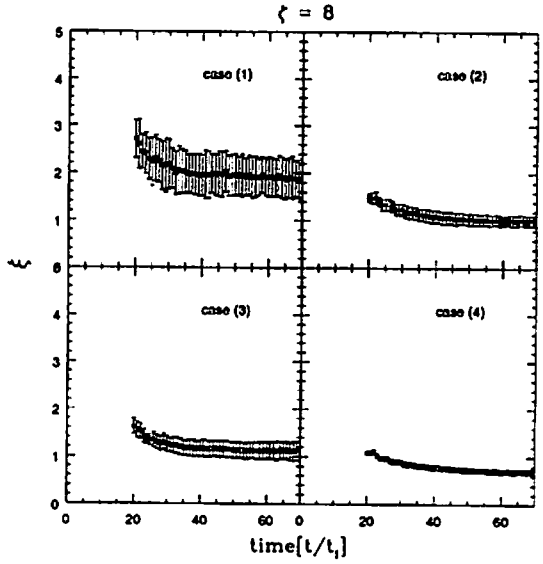

Figure 2: Time development of ξ in the cases from (1) to (4) with $\zeta = 8$ under the reflective boundary condition. Symbols(□) represent time development of ξ. The vertical lines denote a standard deviation over different initial conditions.

strings tends to be more than that in the real universe. Figs. 2 and 3 represent time development of ξ with $\zeta = 8$ (case(1)-(4)) and $\zeta = 4$ (case(5)-(7)), where ξ becomes a constant irrespective of time with (1)1.93 ± 0.04, (2)1.03 ± 0.03, (3)1.13 ± 0.02, (4)0.72 ± 0.03, (5)1.36 ± 0.06, (6)1.21 ± 0.04, (7)0.72 ± 0.03. ξ has larger values in smaller-box simulations due to the boundary effect as explained above. Also, for larger-box simulations, ξ depends very little on ζ.

From the results of the largest-box simulations containing the largest number of the Hubble volume at the final epoch, we conclude ξ converges to a constant $\xi \simeq 0.6 \pm 0.1$ irrespective of the boundary conditions. This result will be supported later by comparing with our previous results in the radiation-dominated regime [17, 18] through an analytic model of Albrecht and Turok [3].

Next we investigate the loop distribution, which is predicted by Kibble's one-scale model [19, 20, 21] as

$$n_l(t) = \frac{\nu}{t^2(l + \kappa t)^2}\,, \tag{11}$$

where ν is a constant, l is the length of a loop, and the log-dependence of μ is neglected. In contrast with local strings, the dominant energy loss mechanism of global strings is radiation of the associated Nambu-Goldstone field [10]. We define the radiation power, P, as $P = \kappa\mu$ where κ is a constant.

We determine whether the loop distribution in the simulation coincides with the above function. Since the case (4) with the largest box takes too much time for one realization, we investigate the loop distribution for the case (7) under the reflective boundary condition[4] . The loop distribution is depicted in Fig. 4 in the case (7) at $t = 40, 50, 60$, and 70. Since long strings are rare, we cut the length of loops into bins with the width $5 \times \delta x$. Also, we divide 300 realizations into 6 groups comprised of 50 realizations and we summed the number of loops over 50 realizations for each groups. The dot represents the number of loops averaged over 6 groups and the dashed line represents the standard deviation. They can be simultaneously fitted with the above formula if one takes $\nu \sim 0.040$ and $\kappa \sim 0.48$. Thus, the loop

[4] ξ in the case (7) is about twice as large as that in the case (4) corresponding to the largest box simulation so that ν in the real world may become half as large as that obtained in our simulation.

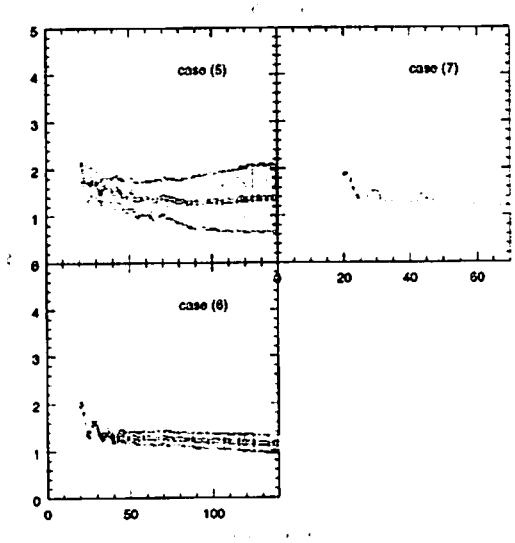

Figure 3: Time development of ξ in the cases from (5) to (7) with $\zeta = 4$ under the reflective boundary condition.

production function as well as the large scale behavior of the string scales together for the global string network. Note that κ takes almost the same value both in the matter and radiation dominated universe, which implies that NG bosons emission is not affected by the background universe and the large-scale behavior of a string network but decided by the fundamental physics near a string segment.

4 Relation of ξ in matter and radiation dominated era

As discussed in [3], assuming the one-scale model, the scaling parameters, ξ_r, in the radiation domination can be related to ξ_m, in the matter domination. From the Nambu-Goto action together with the intercommutation effect, the evolution of the string energy density, ρ, in the expanding universe is given by

$$\begin{aligned} \frac{d\rho}{dt} &= -3H\rho + (1-2V^2)H\rho - c\frac{\rho}{L}, \\ &= -3H\rho + H^2 L\rho - c\frac{\rho}{L}, \end{aligned} \tag{12}$$

where $L = t/\sqrt{\xi}$ is the characteristic scale with $\rho = \mu/L^2$, V^2 is the average velocity squared of a string, and c is a constant representing the intercommutation efficiency [5] . Defining γ as $\gamma = H^{-1}/L$, the evolution of γ is given by

$$\frac{d\gamma}{dt} = -\frac{H}{2}\left[c\gamma^2 - (2\,(\dot{H^{-1}}) - 3)\gamma - 1\right]. \tag{13}$$

Then, in the radiation domination with $(\dot{H^{-1}}) = 2$, we obtain the fixed point, γ_r, given by

$$\gamma_r = \frac{1+\sqrt{1+4c}}{2c}. \tag{14}$$

[5] Though c may be dependent on V, as the zero-th order approximation we set c to be a constant.

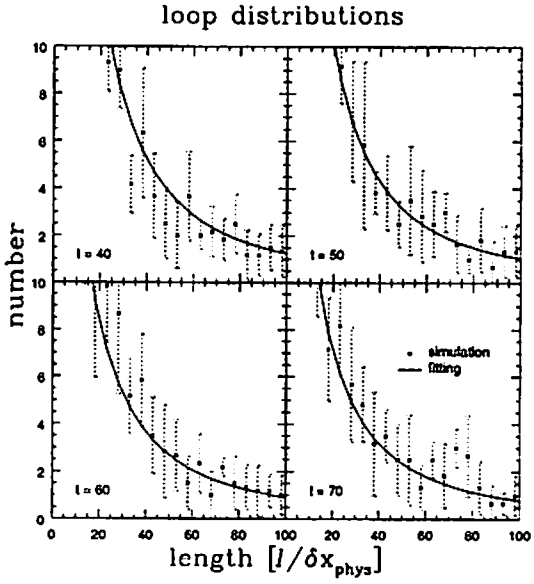

Figure 4: Loop distributions at $t = 40, 50, 60, 70$ are depicted. The number is summed over the box size $(128(\delta x)^3)$ and 50 realizations for each groups. Bins are cut every $5 \times \delta x$.

On the other hand, in the matter domination with $(\dot{H}^{-1}) = 3/2$, we obtain the fixed point, γ_m, given by

$$\gamma_m = \frac{1}{\sqrt{c}}. \tag{15}$$

Considering $\xi_r = \gamma_r^2/4$ and $\xi_m = 4\gamma_m^2/9$, we find the relation between ξ_r and ξ_m,

$$\xi_m = \frac{16}{9} \frac{\xi_r}{2\sqrt{\xi_r} + 1}. \tag{16}$$

Putting $\xi_r \sim (0.9 - 1.3)$ [18] into the relation, ξ_m is predicted to be $(0.6 - 0.7)$, which coincides with our numerical results.

5 Summary

In this paper, we investigated the evolution of a global string network in the matter dominated universe. The network relaxes into the scaling regime as in the radiation dominated universe but the scaling parameter, ξ_m, takes a smaller value, $\xi_m \simeq 0.6 \pm 0.1$, which is consistent with the value predicted from ξ_r by use of the formula obtained by Albrecht and Turok [3]. The loop distribution is also obtained and compared with that predicted by the one scale model, where the number density, $n_l(t)$, of the loop with the length, l, is given by $n_l(t) = \nu/(t^2(l + \kappa t)^2)$. With $\nu \simeq 0.040$ and $\kappa \simeq 0.48$, the loop distribution function can be well fitted with that predicted by the one scale model. Thus, the evolution of the global string network in the matter dominated universe can be well described by the one-scale model as in the radiation dominated universe.

Acknowledgments

This work was partially supported by the Japanese Grant-in-Aid for Scientific Research from the Monbusho, Nos. 10-04558 (MY), 11740146(JY), and "Priority Area: Supersymmetry and Unified Theory of

Elementary Particles (# 707)" (JY & MK).

References

[1] T. W. B. Kibble, J. Phys. **A9**, 1387 (1976).

[2] For a review, A. Vilenkin and E. P. S. Shellard, *Cosmic String and Other Topological Defects* (Cambridge University Press, Cambridge, 1994).

[3] A. Albrecht and N. Turok, Phys. Rev. D**40**, 973 (1989).

[4] A. Albrecht and N. Turok, Phys. Rev. Lett. **54**, 1868 (1985).

[5] D. P. Bennett and F. R. Bouchet, Phys. Rev. Lett. **60**, 257 (1988); **63**, 2776 (1989); Phys. Rev. D**41**, 2408 (1990).

[6] B. Allen and E. P. S. Shellard, Phys. Rev. Lett. **64**, 119 (1990).

[7] D. Austin and E. J. Copeland, and T. W. B. Kibble, Phys. Rev. D**48**, 5594 (1993); E. Copeland, T. W. B. Kibble, and D. Austin, Phys. Rev. D**45**, 1000 (1992).

[8] A. Vilenkin, Phys. Rev. Lett. **46**, 1169 (1981); **46**, 1496(E) (1981).

[9] G. R. Vincent, M. Hindmarsh, and M. Sakellariadou, Phys. Rev. D**56**, 637 (1997); G. R. Vincent, N. D. Antunes, and M. Hindmarsh, Phys. Rev. Lett. **80**, 2277 (1998).

[10] R. L. Davis, Phys. Rev. D**32**, 3172 (1985).

[11] R. L. Davis, Phys. Lett. **180B**, 225 (1986); R. L. Davis and E. P. S. Shellard, Nucl. Phys. **B324**, 167 (1989).

[12] D. Harari and P. Sikivie, Phys. Lett. B**195**, 361 (1987); C. Hagmann and P. Sikivie, Nucl. Phys. **B363**, 247 (1991).

[13] A. Dabholkar and J. M. Quashnock, Nucl. Phys. **B333**, 815 (1990).

[14] R. A. Battye and E. P. S. Shellard, Nucl. Phys. **B423**, 260 (1994); Phys. Rev. Lett. **73**, 2954 (1994).

[15] R. A. Battye and E. P. S. Shellard, Phys. Rev. D**53**, 1811 (1996).

[16] M. Yamaguchi, J. Yokoyama, and M. Kawasaki, Prog. Thor. Phys. **100**, 535 (1998).

[17] M. Yamaguchi, M. Kawasaki, and J. Yokoyama, Phys. Rev. Lett. **82**, 4578 (1999).

[18] M. Yamaguchi, Phys. Rev. D**60**, 103511 (1999).

[19] T. W. B. Kibble, Nucl. Phys. **B252**, 227 (1985).

[20] D. P. Bennet, Phys. Rev. D**33**, 872 (1986); D**34**, 3592 (1986).

[21] C. J. A. P. Martins and E. P. S. Shellard, Phys. Rev. D**53**, 575 (1996); Phys. Rev. D**54**, 2535 (1996); P. P. Avelino, R. R. Caldwell, and C. J. A. P. Martins, Phys. Rev. D**56**, 4568 (1997).

Phase transition and Fractal in self-gravitating ring model

Yasuhide Sota,* Osamu Iguchi, † Masahiro Morikawa, ‡

Department of Physics, Ochanomizu University,
Faculty of Science, 2-1-1 ohtuka, bunkyou-ku, Tokyo, Japan

Takayuki Tatekawa§

Department of Physics, Waseda University,
Shinjuku-ku, Tokyo 169, Japan

Abstract

Fractal and long-tail Lévy-type velocity distribution are well known characters in the self-gravitating viriallized system such as interstellar molecular clouds, so called, interstellar medium (ISM). Here we examined these characters from the viewpoint of the gravitational phase transition by using the one-dimensional ring model with large number of particles interacting with the three-dimensional gravitating force. We got the result that each particle shows Lévy-type random motion whose flight probability has the power-law tail at the critical point. We also examined the fractal dimension of particle distributions at the fixed constant time with the box-counting method. It shows no fractal nature if we allow the particles to rotate the ring many times, until it is captured by a cluster of particles. These results indicate that the fractal nature of self-gravitating system has no correlation with its non-Gaussian velocity natures. However, the nature of these results strongly depends on the fact that the configuration space of particle distribution is compact and the cutoff scale of gravitational force is finite. So in more ideal appropriate limit, we can still expect that both fractal and Lévy flight nature come from the property of phase transition.

I. INTRODUCTION

Self-gravitating system has the exotic statistical characters such as the nonextensivity of supposed-to-be extensive variables [1] and the negative specific heat in microcanonical situation [2]. The latter property makes the system strongly unstable in the canonical situation, that is, if it is immersed in the heat bath. Such a peculiar nature of gravito-statistics is expected to affect the behavior of the gravitationally viriallized system. For example, it is well known that observed ISM meets the viriallized condition and shows the scaling character called Larson's Law [3], which implies the scaling relation among molecular mass (M), molecular size (L) and velocity dispersion (σ^2) as follows,

$$\sigma \sim 1.1 \times L^{0.38}$$
$$\sigma \sim 0.42 \times M^{0.20}. \tag{1}$$

Each ISM also has the characters such as fractal boundary and non-Gaussian, long-tail velocity dispersion [4]. These characters have been explained mainly by the turbulence theory, since their observed Reynolds number is very large. Turbulence theory has succeeded in explaining the observed fractal and non-Gaussian velocity characters in some extents. However, the situation of ISM is quite different from that

*E-mail:sota@skyrose.phys.ocha.ac.jp
†E-mail:osamu@phys.ocha.ac.jp
‡E-mail:hiro@phys.ocha.ac.jp
§E-mail:tatekawa@gravity.phys.waseda.ac.jp

of fluid dynamics in the laboratory, mainly because gravitational interaction plays a key role in triggering the turbulence flow in the former.

There is another approach to explain such phenomena from the viewpoint of the statistics in self-gravitating system [5]. This approach is based on the fact that the main factor to cause turbulence is the gravitational interaction, since the observation indicates that the system is viriallized.

As we mentioned above, there is no stable state in self-gravitating system in the canonical situation. However, if we include the cutoff in the interaction in both large and small scale, we can produce the stationary free-particle state at high temperature and stationary collapsed state at low temperature [2]. In this case, we can regard the gravitationally bound state as the critical point in the phase transition between those two states.

In the case of ISM, the number of each cloud is not fixed, since some of the gas particles can evaporate against gravitational bound. In this sense, it is rather grand canonical as the approach of [5] or [6], especially when we allow for the statistics of ensembles of many different clouds with different numbers. However, if we pay attention to one of those clouds, we can see that it attains to the viriallized micro-canonical state in which all of the element particles are gravitationally bound, although it seems rather canonical after the long time-interval, according to the strength of the interaction with the heat bath. As for the case of ISM, the time scale of relaxation with heat bath seems quite long, since it is weakly interacted with the microwave blackbody radiation. In this sense, it could be fair to say that it is in microcanonical quasi-stable state in the intermediate time interval and finally collapses or diffuses in the long run.

From these considerations, we examine the dynamics of microcanoncial self-gravitating system in this paper, since it would indicate us the plenty of actual phenomena at the critical quasi-stable state in gravitationally viriallized objects such as ISM. In section 2, we introduce the one-dimensional ring model reflecting three dimensional self-gravitating system. In section 3, we will show our numerical results in microcanonical and canonical simulations. Finally, we will briefly comment on the conclusion in section 4.

II. GHMF MODEL ANALYSIS

In this section, we introduce the model of one dimensional self-gravitating system. In general, one-dimensional gravitating model has been analyzed in the context of relaxation [7]. In this context, they examine the model with the force whose potential meets the one-dimensional Poisson's equation and the free boundary condition. Since such a potential is linear and has no upper bound, there is no typical energy scale needed to make each particle escape against gravitational binding energy. This seems unsatisfactory, when it comes to treating the phase transition appearing in the three dimensional self-gravitating system with upper and lower cutoff.

Here we introduce another type of one-dimensional self-gravitating model which reflects the property of such a phase transition. First, we fix the movement of the element particle with the mass m along the one dimensional ring with the radius L and enforce the three dimensional gravitational interaction between each pair of those particles, whose distance is measured by the Euclid measure in the three dimensional Euclid space. The Hamiltonian of such a system becomes as follows,

$$\begin{aligned} H &= \sum_{i=1}^{N} \frac{p_i^2}{2m} - \sum_{i<j}^{N} \frac{Gm^2}{N|2L\sin(\theta_{ij}/2)|} \\ &= \sum_{i=1}^{N} \frac{p_i^2}{2m} - \sum_{i<j}^{N} \frac{Gm^2}{\sqrt{2}LN\sqrt{1-\cos\theta_{ij}}}, \end{aligned} \tag{2}$$

where $\theta_{ij} := \theta_i - \theta_j$ is the angle between i'th and j'th particle on the ring.

Here we divide the interaction term by the particle number N, to keep the extensibity of total energy and take the fluid limit as $N \to \infty$.

Secondly, we also include the lower scale cutoff, ϵ as

$$|2L\sin(\theta_{ij}/2)| \approx \sqrt{2}L\sqrt{1-\cos\theta_{ij}+\epsilon}, \tag{3}$$

since the potential and the force becomes infinite, at the moment that each particle crosses one of the other particles. Then the Hamiltonian and canonical equations of each particles finally become as follows,

$$H = \sum_{i=1}^{N} \frac{p_i^2}{2m} - \sum_{i<j}^{N} \frac{Gm^2}{\sqrt{2}LN\sqrt{1-\cos\theta_{ij}+\epsilon}}. \tag{4}$$

$$\dot{p}_i = -\frac{\partial H}{\partial \theta_i} = -\frac{Gm^2}{2\sqrt{2}LN} \sum_{i\neq j}^{N} \frac{\sin\theta_{ij}}{(1-\cos\theta_{ij}+\epsilon)^{3/2}}$$

$$\dot{\theta}_i = \frac{\partial H}{\partial p_i} = \frac{p_i}{m} \tag{5}$$

In this model, the particle interaction disappears, if the distance of the two particles, $L\delta\theta$, is smaller than the physical scale $\xi \equiv \sqrt{\epsilon}L$. If we take the Fourier expansion for the potential of this model and take only the smallest Fourier mode, we can derive a well-known one dimensional ring model, called Hamilton mean field (HMF) model [8]. Hence we call our model Gravitational HMF (GHMF) model, since it is the extension of HMF model to the case with the gravitational interaction. In the next section, we numerically examine the statistical aspects of GHMF system and compare it with the results of HMF.

III. NUMERICAL RESULTS

Here we numerically solved the canonical equations (5) with the symplectic integrator [9], which keeps the total Hamiltonian highly accurate, even after a long time-interval of numerical simulation. As well as such a microcanonical case, we also examined the canonical case by using Nose's method, where the above N-body system interacts with the heat bath and approaches the canonical equilibrium [10]. In our simulation, we fixed the value of ϵ as 0.01, since it is much harder to keep the total Hamiltonian an accurate value for smaller value of ϵ even with the symplectic method. For the simulation, we take the unit of $G = m = L = 1$.

A. T-U relation

Here, we examine the relation between the total energy U defined by H/N and the temperature T defined by the time averaged one-particle Kinetic energy averaged over all of the particles. This make it clear which type of phase-transition occurs in this system. For example, HMF model shows second-order phase transition, in which the first order derivative of partition function is continuous, while second one is not. This can be shown with the saddle point approximation in canonical system [8]. In the microcanonical numerical simulation, the system stays in the quasi-stable state with the negative specific heat during the long time interval, and then finally moves to the point on the canonical line in T-U plane.

We showed that in GHMF model, the things are more drastic, that is, the system shows the first order phase transition in canonical simulation, as we can see in three dimensional self-gravitating system (Fig.1). So although the state with a negative specific heat exists in GHMF as well as in HMF, we cannot see any counterpart on canonical T-U line in GHMF, which would be finally attained from the microcanonical quasi-stable state with negative specific heat in HMF.

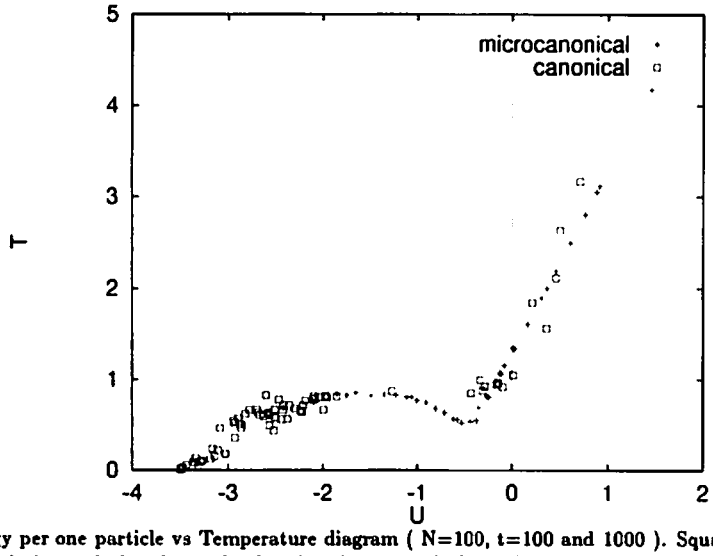

FIG. 1. Energy per one particle vs Temperature diagram (N=100, t=100 and 1000). Square shows the data in canonical simulation and plus shows the data in microcanomical simulation. The jump of the data points can be seen in canonical plot at the energy scale where the specific heat becomes negative in microcanonical plot.

B. Lévy motion and Fractal

Here we examined the particle motions at the state with the negative-specific heat in microcanonical simulation. We can expect some exotic statistical character around this critical state, since the fluctuation becomes large at a critical point, as is well known at phase transition. There are two sorts of flight motion for these particles. First one is the flight motion of the particle captured by gravitationally bounded cluster region. This motion can be expected, if the size of the cluster is much larger than the cutoff scale ξ. Second one is the flight motion of the particles moving along the ring so many times, until it is captured by a cluster of particles. This motion can be expected, if the perimeter of the ring, $2\pi L$, is not much larger than the size of the cluster. In our analysis, the size of the cluster is almost equal to L and ten times larger than ξ. So the second type of flight is more likely to occur than the first one.

It is shown that the second type of Lévy type motion and anomalous diffusion appear in HMF model at the state with the total energy almost equal to the critical one [11]. Here we took the same analysis to see if the Lévy motion occurs in GHMF. We also examined the jump probability to check if it really follows the power-law tail probability. At the energy level $U = U_{cr} \approx -0.45$, we certainly got the result that the probability distribution has a non-Gaussian tail (Fig.2), as is seen in turbulent flow or in foreign exchange markets [12]. The averaged jump probability follows the power-law tail whose exponent is nearly equal to 1.0 between the time interval $dt = 10$ and $dt = 500$.

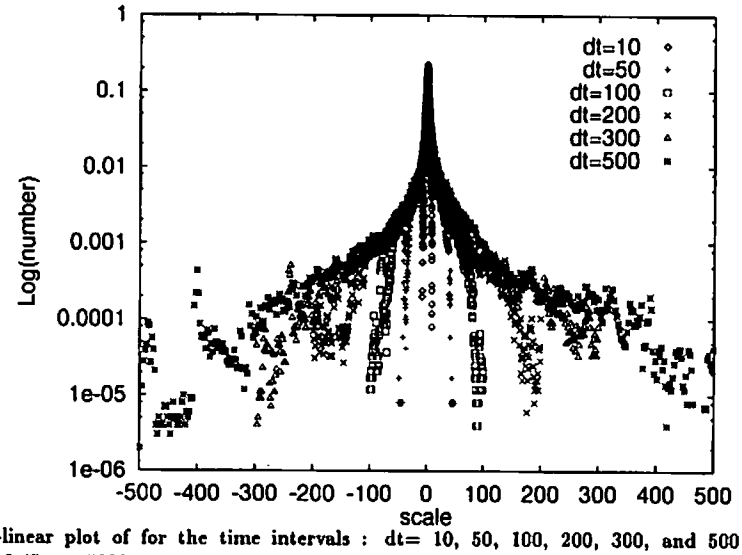

FIG. 2. Log-linear plot of for the time intervals : dt= 10, 50, 100, 200, 300, and 500 for the case of $N = 100, U = -0.45, t = 5000$.

We also compared it with the fractal dimension of the particle distribution at the constant time with the box-counting method [13], when the temperature almost attains to the relaxed value. The averaged distance between the two particles approximately becomes

$$L_{\rm av}(\xi) \approx \frac{L}{N_{\rm free}(\xi)}, \tag{6}$$

where $N_{\rm free}(\xi)$ is the number of the free particles which move independently of a cluster. If the box size r satisfies the condition $r > L_{\rm av}(\xi)$, we cannot expect the fractal dimension $D < 1.0$, since almost all of the boxes include at least one particle in this case. On the other hand, if $r < \xi$, we cannot see any gravitational nature, since the motions of particles become completely free within this box size. So we can expect to get fractal nature caused by the gravitational force only in the scale

$$\xi < r < L_{\rm av}(\xi). \tag{7}$$

In our simulation, $\xi = 0.1$ ($\epsilon = 0.01$) and $L_{\rm av}(\xi) \approx 0.56$ (Fig.3 and Fig.4). So the range (7) is too narrow to get the broad range of fractal region. (The scaling region can be seen only at $\theta \approx 0.056$ in Fig.4, which is much shorter than ξ.) So, we cannot see any fractal nature induced by gravitational interaction in our numerical results. This situation would be improved, if we took much smaller value of ϵ than the value 0.01 in our model.

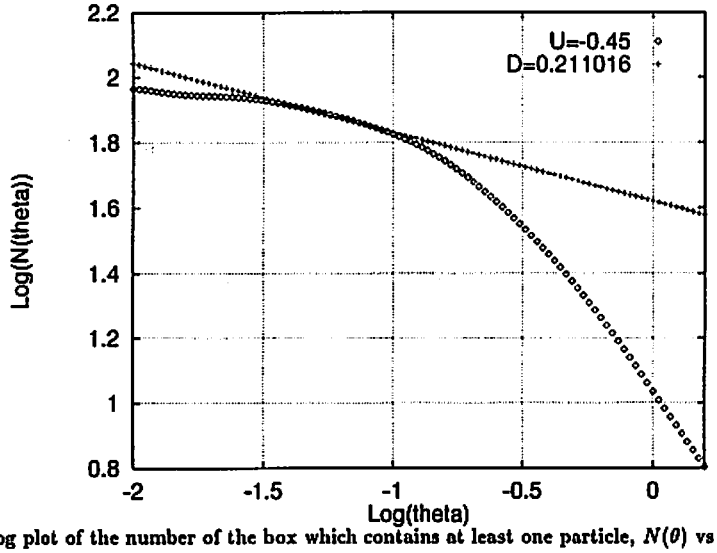

FIG. 3. Log-log plot of the number of the box which contains at least one particle, $N(\theta)$ vs the box size angle , $\theta = r/L$ for the case of $N = 100, U = -0.45, t = 5000$.

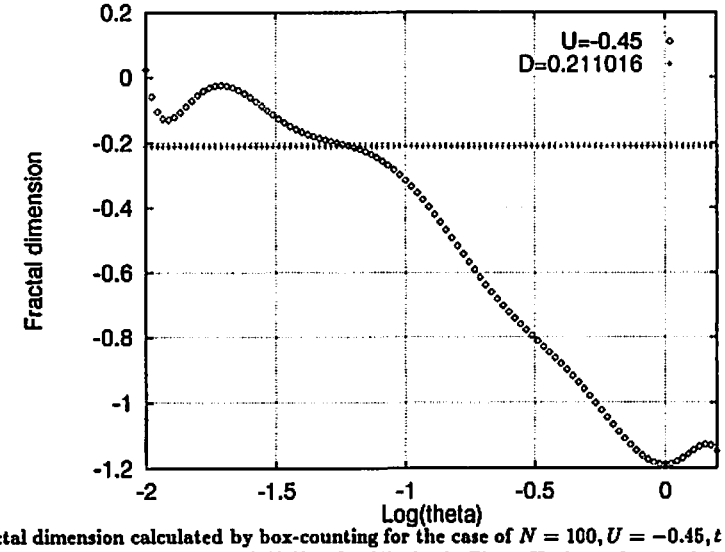

FIG. 4. Fractal dimension calculated by box-counting for the case of $N = 100, U = -0.45, t = 5000$. The curve shows the slope of the tangent line of $Log(N(\theta)) - Log(\theta)$ plot in Fig.3. Horizontal part of the curve can be seen at $\theta = 10^{-1.25} \approx 0.056$,which intersects with the horizontal line in the figure. Fractal dimension departs from one at the scale less than $\theta = 10^{-0.25} \approx 0.56$ corresponding to $L_{\rm av}(\xi)$.

IV. CONCLUSION

Here we got the result that the statistical state at the critical energy in GHMF is characterized by the Lévy motion. This motion is reasonable, from the viewpoint of phase transition, since the fluctuation of the physical variables become so large at the critical point. On the other hand, we cannot see any fractal nature in our model. This is mainly because the size of the configuration space is not much bigger than

that of cluster, which enables the free particle to visit the same cluster so many times. The periodicity of configuration space also prevents particles captured by a cluster from jumping within the cluster, since the particle departing from the cluster by chance is more likely to rotate along the ring. So the Lévy type motion in this model is not directly connected with the non-Gaussian motion and fractal nature in ISM, because the configuration space of the observed ISM has neither such a boundary nor periodicity. However, we can still expect that these natures are fulfilled in the limit of $\xi \to 0$ in our model, since the cluster size becomes much shorter than the perimeter of the ring in this limit. These analyses should be our future challenge, although it is technically hard to accomplish such a limit in the simulation.

From these respects, our results could give the hint for the mechanism of the observed character of gravitationally viriallized objects such as ISM. These statistical approach characterized by the phase transition could be the alternative tactics to treat the highly non-linear large-number systems with the large fluctuations, compensating for the turbulence fluid approach. It is also interesting, in that it gives the hint for the statistics of self-gravitating system. It has been insisted that self-gravitating system do not follow the Maxwell-Boltzmann statistics, since the entropy is not extensive in the system with long-range force interactions [1]. Our results of Lévy motion at phase transition indicates that the variance of statistics diverges in such a highly jump probability. So the nonextensivity of self-gravitating system could be attributed to such a divergence.

V. ACKNOWLEDGMENTS

We thank: K. Maeda, A.Nakamichi, I. Joichi and K.Nakamura for useful discussions and comments on this subject.

---

[1] C. Tsallis, Braz. J. Phys. **29** (1999) 1.
[2] T. Padmanabhan, Phys. Rep. **188** (1990), 285.
[3] R. B. Larson, Mon. Not. R. astr. Soc. **194** (1981), 809.
[4] E. Falgarone, T. G. Phillips and C. K. Walker, ApJ **378** (1991), 186.
[5] H. J. de Vega, N. Sánchez and F. Combes, Phys. Rev. D **54** (1996), 6008.
[6] W. C. Saslaw and A. J. S. Hamilton, ApJ **276** (1984), 13.
[7] T. Tsuchiya, N. Gouda and T.Konishi, Phys.Rev.E **53** (1996),2210.
[8] M. Antoni and S. Ruffo, Phys. Rev. E **52** (1995),2361.
[9] M. Suzuki, Phys. Lett. A **146** (1990), 319.
[10] S. Nose, Molec. Phys. **52**(1984),255.
[11] V. Latora , A. Rapisarda and S. Ruffo, Phys.Rev.Lett. 83 (1999) 2104.
[12] S. Ghashghaie, W.Breymann, J.Peinke, P. Talkner and Y. Dodge, Nature **381** (1996),767.
[13] K. Falconer, Fractal Geometry (1990, John WileySons).

Origin and Evolution of Stochastic Biasing

Atsushi Taruya,[1] Yasushi Suto[2]

Research Center for the Early Universe (RESCEU), School of Science, University of Tokyo, Tokyo 113-0033, Japan

Abstract

The observational study of large-scale structure and the cosmological simulation recently show that the statistical relation between the galaxies and the total mass could become stochastic, non-linear and time-dependent, which significantly affect the determination of cosmological parameters from galaxy sky surveys. Therefore, the understanding of the stochastic and non-linear galaxy biasing is one of the most important problem in observational cosmology. In this article, we explore the origin of the stochasticity in the dark matter halo biasing, which might play an important role for the stochasticity of the galaxy biasing. Based on the formalism of the extended Press-Schechter mass function, we argue that the halo formation time could be a physically important source for the halo biasing being stochastic. The quantitative estimation of the influences of halo formation time is investigated by analyzing the averaged biasing relation. Compared it with the numerical simulation, we find that the averaged biasing relation taking into account the halo formation time reasonably reproduces the N-body result.

1 Introduction

The understanding of large-scale structure in the universe is one of the most important issues in the observational cosmology. Currently, the two wide-angle and deep galaxy sky surveys are working, i.e, the Sloan Digital Sky Survey (SDSS) and the Two degree Field (2dF) survey. The enormous observational data will be obtained from these surveys and it provides us with the powerful constraint on the theory of structure formation in the universe.

When we compare the theoretical prediction for the density fluctuation with the observation of galaxy sky survey, however, the relation between the total mass and the galaxies must be clarified. Since we do not yet have any reliable theory of galaxy/star formation history, there exists the statistical uncertainty between the galaxies and the total mass. This uncertainty is called the *galaxy biasing*, which hampers the efforts to obtain the cosmological information such as the density parameter.

Recently, it has been recognized that the galaxy biasing would be non-linear, stochastic and time-dependent [1] [2]. Denoting the fluctuation of the total mass as δ_m and the distribution of galaxies as δ_g, we generally have

$$\delta_g(x,t) = \mathcal{F}[\delta_m(x,t),\ X_1(x,t),\ X_2(x,t),\cdots], \tag{1}$$

where variables X_i characterize the galaxy/star formation process, which cannot be observed from the galaxy sky surveys. Eq.(1) states that the non-linearity of the biasing comes from the functional form $\mathcal{F}$ for δ_m. Further, the distribution δ_g cannot be characterized by the total mass δ_m completely, due to the hidden variables X_i. The framework to treat the above situation is referred to as the *stochastic biasing*, which might cause a more serious problem in the quantitative study of the large-scale structure formation.

Therefore, the understanding of the stochastic biasing should be paid much attention. Dekel & Lahav has proposed the general formalism for the non-linear stochastic biasing [3]. Pen discussed an observational method to determine the stochasticity [4]. Further, Blanton *et al.* and Blanton, Cen & Tegmark performed the cosmological simulation of galaxy formation [1][2]. Taruya, Koyama & Soda and Taruya analytically studied the gravitational evolution of the stochastic biasing [5][6].

[1] E-mail:ataruya@utap.phys.s.u-tokyo.ac.jp
[2] E-mail:suto@phys.s.u-tokyo.ac.jp

Here, we develop the theoretical study to clarify the origin and the evolution of stochastic biasing, which has not been studied in detail. Although Blanton *et al.* [1] explore the hidden variable X as the sources of stochasticity by using the numerical simulation, the analytical consideration will shed light on the qualitative and quantitative understanding. To investigate this issue, as a first step, we will discuss the stochasticity for the halo biasing. According to the scenario of hierarchical galaxy formation, the galaxies are formed in the dark matter halo region [7]. Although the halo biasing is not directly related to the galaxy biasing, the stochasticity of the halo biasing can lead to the important sources for the stochasticity of galaxy biasing.

In this article, to explore the origin of stochastic halo biasing, we discuss the prescription for the spatial clustering of dark matter halos. In Sec.2, we start to review the extended Press-Schechter formalism, which can explain how the halos are spatially distributed in the dark matter fields. Then, we argue that the halo formation time z_f might be one of the important sources of stochasticity. In Sec.3, we quantify the influence of its stochasticity, that is, we examine the averaged halo biasing relation. We find that the analytical estimation of the averaged biasing relation is remarkablely reproduced the results obtained by N-body simulation if we take into account the distribution of halo formation time. Last section 4 is devoted to the summary and the discussions.

2 Exploring the origin of stochasticity in the halo-biasing

2.1 Extended Press-Schechter Formalism

The prescription for calculating the number abundance of the dark matter halos is originally given by Press and Schechter [8] and reformulated later by several authors to resolve the cloud-in-cloud problem (e.g. [9]). The stochastic description for the mass function (MF) is referred to as the extended Press-Schechter (EPS) formalism, which enables us to model the spatial clustering of the halo distribution [10]. In the EPS formalism, we could have the two types of the MF; the constrained MF and the conditional MF.

The constrained MF is the original version defined by Press and Schechter and it gives the number fraction for a given halo mass M collapsed with the critical threshold δ:

$$n(M,\delta;z)dM = \frac{1}{\sqrt{2\pi}}\frac{\bar{\rho}}{M}\frac{\delta}{\sigma^3(M,z)}\exp\left[-\frac{\delta^2}{2\sigma^2(M,z)}\right]\left|\frac{d\sigma^2(M,z)}{dM}\right|dM, \tag{2}$$

where the mass variance $\sigma(M,z)$ is related to the linearly extrapolated power spectrum of density perturbation $P(k)$ at present through

$$\sigma^2(M,z) = D^2(z)\int\frac{d^3k}{(2\pi)^2}W^2(kR)P(k) \;\;;\;\; M = \frac{4\pi}{3}\bar{\rho}R^3 \tag{3}$$

with the top-hat window function

$$W(x) = \frac{3}{x^3}(\sin x - x\cos x).$$

Here, the function $D(z)$ is the linear growth factor normalized to unity at the present epoch. On the other hand, the conditional MF gives the conditional number density of the halo (M_1, δ_1) in the background overdensity (M_0, δ_0):

$$\begin{aligned} n(M_1,\delta_1|M_0,\delta_0;z)dM_1 \;=\; & \frac{1}{\sqrt{2\pi}}\frac{\bar{\rho}}{M_1}\frac{\delta_1-\delta_0}{[\sigma^2(M_1,z)-\sigma^2(M_0,z)]^{3/2}} \\ & \times\exp\left[-\frac{(\delta_1-\delta_0)^2}{2\{\sigma^2(M_1,z)-\sigma^2(M_0,z)\}}\right]\left|\frac{d\sigma^2(M_1,z)}{dM_1}\right|dM_1, \end{aligned} \tag{4}$$

where the mass of the background overdensity is related to the smoothing radius R_0 through the relation $M_0 = (4\pi/3)\bar{\rho}R_0^3$.

Using these MFs, we can obtain the fluctuation of halo number density δ_h as follows. Equation (4) means that the number density of the halos can be evaluated in the Lagrangian radius of sphere R_0 with

the linearly extrapolated overdensity δ_0. Since we wish to know the halo biasing relation δ_h *v.s* δ_m, the Lagrangian variables (R_0, δ_0) should be transformed to the Eulerian variables (R, δ_m). To relate these variables, Mo & White use a spherical collapse model [10]: $R = R_0/(1+\delta_m)^{1/3}$ and δ_m are calculated for given R, R_0 and δ_0 using the solutions of spherical collapse, i.e, $\delta_m = f(\delta_0)$. Here, we will adopt their approach. Having made the transformation (R_0, δ_0) to (R, δ_m), we can calculate the averaged halo overdensity in the spheres of the observed radius R and for the dark matter overdensity δ_m as

$$\delta_h(M|R,\delta_m;z) = (1+\delta_m)\frac{n(M,\delta_c|R,\delta_0;z)}{n(M,\delta_c;z)} - 1. \tag{5}$$

The critical threshold δ_c is evaluated using a spherical collapse model, which gives the dynamical time scale of the virialization. When we take

$$\delta_c = 1.69\ D(z), \tag{6}$$

the expression (5) denotes the fluctuation of the number density of halos formed at $z = 0$. The linearly extrapolated overdensity δ_0 in equation (5) can be obtained from the inverse function $\delta_0 = f^{-1}(\delta_m)$, which is accurately described by the following fitting formula [10]:

$$\delta_0 = 1.69 - \frac{1.35}{(1+\delta_m)^{3/2}} + \frac{0.789}{(1+\delta_m)^{0.587}} - \frac{1.12}{(1+\delta_m)^{1/2}}. \tag{7}$$

The expression (7) is valid for $\delta_m \lesssim 20 - 30$ and almost independent of the cosmological parameters.

2.2 Halo-formation epoch as a possible candidate for the stochastic biasing

Equation (5) with (6) shows that the halo biasing relation δ_h *v.s.* δ_m at present time can be obtained when we specify the dark matter density δ_m, the smoothing radius R and the halo mass M. In the limit $\delta_0 \ll \delta_c$ and $M \ll M_0$, we reach at the formula of the linear biasing parameter $b \equiv \delta_h/\delta_m$ [10]:

$$b(M,z) = 1 + \frac{\nu^2 - 1}{\delta_c}\ ; \quad \nu = \frac{\delta_c}{\sigma(M,z)}. \tag{8}$$

which is frequently used in the literature.

To evaluate the fluctuation δ_h at an arbitrary redshift z, we incorporate the formation time z_f to the expression (5), at which the density peak of the dark matter distribution can experience the gravitational collapse and a virialized dark matter halo is formed. Since the linear overdensity must exceed the critical value 1.69 at $z_f > z$, the critical threshold (6) should be replaced with

$$\delta_c = 1.69\frac{D(z)}{D(z_f)}. \tag{9}$$

However, unless provided the information when the halo is formed, we cannot evaluate the fluctuation δ_h. To develop the analysis, several authors assume that the only objects existing at any epoch z are those that have just formed by the merging of smaller mass units, i.e, $z_f = z$ (e.g, [11]).

The assumption $z_f = z$ is questionable. The halos with the same mass M need not to be formed at the same time z. The halos with the different formation time could lead to the different growth of fluctuations δ_h due to the gravitational evolution, which significantly affects the clustering property of the dark matter halos. Further, in the hierarchical picture of structure formation, the merging and destruction processes are essential to obtain the correct value of the halo abundance and the formation time can thus have the strong dependence on the merging history. This implies that the halo formation time becomes the stochastic random variable.

We think the halo formation time might be one of the most important variable characterizing the halo biasing. In fact, the halo formation time z_f cannot be observed. It could become a plausible candidate for the hidden variable X contributing to the stochasticity of the halo biasing (see eq.[1]).

Let us investigate the roles of formation time z_f for evaluating the fluctuation δ_h. Hereafter, we denote the formation time z_f for the halo mass M as the time when the progenitor of its halo acquires a mass

greater than $M/2$ for the first time. The randomness of the halo formation epoch can be characterized by the distribution function of z_f. Based on the excursion set approach of the MFs, the EPS formalism can provide us the differential distribution of halo formation epoch $\partial p/\partial z_f$. According to Lacey & Cole [12] (see also Kitayama & Suto [13]), we obtain

$$\frac{\partial p}{\partial z_f}(z_f\,;M,\,z)dz_f = \frac{\partial p}{\partial \tilde{\omega}_f}(\tilde{\omega}_f,\,M)\frac{\partial \tilde{\omega}_f}{\partial z_f}dz_f, \tag{10}$$

$$\frac{\partial p}{\partial \tilde{\omega}_f}(\tilde{\omega}_f,\,M) = -\frac{1}{\sqrt{2\pi}}\int_0^1 \frac{d\tilde{S}}{\tilde{S}^{3/2}}\frac{M}{M'(\tilde{S})}\left(1-\frac{\tilde{\omega}_f^2}{\tilde{S}}\right)e^{-\tilde{\omega}_f^2/(2\tilde{S})}, \tag{11}$$

where

$$\tilde{\omega}_f(z_f,M,z) \equiv 1.69\,\frac{D^{-1}(z_f)-D^{-1}(z)}{\sqrt{\sigma^2(M/2)-\sigma^2(M)}}, \qquad \tilde{S}(M',M) \equiv \frac{\sigma^2(M')-\sigma^2(M)b}{\sigma^2(M/2)-\sigma^2(M)}. \tag{12}$$

The function $M'(\tilde{S})$ can be obtained by solving equation (12) for M'. Equations (10), (11) and (12) say that provided the cosmological parameters and the linear power spectrum, we can obtain the formation epoch distribution at z for a given mass M. Hence, the cumulative fluctuation of the halo number density δ_h is evaluated from

$$\bar{\delta}_h(M|R,\delta_m;z) = \mathcal{N}^{-1}\int_z^\infty dz_f\,\frac{\partial p}{\partial z_f}\,\delta_h(M,z_f|R,\delta_m;z) \;:\; \mathcal{N} \equiv \int_z^\infty dz_f\,\frac{\partial p}{\partial z_f}, \tag{13}$$

where the fluctuation $\delta_h(M,z_f|R,\delta_m;z)$ is the same variable as defined in (5) except for replacing δ_c with (9). The fluctuation $\bar{\delta}_h$ can give us a correct expression for the mean biasing relation, rather than the pre-weighted one δ_h.

3 Time evolution of the averaged halo-biasing relation

In Sec.2.2, we have addressed that the halo formation time z_f could be a possible and a physically plausible candidate for the origin of of the stochastic halo biasing. Now, we will consider how the formation epoch distribution affects the halo biasing relation quantitatively. The simple analysis to estimate this effect is to compare the averaged biasing relation $\bar{\delta}_h$ *v.s.* δ_m given by (13) with the result of N-body simulation.

Recently, Kravtsov and Klypin performed the high-resolution N-body simulation and studied the halo biasing property in the ΛCDM cosmology [15]. In their simulation, the halos are identified using the algorithm called ***bound density maxima***, which enables us to obtain both isolated halos and satellite halos orbiting within the larger halos. Using this halo catalog, they investigate the origin and evolution of halo biasing and found that the analytic expression given by (5) with $z_f = z$ cannot reproduce the N-body result. Rather, they assume the formation redshift $z_f = z+1$. Then, the EPS prediction reasonably recovers the mean biasing relation of the simulation. The results suggest that the halos are formed at an earlier time than the observed time z and the averaged formation time could be approximated by $z_f \approx z+1$ in their halo catalog, if the halo formation time plays an important role for the halo biasing.

In rest of this section, choosing the cosmological parameters as $\Omega_0 = 0.3, \lambda_0 = 0.7$, $\sigma_8 = 1.0$ and $h = 0.7$, we will investigate this conjecture using the analytic prediction in previous section.

First, we evaluate the differential distribution of halo formation time (10). In Figure 1, we plot $\partial p/\partial z_f$ for the various redshift $z = 0,\ 1,\ 2,\ 3$. For each panel, the solid, long-dashed and short-dashed lines respectively show the distribution for the halo mass 10^{11}, 10^{12}, $10^{13} M_\odot$. These mass scales are chosen within a suitable range of their halo catalog [15]. According to the merging history of halos, the massive halos tend to form at later epoch and thereby the formation epoch is sharply distributed near the observed time. In contrast, the low mass objects are early formed and it is expected that we have the broad distribution. Figure 1 shows these trends clearly. Moreover, we see that all of the distribution function have the single peak around $z_f \approx z+1$, which seems to be consistent with the suggestion of N-body simulation.

To prove our conjecture more concretely, we evaluate the averaged biasing relation $\bar{\delta}_h$-δ_m and investigate its time evolution. Recall that the halo catalog created by simulation has the finite range of the mass

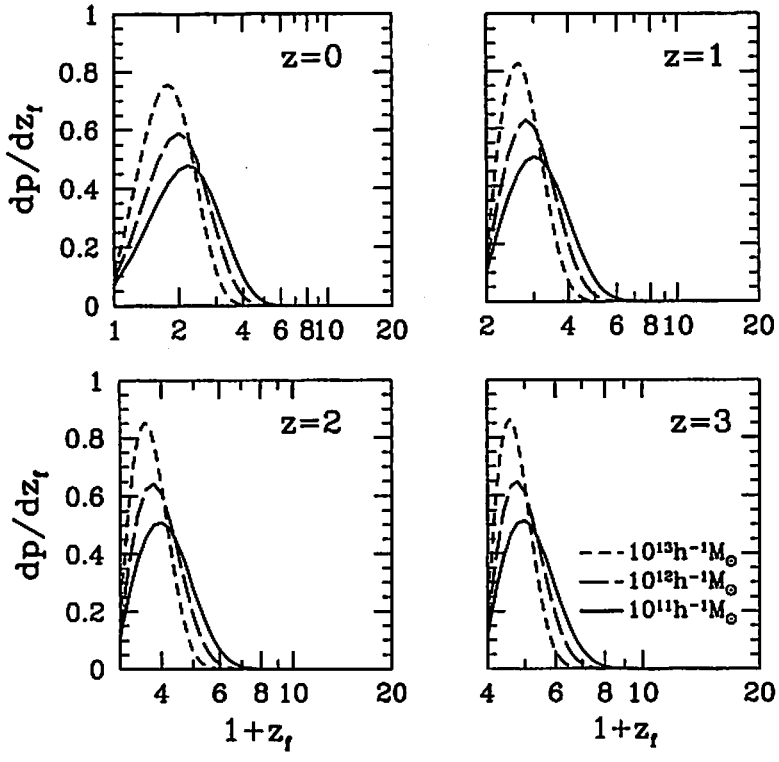

Figure 1: The differential distribution of halo formation time $\partial p/\partial z_f$ in ΛCDM cosmology ($\Omega_0 = 0.3$, $\lambda_0 = 0.7$, $\sigma_8 = 1.0$, $h = 0.7$). To evaluate $\partial p/\partial \bar{\omega}_f$ (eq.[11]), we have used the fitting formula (C4) of Kitayama & Suto [13].

$[M_{min}, M_{max}]$. For our purpose, it is better to compute the number-weighted average over the expression (13), using the Press-Schechter MF (2):

$$\tilde{\delta}_h(R, \delta_m; z) = \tilde{N}^{-1} \int_z^\infty dz_f \frac{\partial p}{\partial z_f} \int_{M_{min}}^{M_{max}} dM\ n(M, \delta_c(z, z_f); z)\ \ \delta_h(M, z_f | R, \delta_m; z), \tag{14}$$

where the normalization factor $\tilde{N}$ becomes

$$\tilde{N} = \int_z^\infty dz_f \frac{\partial p}{\partial z_f} \int_{M_{min}}^{M_{max}} dM\ n(M, \delta_c(z, z_f); z), \tag{15}$$

and δ_c is given by (9). The range of the mass scales is summarized in Table 1.

In Figure 2, we show the averaged halo biasing relation (14) for the different redshift $z = 0$, 1, 2, 3 (*solid lines*). Here, we choose the same smoothing size $R = 5\ h^{-1}$Mpc as used in [15]. In Figure 2, the line draws the steep curve at past $z = 3$ and it implies that the halos are highly biased, because the early formed halos are the rare objects. However, the time evolution gradually reduces this feature. This tendency can be understood from the attractive nature of gravitational force and the continuous process of halo formation. As the fluctuation δ_m grows due to the gravitational instability, a lot of virialized

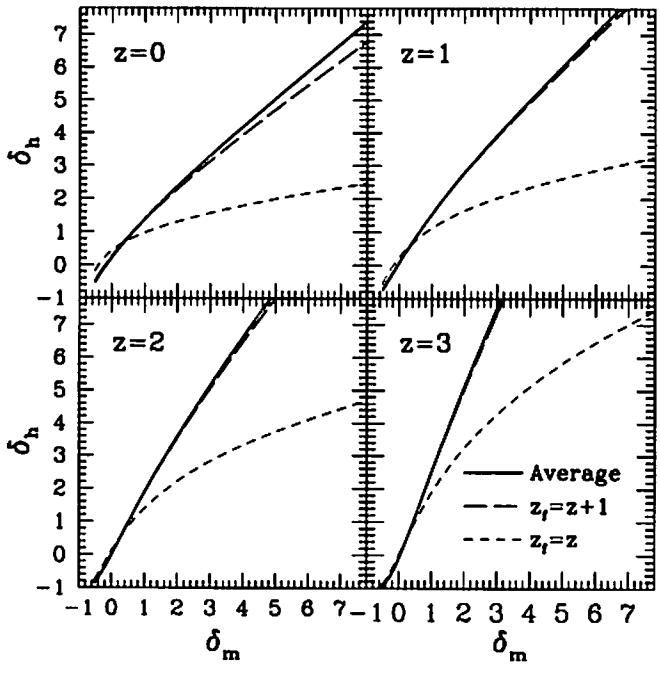

Figure 2: The averaged halo biasing relation as the function of δ_m in the ΛCDM model. The thick-solid line shows the number-weighted fluctuation $\bar{\delta}_h$ taking account of the formation time (eq.[14]). The long-dashed and short-dashed lines respectively denote the fluctuation $\bar{\delta}_h$ with $z_f = z+1$ and $z_f = z$, both of which are averaged over M using the constrained MF (2). The results are similar to those obtained by the N-body simulation (see Figure 4 of Ref.[15])

objects are formed and the distribution of halos falls off the bottom of gravitational potential determined by the total mass δ_m. Note that these processes may not proceed monotonically. In the high density region $\delta_m \gtrsim 1$ at a later time, the relation between the halo and the dark matter becomes anti-biased, due to the finite volume of the virialized halos. The behaviors in Figure 2 shows the generic feature of the halo biasing known in the N-body simulation [16]. As the reference, we also plot the mean biasing relation (5) with z_f (*short-dashed line*) and $z_f = z+1$ (*long-dashed line*), both of which are weighted over the mass range $[M_{min}, M_{max}]$. Remarkably, the averaged fluctuation $\bar{\delta}_h$ is well reproduced by the fluctuation $\bar{\delta}$ with $z_f = z+1$, which agrees with the N-body simulation. This result is more illuminated by comparing with Figure 4 of [15] and fully consistent with Figure 1. Therefore, we can say that the formation epoch distribution is an essential ingredient for the stochasticity and non-linearity of the halo biasing.

4 Summary & Discussions

In this article, we have investigated how the halo formation epoch affects the halo biasing. Within the EPS formalism, the distribution function of formation epoch can be evaluated and using this function, we have analyzed the averaged biasing relation $\bar{\delta}_h$-δ_m over the formation epoch (eq.[14]). The results are in good agreement with the numerical simulation and the time evolution shows that the averaged biasing relation has the strong dependence on the halo formation time.

z	$M_{min}[h^{-1}M_\odot]$	$M_{max}[h^{-1}M_\odot]$
0.0	3.0×10^{11}	10^{13}
1.0	2.0×10^{11}	10^{13}
2.0	1.1×10^{11}	10^{13}
3.0	8.0×10^{10}	10^{13}

Table 1: Range of the mass scales to calculate the expression(14)

The important point in our result is that the influence of the hidden variable as a source of stochasticity can be quantified explicitly. A more detailed evaluation of the degree of scatter and the basic formalism for the halo stochastic biasing arising from the formation epoch distribution will be reported elsewhere.

An interesting application using our formalism is the theoretical prediction for the two-point correlation function of clusters of galaxies, which can give a powerful constraint on the initial amplitude or the initial distribution of large scale structures [17][18]. Although we here restrict our analysis to the one-point statistics, the generalization of our formalism to the two-point statistics is straightforward. The ultimate goal of our study is to reconstruct the dark matter density field from the galaxy catalogs. To establish a reliable theory of the stochastic and non-linear galaxy biasing, we must keep developing our research.

References

[1] M.Blanton, R.Cen, J.P.Ostriker and M.A.Strauss, ApJ. **522** (1999) 590.

[2] M.Blanton, R.Cen, J.P.Ostriker, M.A.Strauss and M.Tegmark, astro-ph/9903165.

[3] A.Dekel and O.Lahav, ApJ. **520** (1999) 24.

[4] U.L.Pen, ApJ **504** (1998) 601.

[5] A.Taruya, K.Koyama and J.Soda, ApJ. **510** (1999), 541.

[6] A.Taruya, astro-ph/9909124, submitted to ApJ.

[7] S.D.White and M.J.Rees, MNRAS **188** (1978) 341.

[8] W.H.Press and P.Schechter, MNRAS **187** (1974) 425.

[9] J.R.Bond, S.Cole, G.Efstathiou, N.Kaiser, ApJ. **379** (1991), 440.

[10] H.J.Mo and S.D.M.White, MNRAS **282** (1996), 347.

[11] S.Matarrese, P.Coles, F.Lucchin and L.Moscardini, MNRAS **286** (1997) 115.

[12] C.G.Lacey and S.Cole, MNRAS **262** (1993), 627.

[13] T.Kitayama and Y.Suto, ApJ. **469** (1996), 480.

[14] J.M.Bardeen, J.R.Bond, N.Kaiser and A.S.Szalay ApJ. **304** (1986), 15.

[15] A.V.Kravtsov and A.A.Klypin, ApJ. **520** (1999), 437.

[16] R.K.Sheth and G.Lemson, MNRAS (1999), in press (astro-ph/9808138).

[17] T.Kitayama and Y.Suto, ApJ **490** (1997) 557.

[18] K.Koyama, J.Soda and A.Taruya, to appear in MNRAS (1999), astro-ph/9903027.

Naked Singularity Explosion

Tomohiro Harada [1] , Hideo Iguchi [2]

Department of Physics, Kyoto University, Kyoto 606-8502, Japan

Ken-ichi Nakao [3]

Department of Physics, Osaka City University, Osaka 558-8585, Japan

Abstract

It is known that the gravitational collapse of a dust ball results in naked singularity formation from an initial density profile which is physically reasonable. In this letter, we show that explosive radiation is emitted during the formation process of the naked singularity.

It is known that the gravitational collapse of an inhomogeneous dust ball results in shell-focusing naked singularity formation. It has been also shown that the naked singularity formation is possible from the spherical collapse of a perfect fluid with a very soft equation of state. Moreover, a kind of runaway collapse in Newtonian gravity is similar to the naked singularity formation in general relativity in many respects. These strongly suggest that the gravitational collapse will often involve drastic growth of spacetime curvature outside the event horizon.

We consider both minimally and conformally coupled massless scalar fields in four dimensional spacetime which is spherically symmetric and asymptotically flat. Let u and v be null coordinates such that they are written as $u \approx T - R$ and $v \approx T + R$ in the asymptotic region with the quasi-Minkowskian spherical coordinates (T, R, θ, ϕ). An outgoing null ray $u = \text{const}$ arriving on $\Im^+$ can be traced back through the geometry becoming an incoming null ray $v = \text{const}$ originating from $\Im^-$ with v. This gives the relation between u and v and we define the function $G(u)$ by $v \equiv G(u)$. Here, we assume that geometrical optics approximation is valid, which implies that the trajectory of the null ray gives a surface of constant phase of the scalar field. Then, the luminosity L_{lm} for the minimally coupled scalar field and the luminosity $\hat{L}_{lm}$ for the conformally coupled scalar field for fixed l and m are given through the point-splitting regularization as [1]

$$L_{lm} = \frac{1}{48\pi}\left(\frac{G''}{G'}\right)^2 - \frac{1}{24\pi}\left(\frac{G''}{G'}\right)', \quad \hat{L}_{lm} = \frac{1}{48\pi}\left(\frac{G''}{G'}\right)^2. \tag{1}$$

This implies that the luminosity depends on how the scalar field couples with gravity. However, if $G''/G'|_{u=a} = G''/G'|_{u=b}$ holds, the amounts of the radiated energy during $a \le u \le b$ for the both fields are the same. We should note that the geometrical optics approximation is only valid for smaller l. Hereafter we omit the suffix l and m. It is noted that these results are free of ambiguity coming from local curvature because the regularization is done in flat spacetime.

The spherically symmetric collapse of a dust fluid is exactly solved [2, 3]. The solution is called the Lemaître-Tolman-Bondi (LTB) solution. For simplicity, we assume the marginally bound collapse. The metric is given by

$$ds^2 = -dt^2 + R_{,r}^2(t,r)dr^2 + R^2(t,r)d\Omega^2 \tag{2}$$

in the synchronous comoving coordinates with $d\Omega^2 \equiv d\theta^2 + \sin^2\theta d\phi^2$. The energy density is given by

$$\epsilon = \frac{F'(r)}{8\pi R^2 R_{,r}}, \tag{3}$$

[1] E-mail address: harada@tap.scphys.kyoto-u.ac.jp
[2] E-mail address: iguchi@tap.scphys.kyoto-u.ac.jp
[3] E-mail address: knakao@sci.osaka-cu.ac.jp

where $F(r)$ is equal to twice the Misner-Sharp mass. We rescale the radial coordinate r as $R(0,r) = r$. Then, R is given as

$$R = r\left(1 - \frac{3}{2}\sqrt{\frac{F}{r^3}}t\right)^{2/3}. \tag{4}$$

The singularity occurs at the time $t_s(r) \equiv (2/3)\sqrt{r^3/F}$. We denote the time of occurrence of singularity at the center as $t_0 \equiv t_s(0)$. From Eq. (3), if we require that an initial density profile at $t = 0$ is a C^∞ function with respect to the local Cartesian coordinates, $F(r)$ is expanded around $r = 0$ as

$$F(r) = F_3 r^3 + F_5 r^5 + F_7 r^7 + \cdots, \tag{5}$$

where we assume that F_3 is positive. If we assume the marginally bound collapse and the mass function as Eq. (5), then the central shell-focusing singularity is naked if and only if F_5 is negative. At an arbitrary radius $r = r_{sf}$, the LTB spacetime can be matched with the Schwarzschild spacetime

$$ds^2 = -\left(1 - \frac{2M}{R}\right)dT^2 + \left(1 - \frac{2M}{R}\right)^{-1}dR^2 + R^2 d\Omega^2, \tag{6}$$

with $M = F(r_{sf})/2$. The relation between T and t is given at $r = r_{sf}$ as

$$T = t - \frac{2r^{3/2}}{3\sqrt{2M}} - 2\sqrt{2MR} + 2M\ln\frac{\sqrt{R} + \sqrt{2M}}{\sqrt{R} - \sqrt{2M}}. \tag{7}$$

The null coordinates u and v in the Schwarzschild spacetime are defined as

$$u \equiv T - R_*, \quad v \equiv T + R_*. \tag{8}$$

with $R_* \equiv R + 2M\ln[(R/2M) - 1]$.

We can determine the function G by solving the trajectories of outgoing and ingoing null rays in the dust and calculating u and v through Eq. (8) at the time when the outgoing and ingoing null rays reach the surface boundary. The trajectories of null rays in the dust are given by the following ordinary differential equation

$$\frac{dt}{dr} = \pm R_{,r}, \tag{9}$$

where the upper and lower signs denote outgoing and ingoing null rays, respectively. We have numerically solved Eq. (9) by the Runge-Kutta method of the fourth order. We have carried out the quadruple precision calculation for retaining accuracy. We have chosen the mass function as $F(r) = F_3 r^3 + F_5 r^5$. We find that the central singularity is globally naked for very small r_{sf} if we fix the value of F_3 and F_5. Although we have calculated several models, we only display the numerical results for the model with $F_3 = 1$, $F_5 = -2$ and $r_{sf} = 0.02$ in an arbitrary unit because the features are the same if the singularity is globally naked. The total gravitational mass M is given by $M = 3.9968 \times 10^{-6}$ for this model.

See Fig. 1. We define u_0 as the retarded time of the earliest light ray which originates from the singularity. In Fig. 1(a), the first derivative $G'(u)$ is plotted. This shows that $G'(u)$ does not diverge but converge to some positive value A with $0 < A < 1$. In Fig. 1(b), it is found that the second derivative $G''(u)$ does diverge as $u \to u_0$. This figure shows that the behavior of growth of $G''(u)$ is different from each other for $10^{-4} \lesssim u_0 - u$ and for $0 < u_0 - u \lesssim 10^{-4}$. For $10^{-4} \lesssim u_0 - u$, the dependence on u is written as $G'' \propto -(-u)^{-2}$, while, for $0 < u_0 - u \lesssim 10^{-4}$, the dependence is written as $G'' \propto -(u_0 - u)^{-1/2}$. Here we determine a dimensionful constant of proportion by physical consideration. We assume that the early time behavior is due to the collapse of the dust as a whole while the late time behavior is due to the growth of the central curvature. This assumption will be justified later. First we should note that the coefficient must be written using the initial data because it must not depend on time. Next we should note that we can regard any $t = \text{const} < t_0$ hypersurface as an initial hypersurface. Therefore, the coefficient must be independent of the choice of an initial slice. For the early time behavior, the only possible quantity is the gravitational mass M of the dust cloud. For the late time behavior, the only possible quantity is $\omega_s \equiv l_0^6/t_0^7 = (3/2)^7 F_3^{13/2}(-F_5)^{-3}$, where t_0 is given as $t_0 = (2/3)F_3^{-1/2}$ and

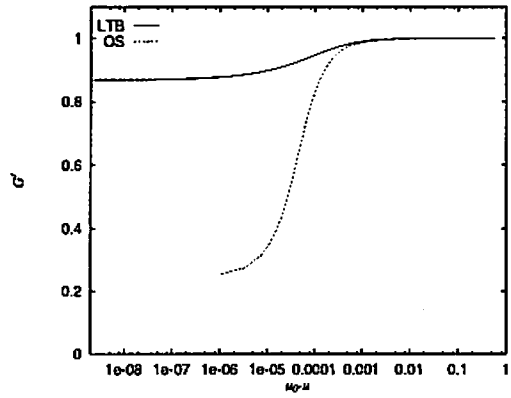

(a)

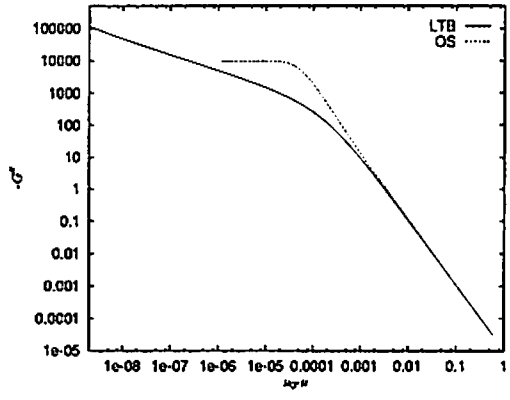

(b)

Figure 1: (a) $G'(u)$ and (b) $G''(u)$ for the LTB spacetime and the OS spacetime.

l_0 denotes the scale of inhomogeneity defined as $l_0 \equiv (-F_5/F_3)^{-1/2}$. We call ω_s a singularity frequency. The ω_s is independent of the choice of an initial slice because the mass function $F(r)$ is written in terms of R as

$$F(r) = F_3 \left(\frac{t_0 - t}{t_0}\right)^{-2} R^3 + F_5 \left(\frac{t_0 - t}{t_0}\right)^{-13/3} R^5 + \cdots, \tag{10}$$

around the center. Thus, we can write $G'' \approx -f_e M(-u)^{-2}$ for $-u \gg M$, and $G'' \approx -f_l A \omega_s^{1/2}(u_0 - u)^{-1/2}$ for $0 < u_0 - u \ll \omega_s^{-1}$, where f_e and f_l are dimensionless positive constants of order unity. The turning point from the early time behavior to the late time behavior is roughly estimated as $u_0 - u \approx (M\omega_s)^{2/3}\omega_s^{-1}$. These estimates show a good agreement with the numerical results.

Let us consider the luminosity which is calculated by Eq. (1). The numerical results are displayed in Fig. 2. We can also write an analytic expression for the luminosity using Eq. (1). In Fig. 1(a), we can find $G' \approx A$ for the late time behavior. Then, the luminosity for the late time behavior is obtained as

$$L \approx \frac{1}{48\pi} f_l \omega_s^{1/2}(u_0 - u)^{-3/2}, \quad \dot{L} \approx \frac{1}{48\pi} f_l^2 \omega_s (u_0 - u)^{-1}. \tag{11}$$

Therefore the luminosity diverges to positive infinity for the both fields as $u \to u_0$. The radiated energy is obtained by integrating the luminosity with u. The radiated energy for the late time behavior is

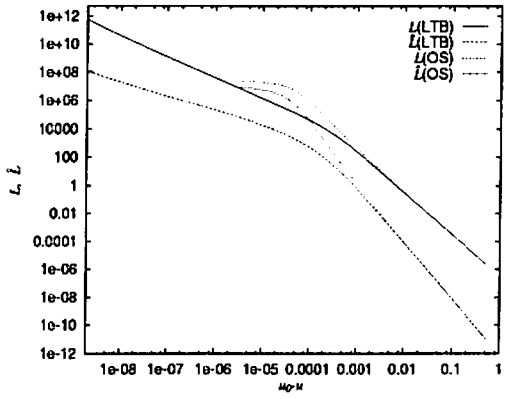

Figure 2: Luminosity for minimally and conformally coupled scalar fields in the LTB spacetime and in the OS spacetime

estimated as

$$E \approx \frac{1}{24\pi} f_l \omega_s^{1/2} (u_0 - u)^{-1/2}, \ \hat{E} \approx \frac{1}{48\pi} f_l^2 \omega_s \ln \frac{(M\omega_s)^{2/3}}{\omega_s (u_0 - u)}. \tag{12}$$

Therefore, the amounts of the total radiated energy diverge to positive infinity for the both fields as $u \longrightarrow u_0$. In realistic situations, we may assume that the naked singularity formation is prevented by some mechanism and that the quantum particle creation is ceased at the time $u_0 - u \approx \Delta t$, which implies that G''/G' vanishes for $u_0 - u \lesssim \Delta t$. Then, the second term in the expression of the luminosity L gives no contribution to the total radiated energy. Therefore, the amounts of the total energy for the both fields are the same, i.e.,

$$E = \hat{E} \approx \frac{1}{48\pi} f_l^2 \omega_s \ln \frac{(M\omega_s)^{2/3}}{\omega_s \Delta t}. \tag{13}$$

From the numerical results and physical discussion above, we obtain the following formula for the late time behavior

$$G(u) \approx A(u - u_0) - \frac{4}{3} A f_l \omega_s^{1/2} (u_0 - u)^{3/2} + \text{const.} \tag{14}$$

For comparison and for a test of our numerical code, we have also calculated the function G for the Oppenheimer-Snyder (OS) collapse to a black hole which is given by $F(r) = F_3 r^3$. We only display the numerical results for the model with $F_3 = 1$ and $r_{sf} = 0.02$ in an arbitrary unit. M is given by $M = 4 \times 10^{-6}$ for this model. The results are plotted also in Figs. 1 and 2. Because we cannot define u_0 for the OS spacetime, we plot the numerical results by setting $u_0 = 0$. For $u > 0$, the numerical results show the well-known behavior

$$G(u) \approx -\text{const} \cdot \exp\left(\frac{-u}{4M}\right) + v_h, \tag{15}$$

$$L \approx \hat{L} \approx \frac{1}{768\pi M^2}, \tag{16}$$

where the ingoing null ray with v_h is reflected to the outgoing null ray which is on the event horizon. The numerical results of L and $\hat{L}$ for the OS collapse show a good agreement with Eq. (16). In Figs. 1 and 2, we can find that the assumption concerning the early time and late time behaviors is justified.

If a back reaction of quantum effects would not become important until a considerable fraction of the total energy of the system is radiated away, the emitted energy could amount to $E \sim 10^{54}(M/M_\odot)$erg. Thus, the naked singularity explosion would be a new candidate for a source of ultra high energy cosmic rays. It may also be a candidate for the central engine of a gamma ray burst. In order to study such possibilities, we need to transform the obtained intrinsic quantities to observed quantities by taking possible reactions of created energetic particles into consideration. It is noted that, since we have obtained

the formula for the late time behavior of the function of $G(u)$, we can determine the spectrum of the radiation and thereby estimate the validity of the geometrical optics approximation [4]. We have obtained the result that the geometrical optics approximation is valid for rough order estimate.

References

[1] L.H. Ford and L. Parker, Phys. Rev. D 17, 1485 (1978)

[2] R.C. Tolman, Proc. Nat. Acad. Sci. **20**, 169 (1934).

[3] H. Bondi, Mon. Not. R. astron. Soc. **107**, 410 (1947).

[4] T. Harada, H. Iguchi and K. Nakao, in preparation.

Formation of Q-balls through Affleck-Dine Mechanism

Shinta Kasuya,[1]

Department of Physics, Ochanomizu University, Tokyo 112-8610, Japan

Masahiro Kawasaki[2]

Research Center for the Early Universe, University of Tokyo, Tokyo, 113-0033, Japan

Abstract

We present the full nonlinear calculation of the formation of Q-ball through the Affleck-Dine (AD) mechanism by numerical simulations. It is shown that large Q-balls are actually produced by the fragmentation of the condensate of a scalar field whose potential is very flat. We find that the typical size of Q-balls is determined by that of the most developed mode of linearized fluctuations when the amplitude of fluctuations grow as large as that of the homogeneous mode: $\langle \delta\phi^2 \rangle \sim \phi^2$. Almost all the initial charges which the AD condensate carries are absorbed into the formed Q-balls, leaving only a small fraction in the form of coherently oscillating AD condensate. Moreover, the actual sizes and the charges stored within Q-balls depend on the initial charge densities. We also find that the evolution of the Q-ball crucially depends on its spatial dimensions, and the stable Q-ball can exist only in the form of three dimensional object.

1 Introduction

A Q-ball is a non-topological soliton with some conserved global charge in the scalar field theory [1]. A Q-ball solution exists if the energy minimum develops at non-zero ϕ with fixed charge Q. In terms of the effective potential of the field ϕ, $V(\phi)/\phi^2$ takes the minimum at $\phi \neq 0$ [1, 2]. The Q-ball naturally appears in the spectrum of the Minimal Supersymmetric Standard Model (MSSM) [3]. In particular, very large Q-balls could exist in the theory with a very flat potential [4], such as in the MSSM which has many flat directions, which consist of squarks and sleptons, carrying baryonic and/or leptonic charges [5]. It provides interesting attention to phenomenology and astrophysics [4, 6, 7].

Cosmologically, it is interesting that large Q-balls carrying baryonic charge (B-ball) can be promising candidate for the dark matter of the universe, and/or the source for the baryogenesis [8, 9, 10]. Moreover, they can explain why the energy density of baryons is as large as that of the dark matter (at least within a few orders of magnitude). If the effective potential of the field ϕ carrying the baryonic charge is very flat at large ϕ, as in the theory that the supersymmetry (SUSY) breaking occurs at low energy scales (gauge-mediated SUSY breaking), B-ball energy per unit charge decreases as the charge increases [4]. For large enough charge, such as $B \gtrsim 10^{12}$, the B-ball cannot decay into nucleon, and is completely stable, which implies that B-balls themselves can be the dark matter [8] with charges $B = 10^{14} - 10^{26}$ [11], while baryons are created by the conventional AD mechanism. In the case of gravity-mediated SUSY breaking scenario, the B-balls can decay into quarks or nucleons, with the decay (evaporation) rate of the Q-ball proportional to the surface area [12], and if they decay after the electroweak phase transition, there are some advantage over the conventional AD baryogenesis [9, 10]. For example, B-balls can protect the baryon asymmetry from the effects of lepton violating interactions above the electroweak scale when anomalous $B + L$ violation is in thermal equilibrium. Another one is that Q-balls with $B - L$ charge survive the sphaleron effects to create the same amounts of baryon and lepton numbers. In either

[1] E-mail:kasuya@cc.ocha..ac.jp
[2] E-mail:kawasaki@resceu.s.u-tokyo.ac.jp

case, it is necessary for Q-balls to have large charges, such as $Q = 10^{22} - 10^{28}$ [9, 10]. In this scenario, dark matter is LSP which arises from the Q-ball decay, and parameters of MSSM could be constrained by investigating the Q-ball cosmology [13]. Note that it is also possible to have stable Q-balls in the gravity-mediated SUSY breaking theory depending on the details of the features of the hidden sector [14].

Those large Q-balls are expected to be created through Affleck-Dine (AD) mechanism [15] in the inflationary universe [8, 9, 10]. The coherent state of the AD scalar field which consists of some flat direction in MSSM becomes unstable and instabilities develop. These fluctuations grow large to form Q-balls.

The formation of large Q-balls has been studied only linear theory analytically [8, 9, 10] and numerical simulations was done in one dimensional lattices [8]. Both of them are based on the assumption that the Q-ball configuration is spherical so that we cannot really tell that the Q-ball configuration is actually accomplished. Recently, some aspects of the dynamics of AD scalar and Q-ball formation were studied in Ref. [16], but the whole evolution was not investigated, which is important for the investigation of the Q-ball formation. (In the context of non-relativistic Bose gas, dynamics of drops of Bose-Einstein condensate which is a non-topological soliton is studied in Ref. [17].) Here, we show the dynamics of a complex scalar field with very flat potential numerically in one, two, and three dimensional lattices, without assuming spherical Q-ball configuration, which is based on the work of Ref. [18]. On one dimensional lattices, it is equivalent to the system independent of other two dimensions, so that we are observing plane-like objects. We call them *Q-walls*. Likewise, string-like objects, which we call *Q-strings*, appear on two dimensional lattices.

2 Instabilities

First we show where instabilities of a scalar field comes from. To be concrete, let us assume that the complex scalar field Φ has an effective potential of the form [8]

$$V(\Phi) = m^4 \ln\left(1 + \frac{|\Phi|^2}{m^2}\right) - cH^2|\Phi|^2 + \frac{\lambda^2}{M^2}|\Phi|^6, \tag{1}$$

where m is the mass of the field, H is the Hubble parameter, λ is a dimensionless coupling constant, $M \simeq 2.4 \times 10^{18}$ GeV is the (reduced) Planck mass, and c is a constant. Hereafter, we assume the matter-dominated universe, where $H = 2/3t$. This form of the potential arises naturally in the gauge-mediated SUSY breaking scenario in MSSM [8]. In addition to Eq.(1), the A-term (e.g., $A(\Phi^4 + \Phi^{*4})$) is necessary for baryogenesis, since it makes the AD field rotate to create baryon numbers. Here we assume that the A-term does not crucially affect other terms of the potential, and take *ad hoc* initial conditions neglecting the A-term. The AD field thus has the initial charge density. Notice that the effective potential for the flat direction has very similar form in the gravity-mediated SUSY breaking scenario [9], and the features of the Q-ball formation are expected to be the same.

If we regard that the field is dominate by the logarithmic potential and the homogeneous mode has only a real part (i.e., no rotational motion), neglecting the second and third term in Eq.(1), instability band is approximately estimated as [19]

$$\frac{k}{a} \lesssim \frac{m^2}{|\Phi|}, \tag{2}$$

for large field value $|\Phi|$, which is exactly the same with the result of Ref. [8] (Note that there are additional instability bands which come from the parametric resonance effects because of the oscillation of the homogeneous field, but they are subdominant effects). Therefore, the instability band grows as time goes on, since the amplitude of the homogeneous mode $|\Phi|$ decreases as a^{-3} for the logarithmic potential. These fluctuations originate from the negative curvature of the logarithmic potential, which produces negative pressure [9]. It is expected that Q-balls with corresponding scales are formed.

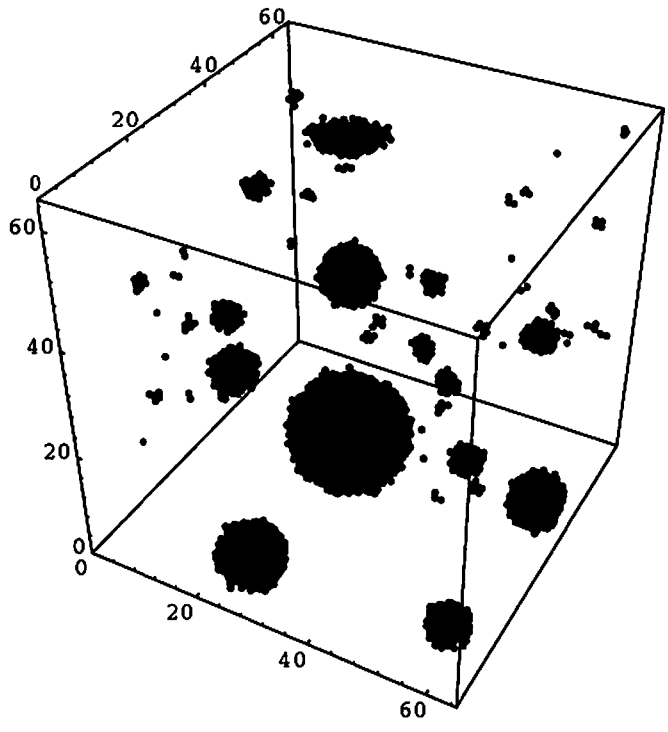

Figure 1: Configuration of Q-balls on three dimensional lattice. More than 30 Q-balls are formed, and the largest one has the charge with $Q \simeq 1.96 \times 10^{16}$

3 Simulations on the lattice

As we mentioned, we calculate the dynamics of the complex scalar field on one, two, and three dimensional lattices. We formulate the equation of motion for the real and imaginary part of the field: $\Phi = \frac{1}{\sqrt{2}}(\phi_1 + i\phi_2)$. Rescaling variables with respect to m, we have dimensionless variables

$$\varphi = \frac{\phi}{m}, \qquad h = \frac{H}{m}, \qquad \tau = mt, \qquad \xi = mx. \tag{3}$$

We have exhaustedly calculated the dynamics of the scalar field and Q-balls for various parameters, and find that Q-balls are actually formed through the Affleck-Dine mechanism in three dimensional lattices. They have thick-wall profiles which are approximately spherical, and its charge is conserved as time goes on. Here we show one example. Figure 1 shows the configuration of Q-ball at $\tau = 10^6$ on 64^3 three dimensional lattices with $\Delta\xi = 1.0$ in matter dominated universe. Initial conditions are $\varphi_1(0) = 2.5 \times 10^6, \varphi_1'(0) = 0, \varphi_2(0) = 0, \varphi_2'(0) = 4.0 \times 10^4, \tau(0) = 100$. We can see more than 30 Q-balls in the box. The charge of the largest Q-ball is $Q \simeq 1.96 \times 10^{16}$ evaluated by

$$Q = \int d^3\xi q = \int d^3\xi \frac{1}{2}(\varphi_1\varphi_2' - \varphi_2\varphi_1'). \tag{4}$$

Though the best way to investigate the nature of Q-ball formation is to calculate in three dimensions, but we must take large box size to take into account low momenta effects and large number of lattices to have the enough resolution. Therefore, we have calculated in one and two dimensions, and use these results complementarily with results in three dimensions.

4 Time evolution of Q-ball configurations

As mentioned in the previous sections, it is necessary to compare the evolutions of Q-balls in one, two, and three dimensions. We have already known that a Q-ball is a non-trivial configuration of the scalar field, which we can obtain by estimating the energy minimum with finite charge Q fixed. From Eq.(4) we can approximately estimate the charge of a Q-ball as

$$Q = a^3 Q_D \sim a^3 R^D \tilde{q} \sim \text{const.}, \tag{5}$$

where $\tilde{q} = \phi_1 \dot{\phi}_2 - \dot{\phi}_1 \phi_2$ is the charge density, and Q_D is the charge in D dimension. Charge conservation tells us that Q is constant. If we assume the form of a Q-ball as

$$\phi(\mathbf{x}, t) = \phi(\mathbf{x}) \exp(i\omega t), \tag{6}$$

the energy of a Q-ball can be calculated as

$$\begin{aligned} E &= \int d^3x \left[\frac{1}{2}(\nabla\phi)^2 + V(\phi) - \frac{1}{2}\omega^2\phi^2 \right] + \omega Q, \\ &= \int d^3x [E_{grad} + V_1 + V_2] + \omega Q, \end{aligned} \tag{7}$$

where

$$\begin{aligned} E_{grad} &\sim \frac{\phi^2}{a^2 R^2}, \\ V_1 &\sim m^4 \log\left(1 + \frac{\phi^2}{2m^2}\right) \sim \text{const.}, \\ V_2 &\sim \omega^2 \phi^2. \end{aligned} \tag{8}$$

When the energy take the minimum value, the equipartition is achieved: $E_{grad} \sim V_1$ and $E_{grad} \sim V_2$. From these equations addition to the charge conservation, we obtain the following evolutions:

$$\begin{aligned} R &\propto a^{-4/(D+1)}, \\ \phi &\propto a^{(D-3)/(D+1)}, \\ \omega &\propto a^{-(D-3)/(D+1)}, \end{aligned} \tag{9}$$

which we observed approximately the same features numerically [19]. Therefore, the physical size $R_{phys} = Ra$ of the Q-balls for $D = 1, 2$ shrinks, while remains constant for $D = 3$. Thus, stable Q-balls (three dimensional objects) can be formed, but Q-walls or Q-strings shrink because of the charge conservation.

5 Charge and size of Q-balls

Figure 2 shows power spectra of the cases of one dimensional lattices with the box size $L = 4096$ and linearized fluctuations at $\tau = 4.5 \times 10^5$ and 5×10^5. As expected, both spectra are very similar at $\tau = 4.5 \times 10^5$, since fluctuations have not fully developed yet. After they are fully developed ($\tau = 5 \times 10^5$), the spectrum becomes smooth and broad because of rescattering [20] (panel (c)). But, even at this time, the most developed mode is the same as that of linearized fluctuations (Compare panels (c) and (d)). Therefore, we conclude that the size of Q-balls is determined by the most developed mode of linearized fluctuations when the amplitude of fluctuations becomes as large as that of the homogeneous mode: $\langle \delta\phi^2 \rangle \sim \phi^2$. For the case of Fig. 2, the typical size is $k_{max} \sim 0.04$, which implies that $R_{phys} \sim a(\tau_f)/k_{max} \sim 7.3 \times 10^3$, where $\tau_f = 5 \times 10^5$ is the Q-ball formation time. At this time, the ratio to the horizon size is $\sim 10^{-2}$, which corresponds to the results of Ref. [8], but this value may not have important meaning, since the sizes of the horizon and Q-balls have different time evolutions. This size is consistent with the actual sizes appeared on three dimensional lattices, where the largest Q-ball has the size $R_{phys} \approx 1.1 \times 10^4$, and the average size of the second to fifth largest Q-balls is $\simeq 5.2 \times 10^3$.

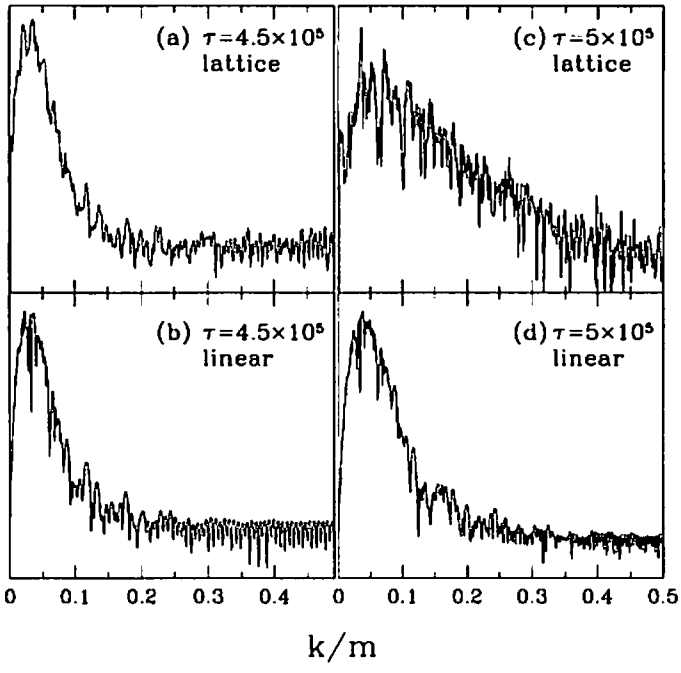

Figure 2: Power spectrum of fluctuations of AD scalar field when the amplitude of fluctuations becomes as large as that of the homogeneous mode: $\langle \delta\phi^2 \rangle \sim \phi^2$. The top panels (a) and (c) show the full fluctuations calculated on one dimensional lattices, while the bottom panels (b) and (d) show the linearized fluctuations without mode mixing.

We also observed that almost all the initial charges carried by the condensate of AD field are absorbed into Q-balls formed from the fragmentations of the condensate, and the amplitude of homogeneous mode is highly damped, which means that they carries only a small fraction of the total initial charges. In the case of Fig. 1, more than 95% of the charges are stored in the Q-balls.

Actually, the charges and sizes of Q-balls depend on the initial value of the charge carried by the AD condensate. Since the initial charge density of AD scalar is written as $q(0) = \varphi_1(0)\varphi_2'(0)$, the larger the initial amplitude or angular velocity of the AD condensate, the larger the charge stored in Q-balls. The dependences of the charge and the (comoving) size of the (largest) Q-ball on the initial charge density are shown in Fig. 3. Here we take one dimensional lattices, so actually we observe Q-walls. We thus estimate their conserved charges as $Q_{max} = a^3 \int dx q(x)$ according to Eq.(5). We find that one large Q-ball and a few small Q-balls are formed in most of the cases, while one Q-ball is formed in some cases such that the initial charge density $q(0)$ is relatively small. Open circles denote the dependence on $\varphi_2'(0)$ for fixed $\varphi_1(0)$, while solid triangles denote the dependence on $\varphi_1(0)$ for fixed $\varphi_2'(0)$ with $L = 256$. Since both results show the same dependence, the only relevant variable which determines the charge and the size is the initial charge density $q(0)$. The dashed line represents the fitted line, $Q_{max} = 94.3(q(0))^{1.03}$. Crosses are obtained on $L = 512$ lattices. They seem to be a little larger, and the box size effect might be remained. Notice that those Q-balls with negative charge can be produced when the initial angular velocity of the AD condensate (or, in our simulations, $\varphi_2'(0)$) is small enough [19].

Since (comoving) size of the Q-balls changes as time goes on, as we mentioned above, the actual values of the size at $\tau = 5 \times 10^7$ in one dimension is not so important. What is important is how the size depends on $q(0)$. The dotted line shows the fitted line written as $R = 9.46 \times 10^{-7}(q(0))^{0.464}$, though

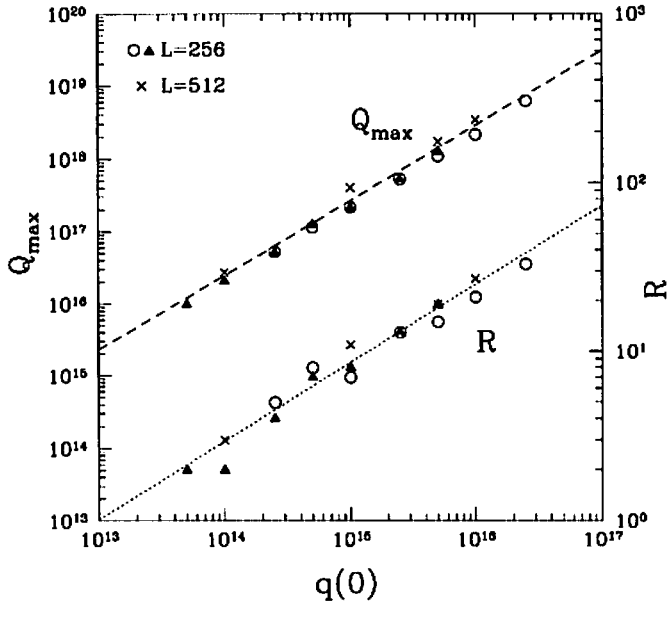

Figure 3: Dependence of charges and sizes on the initial charge $q(0) = \varphi_1(0)\dot{\varphi_2}(0)$ carried by the AD condensate on one dimensional lattices. Open circles and solid triangles denote the dependence on $\dot{\varphi_2}(0)$ and $\varphi_1(0)$, respectively. Crosses are obtained on larger box size. R is evaluated at $\tau = 5 \times 10^7$. Note that the relevant variable is only $q(0)$, since both dependences lie on the same lines.

we expect the relation $R \propto (q(0))^{1/3}$, which means that the charge is proportional to the volume as in Eq.(5). It may be one of the reasons for the discrepancy that the values of R for small charge Q-balls may have considerable error because of poor resolution in spatial lattices.

6 Summary

In conclusion, we consider the full nonlinear equations of motion of the Affleck-Dine scalar field in order to see the formation of Q-ball through the Affleck-Dine mechanism by numerical simulations. It is shown that large Q-balls are actually produced by the fragmentation of the condensate of a scalar field whose potential is very flat, as appeared in the supersymmetric standard theory.

We find that the typical size of Q-balls is determined by that of the most developed mode of linearized fluctuations when the amplitude of fluctuations grow as large as that of the homogeneous mode: $\langle \delta\phi^2 \rangle \sim \phi^2$. Almost all the initial charges carried by the AD condensate are absorbed into the Q-balls formed, leaving only a small fraction in the form of the remaining coherently oscillating AD condensate. We thus can constrain parameters of MSSM through the fraction of the baryon in Q-balls (f_B) in the context of the Q-ball decay producing LSP dark matter [13]

Moreover, the actual sizes and the charges stored within Q-balls depend on the initial charge density of the AD condensate, which is in good agreement with the condition of the existence of the Q-ball that it exists if the scalar field can take non-trivial energy minimum configuration with a fixed charge. Therefore, Q-balls with huge charges necessary for Q-balls to be dark matter could be produced if the initial charge

density that the AD condensate carries is large enough.

We also find that the evolution of Q-balls crucially depends on the form of their dimensions, and the stable Q-balls can only exist in the form of three dimensional objects. Smaller dimensional objects such as Q-walls and Q-strings shrink as the universe expands.

Finally, we will mention the Q-axiton (the higher energy state Q-ball), which was studied in Ref. [16]. In our simulations, Q-balls are actually formed. The field orbits in the complex plane inside Q-balls are almost complete circles. Moreover, even if the initial AD field orbit is extremely oblique such that the initial angular velocity is very small so as to create the negative charged Q-balls, circular orbits can be seen inside both positive and negative Q-balls [19]. It thus seems that Q-axitons may appear, if ever, at the very beginning of the Q-ball formation.

References

[1] S. Coleman, Nucl. Phys. **B262**, 263 (1985).

[2] A. Kusenko, Phys. Lett. **B404**, 285 (1997).

[3] A. Kusenko, Phys. Lett. **B405**, 108 (1997).

[4] G. Dvali, A. Kusenko, and M. Shaposhnikov, Phys. Lett. **B417**, 99 (1998).

[5] M. Dine, L. Randall, and S. Thomas, Nucl. Phys. **B458**, 291 (1996).

[6] A. Kusenko, M. Shaposhnikov, P.G. Tinyakov, and I.I.Tkachev, Phys. Lett. **B423**, 104 (1998).

[7] A. Kusenko, V. Kuzmin, M. Shaposhnikov, and P.G. Tinyakov, Phys. Rev. Lett. **80**, 3185 (1998).

[8] A. Kusenko and M. Shaposhnikov, Phys. Lett. **B418**, 46 (1998).

[9] K. Enqvist and J. McDonald, Phys. Lett. **B425**, 309 (1998).

[10] K. Enqvist and J. McDonald, Nucl. Phys. **B538**, 321 (1999).

[11] M. Laine and M. Shaposhnikov, Nucl. Phys. **B532**, 376 (1998).

[12] A. Cohen, S. Coleman, H. Georgi, and A. Manohar, Nucl. Phys. **B272**, 301 (1986).

[13] K. Enqvist and J. McDonald, Phys. Lett. **B440**, 59 (1998).

[14] K. Enqvist and J. McDonald, Phys. Rev. Lett. **81**, 3071 (1998).

[15] I. Affleck and M. Dine, Nucl. Phys. **B249**, 361 (1985).

[16] K. Enqvist and J. McDonald, hep-ph/9908316.

[17] S.Yu. Khlebnikov and I.I. Tkachev, hep-ph/9902272.

[18] S. Kasuya and M. Kawasaki, to appear in Phys. Rev. **D61** (2000), hep-ph/9909509.

[19] S. Kasuya and M. Kawasaki, in preparation.

[20] S.Yu. Khlebnikov and I.I. Tkachev, Phys. Rev. Lett. **77**, 219 (1996).

Topological Defect Inflation*

Nobuyuki Sakai†

Yukawa Institute for Theoretical Physics, Kyoto University, Kyoto 606-8502

Abstract

We address some issues of topological defect inflation. (1) We clarify the causal structure of an inflating magnetic monopole. The spacetime diagram shows explicitly that this model is free from the "graceful exit" problem, while the monopole itself undergoes "eternal inflation". (2) We extend the study of inflating topological defects to Brans-Dicke gravity. Contrary to the case of Einstein gravity, any inflating monopole eventually shrinks and takes a stable configuration. (3) We reanalyze chaotic inflation with a non-minimally coupled massive scalar field. We find a new solution of domain wall inflation, which relaxes constraints on the coupling constant for successful inflation.

1 Introduction

Guendelman & Rabinowitz, Linde, and Vilenkin independently claimed that topological defects expand exponentially if the vacuum expectation value of the Higgs field η is of the order of the Planck mass $m_{\rm Pl}$ [1, 2]. Their arguments were later verified in numerical simulations [3, 4]: it was shown in particular that the critical value of η for domain walls and global monopoles is $\eta_{\rm inf} \approx 0.33 m_{\rm Pl}$, regardless of initial conditions.

Because this "topological defect inflation" (TDI) model is free from the fine-tuning problem of initial conditions, it has been attracting attention. In particular, recently it has been argued that TDI takes place in some of the plausible models in particle physics [5].

In this paper, concerning the TDI model, we address the following three issues.
(1) Causal structure of an inflating magnetic monopole [6].
(2) TDI in Brans-Dicke (BD) theory [7].
(3) TDI induced by non-minimally coupled massive scalar field [8].

2 Causal Structure of an Inflating Magnetic Monopole

Among various topological defects, spacetime solutions of magnetic monopoles have been studied the most intensively in the literature [9, 10, 11]. This originated from the rather mathematical interest in static solutions with non-Abelian hair [9]. It was shown [10] that static regular solutions are nonexistent if η is larger than a critical value $\eta_{\rm sta} (\sim m_{\rm Pl})$. Our previous work [4] revealed the properties of monopoles for $\eta > \eta_{\rm sta}$. There are three types of solutions, depending on coupling constants and initial configuration: a monopole either expands, collapses into a black hole, or comes to take a stable configuration. The first type corresponds to TDI.

Recently, the causal structure of an inflating magnetic monopole was discussed in Ref.[12]. The spacetime diagrams in Ref.[12] showed, for instance, that the inflationary boundary expands along outgoing null geodesics, that is, no observer can exit from an inflationary region. The above argument would be fatal to TDI because it implies that reheating never occurs. Therefore, the spacetime structure of TDI deserves close examination. Here we discuss the causal structure of an inflating magnetic monopole, based on the numerical solution in Ref.[4].

In order to see the spacetime structure for numerical solutions, we observe the signs of the expansion of a null geodesic congruence. For a spherically symmetric metric,

$$ds^2 = -dt^2 + A^2(t,r)dr^2 + B^2(t,r)r^2(d\theta^2 + \sin^2\theta d\varphi^2), \tag{1}$$

*This talk is based on Refs.[6, 7, 8].

†E-mail:sakai@yukawa.kyoto-u.ac.jp

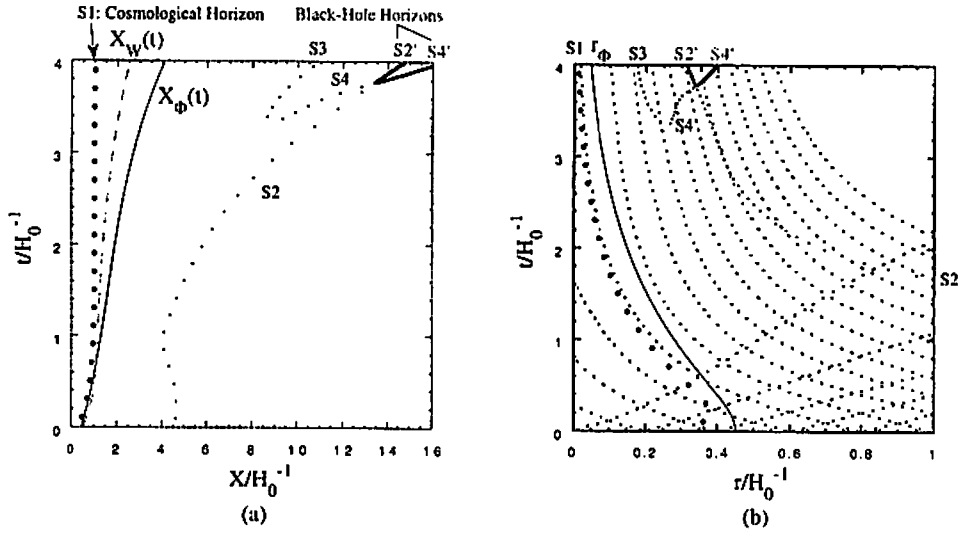

Figure 1: A solution of an inflating magnetic monopole. (a) is the reproduction of Fig. 4(a) of [4]: we plot the trajectories of monopole boundaries and of apparent horizons in terms of the proper distance from the center, X; dotted lines denote apparent horizons; we normalize time and length by the horizon scale defined as $H_c^{-1} \equiv [8\pi V(0)/3m_{\rm Pl}^2]^{-1/2}$. In (b) we plot ingoing and outgoing null geodesics (dotted lines) besides the above-mentioned trajectories in a $t-r$ diagram; the boundary moves *inward* and eventually becomes *spacelike*.

an outgoing (+) or ingoing (−) null vector is given by $k_\pm^\mu = (1, \pm A^{-1}, 0, 0)$, and its expansion $\Theta_\pm$ is written as

$$\Theta_\pm = k^\theta_{\pm;\theta} + k^\varphi_{\pm;\varphi} = \frac{2}{B}\left(\frac{\partial B}{\partial t} \pm \frac{1}{Ar}\frac{\partial (Br)}{\partial r}\right), \tag{2}$$

which is defined as the trace of a *projection* of $k^\mu_{;\nu}$ onto a relevant 2-dimensional surface [13]. We define an "apparent horizon" as the surface with $\Theta^+ = 0$ or $\Theta^- = 0$ [‡]. We label those surfaces as S1, S2, etc. in our figures.

In Fig. 1(a), we plot the trajectories of monopole boundaries and of apparent horizons in terms of the proper distance from the center: $X \equiv \int_0^r A dr'$. Here we define the boundary in two ways: X_ϕ as the position of $\phi = \eta/2$ and X_w as the position of $w = 1/2$, where ϕ and w are the Higgs field and a gauge-field function, respectively. An apparent horizon S1 almost agrees with $X = H_c^{-1} \equiv [8\pi V(0)/3m_{\rm Pl}^2]^{-1/2}$, which implies that the monopole core is almost de Sitter spacetime. Figure 1(a) also illustrates that a wormhole structure with black hole horizons appears around an inflating core. Because the inflating core becomes causally disconnected from the outer universe, such an isolated region is called a "child universe". The production of child universes was originally discussed by Sato, Sasaki, Kodama, and Maeda [14] in the context of old inflation [15].

To see the causal structure of the inflating monopole more closely, we also plot ingoing and outgoing null geodesics in Fig. 1(b). An important feature for the magnetic monopole as well as the global monopole [16] is that the boundary moves *inward* and, moreover, it eventually becomes *spacelike*.

To understand the global structure, which is not completely covered by the numerical solution, we make a reasonable assumption that the core region approaches to de Sitter spacetime and the outside to Reissner-Nordström, as in Refs.[11, 12]. In each static spacetime, apparent horizons and event horizons are identical; the signs of (Θ^+, Θ^-) are determined as is shown in Fig. 2. The above assumption implies that, although the whole space in the early stage is quite dynamical and an apparent horizon does not

[‡]In the literature an "apparent horizon" usually refers to the outermost surface with $\Theta^+ = 0$ in an asymptotically flat spacetime. In this article, however, we call any marginal surface with $\Theta^+ = 0$ or $\Theta^- = 0$ an apparent horizon.

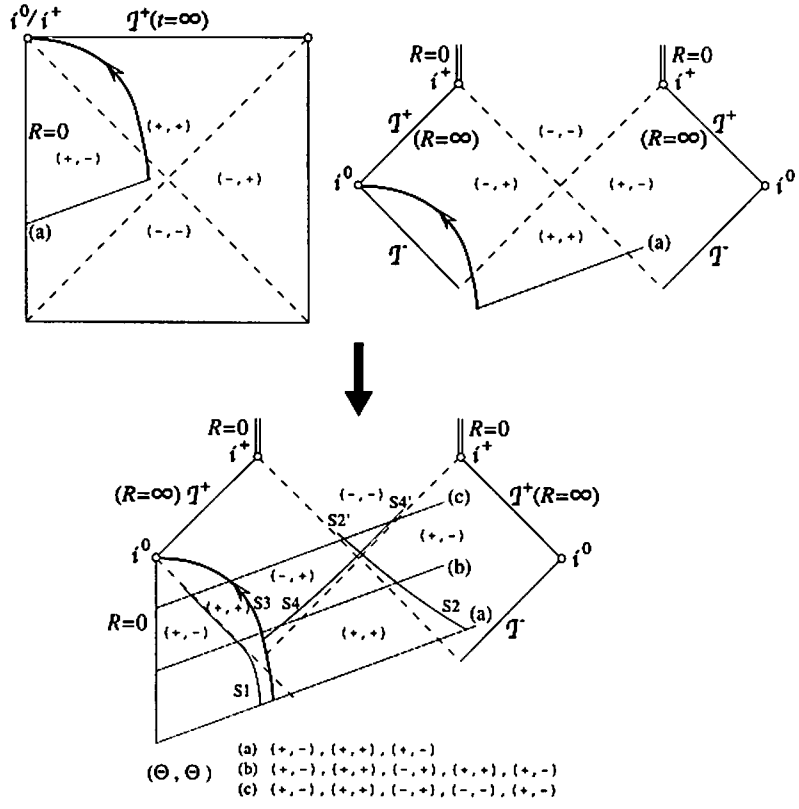

Figure 2: Possible conformal diagram for the spacetime of an inflating magnetic monopole. The core region is approximated to be de Sitter spacetime and the outside to be Reissner-Nordström. The upper figure shows how the monopole boundary is embedded in each spacetime separately, and the lower figure shows a complete spacetime. $\mathcal{I}^+$ and $\mathcal{I}^-$ represent future and past null infinity, i^+ represents future timelike infinity, and i^0 represents spacelike infinity. Long-dashed lines denote event horizons, which are identified with apparent horizons in de Sitter or Reissner-Nordström spacetime. Short-dashed lines (a), (b), and (c) denote time-slices, which correspond to the embedding diagrams (a), (b), and (c) of Fig. 5 of [4], respectively. For reference, we schematically depict the trajectories of apparent horizons. We also write down the signs of the expansion Θ. The structure of apparent horizons, which is determined by the signs of $\Theta^{\pm}$, completely agrees with that in Fig. 1 and Fig. 5 of [4].

coincide with an event horizon, the two horizons later approach each other. Hence, we can extrapolate the global structure from the structure of apparent horizons in the local numerical solution. From the consistency of the spatial distribution of the signs of (Θ^+, Θ^-), we conclude that Fig. 2 gives the only possible embedding.

Cosmologically, Fig. 2 tells us that any inflationary region eventually enters a reheating phase because any observer inside the core finally goes out. On the other hand, the monopole boundary continues to expand in terms of the physical size and approaches spatial infinity (i^0). Figure 2 thus proves that this model is free from the "graceful exit" problem, while the monopole itself undergoes "eternal inflation".

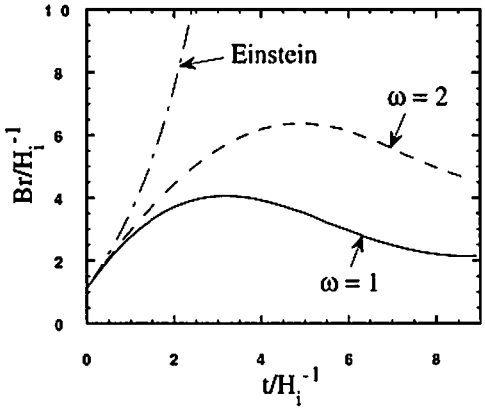

Figure 3: Dynamics of a global monopole for several values of ω. We set $\lambda = 0.1$ and $\eta/m_{\rm Pl}(\Phi_i) = 1$. We plot trajectories of the position of $\phi = \eta/2$.

3 Topological Defect Inflation in Brans-Dicke Theory

The Brans-Dicke-Higgs system, which we consider here, is described by the action

$$S = \int d^4x\sqrt{-g}\left[\frac{\Phi}{16\pi}\mathcal{R} - \frac{\omega}{16\pi\Phi}(\nabla_\mu\Phi)^2 - \frac{1}{2}(\nabla_\mu\phi^a)^2 - V(\phi)\right], \quad \text{with} \quad V(\phi) = \frac{\lambda}{4}(\phi^a\phi^a - \eta^2)^2, \qquad (3)$$

where Φ and ω are the BD field and the BD parameter, respectively.

In extended inflation [17], where the BD theory was originally introduced in inflationary cosmology, the universe does not expand exponentially but expands with a power law. This slower expansion solved the graceful exit problem of old inflation [15]. We thus expect that the BD field also affects the dynamics and global spacetime structure of inflating monopoles.

Let us begin with a discussion of the fate of an inflating topological defect. Once inflation begins, the core region can be approximated to be a homogeneous spacetime, where the scale factor and the BD field are described by the solution of extended inflation [17]: $a(t) \propto t^{\omega+\frac{1}{2}}, \Phi(t) \propto t^2$. Hence, the effective Planck mass,

$$m_{\rm Pl}(\Phi) = \sqrt{\Phi} \propto a^{\frac{1}{\omega+\frac{1}{2}}}, \qquad (4)$$

continues to increase until inflation ends. This implies that, even if $\eta/m_{\rm Pl}(\Phi)$ is large enough to start inflation initially, it eventually becomes smaller than the critical value (≈ 0.33). We thus speculate that any defect comes to shrink after inflation.

In order to ascertain the above argument, we carry out numerical analysis for spherical global monopoles, using the coordinate system (1). The above arguments are verified by this numerical result: as $\eta/m_{\rm Pl}(\Phi)$ gets close to the critical value, the monopole stops expanding and begins to shrink.

Figure 3 shows the trajectories of the position of $\phi = \eta/2$ for several values of ω. The curves indicate that a monopole does not shrink toward the origin but tends to take a stable configuration.

The result that inflation eventually ends stems merely from the change of the local values of $m_{\rm Pl}(\Phi)$. We may therefore extend this result to models of other topological defects.

Next, we discuss constraints for this model to be a realistic cosmological model. One of the distinguishing features of this model is that there are two scenarios of exiting from an inflationary phase and entering a reheating phase. This is illustrated by the slow-roll conditions,

$$\epsilon^{-1} \equiv \frac{\sqrt{6\pi}\eta}{m_{\rm Pl}(\Phi)} \gg 1, \quad \text{with} \quad \phi \ll \eta\left(1 - \frac{\epsilon}{2}\right) \equiv \phi_f. \qquad (5)$$

When the condition $\epsilon^{-1} \gg 1$ (a more precise condition is $\eta/m_{\rm Pl}(\Phi) > 0.33$) breaks down, inflation stops globally. Before this time, many local regions with the present-horizon size enter a reheating phase when

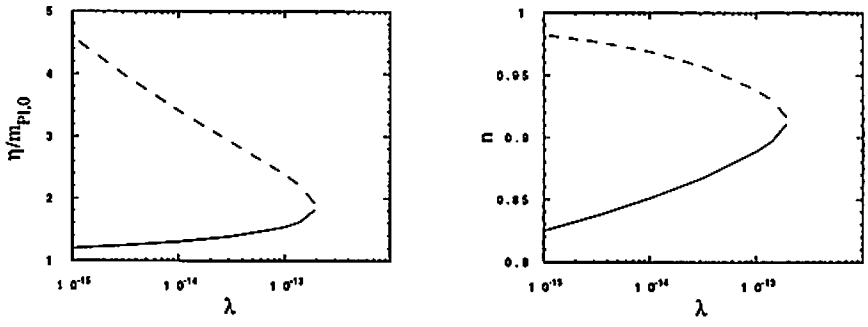

Figure 4: Constraints from COBE-normalized amplitudes of density perturbations. (a) Concordant values of λ and $\eta/m_{\rm Pl,0}$. (b) The spectral indices of density perturbations.

the second condition $\phi \ll \phi_f$ breaks down. The second scenario is just like that of standard TDI or other slow-roll inflationary models. In the first scenario a microscopic monopole might remain in the observable universe. Unfortunately, however, this possibility turns out to be ruled out because $\eta/m_{\rm Pl}(\Phi_f)$ must be larger than 1 from the COBE normalization, as will be seen in Fig. 4(a) later. Thus we only consider the second (standard) reheating scenario.

Starobinsky & Yokoyama [18] derived the amplitude of a density perturbation on comoving scale $l = 2\pi/k$ in terms of Bardeen's variable Φ_A [19] as

$$\Phi_A(l)^2 = \frac{48V}{25m_{\rm Pl}(\Phi)^4}\left[\frac{8\pi V^2}{m_{\rm Pl}(\Phi)^2 V_{,\phi}^{\ 2}} + \frac{(e^{2\gamma^2 N}-1)^2}{4\gamma^2}\right], \quad \text{with} \quad \gamma \equiv \sqrt{\frac{2}{2\omega+3}} \tag{6}$$

where all quantities are defined at the time t_k when the k-mode leaves the Hubble horizon, *i.e.*, when $k = aH$. N is defined as $N \equiv \ln(a_f/a_k)$, where the subscript f denotes the time at the end of inflation.

Since the large-angular-scale anisotropy of the microwave background due to the Sachs-Wolfe effect is given by $\delta T/T = \Phi_A/3$, we can constrain the values of λ and $\eta/m_{\rm Pl}$ by the 4yr COBE-DMR data normalization [20]: $\Phi_A/3 \cong 10^{-5}$, on the relevant scale. We choose $N_{k=a_0H_0} = 65$ typically, where a subscript 0 denotes the present epoch. Figure 4(a) shows the allowed values of λ and $\eta/m_{\rm Pl}$ for $\gamma = 0.045$ ($\omega = 500$). The concordant values are represented by two curves, which is a distinguishing feature for the double-well potential. Unfortunately, fine-tuning of $\lambda \lesssim 10^{-13}$) is needed, just like other models [18]. The constraints for $\omega > 500$ are practically no different from those in the Einstein gravity.

Using the relation $d\ln k = da/a + dH/H$ and the field equations, we obtain [21]

$$n - 1 \equiv \frac{d\ln\Phi_A^2}{d\ln k} \cong -\frac{3m_{\rm Pl}(\Phi)^2 V_{,\phi}^{\ 2}}{8\pi V^2} + \frac{m_{\rm Pl}(\Phi)^2 V_{,\phi\phi}}{4\pi V} - 6\gamma^2. \tag{7}$$

The spectral indices are plotted in Fig. 4(b); the two lines correspond to the two lines of COBE-normalized amplitudes in Fig. 4(b). As Eq. (7) suggests, the deviation from the Einstein theory is only $6\gamma^2 \cong 0.01$ for $\omega = 500$. Therefore, the relatively large shift from $n = 1$ is caused not by the BD field but by the double well potential.

Finally, we consider the detectability of relic monopoles in this model. Due to the sufficient expansion, $N > 65$, the core of a monopole is located so far from the observed region that even the long-range term of a global monopole, $\rho = \eta^2/R^2$, does not exert any effective astrophysical influence.

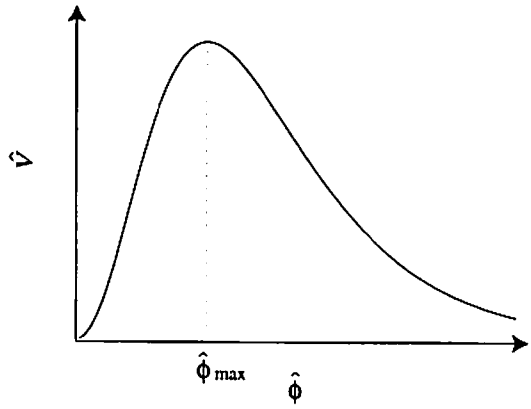

Figure 5: The potential $\hat{V}(\hat{\phi})$ in a fictitious world for $\xi < 0$ [22]. A plateau at $\hat{\phi} = \hat{\phi}_{\max}$ leads TDI.

4 Topological Defect Inflation Induced by Non-Minimally Coupled Massive Scalar Field

The model with a non-minimally coupled massive scalar field is described by the action,

$$S = \int d^4x\sqrt{-g}\left[\frac{\mathcal{R}}{2\kappa^2} - \frac{1}{2}\xi\phi^2\mathcal{R} - \frac{1}{2}(\nabla\phi)^2 - V(\phi)\right], \quad \text{with } V(\phi) = \frac{1}{2}m^2\phi^2 \text{ and } \kappa^2 \equiv \frac{8\pi}{{m_{\rm Pl}}^2}. \tag{8}$$

Futamase & Maeda [22] investigated how the nonminimal coupling term $(1/2)\xi\mathcal{R}\phi^2$ affects realization of chaotic inflation [23], and derived constraints on the coupling constant ξ from the condition for sufficient inflation. For the massive scalar model (8), they obtained $|\xi| \lesssim 10^{-3}$. Here we show that another type of inflation may be possible if $\xi < 0$, which relaxes the constraint on ξ.

Following Futamase & Maeda, we apply the conformal transformation and redefine a scalar field so that the model is described by the Einstein gravity with a canonical scalar field:

$$\hat{S} = \int d^4\hat{x}\sqrt{-\hat{g}}\left[\frac{\hat{\mathcal{R}}}{2\kappa^2} - \frac{1}{2}(\hat{\nabla}\hat{\phi})^2 - \hat{V}(\hat{\phi})\right], \quad \text{with } \hat{V}(\hat{\phi}) = \frac{V(\phi)}{(1+\psi)^2} \text{ and } \psi \equiv -\xi\kappa^2\phi^2. \tag{9}$$

Thanks to this standard form of the theory, we can discuss the qualitative behavior of $\hat{\phi}$ (or ϕ) in terms of the potential shape. We depict $\hat{V}(\hat{\phi})$ for $\xi < 0$ in Fig. 5. A distinguishing feature of this potential is that it has a maximum at $\hat{\phi} = \hat{\phi}_{\max}$ corresponding to $\psi = 1$ or $\phi = 1/\kappa\sqrt{-\xi} \equiv \phi_{\max}$. Hence, if the initial value of the scalar field, $\hat{\phi}_i$, is larger than $\hat{\phi}_{\max}$ and if the energy density of the scalar field $E_{\hat{\phi}} = \dot{\hat{\phi}}^2/2 + \hat{V}(\hat{\phi})$ is below $\hat{V}(\hat{\phi}_{\max})$, Φ cannot reach the origin $\hat{\phi} = \phi = 0$, but it will run away to infinity as long as the universe is expanding in the conformal frame with $\hat{H} > 0$. This runaway solution is irrelevant to our Universe, and Futamase & Maeda [22] obtained a constraint $|\xi| < 10^{-3}$ so that $\hat{\phi}_{\max} > 5m_{\rm Pl}$ and the initial value of $\hat{\phi}$ required for sufficient chaotic inflation $\hat{\phi}_i \sim 5m_{\rm Pl}$ lies on the left of the potential peak.

We can argue, however, that sufficient inflation may be possible even if $\hat{\phi}_{\max} < 5m_{\rm Pl}$ because the plateau around $\hat{\phi} = \hat{\phi}_{\max}$ may cause another channel of inflation. Seen in the conformal frame, some domains of the universe relax to $\hat{\phi} = 0$ and others run away to $\hat{\phi} \to \infty$ as the universe expands. In between these two classes of regions exist domain walls where large potential energy density $\hat{V}(\hat{\phi}_{\max})$ is stored. If the curvature of the potential is sufficiently small there, such domain walls will inflate. This is nothing but TDI.

Let us discuss whether inflation can take place at $\hat{\phi} = \hat{\phi}_{\max}$, following the arguments of Linde & Vilenkin [2]. The standard conditions for slow-roll inflation lead to

$$\frac{|\xi|}{1+3|\xi|} \ll \frac{3}{4}. \tag{10}$$

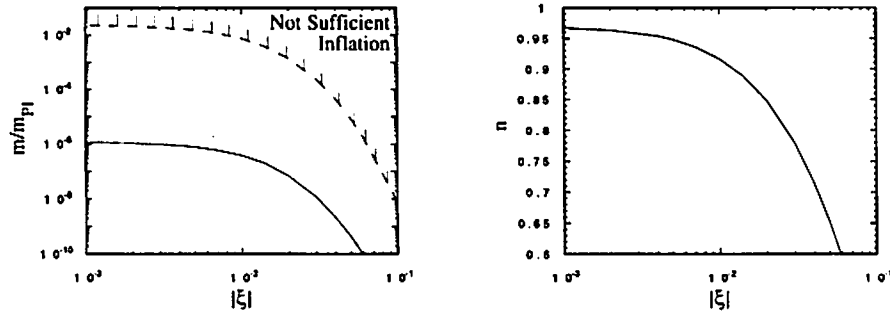

Figure 6: Constraints from COBE-normalized amplitudes of density perturbations. (a) Constraints on ξ and $m/m_{\rm Pl}$. The dashed curve is a constraint from sufficient inflation. The solid curve represents the concordant values with the amplitude of the COBE-DMR data. (b) The spectral indices of density perturbations.

A similar relation is derived from the condition that the thickness of the wall characterized by the curvature scale of the potential at the maximum, $\hat{R}_w$, is greater than the horizon, $\hat{H}^{-1}$:

$$\hat{R}_w \hat{H} = \sqrt{\frac{\kappa^2 \hat{V}(\hat{\phi}_{\rm max})}{3\hat{V}_{,\hat{\phi}\hat{\phi}}(\phi_{\rm max})}} = \sqrt{\frac{1+3|\xi|}{12|\xi|}} \gtrsim 1. \tag{11}$$

Inequalities (10) and (11) suggest that inflation actually takes place at the top of the potential if $|\xi| \ll 1$. Once inflation sets in, it continues forever inside a domain wall.

In order to obtain more precise conditions for sufficient inflation, we solve the (homogeneous and isotropic) field equations numerically. We assume initial values as $\hat{\phi}_i = \delta\hat{\phi}_{\rm Q} \equiv \hat{H}/2\pi$ and $(\hat{\phi}_{,i})_i = 0$, and observe the e-fold number of inflation after the classical dynamics dominates over quantum fluctuations, *i.e.*, $|\hat{\phi}_{,i}|/\hat{H} > \delta\hat{\phi}_{\rm Q}$. Sufficient expansion typically requires $a_f/a_c > e^{65}$, where c denotes the time when $|\hat{\phi}_{,i}|/\hat{H} = \delta\hat{\phi}_{\rm Q}$. The allowed region is plotted in Fig. 6(a). This shows that inflation continues sufficiently even if $|\xi| \cong 0.1$, contrary to the previous result [22].

Next, we investigate density perturbations generated during inflation, and constrain the model from the 4yr COBE-DMR data [20]. Because Makino & Sasaki [24] showed that the density perturbation in the original frame exactly coincides with that in the conformal frame, we can easily calculate the amplitude and the spectral index with the well-known formulas. The amplitude of perturbation is given as

$$\Phi_A\left(l = \frac{2\pi}{k}\right) = \frac{\sqrt{3}\kappa^3 \hat{V}^{\frac{3}{2}}}{10\pi \hat{V}_{,\hat{\phi}}} = \frac{\sqrt{3}\kappa^3 m\hat{\phi}^2\sqrt{1+(1-6\xi)\psi}}{20\sqrt{2}\pi(1-\psi^2)}. \tag{12}$$

The large-scale anisotropy of the cosmic microwave background measured by COBE-DMR leads to [20] $\delta T/T = \Phi_A/3 \cong 10^{-5}$. The concordant values of ξ and m are also plotted in Fig. 6(a).

The spectral index n is given as [21]

$$n - 1 \equiv \frac{d\ln\Phi_A^2}{d\ln k} = \frac{4}{\kappa^2\hat{\phi}^2}\left[-\frac{3(1-\psi)^2}{1+(1-6\xi)\psi} + \frac{1-6\psi-(5-35\xi)\psi^2+2(1-6\xi)\psi^3}{\{1+(1-6\xi)\psi\}^2}\right]. \tag{13}$$

The values of n which satisfy the COBE-DMR normalization are plotted in Fig. 6(b). With the observational data, $n = 1.2 \pm 0.3$ [20], we have a constraint $|\xi| \lesssim 10^{-2}$, which is still less stringent than the previous result [22].

Acknowledgments

I would like to thank Tomohiro Harada, Kei-ichi Maeda, Ken-ichi Nakao, and Jun'ichi Yokoyama, with whom the present work was done. Thanks are also due to Paul Haines for reading the manuscript. Numerical Computation of this work was carried out at the Yukawa Institute Computer Facility. I was supported by JSPS Research Fellowships for Young Scientist, No. 9702603.

References

[1] E.I. Guendelman & A. Rabinowitz, Phys. Rev. D. **44**, 3152 (1991).

[2] A. Linde, Phys. Lett. B **327**, 208 (1994); A. Vilenkin, Phys. Rev. Lett. **72**, 3137 (1994).

[3] N. Sakai, H. Shinkai, T. Tachizawa & K. Maeda, Phys. Rev. D **53**, 655 (1996).

[4] N. Sakai, Phys. Rev. D **54** 1548 (1996).

[5] J. Ellis, N. Kaloper, K.A. Olive & J. Yokoyama, Phys. Rev. D **59**, 103503 (1999); Izawa K.-I., M. Kawasaki & T. Yanagida, Prog. Theor. Phys. **101**, 1129 (1999).

[6] N. Sakai, K. Nakao & T. Harada, preprint gr-qc/9909027.

[7] N. Sakai, J. Yokoyama & K. Maeda, Phys. Rev. D **59**, 103504 (1999).

[8] N. Sakai & J. Yokoyama, Phys. Lett. B **456**, 113 (1999).

[9] For a review of spacetime solutions with non-Abelian fields, see, e.g., M.S. Volkov & D.V. Gal'tsov, preprint hep-th/9810070.

[10] M.E. Ortiz, Phys. Rev. D **45**, R2586 (1992); K. Lee, V.P. Nair & E.J. Weinberg, *ibid.* **45**, 2751 (1992); P. Breitenlohner, P. Forgàcs & D. Maison, Nucl. Phys. **B383**, 357 (1992); *ibid.* **B442**, 126 (1995).

[11] T. Tachizawa, K. Maeda & T. Torii, Phys. Rev. D **51**, 4054 (1995).

[12] A. Borde, M. Trodden & T. Vachaspati, Phys. Rev. D **59**, 43513 (1998); T. Vachaspati & M. Trodden, preprint gr-qc/9811037.

[13] T. Nakamura, K. Oohara & Y. Kojima, Prog. Theor. Phys. Suppl. **90**, 1 (1987).

[14] K. Sato, M. Sasaki, H. Kodama & K. Maeda, Prog. Theor. Phys. **65**, 1443 (1981); K. Sato, H. Kodama, M. Sasaki & K. Maeda, *ibid.* **108B**, 103 (1982).

[15] K. Sato, Mon. Not. Roy. Astron. Soc. **195**, 467 (1981); Phys. Lett. **99B**, 66 (1981); A.H. Guth, Phys. Rev. D **23**, 347 (1981).

[16] I. Cho & A. Vilenkin, Phys. Rev. D **56**, 7621 (1997).

[17] D. La & P.J. Steinhardt, Phys. Rev. Lett. **62**, 376 (1989).

[18] A. Starobinsky & J. Yokoyama, Proc. 4th Workshop on *General Relativity and Gravitation* eds. K. Nakao *et al.* (Yukawa Institute for Theoretical Physics), 381 (1994).

[19] J.M. Bardeen, Phys. Rev. D **22**, 1882 (1980).

[20] C.L. Bennet *et al.*, Astrophys. J. **464**, L1 (1996).

[21] A.R. Liddle & D.H. Lyth, Phys. Lett. B **291**, 391 (1992).

[22] T. Futamase & K. Maeda, Phys. Rev. D **39**, 399 (1989).

[23] A. Linde, Phys. Lett. B **129**, 177 (1983).

[24] N. Makino & M. Sasaki, Prog. Theor. Phys. **86**, 103 (1991).

False Vacuum Decay with Gravity in Non-Thin-Wall Limit

Uchida Gen,[1] Misao Sasaki[2]

Osaka University, Toyonaka 560-0043, Japan

Department of Physics, The University of Tokyo, Tokyo 113-0033, Japan

Abstract

We consider a wave-function approach to the false vacuum decay with gravity and present a new method to calculate the tunneling amplitude under the WKB approximation. The result agrees with the one obtained by the Euclidean path-integral method, but gives a much clearer interpretation of an instanton (Euclidean bounce solution) that dominates the path integral. In particular, our method is fully capable of dealing with the case of a thick wall with the radius of the bubble comparable to the radius of the instanton, thus surpassing the path-integral method whose use can be justified only in the thin-wall and small bubble radius limit. The calculation is done by matching two WKB wave functions, one with the final state and another with the initial state, with the wave function in the region where the scale factor of the metric is sufficiently small compared with the inverse of the typical energy scale of the field potential at the tunneling. The relation of the boundary condition on our wave function for the false vacuum decay with Hartle-Hawking's no-boundary boundary condition and Vilenkin's tunneling boundary condition on the wave function of the universe is also discussed.

1 Introduction

In the previous literature, the false vacuum decay with gravity was investigated, in essence, by a naive extrapolation of well-established methods used for the Minkowski background[2]. There are two methods to calculate the decay rate of false vacuum, one using the Euclidean path integral and the other constructing a WKB wave function. However, in both approaches such extrapolation is valid only for a tunneling potential $V(\phi)$ satisfying the thin-wall condition (we shall come back to this point below).

The false vacuum decay in quantum field theory on the Minkowski background is analyzed in the semiclassical way (i.e., in the WKB approximation) as follows[3]. First, the Euclidean classical equation of motion for the field ϕ is solved by assuming the $O(4)$ symmetry on the field configuration with the boundary condition that the solution is regular at the origin and asymptotically approaches the false vacuum at infinite radius. There will be two such solutions; one trivially sitting at the false vacuum and the other that leaves the origin from a field value near the true vacuum and goes over the potential barrier. We call the former the false vacuum instanton and the latter the bounce instanton. We can take either the path-integral approach or the wave-function approach.

In the path-integral approach, we sum up the contribution of instantons and fluctuations around them to obtain the tunneling amplitude or the decay rate of false vacuum. If we denote the Euclidean action of the false vacuum instanton by S_F and that of the bounce instanton by S_B, the decay rate is given by $\Gamma \sim e^{-(S_B - S_F)}$.

In the wave-function approach, we construct a one-parameter family of 3-dimensional field configurations from the everywhere-false-vacuum configuration to the configuration with the true vacuum bubble about to expand in the false vacuum sea (the critical bubble configuration). Then, exponentiating the action of these configurations we obtain the WKB wave function(al) describing the tunneling of the field from the false vacuum state to the state of the critical bubble [4]. Then the tunneling amplitude is obtained by taking the square of the ratio of the final state wave function to the initial state wave function, which is also given by $e^{-(S_B - S_F)}$.

[1] E-mail:gen@vega.ess.sci.osaka-u.ac.jp
[2] E-mail:misao@vega.ess.sci.osaka-u.ac.jp

Since these two different approaches give the same result, and since there is one-to-one correspondence between a classical solution and a WKB wave function, we may justify the interpretation of the bounce instanton as describing the tunneling process and its analytic continuation to the Lorentzian space-time as describing the classical configuration of the field after false vacuum decay.

A trouble arises when one attempts to extrapolate the above procedure to the case of false vacuum decay with gravity. First, the scalar field equation is now coupled with the Friedmann equation that governs the scale factor of the $O(4)$ symmetric metric. Second, and most problematically, the 4-dimensional Euclidean space becomes inevitably compact with topology of S^4 when gravity is taken into account (we assume $V(\phi_F) > 0$ where ϕ_F is the field value at the false vacuum and a potential of the shape depicted in Fig. 1), i.e., not $\mathbb{R}^4$ as in the case of flat space-time. Of course a bounce solution still exists in the presence of gravity, first obtained by Coleman and DeLuccia[2]. However, there will be no bounce solution that admits a 3-dimensional slice on which the field is *asymptotically* at false vacuum everywhere; an instanton leaving, say, the north pole of S^4 from the true vacuum side does not reach the false vacuum when arriving even at the south pole. Furthermore, the standard dilute gas approximation to obtain the decay rate in the path-integral approach, in which the 4-volume occupied by a vacuum bubble is assumed to be negligible compared with the whole Euclidean 4-volume, fails.

Nevertheless, there is one special case in which the extrapolation can be almost justified. It is the thin-wall limit[6]. In this case, the field ϕ, which is sitting on the true vacuum side of the barrier at the north pole, varies abruptly at the position of the bubble wall sharply located in the northern hemisphere and $\phi = \phi_F$ everywhere outside the bubble. Then, the solution admits a maximal 3-surface on which the extrinsic curvature of the 3-surface vanishes and $\phi = \phi_F$ everywhere. Through this surface, we can analytically continue to the Lorentzian solution that describes the false vacuum state. The critical bubble configuration that describes the moment of bubble nucleation is also a maximal 3-surface, and analytic continuation through the surface gives the space-time with an expanding bubble. Thus we obtain a one-parameter family of 3-dimensional configurations that interpolates between the false vacuum and critical bubble configurations.

However, only a very restricted class of potentials admits bounce instantons in the thin-wall limit. Namely, the ratio of the mass scale m of the curvature at the top of the potential barrier, $m^2 = -d^2V/d\phi^2(\phi_{top})$, to the typical mass scale M of the potential energy density must be very large (rigorously speaking, it must be infinitely large in the exact thin-wall limit). In other words, the barrier must be extremely sharply peaked. We note that this is somewhat different from the definition of the thin-wall limit originally discussed by Coleman and DeLuccia[2]. In our definition, since the Euclidean 4-volume is proportional to $(GM^4)^{-2}$ while the 4-volume of a bubble is $O(m^{-4})$, the thin-wall limit implies small bubble radius, provided M is smaller than the Planck scale, i.e., $GM^2 < 1$. Field potentials with such a feature are apparently not general. However, previous discussions on the false vacuum decay with gravity have been relied on the picture of a bounce instanton having the feature of the thin-wall limit. For example, it is widely believed that the formula $\Gamma \sim e^{-(S_B - S_F)}$ is still valid even when the bounce solution does not have the thin-wall feature at all. Furthermore, the interpretation of such a bounce as describing the tunneling process and describing the classical evolution from the critical bubble state has been adopted without serious considerations.

In this paper, we propose a new method to calculate the wave function describing false vacuum decay with gravity, which is not restricted to the thin-wall limit. Our method gives a picture of tunneling substantially different from that in the Minkowski background, but nevertheless our wave function interpolates between the false vacuum state, which is described by the trivial instanton sitting at false vacuum, and the state at the bubble nucleation, which is a maximal 3-slice containing the critical bubble of the bounce solution.

In the rest of the paper, we keep $\hbar$ and G explicit to clarify the WKB order as well as the effect of gravity.

2 Formulation

In this section, we describe our method to construct a relevant classical path in the Euclidean regime that determines the WKB tunneling wave function.

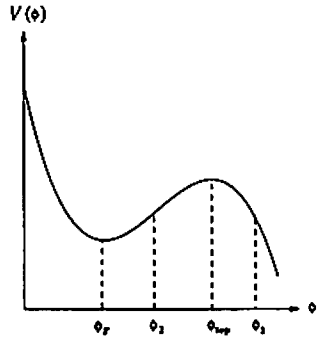

Figure 1: A schematic picture of the potential $V(\phi)$ of a scalar field discussed in the text.

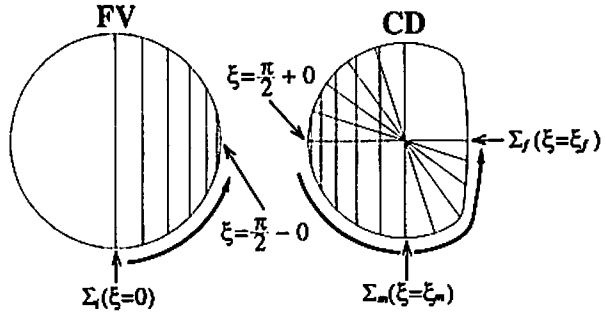

Figure 2: Schematic pictures of the false vacuum (FV) instanton and the Coleman-DeLuccia (CD) instanton with 2-dimensions suppressed. The arrow indicates the direction of the increase in the parameter ξ defined in the text.

2.1 Instantons and WKB approximation

We consider the action,

$$S = \int d^4x\sqrt{g}\left[\frac{\mathcal{R}}{24\pi^2\kappa} - \frac{1}{2}g^{\mu\nu}\partial_\mu\phi\partial_\nu\phi - V(\phi)\right], \tag{1}$$

where $\kappa := 2G/3\pi$, and the potential $V(\phi)$ as illustrated in Fig. 1. We confine our attention to WKB wave functions that are described by classical solutions having $O(4)$ symmetry. Hence we consider the metric in the form, $ds^2 = -N^2(t)dt^2 + a^2(t)d\Omega^2_{(3)}$ in which $d\Omega^2_{(3)}$ is the metric on a unit 3-sphere, and $\phi = \phi(t)$. Then the Wheeler-DeWitt equation is written down as

$$\frac{\kappa}{2a}\left[h^2\frac{\partial^2}{\partial a^2} + h^2\frac{p}{a}\frac{\partial}{\partial a} - \frac{h^2}{(2\pi^2\kappa)\,a^2}\frac{\partial^2}{\partial\phi^2} - \frac{a^2}{\kappa^2}Q(a,\phi)\right]\Psi = 0, \quad \text{where} \quad Q(a,\phi) = 1 - (4\pi^2\kappa)\,a^2V(\phi), \tag{2}$$

and p is an arbitrary constant that determines the operator-ordering; $p = 1$ corresponds to making the ordering covariant with respect to the superspace metric (see [1]).

The construction of a WKB wave function describing multi-dimensional quantum tunneling was discussed much in the literature [4] and reformulated in a covariant manner in [5]. Given a one-parameter family of configurations that satisfies the Euclidean equations of motion, the WKB wave function along the family can be obtained with this method. Following this method, we first express the wave function in the form, $\Psi = \exp[-W_0(a,\phi)/h - W_1(a,\phi) + \cdots]$. Then at the lowest WKB order, we have

$$\left\{\frac{\kappa}{a}\left(\frac{\partial W_0}{\partial a}\right)^2 - \frac{1}{2\pi^2a^3}\left(\frac{\partial W_0}{\partial\phi}\right)^2\right\} - \frac{a}{\kappa}Q(a,\phi) = 0, \tag{3}$$

which is, of course, free from the operator-ordering ambiguity.

Introducing a parameter τ such that

$$\frac{da(\tau)}{d\tau} := -\frac{\kappa}{a}\frac{\partial W_0}{\partial a} \qquad \text{and} \qquad \frac{d\phi(\tau)}{d\tau} =: \frac{1}{2\pi^2a^3}\frac{\partial W_0}{\partial\phi}, \tag{4}$$

we find

$$\frac{d}{d\tau}W_0(a,\phi) = -\frac{a}{\kappa}Q(a,\phi). \tag{5}$$

The Euclidean equations of motion for $O(4)$ symmetric configurations, $(a(\tau),\phi(\tau))$, with the choice of the lapse $N = 1$ are obtained from Eqs. (3), (4) and (5) as

$$\dot{a}^2 - (2\pi^2\kappa)a^2\dot{\phi}^2 - Q(a,\phi) = 0, \qquad \ddot{\phi} + 3\frac{\dot{a}}{a}\dot{\phi} = \frac{dV}{d\phi}, \qquad a\ddot{a} + 2\dot{a}^2 + 1 = 3Q(a,\phi). \tag{6}$$

The first equation is the (Euclidean) Friedmann equation that corresponds to the energy integral of the remaining two equations. The regularity of the solution requires $\dot{\phi} = 0$ at $a = 0$.

Equation (5) readily gives the relative amplitudes of the leading-order WKB wave function at two different configurations at $\tau = \tau_1$ and τ_2.

$$\Psi(\tau_2) = \exp\left[-W_0(\tau_2;\tau_1)\right]\Psi(\tau_1); \quad W_0(\tau_2;\tau_1) = -\frac{1}{\kappa}\int_{\tau_1}^{\tau_2} d\tau'\, a(\tau')Q\left(a(\tau'),\phi(\tau')\right). \tag{7}$$

As is well-known, $W_0(\tau_2;\tau_1)$ is just the Euclidean action integral of the system from the configuration at τ_1 to that at τ_2.

The solutions relevant to our discussion are the trivial solution sitting at the false vacuum and the bounce instanton. The trivial instanton is explicitly given by $(a^{FV}(\tau),\phi^{FV}(\tau)) = (H_F^{-1}\sin(H_F\tau),\phi_F)$; $\tau \in [0,\pi/H_F]$, where $H_F = 2\pi\sqrt{\kappa V(\phi_F)}$. We call it the false vacuum (FV) instanton hereafter. The bounce instanton is known as the Coleman-DeLuccia (CD) instanton [2, 6]. We denote it by $(a^{CD}(\tau),\phi^{CD}(\tau))$ with $\tau \in [\tau_1,\tau_2]$. For later convenience, we set $(a^{CD}(\tau_1),\phi^{CD}(\tau_1)) = (0,\phi_1)$ where ϕ_1 is on the true vacuum side of the barrier, and $(a^{CD}(\tau_2),\phi^{CD}(\tau_2)) = (0,\phi_2)$ where ϕ_2 is on the false vacuum side of the barrier. See Fig. 1. The FV and CD instantons embedded in $\mathbb{R}^5$ are schematically shown in Fig. 2 with 2-dimensions suppressed.

2.2 One-parameter family of tunneling configurations

As we noted in Introduction, the CD instanton itself does not admit a maximal 3-surface on which $\phi = \phi_F$ everywhere, unless the potential satisfies the thin-wall condition. Hence the CD instanton alone cannot describe the tunneling wave function. It is then natural to suppose that the FV instanton plays a role as well. In fact, there is already a hint in the formula for the decay rate, $\Gamma \sim e^{-(S_B-S_F)/\hbar}$, valid in the thin-wall limit, where the action of the FV instanton comes into play.

We therefore consider a possibility to construct a one-parameter family of spatial configurations that connect the false vacuum state and the critical bubble state by matching these two instantons. We combine and re-organize the $O(4)$ symmetric families of configurations of the two instantons discussed in the previous subsection to a one-parameter family of configurations which adequately describes the false vacuum decay. We denote this one-parameter family by $(h_{ij}(x^i;\xi),\phi(x^i;\xi))$ where ξ is a non-dimensional parameter. The parameter ξ is assumed to run through a range $[0,\xi_f]$ with the initial $(\xi = 0)$ and final $(\xi = \xi_f)$ configurations given by the the maximal 3-slice of the FV instanton and the critical bubble configuration of the CD instanton, respectively.

The initial configuration, denoted by Σ_i in Fig. 2, is given by $H_F\tau = \pi/2$. We thus set $\xi = H_F\tau - \pi/2$ until the scale factor a vanishes, $(h_{ij}(x^i;\xi),\phi(x^i;\xi)) = (H_F^{-2}\sin^2(\xi+\pi/2)d\Omega^2_{(3)},\phi_F)$ $\xi \in [0,\pi/2)$.

We match $a = 0$ of the above to the point $(a^{CD},\phi^{CD}) = (0,\phi_2)$ of the CD instanton, where ϕ_2 is the field value at the 'south pole', see Figs. 1 and 2. Note that the values of ϕ are different at these two points where the WKB breaks down. However, as we shall see in the next section, this will not be an obstacle since the wave function will be independent of ϕ in the vicinity of $a = 0$.

For $\xi > \pi/2$, we take the $O(4)$ symmetric configurations of the CD instanton up to the slice Σ_m shown in Fig. 2, where Σ_m is the $O(4)$ symmetric slice at $\dot{a}^{CD} = 0$ where the 3-volume is maximum, which we denote by $(h_{ij},\phi) = (H_m^{-2}d\Omega^2_{(3)},\phi_m)$. Thus, $(h_{ij}(x^i;\xi),\phi(x^i;\xi)) = (a^{CD}(\xi)d\Omega^2_{(3)},\phi^{CD}(\xi);\ \xi \in (\frac{\pi}{2},\xi_m]$, where $(a^{CD}(\pi/2),\phi^{CD}(\pi/2)) = (0,\phi_2)$, $\quad(a^{CD}(\xi_m),\phi^{CD}(\xi_m)) = (H_m^{-1},\phi_m)$.

For $\xi > \xi_m$, we slice the CD instanton in such a way that all of the configurations contain the common 2-sphere the slice Σ_m and the final slice Σ_f of the critical bubble configuration intersect. These slices do not respect the $O(4)$ symmetry but are analogous to the static slices of the de Sitter space of radius H^{-1}. As mentioned above, we label the final configuration by $\xi = \xi_f$. Thus $(h_{ij}(\xi_f),\phi(\xi_f)) =$ (the critical bubble 3-geometry).

As it is clear from the above construction, the lapse function N vanishes at Σ_m, and the geometry is degenerate there. However, this will not be a problem since we have started from the Wheeler-DeWitt equation (2), in which the dynamical variables are $(h_{ij}(x^i),\phi(x^i))$ of a 3-geometry. Hence, although the lapse function plays a role when a Euclidean classical solution is considered, the vanishing of it is irrelevant to our discussion (in this connection, see [8]).

3 Tunneling wave function

Let us now construct the tunneling wave function. Since we are interested in the false vacuum decay, we want the wave function to describe the *expanding* universe after tunneling. Thus the appropriate boundary condition for the wave function is the tunneling boundary condition, which demands the wave function describing the classical universe after tunneling to have a positive eigenvalue for the momentum operator $P_a = -ih\partial/\partial a$ [7].

In accordance with the construction of the classical path given in the previous section, we assume the universe after tunneling is described by analytic continuation of the CD instanton through the critical bubble configuration. We choose the moment of nucleation ($\xi = \xi_f$) as $t = \tau = 0$. Thus we set

$$\Psi(\xi > \xi_f) = N \exp\left[\frac{i}{h}\int_0^{t(\xi)} dt' L^{CD}(t') + i\frac{\pi}{4}\right], \tag{8}$$

where N is a normalization constant and $L^{CD}(t)$ is the Lagrangian of the Lorentzian CD solution. The phase $\pi/4$ is inserted for convenience, and we have neglected the prefactor arising from the next WKB order. Then, the standard WKB connection formula gives the under-barrier wave function for $\xi \in (\pi/2, \xi_f]$ as

$$\Psi(\pi/2 < \xi < \xi_f) = N \exp\left[\frac{1}{h}\int_{\tau(\xi)}^{0} d\tau' L_E^{CD}(\tau')\right] + \frac{i}{2} N \exp\left[-\frac{1}{h}\int_{\tau(\xi)}^{0} d\tau' L_E^{CD}(\tau')\right], \tag{9}$$

where $L_E^{CD}(\tau)$ is the Euclidean Lagrangian of the CD solution.

For $\xi \in (\pi/2, \xi_m]$ where the 3-geometries are $O(4)$ symmetric, we have from Eq. (7),

$$\int_{\tau(\xi)}^{0} d\tau' L_E^{CD}(\tau') = W_0(\xi_f; \pi/2) - W_0(\xi; \pi/2) = \frac{S_B}{2} - W_0(\xi; \pi/2), \tag{10}$$

where S_B is the total action of the CD bounce instanton and

$$W_0(\xi; \pi/2) = -\frac{1}{\kappa}\int_{\tau(\pi/2)}^{\tau(\xi)} d\tau' a^{CD}(\tau') Q\left(a^{CD}(\tau'), \phi^{CD}(\tau')\right) =: W_0^{CD}(\xi), \tag{11}$$

where $a^{CD}(\tau(\pi/2)) = 0$. Hence

$$\Psi(\pi/2 < \xi < \xi_m) = A \exp\left[-\frac{1}{h} W_0^{CD}(\xi)\right] + B \exp\left[\frac{1}{h} W_0^{CD}(\xi)\right] \tag{12}$$

where the coefficients A and B are given by $A = N e^{S_B/2h}$, $B = \frac{i}{2} N e^{-S_B/2h}$. Likewise, the WKB wave function for $\xi \in (0, \pi/2)$ is expressed as

$$\Psi(0 < \xi < \pi/2) = C \exp\left[-\frac{1}{h} W_0^{FV}(\xi)\right] + D \exp\left[\frac{1}{h} W_0^{FV}(\xi)\right], \tag{13}$$

$$\text{where} \quad W_0^{FV}(\xi) := W_0(\pi/2; \xi) = -\frac{1}{\kappa}\int_{\tau(\xi)}^{\pi/H_F} d\tau' a^{FV}(\tau') Q\left(a^{FV}(\tau'), \phi_F\right), \tag{14}$$

and C and D are constants and

We consider the matching of the above wave functions in a region $a \sim 0$. Noting that $V(\phi) \geq V(\phi_F)$ in the vicinity of $\xi = \pi/2$, it is convenient to introduce a re-scaled (non-dimensional) scale factor,

$$\hat{a} := \epsilon \frac{a}{\ell_{pl}} \quad \text{where} \quad \epsilon := 2\pi\sqrt{\frac{h^4 V(\phi_F)}{m_{pl}^4}}, \tag{15}$$

and $\ell_{pl} := \sqrt{h\kappa} = \sqrt{2hG/3\pi}$ is the Planck length and $m_{pl} := \sqrt{h/\kappa} = \sqrt{3\pi h/2G}$ the Planck mass. We assume the potential energy scale is much below the Plank scale, $\epsilon \ll 1$.

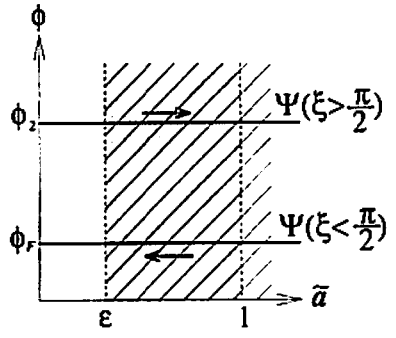

Figure 3: The superspace $(\tilde{a},\phi)$ near the matching region. The thick lines are $(h_{ij}(\xi),\phi(\xi))$ in the range $\xi\in[0,\pi/2)$ and $\xi\in(\pi/2,\xi_f]$. The arrow indicates the direction of increase in ξ along the family. The WKB approximation and the wave function (19) are, repspectively, valid in the hatched and the grayed region. The overlapping region is where the matching is performed.

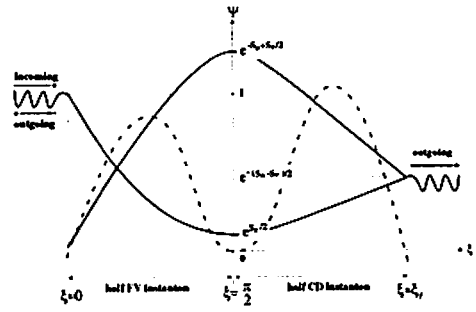

Figure 4: A schematic behavior of the tunneling wave function. The point $\xi=\pi/2$ is where the scale factor a vanishes, and towards both right and left directions from there the 3-volume increases. The dotted curve indicates the effective potential barrier.

In the region $a\ll 1/(2\pi\sqrt{\kappa V(\phi_F)})$, which corresponds to $\tilde{a}\ll 1$, $Q(a,\phi)$ is independent of ϕ; $Q\approx 1$, but the WKB approximation is valid as long as $\tilde{a}\gg\epsilon$. Hence, $W_0^{CD}(\xi)$ and $W_0^{FV}(\xi)$ in this region reduce to the same form, $W_0^{CD}(\xi)=W_0^{FV}(\xi)=-\frac{a^2(\xi)}{2\kappa}=-h\frac{\tilde{a}^2(\xi)}{2\epsilon^2}$. The prefactor due to the first-order WKB correction is calculated to be (see [1]) $\exp(-W_1)=\tilde{a}^{-\frac{p+1}{2}}\times$ const. Although we are not interested in this first order correction, we recover it in the region $\epsilon\ll\tilde{a}\ll 1$ to show explicitly that the matching we perform below is independent of the operator-ordering. Thus the WKB wave function in the region $\epsilon\ll\tilde{a}\ll 1$ becomes

$$\Psi(\xi>\pi/2) = A\tilde{a}^{-\frac{p+1}{2}}\exp\left[+\frac{\tilde{a}^2(\xi)}{2\epsilon^2}\right]+B\tilde{a}^{-\frac{p+1}{2}}\exp\left[-\frac{\tilde{a}^2(\xi)}{2\epsilon^2}\right], \tag{16}$$

$$\Psi(\xi<\pi/2) = C\tilde{a}^{-\frac{p+1}{2}}\exp\left[+\frac{\tilde{a}^2(\xi)}{2\epsilon^2}\right]+D\tilde{a}^{-\frac{p+1}{2}}\exp\left[-\frac{\tilde{a}^2(\xi)}{2\epsilon^2}\right]. \tag{17}$$

To match these two wave functions, we directly solve the Wheeler-DeWitt equation in the region $0<\tilde{a}\ll 1$ and compare the coefficients in the region $\epsilon\ll\tilde{a}\ll 1$. See Fig. 3. In terms of $\tilde{a}$, the Wheeler-DeWitt equation (2) reduces to

$$\left[\frac{\partial^2}{\partial\tilde{a}^2}+\frac{p}{\tilde{a}}\frac{\partial}{\partial\tilde{a}}-\frac{\tilde{a}^2}{\epsilon^4}\right]\Psi=0. \tag{18}$$

The general solution is $\Psi(\tilde{a},\phi)=\pi^{1/2}E\tilde{a}^{2\nu}I_\nu(\frac{\tilde{a}^2}{2\epsilon^2})+\pi^{-1/2}F\tilde{a}^{2\nu}K_\nu(\frac{\tilde{a}^2}{2\epsilon^2})$, where $\nu=(1-p)/4$, E and F are constants, and $I_\nu(z)$ and $K_\nu(z)$ are the modified Bessel functions. The asymptotic form of this wave function at $\tilde{a}\gg\epsilon$ is given by

$$\Psi(\tilde{a},\phi)=\left[\epsilon E\tilde{a}^{-\frac{p+1}{2}}\exp\left[+\frac{\tilde{a}^2}{2\epsilon^2}\right]+\epsilon(E\epsilon^{(\nu+\frac{1}{2})\pi i}+F)\tilde{a}^{-\frac{p+1}{2}}\exp\left[-\frac{\tilde{a}^2}{2\epsilon^2}\right]\right](1+O(\frac{2\epsilon^2}{\tilde{a}^2})). \tag{19}$$

Since Eqs. (16) and (17) have exactly the same $\tilde{a}$ dependence, the comparison of them with (19) readily gives $A=\epsilon E=C$, $B=\epsilon(E\epsilon^{(\nu+\frac{1}{2})\pi i}+F)=D$, independently of the choice of the operator-ordering.

Plugging this result into Eq. (13), we find the wave function for $\xi\in(0,\pi/2)$ as

$$\Psi(0<\xi<\pi/2)=N\epsilon^{S_B/2\hbar}\exp\left[-\frac{1}{\hbar}W_0^{FV}(\xi)\right]+\frac{i}{2}N\epsilon^{-S_B/2\hbar}\exp\left[\frac{1}{\hbar}W_0^{FV}(\xi)\right]. \tag{20}$$

Noting the fact $W_0^{FV}(0) = S_F/2$, we connect this to the Lorentzian region $\xi < 0$ of the false vacuum to obtain

$$\Psi(\xi < 0) = Ne^{(S_B - S_F)/2\hbar}(e^{iW_L^{FV}(t)/\hbar} + e^{-iW_L^{FV}(t)/\hbar}) + \frac{i}{2}Ne^{-(S_B - S_F)/2\hbar}(e^{iW_L^{FV}(t)/\hbar} + e^{-iW_L^{FV}(t)/\hbar}). \quad (21)$$

where $W_L^{FV}(t) := \int_0^{t(\xi)} dt' L^{FV}(t')$. Since $S_B > S_F$, the first two terms in the brackets dominate. Thus, the tunneling amplitude Γ of the false vacuum decay is found to be

$$\Gamma \sim \frac{|\Psi(\xi_f)|^2}{|\Psi(0)|^2} = \exp\left[-\frac{1}{\hbar}(S_B - S_F)\right]. \quad (22)$$

This agrees with the result in the thin-wall limit. The overall behavior of the wave function is shown schematically in Fig.4, in which the normalization constant N is chosen to be $\exp[-(S_B - S_F)/2\hbar]$ so that the amplitude of the wave function at the false vacuum equals unity.

4 Discussion and conclusion

We have presented a new method to calculate the tunneling wave function that describes the false vacuum decay with gravity. In this method, the tunneling wave function is constructed by matching the false vacuum (FV) instanton and the Coleman-DeLuccia (CD) instanton through the point at which the scale factor vanishes. We found the resulting tunneling amplitude agrees with the naive extrapolation of the formula whose validity had been justified only in the thin-wall limit or in the flat background. Our result is a strong support for the standard interpretation that analytic continuation through the critical bubble configuration of the CD instanton describes the universe after false vacuum decay.

In our picture, the false vacuum decay with gravity becomes more or less quantum cosmological. For example, as can be seen from Fig. 4, interpreting the wave function as describing the actual tunneling path, the tunneling under consideration is quite similar to a case of standard quantum tunneling with a resonant state inside the barrier, except for the sign of the Euclidean actions S_F and S_B which are negative. The difference is that the resonant state here is not a state of something but the state of 'nothing'. This gives us a very interesting picture that the false vacuum decay is first proceeded by pumping up the amplitude in the state of nothing and subsequently a universe with an expanding bubble is created from nothing.

A similar idea of joining the two instantons was previously proposed by Bousso and Chamblin in the context of path-integral approach[9]. But the principles behind his approach and ours seem rather different. Our method is completely within the scope of the standard WKB approximation, while they had to introduce a Planck size wormhole and reverse the sign the 4-volume after traversing the wormhole in an ad hoc way. Nevertheless, it is of interest to see if these two methods correspond to each other at certain level of approximations. Recently, Rubakov and Sibiryakov proposed another method to deal with the false vacuum decay with gravity[10], by considering complex paths and adding a constraint to the action to realize the initial false vacuum state. It is, however, not clear how the complex path they considered joins the false vacuum and the critical bubble configuration, particularly because of the constraint that modifies the equations of motion.

We have demanded the wave function to have only the component describing an expanding universe after false vacuum decay. In this respect, our boundary condition is very similar to the tunneling boundary condition proposed by Vilenkin [7] in the context of quantum cosmology. However, in Vilenkin's picture, only the wave function for an expanding universe appears in the Lorentzian region of the superspace. This means there is a steady flux coming out from the Euclidean boundaries of the superspace. On the other hand, our wave function is outgoing only for the universe after false vacuum decay. Indeed, along the line $\phi = \phi_F$ in the superspace, where the universe is in the false vacuum, our wave function has both expanding and contracting components. See Fig. 5. The latter feature is similar to the one of the Hartle-Hawking wave function [11]. See Fig. 4: If we consider only the right-hand side ($\xi > \pi/2$) of the figure, the amplitude at $a = 0$ ($\xi = \pi/2$) is dominated by the component that decreases exponentially as a increases, as is the case of the Vilenkin wave function. On the other hand, if we consider only the left-hand side ($\xi < \pi/2$) of the figure, our wave function can be approximately regarded as a Hartle-Hawking wave function. The exponentially decreasing component becomes totally negligible when it

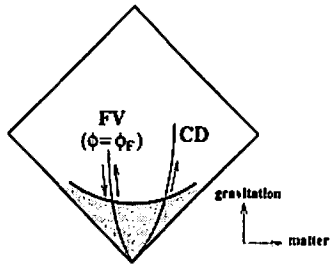

Figure 5: Schematic picture of the causal structure of superspace and the one-parameter family of configurations used to construct the wave function. The Euclidean region is shaded. The lines indicated by FV and CD correspond to the configurations of the false vacuum and Coleman-DeLuccia solutions, respectively. The up or down arrows along the lines indicate the expanding or contracting components contained in the wave function.

appears in the Lorentzian region, hence it is an irrelevant component, while the exponentially increasing component dominates the wave function in the Lorentzian region, which consists of both outgoing and ingoing components with equal weight.

We have considered only the leading order behavior of the WKB wave function. We need to analyze the next order to determine the quantum state of fluctuations after tunneling. It seems, however, that there is no reason to expect the result should differ from the ones obtained previously under the assumption of the Euclidean vacuum associated with the CD instanton. This is because all the properties of the quantum fluctuations are determined by the Euclidean structure of a single classical solution, which is the CD instanton, as far as we are interested only in the state after false vacuum decay: The quantum fluctuations around the CD instanton is completely decoupled from those around the FV instanton. Then once we focus only on the CD instanton, our wave function satisfies the outgoing boundary condition, and it is known to give the Euclidean vacuum state[12]. This reassures the validity of previous calculations of quantum fluctuations in the one-bubble open inflation scenario[13].

Acknowledgment

We would like to thank J. Garriga and T. Tanaka for useful discussions and comments at the early stages of this work. This work was supported in part by the Monbusho Grant-In-Aid for Scientific Research, No. 09640355.

References

[1] U. Gen and M.Sasaki, gr-qc/9912096

[2] S. Coleman and F. De Luccia, Phys. Rev. D **21**, 3305 (1980)

[3] S. Coleman, Phys. Rev. D **15**, 2929 (1977)

[4] T. Banks, C.M. Bender and T.T. Wu, Phys. Rev. D **8**, 3346 (1973); T. Banks and C.M. Bender, *ibid.* **8**, 3366 (1973); J.L. Gervais and B. Sakita, *ibid.* **15**, 3507 (1977); K.M. Bitar and S.J. Chang, *ibid.* **18**, 435 (1978)

[5] T. Tanaka, M.Sasaki and K.Yamamoto, Phys. Rev. D **49**, 1039 (1994)

[6] L.G. Jensen and P.J. Steinhardt, Nucl. Phys. **B237**, 176 (1984)

[7] A. Vilenkin, Phys. Rev. D **30**, 509 (1984); A. Vilenkin, Phys. Rev. D **33**, 3560 (1986)

[8] W. Fischler, D.Morgan and J. Polchinski, Phys. Rev. D **42** (1990)

[9] R. Bousso and A. Chamblin, Phys. Rev. D **59**, 084004 (1999)

[10] V.A. Rubakov and S.M.Sibiryakov, gr-qc/9905093

[11] J.B. Hartle and S.W. Hawking, Phys. Rev. D **28**, 2960 (1983)

[12] T. Vachaspati and A. Vilenkin, Phys. Rev. D **37**, 898 (1988)

[13] J. Garriga, X. Montes, M. Sasaki and T. Tanaka, Nucl.Phys. **B513**, 343 (1998); *ibid.* **B551**, 317 (1999)

An Open Universe from Valley Bounce

Kazuya Koyama[1]

Graduate School of Human and Environment Studies,
Kyoto University, Kyoto 606-8501, Japan

Kayoko Maeda[2] Jiro Soda[3]

Department of Fundamental Sciences, FIHS, Kyoto University,
Kyoto, 606-8501, Japan

Abstract

It appears difficult to construct a simple model for an open universe based on the one bubble inflationary scenario. The reason is that one needs a large mass to avoid the tunneling via the Hawking Moss solution and a small mass for successful slow-rolling. However, Rubakov and Sibiryakov suggest that the Hawking Moss solution is not a solution for the false vacuum decay process since it does not satisfy the boundary condition. Hence, we have reconsidered the arguments for the defect of the simple polynomial model. We find the valley bounce belonging to a valley line in the functional space represents the decay process instead of the Hawking Moss solution. The point is that the valley bounce gives the appropriate initial condition for the inflation. We show an open inflation model can be constructed within the polynomial form of the potential so that the fluctuations can be reconciled with the observations. Details of the analysis can be seen in Ref.[1].

1 Introduction

Recent observations suggest the matter density of the universe is less than the critical density. Hence, it is desirable to have a model for an open universe, say $\Omega_0 \sim 0.3$. The realization of an open universe is difficult in the ordinary inflationary scenario. This is because if the universe expands enough to solve the horizon problem, the universe becomes almost flat. One attempt to realize an open universe in the inflationary scenario is to consider inside the bubble created by the false vacuum decay [2]. The scenario is as follows. Consider the potential which has two minimum. One is the false vacuum which has non-zero energy and the other is the true vacuum. Initially the field is trapped at the false vacuum. Due to the potential energy, universe expands exponentially and the large fraction of the universe becomes homogeneous. As the false vacuum is unstable, it decays and creates the bubble of the true vacuum. If the decay process is well suppressed, the interior of the bubble is still homogeneous. The decay is described by the $O(4)$ symmetric configuration in the Euclidean spacetime. Then, analytical continuation of this configuration to the Lorentzian spacetime describes the evolution of the bubble which looks from the inside like an open universe. Unfortunately, since the bubble radius cannot be greater than the Hubble radius, the created universe is curvature dominated even if the whole energy of the false vacuum is converted to the energy of the matter inside the bubble [3]. Thus, the second inflation in the bubble is needed. If this second inflation stopped when $\Omega < 1$, our universe becomes homogeneous open universe.

Though the basic idea is simple, the realization of this scenario in a simple model has been recognized difficult [4]. The difficulty is usually explained as follows. Consider the model involving one scalar field. For the polynomial form of the potential like $V(\phi) = m^2\phi^2 - \delta\phi^3 + \lambda\phi^4$, the tunneling should occur at sufficiently large ϕ to ensure that the second inflation gives the appropriate density parameter. Then,

[1]E-mail:kazuya@phys.h.kyoto-u.ac.jp
[2]E-mail:maeda@phys.h.kyoto-u.ac.jp
[3]E-mail:jiro@phys.h.kyoto-u.ac.jp

the curvature around the barrier which separates the false and the true vacuum is small compared with the Hubble scale which is determined by the energy of the false vacuum. In this case, the field jumps up onto the top of the barrier due to the quantum diffusion. When the field begins to roll down from the top of the barrier, large fluctuations are formed due to the quantum diffusion at the top of the barrier. Then the whole scenario fails. This problem is rather generic. To avoid jumping up, the curvature around the barrier should be large compared with the Hubble scale $V'' > H^2$. On the other hand, to realize the second inflation, the field should roll down slowly, then we need $V'' < H^2$. These two conditions are incompatible.

There are several attempts to overcome this problem. Recently Linde constructs the potential which has sharp peak near the false vacuum [5]. In this potential, the tunneling occurs and at the same time slow-rolling is allowed after tunneling, then the second inflation can be realized. But, it is still unclear what is the physical mechanism for the appearance of the sharp peak in the potential.

We will reconsider this problem from different perspective. The point is the understanding of the tunneling process. In the imaginary-time path-integral formalism, tunneling is described by the solution of the Euclidean field equation. This solution gives the saddle-point of the path-integral. Then this determines the semi-classical exponent of the decay rate $\exp(-S_E(\phi_B))$, where S_E is the Euclidean action. In the case the curvature around the barrier is small compared with the Hubble, the solution is given by the Hawking Moss (HM) solution, which stays at the top of the barrier through the whole Euclidean time [6]. Recently Rubakov and Sibiryakov give the interpretation of this tunneling mode using the constrained instanton method [7, 8]. They show the HM solution does not represent the false vacuum decay if one takes into account the analytic continuation to the Lorentzian spacetime. This is because this solution does not satisfy the boundary condition that the field exists in the false vacuum at the infinite past. However, this does not imply the decay does not occur. One should consider a family of the almost saddle-point configurations instead of the true solution of the Euclidean field equation. They show although the decay rate is determined by the HM solution, the structure of the field after tunneling is determined by the other configuration which is one of the almost saddle-point solutions. In this method, one must choose the constraint so that a family of almost saddle-point solutions well covers the region which is expected to dominate the path-integral. One way to realize this is to cover the valley region of the functional space of the action [9, 10]. Along the valley line, the action varies most gently. Then it is reasonable to take the configurations on the valley line as a family of the almost saddle-point configurations. We will call the configuration on the valley line of the action the valley bounce ϕ_V.

This analysis gives the possibility to overcome the problem. Even if the curvature around the barrier is small compared with the Hubble scale, it implies there is a possibility to occur the tunneling described by the valley bounce. If the field appears sufficiently far from the top, one can avoid the large fluctuations. During the tunneling, fluctuations of the tunneling field are generated. These fluctuations are stretched during the second inflation and observed in the open universe. These should be compatible with the observation. Once this can be confirmed, there is no difficulty in constructing the one bubble open inflationary model in the simple model with the polynomial form of the potential.

In this paper, we show this is true as long as the tunneling is described by the valley bounce. We clarify the structure of the valley bounce extending the method developed by Aoyama.et.al [10] to the de Sitter spacetime. We show the fluctuations can be reconciled with the observations.

2 Valley method in de Sitter spacetime

First we review the formalisms which are necessary to describe the false vacuum decay in the de Sitter space. We want to examine the case in which the gravity comes to play a role. Unfortunately, we have not known how to deal with quantum gravity effect yet. So, we study the case in which we can treat gravity at the semi-classical level. That is, we treat the problem within the framework of the field theory in a fixed curved spacetime [7]. The potential relevant to the tunneling is given by

$$V(\phi) = \epsilon + V_T(\phi). \tag{1}$$

We assume ϵ is of the order M_*^4 and $V_T(\phi)$ is of the order M^4. We study the case M is small compared to M_*, $M \ll M_*$. Then the geometry of the spacetime is fixed to the de Sitter spacetime with $H = M_*^2/M_p$,

where $M_p^{-2} = 8\pi G/3$. We consider the situation in which the potential $V_T(\phi)$ has the false vacuum at $\phi = \varphi_F$ and the top of the barrier at $\phi = \varphi_T$. Since the background metric is fixed, we can change the origin of the energy freely. We choose $V_T(\phi_F) = 0$. Following, we work in units with $H = 1$.

The decay rate is given by the imaginary part of the path-integral

$$Z = \int [d\phi] \exp\left(-S_E(\phi)\right), \tag{2}$$

where S_E is the Euclidean action relevant to the tunneling. The dominant contribution of this path-integral is given by the configurations which have $O(4)$ symmetry [11]. So, we assume the background metric and the field to have the form

$$\begin{aligned} ds^2 &= d\sigma^2 + a(\sigma)^2 \left(d\rho^2 + \sin^2\rho d\Omega\right), \\ \phi &= \phi(\sigma), \end{aligned} \tag{3}$$

where $a(\sigma) = \sin\sigma$. Then, the Euclidean action of $\phi(\sigma)$ is given by

$$S_E = 2\pi^2 \int d\sigma \left(a^3 \left(\frac{1}{2}\phi'^2 + V_T(\phi)\right)\right). \tag{4}$$

The saddle-point of this path-integral is determined by the Euclidean field equation $\delta S_E/\delta\phi$=0;

$$\phi'' + 3\cot\sigma\, \phi' - V_T'(\phi) = 0. \tag{5}$$

We impose the regularity conditions at the time when $a(\sigma) = 0$ as

$$\phi'(\sigma = 0) = \phi'(\sigma = \pi) = 0. \tag{6}$$

We represent the solution of this equation as $\phi_B(\sigma)$. If the fluctuations around this solution have a negative mode, this gives the imaginary part to the path-integral and this solution contributes to the decay dominantly. The decay rate Γ is evaluated by

$$\Gamma \sim \exp(-S_E(\phi_B)). \tag{7}$$

The equation has two types of the solutions depending on the shape of the potential. If the curvature around the barrier is large compared with the Hubble scale, then the Coleman De Luccia (CD) solution and the Hawking Moss (HM) solution exist [6, 11]. In this case, the decay is described by the CD solution. The analytic continuation of this solution to Lorentzian spacetime describes the bubble of the true vacuum. On the other hand, in the case the curvature around the barrier is small compared with the Hubble scale, only the HM solution exists. This solution is a trivial solution $\phi = \varphi_T$. The meaning of the HM solution is somewhat ambiguous. There are several attempts to interpret this tunneling mode. One way is to use the stochastic approach [12]. Within this approach, it has been demonstrated that the decay rate given by eq.(7) coincides with the probability of jumping from the false vacuum φ_F onto the top of the barrier φ_T due to the quantum fluctuations.

Recently, Rubakov and Sibiryakov give the interpretation of the HM solution using the constrained instanton method [7, 8]. The main idea is to consider a family of the almost saddle-point configurations instead of the true solution of the Euclidean field equation, i.e. the HM solution. The motivation comes from the boundary condition. They take the boundary condition that the state of the quantum fluctuations above the classical false vacuum is the conformal vacuum. In this case they show the field should not be constant at $0 < \sigma < \pi$ and the HM solution is excluded by this boundary condition. Then one should seek the other configurations which obey the boundary condition and dominantly contribute to the path-integral. In the functional integral, the saddle-point solution gives the most dominant contribution, but the contribution from a family of almost saddle-point configurations which have almost the same action with that of the saddle-point solution should also be included. To realize this in the functional integral, one introduces the identity $1 = \int d\alpha \delta(\mathcal{C} - \alpha)$ into the path integral for some constraint $\mathcal{C}$. First choose one α. This selects the subspace of the functional space. In this subspace, we can perform the integral of the field using saddle-point method under the constraint. The minimum in this subspace

satisfies the equation of motion with constraint instead of the field equation. This minimum corresponds to the almost saddle-point configuration ϕ_α which is slightly deformed from the HM solution. Changing α, these configurations form a trajectory. We can evaluate the path-integral by integrating over α along this trajectory. Since along this trajectory the HM solution gives the minimum action, integrating over α gives the decay rate determined by the HM solution. But the structure of the field after tunneling can be determined by the other configuration on this trajectory ϕ_α. They found the configuration which describes the bubble of the true vacuum if we continue it to the Lorentzian spacetime. Then, they conclude that even in the case only the HM solution exists, the result of the tunneling process can be the bubble of the true vacuum which is described by one of the almost saddle-point configurations.

In this formalism, the validity of the method depends on the choice of the constraint [10, 13]. This is because, in practice, we do the Gaussian integral around the almost saddle-point solutions. To evaluate the path-integral properly we should choose the constraint so that a family of almost saddle-point solutions well covers the region which is expected to dominate the path-integral. Since the action varies most gently along the valley line, one way to realize the aim is to cover the valley region of the action [9, 10]. One can identify the configurations on the valley line and make Gaussian integral around these configurations.

Taking into account the above fact, it is desirable to analyze the structure of not only the solution of the Euclidean field equation but also the configurations on the valley line. One way to define the configurations on this valley line is to use the valley method developed by Aoyama.et.al [10]. To obtain the intuitive understanding of this method, consider the system of the field ϕ_i. Here i stands for the discretized coordinate label and we take the metric as δ_{ij}. In the valley method the equation which identifies the valley line in the functional space is given by

$$D_{ij}\partial_i S = \lambda\,\partial_i S, \quad D_{ij} = \partial_i\partial_j S, \tag{8}$$

where $\partial_i = \partial/\partial\phi_i$. Since this equation has one parameter λ, this defines a trajectory in the space of ϕ. The parameter λ is one of the eigen value of the matrix D_{ij}. On this trajectory the gradient vector $\partial_i S$ is orthogonal to all the eigenvectors of D_{ij} except for the eigenvector of the eigen value λ. This equation can be rewritten as

$$\partial_i\left(\frac{1}{2}(\partial_j S)^2 - \lambda S\right) = 0. \tag{9}$$

This allows the interpretation of the solution for the equation. It extremizes the norm of the gradient vector $\partial_i S$ under the constraint S =const., where λ plays the role of the Lagrange multiplier. Such solution can be found each hypersurface of constant action, then the solutions of the equation form a line in the functional space. If we take λ as the one with the smallest value, then the gradient vector is minimized. In this case, the action varies most gently along this line. This is a plausible definition of the valley line. We will call the configuration on the valley line of the action the valley bounce ϕ_V and the trajectory they form the valley trajectory.

Following we formulate this method in the de Sitter spacetime. The most convenient way is to use the variational method eq.(9). We shall define the valley action by

$$S_V = S_E - \frac{1}{2\lambda}\int d\sigma\sqrt{g}\left(\frac{1}{\sqrt{g}}\frac{\delta S_E}{\delta\phi}\right)^2. \tag{10}$$

The valley bounce is obtained by varying this action. The equation which determines the valley bounce $\delta S_V/\delta\phi = 0$ is a fourth order differential equation. We introduce the auxiliary field f to cancel the fourth derivative term [14];

$$S_f = \frac{1}{2\lambda}\int d\sigma\sqrt{g}\left(f - \frac{1}{\sqrt{g}}\frac{\delta S_E}{\delta\phi}\right)^2. \tag{11}$$

Then the valley action becomes

$$S_V + S_f = S_E + \frac{1}{2\lambda}\int d\sigma\sqrt{g}f^2 - \frac{1}{\lambda}\int d\sigma f\frac{\delta S_E}{\delta\phi}. \tag{12}$$

Taking the variation of this action with respect to f and ϕ, we obtain the equations for ϕ and f;

$$\frac{1}{\sqrt{g}}\frac{\delta S_E}{\delta\phi} = f,$$

$$\int d\sigma' \frac{\delta^2 S_E}{\delta\phi(\sigma)\delta\phi(\sigma')} f(\sigma) = \lambda\sqrt{g} f(\sigma). \tag{13}$$

Using $a(\sigma) = \sin\sigma$, the valley equation which determines the structure of the valley bounce is given by

$$\begin{aligned} \phi'' + 3\cot\sigma\,\phi' - V_T'(\phi) &= -f, \\ f'' + 3\cot\sigma\, f' - V_T''(\phi) f &= -\lambda f. \end{aligned} \tag{14}$$

We analyze the structure of the valley bounce for the case only the HM solution exists. We construct the piece-wise quadratic potential in which we can solve the valley equations analytically. The potential which we study is

$$V_T(\phi) = \begin{cases} \frac{1}{2} m_F^2 (\phi - \varphi_F)^2, & -\infty < \phi < 0, \\ -\frac{1}{2} m_T^2 (\phi - \varphi_T)^2 + \eta, & 0 \le \phi < \infty, \end{cases} \tag{15}$$

where η is of the order M^4. For $m_T^2 < 4$, only the HM solution exists. For example we take $m_T^2 = 2$, $m_F^2 = 0.5$ and $\eta = 0.1M^4$. The HM solution has one negative eigenvalue $\rho_{HM,-} = -2$ and the smallest positive eigenvalue is given by $\rho_{HM,+} = 2$. The generic feature of the valley bounce is understood by the simple analysis of the case in which the valley bounce exists only in one parabola. First consider the valley trajectory associated with the negative eigenvalue. The solution of the valley equation is essentially has a form $f = \lambda(\phi - \varphi_T) = \text{const}$. This solution does not represent the tunneling, so we seek the trajectory associated with the smallest positive eigenvalue $\lambda(\phi_{HM}) = \rho_{HM,+}$. The solution of the valley equation is given by $\phi - \phi_T \propto \cos\sigma$ and $f = \lambda(\phi - \phi_T)$ (Fig.1). In this trajectory, the HM solution gives the minimum of the action (Fig.2). The horizontal coordinate is the norm of the filed $\Phi = \sqrt{\int d\sigma a(\sigma)^3 |\phi(\sigma) - \varphi_T|^2}$. The action grows as the variation of the field becomes large, but this increase is relatively gentle.

Although the HM solution gives the dominant contribution to the path-integral, this solution does not satisfy the boundary condition for the false vacuum decay as shown by Rubakov and Sibiryakov [7]. Making Analytic continuation to the Lorentzian spacetime at $\sigma = 0 (z = -1)$, the field moves according to the field equation. If the field reaches φ_F, this solution represents the false vacuum decay. The behavior of the field in this Lorentzian spacetime is determined by the initial position of the field. This is determined by the behavior of the field at $\sigma = 0$ in the Euclidean region. Provided that its initial position is different from φ_T, this boundary condition can be satisfied. From this fact, the HM solution does not satisfy the boundary condition. On the other hand the valley bounce does satisfy the boundary condition. Furthermore the fluctuations around the valley bounce should have one negative mode to ensure that the valley bounce plays a role instead of the HM solution. The valley bounce has a lowest eigenvalue $\rho_{V,-} < \lambda(\phi_V)$. We find this is negative on this trajectory. Since this is the unique negative eigenvalue, the gaussian integration of the fluctuations around this valley bounce gives the imaginary part to the path-integral. Then, the valley bounce contributes to the false vacuum decay and describes the creation of the bubble of the true vacuum.

3 An open universe from valley bounce

We will see an open inflation model can be constructed using the valley bounce. Following, we restore the Hubble scale H. Since the radius of the bubble R is small compared with the Hubble horizon [11], then the curvature scale is greater than the energy of the matter inside the bubble ρ_M even if the whole energy of the false vacuum is converted to it, $\rho_M/M_p^2 \sim H^2 < 1/R^2$ [3]. Then, we need the second inflation in the bubble. To realize the second inflation inside the bubble, the field should roll slowly down the potential. This implies the curvature of the potential is small compared with the Hubble. To avoid the *ad hoc* fine-tuning of the potential, we will assume this is true for all region of the potential. In this case, since $m_T < H$ the solution of the Euclidean equation is given by the HM solution and the valley bounce is shown as in Fig.7. We connect the linear potential at the point the field appears after the tunneling $\phi = \phi_*$,

$$V(\phi) = V_* - \mu^3(\phi - \phi_*), \qquad (\phi > \phi_*). \tag{16}$$

We demand the potential and its derivative are connected smoothly at the connection point ϕ_*. Then we obtain

$$\begin{aligned} V_* &= \epsilon + \eta - \frac{1}{2} m_T^2 (\phi_* - \varphi_T)^2, \\ \mu^3 &= m_T^2 (\phi_* - \varphi_T). \end{aligned} \tag{17}$$

The initial conditions of the field are given by the valley bounce

$$\phi(t=0) = \phi_0(z=1) = \phi_*, \quad \dot{\phi}(t=0) = 0. \tag{18}$$

If the field obeys the classical field equation;

$$\ddot{\phi} + 3 \coth t \, \dot{\phi} + V'(\phi) = 0, \tag{19}$$

then the solution of ϕ satisfies

$$\dot{\phi}(t) = \mu^3 \frac{\cosh^3 t - 3 \cosh t + 2}{3 \sinh^3 t}. \tag{20}$$

In the small t this behaves as $(1/4)\mu^3 t$. The classical motion during one expansion time is given by $|\dot{\phi}| H^{-1}$. On the other hand the amplitude of the quantum fluctuations is given by $\delta\phi \sim H$. The curvature perturbation $\mathcal{R}$ produced by the quantum fluctuations is approximately given by the ratio of these two quantities;

$$\mathcal{R} \sim \frac{\delta\phi}{|\dot{\phi}| H^{-1}} \sim \frac{H^3}{\mu^3} \sim \frac{H^2}{m_T^2} \left(\frac{H}{\phi_* - \varphi_T} \right). \tag{21}$$

This should be of the order 10^{-5} from the observation of the cosmic microwave background (CMB) anisotropies. If $|\phi_* - \varphi_T| < H$, as in the case the HM solution describes the tunneling, $\mathcal{R} > 1$ and the scenario cannot work well. This is because at $\phi_* \sim \varphi_T$, the field experiences the quantum diffusion rather than the classical potential force. Fluctuations in this diffusion dominated epoch make the inhomogeneous delay of the start of the classical motion, thus make large fluctuations. Fortunately, from Fig.7, we see for appropriate λ, the valley bounce gives the initial condition as $|\phi_* - \varphi_T| \sim O(1)(M^2/m_T)$, which is larger than the Hubble if $M > H$. In this case, the potential force works and the field rolls slowly down the potential. We expect the curvature perturbation can be suppressed for the valley bounce. In fact, we find the power of the curvature purturbations is given by

$$\lim_{p \to \infty} \frac{p^3}{2\pi^2} P_{\mathcal{R}}(p, \lambda) = \frac{1}{4\pi^2} \left(\frac{3H^3}{\mu^3} \right)^2 \sim \left(\frac{M_*^2}{M_p M} \right)^4 \left(\frac{H}{m_T} \right)^2. \tag{22}$$

Here we use the fact the valley bounce gives the initial condition as $|\phi_* - \varphi_T| \sim M^2/m_T$, then $\mu^3 = m_T M^2$. This quantity should be of the order 10^{-10} from the observation. This can be achieved by taking $(M_*^2/M) \ll M_p$.

4 Conclusion

It is difficult to provide the model which solves the horizon problem and at the same time leads to the open universe in the context of the usual inflationary scenario. In the one bubble open inflationary scenario, the horizon problem is solved by the first inflation and the second inflation creates the universe with the appropriate Ω_0.

Many works have been done within this framework of the scenario and it is recognized this scenario requires additional fine-tuning [4, 5]. The defect is thought to arise because the curvature around the barrier should be larger than the Hubble scale to avoid large fluctuations, which contradicts to the requirement that the curvature of the potential should be small to realize the second inflation inside the bubble.

Thus to complete the scenario, we should solve this problem. The main claim of this paper is that this problem can be solved in the simple model with the polynomial form of the potential. We reconsidered

the tunneling process from the different perspective. If the curvature around the potential is small, the tunneling is described by one of a family of the almost saddle-point solutions [7]. This is because the true saddle-point solution, that is, the Hawking Moss solution does not satisfy the boundary condition for the false vacuum decay. The main idea is that the almost saddle-point solution can give the appropriate initial condition for the second inflation. A family of the almost saddle-point solutions generally forms a valley line in the functional space. We called the configurations on the valley line valley bounces. To identify valley bounces, we applied the valley method developed by Aoyama.et.al [10]. In this method these configurations can be identified using the fact the trajectory they form in the functional space corresponds to the line on which the action varies most gently. We formulated this method in the de Sitter spacetime and clarified the structure of the valley bounces. We found the valley bounce which gives the appropriate initial condition of the second inflation even if the curvature around the barrier is small compared with the Hubble scale. Consider the case this valley bounce describes the tunneling. It is possible the field appears sufficiently far from the top of the barrier after the tunneling, then we can avoid the large fluctuations. Hence, using the valley bounce, we can solve the problem which arises in the open inflationary scenario besides the usual fine-tuning of the inflationary scenario. The one bubble open inflation model can be constructed without difficulty.

Acknowledgements

The work of J.S. was supported by Monbusho Grant-in-Aid No.10740118 and the work of K.K. was supported by JSPS Research Fellowships for Young Scientist No.04687

References

[1] K. Koyama, K. Maeda and J. Soda, hep-ph/9910556.

[2] J.R. Gott III, Nature **295**, 304 (1982);
J.R. Gott III and T.S. Statler, Phys. Lett. **B136**, 157 (1984).

[3] M. Sasaki, T. Tanaka, K. Yamamoto, and J. Yokoyama, Phys. Lett. **B317**, 510 (1993).

[4] A.D. Linde, Phys. Lett. **B351**, 99 (1995); A.D. Linde and A. Mezhlumian, Phys. Rev. D **52**, 6789 (1995).

[5] A.D. Linde, Phys. Rev. **D59**, 023503 (1999);

[6] S.W. Hawking and I.G. Moss, Phys. Lett. **B110**, 35 (1982).

[7] V.A. Rubakov and S.M. Sibiryakov, preprint, gr-qc/9905093 (1999).

[8] I. Affleck, Nucl. Phys. **B191**, 429 (1981).

[9] I.I. Balitsky and A.V. Yung, Phys. Lett. **B168**, 113 (1986).

[10] H. Aoyama and H. Kikuchi, Nucl. Phys. **B369**, 219 (1992); for a review see H. Aoyama, T. Harano, H. Kikuchi, I. Okouchi, M. Sato and S. Wada, Prog. Theor. Phys. Suppl. **127**, 1 (1997).

[11] S. Coleman and F. De Luccia, Phys. Rev. **D21**, 3305 (1980).

[12] A. Goncharov and A. Linde, Sov. J. Part. Nucl. **17**, 369 (1986); A.D. Linde, Nucl. Phys. **B216**, 421 (1983).

[13] H. Aoyama, T. Harano, M. Sato and S. Wada, Nucl. Phys. **B466**, 127 (1996).

[14] H. Aoyama and S. Wada, Phys. Lett. **B349**, 279 (1995).

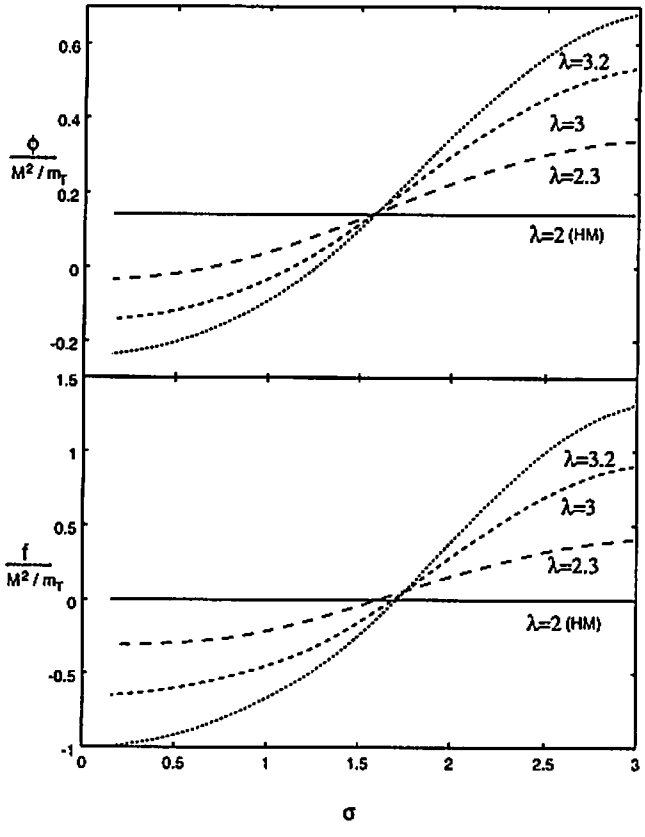

Figure 1:

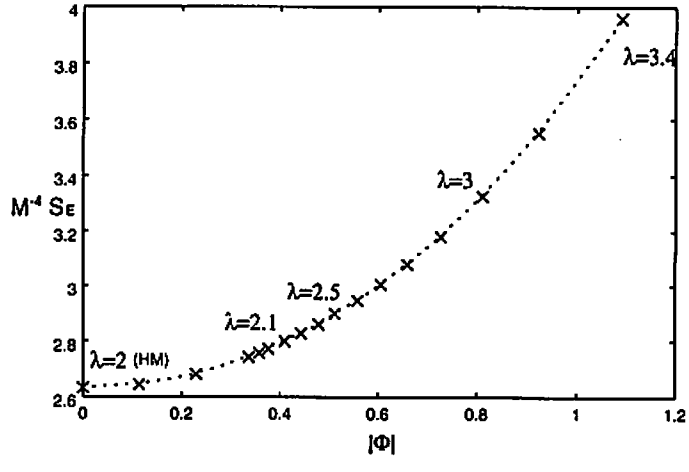

Figure 2:

What happens when the inflaton stops during inflation

Osamu Seto,[1]

Yukawa Institute for Theoretical Physics, Kyoto University, Sakyo-ku, Kyoto 606-8502, Japan

Jun'ichi Yokoyama[2]

Department of Earth and Space Science, Graduate School of Science, Osaka University, Toyonaka 560-0043, Japan

Hideo Kodama[3]

Yukawa Institute for Theoretical Physics, Kyoto University, Sakyo-ku, Kyoto 606 8502, Japan

Abstract

The spectrum of adiabatic density perturbation generated during inflation is studied in the case the time derivative of an inflation-driving scalar field (inflaton) vanishes at some time during inflation. It is shown that the nondecaying mode of perturbation has a finite value even in this case and that its amplitude is given by the standard formula with the time derivation of the scalar field replaced by the potential gradient using the slow-roll equation.

1 Introduction

It is now widely believed that the large-scale homogeneity and isotropy observed in the Universe were realized as a result of accelerated expansion or inflation in the early universe [1]. It also provides a mechanism to account for the origin of primordial density fluctuations out of quantum fluctuations of the inflation-driving scalar field which we call the *inflaton* [2]. In the standard inflation models such as new [3] and chaotic [4] inflation, inflation is driven by the potential energy of the inflaton as it slowly rolls the potential hill and is predicted to produce adiabatic fluctuations with a nearly scale-invariant spectrum.

More specifically, the amplitude of curvature perturbation, Φ, on comoving scale $r = 2\pi/k$ is given by the formula,

$$\Phi(r) \approx \left.\frac{H^2}{|\dot{\phi}|}\right|_{t_k}, \tag{1}$$

where ϕ is the inflaton and H is the Hubble parameter during inflation, and the right-hand-side should be evaluated when the relevant scale left the Hubble radius during inflation. The above formula also gives an estimate of the amplitude of density perturbation on the comoving scale r when this scale reentered the Hubble horizon after inflation as well as that of large-scale anisotropy of CMB due to the Sachs-Wolfe effect [5], which has been probed by the COsmic Background Explorer (COBE) satellite [6]. The reason why (1) gives an almost scale-invariant spectrum is that both H and $\dot{\phi}$ change very slowly during slow-roll inflation.

Recently, however, new classes of inflation models have been proposed such that ϕ is not necessarily slowly rolling during the entire period of inflation and that it changes direction of motion during inflation. One example is the oscillating inflation proposed by Damour and Mukhanov [7, 8] in which accelerated

[1] E-mail:oseto@yukawa.kyoto-u.ac.jp
[2] E-mail:yokoyama@vega.ess.sci.osaka-u.ac.jp
[3] E-mail:kodama@yukawa.kyoto-u.ac.jp

expansion is realized as the inflaton oscillates around a minimum of a nonconvex potential. In this model $\dot{\phi}$ vanishes twice in each period of oscillation during inflation. Another example is the chaotic new inflation model proposed by one of us [9]. This model assumes a potential with a local maximum at the origin like new inflation but start with the same initial condition as chaotic inflation. If model parameters are appropriately chosen, the inflaton climbs up the potential hill near to the origin after chaotic inflation and new inflation can be realized there. In the early stage of new inflation $\dot{\phi}$ may vanish and ϕ changes its direction of motion if it does not have sufficient energy to go over the origin.

In both models, if we apply the formula (1) as it is, the amplitude of fluctuation apparently diverges when $\dot{\phi}$ vanishes. The above formula, however, has been derived under the slow-roll approximation, namely, under the assumption that both ϕ and Φ changes slowly during inflation. On the other hand, motion of ϕ is not given by the slow-roll formula when ϕ changes its direction, because $\dot{\phi}$ vanishes where the gradient of the potential does not vanish.

Thus we expect that it is inappropriate to apply (1) to the case $\dot{\phi}$ vanishes during inflation. The purpose of the present paper is to derive a formula of curvature perturbation in such a situation. This is accomplished by a proper account of not only the growing (or nondecreasing) mode but also the decaying mode as seen below. The rest of the paper is organized as follows. In §II we give the formulation with an appropriate choice of a variable and present solutions in the long- and the short-wavelength limit. Then these solutions are matched for the case of the linear potential in §III and for the quadratic potential in §IV. §V is devoted to the conclusion.

2 Equations of motion and the solutions in the long- and the short-wavelength limit

We consider a minimally coupled singlet scaler field ϕ in the spatially flat Robertson-Walker background metric,

$$ds^2 = -dt^2 + a^2(t)d\mathbf{x}^2, \tag{2}$$

where $a(t)$ denotes the scale factor. Then the total action is

$$S = \frac{1}{2\kappa^2}\int R\sqrt{-g}d^4x + \int\left[-\frac{1}{2}(\partial\phi)^2 - V(\phi)\right]\sqrt{-g}d^4x, \tag{3}$$

where R is the scalar curvature and $\kappa^2 = 8\pi G$ with G being the gravitational constant. The Einstein equation and the field equation of ϕ read

$$H^2 = \left(\frac{\dot{a}}{a}\right)^2 = \frac{\kappa^2}{3}\left(\frac{1}{2}\dot{\phi}^2 + V(\phi)\right). \tag{4}$$

$$\ddot{\phi} + 3H\dot{\phi} + V'(\phi) = 0. \tag{5}$$

with H being the Hubble parameter. Here a dot denotes time differentiation and a prime represents differentiation with respect to ϕ. These are the equations for the unperturbed variables.

Next we incorporate a linear perturbation, writing the perturbed metric in terms of the gauge-invariant variables [10] in the longitudinal gauge,

$$ds^2 = -[1 + 2\Psi(\mathbf{x},t)]dt^2 + a^2(t)[1 + 2\Phi(\mathbf{x},t)]d\mathbf{x}^2, \tag{6}$$

where we use the notation of [11] for the perturbation variables. Hereafter all perturbation variables represent Fourier expansion coefficients like

$$\Phi_{\mathbf{k}} = \int\frac{d^3\mathbf{x}}{(2\pi)^{3/2}}\Phi(\mathbf{x},t)e^{i\mathbf{k}\mathbf{x}}. \tag{7}$$

and we omit the wave-number suffix k. We use the following combination of gauge-invariant variables [12, 13, 14],

$$Y = X - \frac{\dot{\phi}}{H}\Phi, \tag{8}$$

where

$$X = \delta\phi - \frac{a}{k}\dot{\phi}\sigma_g, \tag{9}$$

is the gauge-invariant scalar field fluctuation with σ_g being the shear of each constant time slice. The latter vanishes on Newtonian slice including the longitudinal gauge.

The above quantity Y is related to the gauge-invariant variable

$$Z \equiv \Phi - \frac{aH}{k}V = \Phi + \frac{2}{3}\frac{\Phi + H^{-1}\dot{\Phi}}{1+w}, \tag{10}$$

as

$$Z = -\frac{H}{\dot{\phi}}Y, \tag{11}$$

in the present case where matter consists of a scalar field. Here V is a gauge-invariant velocity perturbation [11] and w denotes the ratio of pressure to energy density. Although the definition of Z is slightly different from the Bardeen's ζ [15], which was originally defined by

$$\zeta = \left[1 + \frac{2}{9}\frac{k^2}{(1+w)H^2a^2}\right]\Phi - \frac{aH}{k}V, \tag{12}$$

it enjoys the same property as ζ, that is, both quantities are constant during $k \ll aH$ if only adiabatic fluctuation is present and sound velocity is nonsingular.

From the perturbed Einstein equations, we obtain the following equations:

$$\dot{X}\dot{\phi} - \ddot{\phi}X + \dot{\phi}^2\Phi = \frac{2}{\kappa^2}\frac{k^2}{a^2}\Phi, \tag{13}$$

$$\dot{\Phi} + H\Phi = -\frac{\kappa^2}{2}\dot{\phi}X. \tag{14}$$

From these equations and (8), the equation of motion of Y reads

$$\ddot{Y} + 3H\dot{Y} + \left[\left(\frac{k}{a}\right)^2 + M^2_{Y\mathrm{eff}}\right]Y = 0, \tag{15}$$

with

$$M^2_{Y\mathrm{eff}} \equiv V''(\phi) + 3\kappa^2\dot{\phi}^2 - \frac{\kappa^4}{2H^2}\dot{\phi}^4 + 2\kappa^2\frac{\dot{\phi}}{H}V'(\phi). \tag{16}$$

This equation has the following exact solution in the long-wavelength limit $k \longrightarrow 0$ [13, 16].

$$Y(t) = \tilde{c}_1(k)Y_1(t) + \tilde{c}_2(k)Y_2(t), \tag{17}$$

$$Y_1(t) = \frac{\dot{\phi}}{H}, \tag{18}$$

$$Y_2(t) = \frac{\dot{\phi}}{H}\int_T^t \frac{H^2}{a^3\dot{\phi}^2}dt, \tag{19}$$

where $\tilde{c}_1(k)$ and $\tilde{c}_2(k)$ are integration constants to be determined by quantum fluctuations generated during inflation, and T is some initial time which may be chosen arbitrarily because its effect can be absorbed by a redefinition of $\tilde{c}_1(k)$. The solution $Y_2(t)$ is apparently singular at $\dot{\phi} = 0$. But in fact it is regular there [13].

Since $Y_2(t)$ has a different dimension than $Y_1(t)$, it is more convenient to redefine the coefficients as

$$c_1(k) \equiv \tilde{c}_1(k), \qquad c_2(k) \equiv \tilde{c}_2(k)/k^3, \tag{20}$$

for which the scale factor appears in the rescaling-invariant form of $k/a(t)$, and $c_1(k)$ and $c_2(k)$ have the same dimension.

We next consider the evolution of Y in short-wavelength regime in order to set the initial condition of Y out of quantum fluctuations. Since we are interested in generation of perturbations around the turning

point of the inflaton, we only consider the evolution of Y in the inflationary stage around and after the time $\dot{\phi} = 0$ and assume that $|\dot{H}/H^2| \ll 1$ holds in this stage. We further assume that $\mu \equiv V'/(\kappa V)$ satisfies the condition

$$\mu' \leq 0, \quad \mu\mu'' \geq 0, \tag{21}$$

for the value of ϕ in this stage. This condition is satisfied for quite a large class of potentials including the pure exponential potential and those which are approximately given by $c|\phi|^n$ or $V_0 - c|\phi|^n$ around the turning point where $c > 0$ and n is a positive integer.

$M^2_{Y\text{eff}}$ defined by (16) can be rewritten in terms of μ as

$$\frac{M^2_{Y\text{eff}}}{\kappa^2 V} = \frac{1}{\kappa}\mu' + \left(\frac{\kappa\dot{\phi}}{H} + \mu\right)^2. \tag{22}$$

Under the condition (21), the value of $|\mu'|/\kappa$ at the turning point should be smaller than $1/N$, where N is the number of e-folds of inflation after the turning point, *i.e.*, the increase of $\ln a$. It is also shown that $|\kappa\dot{\phi}/(H\mu)|$ is always less than unity and approaches unity, *i.e.*, $\kappa\dot{\phi}/(H\mu) \to -1$, in a few expansion time after ϕ passes the turning point. This implies that the second term in the right-hand side of (22) is equal or less than the value of $2|\dot{H}/H^2|$ at the slow-roll phase following the short transient period around the turning point. To be precise, this term is approximately given by $(2/9)(|\mu'|/\kappa)^2|\dot{H}/H^2|$ in the slow-roll phase.

From these estimates we see that $M^2_{Y\text{eff}}$ in (15) can be neglected in the regime

$$\left(\frac{k}{aH}\right)^2 > \frac{1}{N}, \tag{23}$$

which extends to a wavelength much larger than the Hubble horizon size. Thus in this regime (15) becomes

$$\ddot{Y} + 3H\dot{Y} + \left(\frac{k}{a}\right)^2 Y = 0. \tag{24}$$

Under the condition $|\dot{H}/H^2| \ll 1$ the solution of this equation satisfying the normalization condition for positive frequency modes to define the vacuum state,

$$a^3(Y\dot{Y}^* - \dot{Y}Y^*) = i, \tag{25}$$

is approximately given by

$$Y = \frac{iH}{\sqrt{2k^3}}\left[\alpha_{\mathbf{k}}(1 + ik\eta)e^{-ik\eta} - \beta_{\mathbf{k}}(1 - ik\eta)e^{ik\eta}\right], \tag{26}$$

where $\eta = -1/(Ha)$, and $\alpha_{\mathbf{k}}$ and $\beta_{\mathbf{k}}$ are constants which satisfy

$$|\alpha_{\mathbf{k}}|^2 - |\beta_{\mathbf{k}}|^2 = 1. \tag{27}$$

We shall choose $(\alpha_{\mathbf{k}}, \beta_{\mathbf{k}}) = (1, 0)$ so that the vacuum reduces to the one in Minkowski spacetime at the short-wavelength limit $(-k\eta \to \infty)$. Therefore we obtain

$$Y = \frac{iH}{\sqrt{2k^3}}(1 + ik\eta)e^{-ik\eta}. \tag{28}$$

3 Matching the short- and the long-wavelength regimes: The case of a linear potential

Having obtained the short- and the long-wavelength solutions we next connect these two regimes in order to determine the coefficients $c_1(k)$ and $c_2(k)$. In this section we consider the simplest case in which the

inflaton's potential can be approximated by a linear function near the point where the inflaton switches its direction of motion. That is, we take,

$$V(\phi) = V_0 + V'\phi, \tag{29}$$

with V_0 and V' being constants and assume $|V'\phi| \ll V_0$. Then the solution of (5) is

$$\dot{\phi}(t) = \dot{\phi}_s \left(1 - e^{-3H(t-t_0)}\right) = \dot{\phi}_s \left[1 - \left(\frac{a(t_0)}{a(t)}\right)^3\right], \tag{30}$$

where $\dot{\phi}_s \equiv -V'/3H$ is the velocity of ϕ in the slow-roll limit and we have set

$$\dot{\phi}(t_0) = 0. \tag{31}$$

In this case (17) is rewritten as

$$Y(t) = c_1(k)\frac{\dot{\phi}_s}{H}\left[1 - \left(\frac{a(t_0)}{a(t)}\right)^3\right] + c_2(k)\frac{-1}{3\dot{\phi}_s}\left(\frac{k}{a(t)}\right)^3, \tag{32}$$

where we have chosen $T \longrightarrow \infty$ so that $Y_2(t)$ becomes pure decaying mode. It should be noted that it is nontrivial that $Y_2(t)$ is described like this all the time because the integrand is singular at $t = t_0$ [13]. We emphasize that $Y_1(t)$, which is the nondecreasing mode, has a decaying component in contrast to the case of slow-roll inflation.

We next match (32) with the short-wavelength solution (28).

We adopt is to use the series expansion of (28) with respect to $k/a(t)$, namely,

$$Y = \frac{iH}{\sqrt{2k^3}}\left[1 + \frac{1}{2}\left(\frac{k}{a(t)H}\right)^2 + \frac{i}{3}\left(\frac{k}{a(t)H}\right)^3 + \ldots\right], \tag{33}$$

and match each coefficient of the power series with that of the long-wavelength solution. As is seen here the zeroth-order term matches the main part of the nondecreasing term and the third-order term corresponds to the decaying mode. However, the second-order term, which is present in (33), is absent in (32). In fact, this term should be regarded as a finite-wavenumber correction to the nondecreasing mode Y_1 as we see now.

With the help of the $k = 0$ solutions $Y_1(t)$ and $Y_2(t)$ and the Green function method, we obtain from (15) the following iterative expression for arbitrary k [13].

$$Y = c_1(k)Y_1 + c_2(k)k^3Y_2 + k^2Y_1\int aY_2Y\,dt - k^2Y_2\int aY_1Y\,dt. \tag{34}$$

The lowest-order iterative solution valid for small k reads

$$Y(t) \cong c_1(k)Y_1(t) + c_2(k)k^3Y_2(t) + c_1(k)\left(\frac{k}{a(t)}\right)^2\frac{\dot{\phi}_s}{2H^3} + \mathcal{O}\left(\left(\frac{k}{a(t)}\right)^5\right). \tag{35}$$

The new term corresponds to the second term in (33) and we can now determine $c_1(k)$ and $c_2(k)$ consistently up to the third order in $(k/a)^3$, to yield.

$$c_1(k) = \frac{iH}{\sqrt{2k^3}}\frac{H}{\dot{\phi}_s}, \tag{36}$$

$$c_2(k) = \frac{\dot{\phi}_s}{\sqrt{2k^3}H^2}\left[1 - 3i\left(\frac{a(t_0)H}{k}\right)^3\right]. \tag{37}$$

We note that $a(t_0)H/k = 1$ for the mode leaving the Hubble radius when $\dot{\phi}$ vanishes.

4 The case of a quadratic potential

Next we consider the case for which the potential is locally given by,

$$V(\phi) = V_0 - \frac{1}{2}m^2\phi^2, \tag{38}$$

near the turning point, where V_0 and m are constants satisfying $H^2 \equiv 8\pi G V_0/3 \gg m^2$. We assume $V_0 \gg m^2\phi^2$. Then the solution of (5) reads

$$\dot{\phi}(t) = \frac{\lambda_+}{1-\frac{\lambda_+}{\lambda_-}}\phi_0\left(e^{\lambda_+(t-t_0)} - e^{\lambda_-(t-t_0)}\right), \tag{39}$$

$$\lambda_\pm \equiv -\frac{3}{2}H \pm \sqrt{\frac{9}{4}H^2 + m^2}, \tag{40}$$

where we have set

$$\dot{\phi}(t_0) = 0, \tag{41}$$

$$\phi(t_0) = \phi_0. \tag{42}$$

By virtue of the inequality $H \gg m$ we find

$$\lambda_- \cong \frac{m^2}{3H^2}, \qquad \lambda_- \cong -3H. \tag{43}$$

To the lowest order in $m^2/(3H^2)$, (17) is expressed as

$$Y = c_1(k)\frac{m^2}{3H^2}\phi_0\left[1 - \left(\frac{a(t_0)}{a(t)}\right)^3\right] - c_2(k)\frac{H}{m^2\phi_0}\left(\frac{k}{a(t)}\right)^3. \tag{44}$$

We can repeat the same argument as the case of a linear potential. As is suggested by the fact that (44) coincides with (32) by the replacement,

$$-\frac{m^2\phi_0}{3H} = -\frac{V'(\phi_0)}{3H} \Longleftrightarrow \dot{\phi}_* = -\frac{V'}{3H},$$

we obtain in this case,

$$c_1(k) = -\frac{3iH^3}{\sqrt{2k^3}V''(\phi_0)}. \tag{45}$$

Thus in both cases the coefficient of the nondecaying mode is given by the standard formula as if ϕ is slowly rolling with the speed,

$$\dot{\phi} = -\frac{V'(\phi)}{3H}, \tag{46}$$

even for the k−mode leaving the horizon when $\dot{\phi}$ vanishes.

5 Conclusion

In the present paper we have derived a formula for the spectrum of density perturbation generated by inflation in the case the time-derivative of the inflaton, $\dot{\phi}$, vanishes at some time during inflation. Calculation in such a situation is not straightforward because the amplitude of growing mode in the long-wavelength limit vanishes at the turning point of the inflaton, which implies that the Bardeen parameter estimated for quantum fluctuations at horizon crossing diverges at that time. This is the origin of the divergence of the standard formula at $\dot{\phi} = 0$. Of course, the amplitude of perturbations generated around the turning point do not diverge in reality because the Bardeen parameter becomes finite when the inflaton moves away from the turning point. This implies that we must subtract a contribution of

decaying mode, for which the Bardeen parameter is not constant, from the perturbation generated from quantum fluctuation in order to obtain a correct formula for the amplitude of growing mode.

In order to treat this problem properly, we have first shown that the standard expression for quantum fluctuations in the short-wavelength limit gives a good approximation for the evolution of perturbations during inflation, at least in the case we are concerned with, even when wavelengths are much larger than the Hubble horizon size. Then we have matched this expression with an exact long-wavelength expression for the evolution of the perturbation variable, Y, which does not show any singular behavior when $\dot{\phi}$ vanishes, in a range of wavelength in which both expressions are valid to determine the amplitude of growing mode in quantum fluctuations. As a result we have obtained the new formula for the amplitude of curvature perturbation

$$\Phi\left(r=\frac{2\pi}{k}\right)=f\left.\frac{3H^3}{2\pi|V'(\phi)|}\right|_{t_k}, \tag{47}$$

where $f=3/5$ $(2/3)$ in the matter- (radiation-) dominated stage. Apparently this formula coincides with the standard formula with $\dot{\phi}$ in the denominator replaced by the slow-roll velocity,

$$\dot{\phi}=-\frac{V'(\phi)}{3H}, \tag{48}$$

but it is valid not only in the slow-roll regime but also in an extreme situation $\dot{\phi}=0$ when the relevant mode leaves Hubble radius during inflation.

Although we have done calculations only for two simple models in the present paper, the above formula seems to hold for perturbations generated around and after the turning point of the inflaton in generic models for the following reason. First recall that the expression (28) for perturbations generated from quantum fluctuations gives a good approximation during inflation even when the wavelength is much larger than the Hubble horizon size. Though it is a combination of a growing mode and a decaying mode at the horizon crossing, the amplitude of the latter component decreases rapidly with cosmic expansion after the horizon crossing. In that stage the Bardeen parameter $Z=-HY/\dot{\phi}$ should approach a constant. In a several Hubble time after passing the turning point, the slow-roll approximation becomes good and $\dot{\phi}/H$ is expressed as $-V'/3H^2$, which is constant with a good accuracy in the early phase of inflation after the turning point. In the meanwhile Y given by (28) also becomes a constant $iH/\sqrt{2k^3}$. Hence the value of the Bardeen parameter for the growing mode should be given by

$$Z=-i\frac{H}{\sqrt{2k^3}}\frac{3H^2}{V'}. \tag{49}$$

This expression coincides with Z obtained from $c_1(k)Y_1$ with $c_1(k)$ given by (36). This argument does not determine the amplitude of the decaying-mode component, but it has no importance in the estimation of curvature perturbation in later states.

acknowledgements

One of the authors (JY) would like to thank Isaac Newton Institute for Mathematical Sciences for its hospitality where this research was completed. This work was supported in part by the Monbusho Grant-in-Aid for Scientific Research Nos. 11740146 (JY) and 11640273 (HK), and "Priority Area: Supersymmetry and Unified Theory of Elementary Particles (No. 707)" (JY).

References

[1] For a review of inflation, see, e.g. A.D. Linde, Particle Physics and Inflationary Cosmology (Harwood, Chur, Switzerland, 1990); K.A. Olive, Phys. Rep. **190**.181(1990).

[2] S.W. Hawking, Phys. Lett. **115B**. 295(1982); A.A.Starobinsky, Phys. Lett. **117B**. 175(1982); A.H. Guth and S-Y. Pi, Phys. Rev. Lett. **49**. 1110(1982).

[3] A.D. Linde, Phys. Lett. **108B**, 389(1982); A. Albrecht and P.J. Steinhardt, Phys. Rev. Lett. **48**, 1220(1982).

[4] A.D. Linde, Phys. Lett. **129B**, 177(1983).

[5] R.K. Sacks and A.M. Wolfe, Astrophys. J. **147**, 73(1967).

[6] C.L. Bennet *etal.*, Astrophys. J. Lett. **464**, L1(1996).

[7] T. Damour and V.F. Mukhanov, Phys. Rev. Lett. **80**, 3440(1998).

[8] A.R. Liddle and A. Mazumdar, Phys. Rev. **D58**, 083508(1998); A. Taruya, Phys. Rev. **D59**, 103505(1999).

[9] J. Yokoyama, Phys. Rev. **D58**, 083510(1998); J. Yokoyama, Phys. Rev. **D59**, 107303(1999).

[10] J.M. Bardeen, Phys. Rev. **D22**, 1882(1980).

[11] H. Kodama and M. Sasaki, Prog. Theor. Phys. Suppl. **78**, 1(1984).

[12] V.F. Mukhanov, Sov. Phys. JETP **68**, 1297(1988).

[13] H. Kodama and T. Hamazaki, Prog. Theor. Phys. **96**, 949(1996).

[14] Y. Nambu and A. Taruya, Prog. Theor. Phys. **97**, 83(1997).

[15] J.M. Bardeen, P.J. Steinhardt and M.S. Turner, Phys. Rev. **D28**, 679(1983).

[16] J. Hwang, Phys. Rev. D **48**, 3544(1993).

Thick Domain Walls Interacting with a Black Hole

Yoshiyuki Morisawa[1] , Ryo Yamazaki[2] , Daisuke Ida[3] , Akihiro Ishibashi[4] and Ken-ichi Nakao[5]

[1,4] *Yukawa Institute for Theoretical Physics, Kyoto University, Kyoto 606-8502, Japan*
[2,3] *Department of Physics, Kyoto University, Kyoto 606-8502, Japan*
[5] *Department of Physics, Osaka City University, Osaka 558 8585, Japan*

Abstract

We discuss the gravitationally interacting system of a thick domain wall and a black hole. We numerically solve the scalar field equation in the Schwarzchild spacetime and show that there exist scalar field configurations representing thick domain walls intersecting the black hole.

1 Introduction

Unified gauge theories suggest that phase transitions occur in the early universe. Topological defects such as cosmic strings and domain walls are the evidence of the phase transitions (see for example, [1]). To seek the existence of such defects is therefore crucially important in cosmology and elementary particle physics.

As a possible case, one can consider the situation that topological defects are captured by a black hole via its strong gravity and located around the black hole. Topological defects are extended relativistic objects due to their large tension. It is intriguing in general relativity to study the gravitational interaction between two extended relativistic objects: a topological defect and a black hole.

Within this context, the scattering problem of a cosmic string by a black hole has been studied in detail by De Villiers and Frolov [2]. In the domain wall case, recently Frolov *et al* considered test membranes embedded in the Schwarzchild black hole spacetime and found the stationary membranes [3]. They showed that there exist a family of membranes which intersect the black hole event horizon. In these work, however, topological defects have been treated as infinitely thin objects, whereas a 'realistic' topological defect arises from a scalar field as a topologically stable configuration and thus has a finite thickness.

In the system of a topological defect and a black hole, there are two characteristic scales: the thickness w of the defect and the black hole radius r_g. The defect is said to be "thin" when w is sufficiently smaller than r_g. In the case that the system consists of an astrophysical black hole with the mass $\sim M_\odot$ and a defect formed during a GUT phase transition, the thickness of the defect is much smaller than the black hole radius and therefore thin wall approximation is valid.

On the other hand, during the last few decades, many authors have studied the formation of small black holes or primordial black holes (PBHs), which are much smaller than astrophysical ones (see for example, [4]). Besides, it has been discussed the possibility of thick defects and their cosmological implications, e.g. as a source of large-scale structure in the universe [5], or as a candidate for some kind of dark matter [6]. Then, when one treats the defects and black hole system, it is not so hard to consider the situation that the thickness of defects cannot be negligible as compared with the size of a small black hole. For example, it is thought that the typical mass of PBHs evaporating in the present time is 10^{15}g, so $r_g \sim 10^{-13}$cm. When one considers the topological defects formed during a phase transition at $\sim$ 100MeV, the thickness of such defects becomes comparable to the size of PBHs.

So far, there are many studies about the properties of thick domain walls in the flat and de Sitter spacetime backgrounds [1]. However, little is known about the existence of thick wall configurations on inhomogeneous, strongly curved background such as a black hole spacetime.

[1] E-mail:morisawa@yukawa.kyoto-u.ac.jp
[2] E-mail:yamazaki@tap.scphys.kyoto-u.ac.jp
[3] E-mail:ida@tap.scphys.kyoto-u.ac.jp
[4] E-mail:akihiro@yukawa.kyoto-u.ac.jp
[5] E-mail:knakao@sci.osaka-cu.ac.jp

In this paper, we will investigate the gravitational interaction between a domain wall and a black hole with taking the thickness of the wall into account. We deal with a scalar field with ϕ^4-potential in the Schwarzchild black hole spacetime and explicitly show that static thick domain walls intersecting the black hole do exist by numerical investigation. We consider a non-gravitating scalar field for simplicity.

This paper is organized as follows. In section 2, we derive the basic equation and discuss the boundary conditions which represent the situation we want to study. In section 3, we show the numerical result. We summarize our work in section 4.

2 Model

We consider the Schwarzchild black hole, whose metric is written as

$$ds^2 = -\left(\frac{1-M/2R}{1+M/2R}\right)^2 dt^2 + \left(1+\frac{M}{2R}\right)^4 \left[dR^2 + R^2(d\theta^2 + \sin^2\theta d\varphi^2)\right] \tag{1}$$

in the isotropic coordinates (t, R, θ, φ). Here M is the mass of the black hole and the event horizon is located at $R = M/2$.

On this background we consider a real scalar field ϕ whose Lagrangian density is given by

$$\mathcal{L} = -\sqrt{-g}\left[\frac{1}{2}g^{ab}\nabla_a\phi\nabla_b\phi + V(\phi)\right]. \tag{2}$$

Then, we have the equation of motion

$$\Box\phi = \frac{\partial V}{\partial\phi}, \tag{3}$$

where $\Box \equiv g^{ab}\nabla_a\nabla_b$. In particular, we deal with the ϕ^4-potential

$$V(\phi) = \frac{\lambda}{4}(\phi^2 - \eta^2)^2. \tag{4}$$

As is well known, if the background spacetime is flat, eq.(3) has an exact solution $\phi(z) = \eta\tanh\sqrt{\lambda/2}\eta z$, which represents a domain wall with the thickness $w \sim 1/\sqrt{\lambda}\eta$.

Since we are concerned with stationary domain walls intersecting the black hole, we assume that the configuration of the scalar field is static and axially symmetric, *i.e.* $\phi = \phi(R, \theta)$. Then, eq.(3) is reduced to

$$\frac{\partial^2\Phi}{\partial\rho^2} + \frac{2\rho}{(\rho+1)(\rho-1)}\frac{\partial\Phi}{\partial\rho} + \frac{1}{\rho^2}\frac{\partial^2\Phi}{\partial\theta^2} + \frac{\cot\theta}{\rho^2}\frac{\partial\Phi}{\partial\theta} = \epsilon\left(\frac{\rho+1}{\rho}\right)^4\Phi(\Phi^2-1) \tag{5}$$

by the rescaling:

$$R = \frac{M}{2}\rho, \tag{6}$$

$$\phi = \eta\Phi. \tag{7}$$

Note that the basic equation (5) includes only one parameter:

$$\epsilon = \left(\frac{M/2}{(\sqrt{\lambda}\eta)^{-1}}\right)^2, \tag{8}$$

i.e. the square of a ratio of the horizon radius to the wall thickness measured in the asymptotic region. When ϵ is smaller (larger) than unity, the wall is said to be thick (thin) as compared to the size of the black hole.

To simplify the problem, we shall confine ourselves to the case that the wall's core is located at the equatorial plane of the black hole, and accordingly we assume

$$\Phi = 0 \qquad \text{at } \theta = \tfrac{\pi}{2}. \tag{9}$$

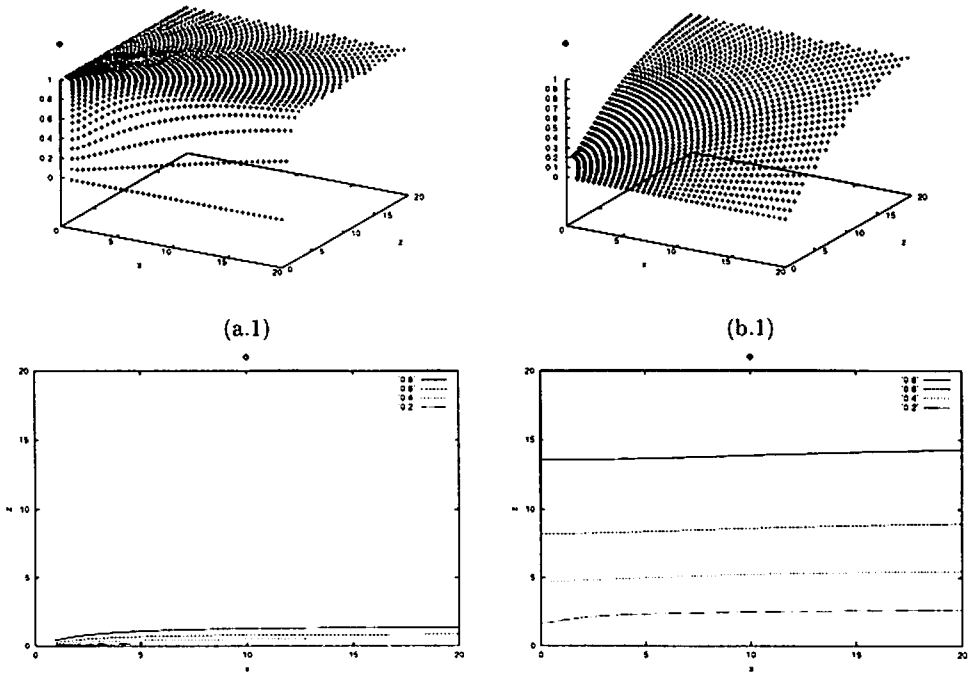

(a.1) (b.1)

(a.2) (b.2)

Figure 1: The scalar field configurations. $\Phi(x, z)$ are plotted for $\epsilon = 1$ (a.1) and $\epsilon = 0.01$ (b.1). (a.2) and (b.2) are contour maps of (a.1) and (b.1), respectively.

Then, it is enough to investigate the 'north' region (*i.e.* $0 \leq \theta \leq \frac{\pi}{2}$, $\rho \geq 1$) of the spacetime. We also require the boundary conditions

$$\frac{\partial \Phi}{\partial \theta} = 0 \qquad \text{at } \theta = 0, \tag{10}$$

and

$$\frac{\partial \Phi}{\partial \rho} = 0 \qquad \text{at the black hole horizon, } \rho = 1, \tag{11}$$

for the regularity of the scalar field at the symmetric axis and at the black hole event horizon, respectively. It is worth noting that the second condition (11) is derived from a natural requirement that the energy density observed by free fall observers do not diverge at the event horizon. Since the background spacetime is asymptotically flat, the scalar field configuration should approach an exact wall solution in the flat background case:

$$\Phi = \tanh(\sqrt{\frac{\epsilon}{2}}\rho_{\max}\cos\theta) \qquad \text{at outer boundary } (\rho_{\max} \gg 1). \tag{12}$$

We solve the equation of motion (5) for ϕ under these boundary conditions (9)–(12). We numerically integrate eq.(5) using relaxation method.

3 Results

The scalar field configuration $\Phi(x, z)$ satisfying (5) is shown in fig.1. Here x and z are the Cartesian coordinates: $(x, z) = (\rho\sin\theta, \rho\cos\theta)$. We plot $\Phi(x, z)$ in figures 1(a.1) and (b.1), and represent contour maps of them in figures 1(a.2) and (b.2).

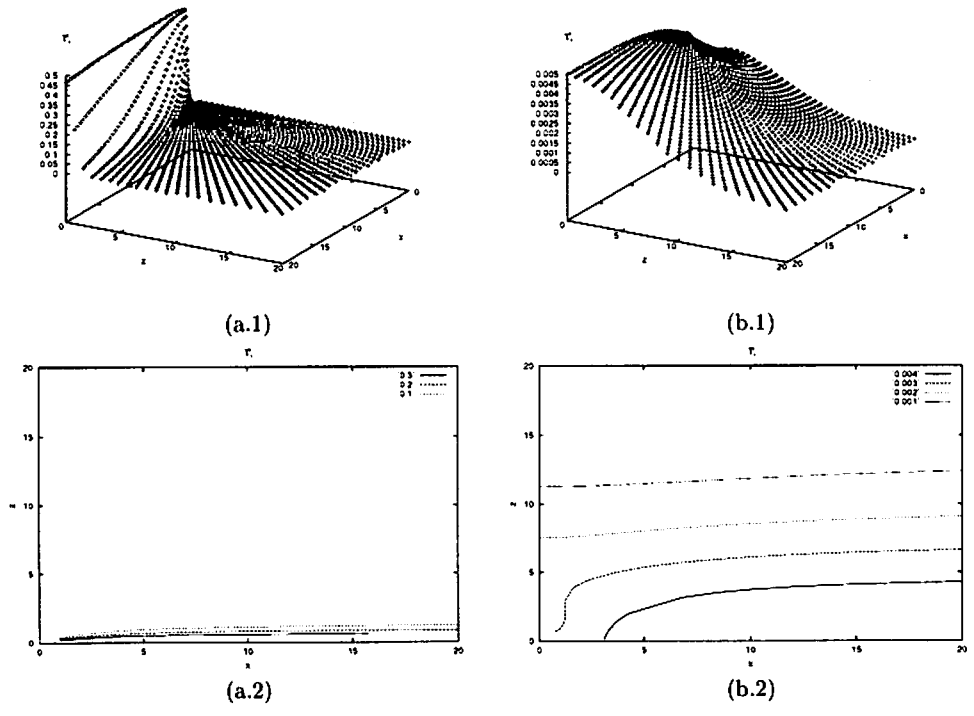

Figure 2: The energy density. $T^t{}_t(x,z)$ are plotted for $\epsilon = 1$ (a.1) and $\epsilon = 0.01$ (b.1). (a.2) and (b.2) are contour maps of (a.1) and (b.1), respectively.

We have investigated in the two cases: One is that the thickness of a wall is comparable to the size of the black hole ($\epsilon = 1$, in (a.1) and (a.2)), and the other is that the wall is ten times as thick as the size of the black hole ($\epsilon = 0.01$, in (b.1) and (b.2)). We obtain the domain wall configuration by extending Φ to the 'south' region as an odd function of z, *i.e.* $\Phi(x,-z) = -\Phi(x,z)$.

It can be seen by plotting energy density that the configuration have a truly wall-like structure. In fig.2, we show the energy density $T^t{}_t$ in the similar way to fig.1. In both cases, the energy density is localized about the equatorial plane with a certain thickness corresponding to ϵ.

4 Summary

We have numerically solved the equation of motion for scalar field with double well potential in the Schwarzchild black hole spacetime and obtained the static solution representing a domain wall intersecting the black hole.

One might wonder about our present results; one naively expects that the scalar field could have no stationary distribution around a black hole and inevitably fall into the horizon as usual objects do. However, being different from usual matter such as dust or perfect fluids, domain walls have negative pressure, or tension. Furthermore in our study we examined the domain walls which are extended infinitely in space. Then we can understand that the domain wall is suspended from the asymptotic region and supported against falling into the black hole by its tension, so that the stationary configuration is realized.

As a generalization of the present analysis, it is interesting to consider the system of a thick cosmic string and a black hole.

Acknowledgments

We would like to thank Hideki Ishihara, Hideo Kodama and Takashi Nakamura for many useful suggestions and comments. We also thank Susumu Higaki for stimulating discussions. This work was partially supported by Handai Yukawa Shogakukai (A.I.).

References

[1] A. Vilenkin and E.P.S. Shellard, *Cosmic Strings and other Topological Defects* (Cambridge University Press, New York, 1994).

[2] J. De Villiers and V. Frolov, Phys. Rev. **D58**, 105018 (1998) gr-qc/9804087. J. De Villiers and V. Frolov, Class. Quant. Grav. **16**, 2403 (1999) gr-qc/9812016.

[3] M. Christensen, V.P. Frolov and A.L. Larsen, Phys. Rev. **D58**, 085008 (1998) hep-th/9803158. V.P. Frolov, A.L. Larsen and M. Christensen, Phys. Rev. **D59**, 125008 (1999) hep-th/9811148.

[4] D. B. Cline ed.: *"Sources and detection of dark matter in the universe. Proceedings, 3rd International Symposium, and Workshop on Primordial Black Holes and Hawking Radiation, Marina del Rey, USA, February 17-20, 1998,"* Phys. Rept. **307**, 1 (1998).

[5] C.T. Hill, D.N. Schramm and J.N. Fry, Comments Nucl. Part. Phys. **19**, 25 (1989).

[6] R.A. Battye, M. Bucher and D. Spergel, astro-ph/9908047.

[7] A. Vilenkin, Phys. Lett. **B133**, 177 (1983). J. Ipser and P. Sikivie, Phys. Rev. **D30**, 712 (1984).

Theoretical formulation for two-point statistics on a light cone

Hiroaki Nishioka [1]

Department of Physics, Hiroshima University,
Higashi-hiroshima, 739-8526, Japan

Abstract

We examine the effect of the redshift-space distortion on the power spectrum and the two-point correlation function on a light cone. We develop theoretical formulae for the power spectrum and the two-point correlation function in linear theory of density perturbations in a rigorous manner. Approximate formulae, which are useful properly to incorporate the light-cone effect and redshift-space distortion into the power spectrum and the two-point correlation function are derived, and the validity is examined. Applying our formulae to galaxy and quasar samples which roughly match the SDSS survey, we will show how the light-cone effect and redshift-space distortion distort the power spectrum and the two-point correlation function.

1 Introduction

The wide-field redshift surveys of galaxies and quasars like 2dF and SDSS provide the three dimensional maps of the distribution of cosmological objects extended to high-redshifts. The dependence of various properties of the universe (initial density fluctuation, formation process of the cosmological objects, bias mechanism, luminosity function, cosmological parameters, dark matter, etc.) on the spatial distribution of the cosmological objects can be used to constrain these properties by comparison of the observational data with theoretical prediction.

The most used tools to quantify the clustering property of cosmological objects are the two-point correlation function and the power spectrum. Because the observation of the universe contains the various contaminations like the light-cone effect, redshift-space distortion, cosmological redshift-space distortion, and gravitational lensing effect, the statistical quantities calculated from the observational data are distorted by these effect. Then, to compare the theoretical prediction and observation, we should take these effects properly into account. Recently, a rigorous framework to incorporate the light-cone effect and redshift-space distortion into the two-point correlation function and the power spectrum has been developed [1,2,3,4]

In this paper, we focus on the light-cone effect and redshift-space distortion. We derive the theoretical formulae for the two-point correlation function and the power spectrum of cosmological objects distributed on a light-cone hypersurface in redshift space within the linear perturbation theory of the density fluctuation. And we examine how these effects distort the two-point correlation function and the power spectrum measured in wide- and deep-fields surveys, by modelling the galaxy and quasar samples which roughly match the SDSS samples.

This paper is organized as follows: In section 2 we define the estimator of the two-point correlation function and the power spectrum. In section 3 we derive the two-point correlation and the power spectrum on a light cone in redshift space by calculating the ensemble average of the estimator within the linear perturbation theory of the density fluctuation. In section 4 we discuss the light-cone effect and redshift-space distortion by numerical calculation. In section 5 we summarize the present paper. Throughout this paper, we use the unit in which the light velocity c is unity.

2 Definition of the estimator

In this section we define the estimators of the two-point correlation function and the power spectrum. And we show that these two estimators are the Fourier transform pairs, as the conventional two-point correlation function and the power spectrum.

[1] E-mail:nishioka@aqua.phys.sci.hiroshima-u.ac.jp

In a redshift survey, the position of a cosmological object is specified by the redshift z and the direction (unit) vector $\boldsymbol{\gamma}$. The cosmological distance to the cosmological object is evaluated from the redshift z through some converting formula. And a map of the cosmological objects is obtained eventually. The statistical quantities, the power spectrum and the two-point correlation function, are computed from the map. Introducing the variable s in order to specify the cosmological distance (the radial coordinate) in the redshift space, then we write the number density field of the cosmological objects in the redshift space $n^{\rm S}(s,\boldsymbol{\gamma})$ and the mean number density $n_0^{\rm S}(s)$. Following the conventional treatment of the power spectrum (e.g., [5]), we introduce the number density field

$$F(s,\boldsymbol{\gamma}) = \frac{n^{\rm S}(s,\boldsymbol{\gamma}) - n^{\rm S}_{\rm syn}(s,\boldsymbol{\gamma})}{\left[\int d^3s n_0^{\rm S}(s)^2\right]^{\frac{1}{2}}}, \tag{1}$$

where $n^{\rm S}_{\rm syn}(s,\boldsymbol{\gamma})$ is the number density field of objects for a synthetic catalog without structure which has the same mean number density $n_0^{\rm S}(s)$ as that of the cosmological objects $n^{\rm S}(s,\boldsymbol{\gamma})$. To be specific for the synthetic catalog, if we write $n^{\rm S}(s,\boldsymbol{\gamma})$ and $n^{\rm S}_{\rm syn}(s,\boldsymbol{\gamma})$ as

$$n^{\rm S}(s,\boldsymbol{\gamma}) = n_0^{\rm S}(s)[1+\Delta^{\rm S}(s,\boldsymbol{\gamma})], \tag{2}$$

$$n^{\rm S}_{\rm syn}(s,\boldsymbol{\gamma}) = n_0^{\rm S}(s)[1+\Delta^{\rm S}_{\rm syn}(s,\boldsymbol{\gamma})], \tag{3}$$

respectively, then we write

$$\left\langle \Delta^{\rm S}_{\rm syn}(s_1,\boldsymbol{\gamma}_1)\Delta^{\rm S}_{\rm syn}(s_2,\boldsymbol{\gamma}_2)\right\rangle = \left\langle \Delta^{\rm S}(s_1,\boldsymbol{\gamma}_1)\Delta^{\rm S}_{\rm syn}(s_2,\boldsymbol{\gamma}_2)\right\rangle = 0. \tag{4}$$

When the density field $F(s,\boldsymbol{\gamma})$ is given, one may compute the following two-point statistics,

$$\xi^{obs}(R) = \int \frac{d\Omega_{\hat{\boldsymbol{R}}}}{4\pi}\int d^3s_1 \int d^3s_2 F(s_1,\boldsymbol{\gamma}_1)F(s_2,\boldsymbol{\gamma}_2)\delta^{(3)}(\boldsymbol{s}_1-\boldsymbol{s}_2-\boldsymbol{R}), \tag{5}$$

where $\boldsymbol{s}_1 = s_1\boldsymbol{\gamma}_1$ and $\boldsymbol{s}_2 = s_2\boldsymbol{\gamma}_2$ and $R = |\boldsymbol{R}|$, and $\hat{\boldsymbol{R}} = \boldsymbol{R}/R$. Then the ensemble average of the estimator is written as

$$\xi^{\rm LC}_{\rm S}(R) = \left\langle \xi^{obs}(R)\right\rangle = \int \frac{d\Omega_{\hat{\boldsymbol{R}}}}{4\pi}\int d^3s_1 \int d^3s_2 \left\langle F(s_1,\boldsymbol{\gamma}_1)F(s_2,\boldsymbol{\gamma}_2)\delta^{(3)}(\boldsymbol{s}_1-\boldsymbol{s}_2-\boldsymbol{R})\right\rangle, \tag{6}$$

which we define as the two-point correlation function in the redshift space.

Next we consider the power spectrum. When the density field $F(s,\boldsymbol{\gamma})$ is given, one can compute the Fourier coefficient of equation (1)

$$\mathcal{F}(\boldsymbol{k}) = \int d^3s F(s,\boldsymbol{\gamma})e^{i\boldsymbol{k}\cdot\boldsymbol{s}} = \frac{\int d^3s[n^{\rm S}(s,\boldsymbol{\gamma}) - n^{\rm S}_{\rm syn}(s,\boldsymbol{\gamma})]e^{i\boldsymbol{k}\cdot\boldsymbol{s}}}{\left[\int d^3s n_0^{\rm S}(s)^2\right]^{\frac{1}{2}}}, \tag{7}$$

and the power spectrum may be computed as follows [5],

$$P^{obs}(k) = \int \frac{d\Omega_{\hat{\boldsymbol{k}}}}{4\pi}|\mathcal{F}(\boldsymbol{k})|^2, \tag{8}$$

where $\boldsymbol{k}$ denotes the wavenumber vector, and $k = |\boldsymbol{k}|$, and $\hat{\boldsymbol{k}} = \boldsymbol{k}/k$. The ensemble expectation value of the estimator is written as

$$P^{\rm LC}_{\rm S}(k) = \left\langle P^{obs}(k)\right\rangle = \int \frac{d\Omega_{\hat{\boldsymbol{k}}}}{4\pi}\left\langle |\mathcal{F}(\boldsymbol{k})|^2\right\rangle, \tag{9}$$

which we define as the power spectrum on a light cone in the redshift space.

In the case adopting the above definitions, we show the familiar fundamental relation which holds between the two-point correlation function and the power spectrum, as follows. With the use of the relation

$$\delta^{(3)}(\boldsymbol{s}_1 - \boldsymbol{s}_2 - \boldsymbol{R}) = \int \frac{d^3\boldsymbol{k}}{(2\pi)^3} e^{i\boldsymbol{k}\cdot(\boldsymbol{s}_1 - \boldsymbol{s}_2 - \boldsymbol{R})}, \tag{10}$$

equation (6) is written as

$$\begin{aligned} \xi_{\rm S}^{\rm LC}(R) &= \int \frac{d\Omega_{\hat{\boldsymbol{R}}}}{4\pi} \int \frac{d^3\boldsymbol{k}}{(2\pi)^3} \Big\langle |F(k)|^2 \Big\rangle e^{-i\boldsymbol{k}\cdot\boldsymbol{R}} \\ &= \frac{1}{2\pi^2} \int dk k^2 P_{\rm S}^{\rm LC}(k) j_0(kR). \end{aligned} \tag{11}$$

The inverse Fourier transformation yields,

$$P_{\rm S}^{\rm LC}(k) = 4\pi \int dR R^2 \xi_{\rm S}^{\rm LC}(R) j_0(kR). \tag{12}$$

Equations (11) and (12) are the familiar formulae which hold for the conventional two-point correlation function and the power spectrum defined on a constant-time hypersurface.

In this paper, we use a superscript LC to indicate quantities on the light cone explicitly. The power spectrum without the superscript $P(k)$ denotes the CDM power spectrum defined on the constant-time hypersurface at present. And we use subscripts (superscripts) R and S to indicate quantities in real and redshift space, respectively.

3 Formulation

In this section we derive the formula for two-point correlation function and the power spectrum, taking the light-cone effect and the redshift-space distortion into account within the linear perturbation theory of the density fluctuation based on the CDM scenario.

Throughout the present paper, we consider the spatially-flat Friedmann-Lemaitre universe, whose line element is expressed as

$$ds^2 = a^2(\eta)\Big[-d\eta^2 + d\chi^2 + \chi^2 d\Omega_{(2)}^2\Big], \tag{13}$$

where η is the conformal time, a is the scale factor, and χ is the radial coordinate. We normalize the scale factor to be unity at present, $a(\eta) = 1$. Then the Friedmann equation is

$$\left(\frac{\dot{a}}{a}\right)^2 = H_0^2\left(\frac{\Omega_0}{a} + a^2\Omega_\lambda\right), \tag{14}$$

where $H_0 = 100h$km/s/Mpc is the Hubble parameter, $\Omega_0 (= 1 - \Omega_\lambda)$ is the density parameter, and the dot denotes η-differentiation. In this section we assume that the cosmological model is exact.

Since we locate a fiducial observer at the origin of coordinates ($\eta = \eta_0, \chi = 0$), a cosmological object at χ and η on the light cone hypersurface of the observer satisfies a simple relation $\eta = \eta_0 - \chi$. Then the real- space position of source is specified by (χ, γ), where γ is an unit vector along the line of sight. We introduce the radial coordinate r instead of χ, and we denote the metric of the three dimensional real space on a light cone hypersurface as

$$ds_{LC}^2 = dr^2 + r^2 d\Omega_{(2)}^2. \tag{15}$$

Then we denote the number density of sources on the light cone by $n^{\rm R}(r, \gamma)$, which is simply related to the comoving number density of objects at a conformal time η and at a position (χ, γ) , $n(\eta, \chi, \gamma)$ as

$$n^{\rm R}(r, \gamma) = n(\eta, \chi, \gamma)|_{\eta \to \eta_0 - r, \chi \to r}. \tag{16}$$

By using the mean observed comoving number density $n_0(\eta)$ at time η and the density fluctuation of luminous objects $\Delta(\eta, \chi, \gamma)$, we write

$$n(\eta, \chi, \gamma) = n_0(\eta)[1 + \Delta(\eta, \chi, \gamma)]. \tag{17}$$

Then equation (16) is rewritten as

$$n^{\rm R}(r,\gamma) = n_0^{\rm R}(r)[1+\Delta^{\rm R}(r,\gamma)], \tag{18}$$

where we defined

$$n_0^{\rm R}(r) \equiv n_0(\eta)|_{\eta\to\eta_0-r}, \qquad \Delta^{\rm R}(r,\gamma) \equiv \Delta(\eta,\chi,\gamma)|_{\eta\to\eta_0-r,\chi\to r}. \tag{19}$$

Note that the mean observed number density $n_0(\eta)$ is different from the mean number density of the objects at η by a factor of the selection function.

Now we consider the two-point correlation function (6) in the redshift space. The relation between the redshift space and the real space is specified as follows,

$$n^{\rm S}(s,\gamma)s^2 ds d\Omega_\gamma = n^{\rm R}(r,\gamma)r^2 dr d\Omega_\gamma, \tag{20}$$

$$n^{\rm S}_{\rm syn}(s,\gamma)s^2 ds d\Omega_\gamma = n^{\rm R}_{\rm syn}(r,\gamma)r^2 dr d\Omega_\gamma, \tag{21}$$

and

$$s = r + \delta r(r,\gamma), \tag{22}$$

where $\delta r(r,\gamma)$ in equation (22) represents the apparent shift in the comoving radial coordinate due to the peculiar velocity. $\delta r(r,\gamma)$ is of order of the velocity perturbation. Equation (21) defines the number density of the synthetic catalog in the real space $n^{\rm R}_{\rm syn}(r,\gamma)$.

With the use of the above equations we obtain the following expression from (6),

$$\begin{aligned}\xi^{\rm LC}_{\rm S}(R) &= \left[\int d^3 r n_0^{\rm R}(r)^2\right]^{-1} \int \frac{d\Omega_{\hat{\boldsymbol{R}}}}{4\pi} \int dr_1 r_1^2 d\Omega_{\gamma_1} \int dr_2 r_2^2 d\Omega_{\gamma_2} \\ &\times \Big\langle [n^{\rm R}(r_1,\gamma_1) - n^{\rm R}_{\rm syn}(r_1,\gamma_1)][n^{\rm R}(r_2,\gamma_2) - n^{\rm R}_{\rm syn}(r_2,\gamma_2)] \\ &\times \delta^{(3)}(\boldsymbol{r}_1 + \delta\boldsymbol{r}_1 - \boldsymbol{r}_2 - \delta\boldsymbol{r}_2 - \boldsymbol{R})\Big\rangle,\end{aligned} \tag{23}$$

where $\boldsymbol{r} + \delta\boldsymbol{r} = (r+\delta r)\gamma$ and we have assumed

$$\int d^3 s n_0^{\rm S}(s)^2 = \int d^3 r n_0^{\rm R}(r)^2. \tag{24}$$

Note that the number density field of the synthetic catalog in the redshift space $n^{\rm S}_{\rm syn}(s,\gamma)$ has no structure. Then the number density field in the real space $n^{\rm R}_{\rm syn}(r,\gamma)$, which is defined by equation (21), has a structure. Writing the number density field as

$$n^{\rm R}_{\rm syn}(r,\gamma) = n_0^{\rm R}(r)[1+\Delta^{\rm R}_{\rm syn}(r,\gamma)], \tag{25}$$

the density contrast $\Delta^{\rm R}_{\rm syn}(r,\gamma)$ is expressed as [6],

$$\Delta^{\rm R}_{\rm syn}(r,\gamma) = \Delta^{\rm S}_{\rm syn}(r,\gamma) + \left(\frac{\partial}{\partial r} + \frac{\alpha(r)}{r}\right)\delta r(r,\gamma), \tag{26}$$

where

$$\alpha(r) = \frac{\partial \ln r^2 n_0^{\rm R}(r)}{\partial \ln r}, \tag{27}$$

and we use $\Delta^{\rm S}_{\rm syn}(r,\gamma) = \Delta^{\rm S}_{\rm syn}(s,\gamma)$ within the linear order of perturbation. In the leading order of the perturbative expansion, equation (23) is rewritten as

$$\begin{aligned}\xi^{\rm LC}_{\rm S}(R) &= \left[\int d^3 r n_0^{\rm R}(r)^2\right]^{-1} \int \frac{d\Omega_{\hat{\boldsymbol{R}}}}{4\pi} \int dr_1 r_1^2 d\Omega_{\gamma_1} \int dr_2 r_2^2 d\Omega_{\gamma_2} n_0^{\rm R}(r_1) n_0^{\rm R}(r_2) \\ &\times \Big\langle [\Delta^{\rm R}(r_1,\gamma_1) - \left(\frac{\partial}{\partial r_1} + \frac{\alpha(r_1)}{r_1}\right)\delta r_1(r_1,\gamma_1)] \\ &\times [\Delta^{\rm R}(r_2,\gamma_2) - \left(\frac{\partial}{\partial r_2} + \frac{\alpha(r_2)}{r_2}\right)\delta r_2(r_2,\gamma_2)]\Big\rangle \delta^{(3)}(\boldsymbol{r}_1 - \boldsymbol{r}_2 - \boldsymbol{R}),\end{aligned} \tag{28}$$

where we used (18), (25), (26), and (4). Based on the CDM model with the linear biasing,

$$\Delta_{klm}(\eta) = b(k;\eta)\delta^{(c)}_{klm}(\eta), \tag{29}$$

the straightforward calculation leads to the following expression,

$$\begin{aligned}
\xi^{\rm LC}_{\rm S}(R) &= \left[\int dr r^2 n^{\rm R}_0(r)^2\right]^{-1} \frac{1}{2R}\iint_S dr_1 dr_2 r_1 r_2 n^{\rm R}_0(r_1) n^{\rm R}_0(r_2) \\
&\times \frac{1}{2\pi^2}\int dk k^2 P(k) \prod_{i=1}^{2}\left[b(k;\eta_0 - r_i) D_1(\eta_0 - r_i)\right] \\
&\times \Big[j_0(kR) + \beta(k;\eta_0 - r_2) I(k;R;r_1,r_2) + \beta(k;\eta_0 - r_1) I(k;R;r_2,r_1) \\
&+ \beta(k;\eta_0 - r_1)\beta(k;\eta_0 - r_2) J(k;R;r_1,r_2)\Big],
\end{aligned} \tag{30}$$

where S denotes the region $|r_1 - r_2| \le R \le r_1 + r_2$, $P(k)$ is the CDM power spectrum at present, $D_1(\eta)$ is the linear growth rate normalized to be unity at present, $I(k;R;r_1,r_2)$ and $J(k;R;r_1,r_2)$ are defined as

$$I(k;R;r_1,r_2) = \frac{j_1(kR)}{kR} - \frac{j_2(kR)}{R^2}\left\{\frac{R^2 + r_2^2 - r_1^2}{2r_2}\right\} \tag{31}$$

$$\begin{aligned}
J(k;R;r_1,r_2) &= \frac{j_2(kR)}{(kR)^2}\left[2\left\{\frac{r_1^2 + r_2^2 - R^2}{2r_1 r_2}\right\}^2 + 1\right] \\
&+ \frac{j_4(kR)}{R^4}\left\{\frac{R^2 + r_1^2 - r_2^2}{2r_1}\right\}^2\left\{\frac{R^2 + r_2^2 - r_1^2}{2r_2}\right\}^2 \\
&- \frac{j_3(kR)}{kR^3}\left[\left\{\frac{R^2 + r_1^2 - r_2^2}{2r_1}\right\}^2 + \left\{\frac{R^2 + r_2^2 - r_1^2}{2r_2}\right\}^2\right. \\
&\left. + \frac{R^2 + r_1^2 - r_2^2}{r_1}\frac{R^2 + r_2^2 - r_1^2}{r_2}\frac{r_1^2 + r_2^2 - R^2}{2r_1 r_2}\right],
\end{aligned} \tag{32}$$

and $\beta(k;\eta)$ is defined as

$$\beta(k;\eta) = \frac{1}{b(k;\eta)}\frac{d\ln D_1(\eta)}{d\ln a(\eta)}. \tag{33}$$

Applying the plane-parallel, or distant observer, approximation, equation (30) reduces to the simple form. In the case where R is small compared with the size of the survey volume, we use the approximation

$$\iint_S dr_1 dr_2 \simeq \int dr_1 \int_{-R}^{R} dx \tag{34}$$

where $x = r_2 - r_1$, and $I(k;R;r_1,r_2)$ and $J(k;R;r_1,r_2)$ are approximated as

$$I(k;R;r_1,r_2) = \frac{j_1(kR)}{kR} - \frac{j_2(kR)}{R^2}x^2, \tag{35}$$

$$J(k;R;r_1,r_2) = 3\frac{j_2(kR)}{(kR)^2} - 6\frac{j_3(kR)}{kR^3}x^2 + \frac{j_4(kR)}{R^4}x^4, \tag{36}$$

respectively. Integration over x yields,

$$\xi^{\rm LC}_{\rm S}(R) \simeq \frac{\int dr r^2 n^{\rm R}_0(r)^2 \xi[R, z(r)]_{\rm source}}{\int dr r^2 n^{\rm R}_0(r)^2}, \tag{37}$$

where we defined

$$\xi[R, z(r)]_{\rm source} = \frac{1}{2\pi^2}\int dk k^2 P(k) D_1(\eta_0 - r)^2 b(k;\eta_0 - r)^2 \times\left[1 + \frac{2}{3}\beta(k;\eta_0 - r) + \frac{1}{5}\beta(k;\eta_0 - r)^2\right] j_0(kR). \quad (38)$$

This formula indicates that the two-point correlation function on a light cone is obtained by averaging the correlation function at each time defined on the constant-time hypersurface $\xi[R, z(r)]_{\rm source}$ by weighting $n_0^{\rm R}(r)^2$. We note that this formula is rigorously derived only in the framework of linear theory.

The power spectrum on the light-cone, $P_{\rm S}^{\rm LC}(k)$, is obtained from the two-point correlation function by substituting equation (30) into (12).The approximate formula for the power spectrum is easily obtained by substituting equation (38) into equation (12),

$$P_{\rm S}^{\rm LC}(k) \simeq \alpha(k) P(k), \quad (39)$$

where

$$\alpha(k) = \frac{\int dr r^2 n_0^{\rm R}(r)^2 b(k;\eta_0 - r)^2 D_1(\eta_0 - r)^2 \left[1 + \frac{2}{3}\beta(k;\eta_0 - r) + \frac{1}{5}\beta(k;\eta_0 - r)^2\right]}{\int dr r^2 n_0^{\rm R}(r)^2}. \quad (40)$$

In the case that the bias does not depend on the scale of the density fluctuation or k, i.e., $b(k;\eta) = b(\eta)$, $\alpha(k)$ becomes a constant α. Thus in this case the light-cone effect and the linear redshift-space distortion is described by the constant α.

4 Numerical results and discussion

In this section we apply the formulae developed in the previous section to galaxy and quasar samples. For the galaxy luminosity function, we adopt a B-band luminosity function of the APM galaxies [7] fitted to Schechter function

$$\phi(L) = \phi^*\left(\frac{L}{L^*}\right)^{\nu} \exp\left(-\frac{L}{L^*}\right) d\left(\frac{L}{L^*}\right), \quad (41)$$

with $\phi^* = 1.40 \times 10^{-2} h^3 {\rm Mpc}^{-3}$, $\nu = -0.97$, and $M_B^* = -19.50 + 5\log_{10} h$. Then the comoving number density of galaxies at z which are brighter than the limiting magnitude $B_{\rm lim}$ is given by

$$n_0(z, < B_{\rm lim}) = \int_{L(B_{\rm lim}, z)}^{\infty} \phi(L) dL = \phi^* \Gamma[\nu + 1, x(B_{\rm lim}, z)], \quad (42)$$

where,

$$x(B_{\rm lim}) \equiv \frac{L(B_{\rm lim}, z)}{L^*} = \left[\frac{d_L(z)}{1h^{-1}{\rm Mpc}}\right]^2 10^{2.2 - 0.4 B_{\rm lim}}, \quad (43)$$

and $\Gamma[\nu, x]$ is the incomplete Gamma function. We consider the galaxy samples in the range of redshift $0 \le z \le 0.2$, and adopt the B-band limiting magnitude 19 to match the SDSS spectroscopic sample.

We also assume quasar samples which roughly match the SDSS quasar survey, where we use a selection function for B-band magnitude limited samples on the basis of the luminosity function by Wallington and Narayan [8] and adopt the B-band limiting magnitude 20. And we assume the depth of the survey volume to be $z_{\rm max} = 5$.

As for the bias we adopt the model by Fry [9].

$$b(\eta) = 1 + \frac{1}{D_1(\eta)}(b_0 - 1), \quad (44)$$

Figure 1 plots the galaxy and quasar correlation function and power spectrum in which we adopted the LCDM model and the case of no bias. The solid line which represent the exact two-point correlation

function and power spectrum are compared with the approximate ones. The approximation for the two-point correlation function and the power spectrum is good for small R or large k, but for larger R or smaller k, the deviation becomes significant. This behavior originates from the finite size effect of the survey volume. Then we cannot evaluate the power spectrum properly at $1/k \gtrsim r_{\rm max}$.

Figure 2 plots the factor α/b_0^2 as a function of Ω_0. The solid and the dotted lines represent the factor α/b_0^2 in the redshift space and the real space, respectively. Here we adopt the same model for the galaxy and quasar luminosity function as in Figure 1. From Figure 2 it is apparent that the light-cone effect and the linear redshift-space distortion becomes more effective as Ω_0 increases. This is traced to the behavior of the linear growth rate. For the galaxy sample, the increase of amplitude due to the redshift-space distortion is effective than the decrease due to the light-cone effect. In contrast to this, for the quasar sample, the light-cone effect and the time-evolution of bias becomes important.

5 Summary

In the present paper we derived the formulae for the two-point correlation function and the power spectrum on light-cone in redshift space within the linear theory of the CDM density perturbation. Using the distant observer approximation we get the simple relation (eqs.(38) and (39)) which is valid for $k \gtrsim 1/r_{\rm max}$.

Applying our formulae to galaxy and quasar samples which is roughly match the SDSS survey, we get the following results. For galaxy samples the light-cone effect suppress the power spectrum amplitude $\sim 10\%$ and redshift-space distortion enhance it $\sim 60\%$. For quasar samples, the light-cone effect is highly influential. Then the time dependence of bias would have the significant influence to the amplitude of the power spectrum.

For more precise prediction, we need to consider the nonlinear effect, the cosmological redshift-space distortion, and the realistic models for bias and luminosity function.

ACKNOWLEDGMENTS

This work is based on the collaboration with K. Yamamoto and Y. Suto. The author would like to thank Yasufumi Kojima for useful discussions. Numerical computations were carried in part on INSAM of Hiroshima University.

References

[1] K. Yamamoto and Y. Suto, 1999, ApJ, 517, 1

[2] K. Yamamoto, H. Nishioka and Y. Suto, 1999, ApJ in press

[3] Y. Suto, H. Magira, Y. P. Jing, T. Matsubara, and K. Yamamoto, 1999, Prog. Theor. Phys. Supp., 133, 183

[4] H. Nishioka and K. Yamamoto, 1999, ApJ, 520, 426

[5] H. A. Feldman, N. Kaiser, and A. A. Peacock, 1994, ApJ, 426, 23

[6] A. J. S. Hamilton, 1998, in " The Evolving Universe. Selected Topics on Large-Scale Structure and on the Properties of Galaxies", (Kluwer: Dordrecht), p.185

[7] J. Loveday, B. A. Peterson, G. Efsathiou, and S. J. Maddox, 1992, ApJ, 390, 338

[8] S. Wallington and R. Narayan, 1993, ApJ, 403, 517

[9] N. J. Fry, 1996, ApJ, 461, L65

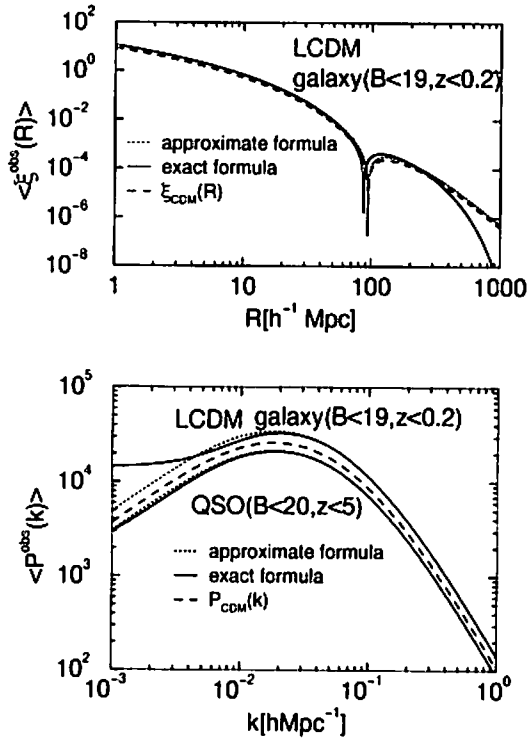

Figure 1: The galaxy and quasar two-point correlation function and power spectrum. The upper panel plots the two-point correlation function and the lower panel does the power spectrum. The solid and dotted lines represent the exact and approximate formulae for two-point correlation function and power spectrum. For comparison the CDM correlation function and power spectrum at present are plotted (dashed lines).

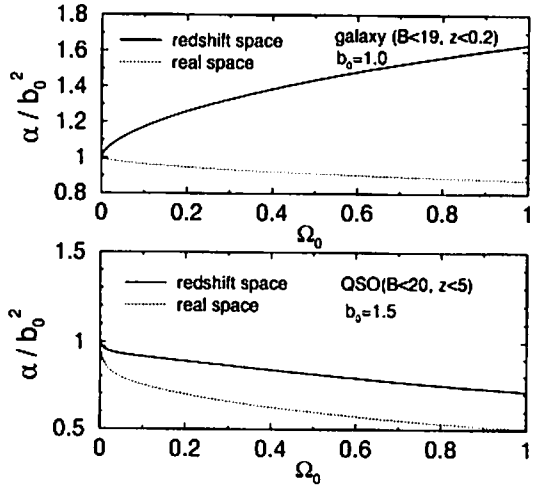

Figure 2: The factor α/b_0^2 for galaxy and quasar as a function of Ω_0 is plotted. The solid and the dotted lines represent the factor in the redshift and the real spaces, respectively. We adopt the galaxy and quasar samples in upper and lower panel, respectively.

Second-order rotational effects on the r-mode oscillations in GR

Masayasu Hosonuma[1] and Yasufumi Kojima[2]

Department of Physics, Hiroshima University,
Higashi-Hiroshima 739-8526, Japan

Abstract

We study the r-mode oscillations including both the effects of second-order rotational corrections and metric perturbations in a general relativistic framework. In this paper, we extend the methods used in the previous work in which we studied the axial mode oscillations with the Cowling approximation. We obtain the analytic representations of the equation governing mode functions. We take the first step to examine the nonlinear effects of fluid and metric perturbations.

1 Introduction

The Andersson's surprising discovery [1], that rotating relativistic stars are generically unstable against the r-mode instability, makes the r-mode oscillations one of the most attractive astrophysical subjects. A large literature have been published by many authors in recent few years. In these papers, they have investigated astrophysical implications of pulsations and estimated the detectability of gravitational waves associated with this instability [2]-[8]. Most of these studies have done within the Newtonian theory of gravity and the lowest-order of rotation have been considered alone. When the gravitational waves associated with the r-mode instability are concerned, the general relativistic aspect plays an important role. Moreover, the higher-order of rotational effects on the r-mode frequency are not well understood as yet.

The stellar oscillations can be divided into two classes by parity, axial and polar. The r-mode we will discuss belongs to the axial mode. The axial oscillation is trivial in the non-rotating stars, since there is no restoring force in the fluid stars. The oscillation becomes possible in the rotating stars. We therefore have to consider the oscillation on the rotating stars, which will be a difficult task. In the spherically symmetric case, the perturbations can be decoupled into the axial and polar perturbations with spherical harmonic index (l, m). In the presence of rotation, the perturbations are described by the mixed state of them. We expand the mode functions by a rotational parameter, then axial-led functions are induced by lower order of the polar-led functions and *vice versa*. The second-order axial mode or r-mode means the mode of higher order induced by the lowest order of polar mode. We investigate second-order of axial-led functions here. The effects on the r-mode frequency caused by the higher order of fluid and metric perturbations should be studied.

For quest of this problem, as the first step, we have investigated the r-mode oscillations on a rotating relativistic star with neglecting metric perturbations, i.e., the Cowling approximation in a recent our paper [7] (referred to hereafter as Paper I). We have showed that the higher rotational corrections make mode frequency undegenerated even in Newtonian limit. The importance of higher order of rotation on the fluid have been recognized. In Paper I, we have treated with the fluid perturbations only. We have to extend this perturbation scheme to the version including metric perturbations.

In Section 2, we formulate the linearized Einstein field equations and linear perturbation method. In Section 3, the lowest order of axial-led functions are shown. In Section 4, we derive equations which the polar-led functions obey. The axial-led functions including second-order corrections are given in Section 5. Finally, we summarize we have obtained in Section 6.

[1]E-mail:numa@theo.phys.sci.hiroshima-u.ac.jp
[2]E-mail:kojima@theo.phys.sci.hiroshima-u.ac.jp

2 Perturbation scheme

We consider a rotating star with uniform angular velocity $\Omega \sim O(\varepsilon)$, where ε is a small rotational parameter. The metric and fluid quantities describing the equilibrium state can be calculated by the slow-rotation formalism [9]. They are summarized in the Appendix. We next investigate the perturbations from the state. The metric perturbations can be described by six functions. Working in the Regge-Wheeler gauge [12], the perturbations are expressed as

$$h_{\mu\nu} = \sum_{l,m} \begin{pmatrix} e^{\nu} H_{0lm}(t,r) Y_{lm} & H_{1lm}(t,r) Y_{lm} & -h_{0lm}(t,r) \frac{\partial_\phi Y_{lm}}{\sin\theta} & h_{0lm}(t,r) \sin\theta \partial_\theta Y_{lm} \\ \mathrm{sym} & e^{\lambda} H_{2lm}(t,r) Y_{lm} & -h_{1lm}(t,r) \frac{\partial_\phi Y_{lm}}{\sin\theta} & h_{1lm}(t,r) \sin\theta \partial_\theta Y_{lm} \\ \mathrm{sym} & \mathrm{sym} & r^2 K_{lm}(t,r) Y_{lm} & 0 \\ \mathrm{sym} & \mathrm{sym} & \mathrm{sym} & r^2 \sin^2\theta K_{lm}(t,r) Y_{lm} \end{pmatrix}, \quad (1)$$

where $Y_{lm} = Y_{lm}(\theta,\phi)$ represents spherical harmonics. The angular part is expanded with an appropriate combination of the harmonics. In a same way, the fluid perturbations are described by five functions. They are the pressure perturbation δp, density perturbation $\delta\rho$ and three components of the 4-velocity $(\delta u_r, \delta u_\theta, \delta u_\phi)$. The component δu_t can be determined by the condition, $\delta u_\mu u^\mu = 0$. These perturbed quantities are also expanded as

$$\delta p = \sum_{l,m} \delta p_{lm}(t,r) Y_{lm}(\theta,\phi), \quad (2)$$

$$\delta\rho = \sum_{l,m} \delta\rho_{lm}(t,r) Y_{lm}(\theta,\phi), \quad (3)$$

$$(\rho+p)\delta u_r = e^{\nu/2} \sum_{l,m} R_{lm}(t,r) Y_{lm}(\theta,\phi), \quad (4)$$

$$(\rho+p)\delta u_\theta = e^{\nu/2} \sum_{l,m} \left[V_{lm}(t,r) \partial_\theta Y_{lm}(\theta,\phi) - \frac{U_{lm}(t,r)}{\sin\theta} \partial_\phi Y_{lm}(\theta,\phi) \right], \quad (5)$$

$$(\rho+p)\delta u_\phi = e^{\nu/2} \sum_{l,m} \left[V_{lm}(t,r) \partial_\phi Y_{lm}(\theta,\phi) + U_{lm}(t,r) \sin\theta \partial_\theta Y_{lm}(\theta,\phi) \right]. \quad (6)$$

These eleven functions are determined by ten components of the linearized Einstein field equations,

$$\delta G_{\mu\nu} = 8\pi \delta T_{\mu\nu}, \quad (7)$$

and the adiabatic condition for the perturbations,

$$\delta p + \xi \cdot \nabla p = \frac{\Gamma p}{p+\rho} (\delta\rho + \xi \cdot \nabla\rho), \quad (8)$$

where Γ is the adiabatic index and ξ is the Lagrange displacement.

Now we will solve the pulsation equations by the expansion of the spherical harmonics. In the spherically symmetric star, the equations are decoupled for each harmonic index (l,m). The perturbations can also be decoupled into the axial and polar perturbations. They are respectively described by the axial functions $\mathcal{A}_{lm} \equiv (U_{lm}, h_{0,lm}, h_{1,lm})$, and the polar functions $\mathcal{P}_{lm} \equiv (\delta p_{lm}, \delta\rho_{lm}, R_{lm}, V_{lm}, H_{0,lm}, H_{1,lm}, H_{2,lm}, K_{lm})$. In the presence of rotation, the perturbations are described by the mixed state of them. From now on, we call these functions as the axial-led ones for $\mathcal{A}_{lm}$ and the polar-led ones for $\mathcal{P}_{lm}$. Since the slow rotation corresponds to the perturbation with $l = 1$, the formal relation between $\mathcal{A}_{lm}$ and $\mathcal{P}_{lm}$ in the eqs. (7)-(8) can schematically be expressed as

$$0 = [\mathcal{A}_{lm}] + \mathcal{E} \times [\mathcal{P}_{l\pm1m}] + \mathcal{E}^2 \times [\mathcal{A}_{lm}, \mathcal{A}_{l\pm2m}] + \cdots, \quad (9)$$

$$0 = [\mathcal{P}_{lm}] + \mathcal{E} \times [\mathcal{A}_{l\pm1m}] + \mathcal{E}^2 \times [\mathcal{P}_{lm}, \mathcal{P}_{l\pm2m}] + \cdots, \quad (10)$$

where the symbol $\mathcal{E}$ denotes some functions of order ε, and the square bracket formally represents the relation among the perturbation functions therein. We moreover assume that the axial-led functions are

dominant in the slowly rotating star, i.e., $\mathcal{A}_{lm} \gg \mathcal{P}_{lm}$. This assumption is not valid for the some cases. If the star and its perturbations obey the same one-parameter equation of state, r-modes and g-modes are coupled at the lowest order in general. They are respectively described by $\mathcal{P}_{lm}$ and $\mathcal{A}_{lm}$, which have zero frequency in the spherical isentropic star. They form hybrid modes in the rotating star. However, the r-modes are discriminated from the g-modes for non-isentropic stars, since the g-mode frequencies are non-zero in the spherical limit. In that case, we may use the assumption $\mathcal{A}_{lm} \gg \mathcal{P}_{lm}$ to solve the r-mode oscillations, and expand as

$$\mathcal{A}_{lm} = \mathcal{A}^{(1)}_{lm} + \varepsilon^2 \mathcal{A}^{(2)}_{lm} + \cdots, \quad \mathcal{P}_{lm} = \varepsilon(\mathcal{P}^{(1)}_{lm} + \varepsilon^2 \mathcal{P}^{(2)}_{lm} + \cdots). \tag{11}$$

Substituting these functions into eqs.(9)-(10), and comparing each order of ε, we have the following equations of $\varepsilon^n (n = 0, 1, 2)$,

$$0 = [\mathcal{A}^{(1)}_{lm}], \tag{12}$$

$$0 = [\varepsilon \mathcal{P}^{(1)}_{l\pm1m} + \mathcal{E} \times \mathcal{A}^{(1)}_{lm}], \tag{13}$$

$$0 = [\varepsilon^2 \mathcal{A}^{(2)}_{lm}] + \mathcal{E} \times [\varepsilon \mathcal{P}^{(1)}_{l\pm1m}] + \mathcal{E}^2 \times [\mathcal{A}^{(1)}_{lm}, \mathcal{A}^{(1)}_{l\pm2m}] \tag{14}$$

$$= [\varepsilon^2 \mathcal{A}^{(2)}_{lm} + \mathcal{E}^2 \times \mathcal{A}^{(1)}_{lm}]. \tag{15}$$

We have here assumed that the perturbation is described by a single spherical harmonic in the lowest order, that is, $\mathcal{A}^{(1)}_{l'm} = 0$, for $l' \neq l$. The polar-led functions in eq.(14) are eliminated by eq.(13). Equation (12) represents the axial oscillation at the lowest order. Equation (15) is the second-order form of it, and the term $\mathcal{E}^2 \times \mathcal{A}^{(1)}_{lm}$ can be regarded as the rotational corrections. The method to solve the equations is straightforward. The first-order equations are solved by the axial-led functions. The polar-led functions are expressed using them. We have the second-order equations with the corrections expressed by the axial-led functions at the lowest-order. These equations are successively solved in the following sections. In the actual calculations, we also assume that the time variation of the oscillation is slow and proportional to Ω, i.e., $\partial_t \sim \Omega \sim O(\varepsilon)$. This is true in the r-mode oscillation, as will be confirmed soon.

3 Lowest-order calculation

In this section, we review the equations governing the axial oscillations at the lowest order. The radial functions are decoupled for each spherical harmonic index. We denote it as $L \equiv (l, m)$ for the abbreviation. The relevant functions are $h_{0,L}, h_{1,L}$ and U_L and are calculated from three components of the Einstein equations. They are essentially $(t\phi)$ $(r\phi)$ and $(\theta\phi)$ components. We define a function $\Phi^{(1)}_L$ as

$$\Phi^{(1)}_L = \frac{h^{(1)}_{0,L}}{r^2}. \tag{16}$$

The relation between the metric functions is given by

$$h^{(1)}_{1,L} = \frac{r^4 e^{-\nu}}{[l(l+1)-2]} \left[(\partial_T - im\varpi)\Phi^{(1)\prime}_L + \frac{2im\varpi'}{l(l+1)} \Phi^{(1)}_L \right], \tag{17}$$

where $\partial_T = \partial_t + im\Omega$ denotes a time-derivative in a co-rotating frame and a prime denotes a derivation with respect to r. The axial velocity function is expressed by two ways:

$$(\partial_T - im\chi) U^{(1)}_L = -4\pi(p_0 + \rho_0) r^2 e^{-\nu} \partial_T \Phi^{(1)}_L, \tag{18}$$

$$U^{(1)}_L = \frac{j^2 r^2}{4} \left[\frac{1}{jr^4} (jr^4 \Phi^{(1)\prime}_L)' - (v + 16\pi(p_0 + \rho_0) e^{\lambda}) \Phi^{(1)}_L \right], \tag{19}$$

where

$$\chi = \frac{2}{l(l+1)} \varpi = \frac{2}{l(l+1)} (\Omega - \omega), \tag{20}$$

$$v = \frac{e^{\lambda}}{r^2} [l(l+1) - 2], \tag{21}$$

$$j = e^{-(\lambda+\nu)/2}. \tag{22}$$

Eliminating $U_L^{(1)}$ in eqs.(18)-(19), we have a second-order differential equation for $\Phi_L^{(1)}$.

$$0 = \mathcal{L}[\Phi^{(1)}] \tag{23}$$

$$= (\partial_T - im\chi)\left[\frac{1}{jr^4}\left(jr^4\Phi_L^{(1)\prime}\right)' - v\Phi_L^{(1)}\right] + 16\pi im\chi(p_0+\rho_0)e^{\lambda}\Phi_L^{(1)}. \tag{24}$$

When one can solve equation (24), other functions, $h_{1,L}^{(1)}$ and $U_L^{(1)}$ can be determined from eqs. (17) and (19). As we will show in the subsequent sections, the function $\Phi^{(1)}$ can also affect the polar-led functions. When one considers the equations for the next order, $\Phi^{(2)}$, additional higher order terms should be included in the form (24).

This equation is reduced to an eigen-value equation [3], by assuming $\exp(-i\sigma t)$:

$$(\varpi - \mu)\left[\frac{1}{jr^4}(jr^4\Phi_L^{\prime(1)})' - v\Phi_L^{(1)}\right] = q\Phi_L^{(1)}, \tag{25}$$

$$\mu = -\frac{l(l+1)}{2m}(\sigma - m\Omega), \tag{26}$$

$$q = \frac{1}{jr^4}\left(jr^4\varpi'\right)' = 16\pi(p_0+\rho_0)e^{\lambda}\varpi \geq 0. \tag{27}$$

with assuming the time dependence for the mode as the form $e^{-i\sigma t}$, σ is the frequency of the mode.

Equation (25) is called singular eigen-value equation, since it has a singular point r_0 unless $q(r_0) = 0$, corresponding to the real value of $\mu = \varpi(r_0)$. This kind of singular eigen-value equation is studied for the incompressible shear flow. See the Appendix for the Rayleigh equation in two dimensional parallel flows. Some important conclusion can be derived from the behavior of the background flow, i.e., the function ϖ in this problem. For example, the necessary condition of the instability is that the function ϖ has inflection point, i.e., $q = 0$. This condition is never satisfied inside the star. As a result, the frequency is real and the flow is stable in this order.

4 First-order corrections in polar-led functions

In this section, we will derive the equations governing the polar-led functions, $H_0^{(1)}$, $H_1^{(1)}$, $H_2^{(1)}$, $K^{(1)}$, $\delta p^{(1)}$, $\delta\rho^{(1)}$, $R^{(1)}$ and $V^{(1)}$. As shown in section 2, the functions with $(l \pm 1, m)$ are coupled with the axial-led functions with (l, m). We will shorten the subscript of the spherical harmonic index as e.g., $\delta p_{\pm}^{(1)} \equiv \delta p_{l\pm1m}^{(1)}$. These eight functions are determined by seven components of the linearized Einstein field equations and one thermodynamical relation. The calculations are straightforward, but results are sometimes messy. The pressure $\delta p_{\pm}^{(1)}$ and density perturbations $\delta\rho_{\pm}^{(1)}$ are expressed by

$$\delta p_{\pm}^{(1)} = \frac{1}{2}(p_0+\rho_0)(H_{0,\pm}^{(1)} + 2T_{\pm}\Omega r^2 e^{-\nu}\Phi_L^{(1)}) + 2S_{\pm}\varpi U_L^{(1)}, \tag{28}$$

$$\delta\rho_{\pm}^{(1)} = -\frac{\rho_0'}{\nu'}(H_{0,\pm}^{(1)} + 2T_{\pm}\Omega r^2 e^{-\nu}\Phi_L^{(1)}) - 4S_{\pm}\frac{e^{-\nu/2}}{\nu'}\left(e^{\nu/2}\varpi U_L^{(1)}\right)' + 2T_{\pm}\frac{e^{\nu}}{\nu' r^2}(\varpi r^2 e^{-\nu})' U_L^{(1)}, \tag{29}$$

where

$$S_+ = \frac{l}{l+1}Q_+, \quad S_- = \frac{l+1}{l}Q_-, \quad T_+ = lQ_+, \quad T_- = -(l+1)Q_-, \tag{30}$$

$$Q_- = \sqrt{\frac{(l+1)^2 - m^2}{(2l+1)(2l+3)}}, \quad Q_- = \sqrt{\frac{l^2 - m^2}{(2l-1)(2l+1)}}. \tag{31}$$

These quantities are expressed by the axial-led functions $(\Phi_L^{(1)}, U_L^{(1)})$ and $H_{0,\pm}^{(1)}$. There is another relation between $H_{0\pm}^{(1)}$ and $\delta\rho_\pm^{(1)}$ in the field equations. Eliminating $\delta\rho_\pm^{(1)}$, we have a second-order differential equation for the metric perturbations. The equation can be regarded as relativistic version of the Poisson equation, $\nabla^2\delta\phi = 4\pi\delta\rho$, for the gravitational potential $\delta\phi$ and the density perturbation $\delta\rho$. In the relativistic case, the Newtonian potential is replaced by $H_0^{(1)}$ or $K^{(1)}$. Therefore, the second-order differential equation is explicitly given by

$$K_\pm^{\prime(1)} - \frac{e^\lambda}{\nu' r^2}\{n_\pm(K_\pm - H_{0,\pm}) + 2((p_0+\rho_0)r^2 + e^{-\lambda} - 1)H_{0,\pm}\} = s_1, \tag{32}$$

$$(K_\pm^{(1)} - H_{0,\pm}^{(1)})' - \nu' H_{0,\pm}^{(1)} = (1 + \frac{\nu' r}{2})s_1 + s_2, \tag{33}$$

where

$$n_\pm = -2 + l'(l'+1)|_{l'=l\pm1} \tag{34}$$

$$\begin{aligned} s_1 = & -Q_\pm\left[8\varpi r U_L + 8(p_0+\rho_0)\varpi r^3 e^{-\nu}\Phi_L + 2\varpi' j^2 r^3 \Phi_L'\right] \\ & + S_\pm\left[8\left\{r + \frac{e^\lambda}{\nu'}\right\}\varpi U_L - \frac{4}{(e^\nu)'}\left\{l(l+1)\omega e^\lambda + 4p_0'\varpi r^3 - \varpi' r\right\}\Phi_L + 2\varpi' j^2 r^3 \Phi_L'\right] \\ & + T_\pm\left[\frac{2}{(e^\nu)'}\left\{(2 - 2e^\lambda - l(l+1)e^\lambda)\omega + 2\Omega(p_0+\rho_0)r^2 e^\lambda - \varpi' r\right\}\Phi_L - \frac{\varpi' r^2}{(e^\nu)'}\Phi_L'\right]. \end{aligned} \tag{35}$$

$$\begin{aligned} s_2 = & \left(r + \frac{2}{\nu'}\right)\left[-S_\pm\left[4\varpi e^\lambda U_L - 2\left\{l(l+1)\omega e^\lambda - 2\varpi' r\right\}e^{-\nu}\Phi_L\right]\right. \\ & \left. + T_\pm\left\{\frac{1}{2}\varpi' r^2 e^{-\nu}\Phi_L' + \left[\left\{(l(l+1)+2)\omega - 2(p_0+\rho_0)\Omega r^2\right\}e^{\lambda-\nu} + 2\omega e^{-\nu}\right]\Phi_L\right\}\right] \\ & + \left[4S_\pm\frac{\varpi' r}{(e^\nu)'}\Phi_L + T_\pm\left(2\omega r^2 e^{-\nu}\Phi_L' + \frac{2\varpi' r - 8\omega}{(e^\nu)'}\Phi_L\right)\right]. \end{aligned} \tag{36}$$

When the axial-led function at the lowest order $\Phi_L^{(1)}$ is given, the functions $H_{0,\pm}^{(1)}$, $K^{(1)}$ are solved with appropriate boundary conditions. In a similar way, we can solve the other polar-led functions, $H_{1,\pm}^{(1)}$, $H_{2,\pm}^{(1)}$, $R_\pm^{(1)}$ and $V_\pm^{(1)}$ by $(\Phi_L^{(1)}, U_L^{(1)})$ and $(H_{0,\pm}^{(1)}, K^{(1)})$. These five functions are eliminated in the following calculations, and the expressions are omitted here. However, here is a comment on using the adiabatic condition (8). The time derivative of it can be written as

$$\partial_T\left(\delta p_\pm^{(1)} - \frac{\Gamma p_0}{p_0+\rho_0}\delta\rho_\pm^{(1)}\right) = \frac{A\Gamma p_0 e^\nu}{p_0+\rho_0}\left(e^{-\lambda}R_\pm^{(1)} - \frac{3im\xi_2}{r^2}Q_\pm U_L^{(1)}\right), \tag{37}$$

where

$$\xi_2 = -\frac{2}{\nu'}\left(h_2 + \frac{1}{3}\varpi^2 r^2 e^{-\nu}\right), \tag{38}$$

$$A = \frac{\rho_0'}{p_0+\rho_0} - \frac{p_0'}{\Gamma p_0}. \tag{39}$$

This thermodynamical relation determines the function $R_\pm^{(1)}$ unless the Schwarzschild discriminant A vanishes. Otherwise, we have one constraint for the function $U_L^{(1)}$ through eqs.(28-29), and the function $R_\pm^{(1)}$ should be specified in another way. The mathematical drawback for the isentropic case $A = 0$ is related with the coupling of the g-modes. A particular treatment is necessary since both r-modes and g-modes are degenerate in the non-rotating star. We will consider the case $A \neq 0$ only from now on.

5 Including second-order corrections

We reconsider the same components of the Einstein equations, which are used in the leading order calculations, i.e., essentially $(t\phi)$ $(r\phi)$ and $(\theta\phi)$ components. When we consider the next order terms,

we have the relations among the functions $h^{(2)}_{0,L}, h^{(2)}_{1,L}$ and $U^{(2)}_L$. They are also affected by the functions calculated in the previous sections. The equation governing the axial oscillations can be written in the following form

$$\mathcal{L}[\Phi^{(2)}_L] = \mathcal{D}[\Phi^{(1)}_L, h^{(1)}_{1,L}, U^{(1)}_L] + \mathcal{G}[H^{(1)}_{0,\pm}, K^{(1)}_{\pm}], \tag{40}$$

where the operator $\mathcal{L}$ is defined in eq.(24) and the right hand side is the second-order rotational corrections. They consist of several types of equations as

$$\mathcal{D}[\Phi^{(1)}_{lm}, h^{(1)}_{1,lm}, U^{(1)}_{lm}] = \mathcal{D}_0 + \alpha_1 h^{(1)}_{1,L} + \alpha_2 \partial_T \Phi^{(1)}_L + im(\beta_1 U^{(1)}_L + \beta_2 \Phi'^{(1)}_L + \beta_3 \Phi^{(1)}_L) \tag{41}$$

where

$$\begin{aligned}
\mathcal{D}_0 = & -e^{\lambda-\nu}(\partial_T - im\chi)(\partial_T - im\varpi)^2 \Phi^{(1)}_L \\
& + (\partial_T - im\chi)\left\{\left(\frac{\nu'}{r^2} - \frac{2}{r^3}\right)(\partial_T - im\varpi) + 2im\frac{\varpi'}{r^2}\right\} h_{1,L} \\
& + 32c_3 \frac{\varpi e^{-\nu}}{jr^2}\left\{\frac{(\rho_0 + p_0)r^2}{jA\nu'}\left(\frac{\varpi \partial_T U^{(1)}_L}{\rho_0 + p_0}\right)'\right\}' \\
& + \left\{\frac{16c_2\varpi^2 e^{-\nu}}{(\rho_0 + p_0)jr^2}\left[\frac{(\rho_0 + p_0)e^{\nu}}{A\varpi j\nu'}(\varpi r^2 e^{-\nu})'\right]' - \left(\frac{8c_1 e^{\nu}}{Aj^2\nu' r^4}\right)[(\varpi r^2 e^{-\nu})']^2\right\} \partial_T U^{(1)}_L.
\end{aligned} \tag{42}$$

6 Summary

We have formulated the relativistic r-mode oscillations with the metric perturbations. We have obtained the equation governing the axial-led functions including the second-order of rotational corrections. The second-order equation seems not to be identical with that of the Cowling approximation in neglecting metric perturbations. However there are relations among $\Phi^{(1)}_{lm}$, $U^{(1)}_{lm}$ and $h^{(1)}_{lm}$, we have neglected the terms such as $\Phi^{(1)}_{lm}$ and $h^{(1)}_{lm}$ in this approximation. Moreover, in barotropic case, i.e., $A = 0$, we can not show that the terms including A cancel as the same way of the Cowling case. Hence, we can not compare between these two cases simply.

References

[1] Andersson, N., 1998, ApJ, 502, 708.

[2] Friedman, J.L. and Morsink, S.M., 1998, ApJ, 502, 714.

[3] Kojima, Y., 1998, MNRAS, 293, 49.

[4] Lindblom, L., Owen, B.J. and Morsink, S.M., 1998, Phys. Rev. Lett., 80, 4843.

[5] Owen, B.J., Lindblom, L., Cutler, C., Schutz, B.F., Vecchio, A., and Andersson, N., 1998, Phys. Rev. D58, 084020.

[6] Andersson, N., Kokkotas, K. and Schutz, B.F., 1999, ApJ, 510, 846.

[7] Kojima, Y. and Hosonuma, M., 1999, ApJ, 520, 788.

[8] Yoshida, S. and Lee, U., 1999, [astro-ph/9908197].

[9] Hartle, J.B., 1967, ApJ, 150, 1005.

[10] Kojima, Y., 1992, Phys. Rev. D46, 4289.

[11] Kojima, Y. 1997, Prog. Theor. Phys. Suppl., 128, 251.

[12] Regge, T. and Wheeler, J.A., 1957, Phys. Rev., 108, 1063.

General Relativistic Approach to Magnetized Stars

Kohkichi Konno[1], Tomohiro Obata, Yasufumi Kojima[2]

Department of Physics, Hiroshima University,
Higashi-Hiroshima 739-8526, Japan

Abstract

Magnetized stars are formulated within a general relativistic framework based on the perturbation theory. Considering a magnetic field firstly on a background non-rotating, spherically symmetric star, we discuss the effect of the stellar rotation on the electromagnetic field around the star and the effect of the magnetic stress on the structure of the star. We have obtained the solution analytically outside the star.

1 Introduction

New classes of objects such as soft-gamma repeaters (SGRs) and anomalous X-ray pulsars (AXPs) attract attentions of many astrophysicists. This is because the very strong magnetic fields in excess of $B_{\rm cr} \sim 10^{13}$G are expected from the observation of the period and period derivative[1], so that these objects are most likely candidates of *magnetars*[2]. Under these observational situations, the studies on magnetized stars become more important than before. We deal with magnetized stars within a general relativistic framework. The relativistic magnetized stars are discussed by authors of Refs. [3, 4] previously. However, their approach is fully numerical. Contrastingly, we give a formulation of relativistic magnetized stars based on a perturbative approach, which is more analytical. Our formulation is regarded as a direct general-relativistic extension of the Newtonian treatment by Ferraro[5]. The most parts is based on our recent paper[6].

Two factors, rotation and magnetic fields, are considered to be perturbations to spherically symmetric structure of stars, because each effect is small compared with gravity in most cases. Thus, we specify the angular velocity Ω and the magnetic field strength B by small quantities ε and η, respectively, i.e., $\Omega \sim O(\varepsilon)$ and $B \sim O(\eta)$. Hartle[7] gave a formulation describing deformation of stars due to the rotational effect only, by considering the perturbation up to second order in ε. We now take into account the magnetic effect. To develop the formalism, we introduce several assumptions. Firstly, we assume that the star is at least in stationary configurations. In this relation, we consider only axisymmetric, poloidal magnetic fields, and suppose that the magnetic axis is aligned with the rotational axis if the star rotates. This situation leads to the following form of the 4-current J_μ and 4-potential A_μ in the spherical coordinates: $J_\mu = (J_t, 0, 0, J_\phi)$ and $A_\mu = (A_t, 0, 0, A_\phi)$ (see also Ref. [8] and references therein). Furthermore, we assume a perfectly conducting interior, which is expressed by $n^\mu F_{\mu\nu} = 0$ (n^μ is the unit vector normal to the $t =$ const hypersurfaces, and $F_{\mu\nu}$ is the Faraday tensor). Using the 4-potential A_μ mentioned above, we derive a relation $A_t = -\Omega A_\phi + C$ (C is a constant of integration). From this relation, it follows that we can neglect the t-component of the 4-potential A_μ in non-rotating configurations.

For our purpose of the formulation of relativistic magnetized stars, we take non-rotating, spherically symmetric stars as backgrounds firstly. Next, we consider the magnetic fields, which are the first-order perturbation in η, on this space-time. Although our formalism can be applied to any configurations of the magnetic fields, we restrict ourselves to a dipole magnetic field. The solution of the magnetic field is derived from the Maxwell equation for A_ϕ, in which the current distribution is introduced as the first-order quantity as well. For the next steps, we can consider two situations: the one is a case that the rotation of stars is taken into account, and the other is a situation that the non-rotating star is deformed by the magnetic stress, which is of second order in η. In the former case, we have to solve the Maxwell equation for A_t, which is of order $\varepsilon\eta$, while in the latter case, we can obtain the solution describing the distorted star by solving the second-order perturbative equations of the Einstein equation. The details

[1]E-mail:konno@aqua.phys.sci.hiroshima-u.ac.jp
[2]E-mail:kojima@theo.phys.sci.hiroshima-u.ac.jp

of this perturbative scheme are given in §2. Finally, we give summary and discussion in §3. We use the units in which $c = G = 1$.

2 Formulation of relativistic magnetized stars

We now consider a non-rotating, spherically symmetric star to be background, whose space-time is described by

$$ds^2 = -e^{\nu(r)}dt^2 + e^{\lambda(r)}dr^2 + r^2 d\theta^2 + r^2 \sin^2\theta d\phi^2, \tag{1}$$

where ν and λ are functions of the radial coordinate r only. In §2.1, we discuss a dipole magnetic field, which is regarded as the first-order perturbation in η, in this space-time. The rigid rotation of the star is taken into account within stationary configurations in §2.2. The electric field $E \sim O(\varepsilon\eta)$ is induced in this situation. In §2.3, neglecting the rotation, we discuss deformation of the star arising from an effect of the magnetic stress, which is of second order in η.

2.1 Dipole magnetic field in spherically symmetric space-time

For a dipole magnetic field in the non-rotating configurations, it is sufficient to consider only the ϕ-components of the 4-potential A_μ and 4-current J_μ, which obey the ϕ-component of the Maxwell equation $F^{\mu\nu}{}_{;\nu} = 4\pi J^\mu$,

$$e^{-\lambda}\frac{\partial^2 A_\phi}{\partial r^2} + \frac{1}{2}(\nu' - \lambda')e^{-\lambda}\frac{\partial A_\phi}{\partial r} + \frac{1}{r^2}\frac{\partial^2 A_\phi}{\partial \theta^2} - \frac{1}{r^2}\cot\theta\frac{\partial A_\phi}{\partial \theta} = -4\pi J_\phi, \tag{2}$$

where the prime denotes the differentiation with respect to r. The potential A_ϕ and the current J_ϕ are expanded as

$$A_\phi(r,\theta) = \sum_{l=1}^{\infty} a_{\phi l}(r)\sin\theta\frac{dP_l(\cos\theta)}{d\theta}, \tag{3}$$

$$J_\phi(r,\theta) = \sum_{l=1}^{\infty} j_{\phi l}(r)\sin\theta\frac{dP_l(\cos\theta)}{d\theta}. \tag{4}$$

The dipole fields correspond to $l = 1$ for these expansions. The radial part of Eq. (2) is then written as

$$e^{-\lambda}\frac{d^2 a_{\phi 1}}{dr^2} + \frac{1}{2}(\nu' - \lambda')e^{-\lambda}\frac{da_{\phi 1}}{dr} - \frac{2}{r^2}a_{\phi 1} = -4\pi j_{\phi 1}. \tag{5}$$

Using $e^{\nu} = e^{-\lambda} = 1 - 2M/r$ and $j_{\phi 1} = 0$ outside the star, the exterior solution is given by[9]

$$a_{\phi 1} = \frac{3\mu}{8M^3}r^2\left[\ln\left(1 - \frac{2M}{r}\right) + \frac{2M}{r} + \frac{2M^2}{r^2}\right], \tag{6}$$

where μ is a constant corresponding to the magnetic dipole moment with respect to an observer at infinity, and M is the total mass of the background star. The tetrad components of the dipole magnetic field are written as

$$B_{(r)} = -\frac{3\mu}{4M^3}\left[\ln\left(1 - \frac{2M}{r}\right) + \frac{2M}{r} + \frac{2M^2}{r^2}\right]\cos\theta, \tag{7}$$

$$B_{(\theta)} = \frac{3\mu}{4M^3}\left[\sqrt{1 - \frac{2M}{r}}\ln\left(1 - \frac{2M}{r}\right) + \frac{2M(r-M)}{r\sqrt{r(r-2M)}}\right]\sin\theta. \tag{8}$$

Furthermore, inside the star, we can obtain the interior solution numerically by assuming an equation of state (EOS) and the current distribution $j_{\phi 1}$ which satisfies a integrability condition (see Appendix A).

2.2 Induced electric field in the stationary configurations

We now take into account the rigid rotation of the star, whose angular velocity is given by $\Omega(\sim O(\varepsilon))$. The metric of the space-time has the form

$$ds^2 = -e^{\nu(r)}dt^2 - 2\omega(r)r^2\sin^2\theta dt d\phi + e^{\lambda(r)}dr^2 + r^2 d\theta^2 + r^2\sin^2\theta d\phi^2, \tag{9}$$

where $\omega(\sim O(\varepsilon))$ is angular velocity acquired by an observer falling freely from infinity to a point r, and leads to the frame-dragging effect. The solution for ω is derived by solving the $(t\phi)$-component of the Einstein equation. In particular, outside the star, we have $\omega = 2J/r^3$, where J is the angular momentum of the star.

As mentioned in the Introduction, we further have to deal with the t-components of the 4-potential A_μ and 4-current J_μ when the stellar rotation is taken into account. These are governed by the t-component of the Maxwell equation, which is written as

$$\begin{aligned} e^{-\lambda}\frac{\partial^2 A_t}{\partial r^2} - \left(\frac{\nu'+\lambda'}{2} - \frac{2}{r}\right)e^{-\lambda}\frac{\partial A_t}{\partial r} + \frac{1}{r^2}\frac{\partial^2 A_t}{\partial\theta^2} + \frac{1}{r^2}\cot\theta\frac{\partial A_t}{\partial\theta} \\ - \left[\left(\nu' - \frac{2}{r}\right)\omega - \omega'\right]e^{-\lambda}\frac{\partial A_\phi}{\partial r} + \frac{2}{r^2}\omega\cot\theta\frac{\partial A_\phi}{\partial\theta} &= -4\pi J_t. \end{aligned} \tag{10}$$

The last two terms on the left-hand side in Eq. (10) denote the general relativistic frame-dragging effect coupled to the magnetic field. We expand the t-components of the 4-potential and 4-current as follows:

$$A_t(r,\theta) = \sum_{l'=0}^{\infty} a_{tl'}(r)P_{l'}(\cos\theta) \tag{11}$$

$$J_t(r,\theta) = \sum_{l'=0}^{\infty} j_{tl'}(r)P_{l'}(\cos\theta). \tag{12}$$

When we discuss a dipole magnetic field, only the monopole and quadrupole parts are relevant. Hence, we have two equations for the radial parts,

$$\begin{aligned} e^{-\lambda}\frac{d^2 a_{t0}}{dr^2} - \left(\frac{\nu'+\lambda'}{2} - \frac{2}{r}\right)e^{-\lambda}\frac{da_{t0}}{dr} \\ + \frac{2}{3}\left[\left(\nu' - \frac{2}{r}\right)\omega - \omega'\right]e^{-\lambda}\frac{da_{\phi 1}}{dr} - \frac{4}{3r^2}\omega a_{\phi 1} &= -4\pi j_{t0}, \end{aligned} \tag{13}$$

$$\begin{aligned} e^{-\lambda}\frac{d^2 a_{t2}}{dr^2} - \left(\frac{\nu'+\lambda'}{2} - \frac{2}{r}\right)e^{-\lambda}\frac{da_{t2}}{dr} - \frac{6}{r^2}a_{t2} \\ - \frac{2}{3}\left[\left(\nu' - \frac{2}{r}\right)\omega - \omega'\right]e^{-\lambda}\frac{da_{\phi 1}}{dr} - \frac{8}{3r^2}\omega a_{\phi 1} &= -4\pi j_{t2}. \end{aligned} \tag{14}$$

The exterior solution is obtained analytically in the following way:

$$a_{t0} = \frac{c_0}{r} + \frac{J\mu}{2M^3r^2}(3r - M) + \frac{J\mu}{4M^4 r}(3r - 4M)\ln\left(1 - \frac{2M}{r}\right), \tag{15}$$

$$\begin{aligned} a_{t2} = {} & \frac{c_1}{M^2}(r - M)(r - 2M) \\ & + c_2\left[\frac{2}{Mr}\left(3r^2 - 6Mr + M^2\right) + \frac{3}{M^2}\left(r^2 - 3Mr + 2M^2\right)\ln\left(1 - \frac{2M}{r}\right)\right] \\ & - \frac{J\mu}{2M^6r^2}\left(9r^4 - 3Mr^3 - 30M^2r^2 + 8M^3r + 2M^4\right) \\ & - \frac{J\mu}{2M^6 r}\left(12r^3 - 36Mr^2 + 24M^2r + M^3\right)\ln\left(1 - \frac{2M}{r}\right), \end{aligned} \tag{16}$$

where c_0, c_1 and c_2 are constants of integration. Since c_0 is understood as the net charge of the star, we assume $c_0 = 0$. Furthermore, from the regularity condition at infinity, we derive

$$c_1 = \frac{9J\mu}{2M^4}. \tag{17}$$

Consequently, we have

$$a_{t0} = \frac{J\mu}{2M^3r^2}(3r-M) + \frac{J\mu}{4M^4r}(3r-4M)\ln\left(1-\frac{2M}{r}\right), \tag{18}$$

$$\begin{aligned} a_{t2} = {} & c_2\left[\frac{2}{Mr}\left(3r^2-6Mr+M^2\right)+\frac{3}{M^2}\left(r^2-3Mr+2M^2\right)\ln\left(1-\frac{2M}{r}\right)\right] \\ & -\frac{J\mu}{M^5r^2}\left(12r^3-24Mr^2+4M^2r+M^3\right) \\ & -\frac{J\mu}{2M^6r}\left(12r^3-36Mr^2+24M^2r+M^3\right)\ln\left(1-\frac{2M}{r}\right). \end{aligned} \tag{19}$$

From this result, we can construct the induced electric field, whose tetrad components are written as

$$\begin{aligned} E_{(r)} = {} & \frac{1}{2M^6r^3}\left[c_2\left\{4M^5r\left(6r^2-3Mr-M^2\right)+6M^4r^3\left(2r-3M\right)\ln\left(1-\frac{2M}{r}\right)\right\}\right. \\ & -2MJ\mu\left(24r^3-12Mr^2-4M^2r-3M^3\right) \\ & \left.-3rJ\mu\left(8r^3-12Mr^2-M^3\right)\ln\left(1-\frac{2M}{r}\right)\right]P_2\left(\cos\theta\right), \end{aligned} \tag{20}$$

$$\begin{aligned} E_{(\theta)} = {} & -\frac{3}{M^6r^3\sqrt{r(r-2M)}}\left[c_2\left\{2M^5r^2\left(3r^2-6Mr+M^2\right)\right.\right. \\ & \left.+3M^4r^3\left(r^2-3Mr+2M^2\right)\ln\left(1-\frac{2M}{r}\right)\right\} \\ & -MJ\mu\left(12r^4-24Mr^3+4M^2r^2-M^4\right) \\ & \left.-6r^3J\mu\left(r^2-3Mr+2M^2\right)\ln\left(1-\frac{2M}{r}\right)\right]\sin\theta\,\cos\theta. \end{aligned} \tag{21}$$

At infinity, we have

$$E_{(r)} = \left(-\frac{12M^3c_2}{5r^4}+\frac{9J\mu}{5Mr^4}\right)P_2\left(\cos\theta\right), \tag{22}$$

$$E_{(\theta)} = \left(-\frac{12M^3c_2}{5r^4}+\frac{9J\mu}{5Mr^4}\right)\sin\theta\,\cos\theta. \tag{23}$$

Thus, the quadrupole moment Q takes the form

$$Q = -\frac{2}{5}M^3c_2+\frac{3}{10}\frac{J\mu}{M} \tag{24}$$

(see also Ref. [10]).

Inside the star, without solving the Maxwell equation, we can derive the t-component of the 4-potential, from the assumption of the perfectly conducting interior, in the way

$$A_t = -\Omega A_\phi + C, \tag{25}$$

namely,

$$a_{t0} = \frac{2}{3}\Omega a_{\phi 1}+C, \tag{26}$$

$$a_{t2} = -\frac{2}{3}\Omega a_{\phi 1}. \tag{27}$$

By solving the Maxwell equation inversely, we can also derive the t-component of the 4-current inside the star,

$$\begin{aligned} J_t = {} & \frac{2}{3}\Omega j_{\phi 1}+\frac{e^{-\lambda}}{6\pi}\left\{\left(\nu'-\frac{2}{r}\right)(\Omega-\omega)+\omega'\right\}a'_{\phi 1}-\frac{1}{3\pi r^2}(\Omega-\omega)a_{\phi 1} \\ & -\left[\frac{2}{3}\Omega j_{\phi 1}+\frac{e^{-\lambda}}{6\pi}\left\{\left(\nu'-\frac{2}{r}\right)(\Omega-\omega)+\omega'\right\}a'_{\phi 1}+\frac{2}{3\pi r^2}(\Omega-\omega)a_{\phi 1}\right]P_2, \end{aligned} \tag{28}$$

where $j_{\phi 1}$ is the current distribution satisfying the integrability condition, and $a_{\phi 1}$ is the numerically derived solution of Eq. (5).

2.3 Deformation of star due to the magnetic stress

In this subsection, neglecting the rotation, we consider the deformation of the star due to the magnetic stress, which arises as the second-order effect in η. Following the method of Hartle[7], we specify the deformation of the star by adding the second-order quantities to the metric (1),

$$\begin{aligned} ds^2 &= -e^{\nu(r)}\left[1+2\left(h_0(r)+h_2(r)P_2(\cos\theta)\right)\right]dt^2 + e^{\lambda(r)}\left[1+\frac{2e^{\lambda(r)}}{r}\left(m_0(r)+m_2(r)P_2(\cos\theta)\right)\right]dr^2 \\ &\quad + r^2\left[1+2k_2(r)P_2(\cos\theta)\right]\left(d\theta^2+r^2\sin^2\theta d\phi^2\right), \end{aligned} \tag{29}$$

where h_0, h_2, m_0, m_2 and k_2 are of second order in η.

The total energy-momentum tensor is the sum of the perfect-fluid part $T_{(m)}{}^{\mu}{}_{\nu}$ and the electromagnetic part $T_{(em)}{}^{\mu}{}_{\nu}$:

$$T^{\mu}{}_{\nu} = T_{(m)}{}^{\mu}{}_{\nu} + T_{(em)}{}^{\mu}{}_{\nu}, \tag{30}$$

where

$$T_{(m)}{}^{\mu}{}_{\nu} = (\rho+p)\,u^{\mu}u_{\nu} + p\delta^{\mu}{}_{\nu}, \tag{31}$$

$$T_{(em)}{}^{\mu}{}_{\nu} = \frac{1}{4\pi}\left(F^{\mu\lambda}F_{\nu\lambda} - \frac{1}{4}F_{\sigma\lambda}F^{\sigma\lambda}\delta^{\mu}{}_{\nu}\right). \tag{32}$$

The pressure p and the energy density ρ can be expanded in multipoles as

$$p(r,\theta) = p_0 + \left(\delta p_{(l=0)} + \delta p_{(l=2)}P_2\right), \tag{33}$$

$$\rho(r,\theta) = \rho_0 + \frac{\rho_0'}{p_0'}\left(\delta p_{(l=0)} + \delta p_{(l=2)}P_2\right), \tag{34}$$

where $\delta p_{(l=0)}$ and $\delta p_{(l=2)}$ depend on r only, and we have assumed a barotropic case.

From the Einstein equation, we can obtain

$$m_0' = 4\pi r^2\frac{\rho_0'}{p_0'}\delta p_{(l=0)} + \frac{1}{3}\left[e^{-\lambda}\left(a_{\phi 1}'\right)^2 + \frac{2}{r^2}a_{\phi 1}^2\right], \tag{35}$$

$$h_0' = 4\pi r e^{\lambda}\delta p_{(l=0)} + \frac{1}{r}\nu' e^{\lambda}m_0 + \frac{1}{r^2}e^{\lambda}m_0 + \frac{e^{\lambda}}{3r}\left[e^{-\lambda}\left(a_{\phi 1}'\right)^2 - \frac{2}{r^2}a_{\phi 1}^2\right], \tag{36}$$

$$h_2' + k_2' = h_2\left(\frac{1}{r}-\frac{\nu'}{2}\right) + \frac{e^{\lambda}}{r}m_2\left(\frac{1}{r}+\frac{\nu'}{2}\right) + \frac{4}{3r^2}a_{\phi 1}a_{\phi 1}', \tag{37}$$

$$h_2 + \frac{e^{\lambda}}{r}m_2 = \frac{2}{3}e^{-\lambda}\left(a_{\phi 1}'\right)^2, \tag{38}$$

$$\begin{aligned} h_2' + k_2' + \frac{1}{2}r\nu' k_2' &= 4\pi r e^{\lambda}\delta p_{(l=2)} + \frac{1}{r^2}e^{\lambda}m_2 + \frac{1}{r}\nu' e^{\lambda}m_2 \\ &\quad + \frac{3}{r}e^{\lambda}h_2 + \frac{2}{r}e^{\lambda}k_2 - \frac{1}{3r}e^{\lambda}\left[e^{-\lambda}\left(a_{\phi 1}'\right)^2 + \frac{4}{r^2}a_{\phi 1}^2\right]. \end{aligned} \tag{39}$$

Furthermore, from the conservation law of the total energy-momentum tensor, we obtain

$$\delta p_{(l=0)}' = -\frac{1}{2}\nu'\left(\frac{\rho_0'}{p_0'}+1\right)\delta p_{(l=0)} - (\rho_0+p_0)\,h_0' + \frac{2}{3r^2}a_{\phi 1}'j_{\phi 1}, \tag{40}$$

$$\delta p_{(l=2)} = -(\rho_0+p_0)\,h_2 - \frac{2}{3r^2}a_{\phi 1}j_{\phi 1}, \tag{41}$$

$$\delta p_{(l=2)}' = -\frac{1}{2}\nu'\left(\frac{\rho_0'}{p_0'}+1\right)\delta p_{(l=2)} - (\rho_0+p_0)\,h_2' - \frac{2}{3r^2}a_{\phi 1}'j_{\phi 1}. \tag{42}$$

The integrability condition for Eqs. (40) and (42) leads to

$$\frac{j_{\phi 1}}{r^2(\rho_0+p_0)} = \text{const} \tag{43}$$

(see also Appendix A). From this condition, Eq. (40) can be integrated as

$$\delta p_{(l=0)} = -(\rho_0+p_0)h_0 + \frac{2}{3r^2}a_{\phi 1}j_{\phi 1} + \alpha(\rho_0+p_0), \tag{44}$$

where α is a constant of integration.

Consequently, we have two set of differential equations,

$$m_0' = -4\pi r^2\frac{\rho_0'}{p_0'}(\rho_0+p_0)(h_0-\alpha) + \frac{1}{3}e^{-\lambda}(a_{\phi 1}')^2 + \frac{2}{3r^2}a_{\phi 1}^2 + \frac{8\pi}{3}\frac{\rho_0'}{p_0'}a_{\phi 1}j_{\phi 1}, \tag{45}$$

$$h_0' = \left(\frac{1}{r^2}+\frac{\nu'}{r}\right)e^{\lambda}m_0 - 4\pi r e^{\lambda}(\rho_0+p_0)(h_0-\alpha) + \frac{1}{3r}(a_{\phi 1}')^2 - \frac{2}{3r^3}e^{\lambda}a_{\phi 1}{}^2 + \frac{8\pi}{3r}e^{\lambda}a_{\phi 1}j_{\phi 1}, \tag{46}$$

and

$$v_2' = -\nu' h_2 + \frac{2}{3}e^{-\lambda}\left(\frac{1}{r}+\frac{\nu'}{2}\right)(a_{\phi 1}')^2 + \frac{4}{3r^2}a_{\phi 1}a_{\phi 1}', \tag{47}$$

$$h_2' = -\frac{4e^{\lambda}}{r^2\nu'}v_2 + \left[8\pi\frac{e^{\lambda}}{\nu'}(\rho_0+p_0) + \frac{2}{r^2\nu'}(1-e^{\lambda}) - \nu'\right]h_2 + \frac{8}{3r^4\nu'}e^{\lambda}a_{\phi 1}^2 + \frac{8}{3r^3\nu'}\left(1+\frac{r\nu'}{2}\right)a_{\phi 1}a_{\phi 1}' + \left(\frac{1}{3}\nu' e^{-\lambda} + \frac{2}{3r^2\nu'}\right)(a_{\phi 1}')^2 + \frac{16\pi}{3r^2\nu'}e^{\lambda}a_{\phi 1}j_{\phi 1}, \tag{48}$$

where $v_2 \equiv h_2 + k_2$. These equations govern the relativistic magnetized star. We have to solve four differential equations (45)–(48) and one algebraic equation (38) for the unknown functions $(m_0, m_2, h_0, h_2, v_2)$. Furthermore, we can derive $\delta p_{(l=0)}$ and $\delta p_{(l=2)}$ by substituting the solution for h_0 and h_2 into Eqs. (44) and (41).

Outside the star, we can obtain the analytic solution for m_0, h_0, v_2 and h_2 in the following way:

$$m_0 = \frac{3\mu^2}{8M^4r}(r^2-M^2) + \frac{3\mu^2}{8M^5}(r^2-Mr-M^2)\ln\left(1-\frac{2M}{r}\right) + \frac{3\mu^2}{32M^6}r^2(r-2M)\left[\ln\left(1-\frac{2M}{r}\right)\right]^2 + \beta, \tag{49}$$

$$h_0 = -\frac{3\mu^2}{8M^3}\frac{4r-M}{r(r-2M)} + \frac{3\mu^2}{8M^5}\frac{(r-M)(r-3M)}{r-2M}\ln\left(1-\frac{2M}{r}\right) + \frac{3\mu^2}{32M^6}r^2\left[\ln\left(1-\frac{2M}{r}\right)\right]^2 - \frac{\beta}{r-2M} + \frac{3\mu^2}{8M^4}, \tag{50}$$

$$v_2 = \frac{2K}{\sqrt{z^2-1}}Q_2^1(z) - \frac{3\mu^2}{4M^4\sqrt{z^2-1}}P_2^1(z) + \frac{9\mu^2}{4M^4}z + \frac{3\mu^2}{8M^4}\frac{7z^2-4}{z^2-1} + \frac{3\mu^2}{16M^4}\frac{z(11z^2-7)}{z^2-1}\ln\frac{z-1}{z+1} + \frac{3\mu^2}{16M^4}(2z^2+1)\left(\ln\frac{z-1}{z+1}\right)^2 \tag{51}$$

$$h_2 = KQ_2^2(z) - \frac{3\mu^2}{8M^4}P_2^2(z) - \frac{3\mu^2}{16M^4}\left[6z^2+3z-6-\frac{4z^2+2z}{z^2-1}\right] - \frac{3\mu^2}{32M^4}\left[3z^2-8z-3-\frac{8}{z^2-1}\right]\ln\frac{z-1}{z+1} + \frac{3\mu^2}{16M^4}(z^2-1)\left(\ln\frac{z-1}{z+1}\right)^2, \tag{52}$$

where z is defined as $z \equiv r/M - 1$, and P_l^m and Q_l^m are the associated Legendre functions, and β and K are constants of integration, which are fixed by the junction condition at the surface. The remaining functions m_2 and k_2 can be derived through the algebraic equations (38) and $k_2 = v_2 - h_2$, respectively.

Inside the star, we can obtain the solution numerically for a given EOS (see also Ref. [6]).

3 Summary and discussion

Some classes of neutron stars with very strong magnetic fields stimulate studies on magnetized stars. We have developed a formulation for constructing relativistic magnetized stars, based on a perturbative approach. Firstly, we have regarded a non-rotating, spherically symmetric star as a background, and considered a dipole magnetic field on this space-time. Next, we have discussed the rotational effect and the deformation of the star arising from the second-order effect of the magnetic field. In the rotating case, we have derived the induced electric field, which is of order $\varepsilon\eta$, within general relativity. For the deformation of the star, we have obtained the solution describing the distortion, following the method of Hartle[7]. Our formulation gives much simpler calculations of ellipticity of the deformed stars etc. The numerical results of the ellipticity are given in our recent paper[6].

The induced electric fields in more general cases, that is, non-aligned configurations of magnetic rotators will be the subject of future works. Furthermore, higher-order effects of the coupling of the rotation and the magnetic field on structure of stars are also of interest. These will be discussed elsewhere.

A Integrability condition

In this appendix, we review the integrability condition (see also Refs. [5, 8]).

From the conservation law of the stress-energy tensor

$$T_{(m)\mu}{}^{\lambda}{}_{;\lambda} = F_{\mu}{}^{\nu} J_{\nu}, \tag{53}$$

we can obtain the hydrostatic equilibrium equation

$$\partial_i \tilde{P} + \frac{1}{2}\partial_i \nu + \partial_i \left[\frac{1}{2} \ln \left(1 - r^2 \sin^2\theta \, e^{-\nu} (\Omega - \omega)^2 \right) \right] = \frac{1}{\rho + p} F_{i\nu} J^{\nu}, \tag{54}$$

where $\tilde{P}$ is defined as

$$\tilde{P} \equiv \int^{p} \frac{dp}{\rho + p}, \tag{55}$$

and i denotes r or θ. In order that the star is in a hydrostatic equilibrium configuration, the right-hand side in Eq. (54) must be written as a gradient of some function as well. The right-hand side is rewritten as follows:

$$\frac{1}{\rho + p} F_{i\nu} J^{\nu} = \frac{1}{\rho + p} \left(\partial_i A_t \cdot J^t + \partial_i A_\phi \cdot J^\phi \right) \tag{56}$$

$$= \frac{1}{\rho + p} \left(J^t - \Omega J^\phi \right) \partial_i A_\phi. \tag{57}$$

Therefore, the hydrostatic equilibrium condition is given by

$$J^t - \Omega J^\phi = (\rho + p) \, f(A_\phi), \tag{58}$$

where f is an arbitrary function of A_ϕ. This condition is rewritten as

$$J_\phi = g_{\phi\phi} (\rho + p) \, f(A_\phi), \tag{59}$$

which is called *integrability condition*. The dipole field is created by a case of $f = \text{const}$, which reproduces the result of Eq. (43).

References

[1] See, e.g., C. Kouveliotou, et al., Nature **393** (1998), 235; Astrophys. J. **510** (1999), L115; S. Mereghetti and L. Stella, Astrophys. J. **442** (1995), L17.

[2] C. Thompson and R.C. Duncan, Astrophys. J. **473** (1996), 322.

[3] M. Bocquet, S. Bonazzola, E. Gourgoulhon and J. Novak, Astron. Astrophys. **301** (1995), 757.

[4] S. Bonazzola and E. Gourgoulhon, Astron. Astrophys. **312** (1996), 675.

[5] V.C.A. Ferraro, Astrophys. J. **119** (1954), 407.

[6] K. Konno, T. Obata and Y. Kojima, Astron. Astrophys. **352** (1999), 211.

[7] J.B. Hartle, Astrophys. J. **150** (1967), 1005.

[8] S. Bonazzola, E. Gourgoulhon, M. Salgado and J.A. Marck, Astron. Astrophys. **278** (1993), 421.

[9] V.L. Ginzburg and L.M. Ozernoĭ, Sov. Phys. JETP **20** (1965), 689.

[10] P. Mészáros, *High-Energy Radiation from Magnetized Neutron Stars* (The University of Chicago Press, Chicago, 1992), p.349.

Magnetized stars on relativistic perturbation theory

Tomohiro Obata,[1] Kohkichi Konno,[2] and Yasufumi Kojima[3]

Department of Physics, Hiroshima University,
Higashi-Hiroshima 739-8526, Japan

Abstract

We study the deformation of relativistic magnetized stars with the dipole fields. The magnetic effect is assumed to be small and treated as perturbation from the spherical symmetric star. Using the ellipticity of the equilibrium shape, we estimate the quadrupole deformation due to the magnetic effect. We also compare the magnetic deformation with the rotational one. We have found that the magnetic distortion becomes significant for strong magnetized objects such as a candidate of magnetars.

1 Introduction

From recent observations, several interesting astrophysical objects are found: soft gamma-ray repeaters (SGRs) and anomalous X-ray pulsars (AXPs) (see e.g. Kouveliotou et al. [1],[2]; Mereghetti & Stella [3]). Measurements of the period and period derivative yield an evidence for these objects to be strong magnetized stars ($B \sim 10^{14} - 10^{15}$G), which seem to be *magnetars* (Thompson & Duncan [4]). In these strong magnetized stars, the magnetic influence would not be neglected. Hence, taking into account the magnetic field, we should investigate the structure of the stars.

In general, stars are deformed by strong magnetic pressure, which corresponds to the Lorentz force. Rotating stars are also deformed by centrifugal force. The both forces cause a flattening equilibrium star, i.e., quadrupole deformation. There are a few classes of neutron stars with slow/fast rotation and weak/strong magnetic field (see e.g. Taylor et al. [5]), i.e., well-known typical pulsars (the period $T \sim 10^{-1} - 1$sec, $B \sim 10^{11} - 10^{13}$G), millisecond pulsars ($T \sim 10^{-3}$sec, $B \sim 10^{-8}$G), and candidates of magnetars ($T \sim 1$sec, $B \sim 10^{14} - 10^{15}$G). We are interested which effect on the deformation is larger magnetic or rotational. Moreover, the deformation is important, because it may play a significant role in spin-down process of the pulsars (e.g. Melatos [6]), glitch of pulsars, and gravitational radiation.

The quadrupole deformation of magnetized Newtonian stars was discussed by Chandrasekhar & Fermi [7] and Ferraro [8]. That of rotating stars was discussed by Chandrasekhar [9] and Chandrasekhar & Roberts [10] for Newtonian cases, Hartle [11] and Chandrasekhar & Miller [12] for relativistic cases. The general relativistic approach for magnetized stars has appeared recently (Bocquet et al. [13], Bonazzola & Gourgoulhon [14], and Konno et al. [15]) . In this paper, we consider the deformation due to the magnetic effect within general relativity, the effect is assumed to be small and treated as perturbation. Furthermore, we compare the deformation due to the magnetic effect with the rotational effect. We investigate which deformation is larger-by the magnetic effect or the rotational effect for many rotating magnetized objects.

The plan of the present paper is as follows. In Sect.2, we investigate static and dipole magnetic fields in spherical symmetric background. We assume that the magnetic field is weak compared with gravity; the magnetic field strength is treated as first-order quantity η_B. This assumption is valid even for the magnetars. In Sect.3, we consider the quadrupole deformation arising from the magnetic effect based on relativistic perturbation theory. In order to investigate the quadrupole deformation, we use *ellipticity* of the equilibrium shape. Next, in Sect.4, we briefly review the deformation due to slow rotation [11, 12]. In this, we treat the rotation and the magnetic field as each perturbation separately. Using of the ellipticity, furthermore, we compare the magnetic effect with the rotational effect on stellar deformation. Finally, we give summary and discussion in Sect.5. Throughout the paper, we use the units in which $c = G = 1$, and the Gaussian system of units for electromagnetic fields.

[1] E-mail:obata@aqua.phys.sci.hiroshima-u.ac.jp
[2] E-mail:konno@aqua.phys.sci.hiroshima-u.ac.jp
[3] E-mai:kojima@theo.phys.sci.hiroshima-u.ac.jp

2 Magnetic field in spherical symmetric space-time

Before considering deformation of magnetized star, we investigate magnetic field of relativistic stars (see also Konno et al.[15]). For simplicity, we deal with static case, i.e., non-rotating case. We assume that the magnetic field strength and electric current are weak compared with the gravitational field, i.e., $B, J \sim O(\eta_B)$: the magnetic field and the current are the first-order quantities. Taking spherical symmetric space-time as background, the line element is given by

$$ds^2 = -e^{\nu(r)}dt^2 + e^{\lambda(r)}dr^2 + r^2(d\theta^2 + \sin\theta^2 d\phi^2), \tag{1}$$

where ν and λ are functions of the radial coordinate r only.

Furthermore, we assume an axisymmetric magnetic field and a perfectly conducting interior. This implies that there is no electric charge inside the star and the electric field vanishes. From these assumptions, we can write the 4-electric current as $J_\mu = (0, 0, 0, J_\phi)$, and the 4-electromagnetic potential as $A_\mu = (0, 0, 0, A_\phi)$ (see also Bocquet et al.[13]). In this case, the Maxwell equation is reduced to

$$e^{-\lambda}\frac{\partial^2 A_\phi}{\partial r^2} + \frac{1}{2}(\nu' - \lambda')e^{-\lambda}\frac{\partial A_\phi}{\partial r} + \frac{1}{r^2}\frac{\partial^2 A_\phi}{\partial \theta^2} - \frac{1}{r^2}\cot\theta\frac{\partial A_\phi}{\partial \theta} = -4\pi J_\phi, \tag{2}$$

where the prime denotes the differentiation with respect to r.

We consider the axisymmetric poloidal magnetic field ($\boldsymbol{B} = (B_r, B_\theta, 0)$) produced by the toroidal electric current J_ϕ and potential A_ϕ. For astrophysical application, we restrict the magnetic field to a dipole field. The toroidal electric current J_ϕ and potential A_ϕ are therefore written as

$$J_\phi = -\sin^2\theta j_1(r), \tag{3}$$

$$A_\phi = -\sin^2\theta a_1(r). \tag{4}$$

Substituting Eqs.(3)-(4) into the Maxwell Eq.(2), and being given a current J_ϕ, we can obtain the potential A_ϕ, therefore, the magnetic field $\boldsymbol{B}$.

In order to describe the magnetic field, we require the current J_ϕ. From integrability condition for the conservation law of the total energy-momentum tensor, this current is given by

$$J_\phi = -c_0 r^2(\rho_0(r) + p_0(r))\sin^2\theta, \tag{5}$$

where c_0 is an arbitrary constant, and ρ_0 and p_0 are the density and pressure, respectively, of background star. We now obtain the potential inside star. The potential outside star (the current $J_\phi = 0$) can easily be solved in the form

$$A_\phi = \frac{3\mu}{8M^3}r^2\left[\ln\left(1 - \frac{2M}{r}\right) + \frac{2M}{r} + \frac{2M^2}{r^2}\right]\sin^2\theta, \tag{6}$$

where μ is a constant corresponding to the magnetic dipole moment as seen by an observer at infinity, and M is the total mass of the star. In this way, we can investigate the distribution of the magnetic field in the whole space-time.

Fig. 1 displays the tetrad component of the magnetic field,

$$B_{\hat{r}} = -\frac{1}{r^2\sin\theta}\partial_\theta A_\phi \tag{7}$$

on the symmetry axis (i.e., $\theta = 0$), and Fig. 2 displays the tetrad component

$$B_{\hat{\theta}} = \frac{e^{-\lambda/2}}{r\sin\theta}\partial_r A_\phi \tag{8}$$

on the equatorial plane (i.e., $\theta = \pi/2$) with respect to the radial coordinate r. We have normalized them by the typical magnetic field strength μ/R^3, where R is the radius of the star. The solid lines denote a relativistic case, whereas the dashed lines correspond to a Newtonian case. In these calculations, we have used the polytropic equation of state (EOS): $p_0 = \kappa\rho_0^{1+1/n}$ ($n = 1$). From these figures, we can see that the intensity of the magnetic field increases as r becomes closer to the center. Furthermore, these two figures show that despite the same magnetic moment with respect to an observer at infinity, the central magnetic field of the relativistic star is stronger than that of the Newtonian star by about 50% of the Newtonian case. Therefore, it follows that the relativistic effect strengthens the internal magnetic fields.

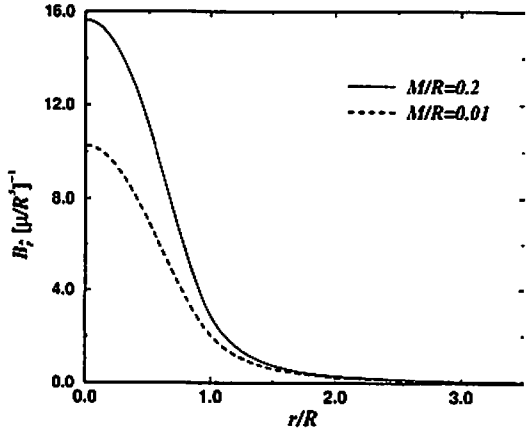

Figure 1: The tetrad component of the magnetic fields, $B_{\hat{r}}$ on the symmetry axis ($\theta = 0$), plotted against r/R. The solid line denotes a relativistic case ($M/R = 0.2$), while the dashed line corresponds to a Newtonian case ($M/R = 0.01$). The magnetic fields are normalized by the typical field strength μ/R^3.

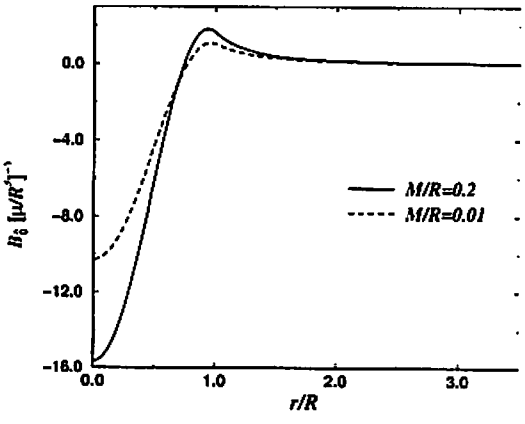

Figure 2: The tetrad component of the magnetic fields, $B_{\hat{\phi}}$ on the equatorial plane ($\theta = \pi/2$), plotted against r/R. The solid line denotes a relativistic case ($M/R = 0.2$), while the dashed line corresponds to a Newtonian case ($M/R = 0.01$). The magnetic fields are normalized by the typical field strength μ/R^3.

3 Deformation of magnetized stars

Since we have investigated the magnetic field of stars, let now us consider deformation due to the magnetic effect (see also Konno et al.[15]). The deformation can be expressed by the second-order corrections in η_B. The poloidal magnetic field and the toroidal electric current produce magnetic pressure corresponding to the Lorentz force $\boldsymbol{J} \times \boldsymbol{B}$. The force causes a flattening star, i.e., equilibrium with quadrupole deformation. The deformation of the equilibrium star is characterized by the ellipticity ε, which is defined by

$$\varepsilon = \frac{\text{equatorial radius} - \text{polar radius}}{\text{mean radius}}. \tag{9}$$

In order to consider the deformation, i.e., ellipticity, we must calculate the perturbation of the space-time metric, which is caused by the magnetic field. Considering the magnetic dipole field, the metric can be expanded as (see also Hartle [11])

$$\begin{aligned} ds^2 &= -e^{\nu(r)}\left[1 + 2\left(h_0(r) + h_2(r)P_2(\cos\theta)\right)\right]dt^2 \\ &\quad + e^{\lambda(r)}\left[1 + \frac{2e^{\lambda(r)}}{r}\left(m_0(r) + m_2(r)P_2(\cos\theta)\right)\right]dr^2 \\ &\quad + r^2\left[1 + 2k_2(r)P_2(\cos\theta)\right]\left(d\theta^2 + \sin^2\theta d\phi^2\right). \end{aligned} \tag{10}$$

where P_2 is the Legendre's polynomial of degree 2, and $(h_0, h_2, m_0, m_2, k_2)$ are the second-order corrections in η_B. The total energy-momentum tensor is the sum of the perfect fluid part ${T_{(m)}}^{\mu}{}_{\nu}$ and the electromagnetic part ${T_{(em)}}^{\mu}{}_{\nu}$:

$${T_{(total)}}^{\mu}{}_{\nu} = {T_{(m)}}^{\mu}{}_{\nu} + {T_{(em)}}^{\mu}{}_{\nu}, \tag{11}$$

where

$${T_{(m)}}^{\mu}{}_{\nu} = (\rho + p)\, u^{\mu}u_{\nu} + p\delta^{\mu}{}_{\nu}, \tag{12}$$

$${T_{(em)}}^{\mu}{}_{\nu} = \frac{1}{4\pi}\left(F^{\mu\lambda}F_{\nu\lambda} - \frac{1}{4}F_{\sigma\lambda}F^{\sigma\lambda}\delta^{\mu}{}_{\nu}\right). \tag{13}$$

From the definition Eq. (9) and the hydrostatic equilibrium condition, the ellipticity of the magnetized star can be written by

$$\varepsilon_B = \frac{2r}{\nu'(\rho_0 + p_0)}J^{\phi}A^{\phi} + \frac{3}{r\nu'}h_2 - \frac{3}{2}k_2. \tag{14}$$

By using of the first-order quantities A_ϕ and J_ϕ, we can solve the second-order Einstein equations. Hence we can obtain the metric functions $(h_0, h_2, m_0, m_2, k_2)$, and the ellipticity ε_B.
The first term of the right-hand side in Eq. (14) corresponds to the effect of the 'Lorentz force', the second term represents the effect of the perturbation of the 'gravitational potential' induced by the magnetic effect, and the third term is a 'purely relativistic term' which arises from a definition of the radius, that is, the circumferential radius.

Fig. 3 displays the ellipticity ε_B and the contribution from each three terms. These are plotted as a function of the relativistic factor M/R, and we have normalized by μ^2R^2/I^2. The quantity I is the moment of inertia; μ^2R^2/I^2 is the ratio of the magnetic energy to the gravitational energy. In our numerical calculations, we have used the polytropic EOS with $n = 1$. From this figure, we can see that the ellipticity becomes large as the relativistic factor, and that the 'Lorentz force' term (unlike the other two terms) strongly influences the ellipticity. An important thing is that the relativistic calculation leads to larger the ellipticity for a fixed value of μ^2R^2/I^2.

4 Comparison of two types of star deformation: magnetic fields and rotation

Not only the magnetic effect, but also rotational effect cause quadrupole deformation. In this section, we also calculate the deformation due to the rotational effect. From the results calculated separately, we compare the magnetic effect with the rotational effect on the quadrupole deformation.

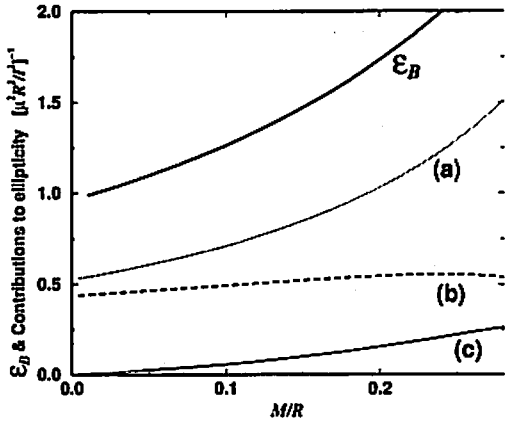

Figure 3: The ellipticity ε_B and the three contributions to the ellipticity: ε_B, and (a) the effect of the 'Lorentz force', (b) the effect of the perturbation of the 'gravitational potential', (c) the 'purely relativistic effect' (see text). These are plotted against M/R.

Before the comparison, we review the rotational deformation following Chandrasekhar & Miller [12], and Hartle [11]. The star has uniform angular velocity $\Omega \sim O(\eta_\Omega)$. The line element of the slowly rotating star is written as

$$\begin{aligned} ds^2 &= -e^{\nu(r)}\left[1+2\left\{h_0(r)+h_2(r)P_2\left(\cos\theta\right)\right\}\right]dt^2 \\ &\quad + e^{\lambda(r)}\left[1+\frac{2e^{\lambda(r)}}{r}\left\{m_0(r)+m_2(r)P_2\left(\cos\theta\right)\right\}\right]dr^2 \\ &\quad + r^2\left(1+2k_2(r)P_2\left(\cos\theta\right)\right)\left[d\theta^2+\sin^2\theta(d\phi-\omega(r)dt)^2\right], \end{aligned} \tag{15}$$

where P_2 is the Legendre's polynomial of degree 2, and $(h_0, h_2, m_0, m_2, k_2)$ are the second-order corrections in η_Ω. The quantity ω is angular velocity as seen by an observer falling freely from infinity to a point r. In a similar way as the deformation of the magnetized star, the ellipticity of the slowly rotating star can be calculated as

$$\varepsilon_\Omega = \frac{r}{\nu'}e^{-\nu}(\Omega-\omega)^2 + \frac{3}{r\nu'}h_2 - \frac{3}{2}k_2. \tag{16}$$

The first term of the right-hand side in Eq. (16) corresponds to the effect of the 'centrifugal force'; this term largely affects the ellipticity of the rotating star ε_Ω. Solving the Einstein equations, we can obtain the metric functions $(h_0, h_2, m_0, m_2, k_2)$ in Eq. (15), and the ellipticity ε_Ω. Now we can see the deformation of the rotating star.

Furthermore, using of the two ellipticities ε_B Eq. (14) and ε_Ω Eq. (16), we can give the comparison of two types of the star deformation: the magnetic effect and the rotational effect. Fig. 4 shows which effect is dominant in the relativistic star with magnetic field strength B and angular velocity Ω. The quantity B denotes the typical magnetic field strength on the surface, which is defined by $B = \mu/R^3$. The critical line on which $\varepsilon_\Omega = \varepsilon_B$ and the two regions divided by this line in B-Ω space. We have used the stellar model with $n = 1$ and $M/R = 0.2$. In the region I, the magnetic effect dominates the rotational effect, i.e., $\varepsilon_B > \varepsilon_\Omega$, while in the region II vice versa, i.e., $\varepsilon_\Omega > \varepsilon_B$. From this figure, we find that the objects having magnetic field strength $B \sim 10^{14}$–10^{15}G and period $T \sim 1$ sec such as SGRs and AXPs belong to the region I. Thus, the magnetic effect overwhelms the rotational effect for such observed candidates of magnetars. On the other hand, well-known typical pulsars with $B \sim 10^{11}$–10^{13}G and $T \sim 10^{-1}$–1 sec obviously belong to the region II. Millisecond pulsars also belong to the region II. The magnetic deformation is neglected for these pulsars. Therefore, in the candidates of magnetars only, the deformation due to the magnetic effect is larger than the rotational effect.

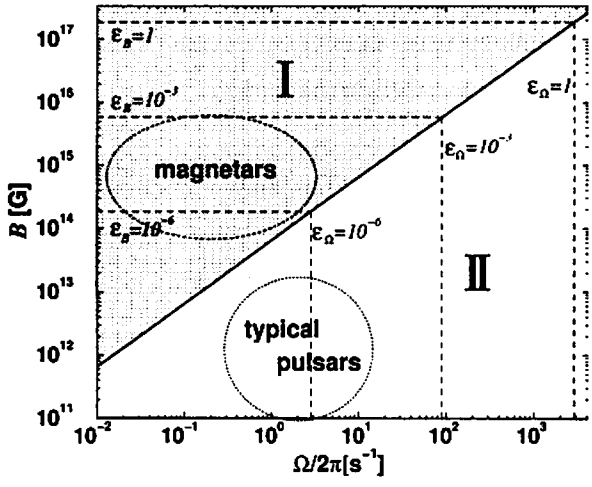

Figure 4: The critical line on which $\varepsilon_\Omega = \varepsilon_B$ in B-Ω space for $M/R = 0.2$. This line divides the B-Ω space into two regions. In the region I, the magnetic effect dominates the rotational effect, while in the region II vice versa.

5 Summary and discussion

We have studied the magnetized star on the relativistic perturbation theory. The summarized results are as follows. (1) the interior magnetic field of the relativistic star is stronger than that of the Newtonian star by about 50% of the Newtonian case (Fig. 1, 2). (2) the ellipticity of the stars is larger as the relativistic factor M/R increases, for the same energy ratio of the magnetic energy to the gravitational energy (Fig. 3). These are important effects of the relativity. (3) the new classes of objects, which seem to be magnetars, are more deformed by the magnetic effect than by the rotational effect (Fig. 4). This implies that the deformation due to magnetic effect becomes a significant factor in many astrophysical phenomena, for example, irregular spin-down process of AXPs, glitch of pulsars, and gravitational radiation.

We have investigated the quadrupole deformation due to the magnetic effect separately from the rotational effect. To consider the deformation more precisely, we have to take into account the both effects at the same time. In this case, the calculations become complicated because of non-vanishing electric field. Moreover, electromagnetic radiation is produced when the rotational axis is non-aligned with the magnetic one. In summary, the couplings in the rotating magnetized objects are quite interesting, and will be the subject of further investigation.

References

[1] C. Kouveliotou, et al., Nature, **393**(1998), 235.

[2] C. Kouveliotou, et al., ApJ, **510**(1999), L115.

[3] S. Mereghetti and L. Stella, ApJ, **442**(1995), L17.

[4] C. Thompson and R. C. Duncan, ApJ, **473**(1996), 322.

[5] J. H. Taylor, R. N. Manchester and A. G. Lyne, ApJ Suppl., **88**(1993), 529.

[6] Melatos A., ApJ, **519**(1999), L77.

[7] Chandrasekhar S., Fermi E., ApJ, **118**(1953), 116.

[8] Ferraro V. C. A., ApJ **119**(1954), 407.

[9] Chandrasekhar S., MNRAS **93**(1933), 539.

[10] Chandrasekhar S., Roberts P. H., ApJ, **138**(1963), 801.

[11] Hartle J. B., ApJ **150**(1967), 1005.

[12] Chandrasekhar S., Miller J. C., MNRAS **167**(1974), 63.

[13] M. Bocquet, S. Bonazzola, E. Gourgoulhon and J. Novak, A & A, **301**(1995),757.

[14] S. Bonazzola and E. Gourgoulhon, A & A, **312**(1996),675.

[15] Konno K., Obata T., Kojima Y., A&A, **352**(1999), 211.